Lecture Notes in Civil Engineering

B. B. Das
Hiroshan Hettiarachchi
Prasanta Kumar Sahu
Satyajeet Nanda *Editors*

Recent Developments in Sustainable Infrastructure (ICRDSI-2020)—GEO-TRA-ENV-WRM

Conference Proceedings from ICRDSI-2020 Vol. 2

Springer

Lecture Notes in Civil Engineering

Volume 207

Lecture Notes in Civil Engineering (LNCE) publishes the latest developments in Civil Engineering - quickly, informally and in top quality. Though original research reported in proceedings and post-proceedings represents the core of LNCE, edited volumes of exceptionally high quality and interest may also be considered for publication. Volumes published in LNCE embrace all aspects and subfields of, as well as new challenges in, Civil Engineering. Topics in the series include:

- Construction and Structural Mechanics
- Building Materials
- Concrete, Steel and Timber Structures
- Geotechnical Engineering
- Earthquake Engineering
- Coastal Engineering
- Ocean and Offshore Engineering; Ships and Floating Structures
- Hydraulics, Hydrology and Water Resources Engineering
- Environmental Engineering and Sustainability
- Structural Health and Monitoring
- Surveying and Geographical Information Systems
- Indoor Environments
- Transportation and Traffic
- Risk Analysis
- Safety and Security

To submit a proposal or request further information, please contact the appropriate Springer Editor:

– Pierpaolo Riva at pierpaolo.riva@springer.com (Europe and Americas);
– Swati Meherishi at swati.meherishi@springer.com (Asia - except China, and Australia, New Zealand);
– Wayne Hu at wayne.hu@springer.com (China).

All books in the series now indexed by Scopus and EI Compendex database!

More information about this series at https://link.springer.com/bookseries/15087

B. B. Das · Hiroshan Hettiarachchi ·
Prasanta Kumar Sahu · Satyajeet Nanda
Editors

Recent Developments in Sustainable Infrastructure (ICRDSI-2020)—GEO-TRA-ENV-WRM

Conference Proceedings from ICRDSI-2020
Vol. 2

Springer

Editors
B. B. Das
Department of Civil Engineering
National Institute of Technology Karnataka
Surathkal, India

Hiroshan Hettiarachchi
Independent Geotechnical
Engineering/Waste Management Consultant
Michigan, USA

Prasanta Kumar Sahu
Department of Civil Engineering
Birla Institute of Technology and Science
Hyderabad, India

Satyajeet Nanda
School of Civil Engineering
KIIT Deemed to be University
Bhubaneswar, India

ISSN 2366-2557 ISSN 2366-2565 (electronic)
Lecture Notes in Civil Engineering
ISBN 978-981-16-7508-9 ISBN 978-981-16-7509-6 (eBook)
https://doi.org/10.1007/978-981-16-7509-6

Contents

Impact Assessment and Mitigation Measures of Stack Emission from a Pelletisation Unit

Chittaranjan Panda, Sudhansu Sekhar Biswal, Trilochan Jena, and Kishor Chandra Panda

Abstract As a part of value addition, one organisation is planning to set up 0.6 MTPA pelletisation unit by collecting the rejected iron ore fines and preparing them into desirable sizes of pellets. The objective of this study is to assess the adverse impact due to emission on the environment in the study area, which can arise due to the proposed project activities. Based on the results of assessment various mitigation measures are planned. Various adverse impacts mainly due to point source emission from stacks and fugitive emission from different area source. Ground level concentrations (GLC) of different pollutants are predicted using USEPA and MoEFFCC recognised software AERMOD ISCST Version 3 by Lakes Environment, Canada. Different input data of control, source and emission, receptor, meteorological source are to be fed to the model. Accordingly, the output results are obtained and are shown graphically as different pollutant isopleths. In order to control the pollutant emission, the different mitigation measure will be planned so that the predicted GLC will be under National Ambient Air Quality Standard (NAAQS) norms.

Keywords Pelletisation · Impacts · Mitigation measure · Isopleth · GLC

C. Panda (✉) · T. Jena
Department of Civil Engineering, Siksha 'O' Anusndhan (Deemed To be University), Bhubaneswar, Odisha 751030, India
e-mail: chittaranjanpanda@soa.ac.in

S. S. Biswal
Environmental Science (Department of Chemistry), Siksha 'O' Anusndhan (Deemed To be University), Bhubaneswar, Odisha 751030, India

K. C. Panda
Department of Civil Engineering, Government College of Engineering, Kalahandi, Bhawanipatna, Odisha, India

B. B. Das et al. (eds.), *Recent Developments in Sustainable Infrastructure (ICRDSI-2020)—GEO-TRA-ENV-WRM*, Lecture Notes in Civil Engineering 207,
https://doi.org/10.1007/978-981-16-7509-6_1

1 Introduction

Iron ore is mined in Keonjhar district in the eastern parts of India. A lot of ore fines are released in the process and are rejected as a subgrade ore. As a part of value addition, some organisation are collecting these fines for beneficiation to higher grade fines and then beneficiated ore are agglomerated into pellets. In the process of palletisation, agglomerated ore are heat dried into form of dry and hard pellets for effective use in our steel plant. Hot gases are formed usually by mixtures of coal gas and furnace oil and is the major source of pollutants. The main pollutant emissions from the stack of pelletisation unit are sulphur dioxide (SO_2), oxides of nitrogen (NO_x) and particulate matter (PM).

ISCST3 model was used to predict NO_2 and PM_{10} emissions from line sources and the results were compared with CALINE4 model. It was observed that CALINE4 model was not suitable to predict pollutants with lower concentrations (Majumdar 2019). It had been found from ISCST prediction of the pollutants from stack emission agreed with the measured value of the ambient GLC value of SO_2, NO_2, CO and particulates from an aluminium foundry within the standard limit values (Cirtina et al. 2016). AERMOD modelling output data for the assessment of SO_2 emission from Patalganga industrial complex, India was found to comply with the NAAQS 2009 norms (Zade and Ingole 2015). Suspended particulate matter emission from a poultry farm was predicted successfully using AERMOD (Hadlocon et al. 2015). Dispersion models like AERMOD and ISCST were successfully assessed during the winter period (Rood 2014). Linear and nonlinear modelling and prediction of NO_x emission was carried out for a coal based thermal power plant (Smrekar et al. 2013). Ground level concentration of SO_2 in Mangalore industrial complex, India was successfully predicted using ISCST3 model (Bandyopadhyay 2009). The dispersion model ISCST-3 prediction of GLC in sponge iron industry location exceeded the NAAQS norms thus necessitating the use of air pollution control devices (Rao et al. 2009). The General Plume Dispersion Model (GPDM) using Java and Visual basic tools was developed based on Gaussian plume dispersion equation (Awasthi et al. 2006).

Pelletisation unit in iron ore rich Keonjhar district will beneficiate iron ore fines to heat dried hard pellet to be used as feed material in iron making industries. The process will use the raw materials like iron ore fines, bentonite, limestone, coal and furnace oil. Grinding and handling of raw materials will release a lot of dust particles and in indurating furnace the green pellets are heat dried by the hot gas produced by burning of furnace oil and coal, thus emitting gaseous pollutants like sulphur dioxide and oxides of nitrogen. In the present work, corresponding to different point

source stack emissions, the ground level concentration of pollutants is predicted using ISCST-3 modelling software without air pollution control measures and then with air pollution control devices.

2 Materials and Methods

2.1 Air Quality Modelling

The Industrial Source Complex-Short Term Version 3 (ISCST-3) by Lakes environment, Canada is the model used for predicting the ground level concentration (GLC) of the pollutants from different point sources as per the Central Pollution Control Board guidelines. The model uses rural dispersion and regulatory defaults options as per guidelines on air quality models. This model uses Gaussian Plume dispersion equation for computing the pollutant concentration for any point co-ordinates X and Y (in meters) with respect to the central stack. The GLC of the pollutant C is given by the equation

$$\mathrm{C\,(X,\,Y,\,0:H)} = \frac{Q}{\pi\sigma y\sigma zU}\exp\left[-1/2\,(\mathrm{y}/\sigma_{\mathrm{y}})^2\right]\left[\exp\{-1/2\,(\mathrm{H}/\sigma_{\mathrm{z}})^2\right]$$

Q = Emission rate in gm/sec.
U = Wind speed at Stack (m/s) in X direction (down wind direction).
$\boldsymbol{\sigma_{\mathrm{y}}}$, $\boldsymbol{\sigma_{\mathrm{z}}}$ = Dispersion coefficient in **Y** and Z direction.
H = Effective stack height (Physical height + Plume rise) in m.

2.2 Model Input

2.2.1 Control Option

Among the various control options include that plume rise is calculated by using Brigg's formula. It considers buoyancy induced dispersion, calm processing routine and 24 h averaging. The pollutants will not undergo physico-chemical changes.

Table 1 Stack and emission data

Parameters	Induration furnace	RMH section	Proportionating system	Ball mill	Coke grinding section
No of stack	1	1	1	1	1
Height in m	60	30	30	30	30
Diameter (m)	3	1	1	1	0.8
Temperature (°C)	150	40	40	40	40
Velocity (m/s)	20.1	7.38	5.56	7.38	5.77
Gas flow (m^3/s)	360,000	21,000	15,000	21,000	10,000
PM_{10} (gm/s)	3.0	0.37	0.25	0.37	0.17
$PM_{2.5}$ (gm/s)	2.0	0.29	0.17	0.29	0.11
SO_2 (gm/s)	11.32	–	–	–	–
NO_x (gm/s)	15.0	–	–	–	–
APC equipment	ESP	Bag house	Bag house	Bag house	Bag house

2.2.2 Source and Emission Data

The emission from stacks are the main point sources of air pollution from the proposed plant. The proposed plant is to be provided with adequate air pollution control devices like electrostatic precipitators (ESP) and, bag houses. The emission inventory is prepared on the basis of following assumptions and calculations. Particulate emission is based upon the air pollution control device (APCD) with design stack emission limited to <50 mg/Nm^3. PM_{10} and $PM_{2.5}$ was assumed to be 60 and 40% of the particulate matter. SO_2 Emission in power plant is based on sulphur content in furnace oil, coal, coke and 60% SO_2 emission will be reduced by limestone dosing along with other raw materials. NO_x emission is taken from the emission data at the rate of 100 mg/Nm^3. Stack and emission data are presented in Table 1.

2.2.3 Meteorological Data

The primary meteorological data was recorded at the 8 number of sampling points which were input to the model. For the present study, wind speed (ms^{-1}), wind direction (degrees), Temperature (C); Pressure (mbar), cloud cover and Relative humidity (%) were measured at the station with the meteorological data, the wind rose diagram is constructed for the winter seasons ranging from December to February in 2019 and is shown in Fig. 1. The predominant wind directions were found to be from

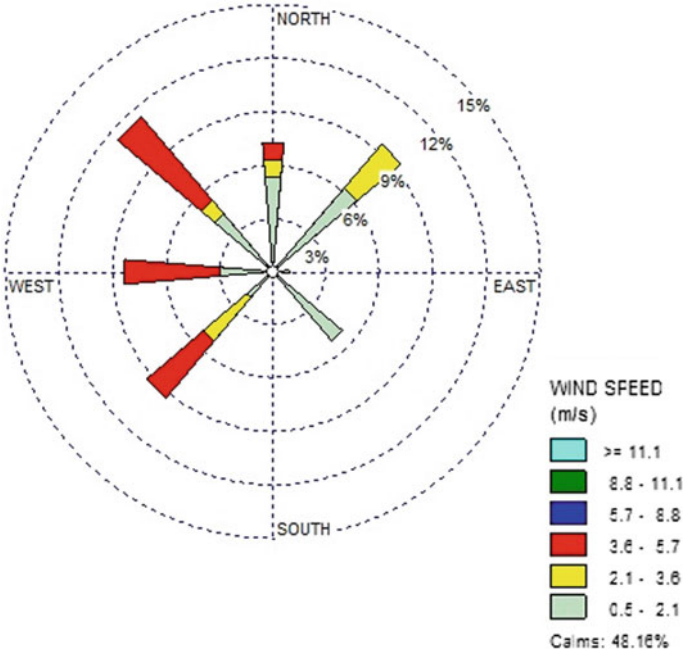

Fig. 1 Wind rose diagram

southwest directions to north east direction followed by west to east and south-west to north east.

2.2.4 Receptor Options

In a polar coordinate system with respect to the central stack in 16 possible wind directions (N to NNW). Total of 336 grid points with 500 m spacing were chosen to predict the incremental GLC at different sampling location. Maximum incremental GLCs have been calculated at every 500 m grids spacing.

3 Result and Discussion

Model output results show the incremental GLC at different sampling locations without the mitigation measures and then with the mitigation measures.

Table 2 Maximum GLC of pollutants without mitigation measures

Sl No	Pollutant parameters	Incremental GLC in $\mu g/m^3$	NAAQS-2009
1	PM10	336.9	100
2	PM2.5	235.4	60
3	SO_2	1.2	80
4	NO_x	1.37	80

3.1 Incremental GLC of Pollutants Without Mitigation Measures

Pellet plant shall use huge amounts of iron ore, limestone, dolomite and coal in granulated and powdered form resulting in considerable amount of particulates. Similarly, large amount of use of coal and fuel oil shall contribute to significant gaseous pollution. With no mitigation measures, the modelling results indicate that there will be release of very high unacceptable levels of incremental particulate and gaseous emissions and hence adequate mitigation measures must be taken up. The modelling results without mitigation measures are mentioned in Table 2

Obviously, there will be serious emission problems with respect to particulate matter plant operations. Adverse impacts on the various environmental attributes are listed below.

Due to high particulate emission.

- Very Serious human health disorders particularly in respiratory, digestive and other system.
- Contamination of surface water leading to water pollution related health problems.
- Dust deposition on plant leaves reduce the photo-synthetic activities in plants.
- Dust depositions cause material damage.

3.2 Mitigation Measures Suggested for Stack Emissions Control

Electrostatic Precipitator (ESP) will be installed to minimize particulate matter to be generated from the flue gas from the furnace. The collected particulate matter will be recycled in the palletisation process. Suitable dust extraction system followed by adequate capacity bag houses shall be provided at ball mill, grinding units and raw material handling facilities to control the particulate matter and prevent them

Table 3 Details of air pollution control (APC) system

Sl. No	Department	APC proposed	Design stack emissions	APC efficiency
1	RMHS	Dust extraction with Bag house	<50 mg/Nm^3	>99%
2	Coke grinding	Dust extraction with Bag house	<50 mg/Nm^3	>99%
3	Proportioning	Dust extraction with Bag house	<50 mg/Nm^3	>99%
4	Ball mill	Dust extraction with Bag house	<50 mg/Nm^3	>99%
5	Indurating furnace	Elecrostatic pecipitator (ESP)	<50 mg/Nm^3	>99%

becoming air borne. The various APCD attached to different stacks with efficiency are presented in Table 3.

3.3 Model Output: Maximum Anticipated Ground Level Concentration (GLC) of Pollutants with Mitigation Measures

The predicted maximum incremental contribution of GLC found at different sampling locations are 3.37 μg/m^3 for PM_{10}, 2.35 μg/m^3 for $PM_{2.5}$, 0.78 μg/m^3 for SO_2 and 1.37 μg/m^3 for NO_X respectively. The predicted contributions of different pollutants from the proposed plant when added with the monitored existing background levels of PM, SO_2 and NO_X, the resultant shall be well within the norms of Industrial/residential area norms (NAAQS 2009). The results are presented in Table 4 and they are illustrated in Figs. 2, 3, 4 and 5.

Table 4 Maximum predicted GLC (with mitigation measures)

Pollutant parameter	Sampling location code	Distance (km) and direction	Max ambient GLC in μg/Nm^3	Max. predicted incremental GLC μg/Nm^3	Max. resultant values of GLC in μg/Nm^3	NAAQS-industrial residential area norm μg/Nm^3
PM_{10}	A6	W-3.5	31.7	3.37	35.07	100
$PM_{2.5}$	A6	W-3.5	26.3	2.35	28.65	60
SO_2	A3	NE-2.5	9.4	0.77	10. 17	80
NO_X	A3	NE-2.5	14.4	1.37	15.77	80

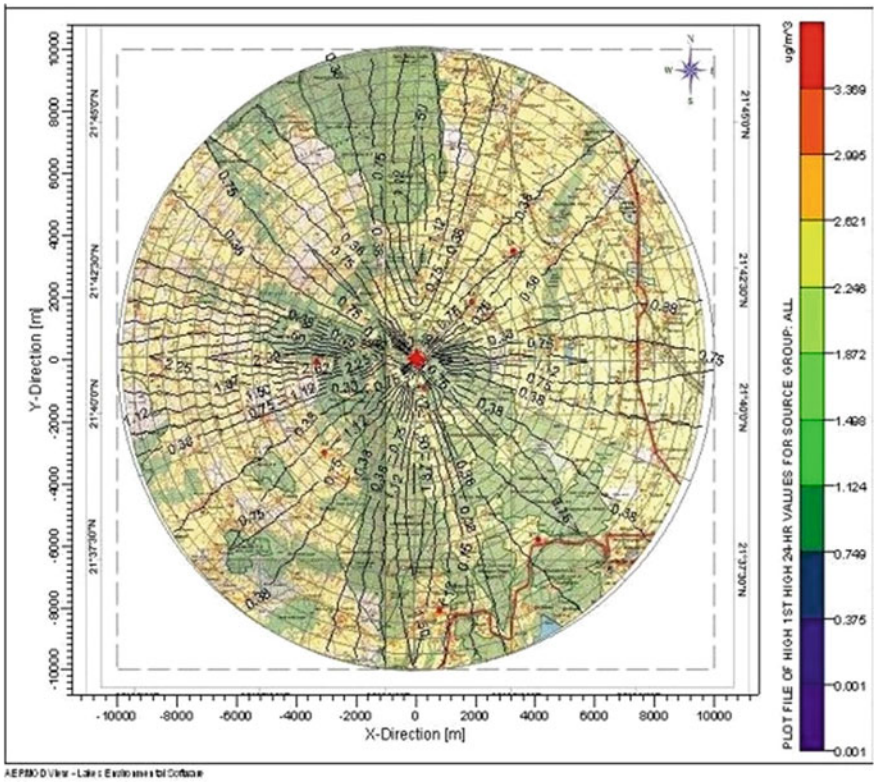

Fig. 2 Isopleth of PM_{10}

Sampling location are chosen and are coded in the downwind and crosswind directions of the predominant wind direction and are mentioned in Table 5. From the model output data sheets, the maximum incremental GLC values for PM_{10}, $PM_{2.5}$, SO_2 and NO_x are observed at different sampling locations and the same are plotted against different down wind and cross wind distances at a receptor interval of 500 m. The results are depicted graphically in Figs. 6, 7, 8 and 9.

4 Conclusion

The point source emission particularly the particulate emission from different stacks without adequate air pollution control measures exceeds the NAAQS norms for

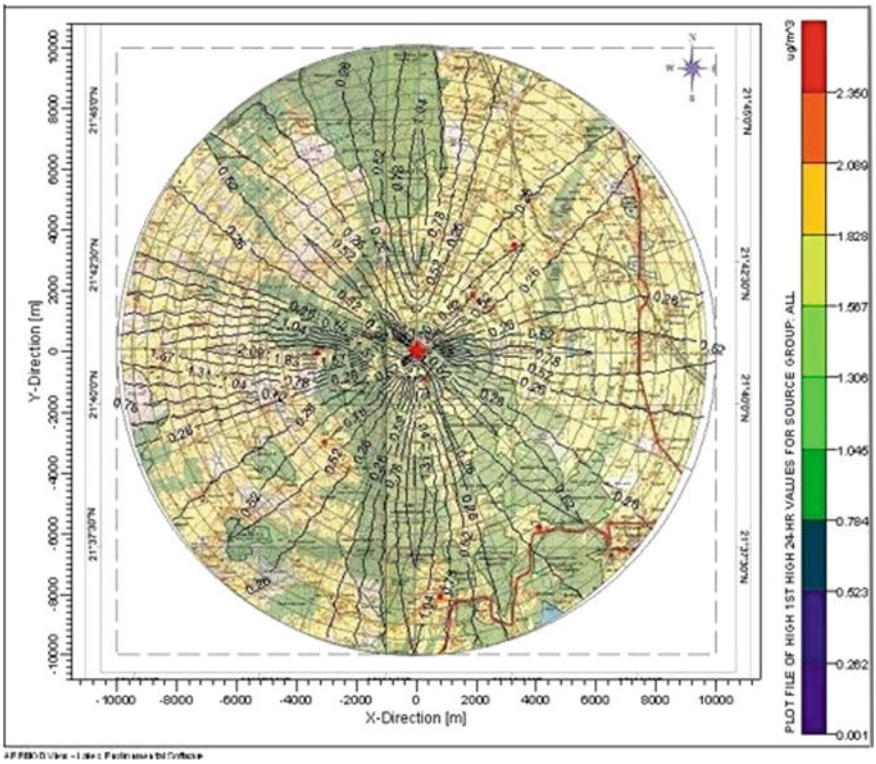

Fig. 3 Isopleth of $PM_{2.5}$

almost at all sampling points. So the adequate capacity bag houses and electrostatic precipitators is to be provided at each stack so that particulate emission will be below 50 mg/Nm^3. For SO_2 emission is controlled by the lime addition with the raw material that effectively reduces SO_2 emission by 60%. With the use of tall stack, the flue gas SO_2 is effectively dispersed to the atmosphere and GLC of SO_2 remains well within the NAAQS norm. Therefore, it may be concluded, with adequate pollution control measures, GLC of pollutants comply the norms set by National Ambient Air Quality Standard (NAAQS 2009).

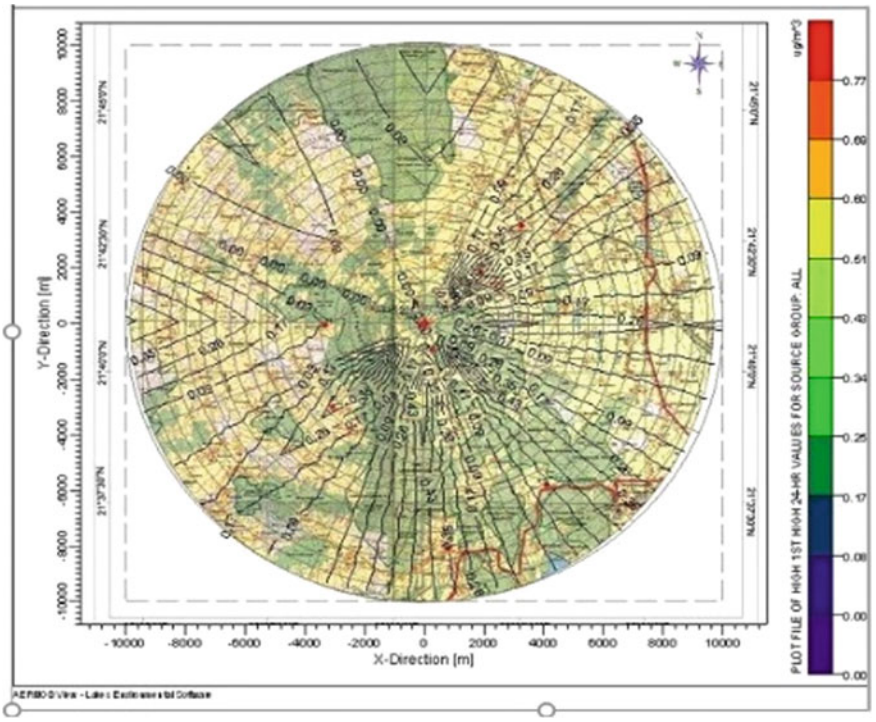

Fig. 4 Isopleths of SO_2

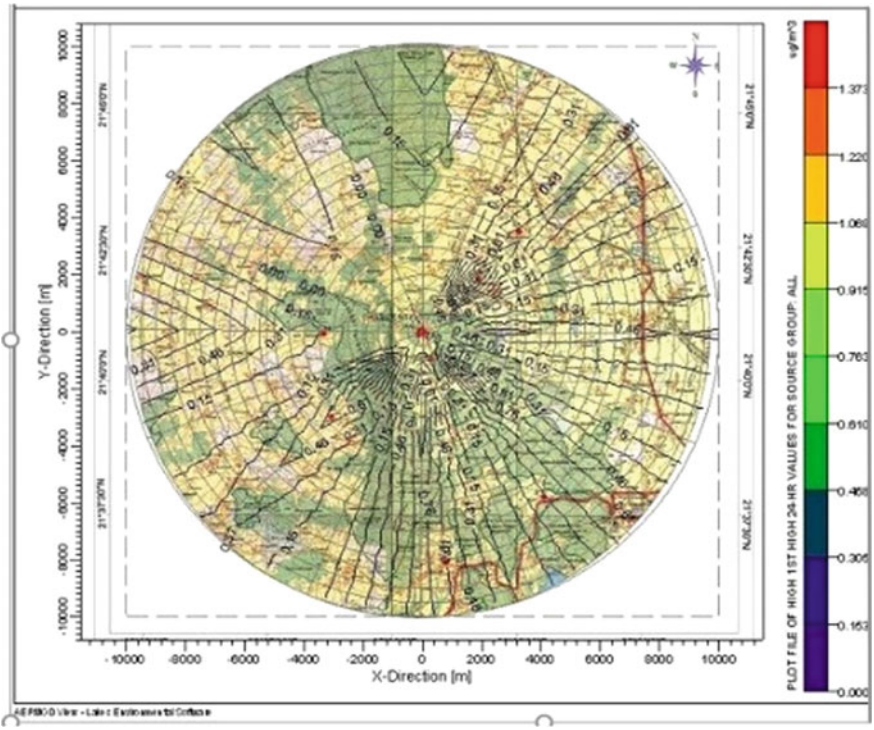

Fig. 5 Isopleths of NO_x

Table 5 Sampling locations from the plant site with distance and direction

Locations code	A1	A2	A3	A4	A5	A6	A7	A8
Distance km	Plant site 0 km	5.0	2.5	2.0	5.0	3.5	7.0	8.0
Direction	0	SW	NE	SE	NE	W	SE	S

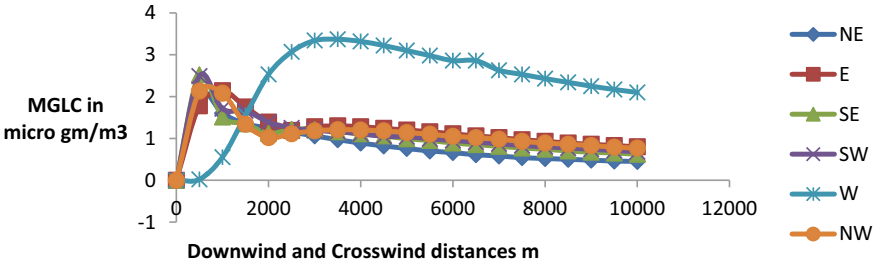

Fig. 6 MGLC for PM_{10} in different locations

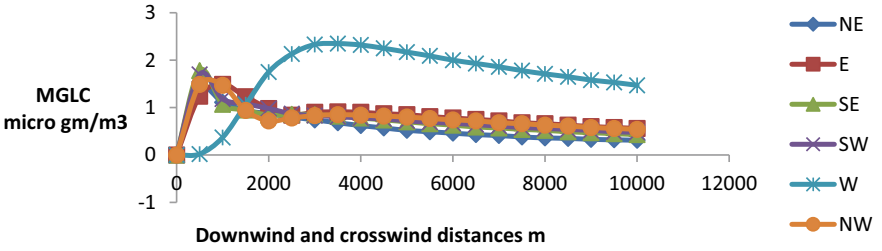

Fig. 7 MGLC for $PM_{2.5}$ in different locations

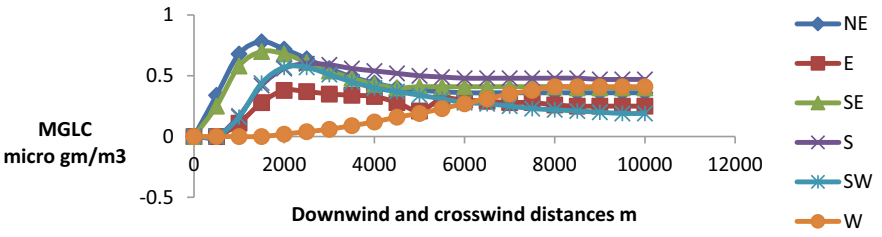

Fig. 8 MGLC for SO_2 in different locations

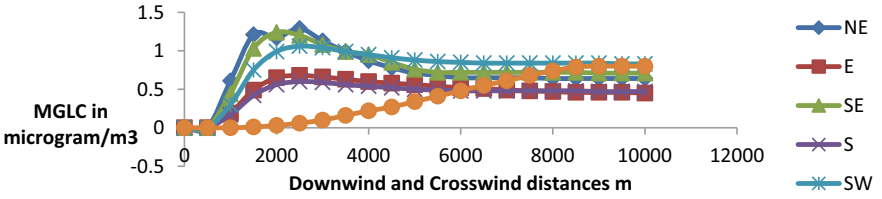

Fig. 9 MGLC for NO_x in different locations

References

Awasthi S, Khare M, Gargava P (2006) General plume dispersion model (GPDM) for point source emission. Environ Model Assess 11:267–276

Bandyopadhyay A (2009) Prediction of ground level concentration of sulphur dioxide using ISCST3 model in Mangalore industrial region of India. Clean Tech Environ Policy 11:173–188

Cirtina D, Chivu O, Cirtina M (2016) Assessment of air pollutants produced by industrial activity from an aluminium alloys foundry. Metalurgija 55(1):11–14

Hadlocon LS, Zhao LY, Bohrer G, Kenny W, Garrity SR, Wang J, Wyslouzil B, Upadhyay J (2015) Modeling of particulate matter dispersion from a poultry facility using AERMOD. J Air Waste Manage Assoc 65:206–217

Majumdar S (2019) Emission load distribution and prediction of NO_2 and PM10 using ISCST3 and CALINE4 line source modeling. Appl J Environ Eng Sci 5:121–135

Rao PS, Kumar A, Ansari MF, Pipalatkar P, Chakrabarti T (2009) Air quality impact of sponge iron industries in Central India. Bull Environ Contam Toxicol 82:255–259

Rood AS (2014) Performance evaluation of AERMOD, CALPUFF, and legacy air dispersion models using the winter validation tracer study dataset. Atmos Environ 89:707–720
Smrekar J, Potocnik P, Senegacnik A (2013) Multi-step-ahead prediction of NOx emissions for a coal-based boiler. Appl Energy 106:89–99
National Ambient Air Quality Standard, Central pollution control board (2009)
Zade S, Ingole NW (2015) Air dispersion modelling to assess ambient air quality impact due to carbon industry. Int J Res Stud Sci Eng Technol 2(7):45–53

Bearing Capacity of Square Footing on Cohesive Soil Reinforced with Geocomposite

Stutee Mohanty and Kajal Swain

Abstract Various reinforcing techniques have been used till now for the bearing capacity improvement of Shallow Foundations over soft clay. Of all the techniques, Geosynthetic reinforcement has proved to be a cost-effective solution. Many researchers have focused on behaviour of Geotextile or Geogrid alone as a reinforcing material. But less research is available on Geocomposites. In this study, the combination of Geotextile and Geogrid (i.e. Combigrid) is used as a single reinforcing material in a single layer which is more economical than using different materials in different layers, hence the purpose of my research is to provide a cost-effective ground improvement technique in soft soil by using a single layer of geocomposite at optimum depth and length. Laboratory tests are performed on various configurations of the reinforcement layout to investigate the bearing capacity of reinforced clay. The model test tank of size 280 mm × 280 mm × 240 mm and square footing of width 5 cm is used. First the model tank is tested in a Universal Testing Machine with clay only and the Bearing capacity of unreinforced clay is recorded, then for 0.3B depth of reinforcement, three varied lengths of reinforcement (3B, 4B, 5B) are tested. Similarly, for 0.5B, 0.7B and 0.9B depth, the length of reinforcement varied from 3 to 5B (B = width of footing) and for each case, the bearing capacity is calculated. Results are compared in terms of BCR and it is found that Combigrid helps in bearing capacity improvement of soft clay upto four times more than the Unreinforced Bearing Capacity.

Keywords Bearing capacity · Reinforcement · Combigrid · Universal Testing Machine · Geogrid

S. Mohanty (✉)
School of Civil Engineering, KIIT University, Bhubaneswar, India

K. Swain
Department of Civil Engineering, VSSUT, Burla, India

B. B. Das et al. (eds.), *Recent Developments in Sustainable Infrastructure (ICRDSI-2020)—GEO-TRA-ENV-WRM*, Lecture Notes in Civil Engineering 207,
https://doi.org/10.1007/978-981-16-7509-6_2

1 Introduction

Over the last three decades, the availability of good construction sites has decreased. This has inversely resulted in the increased use of low-quality construction sites where the bearing capacity of the soil is very poor and any construction on these sites will result in differential settlement and collapse of the structure. Therefore, it is important to improve the bearing capacity of weak foundation soils through various economical and durable methods. Extensive research has been conducted by multiple researchers to analyze the function of various reinforcing materials in improving the bearing capacity of foundation soils. Of all the reinforcing material used in the experiments, Geosynthetic is found out to be a promising material whose inclusion in soil with proper layout and configuration can drastically improve the bearing capacity of weak soil. Apart from these, there are various other factors which effects the level of improvement such as soil type, geosynthetic type, foundation type and foundation depth. Geosynthetic material are found in various forms such as geogrids, geotextiles, geocell, etc. and all of these forms are popular for their different functions related to improvement of soil properties. Khing et al. (1993) performed a study to evaluate the bearing capacity of strip foundation resting on geogrid reinforced sand bed. In their study, after giving six layers of reinforcement, the bearing capacity increased about 1.5 times. Several other researchers such as Das and Omar et al. (1994), Yetimoglu (1998), Adams and Collin (1997), Latha and Somwanshi (2009) and Ronad (2014) also conducted experimental studies on sand bed using geogrid as a reinforcement material. Guido et al. (1985) performed tests on sand bed with geotextile as reinforcement and concluded that the bearing capacity of reinforced soil increased by a factor greater than three. In Guido et al. (1986) did a comparative study between geogrid and geotextile to show their role in improvement of Soil's bearing capacity. The results showed that the bearing capacity increases with either type of reinforcement. It was observed from the results that for geotextiles to perform suitably as reinforcement material, friction should build up between the soil and the reinforcing material to prevent slipping of the material. Whereas for geogrids, the interlocking of the soil through the grid openings accomplishes an effective anchorage effect. Basudhar et al. (2007) also performed tests on geotextile reinforced sand bed. A combination of experimental and numerical studies was performed to evaluate the effects of reinforcement. Tests were carried out with the number of reinforcement layers varying from 0 to 3 and sand bed's relative density varying from 45 to 84%. It is reported that with three layer of reinforcement the ratio of bearing capacity increased about 4.5 times than of unreinforced case. Regarding settlement reduction, it was concluded that bending stiffness is not present in geotextiles for which the settlement could not be reduced appreciably. Chen ety al. (2007) studied the performance of geosynthetic-reinforced sandy soil foundations in terms of increasing the bearing capacity and settlement reduction. The parameters investigated were the uppermost layer spacing, number of reinforcement layers and spacing between them, the depth of embedment and the effect of shape of footing. Two different geosynthetics were used for comparision- (1) geogrid and (2) geotextile, both were used separately as

well as combined to investigate the difference. The results of the test showed that the settlement can be reduced upto 20% at all pressure levels of the footing when more than two layers of reinforcement was provided. The geogrid and geotextile combination performed better in improving the bearing capacity of sand than those reinforced by single geosynthetic material. The outcomes test also stated that the optimum top layer spacing was 0.33B for the embedded square model footing ($D_f/B = 1$) on sand reinforced with geogrid and the effective reinforcement length is 6B. The inclusion of reinforcement could appreciably distribute the applied load to a more enhanced uniform pattern, thus reducing concentration of stress, which resulted in settlement reduction. Ramaswamy and Purushottaman (1992) performed experimental studies of model circular footings on the clayey soil foundation reinforced with geogrid. Their results revealed that the optimal upper layer spacing was found to be about 0.5 times the diameter of the footing and the effective reinforcement length was found to be about four times the footing diameter. With the increase in number of layers from one to three, the BCR value increased from 1.15 to 1.70. Mandal and Sah (1992) performed a series of model tests on 100 mm square footings supported on clay reinforced with geogrid from the model test results it was observed that when the top layer spacing was 0.175 times the width of footing, the maximum BCR achieved was 1.36 was and the minimum settlement reduction factor (SRF) was obtained when top layer spacing was 0.25 times the width of footing. The settlement could be reduced upto 45% with the use of geogrid material. Shin et al. (1993) led a trial investigation of strip footings on clay bed reinforced with geogrid. The outcomes demonstrated that the optimal upper sheet spacing was about 0.4 times the width of footing and the effective reinforcement length was about 4.5 to 5 times the width of footing. With the increasing number of layer from 1 to 5, the BCR value also increased from 1.06 to 1.45 and nearly kept consistent from that point. Sakti and Das (1987) performed a study on the clay foundation reinforced with geotextile. Their results elucidated the following;—(1) The maximum geotextile reinforcement advantage was obtained when the upper sheet of reinforcement was placed at a depth of 0.35 times the footing width, (2) With the increasing number of layers from 1 to 3, the BCR estimation also increased from 1.1 to 1.5 and then remained consistent. The influence depth of geotextile placement was found to be same as the width of the footing, and (3). The effective geotextile length was equal to 4 times the strip footing width. Chen et al. (2007) performed an experimental study on a geosynthetic reinforced clay foundation, where the geosynthetics were geogrid and geotextile, both used separately. The model footing was a square footing of size 152 mm × 152 mm. The test gave the following results (1) the reinforcement inclusion could insignificantly increase the bearing capacity of soil and reduce the settlement of footing, (2) the optimal spacing of the top layer was found to be 0.33 times the width of square footing on clay reinforced with geogrid, (3) geogrid beyond the effective length (6B) resulted in negligible mobilized tensile strength.

2 Objectives and Scope

It is known that some previous work along this sector has been done by some of the researcher by taking reinforced sand and different types of footings but the results have been no conclusive and furthermore very little has been published by using square footing. Many test have been done with various types of reinforcement to improve the bearing capacity of sand but hardly very few have been made with square footing on clay. The majority of the previous research is oriented towards reinforcing the soil with geogrids and geotextiles as two separate reinforcing materials and both of the materials have shown good results in the past studies. It will be interesting to study how the combination of these materials works. Therefore a Geocomposite known as Combigrid will be used in the proposed study to be used as a reinforcing material for the foundation bed. Apart from highway engineering and railway engineering, this Geocomposite i.e. Combigrid has not been used much in other areas. This will be a new attempt in the field of geotechnical engineering where combigrid will be used to reinforce the foundation bed.

3 Experimental Investigation

3.1 Materials

Clayey Soil samples were collected from the local sites of Burla, Sambalpur. Tests are conducted on representative sample for index properties. The liquid limit and plasticity index values of tested sample are 38% and 21.22 respectively and the soil is classified as clay of intermediate clay as per USCS. The properties of this clay are listed in Table 1.

For the reinforcement a geosynthetic material Combigrid was used in the model study (Table 2).

Table 1 Properties of clay

Parameters	Value
Specific gravity	2.27
Liquid limit (%)	38
Plastic limit (%)	16.78
Plasticity index (%)	21.22
Natural moisture content (%)	7.6
Optimum moisture content (%)	13.12
Maximum unit weight	21.5
Shear strength (kPa)	30
USCS classification symbol	CI

Table 2 Properties of combigrid

Quality assurance parameters secugrid 30/30 Q1 (A)	Standard/unit	Values
Material/type	Polypropylene/bi oriented—biaxial	
Aperture size	(mm)	32 × 32
Max tensile strength MD/CD	EN ISO 10319 (kN/m)	≥ 30/ ≥ 30
Elongation at nominal tensile strength	EN ISO 10319 (%)	≤ 7%
Tensile strength @ 0.5% strain MD/CD	EN ISO 10319 (kN/m)	3.0
Tensile strength @ 2% strain MD/CD	EN ISO 10319 (kN/m)	12.0/12.0
Tensile strength @ 5% strain MD/CD	EN ISO 10319 (kN/m)	24.0/24.0

- Combigrid is a combination of secugrid, geogrid made of stretched monolithic polypropylene bars with welded junction and a mechanically bonded filter geotextile welded with the geogrid structure. This material therefore has functions of reinforcement, filtration and separation. The properties of combigrid as provide by the manufacturer is as follows.

3.2 Test Setup

The model test was set up in a wooden tank of dimensions 280 mm × 280 mm × 240 mm. The model footing used is a mild steel plate with dimensions 50 mm × 50 mm (sides) and 10 mm (thickness). The footing was loaded by universal testing machine and the load settlement data was recorded under various reinforcement arrangements.

3.3 Preparation of Test Bed

The model tank is cleaned from inside and inner wall is greased with thin coat to avoid friction between the clay and the tank wall. The test tank's volume was calculated by measuring the inner dimensions of the tank correctly. Then the weight of the clay required to fill up the tank of required density of 21 kN/m^3 was computed. The soil is prepared in layers and is filled upto bottom layer of reinforcement. Each layer was compacted and the compaction energy was kept constant throughout the tests. Random arrangements have been made by varying number of reinforcement and depth of reinforcement and then load is applied and settlement of footing is noted (Fig. 1).

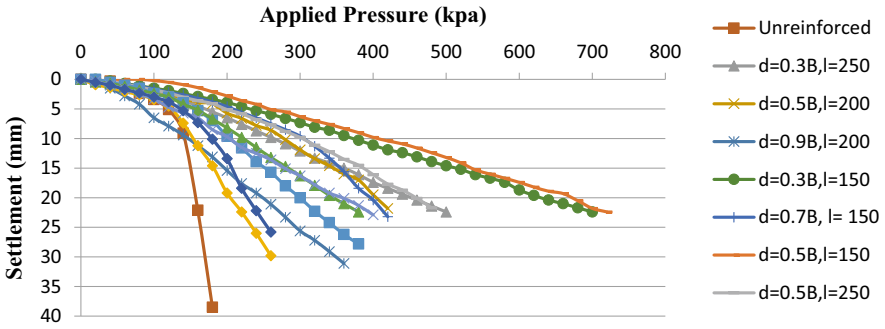

Fig. 1 Summary of tests

3.4 Testing Procedure

After the soil bed was prepared, the footing was placed exactly at the centre of the loading assembly. The tests have been performed for unreinforced and reinforced condition of soil. The load is applied using UTM at a constant rate of settlement of 1 mm per minute. The load and settlement are recorded from the digital display system. The loading was stopped when the settlement exceeded 40% of the width of the footing which is the criteria used for determination of the ultimate bearing pressure in this study). After the load tests, the equipment were removed, the test tank was emptied and due preparations were made for the next set of loads. A total of 13 load tests on model footings were conducted in the laboratory as per the following breakup (Table 3).

4 Results and Analysis

The laboratory model test results are summed up in table. In this table, the BCR obtained at settlement ratios (s/B) = 10%, 20%, 30% and 40% are presented. One test is for unreinforced clay and the other test series data is as below in Table 4.

Figure 2a, b and c shows the results of the tests performed on 50 mm square footing on clay bed reinforced with combigrid of length 3B, 4B and 5B respectively (Fig. 3). In all the three different lengths, the variation of depth was 0.3B, 0.5B, 0.7B and 0.9B respectively. The Fig. 4 illustrates the effect of reinforcement depth on bearing capacity for length 3B placed at four different depths. The bearing capacity is higher when the reinforcement is provided at a depth of 0.5B and 0.3B. However the load carrying capacity decreased when the depth of reinforcement was increased. So, for this case, the optimum depth of reinforcement was 0.5B. Load tests were also conducted for 200 mm long reinforcement placed at different depths and the results illustrated that 0.5B was the optimum depth followed by 0.3B. On increasing the depth beyond 0.5B, the load carrying capacity gradually decreased (Fig. 5). When

Table 3 Tests conducted

Description of load test	No. of test conducted
Without reinforcement	1
With reinforcement at depth 0.3B	
Of length 3B	1
Of length 4B	1
Of length 5B	1
With reinforcement at depth 0.5B	
Of length 3B	1
Of length 4B	1
Of length 5B	1
With reinforcement at depth 0.7B	
Of length 3B	1
Of length 4B	1
Of length 5B	1
With reinforcement at depth 0.9B	
Of length 3B	1
Of length 4B	1
Of length 5B	1
Total number of tests	13

Table 4 Summary of tests

				s/B = 10%		s/b = 20%		s/B = 30%		s/B = 40%	
Test No	Reinforced configuration	*l*, mm	*d*	*q*, kpa	BCR	*q*, kpa	BCR	*q*, kpa	BCR	*q*, kpa	BCR
1	Unreinforced			120		145		150		155	
2		150	0.7B	200	1.6	300	2.06	358	2.38	400	2.58
3		150	0.3B	220	1.83	360	2.48	500	*3.33*	630	*4.06*
4		**150**	**0.5B**	258	2.15	400	2.75	530	*3.53*	670	**4.32**
5		150	0.9B	158	1.31	224	1.54	280	1.86	340	2.19
6		200	0.7B	160	1.33	200	1.37	250	1.66	300	1.93
7		200	0.3B	120	1	200	1.37	280	1.86	360	2.32
8	Reinforced	200	0.5B	190	1.58	278	1.91	340	2.26	400	2.58
9		200	0.9B	85	0.7	145	1	200	1.3	250	1.61
10		250	0.7B	137	1.14	180	1.24	205	1.36	230	1.48
11		250	0.3B	160	1.33	260	1.79	360	2.4	450	2.9
12		250	0.5B	198	1.65	300	2.06	380	2.5	460	2.96
13		250	0.9B	121	1	157	1.08	180	1.2	205	1.32

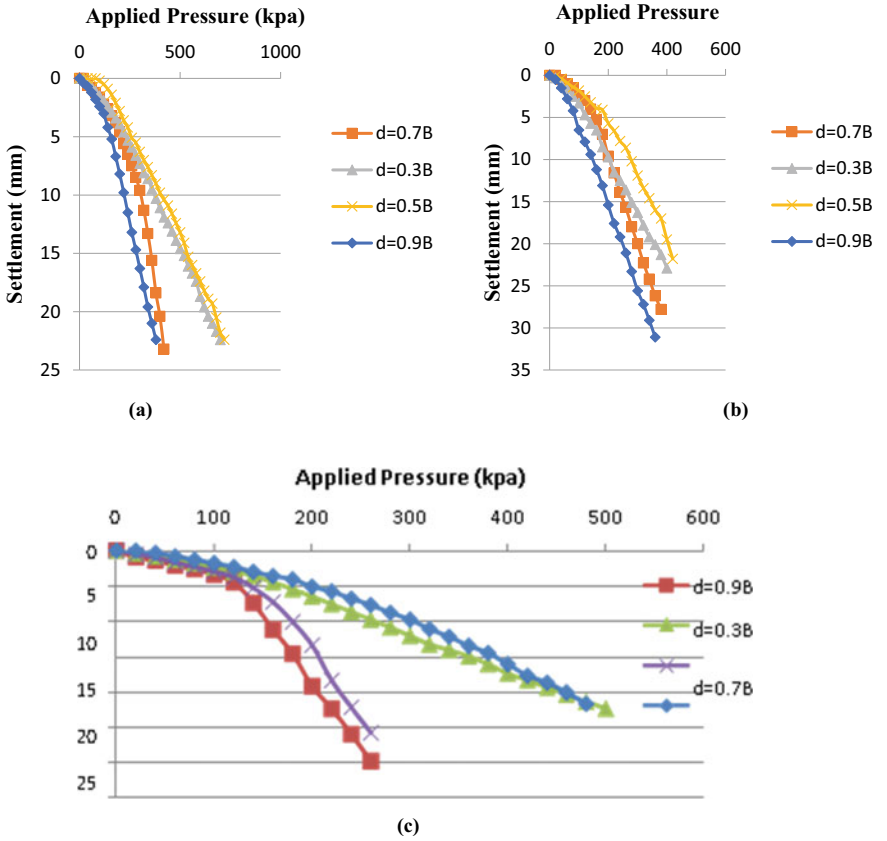

Fig. 2 **a** Bearing pressure—settlement behaviour of reinforced soil at reinforcement length = 3B and varying depths, **b** Bearing pressure—settlement behaviour of reinforced soil at reinforcement length = 4B and varying depths. **c** Bearing pressure—settlement behaviour of reinforced soil at length = 5B and varying depths

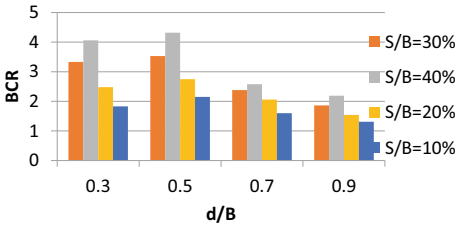

Fig. 3 BCR based on 10, 20, 30, 40% settlement ratios for reinforcement length of 150 mm at different depths

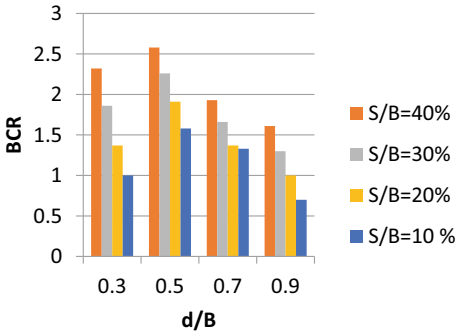

Fig. 4 BCR based on 10, 20, 30, 40% settlement for reinforcement length of 200 mm at different depth

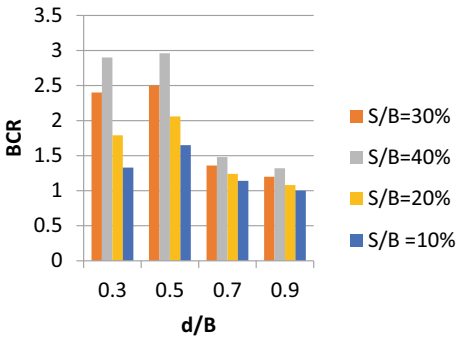

Fig. 5 BCR based on 10, 20, 30, 40% settlement for reinforcement length of 250 mm at different depths

the reinforcement of length 5B was placed at different depths, the outcomes are as shown in Fig. 6. In this case too, the best results are obtained at d/B = 0.5.

4.1 Effect of the Reinforcement Depth

The load settlement behaviour of the reinforced clay for different depths of reinforcement i.e. 0.3B to 0.9B is compared with that of the unreinforced clay. For all the three different lengths of reinforcement, the variation of BCRs obtained at settlement ratios of s/B = 10%, 20%, 30% and 40% for different depths of reinforcement are shown in Figs. 7, 8, 9. It can be seen from the figures that BCRs at a reinforcement depth of 0.5B is higher when compared to other depths and the BCR values are also increasing with the increase in settlement ratios. From the figures, it can

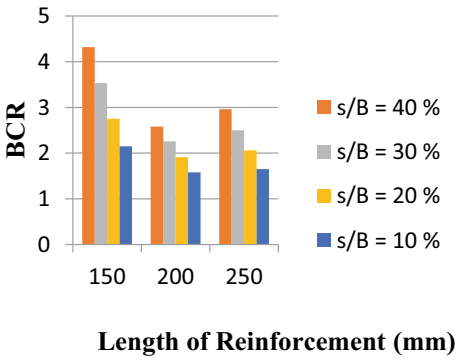

Fig. 6 BCR based on 10, 20, 30, 40% settlement for d/B = 0.5 at different lengths of reinforcement

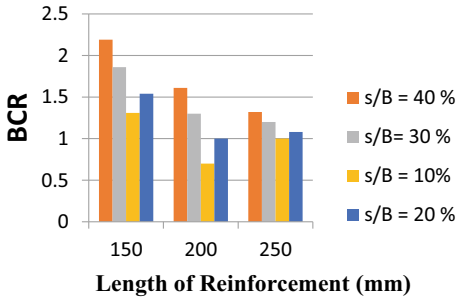

Fig. 7 BCR based on 10, 20, 30, 40% settlement for d/B = 0.9 at different lengths of reinforcement

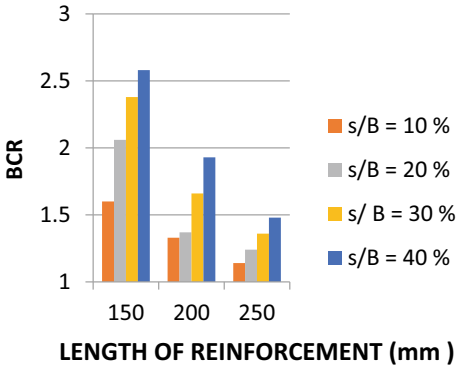

Fig. 8 BCR based on 10, 20, 30, 40% settlement for d/B = 0.7 at different lengths of reinforcement

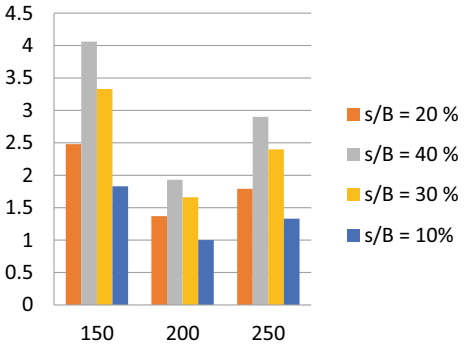

Fig. 9 BCR based on 10, 20, 30, 40% settlement for d/B = 0.3 at different lengths of reinforcement

be observed that at different settlement ratios, the bearing capacity is improving by factors 2.15–4.32 at optimum depth and optimum length of reinforcement.

4.2 Effect of the Reinforcement Length

The load tests were performed at the optimal reinforcement depth with reinforcement length varying from 3B to 5B.The results have been presented in Table 4. From the results it can be noticed that the BCR values at different settlement ratios are higher at a shorter length of reinforcement i.e. at L = 3B (B = width of the footing) irrespective of the depth of reinforcement. On increasing the length, the BCR values are generally decreasing. By using economic size of reinforcement at optimum depth, it is found that the bearing capacity increased to a maximum value of 4.32.

5 Conclusion

13 model tests were conducted for the evaluation of the potential of combigrid for improvement in bearing capacity. Only a single layer of Combigrid was placed beneath the 50 mm square footing in clayey soil. The ratio of the reinforcement depth to width of footing (d/B) varied from 0.3 to 0.9. The length of the reinforcement varied from 3 to 5B. The results clearly demonstrate that Combigrid reinforcement could significantly improve the ultimate bearing capacity of shallow footings on clay.

On the basis of the outcomes, the following points are concluded:

- The optimal Length of reinforcement is found to be 3B.
- The optimal depth of reinforcement is 0.5 B beyond which the load carrying capacity decreased at particular settlement values.

- Immediate settlement could be significantly reduced when reinforcement is included in the soil.
- Only with a single reinforcement layer, the bearing capacity of model footing on clay could be increased upto 4.3 times its unreinforced bearing capacity.
- The reinforcement inclusion can develop a surcharge effect that can prevent soil from upward movement. This can be helpful in improving the bearing capacity of clay.
- The improvement in bearing capacity is directly proportional to the rate of settlement.
- Combigrid has great potential in boosting the bearing capacity of weak clay upto four times than its unreinforced bearing capacity and therefore is a great source of reinforcement in engineering works.
- One layer of reinforcement is economical than using more number of reinforcement layers, so if the Bearing capacity of clay can be improved upto 4 times only by using single layer of Combigrid, then it is one of the best reinforcing material that can be used to reduce the construction cost.

The bearing capacity improvement of reinforced soil is directly proportional to the footing size. Prototype foundations being larger in size, bearing capacity improvement is expected to be more than the improvement exhibited here.

References

Adams MT, Collin JG (1997) Large model spread footing load tests on geosynthetic reinforced soil foundations. J Geotech Geoenviron Eng ASCE 123(1):66–72

Basudhar PK, Saha S, Deb K (2007) Circular footings resting on geotextile reinforced sand bed. Geotext Geomembr 25:377–384

Chen Q, Abu-farsakh M, Sharma R, Zhang X (2007) Laboratory investigation of behavior of foundations on geosynthetic-reinforced clayey soil. Transp Res Record J Transp Res Board 2004:28–38

Das BM, Omar MT (1994) The effects of foundation width on model tests for the bearing capacity of sand with geogrid reinforcement. Geotech Geol Eng 12:133–141

Guido VA, Chang DK, Sweeney MA (1986) Comparison of geogrid and geotextile reinforced slabs. Can Geotech J 23:435–440

Guido VA, Biesiadecki GL, Sullivan MJ (1985) Bearing capacity of a geotextile-reinforced foundation. In: Proceedings of 11th international conference on soil mechanics and foundation engineering. San Francisco, USA, pp 1777–1780

Khing KH, Das BM, Puri VK, Cook EE, Yen SC (1993) The bearing-capacity of a strip foundation on geogrid-reinforced sand. Geotext Geomembr 12(4):351–361

Latha GM, Somwanshi A (2009) Bearing capacity of square footings on geosynthetic reinforced sand. Geotext Geomembr 27:281–294

Mandal JN, Sah HS (1992) Bearing capacity tests on geogrid-reinforced clay. Geotext Geomembr 11(3):327–333

Mirzaeifar H, Ghazavi M (2010) Bearing capacity of multi-edge shallow foundations on geogrid-reinforced sand. In: The 4th International conference on geotechnical engineering and soil mechanics. Tehran, Iran Paper No. & Code: 600 (BCOGHA)

Mosallanezhad M, Hataf N, Ghahramani A (2010) Three dimensional bearing capacity analysis of granular soils, reinforced with innovative grid-anchor system. Iranian J Sci Technol 34(B4):419–431

Ramaswamy SD, Purushothaman P (1992) Model footings of geogrid reinforced clay. Proc Indian Geotech Conf Geotech Today 1:183–186

Ronad H (2014) An experimental study of square footing resting on geogrid reinforced sand. Int J Res Eng Technol 3:117–181

Sakti JP, Das BM (1987) Model tests for strip foundation on clay reinforced with geotextile Layers. (Transportation Research Record No. 1153). National Academy of Sciences, Washington, DC, pp. 40–45

Shin EC, Das BM, Puri VK, Yen SC, Cook EE (1993) Bearing capacity of strip foundation on geogridreinforced clay. Geotech Testing J ASTM 16(4):534–541

Yetimoglu T (1998) Discussion: large model spread footing load tests on geosynthetic reinforced soil foundations. J Geotech Geoenviron Eng ASCE 124(11):1157–1158

Zidan AF (2012) Numerical study of behavior of circular footing on geogrid-reinforced sand under static and dynamic loading. Geotech Geol Eng 30:499–510

Waste Utilization and Preservation of Resources

Benazeer Sultana and Ajit Barik

Abstract Developing country like India, the requirement of power or energy is satisfied through the coal-based power stations. From this thermal power station near about 180–185MT of ash generates and this huge amount of coal ash creates major problem for their disposal. Only 40–45% of that ash is able to dispose in proper way and the rest 60% are dumped randomly, this result in pollution of the environment and creates health hazards. Only 20–25% of that ash is disposed in construction of upstream ash dyke method and in construction of ash pond. The downstream construction method of ash dyke can be a good alternative for increasing the rate of disposal of ash. This method requires a good filter material because the filter media helps in protecting the fly ash material to carry away with the seepage. As we know the sand is good in filter material but here the alternative of this sand is found out i.e. ROBO sand (a waste product as it is manufactured from the waste stones). From investigation, it was found that the ROBO Sand has high permeability than river sand and less cohesion & high internal angle of friction. It also satisfies all the IS criteria for filter material. Then the results are analyzed by the PLAXIS 2D software based on Finite element analysis. The analysis is made in three different conditions. In this the factor of safety of dyke are found to be much higher than the required factor of safety (1.5).

Keywords Waste material · ROBO sand · Filter material · Slope stability · PLAXIS 2D

B. Sultana (✉)
Department of Civil Engineering, College of Engineering & Technology, Bhubaneswar, Odisha, India

A. Barik
Bargarh, Odisha, India

B. B. Das et al. (eds.), *Recent Developments in Sustainable Infrastructure (ICRDSI-2020)—GEO-TRA-ENV-WRM*, Lecture Notes in Civil Engineering 207,
https://doi.org/10.1007/978-981-16-7509-6_3

1 Introduction

Now a day's India is facing serious environmental challenges associates with waste generation & inadequate waste collection. It will not be a surprise if we quoted "India is getting buried in its own garbage's." Our country is 3rd largest producer of coal & it has high ash content. Where more than 65–68% of the power station is coal based and it give rise to the production of Fly ash & Bottom ash. In the year 2019–2020 about 180–185 Million Tons of fly ash is generated from all the power station present all over India and the value may increase further. Although the utilization of fly ash growing rapidly, but it is still not sufficient at all to succeed the rate of production. Only 40–45% of fly ash has been successfully utilized in India and the rest are disposed & restored. It has been utilized by the coal industries by two methods of disposal technique, one is wet disposal method which is widely used and another is dry disposal method (dyke construction). The construction of ash dyke is not easy as we were thinking about. It gives a very tough challenge for the engineers to construct a stable & environmental friendly ash dyke (Aaron 2010, Day 2012, Gandhi 2005). Failure of the dyke can land us in very big critical stage, because it will suddenly affect the environment & if it mixes with river bodies then it pollute the entire aquatic life as well as the living being (human life).

Generally the failure of ash dyke may be occurred due to the following factors which were investigated in the field of ash dam. Different factors are –Seepage of water through ash dyke, Stability of embankment, Properties of soil & fly ash in the starter dyke, Compaction method & absence of drainage filters.

1.1 About PLAXIS

Three stages analysis of the soil model has been done by using PLAXIS i.e. Input stage, Calculation stage & Post processing stage (curve stage). Input stage consists of model design, assigning of material parameter, loading & meshing. In Calculation stage load assignment are activated & analyzed the type of soil like plastic, dynamic, consolidation & Phi-C reduction. In Post processing stage plotting of required curves between various calculated parameter is done i.e. load v/s displacement curves. Input parameters like Poisson's ratio & stiffness of soil guide the displacement of slope. Calculation of safety factor (FOS) for stability analysis of ash dyke is done by the Phi-C reduction method. Next the total multiplier ΣMsf will represent the safety factor value at failure.

2 Literature Review and Objective of Work

Biswas et al. (2000) have studied all the geotechnical properties of expansive soil by adding different dosage of ROBO sand on. It was found to be very useful in the effect on MDD to controlling permeability and moisture strength & also increased the shear strength of soil. It is studied that the fine particles present in the bottom dyke could be the main reason for the failure of slopes on 2018. By using PLAXIS 2D the stability of the existing slope was successfully carried out. It was also analyzed that the slope will deform slightly due to the gravity loading.

Pant et al. (2017) and Sarkar (1999), reviews about the influence of engineering behavior of coal ash on design of ash dyke. Maximum percentage of coarse ash particle is highly recommended for the strength of the ash dykes. In the stable construction of ash dyke the shear strength & the compacted density of fly ash plays an important role.

The main objective of this research work is (i) Using of ROBO SAND instead of RIVER SAND as filter material for downstream design of ash dyke. (ii) Then to analyze the seepage & stability of the as dyke section using FEM based software PLAXIS. (Checking Factor of safety). (iii) Finally the optimum & economical design is to be recommended for the design of ash dyke.

3 Experimental Program

In this present study all the geotechnical properties (particle size, specific gravity, and strength parameter and permeability tests) are studied thoroughly & the results of these tests are discussed on result and discussion section.

3.1 Test Methodology

All the test methodology are carried as per Indian Standards (Fig. 1, Table 1).

Fig. 1 Downstream model

Table 1 Parameters used in PLAXIS

Parameter	Fly ash fill	Sand	ROBO sand
Material model	MOHR–COULOMB	MOHR–COULOMB	MOHR–COULOMB
Material type	drained	drained	drained
unsaturated unit weight (KN/m^2)	7.56	17.39	20.24
Saturated unit weight (KN/m^2)	11.38	19.51	22.43
Permeability (m/day)	0.00008	4.79E-08	0.000000244
E (KN/m^2)	1300	2500	3000
Poisson ratio	0.28	0.3	0.3
C (KN/m^2)	20.8	6.57	3.926
Angle of internal friction	19.39	33.265	39.215

(a) Sieve analysis and hydrometer analysis are used to find the grain size of sample, uniformity coefficient and coefficient of curvature. The set of sieves used for the test are less than 4.75 mm and it is done as per IS 2720 Part IV. Results are shown in Graph 2 and Table 2.

(b) Density bottle and Pycnometer analysis for Specific gravity is done as per IS 2720 (Part III): 1980. Samples are oven dried for a duration of 24 h and the average specific gravity of all materials are in Table 3.

(c) Standard proctor test for Maximum dry density and optimum moisture content is done as per IS 2720 (PART 7): 1985. This test helps in finding out the saturated unit weight and the unsaturated unit weight of the sample which required in PLAXIS. Results are shown in Graph 3.

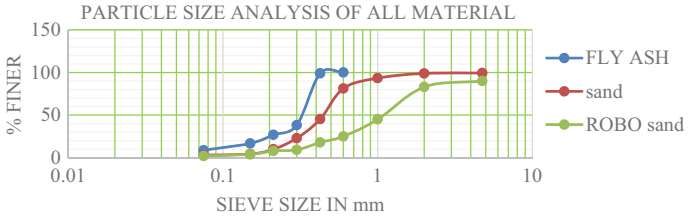

Graph 2 Particle size analysis

Table 2 Analysis table for particle size

Parameter	For sand	For ROBO sand
Cu	2.3464	6.0444
Cc	1.0968	1.00371
Types	Poorly graded sand	Well graded sand

Table 3 Specific gravity

Material	Average specific gravity
Fly ash	2.12
Sand	2.64
ROBO sand	2.67

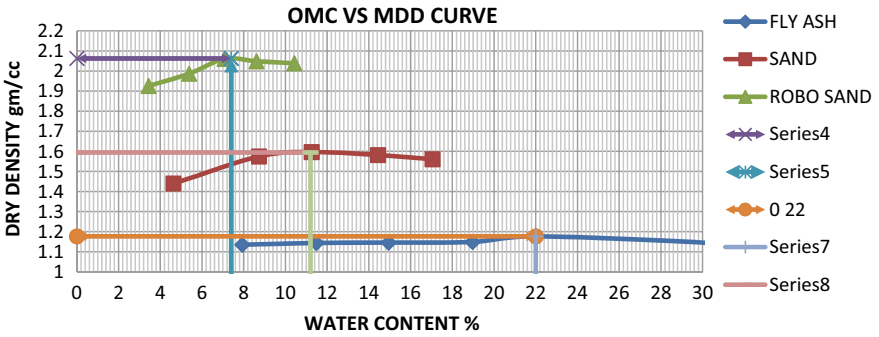

Graph 3 OMC v/s MDD graph for all materials

(d) Direct shear test for internal friction angle and value of cohesion is done as per IS 2720 (PART 13): 1985. The samples are prepared with their required moisture content and compacted with the required dry densities (Table 4). The used specimen size are 60 × 60 × 20 mm and the rate of shearing value is 1.25 mm/min. Results are shown in Graph 4 and Table 5.

(e) Crumb test is done to determine the depressiveness of the material. Here it is used to check for the fly ash whether it is dispersive or not. It is done as per ASTM D6572-06 specification. 1.5 cm × 1.5 cm × 1.5 cm size of mould is prepared with the fly ash

(f) The Permeability of sample is determined by using permeability apparatus. The coefficient of permeability can be determine as per IS 2720 Part 17. The result of coefficient of permeability for Sand and ROBO sand is found out (Table 6) and checked in filter criteria (Graph 5, Tables 7 and 8).

Table 4 Value of maximum dry density and moisture content of all materials

Sl. NO	Material type	Maximum dry density gm/cc	Moisture content %
1	Fly ash	1.771	22
2	Sand	1.594	11.2
3	ROBO sand	2.063	7.4

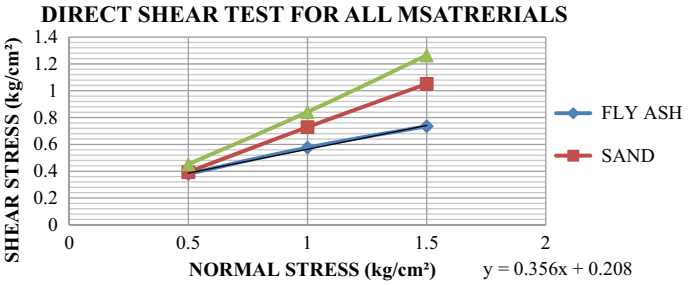

Graph 4 Direct shear analysis of all materials

Table 5 Cohesion and Internal friction angle for all materials

Materials	Cohesion value (C) kg/cm^2	Angle of internal friction (Φ)
Fly ash	0.208	19.39
Sand	0.067	33.265
ROBO sand	0.04	39.215

Table 6 Permeability result

Sl. No	Material	Coefficient of permeability cm/sec
1	Sand	4.14026E-06
2	ROBO sand	0.000211

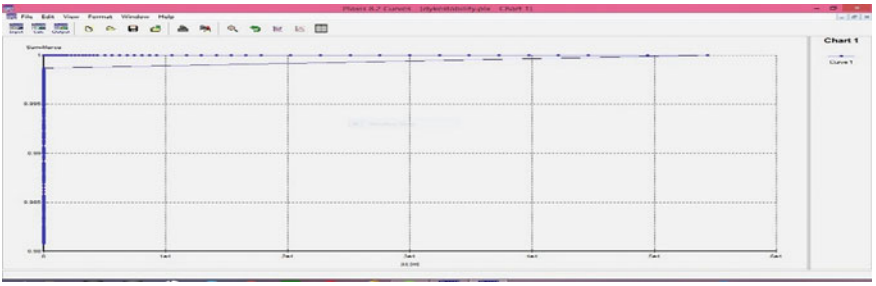

Graph 5 Curve for full dry condition

Table 7 Filter check for river sand

D15(F)/D15(B) > 5	D15(F)/D85(B) < 5	D50(F)/D50(B) < 25	Material passing 75 micron sieve is less than 5%
1.77	0.62	1.38	Satisfied
Not satisfying IS criteria	Satisfying IS criteria	Satisfying IS criteria	

Table 8 Filter check for ROBO sand

D15(F)/D15(B) > 5	D15(F)/D85(B) < 5	D50(F)/D50(B) < 25	MATERIAL PASSING 75 MICRON SIEVE IS LESS THAN 5%
5.02	1.759	3.489	SATISFIED
Satisfying IS criteria	Satisfying IS criteria	Satisfying IS criteria	

3.2 Material Properties Used for PLAXIS Analysis

All the properties given below are found from the experiment except the E values of different materials. The reference E value is considered for all the material for better assessment. Saturated and the unsaturated unit weight of all the materials can be found from the maximum dry density and optimum moisture content value. Void ratio of all the sample can be calculated further. Here we are considered the material model on MOHR–COULOMB analysis and the type of material to be considered as drained. All the obtained parameters are shown in Table 1.

3.3 Downstream Model in PLAXIS

See Fig. 1.

3.4 Analysis of Models

The above ash dyke model is analyzed in different site conditions which is mentioned below.

i)Full dry condition.
ii)By changing the height of water table.
iii)Steady seepage analysis.

4 Result and Discussion

4.1 Particle Size Analysis

See Graph 2 and Table 2.

4.2 Specific Gravity

See Table 3.

4.3 Standard Proctor Test

See Graph 3 and Table 4.

4.4 Direct Shear Test

See Tables 5, 6 and Graph 4.

4.5 Permeability Test

See Table 7.

4.6 Is Filter Criteria

From Graph 2 the particle size value required for the IS Filter criteria has been noted down (Table 9).

4.6.1 In this case natural river sand is taken as filter material and fly ash is taken as base material. The following test results are found as per the IS: 9429, which is given in the tables.

4.6.2 In this case crushed ROBO sand is taken as filter material and fly ash is taken as base material. The following test results are found as per the IS: 9429, which is given in the tables (Graphs 6, 7).

Table 9 Factor of safety analysis

Conditions	Factor of safety
Full dry	1
GWL varied	5.8
Steady seepage	3.51

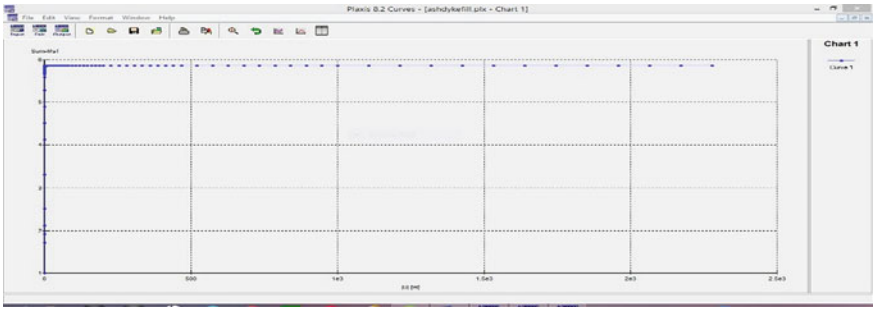

Graph 6 Curve for varying ground water level condition

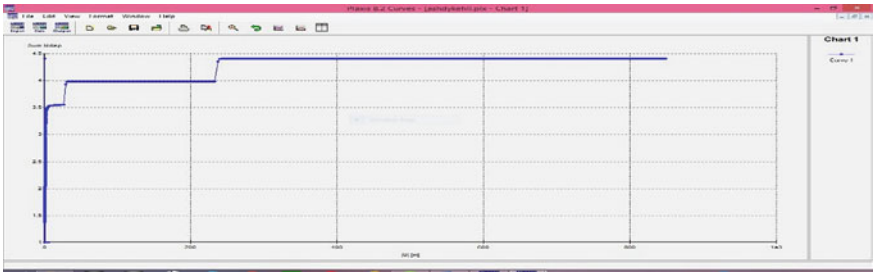

Graph 7 Curve for steady seepage condition

4.7 From PLAXIS 2D

Graphs 5, 6, 7

4.8 Discussion

Comparison was done between natural river sand and the material taken from manufacturing site which is known as ROBO sand to know the better filter material. As we all know the river sand is good at filter but in this present study we found that the sand we have considered was poorly graded sand. Whereas the ROBO sand was found to be well graded sand. While analyzing the stability of ash dyke in PLAXIS software which is based on finite element method we found that in dry condition the factor of safety was below 1.5. But in varying ground water table condition and steady seepage condition the factor safety was found to be well above 1.5. The factor of safety was found to be higher in both condition due to ROBO sand is provided below the ash fill. The steady seepage and ground water level is very much important during the construction of ash dyke because the main reason for the ash dyke failure is seepage.

5 Conclusion

From the above experiment and software analysis the following results can be concluded that the specific gravity of all three materials are found to be 2.119, 2.639 and 2.673 respectively & Fly ash are found to be dispersive material. ROBO sand is more found to be well graded sand as compared to the normal river sand. Here we can also conclude that the ROBO sand is the good filter materials than river sand. Using of filter medium in ash dyke reduces the effect of failure from seepage and increases the stability of ash dyke. Provision of filter material below the ash fill results in high stability in ash dyke as the FOS are above 1.5. In India engineers prefer the upstream design method but it has more demerit. So construction of ash dyke in downstream method can be a good alternative.

References

Aaron B (2010) Slope stability analysis of fly ash containment dyke. Thesis submitted to University of British Columbia, Canada. Brisbin_Aaron_UBC_2010_EOSC_Honours_Thesis.pdf

Biswas et al (2000) Characteristics of coal ash and their role in hydraulic design of ash disposal pipelines by A. Department of Applied mechanics, IIT, Delhi

Arindam Day (2012) Stability of ash dykes: peeping through case studies conference: GIT-NE 2012. National Workshop on Ground Improvement Techniques with reference to NE region At: Guwahati, India

Gandhi SR (2005) Design & maintenance of ash pond for fly ash disposal. Indian Geotechnical Conference, Warangal

Pant A, Datta M, Ramana GV (2017) Influence of variability of coal ash on the requirement of reinforcement and cost of reinforced earth wall. Sixth Indian young geotechnical engineers conference

Sarkar P (1999) Fly ash utilization-present vision. CSIR-Central Institute of Mining and Fuel Research, 2013. Dhanbad, India

Thermal Behavior of a PCM Incorporated Concrete Pavement

B. R. Anupam, Umesh Chandra Sahoo, and Prasenjit Rath

Abstract Conversion of natural landscapes to artificial structures that store sensible heat has led to urban heat island (UHI) effect and thermal distresses in the pavements. Reducing the pavement temperature without affecting its structural and service properties is an emerging problem of research importance. The current study evaluates the thermal behavior of phase change material (PCM) incorporated concrete pavement. A commercially available organic PCM with melting temperature 35–65°C was used in this work. As direct incorporation of PCM adversely affects the mechanical strength of concrete, the PCM was impregnated into expanded clay aggregates (ECA) and coated with cement paste for encapsulation. The thermal and mechanical performances of this PCM incorporated concrete pavement was evaluated for a period of 1 month. A maximum temperature reduction of up to 3.68°C was observed by the incorporation of the PCM.

Keywords Cool pavements · Pavement temperature · Phase change materials · Urban heat island

1 Introduction

Stresses developed in concrete pavements are mainly attributed to vehicular loads and temperature gradient between the top and bottom of the pavement surface (Oh et al. 2017). This temperature gradient leads to repeated temperature curling of the slabs, resulting in transverse, longitudinal, and corner cracks (Lines et al. 2005). Therefore,

B. R. Anupam (✉) · U. C. Sahoo
School of Infrastructure, Indian Institute of Technology, Bhubaneswar, India
e-mail: abr10@iitbbs.ac.in

U. C. Sahoo
e-mail: ucsahoo@iitbbs.ac.in

P. Rath
School of Mechanical Sciences, Indian Institute of Technology, Bhubaneswar, India
e-mail: prath@iitbbs.ac.in

B. B. Das et al. (eds.), *Recent Developments in Sustainable Infrastructure (ICRDSI-2020)—GEO-TRA-ENV-WRM*, Lecture Notes in Civil Engineering 207,
https://doi.org/10.1007/978-981-16-7509-6_4

a reduction in pavement surface temperature can reduce the thermal stresses induced in the slabs and significantly improve the pavement life. Moreover, a reduction in pavement surface temperate can contribute towards the UHI mitigation efforts. The elevated urban temperature with respect to the surrounding rural areas, due to the conversion of natural vegetation to artificial structures that stores heat energy, is termed as UHI (Yang et al. 2016).

According to the United States Environmental Protection Agency (USEPA), "Cool pavements include a range of established and emerging technologies that communities are exploring as part of their heat island reduction efforts. The term currently refers to paving materials that reflect more solar energy, enhance water evaporation, or have been otherwise modified to remain cooler than conventional pavements". Even though conventional cool pavement technologies such as enhancing the water evaporation in pavements (evaporative pavements) can reduce the pavement temperature, its cooling efficiency is highly dependent on the water content. Due to the lower thermal mass and solar reflectance, evaporative pavements are found to be hotter than conventional pavements in the absence of water (Qin 2017). Cool pavements having higher solar reflectance (reflective pavements) may lead to glare related issues, thermal load on pedestrian traffic, and increase the temperature of the nearby buildings (Pomerantz et al. 2016).

PCMs are capable to store heat energy in the form of latent heat without an increase in the temperature (Ma et al. 2011). These materials are now being introduced into the pavements with an objective to reduce the pavement surface temperature. During the daytime, with rise in the temperature, PCM undergoes solid–liquid phase change at its melting temperature and restricts the pavement temperature from rising. During night time, this stored latent heat is released and the PCM solidifies. Therefore incorporation of PCM in pavements decreases the pavement temperature during daytime and increases during night time. However, the direct incorporation of these PCMs interfere with the cement hydration process and adversely affects the mechanical strength of concrete. To address this issue, encapsulated PCMs are usually recommended for pavement applications. Encapsulation is the process of covering or coating the PCM with a suitable medium to avoid its direct interaction with the pavement materials (Anupam et al. 2020).

The primary aim of this study was to develop a suitable encapsulated PCM for concrete pavement applications and to evaluate the thermal and mechanical performance of the PCM incorporated concrete. A PCM incorporated concrete slab was casted and the monthly variation in pavement temperature has been analyzed under this study.

2 Materials and Methods

Generally, organic PCMs are suitable for pavement applications as they do not require super-cooling during phase change and have good resistance against corrosion (Sharma et al. 2009). Therefore, a commercially available organic PCM (OM

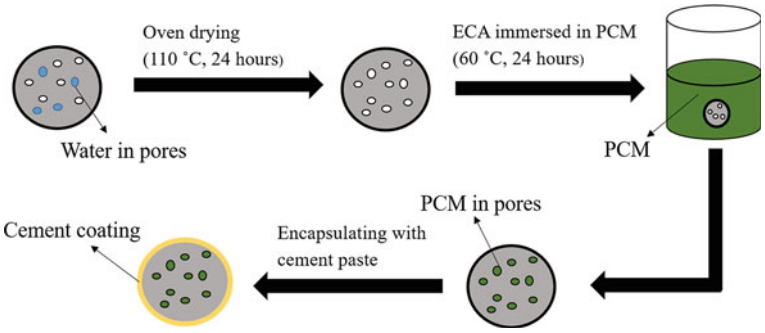

Fig. 1 Preparation of PCM impregnated ECA

35) supplied by PLUSS Technology Pvt. Ltd., India was used in this study. ECA supplied by PERL TECH Pvt. Ltd., India was used as the encapsulation medium for this study due to its higher water absorption properties.

In order to prepare the PCM impregnated ECA, the ECAs were first oven dried for 24 h to remove any water content present in the pores. The oven-dried ECAs were then immersed in molten PCM for 24 h for PCM abortion. Afterward, the ECAs were filtered out from the molten PCM and the surfaces were cleaned with a cloth. A cement coating was the applied over the ECA to avoid PCM leakage. A schematic representation of this process is shown in Fig. 1.

The phase change temperature and latent heat of fusion of PCM and developed PCM impregnated ECA was evaluated by using a differential scanning calorimeter (DSC). The thermal stability of PCM was evaluated by thermogravimetric analysis (TGA). To quantify the PCM leakage, the diffusion-oozing circle test as suggested by Ma et al. (2013) was conducted in this study. Further, PCM impregnated ECAs were added as a partial replacement to coarse aggregates, and the 7th and 28th day compressive and flexural strengths were evaluated. M30 grade of concrete was designed for this study. In a 300 mm thick concrete slab, the PCM incorporated concrete mix was provided only in the top 100 mm and the variation in the surface temperature of the slabs was monitored continuously for a period of 1 month (Fig. 2).

3 Results and Discussion

From the DSC results as shown in Fig. 3a, it may be observed that the phase change process of the PCM initiates at 35°C and ends at 65°C. This indicated that the phase change temperature range is suitable for pavement cooling applications in Indian climatic conditions. Moreover, the PCM could store a latent heat of 115.9 J/g during phase change. However, the latent heat of PCM impregnated ECA was less than that of the pure PCM, maybe due to the lower mass fraction of PCM in the composite. Further, the TGA as shown in Fig. 3b indicates that there is no mass loss up to 190°C

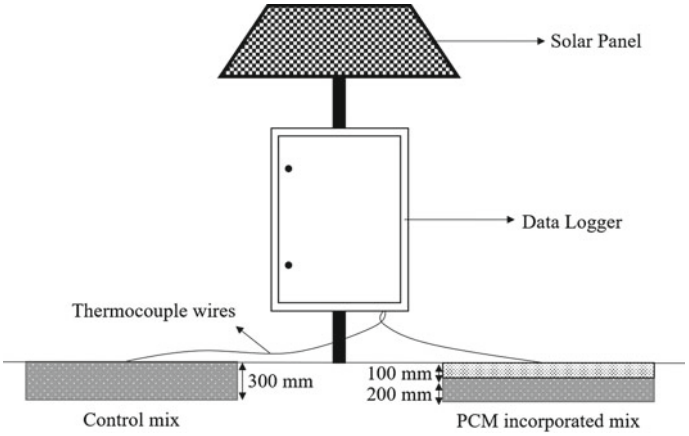

Fig. 2 Solar-powered thermocouple and datalogger set up

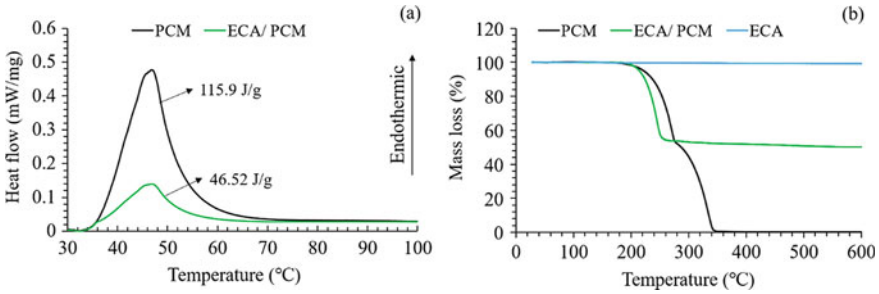

Fig. 3 **a** Differential scanning calorimeter results, **b** Thermogravimetry results

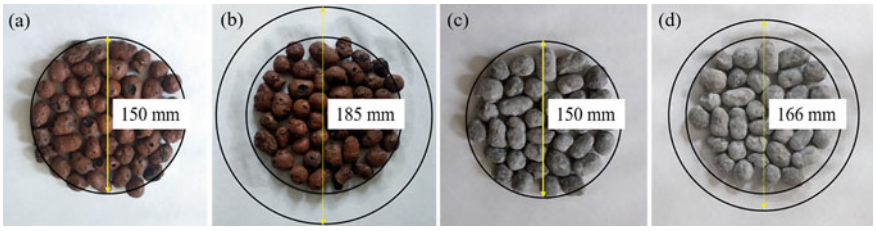

Fig. 4 Diffusion oozing circle test results (**a**) Standard circle, (**b**) Leakage circle, (**c**) Standard circle of cement coated ECA, (**d**) Leakage circle of cement coated ECA

and hence there will be no mass loss during the pavement construction and operation phases.

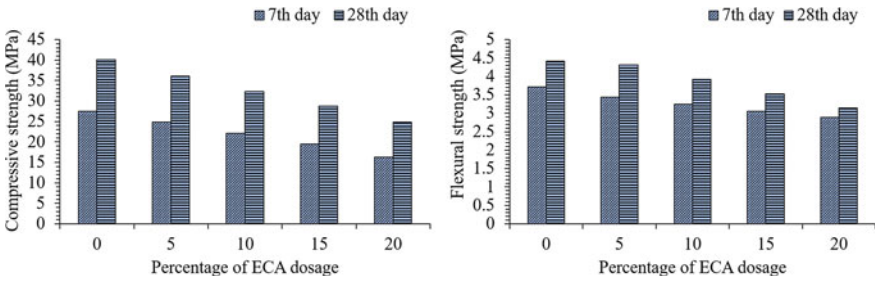

Fig. 5 Mechanical strength test results

The diffusion oozing circle test results (Fig. 4) indicate that the cement coating could significantly reduce the PCM leakage from the ECA. The leakage circle diameter was reduced from 285 to 166 mm, after the cement coating. i.e., the encapsulation efficiency (η), which is the ratio of leakage circle to standard circle, improved from 0.123 to 0.110 by providing cement coating. According to Sun and Wu (2004), an encapsulation efficiency value of up to 0.115 is safe and may be considered acceptable for civil engineering works concerning the PCM leakage.

The compressive and flexural strength test results of the designed M30 grade of concrete are as indicated in Fig. 5. A reduction in mechanical strength was observed with an increase in the replacement of coarse aggregates with ECA. However, the concrete exhibited satisfactory mechanical strength up to 10% replacement dosage and hence suitable for concrete pavement applications.

The variation in pavement surface temperatures measured continuously for 30 days is shown in Fig. 6. A reduction in pavement surface temperature was observed for the PCM incorporated concrete pavements. The maximum reduction in pavement temperatures for 30 days is shown in Fig. 7, which indicates a maximum reduction of 3.68°C with PCM incorporation. This reduction in pavement surface temperature will help to mitigate the UHI effect. Moreover, the surface temperature of PCM incorporated pavement was found to be higher than that of normal concrete pavements during night time, which is due to the latent heat release during PCM solidification. A decreased surface temperature during day time and increased surface temperature during night time reduces the temperature gradient developed in concrete pavements and will lead to an increase in the pavement life.

4 Conclusions

The present study evaluated the thermal behavior of a commercially available organic PCM incorporated concrete slab for 1 month. The key findings of the study may be summarized as follows.

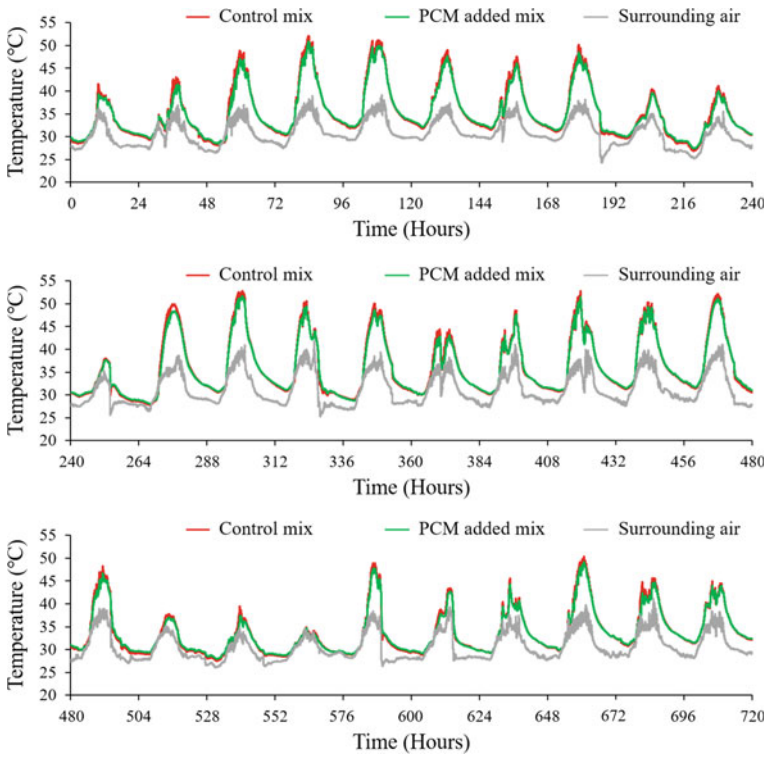

Fig. 6 Monthly variation in pavement surface temperature

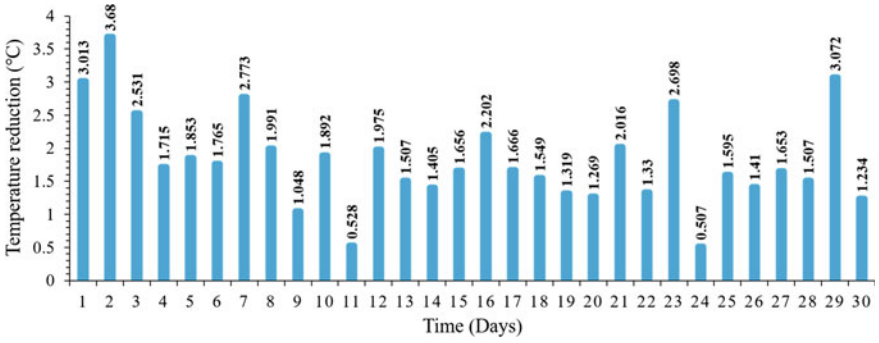

Fig. 7 Maximum reduction in pavement surface temperature

- Impregnating PCM into ECA and coating it with cement can significantly reduce the PCM leakage and hence this composite may be considered suitable for civil engineering works. The diffusion oozing circle test results indicate that the encapsulation efficiency improved from 0.123 to 0.110 by providing cement coating.
- The developed ECA-PCM composite can be added as a partial replacement to coarse aggregates in cement concrete pavements. Mechanical strength results indicate that up to 10% replacement of coarse aggregates by ECA can be considered without affecting the strength.
- Incorporation of PCM can significantly reduce the higher and lower temperature extremes in concrete pavements. A peak reduction of up to 3.68°C during daytime was observed PCM incorporated pavement.

Further studies in this area consist of analyzing the seasonal thermal performance of these PCM incorporated concrete pavements, and developing a numerical model to predict the thermal behavior of PCM incorporated concrete pavements.

References

Anupam BR, Sahoo UC, Rath P (2020) Phase change materials for pavement applications: a review. Constr Build Mater 247:118553. https://doi.org/10.1016/j.conbuildmat.2020.118553

Kim S-M, Nam JH (2010) Measurements and experimental analysis of temperature variations in portland cement concrete pavement systems. Road Mater Pavement Des 11(3):745–771. https://doi.org/10.3166/rmpd.11.745-771

Lines I, Hiller JE, Asce M, Roesler JR, Asce M (2015) Determination of critical concrete pavement fatigue damage locations using influence lines 8, August 2005. https://doi.org/10.1061/(ASCE)0733-947X(2005)131

Ma B, Li J, Wang XM, Xiao N (2011) Effect of composite shape-stabilized phase change material on asphalt mixture temperature. Adv Mater Res 311–313:2151–2154. https://doi.org/10.4028/www.scientific.net/amr.311-313.2151

Ma B, Adhikari S, Chang Y, Ren J, Liu J, You Z (2013) Preparation of composite shape-stabilized phase change materials for highway pavements. Constr Build Mater 42:114–121. https://doi.org/10.1016/j.conbuildmat.2012.12.027

Oh HJ, Cho YK, Kim S-M (2017) Experimental evaluation of crack width movement of continuously reinforced concrete pavement under environmental load. Constr Build Mater 137:85–95. https://doi.org/10.1016/j.conbuildmat.2017.01.080

Pomerantz M, Akbari H, Berdahl P, Konopacki SJ, Taha H (2016) Reflective surfaces for cooler buildings and cities 2812(June). https://doi.org/10.1080/13642819908216984

Qin Y (2017) A review on the development of cool pavements to mitigate urban heat island effect. Renew Sustain Energy Rev 52(December):445–459. https://doi.org/10.1016/j.rser.2015.07.177

Sharma A, Tyagi VV, Chen CR, Buddhi D (2009) Review on thermal energy storage with phase change materials and applications 13:318–345. https://doi.org/10.1016/j.rser.2007.10.005

Sun J, Wu Z (2004) Study on evaluation method of exudation of phase transition working substance for building materials. New Build Mater 7:43–46

Yang J, Wang Z, Kaloush KE, Dylla H (2016) Effect of pavement thermal properties on mitigating urban heat islands : a multi-scale modeling case study in phoenix 108:110–121. https://doi.org/10.1016/j.buildenv.2016.08.021

Hydrogeochemical Characterization, Groundwater Quality and Water Resource Management in Salem, Tamil Nadu, India

D. Venkatesan, M. Suresh Gandhi, K. Sandeep Vamsi, Priyanko Das, Narala Gangadhara Reddy, and G. S. Gayathri

Abstract This work investigates the Physico-chemical characteristics of groundwater, in the district of Salem, Tamil Nadu, India. For this purpose, 47 groundwater samples are collected and analyzed for electrical conductivity (EC), total dissolved solids (TDS), pH, sodium, magnesium, calcium, potassium, bicarbonate, carbonate, sulphate, chloride, fluoride and nitrate. Piper trilinear diagram is used to identify the contamination of major Physico-chemical facies and quality characteristics. USSL diagram stated that the C3S1 and C4S2 classes were suitable for irrigation purposes under the special management for salinity control. The geochemical analysis of TDS (325–6018 mg/l) and EC (464–8597 μs/cm) shows that the values are above the world health organization (WHO) standard limits, which is not suitable for drinking purpose. Spatial distribution result shows high EC values near Thirumanimuthar river. The samples pH values show alkaline nature (6.73–8.5) with a high concentration of Na and Cl. The Mg, Ca, K, SO_4^- and NO_3^- of groundwater samples exceed the limits of WHO, due to industrial waste and anthropogenic activity and possess health risk. Low values of permeability index (PI), sodium adsorption ratio (SAR) and residual sodium carbonate (RSC) are suitable for plant growth and irrigation purpose in the studied region.

Keywords Groundwater · Hydro-geochemistry · Contamination · SAR · RSC

D. Venkatesan
Department of Geology, AVS College of Arts and Science, Salem, India

M. S. Gandhi · K. S. Vamsi (✉) · G. S. Gayathri
Department of Geology, University of Madras, Chennai, India

P. Das
School of Geography and Oceanography Sciences, Nanjing University, Nanjing, China

N. G. Reddy
Department of Civil Engineering, Kakatiya Institute of Technology and Science, Warangal, India

B. B. Das et al. (eds.), *Recent Developments in Sustainable Infrastructure (ICRDSI-2020)—GEO-TRA-ENV-WRM*, Lecture Notes in Civil Engineering 207,
https://doi.org/10.1007/978-981-16-7509-6_5

1 Introduction

Groundwater is the primary source of water in arid regions for industrial, agricultural, and domestic sectors. Evaluating the quality of groundwater is necessary for better utilization. Hydro-geochemistry and its processes differ according to the geology and chemical properties of the aquifer spatially and temporally (Lakshmanan et al. 2003). Water quality is based on the action of the waters through transpiration, evaporation, degradation or reduction of cation exchange, algae, mineral dissociation, mineral deposition, waters mixing, fertilizer and manure leaching, biological and lake/sea processes (Prasanna et al. 2011). The quality of groundwater mostly affected by both human and natural activities (Andrade et al. 2008). Rapid urbanization and increase in population have resulted in declining of groundwater quality (Ramesh and Elango 2011; Brindha et al. 2011). Agro-chemicals may also contaminate groundwater. The study region is a metropolitan area with an inadequate surface water supply and the majority population dependent on groundwater for household, industrial, and agricultural purposes. This research, performed in 2018, will serve as the basis for assessing potential groundwater quality.

2 Study Area

The study area Salem and Valapadi taluks (Fig. 1) lies in Salem district in Tamil Nadu. It is geographically situated between 77° 59′ 57″ to 78° 28′ 34″ E and 11° 52′ 43″ to 11° 30′ 44″ N covering an area about 986 sq km with toposheets numbers 58 I/2, 5 and 6 (Survey of India).

3 Methodology

Forty-seven samples are collected and tested using standard methods for knowing the Physico-chemical changes in water quality parameters. Digital metres are used to measure EC and pH in the location area itself. Collected samples were analyzed to determine K, Mg, Ca, CO_3, Na, Cl, SO_4 and HCO_3 concentrations on the same day. Spatial variation maps (isoline maps) are created using the GIS software for many major ions. Further, the concentration of different ions of groundwater samples was compared with the Bureau of Indian Standards, World Health Organisation and various international standards for understanding the suitability for domestic and agriculture use.

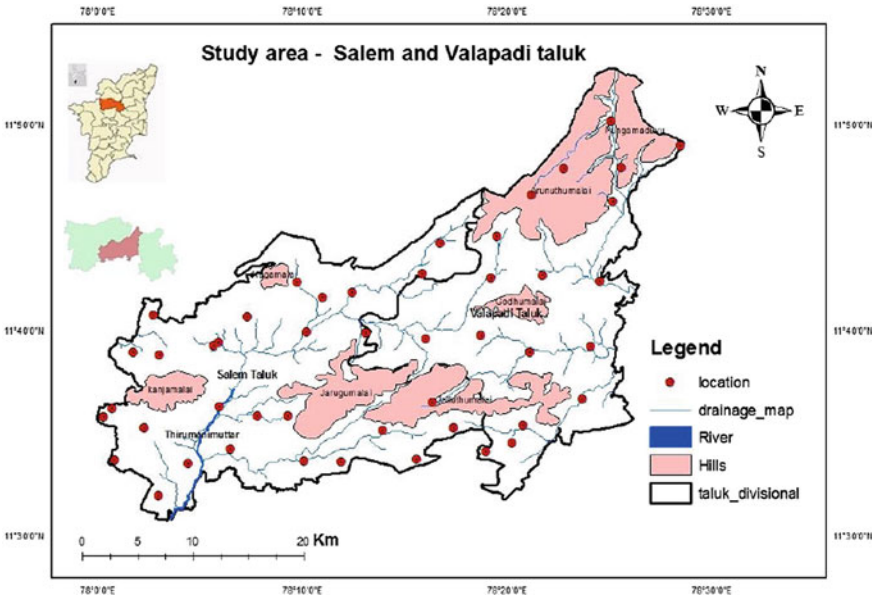

Fig. 1 Study area with well locations

4 Result and Discussion

4.1 Hydro-chemical Facies

Hydro-chemical facies concept helps to understand the transport and flow processes in groundwater and reveals the information on paleoenvironmental conditions. Hydro-geo-chemical faces show the regional relationship between chemical characteristics, lithology and patterns of regional flow. The Piper diagram (1944) helps define groundwater variations and similarities since it identifies similar attributes as a category (Todd 1980). Also, it is used to classify types of water for determining hydrogeochemical facies and hard rock geochemical characteristics (Thivya et al. 2014). The Piper plot is used to infer the two samples mixing ratio (Karmegam et al. 2011) which is measured using AQUACHEM 4.0 software. The obtained values from the groundwater analysis and the plot on the Piper trilinear diagram indicate that the dominant anions are Cl and HCO_3 and the cations are Ca and Na. Figure 2 indicate that the water samples plot in the Na–Ca–Mg–Cl–HCO_3 and Na–Ca–Mg–HCO_3–Cl field, and the samples are influenced by agriculture processes due to overexploitation and irrigation practice. From the plot, it is inferred that the alkalis (K, Na) exceed alkaline earth (Mg, Ca), and strong acids (SO_4 and Cl) exceed weak acids (HCO_3).

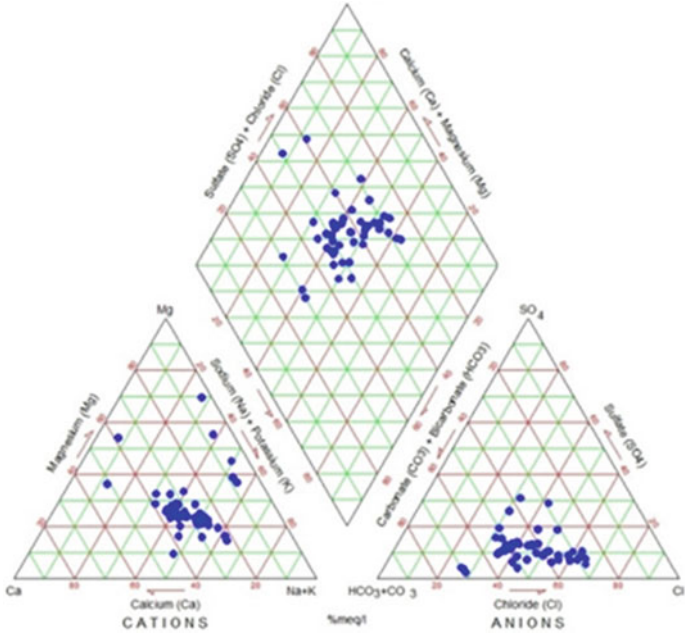

Fig. 2 Piper trilinear diagram

4.2 Physico-chemical Parameters

The total solids dissolved (TDS) range between 325 and 6018 mg/l (Fig. 3). These findings show very high values in certain samples of groundwater. According to David and DeWeist classification, the TDS values of only four samples are desirable for drinking purpose (<500 mg/l). Among the total number of samples, 27 are useful for irrigation (1000–3000 mg/l). The TDS value vary from 325 to 6018 mg/l, averaging (Fig. 3) 5128 mg/l. Unsuitable for irrigational and drinking purposes of groundwater

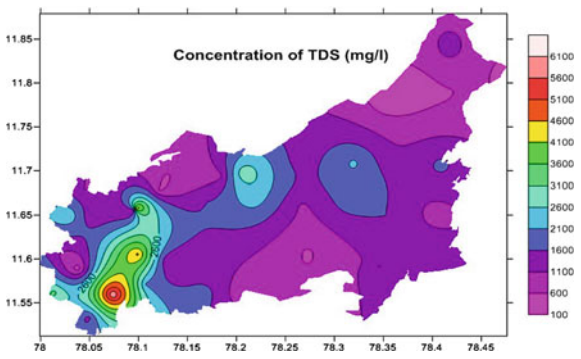

Fig. 3 Spatial variation of TDS (mg/l)

were recorded due to industrial activity. Uthamasolapuram and Vadarasampatti have a very high concentration of TDS because of dyeing factory effluents mixing with the stream, which is located nearby wells (Venkatesan et al. 2016).

Electric conductivity (EC) is used to calculate water capacity to transport the electric current. Pure water is a poor electrical conductor and exhibits higher conductivity when the salt is present. The conductivity is proportional to the amount of salts present in water. The values of EC (Fig. 4) vary in range from 464 to 8597 µs/cm, with 2229 µs/cm as an average. The spatial distribution showed higher EC values near the Thirumanimutar River tributary, where the effluents are mixed from dyeing factories. Discharges from intense and prolonged farming activities, releases of industrial and household waste are local anthropogenic activities (Dinkaa et al. 2015). The pH varied from 6.73 to 8.5 indicating mild alkaline nature of groundwater (Fig. 5).

Figure 6 shows the spatial distribution of calcium concentrations with 134 mg/l as an average, where the values vary from 8 to 948 mg/l, magnesium varying from 7 to 408 mg/l, averaging 70 mg/l (Fig. 7). As per WHO, it is observed that 13 samples exceeded the allowable limits of 200 mg/l. Higher Ca values are contained in samples of Vadarasampatti (948 mg/l) and Uthamasolapuram (448 mg/l). The concentration

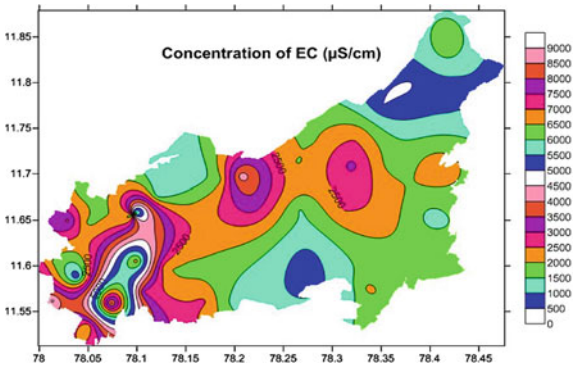

Fig. 4 Spatial variation of EC (µs/cm)

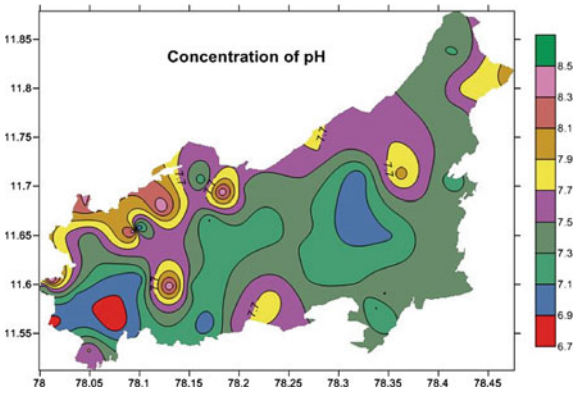

Fig. 5 Spatial variation of pH

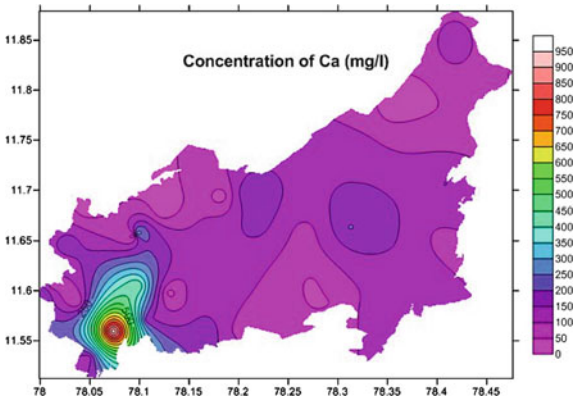

Fig. 6 Spatial variation of Ca (mg/l)

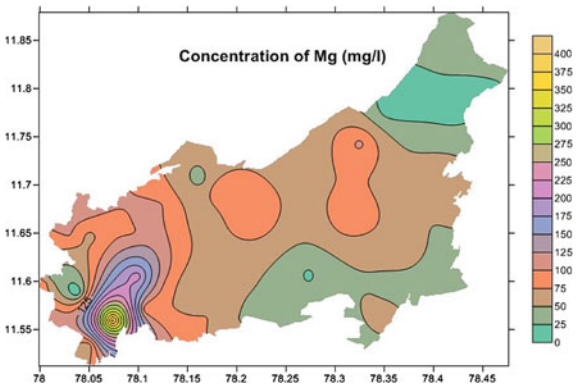

Fig. 7 Spatial variation of Mg (mg/l)

of Na ion (Fig. 8) is 216 mg/l as an average value, and the values vary in-between 25 and 846 mg/l. A total of 19 groundwater samples shows above the desired WHO limit

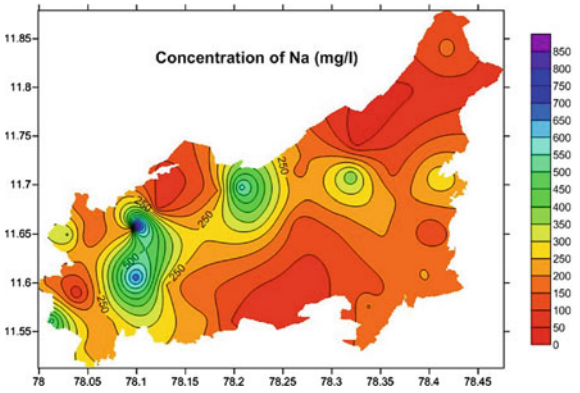

Fig. 8 Spatial variation of Na (mg/l)

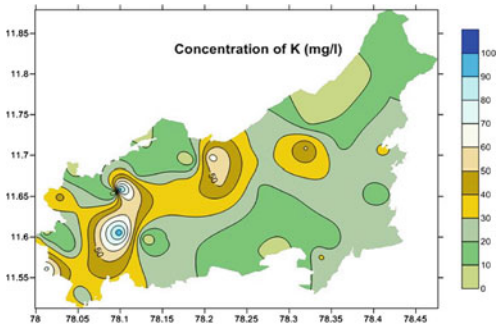

Fig. 9 Spatial variation of K (mg/l)

of 200 mg/l. The Na content of groundwater samples found to be high in Salem taluk compared with Valapadi taluk. Na is mainly linked to high chloride levels resulting in salinity (Nandhakumar et al. 2015). The cation exchange process also affects Na concentrations. The potassium concentration (Fig. 9) have 25 mg/l as a mean value, where the values vary from 1 to 99 mg/l, owing to agricultural and industrial activities (Selvakumar et al. 2017).

The permitted chloride limit for groundwater is 250 mg/l, which can be increased to 1000 mg/l in BIS 1991 standards. The concentration of Cl (Fig. 10) having 488 mg/l as an average, where the values range between 136 and 1600 mg/l. The highest (1600 mg/l) potassium value in the Vadarasampatti region has been reported. The bicarbonate has 481 mg/l as an average value, where the values vary from 65 to 1980 mg/l, (Fig. 11).

The ranges of sulphate and nitrate (Fig. 12) having 101–47 mg/l as a mean value vary from 8 to 288 mg/l and 1 to 188, respectively. In Salem Taluk, the concentration of nitrate and sulphate in the study area surpassed the desired amount. Fluoride is one of the major groundwater contaminants. A fluoride-containing country-rock typically accounts for the elevated amounts of ion in groundwater (Fig. 13, Currell et al. 2011). Fluoride amounts (Fig. 14) in groundwater vary from 0 to 3.2 mg/l,

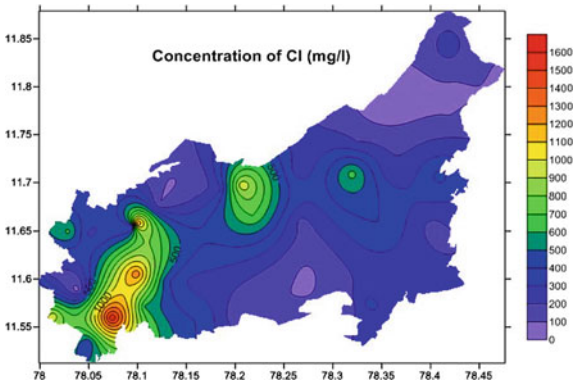

Fig. 10 Spatial variation of Cl (mg/l)

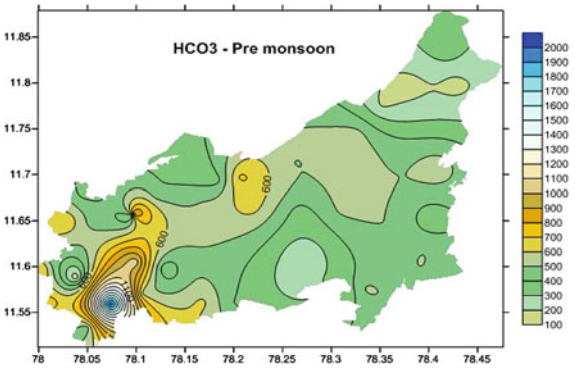

Fig. 11 Spatial variation of HCO

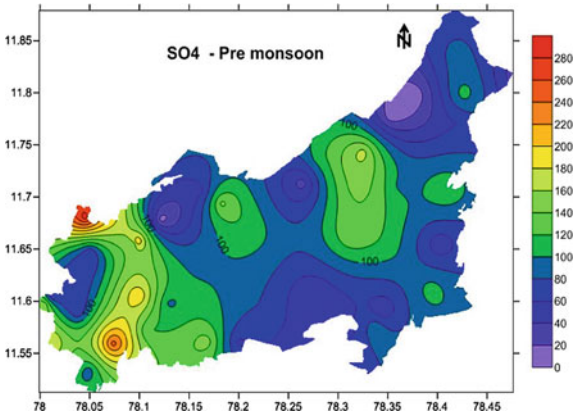

Fig. 12 Spatial variation of SO_4

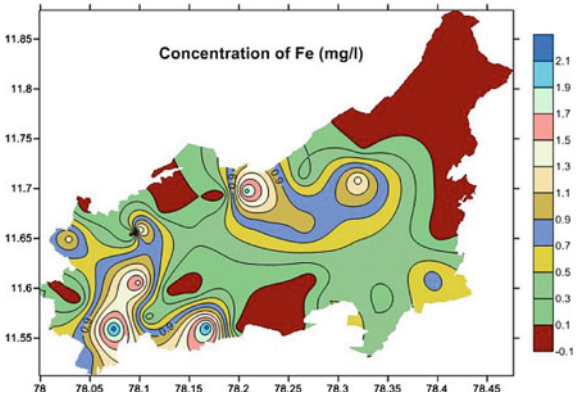

Fig. 13 Spatial variation of Fe (mg/l)

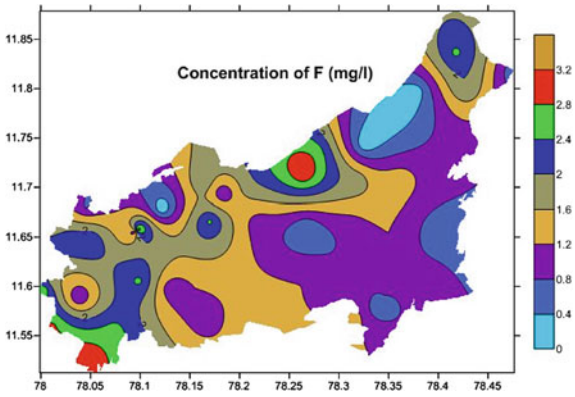

Fig. 14 Spatial variation of F (mg/l)

averaging 1.44 mg/l. In the study area, 18 groundwater samples exceeded the WHO permissible limits (1.5 mg/l).

4.3 Sodium Adsorption Ratio (SAR)

SAR is a critical component in evaluating groundwater suitability for irrigation. If the water has high Na and low Ca concentrations, the cation exchange complex can be saturated with Na. Sodium in the aquifer is introduced from rainwater and rock dissolution. The potential of sodium risk in the water rises with higher SAR values (>18). The SAR is calculated by using the formula (Richards 1954).

$$\mathrm{SAR} = \frac{\mathrm{Na}^{+}}{\sqrt{\mathrm{Ca}^{2+} + \mathrm{Mg}^{2+}/2}} \tag{1}$$

Ions are expressed in meq/l.

The SAR results are observed in between 0.39 and 10.84. A more comprehensive study of irrigation water suitability has been carried out by plotting the diagram given by US Salinity Laboratory. All other samples except for one were excellent based on the SAR that can be used for irrigation. The SAR vs. EC values for groundwater samples are shown in the USSL irrigation water diagram (Fig. 15). From the USSL diagram, it is revealed that the quality of water of 34 samples fall in S1 category (high sodium salinity) that is desirable for irrigation, S2 category (Very high salinity with moderate sodium), one sample fall into the S3 category (Very high sodium salinity), which is appropriate for irrigation under special treatment for salinity control due to high salinity risk.

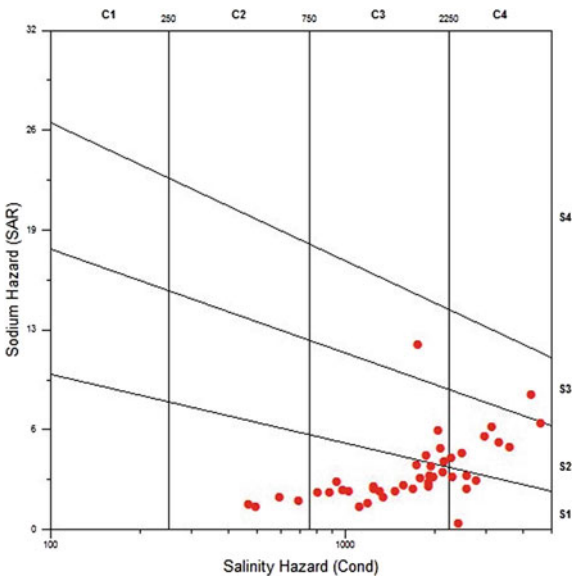

Fig. 15 USSL groundwater classification in the research area

4.4 Residual Sodium Carbonate (RSC)

The RSC index of soil or irrigation water is used to determine the risk of soil alkalinity. The RSC index identifies the irrigation suitability of the water in clay soils with a high cation exchange capacity. High sodium content in water, when compared with magnesium and calcium, leads to dispersion or swelling of clayey soils.

$$\mathrm{RSC} = \left[(\mathrm{HCO_3} + \mathrm{CO_3}) - (\mathrm{Ca} + \mathrm{Mg})\right] \tag{2}$$

The concentrations are expressed in meq/l.

A high value of RSC in water results in increase sodium adsorption (Eaton 1950) in soil. RSC > 5 meq/l is found to be hazardous for plant growth although, RSC > 2.5 meq/l are not ideal for irrigation (Sudhakar and Narsimha 2013). All 47 samples of the study area groundwater samples were analyzed for RSC. As per RSC values, 47 samples have less than 1.25 values and are fit for irrigation. The positive RSC value reveals that the dissolved Mg and Ca ions are less than HCO_3 and CO_3 (Selvakumar et al. 2017). The carbonate and bicarbonate concentration also affect the groundwater quality for irrigation.

4.5 Sodium Percentage

Sodium is a significant irrigation water parameter and is referred to as Na%, which is measured using the formula given below (Wilcox 1955).

$$\text{Na\%} = \frac{\left(\text{Na}^{+} + \text{K}^{+}\right) \times 100}{\text{Na}^{+} + \text{Mg}^{2+} + \text{K}^{+} + \text{Ca}^{2+}} \tag{3}$$

Na% in the research location ranged from 7.4 to 63 meq/l, and only Vadarasampatti and Velampatti samples were considered suitable for excellent in irrigation purpose. The samples are mostly in the permissible limit; meanwhile, 2 and 12 samples are considered excellent and good, respectively. 31 samples belong to permissible, and 2 samples are under doubtful condition.

EC and concentrations of sodium are essential parameters for the classification of irrigation water. Water used for irrigation often includes detectable concentrations of dissolved compounds such as salts. Besides explicitly influencing the growth of plants, the salts also affect soil structure, aeration and permeability that influence plant growth indirectly (Tiwari and Singh 2014). The high sodium water induces the water exchange in the soil for Na and Mg ions and decreases the permeability and consequently result in the soil with low internal drainage (Collins and Jenkins 1996).

The Na% and EC diagram of the Wilcox (1955) indicate that 8.5% of the samples fall into the "excellent to good" while the other 45% fall into the "permissible to good" category. Meanwhile, 28% of groundwater falls under "Doubtful to Unsuitable" range and 17% of samples coming under "Unsuitable" range. Na% and the Wilcox diagram indicate the groundwater as permissible to good (Fig. 16).

4.6 Permeability Index

Doneen (1964) has established a criterion for determining PI-based irrigation water suitability (Srinivasamoorthy et al. 2014). This formulation is used to measure PI (represented in meq/l).

$$\text{Permeability index (PI)} = \text{Na} + \sqrt{\text{HCO}_3}/(\text{Ca} + \text{Mg} + \text{Na}) \times 100 \tag{4}$$

PI varies from 17.67 to 76.7 meq/l with an average of approximately 58.2. Doneen (1964) classifies groundwater suitability for both seasons under classes I and II, demonstrating that water for irrigation purposes is of moderate to good quality.

Gibbs plot is used to illustrate the effect of weathering, evaporation and precipitation (Gibbs 1970). Most samples are identified within the water–rock interaction and evaporation zone (Fig. 17). The effect of agricultural operations may be attributed

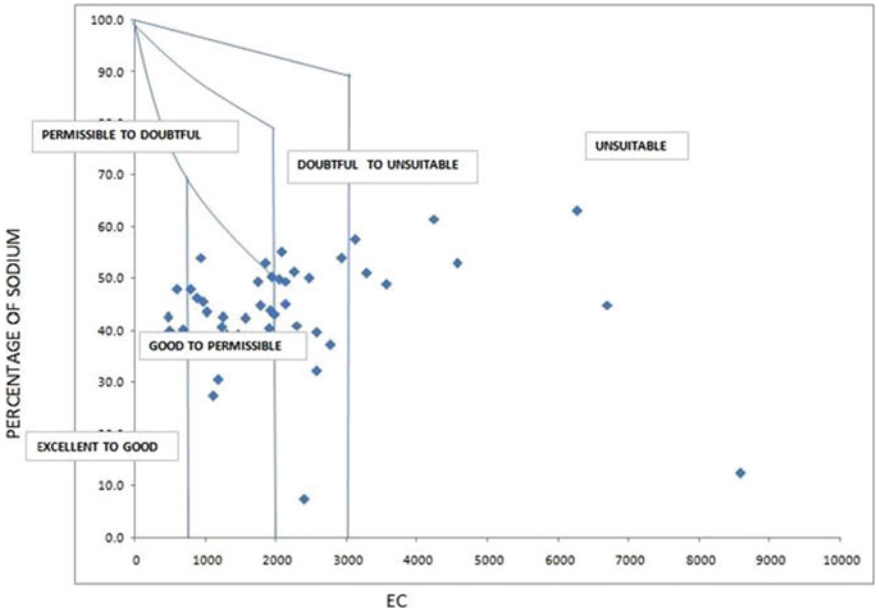

Fig. 16 Gibbs plot for groundwater in the research area

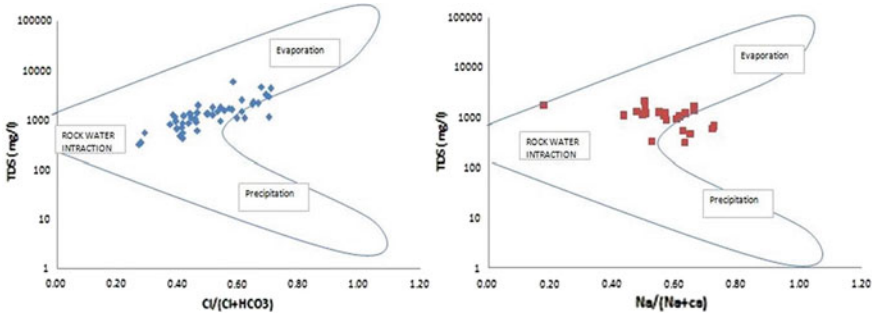

Fig. 17 Wilcox diagram for groundwater in the research area

to the sample representation in the evaporated zone (Gupta et al. 2008). Most of the samples indicate that the primary process in the research region is the weathering of rock. The mixing system indicates samples that fall in-between the evaporation and weathering zone (Thivya et al. 2013).

5 Conclusions

The groundwater chemical composition in the research area demonstrates the dominance of anions such as Cl and HCO_3 and cations like Ca and Na. The analysis revealed that most of the samples were slightly acidic to alkaline in nature. TDS, pH, and EC values were higher in samples of Uthamasolapuram, Karevappilankadu, Vadarasampatti and Selathampatti, which are nearby stream polluted by dyeing factory effluents. Two major hydro-chemical facies Na–Ca–Mg–HCO_3-Cl and Na–Ca–Mg–Cl–HCO_3 were identified using the Piper diagram. The SAR values suggest that groundwater samples fall under the excellent category for irrigation. The Na% of samples indicated the groundwater suitability for agricultural purpose. The C3S1 and C4S2 categories for most of the samples that are desirable for irrigation purposes under a special salinity control management for high salinity is indicated in the USSL diagram. In Salem and Valapadi Taluk, the most detrimental effect of garment dyeing factories on the local ecosystem is the dangers posed by colouring effluents that include both chemical and organic contaminants. With the rising amount of garment dyeing factories, the concentration of these toxins rises alarmingly. The concentration of fluoride exceeds the permissible level (1.5 mg/l) and is not ideal for consumption. An effluent treatment plant is needed to mitigate the potential risk of untreated water discharge. Effluent shall meet national standard norms for effluent discharge. Pollutants are eliminated as water flows into the effluent treatment system, and water quality is improved to enable final discharge without any significant harm to the ecosystem.

References

Andrade E, Palacio HAQ, Souza IH, Leao RA, Guerreio MJ (2008) Land use effects in groundwater composition of an alluvial aquifer by multivariate techniques. Environ Res 106:170–177

Brindha K, Rajesh R, Murugan R, Elango L (2011) Fluoride contamination in groundwater in parts of Nalgonda district, Andhra Pradesh, India. Environ Monit Assess 172:481–492

Collins R, Jenkins A (1996) The impact of agricultural land use on stream chemistry in the Middle Hills of the Himalayas, Nepal. J Hydrol

Currell M, Cartwright I, Raveggi M, Han D (2011) Controls on elevated fluoride and arsenic concentrations in groundwater from the Yuncheng Basin, China. Appl Geochem

Dinkaa MO, Loiskandlb W, Ndambukic JM (2015) Hydro-chemical characterization of various surface water and groundwater resources available in Matahara areas, Fantalle Woreda of Oromiya region. J Hydrol Reg Stud 3:444–456

Doneen LD (1964) Notes on water quality in agriculture. Published as water science and engineering, paper 4001 science and engineering, University of California, Davis Department of water

Eaton FM (1950) Significance of carbonates in irrigation waters. Soil Sci 39:123–134

Gibbs RJ (1970) Mechanisms controlling world's water chemistry. Science 170:1088–1090

Gupta S, Mahato A, Roy P, Datta JK, Saha RN (2008) Geochemistry of groundwater, Burdwan District, West Bengal, India. Environ Geol 53:1271–1282

Karmegam U, Chidambaram S, Prasanna MV, Sasidhar P, Manikandan S, Johnsonbabu G, Dheivanayaki V, Paramaguru P, Manivannan R, Srinivasamoorthy K, Anandhan P (2011) A study on the mixing proportion in groundwater samples by using Piper diagram and phreeqc model. Chin J Geochem 30:490–495

Lakshmanan E, Kannan R, Senthil KM (2003) Major ion chemistry and identification of hydrogeochemical processes of groundwater in a part of Kancheepuram district, Tamil Nadu, India. Environ Geosci 10:157–166

Nandhakumar S, Varun K, Sathyanarayanan N (2015) Interpretation of groundwater quality around Ambattur Lake, Chennai, Tamil Nadu. J Chem Pharm Res 7:1626–1633

Piper AM (1944) A graphic procedure in the geochemical interpretation of water analysis. Trans Am Geophys Union 25:914–923

Prasanna MV, Chidambaram S, Gireesh TV, Ali TVJ (2011) A study on hydro-chemical characteristics of surface and sub-surface water in and around Perumal Lake, Cuddalore district, Tamil Nadu, South India. Environ Earth Sci

Ramesh K, Elango L (2011) Groundwater quality and its suitability for domestic and agricultural use in Tondiar river basin, Tamil Nadu, India. Environ Monit Assess 184:3887–3899

Richards LA (1954) Diagnosis and improvement of saline and alkali soils. Agricultural Handbook 60, US Department of Agriculture, Washington, DC, p 160

Selvakumar S, Ramkumar K, Chandrasekar N, Magesh NS, Kaliraj S (2017) Groundwater quality and its suitability for drinking and irrigational use in the Southern Tiruchirappalli district, Tamil Nadu, India. Appl Water Sci 7:411–420

Srinivasamoorthy K, Gopinath M, Chidambaram S, Vasanthavigar, M, Sarma VS (2014) Hydrochemical characterization and quality appraisal of groundwater from Pungar sub basin, Tamilnadu, India. J King Saud Univ Sci

Sudhakar A, Narsimha A (2013) Suitability and assessment of groundwater for irrigation purpose: a case study of Kushaiguda area, Ranga Reddy district, Andhra Pradesh, India. Adv Appl Sci Res 4:75–81

Thivya C, Chidambaram S, Singaraja C, Thilagavathi R, Prasanna MV, Jainab I (2013) A study on the significance of lithology in groundwater quality of Madurai district, Tamil Nadu (India). Environ Develop Sustainability. https://doi.org/10.1007/s10668-013-9439-z

Thivya C, Chidambaram S, Thilagavathi R, Prasanna MV, Singaraja C, Nepolian M, Sundararajan M (2014) Identification of the geochemical processes in groundwater by factor analysis in hard rock aquifers of Madurai district, South India. Arab J Geosci. https://doi.org/10.1007/s12517-013-1065-4

Tiwari AK, Singh AK (2014) Hydrogeochemical investigation and groundwater quality assessment of Pratapgarh district, Uttar Pradesh. J Geol Soc India. https://doi.org/10.1007/s12594-014-0045-y

Todd DK (1980) Groundwater hydrology. Wiley, New York, p 535

Venkatesan D, Suresh Gandhi M, Thivya C (2016) Quality of groundwater and hydrogeochemical processes in hard rock region of Salem taluk, Tamilnadu. Enviro Geo Chimica Acta 3:63–70

Wilcox LV (1955) Classification and use of irrigation waters. US Department of Agriculture. Circ. 969. Washington, DC

Effect of Softer Binder on Bituminous Mixture Containing Reclaimed Asphalt Pavement (RAP) Material

Sujit Kumar Pradhan and Umesh Chandra Sahoo

Abstract Because of the increasing cost of bitumen and aggregate, there is increasing interest for utilizing higher rates of Reclaimed Asphalt Pavement (RAP) material in new hot mix asphalt (HMA) as a result of the gainful effect on the climate, preservation of energy, and saving natural resources. Yet these RAP materials are highly stiff due to the aged binder present in it, making untimely damage to the pavement. To adjust the negative effect of the aged RAP binder, a softer binder is a reasonable choice that reestablishes the properties of the aged binder. This exploration focused on the impact of suitable grade softer binder on the HMA mixture containing RAP. All mixes were designed according to Superpave specification ($N_{initial} = 8$, $N_{design} = 100$, and $N_{final} = 160$ gyrations) by considering the 12.5 mm nominal size of the aggregate. RAP utilized in HMA mixes at four varying percentages, such as 0%, 30%, 40%, and 50%. The suitable grade of the softer binder is controlled by the blending chart technique. Performance properties of these mixes were assessed by volumetric, indirect tensile strength (ITS), moisture sensitivity, and rutting. Later these outcomes constrated with the performance of the control mixture containing PG70-X binder. Results of the laboratory experiment show that ITS value increases, as RAP quantity increases. TSR of the mixes lies above the acceptance criteria of 80%. On the other hand, resistance to rutting increasing with RAP. In light of the results, it might be concluded that the softer binder has a significant effect on the RAP mixture, and RAP up to 50% may be used for the construction of bituminous pavement.

Keywords RAP · Softer binder · Volumetric · Moisture sensitivity

S. K. Pradhan (✉)
Department of Civil Engineering, IGIT Sarang, Dhenkanal, India
e-mail: sujitpradhan@igitsarang.ac.in

U. C. Sahoo
School of Infrastructure, IIT Bhubaneswar, Bhubaneswar, India
e-mail: ucsahoo@iitbbs.ac.in

B. B. Das et al. (eds.), *Recent Developments in Sustainable Infrastructure (ICRDSI-2020)—GEO-TRA-ENV-WRM*, Lecture Notes in Civil Engineering 207,
https://doi.org/10.1007/978-981-16-7509-6_6

1 Introduction

Now-a-days, utilizing Reclaimed asphalt pavement (RAP) material in asphalt mixes brings about significant economic savings and sustainability. According to National Asphalt Pavement Association, more than 76.9 million tons of RAP were utilized in new pavement construction (Hansen and Copeland 2017). Reusing of existing pavement material lessens the use of virgin material, which reduce the cost for the construction of new pavement. Efforts are still to utilize higher amount of RAP in hot mix asphalt. One of the essential purpose behind utilizing RAP restricted because of the variability in aggregate gradation. Also, presence of fines particles in RAP accelerated stiffness of the RAP binder. Regardless, RAP comprises of aged binder and aggregates that lead to fatigue and low temperature cracking, thereby affecting its workability. For recompensing the RAP binder and establishing better pavement performance includes the utilization of a rejuvenator or softer binder. The softer binder act as an preservative to soft the RAP binder and reinstate the physical and rheological properties of the aged binder. So it is a requirement for the investigation to concentrate on mechanical assessment of mixture that contains RAP with or without the softer binder.

Presently, the experimental studies have demonstrated that softer binder or rejuvenator can enhance the various properties of the RAP mixture (Chen et al. 2015; Shen et al. 2007; Mogawer et al. 2012; Willis et al. 2012; Zaumanis et al. 2014; Zaumanis 2014; Pradhan and Sahoo 2020a, b).

2 Objectives

The primary objective of this research was focussed on the following points:

- Impact of high RAP (30–50%) in HMA with a softer binder and compared its performance properties (i.e., indirect tensile strength, tensile strength ratio, rutting, and resilient modulus) with the control mixture containing no RAP.
- Statistical analysis of the mixtures on the performance properties.
- Comparison between the simple cost analysis of the control mixture and mixes containing RAP.

3 Materials and Methodology

3.1 RAP and Virgin Aggregate

For the study, RAP and virgin aggregate was collected from a nearby area from Bhubaneswar in the state of Odisha. Centrifugal extractors are used to determine the percentage of asphalt and aggregate gradation of bituminous paving materials based

Table 1 Physical properties of virgin and RAP aggregate

Particulars	Virgin aggregate	RAP aggregate
Specific gravity	2.235	2.724
Impact value (%)	14.25	25.46
Crushing value (%)	15.30	27.04
Combined flakiness and elongation index (%)	17.22	28.11
Water absorption (%)	0.38	0.89

on the weight of an asphalt and aggregate mixture. The aged binder content found in 100% RAP is 3.64%.

3.2 Characterization of RAP and Virgin Aggregate

The aggregate used for pavement construction should be of sufficient quality. To ensure this basic laboratory tests were conducted for both RAP and virgin aggregates and results were shown below (Table 1).

3.3 Methodology

A methodology was designed to identify the impact of RAP in HMA. All the mixes are designed according to the Superpave mix design method for 12.5 mm nominal size of aggregate.

Control mixture was set up with 100% fresh aggregate with target virgin binder VG 30 or PG 70-X and RAP mixes were prepared with 30, 40, 50% of RAP with a suitable grade of virgin binder determined from the blending chart technique (MS2 2014). Results of both control and RAP mixes were compared with various performance tests, including indirect tensile strength, TSR in terms of moisture susceptibility, wheel tracking to determine the rut depth and resilient modulus.

3.3.1 Indirect Tensile Strength Test (IDT)

IDT measure the tensile strength of the bituminous mixture and conducted as per ASTM D6931 (2017).

IDT was then determined by Eq. (1).

$$\text{IDT (kPa)} = 2000P/\pi Dt \tag{1}$$

where, P = Load (N), t = thickness before test (mm) and D = Sample diameter (mm).

3.3.2 Tensile Strength Ratio

Tensile strength ratio was found out following ASTM D 4867 (2014). Samples were compacted by gyratory compactor at 7 ± 0.5% air voids. Samples prepared were 100 mm in diameter and 63.5 mm in height. IDT was performed on 3 nos. conditioned samples and 3 nos. of dry samples. TSR are calculated by taking the ratio between IDT of the conditioned and unconditioned samples.

3.3.3 Rutting

Rutting was conducted according to BS EN 12697-22 (2003). Mixture was compacted to 6.5–7.5% by a roller compactor with a size 30.5 cm × 30.5 cm and a thickness of 0.5 cm. Before conducting wheel tracking test, sample was conditioned at 60 °C. The test was performed under dry conditions at wheel load of 700 N with 10,000 cycles.

3.3.4 *Resilient Modulus Test (M_R)*

Resilient modulus test was performed following ASTM D7369 (2011) and conducted at 25 °C. M_R (MPa) was then obtained by using the Eq. (2). Load is considered here 20% of the failure load.

$$M_R = P/Ht\ (0.27 + \mu) \tag{2}$$

where P = load (N), H = deformation (m), t = thickness (m) and μ = Poisson ratio.

4 Results and Discussions

4.1 Gradation

Blends must be intended to have sufficient resistance and reliability to withstand traffic loads and impacts due to change in temperature. An appropriately designed bituminous mixture gives an equalization of designing properties and economics that ensure a stable pavement. Mix gradations were selected according to the Superpave specification for the 12.5 mm nominal size of the aggregate according to SHRP (1987) (Table 2).

Table 2 Particle size distribution of mixes

Sieve size	Virgin	R30	R40	R50
19.00	100	100	100	100
12.50	93.56	94.22	94.52	93.12
9.50	82.61	84	84.45	81.52
4.75	48.14	50.84	51.98	45.12
2.36	33.54	35.22	34.44	31.88
1.18	22.12	20.42	19.55	18.21
0.60	15.26	13.43	14.02	12.02
0.30	11.18	9.71	10.05	6.52
0.15	7.15	6.58	6.87	5.83
0.08	2.95	3.21	3.39	3.48

4.2 Selection of Softer Binder Grade

The selection of binder grade to use in a RAP mixture is generally decided by MS2 (2014). Also, binder grade selection depend upon many factors such as climate and traffic intensity. When a 15% extracted RAP binder mixed with target binder, not required to change the binder grade. But, mixing of 15–25% RAP binder with virgin binder leading to lower the softer binder grade one grade than target binder grade. When mixtures containing more than 25% RAP, the binder grade used here one or two grade softer than the target grade of the binder. In this research, the target binder grade is PG 70-X and RAP used here is 30, 40, and 50% which is more than the limiting value of 25%. Blending chart approach, applied here to determine the softer binder grade of the 30, 40, 50% RAP mixes. To attain the target binder grade (PG 70-X), PG64-X, PG64-X and PG 58-X blended with the 30, 40, 50% RAP mixtures respectively.

4.3 Indirect Tensile Strength (IDT)

IDT tests were performed at 25 °C and results presented in Fig. 1. It is observed virgin mixture showed lesser strength related to the RAP mixes. As we increasing the RAP content, the IDT value increasing. Higher IDT value of RAP mixes illustrated higher cracking resistance. Aside from that, softer binder rejuvenated RAP mixes have highest tensile strength could be allocated to the high stability of the RAP mixes. The addition of softer binder improves the tensile strength of 30, 40, 50% RAP mixes by 6.66, 32.38, 42.35% respectively in comparison with the virgin mixture which prompted to high internal quality in terms of strength due to impact load. It also demonstrated average stiffness more than virgin mixture. Softer binders are

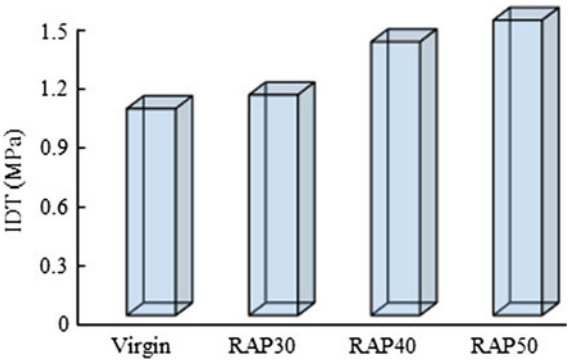

Fig. 1 IDT of mixes

efficiently in lowering stiffness of RAP mixtures at a transitional temperature that is appropriate for assessing the probability of cracking due to fatigue.

4.4 Tensile Strength Ratio (TSR)

To calculate the TSR value, IDT was performed on 3 nos. dry samples and 3 nos. conditioned samples. Figure 2 presents all the mixes achieved the limiting criteria of 80% TSR as per SHRP (1987). TSRs reduced with an increment in RAP content. Generally, moisture damage is due to the loss in the cohesion or adhesion between the interface between binder and aggregate interface. Generally, strength increment due to the existence of the RAP binder as strength comparatively depend on the binder. Noticeable stripping investigation was led after IDT test. The samples affirmed that the stripping of mixtures with RAP is less as compared with virgin mixture which means minimal stripping between aggregate and binder.

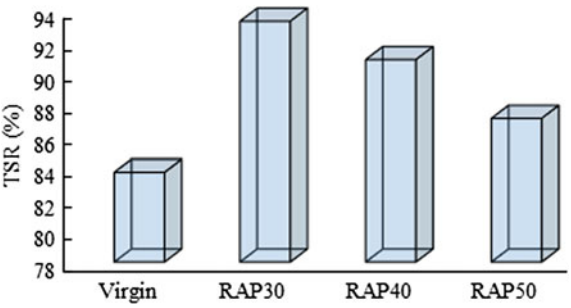

Fig. 2 TSR of mixes

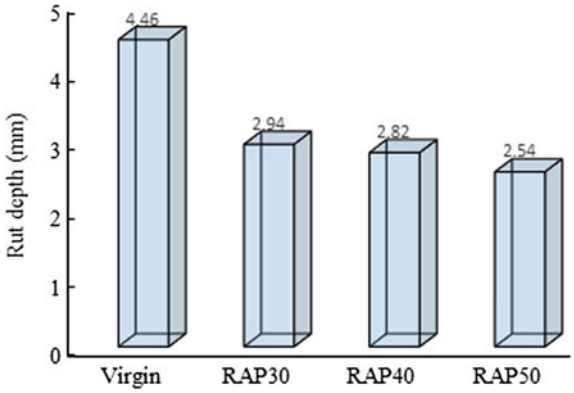

Fig. 3 Rut depth of mixes

4.5 Rutting

Figure 3 shows the impact of RAP on HMA rut depth for virgin mixture and RAP mixes containing a softer binder. The outcomes indicated that rut depth of virgin and RAP mixes are less than 12.5 mm which suggested by BS EN 12697-22 (2003). The control mixture has the highest rut depth as compared to the RAP mixture. Reduction of rut depth was noticed as mixture containing RAP raised from 30 to 50%. Softer binder added RAP mixture achieved lower rut depth due to the stiffness of the mixture and produce the rut depth of 30, 40, and 50% RAP mixes lesser by 34.08, 36.77, 43.04% with respect to the virgin mixture. Due to increasing in RAP content rutting resistance of the RAP mixes increases.. This divulged that incorporation of RAP accelerates the inflexibility of the RAP due to aged binder present in it and decreases the rutting.

4.6 Resilient Modulus

Modulus of the virgin, RAP mixtures with softer binder presented in Fig. 4. It tends

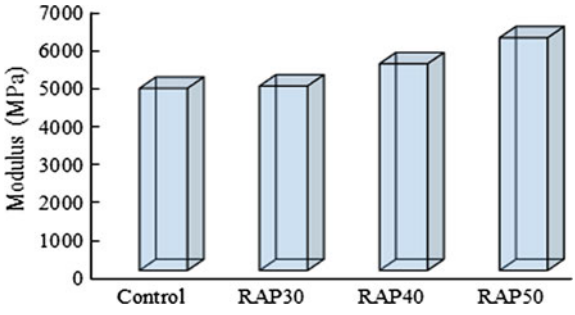

Fig. 4 Modulus of mixes

to be seen that RAP mixes having a resilient modulus higher than the virgin mixture at temperature 25 °C. As RAP content increases from 30 to 50%, the modulus value increases. At 25 °C, modulus values improved about 1.25%, 13.48, 27.76% for 30, 40, and 50% RAP mixes respectively, compared to control mixture. Higher resilient modulus impact elasticity to RAP mixes after loading. This indicated that it have a superior endurance to fatigue at moderate temperatures. Likewise, the high modulus of RAP mixes suggested stiffer mix and have a superior endurance to rutting in as compared to virgin mixture. Accordingly, the softer binder rejuvenated RAP mixture remarkably enhanced fatigue and rutting.

4.7 Statistical Analysis

One way Analysis of Variance (ANOVA) was implemented to assess the significant difference between the RAP mixes with respect to IDT, TSR, Rut depth and resilient modulus. The tests were performed at 95% significant level. These two hypotheses were considered:

Null Hypotheses: No significant difference between the mixes.
Alternate Hypotheses: Significant difference between the mixes (Tables 3, 4, 5 and 6).

As *p*-value is less than 0.05, there is significant difference between the RAP mixes on performance properties.

Table 3 ANOVA single factor RAP on ITS value

Source of variation	SS	df	MS	F	*P*-value	F crit
Between groups	0.448425	3	0.149475	70.89723	4.1872E−06	4.066181
Within groups	0.01686667	8	0.002108			
Total	0.46529167	11				

Table 4 ANOVA single factor RAP on TSR value

Source of variation	SS	df	MS	F	*P*-value	F crit
Between groups	157.665825	3	52.55528	13.46423	0.001711932	4.066181
Within groups	31.2266	8	3.903325			
Total	188.892425	11				

Table 5 ANOVA single factor RAP on RUT value

Source of variation	SS	df	MS	F	*P*-value	F crit
Between groups	6.7044	3	2.2348	502.2022	1.91136E−09	4.066181
Within groups	0.0356	8	0.00445			
Total	6.74	11				

Table 6 ANOVA single factor RAP on RM value

Source of variation	SS	df	MS	F	*P*-value	F crit
Between groups	3,173,016	3	1,057,672	102.4628	1.00838E−06	4.066181
Within groups	82,580	8	10,322.5			
Total	3,255,596	11				

4.8 Cost Evaluation

A simple cost evaluation was performed to know the suitability of the RAP in the bituminous mixes leading to the sustainability and economy. Several factors generally involved in the cost analysis. Here, only material cost taken in to account as per PWD, Government of Odisha schedule of rates (Table 7).

It is seen from the above table that the cost of control mix, 30%, 40%, 50% RAP mixes are Rs. 2986/-, Rs. 2436/-, Rs. 2251/- and Rs. 2063/- respectively. Reduction of cost of 30, 40, and 50% RAP by 18.42%, 24.61%, and 30.91% respectively as compared to control mix.

5 Conclusions

Based on the outcomes of the research, findings are described below:

- Increasing in RAP content lead to increase the strength and modulus of the mixture.
- RAP mixtures passed the limiting criteria of TSR (80%) even better than the control mixture.
- Rutting resistance increases with RAP content.
- When RAP content in the mixes more than 25%, it is required to include a softer binder in the mix to reduce the stiffness.
- Higher RAP utilization saves costs up to 30.91% in comparison to the control mixture.

Table 7 Cost analysis

	Quantity	Unit
Virgin aggregate and virgin binder		
Total weight of mixture	1000	kg
Weight virgin binder (OBC 5.5%)	55	kg
Weight of virgin aggregate	945	kg
Total cost = Rs. 2986.00 per ton		
Virgin aggregate, softer binder and RAP (30%)		
Total weight of mixture	1000	kg
RAP (30%)	300	kg
Bitumen content in RAP (3.64%)	10.92	kg
Virgin binder in total mix (OBC 5.4%)	53.1	kg
Weight of virgin binder required	42.18	kg
Weight of virgin aggregate	657.82	kg
Total cost = Rs. 2436.00 per ton		
Virgin aggregate, softer binder and RAP (40%)		
Total weight of mixture	1000	kg
RAP (40%)	400	kg
Bitumen content in RAP (3.64%)	14.56	kg
Virgin binder in total mix (OBC 5.36%)	53.6	kg
Weight of virgin binder required	39.04	kg
Weight of virgin aggregate	560.96	kg
Total cost = Rs. 2251.00 per ton		
Virgin aggregate, softer binder and RAP (50%)		
Total weight of mixture	1000	kg
RAP (50%)	500	kg
Bitumen content in RAP (3.64%)	18.2	kg
Virgin binder in total mix (OBC 5.31%)	53.1	kg
Weight of virgin binder required	34.9	kg
Weight of virgin aggregate	465.1	kg
Total cost = Rs. 2063.00 per ton		

References

Asphalt Institute (2014) Asphalt mix design method. Manual series No-02 (MS-2). AI, Lexington, KY, USA

ASTM D7369 (2011) Standard test method for determining the resilient modulus of bituminous mixtures by indirect tension test

ASTM D4867 (2014) Standard test method for effect of moisture on asphalt concrete paving mixtures

ASTM D6931 (2017) Standard test method for indirect tensile strength of asphalt mixtures

BS EN 12697:22 (2003) Bituminous mixtures-test methods for hot mix asphalt-wheel tracking

Chen JS, Chen SF, Liao MC, Huang SW (2015) Laboratory evaluation of asphalt blends of recycling agents with aged binders. J Mater Civ Eng 27(4)

Hansen KR, Copeland A (2016) Asphalt pavement industry survey on recycled materials and warm-mix asphalt usage. Report no. IS-138. National Asphalt Pavement Association, Lanham, MD

Mogawer W, Bennert T, Daniel JS, Bonaquist R, Austerman A, Booshehrian A (2012) Performance characteristics of plant produced high RAP mixtures supplement. Road Mater Pavement Des 13(S1):183–208

Pradhan SK, Sahoo UC (2020a) Effectiveness of Pongamia pinnata oil as rejuvenator for higher utilization of reclaimed asphalt (RAP) material. Innovative Infrastruct Solution. https://doi.org/10.1007/s41062-020-00343-6

Pradhan SK, Sahoo UC (2020b) Evaluation of recycled asphalt mixtures rejuvenated with Madhuca Longifolia (Mahua) oil. Int J Pavement Res Technol. https://doi.org/10.1007/s2947-020-0279-6

Shen J, Amirkhanian S, Miller JA (2007) Effects of rejuvenating agents on superpave mixtures containing reclaimed asphalt pavement. J Mater Civ Eng 9(5):376–384

Strategic Highway Research Program (SHRP) (1987) Superpave series no. 2 (SP-2), asphalt binder specifications and testing. Asphalt Institute, Lexington, KY, USA

Willis JR, Turner P, Julian G, Taylor AJ, Tran N, Padula FDG (2012) Effects of changing virgin binder grade and content on RAP mixture properties. NCAT report 12-03, National Center for Asphalt Technology

Zaumanis M (2014) 100% recycled hot mix asphalt and use of rejuvenators. Thesis dissertation

Zaumanis M, Mallick RB, Frank R (2014) 100% Recycled hot mix asphalt: a review and analysis. Resour Conserv Recycl 92:230–245

Multiple Linear Regression Analysis of Degradation Phenomena of HDPE Geomembrane Using Machine Learning

V. Nikhila Bhavani and S. Sangeetha

Abstract Leachates generated from municipal solid waste landfills, acid mine tailings etc., are toxic and hazardous which are being released into the environment. These leachates when released into the soil highly alter the geo-environmental properties of soil which are becoming biggest alarm in recent days. To avoid these problems, HDPE geomembrane is used as a barrier between soil and landfill waste but due to continuous exposure to leachates, life expectancy of geomembrane will be reduced which has to be analyzed. Oxidative induction time test is the most versatile test being used to estimate the life expectancy of geomembrane. The present study is an attempt to analyze the data digitized from previous research works and to develop a model by considering the combined effect of medium of exposure, thickness, temperature and time on depletion of antioxidants from geomembrane using machine learning.

Keywords HDPE geomembrane · OIT · Machine learning · Multiple linear regression analysis

1 Introduction

High Density Polyethylene (HDPE) geomembranes are most widely used liners for different types of landfills like MSW landfills, mine tailings, heavy leach ponds etc., (Rowe et al. 2008a, b) because of the stupendous physical and chemical resistance. Degradation of HDPE geomembrane is enormous, due to long-effect of above-mentioned contaminants. Hence, verifying the effectiveness of geomembrane is becoming the most important concern in present days. In general, intact geomembrane experiences degradation with ageing due to the physico-chemical effects during its service period (Husan and Koerner 1998). Practically, estimating the service life of geomembrane in field is not feasible for a longer duration. So, accelerated laboratory tests are performed to know the degradation pattern of geomembrane (Rowe et al.

V. Nikhila Bhavani (✉) · S. Sangeetha
Department of Civil Engineering, VNRVJIET, Hyderabad, Telangana 500090, India

B. B. Das et al. (eds.), *Recent Developments in Sustainable Infrastructure (ICRDSI-2020)—GEO-TRA-ENV-WRM*, Lecture Notes in Civil Engineering 207,
https://doi.org/10.1007/978-981-16-7509-6_7

2008a, b). But accelerated tests are also required to be performed for a minimum period of 2 years.

Degradation of geomembrane is defined as depletion of material properties in a slow and irreversible manner under adverse environmental conditions. Due to ageing, geomembrane undergoes adverse effects like loss of additives, plasticizers, change in molecular weight, formation of free radicals and become brittle as well (Kulshershtha 1992). Usually several degradation mechanisms such as ultraviolent degradation, chemical degradation, biological degradation, degradation by swelling, degradation by extraction, oxidative degradation and thermal degradation can take place based on exposure condition (Haxo and Nelson 1984; Koerner et al. 1990).

Effect of these degradations can be in any combinations, of which oxidative degradation is the most destructing phenomenon for HDPE geomembrane (Hawkins 1984). Oxidative degradation leads to formation of free-radicals by development of oxidative chain reactions in geomembrane (Kelen 1983). Due to these chains, HDPE polymer breaks down and leads to decrease in molecular weight of geomembrane; in succession, geomembrane eventually becomes brittle and is vulnerable to environmental stress cracking.

Oxidative degradation of HDPE geomembrane is divided into three stages—stage (I): Depletion time of antioxidants, stage (II): Incubation time, stage (III): Property reduction due to degradation of polymer (Husan and Koerner 1998). During manufacturing of geomembrane, the basic polymeric properties may vary. In order to avert these effects, antioxidants are added to geomembrane. Antioxidants prevents oxidative reactions to occur which usually happen in stage I. Antioxidants get depleted with the ageing process and this depletion depends on type of anti-oxidants, amount of anti-oxidants, combination of antioxidants used during manufacturing. It also depends on temperature, type of exposure medium to which geomembrane is subjected during testing (Fay and king 1994; Hsuan and Koerner 1998).

2 Problem Statement

In previous studies (Rowe et al. 2008a, b, 2010a, b; Gulec et al. 2004; Abdelaal et al. 2011) depletion of antioxidants is measured in terms of Oxidative Induction Time (OIT). Using the computed OIT values the life expectancy of geomembrane is estimated through Arrhenius Equation. The present research included collection of data from various journals and developed a model using Machine Learning after pooling the digitized data that accounted the combined effect of exposure condition, thickness, temperature and time of exposure.

3 Oxidative Induction Time Test

Degradation of geomembrane is generally measured using stress crack resistance test, oxidative induction test, melt flow index test, crystallinity test, and tensile test. The present study has focused on Oxidative Induction Time tests that were previously performed by various researchers in the past as per ASTM D3895. These tests give a detailed data regarding the presence of antioxidants in geomembrane. OIT can be performed in two ways such as Standard Oxidative Induction Time and High-Pressure Oxidative Induction Time. Standard OIT test is conducted using TA instrument Q-100 series differential scanning calorimeter which is provided with auto sampler. Samples of 6–10 g are heated to temperature of 200 °C at a rate of 20 °C/min and maintaining a pressure of 35 kPa in the presence of nitrogen environment, when the temperature reaches to 200 °C flow of nitrogen gas is stopped and maintained for 5 min, later the gas flow is changed to oxygen with the same pressure of 35 kPa. Using Differential Scanning Calorimeter, the level of antioxidant depletion is measured. The procedure for high pressure OIT test is same as standard OIT test but the temperature of 150 °C and pressure of 3500 kPa is maintained. To carry out this test, at least five samples are to be collected and tested; finally, it is concluded with average results and standard deviation.

4 Methodology

4.1 Collecting, Digitizing, Segregating the Data

In the present study multiple linear regression analysis has been performed for the data collected. Data are digitized for different test results given below which are collected from different literatures and weightage for exposure medium is found out based on the obtained OIT values in terms of air. Weightage of exposure medium varies with the different exposed condition like air, water, DI water, acid water, acid mine drainage and leachate. Initially weightage of exposure condition is determined when exposed to air, water, and leachate for testing data 1 in terms of air. Further, weightage of exposure condition for different leachates are determined in terms of air.

The study focusses on developing an inter-relation between independent and dependent variables where independent variables are weightage for exposure medium, thickness, time and temperature and dependent variables are oxidative induction time respectively. Data consist of four independent variables and one dependent variable, between these variables relationship is developed, and statistical measure has been computed for validating the relations. Such type of analysis is called as multiple linear regression analysis. In traditional methods, laboratory tests are conducted to predict the OIT of geomembrane at given conditions but this research aims at predicting the OIT value without going through those tedious and

time-consuming processes if considerable research data are combined in a single program which are available in the literatures. The main purpose of performing this type of analysis is to develop a model such that it predicts the OIT value based on the combined effect of thickness of geomembrane, any given exposure conditions, temperature to which geomembrane is exposed and time period to which geomembrane gets exposed.

4.2 Machine Learning

Machine learning is a language which is used to build a mathematical model and to predict the results based on available data referred as training data. In present research, analysis has been carried out in python language as it is easy, user-friendly, expressive, object oriented, high-level programming language which is widely being used in present days for writing scripts and complex computation program.

In order to perform the analysis, testing data were digitized from seven different studies i.e., Rowe et al. (2002b, 2008a, b, 2010a, b), Gulec et al. (2004), Abdelaal et al. (2011) and all the data were amalgamated. Following are the tables representing the data digitized from above mentioned studies. As data is huge only two digitized data are mentioned in Tables 1 and 2.

4.3 Development of Program Using Machine Learning

The flow chart representing the processing of individual and amalgamated data on Python platform is depicted in Fig. 1.

Initially analysis has been carried out based on the above procedure for individual test data and further all the data are pooled together to evaluate the R square value.

5 Results and Discussions

Multiple Linear Regression Analysis has been carried out for the digitized data and the following equations were developed.

Rowe et al. (2002b):

$$\mathrm{Y} = -0.0477(\mathrm{X}_1) - 9.02 \times 10^{-17}(\mathrm{X}_2) - 0.0576(\mathrm{X}_3) - 0.0119(\mathrm{X}_4) + 9.73,$$
$$\mathrm{R}^2 = 75\% \quad (1)$$

Gulec et al. (2004):

Table 1 Variation of ln (OIT) with varying exposure condition, thickness, temperature and time (Rowe et al. 2002b)

Weightage for exposure medium	Thickness (mm)	Temperature (°C)	Time (months)	ln (OIT) (min)
1	2	55	0	4.9
1	2	55	2	4.8
1	2	55	8	4.7
1	2	55	14	4.6
1	2	55	23	4.3
1	2	55	33	4.1
2	2	55	0	4.9
2	2	55	1	4.8
2	2	55	8	4.5
2	2	55	14	4.2
2	2	55	23	3.8
2	2	55	33	3.3
4	2	55	0	4.9
4	2	55	2	4.2
4	2	55	5	3.8
4	2	55	8	3.7
4	2	55	13	2.7
4	2	55	30	0.23
1	2	85	0	4.8
1	2	85	2	4.7
1	2	85	8	3.6
1	2	85	14	2.8
1	2	85	23	2
1	2	85	33	0.71
2	2	85	0	4.9
2	2	85	2	4.5
2	2	85	8	3.1
2	2	85	14	1.9
2	2	85	23	−1.7
2	2	85	33	−2.6
4	2	85	0	4.9
4	2	85	2	3.5
4	2	85	5	2.8
4	2	85	8	0.8

Table 2 Variation of ln (OIT) with varying exposure condition, thickness, temperature and time (Gulec et al. 2004)

Weightage for exposure medium	Thickness (mm)	Temperature (°C)	Time (months)	ln (OIT) (min)
0.99	1.5	20	0	6
0.99	1.5	20	3	6
0.99	1.5	20	6	6
0.99	1.5	20	9	5
0.99	1.5	20	12	5
0.99	1.5	20	15	5
0.99	1.5	20	18	5
0.99	1.5	20	21	5
1.05	1.5	40	0	5
1.05	1.5	40	3	5
1.05	1.5	40	6	5
1.05	1.5	40	9	5
1.05	1.5	40	12	5
1.05	1.5	40	15	5
1.05	1.5	40	18	5
1.05	1.5	40	21	5
1.05	1.5	60	0	6
1.05	1.5	60	9	5
1.05	1.5	60	12	4
1.05	1.5	60	15	4
1.05	1.5	60	18	4
1.05	1.5	60	21	4
1.09	1.5	80	0	5
1.09	1.5	80	1	5
1.09	1.5	80	2	4
1	1.5	60	0	5.6
1	1.5	60	3	5.5
1	1.5	60	9	5.2
1	1.5	60	12	5
1	1.5	60	15	4.7
1	1.5	60	18	4.7
1	1.5	60	21	4.6
1.05	1.5	60	0	5.6
1.05	1.5	60	3	5.5
1.05	1.5	60	6	5.2

(continued)

Table 2 (continued)

Weightage for exposure medium	Thickness (mm)	Temperature (°C)	Time (months)	ln (OIT) (min)
1.05	1.5	60	9	4.8
1.05	1.5	60	12	4.6
1.05	1.5	60	15	4.5
1.05	1.5	60	18	4.2

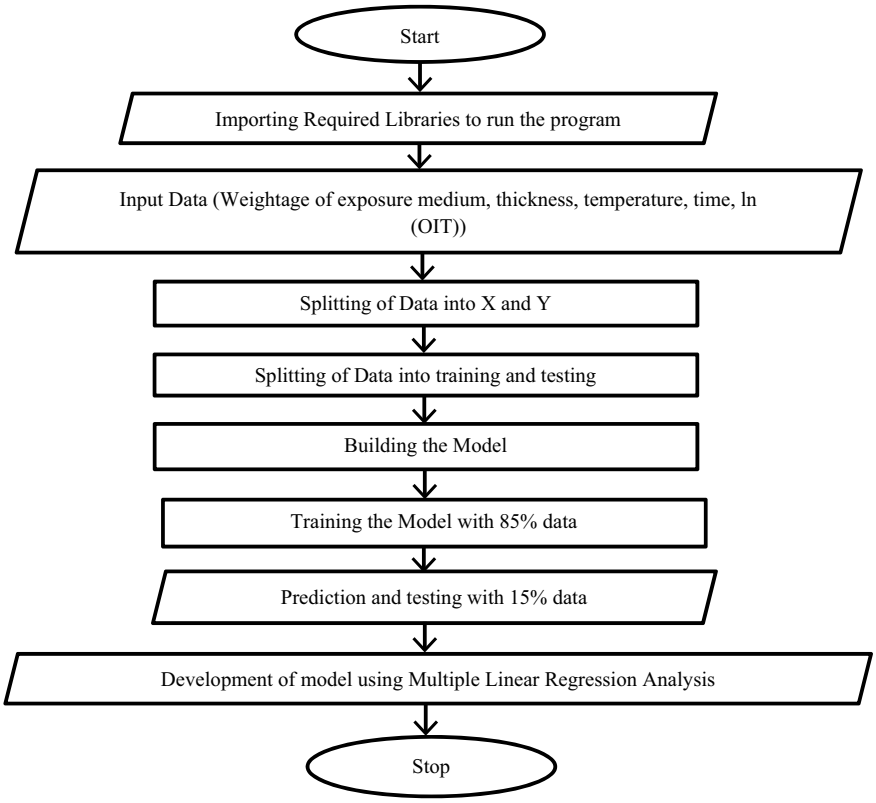

Fig. 1 Workflow in python

$$Y = -5.7(X_1) - 1.27 \times 10^{-13}(X_2) - 0.09(X_3) - 0.054(X_4) + 11.87, R^2 = 78\% \quad (2)$$

Rowe et al. (2008a, b):

$$Y = -0.002(X_1) - 8.32 \times 10^{-17}(X_2) - 0.054(X_3) - 0.077(X_4) + 7.4, R^2 = 77\% \quad (3)$$

Rowe et al. (2008a, b):

$$Y = -1.21(X_1) + 3.9 \times 10^{-14}(X_2) - 0.042(X_3) - 0.078(X_4) + 8.38, R^2 = 66\% \quad (4)$$

Rowe et al. (2010a, b):

$$Y = -1.95(X_1) + 3.5 \times 10^{-14}(X_2) - 0.09(X_3) - 0.14(X_4) + 12.8, R^2 = 75\% \quad (5)$$

Abdelaal et al. (2011):

$$Y = -0.157(X_1) - 1.24 \times 10^{-16}(X_2) - 0.002(X_3) - 0.021(X_4) + 6.2, R^2 = 83\% \quad (6)$$

Combined data

$$Y = -0.13(X_1) + 0.24(X_2) - 0.04(X_3) - 0.09(X_4) + 7.1, R^2 = 83\% \quad (7)$$

where X_1 = Weightage of exposure condition, X_2 = Thickness (mm), X_3 = Temperature (°C), X_4 = Time (months), Y = ln (OIT) (min).

Using above developed equations oxidative induction time of geomembrane can be determined.

Figures 2 and 3 represents the time versus ln (OIT) plot for the data digitized from Rowe et al. (2002b). Time taken for complete loss of antioxidants from geomembrane when exposed to air, water, and leachate at 55 °C is 583, 624, and 573 months and at 85 °C is 433, 474 and 498 months. It is noticed that the consumption of antioxidants from geomembrane takes place at faster rate at 85 °C when compared with the other as shown in the plots. Rate of depletion of antioxidants is dependent on various factors like physical, chemical, mechanical i.e., diffusion, volatilization, reaction with oxygen, free radicals and it is observed that time taken for antioxidant depletion is fast when geomembrane exposed to leachates as there is a extraction of antioxidants

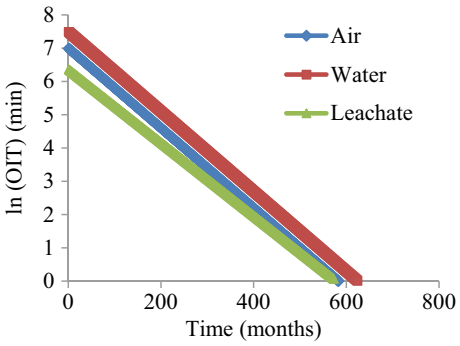

Fig. 2 Estimated OIT of geomembrane at 55 °C in air, water and leachate (Rowe et al. 2002b)

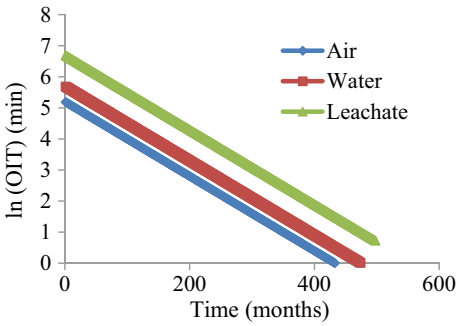

Fig. 3 Estimated OIT of geomembrane at 85 °C in air, water and leachate (Rowe et al. 2002b)

which leads to faster rate of loss of antioxidants at 55 °C when compared to air, water. But the pattern is reverse when geomembrane exposed to 85 °C this may be due to effect of polymerization of chains in geomembrane (Rowe et al. 2008a, b) which lead to increase in time for loss of antioxidants in MSW leachate.

Figure 4 represents variation of estimated OIT of geomembrane at different temperatures for the data digitized from Gulec et al. (2004). Acid mine drainage (AMD) is used as an exposure medium in this study. Based on equation obtained from multiple linear regression analysis for the digitized data OIT is determined. It is observed that effect of increase in temperature on loss of antioxidants is predominant. Time taken for reduction in antioxidants from geomembrane at 20, 40, 60, 80 °C is 111, 101, 98, 90 months. As temperature increases the consumption of antioxidants increases where the pattern followed in loss of antioxidants for this study is same as the previous study, but AMD has higher effect on loss of antioxidants when compared to MSW leachate.

Figure 5 represents plot for ln (OIT) with the time digitized from Rowe et al. (2008a, b) which shows linear response curve. It shows that the consumption of antioxidants is more at higher temperature when compared to lesser temperature. Estimated time taken for loss of antioxidants at different temperatures i.e., 26, 55,

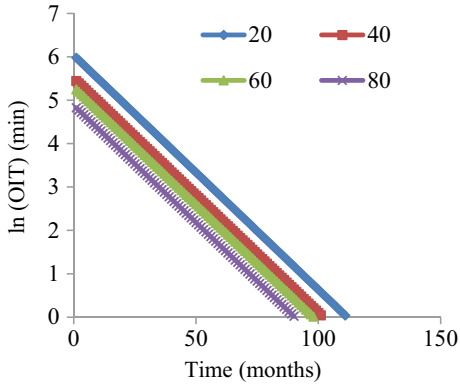

Fig. 4 Estimated OIT of geomembrane at 20, 40, 60 and 80 °C in leachate (Gulec et al. 2004)

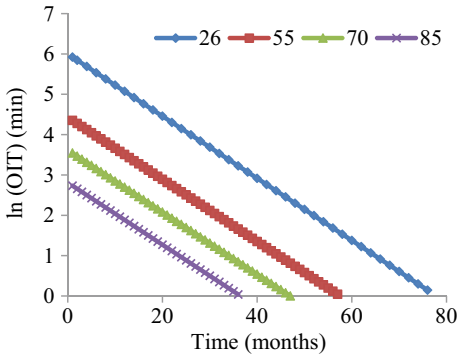

Fig. 5 Estimated OIT of geomembrane at 26, 55, 70 and 80 °C in leachate (Rowe et al. 2008a, b)

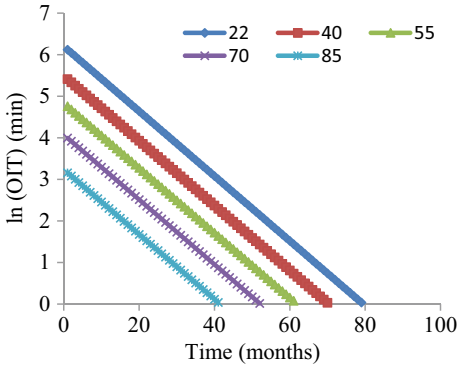

Fig. 6 Estimated OIT of geomembrane at 22, 40, 55, 70 and 80 °C in leachate (Rowe et al. 2008a, b)

70, 85 °C is 76, 57, 47, 36 months. Presence of surfactant in leachate is major source of loss of antioxidant from geomembrane and the effect of consumption increases with increase in temperature.

Variation of estimated OIT of geomembrane for data digitized from Rowe et al. (2008a, b) is shown in Fig. 6. In the present study geomembrane is exposed to four leachates and the above plot represents estimated OIT for leachate 1. It is seemed that the loss of antioxidants is increasing with the increase in temperature alike the other studies and time taken for consumption of antioxidants from geomembrane when immersed in leachate 1 at 22, 40, 55, 70, 85 °C is 79, 70, 61, 52, 41 months whereas in case of leachate 2 at 22, 40, 55, 70, 85 °C is 79, 69, 60, 49, 38 months; leachate 3 at 22, 40, 55, 70, 85 °C is 78, 70, 61, 49, 40 months; leachate 4 at 22, 40, 55, 70, 85 °C is 78, 70, 61, 51, 39 months. Based on above results it is examined that there is not much difference in consumption of antioxidants from geomembrane when exposed to four different types of leachates with varying composition at four different temperatures only the temperature effect is prevailing factor for loss of antioxidants.

Plot shown in Fig. 7 digitized from Rowe et al. (2010a, b) for leachate 1 reveals that pattern followed for consumption of antioxidants from geomembrane is same

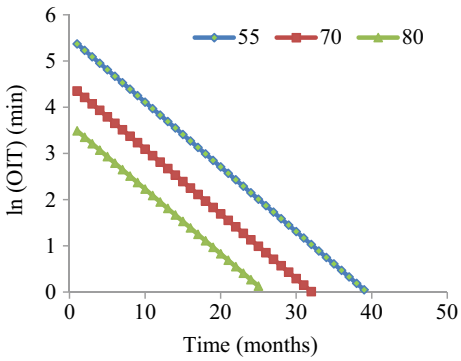

Fig. 7 Estimated OIT of geomembrane at 55, 70 and 80 °C in leachate (Rowe et al. 2010a, b)

as the other studies whereas the effect of temperature is a dominant factor in loss of antioxidants from geomembrane. Based on the developed from multiple linear regression analysis OIT is estimated at different temperatures it is examined that the time taken for complete loss of antioxidants from geomembrane in leachate 1 at 55, 70, 85 °C is 39, 32, 25 months and for leachate 2 at 55, 70, 85 °C is 41, 31, 25 months. It is also noticed that there is no much difference in loss of antioxidants from geomembrane when exposed to both leachates and pattern followed is same for both the leachates and alike other studies where temperature has major effect on depletion of antioxidant from geomembrane.

Multiple linear regression analysis has been carried out for the data digitized from Abdelaal et al. (2011) and estimated OIT is mentioned in the plot given in Fig. 8 which shows that there is an increment in depletion of antioxidants with increase in temperature which follows the same trend alike other studies. Time consumed for the complete loss of antioxidants from geomembrane at 75, 85, 95 °C is 292, 295, 294 months. It is witnessed that for loss of antioxidants, temperature has no effect as there is no much difference in time taken for complete depletion at the three different temperatures considered.

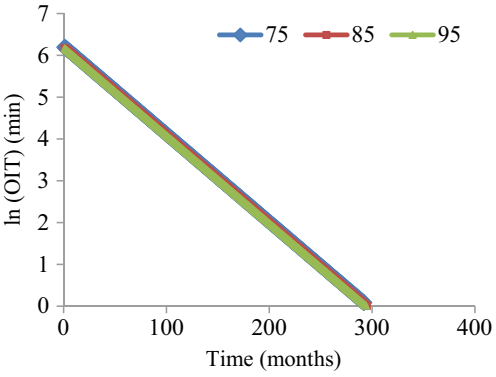

Fig. 8 Estimated OIT geomembrane at 75, 85 and 95 °C in leachate (Abdelaal et al. 2011)

5.1 *Extrapolation of Half-Life of Geomembrane for the Above Digitized Data*

From the estimated OIT, half-life of geomembrane is extrapolated for all testing data using time- temperature superposition model. Half-life of geomembrane is extrapolated for field temperature is given below.

5.1.1 Testing Data 1

Initially time taken for retention of 50% of OIT is tabulated for air, water, leachate at 55, 85 °C using multiple linear regression analysis for Rowe et al. (2002b) in Table 3. According to time–temperature superposition model a plot is made between temperature (K^{-1}) and time ($month^{-1}$) as shown in Fig. 9 and extrapolated half-life of geomembrane at field temperature of 33 °C using Eqs. 8, 9 and 10 in air, water, leachate is 43, 65, 88 years given in Table 4.

$$\text{In water} \quad Y = -5.1506X + 0.0181, R^2 = 1 \tag{8}$$

Table 3 Estimated half-life of geomembrane at 55 and 85 °C in air, water and leachate

Exposure medium	Temperature (°C)	Time (t) (month)	Temperature (T) (K)	1/T (K^{-1})	1/t ($month^{-1}$)
Air	55	379	328.15	0.0030	0.0026
	85	229	358.15	0.0028	0.0044
Water	55	421	328.15	0.0030	0.0024
	85	271	358.15	0.0028	0.0037
Leachate	55	356	328.15	0.0030	0.0028
	85	354	358.15	0.0028	0.0028

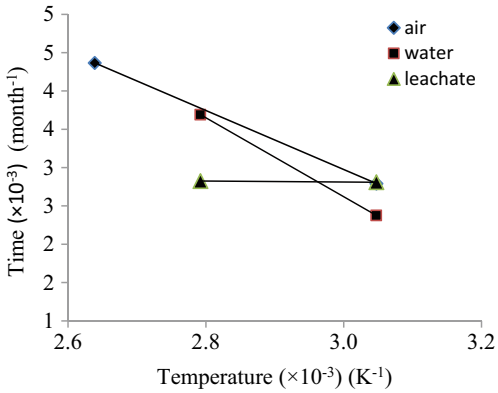

Fig. 9 Variation of half-life of geomembrane at 55 and 85 °C in air, water and leachate

Table 4 Prediction of half-life of geomembrane at field temperature at 33 °C

Exposure medium	Temperature (°C)	Half-life (years)
Air	33	43
Water	33	65
Leachate	33	88

$$\text{In air} \quad Y = -3.8514X + 0.0145, R^2 = 1 \tag{9}$$

$$\text{In leachate} \quad Y = -8.6819X + 0.0293, R^2 = 1 \tag{10}$$

5.1.2 Testing Data 2

Table 5 represents the estimated half-life of geomembrane at 20, 40, 60, 80 °C and a plot is made between temperature (K^{-1}) and time ($month^{-1}$) according to time–temperature superposition model for the estimated half-life of geomembrane using multiple linear regression analysis for Gulec et al. (2004) shown in Fig. 10 and half-life of geomembrane is extrapolated at field temperature of 33 °C using Eq. 11 which is of 4.1 years when exposed to leachate as shown in Table 6.

Table 5 Estimated half-life of geomembrane at 20, 40, 60, 80 °C in leachate

Exposure medium	Temperature (°C)	Time (t) (month)	Temperature (T) (K)	1/T (K^{-1})	1/t ($month^{-1}$)
Leachate	20	56	293.15	0.0034	0.0179
	40	46	313.15	0.0032	0.0217
	60	42	333.15	0.0030	0.0238
	80	30	353.15	0.0028	0.0333

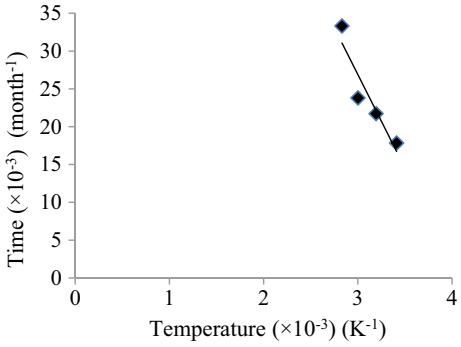

Fig. 10 Variation of Half-life of geomembrane at 20, 40, 60 and 80 °C in leachate

Table 6 Prediction of half-life of geomembrane at 33 °C

Exposure medium	Temperature (°C)	Half-life (years)
Leachate	33	4.1

$$y = -24.696X + 0.101, R^2 = 0.8778 \quad (11)$$

5.1.3 Testing Data 3

A time–temperature plot is made shown in Fig. 11 to extrapolate the half-life of geomembrane at field temperature of 33 °C using estimated half-life of geomembrane at temperatures 26, 55, 70, 85 °C for Rowe et al. (2008a, b) given in Table 7 and using Eq. 12 the half-life of geomembrane is and extrapolated at 33 °C is 3.3 years depicted in Table 8.

$$Y = -40.695X + 0.1585, R^2 = 0.7582 \quad (12)$$

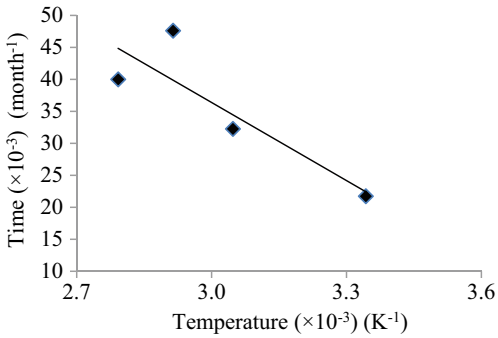

Fig. 11 Variation of half-life of geomembrane at 26, 55, 70 and 80 °C in leachate (Rowe et al. 2008a, b)

Table 7 Estimated half-life of geomembrane at 26, 55, 70, 85 °C in leachate

Exposure medium	Temperature (°C)	Time (t) (months)	Temperature (T) (K)	1/T (K^{-1})	1/t (month $^{-1}$)
Leachate	26	46	299.15	0.00334	0.021
	55	31	328.15	0.00304	0.032
	70	21	343.15	0.00291	0.047
	85	25	358.15	0.00279	0.04

Table 8 Prediction of half-life of geomembrane at field temperature at 33 °C

Exposure medium	Temperature (°C)	Half-life (years)
Leachate	33	3.3

5.1.4 Testing Data 4

Half-life of geomembrane is estimated at 22, 40, 55, 70, 85 °C for leachate 1 using multiple linear regression analysis to data digitized from Rowe et al. (2008a, b) which is mentioned in Table 9 and plot is developed shown in Fig. 12 based time–temperature superposition to extrapolate the half-life of geomembrane at field temperature of 33 °C using Eq. 13 and is 3.7 years shown in Table 10 and at the same field temperature extrapolated half-life for other leachates is 4.3, 3.7, 4.1 years. It is observed that there is no huge difference in extrapolated half-life for four leachates. So, in present study variation in composition of leachate has no effect on half-life of geomembrane

$$Y = -149.7X + 0.5113, R^2 = 0.6821 \tag{13}$$

Table 9 Estimated half-life of geomembrane at 22, 40, 55, 70, 85 °C in leachate 1

Exposure medium	Temperature (°C)	Time (t) (months)	Temperature (T) (K)	1/T (K^{-1})	1/t ($month^{-1}$)
Leachate 1	22	46	295.15	0.0034	0.022
	40	37	313.15	0.0032	0.027
	55	29	328.15	0.0030	0.034
	70	19	343.15	0.0029	0.053
	85	8	358.15	0.0028	0.125

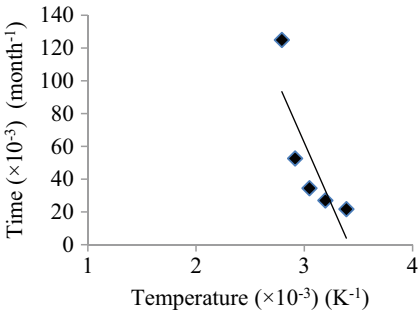

Fig. 12 Variation of half-life of geomembrane at 22, 40, 55, 70 and 80 °C in leachate 1

Table 10 Prediction of half-life of geomembrane at 33 °C

Exposure medium	Temperature (°C)	Half-life (years)
Leachate 1	33	3.7

5.1.5 Testing Data 5

Estimated half-life of geomembrane for leachate 1 and 2 at temperatures 55, 70, 85 °C from Rowe et al. (2010a, b) is tabulated in Table 11 and a time–temperature plot is made shown in Fig. 13 to extrapolate the half-life of geomembrane using Eqs. 14 and 15 at field temperature of 33 °C and the half-life for leachate 1 and 2 is 3.5, 2.6 years shown in Table 12.

$$Y = -325.52X + 1.031, R^2 = 0.9871 \tag{14}$$

$$Y = -301.25X + 0.9604, R^2 = 0.9418 \tag{15}$$

Table 11 Estimated half-life of geomembrane at 55, 75 °C in leachate

Exposure medium	Temperature (°C)	Time (t) (months)	Temperature (T) (K)	1/T (K^{-1})	1/t ($month^{-1}$)
Leachate 1	55	21	328.15	0.0030	0.048
	70	14	343.15	0.0029	0.071
	85	8	358.15	0.0028	0.125
Leachate 2	55	24	328.15	0.0030	0.042
	70	13	343.15	0.0029	0.077
	85	8	358.15	0.0028	0.125

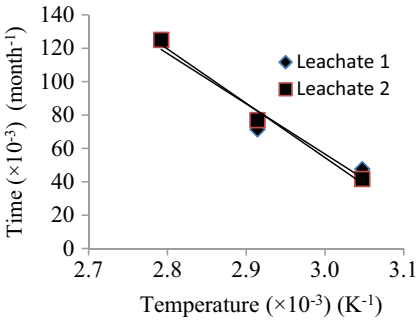

Fig. 13 Variation of half-life of geomembrane at 26, 55, 70 and 80 °C in leachate (Rowe et al. 2010a, b)

Table 12 Prediction of half-life of geomembrane at field temperature at 33 °C

Exposure medium	Temperature (°C)	Half-life (years)
Leachate 1	33	3.5
Leachate 2	33	2.6

Table 13 Estimated half-life of geomembrane at 75, 85, 95 °C

Exposure medium	Temperature (°C)	Time (t) (months)	Temperature (T) (K)	1/T (K^{-1})	1/t ($month^{-1}$)
Leachate	75	186	348.15	0.0029	0.00538
	85	185	358.15	0.0028	0.00541
	95	184	368.15	0.0027	0.00543

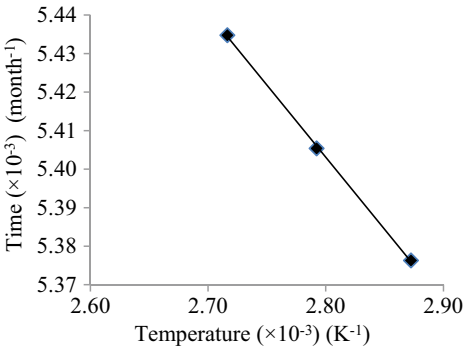

Fig. 14 Variation of half-life of geomembrane at 22, 40, 55, 70 and 80 °C in leachate

Table 14 Prediction of half-life of geomembrane at field temperature at 33 °C

Exposure medium	Temperature (°C)	Half-life (years)
Leachate	33	16

5.1.6 Testing Data 6

Table 13 represents estimated half-life of geomembrane at 75, 85, 95 °C when exposed to leachate digitized from Abdelaal et al. (2011). A time–temperature superposition plot is made for the estimated data shown in Fig. 14 and at field temperature of 33 °C extrapolated half-life of geomembrane is 16 years using Eq. 16 shown in Table 14.

$$Y = -0.3744X + 0.0065, R^2 = 0.9996 \quad (16)$$

5.1.7 Testing Data 7 (Pooled Data)

Multiple linear regression analysis is also performed for pooled data taken from Rowe et al. (2002b, 2008a, b, 2010a, b), Gulec et al. (2004) and Abdelaal et al. (2011). Procedure followed for Half-life estimation for all the data and procedure followed for extrapolation of half-life at field temperature of 33 °C is same as the individual data.

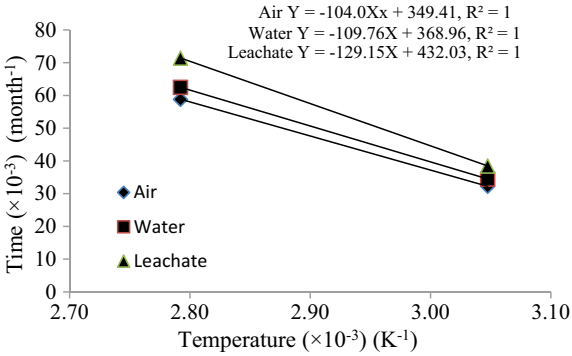

Fig. 15 Variation of half-life of geomembrane at 55 and 80 °C in air, water and leachate

Table 15 Estimated half-life of geomembrane at 55, 85 °C in air, water and leachate

Exposure medium	Temperature (°C)	Time (t) (months)	Temperature (T) (K)	1/T (K^{-1})	1/t ($month^{-1}$)
Air	55	31	328.15	0.0030	0.0323
	85	17	358.15	0.0028	0.0588
Water	55	29	328.15	0.0030	0.0345
	85	16	358.15	0.0028	0.0625
Leachate	55	26	328.15	0.0030	0.0385
	85	14	358.15	0.0028	0.0714

Table 16 Prediction of half-life of geomembrane at field data temperature for at 33 °C

Exposure medium	Temperature (°C)	Half-life (years)
Air	33	8.8
Water	33	7.95
Leachate	33	8.21

For Rowe et al. (2002b)

See Fig. 15 and Tables 15, 16.

For Gulec et al. (2004)

See Fig. 16 and Tables 17, 18.

For Rowe et al. (2008a, b)

See Fig. 17 and Table 19, 20.

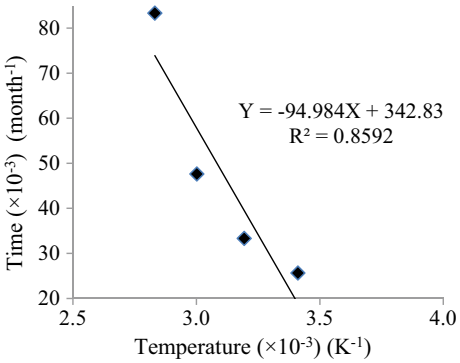

Fig. 16 Variation of half-life of geomembrane at 20, 40, 60 and 80 °C in leachate

Table 17 Estimated half-life of geomembrane at 20, 40, 60, 80 °C in leachate

Exposure medium	Temperature (°C)	Time (t) (months)	Temperature (T) (K)	1/T (K^{-1})	1/t ($month^{-1}$)
Leachate	20	39	293.15	0.0034	0.0256
	40	30	313.15	0.0032	0.0333
	60	21	333.15	0.0030	0.0476
	80	12	353.15	0.0028	0.0833

Table 18 Prediction of half-life of geomembrane at room temperature at 33 °C

Exposure medium	Temperature (°C)	Half-life (years)
Leachate	33	2.56

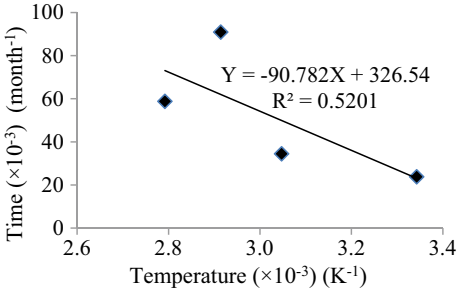

Fig. 17 Variation of half-life of geomembrane at 26, 55, 70 and 85°C in leachate

Table 19 Estimated half-life of geomembrane at 26, 55, 70, 85 °C in leachate

Exposure medium	Temperature (°C)	Time (t) (months)	Temperature (T) (K)	1/T (K^{-1})	1/t ($month^{-1}$)
Leachate	26	42	299.15	0.0033	0.0238
	55	29	328.15	0.0030	0.0345
	70	11	343.15	0.0029	0.0909
	85	17	358.15	0.0028	0.0588

Table 20 Prediction of Half-life of geomembrane at field temperature at 33 °C

Exposure medium	Temperature (°C)	Half-life (years)
Leachate 1	33	2.8

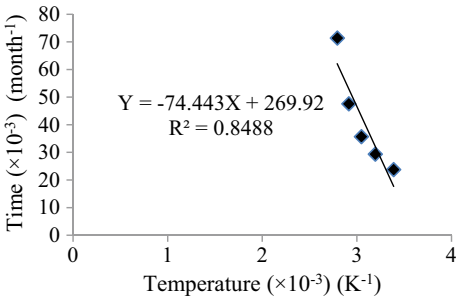

Fig. 18 Variation of half-life of geomembrane at 20, 40, 55, 70 and 85 °C in leachate

Table 21 Estimated half-life of geomembrane at 22, 40, 55, 70, 85 °C in leachate

Exposure medium	Temperature (°C)	Time (t) (months)	Temperature (T) (K)	1/T (K^{-1})	1/t ($month^{-1}$)
Leachate 1	22	42	295.15	0.0034	0.0238
	40	34	313.15	0.0032	0.0294
	55	28	328.15	0.0030	0.0357
	70	21	343.15	0.0029	0.0476
	85	14	358.15	0.0028	0.0714

Table 22 Prediction of half-life of geomembrane at field temperature at 33 °C

Exposure medium	Temperature (°C)	Half-life (years)
Leachate 1	33	3.1

For Rowe et al. (2008a, b)

See Fig. 18 and Tables 21, 22.

For Rowe et al. (2010a, b)

See Fig. 19 and Tables 23, 24.

For Abdelaal et al. (2011)

See Fig. 20 and Tables 25, 26.

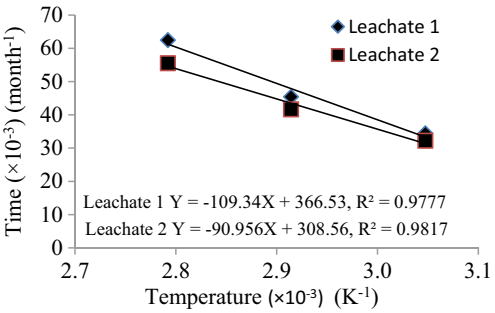

Fig. 19 Variation of half-life of geomembrane at 55, 70 and 85 °C in leachate

Table 23 Estimated half-life of geomembrane at 55, 70, 85 °C in leachate

Exposure medium	Temperature (°C)	Time (t) (months)	Temperature (T) (K)	1/T (K^{-1})	1/t ($month^{-1}$)
Leachate 1	55	29	328.15	0.0030	0.0345
	70	22	343.15	0.0029	0.0455
	85	16	358.15	0.0028	0.0625
Leachate 2	55	31	328.15	0.0030	0.0323
	70	24	343.15	0.0029	0.0417
	85	18	358.15	0.0028	0.0556

Table 24 Prediction of half-life of geomembrane at field temperature at 33 °C

Exposure medium	Temperature (°C)	Half-life (years)
Leachate 1	33	9
Leachate 2	33	7

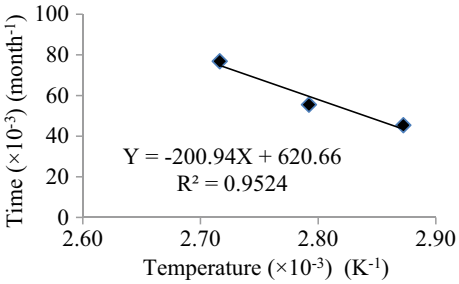

Fig. 20 Variation of half-life of geomembrane at 55, 70 and 85°C in leachate

Table 25 Estimated half-life of geomembrane at 75, 85, 95 °C in leachate

Exposure medium	Temperature (°C)	Time (t) (months)	Temperature (T) (K)	1/T (K^{-1})	1/t ($month^{-1}$)
Leachate	75	22	348.15	0.0029	0.0455
	85	18	358.15	0.0028	0.0556
	95	13	368.15	0.0027	0.0769

Table 26 Prediction of half-life of geomembrane at field temperature at 33 °C

Exposure medium	Temperature (°C)	Half-life (years)
Leachate	33	2.34

Table 27 Extrapolated half-life of geomembrane at field temperature of 33°C for all testing data

S. No.	Testing data source	Medium of exposure	Extrapolated half-life of geomembrane at field temperature of 33 °C (Years)		% variation of individual and pooled data
			Individual data	Pooled data	
1	Rowe et al. (2002)	Air	43	8.8	80
		water	65	7.92	87.7
		Leachate	68	8.21	88
2	Gulec et al. (2004)	Acid mine Drainage	4.1	2.56	38
3	Rowe et al. (2008a, b)	Leachate	3.3	2.8	15
4	Rowe et al. (2008a, b)	Leachate 1	3.7	3.1	16
		Leachate 2	4.3	3.1	28
		Leachate 3	3.7	3.2	14
		Leachate 4	4.1	3.2	22
5	Rowe et al. (2010a, b)	Leachate 1	3.5	9	61
		Leachate 2	2.6	7	63
6	Abdelaal et al. (2011)	Leachate	16	2.34	85

OIT obtained by validating the digitized data is almost same when compared with the actual data which was obtained by conducting accelerated laboratory tests. Table 27 gives half-life calculated using individual data, pooled data and percentage variation between them. The main advantage of this type of study is, one can estimate the Oxidative induction time easily as this procedure does not require any kind of laboratory testing and it is possible to estimate the time taken for the complete loss of antioxidants from geomembrane using this method. As the conventional laboratory method is time consuming, one could ignore the degradation study while harnessing geomembrane for field applications.

6 Conclusions

From the above computation, it has been witnessed that half-life of geomembrane estimated from pooled testing data is almost in line with individual data for all the literatures considered except for the testing data 1, 5, 6 this may be due to non-linearity

when data is pooled. As 50% of the obtained results are inline with each other, half-life obtained from both the individual and pooled data are satisfactory. Hence, this procedure can be used to estimate the antioxidant depletion time of geomembrane by performing multiple linear regression analysis for the digitized and amalgamated data sets without any laboratory testing. As this is a new technique to estimate the antioxidant depletion time and is also a preliminary study there is a need to do more research to obtain accurate results by collecting large number of data sets which are required to estimate life of geomembrane.

Scope

Antioxidant depletion rate can be determined by developing a software using machine learning technique so that we can avoid tedious laboratory process which would be generally ignored before field implementation and can save time.

Acknowledgements I would like to extend my sincere indebtedness to Praveen Kumar Pathi working as a Sr. Associate in Cognizant, USA for providing assistance in programming.

References

Abdelaal F, Rowe RK, Thiel R (2011) OIT depletion in HDPE geomembranes used in contact with solutions having very high and low pH. In: Pan AM CGS geotechnical conference

Fay JJ, King RE (1994) Antioxidants for geosynthetic resins and applications. In: Hsuan YG, Koerner RM (eds) Geosynthetic resins, formulations and manufacturing. GRI conference series, IFIA, St Paul, MN, USA, pp 77–96

Gulec SB, Edil TB, Benson CH (2004) Effect of acidic mine drainage on the polymer properties of an HDPE geomembrane. Geosynthetics Int 11(2)

Hawkins WL (1984) In: Harwood HJ (ed) Polymer degradation and stabilization, polymer/properties and applications, vol 8. Springer, Berlin, 119 p

Haxo HE, Nelson NA (1984) Factors in the durability of polymeric membrane liners. In: Proceedings of the international conference on geomembranes, vol II, Denver, CO, IFAI Publishers, St Paul, MN, pp 287–292

Hsuan YG, Koerner RM (1998) Antioxidant depletion lifetime in high density polyethylene geomembranes. J Geotech Geoenviron Eng ASCE 124(6):532–541

Kelen T (1983) Polymer degradation. Van Nostrand Reinhold, New York, 211 p

Koerner RM, Halse YH, Lord Jr AE (1990) Long-term durability and aging of geomembrane. In: Bonaparte R (ed) Waste containment systems: construction, regulation, and performance. ASCE Geotechnical Special Publication No. 26, New York, pp 106–134

Kulshershtha A (1992) Chemical degradation. In: Hamid SH, Amin MB, Madhah AG (eds) Handbook of polymer degradation. Marcel Dekker, New York, pp 55–95

Rowe RK, Islam MZ, Hsuan YG (2008a) Leachate chemical composition effects on OIT depletion in an HDPE geomembrane. Geosynthetics Int 15(2)

Rowe RK, ASCE F, Rimal S (2008b) Depletion of antioxidants from an HDPE geomembrane in a composite liner. J Geotech Geoenviron Eng 134:68–78

Rowe RK, ASCE F, Islam MZ, Hsuan YG (2010a) Effects of thickness on the aging of HDPE geomembranes. J Geotech Geoenviron Eng 136(2)

Rowe RK, ASCE F, Islam MZ, ASCE MR, Brachman WI, Arnepalli DN, Ragab Ewais A (2010b) Antioxidant depletion from a high density polyethylene geomembrane under simulated landfill conditions. J Geotech Geoenviron Eng 136(7)

Sangam HP, Rowe RK (2002) Effects of exposure conditions on the depletion of antioxidants from high-density polyethylene (HDPE) geomembranes. Can Geotech J 30(6):1221–1230

Comparative Study on Rainfall and Water Availability in Irrigation Tanks Using Google Earth Engine

Doggali Raju, Adhugiri Laxmi Sanjana, and Rambabu Palaka

Abstract The rainfall during monsoon season controls many sectors from agriculture, food, and water, to the management of drought. Rainfall is that the primary sources of water for irrigation. Rainfall is not available throughout the year. The stored rain water either in tank or in sub-surface is employed as resources of irrigation water for crop periods mostly for Rabi Season (November–April). So, it is needed to understand rainfall events and availability of rainwater in the irrigation tanks. Where, in Telangana State, this irrigation tanks play major role for the sustainable crop production. This study presents, a comparative study of availability of water in irrigation tanks by the help of rainfall data collected from Automated Weather Stations (AWS) deployed and managed by Telangana State Development Planning Society (TSDPS). In addition, Global Satellite Precipitation Data is used to compare the Rainfall occurrence using Google Earth Engine (GEE) Cloud based Computing Environment. Google Earth Engine is a platform that provides satellite datasets and collection of the tools for analysis of data using JavaScript, without downloading the huge data from Internet. In this study, we have used Global Surface Water (GSW) Dataset prepared for the period of 1984–2019 to map the maximum occurrence of Rainfall and Surface Area of waterbody. The NDWI maps prepared from Sentinel-1 and Sentinel-2 Satellite data were used to know the difference in water availability in different months of monsoon season (July to August) in Irrigation Tanks.

Keywords Rainfall · Water spread area · Google earth engine · Sentinel satellite · Global surface water

1 Introduction

Accurate and reliable information about extent of surface water is critical for various agriculture applications such as drought, flood monitoring, and awareness of surface water availability to irrigate (Mohite et al. 2019). Remote sensing is one of the

D. Raju (✉) · A. Laxmi Sanjana · R. Palaka
Department of Civil Engineering, B.V. Raju Institute of Technology, Narsapur, Medak, India
e-mail: 18211a0122@bvrit.ac.in

B. B. Das et al. (eds.), *Recent Developments in Sustainable Infrastructure (ICRDSI-2020)—GEO-TRA-ENV-WRM*, Lecture Notes in Civil Engineering 207,
https://doi.org/10.1007/978-981-16-7509-6_8

widely accepted technology for monitoring water resources and flooded areas on regular basis. A wide range of satellites is capturing information at various spatial, spectral, temporal and radiometric resolutions. Near real time satellite imagery helps in identifying droughts and floods for quick decisions (Gummadi et al. 2017).

In rainy season the optical remote sensing observations over Indian sub-continent are obstructed due to cloud cover. Synthetic Aperture Radar (SAR) is a useful alternative for monitoring of the surface water bodies even there is cloud cover. Sentinel-1C satellite data with spatial resolution of 10 m and temporal resolution of 12 days is highly useful to monitor the changes in water spread area of Irrigation tanks. In addition, Sentinel-2B MSI (Multispectral Imager) instrument covering 13 spectral bands (443–2190 nm) with a spatial resolution of 10 m (four visible and near-infrared bands) is also useful to detect water spread changes whenever there are no clouds (ESA Online).

Agriculture is an important filed of the national economy of Telangana. It added 13% to the income of the state. Nearly 56% of population in the state is depending on agriculture. It has the net cropped area of 5.12 million hectares and almost 56% of the area is irrigated by different sources of irrigation (Kamraju et al. 2017). The observations of the meteorological parameters of the surface are important in understanding the cycle of rainfall during the rainy season. To facilitate data collection Telangana State Development Planning Society (TSDPS) has installed 1044 Automatic Weather Stations (AWS) with 6 weather parameters such as Rainfall, Wind Speed, Wind Direction, Pressure, Humidity and Temperature. Presently, at least one AWS for each Mandal is installed in a grid of 10 km $\times$ 10 km (https://tsdps.telangana.gov.in).

Detailed information and improvements in the distribution of surface water are of great importance for the management of water and the conservation of biodiversity. Landsat-based assessments of surface water, such as the Global Surface Water (GSW) dataset developed by the European Commission Joint Research Centre (JRC) is useful to know the maximum extent of water spread area. GSW dataset contains maps of the location and temporal distribution of surface water from 1984 to 2019 and provides statistics on the extent and change of those water surfaces (Li et al. 2019).

Currently, cloud infrastructures can provide the flexibility needed to handle and process such enormous volumes of data (both for storage and computation) effectively, thereby making possible analyses that were previously assumed to be unfeasible due to data volume and computational constraints. In this respect, Google Earth Engine (GEE) is a cloud-based platform that makes it easy to access both multi-temporal remote sensing big data and high-performance computing resources for processing these datasets. Also, GEE users can upload their own non-public data in reserved areas and process them together the public ones, performing synergic data fusion and integration (Crespi et al. 2020).

Fig. 1 Location map of Narsapur Tank (Rairao Cheruvu) (78.28536 °E, 17.72608 °N)

2 Study Area

The main aim of this study is to analyse water spread area in Irrigation Tank and its changes during Kharif Season (June to October) located at Narsapur village, Medak District, Telangana State, India, is show in Fig. 1. Narsapur Tank (Rairao Cheruvu) is one of the main sources for Irrigation in Narsapur Mandal. This tank is monitored and maintained by the Dept. of Irrigation and Command Area Development, Govt. of Telangana State.

Salient Features of Narsapur Tank: (as per I&CAD)

- Settled Ayacut: 515.07 acres
- Catchment Area: 22.68 km^2
- Capacity at F.T.L.: 92.92 million ft^3
- Water Spread Area: 0.91 million m^2.

3 Methodology

3.1 Google Earth Engine (GEE) Platform

A cloud computing environment for satellite data analysis that provides free access for the data from various institutions such as the National Aeronautics and Space Administration (NASA) and the European Space Agency (ESA). GEE enable us

to handle large volume datasets of remote sensing and other ancillary datasets in a cloud computing platform without download into local machine. A web-based IDE for the Earth Engine (code.earthengine.google.com) using JavaScript API is used in this study.

3.2 Dataset

3.2.1 Satellite Data

Sentinel-1 SAR

This collection contains all of the C-band Synthetic Aperture Radar Ground Range Detected (GRD) scenes. Each scene has one of 3 resolutions (10, 25 or 40 m), 4 band combinations (corresponding to scene polarization) and 3 instrument modes. The revisit time of this satellite is 12 days.

In this study, SAR Data with a 10 m spatial resolution with VV polarization is used for change detection in Water Spread Area for the Kharif Crop Season (June to October) as most of the time during this period is cloudy.

Sentinel-2B

Sentinel-2 is a multi-spectral, high-resolution, wide-swath imaging mission that supports Copernicus Land Monitoring studies, including vegetation, soil and water cover monitoring. Sentinel-2B satellite was launched on 7 March 2017. When two sensors are operated simultaneously, the mission's revisit time is about 5 days, while about 10 days with one satellite in operation.

In this study, Normalized Difference Water Index (NDWI) is used to differentiate water from the dry land. Water bodies have a low radiation and strong absorbability in the visible infrared wavelengths range.

$$NDVI = \frac{(NIR - RED)}{(NIR + RED)}$$

3.2.2 Global Surface Water (GSW) Dataset

This dataset contains maps of the location and temporal distribution of surface water from 1984 to 2019 and provides statistics on the extent and change of those water surfaces. These data were produced using 4,185,439 scenes acquired between 16 March 1984 and 31 December 2019 from Landsat 5, 7, and 8. Using an expert method, each pixel was individually categorised into water/non-water and the results were collated into a monthly background for the entire time span and two epochs (1984–1999, 2000–2019) for identification of transition. This product for mapping

layers consists of 1 image with 7 bands in it. In this study, GSW data with 1% of accurance, the frequency with which water was present, is used to map the maximum probable extent of water spread area of Narsapur tank.

3.2.3 AWS Rainfall Data

In this study, Rainfall data from nearby Automatic Weather Stations were collected to analyse the Rainfall pattern, Intensity, and Cumulative Rainfall. This data was used in comparative study of water spread area in Irrigation Tank with respect rainfall.

3.2.4 Analysis

We analysed water spread status for the Narsapur Tank for four months i.e., Jul-Oct, 2020. First, Maximum Probable Extent of Water Spread is identified using Global Surface Water (GSW) dataset considering precipitation occurrence greater than or equal to 1%.Second, using Sentinel-1B SAR data is used map the water spread extent for different time series. Third, using Sentinel-2B MSI data is used to verify the Water Spread Extent which was mapped using SAR Data. Finally, Rainfall Data was collected from nearby Automatic Weather Stations (AWS) to make a Comparative Study on Rainfall and Water Availability in Irrigation Tank.

4 Results and Discussion

Rainfall data from the nearby Automatic Weather Station (AWS Id: 10995) of the Narsapur Tank is collected for the period from 1st July 2020. The Cumulative Rainfall which is used into comparative study to understand the change in Water Spread Area is shown in Table 1.

From the above Cumulative Rainfall Data, a chart for Rainfall versus Satellite Data Acquired Dates (Sentinel 1 SAR) is prepared to know the rainfall pattern nearby Narsapur Tank as shown in Fig. 2.

Using Google Earth Engine using JavaScript, Water Spread Area Maps for different time periods was created from the Sentinel 1 (SAR) data. From the maps shown Fig. 3, it is observed that there is no water in Narsapur Tank till 10-Aug-2020 and water accumulation is observed 12 ha (16.44% of Max. Water Spread Extent of 73 ha derived from Global Surface Water (GSW) dataset). And, water accumulation is increased gradually and observed the coverage is 95.89% on 21-Oct-2020 (Fig. 4 and Table 2).

From the Water Spread and Rainfall Data, it is observed that water accumulation is started after 250 mm cumulative rainfall which might be due to initial abstractions like detention and retention of surface run-off after rainfall event. A comparison

Table 1 Rainfall data (AWS Id: 10995)

Rain date	No. of hours	Rain (mm)	Cumulative rainfall (mm)
02-Jul-20	3	8.8	8.8
04-Jul-20	6	14	22.8
05-Jul-20	3	1.5	24.3
06-Jul-20	4	1	25.3
09-Jul-20	2	2.3	27.6
10-Jul-20	5	3.5	31.1
12-Jul-20	1	2.3	33.4
14-Jul-20	7	6.5	39.9
15-Jul-20	9	45.5	85.4
20-Jul-20	1	0.5	85.9
21-Jul-20	2	12.3	98.2
22-Jul-20	1	0.5	98.7
23-Jul-20	8	21.5	120.2
24-Jul-20	1	0.3	120.5
28-Jul-20	3	1.5	122
30-Jul-20	2	69	191
31-Jul-20	4	12.8	203.8
03-Aug-20	4	7.3	211.1
04-Aug-20	2	0.8	211.9
05-Aug-20	1	8.5	220.4
06-Aug-20	1	0.5	220.9
07-Aug-20	1	0.5	221.4
08-Aug-20	1	0.3	221.7
09-Aug-20	5	13	234.7
10-Aug-20	13	15.8	250.5
11-Aug-20	1	0.3	250.8
12-Aug-20	4	12.3	263.1
13-Aug-20	18	34.5	297.6
14-Aug-20	5	8	305.6
15-Aug-20	21	29.2	334.8
16-Aug-20	22	26.5	361.3
17-Aug-20	9	10.8	372.1
18-Aug-20	3	9.5	381.6
19-Aug-20	11	17.3	398.9
20-Aug-20	14	43.8	442.7
21-Aug-20	4	16.5	459.2

(continued)

Table 1 (continued)

Rain date	No. of hours	Rain (mm)	Cumulative rainfall (mm)
27-Aug-20	8	81.8	541
28-Aug-20	2	5.5	546.5
09-Sep-20	3	26.5	573
10-Sep-20	1	1.8	574.8
11-Sep-20	4	1.7	576.5
12-Sep-20	3	4.8	581.3
13-Sep-20	9	26.8	608.1
14-Sep-20	9	34.8	642.9
15-Sep-20	7	6.8	649.7
16-Sep-20	8	39.3	689
17-Sep-20	2	2.5	691.5
19-Sep-20	3	12.3	703.8
20-Sep-20	8	61.2	765
25-Sep-20	8	61.5	826.5
26-Sep-20	12	54.8	881.3
27-Sep-20	1	0.2	881.5
28-Sep-20	1	0.8	882.3
29-Sep-20	1	2.5	884.8
30-Sep-20	1	0.3	885.1
11-Oct-2020	8	75.8	960.9
12-Oct-2020	3	1.2	962.1
13-Oct-2020	16	143.5	1105.6
14-Oct-2020	4	38	1143.6
15-Oct-2020	3	12.3	1155.9
17-Oct-2020	1	5.5	1161.4
18-Oct-2020	5	54.3	1215.7
19-Oct-2020	1	4.3	1220
20-Oct-2020	2	16.7	1236.7

study on Water Spread Area versus Cumulative Rainfall is shown in Table 3 and same was presented in Fig. 5.

5 Conclusions

Sentinel-1 SAR data is more useful for Mapping and Computing Water Spread Area as most of the days are Cloudy in monsoon season. The accumulation of water in

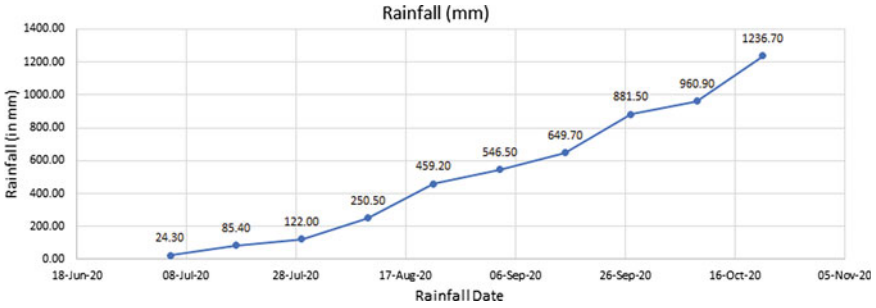

Fig. 2 Cumulative rainfall versus satellite data acquired dates

Narsapur Tank is started in the month of August 2020 even though there is a rainfall of 234.3 mm observed for the period January to June, 2020. Based on the analysis, it is observed that Water Spread Area is increased from 16.44% on 22-Aug-2020 to 95.89% on 21-Oct-2020 out of 73 ha of Maximum Water Spread Area derived from Global Surface Water dataset. Further, it is observed that the Irrigation Tank reached to its Full Tank Level (95.89%) in just 2 months with a total rainfall 986.2 mm. The max. storage capacity of Narsapur Tank and quantity of water accumulated during the above period will be discussed in the future studies.

Source: Global Surface Water
Max. Water Extent: **73 Hectares**

10-Aug-2020
Water Spead Area: **0 Hectares (0%)**

22-Aug-2020
Water Spread Area: **12 Hectares (16.44%)**

03-Sep-2020
Water Spread Area: **26 Hectares (35.62%)**

15-Sep-2020
Water Spread Area: **23 Hectares (31.51%)**

27-Sep-2020
Water Spread Area: **51 Hectares (69.86%)**

09-Oct-2020
Water Spread Area: **60 Hectares (82.19%)**

21-Oct-2020
Water Spread Area: **70 Hectares (95.89%)**

Fig. 3 Water spread area maps for the period from 10-Aug-2020 to 21-Oct-2020

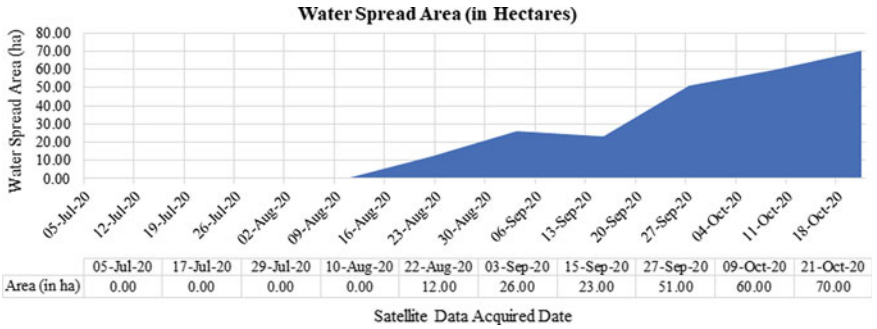

Fig. 4 Water spread area versus date of satellite data acquisition

Table 2 Water spread area versus satellite data acquired dates

Max. water spread area: 73 ha			
Date	Water spread area		Rainfall (mm)
	Hectares	%	
17-Jul-20	0	0.00	85.4
29-Jul-20	0	0.00	122
10-Aug-20	0	0.00	250.5
22-Aug-20	12	16.44	459.2
03-Sep-20	26	35.62	546.5
15-Sep-20	23	31.51	649.7
27-Sep-20	51	69.86	881.5
09-Oct-20	60	82.19	960.9
21-Oct-20	70	95.89	1236.7

Table 3 Water spread area versus cumulative rainfall

Max. water spread area: 73 ha		
Date	Area (in ha)	Rainfall (mm)
10-Aug-20	0.00	250.50
22-Aug-20	12.00	459.20
03-Sep-20	26.00	546.50
27-Sep-20	51.00	881.50
09-Oct-20	60.00	960.90
21-Oct-20	70.00	1236.70

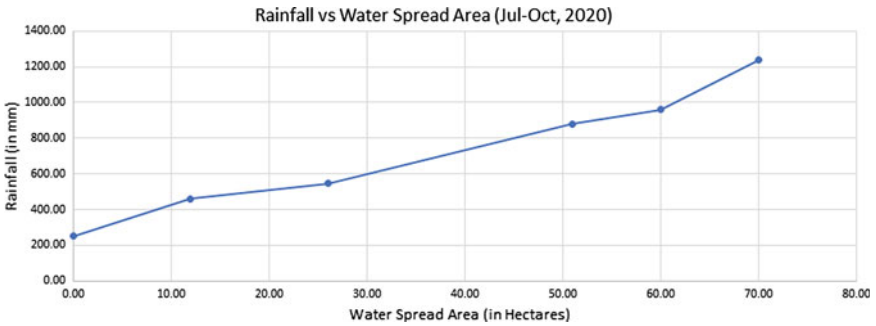

Fig. 5 Rainfall versus water spread area for the period Jul-Oct, 2020

Acknowledgements We would like to express our thanks to the Google Earth Engine (GEE) online forum for their invaluable assistance and inputs. We would also like to thank "Spatial Thoughts" for sharing the code used to Calculate Area using Google Earth Engine.

References

Crespi M, Nascetti A, Ravanelli R (2020) Special issue information—Google earth engine and cloud computing platforms: methods and applications in big geo data science. https://www.mdpi.com/journal/remotesensing/special_issues/GEE_Methods_Applications

Gummadi S, Rao KPC, Seid J, Legesse G, Kadiyala MDM, Takele R, Amede T, Whitbread A (2017) Spatio-temporal variability and trends of precipitation and extreme rainfall events in Ethiopia in 1980–2010. Theor Appl Climatol 134:1315–1328

Kamraju M, Vani M, Anuradha T (2017) Crop diversification pattern: a case study of Telangana state. Int J Innov Sci Res Technol 2(5)

Li L, Skidmore A, Vrieling A, Wang T (2019) A new dense 18-year time series of surface water fraction estimates from MODIS for the Mediterranean region. Hydrol Earth Syst Sci 23:3037–3056

Mohite J, Sawant S, Pappula S (2019) Spatiotemporal surface water mapping using Sentinel-1 data for regional drought assessment. In: Proceedings of SPIE 11149, Remote sensing for agriculture, ecosystems, and hydrology, vol XXI, p 1114905

Treatment of the Wastewater Polluted with Synthetic Microfiber Released from Washing Machine

Sunanda Mishra and Alok Prasad Das

Abstract Microfiber (MFs), are classified as secondary microplastic pollutants with diameter less than 10 μm, mainly released from the laundering of synthetic fabric. Investigations confirmed the universal presence of these fragments throughout the atmosphere including air water and soil. Tiny plastic fibers are the major source of this type of pollutant. Microfiber released by domestic laundering processes of synthetic fabric has recently been detected as the prime source of microfiber pollution in the aquatic environment. However, it is vital to understand the contribution of the synthetic clothes laundering to this environmental problem. Current study mainly focuses on the quantification of data about the release of microplastics, and to identify possible influences of textile characteristics on the release. Washing trials were performed using daily use synthetic garments in the household washing machine in order to record the influence of the washing parameters on the quantity of micro fleeces released. These tiny particles are discharged into the marine environment each year from a variety of sources, of which approximately 700,000 micro fragments are released and 1900 particles from one piece of garment. It can be predicted that, till date, 1.5 million trillion of MF pollutants are currently gathered in the ocean discharged by principal microfiber contributing countries. Domestic washing machines, unable to filter tiny fibers; hence, they can be easily escaped through the outlet to the river and oceans via domestic drainage. Synthetic microfibers are harmful as they are polluting the whole food chain when these pollutants are ingested by smaller aquatic organisms inadvertently. Advancement in the microscopic and spectroscopic techniques is employed for the quick detection of microfleece pollutant in various aquatic systems. Although few and technology with advanced density separation and centrifugation were developed to combat this pollution. However it was scientifically investigated that none of this method and product can filter MFs so competently. Meticulous research in this field is necessary and pre requisite for developing a technique for recycling of these pollutants and sustainable management, which may diminish the pollution level of the water bodies. Future research should primarily aim at developing novel techniques as a solution to this problem. In this present work, primarily the washing machine effluents samples were collected from

S. Mishra · A. P. Das (✉)
Department of Life Science, Rama Devi Women's University, Bhubaneswar, Odisha, India

B. B. Das et al. (eds.), *Recent Developments in Sustainable Infrastructure (ICRDSI-2020)—GEO-TRA-ENV-WRM*, Lecture Notes in Civil Engineering 207,
https://doi.org/10.1007/978-981-16-7509-6_9

5 different house hold regions of Bhubaneswar city, from Odisha state of India. Physiochemical parameters such as pH, Total dissolved solid, Total suspended solid of the collected grey water samples were measured to observe the variation. Morphological feature of the collected microfiber particles such as texture, colour, number and weight were measured. Around 500–520 numbers of visible fiber fleeces were present in 1 L of effluent sample, having biomass 3 mg/L approximately. Dominant presence of deep-red, black and blue coloured microfibers having fiber length 1–2.5 cm was observed. Abundant presence of polyester fiber groups is confirmed through hit description image and peaks 1240.03–2917.38 obtained from FTIR (Fourier transform infrared spectroscopy) analysis.

Keywords Washing machine · Waste water · Synthetic microfiber · Pollution · Treatment

1 Introduction

Both natural and manmade fibers are utilized to form textile products and garments and many valuable economic commodities which have essential role in our society. Recently, artificial and chemically modified fibers have exceeded dominating the clothing market of the whole world. All of us prefer to wear modern synthetic clothing every day, but are unaware of their dumping. Micro sized fiber particles released during the washing process, called microfibers, is omnipresent in all ecosystems and is regarded as an anthropogenic waste that has become a universal problem (Mohanty et al. 2017, 18; Das and Mishra 2008, 2010). It is anticipated that nearly 2 million tons of microfibers are discharged into the ocean each year and that 1.5 million trillion microfibers are present in the marine ecosystem currently (Mishra et al. 2019, 20). Synthetic clothing contributes upto 35% of all primary microplastics in the marine environment are releasing from synthetic garments (Laitala et al. 2018). Although all the sources have not been fully investigated, it was extensively believed until recently that household and commercial laundry liberations were the key source. Approximately 35% of synthetic fiber particles are discharged of primary source of microplastics into the ocean (Boucher and Friot 2017; Baldwin et al. 2016). Over time, large sized fiber particles break into tiny particles called microfibers, which cannot be degraded in the environment for thousands of years. These pollutants have harmful effects for wildlife. Individual animals can ingest large pieces or become entangled in plastic items, such as fishing gear, and suffocate or starve to death (Lamichhane 2018; Singh et al. 2020). Although there is no question that large plastics are harmful to aquatic organisms, the effects of microplastics mainly microfibers are not as straightforward. Many investigations concluded that microfibers can cause the harmful gene alteration, development, reproductive system (Gavigan et al. 2020). The lack of clear information makes it more complicated for decision-makers to perform an efficient policy to lessen this emerging pollution. India lies in the third position producing approximately 8% of total global SMFs. Bhubaneswar, the capital

city of Odisha, state of India has an important geographical location with three major rivers adjoining to the Bay of Bengal. As one of the most developing cities in the country, Bhubaneswar with 10 lakhs population is expected to produce an average of 19,000 lakhs of microfiber particles per wash in a single day. Detection of the microfibers in the water sources is essential in order to identify contribution of sources towards pollution and developing remediation strategies. The objective of our study was to detect the presence of microfibers from densely populated region of Bhubaneswar city, which enable to estimate the average mass of fiber particles discharged into the environment and their morphological characterization (Yang et al. 2019; Hirai et al. 2011; Das et al. 2014; Barrows et al. 2017). These tiny strands of synthetic fabric shed during textile manufacture, utilization have been detected in all types of ecosystems all around the world (De Falco et al. 2020). Synthetic fabric holds huge amounts of chemical and dyes during garment manufacturing, most of which are released during washing of garments. This designates that microfibers are of actual apprehension regarding the release and transportation of hazardous chemicals into the environment (Das and Singh 2011; Das et al. 2011, 15). In fact, microfibers have become one of the most frequently identified types of microplastic pollutants in water samples, found in rivers, soils, lakes, sediments, ocean water, the deep sea, arctic sea ice, seafood, table salt and most recently, public drinking water (Sanchez-Vidal et al. 2018). Such extensive exposure raises concerns about probable effects on aquatic organisms and also on terrestrial animals. As a consequence, microfibers are increasingly attracting the attention of governments, regulators, companies, nongovernmental organizations (NGOs), scientists and the news media. Detection of the microfibers in the water streams is important and essential in order to quantify the amount of microfibers released from various sources and their proper treatment and management. The present study aims at (1) Collecting washing machine effluents from different regions and to study the physio-chemical parameters of the collected samples (2) Characterization of extracted microfibers (3) To detect and analyse the chemical composition, functional groups FTIR (Fourier transform infrared) (4) Filtration and Separation of microfiber pollutants from collected waste sample.

2 Experimental Procedures

2.1 Sample Collection

Washing machine greywaters were collected from domestic drainage of different house from five different regions of Bhubaneswar city, Odisha. Location of sampling sites is latitude 20° 17′ 45.9″ to the North and 85° 49′ 28.5″ to the East in Khordha district of Odisha state of India. 1000 ml of washing machine effluent were collected

in clean, sterilized transparent glass stock bottles and kept safely for further experiments. To minimize contamination sterilized gloves were worn during the wash experiments, and samples were not exposed to the ambient environment.

2.2 Sampling Parameters

1000 ml of washing machine effluent were collected in clean, sterilized glass stock bottles and kept safely for further experiments from different locations of Bhubaneswar city. The washing parameters and washing machine type were recorded to allow for evaluating the effect of washing condition on microfiber release from garments. Washing experiment was carried out with constant speed and time of wash to access the variation in amount of MF release. On-site analyses of pH measurement were conducted out at the site of sample collection following the standard method. Microfiber particles were separated from collected washing machine effluents through filtration using whatman filter paper. The filter paper along with the fibers was air dried using hot air oven at 50 °C for 12 h.

2.3 Microfiber Characterization

The morphometric features of the microfiber particle separated from washing machine effluents through filtration were measured. Reliable identification of these smallest particles is possible with Fourier Transform Infrared Spectroscopy (FTIR). FTIR analysis of microfiber sample was carried out to ascertain the functional groups that are present in the collected sample. (FTIR) of dried MF particles was carried out to study its magnified surface morphology. Microfiber particles were washed, air dried and crumbled prior to spectroscopy. To eradicate natural organic substances prior to FT-IR analyses, the dried samples were treated with hydrogen peroxide followed by distilled water. FTIR analysis of microfiber sample was carried out using PerkinElmer (Spectrum II) to ascertain the functional groups that are present in the collected sample.

2.4 Treatment of Microfibers

The initial step for controlling microfleece pollution is mainly based on using the filtration technique. Collection of microfibers was carried out by straining greywaters from the washing machine using a filtration setup. To filter microfibers from effluent sample, filtration was carried out. For filtration experiment, initially the quadrant-folded filter paper was placed on the conical flask and the washing machine effluent sample was poured into filter paper.

3 Result and Discussion

3.1 Sample Collection and Sampling Parameters

The washing machine effluents were collected from different household regions of Bhubaneswar city, Odisha as shown in Fig. 1. Collected samples were kept in sterilized glass bottles for further experiments (Fig. 2). The washing parameters and washing machine type were recorded to allow for evaluating the effect of washing condition on microfiber release from garments. Synthetic fabric and products such as bed sheet, Shocks, jackets, jogging pants, T-Shirts, Pants Saree, carpets, towels, jackets were washed during washing experiment using top and frontload washing machine. Washing experiment was carried out with constant speed and time of wash to access the variation in amount of MF release. pH, Total suspended solid and Total dissolved solid of the collected washing machine effluents were investigated as in to access the quality status and results in a significant variation as represent in Table 1.

Fig. 1 Geographical location of sampling sites

Fig. 2 Collection of washing machine effluent

Table 1 Physio-chemical parameters

Sample No.	pH	TDS (mg/L)	TSS (mg/L)
S1	10	12	11.4
S2	9.5	12	12.6
S3	9	11	13.8
S4	9	10	15.2
S5	9	11	14

3.2 Sample Preparation and Characterization

The morphometric features of the microfiber particle separated from washing machine effluents through filtration were measured. Approximately 500–520 numbers of particles were present in 1 L of washing machine effluent samples. Dominant presence of yellow, deep-red, black and blue colored microfibers having fiber length 1–2.5 cm was observed (Fig. 3).

3.3 Spectroscopic Analysis

The spectrum was obtained by a mathematical algorithm called Fourier transform, which converts the raw data into a spectrum by converting the output signals into wavelengths. Presence of different types of synthetic fibers was confirmed from peak analysis and hit descriptions obtained from FTIR analysis. Abundant presence of polyester fiber in collected samples was confirmed from Carbonyl (C=O) stretching band at 1711 cm^{-1} and Aldehyde (–C–H) Weak bond at 2917.38 cm^{-1}. Mainly the C=O bond stretching confirmed the Presence of polyethylene terephthalate and C–F bond at 1452.23 cm^{-1} represented the presence of polyamides.

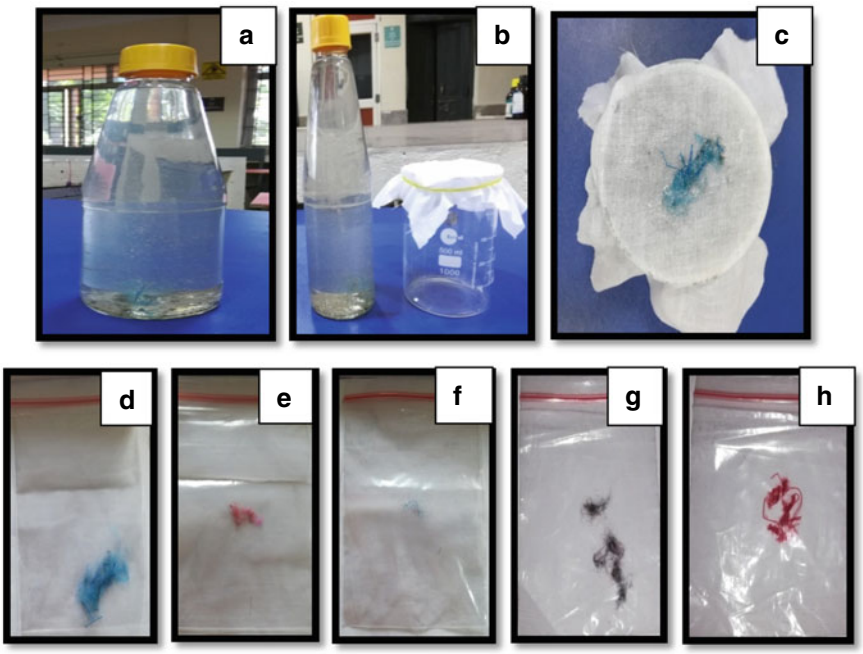

Fig. 3 **a–c** Recovery of microfibers from collected washing machine effluents, **c–g** collected microfibers from the sample

3.4 Treatment of Microfibers Through Filtration and Separation

Filtration intended to develop a trouble-free procedure to determine the concentrations of microfibers in waste waters released during laundering. The collected microfiber samples after filtration, the filtered samples were collected and biomass of the collected microfiber residue is measured. Approximately 4 mg of microfibers were separated from 1 L of washing machine effluents (Fig. 4a, b). After surface sterilization microfiber sample was cut into small fragments for characterization. Fiber particles were observed after the filtration, revealing a higher number of fibers than expected from observation of the filters before filtration.

4 Conclusion

Contaminated water treatment by this type of membrane filtration method is an economic and precisely practicable and substitute for the traditional treatment. Current investigation to the best of our knowledge is the first documented

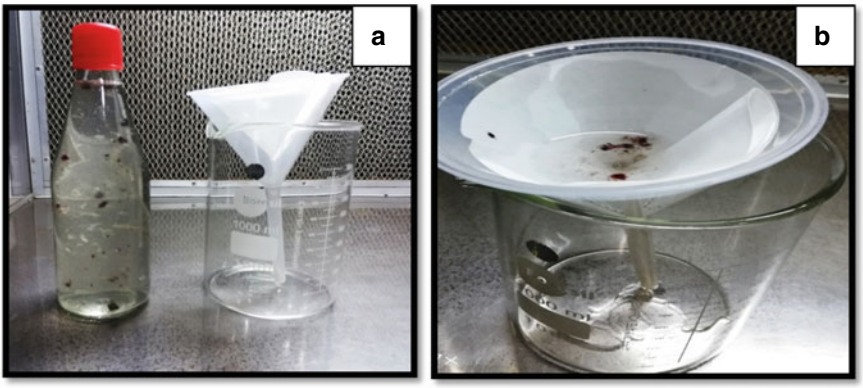

Fig. 4 **a**, **b** Filtration setup and filtration experiment

investigation on the presence of synthetic microfiber particles from the domestic washing machine effluents collected from Bhubaneswar city located in Odisha state of India. Our findings suggest that washing machine effluent could be a key source of MFs and thus can be considered to play an important role for environmental MF pollution. Their detection in the water sources is vital in order to identify contribution of sources towards pollution.

References

Baldwin AK, Corsi SR, Mason SA (2016) Plastic debris in 29 Great Lakes tributaries: relations to watershed attributes and hydrology. Environ Sci Technol 50:10377–10385. https://doi.org/10.1021/acs.est.6b02917

Barrows APW, Neumann CA, Berger ML, Shaw SD (2017) Grab vs. neuston tow net: a microplastic sampling performance comparison and possible advances in the field. Anal Methods 9:1446–1453. https://doi.org/10.1039/c6ay02387h

Boucher J, Friot D (2017) Primary microplastics in the oceans: a global evaluation of sources. Gland, Switzerland

Das AP, Mishra S (2008) Hexavalent chromium (VI): health hazards and environmental pollutant. J Environ Res Dev 2:386–392

Das AP, Mishra S (2010) Biodegradation of the metallic carcinogen hexavalent chromium Cr (VI) by an indigenously isolated bacterial strain. J Carcinog 9:6

Das AP, Singh S (2011) Occupational health assessment of chromite toxicity among Indian miners. Indian J Occup Environ Med 15(1):6–17

Das AP, Sukla LB, Pradhan N, Nayak S (2011) Manganese biomining: a review. Bioresour Technol 102:7381–7387

Das AP, Kumar PS, Swain S (2014) Recent advances in biosensor based endotoxin detection. Biosens Bioelectron 51:62–75

Das AP, Ghosh S, Mohanty S, Sukla LB (2015) Consequences of manganese compounds: a review. Toxicol Environ Chem 96:981–997

De Falco F et al (2020) Microfiber pollution from source to mitigation. In: Cocca M et al (eds) Proceedings of the 2nd international conference on microplastic pollution in the mediterranean sea, ICMPMS 2019. Springer Water. Springer, Cham. http://doi.org/10.1007/978-3-030-45909-3_11

Gavigan J et al (2020) Synthetic microfiber emissions to land rival those to waterbodies and are growing. PLoS ONE. https://doi.org/10.1371/journal.pone.0237839

Hirai H, Takada H, Ogata Y, Yamashita R, Mizukawa K, Saha M, Kwan C, Moore C, Gray H, Laursen D, Zettler ER, Farrington JW, Reddy CM, Peacock EE, Ward MW (2011) Organic micropollutants in marine plastics debris from the open ocean and remote and urban beaches. Mar Pollut Bull 62:1683–1692. https://doi.org/10.1016/j.marpolbul.2011.06.004

Laitala K, Klepp IG, Henry B (2018) Does use matter? Comparison of environmental impacts of clothing based on fiber type. Sustain 10:1–25

Lamichhane G (2018) Analysis of microfibers in waste water from washing machines. Metropolia University of Applied Sciences

Mishra S, Rath CC, Das AP (2019) Marine microfiber pollution: a review on present status and future challenges. Mar Pollut Bull 140:188–197

Mishra S, Singh RP, Rath CC, Das AP (2020) Synthetic microfibers: source, transport and their remediation. J Water Process 38:101612

Mohanty S, Ghosh S, Nayak S, Das AP (2017) Bioleaching of manganese by Aspergillus sp. isolated from mining deposits. Chemosphere 172:302–309

Mohanty S, Ghosh S, Bal B, Das AP (2018) A review of biotechnology processes applied for manganese recovery from wastes. Rev Environ Sci Biotechnol 17:791–811

Sanchez-Vidal A, Thompson RC, Canals M, de Haan WP (2018) The imprint of microfibres in southern European deep seas. PLoS ONE 13(11):e0207033. http://doi.org/10.1371/journal.pone.0207033

Singh RP, Mishra S, Das AP (2020) Synthetic microfibers: pollution toxicity and remediation. Chemosphere. http://doi.org/10.1016/j.chemosphere.2020.127199

Yang L, Qiao F, Lei K, Li H, Kang Y, Cui S, An L (2019) Microfiber release from different fabrics during washing. Environ Pollut 249:136–143

Estimation of PCE for Heterogeneous Traffic Stream in the Dual Carriageway Section

Pratap Kumar Pradhan, Shubhashish Bhoi, and Namrata Bishi

Abstract PCE are used as the factors to transfigure a traffic stream which is composed of various class of vehicles into an equivalent traffic stream composed absolutely of passenger cars. Based on various parameters of traffic stream traffic speed, traffic density, traffic flow and traffic headways PCE values are calculated. Present study analyses that various methods have been used to forecast the PCE values. It is too tough to estimate the traffic volume and traffic capacity of carriageway under heterogeneous traffic conditions. So, to get a standard vehicular unit, PCE has been developed to compare the congestion caused by different vehicles. The PCE values as introduced by developed countries are inappropriate for Indian mixed traffic condition because traffic is more heterogeneous and miscellaneous in nature. HCM utilizes PCE factors to estimate the effect of heavy vehicles on traffic stream under mixed traffic conditions. Different vehicles have significantly various driving performance characteristics to that of passenger cars. Therefore, these vehicles can have a major impact on traffic operations. It is therefore important to account properly for this impact in the traffic stream analysis in order to reflect the functioning quality of carriageway as close as possible. The primary objective of the research is to determine the appropriate PCE values of different vehicles. Additionally, a general PCE value with only one vehicle category was developed for planning purposes. The development of PCE values were based on the relative headway concept. For analysis of PCE, a significant amount of field data was collected during both peak and off-peak hour for the purpose of calibration. The PCE values determined from this study were 4.57, 3.76, 2.13, 0.28, 0.53 and 1.38 for peak hour and 4.6, 3.63, 2.14, 0.29, 0.55 and 1.33 for off peak hour for truck, bus, LCV, 2-wheeler, cycle and 3-wheeler respectively.

Keywords Capacity · Passenger car unit · Headway · Heterogeneous traffic · Traffic stream

P. K. Pradhan (✉)
Assistant Professor, Veer Surendra Sai University of Technology, Burla, Odisha, India
e-mail: pkpradhan88_ce@vssut.ac.in

S. Bhoi · N. Bishi
Transportation Engineering, Veer Surendra Sai University of Technology, Burla, Odisha, India

B. B. Das et al. (eds.), *Recent Developments in Sustainable Infrastructure (ICRDSI-2020)—GEO-TRA-ENV-WRM*, Lecture Notes in Civil Engineering 207,
https://doi.org/10.1007/978-981-16-7509-6_10

1 Introduction

The characteristics of travel, road networks system and other limits are very different and complexity in the developing countries' cities than those of developed. So, it is necessary to determine the various parameters of traffic movements which are appropriate for both study and design of characteristic of local urban transport system. To evaluate the various types of vehicles on mutual basis, a passenger car unit (PCU) or passenger car equivalent (PCE) was introduced.

Demarchi and Selti (1852) describes the truck of varying sizes also influence the PCE. A simple algebraic equation can't calculate the combined impact of the trucks. A work around method is applied to avoid the aggregate of PCE deviation. Botma (1988) describes the effects on traffic operation of a journey of slow vehicle. A special model was developed for congestion branch with the input of flows in both directions, % of trucks, speed and journey length. Outputs were number of overtaken size and duration of disturbance, number of affected vehicles. A computer program for a personal computer with several input procedure and graphical output has been developed, which makes it easy to use (1990).

Sikdar and Chandra (2000) analyse the mix traffic all the vehicles should be converted to PCE. The dynamic nature of PCE has been studied in this paper. The computer program developed to estimate PCE under a given road width, traffic volume and composition. Applicable in all traffic situations with a maximum number of 5 different vehicles.

Chandra and Kumar (2003) utilize the area, as opposed to only length and speed of vehicles. Vehicles were divided into 9 categories and PCE were estimated. It was found that PCE of a vehicle increases linearly with increase in lane width of carriageway. It is due to greater freedom of movement on wider road and greater speed difference between a passenger car and a vehicle.

Basu et al. (2006) shows that PCE of vehicles changes non-linear manner with total traffic volume and composition share of that vehicle type. The Neural Network technology is efficient enough to calculate PCE of vehicle. It require stream speed and measure of equivalence.

Tiwari et al. (2007) says the continuity equation is the basic block of any traffic planning. The modified density method helps in finding the loose lane discipline i.e. Rural non-homogenous traffic like truck, farm vehicles, tractors, 3 wheelers, 2 wheelers, bicycles, and animal drawn carts. Their speed varies too much like for buses, trucks, bicycles etc. Large PCEs of slow moving vehicle explain that these vehicles consume a high capacity of highway which includes non-homogenous flow. Homogenous flow contributes for increased capacity.

Mallikarjuna and Ramachandra (2006) shown that, in heterogeneous traffic condition microscopic characteristic is difficult to measure where as macroscopic characteristic would give enormous result. It expresses how long a particular size of vehicle is moving on that section of road.

Arasan and Krishnamurthy (2008) the PCE values obtained from different types of vehicle for a wide range of traffic volume and roadway condition indicate that

PCE values of a vehicle significantly changes with change in volume and width of roadway.

Do and Ngocle (2010) researched that developing countries having two wheeler as their major travelling mode. The PCE of motor bike depends upon the traffic conditions i.e. homogeneous or heterogeneous. Sarraj and Israa (2012) calculated the PCE using headway method at signalised intersections. They found that PCE for bus was 2 and that for animal driven cart was 1.67.

Metkari et al. (2014) says that PCE developed by developed countries are not suitable for Indian heterogeneous context. This paper reviews the existing basic methods. The paper represented the PCE values for different condition and covering all the sections so that a model can be built which can evaluate PCE of a vehicle for universal adoption.

Mehar et al. (2014) has provided the PCE values of different vehicles under different LOS. Speed-volume relation of car and other vehicles were found out using VISSIM. So the PCE of different vehicle at different LOS and different traffic composition on 4 and 6 lanes were suggested.

2 Method

2.1 PCU Based on Flow Rates and Density

In transportation engineering, the equivalent rate of vehicles passing a point per unit of time is called Traffic flow. According to this method, PCE can be determined by percentage of grade, mixed vehicle flow and truck volume to capacity ratio (John and Glauz):

$$PCU = \frac{q_B - q_M(1 - p_T)}{q_M * P_T}$$

Huber made a model for PCE calculation in multilane vehicle condition, under free flow. According to this, PCU values can be determined by

$$PCU = \frac{1}{P_T}\left(\frac{q_B}{q_M} - 1\right) + 1$$

Demarchi and Setti proposed a formula so as to eliminate the possible error for mixed vehicles in the traffic streams.

$$PCU = \frac{1}{\sum \mathrm{Pt}}\left(\frac{q_B}{q_M} - 1\right) + 1$$

where,

q_M Mixed flow rate
q_B Flow rate of car
P_T Proportion of T type of vehicles
P_i proportion of trucks of type i out of all trucks n in the mixed traffic flow.

$$PCU = \frac{K_c / W_l}{K_i / W_l}$$

where,

K_c Density of car under homogeneous condition
K_i Density of type 'i' vehicle under homogeneous condition
W_l Width of the lane.

2.2 Chandra Method

Here in this method, we focus on two factors, Space mean speed of the vehicle type and Its projected rectangular area. By using these two factors we calculate PCU values.

$$PCU = \frac{V_c / V_i}{A_c / A_i}$$

where;

V_c mean speeds of cars
V_i mean speeds of vehicle of type i
A_c projected rectangular areas on the road of cars
A_i projected rectangular areas on the road of type i vehicle.

2.3 Headway Method

It is one of the most popular method for the calculation of PCU values. in this method we consider relative amount of space taken by a vehicle for the calculation of PCU. Light vehicle takes less space than that of heavy vehicle. In 1976, Werner and Morrall derived the formula for PCU calculation on low terrain as

$$PCU = \frac{\frac{H_M}{H_B} - P_c}{P_T}$$

where,

H_M is the average headway for a sample including all vehicle types.

H_B is the average headway for a sample of passenger cars.
P_C is the proportion of cars.
P_T is the proportion of trucks.

2.4 Relative Delay Method

In this method, Werner and Morrall (1976) used Walker method to determine PCU values based on speed distributions, traffic volume and vehicle type. This method determines the PCU values by using the ratio of delay experienced by a passenger car due to non-passenger vehicles to delay experienced by a passenger car due to other passenger cars. According to this;

$$PCU = \frac{D_{ij} - D_{base}}{D_{base}}$$

where,

D_{ij} delay to passenger cars due to vehicle type i under condition j
D_{base} delay to standard passenger cars due to slower passenger cars.

2.5 Highway Capacity Method

Here we use the PCU factors which are determined in previous studies as here PCU is not calculated in any explicit way.

2.6 Speed Method

This is another method used to calculate the PCU value as the rate of motion of vehicles in a distance per unit time or unit speed. Yagar and Van Aerde (1983) made a methodology to determine PCU based on relative rates of speed for each type of vehicle. According to this PCU value decreases for higher speed percentiles. The speed analysis using the linear regression model structure is

$$\begin{aligned}\textbf{Percentile speed} = {} & \text{free speed} + \text{C1(number of passenger cars)} \\ & + \text{C2(number of passenger trucks)} \\ & + \text{C3(number of RVs)} + \text{C4(number of other vehicles)} \\ & + \text{C5(number of vehicle opposing)}\end{aligned}$$

where,

C1 to C5 speed reduction coefficient of each vehicle.

Using the speed reduction coefficient, the PCU for a vehicle type n is calculated as

$$PCU = \frac{C_n}{C_i}$$

where,

C_n speed reduction coefficient of vehicle type n.
C_1 speed reduction coefficient of passenger cars.

2.7 Greenshield Headway Method

PCU is calculated by the following equation. This method is known as basic headway method.

$$PCU = \frac{H_i}{H_c}$$

where

PCU_i passenger car unit
H_i average headway of vehicle type i
H_c average headway of passenger car.

2.8 Site Selection

The site selected should be such that it should be a straight road and there should not be any connecting road for a stretch of 1 km. We selected a stretch at Katapali area on NH 53. After the site is selected, a starting and ending line is drawn on the road with the help of paint with a distance of 60 m between the two lines. A flag is fixed at the far end for clear visibility. Then the data was collected with the help of a DSLR camera during the peak time for two hours (9:30–11:30 am) and two hours (2:30–4:30 pm) during off peak hours. The camera was kept at a height of nearly 6 ft. for clear visibility of all types of vehicles (Figs. 1 and 2).

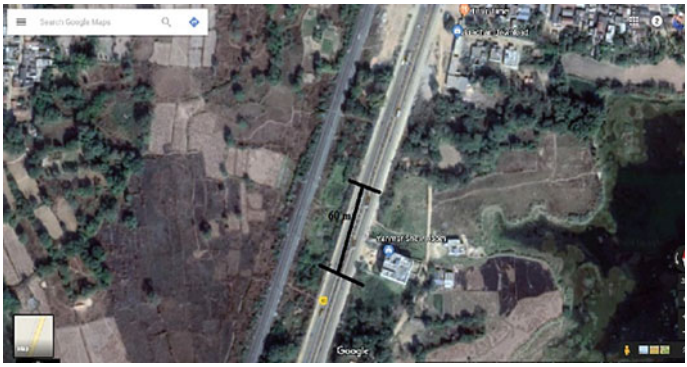

Fig. 1 Map picture and satellite picture

Fig. 2 Data collecting sites

3 Analysis

3.1 Traffic Data Analysis

First of all, we have to count all the vehicles and segregate them with respect to their types for both peak and off-peak hour in order to know their heterogeneity (Table 1).

We found that two wheelers are most on this road for both peak and off-peak hour. So, it is mainly dominated by two wheelers i.e. 56% during peak and 47% during off peak hour.

Table 1 Shows countable number of vehicles for different vehicle class in NH 53

Type of vehicle	Bus	Truck	2-W	3-W	Cars	Cycles	LCV
No. of vehicles during peak hour	49	271	1186	45	371	27	168
No. of vehicles during off peak hour	20	314	719	40	309	23	92

The speed is calculated of all the vehicles and then the speed is segregated for a 15 min time interval to know the fast driving period at that particular area. It was found that car is the fastest vehicle for both the peak and off-peak hour at that area i.e. 64.87 kmph during peak and 68.01 kmph during off peak hour.

Then the cumulative frequency is calculated and a table is prepared, by whose help the cumulative frequency graph is plotted (Figs. 3 and 4).

The above graphs help us to get the 15% speed, 50% speed, 85% speed and the 98% speed, that helps us to know the minimum speed, average speed, safe speed and design speed respectively which will ultimately help to design a pavement (Table 2).

The statistical data are also obtained using the excel sheets i.e. mean, median, mode and standard deviation (Table 3).

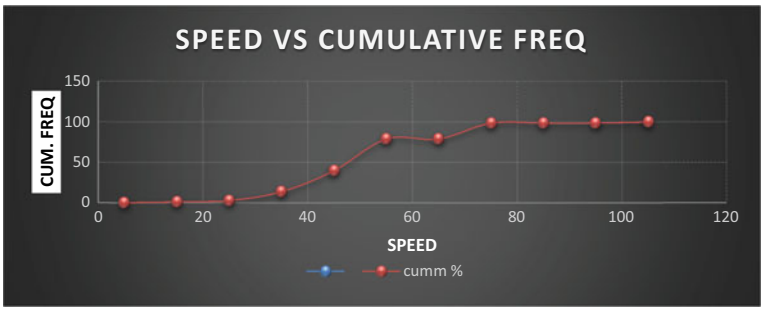

Fig. 3 Graph of speed versus cumulative frequency of vehicles for peak hour

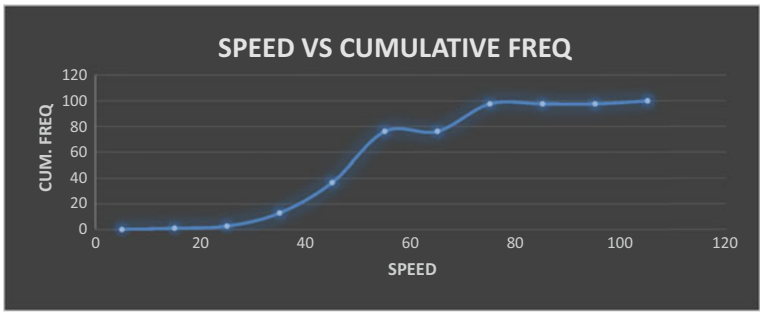

Fig. 4 Speed versus cumulative frequency for off peak period

Table 2 Shows the design, safe, average and minimum speed for peak and off peak hour

Speed types	Peak (kmph)	Off peak (kmph)
Design speed (98%)	74–76	74–76
Safe speed (85%)	68–70	68–70
Average speed (50%)	48	48–50
Minimum speed (15%)	36	36–38

Table 3 Shows the statistical speed data

Statistical data	Mean speed	Median speed	Mode	Standard deviation
Speed (kmph) peak	52.432	54	54	14.44
Speed (kmph) off-peak	53.767	54	54	15.24

Table 4 Shows the PCU using Chandra's method

Vehicle type	Car	Truck	Bus	LCV	2-W	Cycle	3-W
PCU (Peak)	1	4.571	3.76	2.131	0.285	0.528	1.381
PCU (Off)	1.000	4.610	3.634	2.143	0.293	0.553	1.332

Table 5 Show the PCU using traffic flow method for peak and off-peak hour

Vehicle type	Car	Truck	Bus	LCV	2-W	Cycle	3-W
PCU (Peak)	0.952	0.935	0.643	0.896	0.985	0.353	0.582
PCU (Off)	0.96	0.96	0.39	0.98	0.87	0.47	0.70

We found that the mean speed has increased up to some extent during off peak period likewise standard deviation has also increased during off peak hour while median speed and modal speed remains constant.

Over a heterogeneous traffic neither the traffic volume is constant over a period nor the traffic density. They vary with respect to time.

3.2 Calculation of PCU

3.2.1 Chandra's Method

The PCU values for various types of vehicles are cited below using the formula discussed above (Table 4).

3.2.2 Traffic Flow Method

It is another method used for calculation of PCU with respect to the flow of different types of vehicles (Table 5).

3.2.3 Traffic Density Method

In this method the traffic is considered to be in homogeneous condition and the PCU of various vehicles is calculated using their density on a road section (Table 6).

Table 6 Shows the PCU values from traffic density

Vehicle type	Car	Truck	Bus	LCV	3-W
PCU (Peak)	1	2.576	2.048	1.111	0.41
PCU (Off)	1	2.45	2	1.03	0.37

Table 7 Shows PCU values using headway method

Vehicle type	Car	Truck	Bus	LCV	2-W	Cycle	3-W
PCU (Peak)	1	1.11	1.36	0.89	1.18	0.90	1.61
PCU (Off)	1	1.06	1.44	0.94	1.21	0.92	1.6

3.2.4 Greenshield Headway Method

It is one of the oldest methods, introduced by Greenshield which calculates the PCU values using the time headway of various types of vehicles from the collected data (Table 7).

3.2.5 Comparison of PCU of All the Methods to that of IRC Recommended Values for Peak Hour

The above graphs show the comparison of PCU values of different vehicles using the four methods. Mostly the PCU of Chandra's method are closer to the IRC recommended value while the other three methods vary a lot as compared to IRC values. However, it is found that there is not much variation in between PCU of vehicles during peak and off-peak hour (Figs. 5 and 6).

4 Conclusion

The PCU used by IRC was developed for a homogeneous traffic condition. So, we can't consider the same values for the recent heterogeneous traffic. Not only the heterogeneity but also the sizes and shapes of vehicles matter a lot for the change in PCU values. The new vehicles developed in the present days are too much different to the vehicles developed before. They have varied a lot with respect to their sizes and efficiency. PCU is a speed and size dominated entity.

The PCU calculated using Chandra's method is closer to that of the IRC with respect to that of headway, flow and density method. The PCU calculated using the headway, flow and density methods vary a lot to that of IRC and the values are non-recommendable. Moreover, the peak and off-peak hour don't make any large difference in the PCU values rather they are close enough to each other numerically.

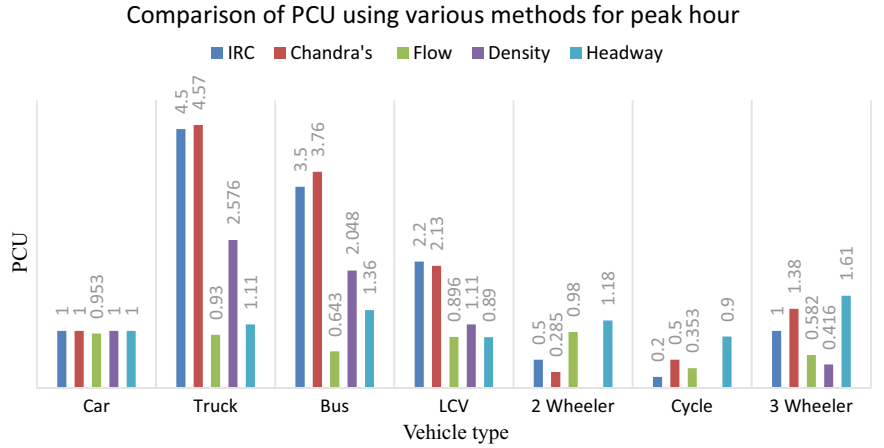

Fig. 5 Shows the comparison of PCU using different methods for peak hour

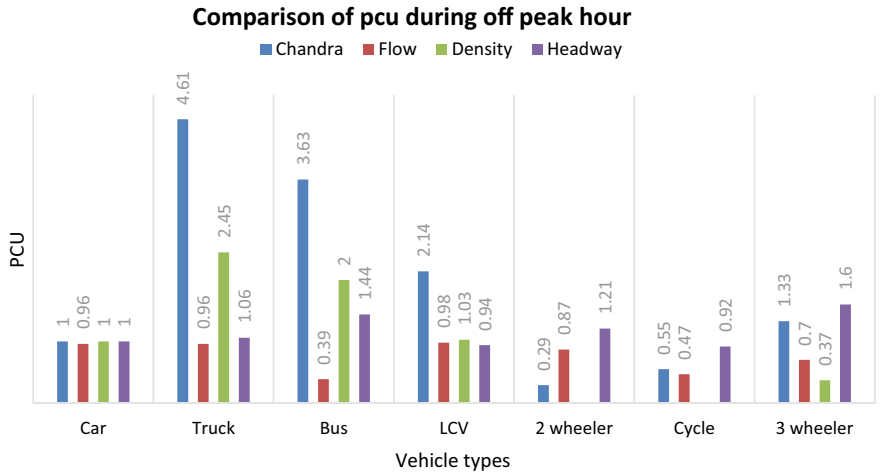

Fig. 6 Shows comparison of PCU using different methods for off peak hour

Finally, we may conclude that PCU is a dynamic value which depends upon the vehicle characteristics, driver characteristics and the road conditions. It varies from place to place according to the efficiency of all the three parameters said above. There is no much changes in the PCU values during the peak and off-peak hour.

References

Arasan VT, Krishnamurthy K (2008) Study of the effect of traffic volume and road width on PCU values of vehicles using microscopic simulation. J Indian Roads Congr 69–2:133–149

Basu D, Maitra B et al (2006) Modelling PCE at an urban mid block using stream speed as measure of equivalence. Eur Transp (34):75–87

Botma H (1988) Effect of traffic operation of a slow moving vehicle on two lane rural roads. In: Proceeding 14th ARRB conference, Canberra, pp 48–55

Chandra S, Kumar U (2003) Effect of lane width on capacity under mixed traffic conditions in India. J Transp Eng 129:155–160

Cunnagin WD, Mess CJ (1983) PCE for rural highways. Transp Res Rec 905

Demarchi SH, Selti JR (1852) Limitation of PCE derivation for traffic stream with more than one truck types. Transp Res Rec 03-3496

Do NA, Ngocle QL (2010) An estimation of passenger car unit of motorbikes. Transp Res Part C 140–15

Indian Roads Congress (1990) Guidelines for capacity of urban roads in plain areas. IRC code of practice, vol 106, New Delhi, India

Mallikarjuna C, Ramachandra Rao K (2006) Area occupancy characteristics of heterogeneous traffic. Transportmetrica 2(3):223–236

Metkari MK, Budhkar AK (2014) Review of passenger car equivalence studies in Indian context. Int J Eng Technol Adv Eng 4(6)

Mehar A, Chandra S, Velmurugan S (2014) Passenger car units at different levels of service for capacity analysis of multilane interurban highways in India. J transport Eng, 140(1), 81–88. https://doi.org/10.1061/(ASCE)TE.1943-5436.0000615

Sarraj Y, Israa J (2012) Estimating passenger car unit factors for buses and animal driven carts in Gaza City, Palestine. IUG J Nat Eng Stud 20(2):99

Sikdar PK, Chandra S (2000) Factors affecting PCU in mixed traffic situations on urban roads. Road Transp Res 40–50

Tiwari G, Fazio J, Gaurav S (2007) Traffic planning for non-homogeneous traffic. Sadhna 32(Part 4):309–328

Werner A, Morrall J (1976) Passenger car equivalencies of trucks, buses and recreational vehicles for two-lane rural highways. Transport Res Rec, pp 10–17

Yagar S, Van Aerde M (1983) Geometric and environmental effects on speeds of 2-lane highways. Transport Res Part A: General, vol 17(4):315–325

Crop Classification Using Machine Learning Algorithm

Pravalika Garipelly, Divya Bujarampet, and Rambabu Palaka

Abstract Agriculture plays a critical role in the global economy. This paper focuses on how agriculture can be merged with Machine learning. Machine learning has emerged with enormous data technologies and high-performance computing to build new opportunities for data-intensive science in the multi-disciplinary Agri-technologies domain. ML is defined as the scientific field that provides machines the ability to learn without being precisely programmed. In this paper, we present a detailed review of the application of ML in agriculture. Crops classification from satellite images is essential due to the use of those images as an input for agricultural and economic planning by government and private agencies. The methodology for this work is the selection of satellite data; use of the suitable method for classification and checking the accuracy. From last four decades, various researchers have been working on these issues up to some extent but still, some challenges are there like multiple crops identification, differentiation of crops of the same type this paper provides an overall review of the work done in this important area. In this paper, we used Random Forest (RF) Classifier using Google Earth Engine Cloud Computing Environment. The study was carried out in Narsapur Mandal comprising 35 villages in Medak District, Telangana State. A training set with more than 100 field samples of various crops like Paddy, Cotton, Jowar, etc., were collected from Mandal Agricultural Officers and used in the Crop Classification. The ML algorithm was applied on the Sentinel-2 Multispectral satellite data for the Kharif Crop Season 2020 and got satisfactory results.

Keywords Crop classification · Google earth engine · Machine learning · Random forest classifier

P. Garipelly (✉) · D. Bujarampet
Civil Engineering (B. Tech), Raju Institute of Technology, B.V, Narsapur, Medak, India
e-mail: 18211a0130@bvrit.ac.in

R. Palaka
Department of Civil Engineering, B.V. Raju Institute of Technology, Narsapur, Medak, India

B. B. Das et al. (eds.), *Recent Developments in Sustainable Infrastructure (ICRDSI-2020)—GEO-TRA-ENV-WRM*, Lecture Notes in Civil Engineering 207,
https://doi.org/10.1007/978-981-16-7509-6_11

1 Introduction

The extent, distribution, and characteristics (e.g., irrigation versus rainfed, cropping intensity, crop types) of croplands are factors that have long been identified as fundamental influences on agricultural development pathways, food security scenarios, and poverty reduction. Crop Mapping with high spatial resolution (10 m) over small areas such as districts or Mandal's or village accurately is of great importance for addressing cultivation of variety of crops and water security challenges. Cropland products capture a specific farm fields crucial for developing precise higher-level cropland products like cropping intensities, crop types, crop watering techniques (irrigated or rainfed), crop productivity, and crop water productivity (Teluguntla et al. 2018).

Crop Mapping brings various challenges that comprise handling massively big data volumes, computing power, and gathering resource-intensive reference training and validation data over geographic and political limitations. In this aspect, Google Earth Engine (GEE) is a cloud-based platform that makes it easy to access both multi-temporal remote sensing big data and high-performance computing resources for processing these datasets. (Crespi et al. 2020).

In this study, Seven Bands such as B2 (Blue), B3 (Green), B4 (Red), B5 (Red Edge 1—703.9 nm), B6 (Red Edge 2—740.2 nm), B7 (Red Edge 3—782.5 nm), B8 (NIR), and NDVI) of Sentinel-1C every 5-day temporal data for the period June-October, 2020 are used for Crop Classification. The crop classification executed by employing a pixel-based supervised Random Forest (RF) machine learning algorithm (MLA) executed on the Google Earth Engine (GEE) cloud computing platform.

2 Study Area

Agriculture is an important filed of the national economy of Telangana. It added 13% to the income of the state. Nearly 56% of population in the state is depending on agriculture. It has the net cropped area of 5.12 million hectares and almost 56% of the area is irrigated by different sources of irrigation (Kamraju et al. 2017).

In this study, an attempt is made for Crop Classification using Sentinel-2 satellite data using Google Earth Engine for Narsapur Mandal, Medak District, Telangana State, India. There are 35 Villages in Narsapur Mandal as shown in Fig. 1. Major Crops observed in this area for the Kharif Season are Paddy, Cotton, Maize, and Red gram.

All 35 villages in Narsapur Mandal are grouped into 5 clusters to facilitate easy administration and crop monitoring as shown in Table 1.

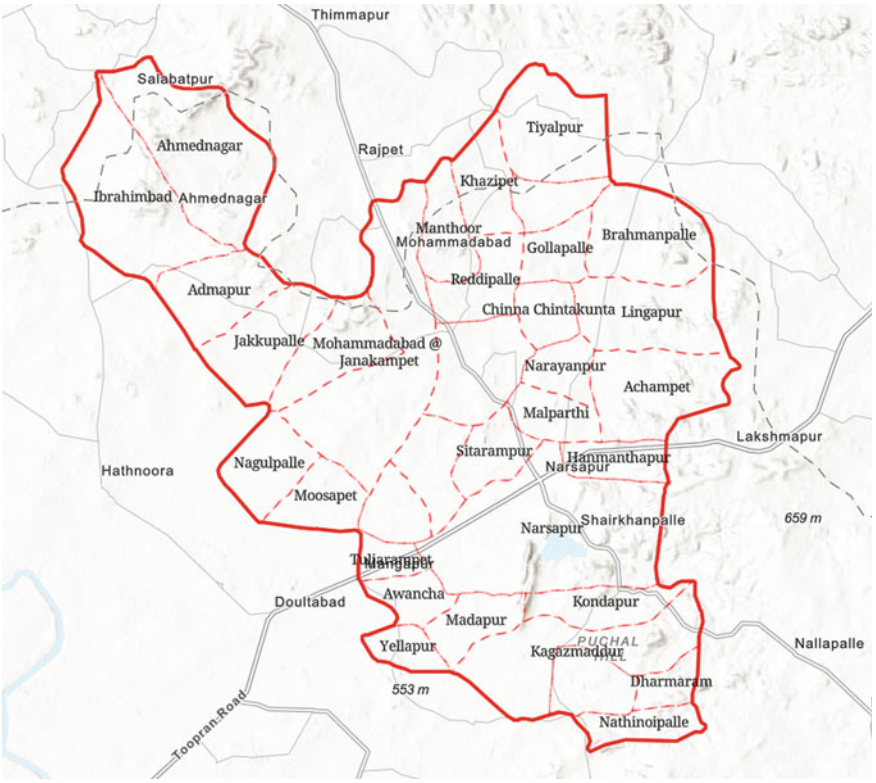

Fig. 1 Location Map of Narsapur Mandal. (78.2665° E, 17.7553° N)

3 Methodology

3.1 Google Earth Engine (GEE) Platform

A cloud computing environment for satellite data analysis that provides free access for the data from various institutions such as the National Aeronautics and Space Administration (NASA) and the European Space Agency (ESA). GEE enable us to handle large volume datasets of remote sensing and other ancillary datasets in a cloud computing platform without download into local machine. A web-based IDE for the Earth Engine (code.earthengine.google.com) using JavaScript API is used in this study.

Table 1 List of Villages in Narsapur Mandal

S. No	Cluster	Revenue Village	GP	Cultivable Area in Acres
1	AWANCHA	Awancha	Awancha	675
2		Madapur	Madapur	824
3		Moosapet	Moosapet	830
4		Nagulpalle	Nagulpalle	700
5		Ramachandrapur	Ramachandrapur	762
6		Tuljarampet	Tuljarampet	207
7		Yellapur	Yellapur	505
		Total		4503
1	IBRAHIMBAD	Admapur	Admapur	490
2		Ahmednagar	Ahmednagar	847
3		Chippalturthi	Chippalturthi	1320
4		Ibrahimbad	Ibrahimbad	990
5		Jakkupalle	Jakkupalle	560
6		Mohammadabad @ Janakampet	Mohammadabad @ Janakampet	598
		Total		4805
1	LINGAPUR	Achampet	Achampet	423
2		Brahmanpalle	Brahmanpalle	590
3		Gollapalle	Gollapalle	300
4		Lingapur	Lingapur	780
5		Malparthi		252
6		Narayanpur	Narayanpur	509
7		Thirmalapur	Thirmalapur	537
8		Tujalpur	Tujalpur	1127
		Total		4518
1	NARSAPUR	Dharmaram		
2		Hanmanthapur	Municipality	332
3		Kagazmaddur	Kagazmaddur	460
4		Kondapur		85
5		Naimatullaguda		117
6		Narsapur	Municipality	1930
7		Nathinoipalle	Nathinoipalle	892
8		Rustumpet	Rustumpet	646
		Sitarampur	Sitarampur	233
		Total		4695
1	REDDIPALLE	Chinna Chintakunta	Chinna Chintakunta	837

(continued)

Table 1 (continued)

S. No	Cluster	Revenue Village	GP	Cultivable Area in Acres
2		Khazipet	Khazipet	764
3		Manthoor	Manthoor	420
4		Pedda Chintakunta	Pedda Chintakunta	839
5		Reddipalle	Reddipalle	2492
				5352
		Grand Total		23,873

Source Narsapur Mandal Agriculture Office

3.2 Dataset

3.2.1 Satellite Data

Sentinel-2 MSI

Sentinel-2 is a multi-spectral, high-resolution, wide-swath imaging mission that supports Copernicus Land Monitoring studies, including vegetation, soil and water cover monitoring. Sentinel-2B satellite was launched on 7 March 2017. When two sensors are operated simultaneously, the mission's revisit time is about 5 days, while about 10 days with one satellite in operation.

In this study, Seven Bands such as B2, B3, B4, B5, B6, B7, B8 and NDVI of Sentinel-2A are used for Crop Classification using Supervised Random Forest Classifier. Normalized Difference Vegetation Index (NDVI) is used to differentiate vegetation from the dry land. Extremely low values of NDVI (0.1 and below) approximate to barren areas of rock, sand, and snow. Moderate values illustrate shrub and grassland (0.2–0.3), while high values specify temperate and tropical rainforests (0.6–0.8).

$$NDVI = \frac{(NIR - RED)}{(NIR + RED)}$$

3.2.2 Crop Field Data

Crop Field Data was collected randomly using Mobile App covering most part of Narsapur Mandal. The data includes GPS Coordinates, Village Name, Crop Type and Photos as shown in Table 2.

The sample photo of Field Data is shown in Fig. 2a–d.

Table 2 Crop field data

Crop Id	longitude	Latitude	Crop type
1	78.26092	17.714997	Mirchi
2	78.260962	17.713391	Paddy
3	78.26103	17.716072	Paddy
4	78.252379	17.711255	Maize
5	78.260769	17.715206	Paddy
6	78.260444	17.719829	Redgram
7	78.261385	17.713388	Cotton
8	78.246229	17.712081	Cotton
9	78.24888	17.71144	Cotton
10	78.247522	17.711577	Redgram
11	78.251743	17.711077	Redgram and cotton
12	78.219689	17.77703	Maize
13	78.219689	17.77703	Maize
14	78.263028	17.769818	Paddy
15	78.250185	17.77837	Paddy
16	78.250185	17.77837	Paddy
17	78.263028	17.769818	Paddy
18	78.216983	17.773062	Paddy
19	78.23158	17.771505	Paddy
20	78.221484	17.775803	Paddy
21	78.236261	17.771966	Paddy
22	78.2316	17.771517	Paddy
23	78.217692	17.777868	Paddy
24	78.217692	17.777868	Paddy
25	78.297036	17.779096	Maize
26	78.274987	17.746903	Paddy
27	78.228008	17.766989	Paddy
28	78.245357	17.7785	Papaya
29	78.231739	17.761499	Cotton

3.2.3 Analysis

In this study, Crop NDVI Extraction, Crop Classification and Crop Yield Estimation is carried out using Google Earth Engine using JavaScript for Narsapur Mandal for four months i.e., Jun-Oct, 2020. The entire process is mentioned below and in Fig. 3.

Step 1: Field Crop Sample Data is collected which includes GPS Coordinates, Crop Type and Photo.

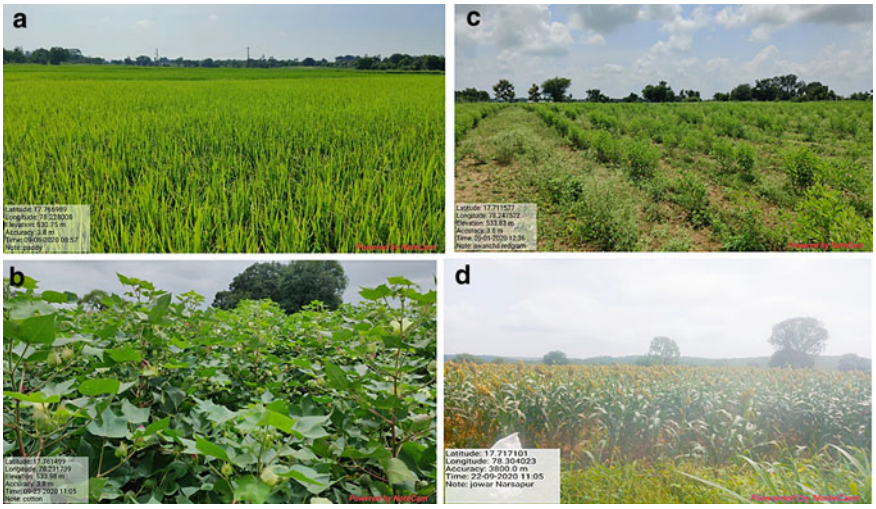

Fig. 2 **a**. Paddy at Awancha Village. **b** Cotton at Awancha Village. **c**. Redgram at Awancha Village. **d** Jowar at Awancha Village

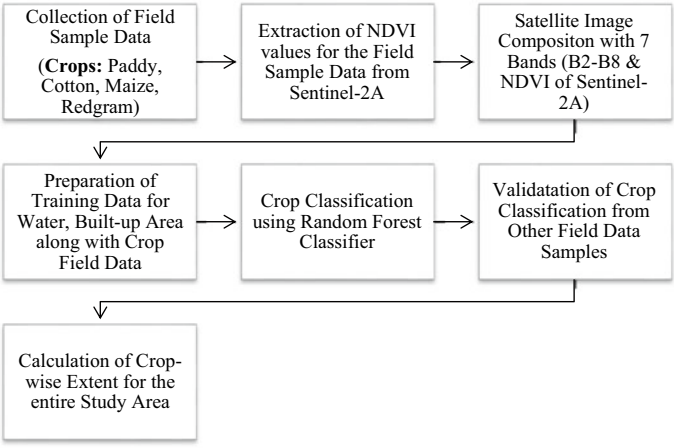

Fig. 3 Methodology

Step 2: Sentinel-2A MSI data is used extract NDVI values for the available data period.

Step 3: Crop Classification using Random Forest Classifier is carried out on 05-Oct-2020 satellite image using Field Crop Sample Data after creating Polygon (Buffer) data from point data.

Step 4: Validation of Crops data classified from other field sample data collected on 26-Oct-2020.

Step 5: Crop Yield Estimation is done and compared with data available for the last 3 years at data.telangana.gov.in portal.

4 Results and Discussion

Total 44 Field Data Samples collected from 5 villages: Awancha, Madapur, Jakkupalle, Admapur and Ibrahimbad of Narsapur Mandal. To analyze Crop Growth and Health, NDVI is extracted for the sample field data for different time periods based on the availability of Sentinel-2A Satellite Data as shown in Table 3 and NDVI values indicating Crop Growth as shown in Fig. 4.

Crop Classification is done using Random Classifier at Google Earth Engine for the Field Sample Data having NDVI greater than 0.66 as shown in Fig. 5.

Finally, Crop Yield Estimation is carried out on the Satellite image dated 05-Oct-2020 for NDVI greater than 0.66 and compared the same with past Crop Yield data available at data.telangana.gov.in as shown in Table 4.

A Comparison graph between Normal Crop Yield, Last 3 years (2016–17, 2017–18, 2018–19) and 2020–21 (estimated based on Crop Classification) is show in Fig. 6.

5 Conclusions

Sentinel-2 MSI satellite data is used for Crop NDVI Extraction to monitor Crop Growth and Health. Radom Forest Supervised Classifier more useful for Crop Classification based on Field Sample Data. Based on the analysis, it is observed that there are four major Crops like Paddy, Maize, Redgram and Cotton in the Narsapur Mandal on 05-Oct-2020 based on NDVI values more than 0.66. A comparative study is carried out between Crop Yield data available at data.telangana.gov.in and Crop Classified data. From this it is observed than there is decrease in Paddy (44.23%) and increase in Cotton (153.60%).

Table 3 Month-wise NDVI for field data

CropId	Longitude	Latitude	Village	Crop Type	Jun	Jul	Aug	Sep	Oct
44	78.20207	17.78632	Admapur	Cotton	0.21	0.29	0.72		
24	78.2007	17.78683	Admapur	Jowar	0.17	0.63	0.52		
40	78.18807	17.79454	Admapur	Paddy	0.17				
17	78.24623	17.71208	Awancha	Cotton		0.2	0.12		0.56
19	78.24888	17.71144	Awancha	Cotton		0.49	0.6		0.62
9	78.25238	17.71126	Awancha	Maize	0.07	0.35	0.55		0.53
10	78.25611	17.71076	Awancha	Paddy		0.42	0.59		
6	78.25347	17.71121	Awancha	Paddy		0.37	0.28		
11	78.25341	17.71095	Awancha	Redgram		0.61	0.64		
20	78.24752	17.71158	Awancha	Redgram		0.34	0.44		0.67
21	78.25174	17.71108	Awancha	Redgram and Cotton	0.18	0.56	0.48		0.67
22	78.21969	17.77703	Chippalturthi	Maize	0.24	0.46	0.78		0.77
23	78.21969	17.77703	Chippalturthi	Maize	0.24	0.46	0.78		0.77
37	78.23626	17.77197	Chippalturthi	Paddy	0.34	0.43	0.24		0.84
38	78.2316	17.77152	Chippalturthi	Paddy	0.17	0.38	0.38	0.39	0.78
30	78.21698	17.77306	Chippalturthi	Paddy	0.22	0.43	0.77	0.54	0.71
31	78.23158	17.77151	Chippalturthi	Paddy	0.17	0.38	0.38	0.39	0.78
32	78.22148	17.7758	Chippalturthi	Paddy	0.17	0.51	0.78	0.75	0.77
49	78.28982	17.80608	Gollapalle	Paddy	0.36	0.38	0.36	0.46	
39	78.18352	17.7959	Ibrahimbad	Cotton	0.17	0.47	0.52	0.56	
35	78.17735	17.80425	Ibrahimbad	Cotton	0.17	0.42	0.77	0.4	
34	78.17775	17.80436	Ibrahimbad	Paddy	0.16	0.34	0.36	0.38	
33	78.20873	17.78501	Jakkupalle	Cotton	0.21	0.46	0.54	0.37	
36	78.2135	17.78139	Jakkupalle	Paddy	0.32	0.42			
41	78.21769	17.77787	Jakkupalle	Paddy	0.29	0.68	0.39		0.78
42	78.21769	17.77787	Jakkupalle	Paddy	0.29	0.68	0.39		0.78
43	78.20847	17.78532	Jakkupalle	Paddy	0.19	0.25	0.78		
48	78.2937	17.70228	Kagazmaddur	Paddy		0.82	0.75	0.65	
45	78.29704	17.7791	Lingapur	Maize	0.33	0.61	0.63	0.44	0.56
15	78.2605	17.71033	Madapur	Cotton	0.12	0.33	0.51		
16	78.26139	17.71339	Madapur	Cotton	0.15	0.36	0.4		0.65
5	78.26096	17.71339	Madapur	Paddy	0.24	0.45	0.37	0.35	0.76
14	78.26077	17.71052	Madapur	Paddy		0.51	0.61		
52	78.23174	17.7615	Mohammadabad @ Janakampet	Cotton	0.13	0.33	0.78		0.78
50	78.22801	17.76699	Mohammadabad @ Janakampet	Paddy	0.23		0.83	0.69	0.76
27	78.25019	17.77837	Mohammadabad @ Janakampet	Paddy	0.26	0.57	0.81		0.8
28	78.25019	17.77837	Mohammadabad @ Janakampet	Paddy	0.26	0.57	0.81		0.8
51	78.24536	17.7785	Mohammadabad @ Janakampet	Papaya	0.22	0.4	0.44	0.51	0.58
47	78.30402	17.7171	Narsapur	Jowar	0.48	0.81	0.86		
4	78.26092	17.715	Narsapur	Mirchi	0.18	0.44	0.51		0.56
8	78.26103	17.71607	Narsapur	Paddy	0.23	0.25	0.72		0.8
12	78.26077	17.71521	Narsapur	Paddy	0.14	0.32	0.41		0.7
13	78.26044	17.71983	Narsapur	Redgram	0.23	0.45	0.62		0.78
25	78.26303	17.76982	Pedda Chintakunta	Paddy		0.41	0.43	0.37	0.29
29	78.26303	17.76982	Pedda Chintakunta	Paddy		0.41	0.43	0.37	0.29
46	78.27499	17.7469	Sitarampur	Paddy	0.16	0.59	0.41	0.63	0.83

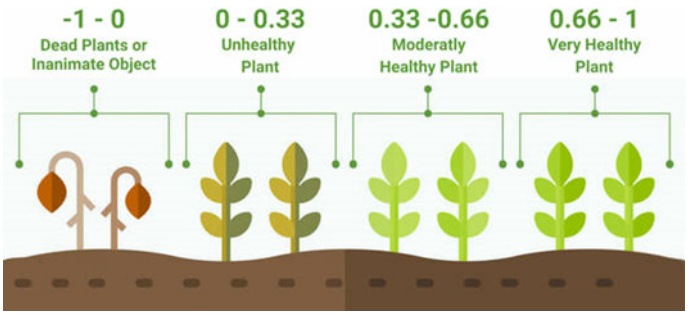

Fig. 4 Normalized difference vegetation index (NDVI). *Source* Earth Observing System—www.eos.com

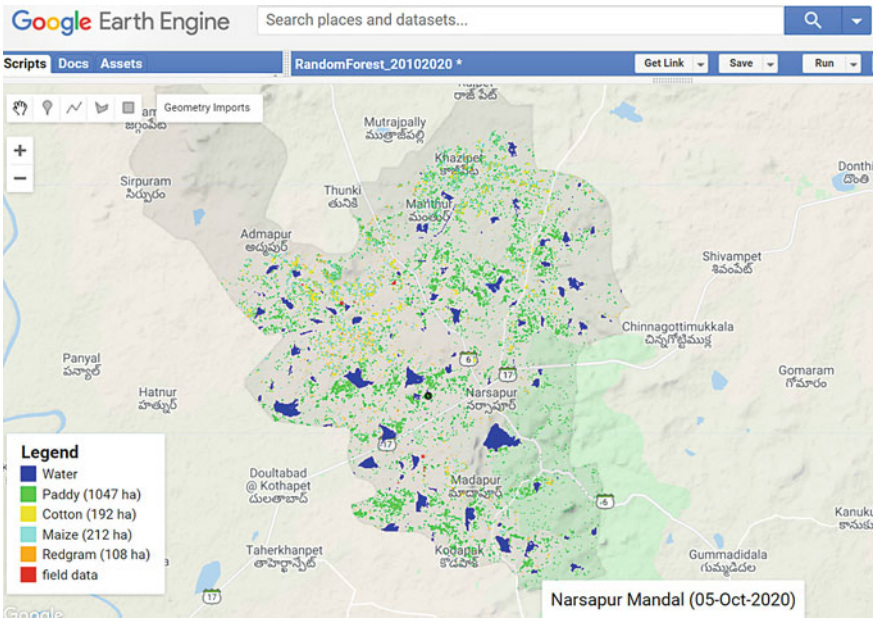

Fig. 5 Crop classification at Narsapur Mandal

Table 4 Crop yield estimate for 2020–21 versus Normal Sown Area for Narsapur Mandal

S. No	Crop sown area (in hectares)					Estimated yield (in hectares)	
	Crop type	Normal	2016–17	2017–18	2018–19	2020–21	Percentage
1	Paddy	2367	1388	2161	1462	1047	44.23
2	Maize	1035	1471	0	1028	212	20.48
3	Red Gram	100	140	0	113	108	108.00
4	Cotton	125	75	0	1365	192	153.60

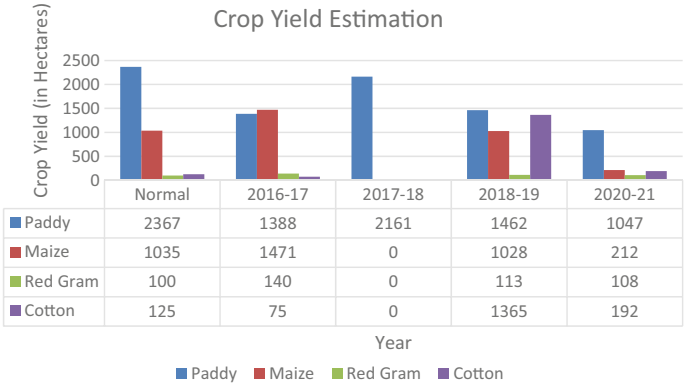

Fig. 6 Crop yield estimation for Narsapur Mandal. *Source* data.telangana.gov.in

Acknowledgements We would like to express our thanks Narsapur Mandal Agriculture Field Officers for their invaluable assistance and inputs. We would also like to thank "geohackweek" for sharing the code for Crop Classification using Random Forest Classifier in Google Earth Engine environment.

References

Crespi M, Nascetti A, Ravanelli R (2020) Special Issue information—google earth engine and cloud computing platforms: methods and applications in big geo data science. https://www.mdpi.com/journal/remotesensing/special_issues/GEE_Methods_Applications

Kamraju M, Vani M, Anuradha T (2017) Crop diversification pattern: a case study of Telangana State. Int J Innov Sci Res Technol 2(5)

Ok A, Akar Ö, Gungor O (2012) Evaluation of random forest method for agricultural crop classification. Euro J Remote Sens 45:421–432

Teluguntla P, Thenkabail PS, Oliphant A, Xiong J, Gumma MK, Congalton RG, Yadav K, Huete A (2018) A 30-m landsat-derived cropland extent product of Australia and China using random forest machine learning algorithm on Google Earth Engine cloud computing platform. ISPRS J Photogram Remote Sens 144:325–340

Su T, Zhang S (2020) Object-based crop classification in Hetao plain using random forest. Earth Sci Inf

Use of Polyacrylamide for Erosion and Fugitive Dust Control of Geomaterials—A Review

Narala Gangadhara Reddy, Preetynanda Nanda, Ramya Sri Mullapudi, and Murala Veera Reddy

Abstract Most of the natural soils and industrial wastes have been identified as problematic geomaterials. Utilization of them for any infrastructural applications have a detrimental effect in the long term. Among the significant problem's the remediation of erosion and fugitive dust of geomaterials not received much attention from previous studies. The erosion and fugitive dust issues are mainly caused by smaller particles, type of minerals present, temperature, water content, thixotropy, the concentration of ions, type of pore fluid. The general practice is the amendment of traditional stabilizers such as cement and lime. However, these materials are not sustainable, that lead to an increased focus on eco-friendly additives for improving the properties of geomaterials. Synthetic polymers and biopolymers have been identified as viable stabilizers for improving soil properties, erosion control, and prevention of infiltration. However, the durability of biopolymers as stabilizers are of great concern. In this study, an attempt was made to review the use of polyacrylamide (PAM) a synthetic polymerfor mitigating the erosion and fugitive dust issues of geomaterials. This review shows that PAM is promising for the alleviation of erosion and dusting issues.

Keywords Problematic soils · Synthetic polymers · Fugitive dust · Erosion control · Water retention

N. G. Reddy · M. V. Reddy
Department of Civil Engineering, Kakatiya Institute of Technology and Science, Warangal, India

P. Nanda (✉)
School of Civil Engineering, KIIT University, Bhubaneswar, India
e-mail: preety.nandafce@kiit.ac.in

R. S. Mullapudi
Department of Civil Engineering, IIT Hyderabad, Kandi, Telangana, India

B. B. Das et al. (eds.), *Recent Developments in Sustainable Infrastructure (ICRDSI-2020)—GEO-TRA-ENV-WRM*, Lecture Notes in Civil Engineering 207,
https://doi.org/10.1007/978-981-16-7509-6_12

1 Introduction

The disintegration of smaller soil or waste particles due to wind speed or water pressure leads to dusting and erosion issues and are main concerns in the environmental and civil engineering point of view. These type of soils or waste materials (geomaterials) generally have low cohesion and poor structure. Inadequate erosion control measures of geomaterials lead to washout and piping andultimately causes failure in earthen civil engineering structures such as embankments (Mohri et al. 2009). For rapid expansion and better use of resources, it is essential to deal with such geomaterials. The use of traditional chemical stabilizers like lime and cement were found to be effective in reducing erosion. However, these are not widely accepted due to the development of heat and makes the geomaterial more brittle in nature (Reddy et al. 2020; Dora et al. 2021). Further, these materials pose various threats to the environment by changing the soil and groundwater pH affecting the vegetation and subsurface native fauna. It also increases the brittle behaviour under cyclic loads, affecting the stability of the structure. Off late, there is an increased search for environmental-friendly materials. Since then, synthetic polymers have gained acceptance for improving physical, engineering, and water retention properties of geomaterials. Synthetic polymers have a good ability to form gel and thickening agent and increase the soil particles stability (Feldman and Barbalata. 1996). Polyacrylamide (PAM) is extensively used for amendment of soils due to its long-chain synthetic polymers. The paper provides a review on the application of PAM amended geomaterial for erosion control and fugitive dust minimization are discussed in detail, and scope for future work is highlighted.

2 Characteristics of PAMand Amendment of Geomaterials

Synthetic polymers as a soil amendment have gained momentum in recent years due to their easy availability and readily mixed properties. The PAM can be synthesized as a simple linear chain or as a cross-linked structure. PAM is water-soluble ionic or anionic material with acrylamide and acrylate units having one or more than other monomers (Zohourian and Kabiri 2008). The specific gravity of PAM varies from 1.1 to 1.3. The PAM is insoluble in non-polar liquids (e.g., kerosene, diesel fuel) but soluble in water. However, at low pH values, the solubility reduces. PAM is stable in the pH range of 3–9. Increase in pH leads to a decrease in the viscosity over time. It is also worth mentioning that the PAM is highly stable till a temperature of 110 °C and the softening point of solid PAM is about 220–230 °C. The PAM has a high molecular weight between 1.2 and 2×10^6 g/mol. The higher molecular weight of PAM leads to increase of chain formation and high viscosity. Non-ionic PAM mainly attracts and binds the particles primarily by Van Der Waals forces; thus, these bonds are weaker. For all practical applications anionic PAM (shown in Fig. 1) is recommended as soil

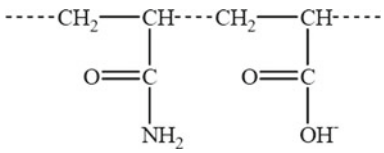

Fig. 1 Chemical structure of synthetic PAM

cations interaction forms ionic or covalent bonds these are stable for a longer time and provides the highest bonding (Yang 2008).

PAM is a hydrophilic synthetic material and is useful for improving the water retention properties and crack remediation and has wide applications in geotechnical and geoenvironmental context. The PAM helps in reducing permeability and enhances the surface stability of geomaterials in preventing surface erosion and fugitive dust emission. For all practical applications, the desired amount of solid PAM will be added and then thoroughly mixed by a mechanical stirrer to make a homogeneous solution (Bjomeberg and Aase 2000). The application of PAM in solid is not feasible due to the hydrophilic nature that leads to non-uniform amended geomaterial. The prepared high viscous solutions are applied for practical or field practices (Ben-Hur 1994).

3 Traditional Materials and Their Mechanism for Soil Remediation

Dusting and erosion are the two problems mainly encountered due to non-contact of smaller particles and dispersive behaviour. Moreover, low electrolyte concentration in the pore fluid leads to internal erosion of soil particles with infiltration of water. Among the various additives, phosphogypsum, a by-product is frequently used material used for the control of erosion. The mechanism behind the addition of gypsum is attributed to increased electrolyte concentration and thereby increases the stability of the particles from internally as well as on the surface aggregation. The gypsum addition on the surface of the soil or mine waste leads to increased soil surface flocculation of clay particles at the soil surface and lesser detachment of particles due to rainfall impact or overland flow (Graber et al. 2006). The study of Vinod et al. (2010) on clayey and silty soil treated with lignosulfonate has an improved erosion parameter like critical shear stress and coefficient of erosion with subsequent increase in the % of lignosulfonate and it can be attributed to decrease in the double layer thickness by the reduction of the surface charges of particles and the subsequent formation of a stable particle cluster or aggregate. Another study showed that the application of bentonite at a rate of 0.4–0.1% reduces the fugitive dust generation by 70–80% over the untreated material. This is attributed to the bonding between the negatively charged surface of the clay with a positively charged surface of limestone and agglomeration of fine particulates with the larger particulates and improved water retention (Bergeson and Brocka 1996). Other traditional methods are the use

of pozzolanic materials like cement and lime for reduction or control of erosion. The mechanism basically involves the aggregation of particles due to formation of C-S-H or C-A-S-H gels. The stabilization increases the strength of the geomaterial several times, and the strength lasts for a longer time (Table 1).

4 Application of PAM for Remediation of Geomaterial Properties

4.1 Erosion Remediation

Erosion is one of the main issues in earthen structures. Continuous surface or internal erosion leads to failure of engineered structures like embankments and storage dams. The internal erosion mainly causes due to water pressure from the upstream side and surface erosion mainly by rainfall and the loosened soil is carried along with runoff. PAM application has gained popularity as an amendment for soil and water remediation problems. A small quantity of PAM (0.5–2%) can improve the physical and engineering properties of soil and waste mines (Ding et al. 2020). He et al. (2008) conducted field erosion tests on the sandy loam soil surface with PAM application and found that 2–4 g/m^2 is effective for soil erosion control which is due to adhesive action of PAM with soil particles. Another such application shows PAM was found to be effective in reducing the depth of sediment by 60% (Sojka et al. 2007). Smith et al. (1990) varied the intensity of rainfall on PAM amended soil and found that it had reduced the erosion of natural soil. Kristian et al. (1998) found that 0.2 g/m^2 application of PAM can reduce the erosion significantly under laboratory sprinkler irrigation tests. The adsorbed properties of the PAM plays a significant role in soil amendment. The anionic PAM binds the soil particles by the process called cation bridging (both soil and PAM are negatively charged) (Ben-Hur 1994). In another case, the divalent cations bridge negatively charged species with a positive charge on clay surface or the anionic PAM. The anionic PAM give more long-term stability compared to the cationic PAM and is effective for soil amendment (reference). The favourable adsorption effect of PAM increases surface aggregation and overall stability. A three-year study by Roa-Espinosa et al. (2000) on use of PAM at construction site reduced 60–97% runoff-sediment for one month between application.

Figure 2 shows the erosion control for the soil amended with PAM. The amendment of PAM has significantly reduced erosion. For 40 mm irrigation depth, it was observed that soil loss reduces from 12.03 to 2.06 g/m^{2}with PAM amendment. Similarly, Bjorneberg and Aase (2000) studies on silt showed that 3 kg/ha with irrigation water reduced the soil loss by 60–80%. Mixing of dry PAM with silty loam soil was most efficient in preventing erosion, because of its increased interparticle bonding by longer polymer chains (Yu et al. 2003a, b). Figure 3 shows the practical performance evaluation for erosion remediation amending with PAM or another synthetic polymer.

Table 1 Existing erosion and fugitive dust control methods

Material name and type	Additive type	Findings	References
Silty sand	Cement	Silty sand amended with 0.5, 1, 1.5, 2% of cement shows greater resistance to soilerosion	Indraratnaet al. (2008)
Soil	Gypsum	Surface- spreading of gypsum releases electrolytes and improves the stability by cation exchange effect of soil. The study observed that 3%-5% of soil erosion	Graber et al. (2006)
Dispersive soil	Fly ash	Fly ash significantly reduced erosion effect when treated with dispersive soil	Indraratna et al. (1991)
Soil	Sodium silicate	Treatment of soil with 20, 35, and 50%of sodium silicate found to be effective inreducing wind erosion. It was observed that wind erosion by 460 times at 50% sodium silicate application	Koohestani et al. (2020)
Clayey and silty soil	Lignosulfonate	Lignosulfonates improved the erosion due to the increase of critical shear stress and coefficient of soil erosion	Vinod et al. (2010) Shulga et al. (2001)
Limestone surface road	Other material Bentonite	Dust reduction by 70% with 9% bentonite treatment	(Bergeson and Brocka 1996)
Surface road	Molasses	Molasses are effective for reduction of dust emission from the road surface. The fines get aggregate due to the addition of molasses	Gotosa et al. (2014) Omane et al. (2018a, b)

(continued)

Table 1 (continued)

Material name and type	Additive type	Findings	References
Fugitive dust	Cementitious materials of biological carbonate	Fugitive dust and rainfall-erosion resistance can be controlled effectively by improving the mechanical and moisture retention properties in a sustainable way	Zhan et al. (2016)

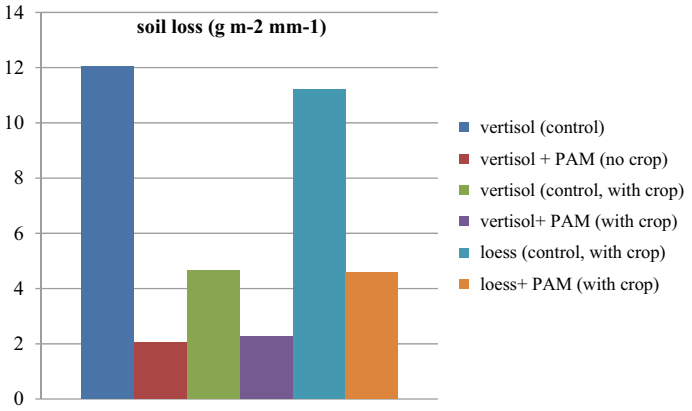

Fig. 2 Erosion control remediation with PAM application

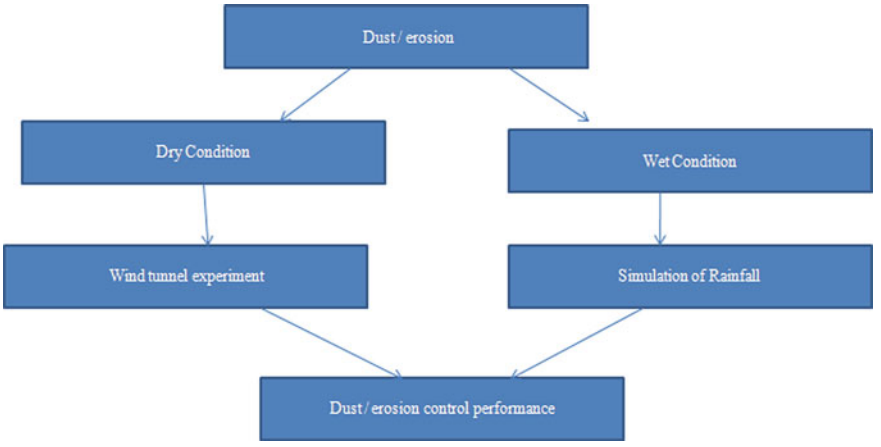

Fig. 3 Typical performance evaluation of dust or erosion with PAM

4.2 Remediation of Fugitive Dust Control

Fugitive dust mainly causes due to low plasticity characteristics and uplift of tiny particles by wind forces, especially in unpaved roads or forest roads. The dust emission is also common in industrial disposal ponds, arid, and semi-arid regions. Many research studies emphasized the importance of penetration resistance and wind tunnel tests for the quantitative estimation of fugitive dust emission. Higher penetration resistance value indicates high strength between particles, and a low value indicates the material causes dust emission. Figure 3 shows the pictorial representation of dust performance evaluation of a geomaterial. Ding et al. (2020) performed wind tunnel experiments on arid soils and found that 0.1 g/m^{2}PAM is sufficient to decrease the dust emission for a longer period. Ding et al. (2020) emphasized the performance of polymer by its ionicity and viscosity. The higher the viscosity and better the dust control and with proved surface mechanical properties. He et al. (2008) highlighted that PAM effective on dust remediation depends on the type of soil, amount of clay content, charge density, and molecular weight of PAM. Most of the studies indicated that 2–4 g/m^2 is effective in soil dust control. Maghchiche et al. (2010) studies showed that the addition of synthetic polymers increases the water retention capacity due to increased surface tension in arid soil and thereby reduction of dust emission. Omane et al. (2018a, b) studies with a variation of climate conditions showed that PAM reduced the dust emission by 99.83, 99.87 and 99.88% after 30 min of exposure to hot, normal and cold temperature and underlined that the PAM efficiency is not affected by temperature. The PAM stabilizes the geomaterial by reduction of repulsive forces among particles by adsorption at the surface and aggregate particles by cation-bridging (Ben-Hur 1994).

In the view environmental concern and nondegradable characteristics of PAM. Cationic PAM is not recommended as these can be toxic to fish and other aquatic life. However, the anionic PAM is completely free from releasing of toxins and typical bacteria in the soil remove the nitrogen from anionic PAM via deamination. Moreover, the divalent cations bridge the negatively charged particles leads to effective stabilization and immobilization of harmful elements.

5 Conclusions

In the present study, the application of synthetic polymer (PAM) as an amendment for remediation of erosion and fugitive dust problems of soils and industrial wastes has been reviewed. It is found that the application rate of PAM plays an important role. Addition of PAM leads to erosion control, dust reduction and improvement in mechanical characteristics of soils. PAM is more effective for clayey soils compared to silty and sandy soils. Based on the review, it is observed that 0.5–4% PAM is sufficient to improve strength characteristics as well as effective in remediation of erosion and dust problems of geomaterial. Overall, PAM can be used for effective

management of soil and waste mines. However, more studies on the durability aspect are not found in the literature, which is essential for the practical usage of PAM. Moreover, cost evaluation comparison and life cycle assessment with traditional stabilizers need further investigations.

References

Bergeson KL, Brocka SG (1996) Bentonite treatment for fugitive dust control. In: Proceedings of the 1996 semi sesquicentennial transportation conference, Ames, IA

Dora et al (2021) Application of biopolymers for enhancing engineering properties of problematic soils and industrial wastes: A Review. LNCE 124: 203–211

Gotosa J et al (2014) Comparative road dust suppression capacity of molasses stillage and water on gravel road in Zimbabwe

Ben-Hur M (1994) Runoff, erosion, and polymer application in moving-sprinkler irrigation. Soil Sci 158(4):283–290

Bjorneberg DL, Aase JK (2000) Multiple polyacrylamide applications for controlling sprinkler irrigation runoff and erosion. Appl Eng Agric 16(5):501

Ding X et al (2020) Effect of synthetic and natural polymers on reducing bauxite residue dust pollution. Environ Technol 41(5):556–565

Feldman D, Barbalata A (1996) Synthetic polymers: technology, properties, applications. Springer

Graber ER, Fine P, Levy GJ (2006) Soil stabilization in semiarid and arid land agriculture. J Mater Civil Eng 18(2):190–205

He J-J, Cai Q-G, Tang Z-J (2008) Wind tunnel experimental study on the effect of PAM on soil wind erosion control. Environ Monit Assess 145(1–3):185–193

Indraratna B et al (2008) Predicting the erosion rate of chemically treated soil using a process simulation apparatus for internal crack erosion. J Geotech Geoenviron Eng 134(6):837–844

Indraratna B, Nutalaya P, Kuganenthira N (1991) Stabilization of a dispersive soil by blending with fly ash. Q J Eng GeolHydrogeol 24(3):275–290

Koohestani B et al (2020) Geopolymerization of soil by sodium silicate as an approach to control wind erosion. Int J Environ Sci Technol 1–12.

Kristian AJ, Bjorneberg DL, Sojka RE (1998) Sprinkler irrigation runoff and erosion control with polyacrylamide—laboratory tests. Soil Sci Soc Am J 62(6):1681–1687

Maghchiche A, Haouam A, Immirzi B (2010) Use of polymers and biopolymers for water retaining and soil stabilization in arid and semiarid regions. J Taibah Univ Sci 4(1):9–16

Mohri Y et al (2009) New direction for earth reinforcement: disaster prevention for earthfill dams. Geosynthetics Int 16(4):246–273

Omane D, Liu WV, Pourrahimian Y (2018a) Comparison of chemical suppressants under different atmospheric temperatures for the control of fugitive dust emission on mine hauls roads. Atmos Pollut Rese 9(3):561–568

Omane D, Liu WV, Pourrahimian Y (2018b) Comparison of chemical suppressants under different atmospheric temperatures for the control of fugitive dust emission on mine hauls roads. Atmos Pollut Res 9(3):561–568

Reddy et al (2020) Application of biopolymers for improving the strength characteristics of red mud waste. Environ Geotech: 1–20

Roa-Espinosa A, Bubenzer GD, Miyashita ES (2000) Sediment and runoff control on construction sites using four application methods of polyacrylamide mix. In: National Conference on Tools for Urban Water Resource Management and Protection, Chicago

Sojka RE et al (2007) Polyacrylamide in agriculture and environmental land management. Adv Agron 92:75–162

Smith HJC, Levy GJ, Shainberg I (1990) Water-droplet energy and soil amendments: effect on infiltration and erosion. Soil Sci Soc Am J 54(4):1084–1087
Shulga G, Rekner F, Varslavan J (2001) SW—soil and water: Lignin-based interpolymer complexes as a novel adhesive for protection against erosion of sandy soil. J Agric Eng Res 78(3):309–316
Vinod JS, Indraratna B, Al Mahamud MA (2010) Stabilisation of an erodible soil using a chemical admixture. Proc Inst Civil Eng-Ground Improv 163(1):43–51
Yang T-H (2008) Recent applications of polyacrylamide as biomaterials. Recent Patents Mater Sci 1(1):29–40
Yu J et al (2003a) Infiltration and erosion in soils treated with dry PAM and gypsum. Soil Sci Soc Am J 67(2):630–636
Yu J et al (2003b) Infiltration and erosion in soils treated with dry PAM and gypsum. Soil Sci Soc Am J 67(2):630–636
Zohourian MM, Kabiri K (2008) Superabsorbent polymer materials: a review: 451–447
Zhan Q, Qian C, Yi H (2016) Microbial-induced mineralization and cementation of fugitive dust and engineering application. Constr Build Mater 121:437–444

Groundwater Depth Forecasting Using Machine Learning and Artificial Intelligence Techniques: A Survey of the Literature

Subhangi Saha, Santanu Mallik, and Umesh Mishra

Abstract Groundwater plays a crucial role in environment and living beings. It maintains the water level and base flow of rivers, lakes and wetlands especially during the dried months. However, current rates of over exploitation, pollution and mismanagement of groundwater pose a great threat to our ecosystem. A crucial aspect in the hydrological analysis is the fluctuation in Groundwater level (GWL), which is affected by numerous factors such as increases in water demand, faulty irrigation practices, mismanagement of soil, and uncontrolled exploitation of aquifers, etc. Traditionally, methods like measuring the water level in a shallow well with tape and surface geophysical methods are mostly used, but they are often time-consuming, costly, and also database dependent. Keeping the groundwater dynamics in mind there is a need to develop a reliable and accurate method for GWL forecast and to meet these challenges, Machine Learning (ML) and Artificial Intelligence (AI) techniques are currently in huge demand. Although a suitable selection of arithmetic or stochastic model building approaches could simulate the discontinuity and complex dynamics of groundwater but they have challenging aspects and require a bit of experience. Therefore various ML and AI techniques and their corresponding methodologies which are mostly used to simulate and predict the GWL alterations have been discussed in this review paper (2011–2020).

Keywords Groundwater · Machine learning · ANN · ANFIS · SVM · RF

1 Introduction

Groundwater is used as a major part of water resources for domestic, industrial, and agricultural purposes. Over-exploitation of groundwater has led to severe fluctuations in their levels over the past decades, ultimately creating a water stressed area. India is the world's largest groundwater user. According to the Water Resources Commission, groundwater is supported by 85% of rural drinking water schemes in about 17.14

S. Saha (✉) · S. Mallik · U. Mishra
Department of Civil Engineering, National Institute of Technology Agartala, Barjala, Jirania, Tripura 799046, India

B. B. Das et al. (eds.), *Recent Developments in Sustainable Infrastructure (ICRDSI-2020)—GEO-TRA-ENV-WRM*, Lecture Notes in Civil Engineering 207,
https://doi.org/10.1007/978-981-16-7509-6_13

hundred thousand households within the country (The Hindi Business Line 2019). The groundwater is acquired from precipitation in Indian landmass and partly from streamflow, lakes, and reservoirs, which is highly nonlinear and dynamic (Amutha and Porchelvan 2011).

When groundwater recharge exceeds exploitation, groundwater depth decreases and may result in water-logging whereas, once groundwater exploitation exceeds recharge, groundwater depth can increase and therefore the geological formation falls, therefore correct assessment and prediction of groundwater depth fluctuation is crucial. Two types of models are generally used, i.e. physical and data-based, to forecast GWL variations (Raghavendra and Deka 2016). The physically-based models were usually the preferred approach over data based in order to capture the complex and dynamic hydrographic occurrence. Physical modeling, however, involves more time and cost expenses and is a major disadvantage of physical-based modeling (Tian et al. 2016). Whereas, as a better alternative approach, data-driven models such as ML Algorithm and AI methods are used to provide more precise predictions within limited time and cost involvement. Data-based models need GWL time-series data and several other variables such as meteorology, geo-hydrology and many more. However, there are several methodologies capable of such data-driven modeling, few questions always arise when choosing a technique such as which model to choose, model performance, model set-up, training samples, input parameters, accuracy and reliability. So, in order to address such issues in this paper author reviews a few of the majorly used ML and AI method i.e. Multilinear regression (MLR), Artificial Neural Network (ANN), Adaptive Neuro-Fuzzy Inference System (ANFIS), Support vector Machine (SVM), Random forest (RF), and performance comparison. This kind of research will help the reader to get a clearer picture of the different methodologies used and their pros and cons associated with them.

2 Data Collection and Preparation

Similar publications were searched using web-based search engines, e-libraries and databases. This search was from the articles and journals that were published for the period of the year 2011–2020. The total number of publication in all the sources per year is shown in Fig. 1. GWL Prediction, ML, MLR, ANN, ANFIS and are some of the Keywords which were used for searching relevant articles in different websites such as Wiley Online, Nature, Elsevier, Taylor Francis Online, Springer are shown in Table 1. Out of all the papers related to this search result in the papers with theoretical concepts and explanation of applied methodologies of GWL forecasting using several soft computation techniques were chosen and included for this review.

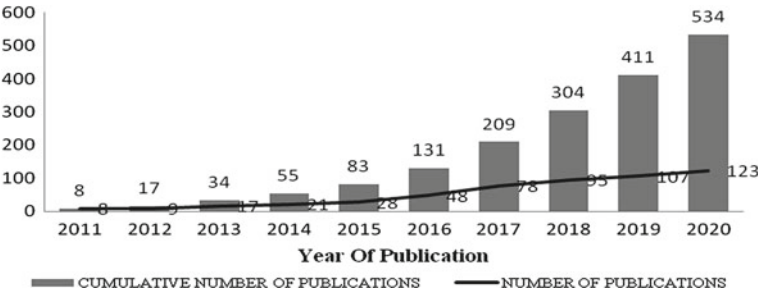

Fig. 1 Publication's statistics per year for the period 2011–2020

Table 1 Number of publication classification under different ML and AI methods

Keywords	No. of articles per website (2011–2020)				
	Wiley Online	Nature	Elsevier	Taylor & Francis	Springer
Groundwater Depth Prediction (GWD-P)	16,807	330	13,107	4566	10,465
(GWD-P) + ML	717	93	2666	958	1652
(GWD-P) + ML + ANN	103	1	184	66	112
(GWD-P) + ML + ANFIS	3	1	40	5	10
(GWD-P) + ML + SVM	21	1	87	14	30
(GWD-P) + ML + MLR	14	0	105	15	19
(GWD-P) + ML + RF	281	10	394	92	205

3 Discussion

3.1 Artificial Intelligence and Machine Learning

Artificial intelligence (AI) is a programmable simulation of human intelligence in machines to mimic human action (Russell and Norvig 2003). It has the capacity like the human brain to reasoning, planning, learning, and problem-solving (Luger et al. 2004). The model building approach includes stages of training, testing and predicting by categorizing the data sets for the three stages respectively.

On the other hand, Machine learning refers to induction algorithms that analyze through automatic, continuous learning from dataset training, analyse knowledge, recognise patterns, and improve prediction accuracy (Machine Learning, wikipedia).

It is a subpart of AI, where machines learn and perform the task without predefine knowledge. Machine learning can be subcategorized into three groups supervised, semi-supervised, and unsupervised learning-based approaches based on the amount of labelled data. The classification algorithm is used to determine the decision boundary whereas; the regression algorithm is used to determine the trend line (Gyansetu 2020).

3.2 Some of the Major AI and ML Techniques

3.2.1 Multi Linear Regression (MLR)

An MLR model may be a technique to model the linear relationship between the dependent and independent variables (Fatih et al. 2019). MLR can give valuable outcomes even with low data availability and less grueling. In addition, it has the adaptability in consideration of any number of autonomous factors within the model (Mohanty et al. 2015). It requires very little skill compared to the other ML methods. It is, however, recommended as an alternative and cost-effective groundwater modeling method considering their functional benefits.

The MLR equation can be written by the following equation

$$Y = a_1x_1 + a_2x_2 + a_3x_3 + \cdots + a_nx_n + C \tag{1}$$

where, X_1, X_2 … X_n are explanatory variables and Y is dependent variable and a_1, a_2 … a_n is the regression co-efficient that indication variable contribution and C is intercept.

3.2.2 Artificial Neural Network (ANN)

ANN is an Artificial Intelligence approach propelled by the human intelligence comprising of input, hidden and output layers with their nodes and activation capacities as shown in Fig. 2 (Yoon et al. 2011). ANN has merits such as clarity, speed, and high adequacy of learning from experimental data (Cerci and Hurdogan 2020). However, it has drawbacks of local minima and over-fitting (Hosseini and Mahjouri 2016). ANN models are more efficient in predicting the abstraction of non-linear complicated input–output rules. To reduce the biasness involved in the input data due to various units or range of data normalization is generally preferred (Mallik et al. 2020; Emamgholizadeh et al. 2014). Figure 2 shows the basic structure of ANN with one hidden layer. The results of the study clearly showed that ANN can be used even in the case when the availability of datasets is inadequate in order to predict groundwater levels with relatively good accuracy in a hard rock field.

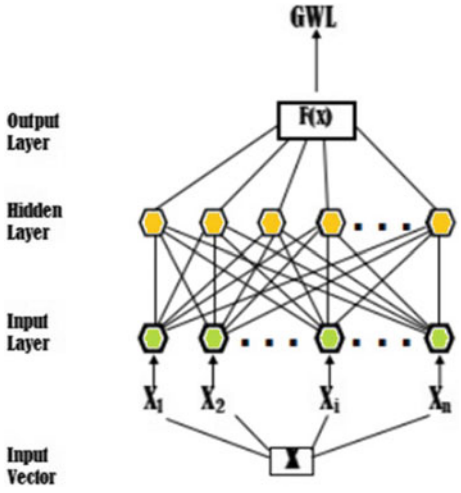

Fig. 2 Structure of ANN

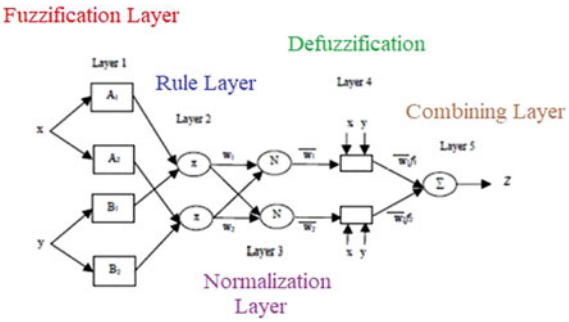

Fig. 3 Structureure of ANFIS

3.2.3 Adaptive Neuro-fuzzy Inference System (ANFIS)

ANFIS is very straightforward to the user and gives less memorization errors as compared to ANN (Şahin and Erol 2017). In addition, the ANFIS model shown in Fig. 3 is capable of altering the values of input and output parameters to get a more strong solution (Kamari et al. 2017; Okwu and Adetunji 2018). Due to its trial and error approach, if–then rules could potentially make the study more complex and time consuming in any case of a large dataset (Azeez et al. 2013). It is a universal predictor capable of approximating any true continuous function to any degree of accuracy in a compact set (Karaboga and Kaya 2019; Fatih et al. 2019). ANFIS outranks ANN in terms of accuracy, becoming an analogous feature of ANN and Fuzzy logic with the merits of both linguistic and numerical knowledge. The groundwater modeling method of ANFIS and ANN can, however, be enhanced by data preprocessing due to the non-linearity and seasonality behavior of data.

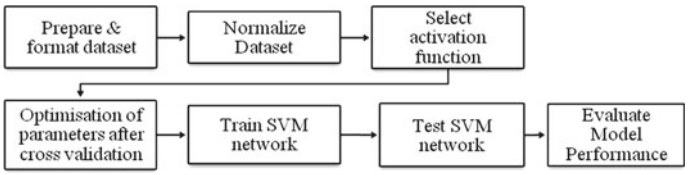

Fig. 4 Flow chart of SVM algorithm on predicting classification

3.2.4 Support-Vector Machines (SVM)

The significance of SVM is to look for the nonlinear link between input and output vectors through nonlinear shift of the input vector into the high-dimensional feature space. Moreover, in the case of sparse data for future prediction, SVM outranks neural systems in terms of accuracy and intensity for the expectation of GWL variation (Yoon et al. 2016; Tapak et al. 2014; Azeez et al. 2013). This differs from ordinary regression techniques as it is based on the statistical learning theory. Despite its superiority to ANN in representing the dynamics of groundwater, it is time consuming due to their trial and error (Raghavendra and Deka 2014). In Fig. 4, the methodology adopted for SVM is shown.

3.2.5 Random Forests (RF)

Random forest is a supervised ML technique consisting of several building blocks called decision trees that produce an ensemble of the predictive model of the same phenomenon and are used to increase their prediction efficiency and over-fitting controls. The method applied to Random forests is illustrated in Fig. 5. Unlike other ML algorithms the random forest and, maximum entropy models can provide useful analysis details, reliability, robust error estimates, low impedance and, low uncertainties (Analytics India Magazine—Rohit Garg 2018; Nhu et al. 2020). However, the drawbacks of the RF model consist of slow real-time prediction, difficulties in implementation and algorithmic complexity. However, in cases of short-term prediction of groundwater level and instances involving low-dimensional data, RF modeling can be approached.

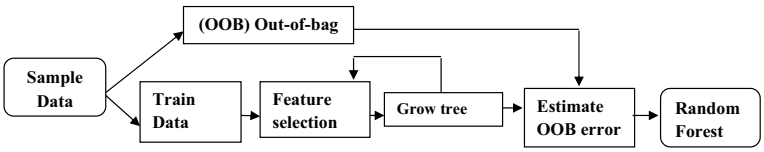

Fig. 5 Flow chart of random forest algorithm

3.3 Overview GWL Prediction Using AI and ML Method

GWL data is deeply irregular and unpredictable in nature, and their prediction depends on various complex natural variables, such as aquifers data, meteorological data, etc. For GWD prediction, various data-driven computation methods such as MLR, SVM, ANN and ANFIS have proven to be more accurate in several cases of groundwater prediction. The trend in the use of soft calculation techniques is shown in Fig. 6. Table 2 summarizes the articles of literature survey. It can be observed from the table that the MLR method can serve as an cost-effective and easy-to-use groundwater modeling tool for hydrogeologists, especially under insufficient field data conditions. There are several training algorithms available in ANN, such as Gradient descent with momentum and back-propagation of adaptive learning rate (GDX), Levenberg–Marquardt (LM) and, Bayesian regularization (BR) , among all LM is often used for data preparation. There are also different optimization strategies available, but the downside is also correlated with each stage of optimization, increasing learning rate and declining performance. The ANFIS model, however, tends to be more adequate for establishing a relationship between multiple input datasets and GWL than ANN. When it is used for trapezoidal membership functions and hybrid optimization approaches, the ANFIS model for various structures has the most precision and less error (Emamgholizadeh et al. 2014). Because of the complex and non-linearity of GWL (Zhou et al. 2017; Moosavi et al. 2013; Zare and Koch 2018; Ebrahimi and Rajaee 2017), combining several techniques may yield good results, such as Wavelet transformation (WT) to obtain better and more accurate performance. SVM can achieve superior performance over longer prediction horizons where data pairs for model creation were sparser due to its ability to present a robust approximating feature and substantial low cost of data-driven model (Behzad et al. 2010). On the other hand, when trained using a sufficient number of training data, RF is a non-complex strong method that works efficiently in regression problems. This method is useful in coping with sparse accessibility of data and is a low-cost method for monitoring groundwater levels in near real time. Different indices are used to estimate the GWD in various literature. Gamma testing or sensitivity analysis can be performed to establish the relative significance of these indices and further evaluate the best model input combination (Tian et al. 2016). Validation is also an important aspect of any output prediction system based on model performance parameters, such as RMSE (should be lower, i.e. closer to observed values), R2 (should be closer to 1), r coefficient, COE, E, etc. Every available validation technique has its own significance and disadvantage, so it is also necessary to choose the correct validation technique.

Table 2 Summarized assessment of the reviewed articles

S. No.	Reference	Input variables	Models used	Data preprocessing	Model performance criteria
1	Kholghi and Hosseini (2009)	• Water level • Hydraulic head • Sink or source	Ordinary kriging (OK), **ANFIS**	–	MSE, MAE, CE
2	Djurovic et al. (2015)	• Precipitation • Climate • Parameters (air temperatures) • Groundwater Levels	**ANN, ANFIS**	–	RMSE, R and COE
3	Amutha and Porchelvan (2011)	• Seasonal rainfall • Past GWL	**ANFIS**,**RBF** (Radial basis function)	–	R, CE, RMSE, MBE
4	Khashei-Siuki and Sarbazi (2015)	• Temperature • Electrical conductivity • Groundwater level pH	Inverse distance weighted (IDW), OK, Cokriging (CK), **ANN**, ANFIS	–	R^2, RMSE, and MAE
5	Yoon et al. (2011)	• Past GWL • Precipitation • Tide level	ANN, **SVM**	–	RMSE, MAPE, ME, CORR, NS, AIC
6	(Behzad et al. 2010)	• Pumping rates • Precipitation • Temperature	**SVM**, ANN	–	R^2, RMSE, E

(continued)

Table 2 (continued)

S. No.	Reference	Input variables	Models used	Data preprocessing	Model performance criteria
7	Tian et al. (2016)	• Irrigation groundwater use • Crop yield • Population • Urbanization rate • Primary and secondary industry output • Tertiary industry output • GDP	PFM (Pulse frequency modulation), BPNN, SVM-LKF(SVM-Lyapunov–Krasovskii functional), **SVM-RBF**	–	RMSE, E
8	Sahoo and Jha (2015)	• Monthly precipitation • River stage • Temperature • Seasonal dummy variables	Several **MLR** models are developed based on different combination of input variables	–	R, R^2, adjusted R^2, F-statistic,p-level
9	Fatih et al. (2019)	• Precipitation • Average air temperature • Relative humidity • Wind speed • GWL time series	MLR, **ANFIS**	–	R^2, MSE, MAE

(continued)

Table 2 (continued)

S. No.	Reference	Input variables	Models used	Data preprocessing	Model performance criteria
10	Sahoo and Jha (2013)	• Rainfall • Ambient temperature • River stage • 11 seasonal dummy variables and influential lags of rainfall • Ambient temperature • River stage • GWL	MLR, **ANN**	–	βj, SE, t-test, F-test, R^2, R, adjusted R^2, p-level and SEE
11	Emamgholizadeh et al. (2014)	• Rainfall recharge • Irrigation returned flow • Pumping rates	ANN, **ANFIS**	–	RMSE, R^2
12	Zare and Koch (2017)	• GWL • Precipitation	**ANFIS**, FCM(Floating Centroids Method)	Wavelet transform	R^2 and RMSE
13	Sreekanth et al. (2011)	• Evaporation • Rainfall • Relative humidity • Temperatures	**FFNN-LM**(Feedforward Neural Network- Levenberg–Marquardt), **ANFIS** and ANN	–	RMSE and R^2
14	Zhou et al. (2017)	• Precipitation • Water use demand • GWL data	ANN, SVM, **WSVM**, WANN	SVM model preprocessed with DWT and ANN model preprocessed with WT	Relative absolute error (RAE), Pearson correlation coefficient (r), RMSE, E

(continued)

Table 2 (continued)

S. No.	Reference	Input variables	Models used	Data preprocessing	Model performance criteria
15	Gong et al. (2018)	• Monthly mean precipitation • Monthly mean temperature • Monthly mean lake level • Monthly maximum temperature	ANN, ANFIS, SVM, EEMD (Ensemble Empirical Mode Decomposition) **EEMD-SVM, EEMD-ANFIS**	–	R, NMSE, RMSE, NS, AIC
16	Yoon et al. (2016)	• Rainfall • GWL	ANN, **SVM**	–	ME, MAPE, RMSE, CORR
17	Mohanty et al. (2015)	• Weekly rainfall • Pan evaporation • River stage • Water level in the surface drain • Pumping rates	Regular ANN, **Developed ANN using GDX** (Variable Learning Rate Back-propagation) **algorithm**	-	RMSE, R, NSE
18	Shiri et al. (2013)	• Water table level • Rainfall • Evapotranspiration	**GEP** (Gene Expression Programming)ANN, ANFIS, SVM	–	R, RMSE, CO, NS
19	Brédy et al. (2020)	• Precipitation • Previous water table depth values • Evapotranspiration	RF and **Extreme Gradient Boosting (XGB)**	–	Mean squared error, coefficient of determination and NSE coefficient

(continued)

Table 2 (continued)

S. No.	Reference	Input variables	Models used	Data preprocessing	Model performance criteria
20	Wang et al. (2018)	• Precipitation • Temperature • Previous groundwater level	Canonical correlation forests with a combination of random features (**CCF-CRF**), LS-SVM and RF Regression	-	R, RMSE, and MAE
21	Kombo (2020)	• Daily mean temperature • Precipitation • Daily maximum solar radiation • Previous day's precipitation • Temperature • Groundwater level	A hybrid K-Nearest Neighbor-RF (**KNN-RF**), ANN, RF, SVM, KNN	Data preprocessing is done with Python Programming Language	RMSE, MAE, NSE and R^2
22	Nhu et al. (2020)	• Daily water level	M5 pruned (**M5P**), RF, Random tree (RT) and reduced error pruning tree (REPT)	–	RMSE, MAE, R^2

Note The bold marked words indicates the best technique out of all the technique used in each research paper

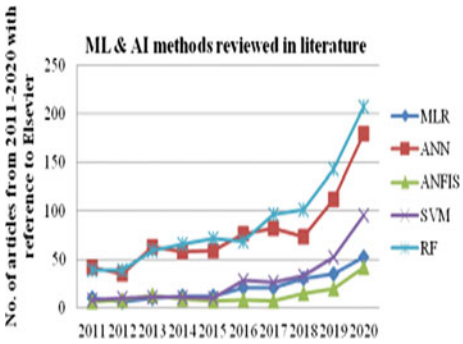

Fig. 6 Major ML and AI methods used for GWL prediction from 2011 to 2020

4 Conclusion

AI and ML techniques have been widely applied to model hydrological processes in recent years, due to its multiple advantage over physical based modeling. Different input variables are used for GWL depth prediction, such as rainfall data, temperature, relative humidity, wind speed and GWL time series, etc. In addition, some pre-processed methods have been added that can be used to improve the performance of all AI and ML methods. By combining these techniques for better GWD prediction, even different hybrid methods can be developed. The review paper will assist multiple readers with GWL fluctuation assessment and prediction for risk-based management of water resource systems based on several AI and ML techniques (whether as singles or hybrids) and different criteria for evaluating model performance. These details can be compiled as a robust tool which can be used to simulate the declining trends in groundwater levels and provide acceptable predetermined criteria.

References

Amutha R, Porchelvan (2011) Seasonal Prediction Of Groundwater Levels Using ANFIS and Radial Basis Neural Network. Int J Geol Earth Environ Sci 1(1): 98–108. ISSN: 2277–2081

Azeez D, Ali MAM et al (2013) Comparison of adaptive neuro-fuzzy inference system and artificial neutral networks model to categorize patients in the emergency department. Springerplus 2(1):416

Barzegar R, Moghaddam AA (2016) Combining the advantages of neural networks using the concept of committee machine in the groundwater salinity prediction. Model Earth Syst Environ 2(26)

Behzad M, Asghari K et al (2010) Comparative Study of SVMs and ANNs in Aquifer Water Level Prediction. J Comput Civil Eng 24(5)

Brédy J, Gallichand J et al (2020) Water table depth forecasting in cranberry fields using two decision-tree-modeling approaches. Agric Water Manage 233: 106090

Cerci KN, Hurdogan E (2020) Comparative study of multiple linear regression (MLR) and artificial neural network (ANN) techniques to model a solid desiccant wheel." *International Communications in Heat and Mass Transfer*, (2020), 116, 104713.

Djurovic N, Domazet M et al (2015) Comparison of groundwater level models based on artificial neural networks and ANFIS. Sci World J 1–13

Ebrahimi H, Rajaee T (2017) Simulation of groundwater level variations using wavelet combined with neural network, linear regression and support vector machine. Global Planetary Change 148:181–191

Emamgholizadeh S, Moslemi K et al (2014) Predicting of the groundwater level of Bastam Plain (Iran) by Artificial Neural Network (ANN) and Adaptive Neuro-Fuzzy Inference System (ANFIS). Water Resour Manage 28:5433–5446

Fatih UNES, Gizem A et al (2019) Ground water level estimation for Dortyol region in HATAY. Int J Environ Agric Biotechnol (IJEAB) 4(3)

Gong Y, Wang Z et al (2018) A comparative study of groundwater level forecasting using data-driven models based on ensemble empirical mode decomposition. Water 10(6):730

Hosseini SM, Mahjouri N (2016) Integrating support vector regression and a geomorphologic artificial neural network for daily rainfall-runoff modeling. J Appl Soft Comput 38:329–345

Http//link—https://en.wikipedia.org/wiki/Machine_learning#cite_note-3. Accessed on 10 Aug 2020

Http//link—https://www.gyansetu.in/regression-vs-classification-in-machine-learning/. Accessed on 10 Aug 2020

Http//link—https://www.thehindubusinessline.com/opinion/its-time-to-tax-groundwateruse/article25994382.ece. Accessed on 10 Aug 2020

Http//link—https://analyticsindiamag.com/7-types-classification-algorithms/. Accessed on 10 Aug 2020

James CD, Davis R et al (2000) Aligned micro contact printing of micrometer-scale poly-L-lysine structures for controlled growth of cultured neurons on planar microelectrode arrays. IEEE Trans Biomed Eng 47(1):17–21

Kamari A, Mohammadi AH et al (2017) Decline curve based models for predicting natural gas well performance. Petroleum 3:242–248

Karaboga D, Kaya E (2019) Adaptive network based fuzzy inference system (ANFIS) training approaches: a comprehensive survey. Artif Intell Rev 52:2263–2293

Khashei-Siuki A, Sarbazi M (2015) Evaluation of ANFIS, ANN, and geostatistical models to spatial distribution of groundwater quality (case study: Mashhad plain in Iran). Arab J Geosci 8:903–912

Kholghi M, Hosseini SM (2009) Comparison of groundwater level estimation using neuro-fuzzy and ordinary kriging. Environ Model Assess 14(72)

Kombo OH, Kumaran S et al (2020) Long-term groundwater level prediction model based on hybrid KNN-RF technique. Hydrology 7(3):59

Luger G et al (2004) Artificial Intelligence: structures and strategies for complex problem solving (5th ed.). The Benjamin/Cummings Publishing Company, ISBN 978–0–8053–4780–7

Mallik S, Bhowmik T, Mishra U, Paul N (2020) Mapping and prediction of soil organic carbon by an advanced geostatistical technique using remote sensing and terrain data. Geocarto International 1–17. https://doi.org/10.1080/10106049.2020.1815864

Mohanty S, Jha MK et al (2015) Using artificial neural network approach for simultaneous forecasting of weekly groundwater levels at multiple sites. Water Resour Manage 29:5521–5532

Moosavi V, Vafakhah M et al (2013) A wavelet-ANFIS hybrid model for groundwater level forecasting for different prediction periods. Water Resour Manage 27:1301–1321

Nhu V-H, Shahabi H et al (2020) Daily water level prediction of Zrebar Lake (Iran): a comparison between M5P, random forest, random tree and reduced error pruning trees algorithms. ISPRS Int J Geo Inform 9:479

Okwu MO, Adetunji O (2018) A comparative study of artificial neural network (ANN) and adaptive neuro-fuzzy inference system (ANFIS) models in distribution system with nondeterministic inputs. Int J Eng Business Manage 10:184797901876842

Raghavendra NS, Deka PC (2014) Support vector machine applications in the field of hydrology: a review. Appl Soft Comput 19:372–386

Raghavendra S, Deka PC (2016) Multistep ahead groundwater level time-series forecasting using Gaussian process regression and ANFIS. Advanced Computing and Systems for Security, Vol 396 of the Series Advances in Intelligent Systems and Computing

Russell SJ, Norvig P (2003) Artificial Intelligence: A Modern Approach (2nd ed.). Prentice Hall, Upper Saddle River, New Jersey. ISBN 0-13-790395-2

Şahin M, Erol R (2017) A comparative study of neural networks and ANFIS for forecasting attendance rate of soccer games. Math Comput Appl 22(4):43

Sahoo S, Jha MK (2013) Groundwater-level prediction using multiple linear regression and artificial neural network techniques: a comparative assessment. Hydrogeol J 21:1865–1887

Sahoo S, Jha MK (2015) On the statistical forecasting of groundwater levels in unconfined aquifer systems. Environ Earth Sci 73:3119–3136

Shiri J, Kisi O et al (2013) Predicting groundwater level fluctuations with meteorological effect implications—A comparative study among soft computing techniques. Computers Geosci 56:32–44

Sreekanth PD, Sreedevi PD et al (2011) Comparison of FFNN and ANFIS models for estimating groundwater level. Environ Earth Sci 62(6):1301–1310

Tapak L, Rahmani AR et al (2014) Prediction the groundwater level of Hamadan-Bahar Plain, West of Iran Using Support Vector Machines. J Res Health Sci Winter 14(1):81–86

Tian J, Li C et al (2016) Groundwater depth prediction using data-driven models with the assistance of gamma test. Sustainability 8(11):1076

Wang X, Liu T et al (2018) Short-term prediction of groundwater level using improved random forest regression with a combination of random features. Appl Water Sci 8(5)

Yoon H, Jun S-C et al (2011) A comparative study of artificial neural networks and support vector machines for predicting groundwater levels in a coastal aquifer. J Hydrol 396(1–2):128–138

Yoon H, Hyun Y et al (2016) A method to improve the stability and accuracy of ANN- and SVM-based time series models for long-term groundwater level predictions. Comput Geosci 90:144–155

Zare M, Koch M (2018) Groundwater level fluctuations simulation and prediction by ANFIS- and hybrid Wavelet- ANFIS/ fuzzy C-means (FCM) clustering models: Application to the Miandarband plain. J Hydro-Environment Res 18:63–76

Zhou T, Wang F et al (2017) Comparative analysis of ANN and SVM models combined with wavelet preprocess for groundwater depth prediction. Water 9(10):781

Management of Bio-medical Wastes in a Multispeciality Hospital in Bhubaneswar

Sneha Sen, Akash Rai, and Sanjib Moulick

Abstract The mushrooming of industrialization over time has not only turned the pollution worse by posing a threat to the natural resources but has also exposed us to an impending doom that the produced wastes might befall, aggravating the environmental problems altogether. Therefore, the management of these mass-produced wastes needs our immediate attention and requires to be catered to as something of utmost importance. In such a scenario, the concept of sustainable waste management plays a huge role which aims at reducing the consumption of natural resources and ensuring their maximum reuse so that the waste produced is kept to a minimum. Achieving this will lessen the repercussions on the environment, improve the water and air quality and contribute to the reduction of greenhouse gas emissions. Being the second-most populated country, India approximately has 16% of the world population. And to cater to their rising needs and demands, new hospitals are cropping up in both the private and government sectors. Associated with them are the heaps of wastes generated every day. Improper management of these wastes will lead to a direct health impact on people and the environment. Thus these wastes (known as biomedical wastes) require proper management and specific treatment previous to its ultimate disposal. To delve deeper into the same, a case study was conducted at one of the best multispeciality hospitals in Bhubaneswar, India wherein the entire procedure of the bio-medical waste management, right after its generation till its disposal was analyzed. An important issue of an environmental protection process is to plan for collecting, transporting, processing and disposing off the hazardous and non-hazardous biomedical wastes and its mandatory compliance with regulatory notifications of Bio medical waste (management and handling) rules 2016. The paper

S. Sen (✉) · A. Rai · S. Moulick
School of Civil Engineering, KIIT Deemed to be University, Bhubaneswar, Odisha, India
e-mail: 1601068@kiit.ac.in

A. Rai
e-mail: 1601090@kiit.ac.in

S. Moulick
e-mail: smoulickfce@kiit.ac.in

B. B. Das et al. (eds.), *Recent Developments in Sustainable Infrastructure (ICRDSI-2020)—GEO-TRA-ENV-WRM*, Lecture Notes in Civil Engineering 207,
https://doi.org/10.1007/978-981-16-7509-6_14

deals with the different processing systems for biomedical waste management—segregation, labeling, packaging, neutralization and disposal (along with their safety precautions) based on the case study at the hospital. Hazards associated with the shortcomings in their existing system are identified and a few recommendations are proposed to lessen the risk of infection and to create awareness among the public in general.

Keywords Biomedical waste · Solid waste management · Waste disposal · Waste segregation · Waste treatment · Incineration

1 Introduction

With an increase in population comes increased demands. Out of the various sectors upon which people are completely dependent, the most salient one is the health care department. Over time, the number of hospitals is seen to thrive all over the country—from private to government. Being a place that runs 24/7 and frequented by people from all walks of life, the amount of waste generated daily is inordinate. The advancement in science and technology has given birth to many sophisticated instruments for treating diseases which altogether has resulted in the generation of wastes based on per capita per patient. Thus, this increasing amount of waste generation has become a thing of concern for the environmentalists and also the people in general (Shrestha et al. 2017; Radha et al. 2009; Jaiswal et al. 2010).

Biomedical wastes are those wastes that are generated during the diagnosis and treatment of human beings and contaminated with the patient's body fluids due to their diseases (Aravindan and Vasumathi 2015; Jaiswal et al. 2010). It has been observed that the amount of waste generated from the hospitals in India ranges between 0.5 and 2.0 kg/bed/day with an average of about 0.33 million tones of wastes per year (Pandit et al. 2004). These generated wastes are mainly of two types—Non-hazardous and Bio-hazardous wastes. The bio hazardous wastes can further be divided into two types—Infectious and Non-infectious wastes. The Infectious wastes include plastic disposables, liquid wastes, etc. whereas, the Non-Infectious wastes include radioactive wastes, discarded glasses, chemical wastes, cytotoxic wastes, incinerate wastes, etc. World Health Organization has declared that 85% of the hospital wastes are non-hazardous, whereas the rest 15–20% (10% are Infectious and 5% are Non-Infectious) are Hazardous Wastes. And about 15–35% of all the hospital wastes fall under Infectious Wastes (Aravindan and Vasumathi 2015; Radha et al. 2009). Besides, there are other wastes like radioactive wastes, mercury-containing instruments, PVC plastics, etc., which are environmentally sensitive and require monitored greater attention (Radha et al. 2009).

If the infectious part gets mixed with the non-infectious part then it will result in the entire mass to be infectious altogether. The Bio-Medical Solid Waste (Management and Handling) Rules 2016, has made it mandatory for any healthcare unit (hospitals, clinics, veterinary institutions, etc.) to dispose of its Bio-Medical solid

wastes as per the law (Aravindan and Vasumathi 2015; Patil and Pokhrel 2005). Thus, improper waste management might not only lead to spreading of diseases and posing serious health risks but also to huge environmental degradation affecting the society at large (Nema et al. 2011). Thus, this study was conducted to ingress and assess the waste management plans, methods used during the different processing systems—segregation, labeling, packaging, neutralization and disposal (along with their safety precautions) based on the case study at the hospital. Hazards associated with the shortcomings in their existing system are identified and a few recommendations are proposed to lessen the risk of infection and to create awareness among the public in general.

2 Survey Methodology

The survey was carried out at one of the best multispeciality hospitals in Bhubaneswar with 1750 beds providing high-quality overall healthcare and medical treatment in a wide range of disciplines to people at an affordable cost. Though being attached to the medical college, the hospital runs like a corporate one with a distinctive corporal culture prevailing throughout. Due to administrative reasons, the hospital's name is not being mentioned here. The required details and statistics were collected from the various departments in the hospital (by observation, interview and a questionnaire survey).

3 Survey Observations

The survey portrays the budding problems faced during the disposal of biomedical wastes. The highlights of this survey incorporated the substantial importance of the generation of the hospital wastes, disposal practices (like—collection, packaging, and handling, storing, autoclaving, incineration, chemical disinfection, etc.) and the disposal sites.

4 Survey Interview

The entire waste management team of the hospital, a member from the infection control department, the sanitary assessor and the supporting staffs involved in the entire management process were conferred with regarding the general management practices carried out by the hospital and the fundamental apprehension of waste management issue. Moreover, the complete process was described by the member of the infection control department and also the sanitary inspector of the hospital. All

the necessary information as obtained during the course of the study were provided by the assigned authorities from the hospital records itself.

5 Questionnaire Survey

To obtain detailed knowledge regarding the present scenario of the hospital to its waste generation and management strategies followed, a set of questions were framed and the corresponding responses were recorded to identify and eventually rectify the shortcomings in their system. The entire questionnaire is summarized as follows:

1. What are the rules and regulations that the hospital follows consistent with the guidelines as issued by the government?
2. What is the method/procedure which is being applied during the management and the accumulation of waste in the different units?
3. How are different types of wastes such as sharps, anatomical waste, and waste generated due to expired or discarded medicines dealt with?
4. Where is the primary area of accumulation of the wastes before its disposal?
5. Do the workers collecting, segregating, storing and disposing the wastes use proper coats and other protective gears?
6. How often are the waste containers/bins emptied?
7. If huge amounts of BMW spill takes place somewhere in the hospital, what immediate steps are taken to cater to the problem, to get rid of it and how?
8. How much waste is generated per day and how much of them (in % per day) is recyclable?

6 Results and Discussions

6.1 Rules and Regulations

According to the Bio-Medical Solid Waste (Management and Handling) Rules 2016, any healthcare unit is subjected to dispose of its generated wastes as per the stated law. The procedures as listed under this law are to be followed during the managing and disposing of the generated biomedical wastes. The most fundamental and essential steps as specified by the BMW rules incorporate—handling, segregation, disinfection, transportation, and finally disposal. An alternative method of the same is proper segregation followed by its disposal by suitable methods. Accordingly, the waste should thus be stored into different colored bags right at the time of its generation, then processed by the properly designated treatment and finally disposed of. Table 1 represents the treatment/disposal methods followed by the hospital as per the stated BMW rules. The wastes are divided under the following subheads—colour coding,

Table 1 BMW categories (segregation, collection, treatment and disposal)

Category	Type of waste	Colour coding	Treatment and disposal
1	Human anatomical waste (human tissues, Yellow organs, body parts)	Yellow	Incineration/deep burial
2	Animal waste (animal tissues, organs, body Yellow parts, carcasses, bleeding parts, blood and experimental animals used in research)	Yellow	Incineration/deep burial
3	Microbiology and biotechnology waste (waste from lab culture, specimens from microorganisms, vaccines, cell cultures, toxins, dishes, devices used to transfer cultures)	Red/yellow	Local autoclaving/microwaving/incineration
4	Waste sharps (needles, syringes, scalpels, blades, glass)	Blue/white	Chemical disinfection autoclaving/microwaving, mutilation and shredding
5	Discarded medicines and cytotoxic drugs (outdated, contaminated, discarded drugs]	Black	Incineration/destruction and disposal in land fills
6	Soiled waste (contaminated with blood and body fluids including cotton, dressings, soiled plasters, linen)	Red/yellow	Autoclaving/microwaving/incineration
7	Solid waste (tubes, catheters, IV sets)	Red/blue	Chemical disinfection/autoclaving/microwaving, mutilation and shredding
8	Liquid waste (waste generated from laboratory and washing, cleaning, disinfection)		Disinfection by chemical treatment and discharge into the drains
9	Incineration ash	Black	Land fills
10	Chemical waste	Black	Chemical disinfection and discharge into the drains

type of wastes, type of bag or container to be used, and the treatment or disposal methods (Nema et al. 2011).

6.2 *Method/Procedure of Management of Waste*

The wastes that are generated in the hospital on a daily basis are mainly of two categories—General wastes and Biomedical waste.

General wastes—both the wet and dry wastes (such as—plastic paper, rubber, leftover food and liquids, house sweepings, soiled papers, etc.) are collected in black colored plastic bags present inside the bins of the same color. This bin is regularly emptied by the waste collectors of the BMC (Bhubaneswar Municipal Corporation) (Fig. 1).

Biomedical Wastes—Each ward in the hospital ensures the usage of four different colour-coded waste collection bins, as per guidelines of the BMW rules 2016. They are—yellow, red, blue and white. Right from the moment of generation of these wastes, they are collected separately and segregated according to their properties into their respective bins (Fig. 2).

Every floor in the hospital has a unit storage room where the generated wastes (from the different wards) are temporarily stored before taking it out to the Main Waste Management Storage Room. The hospital has also put up posters regarding the segregation of wastes in all the storage rooms for an emergency reference. Each bin has its respective colored plastic bag lined inside, as per the rules. The wastes are deposited inside these plastic bags. When 3/4th of the total capacity gets filled, they are tied, labelled and taken out to the main storage room using a closed trolley for their final disposal and treatment. This is done twice daily by the respective staffs on duty. Since September 2019, the hospital has started a new initiative to log the waste generation data by assigning each plastic bag in the main storage room with a special bar code. This, when scanned displays their respective weight, thus making

Fig. 1 Management of general wastes

Fig. 2 Color-coded bins in the unit storage area (left: 1st floor, right: ground floor)

the entire management system more simpler and transparent. Before that, a hand-written record was maintained by their respective authority wherein the weight of the wastes generated per day per bag was recorded and summed up (Figs. 3 and 4).

Fig. 3 Collection of wastes in trolley

Fig. 4 Main storage area for BMW

6.3 Different Types of Biomedical Wastes (Sharps, Anatomical Waste, and Infectious Waste) Dealt with

Sharps—These include needles, syringes with fixed needles, needles from needle tip cutter or burner, scalpels, blades, or any other contaminated sharp object that may cause puncture and cuts (this includes both used, discarded and contaminated metal sharps). With the prior consent from the SPCB (State Pollution Control Board), the hospital treats all of the above stated wastes by autoclaving or dry heat sterilization followed by shredding or mutilation or encapsulation in metal container or cement concrete; combination of shredding cum autoclaving. It is then sent for final disposal to iron foundries or sanitary landfill or designated concrete waste sharp pit.

Anatomical Wastes—It includes human tissues, organs, body parts and fetus below the viability period (as per the Medical Termination of Pregnancy Act 1971, amended from time to time). These wastes undergo incineration or plasma pyrolysis or deep burial.

Waste generated due to expired or discarded medicines—As the name suggests, these wastes incorporate pharmaceutical waste like antibiotics, cytotoxic drugs including all items contaminated with cytotoxic drugs along with glass or plastic ampoules, vials etc. Out of them, the expired and items which is contaminated by cytotoxic drugs are sent back to the respective manufacturer/supplier for their proper sterilization process by incineration (at temperature >1200 °C or treated by common bio-medical waste treatment or hazardous waste treatment. The storage and disposal facility for incineration is maintained at a temperature >1200. Encapsulation or Plasma Pyrolysis is also suggested to be carried out at a temperature >120 °C. All the other medicines that is discarded are either sent back or disposed by incineration.

The followings are bar charts which represent the variation in the weights of the different biomedical wastes generated per day per bin at the hospital, based on the

guidelines as per the BMW rules 2016, over a month's period (from 11th September 2019 to 11th October 2019) (Graphs. 1, 2, 3, 4 and 5).

From the results as obtained from the graphs and the study, the waste generated in the red colored bin was observed to be the highest (4040.165 kg). Followed by yellow (3816.228 kg), blue (511.15 kg) and white (3.6 kg) over the time period of Sept '19 to Oct 19.

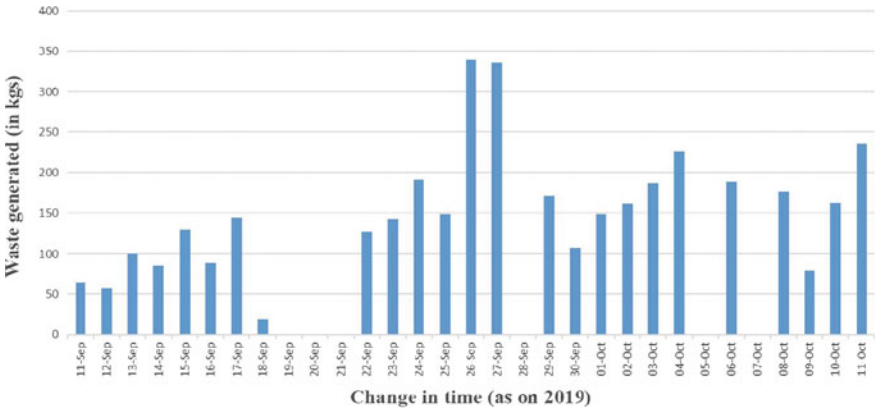

Graph 1 Variation of weight of the waste with time—Yellow Bin

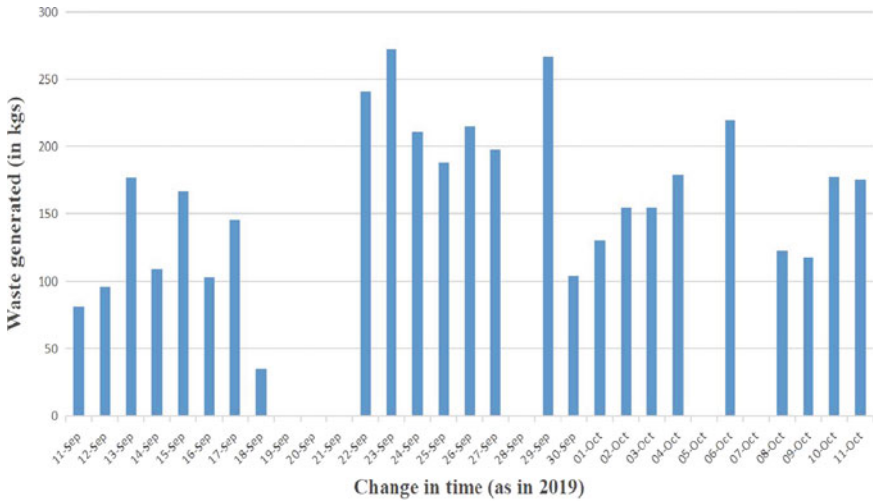

Graph 2 Variation of weight of the waste with time—Red Bin

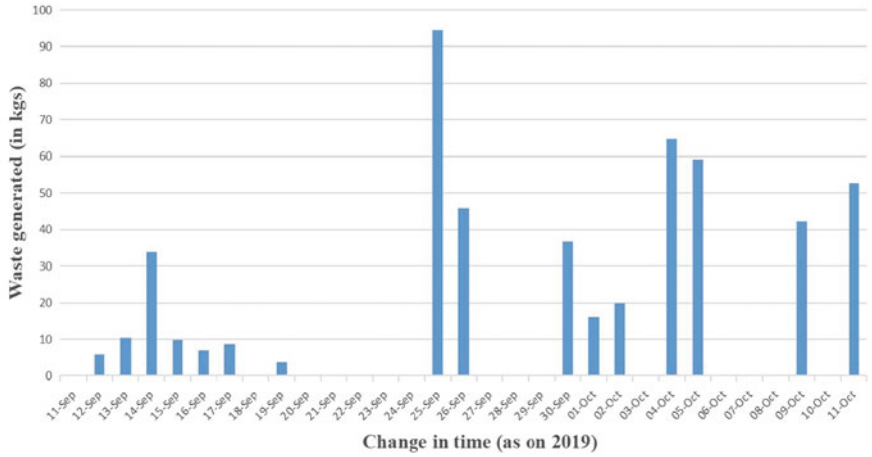

Graph 3 Variation of weight of the waste with time—Blue Bin

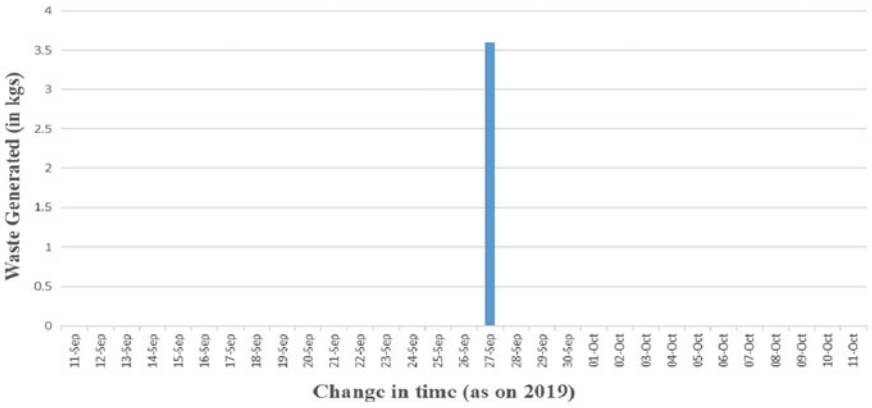

Graph 4 Variation of weight of the waste with time—White Bin

6.4 Precautions and Dress Code of Staff Handling the Wastes

All the staffs at the hospital who are in charge of collecting, segregating, storing and disposing of the wastes are individually supplied with a Personal Protective Equipment (PPE). It includes heavy duty rubber gloves for the hands, boots as shoes and waterproof aprons over their clothes. This combination of PPE acts as a barrier to any infection, virus or pathogen invasion in their body and also protects them from getting hurt while handling sharp objects like needles or broken glass.

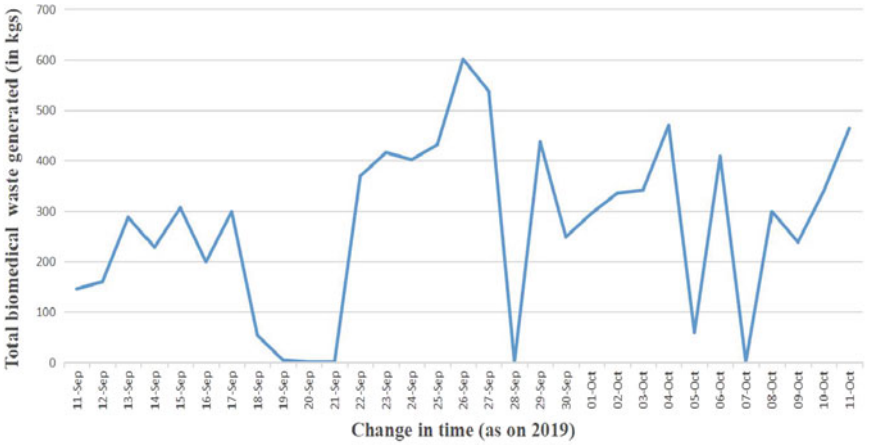

Graph 5 Variation of the total weight of biomedical waste with time

6.5 Emergency Measures Against BMW Spill

The two main types of spills that can occur at any point of time in a hospital is—chemical spill and biological spill. They occur mainly because of faulty equipment or human error. Biological spill incorporates spilling of blood, urine, vomit or faeces whereas, the chemical spill incorporated spilling of (>1L) of ethanol or methanol, strong bases or acids or highly volatile organics and mercury compounds. Whenever any spill takes place in the hospital, the area is marked and caution boards are immediately placed near the spill area. Absorbent material newspaper moistened with hypochlorite solution is introduced on the spilled area and a contact time of 20 min is allowed before wiping it off. Apart from that, every department has supplied the staffs with spill kits that caters to any of the above spillage problems.

6.6 Waste Generated (Per day) and the Amount Recycled

From the data as obtained from the hospital, it was observed that the biomedical wastes formed a weight of about 8400 kgs in one month (11th Sept to 11th Oct, 2019). The average weight of biomedical wastes as obtained from each bed was about 48 kg/month i.e., about 160 g/bed/day.

Estimating the stats as provided by the hospital for a month's time it was observed that about 54% of the biomedical waste generated per month is recyclable (since most of wastes collected in the blue and red bins are recyclable).

7 Conclusion

The entire survey at the hospital complied with most of the criteria as per the Biomedical waste (management and handling) rules 2016. But, it was observed that disinfection practices were at times overlooked due to patient overload. Before September 2019, waste collection records were not properly maintained. Data manipulation was also observed in numerous entries. The main storage room of biomedical wastes had a poor ventilation system that might lead to spreading of infection and diseases and the condition of the main storage room due to negligence was observed to be quite dingy.

8 Recommendations

- The biomedical storage room should have cross ventilation system for the passage of air throughout.
- Main storage room should be repaired as soon as possible or a new storage room should be built maintaining the proper guidelines of Biomedical waste management rules.
- The hospital was observed to use a thermocol box wrapped around by a blue colored paper instead of the blue colored bins as mentioned in the BMW rules which needs to be altered.
- A garbage accumulation was seen in front of the main storage room of the hospital exuding bad odor. This needs to be cleaned immediately as it might lead to infection or diseases.

References

Aravindan A, Vasumathi AM (2015) Case study exploration of biomedical waste in multispecialty hospital in Madurai, 347–363

Jaiswal S, Singh AK, Chowdhury MK, Garg R (2010) Biomedical waste management in a charitable hospital: a case study of Jindal Institute of Medical Science, Hisar District, India 5:115–122

Nema A, Pathak A, Bajaj P, Singh H, Kumar S (2011) A case study: biomedical waste management practices at city hospital in Himachal Pradesh 29:669–673

Pandit NB, Mehta HK, Kartha GP, Choudhary SK (2004) Management of bio-medical waste: awareness and practices in a district of Gujarat. Indian J Public Health 49(4):245–7

Patil GV, Pokhrel K (2005) Biomedical solid waste management in an Indian hospital: a case study 25:592–599

Radha KV, Kalaivani K, Lavanya R (2009) A case study of biomedical waste management in hospitals 41940664

Shrestha D, Gokhe SB, Dhoundiyal A, Bothe P (2017) A case study to review compliance to biomedical waste management rules in a tertiary care hospital 4:511–515

Hydro Economy: Environmental Sustainability of Water and Wastewater Resources and Infrastructure

Soham Kar and Kundan Samal

Abstract Water quality and sustainability is a major challenge worldwide. These challenges arise because of the many factors, such as changes in climate, the natural reservation of water, and human influence. Water resources are the source of survival and interest for all the plants and animals as it keeps the ecosystem balanced. Deficient water quality and over-exploitation of water resources can harm the environment and affect our health and subsistence. Poor management of these resources can even restrict the economic growth and development of a country. The last few decades have seen a massive increase in water resource utilization due to the establishment of new settlements and industries, population growth, increased deforestation, a decrease in groundwater level, climate change, etc. Recent years has seen an increased use of pesticides and fertilizers running off from agricultural lands, forest-clearing for new infrastructure has to lead to suspension of vast chunks of soil into river systems, acid rain due to increased air pollution, waterborne viruses from wastewater discharge, the release of heavy metals into rivers by mining and industries has to lead to damage the ecosystem. In many countries, water treatment systems are not sufficient or adequate to challenge these problems, especially in developing countries. Chances of deceases increases in these countries due to a lack of proper sanitation systems. Water shortages have become more frequent, Continental glaciers have started melting more rapidly due to climate change, floods, and storms caused due to global warming have become more frequent and severe. More attention must be given to growing and conserving the existing water resources. Identification of the multiple impacts and exploitation of these sources should be found and upgraded. New and more effective methods/systems that are both economical and effective should be made applicable to tackle pre-existing water systems. Decision making should be done so that these systems/solutions are economically cheap and easy to use. This paper discusses the various issues, technologies, and potential solutions/alternatives related to water and wastewater treatment sustainability.

S. Kar · K. Samal (✉)
Kalinga Institute of Industrial Technology, Bhubaneswar, India
e-mail: kundan.samalfce@kiit.ac.in

B. B. Das et al. (eds.), *Recent Developments in Sustainable Infrastructure (ICRDSI-2020)—GEO-TRA-ENV-WRM*, Lecture Notes in Civil Engineering 207,
https://doi.org/10.1007/978-981-16-7509-6_15

Keywords Sustainability · Water management · Waste-water treatment · Eco-system · Exploitation

1 Introduction

Growing Urbanization and development has led to the increased usage of water resources. Water is the largest natural resource available to humankind. With more than 95% of the worlds' water supply present in oceans, humans are depended on the 3% of freshwater supply for agricultural, industrial, and domestic purposes. Of these three percent, only 0.5% of water is available and usable to us. As the income of the economies has grown, so has the water demand. Therefore, sustainable and effective use of these water resources is crucial for the survival of humanity and all the living organisms on the planet. It is predicted that by 2025, two-thirds of the world population will face some water scarcity. Local and international ecosystems are also getting affected as water is the source of survival for all the plants and animals due to water pollution and climate change.

According to Rodell et al. (2018), An examination of the distribution of freshwater supplies was carried out by NASA satellite. This included surface waters, soil moisture, groundwater, and snow and ice. This study reported that the climate around the world is changing at an alarming rate, the humid region is receiving more rainfall, and arid regions are becoming drier. Climate change has led to water scarcity in different communities. In 2019, about 2 billion people lived in countries experiencing high water stress (UN 2019). Nations such as Sudan, Qatar, Israel, India, Iran, Pakistan, etc. are at a greater risk of water stress. The rising water stress has caused an economic impact to satisfy the need for water. India is the second-most populous country with more than 1.3 billion people is currently facing one of the worst water crises in its history endangering millions of lives and communities (NITI Aayog 2018, p. 15). The ongoing water crisis is a matter of national importance, with major cities such as Chennai, Delhi, Bengaluru, Hyderabad, Mumbai, and Jaipur are on the verge of facing a water crisis. Apart from the growing scarcity of water, water pollution is another factor affecting water usability and availability. Chemical, physical, or biological contaminants released from factories, mines, refineries, water-treatment plants pollute the water bodies. The water problem has become a significant problem causing scarcity and harming the health of millions around the globe. Lack of infrastructure and low interest for TSS and water turbidity has given rise to disinformation about contamination and water quality, which in turn creates a severe impact on health, environment, and ecosystem (Ahuja 2019; Behrman 2010). More than 200,000 children die every year because of diarrhoeal diseases due to poor sanitation or contaminated water. Diarrhea spreads rapidly in surroundings with poor sanitation, where safe water is unavailable. These areas are often affected due to human or natural calamities. Water-borne diseases are one of the major causes of under-five mortality, along with pneumonia, malaria, and measles.

The usage and burning of fossil products have led to a change in our atmosphere's composition. The release of CO_2 and other greenhouse gasses absorbing the earth's heat is causing a rise in the global temperature. Climate change is one of the significant factors leading to the deprivation of water. The rise in the global temperature has changed the weather and monsoon pattern, which has altered water availability throughout the world.

Scientists and researchers believe that the growing climate change due to the emission of CO_2 is causing additional commination to water resources (Hoff 2009; Kim et al. 2018; Vörösmarty et al. 2010). The rise in a locality's temperature also affects the quality of water available. An increase in the air temperature can lead to a decrease of dissolved oxygen (DO) in water, severely affecting local water bodies such as streams, rivers, and lakes. Scientists and researchers believe that change in the water cycle would result in more precipitation in some areas as compared to others, which could severely affect the economy and ecosystems. The global increase in the world's temperature could lead to the melting of the polar caps and water expansion, leading to sea-level rise. This would have devastating effects on the coastal cities and ecosystems. The water cycle would also undergo a significant change due to the temperature rise.

Over-exploitation of water resources can harm the environment and affect our health and subsistence. Continuous usage of water resources can lead to water level declines and increasing groundwater salinization. Due to an increasing salinity of the extracted groundwater and its negative impacts on soils and land productivity in major aquifers, has led to abandoning of wells and agricultural projects. Due to this, farmlands are abandoned and investments in agriculture has stopped in numerous country. Poor management of the water resources has also led decline and over-exploitation, restricting the economic growth and development of a country.

2 Water Sources

The water used for sanitation, drinking, washing, cleaning, or irrigation, generally comes from different sources (surface water or groundwater). In most developed countries, water is usually collected from one or more sources and is distributed by the municipal or private water provider. These corporations might sometimes mix certain chemicals or disinfectants in water distributed through a network of pipes, reservoirs, and water towers or pump stations (Padowski 2019; Shukla et al. 2018). In many under-developed nation, water may not be available from a water bodies or groundwater. These communities are depended on a communal source, such as a well or tap stand, free or accessible for a nominal fee, water tanker etc. to satisfy their water needs. The source through which water is supplied depends on various reasons such as the quality of the water, the proximity of the water source, and the resource's accessibility. In 2018 India, about 87.6% of the households in the rural areas and about 90.9% of the homes in the urban areas had sufficient drinking water throughout the year from the principal source, and about 51.4% of the households in

the rural areas and about 72.0% of the homes in the urban areas used improved source of drinking water located in the household premises which was sufficiently available throughout (NSS report no. 584, 2018). While drinking water is available to most of the families in India, potential harmful contaminants like arsenic and copper have been found in tap water across the country. Most of the Water quality monitoring programmes are inadequate or are not available in most of the developing countries. Depending on the above factors, water sources can be broadly classified based on its use by industries, farmers, and households.

3 Groundwater

Water stored in aquifers below the land surface in large formations and other small pockets between layers of the earth's crust are called groundwater (Smith et al. 2016). It is reported that the volume of groundwater is much more as compared to the available surface water. Since this water is present below the ground surface, it cannot evaporate and is safe from contamination. Thus, making it is a clean and consistent source of water as compared to other sources. The significant role of groundwater is to maintain the surface water along with flora and fauna, thus making it a significant factor for maintaining and sustaining aquatic ecosystems and provides a reliable discharge to streams, rivers, and wetlands supporting flows during dry seasons and droughts (Chakraborti et al. 2009). Precipitation, location of streams and other surface-water bodies, and evapotranspiration rate are the three significant factors determining the source and amount of water flowing through a groundwater system. In India, groundwater is the primary source of water for agricultural and domestic purposes. The Central Ground Water Board (CGWB 2012) reported that the 92% withdrawal of groundwater is being used for farming purposes that contribute mainly to the country's food security. However, due to recent over-use and groundwater exploitation, groundwater has become unsustainable, and its supply is continuously diminishing in some regions. In India, much of the farmers have installed numerous pumps to extract groundwater, which has led to higher groundwater abstraction leading to depletion and other severe impacts on groundwater resources (Krishan et al. 2020). Agricultural technology has indiscriminately exploited groundwater resources to meet its food requirement. Especially in India's northwestern region (dominant agrarian region), groundwater over-exploitation has led to declining water table problems, deterioration of groundwater quality, water-logging, and soil salinity.

Groundwater salinity is defined as a high concentration of dissolved salts in water present below the earth's crust is more than permissible limits; thus, groundwater salinity is a potential risk to domestic and agricultural productivity if not managed. In India, groundwater salinity is expected in Rajasthan, Haryana, Punjab, Gujarat, Uttar Pradesh, Madhya Pradesh, Maharashtra, Karnataka, Bihar, and Tamil Nadu. Groundwater salinity is a significant threat to the local ecosystems, and it also impacts

agricultural lands and communities living in that area who are dependent on groundwater for drinking and domestic purpose. India's northwestern region (arid and semi-arid areas) has higher evapotranspiration rates, resulting in increased water losses because northwestern states have a diversified geological, climate, and topographic setup, resulting in divergent groundwater situations. Groundwater salinity is present here because of the variability in the climatic and topography of northwestern states. In this region, states of Rajasthan, Punjab, Haryana, and Delhi are most affected as there is an increase in groundwater consumption over the last two decades due to rapid urbanization and industrialization, accompanied by growth agricultural revolution required to feed the growing population. The northwestern region's dry and warm climate is due to the high potential evaporation (Datta et al. 1996; Misra and Mishra 2007). The significant reasons for groundwater salinity are the construction of the canal network and subsequent water table elevation, water-logging, and intensive irrigation (Singh and Kothari 2004; Ifabiyi 2000), along with other factors such as the concentration of dissolved salts through evaporation, the leaching of salts or the mobilization of saline groundwater from deeper aquifer sections (Salama et al. 1999; Tyagi 1988). Salama et al. 1999 also reported that excessive irrigation in the arid and semi-arid regions could result in a loss of soil structure and fertility, and the soil may become more susceptible to water-logging. This loosening of soil could lead to the percolation of salts present on the surface to groundwater the infiltration of rain or irrigation water (Duncan et al. 2005; Fashae and Olusola 2017). Groundwater salinity have adverse effect on the crops grown in these regions. The soil moisture content also decreases in areas with high groundwater salinity. Consumption of exceeded saline in drinking water can cause numerous health problems. Various diseases such as cardiovascular diseases(CVD), diarrhea, and abdominal pain have also been associated with high groundwater salinity. In coastal cities of India, Bangladesh, Vietnam, China, Netherlands, Brazil, groundwater and surface water are susceptible to contamination of salt. Especially, the south-Asian countries, putting more than 30 million at health risk due to consumption of salt water. According to Khan et al. (2014), excess salinity in water has been linked to risk of (pre)eclampsia and gestational hypertension. High salt intake is a significant risk factor for increased blood pressure.. In addition, there are reports of excess water salinity on association with infant mortality, cholera outbreaks, and skin and diarrheal diseases (Grant et al. 2015; Dasgupta et al. 2016; Chakraborty et al. 2019). The problem of groundwater can be controlled with proper policies, climate, morphology, and proper management of surface and subsurface drainage.

Arsenic poising is another common problem in underdeveloped and developing countries. Inorganic arsenic is naturally present at high levels in the groundwater of several countries, including Argentina, Bangladesh, Chile, China, India, Mexico, and the United States of America (WHO 2020). Groundwater used for drinking and agricultural purposes risks the exposure of arsenic poising. More than 100 million people drink water with higher arsenic content than the WHO guideline value of 10 μg/L (Ravenscroft et al. 2009; Liu et al. 2016). Arsenic poising is a significant problem in the state of West Bengal in India and Bangladesh. Despite efforts, it was estimated that in 2012 about 19 million and 39 million people in Bangladesh were exposed

to arsenic concentrations above the WHO provisional guideline value of 10 μg/L (UNICEF 2015). Vomiting, abdominal pain, and diarrhea are common symptoms of arsenic poising. Consumption of too much arsenic can result in numbness and tingling of the extremities, muscle cramping, and can ultimately lead to deaths. The International Agency for Research on Cancer(IARC) has stated that arsenic in drinking-water is carcinogenic, and long time consumption can cause cancer (WHO 2020). In addition to skin cancer, long-term exposure to arsenic may also cause bladder and lung cancers. Adverse health effects associated with long-term ingestion of inorganic arsenic include developmental effects, diabetes, pulmonary disease, and cardiovascular disease. Arsenic-induced myocardial infarction, in particular, is a significant cause of excess mortality in many counties.

Groundwater can be a renewable source of water if appropriate measures are taken to conserve the total amount of water entering, leaving, and being stored in the system is conserved. Since groundwater is a slow and invisible resource, so long-term and adaptive plans should be set on a muti-generational time horizon with clear targets are essential, while acknowledging potential limitations and impacts. Long term and adaptive groundwater management plans should be devised. There are available models that are continuously updated. They are updated with new models and refined for better use. More accurate models should be developed for the monitoring of groundwater resources. Groundwater demands by various industries and sectors should also be metered. In many of the developing and under-developed countries, groundwater data is not sufficient. Government should make legal policies which can help to recharge the decreasing groundwater levels. Involvement of the local community will be essential for implementation of long-term management strategies. People should be made aware of this problem, and government should take initiatives to educate the masses. While devising groundwater management plans, data from previous models should be considered by researchers and groundwater sustainability organization for improved groundwater management plans.

4 Surface Water

Globally, surface water is a commonly used domestic water source and is also the predominant source used by cities. It is estimated that nearly 78% of urban residents (1.2 billion people) rely on surface water sources, employing approximately 504 billion liters per day. Surface water, because it sits on the land surface, is relatively easy to access. Still, the volume and quality available tend to vary more dramatically in response to climatic factors (e.g., precipitation, temperature) and human activity. In the last two decades, surface water pollution has become a significant health hazard in developed and under-developed nations. According to Global Water Status (2018), about 40% of the world's rivers have already been contaminated to different degrees. The need of water for various different purposes have made a variability in supply.

Streams, rivers, or lakes that experience large fluctuations in flow or volume may not ensure a consistent supply. Most of these rivers, streams, and lakes are affected by

water pollution, with most of the major rivers and their branches being firmly over-exploited. Climate change and land usage are significant factors for a difference in surface water quality (Bi et al. 2018; Olusola et al. 2017). Overuse of fertilizers, pesticides, oil, grease, sand, and other chemical agents from factories, animal-livestock industry, agriculture, textile industries can cause runoff. These runoffs pick up and carry away natural and human-made pollutants, finally depositing them into lakes, rivers, wetlands, and coastal waters. Besides land usage, climate change also threatens water quality in rivers, lakes, and streams. Extreme climatic conditions or events such as heavy rainfall, floods, and droughts can increase contamination and affect the local ecosystem. Water pollution is also caused due to drastic changes in temperature and water bodies. This change in temperature and precipitation can directly or indirectly affect the water quality as there would be a change in the hydrological cycle. The water density, viscosity, surface tension, dissolved oxygen content, and other aspects will also change due to temperature variation, thus affecting the local ecosystems and lives (Bi et al. 2018; Hao et al. 2010; Huang and Chiang 2009; Hammond and Pryce 2007). Temperature changes will lead to photosynthesis changes, the chemical reaction rate, the toxicity changes of various pollutants, and the microbial degradation ability of organisms present inside water bodies (Xia et al. 2012). Similarly, precipitation changes will affect the occurrence of rainfall, droughts, and floods and would slightly affect the water quality of different rivers, lakes, and basins. Precipitation decrease would bring about groundwater exploitation and groundwater pollution; On the other hand, precipitation increase will aggravate atmospheric deposition and surface erosion leading to more pollutants being going into water (Curriero et al. 2001). This year (2020), India saw the Brahmaputra River's flooding in the Indian state of Assam along with COVID-19. Assam and Meghalaya's meteorological subdivision saw an excess of approximately 30% of received rainfall; they received 1164 mm compared to an average rainfall of 894 mm during the period; this affected millions and caused over 100 deaths (IMD 2020). Water eutrophication has also become one of the most challenging environmental problems. The excessive nutrient loading into the surface water system is considered to be one of the significant factors. As a result, massive proliferation or prolonged toxic cyanobacteria blooms(TCBs) increase in both frequency and distribution on the water surface. TCBs are an environmental concern due to their ability to produce a wide range of hepatotoxins, neurotoxins, and dermatoxins, affecting health problems. To ensure the safety of drinking water supplies, various physical, chemical, and biological processes, such as coagulation, flocculation, sedimentation, filtration, disinfection, adsorption, and biodegradation, have been applied for the removal of MCs.

The variation in land patterns and land coverage impacts and controls water bodies' physical and biochemical processes (Wang and Zhang 2018). These changes significantly impact the water quality of rivers, streams, and lakes, leading to water pollution. Rapid urbanization and socioeconomic advancement (Wagner et al. 2013) such as deforestation, agricultural activities, industrialization can lead to a change in land use pattern, which has adversely affected the water cycle and has increased the extreme-event possibility, modify land surface characteristics, alter

runoff volume, change water temperature, generate pollution, increase algal production and decrease the concentration of dissolved oxygen in water bodies thus leading to a deteriorating water environment (Fashae et al. 2019). Floods, drought, changes in river and groundwater regimes, and water quality in an area are the four significant direct consequences of land usage on the water cycle (Rogers 2000; Fashae et al. 2017a, b; Fashae et al. 2019). More than 2 billion people worldwide use a drinking water source contaminated with feces (WHO 2020). In cities, wastewater constitutes chemicals and other harmful compounds released from small factories, hospitals, pharmaceutical companies, industrial units located at the towns and outskirts, intensive agricultural practices, indiscriminate disposal of domestic and municipal wastes, and road construction. This wastewater is directly dumped into river systems and streams without adequate treatment. In India, many of these sewer systems do not have any proper enclosure or coverage. Most of the slums are settled near these open drains, which further affects children and adults living near those open drains.

Many surface water sources have been modified as per community needs to help manage variabilities, such as dams, reservoirs, canals, and pumping stations on rivers and aquifers. While developing water management plans, all hydrological cycle components, climate, ecology, and topography should be considered to determine water quality. Evaluation of the natural resources of and near-surface water resources and the impact of their improvements on the hydrology and economy should also be considered. Greater emphasis on planning for droughts and severe floods should be made and efforts to improve or conserve water quality from agricultural, industrial, and wastewater waste. Awareness of water conservation should be promoted on televisions and radios. Improved systems and procedures should be developed along with impacts on the local community, and ecosystems should be taken into account for equal distribution of surface water.

5 Other Sources

Other water sources include water collected from rainwater harvesting, potable and bottled water, desalinized water, and reclaimed (reused) water. There are a lot of communities living without adequate local groundwater or surface water sources. In these communities, people are depended on non-traditional sources to satisfy their water demand. There are water vendors who bring water to rural areas or neighborhoods in many of the underdeveloped countries. Many of these communities also have some local alternatives to withdraw water, such as collecting rainwater for their daily water needs.

Furthermore, depending on their location and finances, communities can access ocean water, or brackish groundwater can adapt and use desalination technology to remove contaminants and minerals to purify water for domestic usage. Some cities lack local freshwater supply have been paid to have large aqueducts or pipelines built to transport water from a distant lake or river sources. The Great Manmade River of Libya, the *Owens Valley aqueduct*, and the *Second Los Angeles Aqueduct* of

Los Angeles, Morgan-Whyalla pipeline, and Mannum-Adelaide pipeline pipelines in Australia are significant examples of this technology.

6 Water Sustainability and Technologies

In last few decades government and private organizations have put in their resources for development of improvement of existing water infrastructures and water management systems. Sustainable water supply is a part of integrated water resource management, the goal of sustainable water systems should be to provide adequate water quantity and quality for a given need, without compromising the future ability to provide this capacity and quality. Economic feasibility, social responsibility and environmental integrity should be assessed and linked to the purpose of water use and management. Governments and scientists are constantly trying to develop new technologies to meet the water requirements and demands of the growing population. Below are some of the new and innovative technologies applied for the treatment of water.

6.1 Membrane Filtration

In recent years, membrane filtration has rapidly become a widely accepted, reliable water treatment technology. Due to membrane technology's benefits, its usability has grown significantly in the last couple of decades for water treatment processes. Companies and researchers have started to adapt microfiltration(MF), ultrafiltration(UF), nanofiltration(NF), forward osmosis(FO), and reverse osmosis(RO) membranes for water treatment due to the extensive research and development of these technologies. Due to the lesser equipment size, energy requirement, and low cost, membrane technology has many potential and prospects in wastewater treatment (Quist-Jensen et al. 2015).

These membranes are categorized as isotropic and anisotropic. Membranes that are uniform in composition and physical structure are called isotropic membranes. In contrast, anisotropic membranes are non-uniform over the membrane area and are made up of different layers with different designs and composition. They can also be classified as either organic or inorganic based on the membrane material. Organic membranes are made from synthetic organic polymers such as polyethylene(PE), polytetrafluorethylene(PTFE), polypropylene, and cellulose acetate (Aliyu et al. 2018; Obotey Ezugbe and Rathilal 2020). Simultaneously, inorganic membranes are made up of ceramic, carbon, silica, zeolite, various oxides(alumina, titania, zirconia), and metals such as palladium, silver, and their alloys. Due to their chemical and thermal stability, inorganic membranes are widely used in industrial applications such as ultra-filtration, and micro-filtration (Baker 2012; Obotey Ezugbe and Rathilal 2020). Often, one or more membranes are combined for desired performance or

result; this type of membrane is called a hybrid membrane. These hybrid membranes are designed to complement a single membrane's disadvantages to achieve better performance to treat water. Hybrid membranes are commonly used in ion exchange, adsorption, or coagulation processes for better performance and results. More hybrid membranes combinations and processes are being researched as an alternative for the traditional treatment methods.

Even though there are many advantages of membrane filtration, there are certain disadvantages related to membranes' use. One of the significant problems for membrane processes is fouling. Membrane fouling can occur when some suspended solids, microbes, or organic materials are trapped within the membrane pores or deposited on the membrane surface, resulting in decreased permeate flux (Speth et al. 1998). Unit processes such as coagulation, flocculation, sedimentation are usually performed before treatment to reduce the risk of fouling of membranes (Stoquart et al. 2012). Fouling can be both reversible as well as irreversible. Fouling is considered reversible when particles or foulants (materials that cause fouling) such as clays, flocs, fungi, oils, humic, and mineral precipitates get deposited on the surface of the membrane, resulting in the formation of a layer that resists the permeate movement. Fouling is considered irreversible when foulants get deposited in the pores of the membrane. There is a perpetual alteration of membrane modules and elements to improve the rebate in membrane fouling (Bui et al. 2020). There are extensive research going on addressing this problem, many of them are also used in field and real-scale experiments.

There is an interminable roster of membrane technology utilization in wastewater treatment. Membrane technology has the potential of linking the economic and sustainability gap, along with the possibilities of low or no chemical practice. It is environmentally friendly and easy to access and use. Membrane technology has proven to be a more favorable option in wastewater treatment processes in recent times.

6.2 Ecological Floating Wetlands

"Ecological floating bed(EFBs) is an economical and sustainable green technology to restore polluted lake water. It is based on nature's self-cleaning capacity, and no toxic byproduct is generated during the treatment process" (Samal et al. 2019). EFBs removal efficiency of pollutants depends upon the temperature, structure, aeration level, and pollutant contents present in wastewater (Headley and Tanner 2012). Due to the fundamental role of hydrophytes in aquatic ecosystems' structure and functioning, they are preferred in EFBs to purify wastewater. Hydrophytes are also used due to their efficiency in accumulating nitrogen and phosphorous and preparing suitable conditions for bio-degradation of organics trapped by roots and rhizomes (Samal et al. 2018; Di Luca et al. 2011).

Constructed wetlands(CWs) are integrated systems that utilize different plant species and bed materials to treat various industrial effluents, sewage, and polluted

water. Constructed floating wetlands (CFWs) or constructed wetlands are based on advanced natural process/technology. Based on the water flow regime and types of macrophytes used, they can be broadly divided into surface flow wetlands (SF) and subsurface wetlands (SSF). Surface flow (SF) wetland has wastewater flowing over the bed materials provided sunlight may reach the system's bottom. Whereas in subsurface flow(SSF) wetland, wastewater flow is maintained below the bed materials. The contaminants present in the wastewater come in contact with bed materials, get attached to the biofilm, and later degraded aerobically (Samal et al. 2018; Vymazal 2007). Biomass and roots play a crucial role in the pollutant removal process in these systems. Aerial tissues, underwater tissues, and root systems optimize wetland performance by trapping various pollutants and metals from the water (Zhang et al. 2017).

Helophytes are also used for the design of CFWs. Helophytes have plenty of aerenchyma tissues, which helps transport oxygen from the above-ground biomass to underground biomass. Since the plant bed needs to be in floating condition, various buoyant materials like PVC pipes, polystyrene sheets, bamboo, and other floating materials are used to design the raft for providing buoyancy to the system. The ecological wetlands' design also depends on the water depth and plant coverage ratio as they affect the atmospheric oxygen diffusion rate to the water body (Samal et al. 2021). Apart from the above factors, macrophyte species, biofilm, and growth media are other significant factors affecting the pollutant removal process. Organics and suspended solids are usually removed by filtration and aerobic degradation process. CFWs are effective for removing exceeded levels of nitrogen and phosphorous present in wastewater along with heavy metals and suspended solids. These systems are being adopted and used worldwide and are one of the sustainable and eco-friendly green technology for the treatment of various types of wastewater.

6.3 Microbial Fuel Cells (MFCs)

In recent decades, a relatively new technology for bioenergy production has emerged in the form of microbial fuel cells (MFCs). It is an environmentally friendly and green technology, significantly growing as an emergent technology in many industries. This technology has seen its implementation in wastewater treatment by simultaneously treating wastewater and generate clean electricity. The microbial fuel cells utilize microorganisms or microbes to convert chemical energy present in a portion of organic matter into direct electric current. Microbial fuel cells (MFCs) are economical and low force alternative to the traditional treatment processes used for wastewater. The available conventional or conventional wastewater treatment systems leave/produce many excess residues, which costs for safe handling and appropriate treatment. Microbial fuel cells are preferable because of their low input energy needs and reduced sludge production by enabling the recovery of energy from wastewater. MFCs can also be used in communities and isolated areas as it does not need external power.

Low-sludge production, low operational costs, energy conservation, water reclamation, no downstream processes, and production of bioenergy are just some of the advantages of Microbial fuel cells. A typical MFC consists of two electrodes present in two different chambers. The anode is the electrode that is kept submerged in a substrate and the side where oxidation takes place. Oxidation occurs at the anode chamber, and the electrons present in the organic matter are transferred to the electrode surface. Microbes present in the anode chamber oxidize reduced substrates generating electrons and protons in the process. The anode is connected to the cathode by an external circuit; the cathode collects the electrons (from the oxidation reactions in the anode compartment) that travel through the external circuit. The concurrent reduction reaction occurs at the cathode; the collected electron is combined with protons with a terminal electron acceptor. An oxidizing agent usually surrounds the cathode since it has limited oxidation capacity (Yazdi et al. 2008). To keep the fuel from being crossed over to the cathode compartment or oxygen from entering the anode compartment, MFC has the anode and cathode compartments separated by a proton exchange membrane(PEM), a microfilter that is used for the transportation of protons. Positively charged hydrogen ions generated at the anode are passed through the PEM to the cathode and combine with electrons and oxygen on the cathode surface to form water, thus completing the electrical circuit.

The growing interest and research on the microbial fuel cells are due to its potential as a clean and self-sustainable water treatment system alternative that concurrently produces current to the pre-existing costly water treatment systems. Researchers and scientists from the various fields have shown their interest and attention to MFCs, which has led to a significant development of this technology (Mathuriya and Yakhmi 2014). MFCs are the only technology that can produce energy out of wastewater without the need for external energy (Santoro et al. 2017). Also, various research and experiments conducted all over the world on MFCs such as microbial desalination cell(MDC), microbial electrolysis cell(MEC), microbial electro-synthesis, and it can also be used to produce hydrogen with low consumption of energy utilizing bioelectrocatalysis supported by additional low energy power sources (Santoro et al. 2017). Besides, integrating microbial fuel cells with other technologies has made significant steps to achieve sustainable energy production and effective water treatment. However, this technology is far from perfect; there are several drawbacks of MFCs, including utilization of new substrates, low power generation, limitation of MFC due to membranes, membrane fouling due to suspended solids soluble contaminants in a large scale application, etc. Microbial fuel cells(MFCs) have shown promise in dealing with the current water and energy needs. Microbial fuel cells are a platform of its own and have extended its use and study into different disciplines. The microbial fuel cell is a cross-disciplinary technology so that the study area has grown to energy, material sciences, biochemistry, etc.

6.4 Hydrodynamic Cavitation

Cavitation (appearance of vapor cavities inside an initially homogeneous liquid medium) is defined as the liquid's breakdown under very low pressure. Cavitation as physical phenomena is environmentally friendly as it does not introduce new chemicals to water and can the water can be easily managed. Cavitation of water results in the generation, growth, and subsequent collapse of gas-filled cavities (bubbles) due to pressure pulses inside a liquid bulk. The bubbles generated through a mechanical device grow in size until the liquid's external pressure decreases to a threshold value, usually around the liquid's vapor pressure; after reaching this threshold, bubbles collapse and implode (). Extreme local pressure and temperature due to cavitation (resulting in various physical and chemical effects) are used to disintegrate tiny organic molecules, which is much harder to decompose by using conventional biological methods. As a result of high temperature, water dissociates into H^+ and OH radicals. The hydroxyl radicals due its strong oxidation tendency oxidizes the chemicals and affects the microbes. Cavitation is also used to increase hydrolysis and biodegradation of organic matter by disintegrating larger particles.

Most of the advanced Oxidation Processes (AOP) are unable to degrade complex compounds completely. The application of cavitation has enabled us to overcome this problem. Cavitation is preferred over AOPs because it is less costly than the advance oxidation process (AOPs), and the by-products are only formed from the oxidation of the contaminants (no products created from other oxidants). Depending upon the device used for generating the bubbles in the liquid medium, cavitation is classified into ultrasonic cavitation (pressure waves generated in an ultrasonic bath or through an ultrasonic horn inside a liquid bulk) and hydrodynamic cavitation (based on the pressure variations due to acceleration/deceleration of a fluid flow). In the last decade, due to the widespread problem such as population rise, increased water consumption, water resources availability has led to innovation and development of hydrodynamic cavitation technologies due to the high cost of ultrasonic cavitation application. The oxidative and mechanical capabilities of hydrodynamic cavitation have been incorporated to treat aqueous effluents polluted by organic, toxic, and bio-refractory contaminants and disintegrate cells of microorganisms in biological applications. Hydrodynamic cavitation releases a large amount of energy. It can be used with other techniques to treat wastewater, ranging from natural processes such as cellular disruption to chemical treatments such as the oxidation of organic pollutants in aqueous effluents, including bio-refractory and toxic chemicals (Mancuso et al. 2016; Mancuso et al. 2017; Mancuso et al. 2019; Mancuso et al. 2020).

As compared to other traditional treatment methods, hydrodynamic cavitation has been reported to have higher removal efficiency, lower operational energy, and few contaminations (Sivakumar and Pandit 2002; Suenaga et al. 2015; Mancuso et al. 2020). Even though the procedures are complex and optimization is harder to achieve, the technique offers some crucial advantages over ultrasonic cavitation. Hydrodynamic cavitation has the potential to become an energy-efficient technique

that can reduce the current use of costly chemical reagents for the water treatment process.

6.5 Biological Filtration

Biological filtration or biofiltration is a natural water treatment technique for effective removal of organic matter present in the wastewater and biologically treated sewage effluent in conventional sewage treatment (Carlson and Amy 1998). The biological component of all biofilters comprises indigenous bacteria that proliferate in biofilms at low nutrient concentrations. Biological filters heavily rely on the microorganisms communities present in the filter; therefore, these microbes decide biological filtration's performance. Biological filtration breaks up the organic matter present in the water utilizing microbes, and therefore microbes' development is essential in biological filtration as they oxidize organic matter in water to produce energy. This technique is the most effective for the production of biologically stable water. Biological filters treat wastewater close to a secondary standard (a higher standard than septic tanks but not as high as aerated wastewater treatment systems). Biological filtration is used in water treatment systems to reduce biodegradable organic matter (BOM). A higher BOM level may lead to biological regrowth after they are introduced in the distribution system. Biological filtration can be an environmentally friendly solution in place of traditional chemical and physical water treatment processes. There are research and experiments going on this method, such as its design, filter media, BOM removal efficiency, etc. to improve the existing systems.

7 Conclusion

The growing demands of water for agriculture, industries, supporting population growth, and the increasing water scarcity have increased in the last few decades. Despite decades of increased international scientific attention and concern, attempts to collect, compile and gain knowledge from consumption, pollution, and abstraction data and information globally are still gradually and in early stages of applicability. Under these circumstances, requirements for finding alternative and cost-effective water treatment technologies with less energy consumption has become a significant area of research. Government and private organizations are pouring tons of money into the development of new technologies. Initiatives are taken by different international as well as national bodies to improve the pre-existing situation. People have become more aware of the problem. Improved water conservation strategies and environmentally friendly approaches, should be taken for the sustainability of this precious resource.

References

Ahuja S (2019) Evaluating water quality to prevent future disasters
Aliyu UM, Rathilal S, Isa YM (2018) Membrane desalination technologies in water treatment: a review. Water Pract Technol 13:738–752
Baker RW (2012) Membrane Technology and Applications; Wiley Online Library: Hoboken. NJ, USA
Behrman N (2010) The waters of the third pole: sources of threat, sources of survival. Humanitarian Future Programme, London.
Bi W, Weng B, Yuan Z, Ye M, Zhang C, Yu Z, Yan D, Xu T (2018) Evolution characteristics of surface water quality due to climate change and LUCC under Scenario Simulations: a case study in the Luanhe River Basin
Bui XT, Chiemchaisri C, Fujioka T, Varjani S (2020) Introduction to recent advances in water and wastewater treatment technologies. Water Wastewater Treat Technol 3–12
Carlson KH, Amy GL (1998) NOM removal during biofiltration. Am Water Works Assoc 90:43–52. (this paper details the removal of NOM using biofilters)
CGWB (2012) Dynamic ground water resources of India (as on 31 March 2009). Central Ground Water Board Ministry of Water Resources Government of India Faridabad November 2011 (p 243)
Chakraborti D, Ghorai SK, Das B, Pal A, Nayak B, Shah BA (2009) Arsenic exposure through groundwater to the rural and urban population in the Allahabad-Kanpur track in the upper Ganga plain. J Environ Monit 11:1455–1459
Chakraborty R, Khan KM, Dibaba DT, Khan MA, Ahmed A, Islam MZ (2019) Health implications of drinking water salinity in coastal areas of Bangladesh. Int J Environ Res Publ Health 16(19):3746
Curriero FC, Patz JA, Rose JB, Lele S (2001) The association between extreme precipitation and waterborne disease outbreaks in the United States, 1948–1994. Am J Public Health 91(8):1194–9
Dasgupta S, Huq M, Wheeler D (2016) Drinking water salinity and infant mortality in coastal Bangladesh. Water Econ Policy 2. https://doi.org/10.1142/S2382624X1650003X
Datta PS, Bhattacharya SK, Tyagi SK (1996) 18O studies on recharge of phreatic aquifers and groundwater flow-paths of mixing in Delhi area. J Hydrol 176:25–36
Di Luca GA, Mufarrege MM, Sánchez GC, Hadad HR, Maine MA (2011) P distribution in different sediment fraction of a constructed wetland. Water Sci Technol 63:2374–2380
Dular M, Griessler-Bulc T, Gutierrez-Aguirre I, Heath E, Kosjek T, Klemenčič AK, Oder M, Petkovšek M, Rački N, Ravnikar M, Šarc A (2015) Use of hydrodynamic cavitation in (waste)water treatment. Ultrason Sonochem 29:577–588
Duncan R, Bethune M, Christen E, Hornbuckle J (2005) A review of salt mobilisation and management in irrigated areas of the Murray-Darling Basin. Cooperative Research Centre for Catchment Hydrology, Monash University, Victoria, Australia
Fashae OA, Olusola AO (2017) Landuse types within channel corridor and river channel morphology of RiverOna, Ibadan, Nigeria. Indones J Geogr 49(2):111–117
Fashae OA, Ayomanor R, Orimoogunje OOI (2017a) Landuse dynamics and surface water quality in a typical Urban Centre of South-Western. Analele Universităţii din Oradea, Seria Geografie, Nigeria
Fashae OA, Ayorinde HA, Olusola AO, Obateru RO (2019) Landuse and surface water quality in an emerging urban city. Appl Water Sci 9(2):25
Fashae OA, Ayomanor R, Orimoogunje OOI (2017b) Landuse dynamics and surface water quality in a typical Urban Centre of South-Western, Nigeria. Analele Universităţii din Oradea, Seria Geografie 27(1):98–107. (Return to ref 2017a in article)
Global Water Status; Available online: http://www.hnsslxh.cn/hnwr/f/view-eb90bc2539f141d681499e2299adb9f3-bca15aa45538471187ccb7533d1b8617.html
Grant SL, Tamason CC, Hoque BA, Jensen PK (2015) Drinking cholera: salinity levels and palatability of drinking water in coastal Bangladesh. Trop Med Int Health 20(4):455–61

Hammond D, Pryce AR (2007) Climate change impacts and water temperature. Environment Agency; Bristol, UK
Hao XP, Xia J, Wang R (2010) Influence of climate change on surface water environment. Hydrology 30:67–72
Headley TR, Tanner CC (2012) Constructed wetlands with flfloating emergent macrophytes: an innovative stormwater treatment technology. Crit Rev Environ Sci Technol 42:2261–2310
Hoff H (2009) Global water resources and their management. Curr Opin Environ Sustain 1:141–147
http://mospi.nic.in/sites/default/files/publication_reports/Report_584_final_0.pdf
https://www.nap.edu/read/9595/chapter/13#230
https://www.unicef.org/media/media_19974.html
Huang CP, Chiang PC (2009) On climate change and sustainable water environment: impact and strategic adaptation. J Nanchang Univ 31:1–15
Ifabiyi IP (2000) (eds) Contemporary issue in environmental studies. Haytee Press and Publishing, Ilorin
IMD hydro-meteorology. IMD. 22 July 2020. Retrieved 22 July 2020
Kim Y, Kong I, Park H, Kim HJ, Kim IJ, Um MJ, Green PA, Vörösmarty CJ (2018) Assessment of regional threats to human water security adopting the global framework: a case study in South Korea. Sci Total Environ 637:1413–1422
Krishan G, Bisht M, Ghosh NC, Prasad G (2020) Groundwater Salinity in Northwestern Region of India: A Critical Appraisal
Liu J, Zhang X, Xia J, Wu S, She D, Zou L (2016) Characterizing and explaining spatiotemporal variation of water quality in a highly disturbed river by multi-statistical techniques
Mancuso G, Langone M, Laezza M, Andreottola G (2016) Decolourization of Rhodamine B: a swirling jet-induced cavitation combined with NaOCl. Ultrason Sonochem 32(18–30):9
Mancuso G, Langone M, Andreottola G (2017) A swirling jet-induced cavitation to increase activated sludge solubilisation and aerobic sludge biodegradability. Ultrason Sonochem 35(489–501):10
Mancuso G, Langone M, Andreottola G, Bruni L (2019) Effects of hydrodynamic cavitation, low-level thermal and low-level alkaline pre-treatments on sludge solubilisation. Ultrason Sonochem 59:104750
Mathuriya AS, Yakhmi JV (2014) Microbial fuel cells–applications for generation of electrical power and beyond. Crit Rev Microbiol 42(1):127–143
Misra AK, Mishra A (2007) Escalation of salinity levels in the quaternary aquifers of the Ganga alluvial plain, India. Environ Geol 53:47–56
Multiple Indicator Cluster Survey 2012–13: Final Report. BBS/UNICEF. Dhaka: Bangladesh Bureau of Statistics/UNICEF, 2015
NITI Aayog (2018). Composite water management index: a tool for water management. Government of India in association with the Ministry of Water Resources, the Ministry of Drinking Water and Sanitation, and the Ministry of Rural Development
Obotey Ezugbe E, Rathilal S (2020) Membrane technologies in wastewater treatment: a review. Membranes 10(5):89
Olusola A, Adeyeye O, Durowoju O (2017) Groundwater: quality levels and human exposure, SW Nigeria. J Environ Geogr 10(1–2)
Padowski JC (2019) Freshwater: the importance of freshwater for domestic use
Quist-Jensen CA, Macedonio F, Drioli E (2015) Membrane technology for water production in agriculture: desalination and wastewater reuse. Desalination 364:17–32. (CrossRef)
Ravenscroft P, Brammer H, Richards K (2009) Arsenic pollution: a global synthesis. Wiley
Rodell M, Famiglietti JS, Wiese DN, Reager JT, Beaudoing HK, Landerer FW, Lo MH (2018) Emerging trends in global freshwater availability. Nature 557:651–659
Rogers P (2000) Landuse change in developing countries: comparing India and China. Harvard University, Cambridge, DEAS/HUCE

Khan AE, Scheelbeek PF, Shilpi AB, Chan Q, Mojumder SK, Rahman A, Haines A, Vineis P (2014) Salinity in drinking water and the risk of (pre) eclampsia and gestational hypertension in coastal Bangladesh: a case-control study. PLoS One 9(9):e108715
Salama RB, Otto CJ, Fitzpatrick RW (1999) Contributions of groundwater conditions to soil and water salinization. Hydrogeol J 7:46–64
Samal K, Dash RR, Bhunia P (2018) Development and optimization of two stage macrophyte assisted vermifiltration for the treatment of dairy wastewater. Sci Total Environ 645:156–169
Samal K, Kar S, Trivedi S (2019) Ecological floating bed (EFB) for decontamination of polluted water bodies: design, mechanism and performance. J Environ Manage 251:109550
Samal K, Kar S, Trivedi S, Upadhyay S (2021) Assessing the impact of vegetation coverage ratio in a floating water treatment bed of Pistia stratiotes. SN Appl Sci 3:120
Santoro C, Arbizzani C, Erable B, Ieropoulos I (2017) Microbial fuel cells: From fundamentals to applications. A review. J Power Sources 356:225–244
Shukla SP, Kumar S, Gita S, Bharti VS, Kumar K, Bhuvaneswari GR (2018) Recent technologies for wastewater treatment: a brief review. Wastewater Manage Through Aquaculture 225–234
Singh J, Kothari M (2004) Waterlogging and salinity studies for the irrigated tracts of South West Punjab using satellite remote sensing and geographical information system. M.Sc. Thesis. Maharana Pratap University of Agriculture and Technology, Udaipur
Sivakumar M, Pandit AB (2002) Wastewater treatment: a novel energy efficient hydrodynamic cavitational technique. Ultrason Sonochem 9:123–131
Smith M, Cross K, Paden M, and Laban P (2016) Spring—managing groundwater sustainably. Gland, Switzerland: International Union for conservation of nature (IUCN)
Song XM, Zhang JY, Zhan CS, Liu CZ (2018) Review of impacts of climate change and human activities on water cycle. J Hydraul Eng 7:779–790
Speth TF, Summers RS, Gusses AM (1998) Nanofiltration Foulants from a Treated Surface Water. Environ Sci Technol 32:3612–3617
Stoquart C, Servais P, Bérubé PR, Barbeau B (2012) Hybrid Membrane Processes using activated carbon treatment for drinking water: A review. J Membr Sci 411–412:1–12
Suenaga T, Nishimura M, Yoshino H, Kato H, Nonokuchi M, Fujii T et al (2015) High-pressure jet device for activated sludge reduction: feasibility of sludge solubilization. Biochem Eng J 100:1–8
Tyagi NK (1988) Managing salinity through conjunctive use of water resources. Ecol Model 40:11–24
Vörösmarty CJ, Mcintyre PB, Gessner MO, Dudgeon D, Prusevich A, Green P, Glidden S, Bunn SE, Sullivan CA, Reidy Liermann C, Davies PM (2010) Global threats to human water security and river biodiversity. Nature 467:555–561
Vymazal J (2007) Removal of nutrients in various types of constructed wetlands. Sci Total Environ 380:48–65
Wagner PD, Kumar S, Schneider K (2013) An assessment of landuse change impacts on the water resources of the Mula and Mutha Rivers catchment upstream of Pune. Hydrol Earth System, India
Wang X, Zhang F (2018) Effects of land use/cover on surface water pollution based on remote sensing and 3D-EEM fluorescence data in the Jinghe Oasis. Sci Rep 8(1):1–3
https://www.who.int/en/news-room/fact-sheets/detail/arsenic
Xia XH, Wu Q, Mou XL (2012) Advances in impacts of climate change on surface water quality. Adv Water Sci 23:124–133
Yazdi HR, Carver SM, Christy AD, Tuovinen OH (2008) Cathodic limitations in microbial fuel cells: An overview. Power Sources 180:683–694
Zhang CB, Liu WL, Han WJ, Guan M, Wang J, Liu SY, Ge Y, Chang J (2017) Responses of dissimilatory nitrate reduction to ammonium and denitrification to plant presence, plant species and species richness in simulated vertical flow constructed wetlands. Wetlands 37:109–122

Network Model for Sustainable and/or Resilient Integrated Stormwater Management of a Water Sensitive City—A Case Study

Lakshmi Raghu Nagendra Prasad Rentachintala, M. G. Muni Reddy, and Pranab Kumar Mohapatra

Abstract Management of stormwater in urban areas have become a challenge due to continuous increase of imperviousness for various requirements, climate change, removal of plantation, constant decay of existing stormwater infrastructure. A few of the challenges which impact stormwater management are in regard to water quantity, quality and change of climate. Sustainable Urban Drainage Systems (SUDS), Low Impact Development (LID), Best Management Practices (BMP), Water Sensitive Urban Design (WSUD) and Sponge City Programme are various efficient stormwater management practices in the world. In the present study, proposed Amaravati city of Andhra Pradesh, India is considered which is envisioned to be the pioneer Smart City of India and to perform as Water Sensitive City as well. This study aimed to develop an efficient stormwater network system by developing a network model using StormCAD software for the proposed Amaravati city. A stormwater network model is build up to carry a discharge of 23 m^3/s including climate change effect and any unanticipated future flows adopting the guidelines and recommendations of CPHEEO manual. Amaravati stormwater network system is designed as an underground gravity system with conduit as most efficient and economical rectangular box section with dimensions as 3.8 m × 2.5 m (rise). Various innovative and efficient stormwater management practices and/or measures are proposed as part of network development. The results obtained are used for further study on developing efficient, sustainable and/or resilient integrated stormwater management system for the study area i.e. proposed Amaravati city to perform as a Water Sensitive City for longer duration.

Keywords Stormwater management · Stormwater network · Runoff · Water sensitive city

L. R. N. P. Rentachintala (✉) · M. G. Muni Reddy
Department of Civil Engineering, A.U. College of Engineering (A), Andhra University, Visakhapatnam, Andhra Pradesh 530003, India

M. G. Muni Reddy
e-mail: dr.mgmreddy@andhrauniversity.edu.in

P. K. Mohapatra
Indian Institute of Technology Gandhinagar, Palaj, Gandhinagar, Gujarat 382355, India
e-mail: pranabm@iitgn.ac.in

B. B. Das et al. (eds.), *Recent Developments in Sustainable Infrastructure (ICRDSI-2020)—GEO-TRA-ENV-WRM*, Lecture Notes in Civil Engineering 207,
https://doi.org/10.1007/978-981-16-7509-6_16

1 Introduction

Stormwater management for an urban area is one of the different facets associated with urban water management. For efficient stormwater management, Sustainable Urban Drainage Systems (SUDS), Low Impact Development (LID) practices with and without Best Management Practices (BMPs) are few practices being chosen as a preference for sustainable and/or resilient urban drainage systems in different regions of the world.

Avellaneda and Jefferson, 2020 assessed the sensitivity of various metrics of hydrology of a continuously rising dense rain garden SCM (Stormwater Control Measure) network using SWAT (Soil and Water Assessment Tool) model. It was found that more than 20% of the impervious area has to be treated for the majority of the metrics of hydrology to alter considerably (Avellaneda and Jefferson, 2020). PySWMM was developed to offer a single framework to assist amending of hydrologic and network parameters (McDonnell et al. 2020). The impacts of climate change due to extreme events were examined using various AOGCMs (Atmospheric-Ocean General Circulation Models) for RCP (Representative Concentration Pathway) 2.6 and RCP8.5 scenarios (Roozbahani et al. 2020). It was found that sustainability of the UWS (urban stormwater system) was slightly more for the base period simulation than those under RCP scenarios (Roozbahani et al. 2020). A broad framework for analysis of risk in urban stormwater systems was provided using FAHP (Fuzzy Analytic Hierarchy Process), FSAW (Fuzzy Simple Additive Weighting) and FTOPSIS (Fuzzy Technique for Order of Preference by Similarity to Ideal Solution) approaches (Shariat et al. 2019). Multicriteria decision-making (MCDM) was carried to assess various options based on four criteria of sustainability for modelling of rainfall-runoff using AHP (Analytic Hierarchy Process) and PROMETHEE II (Preference-Ranking-Organization-Method for Enrichment-Evaluation) and found that Micro-tunnelling as the preferred option (Alhumaid et al. 2018). Structures of various pipe networks for stormwater in the urban environments were assessed and regression models were developed (Lee et al. 2018). A methodology was proposed to appraise the resilience of an urban water system and obtained results revealed that the concept would assist for the enhancement of thinking on resilience for decision making in water infrastructure for water-wiser cities (Makropoulos et al. 2018). A novel procedure of resilience and stochastic approach with an algorithm of multi objective optimization as part of a Copula-based Monte-Carlo framework for Urban Stormwater Drainage Systems (USDSs) was developed (Mohammadiun et al. 2018). Results revealed that the optimal strategies would contain a group of relief tunnels, bypass lines, and storage units for convincing performance with regard to improvement of resiliency of network (Mohammadiun et al. 2018). An integrated methodology for modelling of infrastructure networks was presented with a procedure on probabilistic approach with six-step to evaluate resilience (Guidotti et al. 2016). The results enumerated the functionality loss and the recovery process delay as WN (potable water distribution network) was dependent on the EPN (electric power network) (Guidotti et al. 2016). The index of system performance using the

curves of penalty and the equations was described (Tabesh et al. 2016). The evaluation of benefits of the application of recommended indices was carried (Tabesh et al. 2016). Review of contribution to green/pervious area to urban runoff and its impact on UWS (Urban Stormwater Systems) was performed (Berggren et al. 2013). The results indicated that changes in the infiltration capacity can impact on the urban area and its drainage system in terms of volume and hydraulic system performance (Berggren et al. 2013). A method was recommended to manage network of urban water with controllers of simple nature by integrating SWMM5 (Stormwater Management Model) and Scilab (Degrave et al. 2013). It was suggested to adopt the mixed control approach for affirming the advantages of the local upstream control and the distant downstream control (Degrave et al. 2013). The Model for Urban Stormwater Improvement Conceptualisation (MUSIC) was developed on flows of stormwater and pollution (Dotto et al. 2011). It was found that the MUSIC model was very sensitive to EIF (Effective Impervious Fraction) (Dotto et al. 2011).

1.1 Study Area

Amaravati city of newly formed Andhra Pradesh state, India was chosen as the study area. Amaravati city is located on the bank of Krishna river in Guntur district. Proposed Amaravati city area is 217.50 km^2 and is located at 16.51° N latitude and 80.52° E longitude. The city area is proposed to make up from agricultural lands from 29 number of existing villages and part of 2 number of towns belong to various mandals of Guntur district. This proposed Amaravati city has been envisaged to be the pioneer among various Smart Cities of India and to be efficient Water Sensitive City for number of decades.

Study area map i.e. detailed master plan of Amaravati city is being considered for this research study as provided/available from AP CRDA/AMRDA web portal. This study area master plan map is presented in Fig. 1 for ready reference.

2 Methodology

Stormwater network model is developed using StormCAD software for the study area. Also, various specifications and recommendations are adapted from CPHEEO (Central Public Health and Environmental Engineering Organisation) manual on stormwater drainage systems.

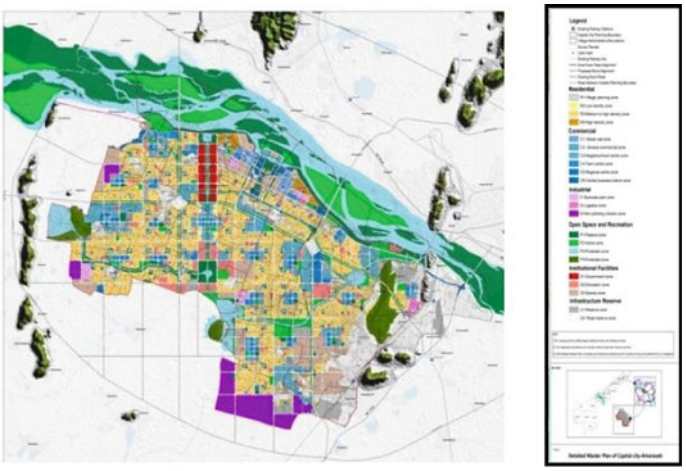

Fig. 1 Detailed master plan of Amaravati city. *Source* AP CRDA/AMRDA

2.1 Development of Amaravati StormCAD Model

Amaravati StormCAD model has been developed to provide stormwater network to proposed Amaravati city as per CPHEEO (Central Public Health and Environmental Engineering Organisation) manual on stormwater drainage systems, August, 2019, prevailing practices, innovative measures and recommendations. This StormCAD network model has designed to convey peak flow through proposed network and discharges stormflow into Krishna river in the vicinity through proposed outlet at Undavalli village and near Prakasam barrage, Vijayawada.

The peak flow which can be allowed through the network is considered as per Cl.4.4.1.3 of CPHEEO Manual on stormwater drainage systems i.e.

$$Q_p = 10\,C\,I\,A \tag{1}$$

where, Q_p: Peak flow at the point of design, m^3/h, C: Runoff coefficient, dimensionless, I: Average rainfall intensity should be taken for the duration of rainfall equal to the time of concentration, mm/h, A: Catchment area, hectares.

The catchment is divided into number of sub-catchments. The division of number of sub-catchments is made as per SWAT model automatic catchment delineation criteria. Based on the specified sub-catchment delineation criteria, area of each sub-catchment is obtained. Runoff coefficient is calculated as the ratio between average annual runoff and average annual precipitation. These hydrologic parameters values are considered from hydrologic cycle diagram for the period of simulation from SWAT model. Time of concentration of flow through each sub-catchment is arrived by finding the distance and time taken by hydraulically remote point to reach the outlet of that particular sub-catchment. Minimum limiting velocity is considered as

0.8 m/s as specified in Table 3.9 of CPHEEO manual on sewerage and sewage treatment for minimum velocity to be ensured in gravity sewers. Maximum velocity is considered as 3 m/s as per Table 5.2 of CPHEEO manual on stormwater drainage systems. Return period of 5 years is considered as per Table 4.1 of CPHEEO manual on stormwater drainage systems for various types of urban catchments. Average rainfall intensity for each sub-catchment is considered for the rainfall which persists up to the duration equal to time of concentration. Average rainfall intensity for each sub-catchment is considered *as average maximum daily rainfall* corresponding to recommended design return period i.e. for 5 years return period as per CPHEEO manual on stormwater drainage systems. The same procedure is repeated for each sub-catchment and peak flow is estimated from each sub-catchment as per Eq. (1). Then, total peak runoff from entire catchment is determined as sum of peak runoff from all sub-catchments. The effect of climate change on rainfall and runoff for the projected period i.e. *for next 30 years is assessed in a different study; it is found as 1.5% on precipitation for 30 years and thus on runoff and also taken into account on peak runoff*. Thus, total peak runoff from entire catchment including climate change effect is determined. This total peak runoff after rounding up is considered as peak flow through stormwater network. RCC box section is considered as conduit section to convey the designed total peak flow. For each conduit of the network, velocity and discharge of flow are obtained from the model and verified to meet/satisfy requirements as per CPHEEO manual on stormwater drainage systems. Slope of each conduit is considered with in 1 in 1000 to 1 in 2000. Cover for each conduit from its crown/top is adopted as 200 mm from existing ground surface at that conduit location. However, to meet velocity and flow requirements, no cover is allowed at few conduit locations which are subject to thickness check as per structural requirements. Also, deep covers up to 15 m is allowed to meet velocity and flow requirements at very few conduit locations as existing ground is abruptly and largely varying/falling at which conduit/box thickness is subject to satisfy structural requirements to take large amount of overburden load and distribution of load from above lying soil. Stormwater network has modelled as an underground gravity flow system. Design Percent Full (%) which is the percent of depth to arrive design capacity is adopted as 80%. Box type manhole of 2.5 m (Length) $\times$ 4.2 m (Width) with a bolted cover is adopted at and as a junction of two conduits and also at start and stop of each conduit. Absolute head loss method is adopted at each manhole with a minimum head loss of 0.1 m.

3 Hydraulic Computations of Design Discharge

Considering daily averaged precipitation data as Tulluru point data (Source: POWER LARC NASA) at latitude 16.53° N and longitude 80.47° E as majority of the considered study area belongs to Tulluru mandal (Table 1).

Thus, Average maximum daily rainfall = 89.41 mm/day = 3.73 mm/h.

Table 1 Maximum daily rainfall for 5-year return period

Start date	End date	Daily rainfall (mm/day)	Start date	End date	Daily rainfall (mm/day)
03-Jan-1981	02-Jan-1986	57.25	03-Jan-2001	02-Jan-2006	73.11
03-Jan-1986	02-Jan-1991	107.24	03-Jan-2006	02-Jan-2011	132.67
03-Jan-1991	02-Jan-1996	97.53	03-Jan-2011	02-Jan-2016	64.35
03-Jan-1996	02-Jan-2001	108.34	03-Jan-2016	25-Feb-2020	74.8

Table 2 Peak flow computations

Sub-basin	Sub-basin area, **A**, km^2	Distance of outlet from hydraulically remote point from SWAT Model (m)	Time taken for the remote point to reach outlet, t_c (s)	Time taken for the remote point to reach outlet, t_c (min)	Intensity of rainfall corresponding to t_c, **I**, mm/h	Peak flow = 10CIA, m^3/h	Peak flow = 10CIA, m^3/s
1	2.222	2025	2531.25	42.19	2.62	2913.77	0.81
2	17.47	945	1181.25	19.69	1.22	10,690.82	2.97
3	1.729	2385	2981.25	49.69	3.09	2670.36	0.74
4	14.88	1185	1481.25	24.69	1.53	11,418.46	3.17
5	11.87	2235	2793.75	46.56	2.89	17,179.66	4.77
6	1.773	1680	2100	35.00	2.18	1928.88	0.54
7	5.346	233	290.625	4.84	0.30	804.89	0.22
8	8.446	1770	2212.5	36.88	2.29	9680.79	2.69
9	2.754	2198	2746.875	45.78	2.85	3919.04	1.09
10	1.957	2325	2906.25	48.44	3.01	2946.46	0.82
11	3.565	4193	5240.625	87.34	5.43	9678.74	2.69

Considering Eq. (1) for peak flow computation, runoff coefficient from SWAT model, $\mathbf{C} = 0.5$. For minimum velocity of 0.8 m/s, considering sub-basin details from Amravati SWAT model (Table 2).

Therefore, Total peak flow, $Q_p = 20.51\ m^3/s$.

4 Design of Conduit Section [As box section]

Consider, conduit section as rectangular box section.

For *most efficient/economical rectangular* section,

$$\text{Bed width, } b = 2 \times \text{depth of flow, } d \tag{2}$$

$$\text{Hydraulic mean radius, } R = \frac{d}{2} \tag{3}$$

Assume, Bed width of the rectangular channel, b = 3.8 m.

Depth of flow, d = $\frac{b}{2} = \frac{3.8}{2} = 1.9$ m.

Assume, Slope of the channel, S = 1 in 950 = $\frac{1}{950} = 0.001$.

As per Table 5.1 of CPHEEO Manual on Stormwater Drainage Systems, Aug 2019, Manning's N for Spun concrete pipes (RCC & PSC) with S/S Joints (Design value) = 0.011.

For most efficient/economical section, Hydraulic mean radius, R = $\frac{d}{2} = \frac{1.9}{2} =$ 0.985 m.

Using Manning's Equation, Velocity of flow, V = $\frac{1}{N} R^{2/3} S^{1/2}$

$$V = 2.85 \text{ m/s} \tag{4}$$

Discharge carrying capacity of the rectangular channel, Q, m^3/s = A × V = 7.22 × 2.85 = 20.58 m^3/s > Discharge required = 20.51 m^3/s **OK**.

Thus, provide, a *most efficient* rectangular channel as box section with dimensions as,

Bed width, b = 3.8 m, Depth of flow, d = 1.9 m, Slope, S = $\frac{1}{950}$, and Free board = 0.6 m.

5 Amaravati Stormwater Network Model

Amaravati stormwater network model has developed using BENTLEY **StormCAD** software CONNECT Update2 10.02.03.03 version.

Considered, 10% additional discharge *to accommodate unanticipated flows including climate change effect*, Design discharge = 1.1 × 20.51 m^3/s = 22.56 $m^3/s \approx 23$ m^3/s = 23,000 l/s.

Design Parameters for each conduit [Manual on Stormwater Drainage Systems, CPHEEO, August, 2019 and IRC: 6-2016 Section-II].

Considered, Design Percent Full (%) = 80%, Velocity = 0.8–3 m/s, Section type as Box.

Material as Concrete [Steel Forms] [**RCC**], Rise = 2.5 m [Depth of flow = 1.9 m, free board = 0.6 m].

Span = 3.8 m [Modified at certain conduit locations i.e. CO_2 (4.2 m), CO18 (4.2 m), CO44 (4.0 m) and CO167 (4.2 m) to satisfy velocity and flow requirements], Cover = 20 cm.

Wall thickness = 72 cm, considering maximum depth of invert from existing ground surface and IRC Class AA tracked vehicle loading, Manning's [n/N] = 0.011.

Table 3 Range of cover

Range	Cover (start) (m)	Cover (stop) (m)
Minimum (m)	0.2	0.2
Maximum (m)	14.39	9.28

Note As per CPHEEO Manual on Stormwater Drainage Systems, CPHEEO, Aug 2019, cover is defined as the distance from the outside top of the pipe to the final grade of the ground surface and *minimum cover to provide is 0.2 m for RCC box drains*

Design Parameters for each manhole

Considered, Section as Box Type, Length = 2.5 m, Width = 4.2 m.

Details of developed Amaravati network model are, number of conduits = 167, number of manholes = 167 and total length of network = 145.59 km (Table 3).

Outfall [Discharge Point]: Outfall is proposed to locate at a position about 1 km from Prakasam Barrage, Vijayawada, Andhra Pradesh and discharging stormwater which is considered to flow through the being developed network into the Krishna river in the vicinity. The type of boundary condition of outfall is considered as *free outfall*. Position of outfall is proposed at an invert level of + 21.30 m. The section of the conduit conveying stormwater towards the proposed outfall is partly above the existing ground level in the vicinity such that the invert [discharging level] may be higher than normal flow level of Krishna river.

6 Various Other Components/Considerations Criteria for Efficient and Sustainable and/or Resilient Integrated Stormwater Management

Proposed Alignment of Stormwater Network: Stormwater network needs to be aligned at the side of a road or a high ground so that any stormwater after falling on the ground flows towards the nearby conduit of the network through suitable inlets and gutter system (Fig. 2).

As per Manual on Stormwater Drainage Systems, CPHEEO, August, 2019. Outfall Structure: Adequate protection mechanism should be provided to check backflow of water in the outfall drain. Cascading and apron structure if necessary may be incorporated in the Outfall Structure System.

Typical drawing of outlet structure for river/streams is given as shown in Fig. 3.

The back flow control systems, flap gates and flood gates are to be used whenever necessary based on flow conditions in the water body which receives the flow.

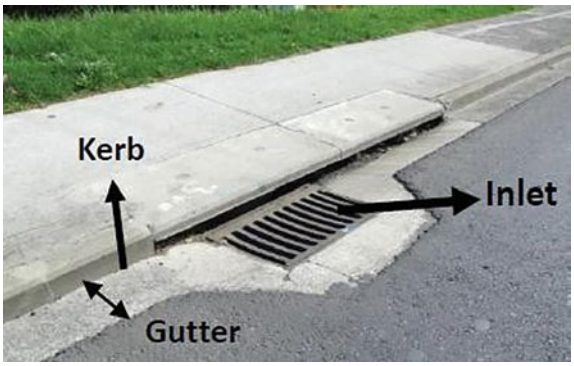

Fig. 2 Inlet and gutter system. *Source* Manual on Stormwater Drainage Systems, CPHEEO, August, 2019)

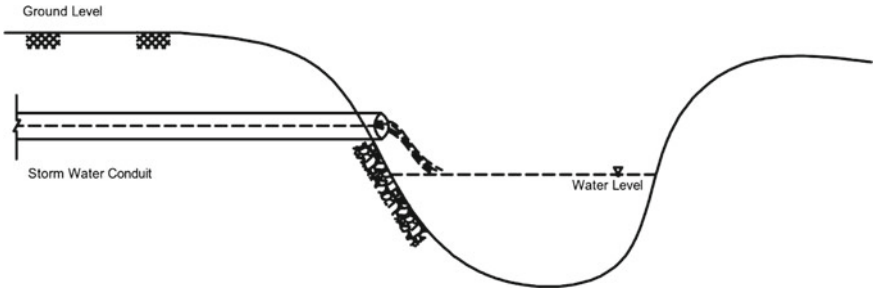

Fig. 3 Stormwater conduit outfall. *Source* Manual on Stormwater Drainage Systems, CPHEEO, August, 2019

7 Conclusions and Recommendations

Following are the various conclusions from the present stormwater network model development of the considered study area i.e. proposed Amaravati city.

Amaravati stormwater network model is designed for a discharge of 23 m^3/s with 10% additional discharge *to accommodate unanticipated flows including climate change effect*.

A most efficient rectangular channel as box section with dimensions as, bed width = 3.8 m, depth of flow = 1.9 m, slope = $\frac{1}{950}$ with a free board = 0.6 m is proposed to adopt for stormwater network of proposed Amaravati city, Andhra Pradesh state, India.

Amaravati stormwater network model contains number of conduits = 167, number of manholes = 167 and total length of network = 145.59 km.

Stormwater which may flow on the road and adjacent to the road may be allowed to flow into the network conduit in the proximity through proper inlet and gutter system.

Suitable outfall arrangement needs to be provided with backflow control system with gates.

During the flood flow to Krishna river in the vicinity with HFL (High Flood Level) exceeds proposed invert of outfall i.e. + 21.30 m of the developed stormwater network, proper pumping arrangements are to be provided to discharge total peak flow through the network to a d/s discharge point where flood flow in the Krishna river is much lower than invert of discharging rising main as per Manual on Stormwater Drainage Systems, CPHEEO, August, 2019 guidelines and/or recommendations.

Total peak flow through Amaravati stormwater developed network would be allowed to discharge in to Krishna river in the vicinity only when there is normal flow in the river.

Although various discharge options proposed as discussed above, it is highly recommended that if there is even flow higher than normal flow in the Krishna river, any amount of flow through proposed network has to be discharged or diverted into the proposed canal system and/or Low Impact Development [LID] controls with Best management Practices [BMPs] which will make stormwater management of proposed Amaravati city as sustainable and/or resilient and ensures the planned city as Water Sensitive City.

The proposed stormwater network model of proposed Amaravati city is useful and necessary to provide efficient stormwater management which will craft the considered proposed city to perform as a Water Sensitive City for longer duration.

References

Alhumaid M et al (2018) Sustainability evaluation framework of urban stormwater drainage options for arid environments using hydraulic modeling and multicriteria decision-making. Water 10(581):1–21

Avellaneda PM, Jefferson AJ (2020) Sensitivity of streamflow metrics to infiltration-based stormwater management networks. Water Resour Res 56:1–18

Berggren K et al (2013) Sensitivity of urban stormwater systems to runoff from green/pervious areas in a changing climate. In: Thematic conference, Novatech

CPHEEO "Engineering" (2013) Manual on sewerage and sewage treatment systems, 3rd edn.

CPHEEO "Engineering Design" (2019) Manual on storm water drainage systems, Part-A, vol I, 1st edn.

Degrave R, Schoorens J, Litrico X (2013) Real-time control of a small urban stormwater network. In: 10th IEEE international conference on networking, sensing and control (ICNSC), Evry, France, pp 526–531

Dotto CBS, Deletic A, McCarthy DT, Fletcher TD (2011) Calibration and sensitivity analysis of urban drainage models: MUSIC rainfall/runoff module and a simple stormwater quality model. Aust J Water Resour 15(1):85–94

Guidotti R et al (2016) Modeling the resilience of critical infrastructure: the role of network dependencies. Sustain Resilient Infrastr 1(3–4):153–168

IRC: 6 "Standard specifications and code of practice for Road bridges" Section-II, Loads and load combinations (seventh revision) (2016)

Lee J et al (2018) Evaluation of the structure of urban stormwater pipe network using drainage density. Water 10(1444):1–11

Makropoulos C et al (2018) A resilience assessment method for urban water systems. Urban Water J 15(4):316–328

McDonnell BE et al (2020) PySWMM: the Python interface to stormwater management model (SWMM). J Open Source Softw 5(52):2292

Mohammadiun S, Yazdi J, Salehi Neyshabouri SAA, Sadiq R (2018) Development of a stochastic framework to design/rehabilitate urban stormwater drainage systems based on a resilient approach. Urban Water J 15(2):167–176

Roozbahani A, Behzadi P, Bavani AM (2020) Analysis of performance criteria and sustainability index in urban stormwater systems under the impacts of climate change. J Clean Prod 271:1–12

Shariat R, Roozbahani A, Ebrahimian A (2019) Risk analysis of urban stormwater infrastructure systems using fuzzy spatial multi-criteria decision making. Sci Total Environ 647:1468–1477

Tabesh M, Azari B, Rezaei HR (2016) Hydraulic performance assessment of stormwater networks. In: International conference on civil, architecture and disaster management (ICCADM-16) 17–18 Nov 2016, Hong Kong

Computation of Storage Capacity and Availability of Water in Irrigation Tanks Using Google Earth Engine

A. Abhishika Bilwani, B. Dhana Lakshmi, and Rambabu Palaka

Abstract Storage capacity of water bodies are useful for understanding the availability of water resources for the crop season in any Agriculture Watershed. Surface water bodies are the major source for Telangana State for the sustainable crop production. Estimation of surface water includes water spread area; volume of water stored in water body. The required reservoir water level and volume of water stored can be acquired from India-WRIS for Large Reservoirs and Dams. However, it is a big challenge to know Storage Capacity and Availability of water for most of the Small Irrigation Tanks which are the major source of water for Irrigation in Telangana State. In this study, an attempt is made to Compute Storage Capacity of Small Irrigation Tanks using Google Earth Engine. Google Earth Engine is a cloud computing platform through which geospatial analysis can be performed without downloading Satellite Data. SRTM (Shuttle Radar Topography Mission) DEM is used to estimate the Storage Capacity of Tanks along with Global Surface Water (GSW) Dataset covers the period 1984–2019. The maximum rainfall occurrence and maximum surface area is considered from GSW Dataset to Compute Storage Capacity of Tanks. Sentinel-1 Multispectral Satellite Data is useful to prepare NDWI Maps for Cloud-Free period. During storm months the optical far off detecting perceptions over semi-bone-dry Indian sub-landmass and deterred because of cover over. At this time Sentinel-1 Synthetic Aperture Radar (SAR) data is helpful to estimate the availability of water in surface water bodies. In this study, we have used both Sentinel-1 and Sentinel-2 satellite data to estimate the availability of water during Kharif Crop Season (June–September, 2020).

Keywords Storage capacity of irrigation tank · Water availability in irrigation tanks · Google earth engine · Sentinel satellite data · SRTM DEM

A. Abhishika Bilwani (✉) · B. Dhana Lakshmi · R. Palaka
Department of Civil Engineering, B.V. Raju Institute of Technology, Narsapur, Medak, India

B. B. Das et al. (eds.), *Recent Developments in Sustainable Infrastructure (ICRDSI-2020)—GEO-TRA-ENV-WRM*, Lecture Notes in Civil Engineering 207,
https://doi.org/10.1007/978-981-16-7509-6_17

1 Introduction

As we know that Surface water bodies are the major source for irrigation everywhere for sustainable crop production. Water spread area; volume of water stored in a water body is much important parameters for availability of water resources for the crop season on surface water bodies. Tanks and Lakes occupy a small part of the Earth's land surface, they are vital elements of the hydrological cycles.

Agriculture is an important filed of the national economy of Telangana. It added 13% to the income of the state. Nearly 56% of population in the state is depending on agriculture. It has the net cropped area of 5.12 million hectares and almost 56% of the area is irrigated by different sources of irrigation (Kamraju et al. 2017).

By using empirical and numerical techniques estimation of reservoir capacity is done which requires large amounts of data and the results are still less accurate. By using Remote Sensing, it becomes very convenient to estimate reservoir capacity and availability of water. Remote sensing techniques are superior to the other conventional techniques, as it provides data availability over a long-time span with a wide spectral range. Satellite data is being used since long time to calculate the water-spread area for different elevations of a reservoir, which as a result in used to estimate the capacity of the reservoir. A wide range of satellites are capturing information at various spatial, spectral, temporal and radiometric resolutions. Near real time satellite imagery helps in identifying water availability in lakes and ponds to take proper decision. In rainy season the optical remote sensing observations over Indian sub-continent are obstructed due to cloud cover. Synthetic Aperture Radar (SAR) is a useful alternative for monitoring of the surface water bodies even there is cloud cover. Sentinel-1C satellite data with spatial resolution of 10 m and temporal resolution of 12 days is highly useful to monitor the changes in water spread area of Irrigation tanks.

Detailed information and improvements in the distribution of surface water are of great importance for the management of water and the conservation of biodiversity. Landsat-based assessments of surface water, such as the Global Surface Water (GSW) dataset developed by the European Commission Joint Research Centre (JRC) is useful to know the maximum extent of water spread area. GSW dataset contains guides of the area and worldly appropriation of surface water from 1984 to 2019 and gives measurements on the degree and change of those water surfaces (Li et al. 2019).

Digital elevation models (DEMs) are crucial in estimation of reservoir capacity as DEM data reflects the actual topographic characteristics. DEMs are records that contain pixels with each point or pixel having an rise esteem. DEM data from a publicly accessible satellite, Shuttle Radar Topography Mission (SRTM) is highly useful and available freely at Google Earth Engine. The Google Earth Engine (GEE) is a framework intended to empower petabyte-scale, logical investigation and perception geospatial datasets. Earth Engine gives a combined climate including a gigantic information co-situated with a huge number of PCs for investigation.

2 Study Area

Our main aim is to estimate reservoir capacity and availability of water and how it would be varying during Kharif Season (June to October) in Irrigation Tank located at Narsapur village, Medak District, Telangana State, India. Narsapur Tank (Rairao Cheruvu) is one of the main sources for Irrigation in Narsapur Village. This tank is monitored and maintained by the Dept. of Irrigation & Command Area Development, Govt. of Telangana State.

Salient Features of Narsapur Tank (as per I&CAD)

- Catchment Area: 22.68 km^2
- Capacity at F.T.L.: 92.92 M cft
- Water Spread Area: 0.91 M m^2
- Length of Bund: 413 m
- Full Tank Level (FTL): + 556.05 m
- Sill Level: 1 Sluice @ Ch. 22.50, + 548.812 m (Fig. 1).

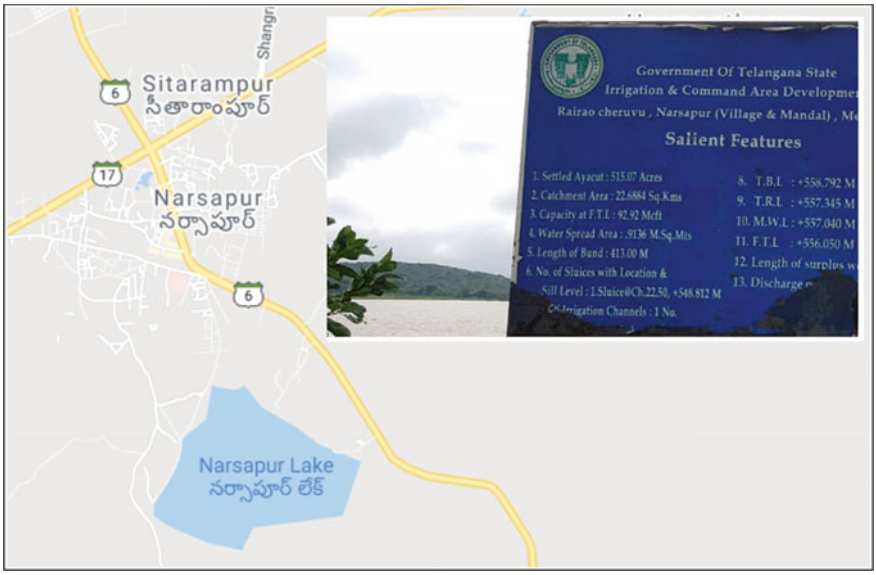

Fig. 1 Location map of Narsapur Tank (Rairao Cheruvu) (78.28536° E, 17.72608° N)

3 Methodology

3.1 Google Earth Engine (GEE) Platform

A cloud computing environment for satellite data analysis that provides free access for the data from various institutions such as the National Aeronautics and Space Administration (NASA) and the European Space Agency (ESA). GEE enable us to handle large volume datasets of remote sensing and other ancillary datasets in a cloud computing platform without download into local machine. A web-based IDE for the Earth Engine (code.earthengine.google.com) using JavaScript API is used in this study.

3.2 Dataset

3.2.1 Satellite Data

Sentinel-1 SAR

This collection contains all of the C-band Synthetic Aperture Radar Ground Range Detected (GRD) scenes. Each scene has one of 3 goals (10, 25, or 40 m), 4 band blends (comparing to scene polarization) and 3 instrument modes. The return to season of this satellite is 12 days.

In this study, SAR Data with a 10 m spatial resolution with VV polarization is used for change detection in Water Spread Area for the Kharif Crop Season (June to October) as most of the time during this period is cloudy.

Sentinel-2B

Sentinel-2 is a multi-unearthly, high-goal, wide-area imaging mission that upholds Copernicus land checking contemplates, including vegetation, soil and water spread observing. Sentinel-2B satellite was launched on 7 March 2017. When two sensors are operated simultaneously, the mission's revisit time is about 5 days, while about 10 days with one satellite in operation.

In this study, Normalized Difference Water Index (NDWI) is used to differentiate water from the dry land. Water bodies have a low radiation and strong absorbability in the noticeable infrared frequencies range.

$$NDVI = \frac{(NIR - RED)}{(NIR + RED)}$$

3.2.2 Global Surface Water (GSW) Dataset

This dataset contains guides of the area and fleeting appropriation of surface water from 1984 to 2019 and gives measurements on the degree and change of those water surfaces. These data were produced using 4,185,439 scenes acquired between 16 March 1984 and 31 December 2019 from Landsat 5, 7, and 8. Using an expert method, each pixel was individually categorised into water/non-water and the results were collated into a monthly background for the entire time span and two epochs (1984–1999, 2000–2019) for identification of transition. This product for mapping layers consists of 1 image with 7 bands in it. In this study, GSW data with 1% of accuracy, the frequency with which water was present, is used to map the maximum probable extent of water spread area of Narsapur tank.

3.2.3 SRTM DEM Data

In this study, The Shuttle Radar Topography Mission (SRTM) digital elevation dataset of 30 m spatial resolution is used which is freely accessible at Google Earth Engine. SRTM rise information offer overall inclusion of void filled information at a goal of 1 curve second (30 m) and flexibly open dispersion of this high goal worldwide dataset. The CartoDEM by National Remote Sensing Centre (NRSC), Hyderabad, is also another DEM data available at free of cost but due to non-availability Google Earth Engine, SRTM DEM is used for analysis in this study.

3.2.4 Analysis

We analysed water spread status for the Narsapur Tank for four months i.e., Jul–Oct, 2020. First, Maximum Probable Extent of Water Spread is identified using Global Surface Water (GSW) dataset considering precipitation occurrence greater than or equal to 1%. Second, using SRTM DEM data, reservoir capacity is estimated for the extent derived from GSW dataset. Third, Sentinel-1B SAR data is used map the water spread extent for different time series. Finally, reservoir capacity and availability of water is computed using Google Earth Engine using JavaScript (Fig. 2).

4 Results and Discussion

Rainfall data from the nearby Automatic Weather Station (AWS Id: 10995) of the Narsapur Tank is collected for the period from 1st July 2020. The Cumulative Rainfall which is used into comparative study to understand the change in Water Spread Area is shown in Table 1.

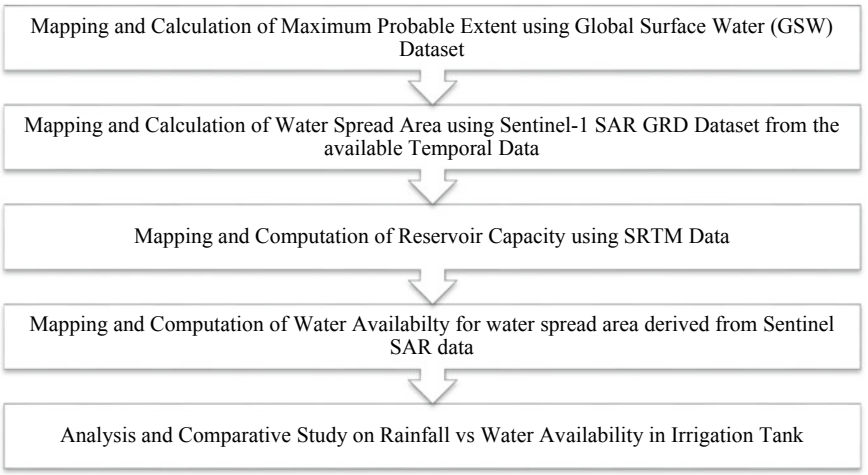

Fig. 2 Methodology

From the above Cumulative Rainfall Data, a chart for Rainfall versus Satellite Data Acquired Dates (Sentinel 1 SAR) is prepared to know the rainfall pattern nearby Narsapur Tank as shown in Fig. 3.

Using Google Earth Engine using JavaScript, Water Spread Area Maps for different time periods was created from the Sentinel 1 (SAR) data. From the maps shown Fig. 4, it is observed that there is no water in Narsapur Tank till 10-Aug-2020 and water accumulation is observed 12 ha (16.44% of Max. Water Spread Extent of 73 ha derived from Global Surface Water (GSW) dataset). And, water accumulation is increased gradually and observed the coverage is 95.89% on 21-Oct-2020.

The Elevation Map as shown in Fig. 5 is prepared from SRTM DEM Data for Narsapur Tank. It is observed that Tank Bottom Level is + 560 m where as actual Sill Level of reservoir is + 548.81 m. Similarly, Water Spread Top Elevations are extracted for different Satellite Dates to calculate the Water Spread Area and Storage Volume as shown in Table 2 and same is presented in Figs. 4, 5 and 6.

From the Storage Volume and Rainfall Data, it is observed that water accumulation is started only after 250 mm cumulative rainfall which might be due to initial abstractions like detention and retention of surface run-off after rainfall event. A comparison study on Storage Volume versus Cumulative Rainfall is shown in Table 3 and same is presented in Fig. 7.

5 Conclusions

SRTM DEM data is used to understand the topography of Irrigation Tank and to calculate its extent. From the DEM data, it is observed that Tank Bottom Elevation

Table 1 Rainfall data (AWS Id: 10995)

Rain date	No. of hours	Rain (mm)	Cumulative rainfall (mm)
02-Jul-20	3	8.8	8.8
04-Jul-20	6	14	22.8
05-Jul-20	3	1.5	24.3
06-Jul-20	4	1	25.3
09-Jul-20	2	2.3	27.6
10-Jul-20	5	3.5	31.1
12-Jul-20	1	2.3	33.4
14-Jul-20	7	6.5	39.9
15-Jul-20	9	45.5	85.4
20-Jul-20	1	0.5	85.9
21-Jul-20	2	12.3	98.2
22-Jul-20	1	0.5	98.7
23-Jul-20	8	21.5	120.2
24-Jul-20	1	0.3	120.5
28-Jul-20	3	1.5	122
30-Jul-20	2	69	191
31-Jul-20	4	12.8	203.8
03-Aug-20	4	7.3	211.1
04-Aug-20	2	0.8	211.9
05-Aug-20	1	8.5	220.4
06-Aug-20	1	0.5	220.9
07-Aug-20	1	0.5	221.4
08-Aug-20	1	0.3	221.7
09-Aug-20	5	13	234.7
10-Aug-20	13	15.8	250.5
11-Aug-20	1	0.3	250.8
12-Aug-20	4	12.3	263.1
13-Aug-20	18	34.5	297.6
14-Aug-20	5	8	305.6
15-Aug-20	21	29.2	334.8
16-Aug-20	22	26.5	361.3
17-Aug-20	9	10.8	372.1
18-Aug-20	3	9.5	381.6
19-Aug-20	11	17.3	398.9
20-Aug-20	14	43.8	442.7
21-Aug-20	4	16.5	459.2

(continued)

Table 1 (continued)

Rain date	No. of hours	Rain (mm)	Cumulative rainfall (mm)
27-Aug-20	8	81.8	541
28-Aug-20	2	5.5	546.5
09-Sep-20	3	26.5	573
10-Sep-20	1	1.8	574.8
11-Sep-20	4	1.7	576.5
12-Sep-20	3	4.8	581.3
13-Sep-20	9	26.8	608.1
14-Sep-20	9	34.8	642.9
15-Sep-20	7	6.8	649.7
16-Sep-20	8	39.3	689
17-Sep-20	2	2.5	691.5
19-Sep-20	3	12.3	703.8
20-Sep-20	8	61.2	765
25-Sep-20	8	61.5	826.5
26-Sep-20	12	54.8	881.3
27-Sep-20	1	0.2	881.5
28-Sep-20	1	0.8	882.3
29-Sep-20	1	2.5	884.8
30-Sep-20	1	0.3	885.1
11-Oct-2020	8	75.8	960.9
12-Oct-2020	3	1.2	962.1
13-Oct-2020	16	143.5	1105.6
14-Oct-2020	4	38	1143.6
15-Oct-2020	3	12.3	1155.9
17-Oct-2020	1	5.5	1161.4
18-Oct-2020	5	54.3	1215.7
19-Oct-2020	1	4.3	1220
20-Oct-2020	2	16.7	1236.7

is + 500 m which is 1.2 m above Sill Level of reservoir. In this study, the bed level of reservoir is assumed at 5 m below i.e., + 445 m to calculate the Dead Storage Capacity of Reservoir. The maximum storage volume including dead storage volume is calculated considering the SRTM DEM Elevation (+561 m) and Maximum Water Spread Extent (73 ha) derived from Global Surface Water dataset.

Sentinel-1 SAR data is found very useful for mapping and estimating Water Spread Area for Rainy season. Rainfall data from July is considered as it is observed that there is no impact or runoff occurred into tank till June-2020. Based on the analysis, it is observed that Water Storage Volume is increased from 1186 ML (20.61%) on

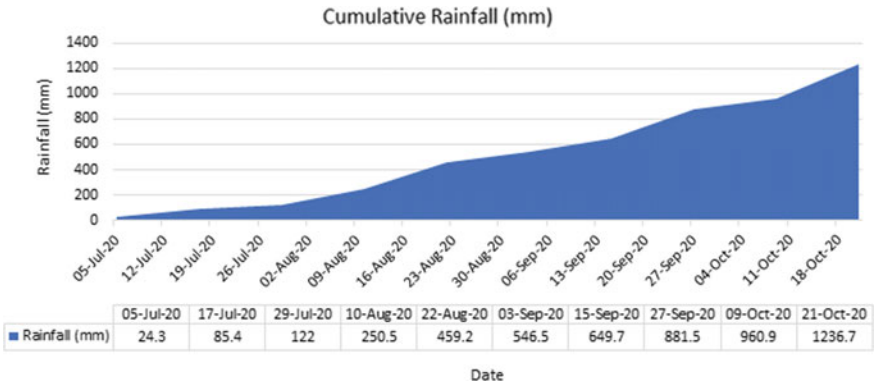

	05-Jul-20	17-Jul-20	29-Jul-20	10-Aug-20	22-Aug-20	03-Sep-20	15-Sep-20	27-Sep-20	09-Oct-20	21-Oct-20
Rainfall (mm)	24.3	85.4	122	250.5	459.2	546.5	649.7	881.5	960.9	1236.7

Fig. 3 Cumulative rainfall versus satellite data acquired dates

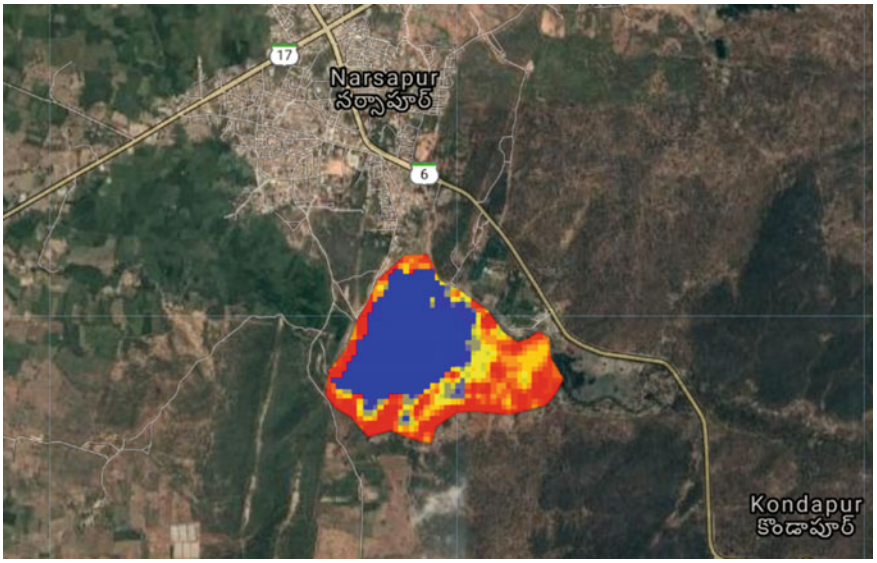

Fig. 4 Elevation map (SRTM DEM) (elevation ranges from + 550 m to + 560 m)

22-Aug-2020 to 5724 ML (99.46%) on 21-Oct-2020. Further, it is observed that the Irrigation Tank reached to its Full Tank Level at an Elevation of + 561 m. The rainfall-runoff pattern during the above period will be discussed in the future studies.

Fig. 5 Water spread area in different time periods. *Note* 1: Min. water spread area observed from Sentinel-1 SAR data on 22-Aug-2020. 2: water spread area observed from SRTM DEM. 3: Max. water spread area observed from Sentinel-1 SAR data on 21-Oct-2020

Table 2 Water spread area versus storage volume of water

Max. water spread area: 73 ha (max. tank level + 561 m)						
Date	Water spread area		Tank top level (m)	Volume (ML)		
	Hectares	%		Above + 550 m[a]	Below + 550 m[b]	Total
22-Aug-20	12	16.44	Below 550	123		123
03-Sep-20	26	35.62	551	255	1063	1318
15-Sep-20	23	31.51	551	229	1063	1292
27-Sep-20	51	69.86	558	3225	1063	4288
09-Oct-20	60	82.19	559	3861	1063	4924
21-Oct-20	70	95.89	560	4661	1063	5724

[a] Storage volume is calculated between tank bottom level observed from SRTM DEM data and top level observed from Sentinel-1 SAR data

[b] Storage volume is calculated between sill level (+445 m) and tank bottom level (+550 m) observed from SRTM DEM data

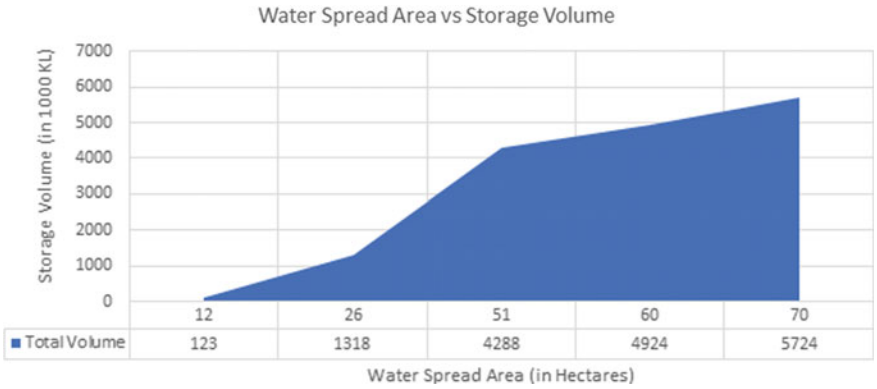

Fig. 6 Water spread area versus volume of water

Table 3 Cumulative rainfall versus volume of water

Max. water spread area: 73 ha, storage volume: 5755 ML			
Date	Rainfall (mm)	Storage volume (ML)	%
10-Aug-20	250.50	0	0.00
22-Aug-20	459.2	1186	20.61
03-Sep-20	546.5	1318	22.90
15-Sep-20	649.7	1292	22.45
27-Sep-20	881.5	4288	74.51
09-Oct-20	960.9	4924	85.56
21-Oct-20	1236.7	5724	99.46

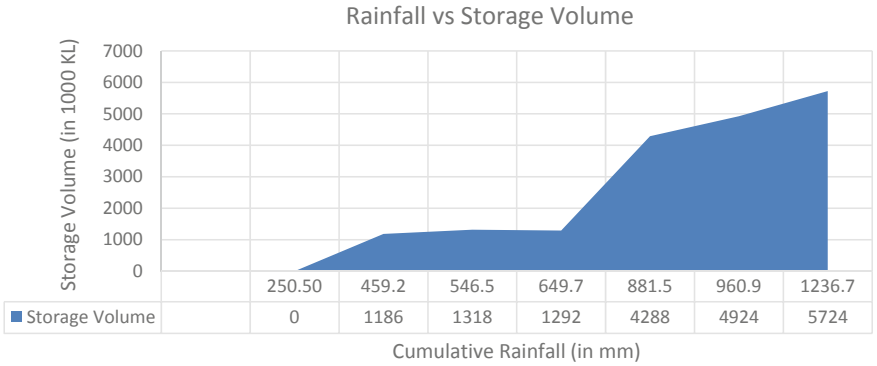

Fig. 7 Rainfall versus volume of water for the period Jul–Oct, 2020

Acknowledgements We would like to express our thanks to the Google Earth Engine (GEE) online forum for their invaluable assistance and inputs. We would also like to thanks "Spatial Thoughts" and "Open Geo Blog" for sharing the code used to Calculate Area and Storage Volume using Google Earth Engine using JavaScript.

References

Crespi M, Nascetti A, Ravanelli R (2020) Special issue information—Google Earth Engine and cloud computing platforms: methods and applications in big geo data science. https://www.mdpi.com/journal/remotesensing/special_issues/GEE_Methods_Applications

Kamraju M, Vani M, Anuradha T (2017) Crop diversification pattern: a case study of Telangana state. Int J Innov Sci Res Technol 2(5)

Li L, Skidmore A, Vrieling A, Wang T (2019) A new dense 18-year time series of surface water fraction estimates from MODIS for the Mediterranean region. Hydrol Earth Syst Sci 23:3037–3056

Mohite J, Sawant S, Pappula S (2019) Spatiotemporal surface water mapping using Sentinel-1 data for regional drought assessment. In: Proceedings of SPIE 11149. Remote sensing for agriculture, ecosystems, and hydrology, vol. XXI, p 1114905

Pekel J-F, Cottam A, Gorelick N, Belward AS (2016) High-resolution mapping of global surface water and its long-term changes. Nature 540:418–422

Yarrakula K, Deb D, Samanta B (2013) Comparative evaluation of Cartosat-1 and SRTM imageries for digital elevation modelling. Geo-spatial Inf Sci 16(2):75–82

Optimizing the Composting Process by Mixing Specific Organic Fractions of Municipal Solid Waste in a Reactor

B. R. Hiremath and Sudha Goel

Abstract Population explosion, rapid urbanization, and industrialization has led to the generation of huge amounts of solid waste. Of the MSW generated, about 50–60% is compostable organic matter. Composting is one of the best options for recycling and treatment of the organic fractions of municipal solid waste. Reactor-based composting was carried out using mixtures of Leaf Litter, Chana Dal, and the aqueous media, Dakshineshwar Ganga Water (DGW) was used to provide the optimum 60% moisture content. From the literature survey it was found that the C:N ratio less than 15 may be good for final compost product and hence the proportions of the three substrates were determined a priori to achieve a final C:N ratio of 10. This study provides an effective methodology for determining the rate and extent of biodegradation of individual OFMSW and how this knowledge can be used to optimize the composting process. The initial TOC of the reactor was 36.18 ± 0.12% and after 81 days of composting, it was reported as 31.08 ± 0.72%. Similar pattern was followed by C:N ratio. Total percent of nitrogen content increased due to decomposition of amino acids and proteins and mineralization of carbon. The initial content of Total Nitrogen in the reactor was reported as 3.7 ± 0.17% and at the last day of decomposition it was recorded as 4.41 ± 0.69. Various macro and micronutrients like, Total Phosphate, Total Potassium, Sodium, Calcium, Magnesium, and Manganese increased during the process of composting were also measured in the experiment.

Keywords Organic fraction · Tannin lignin · Mixed waste · Dakshineshwar Ganga Water · Mineral media

B. R. Hiremath (✉)
Civil Engineering Department, Basaveshwar Engineering College, Bagalkot, Karnataka, India

S. Goel
Civil Engineering Department, IIT Kharagpur, Kharagpur, West Bengal, India

B. B. Das et al. (eds.), *Recent Developments in Sustainable Infrastructure (ICRDSI-2020)—GEO-TRA-ENV-WRM*, Lecture Notes in Civil Engineering 207,
https://doi.org/10.1007/978-981-16-7509-6_18

1 Introduction

Even though MSW is a small part of the total SW generated, it is tremendously important in urban areas, especially in metropolitan cities because of the increase in population growth, migration of people from rural to urban areas, rapid urbanization and industrialization. Waste generation increases in proportion to the rise in population and urbanization. The generation of MSW is also directly proportionate to the population of the area of the city due to which bigger cities generate more waste. Understanding the composition of MSW by characterizing it is useful for developing sustainable MSW management strategies (Astrup et al. 2015; Medina-salas et al. 2019). The process of recycling is one of the best measures to reduce the burden on landfills (Fricke et al. 2005). Waste-to-energy (WTE) options like incineration or bio-fuel generation are attractive alternatives to landfilling. Composting is the most popular treatment method in India and has been promoted by many urban local bodies with some degree of success (Goel 2008; CPCB 2018).

By 2025, the generation of waste in Indian urban areas will be about 0.7 kg/person/day, which is about four times to six times greater than that in the year 1999 (Kumar and Samadder 2017). There are four major treatment and disposal methods in use in India: composting, which had 50% of the market share followed by anaerobic digestion with 30%, and pelletization (refuse-derived fuel) and landfilling with 10% (Palanichamy et al. 2002).

Organic fractions of MSW comprise of complex substrates which are broken down into intermediate and simpler compounds by microorganisms during composting. Due to the activities of various microbes and higher organisms, compounds of nitrogen and carbon are transformed into stable humic substances called compost (Paré et al. 1998).

For the design of efficient bioprocesses like composting, it is important to know the rate and extent of biodegradation of individual organic fractions of MSW. Very little work has been carried out on the biodegradation of lignin by a mixed microbial compost population (Tuomela et al. 2000). Leaf Litter contains cellulose, hemicellulose, and lignin in different proportions. Chana Dal, on the other hand, is high in protein and has fewer carbohydrates and lignin compared to the other substrates. Chana Dal is a common legume used in Indian food.

2 Materials and Methods

2.1 Sample Collection

Sal Leaf Litter (LL) was collected from the parking area in front of the Civil Engineering Department, IIT Kharagpur. Food waste take a lead role as an organic fraction of MSW and Cicer Arietinumb (Chana dal) is one of the most popular legume from the list of Indian dals. Chana Dal was collected from a grocery shop and powdered.

2.2 Reactor Substrates

The rate and extent of biodegradation of mixtures of LL, CD and water media Dakshineshwar Ganga Water (DGW) were measured in the present reactor study. After washing the LL clean, it was sun- dried and then pulverized to three sizes. The weights (dry) in each size fraction were then calculated. Solid waste particles in the first fraction had sizes ranging between 75 μm and 2.33 mm; the second fraction had sizes between 3 mm and 1 cm and the third fraction between 1 and 4 cm. Chana Dal was powdered like clay in a small grinder and the powder was used as sample and added to the mixture. Ganga water was collected from Ganga River at Dakshineshwar, Kolkata and was used for the Reactor.

2.3 Experimental Procedure

Total 7 kg of the mixture of Leaf Litter, Chana Dal and DGW was taken as substrates. Aeration was provided using a stirrer/agitator rotating at 600 rpm for 15 min/day. The reactor contents were mixed daily using the agitator (Fig. 1). After thoroughly mixing the contents using an agitator, triplicate samples were taken from three different places covering the entire volume of the reactor for testing and were analyzed on each of the following days: 0, 1, 2, 3, 5, 8, 13, 21, 34, 55, 81 days. Each of the samples was tested for the following parameters: Moisture content (MC %), temperature, pH,

Fig. 1 Photographs of the reactor

TSS, VSS, and conductivity. Some samples were analyzed for tannin-lignin, HPC, SEM and EDX tests.

2.4 Soil Microbial Seed for Inocula

For microbial seed preparation, 2 g of soil was mixed with 20 mL phosphate buffer (0.008 M) and the volume was made to 200 mL. The buffer solution was added to the soil microbes to create an isotonic media for microbes. This sample was shaken for 1 h and then allowed to settle for half an hour. 84 mL of the supernatant solution was then added to 4.2 L of solution to provide microbial seed for biodegradation.

2.5 Analytical Methods

The samples were analyzed in the laboratory for the following parameters according to Standard methods for water and wastewater analysis (APHA et al. 2005). Methods used and modifications made are described here.

3 Results and Discussion

3.1 Moisture Content

Initial MC (in % of total weight of sample) was 60.56 ± 0.27 and it fluctuated between 59.31 ± 0.59 and 61.18 ± 0.62 up to the 6th day. Then it gradually decreased and was found to be $37.83 \pm 0.43\%$ on the last day of composting, i.e., 81st day (Fig. 2). During the process of composting, microorganisms break down the waste material and water

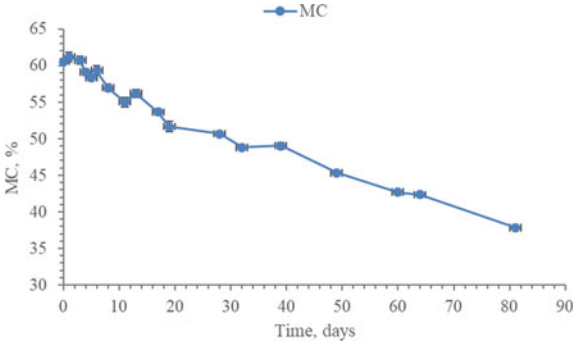

Fig. 2 Change in MC in the reactor

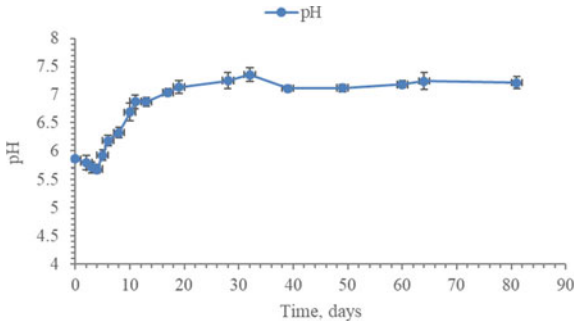

Fig. 3 Change in pH in the reactor

is released by two processes: moisture present in the organic matter is released by compaction (mechanical pressure) and biodegradation of the organic matter results in the generation of water. However, increase in temperature and vaporization of water resulted in net decrease in MC in the present study.

3.2 pH

Initially, pH was 5.85 ± 0.02 and it varied between 5.68 and 5.85 in the first 4 days. On the 5th day, it was 5.92 ± 0.10 and after that it continued to increase steadily up to the 81st day of the experiment when it was 7.21 ± 0.11 (Fig. 3). In the first phase of any biological process, volatile fatty acids are generated leading to an initial decrease in pH. After some time, these acids are degraded and converted to CO_2 and H_2O in aerobic composting resulting in near neutral pH. These results are similar to those reported in most aerobic composting processes (Tchobanoglous et al. 1993).

3.3 Conductivity and Temperature

Electrical Conductivity indicates the compost salinity level and affects plant growth and phytotoxicity when applied to soils. Conductivity increased rapidly from 0th day to 5th day from 1.05 ± 0.01 to 2.78 ± 0.06 dS/m and then more slowly from the 6th day onwards, from 2.84 ± 0.10 to 3.82 ± 0.05 dS/m on the last day of the experiment (Fig. 4).

Increase in conductivity indicates an increase in ionic strength of the solution which may be attributed to solubilization of solids from organic waste. At the beginning of the experiment, the increment in conductivity was rapid due to solubilization of solid waste which is the first step in the degradation process. After that, the increase is slower due to the uptake of ions from solution by the biomass being produced.

Initial temperature was 30.67 ± 0.58 °C and it increased to 39.33 ± 0.58 °C on the last day of the composting process. The reactor was mixed once a day for 15 min.

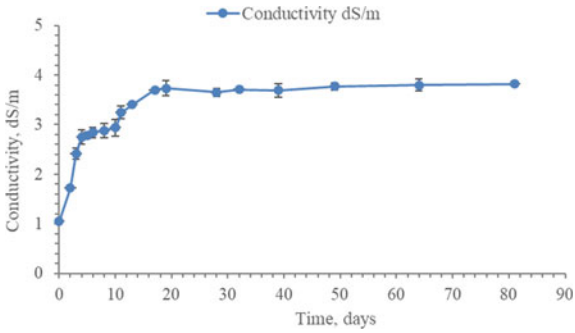

Fig. 4 Change in conductivity in the reactor

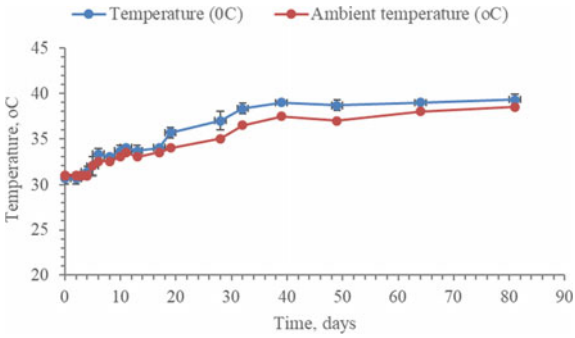

Fig. 5 Similarity between the reactor and ambient temperature

Hence the temperature of the reactor was almost equal to ambient temperature as shown in Fig. 5.

3.4 Total Solids (TS)

The initial TS was recorded as 39.41 ± 0.97% and varied between 39.76 ± 0.81% and 39.20 ± 1.36% and it was recorded as 31.28 ± 0.43% on the last day of composting. The percent decrease in TS was 20.63% (Fig. 6). A simultaneous decrease in TS and MC indicate loss of mass from the reactor due to the degradation of OFMSW.

3.5 Volatile Solids (VS)

VS slowly decreased from 96.83 ± 0.22% on day 0 to 75.68 ± 0.27% after 81 days of the composting period as shown in Fig. 7. There was some decrease in VS, i.e., 21.84%. The decrease in VS in the composting reactor represents the utilization of

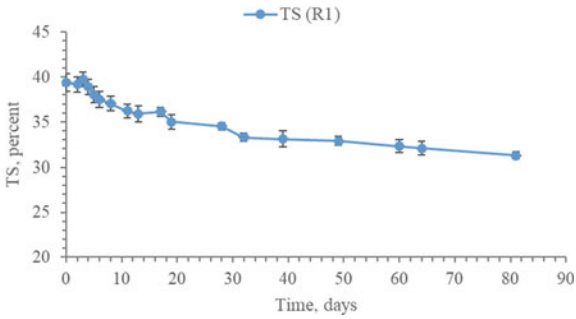

Fig. 6 Change in TS (%) in the reactor

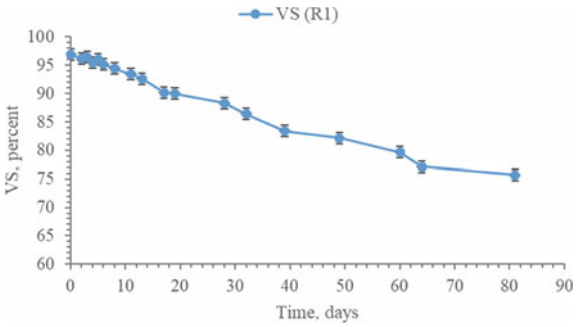

Fig. 7 Change in VS (%) in the reactor

organic carbon by microorganisms (Troy et al. 2012). Similar results were found in Wang et al. (2011) and Soobhany (2018).

3.6 C:N Ratio

The initial C:N ratio was 9.78 and decreased to 7.05 after 81 days of composting (Fig. 8). There was a 27.93% decrease in C:N ratio.

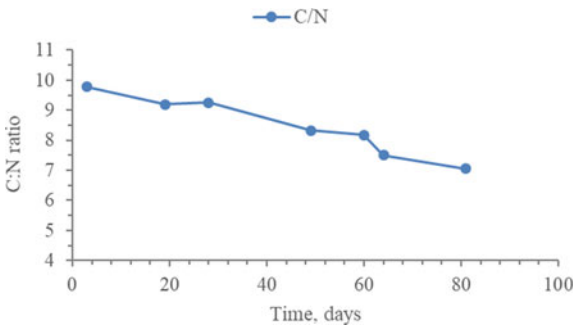

Fig. 8 Change in C:N ratio in the reactor

4 Conclusions

- Aerobic composting of OFMSW, i.e. Leaf Litter (Sal), and Chana Dal was carried out in the reactor with River Ganga water from Dakshineshwar (Kolkata) in the laboratory for 81 days.
- Regular mixing of the reactor contents ensured that an aerobic environment was maintained in the reactor and the temperature in the reactor was slightly higher than the ambient temperature.
- Percentage decrease in VS was 21.84%. Biodegradation in the reactor was because of the nutrients and microbes found in naturally available water at Dakshineshwar.
- Percent decrease in C:N ratio in the reactor was 27.93% which follows the path of VS.
- Compost produced in the present reactor proved to be excellent according to CQI and can be used as a soil conditioner and good supplemental fertilizer for plants thereby reducing consumption of chemical fertilizers.

References

APHA, AWWA, WEF (2005) Standard methods for examination of water and wastewater

Astrup TF, Tonini D, Turconi R, Boldrin A (2015) Life cycle assessment of thermal waste-to-energy technologies: review and recommendations. Waste Manag 37:104–115

CPCB (2018) Consolidated annual report (2016–17) on implementation of solid waste management rules, 2016

Fricke K, Santen H, Wallmann R (2005) Comparison of selected aerobic and anaerobic procedures for MSW treatment. Waste Manag 799–810

Goel S (2008) Municipal Solid Waste Management (MSWM) in India: a critical review. J Environ Sci Eng 50(4):319–328

Kumar A, Samadder SR (2017) A review on technological options of waste to energy for effective management of municipal solid waste. Waste Manag 69:407–422

Medina- LD, Castillo- E, Giraldi-díaz MR, Jamed-boza LO (2019) Valorisation of the organic fraction of municipal solid waste. Waste Manag Res 37(1):59–73

Palanichamy C, Babu NS, Nadarajan C (2002) Municipal solid waste fueled power generation for India. IEEE Trans Energy Convers 17(4):556–563

Paré T, Dinel H, Schnitzer M, Dumontet S (1998) Transformations of carbon and nitrogen during composting of animal manure and shredded paper. Biol Fertil Soils 26(3):173–178

Soobhany N (2018) Assessing the physicochemical properties and quality parameters during composting of different organic constituents of municipal solid waste. J Environ Chem Eng 6(2):1979–1988

Tchobanoglous G, Theisen H, Vigil SA (1993) Physical, chemical, and biological properties of municipal solid waste. Integrated solid waste management: engineering principles and management issues, McGraw-Hill Inc., New York, USA, p 978

Troy SM, Nolan T, Kwapinski W, Leahy JJ, Healy MG, Lawlor PG (2012) Effect of sawdust addition on composting of separated raw and anaerobically digested pig manure. J Environ Manag 111:70–77

Tuomela M, Vikman M, Hatakka A, Itävaara M (2000) Biodegradation of lignin in a compost environment: a review. Biores Technol 72(2):169–183
Wang X, Jennifer MP, Florentino B, la Cruz D, Morton AB (2011) Wood biodegradation in laboratory-scale landfills. Environ Sci Technol 45:6864–6871

Drought Vulnerability Assessment and Analysis in Bidar District

Priyanka Sawale, Anand V. Shivapur, H. S. Shivakumar Naiklal, and A. Bharath

Abstract Drought is one of the significant threats to the sustainable development of India. The Karnataka state's Bidar district often experiences drought because of inadequate rainfall and significant rainfall variation within its geographical area. Hence Bidar district is considered one of the drought-prone districts in the state, and hence there is a need to take up the drought mitigation measures. The primary stage in the development of drought mitigation measures is drought evaluation. In the present study, the meteorological drought assessment is carried out by taking percentage of departure for five rain gauge stations of Bidar district, namely Aurad, Bidar, Bhalki, Basavakalyan, and Humnabad, using 35 years historical data (1985–2019). This study reveals that percentage of departure is the most appropriate drought indices in portraying drought in the study area. The rainfall analysis is carried out to know the rainfall distribution. Also, rainfall variation maps are developed for annual and seasonal mean rainfall in the ArcGIS platform.

Keywords Meteorological drought · Percentage of departure · Rainfall pattern · Drought vulnerability · GIS

1 Introduction

Water is one of nature's valuable blessings to humankind. Being the main thrust of life, water plays a significant role in balancing the entire biological system. When a deficiency of water happens over a region for an extended period, it affects the biology of that place (Bharath et al. 2021b). The dry season is an extended period when a region receives less than normal rainfall. Drought has many effects on human

P. Sawale (✉) · A. V. Shivapur
Department of Civil Engineering, VTU, Belagavi, Karnataka, India

H. S. Shivakumar Naiklal
RS and GIS Department, KSNDMC, Banglore, Karnataka, India

A. Bharath
Department of Civil Engineering, GITAM University, Banglore, Karnataka, India

B. B. Das et al. (eds.), *Recent Developments in Sustainable Infrastructure (ICRDSI-2020)—GEO-TRA-ENV-WRM*, Lecture Notes in Civil Engineering 207,
https://doi.org/10.1007/978-981-16-7509-6_19

activities, human lives and different components of the environment. Conventionally, a decrease in rainfall is considered the cause of drought, which prompts a decrease in water storage and fluxes associated with the hydrological cycle (Cm 2018). A dry season is an unexpected event with a decrease in precipitation over a long time zone, which is not arid (Bharath et al. 2021a). Describing periods of shortage and drought has been challenging for managing water assets frameworks for a long time (Babu 2016). A dry spell is one of the most destructive catastrophic events that influence the human population and low precipitation can prompt severe hydrologic deficiencies (Kant et al. 2014). These deficiencies may affect crop yields, groundwater assets, storage in reservoirs and deficiency of drinking water and, decreased fodder accessibility and so on, which adversely influence the local population (Shah et al. 2015). Therefore, the ability to forecast and anticipate the magnitude of dry spells, particularly their recurrence and severity, are the concerns. Drought assessment and monitoring are fundamental for the agriculture sector as well as the management of water resources. Unlike other catastrophic events like flood, tremors dry spells have a moderate evolution time (Tangadagi et al. 2021).

2 Literature Review

The literature listed below is based on drought evaluation and variability in rainfall. This literature has been used for deciding the methodology, data requirement, and software setting for the project.

Kant et al. (2014) have studied the drought at Agra, Uttar Pradesh, utilizing 31 years of precipitation data from 1970 to 2000. The authors reported a seasonal wise percentage of departure rainfall, yearly precipitation deviation, and dry spell analysis. The region experienced extreme drought conditions during the years 1972 and 1979, and a moderate drought situation was seen during 1970, 1986, 1987, 1990, and 2000. It is estimated that According to this research, dry spell changes from 2 to 2.5 once in 10 years.

Shah et al. (2015) did study on the Surath area to observe and describe drought using SPI (standardized precipitation index) strategy for a long time precipitation data (40 years). They discovered dry season records based on a twelve-month time scale and compared with drought station. The study reports that 50% is appeared from normal to wet and normal to dry by SPI technique and reasoned that this strategy is necessary and sufficient.

Madolli et al. (2015) have analysed the effect on precipitation because of climatic variation experienced in the Upper Cauvery Basin in Karnataka. The study was conducted on rainfall pattern evaluation and SPI over eight districts. Using annual normal precipitation, SPI values and SPI maps were produced for a long time (63 years). SPI value was estimated to be between 3.02 and −2.88, indicating a considerable variation in precipitation. Further, SPI maps (district-wise) of the years 2001 and 2012 indicate considerable variation in the number of dry and wet years. The outcome indicated an increased number of wet years in the locale of Kodagu,

Bengaluru Urban, and Bengaluru Rural, and the number of dry years increased in Hassan, Mysore, Tumkur, Chamarajnagar, and Mandya areas.

Babu (2016) has revealed through his research on fundamental evaluation of meteorological dry spell indicator in Ananthapur District. The author has assessed drought by utilizing meteorological dry spell indicators and evaluated using decision models to determine a suitable indicator. The research presumed that the departure index was the most suitable index for portraying drought intensity compared with RDI and SPI as they demonstrated fickle qualities.

3 Study Area

The Bidar district of Karnataka state, India has been considered for study as the district has been declared as drought-prone area. This district lies between 17°35′ to 18°29′ North latitude and 76°41′ to 77°39′ East longitude (CGWB 2008). The district is bounded by Telangana state towards the east, Latur and Osmanabad districts, Maharashtra state towards the west, Nanded district, Maharashtra towards the north, and Gulbarga district, Karnataka State towards the south. The total geographical area is 5460 km^2. The whole district lies within the drought zone, with inadequate rainfall, non-uniform rainfall over the district, and unstable irrigation sources presenting the district to famines. Hence, historical analysis of droughts using a systematic methodology helps to understand rainfall distribution patterns, identifying the region's drought conditions and dry spells (Fig. 1).

4 Methodology

The study has been done using monthly rainfall data of five rain gauge stations located within Bidar district for 35 years (1985–2019) were collected from the Karnataka State Natural Disaster Monitoring Centre Bengaluru (KSNDMC) to evaluate meteorological drought based on percentage of departure and rainfall variation were examined for annual, seasonal and monthly period. Meteorological drought is generally defined by a precipitation deficiency limit over a predetermined timeframe, and it′s period is based on the number of days with rainfall less than some specified threshold (Babu 2016). The evaluation of drought becomes more significant with increased population and demand for food. Drought assessment is a tedious task for drought researchers and experts since it is hard to decide its beginning and end and its severity (Babu 2016). In this study, drought assessment is carried out using the percentage of departure indices because of its popularity. The monthly rainfall, seasonal rainfall (i.e., Pre-monsoon: January–May, monsoon: June–September, post-monsoon: October–December), and annual rainfall were analysed by rainfall analysis using arithmetic mean method and calculated mean, standard deviation, coefficient variation, and rainfall contribution in Microsoft excel.

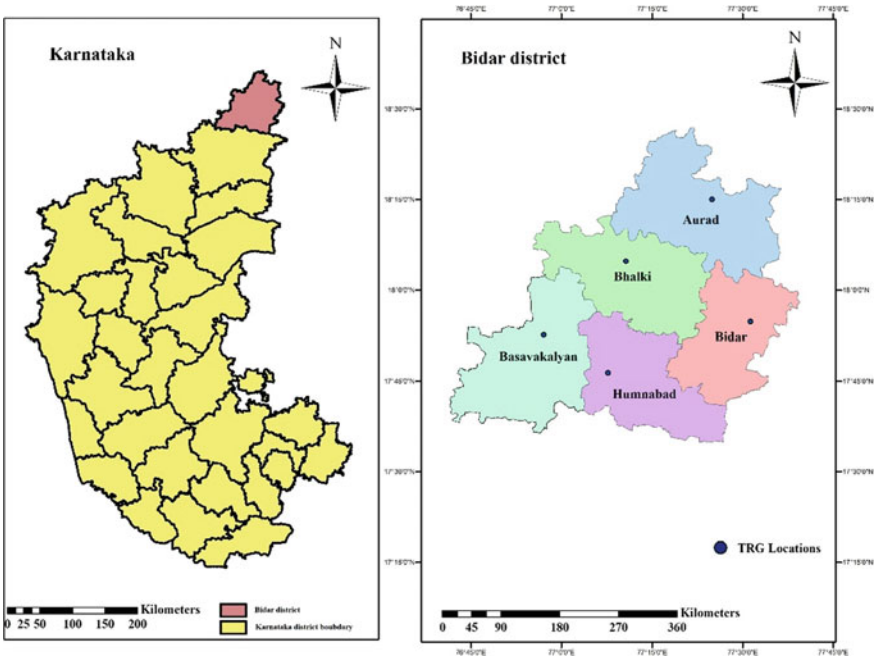

Fig. 1 Location map of the study area

The drought has been analysed using the criteria suggested by the India Meteorological Department (IMD 1971) based on percentage departure from normal rainfall as,

$$\text{Percentage Departure of Rainfall } (\%) = \frac{AR - NR}{NR} \times 100 \tag{1}$$

where AR is the Actual rainfall in mm, NR is the Normal rainfall in mm.

The standard practice of declaring the drought condition, as shown in Table 1, is followed in the present study.

The seamless rainfall data obtained from TRG's (Telemetric rain gauges) system established to have consistent rainfall data is being computed against the normal rainfall to choose the dry spell level at the taluk level weekly. It is also used to

Table 1 Drought conditions

% Departure of rainfall	Drought condition
0.0 to above	No drought
0.0 to −25.0	Mild drought
−26 to −50.0	Moderate drought
> −50	Severe drought

choose the break monsoon condition and spatial appropriation of precipitation in the state. A drought is described as it is a short time of no rainfall or normally a month of less rainfall. This indicator is noteworthy because it assesses the degree of intra-season precipitation variations, which is so fundamental for the prosperity of yields and soil and hydrological system (UNESCO IHE 2011).

The study also deals with the plotting of the rainfall distribution patterns using the rainfall data of 35 years for five rain gauge stations of Bidar district. The annual precipitation (January–December) incorporates three principle seasons Pre-Monsoon (January–May), South-West Monsoon (June–September), and North-West Monsoon (October–December). These rainfall distribution patterns maps were created to know the annual and season wise rainfall variation in Bidar district in the ArcGIS platform.

To achieve the results, Microsoft excel is used for calculation, graphing, pivot tables, and ArcGIS software used to produce rainfall pattern maps. The following section describes results obtained from the study giving seasonal wise annual rainfall variability and meteorological drought evaluation.

5 Results and Discussions

In this study, the assessment of meteorological drought and analysis of rainfall variation pattern has been carried out to monitor the drought severity, drought condition, and plot rainfall variability pattern for the Bidar district of Karnataka. Figure 2 shows normal rainfall graph for five taluks of Bidar district, namely Aurad, Bidar, Bhalki, Basavakalyan and Humnabad. This shows the maximum and minimum normal rainfall month for historical rainfall data ranging from 1985 to 2019 (35 years) for each

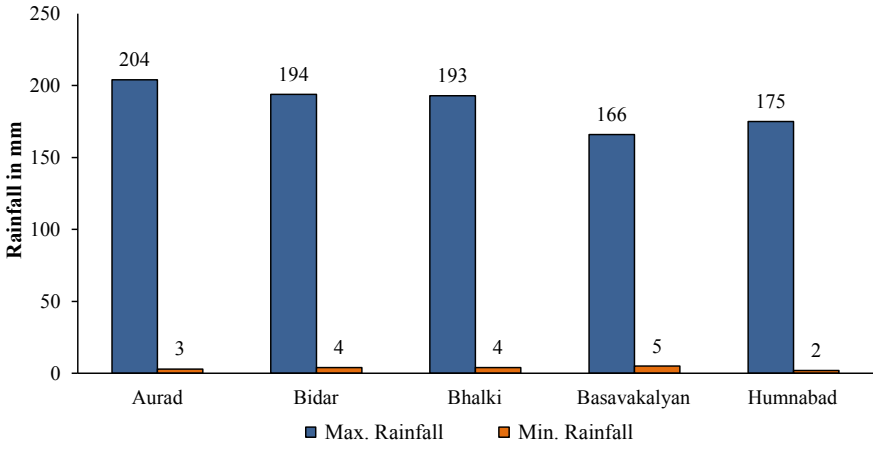

Fig. 2 Normal rainfall for Taluks of Bidar district

Bidar district taluk. The maximum and minimum normal rainfall month was 204 mm at Aurad taluk in August month and 2 mm at Humnabad taluk in February month.

Figure 3 shows the percentage of south-west normal rainfall contribution shown in the pie chart below for five rain gauge stations of Bidar district based on 35 years of rainfall data from 1985 to 2019. The pie chart indicates that maximum rainfall contributes to the south-west monsoon season (June–September) around 82% at Aurad taluk in August month.

Figure 4 shows the annual rainfall plot for five taluks of the Bidar district. This represents the maximum and minimum annual rainfall year within 35 years (1985–2019) for each taluk. The maximum and minimum annual rainfall was found to be 1453 mm at Bidar taluk, which occurred in 1988, and 359 at Aurad taluk, which occurred in 2014, respectively.

Figure 5 shows yearly dry spell weeks for the five rain gauge stations of Bidar district, i.e., dry spell weeks on Y-axis versus year on X-axis. This analysis helps identify maximum dry spell weeks and no dry spell years. In 35 years, it is found

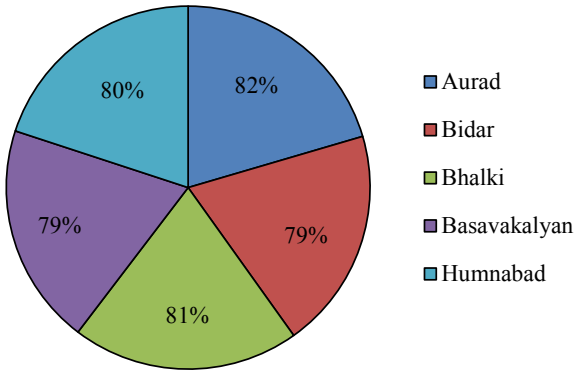

Fig. 3 South-west monsoon normal rainfall contribution in taluks of Bidar district

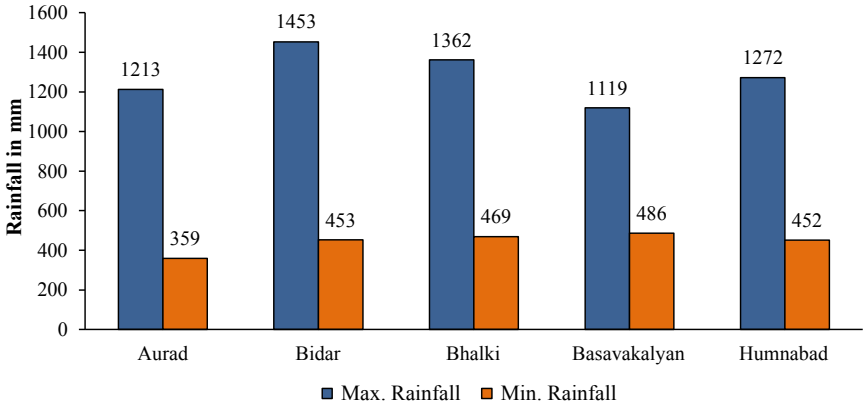

Fig. 4 Annual rainfall for Taluks of Bidar district

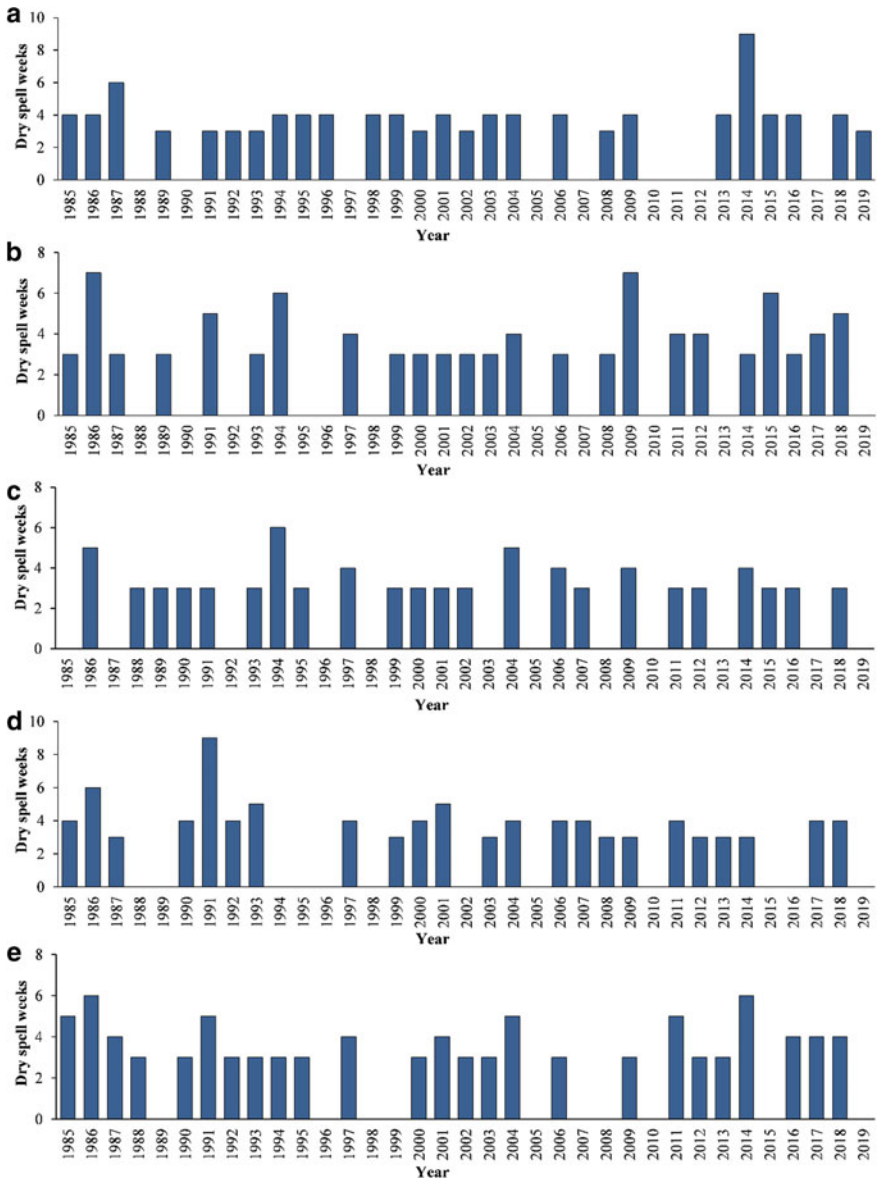

Fig. 5 Dry spell weeks for taluks of Bidar district: A—Aurad, B—Bhalki, C—Bidar, D—Basavakalyan, E—Humnabad

that Aurad, Bidar, Bhalki, Basavakalyan, and Humnabad taluks experience 26, 23, 24, 23, and 25 years of dry spell respectively. The maximum consecutive dry spell weeks were 9 numbers at Aurad in 2014 and Basavakalyan taluk in 1991.

Figure 6 shows the percentage deviation plot for 35 years from 1985–2019 in the Bidar district for five taluks. This helps identify dry and wet years, to know drought conditions (Table 2), and the total number of drought years (Table 3) based on percentage of departure from normal. These graphs show that 1988 was the maximum wettest year with 61% of positive departure at Bidar taluk, and the year 2014 is found to be the driest year with 59% of negative departure at Aurad taluk.

The year-wise percentage deviation and drought condition of 35 years (1985–2019) for five taluks, namely Aurad, Bidar, Bhalki, Basavakalyan, and Humnabad of Bidar district is shown in Table 2. Table 3 shows the total number of drought years of various classifications. In 35 years, Aurad and Bidar taluks have experienced severe drought condition in 2014 and 2018 respectively and the number of years of no drought condition are 18, 15, 17, 15 and 19; mild drought condition are 10, 13, 12, 15 and 8, Moderate drought condition are 6, 6, 6, 5 and 8 in Aurad, Bidar, Bhalki, Basavakalyan and Humnabad taluk respectively.

The season's wise annual rainfall patterns statistics of 35 years (1985–2019) using the data for five rain gauge stations of Bidar district are shown in Table 4. The rainfall patterns for the Bidar district is generated (Fig. 7) in the GIS environment. The annual rainfall variation in the district is more than 900 mm and it varies in three main seasons (Pre-monsoon, Southwest monsoon, North-west monsoon). In Pre-monsoon (January to May month), maximum rainfall varies between 89 and 91 mm at Bidar taluk, South-west monsoon (June to September month) maximum rainfall varies from 670 to 684 mm at Aurad and Bidar taluk and North-east monsoon (October to December month) maximum rainfall varies from 123 to 130 mm at Bidar taluk of Bidar district.

The coefficient of variation refers to the proportion of standard deviations to the mean and is used to know the variability of rainfall within the area. Figure 8 indicates that the central part of Aurad and Basavakalyan taluk with a high coefficient of variation. At the same time, it is least in the southern part of the Humnabad and south-eastern part of Bidar taluk of Bidar district.

6 Conclusions

Precipitation during the monsoon season and its variation within the district directly impact cropping patterns in the Bidar district. The drought happens due to scanty rainfall. Based on the available data, authors have done exercise to understand season's wise annual rainfall analysis and meteorological drought evaluation to understand the rainfall process and year-wise drought conditions based on percentage of departure. The following conclusions have been drawn:

The year-wise percentage deviation and drought condition of 35 years (1985–2019) for five taluks, namely Aurad, Bidar, Bhalki, Basavakalyan and Humnabad

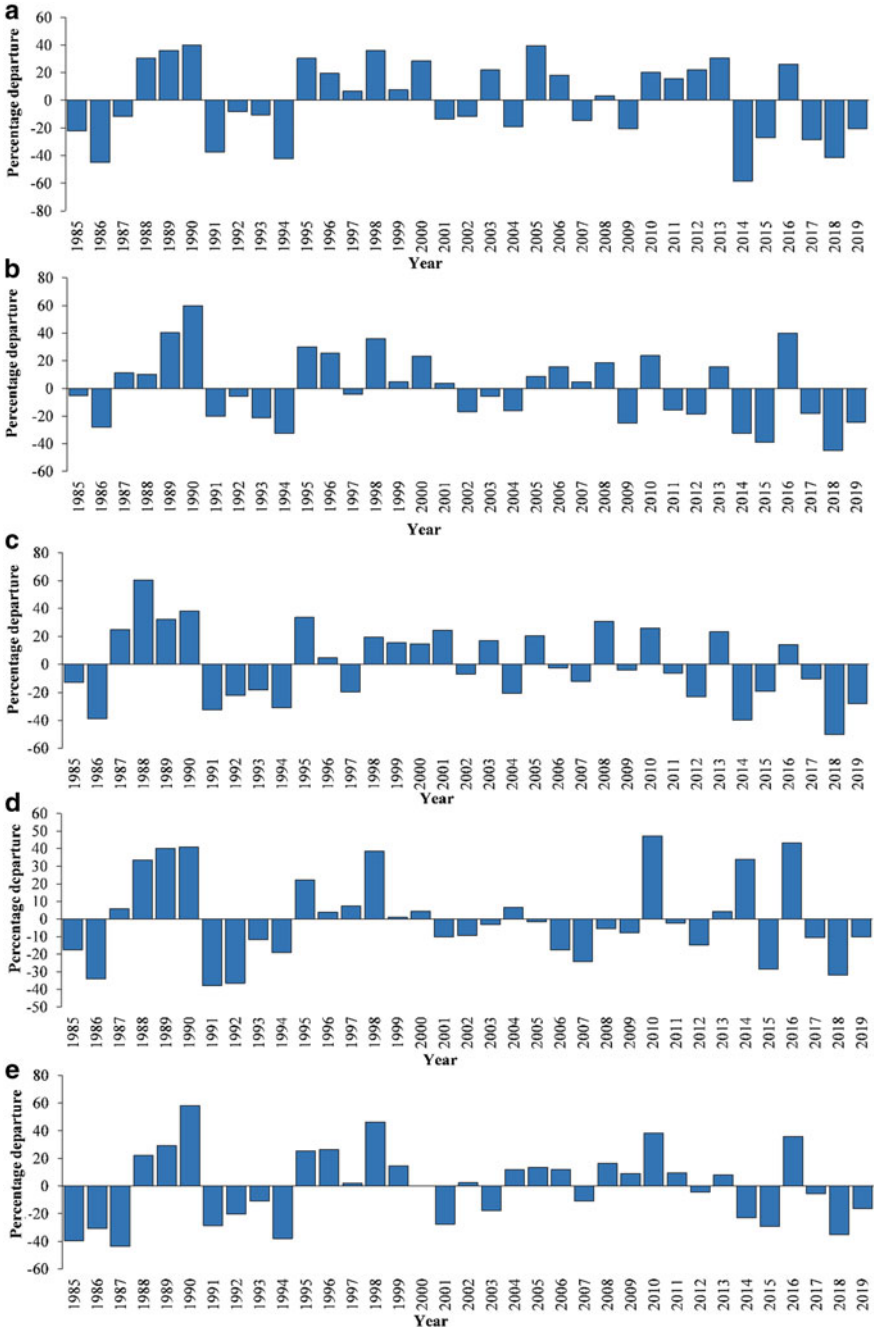

Fig. 6 Percentage of departure from normal rainfall for taluks of Bidar district: A—Aurad, B—Bhalki, C—Bidar, D—Basavakalyan, E—Humnabad

Table 2 Year-wise drought condition for Bidar district

Year	Aurad taluk		Bidar taluk		Bhalki taluk		Basavakalyan taluk		Humnabad taluk	
	% Departure	condition	% Departure	condition	% Departure	condition	% Departure	condition	% Departure	condition
1985	−22	MID	−13	MID	−5	MID	−17	MID	−40	MD
1986	−45	MD	−39	MD	−28	MD	−34	MD	−31	MD
1987	−12	MID	25	ND	11	ND	6	ND	−44	MD
1988	30	ND	61	ND	10	ND	34	ND	22	ND
1989	36	ND	32	ND	40	ND	40	ND	29	ND
1990	40	ND	38	ND	60	ND	41	ND	58	ND
1991	−37	MD	−32	MD	−20	MID	−38	MD	−29	MD
1992	−8	MID	−22	MID	−6	MID	−36	MD	−20	MID
1993	−11	MID	−18	MID	−21	MID	−12	MID	−11	MID
1994	−42	MD	−31	MD	−32	MD	−19	MID	−38	MD
1995	30	ND	34	ND	30	ND	22	ND	25	ND
1996	19	ND	5	ND	26	ND	4	ND	26	ND
1997	7	ND	−20	MID	−4	MID	8	ND	2	ND
1998	36	ND	19	ND	36	ND	38	ND	46	ND
1999	8	ND	15	ND	5	ND	1	ND	15	ND
2000	28	ND	15	ND	23	ND	5	ND	0	ND
2001	−14	MID	25	ND	4	ND	−10	MID	−28	MD
2002	−12	MID	−7	MID	−17	MID	−10	MID	2	ND
2003	22	ND	17	ND	−6	MID	−3	MID	−18	MID
2004	−19	MID	−20	MID	−16	MID	7	ND	12	ND

(continued)

Table 2 (continued)

Year	Aurad taluk		Bidar taluk		Bhalki taluk		Basavakalyan taluk		Humnabad taluk	
	% Departure	condition	% Departure	condition	% Departure	condition	% Departure	condition	% Departure	condition
2005	39	ND	20	ND	9	ND	−1	MID	14	ND
2006	18	ND	−3	MID	16	ND	−18	MID	12	ND
2007	−15	MID	−12	MID	5	ND	−24	MID	−11	MID
2008	3	ND	31	ND	19	ND	−6	MID	16	ND
2009	−21	MID	−4	MID	−25	MD	−8	MID	9	ND
2010	20	ND	26	ND	24	ND	47	ND	38	ND
2011	16	ND	−6	MID	−16	MID	−2	MID	9	ND
2012	22	ND	−23	MID	−18	MID	−15	MID	−4	MID
2013	31	ND	23	ND	16	ND	4	ND	8	ND
2014	−59	SD	−40	MD	−32	MD	34	ND	−23	MID
2015	−27	MD	−19	MID	−39	MD	−29	MD	−29	MD
2016	26	ND	14	ND	40	ND	43	ND	36	ND
2017	−28	MD	−11	MID	−18	MID	−11	MID	−6	MID
2018	−42	MD	−50	SD	−45	MD	−32	MD	−35	MD
2019	−20	MID	−28	MD	−24	MID	−10	MID	−16	MID

ND No drought, *MD* Moderate drought, *MID* Mild drought, *SD* Severe drought

Table 3 Number of drought years in Bidar district

Sl. No.	Drought condition	Number of drought years				
		Aurad	Bidar	Bhalki	Basvakalyan	Humnabad
1	No drought	18	15	17	15	19
2	Mild drought	10	13	12	15	8
3	Moderate drought	6	6	6	5	8
4	Severe drought	1	1	0	0	0

Table 4 Seasons wise annual rainfall patterns statistics for Bidar district

Years	Taluk	Particulars	PM	SW	NE	Annual
1985–2019	Aurad	Mean rainfall (mm)	82	676	108	867
		Standard deviation	55	228	76	244
		C.V (%)	66	34	70	28
		Contribution (%)	9	78	13	100
1985–2019	Bidar	Mean rainfall (mm)	91	685	130	905
		Standard deviation	64	228	91	240
		C.V (%)	70	33	71	26
		Contribution (%)	10	76	14	100
1985–2019	Bhalki	Mean rainfall (mm)	82	659	111	852
		Standard deviation	58	190	86	217
		C.V (%)	71	29	77	25
		Contribution (%)	10	77	13	100
1985–2019	Basavakalyan	Mean rainfall (mm)	85	586	110	781
		Standard deviation	52	186	76	190
		C.V (%)	61	32	69	24
		Contribution (%)	11	75	14	100
1985–2019	Humnabad	Mean rainfall (mm)	89	604	111	804
		Standard deviation	64	190	65	211
		C.V (%)	72	31	59	26
		Contribution (%)	11	75	14	100

PM Pre-monsoon, *SW* South-west monsoon, *NE* North-west monsoon

of Bidar district are shown in Table 2. Table 3 shows the total number of drought years of various classifications. In 35 years, Aurad and Bidar taluks have experienced severe drought condition in 2014 and 2018 respectively, and the number of years of no drought condition are 18, 15, 17, 15 and 19, Mild drought condition are 10, 13, 12, 15 and 8, Moderate drought condition are 6, 6, 6, 5 and 8 in Aurad, Bidar, Bhalki, Basavakalyan and Humnabad taluk respectively.

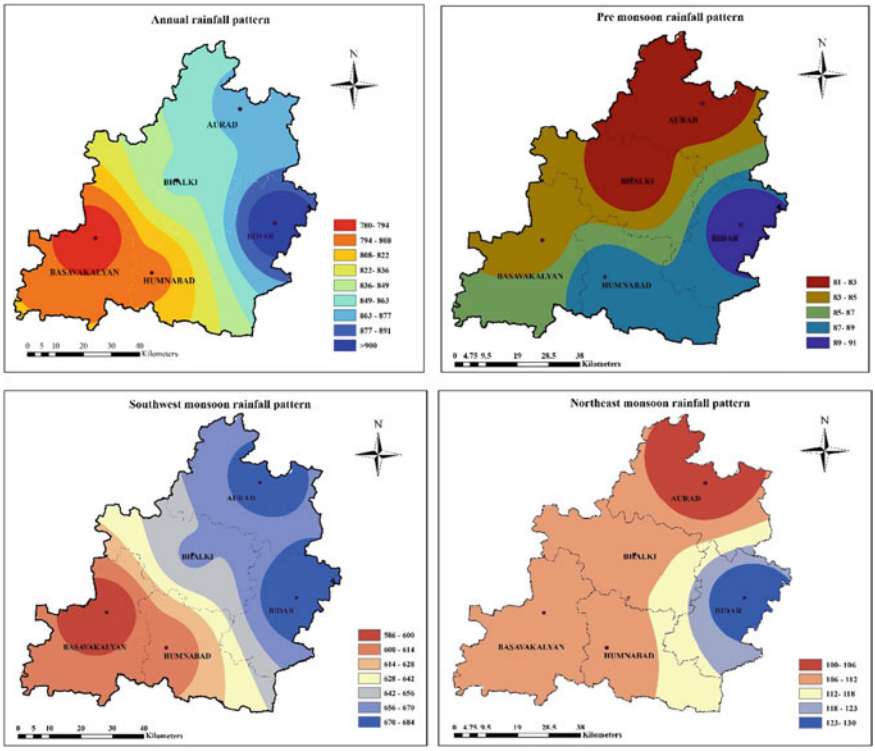

Fig. 7 Rainfall distribution pattern in Bidar district

The annual rainfall variation within the district is more than 900 mm and it varies in three main seasons (Pre-monsoon, South west monsoon, North-west monsoon). In Pre-monsoon (January to May month) maximum rainfall varies between 89 and 91 mm at Bidar taluk, South-west monsoon (June to September month) maximum rainfall varies from 670 to 684 mm at Aurad and Bidar taluk and North-east monsoon (October to December month) maximum rainfall varies from1 23 to 130 mm at Bidar taluk of Bidar district.

The coefficient of variation is high regarding the central part of Aurad and Basavakalyan taluk, i.e., 27–28% indicates that precipitation was pretty much stable throughout the years. While it is least in southern part of Humnabad and south eastern part of Bidar taluk of Bidar district.

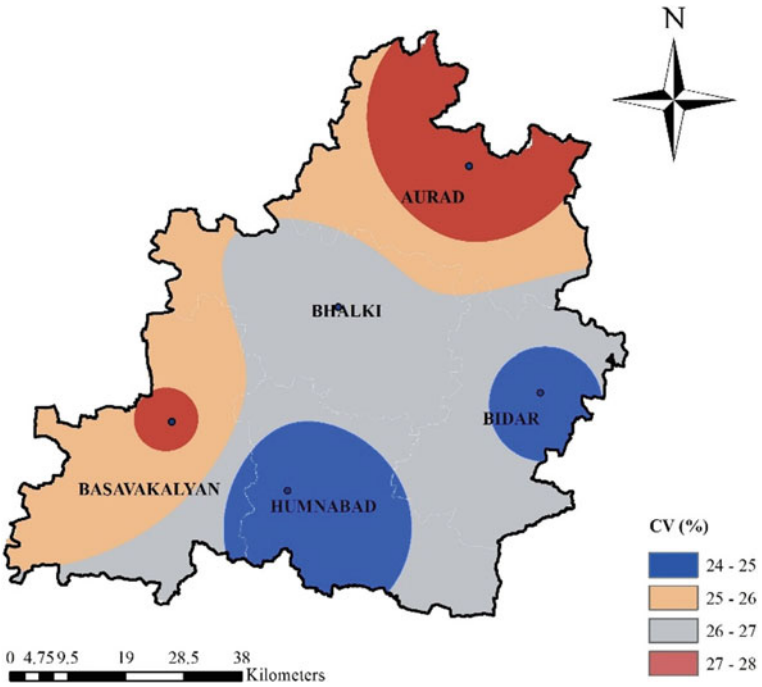

Fig. 8 Coefficient variation rainfall pattern in Bidar district 1985–2019

References

Babu CM (2016) Critical appraisal of meteorological drought indices: a case study on the Ananthapur district. Int J Adv Res 4(3):1705–1717

Bharath A, Kumar KK, Maddamsetty R, Manjunatha M, Tangadagi RB, Preethi S (2021a) Drainage morphometry based sub-watershed prioritization of Kalinadi Basin using geospatial technology. Environ Challenges 5:100277

Bharath A, Shivapur AV, Hiremath CG (2021b) Dam break flood routing and inundation mapping using HEC-RAS and HEC-GeoRAS. In: Water resources management and reservoir operation. Springer, Cham, pp 129–137

Bhuiyan C, Singh RP, Kogan FN (2006) Monitoring drought dynamics in the Aravalli region (India) using different indices based on ground and remote sensing data. Int J Appl Earth Obs Geoinf 8(4):289–302

Goud S et al (2015) Implications of rainfall distribution pattern and its variability for crop planning of crops: a study in North Eastern transitional zone of Karnataka. Karnataka J Agric Sci 28:5

Kant SKS, Meshram S, Sahu KC (2014) Analysis of rainfall data for drought investigation at Agra UP. Recent Res Sci Technol (2014)

Madolli MJ, Kanannavar PS, Ravindra Y (2015) Impact of climate change on precipitation for the upper Cauvery river basin, Karnataka state. International J Agric Sci Res (IJASR) 5(1):99–104

Tangadagi RB, Dangeti M (2021) Assessment of LULC changes for Hesaraghatta watershed using GIS Tools and Remote Sensed Data. Nat Environ Pollut Tech 20(4)

Zarch MAA et al (2011) Drought monitoring by reconnaissance drought index (RDI) in Iran. Water Resour Manag 25(13):3485

Urban Flooding: A Case Study Panaji City

Raasiq Sayed, Shreya Arolkar, Genevieve Fernandes, Naomi Pereira, Ancila Vaz, Tanvisha Bakhale, and K. G. Guptha

Abstract Panaji, the capital city of Goa was initially planned by the Portuguese for a focused population. The city saw tremendous development in the post-liberation period so much so that the planned city started experiencing different problems viz., erratic and unplanned development and its related issues making normal life miserable at times. They were instrumental in the construction of the primary drains which are currently functional and catering to the needs of that time. The design of the drainage system was carried out in a planned manner, but due to the current scenario of haphazard construction, impermeable surfaces and other factors have posed a threat and requires immediate attention. The capacity of the present drainage system is inadequate, with rising populations and urbanization in a disordered manner leading to waterlogging in the city as one of the man-made causes of concern. These shortcomings need investigations immediately before the situation turns beyond anyone's control and capacity and hence the management of urban drainage is critically an important challenge! This is necessary as the city is selected as a "Smart city" by govt. of India. With the futuristic views of modern planners comes words and ideas like 'Zero discharge city, Sustainability, Environmental friendly transportation, pedestrianism' and many such innovations that are designed and implemented to build our world into a better place for our children to live in. This work focuses on assessing the technical reasons leading to urban flooding, using geospatial techniques like QGIS, Google Earth Pro, understanding the current scenario of the dilemma, and intend to provide a credible solution towards the problem.

Keywords QGIS · Flash-floods · Climate · Storm-water · Drainage

R. Sayed (✉) · S. Arolkar · G. Fernandes · N. Pereira · A. Vaz · T. Bakhale · K. G. Guptha
GEC, Farmagudi, Goa, India

B. B. Das et al. (eds.), *Recent Developments in Sustainable Infrastructure (ICRDSI-2020)—GEO-TRA-ENV-WRM*, Lecture Notes in Civil Engineering 207,
https://doi.org/10.1007/978-981-16-7509-6_20

1 Introduction

The all-around arranged Panaji city of the bygone eras adapts up and performs well even with the changes, pressures, and the quick increment in urbanization alongside its advancement. Be that as it may, a few deficiencies should be examined preceding the circumstance is past anybody's ability. Panaji channels are not simply stopped up with the trash descending the slopes of Dona Paula and Altinho yet all the plastic and paper squander that goes unchecked. The absence of room around has driven this study to search for options to the endless issue that is just going to increment in size in the years to accompany the development of populace and endless suburbia. The city is setting out toward this heading and ought to do as such before the current circumstances become disastrous. The main objectives include locating and identifying the flooded areas, establishing technical reasons and causes for drainage congestion based on the existing drainage system. Quantification of flooded areas and suggesting remedies to free the city of waterlogging.

2 Literature Review

The Energy and Resource Institute (TERI) evaluated a yearlong study on 'Climate Resilient Infrastructure Services'. The study aimed to understand the kind of infrastructure that Panaji and Visakhapatnam have and their vulnerability to climate change. All the infrastructure and services are considered.

Miguez et al. (2009) presented a paper titled 'Planning and Design of Urban Flood control Measures: 'Assessing Effects Combination' aims to recover natural flow patterns before urbanization.

Heidari (2010) revealed a study on 'the best plan for flood mitigation: The proposed detention dam master plan is debated, and its effect is assessed in the basin.

3 Data Collection

3.1 Climatic Parameters

Panaji gets precipitation from the South-West storm between the long stretches of June to September. The normal yearly precipitation saw in the city is 3124.06 mm which is higher than the locale normal of 2932 mm. The city encounters a mean everyday temperature of 27.4 °C which increments to 30 °C in the storm season. The MSL esteem was discovered to be 7.02 m dependent on tide check information since 1878.

3.2 Topography and Geology

Panaji is situated at 15°29′56″ N Latitude and 73°49′40″ E Longitude. The landscape of the city is commonly slanting from East to West heading along the course of River Mandovi. The geographical structure of the city is as a bowl having a higher height at Altinho and Old secretariat.

3.3 Groundwater

The city of Panaji, except for the Altinho territory in Goa, most different regions have a high water table. The profundity of the water table is supposed to be 1–1.5 m subterranean.

3.4 Land Use Pattern

The city involves 66% (5.5 km^2) developed territory and 34% (2.8 km^2) of the lacking zone. The development of the city is in the westwards course.

3.5 Road Characteristics

The streets inside the center city region are laid in a Gridiron pattern. All the streets inside the city are 100% surfaced yet have low carriageway. The normal carriageway in the city is 11 m. The most elevated carriageway in the city is 15.5 m while the least is 2.0 m.

3.6 Outline Development Plan

Panaji is limited by the Mandovi River toward the north, Ourem Creek toward the east, the hillock of Altinho toward the southeast, and the Arabian Sea. The city zone has been changing throughout the years as a significant business and vacationer center.

3.7 Population Data

The populace expanded from around 35,000 out in 1971 to 64,764 every 2001 and went up to around 70,991 out in 2011. At present normal thickness in the city is 3668 people for each km^2 which shows a high-thickness design. Populace and development pattern has been fluctuating over the previous many years chiefly because of the change in the authoritative territory due to either consideration or rejection of connecting metropolitan pockets inside the city.

3.8 Water Bodies

The significant water bodies situated in and around the city are the River Mandovi and Zuari spilling out of the Northern side towards the Arabian Sea in the South. The city has two regular water bodies, Mala Lake which is a catchment region for water from more significant levels of the city situated in the north-eastern part, and La Campala Lake in the western part.

3.9 Existing Storm Water Drainage System

The present stormwater seepage network is old and inadequately kept up and has high siltation issue. The city right now has a 70 km channel length which is comparable to 90% street length inclusion as seen in Fig. 1. Unpredictable unloading of strong waste, the release of untreated sewage, and infringement in certain spots have prompted

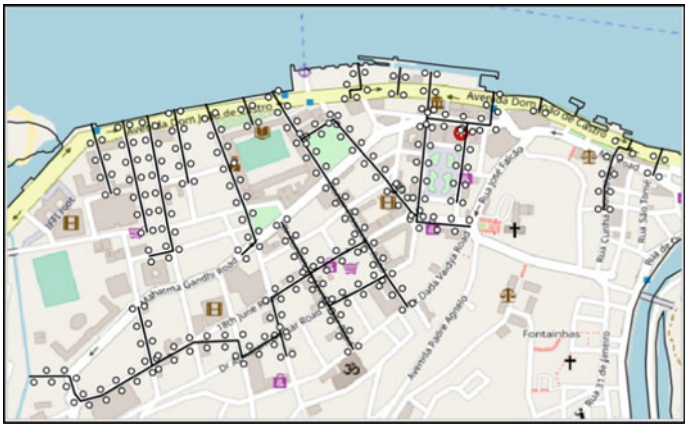

Fig. 1 Existing stormwater drainage network in QGIS

expanded obstructing of the channels. The channels were almost 5 ft. high which are just 1ft. high directly because of high siltation. The whole framework is left to work under gravity and there are mostly 17 outlets draining stormwater into the River. The water level close to the coast to rise which highlights the effect of elevated tides causing the reverse of stormwater.

Likewise, the current foundation empowers stormwater removal on the accompanying lines.

(a) Altino Hill channels into the Mala and Fontainhas zone, prompting Mala Lake which in the long run releases into Mandovi River/Estuary through the Rio de Ourem Creek.
(b) Core city zone (northern part) channels into Mandovi River through surface channels and street-side stormwater waste channels.
(c) St. Inez zones in the north-western part channel into the St. Inez Creek which in the long run joins Mandovi River on the north.
(d) Runoff from the Southern pieces of the town legitimately joins the Arabian Sea.

3.10 Existing Flood Pumping Station

The city of Panaji has no flood siphoning station in focal Panaji. In any case, there exists one siphoning station at Mala zone to siphon floodwater into Ourem Creek. As of now, the limit of the siphon is enlarged from 50 to 100HP.

3.11 Contours of Panaji

The city of Panaji has a normal height of 7 m (23 ft.) along the beachfront belt. The most elevated area is at Altinho at 64 m and the lowermost is at Patto at 2 m and another at Mala Lake. The contours generated in QGIS is shown in Fig. 2.

3.12 Water Supply

Panaji city's water gracefully source is River Khandepar. The general stockpiling limit of the current stores is 12,800 m^3.

Fig. 2 QGIS Generated map showing contour lines of Panaji

3.13 Solid Waste Management

The Corporation of the City of Panaji is dealing with the assortment, transportation, treatment, and removal of Municipal Solid Waste (MSW) Panaji creates around 72 MT/day of waste altogether.

4 Methodology

4.1 Basic Concept of Methodology

From the information gathered, investigations of the current stream designs and found the significant channels which were inclined to flooding were done. Remembering these hotspots, we partitioned our investigation territory into various zones and determined the all-out release.

4.2 General Concept

The flood control sub-area would be impacted by environmental change. The power and event are exacerbated and thusly, the flood will strengthen and increment. Ocean

level ascent will bring about a limit decrease of waste frameworks along these lines dragging out immersion on beachfront territories.

4.3 Vulnerability Assessment

Audit of environmental change situations and investigation models, and target year for variation measures. Venture hydrological angles at the arranged base year utilizing the examination aftereffects of environmental change projection for the objective year. Assess Past and Present Climate Trends and Risks. Assess Future Exposure to Climate Hazards and Perturbations. Study Present Condition of Facilities and Measures. Determine and Project Adaptive Capacity. Assess Vulnerability to environmental change in the objective region by covering the elements.

4.4 Analysis—Methodology

To contemplate the reasons for flooding and assess the current seepage condition, an examination of 2 principle factors was completed utilizing the information gathered, for example, investigation of the development of the city and Stormwater release in the city. The technique for examination was done utilizing QGIS, GPS Essentials, and Google Earth Pro applications to decide the development of the city, forms, and geography of the territory, plan release, and so forth.

4.4.1 Growth of the City Using Google Map

Google maps gives a stage to dissect the development patterns of the city. It assists with understanding the advancement of the city. Over a scope of several years.

4.4.2 Data Creation Using Google Earth

Polygon highlights were made to digitize the investigation zone. These records once made were then sent out as a kml document for additional investigation.

4.4.3 Design Discharge

Computing the peak discharge of the city by dividing into 4 specific zones as shown in Fig. 3.

Computing the peak drainage discharge by the use of the rational formula: If rainfall is applied to an impervious surface at a constant rate, the period after which

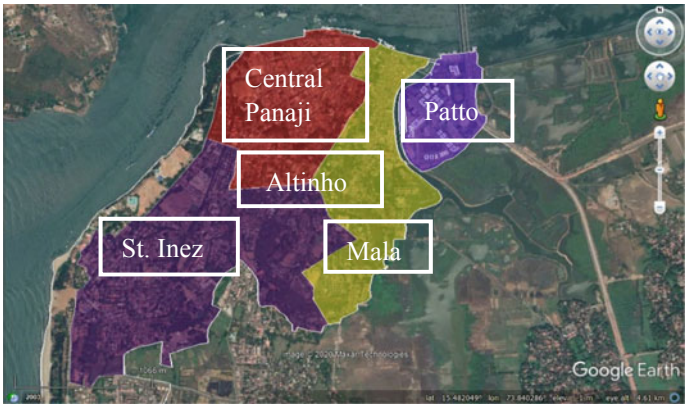

Fig. 3 Zones of study area

the entire area will start contributing to the runoff is called the time of concentration. It has been established that the maximum runoff will be obtained from the rain having a duration equal to the time of concentration, and this is called the critical rainfall duration.

Based on these principles, the rational formula was evolved. This formula states that

$$Q = \frac{1}{36} K p_c A \tag{1}$$

where Q_P = Peak rate of run-off in cumecs,

K = Coefficient of run-off,

A = the catchment area contributing to runoff at the considered point, in hectares,

P_c = Critical rainfall intensity of the design frequency i.e. the rainfall intensity during the critical rainfall duration equal to the time of concentration, in cm/h.

4.4.4 QGIS Analysis

Catchment Area Quantification

The quantification was carried out for the picked 4 zones. QGIS programming was then utilized for the evaluation of the catchment zone. It underpins both raster and vector layers. Vector information is put away as a point, line or polygon include. The shape record sent out from google earth was then brought into QGIS. The implicit highlights and calculations ascertain the catchment zone. The zone counts are accomplished for the picked 4 zones utilizing QGIS as observed underneath in Fig. 4.

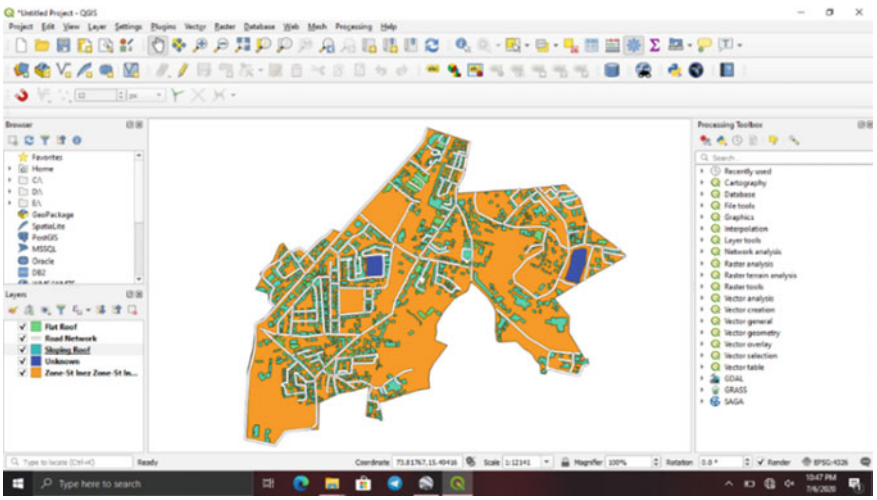

Fig. 4 Calculation of St. Inez area using QGIS software

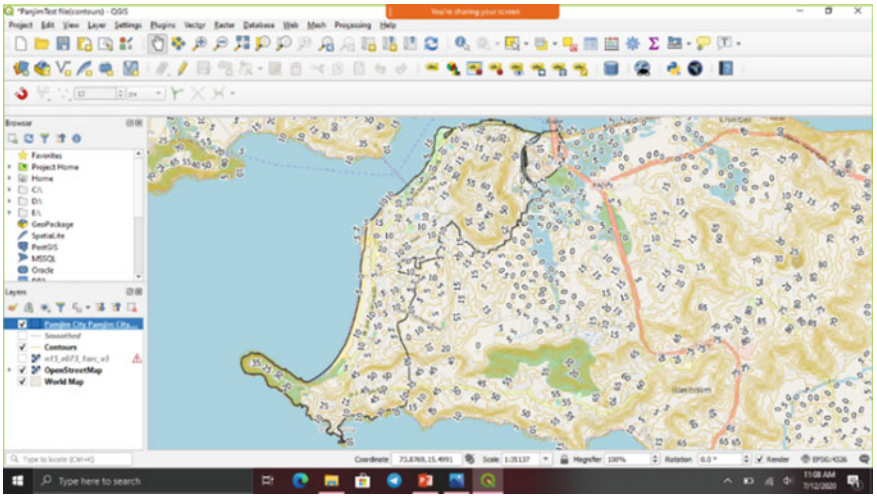

Fig. 5 QGIS generated map showing contour lines of Panaji

Contours of the City Were Generated Using DEM Files

QGIS also renders Contour generation. We generated the contour lines using the DEM file. This was obtained from the SRTM satellite. The analysis is done by using the contour tool and inputting the file into the function as in Fig. 5.

5 Analysis

Based on the data collected the following results were expressed for better understanding.

5.1 Growth of the City Using Google Map

Maps of Panaji were gotten from the year 2003–2019 with a time frame of years. The development of the city was read for the years 2003, 2005, 2010, and 2019. These maps at that point captured demonstrated the advancement in specific segments of the city. Focal Panaji had just been created during the years 2010–2015. In this way from the above perceptions, we can induce that the advancement was found in the North East-South West course.

5.2 Discharge Quantification

Using the data collected and analyzed using Google earth and QGIS, the discharge of the entire Panaji city is calculated as follows in Table 1.

6 Results

6.1 Reasons for Flooding

The causes of floods are varied. Some of the technical reasons are as follows.

6.1.1 Population Growth

Populace development in Panaji city has pressed sewer frameworks. The current populace of the city is 114,405. The transformation of open spaces to structures has left almost no space for racking and drenching of water into the ground.

6.1.2 Climate Change

This climatic change is viewed because of an Earth-wide temperature boost. The ocean level ascent alongside the invasion of blaze flooding, windy breezes during

Table 1 Discharge calculation of the city

Discharge calculations						
Location	Description	Catchment area (ha)	Runoff coefficient	Rainfall intensity (assuming 5 cm/h) (cm/h)	Discharge K*I*A/36 (m^3/s)	Total discharge (m^3/s)
		(A)	(K)	(I)	(Q)	(Q)
Althinho + Main city	Roof area	42.21	0.95	5	5.57	9.08
	Road/paved area	24.45	0.6	5	2.04	
	Open spaces	42.47	0.25	5	1.48	
Althinho + Mala area	Roof area	31.67	0.95	5	4.18	7.42
	Road/paved area	14.278	0.6	5	1.19	
	Open spaces	59.05	0.25	5	2.05	
Althinho + St. Inez	Roof area	44.94	0.95	5	5.93	13.43
	Road/paved area	30.46	0.6	5	2.54	
	Open spaces	142.81	0.25	5	4.96	
Patto	Roof area	5.72	0.95	5	0.76	2.48
	Road/paved area	8.43	0.6	5	0.70	
	Open spaces	29.29	0.25	5	1.02	
Discharge of Panaji City						32.40

the rainstorm, high flowing level, and a rising mean ocean level prompts ponding of water.

6.1.3 Infrastructure

Panaji encounters serious and weighty rainstorm showers which regularly lead to confined flooding. This prompts loss of business, products, and property. Out of the all-out city region of 8.30 km^2 around 33% of the Panaji city comprises of damp terrains and mangroves along the waterfront which go about as a hindrance from the flooding caused during the storms. These normal hindrances are contracting because of quick urbanization and expanding interest for developable land. For example, the first limit of Mala Lake has been decreased from the first zone of 70,000 to 15,000 m^2.

6.1.4 Drains

The regular channel of Saint-Inez nallah was conveying a significant piece of stormwater from the city to River Mandovi. At present this common channel is silted, exceptionally contaminated, and stale. Out of the 6 fundamental channels, it has been seen that just one channel is practical.

The wide range of various underground depletes and surface channel release into this one channel, along these lines expanding its heap. The floodgate entryways present at numerous outlets are non-utilitarian during elevated tides so there is a reverse of water through the channel pipes which brings the seawater back into the city. The floor zone proportion has expanded lately because of improvements abandoning less space so likewise, different links are being laid close by the streets again decreasing the space for the channels and expanding the heap.

6.1.5 Level of Roads

Expanding urbanization has brought about expanded impenetrable surfaces, for example, cleared and established streets and parking areas. The street levels are higher than the shop levels in light of the overlays while fixing the harmed streets without rejecting the current layers. The channels alongside the road; side depletes now and again flood and there is water originating from the housetops. There is an expansion of the water signing in all the low lying territories and streets which are at a rise of about 3 m, for example, eighteenth June street, Mala territory, Ambedkar nursery, and Patto transport stand zone.

6.1.6 High Tides

Due to environmental change there is an ascent in the ocean level, hefty tempests, and change in wind designs. This causes streak floods in the city prompting an unexpected ascent in water level into the city. This happens when the storm is considerably more in an extremely brief period and causes the amassing of increasingly more water. At the point when the water in the ocean ascends because of the elevated tide; typically most elevated tide is about 2.43 m, a mix of this flowing water and the precipitation water prompts high flood level HFL in the city.

6.1.7 Geology, Water Table, and Soil Characteristics

Panaji city has a high groundwater table with water being accessible around 1–1.5 m from the surface. The dirt is profound, inadequately depleted, and less penetrable. High water tables and expanded overflow joined with land-use practices could prompt expanded flooding.

6.1.8 The Lifestyle of People

Change in the way of life of individuals significantly impacts floods. Individuals working periods and conditions increment step by step and thus the requirement for a parking spot, vehicles increment promoting deforestation. The workers chipping away at the building destinations dump their loss in the channels.

7 Conclusions

(1) The flooding occurs at the prevailing of HTL with continuous precipitation. Flooded areas are respectively having contour numbers as follows

   (a) 18th June Road: 8 m.
   (b) 31st January road: 10 m.
   (c) Mala Area-Mala Lake: 1 m.
   (d) St. Inez: 6 m.
   (e) DB road: 3 m.
   (f) Miramar Circle to La Campala: 6 m.
   (g) Dr Babasaheb Ambedkar Park: 3 m
   (h) Patto Area-Bus Stand: 4 m
   (i) Mary Immaculate School: 10 m.

   The HTL is 2.39 m and LTL is 0.07 m.

(2) Looking at the data collected for the period of the last 5 decades it is obvious that many backwaters and areas covered by mangroves are replaced by concrete/construction. The concreted area calculated as per google earth image 2019 works out to be 9.6% of the total.

(3) Poor maintenance, microplastics, and used packaged food containers are indiscriminately thrown by tourists are the main causes of flooding. The quantum of this waste is 8% of the total garbage.

(4) Panaji has 6 drains constructed by Portuguese out of which 5 are out of function. Recently Govt. of Goa added several secondary drains, providing an intricate network that helps in draining the water into a single primary drain running from AB road to the Ferry point.

(5) To control floods, 1 flood pumping station is employed at Mala area. There is no floodwater pumping station at central Panaji. Additional pumps are required at certain locations such as near Ferry point and St. Inez creek.

(6) Deep infiltration wells along the existing drains may be used for recharging. Hence no new spaces are required in this city.

(7) Strict implementation of the law for garbage control on tourists is required

(8) The warning level of Flooding is 1.67 m.

(9) ODP needs to be re-planned taking into consideration the drainage of stormwater too (so far it is not considered).

8 Suggestions

(1) Quality monitoring of the water supply drainage network has to be frequently carried out in monsoons to prevent leakage of water and infiltration of floodwater into the pipelines.
(2) The elevation of the outfall sewer should be above the high tide level, Construction of sluice gates at the outlets, and electrically operated tidal gates.
(3) Regular maintenance of drainage and sewerage systems to avoid blockages during peak time, frequent desilting of the deep drains along with the installation of precast drains instead of concrete drains also lifting of drainage systems to higher levels.
(4) Plantation of vegetation, demarcation, and preservation of ecologically sensitive areas like Khazan lands, mangroves, and creeks; no construction activities to be allowed in these areas.
(5) Solid waste management can be done by adopting waterproofing measures like waterproof covers and rain shelters, creating elevated storages, framing silting regulations, and identifying alternate disposal sites.
(6) Planning of new infrastructure avoiding low lying vulnerable hotspots, adopting appropriate building design solutions, checking building stability and efficiency, constructing buildings 1 m above ground level, terracing hillsides to slow flow downhill.
(7) Tackling climate change by proper planning of construction and development activities such as to enhance climate resilience, using eco-friendly materials, and reduction in the generation of greenhouse gases by avoiding deforestation and burning.
(8) Creation and Protection of wetlands, wooded areas, reforesting upstream areas.
(9) Introducing water storage areas such as flood storage reservoirs, storage tanks, surge tanks, dikes and levees, detention tanks, and jack wells which help in preventing and controlling floods.
(10) Adopting pervious surfaces such as top mix permeable which allows rainwater to drain straight through to the underlying water table e.g. pervious concrete and porous concrete.
(11) Green roofs or rooftop gardening can be adopted, rooftop rainwater harvesting, and a new that cuts the running water can be grown.

References

Final city sanitation plan—Panaji (2015) Ministry of Urban Development, Govt. of India & World Bank
Heidari A (2010) The best plan for flood mitigation: a case study in the north-eastern part of Iran

Miguez MG, Mascarenhas FCB, de Magalhaes LPC, D'Alterio CFV (2009) Planning and design of urban flood control measures: assessing effects combination. J Urban Plann Dev 135(3):100–109
North Goa Planning and Development Authority. Outline development plan for Panaji
TERI Planning "climate-resilient coastal cities: learnings from Panaji and Vishakhapatnam", India (2014)

A-State-of-the-Art Review of Soil Liquefaction Mitigation Methods

Deepak Kumar and Siddhartha Sengupta

Abstract Liquefaction of soil stimulated due to earthquake vibration causes the soil to show its fluidlike characteristics. The process of liquefaction occurs due to accumulation of pore water pressure and subsequent decrease in effective stress. The loses due to liquefaction can be devastating in terms economy as well as human lives. To control the liquefaction phenomenon in soil, many researchers have investigated various methods in the past which are not only purpose effective but cost effective also. This paper tends to bring out the review of the developing techniques in the field of mitigation of soil liquefaction and to compare their effectiveness with the conventional methods of liquefaction mitigation. To begin with, the importance of the conventional methods was discussed and their limitation which led to rapid development of the advanced method. The common ground improvement practices such as soil replacement, vibro-compaction, grouting have been used traditionally. Use of nanomaterial grouting, synthetic fibers, biopolymers, air injection etc. are some major innovative techniques for enhancing the liquefaction resistance. Various researchers have adopted the use of recycle materials like glass, fly ash, tires to increase the liquefaction resistance. Several studies suggested the use of biogeotechnological method. Through this review, the readers will be able to recognize the state-of-the-art trend of liquefaction mitigation, the application of new materials and multidisciplinary approach to suggest innovative methods that could be cost effective, environment friendly along with durability and easy to use. The review of these methods for liquefaction mitigation are encouraging and boost our knowledge of the association between the lately established materials, science and technology, multidisciplinary research, and geotechnical engineering.

Keywords Liquefaction · Nanomaterials · Ground improvement · Fly ash

D. Kumar · S. Sengupta (✉)
Civil and Environmental Engineering, Birla Institute of Technology, Mesra, India
e-mail: siddhartha@bitmesra.ac.in

D. Kumar
e-mail: phdcee10003.17@bitmesra.ac.in

B. B. Das et al. (eds.), *Recent Developments in Sustainable Infrastructure (ICRDSI-2020)—GEO-TRA-ENV-WRM*, Lecture Notes in Civil Engineering 207,
https://doi.org/10.1007/978-981-16-7509-6_21

1 Introduction

In the past decade, substantial progress has taken place in understanding the techniques to assess and scientifically treat soil liquefaction. Earthquake-induced liquefaction reported in the past has motivated researchers to refresh liquefaction mitigation methods from conventional practice to a modern engineering technique. Liquefaction in saturated sandy soils can cause considerable destruction to the foundations of structures leading to economic damages in addition to the loss of human lives (Hazout et al. 2017). Liquefaction is primarily caused due to the loss in shear strength with increased pore water pressure and subsequent reduction in effective stress (Dobry and Abdoun 2017).

The likelihood of liquefaction could be cut by implementing an appropriate ground improvement system to strengthen the soil and increase its liquefaction resistance. Although most of the traditional methods (grouting, gravel columns, dewatering) have evolved over the years, their implementation is challenging because of the high cost involved, the effect on the surrounding structure, environmental impact. The customary techniques involving grouting by chemicals and cement, reinforcement of soil, deep compaction, etc. have been in practice for many years. Chemical groutings are not environmentally friendly as it can contaminate the groundwater and the earth (Benhelal et al. 2013). Vibro-compaction could be a challenging method to achieve the desired density at greater depths and could also affect the close proximity structures (Wang et al. 2017). Hence, new techniques for mitigating the effects of soil liquefaction need to be established, which is cost-effective, environment-friendly, sustainable, and non-detrimental to the adjacent structures (Huang and Wen 2015). Recently, new liquefaction alleviation techniques are continuously budding. Maithili (2017) suggested new ideas like microbial geotechnology, air injection, nanomaterial grouting, biocementation.

This review concentrates on the summary of the conventional and state-of-the-art methods for mitigation of soil liquefaction. The strengths and drawbacks of their application have also been explained. Based on the current review, the researchers will appreciate the relationship between the scientific methods, technology, and multidisciplinary approach.

2 Traditional Methods for Liquefaction Mitigation

Soil improvement techniques serve as essential pre-calamity managing skills. The use of a specific approach primarily varies on the kind of soil, cost, the practicality of the technique, etc. The plan behind these soil improvement methods is principally compaction, strengthening, and proper drainage. Current methods for enhancing the liquefaction resistance of soils comprise soil replacement, compaction piles, stone columns, grouting (by cement, chemicals), dewatering. The implementation of these

methods is complicated and troublesome. For instance, the use of cement and chemicals like sodium silicate and epoxy in the grouting method has an adverse effect on the environment (Karol 2003). Their application also confines due to the available site condition and the behavior of the already developed site with the vibrations. For bigger areas, Vibro compaction and soil replacement are not suitable, and also, the replacement of soils at such an extent would be costlier. The determination of the depth of soil replacement in many circumstances is dubious (Gabr 2012). Excessive settlement in cohesive soils can be checked by using the stone column method and provide better shear resistance than sand columns (Wang 2009). But again, stone column method is not viable in smaller areas. The techniques like dewatering, drainage, and air injection are used only to keep the saturation of the soil low or minimum. Still, these methods do not help in reducing settlement and increasing the strength of the ground. Similarly, the deep foundation/pile foundation has the probability of differential settlements during the earthquake vibrations. Khodadadi and Bilsel (2012) suggested that conventional methods utilize more energy and are not economical.

The brief details of conventional methods for mitigating liquefaction are presented in Table 1.

3 Latest Developed Methods

3.1 Nanomaterials

One of the great examples of a multidisciplinary engineering approach mitigating liquefaction is the use of nanomaterials. The nanomaterials can be injected into the finer soils by pressure diffusion (Huang and Wang 2016). These nanomaterials, when infused, do not disturb the adjacent surroundings. The most investigated nanomaterial is colloidal silica formed from silica acid. The bond of colloidal silica continues to grow over time, and simultaneously, the strength also increases. Hamderi and Gallagher (2015) showed that colloidal silica under small concentration increased the shear strength of sand. Bentonite is also a low-cost, readily available nanomaterial that is highly efficient in improving the shearing property of soils. Static and dynamic triaxial tests were conducted along with resonant column tests to investigate the effect of bentonite treated sand, and it was found that the bentonite would add ten times resistance to dynamic vibration than untreated sand (Mohtar et al. 2012; Drnevich et al. 2014). Figure 1 depicts the variation in the unconfined shear strength of the soil–cement blend added with 2% of nano-silica.

Table 1 Conventional methods used for mitigating liquefaction

Technique	Process	Drawbacks
Soil replacement	Removal of liquefaction susceptible soil and compaction of new fill and best suited for shallow foundations	Not suited for a larger area and vibratory compaction is required
Sand compaction piles	Compacted sand piles are formed by dynamic shock or static stimulation. Provides solidity and reduce ground settlement and cheaper than the stone column method	The stiffness of sandpiles is weak and comparatively less permeable
Stone columns	It helps in more drainage than sand piles and reduces excess pore pressure	Not feasible for the area with limited access
Vibrofloatation	A vibrating vibrofloat is used to densify the clay, and backfilling with gravel is done	Not effective in coarser and overconsolidated soils and is costly
Compaction grouting	Grouts consisting of a mixture of water, sand, bentonite, cement are injected into the soil under pressure	Difficult to penetrate in soil with voids containing more fines. Chemical grouts could pollute the soil and the water. It is quite an expensive method
Deep dynamic compaction	Heavyweight is allowed to drop several times from a height of 30–40 m to densify the soil	It is suitable only for construction at shallow depths and not recommended for depths more than 10 m
Blasting	Explosive charges are used to rearrange particles of soil in a denser state	The uniformity in blasting is questionable and not suitable at shallow depths
Drainage	Installation of gravel drains, sand drains may reduce the excess pore water and reduce liquefaction	Knowledge of the permeability of soil is required. It does not help in lessening the ground settlements
Dewatering	Pore pressure generation could be lowered by dewatering the groundwater	Requires continuous pumping and seepage reduction practice at the site
Deep foundation	A pile is driven deep to the ground to transfer the loads deep below the liquefiable ground	The primary concern of a pile foundation is the differential settlement. Pile driving may affect the neighboring structures
Air injection	This method involves injecting air into the soil pores, which does not allow the pore pressure to rise during seismic vibration	Because of its technical difficulties, seldom this method is used

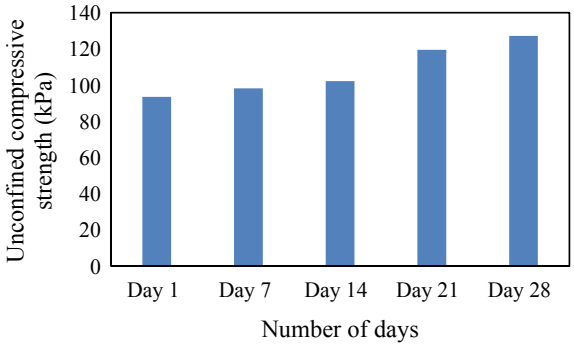

Fig. 1 Variation in unconfined compressive strength of 2% nano-silica added soil–cement mix (Thomas and Rangaswamy 2020)

3.2 Synthetic Fibers

The reinforcement of soils with fibers is not a new concept. Earlier natural fibers were in traditions. However, the scientific application of synthetic fibers has attracted researchers lately, like the orientation of fibers, distribution, aspect ratio, etc. Synthetic fibers provide better durability than natural fibers and have also exhibited improved resistance towards liquefaction susceptibility. Gray and Ohashi (1983) performed the triaxial and direct shear test to study the effect of different types of fibers, orientation, content, and it was observed that the shear strength of the soil increased. Haeri et al. (2000) utilized fiber geotextile to examine dynamic characteristics of sand, and their outcomes proved that geotextile insertion strengthened the bearing capacity and decreased the dilation of the samples. Figure 2 shows the variation in the number of cycles to liquefaction for sand treated with different percentage of polypropylene.

3.3 Use of Recycled/waste Materials

The safe confiscation of waste materials from industries such as fly ash, tires, glass, construction materials was always a challenge. However, nowadays, these materials are utilized by researchers to treat sand/soil for resisting liquefaction. Shredded tires were used by Hazarika et al. (2010) to test its applicability in liquefaction resistance. The result showed a reduction in pore water pressure; however, the relative density reduced significantly. Shake table test of recycled materials like glass, tires, and concrete was conducted with the aim to be used in backfills (Otsubo et al. 2016). The result exhibited satisfactory performance of the backfill with these materials. The materials were readily available, economical, and sustainable at the same time. Again, most of these studies are still under laboratory investigation. Also, there

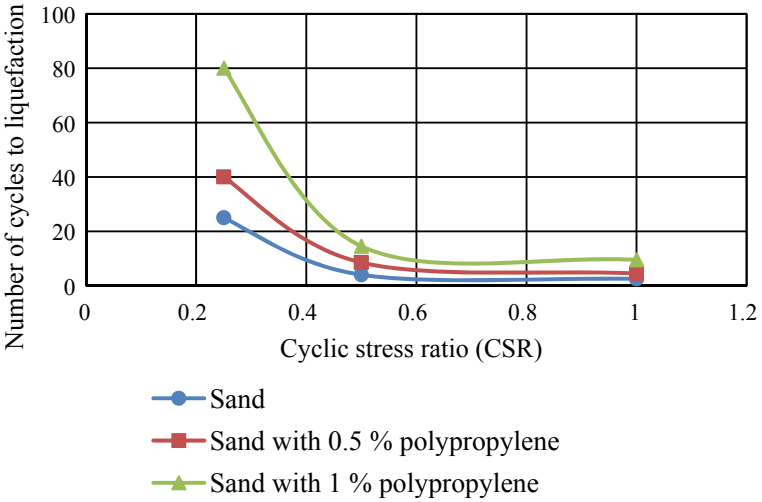

Fig. 2 Effect of polypropylene fiber on liquefaction resistance of sand (Noorzad and Amini 2014)

might be the use of some additives with these materials, and their environmental effect should be studied as well. Figure 3 exhibits the change in the number of cycles for untreated and fly ash treated sand.

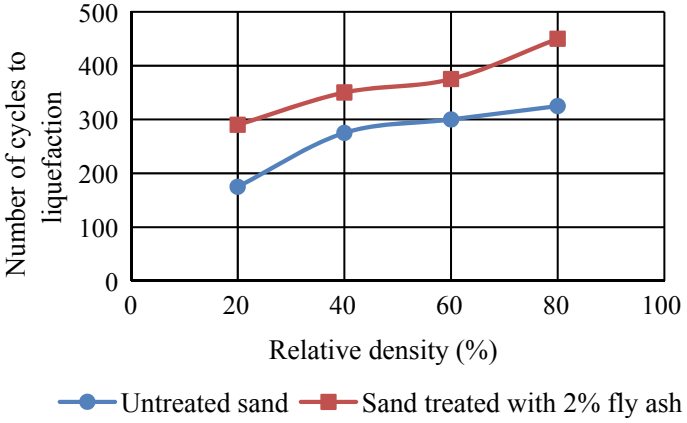

Fig. 3 Effect of fly ash on liquefaction resistance of sand (Keramatikerman et al. 2017)

3.4 Use of Biological Methods in Mitigating Liquefaction

The use of biological microorganisms to resist liquefaction is a new eco-friendly concept. Treating soils using biological materials provides an additional and innovative soil enhancement method to decrease the liquefaction hazard and avoid harm related to seismic loading (Dejong et al. 2013). The sand fragments are bonded together using microorganisms, microbiologically induced calcium carbonate precipitation (MICP), nutrients with urea, and calcium. The process of bond formation is called biocementation. Han et al. (2016) conducted cyclic triaxial tests to examine the dynamic characteristics of microbes in the soil. The findings suggest that the liquefaction resistance and the rigidity of the sand dealt with the microorganism were increased, while the accumulation of pore water and the settlement was reduced. Technological development to cure the liquefiable soil called enzymatically induced calcite precipitation (EICP) is also promising (Simatupang and Okamura 2017). In this process, urease is used to hydrolysis urea generating calcium and carbonate ions giving precipitates of calcium carbonate even at low saturation. Using the biological materials as a ground strengthening technique, liquefaction produced ground distortions, and foundation settlements due to earthquakes were efficiently lowered. Research on achieving the equilibrium between the liquefaction resistance for soil and the diminution of acceleration at the ground is required. On the whole, this approach demonstrated an excellent example of liquefaction improvement in an environmentally friendly manner.

3.5 Use of Biopolymers

Biopolymers such as starch, cellulose, chitosan have also been investigated to discover an alternative for strengthening soils. Biopolymers act as clotting and stabilizing intermediary because of their gelatin characteristics. The thermogelation attributes of biopolymers help in reducing hydraulic conductivity. Chang et al. (2016) suggested the application of gellan gum- cured sand to tackle geotechnical difficulties. The use of biopolymers increases the angle of internal friction and cohesion of the soil, but when it condenses, the strength and rigidity of the soil reduce due to dehydration.

A short summary of advanced methods is shown in Table 2.

4 Challenges in the Application of the Latest Methods to Mitigate Liquefaction

The major problem in the applicability of these current methods is the absence of a scientific standard. Almost every technique is primarily at the laboratory stage and

Table 2 Recent developments in the method of liquefaction mitigation

Materials (categories)	Advantages	Drawbacks	References
Colloidal silica (nanomaterials)	It has low viscosity and manageable gel time. The structure could be least disturbed	Injection of colloidal silica is a slow process. The permeability of the treated soil tends to decrease with an increase in colloidal silica solution	Iler (1979), Gallagher et al. (2007)
Bentonite (nanomaterials)	It is an absorbent aluminum phyllosilicate. It is easy to procure and eco-friendly. It significantly enhanced the resistance towards liquefaction of sand and slow down the time taken for the generation of pore pressure	The gel time of bentonite is slow and has high viscosity. Efficiency in larger areas is not admirable	Mohtar et al. (2012), Drnevich et al. (2014)
Synthetic fibers	Better strength than natural fibers. The load gets transferred between the soil-fiber interface. Studies revealed increased liquefaction resistance of fiber treated soil than untreated soil	The engineering standard for the in-situ application is still not designed	Gray and Ohashi (1983), Haeri et al. (2000)
Fly ash (waste product)	Fly ash mixed sands have better liquefaction resistance than clean sands, and dynamic properties of the mixtures were also improved	The laboratory variation in cyclic resistance of fly ash added sand by different researchers is not uniform. Blending of fly ash in a large field is difficult	Puri et al. (2015), Keramatikerman et al. (2017)

(continued)

Table 2 (continued)

Materials (categories)	Advantages	Drawbacks	References
Biochar	Carbon-containing material obtained from pyrolysis. The mixture of clay and biochar had shown increased shear strength with a decrease in permeability of gas	The method is not yet explored extensively and requires	Ni et al. (2018), Garg et al. (2020)
Metal bars, strips, and glass (recycled materials)	A mixture of glass fibers and cement could be useful in increasing the strength of sand. Metal strips can help in the densification of soil	Application of cement is hazardous for the ground, and the inclusion of metals could reduce the ductility of soil. The field application is also troublesome	Hazarika et al. (2010), Dehghan and Hamidi (2016)
Biopolymers	Cellulose, starch, chitosan are common polymers being tested for soil strengthening for their clogging properties	Biopolymers are biodegradable over time. It also shows swelling properties after dehydration	Chang et al. (2016)

has not been widely applied to direct site conditions at an extensive scale. Also, being the methods under trial, these methods' accurate cost cannot be evaluated until used for in-situ construction. Like for nanomaterials, the overall expenditure is higher than the application of cement or chemicals in the grouting method. Biological methods are cost-efficient on the one hand, but the process is complicated and depends on on-site conditions. Durability is also one of the vital concerns of using these methods. The long-term report on the strength of these techniques is not available.

5 Conclusions and Suggestions

The paper examined the conventional methods for mitigation of liquefaction and the constraints leading to the development of innovative approaches. It also summarizes the mechanism, advantages, drawbacks, problems associated with liquefaction alleviation techniques, and how the multidisciplinary engineering approach could help in problem-solving. The modern methods, in comparison to conventional techniques, are more environmentally friendly, sustainable, and economical. The use of biopolymer or biological processes could cut the operational cost, and the adjacent structures would be left undisturbed. The use of recycled materials in backfills or soil densification is also somewhat significant and effectively increases the shear strength of soils. MICP produced by microorganisms present in soils acts as an adhesive agent between soil particles, increasing the shear strength and decreasing the hydraulic conductivity. Further research is required to test the durability of these methods. Engineering standards should be set up for commercial utilization considering the economic and environmental aspects.

References

Benhelal E et al (2013) Global strategies and potentials to curb CO_2 emissions in cement industry. J Cleaner Prod 51:142–161. https://doi.org/10.1016/j.jclepro.2012.10.049

Chang I et al (2016) Geotechnical engineering behaviors of gellan gum biopolymer treated sand. Can Geotech J 53(10):1658–1670. https://doi.org/10.1139/cgj-2015-0475

Dehghan A, Hamidi A (2016) Triaxial shear behaviour of sand-gravel mixtures reinforced with cement and fibre. Int J Geotech Eng 10(5):510–520. https://doi.org/10.1080/19386362.2016.1175217

Dejong JT et al (2013) Dynamic response of liquefiable sand improved by microbial-induced calcite precipitation. Geotechnique 63(4):302–312

Dobry R, Abdoun T (2017) Recent findings on liquefaction triggering in clean and silty sands during earthquakes. J Geotech Geoenviron Eng 143(10):04017077

Drnevich VP et al (2014) Pore pressure generation in sand with bentonite: from small strains to liquefaction. Geotechnique 64(2):108–117

Gabr AK (2012) The uncertainties of using replacement soil in controlling settlement. J Am Sci 8(12):662–665

Gallagher PM et al (2007) Stabilization of liquefiable soils using colloidal silica grout. J Mater Civ Eng 19(1):33–40. https://doi.org/10.1061/(ASCE)0899-1561(2007)19:1(33)
Garg A et al (2020) Investigation of mechanical factor of soil reinforced with four types of fibers: an integrated experimental and extreme learning machine approach. J Nat Fibers 17(5):650–664. https://doi.org/10.1080/15440478.2018.1521763
Gray DH, Ohashi H (1983) Mechanics of fiber reinforcement in sand. J Geotech Eng 109(3):35–53
Haeri SM et al (2000) Effect of geotextile reinforcement on the mechanical behavior of sand. Geotext Geomembr 18(6):385–402
Hamderi M, Gallagher PM (2015) Pilot-scale modeling of colloidal silica delivery to liquefiable sands. Soils Found 55(1):143–153
Han Z et al (2016) An experimental study on dynamic response for MICP strengthening liquefiable sands. Earthq Eng Eng Vib 15(4):673–679
Hazarika H et al (2010) Investigation of tire chips–sand mixtures as preventive measure against liquefaction. In: Geoshanghai International Conference 207:338–345
Hazout L et al (2017) Evaluation of static liquefaction characteristics of saturated loose sand through the mean grain size and extreme grain sizes. Geotech Geol Eng 3:1–27
Huang Y, Wang L (2016) Experimental studies on nanomaterials for soil improvement: a review. Environ Earth Sci 75(6):1–10
Huang Y, Wen Z (2015) Recent developments of soil improvement methods for seismic liquefaction mitigation. Nat Hazards 76(3):1927–1938
Iler RK (1979) The chemistry of silica—solubility, polymerization, colloid and surface properties and biochemistry. Wiley, New York
Karol RH (2003) Chemical grouting and soil stabilization. Marcel Dekker, New York
Keramatikerman M, Chegenizadeh A, Nikraz H (2017) Experimental study on effect of fly ash on liquefaction resistance of sand. Soil Dyn Earthquake Eng 93:1–6. https://doi.org/10.1016/j.soildyn.2016.11.012
Khodadadi H, Bilsel H (2012) Application of microorganisms for improvement of liquefiable sand. In: Proceedings of 3rd international conference on new developments in soil mechanics and geotechnical engineering, pp 857–863
Maithili KL (2017) A discussion of liquefaction mitigation methods. Int Res J Eng Technol 4(12):1830–1833
Mohtar CSE et al (2012) Liquefaction mitigation using bentonite suspensions. J Geotech Geoenviron Eng 139(8):1369–1380
Ni JJ et al (2018) Effects of biochar on water retention and matric suction of vegetated soil. Geotech Lett 8(2):124–129. https://doi.org/10.1680/jgele.17.00180
Noorzad R, Amini PF (2014) Liquefaction resistance of Babolsar sand reinforced with randomly distributed fibers under cyclic loading. Soil Dyn Earthquake Eng 66:281–292. https://doi.org/10.1016/j.soildyn.2014.07.011
Otsubo M et al (2016) Shaking table tests on liquefaction mitigation of embedded lifelines by backfilling with recycled materials. Soils Found 56(3):365–378
Puri VK et al (2015) Liquefaction potential of sand-fly ash mixtures. In: Proceedings of 50th Indian geotechnical conference
Simatupang M, Okamura M (2017) Liquefaction resistance of sand remediated with carbonate precipitation at different degrees of saturation during curing. Soils Found 57(4):619–631
Thomas G, Rangaswamy K (2020) Dynamic soil properties of nanoparticles and bioenzyme treated clay. Soil Dyn Earthquake Eng 137:106324
Wang Z et al (2017) Review of ground improvement using microbial induced carbonate precipitation (MICP). Mar Georesour Geotechnol 35(8):1135–1146. https://doi.org/10.1080/1064119X.2017.1297877
Wang G (2009) Consolidation of soft clay foundations reinforced by stone columns under time-dependent loadings. J Geotech Geoenviron Eng ASCE 1922–1931

A State of Art Review on Constitutive Modeling of Soft Clays

Uzma Azim and Siddhartha Sengupta

Abstract With the global necessity of developing infrastructure with the concerns of land scarcity and hike in land costs, it has become an utmost need to look for construction alternatives on less feasible sites such as soft ground. Simultaneously there is an emerging need in geotechnical engineering to analyze the behaviour of soft clays in response to the forces acting on them. Abundant researches based on theoretical knowledge, analytical equations, experimental work and numerical studies have been done on constitutive models for soft soils to model their load-deformation behaviour. The models such as Mohr Coulomb, Modified Cam Clay, Soft Soil model and Hardening soil model are made applicable to be employed for finite element and finite discrete element analysis in order to perform the simulation study on soil-structure interaction problems subjected to varying static and dynamic forces. At times, difficulty arises in selecting the model which best suites the simulating conditions and gives the most critic desired results due to non-uniformity in the requirement of parameters computation between different models. This paper addresses to the review study of different researches performed and models prepared in this regard. Accordingly the overview of model's main characteristic features, parameters involved in the widely accepted constitutive model is done. The capabilities and shortcomings of different models and research performed are summarized later in the paper.

Keywords Finite element analysis · Soft clays · Stress-strain behaviour · Modified cam clay model

U. Azim · S. Sengupta (✉)
Civil and Environmental Engineering, Birla Institute of Technology, Mesra, Ranchi, India
e-mail: siddhartha@bitmesra.ac.in

B. B. Das et al. (eds.), *Recent Developments in Sustainable Infrastructure (ICRDSI-2020)—GEO-TRA-ENV-WRM*, Lecture Notes in Civil Engineering 207,
https://doi.org/10.1007/978-981-16-7509-6_22

1 Introduction

With the increased demand of infrastructure development with increasing population, alternatives are looked up to for construction activities. When construction is decided to be done on less feasible sites, there arises an emerging need for geotechnical engineers to analyze the physical and mechanical behaviour of the desired ground in response to the static and dynamic forces acting on them. At times, it becomes difficult to select an appropriate model which best suites the simulating conditions and critically analyses the problem to give the best results. Therefore, the need for studying the soil with suitable model becomes important. Analyzing the problems with finite and discrete element software involves continuum mechanics based algorithms and here constitutive modeling defining the mechanical behaviour of soil plays a crucial role. Various researchers have been performing experiments in this field by employing analytical, experimental and numerical studies as discussed below. The major findings and parameters involved are hence with summarized in Tables 1 and 2.

2 Soft Soil Models

Islam and Gnanendran (2017) prepared an elastic-viscoplastic (EVP) model to study creep effects on isotropic clays. The parameters of the prepared model were taken from conventional oedometer and triaxial tests. The suitability of the model was validated by performing creep tests, relaxation tests, strain-rate effect tests, and overconsolidation ratio effect tests on Kaolin clay. In order to study the long term performance numerical analysis was carried out to compare the settlement characteristics obtained from the prepared EVP model from that of Modified Cam Clay (MCC) model. The model showed better prediction of time dependent settlement characteristics on embankment. For 3.0 m preloading after 590 days, the magnitude of under prediction for surcharging by MCC was 14.25%. The EVP model showed linear variance because of the inclusion of the creep parameter.

Karstunen et al (2006) performed a comparison analysis between elastic–plastic models MCC and Soft soil (SS) model in assessing the behaviour of soft soils. MCC and SS models differ in the way their failure planes are defined and the modeling method on the dry side of the failure plane. The failure surface of MCC model is dependent on the Mohr–Coulomb (MC) failure criterion whereas SS model is independent of failure planes and the yield plane is defined by the incorporation of the coefficient of lateral earth pressure (K_o^{NC}). The MCC model defines softening behaviour of soft soil and plastic analysis is taken care of by the SS model.

Ma et al (2017) developed a 3D elastoplastic model based on characteristic stresses and inspired from MC model. It can be effectively employed to analyze strain softening and cyclic behaviour of wide variety of soils. Since the newly developed model takes into account the multiple loading–unloading cycles, it can be employed

Table 1 Summary of previous studies using different constitutive models for static loading

Author	Proposed model	Major conclusions	Parameters involved
Islam and Gnanendran (2017)	Elastic-viscoplastic (EVP) model	Prepared EVP model to study creep characteristics of isotropic clays. The model showed slight overprediction when compared experimentally on Kaolin clay and performed better than MCC model in settlement prediction	Compression index (λ), swelling index (κ), Poisson's ratio (υ), void ratio at unit mean pressure (e_N), permeability (k), creep parameter (C_α)
Liu and Muraleetharan (2012)	Soil water characteristic curve (SWCC) based model	Found to be capable to model the hydro-mechanical behaviour in saturated and unsaturated soils by taking into account the intergranular stresses effect elastic soil deformation caused due to suction	Mean intergranular stress (p'), deviatoric stress tensor (s), elastic volumetric strain ($\varepsilon_e{}^v$), elastic deviatoric strain ($\varepsilon_e{}^q$), bulk modulus (K), shear modulus (G), and capillary elastic modulus (τ^e)
Ma et al. (2017)	3D elastoplastic model based on characteristic stresses	The newly developed 3D elastoplastic model can be effectively used to model strength and deformation behaviour of soils under general stress conditions It takes into account the principal stress of the material and therefore can predict positive and negative dilatancy and 3D properties of wide category of soils	Plastic volume strain ($\varepsilon_e{}^p$), elastic strain increment ($d\varepsilon_y{}^e$), plastic strain increment ($d\varepsilon_y{}^p$), hardening parameter (H)

(continued)

Table 1 (continued)

Author	Proposed model	Major conclusions	Parameters involved
Mita et al. (2004)	Hvorslev model and MCC model	Effective in modeling the stress–strain behaviour of over consolidated soils up to the subcritical point or until when the specimens remain intact resulting in uniform displacements. The employed models can be used to simulate over consolidated soils under compression, extension and plane strain conditions	Preconsolidation pressure, Compression index (λ), swelling index (κ), shearing resistance angle (ϕ), slope of Hvorslev surface (m_H), slope of critical state line (M_j)
Nagula et al. (2018)	Hardening soil model	The pressure dependent behaviour of the HSM model can be perfectly used to model the hardening and softening behaviour of the pavement granular material. It can also be used to effectively model the repeated loading and unloading cycles observed in the pavement	Secant modulus at 50% material strength (E_{50}^{ref}), unloading elastic modulus (E_{ur}^{ref}), oedometer modulus (E_{oed}^{ref}), cohesion (c), friction angle (ϕ)
Tachibana et al. (2020)	Elasto- plastic rebound version of MCC model	Basically models the swelling characteristics of expansive soils during unloading. It can be effectively employed to determine the stress paths in both axial and radial directions during unloading and swelling The employment of plastic rebound theory can also be utilized in predicting the earth pressure coefficients at rest	Void ratio (e), compression index (λ). Swelling index (κ), K_o value, mean stress (p)

(continued)

Table 1 (continued)

Author	Proposed model	Major conclusions	Parameters involved
Wu et al. (2019)	Equivalent area method (EA), interface elements, MCC and MC model	Irrespective of the constitutive model used, unacceptable numerical results are obtained if interface elements are not employed MCC resulted in overestimation of the involved parameters in the case of over consolidated soils and this was attributed to the elliptical yield surface of the model MC model was attributed as the best suited linear elastic perfectly plastic model but it resulted in inaccurate horizontal displacements	Unit weight of soil (Υ), Initial void ratio (e_0), secant stiffness (E_{50}), Poisson's ratio (υ), compression index (λ), swelling index (κ), permeability coefficient (k), geosynthetic stiffness (J)

Table 2 Summary of previous studies using different constitutive models for dynamic loading

Author	Proposed model	Major conclusions	Parameters involved
Essa and Desai (2017)	Unified constitutive model based on disturbed state concept (DSC)	Effectively models the non-linear behaviour of the ground response during dynamic soil-pile interaction. The model can be used to compute the liquefaction potential and shear stress transfers between the soil and interface elements during the dynamic analysis	Modulus of elasticity (E), Poisson's ratio (υ), critical state parameters (m, e_o^c, λ), disturbance parameters (A, Z, D_u)
Ling et al. (2016)	Sekiguchi-Ohta and MIT-E3 models	Can be used to assess the ground response due to deep excavations such as lateral displacement of diaphragm walls, ground settlements, and bending moments in the diaphragm walls. The simulating results showed great agreement with the field measurements	Compressibility index (λ), swelling index (κ), Poisson's ratio (υ), anisotropy rate (w), bounding surface parameters (C)
Liu et al. (2014)	Unified constitutive model based on critical state soil mechanics	The model was found to be capable to smoothly compute the cyclic hysteresis, cyclic densification, cyclic hardening, and shear-strain accumulation of gravelly soils	Elastic constants (K_o, G_o, m), critical state constants ($e_{\tau 0}$, ϕ_{cr}, λ), bounding surface constant (k_p), dilatancy and plastic flow constants (α, k_m, m_f)
Ni et al. (2014)	Modified Cam Clay (MCC) theory	The proposed model can be effectively used to model the excess pore pressure, bearing capacity, permeability and compressibility of the subgrade material subjected to cyclic loading	Compressibility index (λ), swelling index (κ), initial void ratio (e_o), cyclic degradation parameters (ζ_1, ζ_2)

(continued)

Table 2 (continued)

Author	Proposed model	Major conclusions	Parameters involved
Saberi et al. (2020)	Constitutive model based on shear coupling	Effective in modeling the shear coupling effects in granular and sandy soil-structural element interfaces. The proposed model was found to have wide application in the computation of hardening and softening phenomenon and assessing the stress paths propagations	Average grain size (D_{50}), minimum and maximum void ratio (e_{min}, e_{max}), dry density (Υ_d), relative density (D_r), compressibility index (λ), swelling index (κ)

as a 3D constitutive model to study deformation characteristics for other types of geomaterials as well.

Wu et al (2019) attempted to model cement fly-ash gravel (CFG) pile supported embankment over decomposed granite soils and performed a compatibility analysis between MCC and MC models employing both equivalent area (EA) method and interface elements. When EA method was employed without using interface elements, slight overestimation of stresses was observed in the surrounding soil and underestimation at the pile head which apparently incorrectly interprets the stress concentration ratio. MCC model was found to be dependent on numerous factors such as particle size, degree of saturation, weathering degree and over-consolidation ratio (OCR) and it resulted in inaccurate overestimation of the deformation in the case of over consolidated soils (27% higher than the measured value). MC model gave satisfactory results in the case of normally consolidated soils and was considered as the most acceptable linear elastic perfectly plastic model. In contrast, the maximum horizontal displacement obtained from the MC model was twice of that obtained from the MCC model. Therefore, physical judgment of the results is important regardless of the model used.

3 Hardening Soil Models

Karstunen et al (2006) defined S-Clay1S model to analyse the fabric destructuration during plastic straining. It incorporates 3 hardening laws defining change in yield surface during plastic hardening, rotational hardening law describing orientation changes in the process of plastic straining and destructuration law signifying bond degradation in the course of fabric straining.

Khalilzad et al (2014) used hardening soil model (HSM) to simulate an embankment dam under change in geometry and water level effect conditions. Since the

failure plane of the HSM is not pre-defined and is highly dependent on the deviatoric stress and expands in the case of plastic strain it can be used to model wide variety of soils and shear zones.

Mun and McCartney (2016) prepared constitutive model in order to capture the response of unsaturated and compacted clay subjected to isotropic compression. The proposed model showed agreement with experimental results on unsaturated soils undergoing pressurized saturation up to mean stress of 160 MPa. When confirmed with undrained compression tests, it was observed that all compacted specimens initially followed the elastic compression response until reaching a mean apparent preconsolidation stress.

Nagula et al (2018) modeled pavement granular material using HSM and concluded similarities when compared with static triaxial tests. The yield surface of HSM is stress dependent and responds equally to the confining conditions and being pressure sensitive it gives accurate results for both strain hardening and softening ideally suiting the pavement conditions. Calibration using triaxial tests showed a hyperbolic relationship between axial strain and axial stress as:

$$-\varepsilon_1 = \frac{1}{E_i} - q/\left(1 - \frac{q}{q_a}\right),$$

where q_a = asymptotic value of shear strength and E_i = initial stiffness. The parameters of HSM model can be obtained static triaxial test and oedometer test.

4 Over-Consolidated Soils

Ardebili et al (2015) employed MC, MCC and SS models to compute anchor pull out capacity from saturated soils. The load–displacement curves show that ultimate vertical pullout capacity does not get influenced by the stiffness factor. For shallow plates, the uplift resistance is dependent on soil's effective weight and mobilized shear strength along the failure plane.

Forcelini et al (2020) employed nonlinear poroelastic model to calculate undrained shear strength of transient soils. The analytical equations were confirmed by experimental results from permeability and vane shear tests. The model attempted to analyze the effect on soil stiffness and strength by the vane installation and it was concluded that the radius of the vane's influence critically effects drainage and torque activities of the transient soils.

Mita et al (2004) performed experiments to assess the stress–strain behaviour of overconsolidated soil under triaxial compression, extension, and plane strain conditions. Hvorselv-MCC model was employed in their subcritical regions for the analysis and the failure criterion was generalized using MC model.

Xiao and Desa (2019) used disturbed state concept (DSC) to analyze strain softening, volumetric expansion, undrained shear strength and computation of excess pore pressure during the undrained shearing process of overconsolidated clays. The

model was calibrated against drained triaxial tests and the parameters for disturbance, potential-failure, and plastic modulus were considered as influencing factors in the determination.

Zhang and Hu (2017) carried out a numerical analysis to capture the progressive failure of soil slopes. It incorporated shear zones as they are capable to locate the deformation zones and accordingly pre-determine the failure plane. Centrifuge model tests were used to verify the simulation results and they showed great agreement in the failure plane determination obtained.

5 Expansive Soils

D'onza et al. (2011) compared various constitutive models to analyze the mechanical and water retention behaviour of unsaturated soils employing suction-controlled and constant water content laboratory tests. Models based on hydraulic uncoupled forces proved to coincide better with experimental results. Therefore the major conclusion drawn from this research is that retention based models shows less discrepancies to experimental results as compared to mechanical models.

Liu and Muraleetharan (2012) developed soil water characteristic curve (SWCC) based model to incorporate the suction behaviour in saturated and unsaturated sands and silts. The proposed model was found to simulate the exceptional case of saturated soils which are in the unsaturated zone and the suction value declines below the air entry value. At this point, the suction value is still positive despite all the pores being filled with water. Plastic volumetric strain and irrecoverable water content were found to be the major parameters influencing suction.

Tachibana et al. (2020) prepared an elasto-plastic rebound model to capture the mechanical behaviour of expansive soils. It incorporates a plastic rebound line besides the normal consolidation line in order to employ hardening law to calculate the plastic swelling upon unloading. The slope of semi-log graph between void ratio and mean stress, commonly called normally consolidated line (NCL), gives the compression index (λ) for elasto-plastic loading state and slope of the elastic swelling line (ESL) gives the swelling index (κ). This modified version of the MCC model can be used to simulate both saturated and unsaturated soils as well as their transitions.

6 Dynamic Analysis

Essa and Desai (2017) proposed a discrete state concept (DSC) based model to analyze soil-structural element interaction. The involved parameters were computed by performing triaxial tests on soils and shear tests on interface materials. The discussed model was found capable to simulate the non-linear behaviour of the 2-phase porous media undergoing cyclic or dynamic loading during pile diving.

Ling et al. (2016) attempted to determine effects of deep excavations on adjacent ground surface by employing models made of anisotropic boundaries (namely, Sekiguchi-Ohta and MIT-E3 models). The models adopt a non-associative flow rule. The results obtained from the simulation were in agreement with the field measurements of lateral displacement of diaphragm walls, ground settlements, and bending moments in the diaphragm walls.

Liu et al. (2014) prepared a constitutive soil model to capture the dynamic response of earth structures employing gravelly soils such as rockfill dams and railroad ballasts. The model was designed to incorporate the simulation of particle breakage through translating critical state line, smooth transition from unloading to reloading in the stress space, and proper modeling of cyclic hysteresis, cyclic densification, and cyclic hardening of dense gravelly soils.

Ni et al. (2014) prepared an elastic yield surface based model based on MCC model in order to analyze the behaviour of subgrade materials. The model was found suitable to simulate the materials employed for subgrade in highway pavements, railway tracks, and airport runways which undergo development of excess pore pressure and strain with each successive cyclic loading. The low bearing capacity, high compressibility and low permeability of the subgrade when subjected to cyclic loading can be fairly analyzed by the proposed model.

Saberi et al. (2020) proposed a 3D shear coupling model to simulate extreme interface behaviour (hardening and softening), compaction, dilatancy, stress degradation, partice size deterioration and stress paths for soils subjected to monotonic and cyclic loading involving shear coupling. The simulating parameters were computed using simple interface shear tests.

Tables 1 and 2 show summary of previous studies using static and dynamic constitutive models respectively.

7 Failure Plane and Governing Equations of Major Constitutive Models

7.1 Modified Cam Clay (MCC) Model

$$e - e_o = -\lambda \ln\left(p'/p_o\right) \text{ (for virgin isotropic compression)} \tag{7.1}$$

$$\mathrm{e}-\mathrm{e_o} = -\kappa \ln\left(p'/p_o\right) \text{ (for isotropic unloading/reloading)} \tag{7.2}$$

where e is void ratio, p′ is mean effective stress, λ is compression index, κ is modified swelling index (Fig. 1).

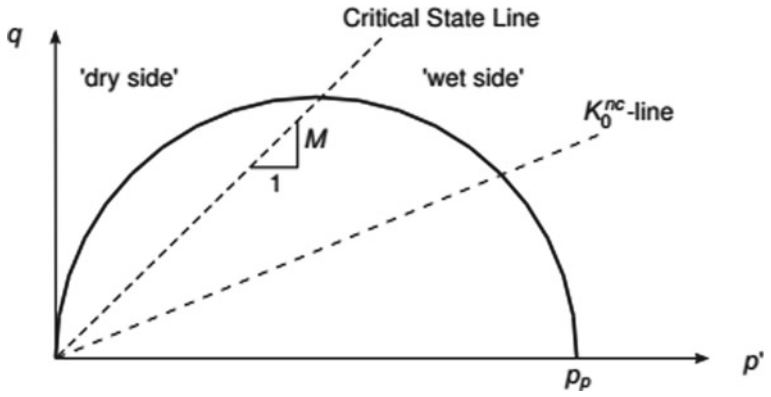

Fig. 1 Yield surface of MCC model in p′-q plane

7.2 Soft Soil (SS) Model

$$\varepsilon_v - \varepsilon_v^o = -\lambda^* \ln\left(\frac{p' + c\cot\varphi}{p^o + c\cot\varphi}\right) \text{ (for virgin compression)} \tag{7.3}$$

$$\varepsilon_v - \varepsilon_v^{eo} = -\kappa^* \ln\left(\frac{p' + c\cot\phi}{p^o + c\cot\phi}\right) \text{ (for unloading/reloading)} \tag{7.4}$$

$$\lambda^* = \frac{\lambda}{1+e};\ \lambda : \text{Cam-Clay compression index},\ \lambda^* : \text{Modified compression index} \tag{7.5}$$

$$\kappa^* = \frac{\kappa}{1+e}\kappa^*,\ \kappa : \text{Cam-Clay swelling index, e : void ratio,}$$
$$\kappa^* : \text{Modified swelling index} \tag{7.6}$$

where ε_v is volumetric strain, p′ is mean effective stress, c is cohesion, φ is angle of internal friction, p^0 is initial stress (Fig. 2).

7.3 Hardening Soil Model (HSM)

See Fig. 3.

7.4 Sekiguchi-Ohta Model

$$\varepsilon_v - \varepsilon_v^o = -\lambda^* \ln\left(\frac{p'}{p^0}\right) \text{ (virgin compression)} \tag{7.7}$$

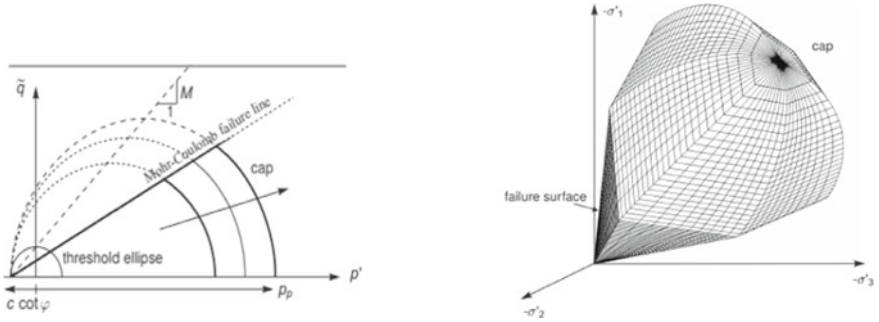

(a) (b)

Fig. 2 **a** Yield surface of SS model in p′-q plane, **b** Yield contour of SS model in principal stresses plane

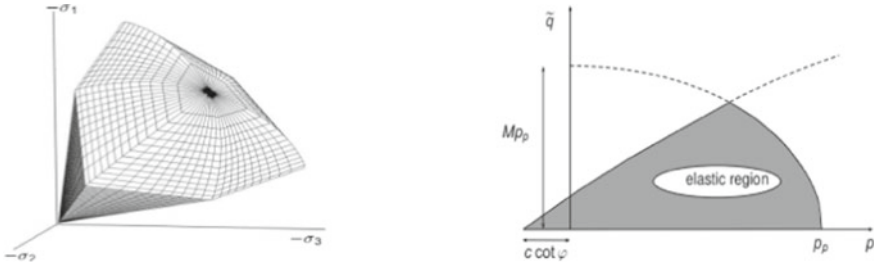

(a) (b)

Fig. 3 **a** Yield contour of HSM in principal stress, **b** yield surface of HSM in p′-q plane

$$\varepsilon_{\mathrm{v}}^{\mathrm{e}} - \varepsilon_{\mathrm{v}}^{\mathrm{eo}} = -\kappa^{*} \ln\left(\frac{p'}{p^{0}}\right) \text{ (unloading and reloading)} \tag{7.8}$$

$$\mathrm{K_{ur}} = \frac{E_{ur}}{3(1-2\upsilon_{ur})} = \frac{p'}{\kappa^{*}} \text{ (unloading/reloading)} \tag{7.9}$$

where ε_{v} is volumetric strain, p′ is mean effective stress, λ* is modified compression index, $\varepsilon_{\mathrm{v}}{}^{\mathrm{e}}$ is elastic volumetric strain, κ* is modified swelling index, $\mathrm{K_{ur}}$ is elastic bulk modulus, $\mathrm{E_{ur}}$ is elastic Young's modulus, υ_{ur} is elastic Poisson's ratio (Fig. 4).

8 Conclusions

Constitutive modeling is employed in numerical analysis in order to analyze the soil critically according to the situation. They assist in providing the crucial mechanical

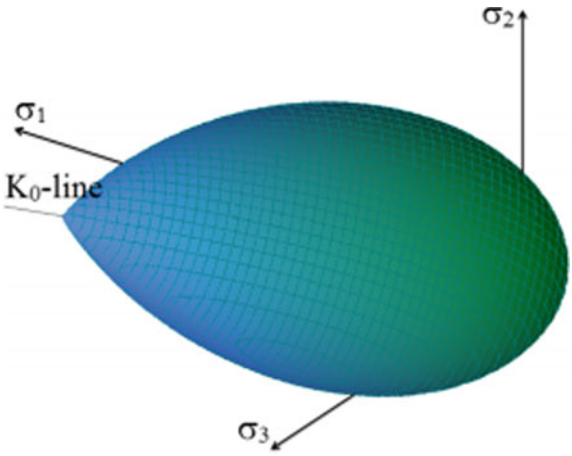

Fig. 4 Sekiguchi-Ohta model yield surface in triaxial space

behaviour of soil emphasizing the prominent aspects of soil behaviour based on mathematical calculations. This paper attempted to summarize some of the commonly used constitutive models employed by different researchers to simulate soft soils, expansive soils, hardening soils and over consolidated soils under static and dynamic analysis. The major conclusions drawn from the review study are listed below:

1. To study soft soil characteristics, Modified Cam Clay (MCC) and Soft Soil (SS) models are appropriate models. The difference between the 2 models arises due to discrepancies in their computing parameters and the way the analysis progresses in the dry side of failure plane.
2. The advantage associated with SS model is that it is independent of failure plane and the yield surface can be used to compute the coefficient of lateral earth pressure (K_0^{NC}) as well.
3. Hardening Soil Model (HSM) has wide applications as it can be employed wide range of soft and stiff type of soils and shear zones since its failure plane is not pre-defined and it expands and contracts depending on the deviatoric stress conditions.
4. Sekiguchi-Ohta and MIT-E3 models can be used to perform dynamic analysis to record ground response due to deep excavations such as lateral displacement of diaphragm walls, ground settlements, and bending moments in the diaphragm walls.
5. The common essential parameters required for constitutive modeling are compressibility index (λ), swelling index (κ), initial void ratio (e_o), bulk modulus (K), shear modulus (G), Young's modulus (E) and unit weight (Υ). These parameters can be derived from simple triaxial and oedometer tests.

References

Ardebili ZA, Gabr MA, Rahman MS (2015) Uplift capacity of plate anchors in saturated clays: analyses with different constitutive models. Int J Geomech 16(2). https://doi.org/10.1061/(ASCE)GM.1943-5622.0000518

D'onza F, Gallipolli D, Wheeler S, Casini F, Vaunat J, Khalili N, Laloui L, Mancuso C, Mas D, Nuth M, Pereira JM, Vassallo R (2011) Benchmark of constitutive models for unsaturated soils. Geotechnique 61(4):283–302. https://doi.org/10.1680/geot.2011.61.4.283

Essa MJK, Desai CS (2017) Dynamic soil–pile interaction using the DSC constitutive model. Indian Geotech J 47:137–149. https://doi.org/10.1007/s40098-016-0197-3

Forcelini M, Maghous S, Schnaid F, Almeida FS, Simplified model for interpretation of undrained shear-strength from field-vane tests in transient soils. J Geotechn Geoenviron Eng 146(6). https://doi.org/10.1061/(ASCE)GT.1943-5606.0002272

Islam MN, Gnanendran CT (2017) Elastic-viscoplastic model for clays: development, validation, and application. J Eng Mech 143(10). https://doi.org/10.1061/(ASCE)EM.1943-7889.0001345

Karstunen C, Wiltafsky, Krenn H, Scharinger F, Schweiger HF (2006) Modelling the behaviour of an embankment on soft clay with different constitutive models. Int J Numer Anal Methods Geomech 30(10), 953–982. https://doi.org/10.1002/nag.507

Khalilzad M, Gabr MA, Hynes ME (2014) Deformation-based limit state analysis of embankment dams including geometry and water level effects. Int J Geomech 15(5). https://doi.org/10.1061/(ASCE)GM.1943-5622.0000435

Ling HI., Hung C, Kaliakin VN (2016) Application of an enhanced anisotropic bounding surface model in simulating deep excavations in clays. J Geotech Geoenviron Eng 142(11). https://doi.org/10.1061/(ASCE)GT.1943-5606.0001533

Liu C, Muraleetharan K (2012) Coupled hydro-mechanical elastoplastic constitutive model for unsaturated sands and silts. I: Formulation. Int J Geomech 12(3):239–247. https://doi.org/10.1061/(ASCE)GM.1943-5622.0000146

Liu H, Zou G, Liu J (2014) Constitutive modeling of dense gravelly soils subjected to cyclic loading. Int J Numer Anal Methods Geomech 38(14). https://doi.org/10.1002/nag.2269

Ma C, Lu D, Du X, Zhou A (2017) Developing a 3D elastoplastic constitutive model for soils: a new approach based on characteristic stress. Comput Geotech 86:129–140. https://doi.org/10.1016/j.compgeo.2017.01.003

Mita KA, Dasari GR, Lo KW (2004) Performance of a three-dimensional Hvorslev-modified cam clay model for overconsolidated clay. Int J Geomech 4(4):296–309. https://doi.org/10.1061/(ASCE)1532-3641(2004)4:4(296)

Mun W, McCartney JS (2016) Constitutive model for the undrained compression of unsaturated clay. J Geotech Geoenviron Eng 143(4). https://doi.org/10.1061/(ASCE)GT.1943-5606.0001635

Nagula SS, Robinson RG, Krishnan JM (2018) Mechanical characterization of pavement granular materials using hardening soil model. Int J Geomech 18(12). https://doi.org/10.1061/(ASCE)GM.1943-5622.0001291

Ni J, Indraratna B, Geng X, Carter JP, Chen Y (2014) Model of soft soils under cyclic loading. Int J Geomech 15(4). https://doi.org/10.1061/(ASCE)GM.1943-5622.0000411

Saberi M, Annan C, Konrad J (2020) Three-dimensional constitutive model for cyclic behavior of soil-structure interfaces. Soil Dyn Earthquake Eng 134. https://doi.org/10.1016/j.soildyn.2020.106162

Tachibana S, Ito S, Iizuka A (2020) Constitutive model with a concept of plastic rebound for expansive soils. Soils Found 60(1):179–197. https://doi.org/10.1016/j.sandf.2020.02.007

Wu L, Jiang G, Ju N (2019) Behavior and numerical evaluation of cement-fly ash-gravel pile-supported embankments over completely decomposed granite soils. Int J Geomech 19(6). https://doi.org/10.1061/(ASCE)GM.1943-5622.0001430

Xiao Y, Desa CS (2019) Constitutive modeling for overconsolidated clays based on disturbed state concept II: Validation. Int J Geomech 19(9). https://doi.org/10.1061/(ASCE)GM.1943-5622.0001475

Zhang G, Hu Y (2017) Numerical modeling of failure process of soil slopes. Int J Geomech 17(4). https://doi.org/10.1061/(ASCE)GM.1943-5622.0000798

Testing the Skill of Hybrid Model Approach for Aerosol Estimates

Dudam Bharath Kumar and Sasmita Sushree

Abstract In this study, we evaluate the performance of aerosol retrieval for surface concentration of PM_{10} (i.e. particulate matter of aerodynamic size less than 10 μm) aerosols and Total Suspended Particulate (TSP) aerosols by combining hybrid model predictions and observations. The 24-hourly aerosol observations during summer (20 February–21 March, 2018) were carried out on the terrace of height of 10 m above ground level near campus-3 of Kalinga Institute of Industrial Technology Deemed to be University (KIIT-DU) Bhubaneswar, India. Estimates of hybrid model approach for surface mass concentration were performed combining a multiplication factor which uses satellite- and model-based aerosol parameters. The satellite parameters include columnar aerosol optical depth (AOD) at 550 nm was obtained from Moderate Resolution Imaging Spectrophotometer (MODIS) estimates of Terra-collection 6 (C6) and Level 3 (L3) combined Dark Target and Deep Blue algorithm (Levy et al. in Atmos Meas Tech 6:2989–3034, 2013); whereas the multiplication factor was obtained from the global model simulations (Reddy et al. in J Geophys Res 110, 2005). The multiplication factor consists of functional constraints (e.g. relative humidity, RH) and constants (e.g. planetary boundary layer in km; mass extinction coefficient in $m^2\ g^{-1}$). The RH, PBLH and MEC were representative of hygroscopy, mixing layer dynamics and extinction efficiency of aerosols. Results showed 24-hourly surface PM_{10} and TSP concentration ranges from 76 to 148 $\mu g\ m^{-3}$ and 142 to 231 $\mu g\ m^{-3}$, respectively. In general, the hybrid model underestimates the observations. The hybrid model predictions of PM10 in February and TSP in March were associated high coherence with the observations. Corresponding normalized bias of model estimates were within the uncertainty of monthly average observations (≈30%). Though few uncertainty, the hybrid model predicts with a considerable skill. However, this uncertainty in the hybrid model is reasoned by error propagated from the satellite observations and emission induced uncertainties in the GCM model. This study may provide scope for the fusion studies that combines vertical profile of aerosols and indirect effects of aerosol-cloud interactions in South Asia.

D. B. Kumar (✉) · S. Sushree
School of Civil Engineering, Kalinga Institute of Industrial Technology Deemed To be University (KIIT-DU), Bhubaneswar, India
e-mail: dudam.kumarfce@kiit.ac.in

B. B. Das et al. (eds.), *Recent Developments in Sustainable Infrastructure (ICRDSI-2020)—GEO-TRA-ENV-WRM*, Lecture Notes in Civil Engineering 207,
https://doi.org/10.1007/978-981-16-7509-6_23

Keywords Synergy · Hybrid model · General circulation model · Skill · Normalized bias

Theme: Sustainability in Environmental Engineering

Subtheme: Aerosol and Air quality

1 Introduction

Achievement of ambient air quality is a challenge for both scientific community and the governing bodies of a city. It has been noticed that most of the urban regions are highly polluted compared to that of rural or adjoining regions (Ramachandran et al. 2012). These studies suggest that rapid growth of population, urbanization, industrialization and elevated vehicular activity escalates the air pollution over the cities. It is observed and reported in previous studies of UNDESAP (2019) that 55% of population lives in urban areas. It was projected a forecast of 13% increase from the latest year towards by 2050. Population growth in state of Odisha reported to be ~31% that is slightly less than Indian average growth rate (i.e. 36%) as suggested in previous studies (BCDP 2019). According to the studies of Swain et al. (2017), city of Bhubaneswar has gained its urban cover by 83% from 2000 till 2014. On the other hand, vegetation or green cover was seen to be reduced by 86% between the corresponding years.

PM pollution?

2 Methodology

2.1 Site Description

Continuous monitoring of PM_{10} and Total Suspended Particulate (TSP) surface level (at a height of 10 m from above ground level, agl) observation was carried out each day for 24 h at terrace of School of Civil Engineering Department the integral building complex of Campus-3 (20.35° N, 85.81° E, 60 m amsl) of Kalinga Institute of Industrial Technology Deemed to be University (KIIT-DU) Bhubaneswar, Odisha. Columnar aerosol properties (e.g. AOD550 nm were obtained from Moderate Resolution Imaging Spectrophotometer (MODIS) estimates of Terra-collection 6 (C6) and Level 3 (L3) combined Dark Target and Deep Blue algorithm (Levy et al. 2013), for the corresponding days of ground-based observation.

2.2 Sources and Transport

Ensemble of seven-day back-trajectories at surface (10, 100 and 500 magl) and elevated (1000, 2500, 500 magl) altitudes were made based on few assumptions including (a) the typical lifetime of aerosol as about a week (i.e. seven days), (b) Arrival height was chosen from above ground level (as the level considered for the aerosol observations were done as the same) and (c) Considered trajectory ensemble at both levels to reduce the uncertainty of wind shear induced by single trajectory use for the representation of mean trajectory of air-parcel.

3 Results and discussion

3.1 Evaluation of Ambient PM_{10} Aerosols

Time series of 24-hourly surface PM_{10} concentration in the ambient air from the model and that from the observations during spring season (February to March) in the year 2018 is shown in Fig. 2. Surface PM_{10} concentration exhibits relatively high during February compared to that of March. It refers that the anthropogenic originated aerosols are predominantly present in the February air mass, less amount of coarser aerosols are reasoned by low PM_{10} concentration (as compared with $PM_{2.5}$ concentration, Figure not shown). Whereas in March, coarser aerosols of low extinction efficiency are likely potential enough to contribute $PM_{10,}$ this was reasoned by the long range transport of dust (from desert or plain regions) originating from regional to continental region level (Refer Fig. 3).

3.2 Chemical Composition

Chemical composition obtained from the model was fed to the aerosol optical depth for the retrieval of surface mass concentration of species as illustrated in Fig. 3. Surface concentration of PM_{10} constituted of mostly naturally emanated emissions including dust and sea spray, those may likely originated from middle east and northern Africa regions (refer Fig. 4). The black carbon, sulfate and organic carbon are predominant in March days (day 6 and day 7) signifying the influence of anthropogenic origin emissions including vehicular emissions, coal combustion and biomass burning emissions, respectively. This was reasoned by back trajectory information obtained as shown in Fig. 1b.

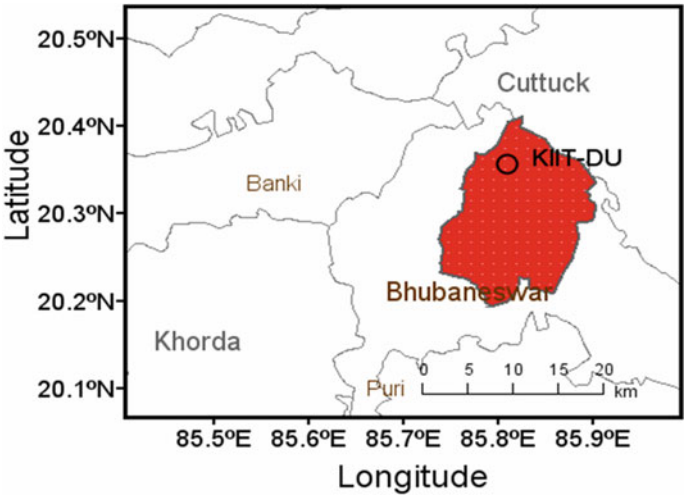

Fig. 1 Site location of present study situated at Kalinga Institute of Industrial Technology Deemed to be University (KIIT-DU) Bhubaneswar. Region mentioned in red background is Bhubaneswar Municipal Corporation (BMC)

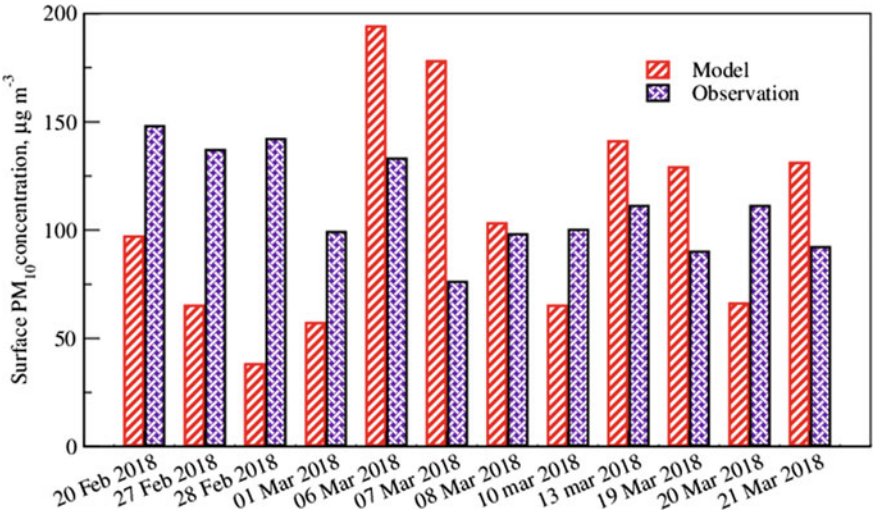

Fig. 2 Time series of 24-hourly (or daily) ambient air particulate matter (of aerodynamic size less than or equal to 10 μm, PM10) for the spring season (February–March) 2018 at Bhubaneswar

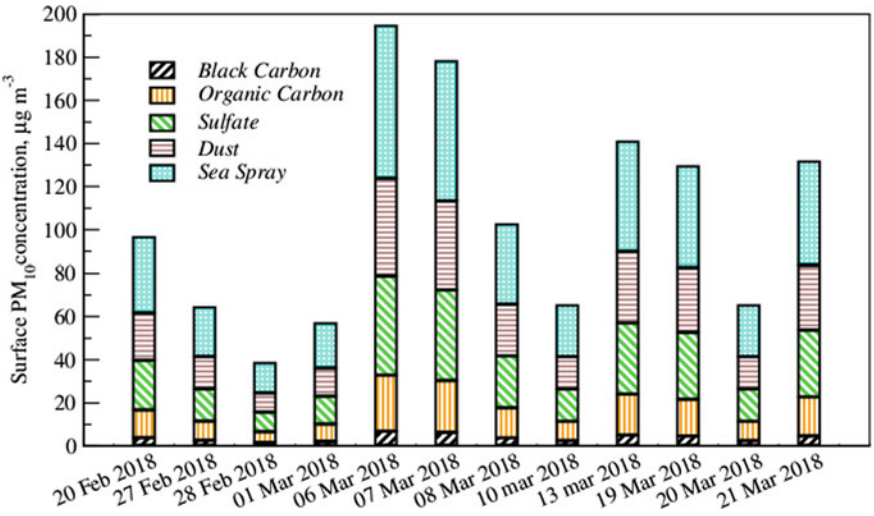

Fig. 3 Species composition including black carbon, organic carbon, sulfate, dust and sea spray to PM_{10} obtained from the model estimations in Spring 2018 over Bhubaneswar

3.3 Back Trajectory Analysis

Coarser size aerosols are predominantly present in the summer air mass, this was reasoned by the long range transport of dust (from desert or plain regions) originating from regional to continental region level. Fine aerosols dominates the air mass in winter due to the prevailing meteorology favors the emissions to accumulate in the lower boundary layer, particularly, at the surface.

A. **Source receptor analysis**

Analysis of source identification using clustering and concentration weighted trajectory was performed as shown in Figs. 5 and 6, respectively. As it was noticed in these figures that most of the source areas or fields lying over local regions (e.g. eastern India over Odisha) at surface level (10–500 m above ground level (agl)) and far-off regions at elevated (1000–5000 m agl) regions (e.g. west Asia and north Africa). However, cluster statistics and potential source regions were analyzed in detain in subsequent sub-sections E and F.

B. **Trajectory clustering**

Grouping of trajectories on the basis of euclidean distance was performed using K-mean clustering algorithm. This was implemented in GIS based MeteoInfo tool.

Analysis of clustering suggests that mean paths for the each cluster signifies the traverse or advection of air mass parcels originating from various source locations or areas towards the receptor location (e.g. Bhubaneswar). Figure 5a shows the 5 paths those originate from both land and oceanic regions. Land region clusters originating from eastern India, Indo-Gangetic plain and central India were associated with high

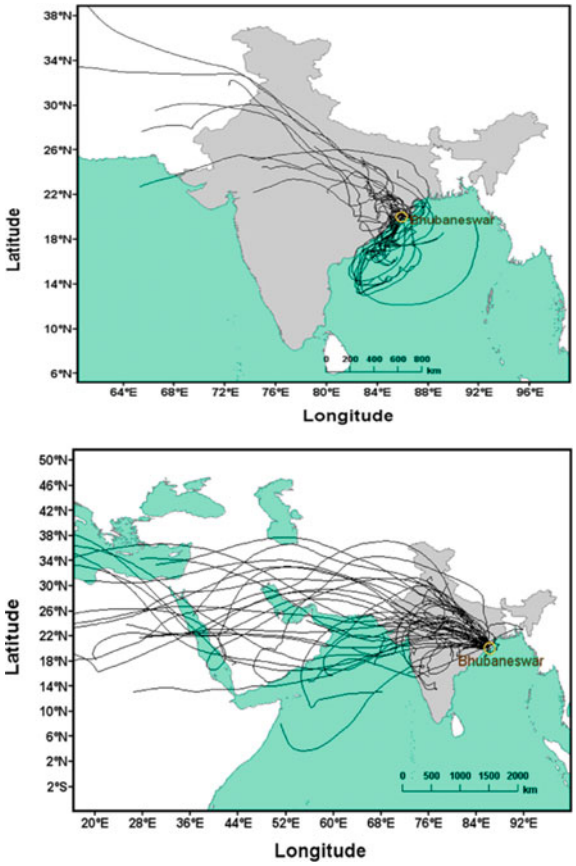

Fig. 4 Back-trajectories traversing from various aerosol emission. Source regions towards the receptor (e.g. Bhubaneswar) at surface (upper panel) and at elevated level (Lower panel) during summer 2018–19

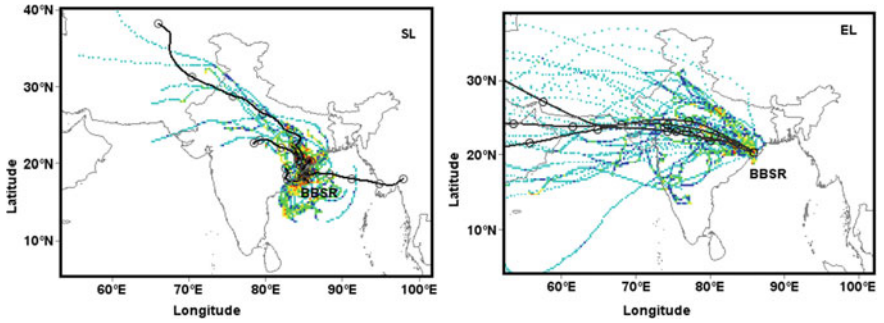

Fig. 5 Trajectory clusters for surface and elevated layers over Bhubaneswar (BBSR) during Summer (February–March) 2018

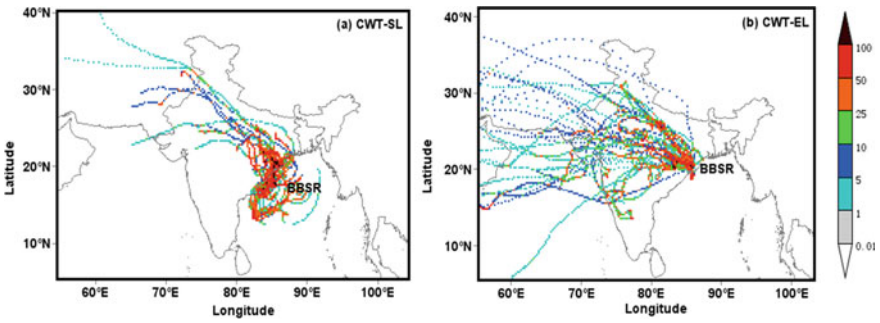

Fig. 6 Residence time weighted concentration weighted trajectory (CWT) at surface and elevated levels for Bhubaneswar during Summer (Feb-March) 2018

frequency, signifying the how often an air mass visits the receptor through transport. Therefore, clusters with high frequency are also observed high concentration of surface level $PM_{10.}$ It indicates that pollution emission transport from the corresponding source regions are found to be significantly contributing to the pollution at a receptor.

Identification of potential source areas are challenging due to the detailed information needed for the assessment including back-trajectory information and pollution concentration data of a receptor. Residence time weighted CWT at surface- and elevated-layers were shown in Fig. 6 that depicts the potential source areas nearby local and far-off long-range source regions. Figure 6a illustrates the accumulation of particulate matter likely source areas on the shore of Bay of Bengal in Odisha at surface level. On the other hand, Fig. 6b shows the long-range source emissions contributing high potential pollution air masses towards the receptor. However, most of the source regions lies over the state of Odisha that signifies the effect of fire events (e.g. forest fires over Odisha) through transporting biomass emissions in March. This is supported by surface level CWT. Dust is likely species contributes in mid of the May till end of the month, which is also supported by elevated level CWT.

4 Conclusion

In summary, we conclude that the coherence of surface PM_{10} concentration was achieved in model estimates on various days of observations. It was found that the uncertainty of the model estimates within the promising value (i.e. 30%).

Sources responsible for the pollution concentration through transport were identified using back trajectory analysis. Various sources for the days of February and March were delineated and found that significant contribution likely from biomass source regions in February and dust or sea spray dominant regions in March, respectively.

Acknowledgements We acknowledge KIIT-DU Bhubaneswar for providing computational facility and laboratory facility.

References

Bhubaneswar City Development Plan (BCDP) (2019) City Development Plan, Bhubaneswar, Orissa, India, Final Report, pp 1–2

Levy RC, Mattoo S, Munchak LA, Remer LA, Sayer AM, Patadia F, Hsu NC (2013) The collection 6 MODIS aerosol products over land and ocean. Atmos Meas Tech 6:2989–3034

Ramachandran S, Kedia S, Srivastava R (2012) Aerosol optical depth trends over different regions of India. Atmos Environ 49338–49347. https://doi.org/10.1016/j.atmosenv.2011.11.017

Reddy MS, Boucher O, Bellouin N, Schulz M, Balkanski Y, Pham M (2005) Estimates of multi-component aerosol optical depths and direct radiative perturbation in the LMDZT general circulation model. J Geophys Res Vol 110. https://doi.org/10.1029/2004JD004757

Swain D, Roberts GJ, Dash J, Lekshmi K, Vinoj V, Tripathy S (2017) Impact of rapid urbanization on the city of Bhubaneswar, India. Proc Natl Acad Sci India Sect A 87(4): 845–853. https://doi.org/10.1007/s40010-017-0453-7

United Nations, Department of Economic and Social Affairs, Population Division (UNDESAP) (2019) World urbanization prospects: the 2018 revision (ST/ESA/SER.A/420). New York, United Nations.

Mapping of Lateritic Rocks in Goa

Mrudula Ingale and Purnanand P. Savoikar

Abstract Various types of rocks found in Goa include the lateritic rock, basalts and gneiss. But the major portion of Goa is covered by lateritic soils and lateritic rocks, which are of rusty-red coloration due to high content of iron oxide. In the Southern and Eastern part of Goa, lateritic highlands are observed; lateritic lowlands and plateaus are observed in the Western and Southern parts of Goa. The laterite rock found at several sites is porous and concretionary in structure and is treated as a soft rock. In the present study, few lateritic rock sites in Goa are selected and their profiles and geotechnical properties are presented. The rock profiles indicate change in the colour, the mineral content, strength properties, water absorption and the safe bearing capacity along the depth and at various locations. The lateritic soil sites are mapped, and their change in the profile, mineral content, safe bearing capacity, unconfined compressive strength (UCS) and other geotechnical properties is observed at different site locations is presented. Also, the core recovery and rock quality designation (RQD) values are presented for classification of rock. This information on variation of various geotechnical properties with depth and at various locations in Goa provides the useful inputs for the engineers for designing various types of foundations resting on the rocks.

Keywords Lateritic Rock · RQD · Core recovery · Unconfined compressive strength

1 Introduction

Goa is covered by rocks of Archaen Protozoic age Dharwar Super Group that stretch in the NW–SE direction while Deccan trap of upper Cretaceous-Lower Eocene age is covered along the NE corner. There are long and narrow stretches of sandy plains

M. Ingale
Badlapur, Thane, Maharashtra 421503, India

P. P. Savoikar (✉)
Civil Engineering Department, Goa Engineering College, Farmagudi, Ponda, Goa 403401, India

B. B. Das et al. (eds.), *Recent Developments in Sustainable Infrastructure (ICRDSI-2020)—GEO-TRA-ENV-WRM*, Lecture Notes in Civil Engineering 207,
https://doi.org/10.1007/978-981-16-7509-6_24

Fig. 1 Map of Goa (www.en.wikipedia.org)

and low flat tops of laterite hills on the western margin of the territory along the Arabian Sea. Much of Goa's soil consists of rich laterites. Figure 1 shows the map of Goa.

Laterite bed has a thickness of 2–25 m and is enclosed in two thirds of the field of Goa. Nearly, to some degree, all rock forms of Goa were lateralized. In general, the laterite profile is around 100 m deep in iron manganese phyllites; laterite cover is seen in ultramafites over a depth of 10 m and Deccan Trap over 5 m. When wet, the lateritic soils are softer and they become harder when they are dry. These are formed as a consequence of lime, silica and organic matter leaching under high-rainfall and high-rainfall action, from the parent rock.

Laterite is formed by intense and sustained chemical weathering, called lateritization, of the underlying parent rock. The main portion of Goa is dominated by laterite and usually appears as plateau landforms (Widdowson and Gunnel 1999). Much of Goa's geological formations are covered by laterite, alluvium and sand, as is expected in the wet tropical climate. Due to its unpredictable behaviour, the analysis of the geotechnical properties of laterites is significant. As compared to other minerals, laterite can be considered a soft rock. Researchers have not yet researched the geotechnical features of laterites in Goa. The present work summarised the occurrence, distribution and mapping of geotechnical properties of laterites in Goa. Mapping will help researchers and consultants to understand laterite better and as guidance in designing structures on lateritic rocks.

2 Literature

The brief review of literature on laterites in Goa is presented below.

Alao (1983) has studied the geology and engineering properties of laterites from Ilorin, Nigeria. Ilorin is a rapidly growing urban centre and capital of Kara state, Nigeria. Samples of laterites were obtained from Ilorin. In this study three varieties of laterites were identified. Mineralogical, chemical and geotechnical analysis was done. This analysis included identification of clay and non-clay minerals by X-ray diffraction (XRD) techniques; moisture contents and specific gravity determination, chemical composition by X-ray fluorescence spectrometer analysis; grain size analysis, pH of soil in water, compaction test by Harvard Compaction Apparatus and unconfined compressive strength determination. Laterites were found to be rich in SiO_2, Fe_2O_3 and Al_2O_3. They are composed of Kaolinite and Illite clay minerals. Topography appears to have some control on the genesis of laterite crust. Widdowson (2009) studied the occurrence, distribution and evolution of laterite in Goa. During the Mesozoic era, the multiphase rift past that influenced western India put major restrictions on this morphotectonic evolution, as well as on the associated erosion, deposition and deep deposition weathering effects that have led to long-term continental margin growth.

Ghosh and Guchhait (2015) studied the characterisation and evolution of primary and secondary laterite in North-western Bengal basin. Geomorphologically, these laterites are found in two settings (i) as continuous crusts on plateau fringe where they act as hard table-like landforms and (ii) at foot slopes and interfluves as deposited ferruginous crust. The age of whole Indian laterite decreases from north to south in concordance with the drift tectonic history of the Indian plate across the equator.

Faldessai and Savoikar (2020) had studied monitoring and mapping of landslides in Goa. Landslides in developed nations are a significant cause of concern. The key causes of landslides are the causing factors such as precipitation, high degree of construction activity, plant cutting, etc. Considering the different factors such as slope height, form of the slope, multiple slope security measures such as RCC retaining walls, strengthened earth walls, soil nailed walls, gabion walls, tie back wall, etc. need to be enforced Soil, building space supply, expense, long-term durability, etc. As preservation steps, new techniques such as cantilever retaining walls with platform relief and managed yielding techniques using EPS geofoam are also being studied. The new analysis of recent landslides in Goa has been used to map Goa's landslide sites on the Goa landslide inventory map and will be useful for planners, architects and engineers to determine the vulnerability of different areas to landslides in Goa before any construction operation is carried out.

Water absorption, unregulated compressive strength, and unit weight were obtained from rock samples collected from different Goa sites (Ingale and Savoikar 2020). The mineral content of both rocks showed larger concentrations of Limonite, followed by Gibsite and Kaolinite. In very small amounts, Hematite and Goethite were found. It is observed that with increase in density, the unconfined compressive strength of the laterite rock does not always increase, but it often decreases and

again increases for the intermediate layer of rock. With the porous and concretionary composition of the laterites located at various depths, differing mineral contents and degree of lateritization may be the reason for this variation in unconfined compressive strength values for laterites.

3 Geology of Goa

The coastal state of Goa is physiographically separated into three forms of terrain:

- Sandy beaches, estuarine mudflats, Khazan lands, salt pans, mangroves, plains and settlement areas of the western coastal estuarine plain
- The middle undulating area or midlands with hills ranging between 100 and 600 m and
- The Western Ghats or Sahyadris in the Eastern and Southern regions range from 600 to 1000 m long.

Goa's geology shows that Goa is part of the Indian Precambrian shield consisting of supracrustal rocks of green schist lying over the trondhjemitic gneiss. The late Cretaceous Deccan Traps are part of the north-eastern outskirts of Goa. On the remaining slopes, laterite cover is found. The alluvium and sand cover of most of Goa's geological formations is observed on the coastal estuarine plains. The Goa geological map is shown in Fig. 2a and distribution map is shown in Fig. 2b.

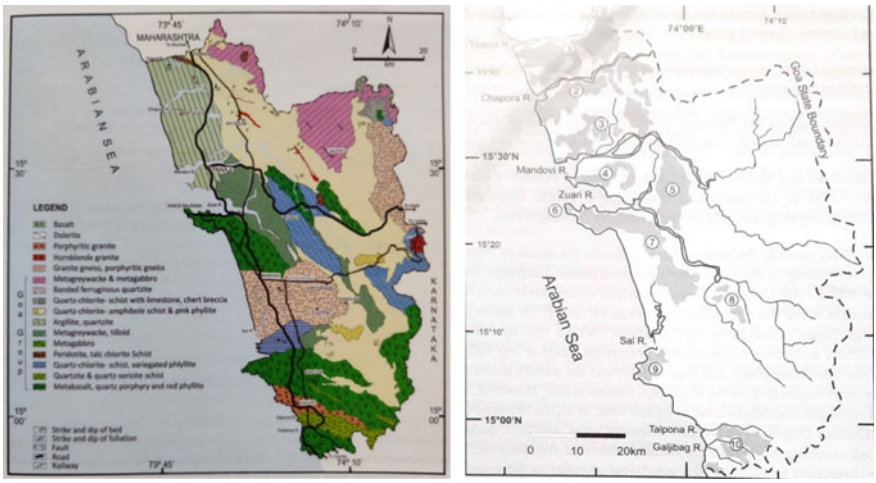

Fig. 2 **a** Geological map of Goa (Gokul et al. 1985) and **b** Map of distribution of key laterite-capped plateaux of Goa (Widdowson 2009)

As per the geological map of Goa (Desai 2011), the geological classification of rocks in Goa comprises of Barcem formation, Ponda (Bicholim and Sanvordem formation) and Vageri formation. Vesicular metabasalts of Barcem formation are found in Canacona taluka while non-vesicular metabasalt extend from Pollem to Usgao-Dharbandora in central Goa. These rocks rest on tonalite-trondhjemite-granodiorite gneiss. Sanvordem formation overlies Barcem formation and comprises of metagreywackes (metamorphosed sandstones) observed in Sanvordem, Calem and also observed in Ribandar Goa and argillites observed in Aguada and Chapora. Bicholim formation overlies Sanvordem formation and comprises of ferruginous and manganiferous phyllites, banded quartzites and limestones found in NW–SE belt of Goa from Naibag in North to Salgini in South Goa. Vageri formation rocks overlies Bicholim formation and comprises of metagreywackes and metabasalts found in Valpoi region. In the Canacona and Chandranath region, Granite and Gneiss rock is observed.

4 Geotechnical Properties of Laterites in Goa

A laterite profile is a typical field-section of a laterite is shown in Fig. 3 from surface to the parent rock. The upper part of the section is red, hard and massive, which is referred to as 'lateritic crust'. It consists of a fretwork of oxides and hydroxides of iron and aluminium. The lower part of it is vermiform in nature and grades into a tubular, semi-indurated laterite. This is underlain by a prominent thick horizon of variegated colours and is dominated by clay minerals is called as 'lithomarge'. It is generally nodular concretionary at the top and mottled below. The mottled portion consists of kaolinite along with patches and accumulations of iron oxyhydroxides. The saprolite beneath the mottled zone is relatively impermeable and corresponds to 'plasmic zone' of the profile. A significant portion of the saprolite shows bleaching and constitutes the 'pallid zone'.

In this section, descriptions of bore hole logs and the geotechnical properties of rocks are described. Typical bore hole logs at the various sites in Goa are presented below in Figs. 4, 5 and 6. The typical variation of layers and interspersed soft strata can be observed in most of the bore hole logs. Although the bore hole log differ from site to site and even within site, the logs attached herewith may give a rough understanding of the strata in a specific location. The geotechnical properties of samples collected from bore holes and shallow open pits at various depths are summarised in Tables 1 and 2, respectively.

Lateritic rock shows uncertain behaviour. It is very soft rock. The strength of lateritic rocks can differ within the site for different locations. These uncertainties of rock characteristics make it imperative to study its strength behaviour. It is observed that, with the increasing density, the unconfined compressive strength of the laterite rock does not always increase, but it often decreases and again increases for the intermediate layer of soil. Unconfined Compressive Strength of laterites in Goa varies from 747 kN/m^2 to 10415.9 kN/m^2 for different sites.

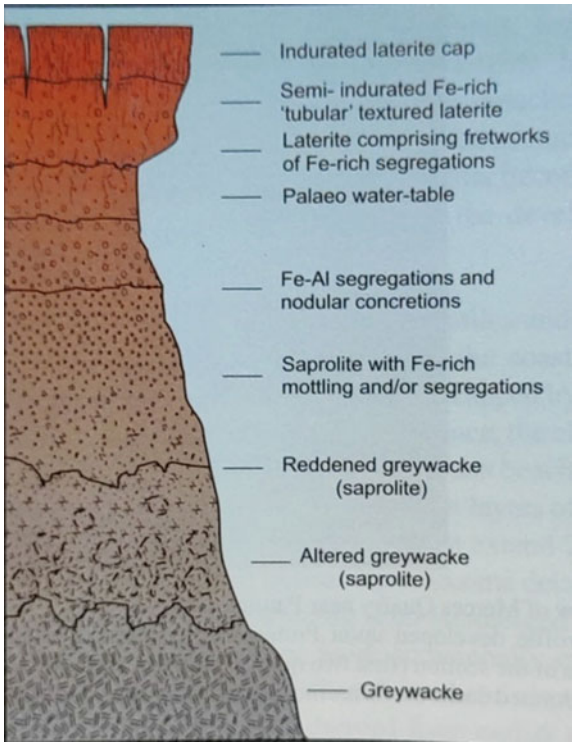

Fig. 3 Typical lateritic profile (Widdowson 2009)

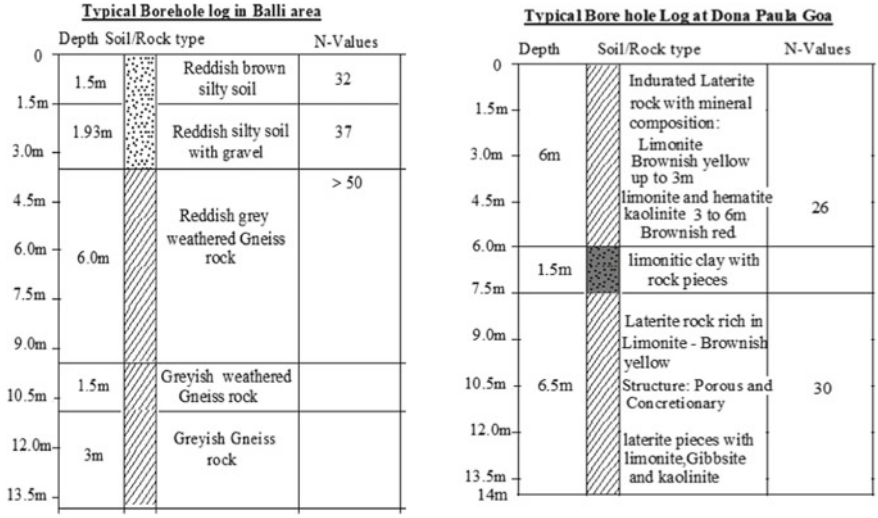

Fig. 4 Typical bore hole logs of Balli area and Dona Paula area

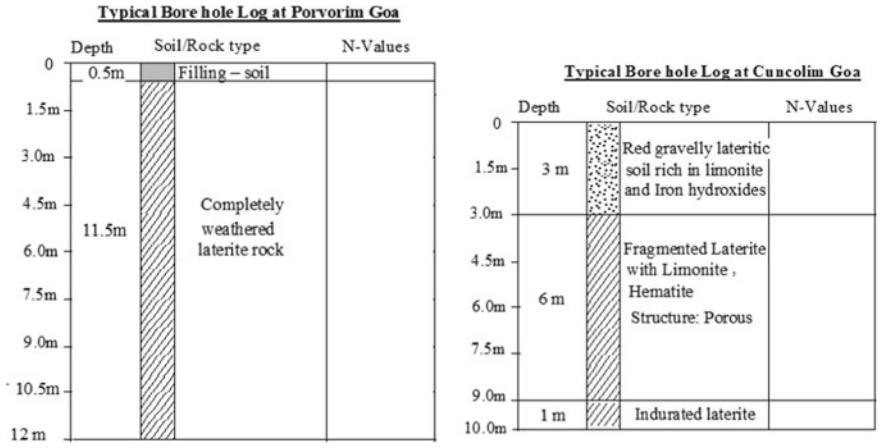

Fig. 5 Typical borehole logs at Porvorim and Cuncolim Goa

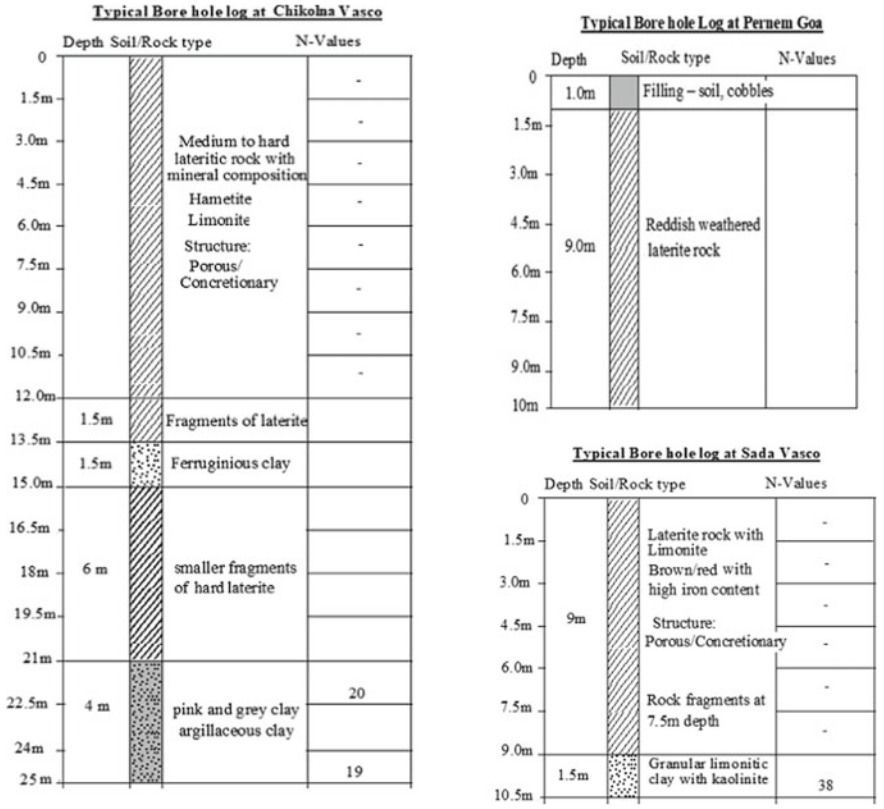

Fig. 6 Typical bore hole logs at Chikolna and Sada in Vasco-da-gama and at Pernem

Table 1 Geotechnical properties of rocks—Bore hole data

Site	Rock	Depth of rock (m)	NMC (%)	Unit weight (kN/m^3)	UCS (kN/m^2)
Dona Paula	Laterite	2–10	18.96–24.08	18.96–24.8	845.18–6374.29
Sada—Vasco	Laterite	2–10	16.36–23.64	16.36–23.64	746.2–3120
Chikolna	Laterite	1.5–10	21.96–24.29	21.96–24.29	5589–6885
Cuncolim	Laterite	2–10	12.88–31.61	12.88–31.61	882–7342
Pernem	Laterite	1.5–10	21.84–34.63	21.84–34.63	753–8095
Porvorim	Laterite	1.5–10	17.4–21.3	17.4–21.3	883- 5481
Balli—Goa	Gneiss	1.5–14	29.4–44.7	29.4–44.7	796–10,415.9
Panjim	Besalt	23–27	21.3–27.7	21.3–27.7	1952.4–9470.5

Table 2 Typical geotechnical properties of rocks—Shallow open pit

Site	Depth of rock (m)	NMC (%)	Unit weight (kN/m^3)	UCS (kN/m^2)
Verna	1.5	27.96	27.96	2637
Dabolim	2	28.75	28.75	2297
Tuem-Pernem	4.5	19.50	19.80	3130
Bandora	2.5	28.2	28.2	6823

5 Mapping of Laterites

Laterite covers major portion of Goa and the properties of laterites are needed to be mapped for the reference. Mapping of laterites in Goa is shown in Fig. 7.

6 Conclusions

Laterite is a soft rock and is formed due to weathering action due to high temperature and rain known as lateritization process, and found in the tropical belt of the world. The laterite rock found in Goa is soft, porous and concretionary in nature. In most of the cases, the lateritic layer is underlain by ferruginous or limonitic clays. Unit weight of laterites varies from 12.88 to 34.6 kN/m^3. Unconfined Compressive Strength of laterites in Goa varies from 747 to 10,415.9 kN/m^2 for different sites. Variation in Geotechnical properties of lateritic rocks is observed at different location within the site or at different sites. This study indicates that proper geotechnical investigation is required while working on sites of laterites, especially when constructing multistoried buildings on laterites, since lateritic rocks are often underlain by soft ferruginous or limonitic soils. This mapping may help as a guide for engineers for designing foundations on laterites.

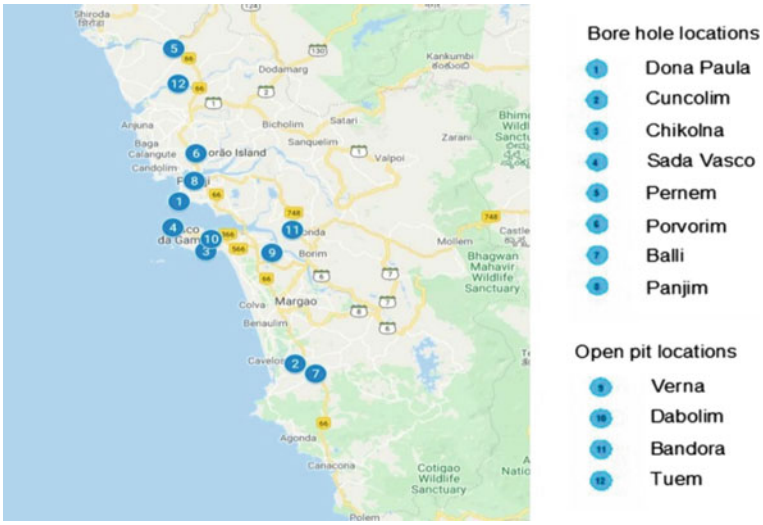

Fig. 7 Locations of laterites in Goa

References

Alao D (1983) Geology and engineering properties of laterites from Ilorin, Nigeria. Eng Geol 19:111–118

Desai AK (2018) Geology and mineral resources of Goa, 1st edn. New Delhi Publishers, New Delhi

Faldesai M, Savoikar P (2020) Monitoring, control and mapping of landslides in Goa. In: Das BB, Barbhuiya S, Gupta R, Saha P (eds) Lecture notes in civil engineering. Recent developments in sustainable infrastructure, Select proceedings of ICRDSI 2019, Springer, Berlin, pp 89–100

Ghosh S, Guchhait SK (2015) Characterization and evolution of primary and secondary laterites in Northwestern Bengal Basin, West Bengal, India. J Palaeogeogr 4(2):203–230

Gokul AR, Srinivasan MD, Gopalkrishnan K, Vishwanathan LS (1985) Stratigraphy and structure of Goa. In: Proceedings of Seminar on Earth Resources for Goa's Development. Geological Survey of India, pp 1–13

Ingale M, Savoikar P (2020) Geotechnical properties of lateritic rocks in North Goa. In: Das BB, Barbhuiya S, Gupta R, Saha P (eds) Lecture notes in civil engineering. Recent developments in sustainable infrastructure, Select proceedings of ICRDSI 2019. Springer, Berlin, pp 79–88

Meshram RR, Randive KR (2011) Geochemical study of laterites of the Jamnagar district, Gujarat, India: Implications on parent rock, mineralogy and tectonics. J Asian Earth Sci 42:1271–1287

Widdowson M (2009) Evolution of laterite in Goa. In: Mascarenhas A, Kalavampara G (eds) Proceedings of natural resources of Goa: a geological perspective. Geological Society of Goa, Miramar Goa, pp 35–68

Widdowson M, Gunnel Y (1999) Lateritization, geomorphology and geodynamics of a passive continental margin: Konkan and Kanara coastal lowlands of Western Penninsula India. In: Thiry M, Simon-Coincon R (eds) Proceedings of Paleoweathering, Paleosurfaces and related continental deposits. International Association of Sedimentologists Special Publication, vol 27, pp 245–274

Effect of Variation of Unit Weight and Friction Angle on Deflection and Bending Moment of Retaining Walls with Shelves

Smita S. Aldonkar and Purnanand P. Savoikar

Abstract Worldwide infrastructure development takes place which involve construction of buildings, dams, canals, bridges, roads, retaining structures, etc. Construction of most of the structures involves cutting and filling of soil like in embankment and retaining walls. The retaining walls are one of the common components of building infrastructure, but cantilever retaining walls cannot be designed for greater heights to retain the soil since it becomes uneconomical to design RCC retaining walls with height more than 6–9 m. For designing cantilever retaining walls to retain soils with heights greater than 9 m is possible by providing relief shelves along the stem height which reduces the active pressures on the stem tremendously making the is possible to design the stem economically. In the present study, a model of cantilever retaining wall retaining soils for the height of 10 m is generated using STAAD software and is analysed for active pressure by using no, single, two and three shelves. The soil property variation used in the present analysis is unit weight (γ) varying from16, 18 and 20 kN/m^{3}and friction angle (ϕ) for soil varying from 25°, 30° and 35°. The deflection and bending moment of the wall are calculated for the above different soil properties and for no shelf, single shelf, two shelves and three shelves conditions. The effect of variation of number of shelves, friction angle and unit weight on deflection of the stem and bending moments in the stem is plotted. It provides useful information on percentage reduction in bending moments and how the economy is brought into design of cantilever retaining walls for retained heights of more than 9 m.

Keywords Cantilever retaining walls · Relief shelves · Deflection · Moment · Friction angle · Unit weight

S. S. Aldonkar · P. P. Savoikar (✉)
Civil Engineering Department, Goa College of Engineering, Farmagudi, Goa 403401, India

S. S. Aldonkar
e-mail: smita@gec.ac.in

B. B. Das et al. (eds.), *Recent Developments in Sustainable Infrastructure (ICRDSI-2020)—GEO-TRA-ENV-WRM*, Lecture Notes in Civil Engineering 207,
https://doi.org/10.1007/978-981-16-7509-6_25

1 Introduction

Retaining walls are often found in places where extra support is needed to prevent the earth from moving downhill with erosion. The most basic function of a retaining wall is to resist lateral forces with help of gravity or cantilever action. Retaining walls can also provide usable land. Reinforced concrete cantilever retaining walls are used in diverse fields of engineering such as roads, dams, tunnels and mines. Different slope stability techniques implemented are gabion walls, soil nailing, rock bolting, reinforced earth structures, counterfort and cantilever retaining walls.

In counterfort retaining wall the stem and the back slab are tied together with counterforts at suitable intervals due to which the vertical stem and the heel slab act as continuous slab in contrast to the cantilevers in the cantilever retaining wall. Use of EPS geofoam to reduce lateral earth pressure behind the rigid retaining wall was investigated using numerical simulation approach. The results shows that placement of EPS geofoam panel behind the retaining wall could reduce the magnitudes of lateral earth pressure and total wall thrust behind the retaining wall approximately 50%. As the surcharge load increases, the efficiency is decreasing, though there is not much difference in the % of reduction.

Reinforced concrete retaining walls are meant to support more height of earth mass. Cantilever retaining wall is constructed up to height of 6 m and above that it becomes uneconomical. To support more height of earth mass advancement is done in cantilever retaining wall by adding relief shelf in it. Due to provision of relief shelf the soil pressure on the stem of retaining wall is reduced resulting in economy in stem design and improvement in stability of retaining wall.

A pressure relief shelf is a thin horizontal cantilever platform of finite width, extending into the backfill at right angles, throughout the length of the retaining wall, constructed monolithically with the stem of the retaining wall. Number of such shelves is constructed at regular spacing along the height of the wall. A few researchers previously proposed this technique with limited theoretical studies but without systematic analysis and proper validation, and demonstrated that provision of relief shelves can reduce lateral earth pressure on retaining walls and subsequently increase the stability of the retaining wall. The benefit of single relief shelf on the reduction of total lateral thrust on a cantilever wall, through stability analysis of wedges as well as small scale model.

2 Literature Review

Yakovlev (1964) studied the effect of relief shelves by conducting experiments. Several experiments were conducted over the years on retaining walls with single shelf to decide the factors that influence the distribution of pressure over the height of the wall as the position of the shelves is changed and the dimensions of the shelves under the effect of variably distributed load and the location of load also the nature

of change in pressure on the wall and the shelf due to forward movement of the wall due to the stress in the backfill soil. The effect of adding one or more relief shelves to the counterfort retaining wall on stability was studied by Jumikis (1964) extending relief shelves up to the theoretical rupture surface. Raychaudhuri (1973) suggested that the cantilever walls with relieving shelves the theory of Coulomb's earth pressure would be applicable and analysed the reduction of the total active earth pressure and its distribution due to provision of relieving shelves. Since simple models used for analysis, the study could not determine the earth pressure behind the wall.

Chauhan et al. (2016) presented numerical study on a 6 m high retaining wall with two relief shelves to understand the influence of width of relief shelves on the contact pressure below base slab, surface settlement, deflection of relief shelves and reduction in lateral earth pressure. It was reported that the retaining wall with relief shelves can considerably reduce the lateral thrust on wall in the range of 10.56–12.5%. Among all the cases studied, relief shelves of width of 0.5 m proved effective in reducing lateral earth pressure and total contact pressure below base slab by 10.56 and 13.4% respectively, without leading to excessive deflection of relief shelves.

Tonne and Mohite (2015) stated that the optimization of counterfort retaining wall is possible due to provision of one relief shelf. Because of relief shelf moment in each component of retaining wall is reduced counterfort retaining wall of heights 10, 12, and 15 m with relief shelf at h/2 gets minimum earth pressure and overturning moment and better stability where h is the height of the stem. Farouk (2016) stated that for high retaining walls and for some repair systems for constructed walls that have problems with stability, it is recommended to provide the cantilever wall with a shelf at a third of the wall height from the top of the wall or more shelves at different levels by conducting a parametric study of the effects of the number of shelves, shelf rigidity, and shelf position on the resulting distribution of the lateral earth pressure, wall top movement, and acting maximum flexural moment of the wall. This was achieved by applying the FEM solution from PLAXIS2D-AE.01 using the hardening soil model.

3 Methodology

Bowles (1996) reported that while constructing the retaining wall with shelves, it is required that the soil must be well compacted up to the relief shelf, the shelf constructed, soil placed and compacted, etc. However, it is difficult to anticipate the amount of consolidation that will occur beneath the shelves and it will regardless of the state of the compaction. The shelf may bend downwards and as a result of this, either the shelf breaks off or the wall above tends to move into the backfill and develop passive pressure. The wall therefore must be well reinforced on both faces and of sufficient thickness to carry this unanticipated shear and moment. There is also the possibility of overall wall stability. It was opined that the relief shelves only increases the design complexity of the wall.

3.1 Parameters Used in the Analysis

In the present study, a model of cantilever retaining wall retaining soils for the height of 10 m is generated using STAAD software and is analysed for active pressure by using no, single, two and three shelves. Figure 2 shows the retaining wall model used in the present analysis with relief shelves of widths B_1, B_2 and $B_3 \ldots B_n$. Considering the moment equilibrium condition $\Sigma M = 0$ at junction 1, if this balancing moment increases, the retaining wall is pushed into the backfill causing the lateral pressure to be more than at rest condition.

To achieve objectives of the study, 27 models were analyzed using STAAD.Pro V8i. The model consists of a retaining wall with a height of 10.0 m and base slab width equal to 6.0 m. The wall and base slab thickness are 0.5 m. The width is analysed based on the bowels moment equilibrium condition, thickness of the shelf is 0.4 m. Mohr–Coulomb soil model is adopted. Unit weight of soil (γ) is assumed to vary from 16, 18, 20 kN/m^3. Soil friction angle varies from $\phi = 25°$, 30°, 35°.

The wall is analysed for the cases of cantilever with one, two and three shelves. The shelves are located at equal heights along the wall. The relief shelf has different widths and uniform thickness is maintained. The models are constructed to study the effect to clarify the effect of number of shelves and the effect of width on deflection and bending moment of the wall under effect of lateral earth pressure and vertical soil pressure on shelf. The result of deflection of the wall and the bending moment is compared for various values of unit weight of soil γ and ϕ.

4 Flexural Behaviour of Stem

4.1 Influence of Shelves

Analysis of retaining wall with and without shelves is performed for the loading as shown in Fig. 1 above and the bending moments in the stem are evaluated. Figure 2 shows the variation of bending moment for $\gamma = 16$ kN/m^3 and $\phi = 25°$ for no shelf, single shelf, two shelves and three shelves cases respectively. It is observed that the stem moment reduces by about 55.65% at the base when single shelf is used, by 74.06 and 78.85% for two shelves and three shelves are used respectively. This is because the entire height of stem is divided in to two to four parts by the shelves and soil pressure is now computed for the reduced height. Table 1 shows the values of bending moments computed over the height of retaining wall for no shelve, single, two and three shelves for $\gamma = 16$ kN/m^3 and $\phi = 25°$.

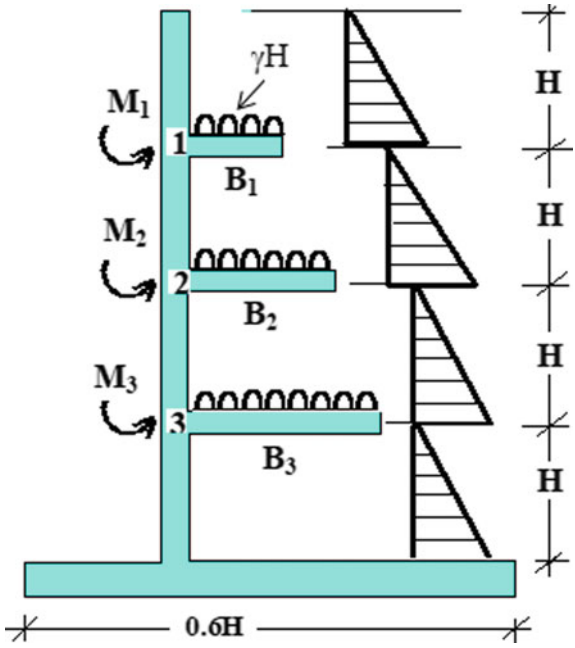

Fig. 1 Retaining wall with varying shelf lengths

4.2 Influence of Friction Angle on the Bending Moments in the Slab

Table 2 shows the values of bending moments for various values of friction angle indication its influence on the bending moments in the stem for constant value of unit weight for retaining walls with single shelf and without shelves. It is observed that higher bending moments are observed for friction angle of 25° for retaining wall without shelf. As friction angle increases, bending moments decreases for retaining wall without shelves. This is because lower friction angle gives higher values of K_a. In the case of stem with shelves, the bending moments also decrease as friction angle increases, unit weight remaining constant. Similar behaviour is obtained in the case of retaining wall with two and three shelves.

4.3 Influence of Unit Weight on Bending Moments in the Stem

Table 3 shows the values of bending moments for various values of unit weight depicting its influence on bending moments in the stem for constant value of friction angle for retaining walls with single shelf and without shelves. It is observed that as unit weight increases, the bending moment also increases for retaining walls without

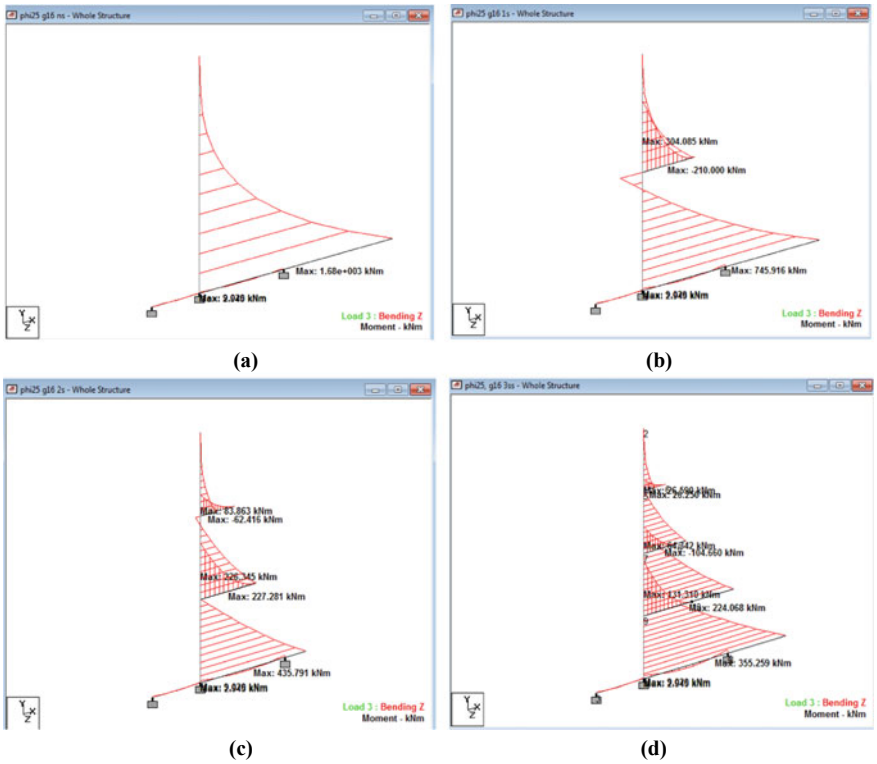

Fig. 2 Bending moment of retaining wall with **a** no shelf and **b** single shelf, **c** two shelves and **d** three shelves for $\gamma = 16$ kN/m^3 and $\phi = 25^o$

Table 1 Variation in bending moments—effect of shelves

Height of stem from base (m)	$\phi = 25°$, $\gamma = 16$ kN/m^3		Bending moments (kN-m)	
	No shelf	Single shelf (% reduction)	Two shelves (% reduction)	Three shelves (% reduction)
0	1680	745.92 (55.65%)	435.791 (74.06%)	355.26 (78.85%)
2.5	708.50	247.165	95.108	**224.07**
3.33	498.525	124.160	**227.28**	153.096
5	210.00	**210.00**	79.651	**104.66**
6.67	66.036	66.036	**62.42**	26.882
7.5	26.25	26.25	26.25	**26.25**
10	0	0	0	**0**

Bold values Indicates maximum moment at shelf

Table 2 Variation in bending moments—effect of friction angle

Height of stem from base (m)	Bending moments (kN m)					
	$\phi = 25°$; $\gamma = 16$ kN/m^3		$\phi = 30°$; $\gamma = 16$ kN/m^3		$\phi = 35°$; $\gamma = 16$ kN/m^3	
	No shelf	Single shelf (% reduction)	No shelf	Single shelf (% reduction)	No shelf	Single shelf (% reduction)
0	1680	745.92 (55.65%)	1320	573.69 (56.54%)	1084	473.94 (56.28%)
2.5	708.50	247.165	556.875	181.82	457.313	152.127
3.33	498.525	124.160	399.11	84.80	321.185	72.458
5	210.00	**210.00**	165	**165.0**	135.50	**135.50**
6.67	66.036	62. 22	48.889	48.89	40.148	40.148
7.5	26.25	26.25	20.625	20.625	16.94	16.94
10	0	0	0	0	0	0

Bold values Indicates maximum moment at shelf

Table 3 Variation in bending moments – effect of unit weight

Height of stem from base (m)	Bending moments (kN m)					
	$\phi = 30°$; $\gamma = 16$ kN/m^3		$\phi = 30°$; $\gamma = 18$ kN/m^3		$\phi = 30°$; $\gamma = 20$ kN/m^3	
	No shelf	Single shelf (% reduction)	No shelf	Single shelf (% reduction)	No shelf	Single shelf (% reduction)
0	1320	643.429 (45.08%)	1485	724.88 (51.19%)	1650	719.94 (56.37%)
2.5	556.88	251.55	626.48	284.02	696.09	230.10
3.33	399.11	154.54	440.00	174.88	488.89	108.83
5	165	165.0	185.63	185.63	206.25	206.25
6.67	48.89	48.89	55.00	55.00	61.11	61.11
7.5	20.63	20.63	23.20	23.20	25.78	25.78
10	0	0	0	0	0	0

shelves. This is due to the fact that soil pressure is higher in the case of higher unit weight i.e. 20 kN/m^3. However, in the case of retaining walls with shelves, higher bending moments are observed in the case of retaining wall with shelves for unit weight of 18 kN/m^3.

5 Deflection Behaviour of Stem

Analysis of retaining wall with and without shelves is performed for the loading as shown in Fig. 1 and the deflection of stem is evaluated for different values of unit weight (γ = 16, 18 and 20 kN/m^3) and internal friction angle ($\phi = 25°$, 30° and

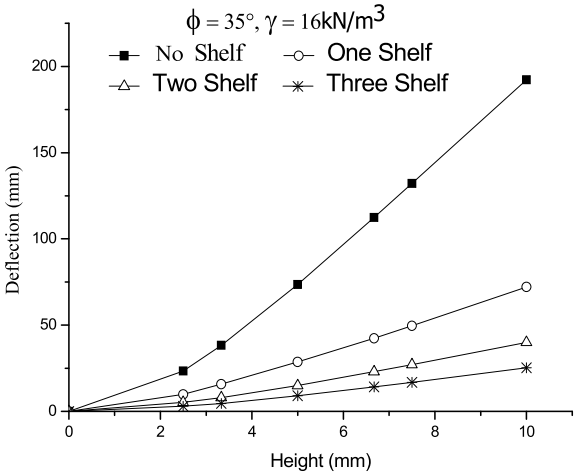

Fig. 3 Variation in deflection of stem for number of shelves

35°). The deflections of the stem for typical cases of friction angle and unit weight for no shelf, single shelf, two shelves and three shelves are shown in Figs. 3, 4 and 5.

5.1 Influence of Shelves

Figure 3 shows variation of deflection for no shelf, single shelf, two shelves and three shelves cases for unit weight of 16 kN/m^3 and friction angle of 35°. It is observed that the stem deflection reduces by about 62.48% when single shelf is introduced, by 79.19 and 86.86% for two shelves and three shelves are introduced respectively. This is because the entire height of stem is divided into two to four parts by the shelves and soil pressure is now computed for the reduced height. Similar behaviour is observed for other cases of unit weight and friction angle.

5.2 Influence of Friction Angle

Figure 4 shows variation of deflection for no shelf and single shelf for unit weight of 20 kN/m^3 and friction angle of 25°, 30° and 35°. As the friction angle increases, the deflection of the top of the stem decreases, unit weight remaining constant, since the thrust of stem decreases due to lesser height of stem on which the soil pressure acts. Also, the weight of soil on shelves restricts the outward deflection of stem. Similar behaviour is observed for other cases of unit weight and friction angle.

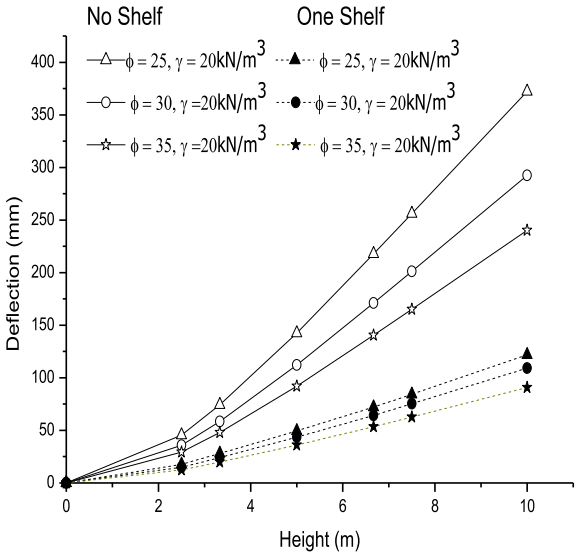

Fig. 4 Variation in deflection of stem showing effect of friction angle

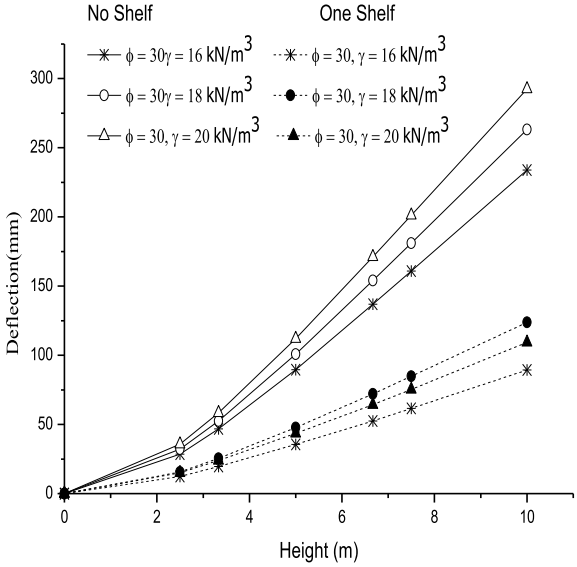

Fig. 5 Variation in deflection of stem showing effect of unit weight

5.3 *Influence of Unit Weight*

Figure 5 shows variation of deflection for no shelf and single shelf for unit weight varying from 16 to 20 kN/m^3 with friction angle remaining constant at 30°. As the unit weight increases, the deflection of the top of the stem also increases, with friction angle of the soil remaining constant, for retaining wall without shelves. This is because soil pressure is directly proportional to the unit weight. It is observed that the stem deflection increases by about 12.50% and 25.4% over and above the deflection for unit weight of 16 kN/m^3 for retaining wall with no shelf for the unit weight values of 18 and 20 kN/m^3 respectively. However, in the case of retaining wall with single shelf, the deflection of top of the stem increases by 38.51% for unit weight of 18 kN/m^3 and by 22.21% over and above the deflection for unit weight of 16 kN/m^3. Higher deflections are observed for unit weight of 18 kN/m^3 as against the expected higher values for unit weight of 20 kN/m^3. Similar, behaviour is observed for retaining wall with two and three shelves and for friction angle values of 25° and 35°.

6 Conclusions

It can be summarized that introduction of shelves reduces the bending moments in the stem and also the outward deflection of stem. As the friction angle increases, the deflection of stem decreases for all values of unit weights and for all shelves. Following conclusions are drawn from the present study:

1. It can be concluded that the introduction of shelves reduces the bending moments in the stem and also the outward deflection of stem. As the friction angle increases, the deflection of stem decreases for all values of unit weights and for all shelves.
2. Keeping shelves of equal lengths reduces the thrust on stem. But moment produced by cantilever bending of shelves introduces higher balancing moments at the junction of stem and shelves which offsets the economy brought about by introduction of shelves. Hence, it is prudent to keep shelves of varying length such that junction moments are balanced without increase in stem moments.
3. However, in the case of variation of stem deflection with unit weight, it is observed that for all shelves, higher stem deflections are observed for unit weight of 18 kN/m^3 rather than for the unit weight of 20 kN/m^3.
4. As the friction angle increases, the deflection of stem decreases for all values of unit weights and for all shelves.

References

Bowles JE (1996) Foundation analysis and design, 5th edn. McGraw Hill Books Company
Chauhan VB, Dasaka SM, Rizwan Khan (2016) Numerical study on the behaviour of rigid retaining wall with relief shelves. In: Proceedings of Indian Geotechnical Conference, IGC2016, Pune
Farouk HS (2016) Retaining wall with relief shelves. Innov Infrastruct Solut 1(4):1–13
Jumikis AR (1964) Mechanics of soils. D Van Nostrand Co., Inc., New Jersey
Raychaudhuri PR (1973) Design of retaining walls with relieving shelves. Paper No. 295, Indian Road Congress J 35(2):289–325
Tonne VR, Mohite PM (2015) Optimization and improvement in stability of counterfort retaining wall with relief shelf. Int J Res Eng Technol 4(4):447–451
Yakovlev PI (1964) Experimental investigations of a new type of relieving device for retaining walls. Scientific papers "Hydraulic Engineering" (in Russian), No. 3, Morskoi Transport

Rainfall Induced Landslides—A Review

Ruchi R. Kadamb and Purnanand P. Savoikar

Abstract Major landslides take place in the world due to several reasons like human activities, heavy rainfall, snow melts and deforestations. A thorough study of landslide prone regions is required for ensuring the safety against this disaster. The triggering factors of landslides include climatic conditions of an area, soil-water characteristics, ground water conditions, quality of soil, topography and slope modifications. In most of the landslides that have occurred in the past, the common reason observed for the slope failure is the heavy rains at hilly regions. The present study aims to analyze slope failures or landslides occurring at several place in India and world due to high and continuous rainfall. Few other uncertainties may also be the root cause of landslide hazards. Rainfall threshold and antecedent rainfall are the elementary parameters of this study. The review includes a vast area of study with different methodologies and remedial systems provided for rainfall includes landslides. Few remedial measures for several landslide locations are discussed in the present study.

Keywords Rainfall · Landslides · Antecedent rainfall · Rainfall thresholds · Slope failures

1 Introduction

Natural disasters are the uncertain and uncontrollable circumstances which needs pre-disaster management installation. Few major disasters are caused due to floods, hurricanes, earthquakes, storms and other geological processes. Some of the common geological disasters include avalanches, rock falls, landslide, and sink holes. Generally, the impact of such disasters is severe in developing countries and in countries with high population. Landslides occur in all parts of world due to several reason like heavy rainfall, snowmelts, changes in ground water, human activities like mining, construction, slope modifications, deforestations etc. Landslides are slope failures

R. R. Kadamb · P. P. Savoikar (✉)
Civil Engineering Department, Goa Engineering College, Farmagudi, Ponda, Goa 403401, India

B. B. Das et al. (eds.), *Recent Developments in Sustainable Infrastructure (ICRDSI-2020)—GEO-TRA-ENV-WRM*, Lecture Notes in Civil Engineering 207,
https://doi.org/10.1007/978-981-16-7509-6_26

caused due to movement of rock mass, debris flow down a slope under gravity. They include different types of slope movements such as topples, slides, spreads, flows and falls. Largely landslides happen due to heavy rainfall that saturates the slope or soil mass by water due to which soil shear strength is reduced and the disasters take place.

Landslides also effects the human settlements, communication modes and land properties. It is a necessity to study these failures to take further precaution for any similar situations. Normally landslides are labelled as shown in Fig. 1. Landslides are classified according to its movements, materials involved, activity and movement velocity. They are also divided into different types with respect to depth of slide as surface slides, shallow slides, deep slides and very deep slides. According to movement type, they are classified as falls, topple, slides, spreads, flows, and complex. The different material classification is rock, debris and earth. Therefore, the landslides types are rock falls, debris fall, Earth fall or Rock topple, debris topple and earth topple. Similarly, the other movements and material types are combined. The different types of landslide are as shown in Fig. 2.

The basic causes of landslides include: physical, geological, morphological and human activities. Physical changes such as ground water level, increase in pore pressures, snow melts, earthquake forces, heavy flooding, rapid drawdown, leaching of salts, heavy rainfalls etc. are the major reason of landslides. The geological causes include bedding, faults, unconformity, weak materials, sheared or jointed materials, and weathered materials. Slope inclinations, uplifts, slope loadings, vegetation

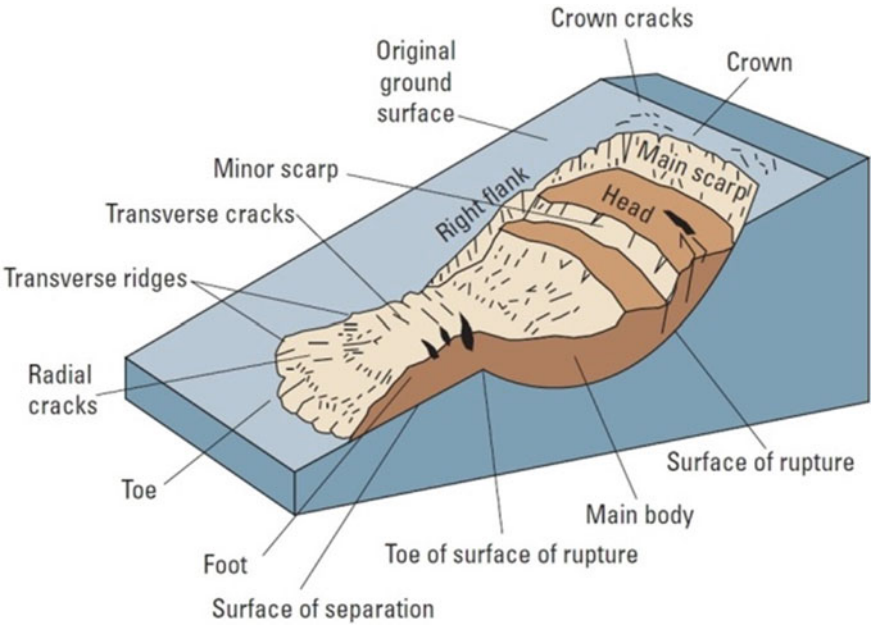

Fig. 1 Nomenclature for labelling the part of landslides (Spiker and Gori 2003)

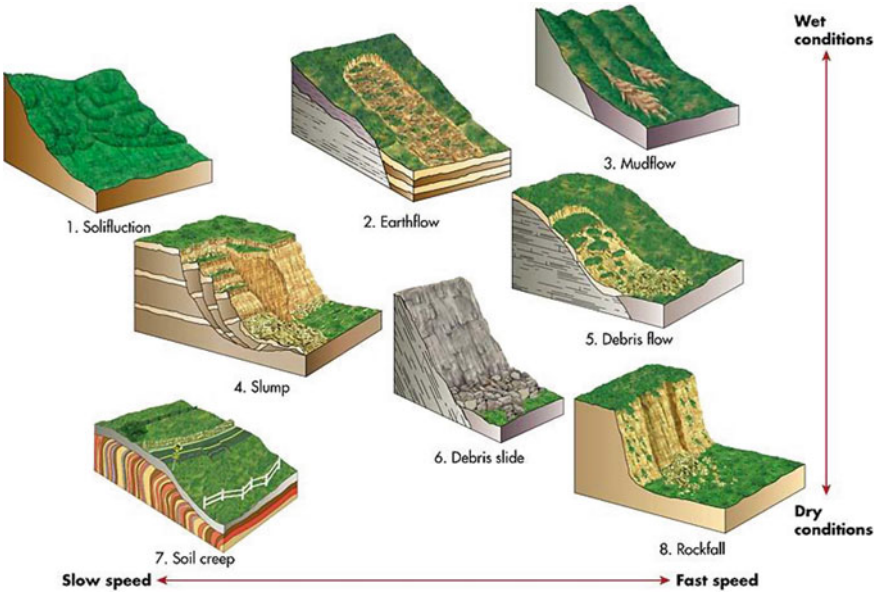

Fig. 2 Types of landslide (www.gsi.org)

removals, tectonic or volcanic uplifts are morphological causes. Human activities like excavation, mining activities, quarrying, vibrations, deforestation, water leakages in pipe line and sewer are few reasons that cause the landslides. But predominantly, increase in shear stress and reduction in material strength are the two main influential parameters of landslides.

2 Rainfall Induced Landslides

In general, landslide occurs in any climatic conditions. But it is mainly observed in area with heavy rainfall. Rainfall induced landslide are common and recurring issue for hilly slopes. The damage caused by rainfall induced landslides incorporates economic losses, property damage, and loss of human and transportation route blockage. Types of landslide that take place due to heavy rainfall are shallow, small but moves rapidly. They further transform into fast moving slurries mixed with water, rock and soil to form debris flow. Landslides induced by rainfall can take place after several hours of rainfall or even immediately after or during its course. In unsaturated areas rainfall induced slides are due to change in ground water conditions. It is the most influential parameter to persuade hill slope instability and reduce the material strength. The effect of pore water pressure also dominates in rainfall induced landslides. Extreme rainfall infiltration mainly forms deep-seated rotational or shallow

translational slides. But if these landslides occur on steep slopes, they are dreadful and dangerous.

According to many researchers, on average short duration high intensity rainfall triggers shallow soil slips and debris flow and long duration, low intensity rainfall triggers deeper debris avalanches and slumps. In general, rainfall increases moisture content of the soil which decreases the soil shear strength. Also, there is increase in pore water pressure and reduction in capillary tension due to continuous rainfall. Therefore, causing slope saturation. This in turn increases the self-weight of soil and leads to collapse.

3 Review of Literature on Landslides

The review study includes several concepts for analysing landslides or slope failures used by several researchers. Different methods of back analysis are referred through literature survey for investigating rain fall induced landslides. Few other uncertainties due to landslide hazards and control measure for such slides occurring at similar location are reviewed in this paper. Rainfall induced landslide are observed in all parts of the world. Few major rainfalls induced landslides are taken for study in this review ranging from year 1980 to 2019.

3.1 Rainfall Induced Landslides in the World

Back in the 1980s some of the rainfall induced landslide studies were conducted by researchers. One such study was viewed by the university of Colorado, the researcher published different records of rainfall intensity and duration in relation with debris flow and shallow land sliding. The data sets of rainfall intensity and rainfall duration were considered from the year of 1960 to 1979. In general, the rainfall threshold for debris flow type of failure was suggested based on rainfall database observation. In most cases the slopes were not modified by any human activities or stream erosions. The threshold was decided based on a graph produced on rainfall duration and intensities. It was observed that a fairly minimum rainfall can also cause slope failure of undisturbed slopes (Caine 1980).

For the landslide that occurred in Tuscany region was evaluated to study the relation between mass movement, interstitial pressures and to find the critical pluviometric threshold for the slide. Here, Gumble's law was used to interpret the annual rainfall. The critical precipitation coefficient was analyzed using probabilistic diagrams of maximum heights distribution of annual precipitation along with cumulative curves of daily rainfall (Canuti et al. 1985). Due to cyclonic rainfall after an abnormally dry summer, North-wales experienced debris flow which caused blockage of road and needed remedial works immediately. After studying all soil properties, it

was found that due to high variable particle parameters colluvial sediments pore pressure rapidly increased and caused failure (Addison 1987).

Every decade improved methods of rainfall induced landslide study has been observed. In china analysis for landslides that happened in 1981 proclaimed that there were two types of serious debris flow, one which triggers by sustained regional rainfall and other that triggers by local heavy rainfall (Ze-Yi 1992). In 1993 the study on slope failure due to rainfall in Hong Kong in a hilly terrain concluded that in large area with heavy rainfall numerous slope failures occur. It was noticed, that the failure occurred when rainfall intensity within 24 h exceed 70 mm and also that possibility of major failure increases with high intensity rainstorms (Au 1993).

Brunetti et al. (2010) analysed the rainfall triggered landslides to provide new rainfall threshold for Italy and Abruzzo region. For study purpose a detailed catalogue of rainfall induced landslides was complied with certain information like time, date, rainfall intensity, rainfall duration, antecedent rainfall, landslide type, rock type, climatic information etc. The new rainfall threshold was decided based on Bayesian inference method (suitable for small data sets) and Frequentist method (suitable for large dataset). The study revealed that national thresholds are lower compared to regional threshold which is usually not the case.

Hasnawir and Kubota (2012) have made a study on 36 landslides occurring in Kelara, Indonesia, water shed areas. The main aim of the study was to determine rainfall thresholds for these shallow landslides. Landslides are also initiated due to transient loss of shear strength due to increase in pore water pressure. The watershed area map and annual rainfall intensity for past 30 years were observed in this study, with a complied inventory of slope failure information over the past years. Empirical threshold method was adopted in which, the regression curve is taken reliable on rainfall intensity—duration threshold. Concluding that for this rainfall induced shallow landslides, threshold rainfall is very important to provide warnings in such watershed areas.

Hasan and Najjar (2013) states that, when there are uncertainties in soil properties, slope failure may occur. A detailed study of slope stability issue that occurred along the highway proposed at Algeria was performed justifying the statement. Using Bayesian technique of back analysis, the effects of pore pressure, prior shear strength, correlation between shear strength parameters, failure location and geometry of slope were obtained. This method is based on limit equilibrium analysis assuming the factor of safety as unity. It was concluded that this approach is suitable when there is uncertainty in pore pressures and shear strength parameters of slope. Ng et al. (2014) presented a slope failure investigation of a man-made slope at Putrajaya Malaysia using numerical back analysis method. In this case remedial measures suggested were designing new slope, installation of slope stabilization methods based on the threshold values.

3.2 Rainfall Induced Landslides in the India

Ering et al. (2015) reported a detailed analysis of slope failure which occurred in the Malin Village, in Pune district of India in July 2014. After detailed investigation of nearby rain gauges it was found that slope failure occurred due to rainfall infiltration and mass movement. Back analysis was conducted to gain in-depth knowledge of slope stability parameter such as pore water pressure and soil shear strength at the moment of failure. For the verification of this analysis, the problem is examined using finite difference program FLAC2D. It was concluded that due to heavy rainfall matric suction in unsaturated part of slope is lowered. As the water starts infiltrating in the soil negative pore pressure dissipates due to increase water content in soil. This decreases the shear strength parameters in soil layers close to the surface which caused failure. Hence unsaturated soil mechanics and rainfall frequency analysis should in-corporate for stability of soil slope subjected to rainfall.

Savoikar and Hede (2018) investigated three landslides in south Goa district involving forensic study. The soil from these site were tested to find the geological properties such as gravel content, sand content, Silt and clay content, specific gravity, dry density, liquid limits and plastic limits. Further using Geo-Studio 2012 software these slopes were analysed for static and seismic slope stability. Morgensten-Price method was used for static analysis and for seismic analysis time history record of Kobe earthquake was used under QUAKE/W module of GEO-STUDIO suite. After the analysis slope protection methods were suggested for the three sites. Ambajim and Canacona sites were suggested soil nailing protection technique and Raia site was suggested Gabion RE wall protection measures. After implementing protection measures Optum G2 software was, used for stability analysis.

It is found that after protection measures were implemented the factor of safety has increased by about 50% in each case. It was concluded that the landslide prone area should follow the land use policies and regulations for better protections. Similarly, suitable landslide protection techniques such as RCC retaining walls, gabion walls, reinforced earth walls, soil nailed walls, and tie back walls should be implemented in such areas. Mardolkar and Souza (2019) investigated the different types of landslides in Ponda–Goa. Goa lies in the west coastal lateritic zone of India. There are around nine major lateritic formations which lie between low lands and high lands. These formations often fail causing spread or rotational type of landslides. Some of the landslides are studied and GeoStudio is used to find its factor of safety. In all six different landslides are presented in this study with its physical and geological properties.

4 Analysis of Rainfall Induced Landslides

Analysis of rainfall induced landslides include forensic investigations of landslides which had occurred in past including finding the water content and geotechnical properties that had resulted in the landslides. Continuous infiltration leads to increase in positive pore pressures which further reduce the shear strength of the soil. Determination of soil water characteristics of the soil is very important for forensic studies of past landslides.

4.1 Stability Analysis of Rain Induced Landslides

New methods were introduced for landslide hazard assessment which utilizes landslide database and geology maps based on GIS. The rainfall data was presented and studied with the help of histogram and antecedent rainfall curves. It was concluded that the assessment of existing landslides and urbanization of hilly areas are the priorities in risk managements (Chowdhury and Flentje 1998). Theoretical approaches of back analysis were demonstrated, which included methods such as Bayesian probability method. On the basis of limit equilibrium method slope stability analysis was performed to learn the effects of three dimensional and two-dimensional failures. It was found that the mobilized strength at the base of slope was of average strength (Gilbert et al. 1998). Certain studies were also conducted using finite element programs. One such case, involved rain records evaluation to identify the cause of failure using SEEP/W to analyze its pore water pressure. It is observed that due to antecedent rainfall, the soil permeability increases due to decrease in matric suction, which causes the failure (Rahardjo et al. 2001). The rainfall data was also analyzed in terms of antecedent rainfall percentage exceedance time (APERT), which determines the relative frequency of rainfall (Chowdhury and Flentje 2002). Another rainfall induced landslide study by Bacchini and Zannoni (2003) revealed that the triggering mechanism of debris flow prove that short duration, high intensity rainfall causes superficial landslides.

Mechanism of rainfall-induced landslide initiation in unsaturated slopes is performed using transient seepage and stability analyses combined with probabilistic back analysis using softwares like FLAC^{2D}. Back analysis determine the causes of failure like the shear strength parameters, pore water pressure and other conditions at the time of failure. It requires determination of soil-water characteristic curve and its parameters (van Genuchten curve fitting parameters). In addition it requires rainfall data, geotechnical properties of soil like natural moisture content, dry and saturated unit weight, specific gravity, liquid and plastic limit, grain size analysis, cohesion and friction angle, etc. Soil-water characteristic curve (SWCC) is the plot between the matric suction (u_a-u_w) and volumetric water content (θ_w). It determines the hydraulic and mechanical behaviour of unsaturated **soils** and to predict **soil water** storage. Matric suction is the difference between pore air pressure (u_a) and pore

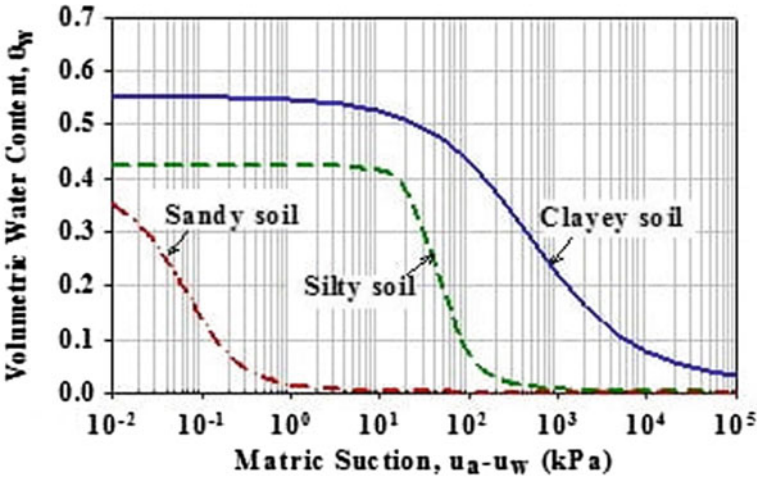

Fig. 3 Typical soil water characteristic curves for different types of soils (Fredlund et al. 2012)

water pressure (u_w). Matric suction influences the behaviour of unsaturated soils in both terms of shear strength and permeability. Figure 3 shows the typical soil water characteristic curves for different types of soils.

4.2 Finding the CRT Value Using Rainfall Data

The rainfall threshold is an important parameter for analysis of rainfall induced landslides. Critical rainfall threshold gives an idea at what value of rainfall, landslides will be triggered. This concept can help in providing warning system to landslide prone regions as well as inform the locals around, regarding such risky situations. The main element to evaluated the CRT value, is the rainfall data such as rainfall intensity, rainfall duration, cumulative rainfall for the past decades. Large data sets can calculate more accurate values and give better predictions. One of the simplest solutions to evaluate the critical rainfall threshold using a probabilistic and empirical method was stated by Huang et al. (2015). This technique is the simplest method to evaluate the rainfall threshold value. In this technique, a curve is plotted for cumulative rainfall (R_t) versus rainfall intensity (I_h). Cumulative rainfall can also be referred to as accumulated precipitation. The total amount of rainfall in 7 days including the day of rainfall that caused the failure is called the accumulated precipitation. In J. Huang's method he has considered two types of envelopes in his graphical representations one is termed as lower envelope of landslide occurrence and the second is termed as upper envelope of landslide occurrence. Figure 4 shows the graph of cumulative rainfall versus rainfall intensity.

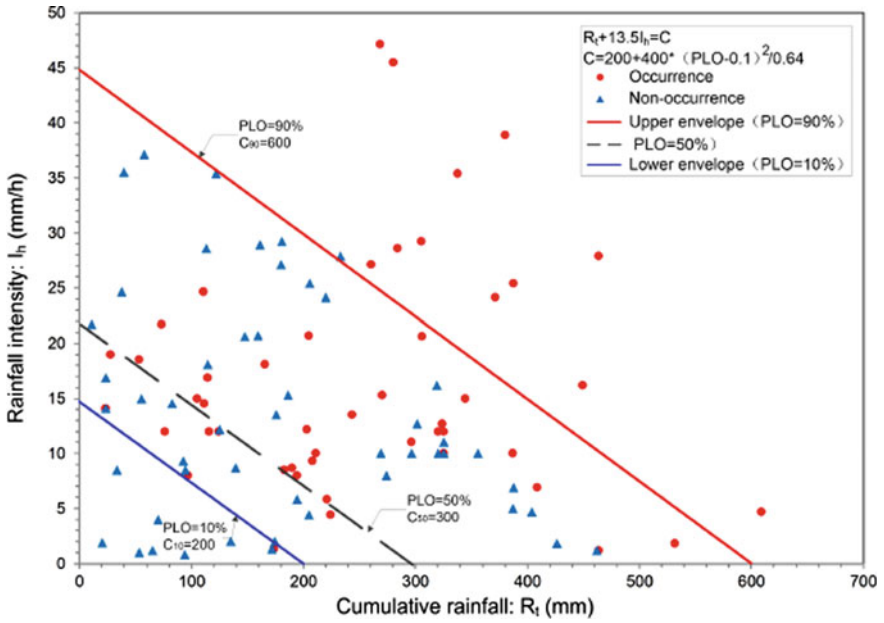

Fig. 4 R_t–I_h graph for occurrence and non-occurrence (Huang et al. 2015)

In the above Fig. 4, the blue line is drawn in such away that the points that are seen below the line are the point that has the minimal possibilities of landslide occurrence (10% probability). This is the lower envelope of landslide occurrence. Similarly, the upper envelope is represented by the red line above which the points that have maximum possibility of landslide occurrence are placed (90% probability). Between the two lines, a dotted black line depicts the probability line which is defined by an algorithm that is in Eq. 1

$$R_t + \alpha I_h = C \tag{1}$$

where R_t = accumulated precipitation in mm; I_h = hourly intensity in mm/hr; C = numerical constant and α = slope of the curve.

The most dangerous area is the one represented with 90% possibility of landslide occurrence which is at high risk where the local habitats are made aware of the situation. Based on this graph, the present situation of rainfall can be superimposed to predict the critical value of rainfall threshold and based on which the warning message can be given to the local habitats of possible landslide.

5 Conclusions

Landslide is a serious natural disaster, that cause intense damage to life and livelihood which needs to be controlled to avoid destruction. The climatic conditions, topography, soil conditions and groundwater table play a significant role in triggering landslides. In most cases, it is observed that the main causes of landslides are human activities like slope modifications and deforestations and further triggered by continuous rainfall. Most of the slopes where landslides occurred were observed with colluviums at the foot-steps of the terrains. Regions with intense heavy rain falls were largely affected by such disaster due to water infiltration, rising of pore water pressure and soil shear strength failures. Back analysis is predominantly used for investigating the reasons of slope failure and to improve knowledge on slope stability parameters and requires geotechnical properties along with determination of soil-water characteristic curves. Determination critical rainfall threshold based on cumulative rainfall data is very important in predicting the impending landslides during prolonged rainfall spells. Based on these studies, possible remedial measures can be suggested and landslide warning systems can be developed.

References

Addison K (1987) Debris flow during intense rainfall in Snowdonia, North Wales: a preliminary survey. Earth Surf Proc Land 12:561–566

Au SWC (1993) Rainfall and slope failure in Hong Kong. Eng Geol 36:143–147

Bacchini M, Zannoni A (2003) Relations between rainfall and triggering of debris-flow: case study of Cancia (Dolomites, Northeastern Italy). Natural Hazards Earth Syst Sci 71–79

Brunetti MT, Peruccacci S, Rossi M, Luciani S, Valigi D, Guzzetti F (2010) Rainfall thresholds for the possible occurrence of landslides in Italy. Nat Hazard 10:448–458

Caine N (1980) The rainfall intensity—duration control of shallow landslides and debris flows. Geogr Ann Ser B 62:23–27

Canuti P, Focardi P, Garzonio CA (1985) Correlation between rainfall and landslides. Int Assoc Eng Geol 32

Chowdhury RN, Flentje PN (1998) Effective urban landslide hazard assessment. 8th congress of the international association of engineering geology and the environment, pp 1–7

Chowdhury R, Flentje P (2002) Uncertainties in rainfall-induced landslide hazard. Q J Eng GeolHydrogeol 35:61–69

Ering P, Kolekar YA, Murty D, Sivakumar Babu GL (2015) Forensic analysis of Malin landslide in India. IOP Conf Ser Earth Environ Sci: Res Gate

Fredlund DG, Rahardjo H, Fredlund MD (2012) Unsaturated soil mechanics in engineering practice. Wiley, New York. ISBN 978-1-118-13359-0

Gilbert RB, Wright SG, Liedtke E (1998) Uncertainity in back analysis of slope: Kettleman Hills case history. J Geotech Geoenviron Eng 124:1167–76

Hasan S, Najjar S (2013) Probabilistic back analysis of failed slopes using Bayesian techniques. Geo-Congress 1013–1022

Hasnawir, Kubota T (2012) Rainfall threshold for shallow landslides in Kelara Watershed, Indonesia. Int J Jpn Erosion Control Eng 5(1):86–92

Huang J, Ju NP, Liao YJ, Liu DD (2015) Determination of rainfall thresholds for shallow landslides by a probabilistic and empirical method. Natural Hazards Earth Syst Sci 2715–2722

Mardolkar T, Souza L (2019) Types of landslides in Ponda lateritic formation. In: ISSMGE TC107 symposium on laterites and lateritic soils, Goa College of Engineering -Ponda Goa, pp 77–86
Ng SM, Ismail MAM, Abustan I (2014) Back analysis of slope failure using finite element with point estimate method (Fem-Pem). J Civ Eng Res 4:31–35
Rahardjo H, Li XW, Toll DG, Leong EC (2001) The effect of antecedent rainfall on slope stability. Geotech Geol Eng 19:371–399
Savoikar P, Hede A (2018) Landslides – stability and control measures. In: 2nd International conference on advances in concrete, structural and geotechnical engineering (keynote paper), 26–28, BITS Pilani, Rajasthan, pp 28–34
Spiker EC, Gori PL (2003) National landslide hazards mitigation strategy a framework for loss reduction. U.S. Department of the Interior, U.S. Geological Survey, Circula 1244
Ze-Yi C (1992) A preliminary study of the relationship between heavy rainfall and serious debris flows. In: The erosion, debris flows and environment in mountain regions (Proceedings of the Chengdu Symposium), Beijing 100080, China

Development of Filter System for Roof Water Harvesting

E. Shijila and K. K. Praveena

Abstract This research work has been taken up with the objective of developing a simple and easy to clean filter system. Under the study, a micro mesh filter has been evaluated thoroughly under actual rainfall conditions. Two additional filters viz. sand and charcoal were also developed as secondary filters and connected to the outlet of the mesh filter to improve the purification efficiency. As rainfall was insufficient to test the performance of the sand and charcoal filter combinations with the mesh filter, synthetic roof water was prepared and test was carried out. The study also included testing the roof water quality from different roofs such as clay tiled, RCC paved with terracotta tiles, clay tiled, old RCC and new RCC. The results showed that pH values of the roof water were not varying with respect to roof materials and their values were very close to 7. EC was varying with respect to roofs and rainfall events but there were no consistency in their variation, also, their values were within the permissible limit of potability. Turbidity and suspended solids were also showing variation and their concentration was higher than the permissible limit. After the filtration, the turbidity and suspended solids concentration reduced by 81% for mesh filter alone and 85% when secondary filter combinations of sand or charcoal were used. BOD5 test of the inflow and outflow water also showed considerable reduction in BOD5 in the outflow water. The study has proved that the micro mesh filter and the filter combinations with sand and charcoal are very effective in the purification of roof water and they are also very user friendly from the point of view of cleaning.

Keywords Roof water harvesting · Mesh filter · Roof materials

1 Introduction

Rainwater harvesting can be an effective and low-cost solution to tide over water scarcity especially the domestic one. The rainwater harvesting is a technique used for collecting and storing rainwater from rooftops, the land surface or rock catchments

E. Shijila · K. K. Praveena (✉)
Kelappaji College of Agricultural Engineering and Technology, Tavanur, Kerala 679573, India

B. B. Das et al. (eds.), *Recent Developments in Sustainable Infrastructure (ICRDSI-2020)—GEO-TRA-ENV-WRM*, Lecture Notes in Civil Engineering 207,
https://doi.org/10.1007/978-981-16-7509-6_27

using simple methods such as pots and tanks as well as more complex techniques such as underground check dams. This can make important contribution in resolving water shortages of the present and the future. Usually rainwater harvesting for domestic use involves collecting water from cleaner surfaces, such as roofs. In such cases, roof is the most direct contamination path in rainwater harvesting. It is well understood that there are a lot of filthy and offensive things on a roof surface that must be removed from the water to make it usable and safe. Rainwater falling on the roof is generally very pure and clean. However, many substances like leaves, bird droppings, dust etc. get mixed up with this pure water on the roof. These contaminants need to be adequately filtered before the rainwater is stored. A wide range of apparatus are used in the removal of fine suspended particles from rainwater, including filtration using membrane, sand, granular activated carbon, and expanded clay and gravel. Despite the growing variety of filters for rainwater purification available in the market worldwide, there are limitations in this technology that need to be addressed. The quality of roof water can be improved considerably if debris is kept out of the system. Filters simply catch the debris and allow clean water to flow through. One of the major limitations of this filter system is its difficulty in cleaning. Because of no periodic cleaning, the filter media will go clogged and the system becomes dysfunctional in a very short span of life. In this context, this study has been proposed to design and develop a more efficient and hassle free filter system for domestic roof water harvesting.

2 Materials and Methods

The study has been conducted on the existing micro mesh filter and the newly developed sand and charcoal filter in the campus of Kelappaji College of Agricultural Engineering and Technology (KCAET), Kerala, India. The details of the design, construction and evaluation of various filters for roof water harvesting systems are presented below.

2.1 Description of the Existing Micro Mesh Filter

The mesh filter was fabricated using PVC pipes of diameter 90 mm as casing pipe and 100 micron mesh wound on 50 mm slotted PVC pipe as filter element, which is placed inside the casing pipe. The filter element was hung concentrically inside the casing pipe and fixed to the casing by means of threaded end cap. Filter element can be taken out of the casing pipe for washing by loosening the threaded end cap. A back wash cleaning provision for the filter unit was also provided at the bottom. Height of the filter element was 30 cm and the surface area of mesh was 470 cm^2. The total height of filter unit with casing was 75 cm.

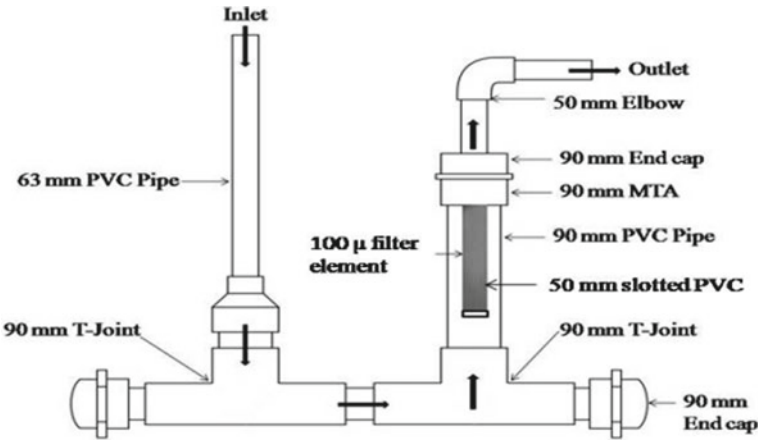

Fig. 1 Existing upward flow micro mesh filter

The region experiences major water scarcity in summer (March to May) due to prolonged summer period and negligible summer showers. Design and arrangement of the existing micro mesh filter is shown in Fig. 1.

2.2 Design of Sand Filter and Charcoal Filter

2.2.1 Design and Development of the Sand Filter

Sand filter was designed and developed using 90 mm diameter PVC pipe of 25 cm long with both ends closed by fine wire mesh of 1 mm^2. Sand passing through 2 mm mesh and retained on 1 mm mesh was used as the filter media. Sand filter was connected as a secondary filter to the outlet of the micro mesh filter. Outlet of the sand filter was connected to the water storage end of the system. The mesh and sand filter combination was used for the roof water purification. The specifications and arrangement of the sand filter is shown in Figs. 2 and 3 respectively.

2.2.2 Design and Development of the Charcoal Filter

A charcoal filter was also designed and developed in the similar line as that of the sand filter. A 90 mm diameter PVC pipe of 25 cm long was used as the casing pipe, both ends were closed with fine wire mesh. Further, muslin cloth was also fixed to the inner end of the wire mesh to act as a barrier to prevent the flow of charcoal along with the flow of water. Charcoal was filled in the casing pipe after 24 h of soaking in water to remove very fine particles which otherwise may go along with the filtered water. Specification of the charcoal filter is shown in Fig. 4. The outlet of the micro

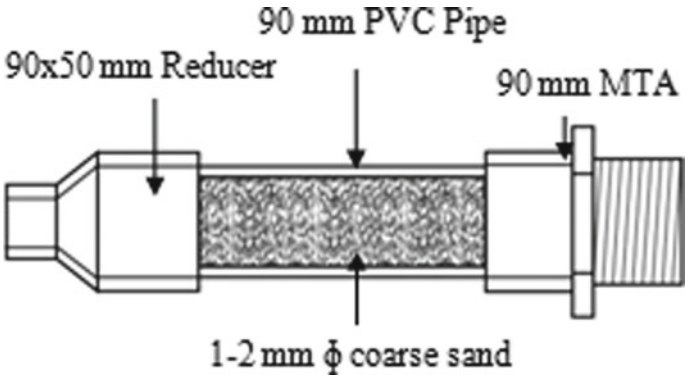

Fig. 2 Sectioned view of sand filter

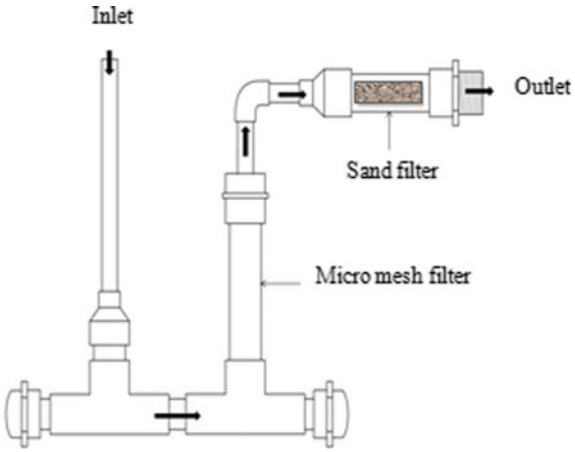

Fig. 3 Arrangement of sand and mesh filter

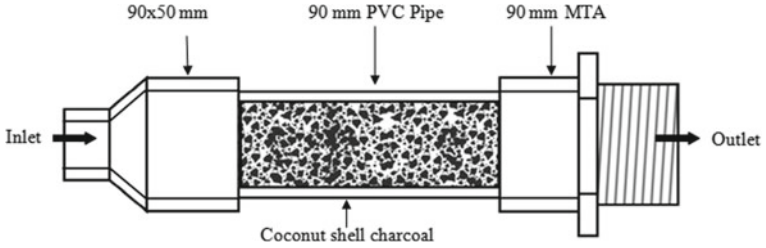

Fig. 4 Sectioned view of charcoal filter

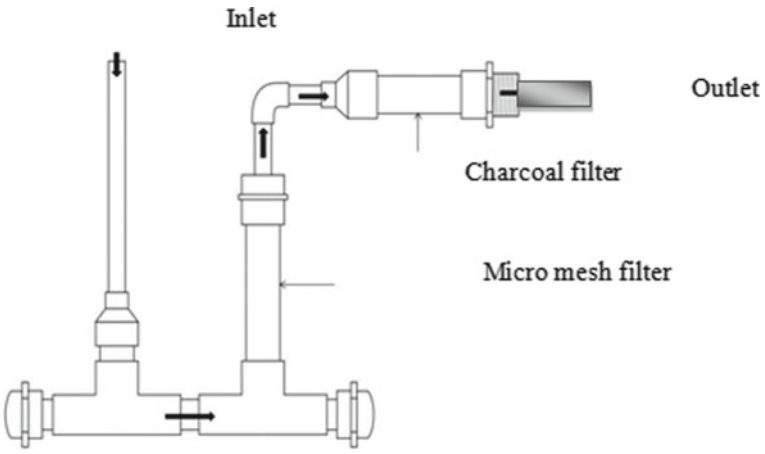

Fig. 5 Arrangement of sand and charcoal filter

mesh filter is connected to the inlet of the charcoal filter and the outlet of the charcoal filter is connected to the conveyance pipe leading to the storage tank. Arrangement of the charcoal filter is shown in Fig. 5.

2.3 Working of Filter Systems

Rainwater coming down from the rooftop through the collector system is conveyed to the filter through a 63 mm pipe which then enters a 90 mm pipe where the incoming flow velocity is reduced and the debris are allowed for initial settlement. Then, the rainwater with reduced velocity of flow move upward through the annular space between the casing pipe and the filter element. Water then passes through the micro mesh of the filter where removal of suspended particles takes place. The filtered water then moves to the storage tank. The entire movement of water from the roof to the storage tank takes place under gravity force without expending any additional energy. The filtered water by the mesh filter will flow through the secondary filter having filter media as sand or charcoal. After the secondary filtration, purified water will flow to the storage tank. The secondary filter is fitted horizontally and water flows through it in horizontal direction.

As the micro mesh filter unit is designed for the pass of water in upward direction, some of the suspended particles is settled at the bottom of its annular space and will reduce the load of impurities for the mesh filter. Impurities settled at the bottom can be removed by opening the end cap provided at the bottom by flushing. Secondary filters are provided for the finer filtration of the roof water. Impurities remaining after the filtration of micro mesh filter may be removed by the sand or charcoal filter.

2.4 Performance Evaluation of the Filter System

Various filter units were evaluated for their performances in respect of filtration efficiency of suspended matter and filtration rate. Evaluation was done under natural rainfall and with synthetic roof water.

During the absence of rainfall, synthetic roof water was prepared similar to natural rainfall roof water. For this, natural rooftop water falling down the roof was collected and the level of suspended impurities was determined through laboratory test (Gravimetric method).The main suspended impurities in roof top rainwater was moss. Hence, the moss was mixed with pure water in varying concentrations to give impurities on higher and lower side with that of natural concentration.

2.4.1 Filtration Rate of Different Filter Systems

The discharge rate and filtration rate of different filters were determined by collecting the filtered water from the filter outlet for a known time by keeping the head constant. Filtration rate is calculated using the following relation.

$$Rf = \frac{v}{t \times A} \tag{1}$$

where,

Rf is the filtration rate, $m^3/min/m^2$.

V is the volume of water collected, m^3.

t is the duration of collection, min.

A is the surface area of the filter, m^2.

2.4.2 Estimation of Filter Efficiency

The concentrations of suspended solids in the water before filtering and after filtering are found out. The efficiency of the filters has been determined by the following equation.

$$\mathrm{E} = \frac{S_\mathrm{b} - S_\mathrm{a}}{S_\mathrm{b}} \times 100 \tag{2}$$

where,

E = Efficiency of the filter, %

Sb = Suspended solids before filtering, mg/l.

Sa = Suspended solids after filtering, mg/l.

2.5 Estimation of Water Quality Parameters

The quality of filtered water is mainly assessed to know the potability of the roof water. Water quality parameters obtained through the test were compared with that of the threshold levels as specified by WHO and BIS.

2.5.1 Physical Analysis Through Water Quality Analyzer

A water quality analyzer, SYSTRONICS WATER QUALITY ANALYSER 371 was used to carry out the physical analysis of the roof water. It is a micro controller based instrument for measuring pH, dissolved oxygen, salinity, conductivity, TDS, temperature, colorimetric and turbidity in water sample one at a time.

2.6 Total Suspended Solids by Gravimetric Method

For measuring suspended solids, the water is filtered through a fine filter (Whattmann®, Grade 1, 110 mm ϕ) and the dry material retained on the filter is weighed. The drying was carried out for one hour in an oven at 105 °C.

$$\text{Total suspended solids in g/l} = \frac{W2 - W1}{V} \times 1000 \tag{3}$$

where, W1 = Initial weight of filter paper, g

W2 = Weight of filter paper and the dry material retained on the filter, g

V = Volume of sample, ml.

2.7 Analysis of Microbial Load

Two tests were conducted to determine microbial load on the rooftop water such as Biochemical Oxygen Demand (BOD) and total coliforms. The tests were undertaken at the Environmental Engineering laboratory of NIT Calicut, Kerala.

3 Results and Discussion

3.1 Effect of Roofing Material on Quality of Roof Water

The pH of roof water collected from different buildings with different roofing materials is tabulated and is shown in Table 1. It can be seen that the average pH of the roof water harvested from four different building through different rainfall events are ranging from 6.1 to 7.1. No appreciable difference in pH between the RCC and clay tiled roof was also seen. As pH values in both the cases were very close to neutral values, both roof catchments can be recommended for roof water collection from drinking purpose. Some studies have reported increase in pH for the water collected from roof compared to that of ambient (direct) rainwater. One sample from building 4 (new RCC) was of considerably acidic in nature. This may be due to the temporary existence of some acidic material on the roof.

The electrical conductivity (EC) of the collected roof water samples determined by water quality analyzer is shown in Table 2. Conductivities of samples were ranging from 20 to 1700 μS/cm. Wide variations for EC was seen between the rainfall events and types of roof. These variations may be due to the varied presence of charged ions in the impurities in the atmosphere and on the roof. EC corresponding to the rainfall event on 11.06.13 was considerably lower in the case of all the roofs. The reason could be the collection of roof water during continuous rainy period, which may yield better quality of water from the atmosphere and that from roof. The rest of the samples were collected after a dry spell of few weeks.

Turbidity of collected samples was tested and the values were varying in the range of 0.5–15 NTU. The occurrence of this turbidity variation may be due to the variations

Table 1 pH of the rooftop water samples

Date	Building 1 (RCC + TC)	Building 2 (clay tiled)	Building 3 (old RCC)	Building 4 (new RCC)
11/06/2013	6.65	6.78	6.94	4.04
28/06/2013	7.08	7.01	7.25	6.97
04/07/2013	6.68	7.26	7.04	6.18
17/07/2013	7.01	7.26	7.04	7.12

Table 2 Electrical conductivity of samples in μS/cm (cell constant = 1.166)

Date	Building 1 (RCC + TC)	Building 2 (clay tiled)	Building 3 (old RCC)	Building 4 (new RCC)
11/06/2013	23.4	25.7	42.6	72.7
28/06/2013	630	1150	1130	1490
04/07/2013	710	802	1030	975
17/07/2013	385	975	939	1630

Table 3 Turbidity of samples in NTU

Date	Building 1 (RCC + TC)	Building 2 (clay tiled)	Building 3 (old RCC)	Building 4 (new RCC)
11/06/2013	13	0.59	1.3	0.59
28/06/2013	1.8	4.5	0.73	2.7
04/07/2013	15	7.3	9.3	2.1
17/07/2013	9.7	3.6	3.0	3.1

Table 4 Suspended solids of given samples in mg/l

Date	Building 1 (RCC + TC)	Building 2 (clay tiled)	Building 3 (old RCC)	Building 4 (new RCC)
11/06/2013	290	250	110	340
28/06/2013	100	200	200	160
04/07/2013	300	300	500	170
17/07/2013	200	100	120	600

in the presence of moss content as well as their susceptibility for dislodgement. It has been reported that particulate matter washes off from smoother surfaces more rapidly than it does from rougher surfaces. According to the USEPA primary drinking water standards for systems using conventional or direct filtration, turbidity should never be above 5 NTU. Therefore, in majority of the samples, the turbidity values were above the allowable limits. Turbidity values were considerably higher in the case of tiled roof compared to RCC roofing. The findings go in conformity with the reported literatures (Kondal et al. 2011) (Table 3).

The selected samples were analyzed for suspended solids by gravimetric method and the values are ranging from 100 to 600 mg/l (Table 4). Different rainfall events showed different values of suspended solids. Between roofs, there were variations, but, that was not consistent. Based on the turbidity and suspended solids concentrations in the roof water harvested after the first-flush, it can be seen that all of the samples were not meeting the potable standards. Thus, treatment is a must to make it potable. The importance of purification of roof water has been highlighted by this result.

3.2 Filtration Rate of Different Filter Systems

Rate of filtration is an important characteristics of filters used in rain water harvesting systems. Considerable filtration rate has to be there in order to collect required quantity of water in a short span of time as the rain lasts only for short durations. The rate of filtration was determined by measuring the volume of outflow for a specified

Table 5 Filtration rate of different filter systems

Type of filter	Discharge (l/s)	Filtration rate ($m^3/min/m^2$)
Mesh filter	3.10	3.83
Sand filter	0.70	6.60
Charcoal filter	0.95	9.42

period of time. The filtration rates of different filters used in the study are shown in Table 5.

The discharge and filtration rates were highest in the case of mesh filter. The combination of mesh and sand filter gave the minimum rate of filtration. In all the cases, the filtration rate was sufficient for a domestic roof water harvesting system. The mesh filter had 3.1 l/s discharge and 3.83 $m^3/min/m^2$ filtration rate. In the case of primary and secondary filter combinations, filtration rate was worked out based on the cross sectional area of the secondary filter.

3.3 Filtration Efficiency of Mesh Filter in Natural Rainfall Conditions

The efficiency of suspended matter removal by the micro mesh filter was quantified and is presented in Table 6. The variation of filtration efficiency was ranging from 78.6 to 84.0%. This efficiency values are appreciable in the light of the simplicity of the filter device developed and also while comparing with the performance of other sand and charcoal filters reported in many research studies. The ease of cleaning feature of the mesh filter makes it more attractive and acceptable.

Table 6 Reduction in the impurity concentration

S. No.	Suspended solid before filtering (mg/l)	Suspended solid after filtering (mg/l)	Efficiency (%)	Average efficiency (%)
1	330	50.0	84.0	81.3
2	380	70.0	81.5	
3	350	65.0	81.4	
4	392	83.2	78.6	
5	450	85.0	81.1	

Table 7 Filtration efficiency of different filter combinations

Filter combinations	Roofing material	Efficiency (%)	Average efficiency (%)
Mesh with charcoal filter	Clay tile	86.31	85.5
	Concrete	85.63	
	Asbestos	84.59	
Mesh with sand filter	Clay tile	83.47	85.0
	Concrete	84.92	
	Asbestos	85.87	
Mesh filter	Clay tile	83.9	84.7
	Concrete	85.7	
	Asbestos	84.6	

3.4 Filter Efficiency of Different Filter Combinations Under Synthetic Roof Water

The filtration efficiency for the two secondary filter combinations have been evaluated extensively using synthetic roof water and is presented in Table 7. It is found that there is a marked reduction in the concentration of impurities. The reduction in impurities ranges from 84 to 86%. The mesh filter in isolation or in combination with sand or charcoal did not show significant variation in their filtration efficiency. Mesh with charcoal filter combination gave maximum filtration efficiency (85.5%).

3.5 Best Filter Combination

It was found that charcoal filter with mesh filter combination results is the maximum filtration efficiency. At the same time, the improvement of filtration efficiency compared to the sand and mesh filter combination was very marginal. Hence, considering the ease of maintenance, a mesh and sand filter combination has been recommended for the purification of roof water.

4 Conclusion

As part of the study, quality of roof water from different kinds of roofing materials has been conducted and the parameters viz. pH, EC, turbidity and suspended matters have been evaluated. Result showed that pH value from tiled and RCC building was very close to 7 indicating neutrality. Variations in pH between rainfall events were also not prominent. In the case of EC value, newly constructed RCC building gave considerably higher values compared to old RCC and tiled building. Presence of ions

in fresh Portland cement could be the reason. However, in all cases the EC values were in the potable limits recommended by national and international agencies. In the case of turbidity, the water samples had slightly higher levels than the values prescribed for drinking water standards. In the case of suspended solids, the values were higher than that is permissible for drinking water standards.

Evaluations of the performance of the micro mesh filter showed that it improves the pH values of outflow water closer to 7.0 and also it reduces the EC and turbidity values. In the case of suspended impurities, the reduction of impurities is to the tune of 85% and this result is very encouraging. Evaluation of the sand and charcoal filter combinations with mesh filter showed a great reduction in EC values compared to the case of mesh filter alone. In the case of pH, turbidity and suspended solids their values did not show any considerable changes in comparison with the unitary mesh filter.

The BOD test with the outflow of synthetic roof water resulted in the marked reduction (about 80%) of BOD for all the three filter combinations put in use in the study. Coliform test indicated that inflow water contained coliform bacteria beyond permissible levels. After the filtration, there were no trace of coliform bacteria and this outcome is worth highlighting.

Estimation of filtration efficiency of the suspended matter gave values of 81.3 for the solitary micro mesh filter and 85.0 and 85.5 for the sand and charcoal secondary filters respectively in combinations with the micro mesh filter as primary filter.

Reference

Kondal RY, Priyanka M, Raghu V, Saireddy NR (2011) Analytical study and microorganisms present in rain water of different areas. Int J Environ Sci 2:194–200

Analysis of Bottleneck at the Midblock in Hyderabad City

Pattepu Naresh, Teja Tallam, and C. Naveen Kumar

Abstract India is experiencing an exponential growth in population which in turn is leading to an increase in vehicular traffic. This increase in traffic is mostly because of private vehicles creating different problems like traffic congestion, increase in environmental pollution, safety issues and vehicular delay. One of the major reasons for traffic congestion in urban scenario is bottlenecking. Bottleneck will have a great impact on human capital hour loss. Three different locations of bottlenecks in Hyderabad, India are selected and video graphic survey was conducted. Vehicular delay, human capital hour loss, percent occupancy and level of service of all the three locations were determined. In this paper, equations for HCL, delay and occupancy were developed using linear regression model using R-Studios which is having MAPE as 24.56%, 18.56%, 11.54% and R-square as 0.62, 0.43 and 0.52 receptively. Level of service for all the three locations were found out with respective percent occupancy from HCM 2010 and based on delay. The obtained level of service was LOS E and LOS F during peak hours.

Keywords Bottleneck · HCL · Delay · Percent occupancy · Level of service

1 Introduction

One of the major concerns of the modern transportation is traffic congestion which has several impacts such as social, environmental and economical. In present scenario, traffic congestion became a severe problem and this situation is becoming worse day by day. Congestion is defined as the scenario where the speeds of vehicles are slower when compared to the normal free flow speed. The main reasons for the cause of congestion is the conflicts at merging for both the traffic streams (enter and exit) due to reducing in the distance from the entrance ramp to the exit ramp. The traffic congestion due to bottleneck is almost 40 percent of traffic congestion. Bottleneck is the situation where the whole capacity of the system is affected by one or more

P. Naresh (✉) · T. Tallam · C. Naveen Kumar
VNR Vignana Jyothi Institute of Engineering & Technology, Hyderabad, Telangana, India

B. B. Das et al. (eds.), *Recent Developments in Sustainable Infrastructure (ICRDSI-2020)—GEO-TRA-ENV-WRM*, Lecture Notes in Civil Engineering 207,
https://doi.org/10.1007/978-981-16-7509-6_28

components of that roadway section. It is also caused by narrowing of lanes which resists the flow of the traffic. Generally, bottleneck is taken from the properties of flow of water. When the water is allowed to flow out of a bottle, the discharge rate effected by the exit width which is a bottleneck. Bottleneck is the roadway section on which there is either greater demand or lesser capacity when compared to other roadway sections. Breakdown occurs when the demand exceeds the capacity of that section which reduces the maximum flow in that section. The major parameters that effect the bottleneck are volume, speed, travel time of the individual vehicles and travel occupancy. In bottleneck situation vehicle tends to move very slowly which increases the travel time of the vehicle. If vehicles move with lesser speeds leads to more consumption of the fuel which in turn results in economic loss of the users. The most harmful effect of the traffic bottleneck is its effect on the environment. When the vehicles are stopped in the traffic it causes additional burning of the fuel which leads to the emission of the carbon particles and more gases which are toxic. Generally due to large delay of the vehicles in the bottleneck. Drivers become impatient and drives more dangerously causing accidents. Delay of vehicles also decreases the surface lifetime of the pavement. Delivery services and the emergency services becomes slow too. A travel time study shall determine the amount of time required to travel on a given route from one point to another. Information on location, duration and causes of delay may also be collected in the conduct of such a study. The data obtained from travel time and delay studies provide a good indicator of the level of service to the study.

1.1 Research Objective

The main objective of the study is:

- To analyze the effect of bottle neck at different locations in Hyderabad.
- To calculate the human capital hour loss and vehicle capital hour loss due to bottleneck.
- Level of service based on delay and percent occupancy for selected locations.

2 Literature Review

Laflamme and Ossenbruggen (2017) analyzed breakdown state from normal flow to congested state and the time interval between congested state and clearance state using regression analysis. Takayama (2015) examined the effect of staggered work hours and trade of between the positive and negative congestion externalities. Optimal distributions of start time of the work and equilibrium characteristics are found out using these intrinsic properties. Yuan et al. (2014) used Ant algorithm for optimization of the signal timing at signalized network. Geng et al. (2014) developed

cell transmission model for the convergence state of bottleneck under the downstream congested state. Li et al. (2015) proposed critical phenomenon is an intrinsic feature of traffic dynamics, during which transition between isolated local flows and global flows occurs. Kim and Coifman (2013) examines traffic behavior in the vicinity of a freeway bottleneck, revisiting commonly held assumptions and uncovering systematic biases that likely have distorted empirical studies of bottleneck formation, capacity drop, and the fundamental relationship (FR). As the affected drivers relax, the high flows become unsustainable so a queue initially forms downstream of the on-ramp (consistent with earlier empirical results) only later receding upstream past the on-ramp. This initial phase of activation often lasts several minutes. Zhang and Levinson (2010) formulated a number of hypotheses to determine the impact of ramp metering on capacity and concluded that ramp metering can increase the bottleneck capacity. Chung et al. (2007) obtained a correlation between density and capacity drop, it ranged from 3 to 18%. They also concluded that capacity drops can be avoided by implementing traffic control schemes that regulate density. Cassidy and Rudjanakanoknad (2005) discovered that via metering the on-ramp, the shoulder lane accumulation decreased and better bottleneck discharge flows have been attained. However, they cautioned that the on-ramp metering schemes should be followed based on limited-access highway situations, which includes automobile accumulations close to the on-ramp, to gain massive growth within the capacities.

3 Methodology

After selecting the study area, data like travel time, travel occupancy, speed, volume are extracted from videography survey. Human Capital hour loss is found out for different classes of vehicles using delay obtained from the travel time survey. Level of service of the bottle neck is calculated using delay and percent occupancy. Methodology of the study is given Fig. 1.

4 Data Collection and Extraction

4.1 Study Area

Three bottlenecks were selected in the city of Hyderabad, Telangana, India for this study. Moosapet, Jubilee Hills, Lingampally are the three locations respectively. Table 1 represents about the inventory data of the locations.

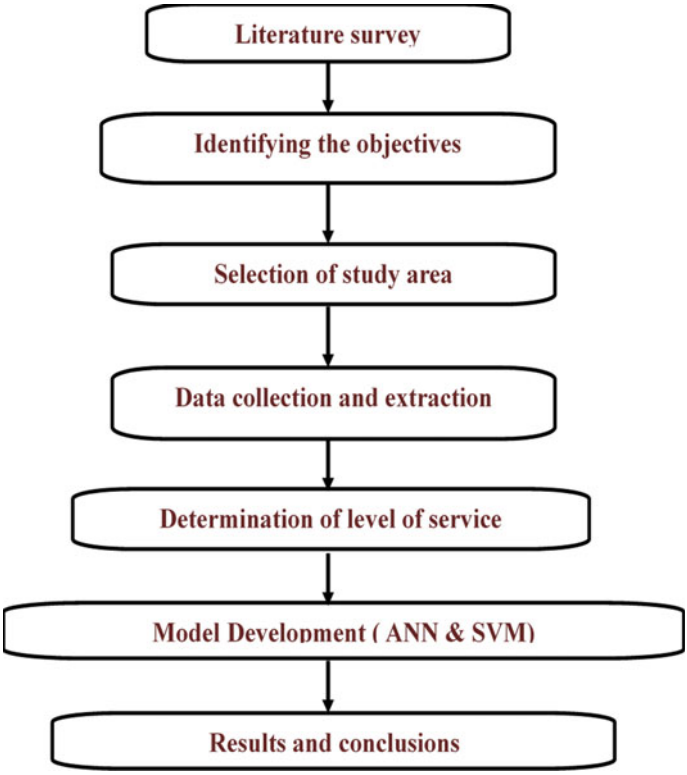

Fig. 1 Methodology flow chart

Table 1 Inventory data for different locations

S. No.	Location	Bottle neck length (m)	Decreased in Number of lanes (No's)
1	Moosapet	30	4–2
2	Jubilee Hills	60	3–2
3	Lingampally	25	3–2

4.2 Data Collection

Data was collected through videography survey at all the locations from 8:00 am to 8:00 pm. Using the videography survey, traffic volume, vehicle composition, speed is extracted. Travel time survey was conducted to calculate the delay due to bottleneck in the stretch. Vehicle occupancy survey is conducted to calculate vehicle occupancy at different locations.

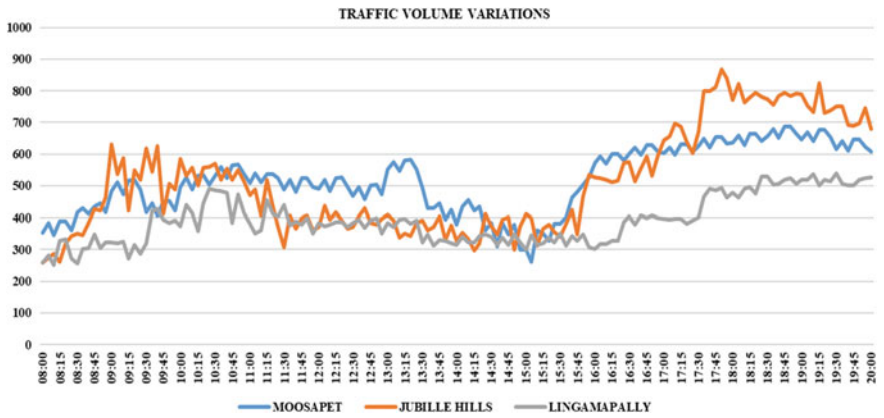

Fig. 2 Traffic volume variation

4.2.1 Volume Survey

The variations in traffic volume for Moosapet, Jubilee Hills, Lingampally are shown in Fig. 2 in vehicles for 5 min interval. The morning peak hours are found to from 8:30 to 11:15. The evening peak is found to be from 16:30 to 20:00.

4.2.2 Travel Time Survey

Travel time survey is conducted to understand the travel time variation and delay calculations.

Figure 3 shows the variation of travel time of different types of vehicles at moosapet. The peak travel times hours are observed from 10:00 am to 12:00 pm and 5:30 pm to 8:00 pm.

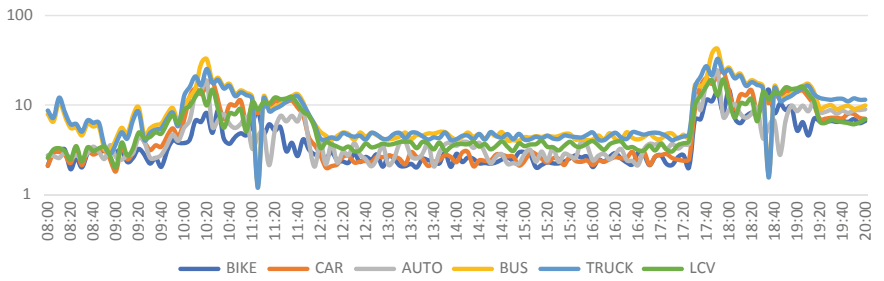

Fig. 3 Travel time variation at moosapet

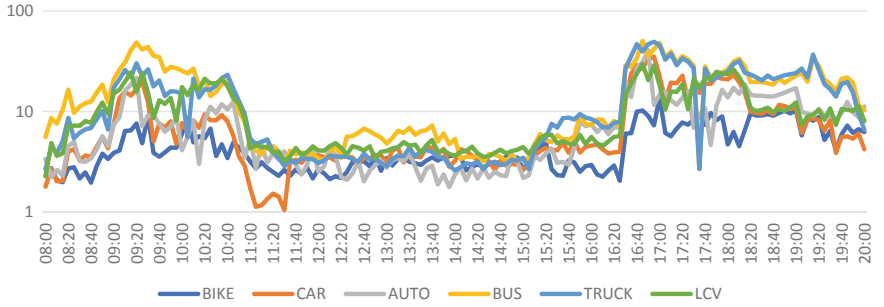

Fig. 4 Travel time variation at Jubilee hills

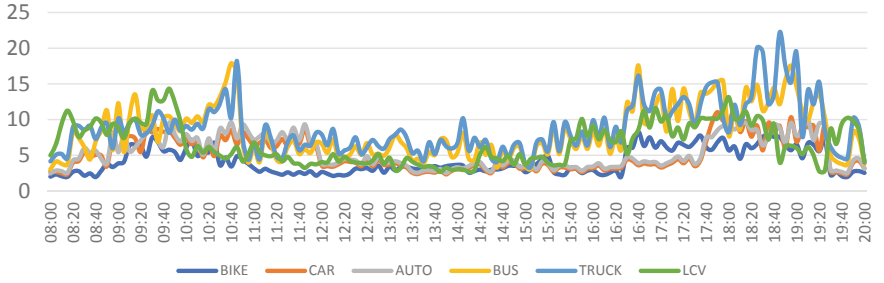

Fig. 5 Travel time variation at Lingampally

Figure 4 shows the variation of travel time of different types of vehicles at jubilee hills. The peak travel times hours are from 09:00 am to 11:00 pm and 4:30 pm to 8:00 pm.

Figure 5 shows the variation of travel time of different types of vehicles at Lingampally. The peak travel times hours are from 09:50 am to 12:00 pm and 5:30 pm to 8:00 pm.

5 Data Analysis

Based on the volume survey, vehicular occupancy survey and travel time survey, human capital hour loss are calculated using travel time, vehicular volume and speeds. Level of service is calculated based on delay and percent occupancy.

5.1 Delay

Travel time in peak hour is extracted and compared with normal travel time in off-peak hour, delay for all vehicles is calculated using Eq. 1.

$$\text{Delay} = \text{Peak Travel Time} - \text{Off - Peak Travel Time} \tag{1}$$

5.2 Human Capital Hour Loss

It is defined as the loss incurred due to delay in the travel time. Equation 2 is used to find out the human capital hour loss.

$$\text{Human Capital Hour} = \text{No. of persons (Vehicular volume} * \text{occupancy)} * \text{Delay} \tag{2}$$

5.3 Percent Occupancy

Percent Occupancy is used to find out the level of service of the bottle neck and is calculated using Eq. 3.

$$\textbf{Percent Occupancy} = \text{Total of Observed duration/Time duration of single point on a roadway is covered by vehicle} \tag{3}$$

5.4 Level of Service (LOS)

It is a mechanism used to determine how well a transport facility operates from a traveler's point of view. Six levels of service are defined and a letter designation from A to F is assigned to each, with LOS A representing the best conditions provided to travelers and LOS F being the worst for the travelers. The level of service is calculated using HCM 2010 and Jenks Natural Breaks Optimization.

Table 2 Human capital hour loss

Time	Total human Capital hour loss (person hours)			Total vehicle hour loss (vehicle hours)		
	Moosapet	Jubilee Hills	Lingampally	Moosapet	Jubilee Hills	Lingampally
8:00	173	603	440	4	34	18
9:00	249	4135	955	7	170	26
10:00	1328	2216	1372	27	174	18
11:00	692	61	693	26	9	16
12:00	144	151	431	7	9	16
13:00	148	227	427	6	10	16
14:00	122	85	492	4	6	16
15:00	127	261	520	4	19	19
16:00	180	3459	1064	6	170	47
17:00	1712	5780	1711	39	296	47
18:00	2109	5342	1650	52	243	52
19:00	1468	4066	1088	44	156	27
Sum	8451	26,386	10,844	227	1295	318

6 Results and Discussions

6.1 Human Capital Hour Loss and Vehicular Hour Loss

Human capital hour loss and total vehicle hour loss are tabulated and are represented in person hours and vehicle hours respectively. Human capital hour loss is calculated for 2-wheeler, 3 wheeler, 4-wheeler and Public mode whereas, vehicle is calculated for commercial vehicles like LCV and trucks. Among all three locations Jubilee Hills location is having highest human capital hour loss and vehicle hour loss. All the calculated values are tabulated in Table 2.

6.2 Delay

Average delay of all class of vehicles in minutes for each location. Jubilee hills area is having more delay when compared to other locations. The average delay calculated is tabulated in Table 3.

Table 3 Delay

Time	Delay		
	Moosapet	Jubilee Hills	Lingampally
8:00	124	188	219
9:00	154	925	423
10:00	667	612	383
11:00	410	32	229
12:00	80	47	146
13:00	83	66	124
14:00	81	35	136
15:00	77	111	159
16:00	79	923	306
17:00	602	1137	453
18:00	706	946	542
19:00	559	704	320
Sum	3623	5726	3440

6.3 Percent Occupancy

Percent occupancy was calculated an are tabulated in Table 4. It is the indication of percentage occupied by the vehicle on the road section with respect to time. Jubilee hills area is having highest percent occupancy compared to others.

Table 4 Percent occupancy

Time	Percent occupancy		
	Moosapet	Jubilee Hills	Lingampally
8:00	96	138	132
9:00	106	387	200
10:00	277	282	187
11:00	191	81	136
12:00	81	87	108
13:00	82	95	101
14:00	82	78	105
15:00	81	113	112
16:00	81	386	162
17:00	256	456	210
18:00	290	394	240
19:00	246	320	171
Sum	156	235	155

6.4 *Level of Service*

Level of service is estimated using delay and percent occupancy and is categorized as LOS A to LOS F based on HCM 2010 and Jenks Natural Breaks Optimization. Figure 6 shows the LOS variation of Moosapet for morning peak (10:00 am to 12:00 pm) and evening peak (5:35 pm to 8:00 pm).

Figure 7 shows the LOS variation of Jubilee Hills for morning peak (09:00 am to 11:00 pm) and evening peak (4:35 pm to 8:00 pm).

Figure 8 shows the LOS variation of Jubilee Hills for morning peak (09:50 am to 11:50 pm) and evening peak (5:30 pm to 8:00 pm).

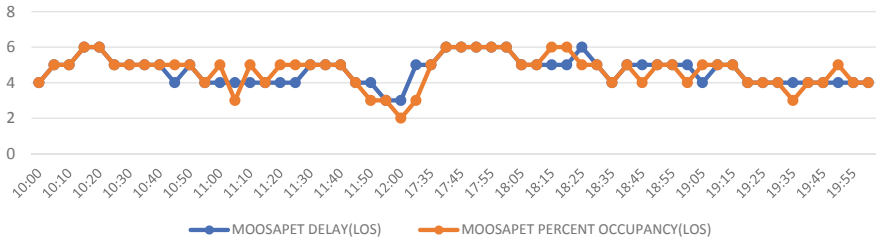

Fig. 6 LOS variation for Moosapet for morning and evening peak

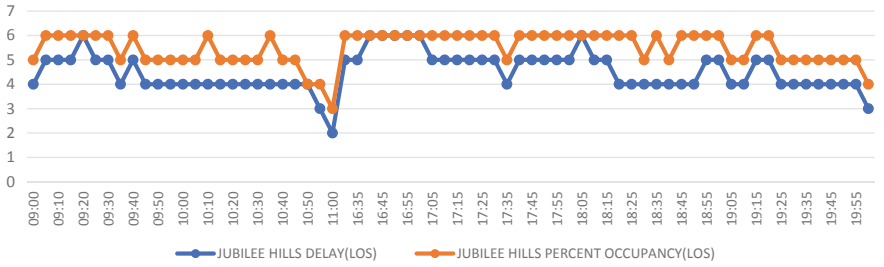

Fig. 7 LOS variation for Jubilee Hills for morning and evening peak

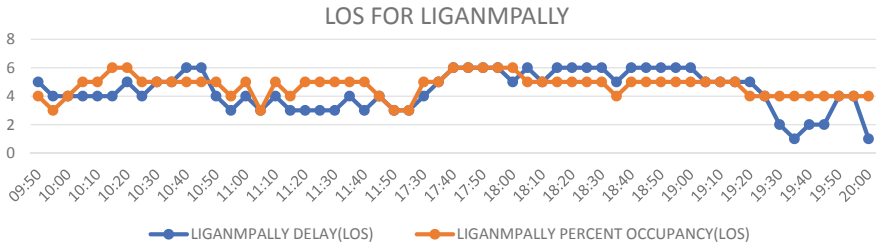

Fig. 8 LOS variation for Lingampally for morning and evening peak

6.5 Model Development

Individual equation is developed for dependent variable as Delay, Percent Occupancy and Human Capital hour loss and independent variables as bike, car, bus, truck, LCV. Equations 4, 5, 6 is having R-Square value as 0.43, 0.62, 0.52 as respectively.

$$\begin{aligned}\text{Delay} = &-38.45 + 0.069 * \text{Bike} + 0.246 * \text{Car} \\ &+ 0.344 * \text{Auto} + 0.328 * \text{Bus} \\ &+ 0.091 * \text{Truck} + 0.021 * \text{LCV}\end{aligned} \tag{4}$$

$$\begin{aligned}\text{HCL} = &-273.99 + 0.32 * \text{BIKE} + 1.31 * \text{CAR} \\ &+ 2.13 * \text{AUTO} + 4.87 * \text{BUS}\end{aligned} \tag{5}$$

$$\begin{aligned}\text{Occupancy} = &-8.83 + 0.02 * \text{Bike} + 0.08 * \text{Car} \\ &+ 0.12 * \text{Auto} + 0.12 * \text{Bus} \\ &+ 0.03 * \text{Truck} + 0.03 * \text{LCV}\end{aligned} \tag{6}$$

6.6 Model Validation

The delay, HCL and occupancy models are developed in R -Studio with 70% of train data and 30% test data. Equations are developed using train data and then tested with the test data, the performance measures are tabulated in Table 5.

From Table 5, based on MAPE of Delay and Occupancy lies between 10 and 20%, which indicates good prediction and HCL model is between 20 and 50%, which states that the model is of Reasonable prediction.

Table 5 Performance measures of the models

Model/performance measures	Delay	HCL	Occupancy
R-Square	0.43	0.62	0.52
RMSE	0.89	1.24	0.75
MAPE	18.56	24.56	11.45
Standard error	21.55	31.15	7.62

7 Conclusions

For decreasing the high human capital hour loss and vehicle hour loss due to the bottle neck, strict rules should be adopted to reduce the losses, like lane discipline should be followed, heavy /bus lanes should be provided if possible. Especially in peak hours there should be supervision as peak hours contribute higher losses. The human capital hour loss for Jubilee hills location is high compared to other location is because of the higher travel time is due to length of bottle neck is more compared to other locations. The Moosapet location is having designated bus lane which contribute to less human capital hour losses. All the locations are under ranging in LOS E and LOS F in peak hours which causes higher human capital hour loss and vehicular hour loss. The model developed for predicting delay, Human Capital Hour loss and Occupancy can be used for the ranking and bottle neck analysis.

References

Cassidy M J, Rudjanakanoknad J (2005) Increasing capacity of an isolated merge by metering its on-ramp. Transp Res 39B:896–913

Chung K, Rudjanakanoknad J, Cassidy M J (2007) Relation between traffic density and capacity drop at three freeway bottlenecks. Transp Res Part B Methodol. 41(1):82–95

Geng N, Zhaoa X, Xiea D (2014) Exploring the influence of the congested downstream on traffic flow at its upstream bottlenecks. In: The 9th international conference on traffic & transportation studies (ICTTS'2014)

Kim S, Coifman B (2013) Driver relaxation impacts on bottlenech activation, capacity and the fundamental relationship. Transp Res Part C Emerg Technol 36:564–580

Laflamme EM, Ossenbruggen PJ (2017) Effect of time-of-day and day-of-the-week on congestion duration and breakdown: a case study at a bottleneck in Salem, NH. J Traffic Transp Eng (JTTE)

Li D, Fu B, Wang Y, Luc G, Berezind Y, Stanleye H E, Havlind S (2015) Percolation transition in dynamical traffic network with evolving critical bottlenecks, PNAS 112(3): 669–672

Takayama Y (2015) Bottleneck congestion and distribution of work start times: the economics of staggered work hours revisited. In: 21st international symposium on transportation and traffic theory

Yuan S, Zhao X, An Y (2014) Identification and optimization of traffic bottleneck with signal timing. J Traffic Transp Eng (JTTE)

Zhang L, Levinson D M (2010) Ramp metering and freeway bottleneck capacity. Transp Res Part A 44(4):218–235

Arrhenius Based High-Temperature Performance Evaluation of Asphalt Binders Modified with Waste Plastic Pyrolytic Char

Abhinay Kumar, Rajan Choudhary, and Ankush Kumar

Abstract Enormous quantities and perplexity in sustainable disposal of plastic wastes pose serious environmental challenge globally and in India. Pyrolysis, a thermo-chemical degradation process, is perceived as a sustainable management approach for the waste plastic. In the pyrolysis process, solid carbonaceous char is generated as a by-product. Possible channels need to be identified for the bulk utilization of char. Plastic pyrolytic char (PPC), being a carbonaceous product, is used in the present study as an asphalt binder modifier as a possible step in the direction of sustainable modification of asphalt binders. Five different blends (asphalt binders modified with 0, 5, 10, 15 and 20% PPC) were evaluated through multiple stress creep and recovery (MSCR) tests performed at four high-service temperatures (40, 50, 60 and 70 °C) and five stress levels (0.1, 3.2, 5.0, 8.0, and 10.0 kPa). To compare rutting performance of asphalt binder on incorporation of PPC, the MSCR test was performed with 30 creep-recovery cycles and the results were compared using the first ten and the last ten cycles. Arrhenius relationship was used to explain and compare the temperature dependence of non-recoverable compliance (J_{nr}). Two ranking parameters were used based on J_{nr} and Arrhenius activation energy (E_a). Based on the ranking parameters, it was concluded that the rutting resistance of binders improved with increasing PPC contents, and that J_{nr} values of first ten cycles slightly overestimated the rutting performance of the binders compared to those obtained from the last ten cycles.

Keywords Sustainable asphalt binders · Pyrolysis · High-temperature performance · Arrhenius · MSCR

A. Kumar · R. Choudhary (✉) · A. Kumar
Department of Civil Engineering, IIT Guwahati, Guwahati, Assam, India
e-mail: rajandce@iitg.ac.in

B. B. Das et al. (eds.), *Recent Developments in Sustainable Infrastructure (ICRDSI-2020)—GEO-TRA-ENV-WRM*, Lecture Notes in Civil Engineering 207,
https://doi.org/10.1007/978-981-16-7509-6_29

1 Introduction

Plastic products find ubiquitous presence in all spheres of the life, especially in a developing economy like India. The rising popularity and use of plastics stems from their numerous advantages such as lightweight, durability, faster production, low cost, and flexibility (Murthy et al. 2020). Most commonly used plastic resins are classified in six types: polyethylene terephthalate (PET), high-density polyethylene (HDPE), polyvinyl chloride (PVC), low-density polyethylene (LDPE), polypropylene (PP), and polystyrene (PS). The mass consumption of plastics has also led to a surge in the generation of plastic wastes. Parker (2018) estimated a total of 8.3 billion metric ton plastic waste in the world. The annual generation is estimated at about 300 million tons per annum (Miandad et al. 2016). Whitcomb (2020) reported that of all plastic waste generated in 2017, a mere 8.4% got recycled. Researchers are therefore making continued efforts to improve and search for better methods to manage plastic wastes.

Pyrolysis of plastic wastes has emerged as one of the promising methods for conversion of plastic waste into products having the potential for energy generation. In the pyrolysis process, plastic is degraded by subjecting to high temperatures (generally 300–500 °C) in an oxygen-deficit environment (Miandad et al. 2016). The end products of plastic pyrolysis include liquid oil, gases, and solid carbonaceous char. Due to calorific value, pyrolytic oil finds applications for diesel engines, generators, and electricity generation (Murthy et al. 2020). Gases produced are mainly utilized to run the pyrolytic reactor. The solid char released as a residue/by-product only finds small applications in treatment of soil and thus raises need of avenues for its bulk utilization. As plastic char is a carbonaceous product like many other asphalt modifiers such as carbon black, carbon nano-tubes, toner ink, the present study attempts the use of plastic pyrolytic char (PPC) in asphalt binder modification.

Almost 90% of the world's roads are asphalt/bituminous pavements (also called flexible pavements) (ul Haq et al. 2020). Asphalt binder is an important and costly constituent of flexible pavement infrastructure and its properties significantly affect the performance of the mix (mixture of asphalt binder and stone aggregates) over a wide range of service temperatures. Asphalt binder is thermoplastic material mainly consisting of carbon and hydrogen along with minor amounts/traces of sulfur, nitrogen and oxygen. Asphalt binders behave as a viscoelastic material in the pavement temperature ranges, and have diverse molecular structures/chemistry depending on the crude source. Continuous increase in traffic volume, tire pressures and axle loads have raised the demand for more durable and long lasting asphalt materials. Asphalt technologists are apprised of these challenges and have made continuous efforts to improve the quality of asphalt binders and mixtures to meet the demands. Modification of asphalt binder has proven to be an effective means to improve the binder's resistance to permanent deformation (rutting resistance), especially at the high pavement service temperatures.

A simple model to describe the temperature dependence of asphalt binder's viscoelastic functions is the Arrhenius model. The Arrhenius law describes the dependency of rate of a reaction (k) on temperature as:

$$k = \alpha \exp\left(\frac{-E_a}{RT}\right) \tag{1}$$

where, α = pre-exponential constant; R = universal gas constant (8.314 J mol^{-1} K), E_a = activation energy (J mol^{-1}), and T = temperature (K). The Arrhenius concept has been used to characterize temperature dependence of asphalt binder and mixture properties such as asphalt binder viscosity (Hussein et al. 2005; Jiang et al. 2019; García-Morales et al. 2004; Salomon and Zhai 2002), carbonyl content (Liu et al. 1996), non-recoverable compliance (J_{nr}) (Narayan et al. 2019; Saboo et al. 2019), complex modulus (G*) (Narayan et al. 2019), shift factor for developing G^* and phase angle (δ) master curves for binders and mixtures (Airey et al. 2008; Pellinen et al. 2004), and asphalt self-healing rate (Garcia 2012).

Rutting is a commonly observed distress mechanism in asphalt pavements caused due to the accumulation of permanent strain in the pavements. Rheology of the asphalt binder plays an important role in characterizing the rutting potential of asphalt binders, especially the modified ones (Domingos and Faxina 2016). Using Eq. (1), the Arrhenius relationship for J_{nr} can be expressed as:

$$J_{nr} = \alpha \exp\left(\frac{-E_a}{RT}\right) \tag{2}$$

A linear form of Eq. (2) in logarithm of J_{nr} and inverse of temperature ($1/T$) is obtained by applying natural logarithm to both sides:

$$\ln J_{nr} = \ln \alpha + \left(\frac{-E_a}{R}\right) \cdot \left(\frac{1}{T}\right) \tag{3}$$

Multiple stress creep and recovery (MSCR) test is generally used for the evaluation of rutting performance of binders. It is usually conducted by applying ten creep-recovery cycles at two stress levels (0.1 and 3.2 kPa). However, it has been found in different studies that during the ten MSCR cycles the binder response is non-homogenous and not stable, and thus leads to higher variability in the results (Golalipour et al. 2017; Golalipour 2011). Further, based on Burger's modeling of MSCR response, Golalipour (2011) concluded that thirty MSCR cycles would suffice to obtain a consistent steady-state response and also capture the delayed elasticity effects. A steady-state response is attained by a binder when the delayed elasticity carried over from previous creep-recovery cycles is reduced (Golalipour et al. 2017), and the strain accumulation rate becomes somewhat constant (Bahia et al. 2001). Golalipour et al. (2017) further demonstrated that for highly modified binders or binders tested well below the high-performance grade temperature, the differences in J_{nr} response can be quite significant comparing the earlier cycles and the later cycles.

The plastic-char modified asphalt binders need to be evaluated for rutting characteristics at different levels of modification. Further it is quite important to characterize

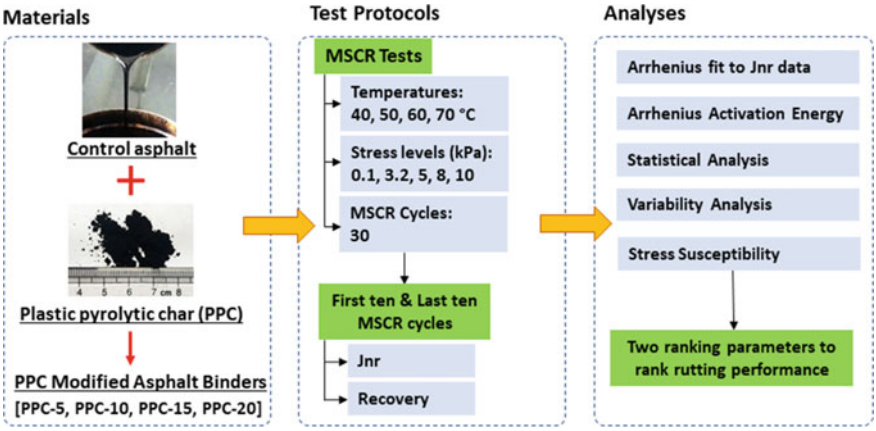

Fig. 1 Flowchart showing materials, test protocols and analyses

the rutting behavior of PPC modified binders considering multiple test temperatures, multiple stress levels, and a higher number of creep-recovery cycles. The objective of the present study is to characterize the rutting behavior of modified binders under different PPC contents (0% (control), 5%, 10%, 15%, and 20% by weight of binder) under different test conditions (stress levels, test temperatures, and test cycles). To characterize rutting behavior based on Arrhenius concept, MSCR test is performed with thirty creep-recovery cycles instead of the conventionally used ten cycles. Comparisons in rutting resistance/characteristics are also made considering J_{nr} derived from the first ten and the last ten cycles. Statistical analysis using analysis of variance (ANOVA) is performed to compare the differences between the J_{nr} values derived from first ten and last ten cycles. Variability analysis of J_{nr} is also performed based on coefficient of variance. Finally, the binders are ranked in terms of rutting performance based on two different ranking parameters. Figure 1 shows the flowchart for materials, nomenclature, test protocols, and analyses used in the present study.

2 Materials and Methodology

The base (unmodified) asphalt binder used was of viscosity grade 30 (VG30) satisfying all requirements of IS: 73 (2013). The PPC was obtained as a by-product from the industrial scale pyrolysis of plastic waste. PPC was obtained from Innova Engineering & Fabrication (Mumbai, India). Details of the pyrolysis process are provided elsewhere (Kumar et al. 2020). A high shear mixer was used to prepare the PPC modified binder blends with following blending conditions: temperature as 160 °C; mixing at 12,000 rpm, and total time of 30 min. Five dosages of PPC were

used: 0, 5, 10, 15 and 20% by weight of binder. A 0.3% by binder weight sulfur was also added to have adequate storage stability.

All modified binder samples were short-term aged using a rolling thin film oven (RTFO) in accordance to ASTM D2872 (2019) at 163 °C for 85 min. RTFO simulates the binder aging process that takes place during the asphalt mix production, transportation, laying and compaction of the bituminous mix. An MCR-102 Anton Paar dynamic shear rheometer (DSR) was used for the MSCR experiments on a 25 mm parallel plate geometry with 1 mm gap. Samples were prepared using silicone rubber moulds and were equilibrated at the desired temperature for 15 min before commencing the test.

MSCR test was conducted at four test temperatures (40, 50, 60 and 70 °C) and five stress levels (0.1, 3.2, 5, 8 and 10 kPa). Four temperatures were selected to evaluate the rutting performance of the PPC modified binders over a wide range of high-service temperatures. It has further been reported that stress levels higher than the currently used 0.1 and 3.2 kPa in the MSCR test are needed to better represent the binder stress state in the mixture (Arshadi 2013; Dreessen et al. 2009). A stress level up to 10 kPa in the MSCR test has been used based on multi-scale micro-mechanical modeling of binder phase in asphalt mixtures (Golalipour et al. 2017). In the present study, five different stress levels were used (0.1, 3.2, 5, 8 and 10 kPa) to capture the rutting behavior under a wide range of stress levels. As discussed earlier, thirty creep-recovery cycles were applied at each stress level. Each cycle consisted of 1 s loading and 9 s recovery. In each MSCR cycle, the non-recovered strain (ε_{nr}) is calculated as:

$$\varepsilon_{nr} = \varepsilon_r - \varepsilon_0 \tag{4}$$

where, ε_r = strain at the end of recovery, ε_0 = strain at the beginning of creep. Percent recovery (PR) is calculated for each MSCR cycle using the following equation:

$$PR = \frac{(\varepsilon_c - \varepsilon_0) - (\varepsilon_r - \varepsilon_0)}{(\varepsilon_c - \varepsilon_0)} \times 100 \tag{5}$$

where, ε_c = strain at the end of creep. Non-recoverable compliance (J_{nr}) at a stress level σ is calculated as follows:

$$J_{nr} = \frac{\varepsilon_{nr}}{\sigma} \tag{6}$$

3 Results and Discussion

3.1 Arrhenius Relationship to MSCR J_{nr}

Figure 2 presents the Arrhenius plots for J_{nr} showing the variation of J_{nr} with the reciprocal of temperature for all binders at two stress levels (3.2 and 8.0 kPa) for first ten and last ten cycles. Dashed lines in the plots are the Arrhenius fits to the data. The J_{nr} value decreases with the increase in the PPC content, showing that the addition of PPC improves the rutting resistance of the binder. Averaged over the four test temperatures, the PPC contents of 5%, 10%, 15% and 20% reduce J_{nr} values by 38.0%, 53.1%, 62.7% and 68.9%, respectively compared to the control binder (i.e., neat binder with 0% PPC content). Furthermore, the addition of PPC also enhances the percent recovery values at all stress levels and test temperatures. The improvements in recovery consistently increase with increase in PPC content. For example, at 40 °C the control binder recovered by 37.6% whereas the recoveries

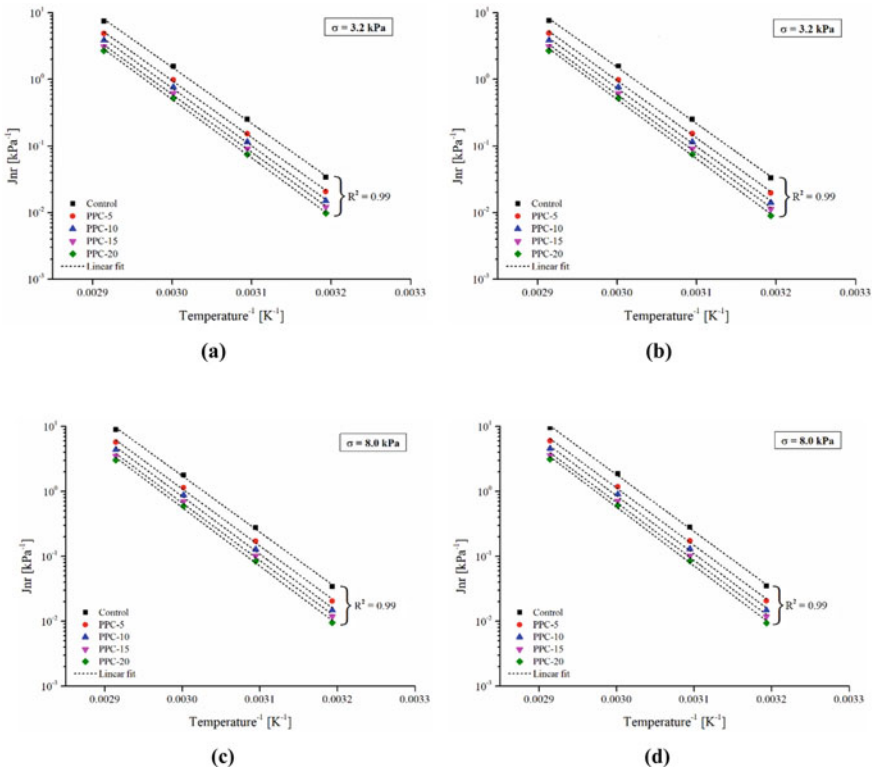

Fig. 2 Arrhenius plot for Jnr at **a** 3.2 kPa for first ten cycles; **b** 3.2 kPa for last ten cycles; **c** 8.0 kPa for first ten cycles; **d** 8.0 kPa for last ten cycles

for different PPC contents were 46.1%, 49.3%, 52.0% and 53.8% at PPC contents of 5%, 10%, 15% and 20%, respectively. Improved recovery results also indicate a well-developed PPC-binder matrix obtained as a result of the modification. A binder with higher recovery potential is further expected to perform better against permanent deformation as it can recover a greater amount of strain it is subjected to. It is also observed that irrespective of stress level, PPC content or selection of cycles, the variation between J_{nr} (on log scale) and reciprocal of temperature follows a straight line with a high coefficient of determination ($R^2 \sim 0.99$ in each case), implying that the J_{nr} response of the control and PPC modified binders is in conformity with the Arrhenius Eq. (2).

3.2 *Arrhenius Activation Energy*

Activation energy (E_a) is determined from the product of slope of Arrhenius graph and the ideal gas constant (R). Figure 3 presents the activation energies of all binders at the five stress levels. The activation energies obtained from last ten cycles are slightly higher than those for the first ten cycles. E_a values for the first ten cycles range from 160.0 to 173.8 kJ/mol whereas those from the last ten cycles range from 161.5 to 174.9 kJ/mol. The magnitude of activation energy values is comparable to those reported for J_{nr} by Narayan et al. (2019) and Saboo et al. (2019).

Narayan et al. (2019) reported a higher J_{nr} activation energy for elastomeric modified asphalt binders (Styrelf) compared to the control (unmodified) binder. Hussein et al. (2005) determined activation energy based on complex viscosity and reported increase in the activation energy with increase in LDPE concentration from 0 to 8% by weight of binder. In their study, LDPE-modified asphalt displayed higher elasticity in comparison to the control (unmodified) asphalt. In both studies (Hussein et al. 2005; Narayan et al. 2019), the increase in activation energy was observed

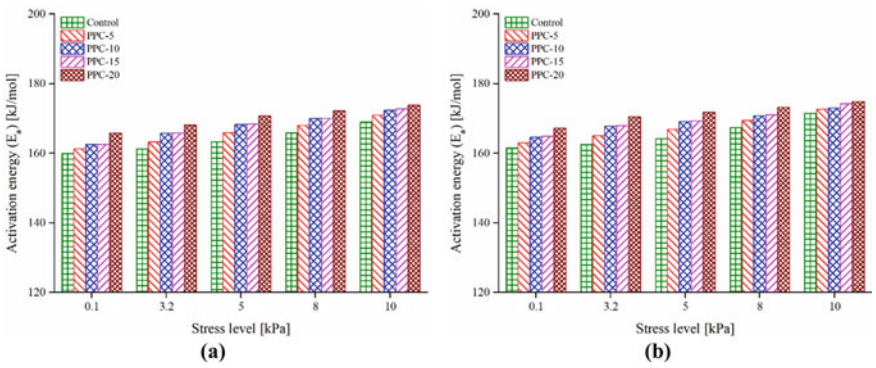

Fig. 3 Activation energy of binders: **a** first ten cycles; **b** last ten cycles

only with elastomeric modification, whereas plastomers reduced the binder activation energy. Jiang et al. (2019) determined activation energy for viscosity at different polyphosphoric acid (PPA) concentrations ranging from 0 to 2.5% by binder weight. It was found that the activation energies monotonically increased with increased PPA concentration. The authors attributed this finding to the higher crosslinking between molecules forming a more stable matrix with the chemical modification effect of PPA. Based on the findings from the literature, Fig. 3 therefore suggests that PPC may act as a pseudo-elastomer in the binder and the effect magnifies at higher PPC concentrations. To further investigate the nature of effect of stress level and PPC content on activation energy, the E_a values were regressed against stress level and PPC content. A fairly good positive linear relationship was found with R^2 ranging from 0.821 to 0.991 for stress level and 0.706 and 0.953 for PPC content. However, no discernible trend could be observed for the slope of the linear fits with respect to either stress level or PPC content.

3.3 *Analysis of J_{nr} of PPC Modified Binders for First Ten and Last Ten Load Cycles in MSCR Test*

Figure 4 compares J_{nr} obtained from first and last ten cycles for all the binders at two stress levels of 8.0 and 10.0 kPa and two test temperatures of 50 and 60 °C. A slightly higher J_{nr} is observed from the last ten cycles. The differences between the two J_{nr} values were lower at lower stress levels and for PPC modified binders compared to the control.

Statistical analysis using one-way ANOVA was performed to quantify the differences in J_{nr} observed from the first ten and the last ten MSCR cycles. For brevity, the results shown in Table 1 are for two stress levels (3.2 and 8 kPa) at the test temperature of 60 °C for all binders. Table 1 shows that the differences in mean J_{nr}

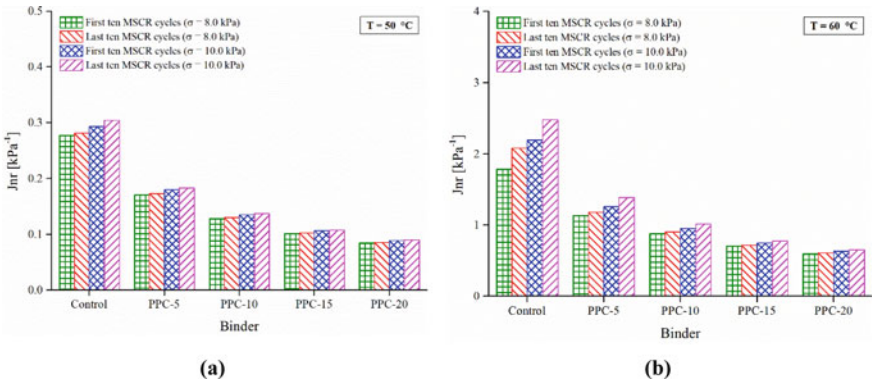

Fig. 4 Comparison of J_{nr} from first and last ten cycles at **a** 50 °C; **b** 60 °C

Table 1 Results of ANOVA for comparison of J_{nr} from first ten and last ten MSCR cycles

Binder	Stress level = 3.2 kPa *p*-value, S/NS	Stress level = 8.0 kPa *p*-value, S/NS
Control	<0.001, S	<0.001, S
PPC-5	0.015, S	<0.001, S
PPC-10	0.006, S	<0.001, S
PPC-15	0.037, S	<0.001, S
PPC-20	0.013, S	<0.001, S

Note 'S'—significant difference; 'NS'—non-significant difference

for the first and last ten cycles are statistically significant at 5% level of significance. The statistical significance is seen for control as well as PPC modified binders. The results were similar at other test temperatures as well and are not presented due to brevity.

The variability in the J_{nr} values obtained from the first ten and last ten MSCR cycles is quantified from the coefficient of variance (CoV), defined as the ratio of standard deviation to mean expressed in percentage. The results of J_{nr} CoV at 40 °C for all binders at 3.2 kPa and 8.0 kPa stress levels are shown in Fig. 5. It can be clearly seen that the last ten MSCR cycles have significantly lower scatter in J_{nr} than that in the first ten MSCR cycles. Therefore, the use of last ten cycles for J_{nr} calculations is expected to produce a more consistent and reliable J_{nr}. Another important observation from these results is the increase in CoV with increase in PPC content for J_{nr} computed from the first ten cycles. This shows that the scatter in J_{nr} is higher for modified binders and further increases with increase in the level of modification. Selection of J_{nr} from the last ten cycles would thus reduce the variability in J_{nr} and yield more reliable results.

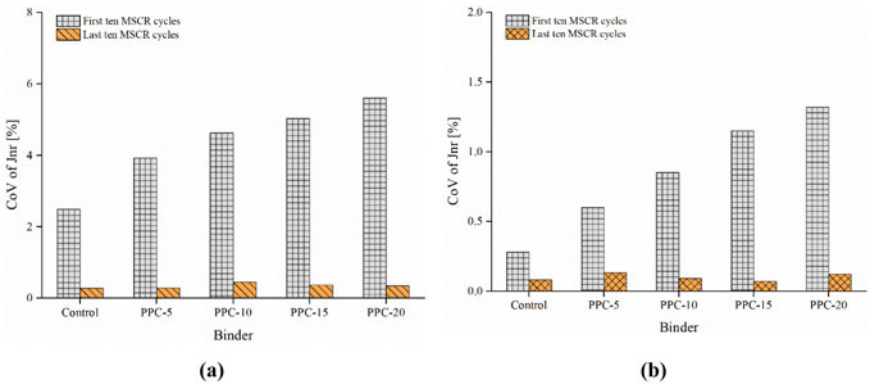

Fig. 5 Coefficient of variance of J_{nr} from first ten and last ten cycles: **a** 3.2 kPa; **b** 8 kPa

3.4 Stress Susceptibility

To measure the stress susceptibility of the binders, the slope of a linear fit between J_{nr} and stress level is used and is denoted by the parameter 'm'. It has the units of kPa^{-2} and quantifies the change in J_{nr} per unit change in the stress level. For example, Fig. 6 presents J_{nr} versus stress level plots for the control and PPC modified binders at 60 °C for J_{nr} calculated for the first ten and last ten cycles. A good linear fit can be observed in both cases for all binders. Graphs at other test temperatures also showed good linear fit and are not shown here for brevity. The parameter m was calculated for binders at all temperatures and Fig. 7 shows the results. For all binders, the value of m increases with increase in the test temperature. Given a unit change in stress level, the change in J_{nr} will be numerically larger at higher temperatures and therefore m increases with temperature. Increase in the PPC modification level generally leads to a lower stress susceptibility as seen from reduced value of m with increasing PPC dosages in Fig. 7. For example, at 60 °C the change in J_{nr} per unit increase in stress

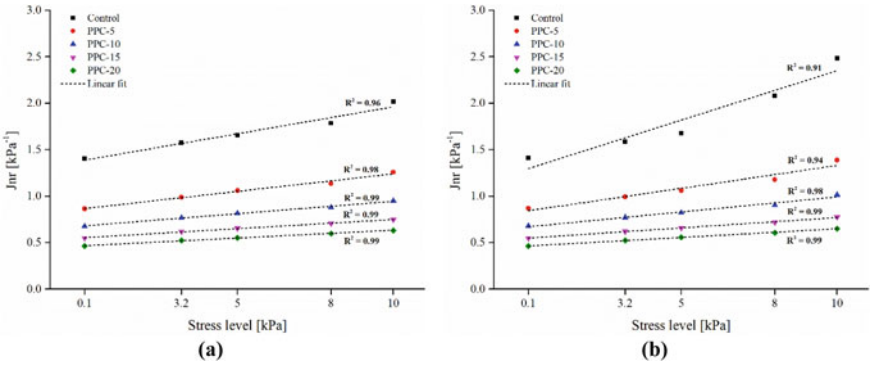

Fig. 6 J_{nr} versus stress level plots at 60 °C for **a** first ten cycles; **b** last ten cycles

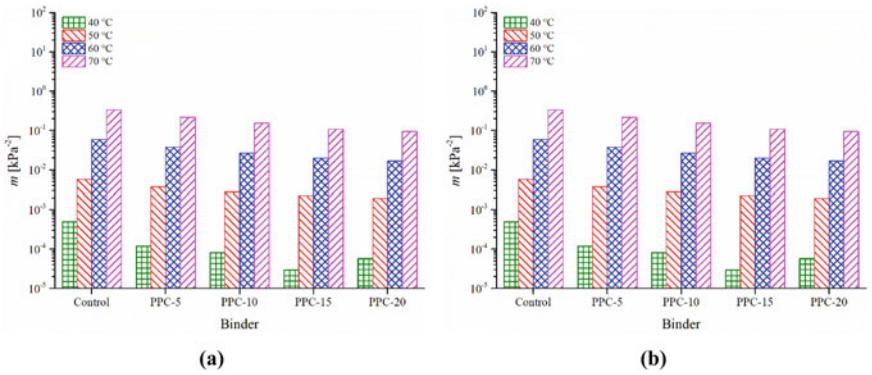

Fig. 7 Stress susceptibility parameter (m) for **a** first ten cycles; **b** last ten cycles

level was 5.9% for the control binder, which successively reduced to 3.8%, 2.7%, 2.0%, and 1.7% at respective PPC contents of 5%, 10%, 15% and 20%. Therefore, the use of PPC for asphalt binder modification is found beneficial from the point of view of reducing the binders' stress susceptibility. A comparison of Fig. 7a, b reveals that m slightly increases when J_{nr} from the last ten MSCR cycles is used.

3.5 Ranking Parameter

Based on MSCR J_{nr} and Arrhenius activation energy results discussed earlier, two ranking parameters are used to rank the rutting performance of the binders investigated in this study. A ranking parameter is a statistic that assigns a rank to the binder based on the relative values of the parameter. Arrhenius plots for J_{nr} (Fig. 2) showed that at all four test temperatures, the J_{nr} of PPC modified binders decreased in the order: control > PPC-5 > PPC-10 > PPC-15 > PPC-20. Further, the percentage decrease in J_{nr} of PPC modified binders compared to the control was slightly higher at lower test temperatures. For example, at 5 kPa stress level, the PPC-20 modified binder reduced the J_{nr} by 72.2%, 69.8%, 66.6%, and 64.7% at the temperatures of 40, 50, 60, and 70 °C, respectively. This observation can be schematically represented by Arrhenius plots shown in Fig. 8. The difference in slope of the Arrhenius plot for the control and a PPC modified binder can be clearly observed, which is also in agreement with higher activation energy values for the modified binders than the control. It therefore follows that a higher activation energy and a lower J_{nr} are expected to contribute towards a better rutting performance. The parameter E_a/J_{nr} can thus capture the effects of both quantities and thus can be used to rank the rutting performance of PPC modified binders. However, for a binder, E_a is calculated at different stress levels, and J_{nr} is obtained at different temperatures and stress levels.

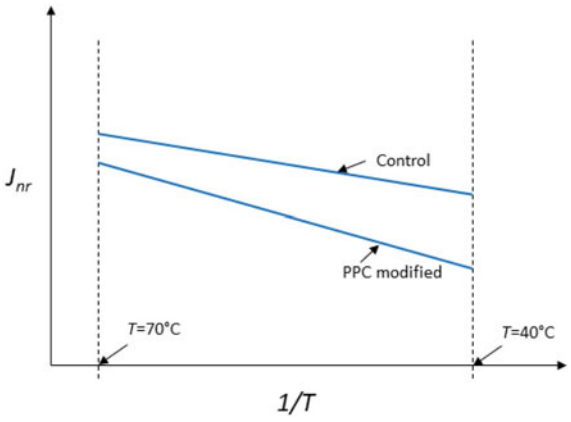

Fig. 8 Schematic Arrhenius plots for control and a PPC modified binder

Averaging these values is therefore needed to arrive at a single value of ranking parameter.

In the present study, two ranking parameters (RP_1 and RP_2) are used with the following expressions.

$$RP_1 = \frac{\overline{E_a}}{\overline{J_{nr,70}}} \tag{7}$$

$$RP_2 = \frac{\overline{E_a}}{\overline{J_{nr,60}}} \tag{8}$$

$\overline{E_a}$, $\overline{J_{nr,70}}$ and $\overline{J_{nr,60}}$ respectively refer to activation energy and J_{nr} (at 70 °C and 60°) averaged for the stress levels. RP_1 is defined based on J_{nr} at 70 °C, the maximum temperature considered in this study to evaluate rutting performance. RP_2 is defined based on J_{nr} at 60 °C as this temperature very commonly represents the high pavement service temperature in India. A higher value of the ranking parameter will assign a higher rank to a binder. The results of the ranking parameters are presented in Fig. 9. RP_1 ranges from 19.9 to 60.1 kPa·kJ/mol for the first ten cycles and 19.5 to 59.5 kPa·kJ/mol for the last ten cycles. RP_2 ranges from 97.5 to 307.5 kPa·kJ/mol for the first ten cycles and 91.9 to 306.3 kPa·kJ/mol for the last ten cycles. The magnitude of RP_1 is smaller than RP_2 as J_{nr} at 70 °C is higher than at 60 °C. Among all five binders, the ranking parameters rank PPC-20 binder the highest followed by PPC-15, PPC-10, PPC-5 and the control. It is pertinent to note that the ranking parameters encompass all five stress levels and four test temperatures and therefore provide a single measure to rank the binders' rutting performance. A lower J_{nr} and a higher activation energy obtained at higher contents of the PPC explain the better rutting performance of the PPC modified binders. The parameters derived from first ten MSCR cycles slightly over-estimate the ranking parameter and hence the rutting performance. Using the last ten MSCR cycles is therefore recommended

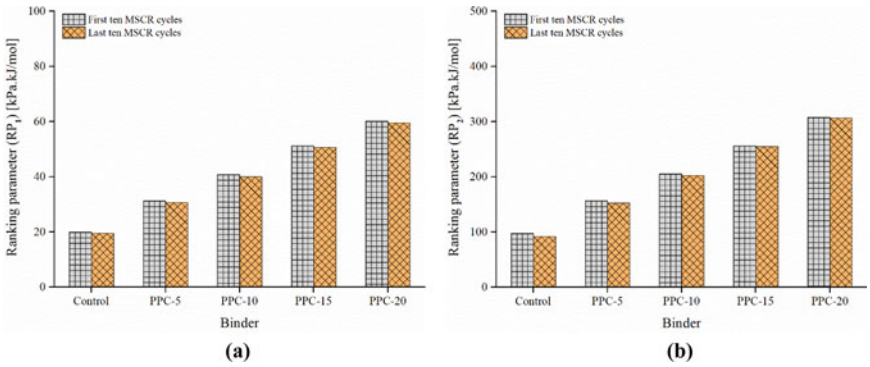

Fig. 9 Results of the two ranking parameters: **a** RP_1; **b** RP_2

since the J_{nr} values derived from these cycles are steady-state and correspond to a more homogeneous response of the control and PPC modified binders.

4 Conclusions

Based on the results and analyses in the present study, the following conclusions are drawn:

- Asphalt binder modification through different contents of plastic pyrolytic char (PPC) yielded binders with improved rutting resistance and enhanced elastic behavior.
- PPC modified binders showed a lower J_{nr} and a higher recovery as compared to the base (unmodified) binder. The improvements became more pronounced at higher PPC contents.
- J_{nr} from the last ten cycles had significantly lower variability compared to those from the first ten MSCR cycles, as measured from the coefficient of variance.
- The J_{nr}-temperature plots for the control and PPC modified binders at all stress levels followed the Arrhenius relationship.
- PPC modified binder with 20% modification was ranked the highest among all binders based on two ranking parameters. PPC modified binders were ranked higher than the control binder and therefore the addition of PPC derived from the pyrolysis of waste plastics helps to improve the rutting performance and reduce the stress susceptibility of asphalt binders. The experimental results obtained are quite encouraging for the use of char from waste plastic pyrolysis as a modifier.

References

Arshadi A (2013) Importance of asphalt binder properties on rut resistance of asphalt mixture. Diss
ASTM D2872 (2019) Standard test method for effect of heat and air on a moving film of asphalt (rolling thin-film oven test). ASTM International, West Conshohocken, PA
Bahia HU et al (2001) Characterization of modified asphalt binders in superpave mix design. No. Project 9-10 FY'96. National Cooperative Highway Research Program, Transportation Research Board, National Research Council, Washington, DC
Domingos MDI, Faxina AL (2016) Susceptibility of asphalt binders to rutting: literature review. J Mater Civ Eng 28(2):04015134
Dreessen S, Planche JP, Gardel V (2009) A new performance related test method for rutting prediction: MSCRT. Adv Test Charact Bituminous Mater 1:971–980
García Á (2012) Self-healing of open cracks in asphalt mastic. Fuel 93:264–272
García-Morales M et al (2004) Viscous properties and microstructure of recycled eva modified bitumen. Fuel 83(1):31–38
Golalipour A, Bahia HU, Tabatabaee HA (2017) Critical considerations toward better implementation of the multiple stress creep and recovery test. J Mater Civ Eng 29(5):04016295

Golalipour A (2011) Modification of multiple stress creep and recovery test procedure and usage in specification. Diss
Hussein IA et al (2005) Influence of M w of LDPE and vinyl acetate content of EVA on the rheology of polymer modified asphalt. Rheologica acta 45(1):92–104
IS 73 (2013) Paving bitumen - specification. Bureau of Indian Standards, New Delhi
Jiang X et al (2019) Investigations on viscosity and flow behavior of polyphosphoric acid (PPA) modified asphalt at high temperatures. Constr Build Mater 228:116610
Kumar A, Choudhary R, Kumar A (2020) Use of char derived from waste plastic pyrolysis for asphalt binder modification. RILEM Book Series-ITCSD 2020, Springer, Berlin
Liu M et al (1996) The kinetics of carbonyl formation in asphalt. AIChE J 42(4):1069–1076
Miandad R et al (2016) Influence of temperature and reaction time on the conversion of polystyrene waste to pyrolysis liquid oil. Waste Manage 58:250–259
Murthy K, Shetty RJ, Shiva K (2020) Plastic waste conversion to fuel: a review on pyrolysis process and influence of operating parameters. Energy Sources Part A: Recov Util Environ Effects 1–21
Narayan SPA, Little DN, Rajagopal KR (2019) Incorporating disparity in temperature sensitivity of asphalt binders into high-temperature specifications. J Mater Civ Eng 31(1):04018343
Parker L (2018) A whopping 91% of plastic isn't recycled. Accessed from https://www.nationalgeographic.com/news/2017/07/plastic-produced-recycling-waste-ocean-trash-debris-environment/
Pellinen TK, Witczak MW, Bonaquist RF (2004) Asphalt mix master curve construction using sigmoidal fitting function with non-linear least squares optimization. In: Recent advances in materials characterization and modeling of pavement systems, pp 83–101
Saboo N, Singh B, Kumar P (2019) Development of high-temperature ranking parameter for asphalt binders using Arrhenius model. J Mater Civ Eng 31(12):04019297
Salomon D, Zhai H (2002) Ranking asphalt binders by activation energy for flow. J Appl Asphalt Binder Technol 2(2):52–60
ul Haq MF et al (2020) Carbon nanotubes and their use for asphalt binder modification: a review. Emerg Mater Res 1–14
Whitcomb I (2020) How much plastic actually gets recycled?. Accessed from https://www.livescience.com/how-much-plastic-recycling.html

Use of Banana Natural Fiber as a Stabilizing Additive in Open Graded Friction Course

Rajan Choudhary, Vishal Kumar, Ankush Kumar, Santanu Pathak, and Abhinay Kumar

Abstract Open graded friction courses (OGFC) are special-purpose asphalt mixes with a porous structure (percentage air voids usually in the range of 18–25%) and are used to quickly remove the rain water from the pavement surface. A porous asphalt mix structure is typically designed utilizing a higher fraction of coarse aggregates and a low fine/filler content. An open asphalt mix structure is however prone to asphalt binder draindown under gravity during production, storage, and transportation of the OGFC mixes. Synthetic and organic fibers are generally used as stabilizing additives in OGFC mixes to alleviate the binder draindown and the abrasion loss. Synthetic fibers (e.g. polypropylene and polyester fibers) are widely used as stabilizing additive but are costly. In this study, natural fiber derived from the banana plant waste is evaluated for use as a stabilizing additive in OGFC mixes. Banana fiber is extracted from the bast/pseudo-stem of the banana plant dumped as waste after harvesting. The main aim of this study is to investigate the draindown and abrasion loss characteristics of OGFC mixes fabricated using variable length and dosages of natural banana fiber as stabilizing additive. One aggregate gradation and a polymer modified binder were used to fabricate the OGFC mixes. A total of twenty-seven combinations of OGFC mixes were evaluated accommodating three bitumen dosages, three fiber lengths, and three contents of banana fiber. Results showed that both the length and dosage of banana fiber had a significant effect on the draindown and abrasion loss characteristics.

Keywords Natural fiber · Banana fiber · OGFC mix · Draindown · Abrasion loss

1 Introduction

Open graded friction course (OGFC) is a special type of hot mix asphalt (HMA) surface course designed with a high percentage (usually in the range of 18–25%) of air voids. The porous structure of OGFC mixes due to high air void content permit quick

R. Choudhary (✉) · V. Kumar · A. Kumar · S. Pathak · A. Kumar
Department of Civil Engineering, IIT Guwahati, Guwahati, Assam, India
e-mail: rajandce@iitg.ac.in

B. B. Das et al. (eds.), *Recent Developments in Sustainable Infrastructure (ICRDSI-2020)—GEO-TRA-ENV-WRM*, Lecture Notes in Civil Engineering 207,
https://doi.org/10.1007/978-981-16-7509-6_30

removal of stormwater from the pavement surface (Alvarez et al. 2011; Choudhary et al. 2017; Kumar et al. 2018). The aggregate structure of OGFC mixes is composed of about 50–60% uniform-sized aggregate particles. To warrant high proportions of internal voids, OGFC mixes generally have a low fine aggregate and filler content. OGFC mixes demand higher asphalt content compared to the dense graded mixes to enable a good coating/film over the aggregate surface so as to ensure adequate abrasion, aging, and moisture damage resistance. Some of the typical benefits offered by the OGFC mixes include improved pavement friction, minimized hydroplaning, reduced splash and spray, improved night visibility, and lower pavement noise levels. (Allen Cooley et al. 2000; Mallick et al. 2000; Kumar et al. 2018; Pattanaik et al. 2019, 2020; Pathak et al. 2019, 2020).

In OGFC mixes, the use of a higher proportion of uniformly graded coarse aggregate with low fine aggregate and filler content makes them prone to binder draindown and abrasion loss. The phenomenon of downward movement of bituminous binder/mastic in OGFC mixes under the action of gravity mainly during production, transportation, and laydown is termed as draindown (Allen Cooley et al. 2000). The draindown of bituminous binder in mixes with an open aggregate gradation is more likely to happen during the high production and construction temperatures. Binder draindown also occurs during storage or hauling, triggering the vertical draining of binder from the mix. It can lead to a non-homogeneous distribution of bitumen in the mix creating few sections of the mix with comparatively low asphalt percentages which can be vulnerable to raveling/stripping while other portions may have higher bitumen dosages that can create a flushed surface with a reduced amount of void and permeability (Putman and Lyons 2015). One of the effective and popular aid to reduce or control the binder drain out from the OGFC mixes is the addition of fibers as a stabilizing additive. The various benefits of incorporating fibers to these mixes include enhanced binder stiffness and aggregate-binder coating, higher tensile strength, reduced severity of cracking, and increased fatigue resistance (Abtahi et al. 2010; Gupta et al. 2019). Different types of fibers have been tried in asphalt mixes such as: synthetic fibers derived from petroleum crude; mineral fibers that are produced through melting of the feedstock minerals followed by the spinning technique to form fibers; and the natural fibers obtained from plants or other natural resources (McDaniel 2015).

Natural fibers from different sources such as cellulose, coir (coconut), sisal, jute, date-palm, hemp, etc. have been used in different asphalt mixes (Allen Cooley et al. 2000; Hassan et al. 2005; Hassan and Al-Jabri 2005; Lei et al. 2010; Oda et al. 2012; Afonso et al. 2017; Dash and Panda 2016; Ramalingam et al. 2017; Shanbara et al. 2018; Kumar and Ravitheja 2019; Ferreira da Costa et al. 2020a, b). Natural fibers have shown to impart improvement to asphalt mixes in terms of reduced binder draindown, higher resistance to raveling, improved tensile strength, and increase in an overall performance (Abtahi et al. 2010; Gupta et al. 2019).

Limited studies are available on the use of banana fiber as a stabilizing agent in bituminous mixes, especially in OGFC mixes. The banana plant is a perennial plant that thrives in a tropical region and grows from a bulb or rhizome and its sowing to harvesting duration is 9–12 months. India tops the chart of banana-producing

Table 1 Aggregate gradation selected as per ASTM D7064 (2013)

Sieve (mm)	Specified gradation, % passing	Selected gradation, % passing
19	100	100
12.5	85–100	92.5
9.5	35–60	47.5
4.75	10–25	17.5
2.36	5–10	7.5
0.075	2–4	3

countries with a total production of about 14.2 million tonnes where the total annual global yield of banana fruit is about 86 million tonnes. After harvesting the fruit, the banana plant becomes waste biomass since it cannot be harvested after one cycle. It has been reported that about 200 tons of waste biomass from the banana plant (including leaf, pseudo-stem, rotten fruit, rhizome, etc.) gets generated from each hectare of banana farming. Banana fibers are extracted out from the bast (pseudo-stem) of the banana plant by a decorticator machine (Subagyo and Chafidz 2018).

It is quite important to understand the effect of both fiber length and fiber content on OGFC mix performance. This study aims at investigating the use of banana fiber obtained from banana plant waste as a stabilizing agent in OGFC mixes. This study addresses the effect of banana fiber dosages and lengths on the draindown and abrasion resistance of OGFC mixes at different asphalt binder contents.

2 Materials and Methodology

2.1 Materials

2.1.1 Aggregate

Aggregates used in this study were procured from a stone crusher plant located in Shillong, Meghalaya, India. The physical properties of aggregate satisfied the requirements of MoRTH (2013). The mid gradation of the specified aggregate gradation in ASTM D7064 (2013) has been selected for the preparation of OGFC mixes. Table 1 shows the aggregate gradation selected for the preparation of OGFC mixes.

2.1.2 Asphalt Binder

The binder selected in this study for the fabrication of OGFC mixes was a polymer modified binder grade 40 (PMB40), elastomeric type, satisfying all the required

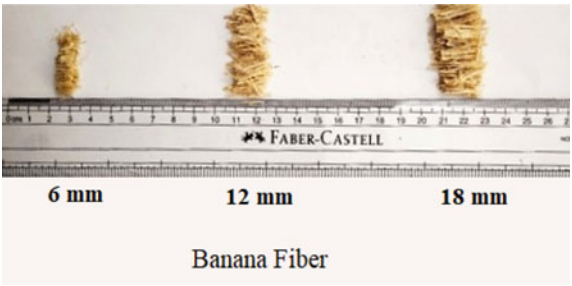

Fig. 1 Different sizes of banana fiber

Table 2 Properties of banana fiber (GoGreen Products, Chennai)

Parameter	Values
Diameter (μm)	1000–3000
Density (g/cm^3)	1.3
Tensile strength (MPa)	650–780
Elongation at break (%)	2–4
Young's modulus (GPa)	29–32

criteria of IS 15462 (2004) specifications and was made available by Tikitar Industries, Gujarat, India.

2.1.3 Banana Fiber

The banana fiber used in the study was procured from GoGreen Products (Chennai, India). Three different banana fiber lengths of 6 mm, 12 mm, and 18 mm were used in this study (shown in Fig. 1). The banana fiber contents selected for the study were 0.15, 0.30, and 0.45% by weight of the dry aggregate. Table 2 shows the properties of banana fiber.

2.1.4 Fabrication of OGFC Mixes

In this study, natural fibers extracted from bast (pseudo-stem) of banana plants were used as stabilizing additive in OGFC mixes. Three binder contents (5.5, 6.0, and 6.5% by mix weight), three different fiber dosages (0.15, 0.30, and 0.45% by weight of the dry aggregate), and three lengths of fibers (6 mm, 12 mm, and 18 mm) were used to prepare 27 different combinations of OGFC mixes. Three replicates for each combination were prepared for evaluation. The OGFC mixes without fiber were also fabricated as the control mix for comparison. The mixing and compaction temperatures used for the fabrication of all OGFC specimens were 170 °C and 160 °C, respectively. For specimen preparation, stabilizing additive (banana natural fiber) and hot aggregate were dry-mixed uniformly to warrant a uniform dispersal of the fiber

during the mixing process. A little longer mixing duration is expected in OGFC mixes with fiber due to the increased surface area, compared to the mixes without fibers. After uniform mixing of aggregate and banana fiber, the given content of preheated asphalt binder (PMB40) was added and thoroughly mixed. The loose OGFC mix for each combination was first conditioned and then compacted using a Superpave Gyratory Compactor (SGC).

2.2 Test Methods

2.2.1 Binder Draindown

The draindown test was carried out as per the specifications laid out in ASTM D6390 (2017). For the draindown test, a basket with a 6.3 mm sized mesh was weighed empty as *A* and then the loose mix was transferred to the basket immediately after preparation and the combined weight of the basket and the loose mix was noted as *B*. The basket was then placed on a plate of weight *C*, and the entire set of plate, basket, and the loose mix was placed in an oven for 1 h. The inside temperature of the oven was maintained at 10 °C above the mixing temperature. After completion of 1 h, the entire set was removed from the oven and kept to cool down to room temperature. Then the drained material along with the plate was noted as *D*. The draindown was calculated using Eq. 1:

$$\text{Draindown}(\%) = \frac{D - C}{B - A} \times 100 \tag{1}$$

2.2.2 Cantabro Abrasion Loss

Cantabro abrasion loss was conducted to measure the resistance of OGFC mixes towards raveling due to inadequate bonding between aggregate particles. The test was accomplished in a Los Angeles abrasion machine following the protocols mentioned in ASTM D7064 (2013). SGC specimens of 100 mm diameter and 63.5 mm height were used for testing and weighed as P_1. The compacted specimen was rotated in the Los Angeles abrasion machine for 300 revolutions with a speed of 30–33 rpm at 25 °C. After completion of revolutions, the remains of the compacted OGFC mix specimen was cleaned and weighed as P_2. The Cantabro abrasion loss was calculated using Eq. 2:

$$\text{Abrasion loss}(\%) = \frac{P_1 - P_2}{P_1} \times 100 \tag{2}$$

3 Results and Discussion

3.1 Binder Draindown

Binder draindown results of OGFC mixes with banana fiber at binder contents 5.5%, 6.0%, and 6.5% are presented in Fig. 2a–c, respectively. Draindown values witnessed appreciable reduction with the addition of banana fiber at all the three binder contents which further alleviated with increment in fiber dosages. At all three binder contents, the incorporation of banana fiber resulted in a reduction in binder draindown of OGFC mixes when compared to control mixes (without fiber). All the mixes satisfied the maximum draindown threshold of 0.3%. For each fiber length, OGFC mixes fabricated with 0.45% banana fiber dosages showed maximum reduction in binder draindown. The trend observed for a decrease in binder draindown with an increase in fiber dosages is also in agreement with the findings of other studies where banana fiber is used as a stabilizing additive (Beena and Bindu 2014; Shiva Kumar et al.

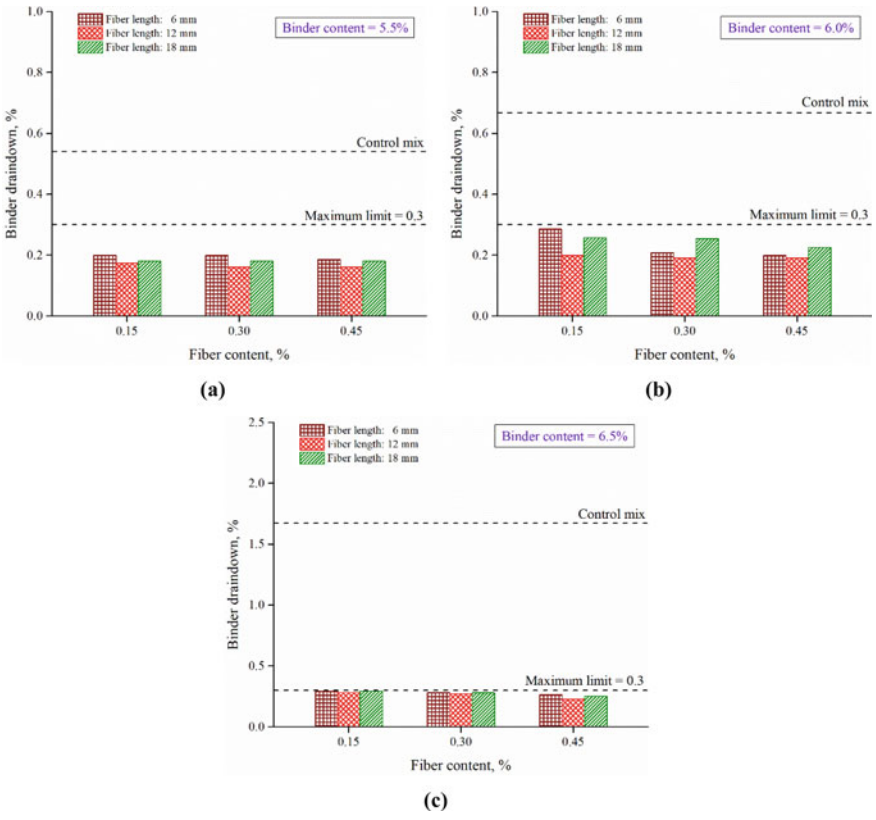

Fig. 2 Binder draindown results

2019; Ferreira da Costa et al. 2020a, b). The decrease in draindown observed on the addition of banana natural fibers shows the absorptive nature of the banana fibers which enhances the stiffness of the asphalt binder and reduces the binder draindown.

Incorporation of 12 mm fiber length showed a higher reduction in draindown, compared to the OGFC specimens fabricated and tested with 6 mm banana fiber. However, on use of fiber length of 18 mm the binder draindown increases. The banana fiber of 12 mm length yielded the best performance in terms of binder draindown (lowest draindown values) at all the three fiber contents as compared to 6 and 18 mm fiber in OGFC mixes. The addition of 12 mm banana fiber imparted a reduction of 68, 70, and 70% in binder draindown for 0.15, 0.30, and 0.45% fiber content, respectively at 5.5% binder content, when compared with the control mix (without fiber). At 6.0 and 6.5% binder contents, the observed reduction in draindown values for 12 mm banana fiber length are 70, 71 and 71% and 83, 84 and 86% than control mix for 0.15, 0.30, and 0.45% fiber content, respectively. At all the three binder contents, binder draindown increased for OGFC mixes with 18 mm banana fiber length in comparison with OGFC mixes fabricated with 12 mm banana fiber. This detrimental draindown behavior of 18 mm long banana fiber can be attributed to the "balling" effect of long fibers, which refers to the formation of fiber lumps leading to reducing blending with asphalt and has been observed by other researchers also (Abtahi et al. 2010; Kumar and Ravitheja 2019). It is evident from the observed results that fiber length plays a significant role in controlling binder draindown in OGFC mixes.

3.2 Cantabro Abrasion Loss

Due to higher air void content, OGFC mixes are prone to aging, abrasion loss, and moisture-induced damage/stripping. Cantabro abrasion loss test protocol is used to evaluate the resistance of OGFC mixes against stone loss or raveling (Watson et al. 2004; Qureshi et al. 2015; Tanzadeh et al. 2020). Raveling is defined as the disintegration of a bituminous layer initiating from the surface with dislodgement of aggregate particles due to loss of bond between the aggregate particle and the asphalt coating (Brown et al. 2009). Cantabro abrasion loss results are shown in Fig. 3a–c for OGFC mixes fabricated at three different binder contents and incorporating banana fiber at three dosages and three fiber lengths. The control OGFC mix (without fiber) failed to satisfy the Cantabro abrasion loss threshold of a maximum of 20% at all the three binder contents indicating that control OGFC mixes are vulnerable to raveling in the absence of a stabilizing additive. Incorporating banana natural fiber into the OGFC mixes exhibited improved resistance to raveling with a reduction in Cantabro abrasion loss at all the three binder contents. All the OGFC mixes with different banana fiber contents and lengths showed the Cantabro abrasion loss well within the maximum limit specified (20%). The improvement in resistance to abrasion loss varies with fiber dosages and lengths. It is observed that both banana fiber dosage and length showed optimal results at 0.3% fiber content and 12 mm fiber length, respectively, for all the three binder contents. The increase in abrasion loss with

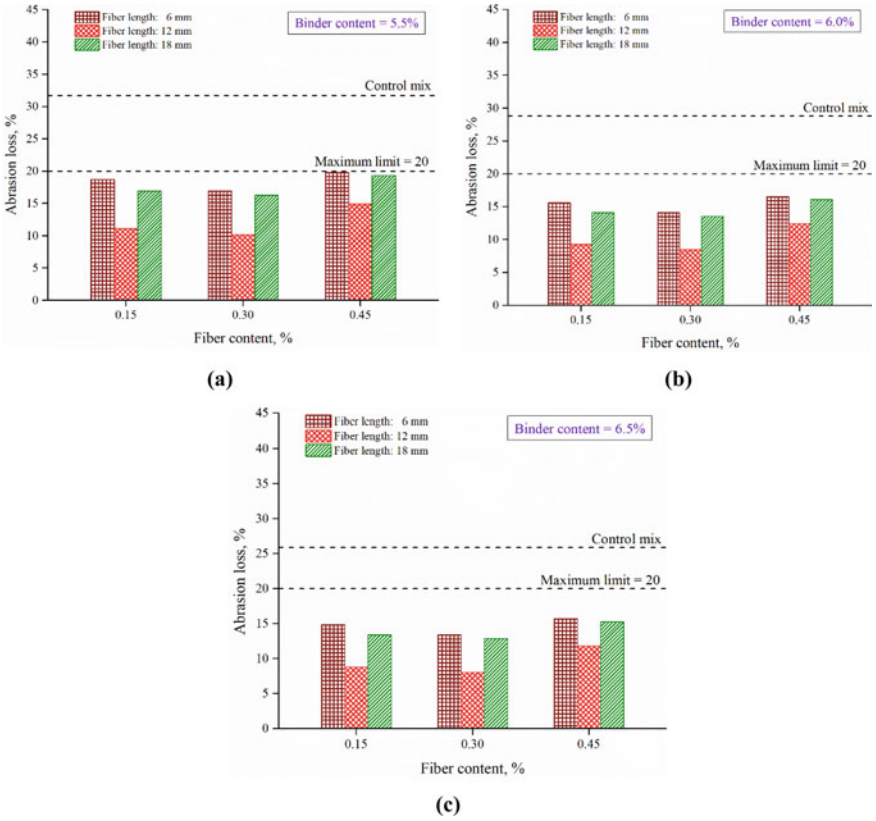

Fig. 3 Cantabro abrasion loss results

the use of longer fiber of 18 mm length can be attributed to the higher draindown observed in OGFC mixes with 18 mm fiber length which reduces the effective binder film/coating on the aggregates and thus make the resulting mix susceptible to raveling. A high fiber content of 0.45% showed a detrimental effect, which may be due to an inadequate mixing and coating at higher fiber contents. Similar results have been reported by other researchers at higher fiber contents (Wang et al. 2019; Zhang et al. 2020). The OGFC mix having banana fiber dosage (0.3%) and length (12 mm) exhibited an optimal reduction of 68, 71, and 69% in abrasion loss at 5.5, 6.0, and 6.5% binder content, respectively, when compared with control mixes (without fiber). The observed trend of results suggests that both banana fiber dosage and lengths are contributing factors in the resistance of OGFC mixes towards raveling or stone loss in terms of Cantabro abrasion loss.

Table 3 ANOVA results for binder draindown

Factor	*p*-value	S/NS
Main effects		
Binder content (BC)	<0.001	S
Fiber content (FC)	0.009	S
Fiber length (FL)	0.008	S
Two-way interactions		
BC:FC	0.535	NS
BC:FL	0.455	NS
FC:FL	0.905	NS

S significant; *NS* non-significant

3.3 Statistical Analysis

The effects of the three variables binder content (BC), fiber content (FC), and fiber length (FL) on binder draindown and abrasion loss were statistically analyzed using analysis of variance (ANOVA) at a 5% level of significance. Tables 3 and 4 shows the ANOVA results for binder draindown and abrasion loss respectively. Each of the three main effects of BC, FC, and FL are found to have a statistically significant effect on the binder draindown and abrasion loss. Further, all two-way interactions are insignificant indicating that the variation of draindown is consistent for a factor at multiple levels of another factor. The binder content, banana fiber dosage, and fiber length showed a significant role in the binder draindown and abrasion loss of OGFC mix fabricated with banana fiber as a stabilizing additive.

Table 4 ANOVA results for abrasion loss

Factor	*p*-value	S/NS
Main effects		
Binder content (BC)	<0.001	S
Fiber content (FC)	<0.001	S
Fiber length (FL)	<0.001	S
Two-way interactions		
BC:FC	0.996	NS
BC:FL	0.931	NS
FC:FL	0.718	NS

S significant; *NS* non-significant

4 Conclusions

Binder draindown and Cantabro abrasion loss characteristics of OGFC mixes with natural fiber from banana plant waste were studied at three different binder contents. OGFC mixes were prepared with a selected gradation and a polymer modified binder. Three asphalt binder dosages (5.5, 6.0, and 6.5% by mix weight), three banana fiber lengths (6 mm, 12 mm, and 18 mm), and three banana fiber dosages (0.15, 0.30, and 0.45% by dry aggregate weight) were used for the fabrication of OGFC mixes to evaluate the use of banana natural fibers as stabilizing additive in OGFC mixes. Based on the experimental data presented and discussed in this study, the following conclusions are drawn:

- The addition of banana natural fiber reduces the draindown of asphalt binder and thus shows promising results as a stabilizing additive in OGFC mixes.
- An increase in banana fiber content leads to a reduction in the asphalt binder draindown in OGFC mixes. The lowest draindown was observed at 0.45% fiber content.
- A banana fiber length of 12 mm showed the best performance with the lowest asphalt binder draindown values of OGFC mixes at all fiber and binder contents.
- OGFC mixes incorporating 12 mm long banana fiber at 0.3% fiber dosage showed best ravelling resistance in terms of the lowest Cantabro abrasion loss value.
- Fibers with longer lengths at higher dosages also act as a hindrance to blending and adhesion and thus show a detrimental effect on the draindown and raveling resistance of OGFC mixes.
- The binder content, banana fiber dosage and length were found statistically significant for binder draindown and abrasion loss in OGFC mixes.
- The use of natural fiber from banana plant waste will also have a socio-economic advantage and will provide a source for additional income to the farmers engaged in cultivation.

References

Abtahi SM, Sheikhzadeh M, Hejazi SM (2010) Fiber-reinforced asphalt-concrete—A review. Constr Build Mater 24(6):871–877

Afonso ML, Dinis-Almeida M, Fael CS (2017) Study of the porous asphalt performance with cellulosic fibres. Constr Build Mater 135:104–111

Allen Cooley Jr L, Ray Brown E, Watson DE (2000) Evaluation of open-graded friction course mixtures containing cellulose fibers. Transp Res Rec 1723(1):19–25

Alvarez AE, Martin AE, Estakhri C (2011) A review of mix design and evaluation research for permeable friction course mixtures. Constr Build Mater 25(3):1159–1166

ASTM D6390 (2017) Standard test method for determination of draindown characteristics in uncompacted asphalt mixtures

ASTM D7064/D7064M-08 (2013) Standard practice for open-graded friction course (OGFC) mix design

Beena KS, Bindu CS (2014) Influence of additives on the drain down characteristics of stone matrix asphalt mixtures
Brown ER et al (2009) Hot mix asphalt materials, mixture design and construction
Choudhary R, Chattopadhyay D, Kumar A, Julaganti A (2017) Use of industrial wastes as filler in open-graded friction courses. Balt J Road Bridge Eng 12(2):106–116
Dash SB, Panda M (2016) A study on use of natural fiber for improvement in engineering properties of dense graded bituminous mixes with coal ash. Transp Dev Econ 2(1):4
Ferreira da Costa L, Grangeiro de Barros A, Lucena LCDFL, Elísio de Figueirêdo Lopes Lucena A (2020) Asphalt mixture reinforced with banana fibres. Road Mater Pavement Des 1–13
Ferreira da Costa L et al (2020) Use of Banana fibers in SMA mixtures. J Mater Civ Eng 32(1):04019341
Gupta A, Rodriguez-Hernandez J, Castro-Fresno D (2019) Incorporation of additives and fibers in porous asphalt mixtures: a review. Materials 12(19):3156
Hassan HF, Al-Jabri KS (2005) Effect of organic fibers on open-graded friction course mixture properties. Int J Pavement Eng 6(1):67–75
Hassan HF, Al-Oraimi S, Taha R (2005) Evaluation of open-graded friction course mixtures containing cellulose fibers and styrene butadiene rubber polymer. J Mater Civ Eng 17(4):416–422
IS 15462 (2004) Polymer and rubber modified bitumen–specification. Bureau of Indian Standards
Kumar NLNK, Ravitheja A (2009) Characteristics of stone matrix asphalt by using natural fibers as additives. Mater Today: Proc 19:397–402
Kumar A, Choudhary R, Nirmal SK (2018) Salient attributes of open graded friction courses towards enhanced road safety in hilly and high rainfall regions of India. J Indian Roads Congress 79(2)
Lei X et al (2000) Effect of sisal fiber on anti-slide performance for asphalt pavement surface. Traffic Transp Stud 2010:1310–1319
Mallick RB et al (2000) Design, construction, and performance of new-generation open-graded friction courses
McDaniel RS (2015) Fiber additives in asphalt mixtures. No. Project 20-05 (Topic 45–15)
MoRTH (Ministry of Road Transport and Highways) (2013) Specifications for road and bridge works. Indian roads congress, New Delhi, India, MoRTH
Oda S, Fernandes Jr JL, Ildefonso JS (2012) Analysis of use of natural fibers and asphalt rubber binder in discontinuous asphalt mixtures. Constr Build Mater 26(1):13–20
Pathak S et al (2019) Feasibility assessment of the use of basic oxygen furnace slag in open graded asphalt courses. Int J Pavement Res Technol 12(6):664–673
Pathak S et al (2020) Evaluation of benefits of open-graded friction courses with basic oxygen furnace steel-slag aggregates for hilly and high-rainfall regions in India. J Mater Civ Eng 32(12):04020356
Pattanaik ML et al (2019) Mechanical properties of open graded friction course mixtures with different contents of electric arc furnace steel slag as an alternative aggregate from steel industries. Road Mater Pavement Des 1–25
Pattanaik ML, Choudhary R, Kumar B (2020) Prediction of frictional characteristics of bituminous mixes using group method of data handling and multigene symbolic genetic programming. Eng Comput 36(4):1875–1888
Putman BJ, Lyons KR (2015) Laboratory evaluation of long-term draindown of porous asphalt mixtures. J Mater Civ Eng 27(10):04015009
Qureshi NA, Farooq SH, Khurshid B (2015) Laboratory evaluation of durability of open-graded friction course mixtures. Int J Eng Technol 7(3):956–964
Ramalingam S, Murugasan R, Nagabhushana MN (2017) Laboratory performance evaluation of environmentally sustainable sisal fibre reinforced bituminous mixes. Constr Build Mater 148:22–9
Shanbara HK, Ruddock F, Atherton W (2018) A laboratory study of high-performance cold mix asphalt mixtures reinforced with natural and synthetic fibres. Constr Build Mater 172:166–175
Shiva Kumar G, Ravi Shankar AU, Ravi Teja BVS (2019) Laboratory evaluation of SMA mixtures made with polymer-modified bitumen and stabilizing additives. J Mater Civ Eng 31(4):04019026

Subagyo A, Chafidz A (2018) Banana pseudo-stem fiber: preparation, characteristics, and applications. Banana Nutrition-Function and Processing Kinetics. IntechOpen

Tanzadeh J, Gamasaei RS, Gilani FR (2020) Laboratory evaluation on the performance comparison between OGFC asphalt reinforcement with fibers and modified with nanosilica. J Test Eval 48(1):487–501

Wang S et al (2019) Investigating the effects of chopped basalt fiber on the performance of porous asphalt mixture. Adv Mater Sci Eng 2019

Watson DE et al (2004) Laboratory performance testing of open-graded friction course mixtures. Transp Res Rec 1891(1):40–47

Zhang J et al (2020) Evaluating four typical fibers used for OGFC mixture modification regarding drainage, raveling, rutting and fatigue resistance. Constr Build Mater 253:119131

Experimental Investigation on the Effect of Polypropylene Fibers with Respect to the Fatigue Behavior of Rigid Pavement

J. Cyril Santhosh, Satya Ranjan Samal, V. Navin Ganesh, Darla Pavani, and R. Sathyanarayan Sridhar

Abstract Fatigue is process of progressive and permanent material damage under repeated loading. It is estimated that 50–90% of structural failure is due to fatigue, thus there is need for quality fatigue design tools. The highway construction industry has made rapid strides in technology up gradation and adaption. With increase in traffic volume and an increased demand for innovative design, there is scope for new concepts in rehabilitation and repair of aging transportation infrastructure. Fiber-reinforced concrete (FRC) is concrete containing fibrous material which increases its structural integrity. By 1960s, steel, glass and synthetic fibers such as polypropylene fibers were used in concrete. The concrete for pavement should be strong and durable necessitating High Performance Concrete (HPC) mixes. The present study attempts to illustrate the effect of length of poly propylene fibers (PPF) on strength and durability characteristics of HPC mixes. Local cement, sand, coarse aggregate were used along with requisite dosage of super plasticizer. A reference mix of M35 concrete with water cement ratio 0.4 has been considered for investigation. Effects of optimum percentage (0.4%) of polypropylene fibers of various lengths on the strength properties like Compressive Strength and durability properties like fatigue characteristics have been studied. Maximum compressive strength and maximum Flexural strength has been achieved at 28 days at an optimum dosage of PPFs of (0.4%) of

J. C. Santhosh (✉) · R. S. Sridhar
Department of Civil Engineering, Coimbatore Institute of Technology, Coimbatore 641014, India
e-mail: cyrilsanthosh.j@cit.edu.in

R. S. Sridhar
e-mail: sathyanarayan@cit.edu.in

S. R. Samal
School of Civil Engineering, KIIT Deemed to be University, Bhubaneswar, India
e-mail: satya.samalfce@kiit.ac.in

V. N. Ganesh
Department of Civil Engineering, PSG Institute of Technology and Applied Research, Coimbatore 641062, India
e-mail: navinganesh@psgitech.ac.in

D. Pavani
Department of Civil Engineering, National Institute of Technology, Trichy 620015, India

B. B. Das et al. (eds.), *Recent Developments in Sustainable Infrastructure (ICRDSI-2020)—GEO-TRA-ENV-WRM*, Lecture Notes in Civil Engineering 207,
https://doi.org/10.1007/978-981-16-7509-6_31

length 12 and 20 mm. This project work aims at studying the fatigue behavior of simply supported beams of known size which are made with plain cement concrete and cement concrete with fibers under flexural loading. Static flexural test was also conducted to determine the flexural strength prior to fatigue testing. The studies briefly present the comparison of fatigue behavior of Plain Cement Concrete and Concrete with Fibers of known lengths with different stress ratios and the results are presented as Fatigue Stress and S–N relationship.

Keywords Fatigue · Fiber- reinforced concrete · Polypropylene fibres · Fatigue stress · Plasticizer

1 Experimental Investigations

The objective of the present investigation is to study the strength properties, durability properties and fatigue characteristics of conventional and PPF concrete mixes. The dosage of super plasticizer used is according to the workability requirement. The physical properties of locally available materials were determined in the laboratory and same materials were used for both controlled and fiber reinforced concrete. Sieve test were done on coarse and fine aggregates and the sample conforming to IS standards was selected. Boasee fibers were collected from MJ suppliers for the experiment.

1.1 Cement

"Coromandal" brand Ordinary Portland Cement of 43 grade was used in this present investigation. The cement was tested for various physical properties according to **IS: 4301-1988**. It is observed that all the values obtained are within the IS specified limits.

1.2 Fine and Graded Aggregates

As mentioned earlier locally available river sand has been used as fine aggregate in the present investigation. Sieve analysis and specific gravity tests were conducted. The fineness modulus obtained was 3.4 and specific gravity was obtained as 2.59. As per **IS 383-1970** the fine aggregate confirms to **zone III**. Coarse aggregate is the strongest and least porous cement component of concrete. The coarse aggregates and fine aggregates filling the voids in between coarse aggregates serves good. For this purpose proper grading should be done. The main concept of gradation is different

Table 1 Mixed aggregate gradations

IS sieve designation (mm)	Percentage passing of 20 mm	Percentage passing of 12.5 mm	Blending 50% 20 mm + 50% 12.5 mm	Limits as per table 1000-1 of MORT&H
40	100	100	100	100
20	91.2	100	95.6	95–100
10	7	65.9	36.45	25–55
4.75	1.55	2.6	2.075	0–10

size of aggregates are used in specific proportions to make dense and good inter locking between the aggregate.

1.3 Mixed Aggregate Gradation

Usage of two or more different materials as aggregate requires separate gradation called mixed gradation, to make it act as a single material. It may however be found more economical to increase the cement content above the minimum required. Mixed aggregate gradation ranges are coming to the specified limits. In mixed gradation the aggregate sizes of 12.5 and 20 mm are added in different proportions as shown in Table 1.

1.4 Polypropylene Fiber

Boasee fiber was used which is a 100% virgin polypropylene fiber supplied by the MJ supplier. In this study two lengths (12 mm and 20 mm with aspect ratio 300 and 500 respectively) of boasee fiber used (Figs. 1 and 2) (Hernandez-Olivares et al. 2006).

Fig. 1 Polypropylene fiber of length 12 and 20 mm length

Fig. 2 Specimens of PC and PPFRC (12 and 20 mm)

1.5 Super Plasticizer

The super plasticizer used in the present study is Conplast SP 430 supplied by M/S FOSROC India Private Ltd. It is a high performance admixture based on selected sulphonated naphthalene polymers. It disperses the fine particles in the concrete mix, enabling the water content of the concrete to perform more effectively. As per supplier for high strength, water reduced concrete the normal dosage range is from 0.6–1.5 L/100 kg of cementitious material. In this study the optimum dosage of Conplast SP 432 was determined by Slump Cone test. Optimum dosage of super plasticizer for 100 mm slump obtained as 1.2 L/100 kg of cementitious material. Mix design details are provided in the Table 2 (Fauzi et al. 2001).

2 Methodology

- The grade of concrete used is M35;
- Super plasticizer is added to obtain workability

Table 2 Mix design-M35

Cement: Fine aggregate: Coarse aggregate	1:1.94:3.43
Water/cement ratio	0.4
Cement (kg/m^3)	356
Fine aggregate (kg/m^3)	691
Coarse aggregate of 20 mm size (kg/m^3)	610
Coarse aggregate of 12.5 mm size (kg/m^3)	610
Water (liters/m^3)	197
Optimum dosage of Super plasticizer for 100 mm slump (%)	1.2
Optimum Percentage of fiber (12 and 20 mm) (%)	0.4

Table 3 Types of tests and specimens and sizes

S. No.	Type of test	Properties studied	Specimen size
1	Concrete strength properties	a. Compressive strength b. Flexure strength For both (7 and 28 days)	150 mm cubes, 100 × 100 × 500 mm beams
2	Durability characteristics	c. Fatigue (28 days) d. Sulphate and acid attack, Water absorption, Abrasion test e. Modulus of elasticity (E)	100 × 100 × 500 mm beams 100 mm cubes Cylinders of 150 mm diameter and 300 mm height

- Concrete mixes were prepared with optimum percentage i.e. 0.4% of polypropylene fiber including super plasticizer are mixed and cubes and beams are casted.
- The 7 days and 28 days strength properties and fatigue behavior and 28, 60- and 90-days durability properties such as water absorption, abrasion, modulus of elasticity, sulphate attack, chloride attack of PPF concrete were studied
- The results obtained are compared with that of conventional concrete.

3 Specimen Casting and Curing

The cube specimens of size 100 and 150 mm, beam specimens of size 100 mm × 100 mm × 500 mm and cylinders of size 150 mm diameter and 300 mm height for M35 grade concrete were casted with mix proportion of 1:1.94:3.43 and water cement ratio of 0.4. The Boasee fiber of lengths 12 and 20 mm were used. A total of 18 cubes and 36 beams were casted. Coarse aggregate and 75% of fine aggregate was added first and mixed thoroughly in the dry condition. After mixing thoroughly, then cement was added. These materials were dry mixed for two minutes. Then 50% of required quantity of water was added followed by remaining 25% of fine aggregate. Super plasticizer was mixed for two minutes to get a homogenous mix.

The mixed concrete was immediately transferred into a metallic tray and then to the moulds. The specimens were compacted using the needle vibrator initially and then vibrated with a table vibrator. After one hour, the specimens were marked. The specimens was demolded after 24 h and then placed for 7 and 28 days (Table 3).

4 Results and Discussions

In the present investigation an attempt has been made to study, the behaviour of concrete mixed with various lengths of PP fiber. Experiments have been conducted to obtain properties like strength, flexural strength, static test and dynamic testing.

Table 4 Comparison of compressive strength in N/mm^2

Sample type	7-days	% of increment compared to conventional concrete	28-days	% of increment compared to conventional concrete
Plain concrete	29.46	–	42.6	–
Concrete with 12 mm fiber	34.9	19	48.73	17
Concrete with 20 mm fiber	36.84	25	51.39	23

4.1 Cube Compressive Strength

Cubes were tested for each type in a digital compression testing machine for determining compressive strength at 7 and 28 days. The cube compressive strength results for different mixes with their comparisons are tabulated in Table 4 Addition of PP fiber to the concrete mix has resulted in higher strength than that of control concrete mix. It was observed that compressive strength of fiber reinforced concrete mixes is increasing by increasing the length of fiber which is shown in Table 4.

4.2 Flexural Strength

The flexural strength of Poly Propylene Fiber Reinforced Concrete (PPFRC) beam was obtained by conducting flexural test on specimens of size 100 × 100 × 500 mm by two-point load method as shown in Table 5. It was observed that flexural strength of fiber reinforced concrete mixes is higher than the control mix. The improvement in flexural strength has been observed for the concrete containing greater length of PP fiber. The percentage of increment in flexural strength for each concrete type is shown in the Table 5 (Manolis et al. 1997).

Table 5 Comparison of flexural strength in N/mm^2

Sample type	7-days	% of increment	28-days	% of increment
Plain concrete	3.46	–	6.73	–
Concrete with 12 mm fiber	4.6	33	9.07	35
Concrete with 20 mm fiber	4.93	42	9.67	44

Table 6 Static test results

S. No.	Plain concrete	Concrete with 12 mm PP fiber	Concrete with 20 mm PP fiber
1	1500	1750	1850
2	1550	1900	1800
3	1750	1800	1950
Average	1600	1817	1867

Table 7 Comparison of static test results

Sample type	Average failure static load	% of increment
Plain concrete	1600	–
Concrete with 12 mm fiber	1817	13
Concrete with 20 mm fiber	1867	17

4.3 Static Flexural Test

The static flexure test was carried out using two-point loading on randomly selected specimens from the set of specimens cast for flexural fatigue test (Heeralal et al. 2009). This test was carried out on specimens selected from each batch of specimens to estimate the average modulus of rupture for the concrete. The load levels to be applied for the flexural fatigue test of the specimens were determined from these results. The support points were marked on the specimens at 50 mm from the ends and two more lines were marked at 133.3 m from support points to mark the loading points for two points loading. The online display of the load application graph also available in the Fatigue testing equipment**.** The failure load was recorded for each set of specimens and average was taken. The loading was applied at a constant rate till the failure of the specimen. The maximum load applied to the specimen at failure was recorded. Tables 6 and 7 shows the tabulated values of Static failure load for conventional concrete and Fiber Reinforced concrete.

4.4 Fatigue Test

The computer system is interfaced with an add on card facility with the accelerated fatigue testing apparatus for controlling the wave form of load application, magnitude of load applied, frequency and to count the number of load repetitions till the failure of specimen. The input details in to the software like dimensions of specimens, load to be applied repeatedly based on stress ratio, frequency of application of load and waveform of load application were entered in the computer. Then the hydraulic system of the accelerated fatigue testing apparatus was switched on simultaneously with the computer system. The waveform applied was half sine form and the load

Table 8 Fatigue test results

Type of concrete	Number of cycles to failure N		
	Stress ratio		
	0.65	0.75	0.85
Plain concrete	11,475	10,205	515
Concrete with 12 mm fiber	15,820	11,135	590
Concrete with 20 mm fiber	16,395	12,130	675

applied was decided based on the stress ratio to be applied. The stress ratio applied was 0.65, 0.75 and 0.85. The load applied, frequency of loading was set in the computer system. The accelerated fatigue testing apparatus hydraulic system was started and continued till the failure of specimen. The number of load application to the failure of specimen was recorded (Hemalatha et al. 2011).

Input data

File Name: PPF 12mm
Specimen: Rectangular Beam
Amplitude: 1545 (0.85 of Static Strength)
Wave form: Half Sine Wave
Frequency: 2 Hz
Rest period: 0

4.4.1 Failure of the Specimen Under Fatigue Loading

During flexural fatigue test the failure of the specimen was sudden and the testing apparatus was switched off. Iron platform was provided below the specimen to avoid the fatling of specimen after failure and also cut-off-switch facility for accelerated testing apparatus to switch off automatically after failure (Naik and Singh 1994). The details of number of cycles to failure for the specimens are tabulated (Table 8). The test set up and failure of specimens is shown in Fig. 3 (Ameen and Szymanski 2006).

4.4.2 S–N Curve

Most of the studies on the fatigue strength of concrete have so for been, interrelate the applied fatigue stress and the fatigue life of concrete. This relationship is shown by *S–N Curve or Wohler curves.*

The analysis of fatigue Test Results arriving the S–N curves is done by Regression analysis. For different stress ratios the behaviour of failure is varying as shown in Figs. 4, 5 and 6 for conventional concrete and concrete with fiber of length 12 and 20 mm.

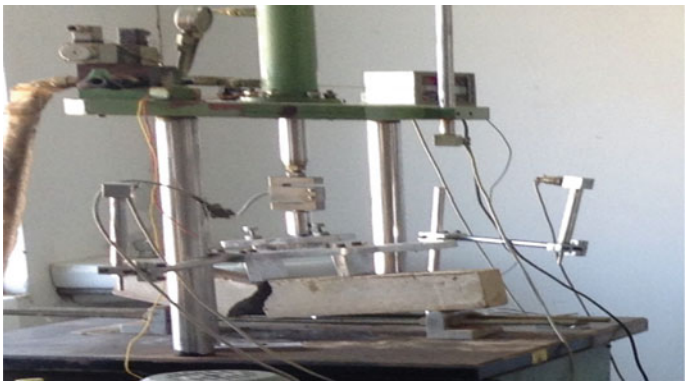

Fig. 3 Failure of the specimen under fatigue test

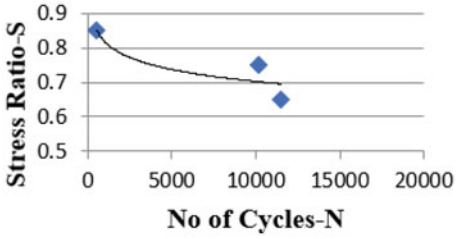

Fig. 4 S–N relationship for conventional concrete specimens

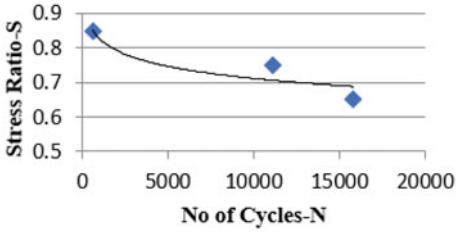

Fig. 5 S–N relationship for concrete with 12 mm PP fiber

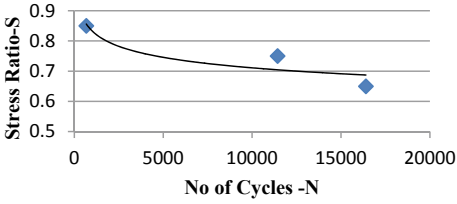

Fig. 6 S–N relationship for concrete with 20 mm PP fiber

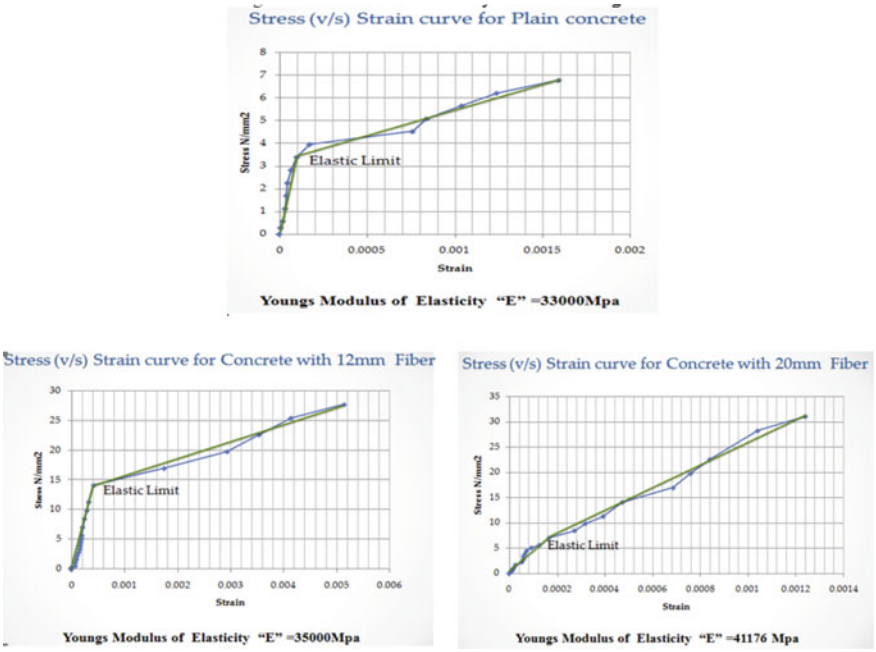

Fig. 7 Young's Modulus of elasticity for three mixes of concrete

4.5 Durability Properties

Water absorption test was conducted for 28, 60 and 90 days change in weight has been measured. Abrasion test has been conducted for concrete mixes and the results shows more resistance to abrasion, and 20 mm length of FRC shows 34% more resistance to abrasion then 12 mm length of FRC.

4.5.1 Modulus of Elasticity (E)

To find the modulus of elasticity graph has been drawn between stress and strain which are obtained from deformations and the applied load. Elastic limit was found out and slope of elastic zone gives the modulus of elasticity as shown in Fig. 7.

PPFRC is more elastic than PC and by increasing the length of fiber elastic nature of concrete is increasing.

4.5.2 Sulphate Attack

Resistance to sulphate attack has been found out by measuring the loss of weight and compressive strength by immersing the samples in $MgSO_4$ solution. Loss of weight

Table 9 Resistance to sulphate attack of FRC in comparison with PC

Sample type	% of increment for 28 days	% of increment for 60 days	% of increment for 90 days
Plain concrete	–	–	–
12 mm fiber concrete	11	12	13
20 mm fiber concrete	16	17	16

Table 10 Resistance to acid attack of FRC in comparison with PC

Sample type	% of increment for 28 days	% of increment for 60 days	% of increment for 90 days
Plain concrete	–	–	–
12 mm fiber concrete	26	25	23
20 mm fiber concrete	24	24	20

due to sulphate attack is more for PC than FRC, 20 mm FRC shows less loss of weight (4%) than 12 mm FRC (Table 9).

Loss of compressive strength (for 90 days) due to sulphate attack for PC is 36%, 12 mm length of FRC is 12% and 20 mm length of FRC is 8%, because more length of fiber there is more resistance for penetration of sulphate solution in to the concrete.

4.5.3 Acid Attack

Resistance to acid attack has been found out by measuring the loss of weight and compressive strength by immersing the samples in H_2SO_4 solution. Loss of weight due to acid attack is more for PC than FRC, 20 mm FRC shows less loss of weight (i.e. 2%) than 12 mm FRC (Table 10).

Loss of compressive strength (for 90 days) due to acid attack for PC is 56%, 12 mm length of FRC is 38% and 20 mm length of FRC is 31%, because more length of fiber there is more resistance for penetration of acid in to the concrete.

5 Conclusions

Within the scope of results available based on the data and discussions presented in the preceding chapters on the limited number of tests conducted. Overall performance of PPFRC in case of strength properties and durability properties was good. From these investigations, the following conclusions are drawn.

- It was observed that addition of PP fiber leads to increase in the strength (Bagherzadeh et al. 2012).

- As compared to conventional concrete there was 17 and 23% of compressive strength and 35 and 44% of flexural strength gained for concrete containing 12 and 20 mm of fiber.
- By increasing the length of fiber (from 12 to 20 mm) compressive strength and flexural strength are increased by 6% and 9% respectively.
- Form Static test it was observed that the ultimate failure load is more for concrete containing 12 and 20 mm lengths of PP fiber and the failure load was 13 and 17% more as compared to conventional concrete.
- Form Fatigue test it was observed that the repetitions are more for PPFRC as compared to PC. By increasing the length of fiber (from 12 to 20 mm) the number of cycles to failure of specimen was more.
- PPFRC shows the better results in durability tests than PC. As compared to 12 mm length of PPFRC, 20 mm length PPFRC is more elastic in nature, more resistant to abrasion (34%) and water absorption is more (4%).
- PPFRC is more resistant to the deterioration than PC. Greater length of fiber shows more resistance to acid attack and sulphate attack.
- For 12 mm length FRC the Loss of weight is more by 2 and 4% due to acid and sulphate attack and loss of compressive strength is more by 7 and 4% by acid attack and sulphate attack than 20 mm length FRC.
- 20 mm length FRC shows the better strength and durability properties than 12 mm length FRC.

5.1 Scope for Future Work

This present study and investigation give the comparison of strength and durability parameters such as Compressive, Flexural, Static, Fatigue tests and durability studies like water absorption, abrasion resistance of concrete, deterioration studies and modulus of elasticity of both conventional concrete and PPF concrete of different length of fiber. There is a further scope to study the effect of temperature on both conventional concrete and Poly Propylene Fiber Reinforced Concrete for rigid pavement. There is possibility to continue the same study by using other fiber and propose the optimum length of fiber.

References

Ameen P, Szymanski M (2006) Fatigue in plain concrete, concrete structures. Chalmers University of Technology Goteborg, Sweden

Bagherzadeh R, Pakravan HR, Sadeghi AH, Latifi M, Merati AA (2012) An investigation on adding polypropylene fiber to reinforce lightweight cement composites. ATMT Institute Research Institute, Amirkabir University of Technology, Tehran, Iran

Fauzi M et al (2001) Influence of admixture and quarry dust on the physical properties of freshly mixed high performance concrete. In: Proceedings of the international conference on structural

engineering, mechanics and computation 2–4 April 2001, vol 2. Cape Town, South Africa, pp 1381–1390

Heeralal M, Rathish P, Rao YV (2009) Flexural fatigue characteristics of steel fiber reinforced recycled aggregate concrete, NIT Warangal, Andhra Pradesh, India. Facta Universitatis, Arch Civil Eng 7(1):19–33

Hemalatha T, Chandra kishen J M, Ramaswamy A (2011) Influence of mineral admixtures on fatigue behaviour of self compacting concrete—scanning electron microscopy and microindentation study. In: VIII International conference on fracture mechanics of concrete and concrete structures. IISC, Bangalore

Hernandez-Olivares et al (2006) Fatigue behaviour of recycled tyre rubber-filled concrete and its implications in the design of rigid pavements, Madrid, Spain. Constr Build Mater 21(2007):1918–1927

Manolis GD, Gareis PJ, Tsonos AD, Neal JA (1997) Dynamic properties of polypropylene fiber reinforced concrete slabs. Cement Concr Compos 19(1997):341–3490

Naik TR, Singh SS (1994) Fatigue property of concrete with and without mineral admixtures. Published in concrete technology—past, present, and future, held in San Francisco, CA, ACI Spring Convention, March 1994

Operational and Constructional Challenges of a Highway Project—A Live Case Study on National Highway No. 67 from km 424/650 to km 487/693 in Anantapur District of Andhra Pradesh

R. Sathish Kumar

Abstract The basic idea involved in the project is to identify the Constructional and Operational challenges faced in the execution of the highway project and to provide the feasible engineering and managerial solutions to the pertaining problems. Constructional challenges and Operational challenges go hand in hand for every construction project. Identification of the challenges before the initiation of the project is practically not possible. It may happen that the list of challenges before the starting of the project may be identified but there is a chance that a new challenge may be faced while execution and that is why most of the projects delay. When it comes to infrastructure projects like highways this problem is predominant. This is the major reason to categorize the challenges that were faced in highway project into challenges before construction, challenges during execution and challenges after construction. Hence this research project identifies some of the constructional and operational challenges in an infrastructure project with the help of a live case study on a highway project "Rehabilitation and Up-gradation of NH-67 from km 424/650 to km 487/693 (Gooty–Tadipatri section)" which is located in Anantapur district of Andhra Pradesh. Some of the constructional and operational challenges in the execution of the project were identified and proper solutions were specified for the successful completion of the project.

Keywords Constructional and operational challenges · Land acquisition · Material and machinery management · Utility shifts · Rehabilitation and up-gradation

1 Introduction

Transportation contributes to the economic, industrial, social and cultural development of any country. Transportation is vital for economic development of any region since every commodity produced whether it is food, clothing, industrial products or medicines needs transport at the production and distribution stages. The inadequate

R. S. Kumar (✉)
National Institute of Construction Management and Research, Hyderabad, India
e-mail: sathishkumar@nicmar.ac.in

B. B. Das et al. (eds.), *Recent Developments in Sustainable Infrastructure (ICRDSI-2020)—GEO-TRA-ENV-WRM*, Lecture Notes in Civil Engineering 207,
https://doi.org/10.1007/978-981-16-7509-6_32

transportation facilities retard the process of socio-economic development of the country. The adequacy of transportation system of a country indicates its economic and social development. In developing countries like India, development cannot be brought through developing urban centers alone, but also the rural areas with the help of a good transportation system. Among the modes of transport, transportation by road is the only mode which gives maximum service to one and all. The other three modes of transportation i.e., Railways, Waterways, Airways, have to depend on roads for the service to and fro from their respective terminals, airports, harbours or stations. The road network is needed not only to serve as feeder systems for other modes of transportation and to supplement them, but also to provide independent facility for road travel by a well-planned network of roads throughout the country.

2 Literature Review

Construction materials management on project sites is required to fill a void created by the absence of proper materials management on construction sites (Patel and Vyas 2011). Research has shown that construction materials and equipment may constitute more than 70% of the total cost for a typical construction project. Therefore the proper management of this single largest component can improve the productivity and cost efficiency of a project and help ensure its timely completion. One of the major problems in delaying construction projects is poor materials and equipment management.

Contracting companies stated that using computer in construction materials management as the main obstacle as there is a shortage of user-friendly computer program and lack of awareness about the importance of computer program (Sawalhi and Kass 2012). Local practices used in construction materials management were explored and construction materials management system was developed to facilitate the management of construction materials mainly in the building construction. A survey questionnaire supported by interviews was used to explore the local practices used in construction materials management.

Organizations that deal with road construction should have appropriate policies on establishment of quantities of materials required (Seboru et al. 2016). The extent to which acquisition of materials influences performance of road construction projects in Kenya were studied. This study was anchored on the theory of controlling, theory of construction management, and stakeholder theory. The model used was pragmatism and the research approach used was mixed methods.

Optimization has to be done in respect to machine output and resource consumption i.e., there is a strong relationship between them (Edwards and Holt 2009). Construction Plant and equipment Management (CPeM) were studied in detail and the principal themes involved in it were identified. CPeM is found well established within the broader subject of construction management. Contractors were in tune with the ideals of the Latham review and characteristics pertaining to the HOLT (Highlight Optimum Legitimate Tender) selection technique (Holt et al. 1996). They presented

a paper involving the findings of a nationwide survey of UK construction contractors assessing their opinion of the Latham procurement recommendations, along with their opinion of the author's proposals for alternative selection procedure.

Competitive tendering may be still efficient and effective in the twenty-first century (Kang et al. 2015). Comparative Study between Clients and Contractors on Competitive Tendering in the Sudan Construction Industry were examined. Construction Industry plays a key role in the process of economic transformation and growth (Patil et al. 2016). The methodology carried out in tendering procedure from pre-bid conference to submission and opening of tender were examined in detail.

3 Case Study

3.1 Introduction

- The research was based on a live case study on a highway project titled "Rehabilitation and Up-gradation of NH-67 from km 424/650 to km 487/693 (Gooty–Tadipatri) to two lane with paved shoulders" located at Vemulapadu in Anantapur district of Andhra Pradesh.
- Package cost was estimated to be Rs. 378.24 Crores.
- Highway passes through 3 main villages namely Rayalacheruvu, Chukkaluru and Vemulapadu.

3.2 Salient Features

- The package was being executed by "M/s HES-RITHWIK Joint Venture" as main Contractor through EPC mode under "NHAI" following the specifications of "Ministry of Road Transport and Highways".
- Construction period of the package is 24 months from appointed date 19/01/2018 to Scheduled date of completion 18/01/2020.
- Designs and drawings of Highways and structures like Bridges; Culverts were handled by a consultant M/s. Aarvee Associates Architects Engineers & Consultants Pvt. Ltd. Hyderabad.
- This package has a total stretch of 61.433 km
- There were 3 major intersections and 16 minor junctions in this package.
- There were 2 Major bridges and 21 minor bridges in which 1 will be newly constructed, 3 will be reconstructed and 17 will be widened. One rail over bridge (ROB) is to be widened.
- There were 38 culverts in which 30 of them will be reconstructed and 8 will be widened.

- A total of 21 Bus bays and Bus shelters were present in this package which will be constructed on both the sides.
- In this 61.433 km stretch of main carriageway, there is one toll plaza and one rest area.

3.3 Observations

3.3.1 General Observations

- The total stretch of the Highway project to be upgraded was 61.433 km.
- The total stretch of Flexible pavement was 42.963 km and total stretch of Rigid pavement was 17.79 km.
- Type of contract followed in the package was EPC contract.
- Civil cost as per agreement was Rs. 288.41 crores and revised cost is Rs. 378.24 crores.
- Construction cost per km was Rs. 6.00 crore.
- Change of scope has been identified in a certain length where the original scope was that only top layer of the pavement has to be reconstructed but the existing pavement does not possess the ability to take loads which may result in early damage of the pavement once it becomes operational. So, in order to improve the strength, all the layers of the pavement have to be reconstructed.
- In the total stretch of 61.433 km, black cotton soil was found in the range from 1 to 23 km and 44 to 61.433 km, the same is unfit for laying of pavement. The black cotton soil has to be removed and filled with the other soil which is fit for construction. The remaining stretch i.e. from 23 to 44 km, the soil found was red soil which is fit for laying of pavement.
- There is no delay in the project i.e., all the targeted milestones as per the tender documents has been achieved within the specified time.
- Total completion of this highway package is around 95.6% as on date.

3.4 Status of Laying of Pavement

3.4.1 Flexible Pavement

- Sections of Flexible pavement laying was as follows:

  (a) Natural Sub-grade-500 mm thickness
  (b) Granular Sub Base (GSB)—2 layers of 200 mm thickness each
  (c) Wet Mix Macadam (WMM) of 250 mm thickness
  (d) Dense Bituminous Mix (DBM) of 95 mm thickness
  (e) Bituminous Concrete (BC) of 40 mm thickness
  (f) Prime coat.

Fig. 1 Flexible pavement

- The proposed road has a formation width of 14 m with carriage way of 10 and 2 m unpaved shoulders on either side (Figs. 1 and 2).

3.4.2 Rigid Pavement

- Laying of 17.74 km completed out of 17.79 km stretch.
- Sections adopted in Rigid pavement laying (from the bottom) was as follows:

  (a) Natural Sub-grade of 500 mm thickness
  (b) Granular Sub Base (GSB) of 150 mm thickness
  (c) Dry Lean Concrete (DLC) of 150 mm thickness
  (d) Pavement Quality Concrete (PQC) of 300 mm thickness.

3.5 Land Acquisition and Utility Shifts

- Shifting of Utilities like Pipe line works of 14.7 km was completed out of 15.5 and 18 km of Electrical line shifting is completed out of 22 km.
- Responsibility of land acquisition was taken by the government and not by the contractor.
- 17.88 Acres of Land has been acquired by the government for the project purpose (Table 1).

Fig. 2 Rigid pavement

Table 1 Land acquisition details

S. No.	Location	Land acquired (acres)	Purpose
1	Englibanda	0.30	For bus lay by
2	Jakkalacheruvu	0.50	For carriage—way
3	High embankment	4.00	For major bridge
4	Truck lay by	2.08	For truck lay by
5	Toll plaza	8.00	For toll plaza
6	Chukkalur	3.00	For carriage way
Total		17.88	

- Some temples were found at a distance of 20 km from project site office in this stretch and there was no problem for construction or widening, but compound walls of church near Chukkaluru was removed as it was constructed in the government land.
- As compensation for land acquisition, government was planning to construct a township for the people near Chukkaluru.

Fig. 3 Minor bridge construction

Fig. 4 Culvert

3.6 Construction Status of Bridges

- There were 2 Major bridges and 21 minor bridges.
- Out of 21 Minor Bridges, 4 Minor Bridges has to be constructed and 17 have to be widened (Shown in Figs. 3 and 4).
- Construction and Widening of 20 Minor Bridges has been completed.

3.7 Construction Status of Culverts

Table 2 shows the construction status of all the types of Culverts which includes Box, Pipe and Slab type of Culverts.

Table 2 Construction status of culverts

Particulars	Box culverts	Pipe culverts	Slab culverts
Total numbers as per the scope	26	38	11
New/Reconstruction	24	26	0
Widening	0	6	9
Total numbers	24	32	9
Status	Completed	Completed	Completed

3.8 Toll Plaza

- Construction of Toll Plaza is in progress.
- Rigid pavement of length nearly 2.145 km at Toll Plaza is totally completed.
- Toll Plaza (shown in Figs. 5 and 6) constitutes for 7 cabins out of which 3 cabins were constructed per side traffic and one cabin is for emergency vehicles.
- The entrance for cabins was through the service room located at the edge of the toll plaza (shown in figure).
- There were a lot of culverts that were to be constructed as per the contract document which were slab and pipe culverts as shown in Figs. 7 and 8.
- There is one Truck lay bay in the stretch and its construction is in progress.

Fig. 5 Cabins in toll plaza

Fig. 6 Service room

Fig. 7 Slab culvert

Fig. 8 Pipe culvert

- Three longitudinal joints were provided for 10 m width of rigid pavement.
- Admixtures like PC (Poly Carboxylate) base, Naphtha base were used in construction.
- Black cotton soil of 20 km was found in the stretch and the soil was replaced and stabilized.
- Lab is located at the project site and it contains all the equipment that is required to test soil, concrete and bitumen.
- Side Drains were to be constructed as per the contract document alongside the proposed road.

4 Questionnaire Survey

The data collected for questionnaire was of primary data type i.e., the data collected freshly from the sources that were available. In statistical terms the population that is selected for the research work is the local people living along the stretch of the project and the technical personnel involved in the execution of the project.

As there were two completely different set of people to take the survey, two separate questionnaires were prepared to ease out the data collection namely general questionnaire and technical questionnaire. General questionnaire was based on the problems that were faced by the local people. A small sample of people were made

part of the survey to analyse and understand the behaviour and problems faced by them during the execution of the project. Technical questionnaire were focused to understand the technical problems.

4.1 Formulation of Questionnaire

When designing the questionnaire, attention was given to make the questions easy to comprehend and to keep it less complicated and precise via proper selection of wording to formulate each question. Another important criteria was to keep it short so that the respondents did not have to spend too much time with the questionnaire thereby ensuring a high response rate within a limited period of time. Technical questionnaire were circulated through Google forms to the technical personnel working with the case study considered. The questions dealt with the following areas:

- General questionnaires related to the problems that the local people might face because of the execution of the project.
- Technical questionnaire related to the challenges that the contractor faced from local people and challenges during the laying of pavement.

General questionnaire was modelled with dichotomous questions i.e., questions having answers as yes/no. Technical questionnaire was modelled with single answer choice. The questions in the technical questionnaire were modelled using Likert scale having the following options: (a) Strongly agree, (b) agree (c) disagree (d) strongly disagree.

4.2 Collection of Data

Collection of data was the important step for the research work to be productive which is why personal interview was chosen as the method of the collection for data. Online Mail survey was also used to collect the data for Technical questionnaire. General questionnaire survey was conducted with the public in the villages present along the National highway mainly Rayalacheruvu, Chukkaluru, Vemulapadu and some other villages that were present behind them like Krishnapadu, Kothapalli, Kothapeta, Tondapadu and Jakkalacheruvu.

4.3 Selection of Software for Analysis

Data analysis plays a vital role in organizations today. It enables effective decision-making by addressing fundamental business questions based on the understanding of the available data. While there were tons of open source and enterprise tools

for conducting data analysis, SPSS has emerged as a popular tool among statistical analysts and researchers. SPSS stands for Statistical package for the Social Science.

5 Discussions from the Data Analysis

5.1 Land Acquisition Problems

The number of people facing acquisition problems were less. The method followed by the government was that, by taking the lands without making any damage to the temples, churches and compensating people with the equal value of the money which helped the contractor in completing the project in a given period of time without going for an extension.

5.2 Traffic Problems

The number of people who were facing traffic problems were less. Contractor provided half way of the pavement for public use and work was carried out in the other half thus making temporary routes for the public use without causing disturbance to the public. This helped the contractors in moving their machineries and helped in the progress of work without any obstructions.

5.3 Compensation Given for Land Acquisition

The number of people who were not satisfied with the compensation were less. The Government compensated the people with equal value of the money and then given lands in the other areas and laying roads inside the villages with the scrap material obtained from the rehabilitation which helped the contractors in completing the project in a given period of time without going for an extension.

5.4 Disturbance to the Local People

The number of people who faced disturbance because of the project works were less. Contractor provided temporary routes for the traffic flow and completed maximum works in the nights than the day and informing ahead about the work helped the contractors in completing the project in a given period of time without causing disturbance to the local people.

5.5 Impact on Natural Resources

The number of people saying that there is no impact on natural resources were more. Reason for less impact on natural resources was that the region where project is going on is one of the driest parts of Rayalaseema district and it comes under semi-arid area recording very less rainfall. There were no plants and greenery near the project area. The project area is full of mountains and barren lands. Contractors did not made any disturbance to the water pipelines during utility shifts helped them in the smooth flow of Project work.

5.6 Impact on Animals

The number of people saying that there is no impact on animals were more. The method followed by the Contractor was by informing people ahead before the start of the work, asking them not to allow animals in the working area and providing barricades on the path of the working is a proper way which helped the contractors in completing the project without causing any impact on animals that helped them in the smooth flow of work.

5.7 Impact on Traditional Livelihood

The number of people saying that there is no impact on traditional livelihood is more. Contractor didn't disturb the daily routine of the people like going to the temples, churches etc. that helped the contractors in completing the project without causing any impact on traditional livelihood.

5.8 Impact on Public Transport (APSRTC)

The number of people thinking that there is an impact on public transport were less. Contractor provided half way of the pavement for public use and carried out the work in the other half making temporary routes for the public use without causing disturbance to the public over there.

5.9 Rural Urban Conflict

The number of people thinking that there is an urban rural conflict were less. Lands that have been acquired for this project were in rural area and were far from the city. There is no urban area in between the stretch of the highway so it is also one of the reasons for the completion of the project in planned time because the traffic were less and works were carried out without interaction. Because of non-existence of urban rural conflict the lands were sold to the government at lesser cost which will be high if an urban area existed in the stretch of highway construction.

5.10 Employment Generation in the Local Place

There is employment generation because of this project. Contractors took the local people for labor work and provide food and shelter to them. They provided transportation facilities from work to stay. This helped contractor in getting labor for lesser money and was able to finish the work early with local language and making them to finish their work quickly.

5.11 Increase in Pollution

As it was very difficult to control the pollution in highway construction, the contractor has taken some precautions like storing of materials in a covered space, slow movement of machineries, avoiding the work on morning times in villages, cleaning of roads at public places in villages, avoiding movement of dumpers inside the villages.

5.12 Project Awareness

The people were aware of the project before the starting of the work. This awareness made people to think about the changes that may be occurring because of the project and this helped government and contractor in land acquisition, informing people before the work.

5.13 Compensation to the Land Acquisition Was Done by Government not by Contractor

The compensation was done by government and not by contractor. This involvement of government in compensation made people to give their land without any hesitation and helped contractor in carrying out the work in fast progress.

5.14 Water and Electricity Problems

The water and electricity problems did not rose because of this project. Contractor managed to make utility shifts in a proper way without causing any problem to the distribution of water and electricity to the people by shifting the electric lines and water pipes as soon as possible.

5.15 Health Issues Because of Pollution

The number of people facing health issues because of this project were less. Though the pollution caused in a highway project is high, contractor took good care by avoiding movement of dumpers in public places and inside the villages, by locating quarry and batching plant at the places far away from the villages which avoided pollution and bad effects on the health of the local people.

6 Conclusion

One of the main challenges that have been identified from both the literature review and from the case study was material management. Material management is more important in the highway project because large amount of money is spent in buying, storing and in usage of materials. These problems were most likely to be faced in all the National highway projects which were to be rehabilitated and upgraded. Other than Material management, machinery management was one of the important challenges that have been identified. Large amount of money was spent and many problems were faced in leasing, renting and operation of machinery.

Utilility shifting was a crucial activity in highway constuction.. Utility shifting activity was carried by contractor because of which many regulations were there resulting in the hault of the activities which happened in the case study considered. In the case study considered, usage of innovative materials was minimal which resulted them in causing pollution in the residential wereas and disturbing the livelihood of

the people. This challenge can be overcomed by using innovative materials which will help replenish the natural resources.

References

Edwards DJ, Holt GD (2009) Construction plant and equipment management research: thematic review. J Eng Des Technol 7(2):186–206

Holt G, Olomolaiye P, Harris F (1996) Tendering procedures, contractual arrangements and Latham: the contractors' view. Eng Constr Archit Manag 1(1):97–115

Kang BG, Elbashier MMME, Goh BH, Song MK (2015) A comparative study between clients and contractors on competitive tendering in the Sudan construction industry. Open J Social Sci 3(7):67–73

Patel KV, Vyas CM (2011) Construction materials management on project sites. In: National conference on recent trends in engineering and technology, Gujarat, India

Patil T, Waghmwere A, Gawande P (2016) Tender and bidding process in construction projects. IJISET—Int J Inno Sci Eng Technol 3(3):492–498

Sawalhi NI, Al Kass MMA (2012) A construction materials management system for Gaza building contractors. In: The 4th international engineering conference—towards engineering of 21st century, Islamic University of Gaza, Gaza, pp 261–267

Seboru MA, Mulwa AS, Kyaloand DD, Rambo C (2016) Acquisition of materials and performance of road construction projects in Kenya: a case of Nairobi county. European Sci J 12(32):223–250

Prediction of Bearing Capacity of Stone Columns Using Type-2 Fuzzy Logic

Manita Das and Ashim Kanti Dey

Abstract Stone column is one of the most widely used soil improvement methods for the improvement of the load carrying capacity and reduction of the settlement of the soft ground. Several theories are available to find out the bearing capacity of the soft ground strengthened by stone columns. But, experimental solution is better than any other solution, because it gives appropriate results with the variation of dependent variables. However, due to some uncertainties occurred during the experiments, the accuracy of the results may not be 100% and some erroneous results may be obtained. In this study, the bearing capacity (q_u) of the stone columns is predicted by using type-2 fuzzy set theory, which deals with the uncertainties. 102 numbers of previously published data were collected and used for this prediction. The prediction results of type-2 fuzzy set model was compared with the results of Artificial Neural Network (ANN) and Adaptive Neuro-Fuzzy Inference System (ANFIS) prediction method with the same data to obtain a better method of bearing capacity prediction. Results showed that the type-2 fuzzy set could be a powerful prediction method for the prediction of q_u as compared to ANN and ANFIS model. The result of sensitivity analysis is also presented in this paper.

Keywords Type-2 fuzzy set · ANN · ANFIS · Bearing capacity · Stone column · Uncertainties

1 Introduction

Building any structure on weak soil is normally a challenging job for all the geotechnical engineers because of its nature i.e. high compressibility and low shear strength. In this type of soil, piles are normally constructed to distribute the stress to the hard

M. Das (✉)
ITER, SOA Deemed to be University, Bhubaneswar, India
e-mail: manitadas@soa.ac.in

A. K. Dey
NIT Silchar, Silchar, India

B. B. Das et al. (eds.), *Recent Developments in Sustainable Infrastructure (ICRDSI-2020)—GEO-TRA-ENV-WRM*, Lecture Notes in Civil Engineering 207,
https://doi.org/10.1007/978-981-16-7509-6_33

and stiff strata below. But, the cost of pile construction is very high for low to medium rise buildings as compared to the structural cost (Golakiya and Lad 2015).

Hence, to solve this problem, some ground improvement methods may be used. Stone column is also a type of soil improvement methods which is most widely used in case of soft clay. Use of stone columns enhances the load carrying capacity and expedites the consolidation rate of the soft clay. To build any structure on soft soil, utility of stone columns are more advantageous than other major type of foundations like pile foundation, because stone columns provide a superior and more economical alternative to pile foundations. Especially, in case of low rise and medium loaded industrial structure, use of stone columns are proved to be simpler and attractive alternative. Shien (2013) also obtained stone columns as a cheap alternative to the other feasible improvement methods.

The theories related to stone column are already described in the IS code (IS 15284-1 2003) and other published papers. In previously published papers, researchers estimated bearing capacity and settlement by conducting experiments (Ambily and Gandhi 2004; Castro 2014; Afshar and Ghazavi 2014a; Mohanty and Samanta 2015) or by conducting some analytical or numerical study (Lee and Pande 1998; Afshar and Ghazavi 2014a, b; Etezad et al. 2015). Etezad et al. (2015) developed an analytical model and obtained an expression to estimate the bearing capacity of group columns by using a limit equilibrium method with the consideration of general shear failure. Castro (2014) performed analytical study to obtain the column settlement below rigid footings.

Although research shows more accuracy in the field test results, yet the importance of analytical studies is not ignorable. The experimental studies may become time-consuming and exhibit a lack of repeatability when multiple variables are involved in a defined solution. Deb (2008) conducted a numerical study on modelling of stone column with the use of finite difference technique. Castro and Sagaseta (2009) discussed on the consolidation property of stone columns by considering the influences of vertical and radial deformations of stone columns. But if column consolidation is considered, the average degree of consolidation of the column-clay composite foundation was found to be reduced (Xie et al. 2009). In civil engineering problems, analytical methods were also used widely (Balaam and Booker 1981; Jellali et al. 2011). The most powerful and error free results can be obtained after validating the experimental results with both the analytical and numerical results (Colas et al. 2008). But conducting experiments along with analytical and numerical solution will be very costly and time consuming. Moreover, the results obtained from experiments may have some uncertainties because of the errors due to the weather forecast, errors caused by installation effects, human errors, etc. If we can deal with these errors, the experimental results will give the most accurate solution. In the present study, considering all the uncertainties associated with the determination of q_u, the magnitude of q_u was obtained with more accuracy with the use of type-2 fuzzy system. In 1965, Prof. L. A. Zadeh first established the type-1 fuzzy set (T1 FS) theory and later on this theory has been successfully utilized in several areas of science and engineering. Normally, the membership function (MF), $\mu X(x)$, of a T1FS is picked on the basis of the user's opinion and hence, the MFs of same T1FS from two individual

experts may be unalike on the basis of their cultures, experiences, and perspectives or by using optimization techniques, this can be designed (Horikawa et al. 1992; Jang 1992; Wang and Mendel 1992). Therefore, in this study, by using type-2 fuzzy system, the bearing capacity of stone column (q_u) was estimated, where membership functions were also considered as fuzzy.

It is important to note here that if in any system, uncertainty is absent, then type-2 fuzzy system will automatically convert into T1FS. To control more uncertainties in a system, the type-2 fuzzy set generates two type-1 fuzzy sets at a time. Since in T1FS, the membership functions do not hold any uncertainty. Therefore, the type-1 system is not a proper way to describe fuzziness. So to describe the fuzziness in its proper way, in 1975, Lotfi Zadeh established type-2 fuzzy system whose membership function is a fuzzy in character too (Zadeh 1975). Interval type-2 fuzzy system (IT2FS) is a special type-2 fyzzy system which is welcomed worldwide and majorly applicable for the more uncertain situation. IT2FS can be used when it becomes more difficult to decide the rules and membership function by an expert (Liu and Mendel 2008; Mendel 2001). Therefore, to increase the accuracy of the result, type-2 fuzzy system is used in this case for the estimation of q_u. In geotechnical engineering, many researchers worked on type-2 fuzzy systems and obtained a very good results, even better than other intelligence method (Olatunji et al. 2011; Dodagoudar and Venkatachalam 2000; Valliappan and Pham 1993; Ayyub 1991). For the comparison purpose, ANN and ANFIS models were also constructed in this study.

ANN is a computational technique, which capability of input–output mapping, is used for finding out an output using a given numbers of inputs. Many researchers utilised ANN in solving geotechnical related problems (Goh et al. 2005; Kostic and Vasovic 2015; Das and Dey 2018b, 2019). Chik et al. (2014), Chik and Aljanabi (2014) used ANN to obtain the settlement occurred due to loading in case of stone columns.

ANFIS system is a combination of both fuzzy logic and neural network. It has the benefits of both the methods i.e. fuzzy and neural network. It has the reasoning power of the fuzzy logic and learning capacity of ANN and it diminishes the overfitting property of neural network. In the present study, the algorithm suggested by Jang (1993) was used for building the model of the determination of load carrying capacity of stone column. Das and Dey (2018a) also used the above mentioned algorithm for constructing the ANFIS model to achieve the bearing capacity of stone columns.

To obtain the interval type-2 fuzzy logic system (IT2FLS) model, data were accumulated from the existing literature. To validate the IT2FLS model, ANN and ANFIS models were constructed with the same data.

2 Collection of Data

In the present study, to construct the IT2FLS model for q_u prediction, 102 numbers of previously published data were collected, the details of which is presented in Table 1. The dataset consists of both laboratory and field results as well as analytical and

Table 1 Description of collected data

Mean value of data					No. of collected data	References
c_u in kPa	s/d	ϕ in degree	*l* in mm	q_u in kPa		
17	3	43	450	1739.08	24	Ambily and Gandhi (2007)
19.44	1.955556	41.11	7888.89	274.44	9	Poorooshasb and Meyerhof (1997)
26.2	2.214	40.1	12.15	173	10	Andreou and Papadopoulos (2014)
13.13	2.13	40	127.5	69.25	4	Etezad (2007)
13.23	2.35	27.35	4250	298.82	17	Ambily and Gandhi (2004)
2.5	2.89	41.5	500	35.67	3	Murugesan and Rajagopal (2008)
6	2	48	217.5	29	10	Malarvizhi and Ilampurthi (2007)
15	2	42	500	550	1	Mohanty and Samanta (2015)
20	3.33	37	300	140	1	Golait et al. (2009)
11.25	2	11.25	10,000	188.13	8	Zhang et al. (2013)
15	1.5	35	20,000	1800	1	Hassen et al. (2010)
11.18	3	39.86	3814.29	357.71	14	Etezad et al. (2015)

numerical results.

These data are from various countries and therefore the environment condition is different, so the soil properties will be different for different dataset. Mainly q_u depends on the parameters like undrained cohesion (c_u) of the surrounding soft ground, friction angle (φ) of column material, spacing to diameter ratio (s/d), and stone column length (*l*). Therefore, all these four parameters were taken as the input and the single output was the column bearing capacity (q_u).

The performance of these model were discussed here using three statistical terms, namely, Root-Mean-Squared Error (RMSE), linear correlation coefficient (*R*), and Mean Absolute Percentage Error (MAPE). It is worth mentioning that the dataset used in the present study were collected from various places and different atmospheric conditions. Moreover, the dataset was included both prototype and laboratory data. Therefore it is very important to normalize the dataset within a range. So, before

constructing the ANN models, the dataset was normalized and taken in the range [0, +1]. In this present study, IT2FLS was used for the prediction of q_u.

3 Uncertainties in the Determination of q_u

In this study, q_u was estimated with the use of type-2 fuzzy set by considering uncertainties. Bearing capacity (q_u) mostly depends on the bulging failure and other parameters like settlement and consolidation associated with bearing capacity of stone column. "Certainty" is only a description for most of the engineering problems, in which situation that the involved parameters and cause-effect relationships are known in a proper way to provide only individual output. The integral problems are included in "uncertainty" where a number of outputs may arise from a result in the prediction of the parameter involved due to the variability and the partial knowledge in the entirety of the casual correlation (Rethati 1988). In a word, the uncertainties of any solutions are unavoidable. The sources of uncertainty in a geotechnical engineering problem may come from the following (Bowels 1996):

- The insufficient understanding of the subsoil conditions.
- Wide variation of soil parameters.
- Less control of environmental changes after completion of construction.
- The inaccuracy of the empirical or theoretical methods for estimating bearing capacity.
- Prediction of the loads applied on the construction such as live loads, dead load, earthquake, wind loads, etc.

The bearing capacity of stone columns (q_u) are normally estimated with plate load test, which is the most reliable test to achieve the load-settlement behavior, may be the unrealistic results may be obtained if not properly conducted (Dasaka et al. 2014). There are many reasons behind this unrealistic results such as if the load increment is not properly maintained, the soil rebounds; and for both the stress maintained and non-maintained laboratory plate load tests give different results. Moreover, the sources of uncertainties may be included as lack of proper equipment and inadequate codal provisions, etc., which may become the reasons for unrealistic results. Uncertainties may be occurred due to variability of the ground, deficiency in design equation and soil-testing errors. For the theoretical studies also, there are many reasons of uncertainties which attack q_u because in the existing formulae for the estimation of q_u, the type of the stone columns were not considered whether it is floating or end bearing, length to diameter ratio and the method of the implementation and many other factors that affect q_u (Fattah et al. 2017).

4 Type-2 Fuzzy Logic Systems Framework

In this study, for the prediction of q_u, type-2 fuzzy logic systems (type-2 FLS) is utilized with the data collected from various investigation. The unique characteristic of the adaptive fuzzy systems is the complete specification of fuzzy logic systems with the use of training data. So, in this case also, the main aim is to state the fuzzy system by using training data. Type-2 FLS is a kind of fuzzy logic systems whose grades of membership function are also fuzzy. The reality of this fuzzy set is very fascinating because the grades of membership function cannot be a crisp value in real life situations. In real life problems, many forms of uncertainties may exist such as uncertainty about the shape of the membership function, uncertainty about the consequent parts of the rule, uncertainty about the training data, and uncertainty about the measurement technique which are used to activate the rules. In all these situations, type-2 FLS can be used. On the basis of type-2 fuzzy sets, type-2 adaptive fuzzy inference systems learn the fuzzy rules and membership functions, from data, which are the adaptive networks in a fuzzy system (Mendel 2009; Cox 1993; Dubois and Prade 1982). Normally the decision of using fuzzy type-1 set or fuzzy type-2 sets will depend on the following situation: when it is hard to decide the membership grade in a set as 0 or 1, then T1FS can be used. In a similar way, when the situation is so fuzzy that it becomes difficult to decide the membership grade as a crisp value in [0, 1], then type-2 fuzzy sets can be used efficiently. A fuzzy set is called a type-n fuzzy set when its membership function is also a fuzzy set of type-n-1, where $n = 2, 3, \ldots$. In case of $n > 2$, the problems can only be visualised and upto $n = 2$, this definition of fuzzy set can be linked with real life situations. Generally type-2 FLS consists of five interconnected components which are fuzzifier, rules, inference engine, type-reducer and defuzzifier. The present study considers four input parameters as mentioned earlier. The fuzzifier takes all these input parameters as inputs. Then after fuzzification in the fuzzifier, the fuzzified value will serve as the input in inference engine. The inference engine will produce the type-2 fuzzy sets from the previously obtained type-1 fuzzy sets. So the output of the inference engine is the type-1 fuzzy set. Then the next step is type reducer. The type reducer reduced the type-2 fuzzy set to type-1 fuzzy set. These type-1 fuzzy sets are the interval sets which give the possible range of values of q_u. Then finally the defuzzifier calculates the predicted crisp output value by averaging the generated interval sets. Figure 1 shows the core components used in type-2 FLS framework to predict q_u.

4.1 Interval Type-2 Fuzzy Sets (IT2 FSS)

As we know that there are many limitations in the capability of type-1 fuzzy logic system (T1FS) for making model and minimization of effect of uncertainties may be because of its crisp values of membership grades. To overcome the demerits of type-1 fuzzy sets, the theory of type-2 fuzzy set (type-2 FS) was established, where

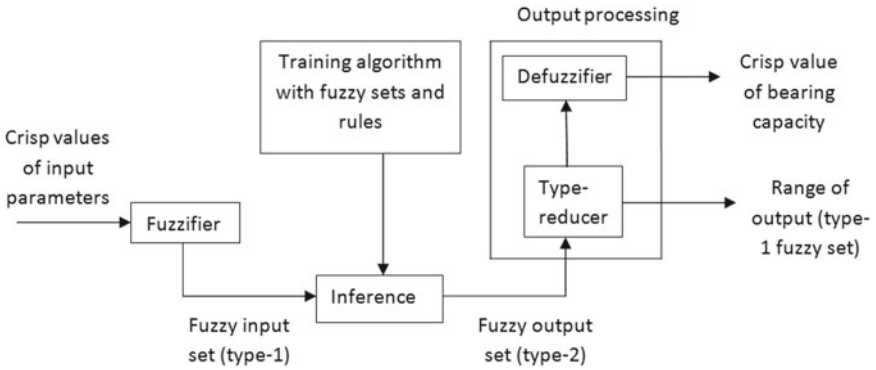

Fig. 1 Schematic diagram of framework based on type-2 FLS to predict the bearing capacity of stone column

the membership functions are also fuzzy. Interval type-2 (IT2) FSs (Mendel 2001), a special case of type-2 FSs, are recently the most widely used in engineering for its reduced computational cost along with other benifits. Two IT1FSs, $\overline{X}$ and $\underline{X}$, bound the IT2FLS from the above and below, which are named as upper membership function (UMF) and lower membership function (LMF), respectively. The area surrounded by the UMF and LMF is called as the footprint of uncertainty (FOU). IT2FLSs are best useful for the situation when it becomes very tough to find out the exact membership function (MF) or in modeling the different opinions for making decisions from the individuals.

4.2 Interval Type-2 Fuzzy Logic System (IT2 FLS)

The schematic diagram of an IT2FLS is presented in Fig. 1. In this figure, the core components of IT2FLS framework proposed for the estimation of q_u are presented. This phenomena is almost similar to the counterpart of type-1 fuzzy set but the main difference is that for IT2FLS, atleast one of the fuzzy sets in the rule base system is an IT2FLS. Therefore the products of the inference engine will be IT2FSs. Then a type reducer is used to convert the IT2FSs to type-1 fuzzy set (T1FS) and then the defuzzification is carried out to obtain the final output.

To describe the IT2 FLS, computation is required. Considering the rulebase of an IT2FLS with N number of rules, the following forms are assumed:

$$R^n : IF\ x_1\ is\ \tilde{X}_1^n\ and\ x_2\ is\ \tilde{X}_2^n \ldots\ and\ x_I\ is\ \tilde{X}_I^n,\ THEN\ y\ is\ Y^n \quad \mathrm{n} = 1, 2, \ldots, \mathrm{N}.$$

where $\tilde{X}_i^n$ are the IT2FSs for i = 1, 2, …, I; $Y^n = \left[\underline{y}^n, \overline{y}^n\right]$ is an interval.

Assuming the input vector as $x' = \left(x'_1, x'_2, \ldots, x'_I\right)$, the following steps are used for the computation of an IT2FLS:

(1) Determination of the membership function of x'_i on each X_i^n, which is represented as $\left[\mu\underline{x}_i^n\left(x'_i\right), \mu\overline{x}_i^n\left(x'_i\right)\right]$, where $i = 1, 2, 3, \ldots, I$, and n = 1, 2, …, N.

(2) Computation of firing interval of nth rule, $F^n\left(x'\right)$, which is expressed as

$$\begin{aligned} F^n\left(x'\right) &= \left[\mu\underline{x}_1^n\left(x'_1\right) \times \mu\underline{x}_2^n\left(x'_2\right) \times \ldots \times \mu\underline{x}_I^n\left(x'_I\right), \mu\overline{x}_1^n\left(x'_1\right)\right. \\ &\quad \left. \times\mu\overline{x}_2^n\left(x'_1\right) \times \ldots \times \mu\overline{x}_1^n\left(x'_I\right)\right] \\ &\equiv \left[\underline{f}^n, \overline{f}^n\right], \quad n = 1, 2, \ldots, N \end{aligned} \tag{1}$$

(3) Application of type-reduction method to unite the firing interval $F^n\left(x'\right)$ and the respective rule consequents. Among all the methods, centre-of-sets (cos) type reduction method is used in this study. The expression of this method is as follows:

$$Y_{\cos}\left(x'\right) = \bigcup_{\substack{f^n \in F^n\left(x'\right) \\ y^n \in Y^n}} \frac{\sum_{n=1}^{N} f^n y^n}{\sum_{n=1}^{N} f^n} = [y_l, y_r] \tag{2}$$

From the literatures (Mendel 2001; Mendel and Wu 2010; Wu and Mendel 2009), the expression of the ranges can be found as

$$y_l = \min_{k\in[1,N-1]} \frac{\sum_{n=1}^{k} \overline{f}^n \underline{y}^n + \sum_{n=k+1}^{N} \underline{f}^n \underline{y}^n}{\sum_{n=1}^{k} \overline{f}^n + \sum_{n=k+1}^{N} \underline{f}^n} \equiv \frac{\sum_{n=1}^{L} \overline{f}^n \underline{y}^n + \sum_{n=L+1}^{N} \underline{f}^n \underline{y}^n}{\sum_{n=1}^{L} \overline{f}^n + \sum_{n=L+1}^{N} \underline{f}^n} \tag{3}$$

$$y_r = \max_{k\in[1,N-1]} \frac{\sum_{n=1}^{k} \underline{f}^n \overline{y}^n + \sum_{n=k+1}^{N} \overline{f}^n \overline{y}^n}{\sum_{n=1}^{k} \underline{f}^n + \sum_{n=k+1}^{N} \overline{f}^n} \equiv \frac{\sum_{n=1}^{R} \underline{f}^n \overline{y}^n + \sum_{n=R+1}^{N} \overline{f}^n \overline{y}^n}{\sum_{n=1}^{R} \underline{f}^n + \sum_{n=R+1}^{N} \overline{f}^n} \tag{4}$$

The switch points L and R are decided as

$$\underline{y}^L \le y_l \le \underline{y}^{L+1} \tag{5}$$

$$\overline{y}^R \le y_r \le \overline{y}^{R+1} \tag{6}$$

where $\overline{y}^n$ and $\underline{y}^n$ are written as the upper and lower limit of Y^n respectively; y_l and y_r can be evaluated by considering the Karnik–Mendel (KM) algorithms as available in the literature (Mendel 2001).

(4) Computation of the final defuzzified value as

$$y = \frac{y_l + y_r}{2} \tag{7}$$

4.3 Computation of the Proposed Type-2 FLS

In this proposed model, the Trapezoidal membership functions are used for the determination of q_u. The computation of IT2FLS was conducted in matlab 2013R, the coding of which was taken from the previous literature (Wu 2014), which used the algorithm from the literature (Mendel 2001) for the computation of y_l and y_r. In this case, 9-point vector method was used for the computation where each IT2FS was denoted by a 9-point vector (p1, p2, …, p9). Mitra et al. (2017) also used type-2 fuzzy sets with Trapezoidal membership functions and obtained a very good result for their work with the considerations of uncertainties.

The membership functions for the four inputs (x_1, x_2, x_3, and x_4) are shown in Fig. 2a–d. Since, the present study deals with four inputs for the determination of q_u, therefore total sixteen rules is formed for the computation of IT2FLS. From the four input, one output model, the following rules are considered for the rulebase:

$$R^1 : IF\ x_1\ is\ \tilde{X}_{11},\ x_2\ is\ \tilde{X}_{21},\ x_3\ is\ \tilde{X}_{31}\ and\ x_4\ is\ \tilde{X}_{41},\ THEN\ y\ is\ Y^1.$$
$$R^2 : IF\ x_1\ is\ \tilde{X}_{11},\ x_2\ is\ \tilde{X}_{22},\ x_3\ is\ \tilde{X}_{31}\ and\ x_4\ is\ \tilde{X}_{41},\ THEN\ y\ is\ Y^2.$$
$$R^3 : IF\ x_1\ is\ \tilde{X}_{11},\ x_2\ is\ \tilde{X}_{22},\ x_3\ is\ \tilde{X}_{32}\ and\ x_4\ is\ \tilde{X}_{41},\ THEN\ y\ is\ Y^3.$$
$$R^4 : IF\ x_1\ is\ \tilde{X}_{11},\ x_2\ is\ \tilde{X}_{22},\ x_3\ is\ \tilde{X}_{32}\ and\ x_4\ is\ \tilde{X}_{42},\ THEN\ y\ is\ Y^4.$$
$$R^5 : IF\ x_1\ is\ \tilde{X}_{11},\ x_2\ is\ \tilde{X}_{21},\ x_3\ is\ \tilde{X}_{31}\ and\ x_5\ is\ \tilde{X}_{42},\ THEN\ y\ is\ Y^5.$$
$$R^6 : IF\ x_1\ is\ \tilde{X}_{11},\ x_2\ is\ \tilde{X}_{21},\ x_3\ is\ \tilde{X}_{32}\ and\ x_4\ is\ \tilde{X}_{41},\ THEN\ y\ is\ Y^6.$$
$$R^7 : IF\ x_1\ is\ \tilde{X}_{11},\ x_2\ is\ \tilde{X}_{21},\ x_3\ is\ \tilde{X}_{32}\ and\ x_4\ is\ \tilde{X}_{42},\ THEN\ y\ is\ Y^7.$$
$$R^8 : IF\ x_1\ is\ \tilde{X}_{11},\ x_2\ is\ \tilde{X}_{22},\ x_3\ is\ \tilde{X}_{31}\ and\ x_4\ is\ \tilde{X}_{42},\ THEN\ y\ is\ Y^8.$$
$$R^9 : IF\ x_1\ is\ \tilde{X}_{12},\ x_2\ is\ \tilde{X}_{21},\ x_3\ is\ \tilde{X}_{31}\ and\ x_4\ is\ \tilde{X}_{42},\ THEN\ y\ is\ Y^9.$$
$$R^{10} : IF\ x_1\ is\ \tilde{X}_{12},\ x_2\ is\ \tilde{X}_{21},\ x_3\ is\ \tilde{X}_{32}\ and\ x_4\ is\ \tilde{X}_{41},\ THEN\ y\ is\ Y^{10}.$$
$$R^{11} : IF\ x_1\ is\ \tilde{X}_{12},\ x_2\ is\ \tilde{X}_{21},\ x_3\ is\ \tilde{X}_{32}\ and\ x_4\ is\ \tilde{X}_{42},\ THEN\ y\ is\ Y^{11}.$$
$$R^{12} : IF\ x_1\ is\ \tilde{X}_{12},\ x_2\ is\ \tilde{X}_{22},\ x_3\ is\ \tilde{X}_{31}\ and\ x_4\ is\ \tilde{X}_{42},\ THEN\ y\ is\ Y^{12}.$$
$$R^{13} : IF\ x_1\ is\ \tilde{X}_{12},\ x_2\ is\ \tilde{X}_{21},\ x_3\ is\ \tilde{X}_{31}\ and\ x_4\ is\ \tilde{X}_{41},\ THEN\ y\ is\ Y^{13}.$$
$$R^{14} : IF\ x_1\ is\ \tilde{X}_{12},\ x_2\ is\ \tilde{X}_{22},\ x_3\ is\ \tilde{X}_{31}\ and\ x_4\ is\ \tilde{X}_{41},\ THEN\ y\ is\ Y^{14}.$$
$$R^{15} : IF\ x_1\ is\ \tilde{X}_{12},\ x_2\ is\ \tilde{X}_{22},\ x_3\ is\ \tilde{X}_{32}\ and\ x_4\ is\ \tilde{X}_{41},\ THEN\ y\ is\ Y^{15}.$$
$$R^{16} : IF\ x_1\ is\ \tilde{X}_{12},\ x_2\ is\ \tilde{X}_{22},\ x_3\ is\ \tilde{X}_{32}\ and\ x_4\ is\ \tilde{X}_{42},\ THEN\ y\ is\ Y^{16}.$$

Considering input vector as $x = [x_1, x_2, x_3, x_4] = (0.35, 0.65, 0.4, 0.7)$. The firing intervals of the IT2FS are

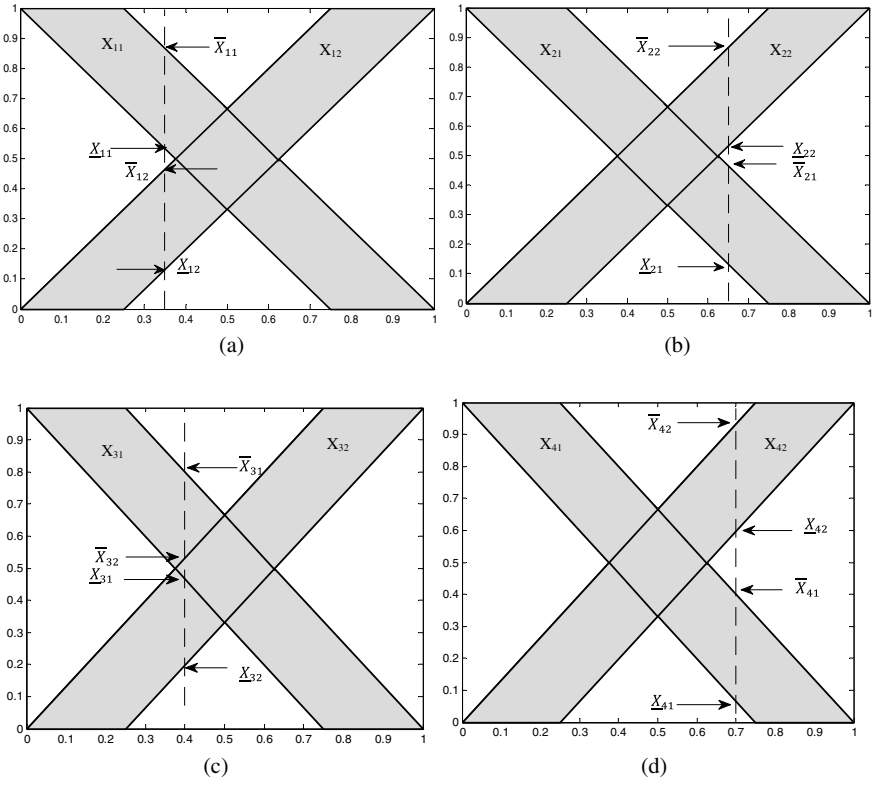

Fig. 2 The membership functions for the inputs: **a** undrained cohesion of clay (c_u) x_1, **b** spacing to diameter ratio (s/d) x_2, **c** friction angle (ϕ) x_3, and **d** length of stone column (l) x_4

$$\left[\mu_{\underline{X}_{11}}(x_1), \mu_{\overline{X}_{11}}(x_1)\right] = [0.54, 0.86]$$
$$\left[\mu_{\underline{X}_{12}}(x_1), \mu_{\overline{X}_{12}}(x_1)\right] = [0.46, 0.12]$$
$$\left[\mu_{\underline{X}_{21}}(x_2), \mu_{\overline{X}_{21}}(x_2)\right] = [0.47, 0.13]$$
$$\left[\mu_{\underline{X}_{22}}(x_2), \mu_{\overline{X}_{22}}(x_2)\right] = [0.53, 0.87]$$
$$\left[\mu_{\underline{X}_{31}}(x_3), \mu_{\overline{X}_{31}}(x_3)\right] = [0.49, 0.81]$$
$$\left[\mu_{\underline{X}_{32}}(x_3), \mu_{\overline{X}_{32}}(x_3)\right] = [0.2, 0.52]$$
$$\left[\mu_{\underline{X}_{41}}(x_4), \mu_{\overline{X}_{41}}(x_4)\right] = [0.05, 0.4]$$
$$\left[\mu_{\underline{X}_{42}}(x_4), \mu_{\overline{X}_{42}}(x_4)\right] = [0.6, 0.93]$$

The firing intervals for all the sixteen rules are listed in Table 2. KM algorithm gives the value of L as 2 and R as 14, therefore y_l and y_r values can be calculated as follows:

Table 2 The firing intervals along with their corresponding consequents

Rule No.	Firing interval	Consequent
R1	$\left[\underline{f}^1, \overline{f}^1\right] = \left[\mu_{\underline{X}_{11}}(x_1).\mu_{\underline{X}_{21}}(x_2).\mu_{\underline{X}_{31}}(x_3).\mu_{\underline{X}_{41}}(x_4), \mu_{\overline{X}_{11}}(x_1).\mu_{\overline{X}_{21}}(x_2).\mu_{\overline{X}_{31}}(x_3).\mu_{\overline{X}_{41}}(x_4)\right]$ $= [0.54 \times 0.47 \times 0.49 \times 0.05, 0.86 \times 0.13 \times 0.81 \times 0.4]$ $= [0.0062, 0.036]$	$\left[\underline{y}^1, \overline{y}^1\right] = [0, 0.07]$
R2	$\left[\underline{f}^2, \overline{f}^2\right] = \left[\mu_{\underline{X}_{11}}(x_1).\mu_{\underline{X}_{22}}(x_2).\mu_{\underline{X}_{31}}(x_3).\mu_{\underline{X}_{41}}(x_4), \mu_{\overline{X}_{11}}(x_1).\mu_{\overline{X}_{22}}(x_2).\mu_{\overline{X}_{31}}(x_3).\mu_{\overline{X}_{41}}(x_4)\right]$ $= [0.54 \times 0.53 \times 0.49 \times 0.05, 0.86 \times 0.87 \times 0.81 \times 0.4]$ $= [0.007, 0.242]$	$\left[\underline{y}^2, \overline{y}^2\right] = [0.09, 0.17]$
R3	$\left[\underline{f}^3, \overline{f}^3\right] = \left[\mu_{\underline{X}_{11}}(x_1).\mu_{\underline{X}_{22}}(x_2).\mu_{\underline{X}_{32}}(x_3).\mu_{\underline{X}_{41}}(x_4), \mu_{\overline{X}_{11}}(x_1).\mu_{\overline{X}_{22}}(x_2).\mu_{\overline{X}_{32}}(x_3).\mu_{\overline{X}_{41}}(x_4)\right]$ $= [0.54 \times 0.53 \times 0.2 \times 0.05, 0.86 \times 0.87 \times 0.52 \times 0.4]$ $= [0.0028, 0.16]$	$\left[\underline{y}^3, \overline{y}^3\right] = [0.15, 0.3]$

(continued)

Table 2 (continued)

Rule No.	Firing interval	Consequent
R4	$\left[\underline{f}^4, \overline{f}^4\right] = \left[\mu_{\underline{X}_{11}}(x_1).\mu_{\underline{X}_{22}}(x_2).\mu_{\underline{X}_{32}}(x_3).\mu_{\underline{X}_{42}}(x_4),\right.$ $\left.\mu_{\overline{X}_{11}}(x_1).\mu_{\overline{X}_{22}}(x_2).\mu_{\overline{X}_{32}}(x_3).\mu_{\overline{X}_{42}}(x_4)\right]$ $= [0.54 \times 0.53 \times 0.6 \times 0.05, 0.86 \times 0.87 \times 0.93 \times 0.4]$ $= [0.0086, 0.28]$	$\left[\underline{y}^4, \overline{y}^4\right] = [0.2, 0.4]$
R5	$\left[\underline{f}^5, \overline{f}^5\right] = \left[\mu_{\underline{X}_{11}}(x_1).\mu_{\underline{X}_{21}}(x_2).\mu_{\underline{X}_{31}}(x_3).\mu_{\underline{X}_{42}}(x_4),\right.$ $\left.\mu_{\overline{X}_{11}}(x_1).\mu_{\overline{X}_{21}}(x_2).\mu_{\overline{X}_{31}}(x_3).\mu_{\overline{X}_{42}}(x_4)\right]$ $= [0.54 \times 0.47 \times 0.49 \times 0.6, 0.86 \times 0.13 \times 0.81 \times 0.93]$ $= [0.0746, 0.0842]$	$\left[\underline{y}^5, \overline{y}^5\right] = [0.35, 0.5]$
R6	$\left[\underline{f}^6, \overline{f}^6\right] = \left[\mu_{\underline{X}_{11}}(x_1).\mu_{\underline{X}_{21}}(x_2).\mu_{\underline{X}_{32}}(x_3).\mu_{\underline{X}_{41}}(x_4),\right.$ $\left.\mu_{\overline{X}_{11}}(x_1).\mu_{\overline{X}_{21}}(x_2).\mu_{\overline{X}_{32}}(x_3).\mu_{\overline{X}_{41}}(x_4)\right]$ $= [0.54 \times 0.47 \times 0.2 \times 0.05, 0.86 \times 0.13 \times 0.52 \times 0.4]$ $= [0.00254, 0.0232]$	$\left[\underline{y}^6, \overline{y}^6\right] = [0.4, 0.6]$
R7	$\left[\underline{f}^7, \overline{f}^7\right] = \left[\mu_{\underline{X}_{11}}(x_1).\mu_{\underline{X}_{21}}(x_2).\mu_{\underline{X}_{32}}(x_3).\mu_{\underline{X}_{42}}(x_4),\right.$ $\left.\mu_{\overline{X}_{11}}(x_1).\mu_{\overline{X}_{21}}(x_2).\mu_{\overline{X}_{32}}(x_3).\mu_{\overline{X}_{42}}(x_4)\right]$ $= [0.54 \times 0.47 \times 0.2 \times 0.6, 0.86 \times 0.13 \times 0.52 \times 0.93]$ $= [0.030, 0.054]$	$\left[\underline{y}^7, \overline{y}^7\right] = [0.45, 0.65]$

(continued)

Table 2 (continued)

Rule No.	Firing interval	Consequent
R8	$\left[\underline{f}^8, \overline{f}^8\right] = \left[\mu_{\underline{X}_{11}}(x_1).\mu_{\underline{X}_{22}}(x_2).\mu_{\underline{X}_{31}}(x_3).\mu_{\underline{X}_{42}}(x_4),\right.$ $\left.\mu_{\overline{X}_{11}}(x_1).\mu_{\overline{X}_{22}}(x_2).\mu_{\overline{X}_{31}}(x_3).\mu_{\overline{X}_{42}}(x_4)\right]$ $= [0.54 \times 0.53 \times 0.49 \times 0.6, 0.86 \times 0.87 \times 0.81 \times 0.93]$ $= [0.0841, 0.564]$	$\left[\underline{y}^8, \overline{y}^8\right] = [0.55, 0.7]$
R9	$\left[\underline{f}^9, \overline{f}^9\right] = \left[\mu_{\underline{X}_{12}}(x_1).\mu_{\underline{X}_{21}}(x_2).\mu_{\underline{X}_{31}}(x_3).\mu_{\underline{X}_{42}}(x_4),\right.$ $\left.\mu_{\overline{X}_{12}}(x_1).\mu_{\overline{X}_{21}}(x_2).\mu_{\overline{X}_{31}}(x_3).\mu_{\overline{X}_{42}}(x_4)\right]$ $= [0.46 \times 0.47 \times 0.49 \times 0.6, 0.12 \times 0.13 \times 0.81 \times 0.93]$ $= [0.0635, 0.018]$	$\left[\underline{y}^9, \overline{y}^9\right] = [0.6, 0.8]$
R10	$\left[\underline{f}^{10}, \overline{f}^{10}\right] = \left[\mu_{\underline{X}_{12}}(x_1).\mu_{\underline{X}_{21}}(x_2).\mu_{\underline{X}_{32}}(x_3).\mu_{\underline{X}_{41}}(x_4),\right.$ $\left.\mu_{\overline{X}_{12}}(x_1).\mu_{\overline{X}_{21}}(x_2).\mu_{\overline{X}_{32}}(x_3).\mu_{\overline{X}_{41}}(x_4)\right]$ $= [0.46 \times 0.47 \times 0.2 \times 0.05, 0.12 \times 0.13 \times 0.52 \times 0.4]$ $= [0.0022, 0.0032]$	$\left[\underline{y}^{10}, \overline{y}^{10}\right] = [0.65, 0.83]$

(continued)

Table 2 (continued)

Rule No.	Firing interval	Consequent
R11	$\left[\underline{f}^{11}, \overline{f}^{11}\right] = \left[\mu_{\underline{X}_{12}}(x_1).\mu_{\underline{X}_{21}}(x_2).\mu_{\underline{X}_{32}}(x_3).\mu_{\underline{X}_{42}}(x_4), \mu_{\overline{X}_{12}}(x_1).\mu_{\overline{X}_{21}}(x_2).\mu_{\overline{X}_{32}}(x_3).\mu_{\overline{X}_{42}}(x_4)\right]$ $= [0.46 \times 0.47 \times 0.2 \times 0.6, 0.12 \times 0.13 \times 0.52 \times 0.93]$ $= [0.026, 0.00754]$	$\left[\underline{y}^{11}, \overline{y}^{11}\right] = [0.7, 0.85]$
R12	$\left[\underline{f}^{12}, \overline{f}^{12}\right] = \left[\mu_{\underline{X}_{12}}(x_1).\mu_{\underline{X}_{22}}(x_2).\mu_{\underline{X}_{31}}(x_3).\mu_{\underline{X}_{42}}(x_4), \mu_{\overline{X}_{12}}(x_1).\mu_{\overline{X}_{22}}(x_2).\mu_{\overline{X}_{31}}(x_3).\mu_{\overline{X}_{42}}(x_4)\right]$ $= [0.46 \times 0.53 \times 0.49 \times 0.6, 0.12 \times 0.87 \times 0.81 \times 0.93]$ $= [0.0935, 0.079]$	$\left[\underline{y}^{12}, \overline{y}^{12}\right] = [0.73, 0.88]$
R13	$\left[\underline{f}^{13}, \overline{f}^{13}\right] = \left[\mu_{\underline{X}_{12}}(x_1).\mu_{\underline{X}_{21}}(x_2).\mu_{\underline{X}_{31}}(x_3).\mu_{\underline{X}_{41}}(x_4), \mu_{\overline{X}_{12}}(x_1).\mu_{\overline{X}_{21}}(x_2).\mu_{\overline{X}_{31}}(x_3).\mu_{\overline{X}_{41}}(x_4)\right]$ $= [0.46 \times 0.47 \times 0.49 \times 0.05, 0.12 \times 0.13 \times 0.81 \times 0.4]$ $= [0.0053, 0.005]$	$\left[\underline{y}^{13}, \overline{y}^{13}\right] = [0.75, 0.9]$
R14	$\left[\underline{f}^{14}, \overline{f}^{14}\right] = \left[\mu_{\underline{X}_{12}}(x_1).\mu_{\underline{X}_{22}}(x_2).\mu_{\underline{X}_{31}}(x_3).\mu_{\underline{X}_{41}}(x_4), \mu_{\overline{X}_{12}}(x_1).\mu_{\overline{X}_{22}}(x_2).\mu_{\overline{X}_{31}}(x_3).\mu_{\overline{X}_{41}}(x_4)\right]$ $= [0.46 \times 0.53 \times 0.49 \times 0.05, 0.12 \times 0.87 \times 0.81 \times 0.4]$ $= [0.006, 0.034]$	$\left[\underline{y}^{14}, \overline{y}^{14}\right] = [0.8, 0.92]$

(continued)

Table 2 (continued)

Rule No.	Firing interval	Consequent
R15	$\left[\underline{f}^{15}, \overline{f}^{15}\right] = \left[\mu_{\underline{X}_{12}}(x_1).\mu_{\underline{X}_{22}}(x_2).\mu_{\underline{X}_{32}}(x_3).\mu_{\underline{X}_{41}}(x_4), \mu_{\overline{X}_{12}}(x_1).\mu_{\overline{X}_{22}}(x_2).\mu_{\overline{X}_{32}}(x_3).\mu_{\overline{X}_{41}}(x_4)\right]$ $= [0.46 \times 0.53 \times 0.2 \times 0.05, 0.12 \times 0.87 \times 0.52 \times 0.4]$ $= [0.00244, 0.022]$	$\left[\underline{y}^{15}, \overline{y}^{15}\right] = [0.85, 0.95]$
R16	$\left[\underline{f}^{16}, \overline{f}^{16}\right] = \left[\mu_{\underline{X}_{12}}(x_1).\mu_{\underline{X}_{22}}(x_2).\mu_{\underline{X}_{32}}(x_3).\mu_{\underline{X}_{42}}(x_4), \mu_{\overline{X}_{12}}(x_1).\mu_{\overline{X}_{22}}(x_2).\mu_{\overline{X}_{32}}(x_3).\mu_{\overline{X}_{42}}(x_4)\right]$ $= [0.46 \times 0.53 \times 0.2 \times 0.6, 0.12 \times 0.87 \times 0.52 \times 0.93]$ $= [0.029, 0.05]$	$\left[\underline{y}^{16}, \overline{y}^{16}\right] = [0.88, 1]$

$$y_l = \frac{\begin{array}{c}\overline{f}^1\underline{y}^1 + \overline{f}^2\underline{y}^2 + \underline{f}^3\underline{y}^3 + \underline{f}^4\underline{y}^4 + \underline{f}^5\underline{y}^5 + \underline{f}^6\underline{y}^6 + \underline{f}^7\underline{y}^7 + \underline{f}^8\underline{y}^8 + \underline{f}^9\underline{y}^9 \\ + \underline{f}^{10}\underline{y}^{10} + \underline{f}^{11}\underline{y}^{11} + \underline{f}^{12}\underline{y}^{12} + \underline{f}^{13}\underline{y}^{13} + \underline{f}^{14}\underline{y}^{14} + \underline{f}^{15}\underline{y}^{15} + \underline{f}^{16}\underline{y}^{16}\end{array}}{\begin{array}{c}\overline{f}^1 + \overline{f}^2 + \underline{f}^3 + \underline{f}^4 + \underline{f}^5 + \underline{f}^{16} + \underline{f}^6 + \underline{f}^7 + \underline{f}^8 \\ + \underline{f}^{10} + \underline{f}^{11} + \underline{f}^{12} + \underline{f}^{13} + \underline{f}^{14} + \underline{f}^{15} + \underline{f}^{16}\end{array}}$$

$$= \frac{\begin{array}{l}0.036 \times 0 + 0.242 \times 0.09 + 0.0028 \times 0.15 + 0.0086 \times 0.2 + 0.0746 \times 0.35 \\ + 0.00254 \times 0.4 + 0.030 \times 0.45 + 0.0841 \times 0.55 + 0.0635 \times 0.6 \\ + 0.0022 \times 0.65 + 0.026 \times 0.7 + 0.0935 \times 0.73 + 0.0053 \times 0.75 \\ + 0.006 \times 0.8 + 0.00244 \times 0.85 + 0.029 \times 0.88\end{array}}{\begin{array}{l}0.036 + 0.242 + 0.0028 + 0.0086 + 0.0746 + 0.00254 + 0.030 + 0.0841 \\ + 0.0635 + 0.0022 + 0.026 + 0.0935 + 0.0053 + 0.006 + 0.00244 + 0.029\end{array}}$$

$$= \frac{0.27316}{0.57234} = 0.47726$$

$$y_r = \frac{\begin{array}{c}\underline{f}^1\overline{y}^1 + \underline{f}^2\overline{y}^2 + \underline{f}^3\overline{y}^3 + \underline{f}^4\overline{y}^4 + \underline{f}^5\overline{y}^5 + \underline{f}^6\overline{y}^6 + \underline{f}^7\overline{y}^7 + \underline{f}^8\overline{y}^8 + \underline{f}^9\overline{y}^9 \\ + \underline{f}^{10}\overline{y}^{10} + \underline{f}^{11}\overline{y}^{11} + \underline{f}^{12}\overline{y}^{12} + \underline{f}^{13}\overline{y}^{13} + \underline{f}^{14}\overline{y}^{14} + \overline{f}^{15}\overline{y}^{15} + \overline{f}^{16}\overline{y}^{16}\end{array}}{\begin{array}{c}\underline{f}^1 + \underline{f}^2 + \underline{f}^3 + \underline{f}^4 + \underline{f}^5 + \underline{f}^6 + \underline{f}^7 + \underline{f}^8 + \underline{f}^9 \\ + \underline{f}^{10} + \underline{f}^{11} + \underline{f}^{12} + \underline{f}^{13} + \underline{f}^{14} + \overline{f}^{15} + \overline{f}^{16}\end{array}}$$

$$= \frac{\begin{array}{l}0.0062 \times 0.07 + 0.007 \times 0.17 + 0.0028 \times 0.3 + 0.0086 \times 0.4 + 0.0746 \times 0.5 \\ + 0.00254 \times 0.6 + 0.030 \times 0.65 + 0.0841 \times 0.7 + 0.0635 \times 0.85 \\ + 0.0022 \times 0.83 + 0.026 \times 0.8 + 0.0935 \times 0.88 + 0.0053 \times 0.9 \\ + 0.006 \times 0.92 + 0.022 \times 0.95 + 0.05 \times 1\end{array}}{\begin{array}{l}0.0062 + 0.007 + 0.0028 + 0.0086 + 0.0746 + 0.00254 + 0.030 + 0.0841 \\ + 0.0635 + 0.0022 + 0.026 + 0.0935 + 0.0053 + 0.006 + 0.022 + 0.05\end{array}}$$

$$= \frac{0.3613}{0.48434} = 0.746$$

Finally, the crisp outcome will be

$$y = \frac{y_l + y_r}{2} = \frac{0.47726 + 0.746}{2} = 0.6116$$

The pictorial representation of estimation of bearing capacity of stone column due to some uncertainties is ellaborated in Fig. 3 in form of flowchart. The uncertainties of different input parameters and the interval of membership functions were considered separately. Firing intervals were calculated separately for every rulebase and type reduction method was applied to combine the firing intervals with the corresponding rule consequents. By using KM algorithm, the ranges (upper and lower limits) of the consequents were evaluated. Figure 4 shows the output versus target graph obtained

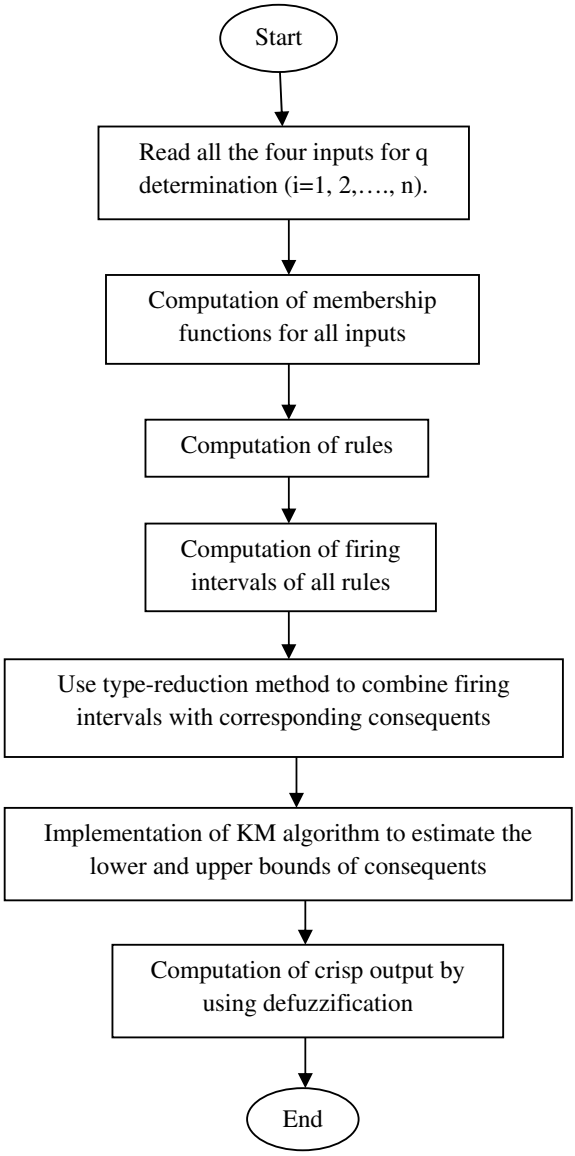

Fig. 3 Flowchart to predict the bearing capacity of stone columns

from IT2FLS, which reflects a very good matching between the output and target data with a high magnitude of coefficient of correlation, R = 0.9986.

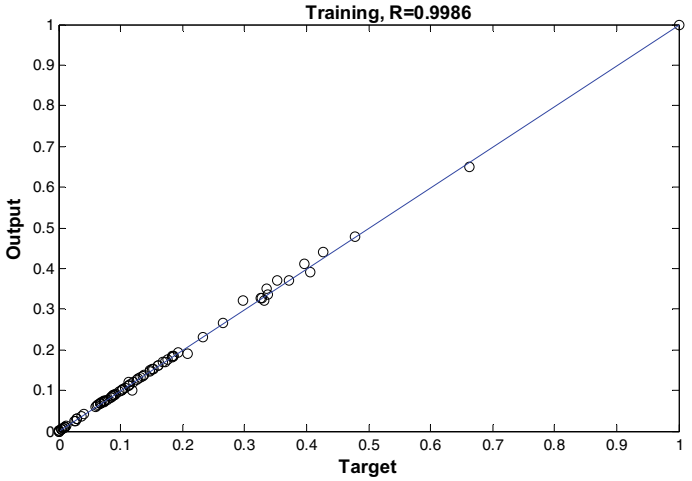

Fig. 4 Output versus target graph obtained from type-2 fuzzy set

5 Formation of ANN

The collected dataset used in this study was split into three sections i.e. training, testing and validation data. The network was generated with the training data, and the trained model was verified with the testing and validation data. In the present study, LM algorithm was utilised for q_u prediction because the network performed the best with this algorithm comparing to other algorithms (Kostic 2015). The description of the ANN results are shown in tabular form (Table 3).

To construct the ANN model, two validation techniques were used i.e. tenfold cross validation technique (TFCV) and non-cross validation technique (NCV). In TFCV model, 90% of the total dataset were utilised as training data and the remaining 10% were utilised as testing data. In NCV model, 70% of the total dataset were utilised as training data and 30% were used as testing data.

The number of hidden neurons was chosen by using trial and error method to achieve the best result. Figure 5 reflects a very good matching between the output network versus training of both TFCV and NCV models. But if we compare the results, the better prediction of TFCV model can be noticed. From Table 4, it is noticed

Table 3 Analysis of ANN models

ANN models	Algorithm	R	RMSE	MAPE	No. of hidden neurons
$q_{90\text{-}10}$	Training	0.95472	1.612	5.0796	11
	Testing	0.95235	1.892	5.235	11
$q_{70\text{-}30}$	Training	0.94846	2.53	6.7131	7
	Testing	0.932	2.65	6.754	7

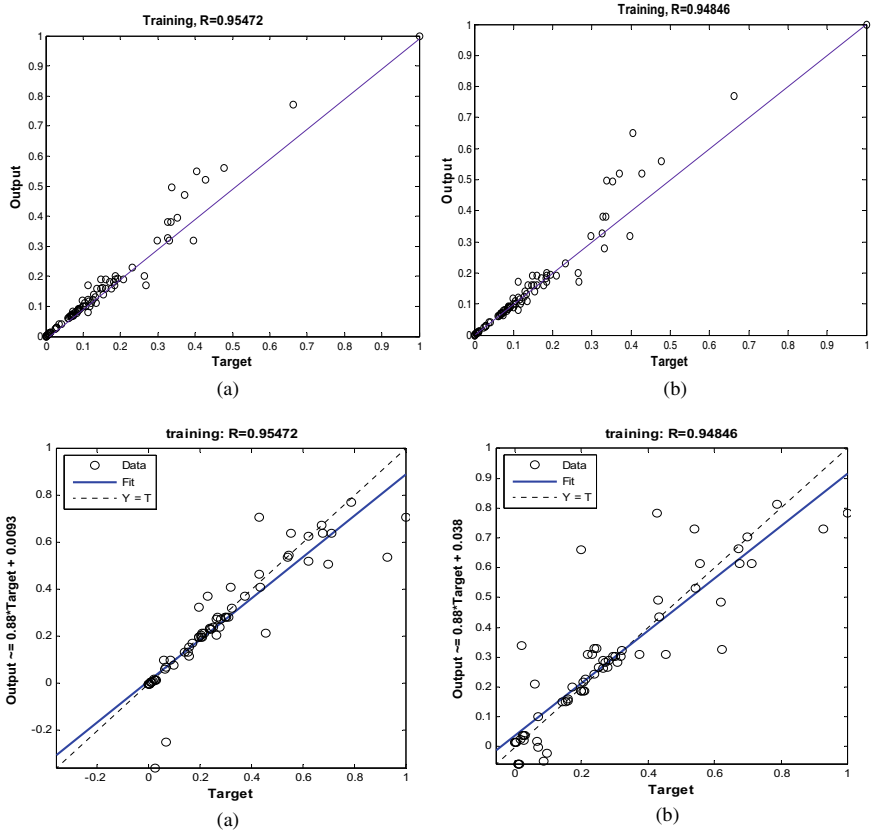

Fig. 5 BPN network output versus training of **a** TFCV (tenfold cross validation) model and **b** NCV (non-cross validation) model for the algorithms LM

Table 4 Error analysis of all the three models

Prediction methods	R	RMSE	MAPE
Type-2 fuzzy model	0.9986	0.884	3.052
Type-1 fuzzy model	0.9133	2.11	4.9735
ANFIS model	0.9643	1.273	4.4881
ANN model	0.95472	1.612	5.0796

that the TFCV model shows the best result because it shows the smallest magnitudes of MAPE, VARE, and MEDAE as compared to $q_{70\text{-}30}$ (non-cross validation) model. Chik et al. (2014), Chik and Aljanabi (2014) also obtained the better result in case of TFCV model than that of NCV model.

6 Formation of ANFIS

ANFIS combines the behavior of both the neural-network and fuzzy logic. To predict q_u, ANFIS was used in the present study. ANFIS includes the advantages of both the system i.e. reasoning power of the fuzzy system and learning power of the neural network. To construct the ANFIS model, the neuro-fuzzy toolbox available in matlab 2013a was used in this study.

Actually, the fuzzy logic, is a method of mapping from a known input to an unknown output, which has the ability of decision making of the fuzzy logic. Fuzzy logic has the capability to classify any kind of data. Generally a fuzzy system consists of five portions such as (i) fuzzification of the input parameter; (ii) utilization of the fuzzy operator (OR or AND) in the antecedent; (iii) implication from the antecedent to the consequent; (iv) accumulation of the consequents over the rules; and (v) defuzzification.

Fuzzification means the procedure by which the input variables are transformed into the linguistic variables. Clustering of the data is a way to generate the rule. Normally meaning of clustering is to split the output data into a number of some fuzzy partitions. By considering the multi-input, single output system, the number of clusters is decided such that the sum of the Euclidian distance of the output data from the cluster center should be minimum. Then, conjunction or a combination of these if–then rules was performed, which is called inferencing method. In defuzzification, the fuzzified output value was converted into a crisp output value. The conjunction operation is conducted by either min or product operation (dot operation). Here, for both the input and outputs, trapezoidal membership functions were considered. ANN is normally inspired by the human brain. It has the capability to learn to store memory and to apply the past experience. In this study, to build the ANFIS model, 90% of the total dataset were utilised as training data and remaining 10% were utilised as testing and validation data. After finishing the training for the model, the trained data were recollected again to verify the trained ANFIS models. The relation between target values and output values is presented in Fig. 6.

7 Comparative Study and Error Analysis

The performance of all these four models i.e. IT2FLS, type-1 fuzzy system, ANN and ANFIS were discussed by using three statistical parameters i.e. R, RMSE and MAPE.

From Table 4, it is seen that type-2 fuzzy model shows the highest R value which is larger than the values obtained from ANN and ANFIS models. In terms of R value, the type-2 fuzzy model shows 8.54, 4.4 and 3.43% improvement than type-1 fuzzy, ANN and ANFIS model respectively. Similarly, in terms of RMSE value, the type-2 fuzzy model shows 58.1, 45.16 and 30.6% improvement than type-1 fuzzy, ANN and ANFIS model respectively. For MAPE value also, type-2 fuzzy model shows least

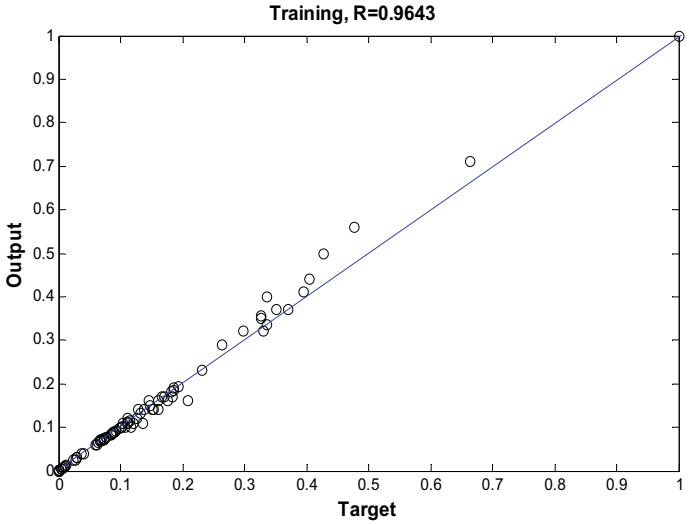

Fig. 6 Output versus target graph obtained from adaptive neuro-fuzzy system

value, as it shows improvement of 38.63%, 40% and 32% over type-1 fuzzy, ANN and ANFIS model respectively.

8 Sensitivity Analysis of the Input Parameters Corresponding to Output Obtained from IT2FLS

In the present study, four input parameters were taken into account to achieve the output q_u. Normally, q_u is affected by all these four input parameters, but among all the four parameters, one should have the strongest effect on the bearing capacity, q_u. Hence, to obtain the parameter which has the highest effect on q_u, a sensitivity analysis was performed. Sensitivity is defined as the amount of variation in output for unit increase in input. In this study, the changes in output parameters were observed by increasing the input parameters by one unit. The sensitivity analysis was conducted in matlab 2013. The sensitivity analysis of each input parameter is shown in Fig. 6.

From Fig. 7, it can be concluded that the third variable i.e. friction angle (ϕ) has the strongest effects on q_u among all other parameters. The spacing to diameter ratio (s/d) shows the second highest effect on q_u. The parameter, length (l) of the column has a negligible effect on q_u. Chik and Aljanabi (2014) also obtained the friction angle, ϕ as the most affecting parameter on the settlement of stone column by using ANN model.

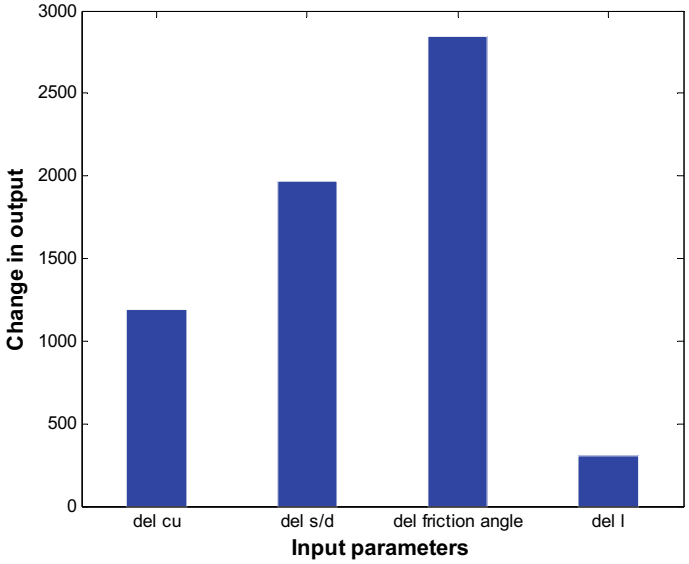

Fig. 7 Sensitivity analysis of each input data

9 Conclusions

In this present work, 102 data were accumulated from previous literatures which were from various places and various weather conditions. These data were used in predicting q_u by constructing IT2FLS model. The performance, feasibility and accuracy of all the IT2FLS model was observed in this research.

The validation of this model has been executed by using T1FS, ANN, and ANFIS with the same dataset. Result shows the superiority of the IT2FLS model than other three models.

The superiority of the model was checked by regression correlation coefficient (R) value and error analysis with RMSE and MAPE. The proposed IT2FLS model achieve 8.54%, 4.4% and 3.43% improvement than type-1 fuzzy, ANN and ANFIS model respectively in terms of R value. From error analysis, it is noticed that in terms of RMSE value, IT2FLS model achieve 58.1, 45.16 and 30.6% improvement over type-1 fuzzy, ANN and ANFIS model respectively. For MAPE value also, IT2FLS model shows least value, as it shows improvement of 38.63%, 40% and 32% over type-1 fuzzy, ANN and ANFIS model respectively.

From the result of the sensitivity analysis, the friction angle (ϕ) of stone column materials was obtained as the most influencing parameter and the length (l) of the stone column was obtained as least effective parameter in the determination of q_u.

Introduce any new data in the IT2FLS model will not create any problem as it has the capability to handle uncertainties and the prediction will give effective, consistent and stable results. Without any extra computational cost the proposed IT2FLS model

gives not only the target values but also the prediction intervals of q_u. Although case studies would be required for the further validation of the model, but the applicability of the proposed model is presented in this study. This model will be beneficial for all the geotechnical engineers as this is a really interesting and useful work because the use of intervals is more important to describe the opinions of more number of experts, so intervals of any prediction value are more realistic.

References

Afshar JN, Ghazavi M (2014a) A simple analytical method for calculation of bearing capacity of stone column. Int J Civil Eng 12(1)

Afshar JN, Ghazavi M (2014b) Experimental studies on bearing capacity of geosynthetic reinforced stone columns. Arab J Sci Eng 39:1559–1571. https://doi.org/10.1007/s13369-013-0709-8

Ambily AP, Gandhi SR (2004) Experimental and theoretical evaluation of stone column in soft clay. In: ICGGE

Andreou P, Papadopoulos V (2014) Factors affecting the settlement estimation of stone column reinforced soils. Geotech Geol Eng 32:1175–1185. https://doi.org/10.1007/s10706-014-9788-x

Ayyub BM (1991) Systems framework for fuzzy sets in civil engineering. Fuzzy Sets Syst 40:491–508

Balaam NP, Booker JR (1981) (1981), Analysis of rigid rafts supported by granular piles. Int J Numer Anal Meth Geomech 5:379–403

Bowels JE (1996) Foundation analysis and design, 5th edn. McGraw-Hill Book Company, p 1175

Castro J (2014) An analytical solution for the settlement of stone columns beneath rigid footings. ActaGeotechnica.https://doi.org/10.1007/s11440-014-0358-4

Castro J, Sagaseta C (2009) Consolidation around stone columns: influence of column deformation. Int J Numer Anal Meth Geomech 33:851–877. https://doi.org/10.1002/nag.745

Chik Z, Aljanabi QA (2014) Intelligent prediction of settlement ratio for soft clay with stone columns using embankment improvement techniques. Neural Comput Appl 25:73–82. https://doi.org/10.1007/s00521-013-1449-0

Chik Z, Aljanabi QA, Kasa A, Taha MR (2014) Tenfold cross validation artificial neural network modeling of the settlement behavior of a stone column under a highway embankment. Arab J Geosci 7:4877–4887. https://doi.org/10.1007/s12517-013-1128-6

Colas AS, Morel JC, Garnier D (2008) Yield design of dry-stone masonry retaining structures—comparisons with analytical, numerical, and experimental data. Int J Numer Anal Meth Geomech 32:1817–1832. https://doi.org/10.1002/nag.697

Cox E (1993) Adaptive fuzzy systems. IEEE Spectrum

Das M, Dey AK (2018a) Determination of bearing capacity of stone column with application of neuro-fuzzy system. KSCE J Civil Eng:1–7

Das M, Dey AK (2018b) Prediction of bearing capacity of stone columns placed in soft clay using ANN model. Geotech Geol Eng 36(3):1845–1861

Das M, Dey AK (2019) Modelling stone columns under a soil-cement bed using an artificial neural network. In: Proceedings of the institution of civil engineers—ground improvement.https://doi.org/10.1680/jgrim.18.00092

Dasaka SM, Jain A, Kolekar YA (2014) Effect of uncertainties in the field load testing on the observed load–settlement response. Indian Geotech J 44(3):294–304. https://doi.org/10.1007/s40098-013-0083-1

Deb K (2008) Modeling of granular bed-stone column-improved soft soil. Int J Numer Anal Meth Geomech 32:1267–1288. https://doi.org/10.1002/nag.672

Dodagoudar GR, Venkatachalam G (2000) Reliability analysis of slopes using fuzzy sets theory. Comput Geotech 27(2000):101–115
Dubois D, Prade H (1982) Fuzzy sets and systems: theory and applications. Academic Press
Etezad M (2007) Geotechnical performance of group of stone columns, a Ph.D. thesis
Etezad M, Hanna AM, Ayadat T (2015) Bearing capacity of a group of stone columns in soft soil. Int J Geomech ASCE 2015. ISSN 1532-3641/04014043(15)
Fattah MY, Al-Neami MA, Al-Suhaily AS (2017) Estimation of bearing capacity of floating group of stone columns. Eng Sci Technol Int J. https://doi.org/10.1016/j.jestch.2017.03.005
Golait YS, Satyanarayana V, Raju SSV (2009) Concept of under reamed cemented stone columns for soft clay ground improvement. In: IGC 2009, Guntur, India
Golakiya HD, Lad MD (2015) Ground improvement by using stone columns. JETIR 2(11). (ISSN-2349-5162)
Hassen G, Buhan PD, Abdelkrim M (2010) Finite element implementation of a homogenized constitutive law for stone column-reinforced foundation soils, with application to the design of structures. Comput Geotech 37(2010):40–49
Horikawa S, Furahashi T, Uchikawa Y (1992) On fuzzy modeling using fuzzy neural networks with back-propagation algorithm. IEEE Trans Neural Netw 3:801–806
IS 15284-1(2003) Design and construction for ground improvement-guidelines. In: Part-1: Stone columns [CED 43: Soil and foundation engineering], ICS 93.020
Jang JSR (1992) Self-learning fuzzy controllers based on temporal back-propagation. IEEE Trans Neural Netw 3:714–723
Jang JSR (1993) ANFIS: adaptive-network-based fuzzy inference system. IEEE Trans Syst Man Cybern 23(3)
Jellali BM, Bouassida PD, Buhan (2011) Stability analysis of an embankment resting upon a column-reinforced soil. Int J Numer Anal Meth Geomech 35:1243–1256. https://doi.org/10.1002/nag.954
Kostic S, Vasovic D (2015) Prediction model for compressive strength of basic concrete mixture using artificial neural networks. Neural Comput Appl 26:1005–1024. https://doi.org/10.1007/s00521-014-1763-1
Lee JS, Pande GN (1998) Analysis of stone-column reinforced foundations. Int J Numer Anal Meth Geomech 22:1001–1020
Liu F, Mendel JM (2008) Encoding words into interval type-2 fuzzy sets using an interval approach. IEEE Trans Fuzzy Syst 16(6):1503–1521
Malarvizhi SN, Ilampurthi K (2007) Comparative study on the behavior of encased stone column and conventional stone column. Soils Found Jpn Geotech Soc 47(5):873–885
Mendel JM (2001) Uncertain rule-based fuzzy logic systems: introduction and new directions. Prentice-Hall
Mendel JM, Wu D (2010) Perceptual computing: aiding people in making subjective judgments. Wiley-IEEE Press, Hoboken, NJ
Mitra R, Goswami AK, Tiwari PK (2017) Voltage sag assessment using type-2 fuzzy system considering uncertainties in distribution system. IET Gener Transm Distrib. https://doi.org/10.1049/iet-gtd.2016.0816
Mohanty P, Samanta M (2015) Experimental and numerical studies on response of the stone column in layered soil. Int J Geosynth Ground Eng 1:27. https://doi.org/10.1007/s40891-015-0029-z
Murugesan S, Rajagopal K (2008) Performance of encased stone columns and design guidelines for construction on soft clay soils. In: Proceedings of the 4th Asian regional conference on geosynthetics, June 17–20, 2008 Shanghai, China
Olatunji SO, Selamat A, Abdulraheem A (2011) Modeling the permeability of carbonate reservoir using type-2 fuzzy logic systems. Comput Ind 62:147–163. https://doi.org/10.1016/j.compind.2010.10.008
Poorooshasb HB, Meyerhof GG (1997) Analysis of behavior of stone columns and lime columns. Comput Geotech 20(1), 47–70
Rethati L (1988) Probabilistic solutions in geotechnics, 451. Elsevier Amsterdam

Shien NK (2013) Numerical study of floating stone column. A thesis submitted for The Degree of Doctor of Philosophy, Department of Civil and Environmental Engineering, National University of Singapore

Valliappan S, Pham TD (1993) Fuzzy finite element analysis of a foundation on an elastic soil medium. Int J Numer Anal Meth Geomech 17:771–789

Wang LX, Mendel JM (1992) Fuzzy basis functions, universal approximation, and orthogonal least-squares learning. IEEE Trans Neural Netw 3:807–813

Wu D (2014)A brief tutorial on interval type-2 fuzzy sets and systems, July 10, 2014

Wu D, Mendel JM (2009) Enhanced Karnik-Mendel algorithms. IEEE Trans Fuzzy Syst 17(4):923–934

Xie KH, Lu MM, Liu GB (2009) Equal strain consolidation for stone columns reinforced foundation. Int J Numer Anal Meth Geomech 33:1721–1735. https://doi.org/10.1002/nag.790

Zadeh LA (1965) Fuzzy sets. Inf Control 8:338–353

Zadeh LA (1975) The concept of a linguistic variable and its application to approximate reasoning-1. Inf Sci 8(4):199–249

Zhang L, Zhao M, Shi C, Zhao H (2013) Settlement calculation of composite foundation reinforced with stone columns. Int J Geomech 13(3):248–256. https://doi.org/10.1061/(ASCE)GM.1943-5622.0000212

Seepage Analysis from an Array of Parallel Triangular Furrows by Inverse Hodograph and Conformal Mapping Technique

Kshyana Prava Samal and G. C. Mishra

Abstract Furrow irrigation is suitable for a wide range of crops. The shape, length and spacing of the furrows are determined by the natural factors, i.e. slope, soil type and available stream size. However, other factors also influence the design of a furrow system, such as the irrigation depth, type of crop and the seepage loss from the furrow. In furrow irrigation, water is conveyed in small channels or furrows. In this case the suitability of furrow irrigation has been clearly checked for shallow rooted, moderately deep rooted crops and deep rooted crops by analyzing the seepage flow from the furrow. The analysis has been done from an array of triangular furrows using inverse hodograph and conformal mapping techinique. The loci of the phreatic lines in the furrow ridge have been found for various side slopes. For a given furrow spacing, variation of the depth of saturation front at the middle of the furrow ridge for different side slopes (i.e. for m = 0.5, 1, 1.5 and 2) of the furrows has been calculated. Here in the analysis the spacing has been properly verified for shallow rooted, moderately deep rooted and deep rooted crops. The spacing of the furrows should be such that, at the middle of the ridge, the sum of depth of saturation and free board less than about 1/4th of the root zone depth (R_d), so that the plant can get proper amount of water which has been properly verified in this analysis. (ii) The suitability of furrow spacing obtained from conformal mapping technique has been verified by published secondary data.

Keywords Seepage · Furrow irrigation · Spacing of furrows · Phreatic line · Conformal mapping

K. P. Samal (✉)
School of Civil Engineering, KIIT Deemed To Be University, Bhubaneswar, India
e-mail: kshyanaprava.samalfce@kiit.ac.in

G. C. Mishra
Water Resources Development and Management, IITR, Roorkee, UK

B. B. Das et al. (eds.), *Recent Developments in Sustainable Infrastructure (ICRDSI-2020)—GEO-TRA-ENV-WRM*, Lecture Notes in Civil Engineering 207,
https://doi.org/10.1007/978-981-16-7509-6_34

Notation

The following symbols are used in this paper:

B (.,.)	Complete beta function
f_b	Free board (L)
k	Hydraulic conductivity (L/T)
L_f	Furrow spacing (L)
m	Side slope of the furrow
Q	Seepage loss per unit length (L^2/T)
Q_0	Seepage per unit length loss from a (L^2/T), non interfering furrow
R_d	Root zone depth (L)
t	Parametric plane
w	$\phi + I\psi$ complex potential
z	x + iy, complex variable

1 Introduction

Furrow irrigation is suitable for mostly for all crops. In furrow irrigation, water is conveyed in small channels or furrows. From field study, it is reported that, about half of the water delivered in the channel or a furrow gets lost as seepage and other losses (Carter 1985). Furrow irrigation has lower application efficiency in comparison to drip irrigation (Tiwari et al. 1998). The obvious reasons for lower efficiency are: (i) excess seepage losses as irrigation water is conveyed in the furrows for a duration more than required and (ii) inappropriate furrow spacing. Close spacing of the furrows leads to unwise use of land resources where as wide spacing leads to non availability of irrigation water to crops grown in the central part of the furrow ridge. There is a need to find the appropriate spacing of the furrows. The spacing of furrows is influenced by the soil type and the cultivation practice. In general, furrows should be spaced quite close so that water can spread laterally to sides into the land between the two successive furrows to replenish the soil moisture in the root zone of crops. As a rule, for sandy soils the spacing should be between 30 and 60 cm. On clayey soils, the spacing between two adjacent furrows should be 75–150 cm (Michael 1999; Brouwer et al. 1990). On clayey soils, double-ridged furrows, sometimes called beds, can also be used. Their advantage is that more plant rows are possible on each ridge, facilitating manual weeding. Depth of irrigation needed, is related to the water holding capacity of the soil and depth of rooting of the crop. In clays the depth of irrigation ranges from 7.5 to 15 cm, in loams the depth varies from 5 to 10 cm and in sands the depth is 5, 7.5 and 10 cm (Michael 1999).

Solutions for seepage from parallel triangular and rectangular canals in a soil layer of finite as well as of infinite thickness have been presented by Bruch and

Street (1967), and Choudhary and Chahar (2007). The Dirichlet boundary condition has been assumed to prevail at the interface of the finite soil layer and an underlying highly pervious draining layer. In this paper, an analysis is presented for seepage from parallel triangular furrows assuming the porous medium to be of infinite depth and Neumann boundary condition prevailing at infinity. In case of interfering furrows, the Neumann type of boundary condition implies that the seepage from a single furrow in parallel furrows system is hydraulic conductivity times the furrow spacing irrespective of shape of the furrow section by Samal and Mishra (2016, 2019). Only locus of the phreatic line is unknown a priori. Inverse hodograph method suitable for solving unconfined flow problems has been used to find the locus of the phreatic line. Vedernikov (1940) (vide. Polubarinova-Kochina 1962) has solved seepage from a single triangular canal in a porous medium of infinite depth for Neumann boundary condition prevailing at infinity.

2 Statement of the Problem

An array of parallel triangular furrows at distance L_f apart is shown in Fig. 1a. The porous medium is of infinite depth having hydraulic conductivity k. The depth of water in a furrow is H; top width of a furrow is 2H cot($\alpha\pi$) and the sides of the furrows make an angle $\alpha\pi$ with the horizontal. D is the point of inflection on the phreatic line. It is aimed to find the locus of the phreatic line.

3 Mapping of the One Half of the Inverse Hodograph (Dz/dw) Plane onto Auxiliary t-plane

The hodograph and the inverse hodograph planes pertaining to one half of the symmetrical flow domain of one of the furrows are shown in Fig. 1b, d. The conformal mapping of the inverse hodograph plane to the lower half of the auxiliary t-plane shown in Fig. 1f is given by

$$\frac{dz}{dw} = M_1 \int_0^t \frac{(\delta - \tau)d\tau}{\tau^{1-\alpha}(1-\tau)^{1-(\frac{1}{2}-\alpha)}} + N_1 \tag{1}$$

the vertices B, C, D being mapped onto 0, 1, and δ respectively on the real axis of the t-plane.

For the vertex 'B', t = 0, and $\frac{dz}{dw} = 0$; hence, the constant $N_1 = 0$. The constant N_1 is governed by the lower limit of integration.

For $0 \leq t \leq 1$,

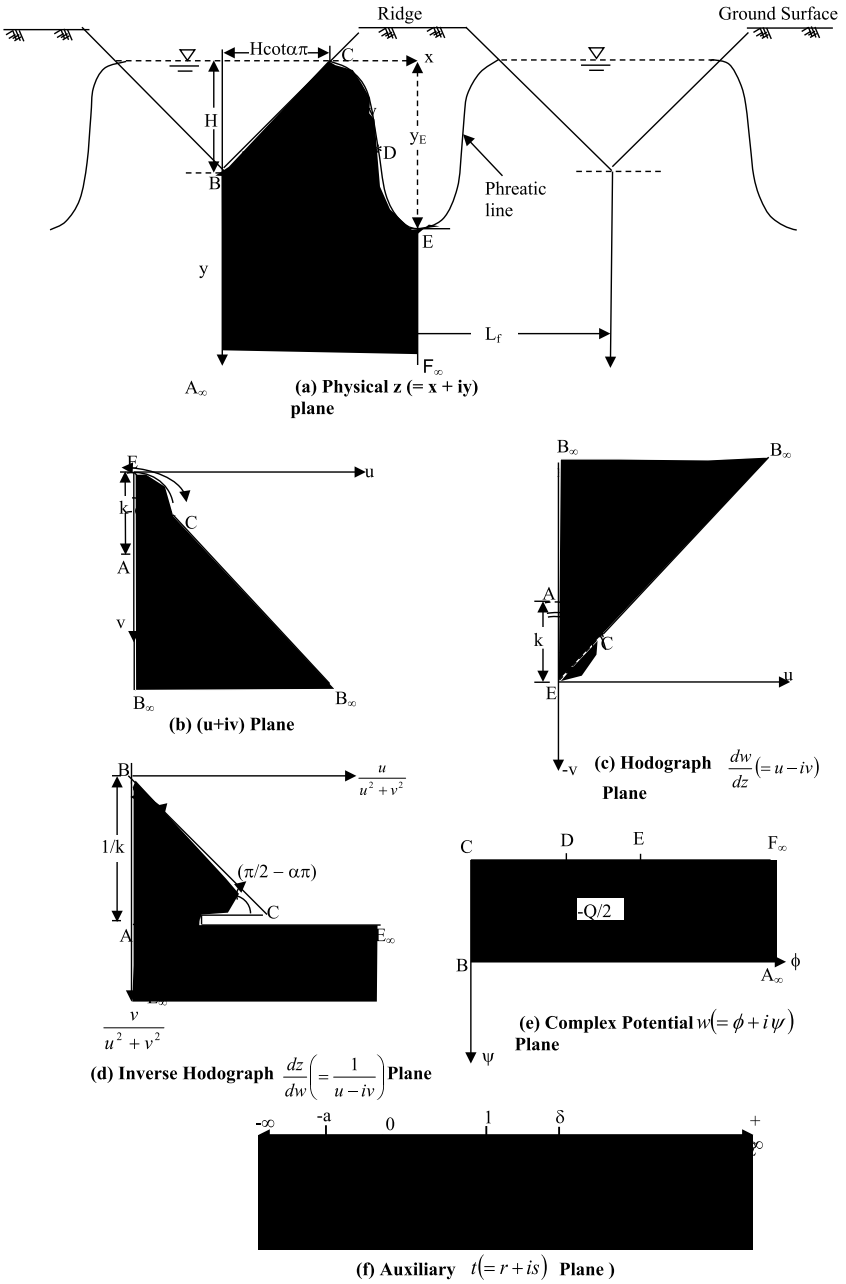

Fig. 1 Steps of conformal mapping for seepage analysis for an array of triangular furrows in soils without capillarity

$$\frac{dz}{dw} = M_1 \int_0^t \frac{(\delta - \tau)d\tau}{\tau^{1-\alpha}(1-\tau)^{1-(\frac{1}{2}-\alpha)}}$$

$$= M_1 \left\{ \delta \, \mathrm{B_t}\left(\alpha, \frac{1}{2} - \alpha\right) - B_t\left(1 + \alpha, \frac{1}{2} - \alpha\right) \right\} \tag{2}$$

where $\mathrm{B_t}\left(\alpha, \frac{1}{2} - \alpha\right)$, $B_t\left(1 + \alpha, \frac{1}{2} - \alpha\right)$ are incomplete beta functions.

For vertex 'C', t = 1 and $\frac{dz}{dw} = \frac{1}{k}\sec(\alpha\pi)\, \mathrm{e}^{\mathrm{i}\pi(\frac{1}{2}-\alpha)}$.

Incorporating this condition in (2)

$$\frac{1}{k}\sec(\alpha\pi)\, e^{i\pi(\frac{1}{2}-\alpha)} = M_1 \left\{ \delta \, B\left(\alpha, \frac{1}{2} - \alpha\right) - B\left(1 + \alpha, \frac{1}{2} - \alpha\right) \right\} \tag{3}$$

Solving for M_1,

$$M_1 = \frac{\frac{1}{k}\sec(\alpha\pi)\,.\,\mathrm{e}^{\mathrm{i}\pi(\frac{1}{2}-\alpha)}}{\delta\, \mathrm{B}\left(\alpha, \frac{1}{2} - \alpha\right) - B\left(1 + \alpha, \frac{1}{2} - \alpha\right)} \tag{4}$$

where $\mathrm{B}\left(\alpha, \frac{1}{2} - \alpha\right)$, $B\left(1 + \alpha, \frac{1}{2} - \alpha\right)$ are complete beta functions.

4 Mapping of the Dz/dw Plane onto the Auxiliary t-plane; $-\infty \le t \le 0$

$$\frac{dz}{dw} = M_1 \int_0^t \frac{(-1)^{1-\alpha}(\delta - \tau)}{(-\tau)^{1-\alpha}(1-\tau)^{1-(\frac{1}{2}-\alpha)}} d\tau \tag{5}$$

For points A_∞ and F_∞ t = −a and $\frac{\mathrm{dz}}{\mathrm{dw}} = \frac{i}{k}$. Incorporating this condition in (5)

$$\frac{i}{k} = M_1(-1)^{1-\alpha} \int_0^{-a} \frac{(\delta - \tau)}{(-\tau)^{1-\alpha}(1-\tau)^{1-(\frac{1}{2}-\alpha)}} d\tau \tag{6a}$$

Substituting $\tau = -\xi$, $\mathrm{d}\tau = -\mathrm{d}\xi$ in (6a)

$$\frac{i}{k} = -M_1(-1)^{1-\alpha} \int_0^a \frac{(\delta + \xi)}{(\xi)^{1-\alpha}(1+\xi)^{1-(\frac{1}{2}-\alpha)}} d\xi = -M_1(-1)^{1-\alpha}\, \mathrm{I_1} \tag{6b}$$

($\mathrm{I_1}$ is evaluated in Appendix 1).

Incorporating M_1 in (6b).

$$\frac{i}{k} = \frac{(-1)^{\frac{1}{k}} \sec(\alpha\pi)}{\delta\, B\left(\alpha, \frac{1}{2} - \alpha\right) - B\left(1 + \alpha, \frac{1}{2} - \alpha\right)} e^{i\pi\left(\frac{1}{2} - \alpha\right)} e^{-i\pi(1-\alpha)} I_1 \tag{6c}$$

Simplification leads to

$$\frac{\sec(\alpha\pi)}{\delta\, B\left(\alpha, \frac{1}{2} - \alpha\right) - B\left(1 + \alpha, \frac{1}{2} - \alpha\right)} I_1 = 1 \tag{7}$$

I_1 is a function of unknown a and δ.

5 Mapping of the Complex Potential w-Plane onto the Auxiliary t-plane

The mapping of the w-plane shown in Fig. 1e onto the lower half of the t plane is given by

$$\frac{dw}{dt} = \frac{M_2}{t^{1/2}(1-t)^{1/2}(t+a)} \tag{8}$$

Integrating,

$$w = M_2 \int_0^{t'} \frac{dt}{t^{1/2}(1-t)^{1/2}(t+a)} + N_2 \tag{9}$$

Corresponding to vertex 'B', w = 0 and t = 0. Hence, constant $N_2 = 0$.
For vertex 'C', t = 1 and $w = -\frac{iQ}{2}$. Incorporating this condition in (9)

$$\frac{-iQ}{2} = M_2 \int_0^1 \frac{dt}{t^{1/2}(1-t)^{1/2}(t+a)} = M_2 I_2 \tag{10}$$

where $I_2 = \int_0^1 \frac{dt}{t^{1/2}(1-t)^{1/2}(t+a)} = \frac{\pi}{\sqrt{a(1+a)}}$. I_2 is evaluated in Appendix 2.
From (10), constant M_2 is given by

$$M_2 = \frac{-iQ}{2I_2} = \frac{-iQ}{2} \frac{\sqrt{a(1+a)}}{\pi} \tag{11}$$

6 Relation Between the Physical Flow Domain *z*-plane and the Auxiliary *t*-Plane for $0 \le t \le 1$

$$\frac{dz}{dt} = \frac{dz}{dw}.\frac{dw}{dt} = M_1\left\{\delta\ B_t\left(\alpha, \frac{1}{2}-\alpha\right) - B_t\left(1+\alpha, \frac{1}{2}-\alpha\right)\right\} \times \frac{M_2}{t^{1/2}(1-t)^{1/2}(t+a)} \tag{12}$$

Integrating,

$$z = M_1 M_2 \int_0^{t'} \left\{\delta\ B_t\left(\alpha, \frac{1}{2}-\alpha\right) - B_t\left(1+\alpha, \frac{1}{2}-\alpha\right)\right\} \times \frac{dt}{t^{1/2}(1-t)^{1/2}(t+a)} + z_B \tag{13}$$

For vertex 'C', $t' = 1$ and $z = z_C$. Incorporating this condition in (13)

$$z_C = M_1 M_2 \int_0^{1} \left\{\delta\ B_t\left(\alpha, \frac{1}{2}-\alpha\right) - B_t\left(1+\alpha, \frac{1}{2}-\alpha\right)\right\} \times \frac{dt}{t^{1/2}(1-t)^{1/2}(t+a)} + z_B \tag{14}$$

or

$$z_C = M_1 M_2 I_3 + z_B \tag{15}$$

where, $I_3 = \int_0^1 \left\{\delta\ B_t\left(\alpha, \frac{1}{2}-\alpha\right) - B_t\left(1+\alpha, \frac{1}{2}-\alpha\right)\right\} \frac{dt}{t^{1/2}(1-t)^{1/2}(t+a)}$ I_3 has been evaluated in Appendix 3.

Substituting M_1 and M_2 in (15)

$$z_C = \frac{1}{k}\frac{\sec(\alpha\pi)}{\delta\ B\left(\alpha, \frac{1}{2}-\alpha\right) - B\left(1+\alpha, \frac{1}{2}-\alpha\right)} e^{i\pi\left(\frac{1}{2}-\alpha\right)}\left(-\frac{iQ}{2I_2}\right) I_3 + z_B$$

$$= \frac{Q}{k}\left\{\frac{\sec(\alpha\pi)}{\delta\ B\left(\alpha, \frac{1}{2}-\alpha\right) - B\left(1+\alpha, \frac{1}{2}-\alpha\right)}\right\}\{\sin(\alpha\pi) + i\cos(\alpha\pi)\}(-i)\frac{I_3}{2I_2} + z_B \tag{16a}$$

Incorporating $z_C = H\cot(\alpha\pi)$, and $z_B = iH$

$$\mathrm{Hcot}(\alpha\pi) = \frac{\mathrm{Q}}{\mathrm{k}}\left\{\frac{\sec(\alpha\pi)}{\delta\ B\left(\alpha, \frac{1}{2}-\alpha\right) - B\left(1+\alpha, \frac{1}{2}-\alpha\right)}\right\}$$

$$\frac{I_3}{2I_2}\{\cos(\alpha\pi) - i\sin(\alpha\pi)\} + iH \tag{16b}$$

Equating the real parts in either side of (16b)

$$\frac{Q}{kH}\left\{\frac{\sec(\alpha\pi)}{\delta\, B\left(\alpha, \frac{1}{2}-\alpha\right) - B\left(1+\alpha, \frac{1}{2}-\alpha\right)}\right\}\left(\frac{I_3}{2I_2}\right)\sin(\alpha\pi) = 1 \tag{17b}$$

The same equation is obtained equating the imaginary parts on either sides of (16b). Equating (7) and (17b)

$$\frac{\sec(\alpha\pi)}{\delta\, B\left(\alpha, \frac{1}{2}-\alpha\right) - B\left(1+\alpha, \frac{1}{2}-\alpha\right)} I_1 = \frac{Q}{kH}\left\{\frac{\sec(\alpha\pi)}{\delta\, B\left(\alpha, \frac{1}{2}-\alpha\right) - B\left(1+\alpha, \frac{1}{2}-\alpha\right)}\right\}\left(\frac{I_3}{2I_2}\right)\sin(\alpha\pi) \tag{18}$$

Incorporating $Q = kL_f$ in (18) and simplifying

$$\frac{L_f}{H}\left(\frac{I_3}{2I_1I_2}\right)\sin(\alpha\pi) = 1 \tag{19}$$

For an assumed value of δ, the corresponding parameter a is evaluated from (19) for a given L_f/H using an iteration procedure.

7 Location of the Phreatic Line

For $1 \le t \le \infty$

$$\frac{dz}{dw} = M_1(-1)^{\left(\frac{1}{2}-\alpha\right)-1}\left\{\delta\int_1^t \tau^{\alpha-1}(\tau-1)^{\left(\frac{1}{2}-\alpha\right)-1}d\tau - \int_1^t \tau^{(1+\alpha)-1}(\tau-1)^{\left(\frac{1}{2}-\alpha\right)-1}d\tau\right\} + \frac{1}{k}\sec(\alpha\pi)\,\mathrm{e}^{\mathrm{i}\pi\left(\frac{1}{2}-\alpha\right)}$$

$$\frac{dw}{dt} = \frac{M_2(-1)^{1/2}}{t^{1/2}(t-1)^{1/2}(t+a)} \text{ and}$$

$$\frac{dz}{dt} = M_1M_2(-1)^{1/2}(-1)^{\left(\frac{1}{2}-\alpha\right)-1}\left\{\delta\int_1^t \tau^{\alpha-1}(\tau-1)^{\left(\frac{1}{2}-\alpha\right))-1}d\tau\right.$$

$$-\int_1^t \tau^{(1+\alpha)-1}(\tau-1)^{\left(\frac{1}{2}-\alpha\right))-1}d\tau\Bigg\} \times \frac{1}{(t)^{1/2}(t-1)^{1/2}(t+a)}$$
$$+\frac{M_2(-1)^{1/2}\sec\alpha\pi}{k}\,\mathrm{e}^{\mathrm{i}\pi\left(\frac{1}{2}-\alpha\right)}\frac{1}{t^{1/2}(t-1)^{1/2}(t+a)} \tag{20}$$

Integrating

$$z(t') = M_1M_2(-1)^{1/2}(-1)^{\left(\frac{1}{2}-\alpha\right)-1}I_4(t') + M_2(-1)^{1/2}e^{i\pi\left(\frac{1}{2}-\alpha\right)}\frac{\sec(\alpha\pi)}{k}I_5(t') + z_C \tag{21}$$

where

$$I_4(t') = \int_1^{t'}\left\{\delta\int_1^t \tau^{\alpha-1}(\tau-1)^{\left(\frac{1}{2}-\alpha\right))-1}d\tau - \int_1^t \tau^{(1+\alpha)-1}(\tau-1)^{\left(\frac{1}{2}-\alpha\right))-1}d\tau\right\} \frac{dt}{(t)^{1/2}(t-1)^{1/2}(t+a)}$$

and

$$I_5(t') = \int_1^{t'}\frac{dt}{(t)^{1/2}(t-1)^{1/2}(t+a)}$$

Incorporating M_1 and M_2

$$z(t') = \left[\left\{\frac{\frac{1}{k}\sec(\alpha\pi)\,\mathrm{e}^{\mathrm{i}\pi\left(\frac{1}{2}-\alpha\right)}}{\delta\,B\left(\alpha,\frac{1}{2}-\alpha\right)-B\left(1+\alpha,\frac{1}{2}-\alpha\right)}\right\}\left\{\frac{(-\mathrm{iQ})}{2\mathrm{I}_2}\right\}(-1)^{1/2}e^{-i\pi\left(-\frac{1}{2}-\alpha\right)}I_4(t')\right]$$
$$+\left[\left\{\frac{(-\mathrm{iQ})}{2\mathrm{I}_2}\right\}(-1)^{1/2}\frac{\sec(\alpha\pi)}{k}\{\sin(\alpha\pi)+i\cos(\alpha\pi)\}I_5(t')\right]+z_C$$
$$=\left\{\frac{(-\mathrm{iQ})}{2\mathrm{kI}_2}(-1)^{1/2}\right\}$$
$$\left[\left\{\frac{\sec(\alpha\pi)}{\delta\,B\left(\alpha,\frac{1}{2}-\alpha\right)-B\left(1+\alpha,\frac{1}{2}-\alpha\right)}\right\}\left\{e^{i\pi}\right\}I_4(t')+\{\tan(\alpha\pi)+\mathrm{i}\}I_5(t')\right]+z_C \tag{22}$$

Incorporating $z_C = H\cot(\alpha\pi)$ in (22)

$$z(t') = \left\{\frac{Q}{k2I_2}\right\}\left[\frac{-\sec(\alpha\pi)}{\delta\,B\left(\alpha,\frac{1}{2}-\alpha\right)-B\left(1+\alpha,\frac{1}{2}-\alpha\right)}I_4(t')\right.$$

$$+\tan(\alpha\pi)I_5(t') + i\,I_5(t')\Big] + H\cot(\alpha\pi) \tag{23}$$

The real part is given by:

$$\frac{x(t')}{H} = \cot(\alpha\pi) + \left\{\frac{Q}{kH\,2I_2}\right\} \left[\frac{-\sec(\alpha\pi)}{\delta\,B\left(\alpha, \frac{1}{2}-\alpha\right) - B\left(1+\alpha, \frac{1}{2}-\alpha\right)} I_4(t') + \tan(\alpha\pi)I_5(t')\right] \tag{24}$$

and the imaginary part is given by:

$$\frac{y(t')}{H} = \left\{\frac{Q}{kH\,2\mathrm{I}_2}\right\} I_5(t') \tag{25}$$

Evaluations of $I_4(t')$ and $\mathrm{I}_5(t')$ are given in Appendices 4 and 5.
The point of inflection is given computing $\frac{x(t')}{H}$ and $\frac{y(t')}{H}$ for $t' = \delta$.

8 Results and Discussion

8.1 Variation of y_E/H with Spacing (L_f/H)

For a given furrow spacing, L_f/H, assigning a value to the parameter δ, the corresponding value of parameter a is obtained using Eq. (19). y_E/H is then computed from (25) after evaluating $I_5\left(t'\right)\ ;\ t' \to \infty$. The variation of y_E/H verses spacing L_f/H for different side slopes (i.e. for m = 0.5, 1, 1.5 and 2) of the furrows are shown in Fig. 2. y_E/H increases with increase in spacing of the furrows. For the spacing for which the furrows do not interfere, $y_E/H \to \infty$. y_E/H also increases with increase in m, i.e. y_E/H is less for steep slope and more for flatter slope. At the minimum furrow spacing i.e. for $L_f/H = 2m$. $y_E/H \to 0$.

8.2 Variation of $Q/Q_0(m)$ with Spacing $\left(L_f/H\right)$

The variations of $Q/Q_0(m)$ with furrow spacing L_f/H is shown in Fig. 3 for various values of m. $Q_0(m)$ is the seepage from a single furrow without interference and it is a function of m. $Q_0(m)/(kH)$ has been computed using an approximate relation $Q_0(m)/(kH) = \left\{\left(4\pi - \pi^2\right)^{1.3} + (2m)^{1.3}\right\}^{0.77}$ derived by Chahar (2000). $Q/Q_0(m)$ increases with increase in spacing till the furrows interfere, beyond which $Q/Q_0(m) = 1$. Q being equal to kL_f as per Neumann boundary condition prevailing

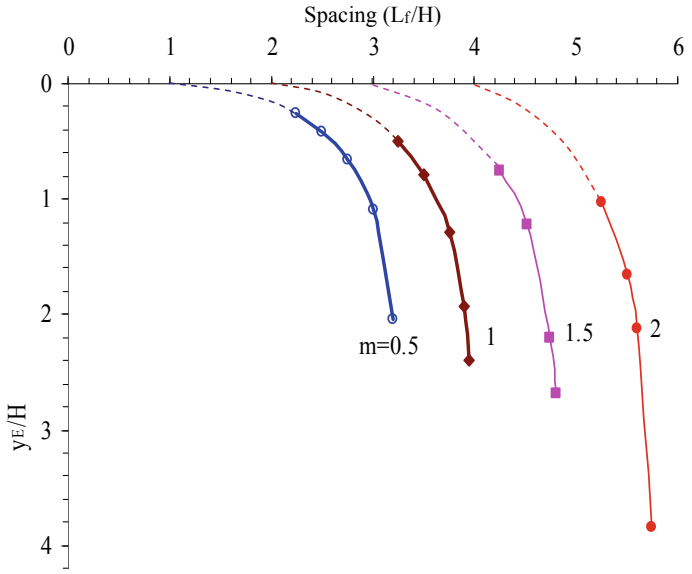

Fig. 2 Variation of y_E/H with spacing, L_f/H for different m

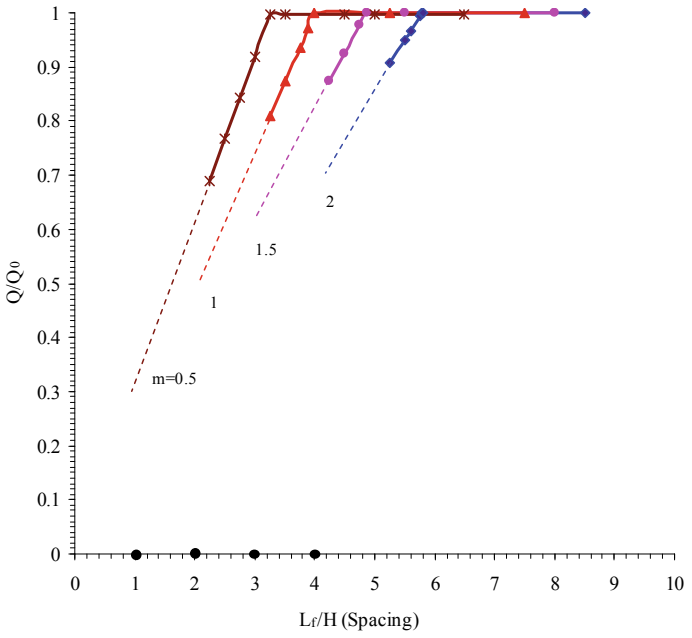

Fig. 3 Variation of Q/Q_0, with, spacing, L_f/H, for an array of triangular furrows

at large depth, for a given m, $Q/Q_0(m)$ varies linearly with L_f/H. At the minimum spacing (starting of the dotted part of the straight line in the figure), $\left(L_f/H\right)_{\min} = 2m$, and $Q/Q_0(m) = \frac{2m}{\left\{\left(4\pi-\pi^2\right)^{1.3}+(2m)^{1.3}\right\}^{0.77}}$.

8.3 *Loci of Phreatic Lines for Different Side Slopes*

The loci of the phreatic lines are plotted in Figs. 4, 5, 6 and 7 for different side slopes and spacing of the furrows. The point of inflection has been shown on the phreatic surface. With increasing spacing the point of inflection shifts towards point E.

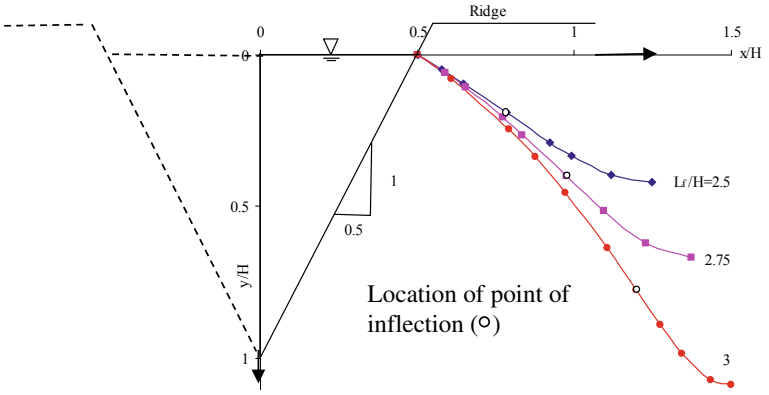

Fig. 4 Loci of phreatic lines for different spacing of an array of triangular furrows for m = 0.5 (α = 0.3524)

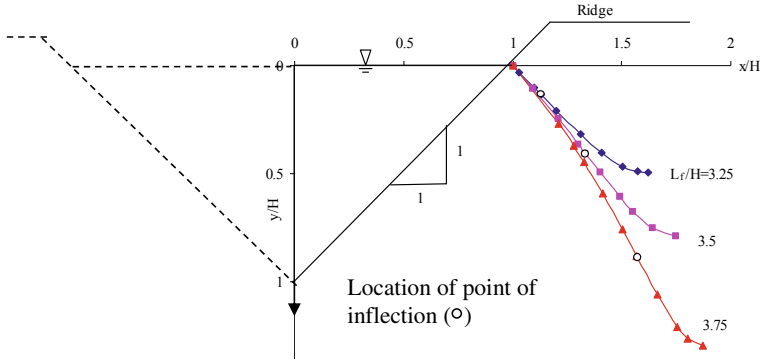

Fig. 5 Loci of phreatic lines for different spacing of an array of triangular furrows for m = 1 (α = 0.25)

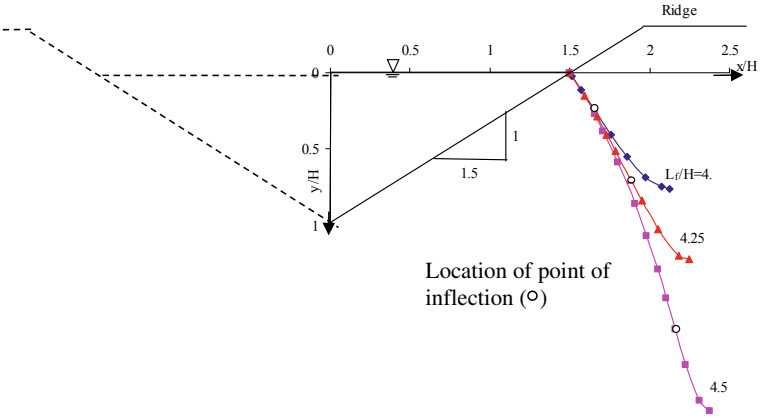

Fig. 6 Loci of phreatic lines for different spacing of an array of triangular furrows for m = 1.5 (α = 0.1872)

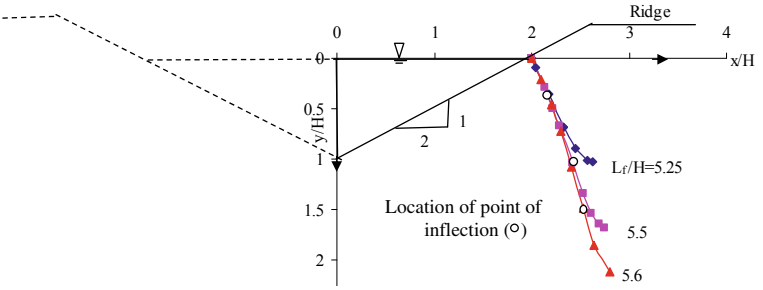

Fig. 7 Loci of phreatic lines for different spacing of an array of triangular furrows for m = 2 (α = 0.1476)

8.4 Variation of Slope of the Tangent to the Phreatic Line

Slope of the tangent to the phreatic line at a point (x, y) on the phreatic line is given by $\frac{dy}{dx}\left\{= \frac{y(t'+\Delta t')-y(t')}{x(t'+\Delta t')-x(t')};\ 1 \le t' < \infty\right\}$. The variation of $\frac{dy}{dx}$ with x for $m = 1$, and $\frac{L_f}{H} = 3.5$ is shown in Fig. 8. 'D' is the point of inflection. At this point the slope of the tangent, $\frac{dy}{dx}$, is the maximum.

8.5 Adequacy in Furrow Spacing

An example is presented here to check the adequacy of furrow spacing. The moisture extraction pattern by plant and extent of saturation of the soil by furrow irrigation are

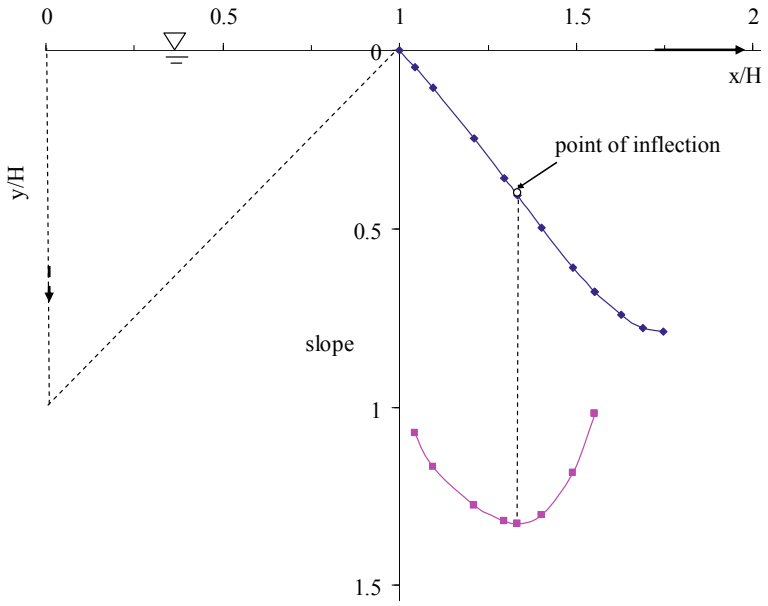

Fig. 8 Slope along the phreatic line

shown in Fig. 9. The root zone depth, (R_d), measured from the ridge of the furrow, is assumed to be 30 cm (Kemble and Sanders 2000).The free board is assumed to be 5 cm (Unger 1992). The depth of water in the furrow H = 10 cm. If a spacing L_f/H = 3.25 is adopted i.e. if L_f = 32.5 cm, then the upper 9.9 cm of the root zone at the middle of the ridge does not get water. Corresponding to spacing L_f = 35, 36, and 37.5 cm, the upper 12.8, 14.5, and 17.9 cm of the root zone do not get water respectively. For such spacings, ($y_E + f_b$) > 0.25 R_d. As the upper 1/4th of the root zone remains in an unsaturated state, such furrow spacings are not recommended for shallow rooted crops.

8.6 Checking the Water Availability in Root zone at Various Furrow Spacing

The spacing of the furrows should be such that, at the middle of the ridge, the sum ($y_E + f_b$) < about 1/4th of the root zone depth. In Table 1, the suitability of furrow spacing is examined corresponding to a free board, f_b = 5 cm, and depth of water in the furrow, H = 10 cm. From Table 1, it is inferred that, the spacings are only suitable for moderately deep and deep rooted crops.

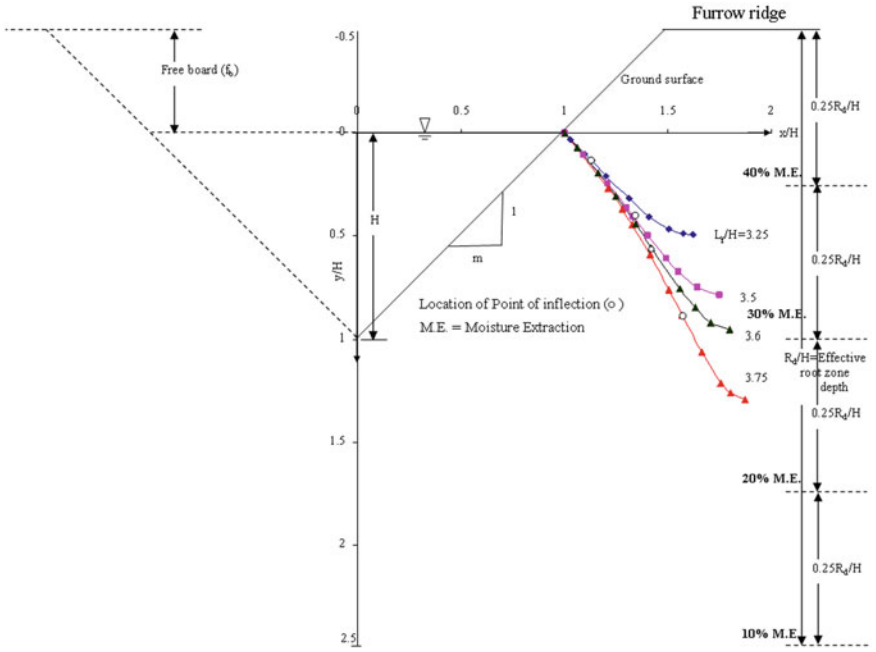

Fig. 9 Furrow profile showing the loci of phreatic lines, root zone depth (R_d/H) and the moisture extraction percentage by plants at different root zone depth for m = 1, H = 10 cm and f_b = 5 cm

9 Conclusions

- An analytical solution for unconfined seepage from parallel triangular furrows in an isotropic porous medium of infinite depth has been derived using the inverse hodograph pertaining to half of the flow domain of one of the furrows and Schwarz–Christoffel transformation. The boundary condition assumed is Neumann-type i.e. at infinity the hydraulic gradient is 1. This boundary condition implies that the seepage from one of the furrows is hydraulic conductivity times spacing of the furrows irrespective of the shape of the furrows. The locus of the phreatic line is governed by the furrow spacing and furrow geometry.
- Saturation of soil under the furrow ridge increases with steeper slope of the furrow banks.
- The slope of the tangent to the phreatic line at point of inflection on the phreatic line attains the maximum.
- With increase in furrow spacing the point of inflection moves downwards
- For side slopes (i.e. for m = 0.5 and 1) of the furrows the sum of depth of saturation and free board is at less depth and hence suitable for deep and moderately deep rooted crops whereas for(m = 1.5 and 2) it is at higher depth and is suitable for only deep rooted crops.

Table 1 The maximum depth to phreatic surface below the middle of ridge, ($y_E + f_b$), for different spacings and side slope of the triangular furrows; $f_b = 5$ cm, depth of water in the furrow, H = 10 cm and suitability of furrow spacings

α	cot απ = m	Spacing (L_f/H)	Spacing L_f, (cm)	y_E/H	y_E (cm)	$y_E + f_b$ (cm)	The spacing suitable for
0.3524	0.5	3.26	32.6	∞	∞	∞	Not suitable
		3.0	30	1.09	10.9	15.9	D
		2.75	27.5	0.67	6.7	11.7	D
		2.5	25	0.42	4.2	9.2	M
0.25	1	4.02	40.2	∞	∞	∞	Not suitable
		3.75	37.5	1.29	12.9	17.9	D
		3.5	35	0.79	7.9	12.9	D
		3.6	36	0.953	9.53	14.53	D
		3.25	32.5	0.49	4.9	9.9	M
0.1872	1.5	4.86	48.6	∞	∞	∞	Not suitable
		4.75	47.5	2.2	22	27	D
		4.5	45	1.2	12	17	D
		4.25	42.5	0.76	7.6	12.6	D
0.1476	2	5.79*	57.9	∞	∞	∞	Not suitable
		5.75	57.5	3.85	38.5	43.5	D
		5.5	55	1.69	16.9	21.9	D
		5.25	52.5	1.03	10.3	15.3	D

* Obtained from Vedernikov's analysis (Vedernikov, 1934) (vide. Harr, 1962)
D Deep rooted crops
M Moderately deep rooted crops

Acknowledgements I am immensely grateful to Prof Nayan Sharma Dept. of WRD&M, IIT Roorkee, for his unwavering support and encouragement to make this manuscript in this present form.

Appendix 1

Evaluation of Integral I_1

$$I_1 = \int_0^a \frac{(\delta + \xi)}{(\xi)^{1-\alpha}(1+\xi)^{1-(\frac{1}{2}-\alpha)}} d\xi$$

$\xi = 0$ is a singular point.

Incorporating $\xi = X^{1/\alpha}$, $d\xi = \frac{1}{\alpha} X^{\frac{1}{\alpha}-1} dX$ for removing the singularity.

$$I_1 = \frac{1}{\alpha}\int_0^{a^\alpha} \frac{(\delta + X^{1/\alpha})X^{\frac{1}{\alpha}-1}}{(X)^{\frac{1-\alpha}{\alpha}}(1+X^{1/\alpha})^{(\frac{1}{2}+\alpha)}}dX = \frac{1}{\alpha}\int_0^{a^\alpha} \frac{(\delta + X^{1/\alpha})}{(1+X^{1/\alpha})^{(\frac{1}{2}+\alpha)}}dX$$

Further substituting $X = \frac{a^\alpha}{2}(1+\eta)\,,\ dX = \frac{a^\alpha}{2}d\eta$

$$I_1 = \frac{a^\alpha}{2\alpha}\int_{-1}^{1} \frac{(\delta + X^{1/\alpha})}{(1+X^{1/\alpha})^{(\frac{1}{2}+\alpha)}}d\eta;\quad \mathrm{X} = \frac{\mathrm{a}^\alpha}{2}(1+\eta)$$
$$= \frac{a^\alpha}{2\alpha}\sum_{i=1}^{N} F(\eta i)w(i)$$

I_1 is evaluated using gaussian weights.

Appendix 2

Evaluation of Integral I_2

$$I_2 = \int_0^1 \frac{dt}{t^{1/2}(1-t)^{1/2}(t+a)}$$

In I_2, t = 0 and t = 1 are singular points. Substituting $\mathrm{t} = \sin^2\theta, \mathrm{dt} = 2\sin\theta\cos\theta\ \mathrm{d}\theta$ for removing the singularities, I_2 reduces to.

$$I_2 = 2\int_0^{\pi/2} \frac{d\theta}{(a+\sin^2\theta)}.$$

Further substituting $\theta = \frac{\pi}{4}(1+\Phi),\ \mathrm{d}\theta = \frac{\pi}{4}d\Phi.$

$$I_2 = \frac{\pi}{2}\int_{-1}^{1} \frac{d\Phi}{a+\sin^2\left\{\frac{\pi}{4}(1+\Phi)\right\}}.$$

I_2 is evaluated using Gaussian weights.

The constant M_2 can also be obtained using the condition at points A and F. Going around a small circle of radius r, $\mathrm{r} \to 0$ around $\mathrm{t} = -\mathrm{a}$, results in a jump equal to $\frac{-iQ}{2}$ in w plane. Substituting $(\mathrm{t}+\mathrm{a}) = re^{i\theta}, dt = re^{i\theta}\ \mathrm{id}\theta$ in (4.8).

$$\frac{-iQ}{2} = \lim_{r\to 0} M_2 \int_0^{\pi} \frac{re^{i\theta} i d\theta}{(re^{i\theta}-a)^{1/2}(1+a-re^{i\theta})^{1/2} re^{i\theta}} = \frac{\pi}{\sqrt{(1+a)a}} M_2$$

$$M_2 = \frac{-iQ\sqrt{a(1+a)}}{2\pi} \quad I_2 = \frac{\pi}{2}\int_{-1}^{1} \frac{d\Phi}{a+\sin^2\left\{\frac{\pi}{4}(1+\Phi)\right\}} = \frac{\pi}{\sqrt{a(1+a)}}$$

Appendix 3

Evaluation of Integration I_3

$$I_3 = \int_0^1 \left\{\delta\, B_t\left(\alpha, \frac{1}{2}-\alpha\right) - B_t\left(1+\alpha, \frac{1}{2}-\alpha\right)\right\} \frac{dt}{t^{1/2}(1-t)^{1/2}(t+a)}$$

Substituting $t = \sin^2\theta$, dt $=$ $2\sin\theta\cos\theta\ \mathrm{d}\theta$

$$I_3 = \int_0^{\pi/2} \left\{\delta\, B_{\sin^2\theta}\left(\alpha, \frac{1}{2}-\alpha\right) - B_{\sin^2\theta}\left(1+\alpha, \frac{1}{2}-\alpha\right)\right\} \frac{2\sin\theta\cos\theta\ \mathrm{d}\theta}{\sin\theta\cos\theta\ (\mathrm{a}+\sin^2\theta)}$$

Further substituting $\theta = \frac{\pi}{4}(1+\Phi)$, $\mathrm{d}\theta = \frac{\pi}{4}\ \mathrm{d}\Phi$

$$I_3 = \int_{-1}^{1} \left\{\delta\ B_{\sin^2\left\{\frac{\pi}{4}(1+\Phi)\right\}}\left(\alpha, \frac{1}{2}-\alpha\right) - B_{\sin^2\left\{\frac{\pi}{4}(1+\Phi)\right\}}\left(1+\alpha, \frac{1}{2}-\alpha\right)\right\} \times \frac{2\frac{\pi}{4}\ \mathrm{d}\Phi}{a+\sin^2\left\{\frac{\pi}{4}(1+\Phi)\right\}}$$

$$= \frac{\pi}{2}\int_{-1}^{1} \left\{\delta\ B_{\sin^2\left\{\frac{\pi}{4}(1+\Phi)\right\}}\left(\alpha, \frac{1}{2}-\alpha\right) - B_{\sin^2\left\{\frac{\pi}{4}(1+\Phi)\right\}}\left(1+\alpha, \frac{1}{2}-\alpha\right)\right\} \times \frac{\mathrm{d}\Phi}{a+\sin^2\left\{\frac{\pi}{4}(1+\Phi)\right\}}$$

Appendix 4

Evaluation of I_4 (t')

$$I_4(t') = \int_1^{t'} \left\{ \delta \int_1^t \tau^{\alpha-1}(\tau-1)^{\left(\frac{1}{2}-\alpha\right)-1} d\tau - \int_1^t \tau^{(1+\alpha)-1}(\tau-1)^{\left(\frac{1}{2}-\alpha\right)-1} d\tau \right\} \times \frac{dt}{(t)^{1/2}(t-1)^{1/2}(t+a)}; \quad 1 \le t \le \infty$$

Substituting $t = \frac{1}{\xi}, dt = -\frac{1}{\xi^2} d\xi$

$$I_4(t') = \int_{1/t'}^{1} \left\{ \delta \int_1^{1/\xi} \tau^{\alpha-1}(\tau-1)^{\left(\frac{1}{2}-\alpha\right)-1} d\tau - \int_1^{1/\xi} \tau^{(1+\alpha)-1}(\tau-1)^{\left(\frac{1}{2}-\alpha\right)-1} d\tau \right\} \times \frac{d\xi}{(1-\xi)^{1/2}(1+a\xi)}$$

$\tau = 1$ is a singular point. The singularity is removed substituting $\tau - 1 = \eta^m$, $\mathrm{d}\tau = \mathrm{m}\eta^{\mathrm{m}-1} d\eta$ and selecting $m = \frac{1}{0.5-\alpha}$. Incorporating the substitution.

$$I_4(t') = \int_{1/t'}^{1} \left\{ \delta\, m \int_0^{\left(\frac{1}{\xi}-1\right)^{1/m}} (1+\eta^m)^{\alpha-1} d\eta - m \int_0^{\left(\frac{1}{\xi}-1\right)^{1/m}} (1+\eta^m)^{(1+\alpha)-1} d\eta \right\} \times \frac{d\xi}{(1-\xi)^{1/2}(1+a\xi)}$$

Further substituting $1 - \xi = V^2, d\xi = -2V dV$

$$I_4(t') = \int_0^{\sqrt{\left(\frac{t'-1}{t'}\right)}} \left\{ \delta\, m \int_0^{\left(\frac{V^2}{1-V^2}\right)^{1/m}} (1+\eta^m)^{\alpha-1} d\eta - m \int_0^{\left(\frac{V^2}{1-V^2}\right)^{1/m}} (1+\eta^m)^{(1+\alpha)-1} d\eta \right\} \times \frac{2dV}{\left\{1+a(1-V^2)\right\}}$$

Let $\frac{1}{2}\sqrt{\frac{t'-1}{t'}}(1+X) = V,\ \mathrm{dV} = \frac{1}{2}\sqrt{\frac{t'-1}{t'}} dX$

$$I_4(t') = \int_{-1}^{1} \left\{ \delta\, m \int_0^{\left(\frac{V^2}{1-V^2}\right)^{1/m}} (1+\eta^m)^{\alpha-1} d\eta - m \int_0^{\left(\frac{V^2}{1-V^2}\right)^{1/m}} (1+\eta^m)^{(1+\alpha)-1} d\eta \right\} \times \frac{\sqrt{\frac{t'-1}{t'}} dX}{\{1+a(1-V^2)\}}$$

Further let $\frac{1}{2}\left(\frac{V^2}{1-V^2}\right)^{1/m}[1+Y] = \eta,\ \mathrm{d}\eta = \frac{1}{2}\left(\frac{V^2}{1-V^2}\right)^{1/m} dY$

$$I_4(t') = \int_{-1}^{1} \left\{ \delta\, mm \int_{-1}^{1} (1+\eta^m)^{\alpha-1} \frac{1}{2}\left(\frac{V^2}{1-V^2}\right)^{1/m} dY - m \int_{-1}^{1} (1+\eta^m)^{(1+\alpha)-1} \frac{1}{2}\left(\frac{V^2}{1-V^2}\right)^{1/m} dY \right\} \frac{\sqrt{\frac{t'-1}{t'}} dX}{\{1+a(1-V^2)\}}$$

$$V = \frac{1}{2}\sqrt{\frac{t'-1}{t'}}(1+X) \quad \eta = \frac{1}{2}\left(\frac{V^2}{1-V^2}\right)^{1/m}[1+Y]$$

$I_4\ (t')$ is evaluated numerically using Gaussian weights.

Appendix 5

Evaluation of I_5(t')

$$I_5(t') = \int_1^{t'} \frac{dt}{t^{1/2}(t-1)^{1/2}(t+a)}$$

Substituting $t = \frac{1}{\xi}, dt = -\frac{d\xi}{\xi^2}$

$$I_5(t') = \int_{1/t'}^{1} \frac{d\xi}{(1-\xi)^{1/2}(1+a\xi)}$$

Further substituting $1-\xi = V^2, \quad \mathrm{d}\xi = -2VdV$

$$I_5(t') = \int_0^{\sqrt{\frac{t'-1}{t'}}} \frac{2dV}{\{1 + a(1 - V^2)\}}$$

Let $\frac{1}{2}\sqrt{\frac{t'-1}{t'}}(1 + X) = V, \quad \mathrm{dV} = \frac{1}{2}\sqrt{\frac{t'-1}{t'}}dX$

$$I_5(t') = \int_{-1}^{1} \frac{\sqrt{\frac{t'-1}{t'}}dX}{\{1 + a(1 - V^2)\}}$$

$I_5\ (t')$ is evaluated using Gaussian weights.

References

Brouwer C, Prins K, Kay M, Heibloem M (1990) Irrigation water management: irrigation methods. Training Manual No-5, FAO, Land and Water Development Division

Bruch JC, Street RL (1967) Seepage from an array of triangular channels. J Engrg Mech Div Proc ASCE 93(EM3):63–82

Carter DL (1985) Controlling erosion and sediment loss on furrow-irrigated land. Reprinted From Soil Erosion and Conservation, Soil Conservation Society of America

Chahar BR (2000) Optimal design of channel sections considering seepage and evaporation losses. Ph.D. Thesis, Department of Civil Engineering, University of Roorkee, Roorkee, India

Choudhary M, Chahar BR (2007) Recharge/seepage from an array of rectangular channels. J Hydrol 343:71–79

Kemble JK, Sanders DC (2000) Basics of vegetable crop irrigation. ACES Publication, ANR-1169

Michael AM (1999) Irrigation theory and practice. Vikas Publishing House Pvt. Ltd., New Delhi

Polubarinova Kochina PI (1962) Theory of groundwater movement. Princeton University Press New Jersey

Samal KP, Mishra GC (2016) Analysis of seepage from a triangular furrow considering soil capillarity using inverse hodograph and conformal mapping technique. ISH J Hydraul Eng. https://doi.org/10.1080/09715010.2016.1213144

Samal KP, Mishra GC, Sharma N (2019) Analysis of seepage from a triangular furrow with negligible free-board considering soil capillarity using inverse hodograph and conformal mapping technique. Int Conf Recent Dev Sustain Infrastruct. KIIT DU, BBSR

Tiwari KN, Mal PK, Singh RM, Chattopadhyay A (1998) Response of okra (Abelmoschus Esculentus (L.) Moench.) to drip irrigation under mulch and non-mulch condition. Agric Water Manage 38:91–102

Unger WP (1992) Ridge height and furrow blocking effects on water use and grain yield. Soil Sci Soc Am J 56(5):1609–1614

Vedernikov VV (1934) Seepage from channels (in Russian). Gosstroyzdat, Moscow, also in German: Wasserkrafts-Wasserwirtsch, 11–13

Impact of Legal Instruments in Improving Domestic Water Supply, Case Study Involving Two Nations Tagged with Most Significant Improvement

Kumarjeeb Pegu, Tanmaya Mohanty, and Kshyana Prava Samal

Abstract According to a worldwide research undertaken by the University of Oxford for the period 1997–2015 to rank nations with 'Most Improved Domestic Water Supply', Cambodia and Malawi were tagged among the best. The ranking was based on the improvement in number of households availing water supply. Such a feat depends on efficient and effective water resource planning and management. The efficacy of the tasks involved in the activities is presumed to be influenced by legal instruments that encompass formulation and implementation of clear and robust water policy and related laws. The present paper brings out the essence in the stated water policies and laws prevailing at these two nations. Secondary data available from academic journals and state websites have been compiled for a doctrinal and analytical methodology. The clarity and robustness as well as the gaps in policy and legal statements are analyzed. Further, the implementation ease and gap are studied considering the locations experiencing significant improvement is access to the domestic water supply.

Keywords Water resource planning and management · Drinking water · Malawi integrated water resources management and water efficiency · MOWRAM

K. Pegu (✉)
School of Law, KIIT Deemed to be University, Bhubaneswar, Odisha 751024, India

T. Mohanty
KIIT School of Mechanical Engineering, KIIT Deemed to be University, Bhubaneswar, Odisha 751024, India

K. P. Samal
School of Civil Engineering, KIIT Deemed to be University, Bhubaneswar, Odisha 751024, India

B. B. Das et al. (eds.), *Recent Developments in Sustainable Infrastructure (ICRDSI-2020)—GEO-TRA-ENV-WRM*, Lecture Notes in Civil Engineering 207,
https://doi.org/10.1007/978-981-16-7509-6_35

1 Introduction

1.1 Drinking Water Status in Malawi

Malawi as of date remains abundant with surface water.[1] However, due to climate change, population growth and over-exploitation of water resources, it is rapidly decreasing (Rijsdijk and Mkwambisi 2016; Laisi 2009, 18–28). The U.N. Country Team in Malawi (UNCTM), in its report (UN Country Team in Malawi 2017) provides an outlook of the Malawi Government's prioritization of access to safe and clean drinking water to households in the Nation. Under this particular effort, role of international agencies and the Malawi Innovation Challenge Funds (herein forth MICF) in promotion of water treatment products and access to affordable drinking water remains an area of significance.

As the populations' access to drinking water is on a raise, there remains a need for more clean drinking water delivery systems as it is estimated that 67% of Malawi households do not treat their drinking water adequately before use (Mulwafu 2010, 752–757; UN Country Team in Malawi 2017). Furthermore, WaterAid estimated that 1 in 3 Malawians do not have excess to clean drinking water.

1.2 Drinking Water Status in Cambodia

Although, Cambodia has abundance of water resources, yet the availability of the resource is highly variable both temporally and spatially (World Bank 2017, 3–9). While, most of Cambodia's water resources are underexploited, yet there remains vulnerability to its water resources and the aquatic ecosystems due to impedance of drainage flows by roads and the effects of irrigation. Further the market forces and food consumption demands of the populace are believed to be only accelerating the pressure on water resources and ecosystems (Asian Development Bank 2012, 4).

As, Cambodia has made strides in improving drinking water supply infrastructure in past 2 decades, challenges reminds in providing universal access to safe drinking water. According to Water.org, today approximately 3 million people in Cambodia lack access to safe water and with approximately 77% of Cambodians living in rural areas, the impact of poor access to safe water and sanitation is disproportionately felt in the rural areas. With a GDP per capita of US $1215, access to affordable and safe drinking water and sanitation services for the people, remains a important object for the government. In Cambodia's Country brief presented at the Sanitation and Water for All Sector Ministers' Meeting held on 4–5 April 2019, in San Jose, it was informed that to cover basic water supply and sanitation service delivery gaps under

[1] Lake Malawi consisting of an area in excess of 9000 square miles and other lakes such as Chilwa, Malombe and Chiuta and multiple rivers including the Shire form part of Malawi's natural water sources.

Cambodian Nation Action Plan 2019–2023 (herein forth NAP 2019–2023), there was a requirement of at least US $898.4 million. The brief further reflected that in terms of total foreign capital investment in the aforementioned service delivery, already US $52.7 million was committed or anticipated through the ADB and UNICEF (Cambodia 2019).

2 Country Analysis—Malawi

2.1 Law and Policy Analysis

In post independent Malawi the first legislation on water resource came about in 1969 in the form of the Water Resources Act. Today, the Water Resource Law of 2013 has superseded the former law and provides for state ownership of water and a system of license or permits of water use. Under the system of permits a fee collection mechanism is implemented for private individuals for the bulk extraction and supply of water resource to the population, so as unabated over-extraction of water resources is regulated. While the Water Law of 1969 provided efforts for institutionalizing water as a public resource, the state only had control of mostly large water bodies while smaller water bodies remained under control of powerful individuals (Mulwafu and Mwamsamali 2017). Today, the efforts of the State and its partnership with Multinational Agencies and private investors in providing access to treated and safer drinking water sources for the people particularly in the rural regions which constitutes 84% of Malawi's population, under government mandated gravity-fed schemes reflects upon the commitment of the State in its steps to provide basic rights of access to drinking water (WHO and UNICEF 2019; African Development Bank 2019). However, areas of concern remain in management and delivery process of improved drinking water including the government's tendency to delegate a significant portion of its responsibilities to the communities and the chronic shortages in staff particularly within the rural water supply sector at the district level, which has severely compromised the states' ability to provide adequate and sustained delivery of water supply to the populace (Oates and Mwathunga 2018, 15–16).

2.1.1 Groundwater Status

It is estimated that although groundwater in Malawi which takes up mere 2% of the total water resource today, it has become the main source of water consumption for 76% of the total population and 86% of the rural population for their day to day domestic use (UNICEF Malawi 2017). Section 38(3) of the 2013 Water Resources Act provides for domestic use of groundwater without a license, while the cap for the extraction through borehole is limited to ten meters for ensuring sustainable

groundwater management. Also, the requirement for Environmental Impact Assessment is not provided in the case of domestic use of ground water. Although, the Law provides for limited groundwater use, State's aim of further strengthening ground water extraction resources on a mass scale by providing basic infrastructural aid for building hand-pump boreholes, to the communities not only increases rapid depletion of groundwater levels, but its subsequent discharge to the rivers and their health (Kelly et al. 2019). Part VI of the 2013 Water Law provides for groundwater protection and licensing of its use for commercial purpose.

2.1.2 Treatment of Extracted Water

The state has initiating major investments to build water treatment and supply infrastructures for distribution in the previous decade, with the prime examples being the Lilongwe Water Investment Programme, Mulanje drinking water project and lilongwe water project. Present estimates indicate that state investment in water infrastructure projects is not sufficient in ensuring access to improved drinking water for the population. Also, presence of pollutants in groundwater indicates the further need for infrastructural focus on its treatment (Rijsdijk and Mkwambisi 2016).

Furthermore, UNICEF's Malawi Country Programme Strategy 2016–2021 has claimed that the financing of its Water, Sanitation and Hygiene program (WASH) in Malawi remains abysmal. The 2013 Law, in general provides for pre-distribution treatment for extracted water resources for license holders on a case by case basis under section 40.1(i). It is observed that under the law, there lacks an express provision on mandatory treatment of extracted water used for drinking water supply.

2.1.3 Water Management—Affordability

The Water Policy of 2005 aimed at addressing the water management issues including affordable supply while Malawi remains a lower income nation (US $100–200 per capita income monthly). However, mismanagement, lack of enforcement of the law, lack of clarity on the definition of water affordability within the water monitoring framework and in certain cases higher cost of supply and distribution by the state of water for household in Malawi remains a concern area leading to rising cost in availing drinking water for the population as people are compelled to spend more in purchasing their own drinking water treatment tools (Adams 2018, 879–884; Smiley 2017, 594–595). The 2005 Water Policy provides for water supply and sanitation services in urban areas and market places, through commercially viable options with equitable accessibility to ensure universal reach. Similarly, for rural areas, the Policy provides for access in water resource management through local community participation. Likewise, the policy sets specific objectives on conservation and investments through both public and private spheres in water management. The application of the policy mandate by the Malawian Government has witnessed more private enterprises accessing the domestic market for creating means of providing clean drinking

water options for people. For instance, Arkay Plastics and SAFI Water Treatment Solutions with support from the Malawi Innovation Challenge Fund (MICF)[2] have created water filter devices for local households at 60% lower price that for similarly imported filters in the market (UN Country Team in Malawi 2017). Currently, under the 2013 Law, for domestic use, people do not need to pay a fee for extraction of water from the water resources.

2.1.4 Transparency and Accountability on Funding Sources in Water Management

UNICEF in a report claims that while 80% of its Water, Sanitation and Hygiene (WASH) funding come from donors, the allocation of funds for WASH in the national budget were a meager 0.08% during 2014/15.The report particularly holds the Malawian State's use of funds under the WASH funding arrangement as non-transparent (WaterAid 2016, 7). Similar to the 2005 Water Policy to on user friendly quality data on water resources, under section 10 (h) of the 2013 Water Law, National Water Resources Authority (herein forth NWRA) is provided the responsibility to gather and maintain information on water resources and from time to time to publish forecasts, projections and information on water resources. Similarly, under section 18(1), the Authority in obligated to maintain a National Monitoring and Information System on Water Resources. Under section 18(5), the information contained in the aforesaid system is accessible to the public for a prescribed fee including the supply of a copy of the Authority's annual report. While, under the 2013 Law, discloser of information of water resource development and its use is provided for to the public, the Law itself is silent on whether information on 'sources of funding' under section 19(1) or on the total percentage use of the Water Resources Trust Fund under section 121 in the area of water resource development, including for financing conservation and management of water resources, constitutes as information under section 18(5).

2.2 Implications

2.2.1 Manpower Staffing in the Water Supply Sector (WSS) and Affordable Access to Drinking Water

The 2013 Water Law is silent on the issue of severe understaffing of manpower in management and delivery process of drinking water supply. The legal framework on Water Resource in Malawi requires a redressal of the issue, and also either through

[2] The MICF is an initiate under the Malawi Government's Private Sector Development Project (PSDP). MICF is funded by UNDP and the Department for International Development of Malawi (DFID), to increase private sector investments in the country.

an amendment to the 2013 Law or under a new legal framework, a portion of the national budget meant for water resource management through the Water Resources Trust Fund must be allocated specifically for staffing of required manpower along with such qualifications as per requirement to ensure drinking water delivery systems under WSS. Similarly, affordability of access to drinking water for the foreseeable future shall remain much dependent on the twin objects of building more water distribution infrastructure and treatment facilities.

2.2.2 Groundwater Treatment and Protection Against Its Depletion

Overdependence of Malawian population on groundwater which only consists of 2% of water resource of Malawi is rapidly causing further decrease in groundwater levels. Although the 2013 Law provides a cap of 10 m for extraction of groundwater through boreholes for domestic use, the legislation do not provide safeguards for limiting the use of groundwater resources. Also, the state's ambitions of providing basic infrastructural aid for building groundwater resource extraction tools reflects upon the state's failure to acknowledge proper water management planning in Malawi.

Presently, the need for a strategy to properly management of groundwater i.e. to reduce overdependence of the State on groundwater resources and to divert most of the funds earmarked for groundwater projects for building a more robust infrastructure capacity for water treatment facilities and surface water management remains the need.

2.2.3 Transparency, Accountability and Public Participation

The 2013 Water Resources Act, do not provide clarity on whether the sources of funding to the National Water Resources Authority (NWRA) and its use by the authority may be disclosed to the public. Similarly at present**,** there exist no legal frameworks to reflect on financial contributions from Nongovernmental Organizations (NGOs) and private donors in Malawi. Hence, a clear and unambiguous legal framework on disclosure of details of funding channels available to NWRA for implementation of water resources management remains an important need for the parliament to enact for ushering in a more responsible and accountable functioning of NWRA.

In term of public participation in water distribution governance, while the erstwhile Water Resources Act, 1969, provided for the Minister responsible for Water Recourses Development to grant water use rights to water users at both rural and urban areas, such actions were taken without involving public discourse or participation of water users on such matter. Under the 2013 Act, one representative of associations of water users is allowed to be a member in the NWRA. The establishment of an Association of Water Users is a rather simple process and may be obtained by an agreement of a simple majority of a group of water users, at their initiative or

at the initiative of the Authority, for the purpose of water resources management at the grassroots level (see section 131 of the Water Resources Act 2013).

The 1969 Act was criticized for not providing any particular structure for appointment of Water Resources Boards' office bearers and for providing vast power solely on the Minister of Water Resources for the functioning of the board. Herein, under the 2013 Act, NWRA's governing body consist of the Minister responsible for Water Resources Development, one representative each from an established Catchment Management Committee, Associations of Water Users, Non-Governmental Organization etc. (see section 8.2). The structure represents a democratic distribution of the decision making process of the NWRA on the matters of water resource distribution and management.

3 Country Analysis—Cambodia

3.1 Law and Policy Analysis

The primary management of water in Cambodia is the Law on Water Resources Management, 2007 (Herein forth Water Resources Law 2007). The law provides a regulatory framework into the system of policy formation with aim for uniformity in water management. Before the enactment of the Water Resources Law, 2007, the responsibility of managing the portfolio of water resources lied with several ministries, leading to the overlapping of the various ministerial plans and hence a resulting situation of administrative conflict. With the enforcement of the Water Resources Law, 2007, while responsibility of water management remains with several ministries,[3] Ministry of Water Resources and Meteorology (Herein forth MoWRAM) has been assigned the primary role to collaboration with all concerned Ministries in planning national strategies on water resources. (See Article 5 and Article 10, Water Resources Management La, 2007). Also, while MoWRAM is provided with the lead responsibility on managing water resources, the Water Resources Law, 2007, ensures that decisions of MoWRAM are not unilateral and consultation with other

[3] The Ministry of Industry, Mines and Energy is provided the portfolios of water supply provision to cities and provincial towns and for hydropower;

The Ministry of Rural Development is provided the portfolio of water supply, sanitation and land drainage in rural areas;

The Ministry of Public Works and Transport is provided the portfolio of water supply and sanitation in Phnom Penh district;

The Ministry of Environment is provided the portfolio of protecting water resources;

The Ministry of Agriculture, Forests and Fisheries is provided the portfolio of implementation of policies on irrigation and catchments in forests and fisheries areas.

The Ministry of Planning is provided the portfolio of development plans;

The Ministry of Health is provided the portfolio of controlling the quality of water used for public water supply;

The Ministry of Finance is provided the portfolio of harmonizing the diverse proposals on water management.

agencies and local authorities of water management and distribution is maintained. (See Article 15, 14, 22, 25 Water Resources Law 2007).

3.1.1 Accountability and Participatory Governance

As result of the inter-ministerial coordination, change has is witnessed in emergence of small- scale irrigation schemes based on principles of decentralized water management with local community participation post the 1990's against large scale irrigation schemes which had impact on regional and environmental ecosystems (Sithirith 2017, 4–8). The implications of such grassroots participation of local communities resulted in the creation of the Farmers' Water User Communities (Herein forth FWUC) through the sub-decree granted to MoWRAM under Article 19 of the Water Resources Law, 2007.

In addressing transparency, Article 9 of the Water Resources Law, 2007, provides for MoWRAM the responsibility of preparing National Water Resources Plan based on information from a water resources inventory of data collected in collaboration with other institutions. The data collected by MoWRAM is open for public access and to other governmental agencies.

However, it is held that weak inter-ministerial coordination in water management even with the overall charge under MoWRAM, has led to hurdles in the enforcement of the Water Resources Law, 2007 (8).

Presently, in the agricultural sector many large-scale irrigation system projects under less decentralized avenues are initiated (8, 9). For the management of such projects, MOWRAM involves Farmers' Water User Communities (FWUC), wherein farmers at the grassroots are taking part in the Participatory Water Management and Development (herein forth PWMD) approach by directly involving with the private sector and donor agencies (8). The advent of the PWMD approach is also reflected in the National Strategy for Rural Water Supply and Sanitation 2011–2025. The involvement of private agencies and people at the grassroots in formulating water resource action plans is provided under Article 7 of the Water Resources Law, 2007, which states;

> The Royal Government of Cambodia shall encourage the collaboration with and participation of the relevant agencies, private sectors, beneficiary groups, NGOs and International Organizations in all activities related to the management, investment, exploitation, conservation and development of the water resources. (Law on Water Resources Management of the Kingdom of Cambodia, 2007).

Also, Article 1 of Water Resources Law, 2007emphasizes on the participation of water users and their associations in the sustainable development of water resources, which reflects on the needs such as access to drinking water for the households in Cambodia. However, participation of the community mainly in the rural areas is effected as decentralization of institutional arrangements not clearly defined and clear procedures of implementation of community management also in not defined under the legal framework (World Bank 2013). Presently, private operators managing

small piped schemes in urban center are entering the rural growth centers and are becoming important players for water supply to rural domestic households (World Bank 2015, 15–16).

3.1.2 Treatment of Extracted Water

In particular, a major concern has been raised on both quality and quantity of data made available to MOWRAM in the past under Article 8 of the Water Resources Law, 2007. As in point, the Phnom Penh Water Supply Authority (PPWSA), which shares its data with MoWRAM, in its previously collected data during 2009–2011, in capital Phnom Penh, had monitored water quality on ISO standard protocols and its water quality testing enabled treated water to be comparable to WHO and Cambodian National Drinking Water Quality Standard for its quality, yet many contaminants including pesticides and some heavy metal were felt out of monitoring and some heavy metals found in PPWSA's water supply, were not included in Cambodian National Drinking Water Quality Standard's (CNDWQS) reports (Vanny et al. 2015, 28). Also, in regards to Arsenic pollution in the water Resources, **t**he Ministry of Industry, Mines, and Energy in the year 2004, while implementing the Cambodian Drinking water Quality Standards (CDWQS) capped the limit for arsenic contains in the drinking water source at 0.05 mg of Arsenic per litre. However, even with the implementation of CDWQS, arsenic was missing from the tests done (37).

Under the Water Resources Law, 2007, for disposition of polluting substances into the water, Article 22 read with Article 23, provides light on an important responsibility of MOWRAM in water resource protection regime. Article 22 provides for subjecting discharge, disposal or deposit of polluting substances which are likely to deteriorate quality of water and endanger human, plant and animal health to license or authorization by MOWRAM. Under Article 23, MoWRAM retains power and authority to declare contingency or protected 'water use' zones in cases of; compromised water quality of serious proportions at both surface and underground water sources,

(a) watershed degradation by humans and
(b) hazardous nature of water for human health. (Article 23, Water Resources Management Law, 2007)

The grant of authorizations under Article 22 stands in contradiction to the Precautionary Principle[4] due to its wording, wherein the term 'endanger' has been used, indicating high severity of the impact of deteriorating water source on life and health. Moreover, even in cases of severe degradation of water quality, MoWRAM acting under the Water Resources Law and in particular under article 23 do not require to

[4] Principle 15 of the Rio Declaration on Environment and Development under United Nations Conference on Environment and Development (1992) state: "*In order to protect the environment, the precautionary approach shall be widely applied by States according to their capabilities. Where there are threats of serious or irreversible damage, lack of full scientific certainty shall not be used as a reason for postponing cost-effective measures to prevent environmental degradation*".

compulsorily declare a contingency or a protected zone, rather provide for measures accordingly as it deems fit, due to the inclusion of the term 'may' in the wording of the article.

3.1.3 Water Management Regime

Certain issues remain in Cambodia's water management regime. For instance 75,000 million m^3 of surface water ran off in Cambodia each year of which only 1% of the total amount of water i.e. 750 million is used of which 95% goes to agriculture (Sithirith 2017, 1). Similarly 80–90% of water abstractions from the Mekong River go back to irrigated agricultural use (WEPA 2004). Recent manmade constructions of hydropower projects across the Mekong river by upstream countries sharing the river with Cambodia has led to severe receding and degradation of the river's resources (Fawthrop 2019). As a result, the Cambodian agriculture industry is now depending more on other water resources of the nation, resulting in further decrease in abstraction of water for domestic water needs including access to drinking water for the population. A relevant approach herein becomes the flood management plans. The National Water Recourse Policy of Cambodia, 2004 (herein forth National Plan 2004) provided for rehabilitation and construction of irrigation, drainage and flood management infrastructure for providing sufficient water to the agriculture sector and alleviate the adverse impact of assess water during floods. Also, the National Plan, 2004 provides for the required need for measures to minimize the impact of chemical substances used in agricultural production and their adverse effect on water resources by encouraging people to implement diversified agricultural methods. However, chemical use in agriculture remains a problem (Vernooy, 2015, 35). Chemical substances from agriculture in Cambodia have not only led to high toxicity of food crops but also the contamination of water recourses (CEDAC et al. 2013; Khmer 2016).

3.2 Implications

3.2.1 Mekong River Diplomacy and Community Participation in Water Resources Management

The relevance of Mekong to Cambodia's economy and water-recourse aspiration is hardly refuted (Piman and Shrestha 2017, 28–32). Article 34 of the Water Resources Law, 2007, emphasizes on equitable and reasonable use of river by the nations sharing the river through observance of International agreements. Herein, the very absence of China and Myanmar from the Mekong River Commission (MRC) of 1995 has greatly eroded the conversation efforts of the river in the region. Hence, the need to emphasize highly on the issue at global forums remains for Cambodia's aspirations as the country's future water resource need depends on the river. At the present, need

for the Government of Cambodia is to allocate more water resources for drinking water supply and accordingly allow for investments in the area. Also, there remains a responsibility on MOWRAM under the Water Resources Law to engage with DWRM and provide training of the local farmers in techniques of farming with limited to zero use of pesticide and chemical substances in agriculture and to build robust infrastructure for elimination of agricultural waste water dumping in water sources. Further, MOWRAM acting under Article 10 of Water Resources Law, 2007, needs to collaborate with the Ministry of Economics and Finances (MEF) and the Ministry of Agriculture, Fisheries and Forest (MAFF) alongside international donors and prepare economic packages at national and regional level to compensate the farmers and mitigate any losses in their income from agriculture during the initial years of shifting towards sustainable diversified agricultural productions which do not depend on chemical use in production. This arrangement has the potential to decrease pollution of the water resources, and ensure cleaner water resource access for the domestic needs for the population. Herein it may be noted that, the National Water Recourse Policy of Cambodia, 2004 (National Policy, 2004) provides for 'preference' of domestic and municipal uses of water by the population during periods of water shortage, over agriculture, hydropower, industries and aquaculture and minimum flow for ecosystem maintenance.

3.2.2 Access to Safe and Affordable Water Supply Services and Participatory Governance

While, 26% of the population remains without access to safely managed drinking water services (UNICEF and WHO 2019, 48, 49), the access is growing. The National Policy on Water Supply and Sanitation, 2004 and the National Strategy for Rural Water Supply and Sanitation 2011–2025 supports affordable drinking water supply. In the urban sector, affordable water supply is gradually becoming more accessible. Particularly, Phnom Penh Water Supply Authority, which has extended reliable and affordable services to 85% of Phnom Penh residents, has been the main driver of progress in the sector (World Bank 2015, 28). In rural areas, as more Private operators managing small piped schemes enter, the need remains for the state to implement a legal framework for inclusion of Rural Water Users Associations under community water governance so as the communities are able to collaborate with private operators and agencies as change agents in ensuring enforcement of regulations on affordable pricing of water distribution and enforcement. In the observation, it was found that Malawian Water legislation provides for strong community participation trough the Water Users Associations**.** Community participation remains vital in implementation of drinking water projects so as decentralization of water management rightfully leads to direct community involvement in the matter related to safe drinking water supply and consumption. (Collignon et al. 2018; Grant et al. 2019).

4 Conclusion

In Malawi and Cambodia, there has been a strategic shift from formerly separating deferent ministries with their own portfolios on water resources to empowering a nodal Ministry for the purpose in both Nations. Today Malawi's Department of Water Resources Development under the Ministry of Irrigation and Water Development and the Ministry of Water Resources and Meteorology (MoWRAM) in Cambodia acts as nodal authorities for implementing the water resources regimes. This arrangement provides for a resolve to break away from the past experience of non-coordinated implementation of National and regional plans by the ministries and the resulting overlapping and mismanagement. Although, similar to Cambodia, problems do exist in the matters of water resources administration under the nodal ministry in Malawi (Chiluwe and Nkhata 2014, 321), this arrangement if enforced properly, allows for a systematic management of water resource with an appropriate structure in both nations.

Also, participation of under privileged classes and vulnerable people in planning and implementation of water supply and sanitation efforts particularly in the rural sectors remains an important goal of the legal framework in the two nations.

Acknowledgment The above work is in reference to the ICSSR Project titled 'Social Determiners of Water Inequity – A Systematic Investigation at Bhubaneswar' (Impress/P 2572/2018–19/ICSSR). Accordingly, the authors would like to thank ICSSR for the opportunity to explore the legal intricacies in Water Management.

References

Adams EA (2018) Thirsty slums in African cities: household water insecurity in urban informal settlements of Lilongwe, Malawi. Int J Water Resour Dev 34(6):879–884

African Development Bank (2019) Malawi: from boreholes to public taps: rural communities to access improved water supply thanks to the African Development Bank. Web. 29 Oct 2008. <https://www.afdb.org/en/news-and-events/malawi-from-boreholes-to-public-taps-rural-communities-to-access-improved-water-supply-thanks-to-the-african-development-bank-19113>

Asian Development Bank (2012) Cambodia: water supply and sanitation sector assessment, strategy, and road map. Mandaluyong City, Philippines: Asian Development Bank, 4

Cambodia (2019) The Cambodia country brief. Sanitation and water for all. Sector Ministers' Meeting

CEDAC, SAEDA and PAN AP (2013) Illegal pesticide trade in the Mekong countries: case studies from Cambodia and Lao PDR. CEDAC, SAEDA and PAN AP (2013) Web 29 Oct 2020. <http://files.panap.net/resources/Illegal-pesticide-trade-in-Lao-and-Cambodia.pdf>

Chiluwe QW, Nkhata B (2014) Analysis of water governance in Malawi: towards a favourable enabling environment? J Water, Sanitat Hyg Dev 321–322

Collignon B, Gallegos M, Rathamony K (2018) Global evaluation of UNICEF's drinking water supply programming in rural areas and small towns 2006–2016: country case study report—Cambodia. Toubkiss J (ed.) UNICEF

Fawthrop T. Something is very wrong on the Mekong river. The Diplomat, 26 August 2019. <https://thediplomat.com/2019/08/something-is-very-wrong-on-the-mekong-river/?fbclid=IwA

R1aRBP_MJ1bLQ2Peqd840BRAUqwAhQq8-Jf9u7QcGQsmRywBVJ01-k9M_8>. Accessed 26 October 2020.
Grant M, Soeters S, Bunthoeun I, Willetts J (2019) Rural piped-water enterprises in Cambodia: a pathway to women's empowerment? Water 11:2541
Kelly L, Bertram D, Kalin RM, Ngongondo C (2019) Characterization of groundwater discharge to rivers in the shire river basin, Malawi. Am J Water Sci Eng 5(4):127–138
Khmer T (2016) Banned pesticide found in water. Khmer times 2 August 2016. <https://www.khmertimeskh.com/26349/banned-pesticide-found-in-water/>. Accessed 26 Oct 2020
Laisi E (2009) National IWRM status report: Malawi. Global Water Partnership, pp 18–28
Mulwafu WO (2010) Water rights in the context of pluralism and policy changes in Malawi. J Phys Chem Earth 30:752–757
Mulwafu W, Mwamsamali O (2017) Water permit systems, policy reforms and implications for equity in Malawi. Pegasys Institute, Int Water Manage Institute Reach 2
Oates N, Mwathunga E (2018) A political economy analysis of Malawi's rural water supply sector. Overseas Development Institute 15–16
Piman T, Shrestha M (2017) Case study on sediment in the Mekong river basin: current state and future trends. UNESCO Stockholm Environ Inst 28–32
Rijsdijk A, Mkwambisi D (2016) Evaluation of the water and sanitation (wash) programme in Malawi (2007–2013). UNICEF
Sithirith M (2017) Water governance in cambodia: from centralized water governance to farmer water user community. Resources 44(6):1, 4–8
Smiley SL (2017) Quality matters: incorporating water quality into water access monitoring in rural Malawi. Water Int 42(5):585–598
The World Bank (2017) Cambodia agricultural sector diversification project (P163264):3–9
UN Country Team in Malawi (2017) The road to safe and affordable drinking water
UNICEF and WHO (2019) Progress on household drinking water, sanitation and hygiene 2000–2017. Special focus on inequalities. UNICEF Fund/WHO, pp 48–49
UNICEF Malawi (2017) Why water is becoming malawi's most precious resource (2017) Web 29 Oct 2008. <https://medium.com/@unicef_malawi/why-water-is-becoming-malawis-most-precious-resource-bb01e9644fe3>
Vanny L, Jiwen G, Seingheng H (2015) Phnom penh's municipal drinking water supply: water quality assessment. Sustain Water Resour Manage 1:28–37
Vernooy R (2015) Effective implementation of crop diversification strategies for cambodia, lao PDR and Vietnam: insights from past experiences and ideas for new research. Bioversity Int 35
WaterAid (2016) Malawi country programme strategy 2016–2021. WaterAid, 8
WEPA (2004) State of water environmental issues: Cambodia. WEPA. Web 29 Oct 2020. <http://www.wepa-db.net/policies/state/cambodia/river2_1_3_2.htm>
WHO and UNICEF (2019) Progress on household drinking water, sanitation and hygiene 2000–2017: special focus on inequalities
World Bank (2015) Water supply and sanitation in cambodia: turning finance into services for the future. World Bank Group 15–16:28
World Bank (2013) Voice choice and decision 2: local basic service delivery. The Asia Foundation and World Bank

Flood Frequency Analysis Using Gumbel's Distribution Method and Log-Pearson Type III Distribution Method in Krishna River, Andhra Pradesh

V. Manohar Reddy

Abstract Extreme rainfall events and the resulting floods can take thousands of lives and cause billions of rupees in damage. Assessment of Flood peak water levels in rivers is required for the design of hydraulic structures across the river by the decision-makers. Frequency analysis is based on fitting a probability distribution to a series of observations to estimate the future probabilities of occurrence of many events of interest. In this research work, Gumbel's distribution method and log-Pearson type (LPT) III distribution used for the finding of peak flows for different return periods in the Krishna river in Andhra Pradesh. 37 years (1980–2016) annual peak discharge data used for the analysis at Wadenepally river point in Krishna River. Frequency analysis of flood peak is done for the different return periods of 10, 25, 50, 100, and 200 years in the Study area. Results reveal that Study area is better adopted for Gumbel's Extreme value distribution, even though the log-Pearson type (LPT) III distribution estimates higher values compared to the Gumbel's distribution for the high return period.

Keywords Flood · Frequency analysis · Gumbel's distribution method · Log-Pearson type (LPT) III distribution method

1 Introduction

Floods are common in the Krishna river basin, and worse in some cases. It is necessary to find the magnitude and frequency of the flooding events for safeguard the lives and economy in the river basins. Historical period flood data is very much useful to predict the flood peak for different return periods. Lower reach of Krishna river in Andhra Pradesh state is mostly less maintained and vulnerable to floods. For the design of Hydraulic structures, flood frequency analyses are mandatory and performed in Rapti basin by the maximum flood values. Log-Pearson type–III distribution and Gumbels

V. Manohar Reddy (✉)
Government College of Engineering Kalahandi, Bhawanipatna, India

B. B. Das et al. (eds.), *Recent Developments in Sustainable Infrastructure (ICRDSI-2020)—GEO-TRA-ENV-WRM*, Lecture Notes in Civil Engineering 207,
https://doi.org/10.1007/978-981-16-7509-6_36

distributions are fitted for the selected basin (Kumar 2019). Flood frequency analyses were done for Jhelum river using the flow data and find that flow values corresponding to the high return periods are exceeding the carrying capacity of the river (Sultan Bhat et al. 2019). Aji River basin was analysed for flood frequency studies using Mathematica software by using the eighteen different probability distributions (Ghorbani et al. 2010). Gumbels distributions used for the flood frequency analysis in Lower Mahi river basin and forecasted the flows corresponding to the higher return periods (Bhagat 2017). Flood frequency distribution of monthly maximum flood at Prakasam barrage in Krishna river is studied by Gumbels distribution. L-moment method is most suited for Gumbels distribution at selected gauging station in Krishna river (Krishna and Verendra 2015). Flood frequency analyses for annual maximum flows at Negeri Sembilan is done by generalized logarithmic distribution (Ahmad et al 2011). Historical observations of flow data effectively useful for predicting the future events by some probabilistic distributions. Frequency analyses of future flood events are beneficial for the management of water resources by constructing the hydraulic structures for future use (Opere and Njogu 2020). Flood inundation mapping of Ogun river basin is done by using the flow values of different return periods by Gumbel probabilistic distribution (Shakirudeen and Raji 2014). Daily rainfall of 59 years used and find the rainfall intensity by using Gumbels distribution and developed the flood hazard maps of Narok town (Houessou-Dossou et al. 2019). Gene Expression Programming (GEP) used for Gumbels extreme value distribution and calculated the flood frequency factor and peak flows of several return periods (Onen and Bagatur 2017). Log-Pearson type–III distribution is good for predicting the flood frequency distributions for 172 streams in Australia (McMahon and R. Srikanthan 1981).

2 Study Area

Krishna river is the lifeline for half of the districts in Andhra Pradesh state. Floods and droughts in the Krishna river basin effect the farmers in Andhra Pradesh. The newly located capital city of Andhra Pradesh, Amaravati is along the banks of Krishna river. so, it is very essential to do the flood frequency analysis by the experts for decreasing the effect of future flood events in the capital and low-lying areas along the river. Wadenepally is one of the river gauging points of the Krishna river in Andhra Pradesh. Selected river gauging point is in upstream of the Amaravati and Vijayawada, which are heart for the state. Accurate measurement of flood frequency analysis at Wadenepally is essential to maintain the water levels in the Prakasam barrage (near Vijayawada) in an effective manner. Regular flooding events are happening on the downstream of Wadenepally and causes severe damage. So strategically chosen the Wadenepally river point for analysing the frequency analysis of floods. Wadenepally river point and downstream of the river reach is shown in Fig. 1.

Fig. 1 Lower Krishna river reach in Andhra Pradesh

3 Methodology

In this study, flood frequency analysis done by using the discharge data from 1980 to 2016. 37 years of discharge data at Wadenepally collected from INDIA—Water Resources Information System (WRIS http://www.india-wris.nrsc.gov.in/wris.html). Annual peak discharge data is plotted against the respective years from 1980 to 2015 is shown in Fig. 2.

Gumbel's Extreme value Distribution and Log-Pearson type–III distribution are statistical methods used for predicting the flood peaks for different return periods. Flood frequency analysis using Gumbel's Extreme value Distribution is explained using a simple flowchart in Fig. 3.

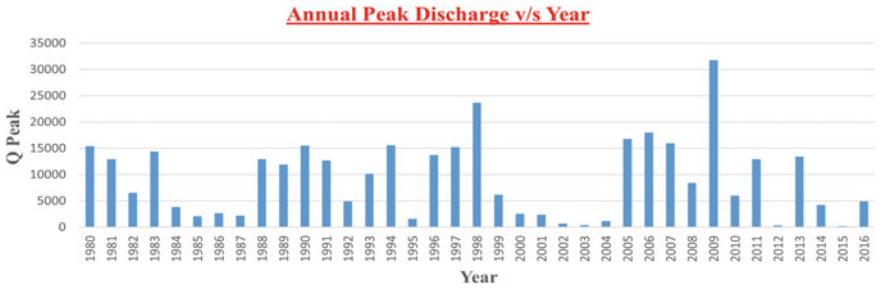

Fig. 2 Annual peak discharge at Wadenepally river gauging point from 1980 to 2016

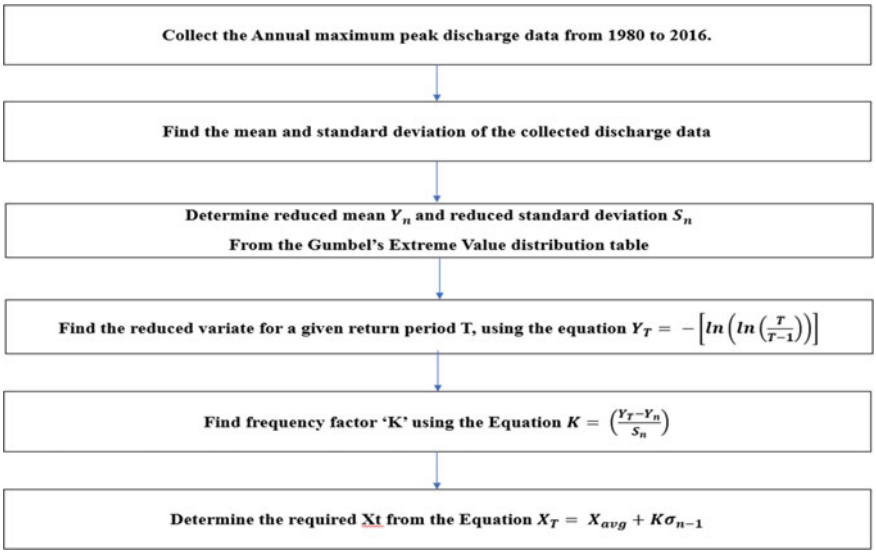

Fig. 3 Schematical procedure of Gumbel's Extreme value distribution

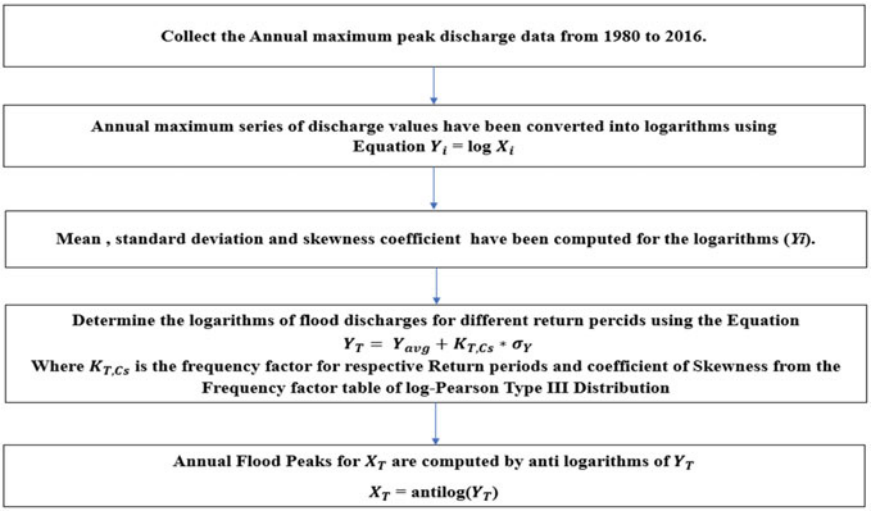

Fig. 4 Schematical procedure of Log-Pearson type–III distribution

Reduced mean Y_n and reduced standard deviation S_n are noted as 0.5418 and 1.1339 respectively, from the Gumbel's Extreme Value distribution table.

Steps for Log-Pearson type–III distribution are explained in a flowchart in Fig. 4.

Coefficient of skewness for the collected sample is calculated from the Eq. 1.

$$C_s = \frac{n\Sigma\left(Y_i - Y_{avg}\right)^3}{(n-1)(n-)S^3} \tag{1}$$

where, n = no of years used for the assessment, S is the standard deviation of the sample, and Y_i is he logarithmic value of annual maximum flow.

4 Results and Discussion

Estimation of flow values for different return period known as flood frequency analysis. Results of flood analysis of Gumbel's Extreme value distribution and Log-Pearson type–III distribution were given Tables 1 and 2, respectively. Maximum and minimum flow values from the assessment sample are 31,802.85 m^3/s and 229.36 m^3/s, respectively. Mean and standard deviation of the sample are 9317.559 and 7385.729.

Maximum flows at the Wadenepally was recorded as 31,802.85 m^3/s n 2009, which is nearly reflects the 50-year return period estimated flows from the above Tables 1 and 2. Graphs between the friction factors and estimated flows for Gumbel's Extreme value distribution and Log-Pearson type–III distribution are given in Figs. 5 and 6,

Table 1 Estimated flow values at Wadenepally for different return periods by Gumbel's extreme value distribution

Return period (T)	Probability (%)	Frequency factor 'K'	Gumbel's varieties (Y_t)	Expected flow X_t (cumec)
5	20	0.845	1.4999	15,558.46
10	10	1.507	2.2504	20,446.42
25	4	2.343	3.1985	26,622.36
50	2	2.963	3.9019	31,204.03
100	1	3.579	4.6001	35,751.87
200	0.5	4.193	5.2958	40,283.12

Table 2 Estimated flow values at Wadenepally for different return periods by Log-Pearson type–III distribution

Return period (T)	Probability (%)	Frequency factor 'K'	Logarithms of flood flows (Y_t)	Expected flow X_t (cumec)
5	20	0.849	4.2093	16,192.69
10	10	1.112	4.3522	22,499.81
25	4	1.335	4.4728	29,704.13
50	2	1.450	4.5351	34,286.34
100	1	1.536	4.5820	38,190.76
200	0.5	1.602	4.6179	41,490.38

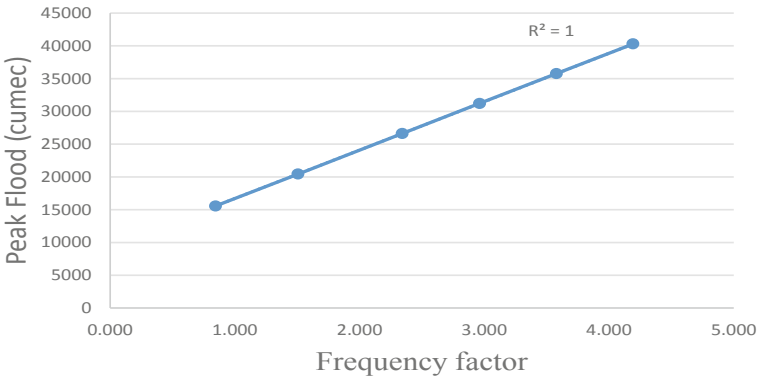

Fig. 5 Plot of peak flood versus frequency factor by Gumbel's extreme value distribution

respectively. Comparison of Flows computed at 5, 10, 25, 50, 100, and 200 years return periods by the two distributions are given in Fig. 7.

From the Fig. 7, we can say that estimated flows from the Log-Pearson type–III distribution were more compared to the Gumbel's Extreme value distribution. But the estimated flows are relatively near to the observed flows. Maximum flow

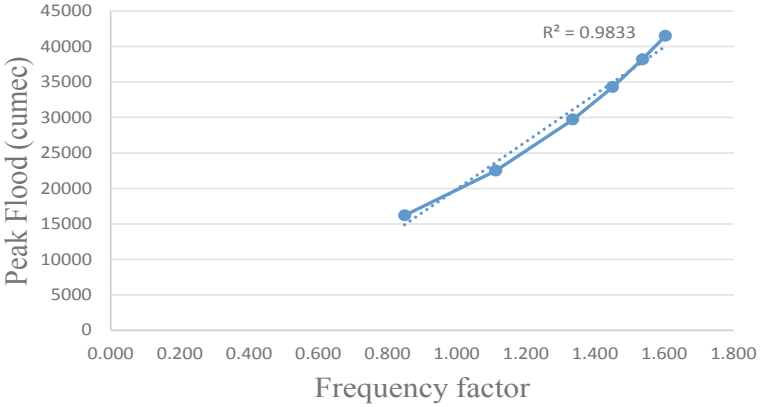

Fig. 6 Plot of peak flood versus frequency factor by Log-Pearson type–III distribution

Fig. 7 Comparison of flows computed using Gumbel's extreme value distribution and Log-Pearson type–III distribution

occurred in the assessment period is 31802.85 cumec which is nearly coincide with the Gumbel's Extreme value distribution 50-year return period flow. From Fig. 5, R2 value for the Gumbel's Extreme value distribution is 1.00 and for the Log-Pearson type–III distribution was 0.9833. Gumbel's Extreme value distribution had better R^2 value and this distribution is suits better for the selected river reach.

5 Conclusions

From the above research work we can conclude that, Lower Krishna river reach was experienced more than 10,000 cumecs flows around 18 times in the selected 37 years. It indicates river reach is frequently experiencing the floods. Maximum flow 31,802.85 cumecs occurred in 2009 which is 3.4 times more than the average

flow in the assessment period indicates, selected river reach experiencing sharp and high floods. Study area is better adopted for Gumbel's Extreme value distribution, even though the Log-Pearson type–III distribution giving more flow values than the Gumbel's Extreme value distribution.

References

Ahmad UN, Shabri A et al (2011) Flood frequency analysis of annual maximum stream flows using L-Moments and TL-Moments approach. Appl Math Sci 5(5):243–253

Bhagat N (2017) Flood frequency analysis using Gumbel's distribution method: a case study of lower Mahi Basin, India. J Water Resour Ocean Sci 6(4):51–54

Ghorbani MA, Ruskeep H et al (2010) Flood frequency analysis using Mathematica. Turkish J Eng Env Sci 34:171–188

Houessou-Dossou EAY, Mwangi Gathenya J et al (2019) Flood frequency analysis using participatory GIS and rainfall data for two stations in Narok Town, Kenya. Hydrology 6:90

Kumar R (2019) Flood frequency analysis of the rapti river basin using log Pearson type-III and Gumbel extreme value-1 methods. J Geol Soc India 94:480–484

McMahon TA, Srikanthan R (1981) Log Pearson III distribution—Is it applicable to flood frequency analysis of Australian streams? J Hydrol 52:139–147

Odunuga S, Raji SA (2014) Flood frequency analysis and inundation mapping of lower Ogun River Basin. J Water Resour Hydraul Eng 3(3):48–59

Onen F, Bagatur T (2017) Prediction of flood frequency factor for Gumbel distribution using regression and GEP model. Arab J Sci Eng 42:3895–3906

Opere AO, Njogu AK (2020) Using extreme value theory to estimate available water in the upper Awach-Kibuon catchment in Nyamira County, Kenya. Am J Water Resour 8(4):200–210

Sai Krishna G, Veerendra GTN (2015) Flood frequency analysis of Prakasam barrage reservoir Krishna District, Andhra Pradesh using Weibull, Gringorten and L-Moments Formula. Int J Civil, Struct Environ Inf Eng Res Dev (IJCSEIERD) 5(2):57–62

Sultan Bhat M, Alam A et al (2019) Flood frequency analysis of river Jhelum in Kashmir basin. Quat Int 507:288–294

A Preliminary Study Exploring the Rooftop Rainwater Harvesting Potential of Bhubaneswar: Scope, Optimization, and Economic Viability

Soumya Kar and Sabyasachi Mohapatra

Abstract Water scarcity and unpredictable weather conditions are an inevitable effect of increasing global temperature. Anthropogenic activities have further aided in the severity of the issues. Bhubaneswar, being the capital city of the state of Odisha, with developing industries and infrastructure establishments, is witnessing an increased annual demand for groundwater, while the annual groundwater recharge has not increased proportionately, leading to a decline in groundwater levels by around 17% (m b.g.l). In contrast, the annual extraction of groundwater has increased quantitatively from about 30% in 2013 to 50% in 2017, while the cumulative annual rainfall for the years has been 1751 mm and 1612 mm, with a mean value of 145.92 mm and 134.33 mm, respectively. Considering a study period of 13 years, from 2008 to 2020, the annual and mean rainfall has been 1375.5 mm and 114.63 mm, and 1286.5 and 160.81 mm, respectively, for 2008 and 2020 (till August). The pattern highlights the importance of harvesting rainfall. In this study, we perform a preliminary analysis evaluating the city of its rainwater harvesting potential and determining the optimal tank size and the associated economic analysis. With an increasing urban infrastructure, rooftop rainwater harvesting (RRWH) shows promising potential. Considering a good case and worst-case scenario, wherein 80% and 30% of households adopt RRWH, the volume of rainwater collected for the year 2018–19 would have been $1.2 * 10^7$ cu.m and $0.44 * 10^7$ cu.m, respectively, while the current harvested amount is meagerly around $0.08 * 10^7$ cu.m. For our study, only taxed houses within the municipal corporation with an average rooftop area of 1000 sq.ft have been adopted. The economic analysis for the breakeven of RRWH shows recovery in 20–25 years, along with the added long-term ecological benefits. This study justifies the RRWH potential of the capital though still at introductory stages.

Keywords Rooftop rainwater harvesting (RRWH) · Bhubaneswar · Economic analysis · Urban infrastructure · Optimization

S. Kar (✉)
Birla Institute of Technology and Science, Pilani, Rajasthan, India

S. Mohapatra
National Institute of Technology, Rourkela, Odisha, India

B. B. Das et al. (eds.), *Recent Developments in Sustainable Infrastructure (ICRDSI-2020)—GEO-TRA-ENV-WRM*, Lecture Notes in Civil Engineering 207,
https://doi.org/10.1007/978-981-16-7509-6_37

1 Introduction

"Thousands have lived without love, not one without water." aptly noted by British poet W H Auden, highlights the unparalleled importance of water for humankind. Even the National Research Council's report on Research Pathways for the Next Decade (National Research Council 1999), quotes "Water is at the heart of both the causes and effects of climate change."

Water is needed for every activity we perform, such as drinking, cooking, washing, cleaning, farming, industries, and recreation. But with industrial development, growing population, and increasing demand, pollution has become a recent problem of our planet, affecting water, air, land, and noise (Dovers and Butler 2017). Pollution is the direct or indirect change in the environment's components harmful to living beings. Pollutants include pesticides, agrochemical and pharmaceutical products, organic matter, metals, and radioactive substances (Özkara et al. 2016).

Water pollution not only degrades the quality of existing water sources, it ultimately leads to scarcity of safe water and increased consumption of polluted or poorly treated water. River water, groundwater, and oceans are all polluted to different magnitudes, which make their safe utilization uncertain. According to one World Health Organization report, 785 million people lack basic drinking water service, 2 billion consume water contaminated with feces and other pollutants, and by 2025 half of the world's population is expected to live in water-stressed areas (Drinking-water 2019). The uneven distribution of Earth's water resources and varying population density has aggravated water pollution and scarcity.

Water pollution kills. According to a study by the Lancet Commission on Pollution and Health, water pollution was responsible for 1.8 million deaths in 2015 alone. Marginalized and low-income communities are disproportionately at risk of illness and death from polluted water.

In India, an exponential rise in population and over-exploitation of existing surface and groundwater sources has led to increased pollution and water stress, resulting in decreased per capita water availability from 5177 cu.m/year in 1951 to a projected 1341 cu.m/year in 2025. When the per capita availability reduces below 1000 cu.m/year, the state is declared water-scarce (Manju and Sagar 2017).

Considering the above scenario, a broader framework incorporating integrated water resources management encouraging aligned water usage according to the needs and demands of different users is necessary. Keeping in view the Government, policymakers, educators, and the country's general masses should adopt and implement efficient water management technology.

In this paper, we are primarily evaluating the rainwater harvesting potential of the developing city of Bhubaneswar. Further, we substantiate our study by an optimization study for tank capacity and associated economic analysis. Using the Net Present Value (NPV) method, the breakeven period was determined. A hypothesis was proposed by considering two scenarios where 80% and 30% of households adopted Rooftop rainwater harvesting (RRWH). The total volume of water collected

for both the scenarios was evaluated and compared to the existing collection capacity to aid our assumption.

1.1 Study Area

Situated in the eastern regions of peninsular India, Odisha boasts rich flora and fauna, maritime history, sprawling agricultural fields, and few perennial rivers. Located around 700 km from the Bay of Bengal, bound by river Mahanadi in the north and Chilika Lake in the south, lies the capital city of Bhubaneswar, defined by highpoints and ridgelines descending into lower elevations. The city's spatial growth was initially slow, but it steadily emerged as one of the country's fastest-growing cities.

With rapid urbanization, the eco-system is getting affected. The existing water bodies are disappearing with dense development, and those that continue to exist are highly polluted. Large parts of the city lack adequate sewage treatment systems, leading to an estimated 173 MLD of untreated sewage flow into adjoining water bodies, polluting rivers, lakes, and groundwater (State of India's Environment 2019 report released by CSE 2019). Further, 19–30% of the city's population is dependent on groundwater for domestic use (Jacob et al. 2012), making them vulnerable to water-related diseases.

1.2 Rainwater Harvesting

Harvesting rainwater is an age-old tradition that is practiced to secure water to meet drinking needs, domestic demands, and agricultural production since the beginning of the Neolithic Revolution (Agarwal and Narain 1997; Gould and Nissen-Petersen 1999; Laureano and Venice 2001; Maliva and Missimer 2012; Friberg and Vahter 1983). Previous studies have documented the development and usage of traditional rainwater harvesting technologies in response to past climate change events, both annual and multi-decadal (Hindson et al. 2011; Pandey et al. 2003). Having a varied climatic condition, India had an assortment of Rainwater harvesting practices such as contouring, micro-dams, rooftop rainwater harvesting, reservoirs, and cisterns.

Though in recent times, rainwater harvesting systems are mostly abandoned due to poor socioeconomic incentives, former colonial policies, increased urbanization, centralization of water resources, increased groundwater extraction abilities, and the alteration of available surface water over long distances through the damming and channeling of rivers (Agarwal and Narain 1997; Castro et al. 2012; Huttenhower et al. 2012; Agarwal et al. 1999; Hoekstra and Mekonnen 2012; Reed et al. 2004). Changes in rainfall and temperature are expected to affect the runoff and water availability, reducing runoff by 10–30% in certain regions (Change, Intergovernmental Panel On Climate 2007). Given these projections, the IPCC (Intergovernmental Panel on

Climate Change) has recommended expanding the practice of rainwater harvesting through water storage and preservation to reduce human vulnerability.

Harvested rainwater is a renewable source of clean water ideal for domestic and landscape uses, providing flexible solutions to meet new and existing demands for both small and large sites (Dos Santos and De Farias 2017; Abu-Zreig et al. 2013). The rainwater harvesting system's larger benefit is the low cost compared to other water supply systems, accessibility, and maintenance at household levels. Further, harvesting rainwater has a long-term impact on local water resources by reducing demands for surface and groundwater withdrawals, simultaneously protecting local water resources' integrity by reducing nonpoint source pollution (Abdulla 2020).

Components for a rooftop rainwater harvesting (RWH) system generally consists of a collection area (roof), a conveyance system, and a cistern or storage tank, aided with or without a filtration unit, delivery system, and treatment depending upon the final usage of the collected water. The study area's common roof material is cement, having good durability, relatively low price, and fairly good quality water (collected after the first flush). The conveyance system usually consists of gutters or pipes that deliver rainwater falling on the rooftop to cisterns or tanks, where the water is ultimately stored. Several options are available for constructing these tanks concerning shape (cylindrical, rectangular, square, or tailored), capacity, and construction material (brickwork, PCC and RCC, plastic, or metal). The storage tanks may be constructed as part of the building or built as a separate unit located at a distance away from the building, which could further channel surplus water to the groundwater table.

2 Analysis of Rainfall Patters with Reporting of Groundwater Level Data

From the fundamental behavior of nature, rainfall is a process that is a part of one of the cyclic processes in nature; the water cycle. As per the water cycle, water gets evaporated from the Earth's surface as vapor (generally during summer months) and later falls back on to it in the form of rain (generally during the monsoon period). This cycle balances the water distribution on the planet. Many places on Earth directly or indirectly depend on the amount of rainfall received, which recharges their lakes, rivers, and groundwater table.

This study's data has been retrieved from the Odisha Rainfall Monitoring System maintained by the State Government (Odisha Rainfall Monitoring System), which shows that the rainfall event is clustered over a period starting from June till the end of October. The data were collected from January 2008 till August of 2020. Figures 1 and 2 represent the rainfall pattern observed through a given year and the total rainfall received during that particular year. Figure 2 further highlights the unpredictable rainfall event, with several years reporting less than average rainfall, i.e., 1522.5 mm, while others witnessed heavy rainfall events. The rainfall received

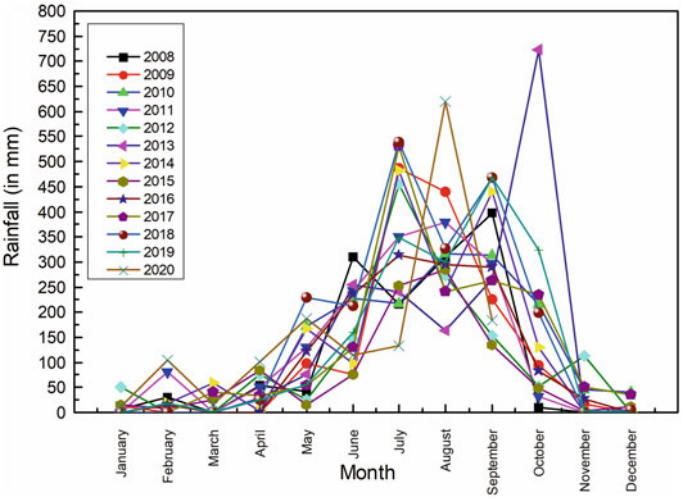

Fig. 1 Rainfall variation throughout a year compared for a period from 2008 to 2020 (till August)

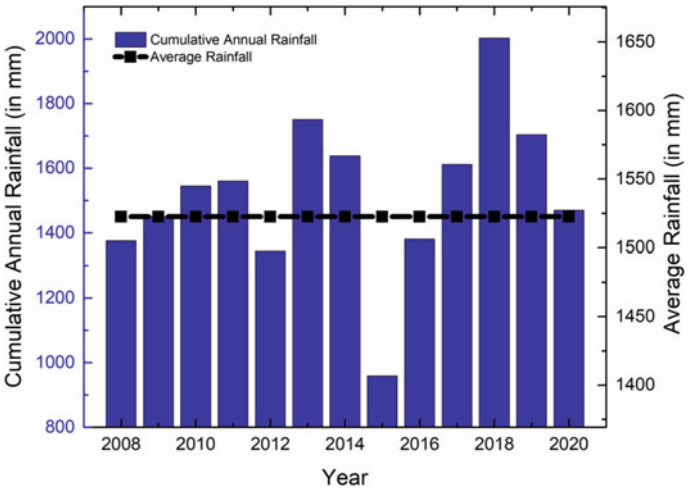

Fig. 2 Cumulative rainfall data along with annual average computed for a period from 2008 to 2020 (till August)

during the first half of the studied years starting from January to June, ranged between 1375.5 and 1751 mm, whereas for the second half starting from July to December, the rainfall varied from 959 mm to as high as 2003 mm, further highlighting the very diverse behavior of annual rainfall. Bhubaneswar, the capital city, and a developing urban center account for the most domestic and commercial groundwater utilization. The state has a tropical climate; hence monsoon rainfall is the major source of water.

Storing this water is imperative for the city's sustenance, and groundwater reserves are the best available option. However, adverse climatic changes accompanied by erratic rainfall events, coupled with the exploitation of existing water resources, reinforce the authors' belief in RWH, RRWH, particularly being adaptable to the studied city's conditions (Abdulla and Al-Shareef 2009).

As per the Dynamic Groundwater Resources Assessment of India (National Compilation on Dynamic Ground Water Resources of India 2017), in the year of 2017, the Khordha district of Odisha had 0.44 bcm of annual extractable groundwater of which around 50% is being extracted, and the demand has grown by 1.5 times over 4 years, starting from 2013 to 2017, with the demand growing continuously year after year. The demand has led to a decrement of 17% in the available water level, i.e., water previously found at an average depth of 12 m below ground level (mbgl) in 2013 to now being found below 14 mbgl. The above statistics prove the decrease in available extractable groundwater, which has been degrading with increased extraction.

3 Rainwater Harvesting Potential and Implementation Data

As most places on Earth have become cemented lands, the water hardly gets the opportunity to recharge the groundwater and mostly runs off to the sea carrying pollutants from the land, making the rainy season's task fail to maintain the cyclic balance. So RRWH becomes an efficient approach to save the water and help in cost-saving, as is discussed later in the article. This preliminary analysis takes into account only the city of Bhubaneswar for estimating the harvesting potential. The Bhubaneswar Municipality Corporation covers 186 sq.km and has around 100,000 (Profile) taxed households. Taxed households are considered for the analysis, assuming they have adequate rooftops and unexplored potential for harvesting rainwater.

$$VR = \mathrm{R} \times \mathrm{A} \times \frac{\mathrm{C}}{1000} \tag{1}$$

Equation 1 (Abdulla and Al-Shareef 2009) is used for calculating the rainwater harvesting potential for the households, where the annual volume of rainfall (VR) is given by the product of average annual rainfall (R), the total roof area in Bhubaneswar (A) (assuming an average of 1000 sq.ft or 93 sq.m of roof area per building), and runoff coefficient (C) (taken as 0.8, assuming 20% rainwater is lost by first-flush, evaporation). Estimation using the equation above shows that for the year 2019, 1.3×10^7 cu.m of water and the current year (available rainfall data till august), 1.1×10^7 cu.m could have been collected.

As part of this study's scope, we estimate two possible scenarios: in the best case, 80%, and in the worst case, 30% of the households opt for rainwater harvesting. For the year 2019, for the best case, the volume of rainfall saved would have been

Table 1 Potential and implemented rainwater harvesting (RRWH) data

Financial year	Potential volume of rainwater harvested (if all 100,000 households implement RRWH) (in 10^7 m^3)	Potential volume of rainwater harvested (if 30% of households implement RRWH) (in 10^7 m^3)	Potential volume of rainwater harvested (if 80% of households implement RRWH) (in 10^7 m^3)	Volume of rainwater currently harvested (considering the average rooftop area and data from Department of Water Resources Odisha) (in 10^7 m^3)
2018–2019	1.3	0.4	1.01	0.08
2019–2020	1.1	0.32	0.87	0.08

1.01×10^7 cu.m, and for the worst-case, the volume would be 0.4×10^7 cu.m. Whereas for the current year till now, the best and worst-case potentials would be 0.87×10^7 cu.m and 0.32×10^7 cu.m, respectively. From the data retrieved from the Department of Water Resources of Odisha (Annual Report 2018-19), as of March 2019, RRWH structures have been installed in 132 government buildings and 5351 private buildings during 2018–19. Considering Eq. 1 and calculating, somewhere around 0.08×10^7 cu.m of rooftop rainwater would have been harvested during this period if the structures are maintained properly. A brief description of the above analysis is represented in Table 1 for clarity. This preliminary analysis shows the potential available for RRWH.

4 Economic Viability with an Optimized Tank Size Recommendation for RRWH

In today's fast-moving and competitive world, economy and ecology have to go hand in hand for sustainable development, and the economic feasibility marks the success of a process. Considering some of the basic requirements of RRWH, which includes pipes or gutters for water collection, a filter unit for removing debris, a storage tank, and finally, a recharge unit, the economy involved were analyzed. Using available market prices for the raw materials and construction charges, a rough estimate of around ₹130,000 was attained to install one system; associated budget estimation is represented in Table 2. The Government of Odisha subsidizes the RRWH under one of its schemes by 50% of the invested amount, up to a maximum of ₹45,000, aiming towards sustainable urban development (Scheme: Rooftop Rainwater Harvesting Ground Water Recharge in Urban Areas of Odisha).

Estimation of economic sustainability requires parameters like the per capita water consumption and the current prevailing prices. As per the Ministry of Housing and Urban Affairs, the per capita water consumption for urban is benchmarked at 135 L per capita per day (lpcd) (Per Capita Availability of Water 2020). Currently, the area's

Table 2 The basic components of RRWH as prescribed by the Government of India and their pricing

Components	Quantity	Specifications	Price (₹)
PVC pipes (rainwater collection roof to filter unit)	10	110–150 mm	10,000
Filter unit	1	Flow rate: 105 lpm, suitable for 1200 sq.ft. roof area, model FL-100 filter	7500
Storage unit	1	PVC tank of 5000 l	15,000
Recharge unit	1	Price varies between ₹60,000–₹80,000 depending on the type	70,000
		Including miscellaneous raw materials and labor charges	27,000
Total			**130,000**

water supply is shifting from the traditional per tap per month pricing to a metered connection system, where the tentative average tariff decided is ₹4.14 per kilolitre (Watco Water Tariff Concept Plan 2017).

Assuming a maximum of 10 persons per household, the rental cost for water estimates to ₹170 for 2020. The Government plans to increase the tariff by 5% per annum, so compounding the current price in 2040, the average price is projected around ₹450, keeping all other factors constant. Substituting the entire water usage for a household from groundwater recharged by the household's RRWH system estimates that a family can save around ₹2000 per year at the supply water's current price. Accounting the increment of water tariffs into calculation shows that the amount invested by the household (i.e., the total amount invested—the amount subsidized) for the RRWH system recovers within 20–25 years, post which, not only the supply of water is free in some sense; it also encourages a sustained approach for future resources, considering the ongoing pollution and irreversible climatic changes.

For the above preliminary analysis for RRWH, we assumed the tank size to be 5000 l or 5 cu.m, as it is the minimum recommended tank size by Water Resource Department, Govt. Of India. But for the actual implementation, the designer needs to provide the system with an adequate storage tank. During the rainy season, this tank will receive huge water inflows compared with the summer days. According to a previous study, author Abdulla (2020) has reviewed some methods for estimating the adequate tank size and using the supply-side approach predicted optimum tank size, taking into account the rooftop area, the average annual rainfall data, and the water demand from the tank. For our study taking an average annual rainfall of 150 mm (data represented in Table 3), for a rooftop area of 1000 m^2, we get an optimum tank volume estimation of 45,000 l, deduced from the plot in Fig. 3 (Abdulla 2020). A tank of capacity 45 cu.m would incur a huge capital cost and require a huge area for installment. Considering the city's financial status, the authors recommend small on-ground storage and encourage more groundwater recharge so that the initial and

Table 3 Annual average rainfall for Bhubaneswar for the period 2008–2020 (till august)

Year	Annual average rainfall (in mm)
2008	114.63
2009	121
2010	128.7
2011	130
2012	112
2013	145.9
2014	136.5
2015	80
2016	115.1
2017	134.33
2018	166.93
2019	141.94
2020	160.81

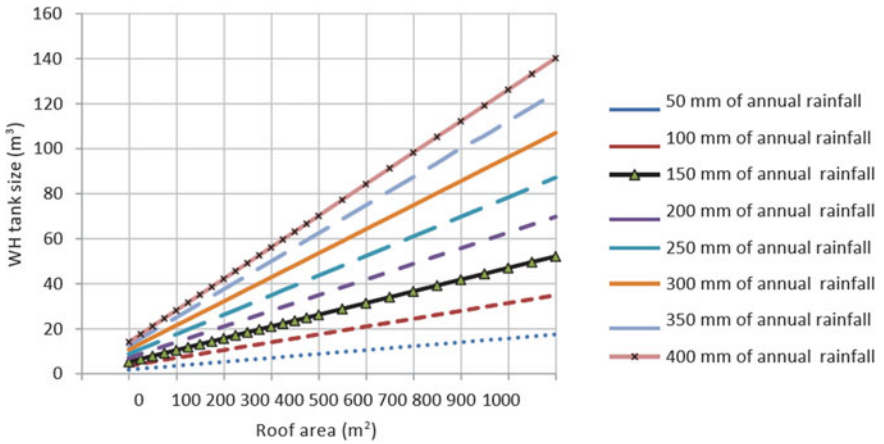

Fig. 3 Optimum tank volume estimated based on Rooftop area and amount of rainfall (empirical relation) (Abdulla 2020)

running cost stays low. Further, Bhubaneswar's groundwater quality is reasonable. Hence, encouraging groundwater recharging is beneficial in the longterm.

5 Conclusions

Bhubaneswar demonstrates the journey of an ancient Indian city standing at the cusp of urbanization while protecting its historical significance. But (re)development on

the cost of degrading ecology is not adaptable in the long run. There has to be a collected vision for long-term sustainability and liveability. Harvested rainwater "has more of a past, and a future than a significant present," stated by Terry Thomas, explains the historical significance of RWH in sustaining civilizations and the future impact it must have when water tariffs, pollution, and scarcity reach unprecedented levels. Several regions depend upon imported water to meet their needs. Collecting natural rainwater and planning ways to store the water and ensure efficient distribution leads to huge economic upliftment. Further rainwater reduces peak demand during summer months, thereby diverting municipal water for more important uses. Groundwater recharging through RWH not only improves the soil moisture and but also benefits irrigation.

From our study, it is established that RRWH is a feasible option for Bhubaneswar to stabilize future water scarcity. A more detailed study can be performed by an optimistic scenario where the entire city adopts RWH, with more precise ground data for a better-optimized proposal, as a suggestion to lawmakers. Bhubaneswar and its twin sister, the city of Cuttack, can be brought under an umbrella initiative for RWH. Social awareness, education, and Government policies and encouragement will inspire the people to adopt a more sustainable lifestyle.

References

Abdulla F (2020) Rainwater harvesting in Jordan: potential water saving, optimal tank sizing and economic analysis. Urban Water J 17(5):446–456

Abdulla FA, Al-Shareef AW (2009) Roof rainwater harvesting systems for household water supply in Jordan. Desalination 243(1–3):195–207

Abu-Zreig M, Hazaymeh A, Shatanawi M (2013) Evaluation of residential rainfall harvesting systems in Jordan. Urban Water J 10(2):105–111

Agarwal A, Narain S (eds) (1997) Dying wisdom: rise, fall and potential of India's traditional water harvesting systems, vol 4. Centre for Science and Environment

Agarwal A, Narain S, Sharma A (1999) Green politics: global environmental negotiations

Annual Report 2018–19. Government of Odisha Department of Water Resources. http://www.dowrodisha.gov.in/AnnualReport/WR_AR18-19.pdf

Castro C et al (2012) Bacterial cellulose produced by a new acid-resistant strain of Gluconacetobacter genus. Carbohydrate Polymers 89(4):1033–1037

Change, Intergovernmental Panel On Climate (2007) Climate change 2007: the physical science basis. Agenda 6(07):333

Dos Santos SM, de Farias MMM (2017) Potential for rainwater harvesting in a dry climate: assessments in a semiarid region in northeast Brazil. J Clean Prod 164:1007–1015

Dovers S, Butler C (2017) Population and environment: a global challenge. Australian Acad Science. https://www.science.org.au/curious/earth-environment/population-environment, Retrieved 15 (2017)

Drinking-water. https://www.who.int/news-room/fact-sheets/detail/drinking-water. Available 14th June 2019

Friberg L, Vahter M (1983) Assessment of exposure to lead and cadmium through biological monitoring: results of a UNEP/WHO global study. Environ Res 30(1):95–128

Gould J, Nissen-Petersen E (1999) Rainwater catchment systems for domestic supply. Intermediate Technol

Hindson BJ et al (2011) High-throughput droplet digital PCR system for absolute quantitation of DNA copy number. Analy Chem 83(22):8604–8610
Hoekstra AY, Mekonnen MM (2012) The water footprint of humanity. Proc Natl Acad Sci 109(9):3232–3237
Huttenhower C et al (2012) Structure, function and diversity of the healthy human microbiome. Nature 486(7402):207
Jacob T et al (2012) Recent contributions of glaciers and ice caps to sea level rise. Nature 482(7386):514–518
Laureano P, Venice UNESCO (2001) The water atlas: traditional knowledge to combat desertification
Maliva R, Missimer T (2012) Arid lands water evaluation and management. Springer Science & Business Media
Manju S, Sagar N (2017) Renewable energy integrated desalination: a sustainable solution to overcome future fresh-water scarcity in India. Renew Sustain Energy Rev 73:594–609
National Compilation on Dynamic Ground Water Resources of India (2017) Government of India Ministry of Jal ShaktiDepartment of Water Resources, RD & GR Central Ground Water Board. http://cgwb.gov.in/GW-Assessment/GWRA-2017-National-Compilation.pdf. Available July 2019
National Research Council (1999) Human dimensions of global environmental change. Global environmental change: research pathways for the next decade. The National Academies Press, Washington, DC. https://doi.org/10.17226/5992
Odisha Rainfall Monitoring System. https://rainfall.nic.in/PubRainChart.asp
Özkara A, Akyıl D, Konuk M (2016) Pesticides, environmental pollution, and health. Environmental Health Risk-Hazardous Factors to Living Species. IntechOpen
Pandey SB et al (2003) The optical afterglow of the not so dark GRB 021211. Astron Astrophys 408(3):L21–L24
Per Capita Availability of Water. Ministry of Jal Shakti. https://pib.gov.in/PressReleasePage.aspx?PRID=1604871. Posted on 02 Mar 2020
Profile. Bhubaneswar Municipal Corporation. https://www.bmc.gov.in/about/profile
Reed KD et al (2004) The detection of monkeypox in humans in the Western Hemisphere. New England J Med 350(4):342–350
Scheme: Rooftop Rainwater Harvesting & Ground Water Recharge in Urban Areas of Odisha. Department of Water Resource Odisha, http://www.dowrodisha.gov.in/Citizen/RRHS/RRHS.htm
State of India's Environment 2019 report released by CSE (2019) Report released at annual media summit held in Rajasthan's Alwar district. Available 11th February 2019
Watco Water Tariff Concept Plan. PMC –WATCO. Posted on 27 Mar 2017

Slope Stability Using Shaking Table

Seema Shringeri and P. G. Rakaraddi

Abstract To study the performance of slopes under seismic conditions, soil strengthening can be utilized to expand the execution of slopes by less deformation and several road embankments and embankment dams failed or suffered severe distress during the earthquake. The instrumentation and monitoring of actual embankments is the best way to study the performance of embankments during earthquakes. However, A series of model tests on a horizontal shaking table were conducted on slopes to study the behavior under seismic conditions. The slopes were built in a model box with a size of about 35 × 30 × 30 cm and the soil collected from nearby city, Bagalkot which is used for the study with the two different slope angles with different heights were considered for each slope to observe the failure of slope during the vibration of table 2 Hz, 3Hz and 4 Hz respectively with constant amplitude. Failure surface were observed horizontally in the upper part of slopes. The response of slope observed with increasing height of slope and angle, displacement increases and Galvanized iron fibers were used as reinforcement in the present work by varying the amount of fibers in slope, to compare the reinforced and unreinforced condition.

Keywords Horizontal shaking table · Slope stability · GI fiber · Reinforced soil slope

1 Introduction

The stability of slope is the capability of protected slopes of the ground to resist and experience the development. Strength of the slope is stated in terms of its shear stress and the shear strength. Effectively steady slope could at first be insecure prohibitively. The initiating components of a slope can be climatic events that could later cause irregularities of the slope, which has caused huge or enormous developments and mass developments caused by the increment in shear stress, for example, load, horizontal pressure, and transient forces. On the other hand, shear strength can be reduced

S. Shringeri (✉) · P. G. Rakaraddi
Basaveshwar Engineering College (Autonomous), Bagalkote 587103, India

B. B. Das et al. (eds.), *Recent Developments in Sustainable Infrastructure (ICRDSI-2020)—GEO-TRA-ENV-WRM*, Lecture Notes in Civil Engineering 207,
https://doi.org/10.1007/978-981-16-7509-6_38

with atmospheric agents, changes in interstitial water pressure and natural material. The reliability range of slope includes the static and dynamic slope stability and drainage dams, the slopes are found in the various types of dams, the excavated slopes and the characteristic slopes in the ground and the weak rocks. To study the performance these slopes there is a critical perspective for the execution of slope under seismic conditions. In spite of the fact that knowledge for the analysis of slope stability and tracking of slope movement and in recent years techniques for stabilization has improved substantially, the instabilities of natural and man-made slopes can cause risks in various areas, particularly during seismic events. The slopes which are truly steady under static conditions can simply fold alongside seismic vibration because of a couple of reasons, including ground shaking that cause excessive vibrations and deformations, loss of bearing strength of the establishment soil due to liquefaction and decrease in the great segment of the slope in view of transient strokes of the pore water pressures. Soil reinforcing can be used to grow the execution of slopes by the less deformation and to make slope steep in less space has been a potential topic that is critical to geotechnical engineers from the past two decades. Be that as it may, the learning on the seismic execution of these reinforced soil slopes under seismic conditions is not observed by many (Vyas et al. 2014). The current earthquakes in India, as, Bhuj Quake (2001), Chamoli Seismic earthquakes (1999), Jabalpur Seismic earthquakes (1997) and Latur Seismic earthquakes (1993) have featured how our present frameworks are to ground developments and that more investigation is expected to properly know the direct of these infrastructures under seismic condition. Among the Bhuj earthquakes a couple of road banks and dam embankment brake or affected firmly (Giria and Sengupta 2009, 2010b). To conduct the slopes under unique condition in the research facility, the model test on the shaking table is one of the best approach to observe the nature. Response of reinforced soil slopes to seismic load conditions is managed by the properties of soil, properties of support and geometry of the slope separated from the beginning parameters of the seismic occasion. Focus specific on the seismic response of the reinforced soil slopes concentrated mainly the examination of failure components, including the impact of support parameters and ground movement parameters on the seismic stability of the slopes. The components impacting the security of the soil slopes are: (i) Soil type and structure (ii) Discontinuity and weaknesses (iii) External load (iv) Slope geometry.

2 Materials and Methodology

2.1 Soil

Soil used for the detail work is collected from close by city, Bagalkot. Also various tests are carried out to determine the index properties of the soil. Coefficient of curvature (C_c) and Coefficient of uniformity (C_u) of the soil is determined to characterize

Table 1 Soil properties

Description	Notation	Result
Specific gravity	G_s	2.51
Grain size (mm)	D_{10}	0.24
	D_{30}	0.81
	D_{60}	2.40
Uniformity coefficient	C_u	10
Coefficient of curvature	C_c	1.167
Liquid limit	W_L	26.50%
Plastic limit	W_P	12.78%
Plasticity index	I_P	13.72%
Soil type	CL	Inorganic clays of medium plasticity
Optimumu mositure content	OMC	16.30%
Max dry density	$\gamma_{d(max)}$	15.69 kN/m^3
Cohesion	C	13 kN/m^2
Friction angle	Φ	30º

the type of soil by conducting grain size distribution analysis according to IS 2720 (Part-4). The estimations of Cc and Cu are obtained from chart. The actual property of the soil like specific gravity (G) is obtained by density bottle test according to IS 2720 (Part-3). The results of these tests are given in Table 1 (Giri and Sengupta 2010a).

Atterberg limits, these test techniques dissimulate the choice of the liquid limit (LL), plastic limit (PL), and the plasticity index (PI) of soils that passes the 425 micron IS sieve. Liquid limit test is directed by casagrande assembly to show the liquid limit of soil and Plastic limit test. Tests are conducted as per IS 2720 (Part-5). The test results of *LL*, *PL* and *PI* are given in Table 1.

As per IS 2720 (Part-7) OMC and MDD of the soil is found by standard proctor test. Cohesion (C) and angle of friction (φ) of the soil is determined by direct shear test according to IS 2720 (Part-13) at its maximum dry unit weight and OMC, the results of OMC, γd(max), C and φ are given in Table 1. The soil classified according to IS 2720 (Part-4) as inorganic clay of medium plasticity (CL) from the outcomes of result.

2.2 Galvanized Iron Fiber

Galvanized iron (*GI*) a layer of zinc is coated to hold the metal to resist corrosion. At the point when metal is in working request, to be utilized in a climate where

Fig. 1 GI fiber of proportion 20

consumption maybe, it is routinely galvanized with the goal that it will be a great idea to experience the conditions.

Approximately 1 mm diameter (*D*) round GI wire was cut to the necessary length (L) of 20 mm and 40 mm giving an proportion or aspect ratio (L/D) of 20, 40. The silent tensile strength fibers are economically available and are usually utilized for electrical work. These GI fiber of proportion 20, 40 are blended in the soil at 2% and 4% by weight. The photograph of the GI fiber of proportion 20 is shown in Fig. 1

3 Experimental Setup

3.1 Shaking Table Equipment

The shaking table is a equipment to reproduce the component of the earthquake, commonly known frequency and amplitude of vibrations. The machine comprises of control panel and drive unit. The fly wheel is having radial scale to change the amplitude. The control board is the most essential part of the shake table as it controls the frequency of the base shaking (Giria and Sengupta 2009). The Shake table tests have the advantage of high controlled information developments and shaking table instrument shown in the Fig. 2. The shake table is having a stage on which revolving table is mounted, rotational table has the tapped openings to fix the various models. This is mounted on straight course and guided in the horizontal direction. The base plate of shake table is mounted over the main concern plate, which is grouted in the concrete bed. The control unit has recurrence drive with ON and OFF pointers and it helps to fit the desired frequency.

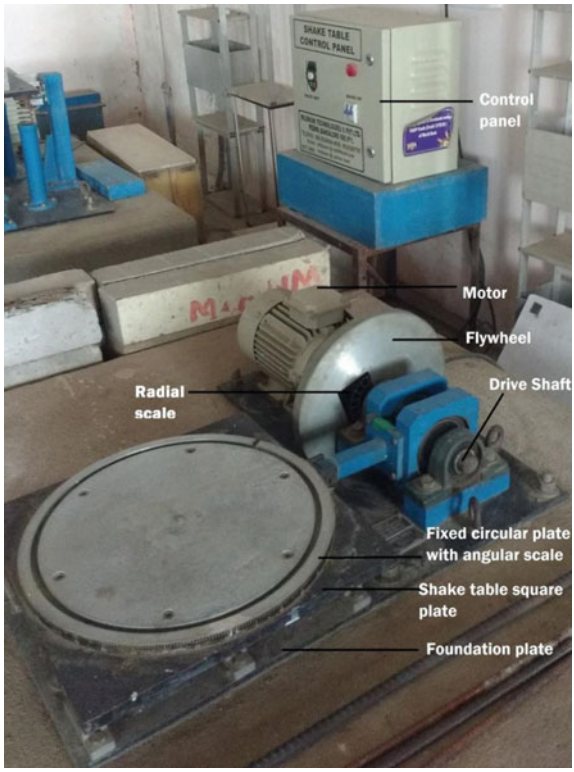

Fig. 2 Shaking table with control unit

3.2 Model Box

Transparent acrylic model box of size 35 cm × 30 cm × 30 cm and having thickness of 5 mm is prepared to conduct the soil slope studies. The acrylic material is strong to oppose the vibration and permit representation of slope surface. Model box opened at one side for soil slope planning and also to measure the displacement of soil slope during testing (Giria and Sengupta 2009; Sahoo et al. 2016). The maximum height maintained in the current work is 20 cm because of load capacity of horizontal shake table (most extreme compensation load 30 kg). The photograph of acrylic model box is shown in Fig. 3.

3.3 Displacement Measurement Device LVDT (Linear Variable Displacement Transformer)

LVDT is equipment, which is utilized measure the displacement of the soil slope. Based on the slope height number of LVDT's is placed at 2, 8, 14 and 18 cm from

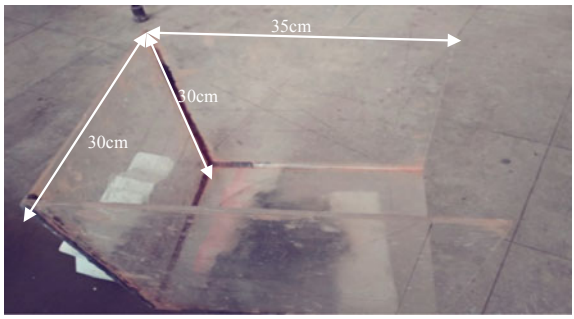

Fig. 3 Model box

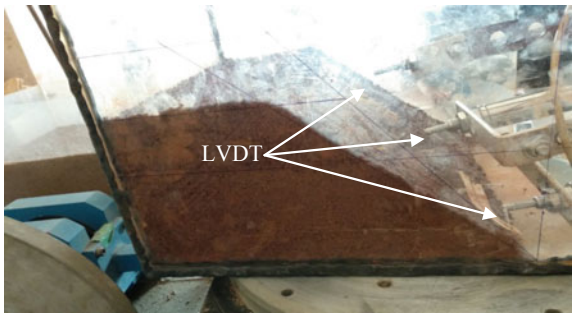

Fig. 4 LVDT setup

the lower part of the container as appeared in Fig. 4 and these are associated with data logger to record the displacement.

3.4 Preparation of Specimen

The dirt slants of point of 40º and 50º were built utilizing clay (moorum) blended in with required amount GI fibers as reinforcement in model box by compacting the soil in 3 layers at OMC of equal height by controlled volume method. Water substance and unit weight were kept as 16.3% and 15.69 kN/m^3 separately in all the soil slope model tests After compacting soil in shape of rectangular, the soil was trimmed to the required slope angle of 40° and 50° with the height of slope as 10 cm and 15 cm individually (Srilatha et al. 2017). Randomly distributed GI fibers shown in Fig. 5.

4 Methodology

All slope models were subjected to the horizontal vibration independently of known constant amplitude and varying frequency. In the current work constant aplitude is

Fig. 5 Randomly distributed fibers mixed in the soil

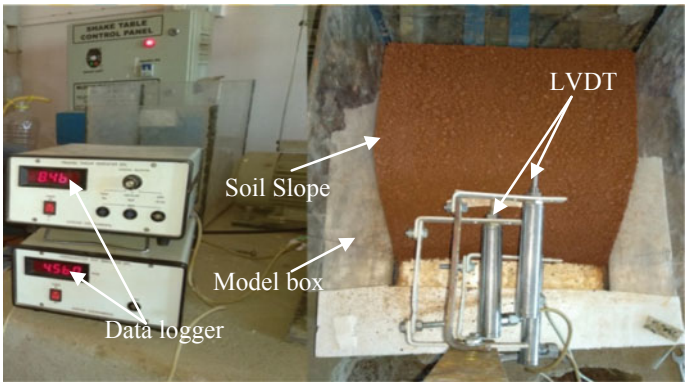

Fig. 6 Experimental setup

maintained as 4 mm. The stability of soil slope for specific soil is studied for varying frequency of 2, 3 and 4 Hz. Slope displacement are measured with LVDT connected at different heights as shown in Fig. 6. The observation is proceeded till the hairline cracks show up on the slope surface. Experimental arrangement is shown in Figs. 6 and 7a, b shows the slope models of shaking table before and after the test.

5 Results and Discussions

5.1 Stability Analysis of Unreinforced Slope

Shaking table tests are carried out on soil slope by different frequency with constant amplitude for varying slope angle and height. Time taken for the slope failure and displacement were measured for frequency of 2 Hz, 3 Hz and 4 Hz.

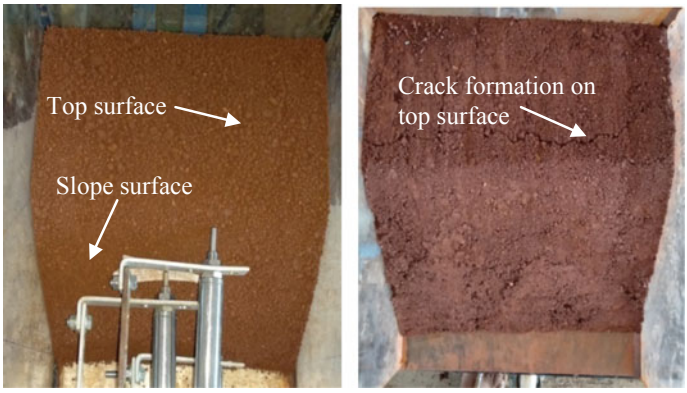

Fig. 7 (a) and (b) Failure plane of horizontal shake table

5.1.1 Stability Analysis of Unreinforced Slopes of 40°

The soil slopes compacted to the required density and test conducted for the slope of 40° and height of 10 cm. The results for the constant amplitude of 4 mm and displacement at 2 cm and 8 cm from the bottom of the slope against time is plotted and shown in Fig. 8a–c respectively for the frequency of 2 Hz, 3 Hz and 4 Hz.

From the Fig. 8, it is found that, the slope will fail (hair cracks will be formed at the top of the slope) for the frequency of 2 Hz, 3 Hz and 4 Hz at the shaking time of 18 min, 16 min and 14 min and the displacement at 2 cm and 8 cm is 5.432 mm and 7.114 mm, 6.385 mm and 8.426 mm and 7.249 mm and 8.62 mm respectively. It is clear that with the increase in the frequency the displacement also increases and displacement measured at 8 cm height is more than at 2 cm height.

The failure of the slope is observed (hair cracks will be formed at the top of the slope) for the frequency of 2 Hz, 3 Hz and 4 Hz is at the shaking time of 24 min, 20 min and 18 min and the displacement at 2 cm, 8 cm and 14 cm is 7.14 mm, 8.174 mm, and 9.87 mm, 7.52 mm, 8.427 mm, and 10.27 mm, and 7.88 mm, 8.845 mm and 10.66 mm respectively observed from the Fig. 9. Here also similar observation was made as increase in the frequency leads to increase in the displacement and displacement measured at 14 cm height is greater than 8 cm and 2 cm height.

5.1.2 Stability Analysis of Unreinforced Slope of 50°

From the Fig. 10, it shows that, the displacement for frequency of 2 Hz at shaking time of 19 min are 7.03 mm and 8.389 mm, for 3 Hz at shaking time of 17 min are 7.81 mm and 8.653 mm and for 4 Hz at shaking time of 15 min are 8.26 mm and 9.826 mm respectively. Slope will fail (hair cracks will be formed at the top of the slope) for the frequency of 2 Hz, 3 Hz and 4 Hz of constant amplitude 4 mm. It is

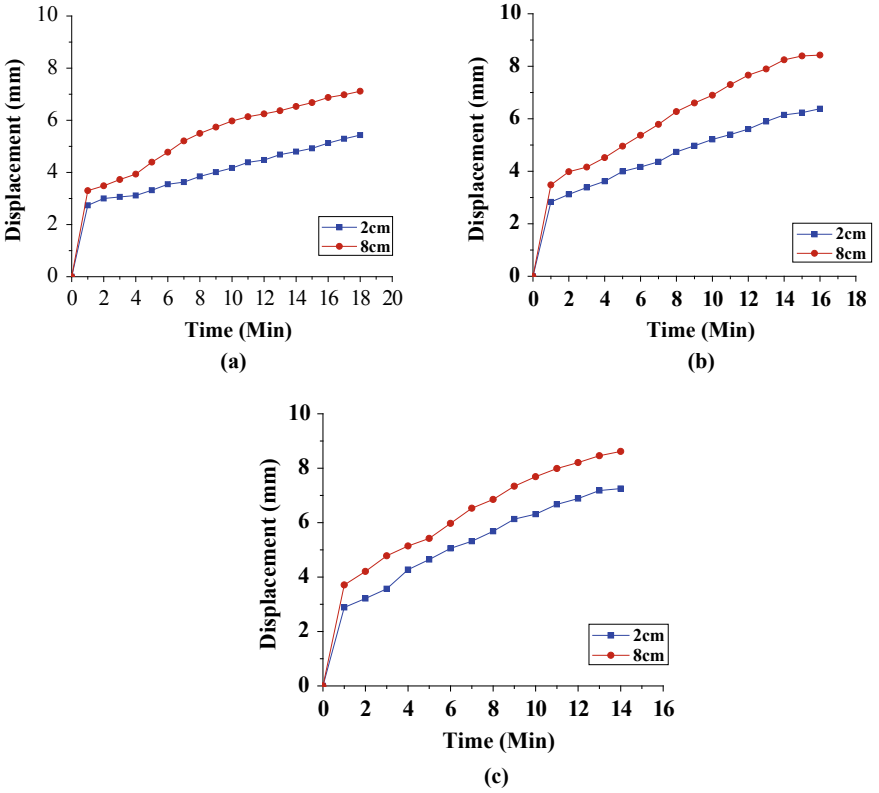

Fig. 8 Variation of displacement of 10 cm height of 40º slope at 2 cm and 8 cm height from the bottom of the embankment for the amplitude of 4 mm with time for the **a** frequency = 2 Hz, **b** 3 Hz, and **c** 4 Hz

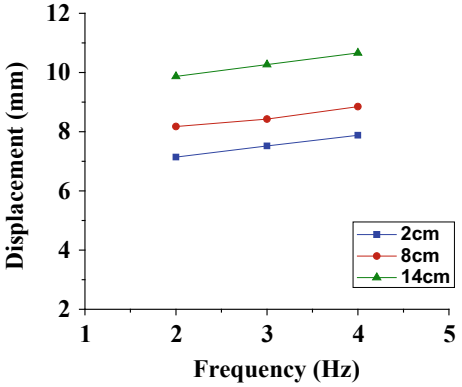

Fig. 9 Displacement variation of 4 mm constant amplitude for 15 cm height of 40º slope at 2 cm, 8 cm and 14 cm height from the bottom of the slope for the Frequency of 2 Hz, 3 Hz, and 4 Hz

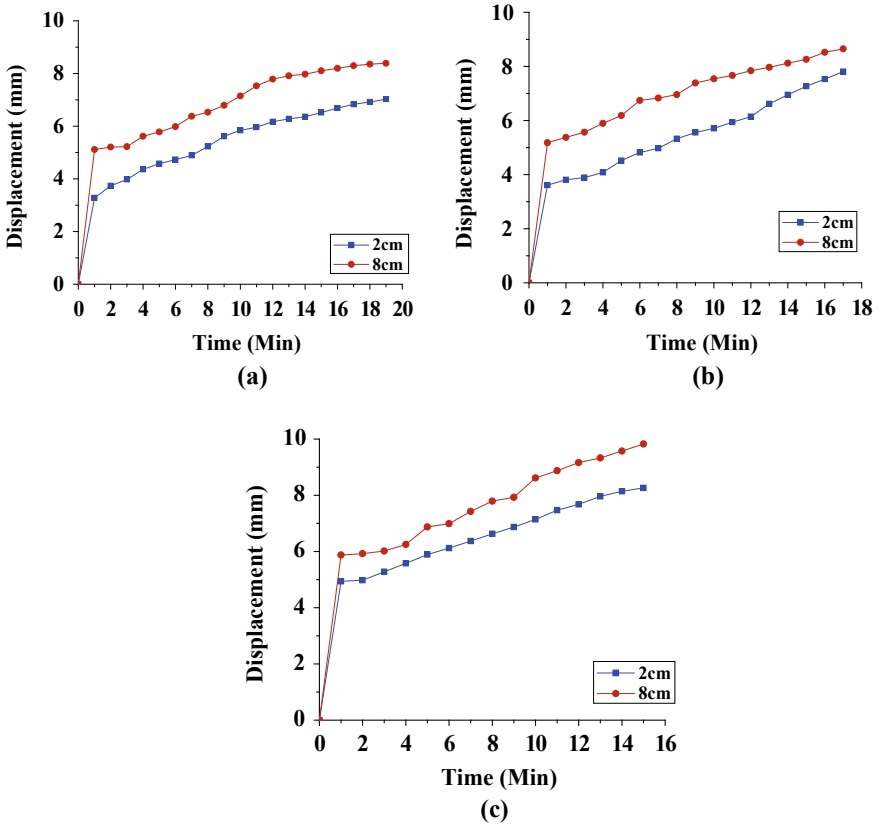

Fig. 10 Displacement variation of 50º slope for 10 cm height, at 2 cm and 8 cm height from the bottom of the embankment of 4 mm amplitude with time for the **a** frequency 2 Hz, **b** 3 Hz, and **c** 4 Hz

observed that the frequency increases displacement also increases and displacement measured at 2 cm height is less than 8 cm height.

It is observed that, the increase in the frequency the displacement also increases and displacement measured at 14 cm height is more than 2 cm and 8 cm height. The shaking time of 25 min, 22 min and 20 min and the displacement at 2 cm, 8 cm is 7.415 mm, 8.58 mm and 10.21 mm, 7.938 mm, 9.07 mm and 10.73 mm, and 8.365 mm, 9.56 mm and 11.12 mm respectively, slope will fail (hair cracks will be formed at the top of the slope) for the frequency of 2 Hz, 3 Hz and 4 Hz shown in the Fig. 11.

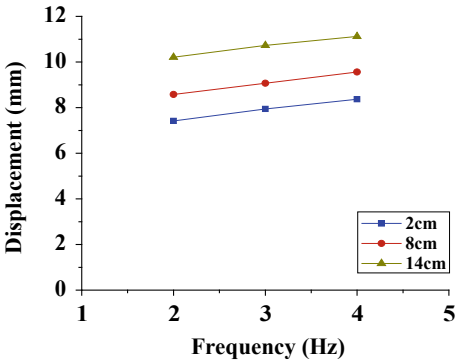

Fig. 11 Variation of displacement for 15 cm height of 50º slope at 2 cm, 8 cm and 14 cm height from the bottom of the embankment for the amplitude of 4 mm with frequency for 2 Hz, 3 Hz, and 4 Hz

5.2 Stability Analysis of Reinforced Slope

Horizontal shaking table tests are carried on soil slope of two different angle and height by varying frequency as 2, 3 and 4 Hz with constant amplitude. As reinforcement 1 mm diameter of Galvanized fiber with 2% and 4% with different aspect ratio were used and displacement were measured at different level on the slope.

5.2.1 Stability Analysis of Reinforced Slope of 40º and (L/D = 20)

The test conducted for the reinforced soil slope compacted to the density of 15.69 kN/m^3 of 40º at height of 10 cm and 1 mm diameter GI fiber reinforcement of 2% and 4% respectively, for L/D = 20 is plotted in Fig. 12a, b for frequency of 2, 3 and 4 Hz with constant amplitude of 4 mm.

From the Fig. 12a, b, it shows that slope reinforced with 2% of *GI* fiber with aspect ratio of 20 (*L/D* = 20) will fail at the shaking period of 19 min, 16 min and 14 min for frequency of 2 Hz, 3 Hz and 4 Hz and displacement at 2 cm and 8 cm from the bottom of the soil slope is 2.14 mm and 2.82 mm, 2.23 mm and 2.96 mm, 2.38 mm and 3.07 mm for constant amplitude of 4 mm. Increase in amount of fiber to 4% slope will fail for the shaking period of 23 min, 18 min and 16 min and displacement at 2 cm and 8 cm is 2.01 mm and 2.78 mm, 2.18 mm and 2.89 mm, 2.23 mm and 2.97 mm. It was observed that frequency increase displacement also increases and displacement at 4% of reinforcement is less than the 2% of reinforcement.

From the Fig. 13a, b, it is observed that, frequency increases the displacement will be more and slope reinforced with 2% of fiber will fail for frequency of 2 Hz, 3 Hz and 4 Hz at the shaking period of 23 min, 18 min and 16 min, displacement at 2 cm, 8 cm and 14 cm is 3.79 mm, 5.216 mm and 6.23, 4.13 mm, 5.368 mm and 6.52, 4.22 mm, 5.635 mm and 6.61 respectively and similarly at 4% of reinforcement

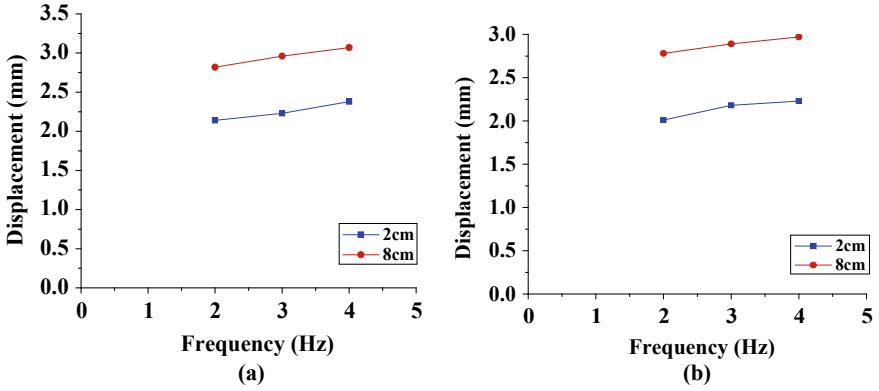

Fig. 12 Variation of displacement verses frequency of 2 Hz, 3 Hz and 4 Hz with reinforcement of 2% (**a**) and 4% (**b**) respectively and *GI* fiber with *L/D* of 20 for the slope of 40º and height of 10 cm for constant amplitude of 4 mm

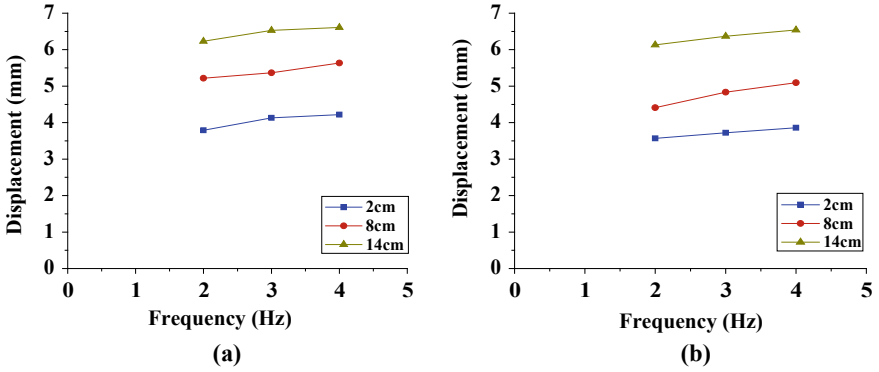

Fig. 13 Slope of 40º for height of 15 cm with reinforcement of 2% (**a**) and 4% (**b**), L/D = 20 for frequency of 2 Hz, 3 Hz and 4 Hz respectively and displacement at 2 cm, 8 cm and 14 cm

slope will fail at shaking time of 27 min, 23 min and 20 min and displacement is 3.57 mm, 4.41 mm and 6.13 mm, 3.72 mm, 4.835, and 6.37 mm, 3.86 mm 5.094, and 6.54.

5.2.2 Stability Analysis of Reinforced Slope of 40º and (L/D = 40)

The test carried out for soil slope reinforced with *GI* fiber of 2% and 4% respectively with *L/D* = 40 for angle of 40° at height of 10 cm density of 15.69 kN/m^3 for frequency of 2 Hz, 3 Hz, and 4 Hz respectively, constant amplitude of 4 mm were plotted in Fig. 14a, b.

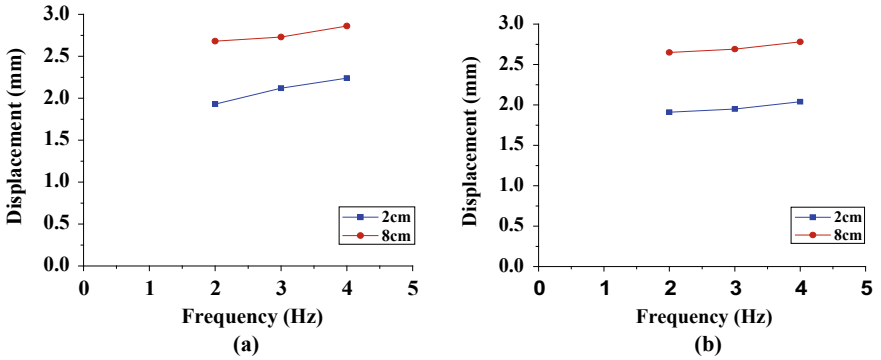

Fig. 14 Shows the displacement variation for frequency of 2 Hz, 3 Hz and 4 Hz. Slope of 40º for height of 10 cm with reinforcement of 2%(a) and 4%(b), L/D = 40 and displacement at 2 cm and 8 cm from the bottom of slope

From the Fig. 14a, b, it shows that slope reinforced with 2% of *GI* fiber with aspect ratio of 40 (*L/D* = 40) for frequency of 2 Hz, 3 Hz and 4 Hz, slope will fail at the shaking time of 22 min, 18 min and 15 min and displacement is 1.93 mm and 2.68 mm, 2.12 mm and 2.73 mm, 2.24 mm and 2.86 mm for constant amplitude of 4 mm. For 4% reinforcement slope will fail for the shaking period of 25 min, 21 min and 18 min and displacement is 1.91 mm and 2.65 mm, 1.95 mm and 2.69 mm, 2.04 mm and 2.78 mm. It was clear that increase in frequency displacement increases and displacement at 4% reinforcement is less than the 2% reinforcement.

From the Fig. 15a, b, it shows that, increase in frequency displacement will be more and slope reinforced with 2% of fiber will fail for frequency of 2 Hz, 3 Hz and 4 Hz at the shaking period of 23 min, 19 min and 14 min, displacement at 2 cm,

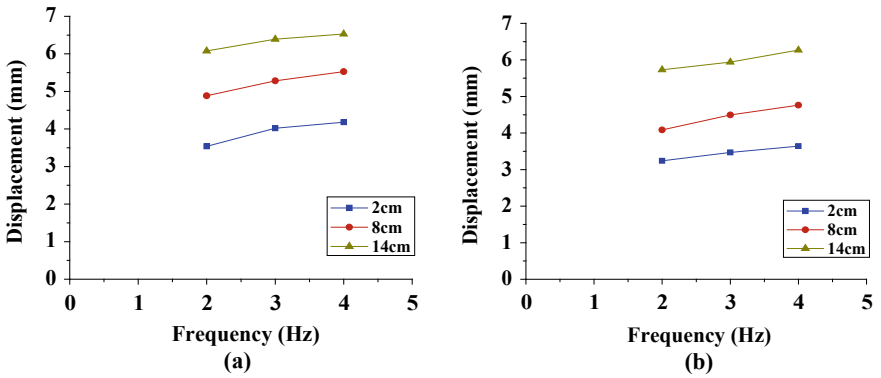

Fig. 15 Variation of displacement against frequency of 2 Hz, 3 Hz, and 4 Hz for slope of 40º at 15 cm height. Soil reinforced with *GI* fiber of 2% and 4% respectively with *L/D* = 40 and displacement at 2 cm, 8 cm and 14 cm height from the bottom of the soil for the constant amplitude of 4 mm

8 cm and 14 cm is 3.54 mm, 4.886 mm and 6.08, 4.02 mm, 5.284 mm and 6.39, 4.18 mm, 5.528 mm and 6.53 respectively a similarly at 4% of reinforcement slope will fail at shaking time of 30 min, 25 min and 22 min and displacement is 3.24 mm, 4.087 mm and 6.73 mm, 3.47 mm, 4.493, and 5.94 mm, 3.64 mm 4.761, and 6.27. Displacement is more at 14 cm than 2 cm and 8 cm height.

5.2.3 Stability Analysis of Reinforced Slope of 50º and Aspect Ratio of 20 (L/D = 20)

From the Fig. 16a, b, it shows that slope reinforced with 2% of *GI* fiber with aspect ratio of 40 ($L/D = 20$) for frequency of 2 Hz, 3 Hz and 4 Hz, slope will fail at the shaking period of 17 min, 14 min and 11 min and displacement is 3.52 mm and 4.54 mm, 3.81 mm and 4.78 mm, 4.13 and 5.26 mm for constant amplitude of 4 mm. Similarly for 4% reinforcement, slope will fail for the shaking period of 23 min, 19 min and 18 min and displacement is 2.70 mm and 3.97 mm, 2.94 mm and 4.22 mm, 3.14 mm and 4.33 mm. It was clearly seen that increase in frequency displacement also increases and displacement at 4% reinforcement is less than the 2% reinforcement and displacement at 2 cm is less than the 8 cm.

From the Fig. 17a, b, it is observed that, as the frequency increases displacement will be more and slope reinforced with 2% of fiber will fail for frequency of 2 Hz, 3 Hz and 4 Hz at the shaking period of 17 min, 14 min and 11 min, displacement at 2 cm, 8 cm and 14 cm is 3.47 mm, 4.461 mm and 5.96, 3.76 mm, 4.624 mm and 6.31, 3.96 mm, 4.723 mm and 6.48 respectively and similarly at 4% of reinforcement slope will fail at shaking time of 22 min, 18 min and 15 min and displacement is 3.34 mm, 4.273 mm and 5.85 mm, 3.72 mm, 4.467, and 6.18 mm, 3.83 mm 4.719, and 6.36.

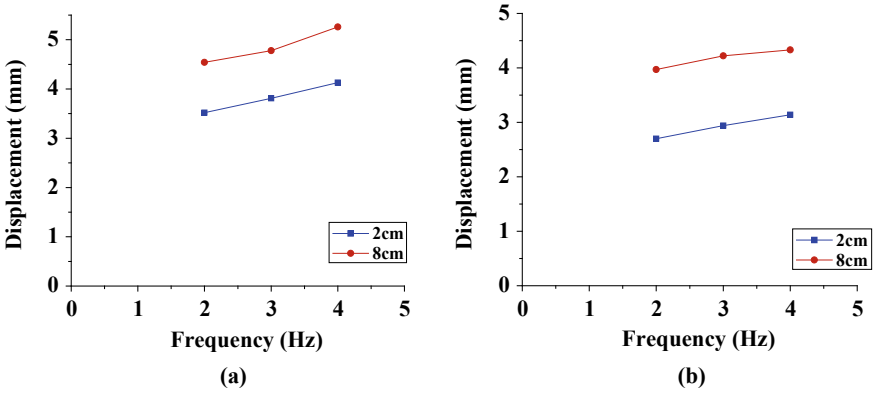

Fig. 16 Variation of displacement against frequency of 2 Hz, 3 Hz and 4 Hz. Slope reinforced with 2% (**a**) and 4% (**b**) of 1 mm diameter GI fiber, L/D = 20 with an angle 0f 50º and height of 10 cm and displacement at 2 cm and 8 cm

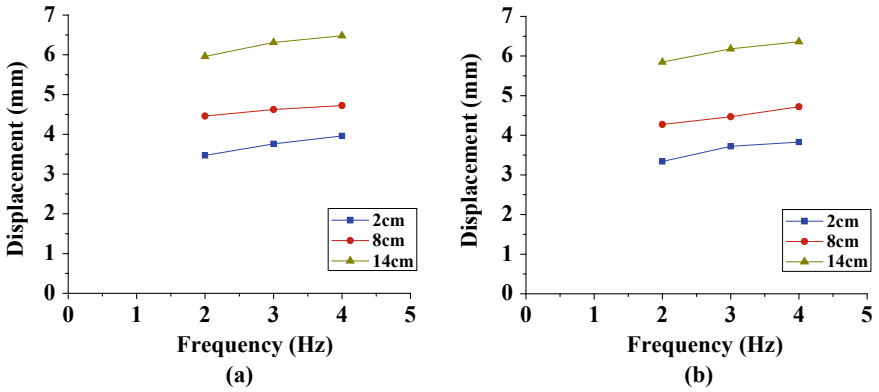

Fig. 17 Shows the variation of displacement against frequency, slope reinforced with of 2% (**a**) and 4% (**b**) angle of 50º and height of 15 cm for L/D = 20 and displacement measured at 2 cm, 8 cm and 14 cm from the bottom of slope f or frequency of 2 Hz, 3 Hz and 4 Hz respectively

5.2.4 Stability Analysis of Reinforced Slope of 50º and Aspect Ratio of 40 (L/D = 40)

The test conducted on the slope of 50º and height of 10 cm compacted with the density of 15.69kN/m^3 and reinforced with the *GI* fiber of 2% and 4%, *L/D* = 40 is plotted in Fig. 18a, b for frequency of 2 Hz, 3 Hz and 4 Hz respectively with 4 mm amplitude.

From the Fig. 18a, b, it shows that slope 50º and height of 10 cm is reinforced with 2% of *GI* fiber with aspect ratio of 40 (*L/D* = 40) for frequency of 2 Hz, 3 Hz and 4 Hz, slope will fail at the shaking period of 20 min, 16 min and 14 min and displacement is 3.19 mm and 4.19 mm, 3.31 mm and 4.34 mm, 4.02 and 5.10 mm

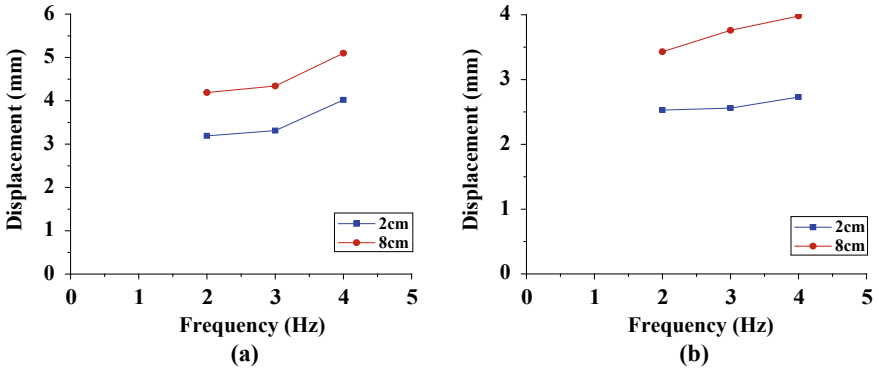

Fig. 18 Variation of displacement against frequency of 2 Hz, 3 Hz and 4 Hz. Slope reinforced with 2% (**a**) and 4% (**b**) of 1 mm diameter GI fiber, L/D = 40 with an angle of 50º and height of 10 cm and displacement at 2 cm and 8 cm

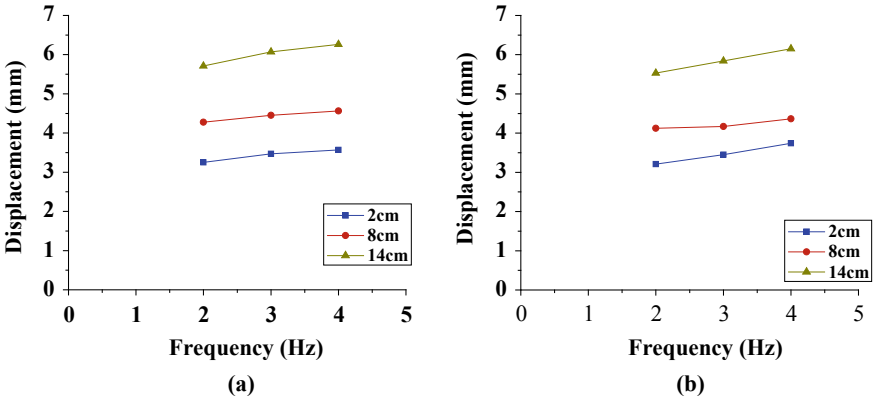

Fig. 19 **a** and **b** Variation of displacement against frequency of 2 Hz, 3 Hz, and 4 Hz for slope of 50º at 15 cm height. Soil reinforced with *GI* fiber of 2% and 4% respectively with $L/D = 40$ and displacement at 2 cm, 8 cm and 14 cm height from the bottom of the soil for the constant amplitude of 4 mm

for constant amplitude of 4 mm. Similarly for 4% reinforcement, slope will fail for the shaking period of 26 min, 21 min and 17 min and displacement is 2.53 mm and 3.43 mm, 2.56 mm and 3.76 mm, 2.73 mm and 3.98 mm. It was clearly seen that the displacement at 2 cm is less than the 8 cm; increase in frequency displacement also increases and at 4% displacement is less than the 2%.

From the Fig. 19a, b, it shows that, slope reinforced with 2% of fiber will fail for frequency of 2 Hz, 3 Hz and 4 Hz at the shaking period of 19 min, 16 min and 13 min, displacement at 2 cm, 8 cm and 14 cm is 3.25 mm, 4.278 mm and 5.71, 3.47 mm, 4.453 mm and 6.07, 3.57 mm, 4.562 mm and 6.26 respectively and similarly at 4% of reinforcement slope will fail at shaking time of 24 min, 20 min and 16 min and displacement is 3.21 mm, 4.122 mm and 5.53 mm, 3.45 mm, 4.168, and 5.84 mm, 3.74 mm 4.364, and 6.15. It was observed that increase in frequency displacement will be more and at 14 cm height displacement is more than 2 cm and 8 cm.

6 Conclusions

Experiments were carried out on reinforced and unreinforced soil slope by varying different parameters. Based on the experimental results and discussions as explained above following conclusions are drawn.

(a) The soil slope stability increases with the inclusion of GI fibers, with the increase in the content of GI fiber the stability increases further.
(b) The slope displacement increases with the height irrespective of frequency and slope.

(c) The slope displacement increases with the increase in the frequency at constant amplitude.
(d) The time taken for the failure of the slope will be decreasing with the increase in the frequency.
(e) With the increase in the angle and height of the slope there is increase in the displacement.
(f) The slope stability increases with the increase in the aspect ratio of fiber.

References

Edincliler A, Toksoy YS (2017) Shake table tests to measure the dynamic performance of geotextile-reinforced embankment. 61(4):803–814
Giri D, Sengupta A (2010a) Performance of small scale model slopes in shaking table. Tests Indian geotechnical conference, Geotrendz December 16–18, IGS Mumbai Chapter & IIT Bombay
Giri D, Sengupta A (2010b) Dynamic behavior of small-scale model slopes in shaking table tests. Int J Geotech Eng 4(1):1–11
Giria D, Sengupta A (2009) Dynamic behavior of small-scale model of nailed steep slopes. Geomech Geoeng 5(2):99–108
Lo Grasso AS, Maugeri M, Recalcati P (2005) Seismic behaviour of geosinthetic-reinforced slopes with overload by shaking table tests. Int J Geotech Eng
Sahoo S, Manna B, Sharma KG (2016) Seismic stability analysis of un-reinforced and reinforced soil slopes. Int J Geosynth Ground Eng 74–81
Srilatha N, Madhavi Latha G, Puttappa CG (2013) Effect of frequency on seismic response of reinforced soil slopes in shaking table tests. Geotext Geomembr 36:27–32
Srilatha N, Madhavi Latha G, Puttappa CG (2017) Effect of slope angle on seismic response of unreinforced and reinforced soil slopes in shaking table tests. Indian Geotech Soc
Vyas M, Rukhaiyar S, Mittal S (2014) Behaviour of slope under dynamic condition—an experimental study. Int J Civil Engg Res 5(2):121–128. ISSN 2278-3652

Trend Analysis of Monsoon Rainfall Over Odisha

Tanmoy Majumder, Bitanjaya Das, and Jyotiprakash Padhi

Abstract The present study was carried out over Odisha, situated in the eastern part of India, to examine the monsoon rainfall trend for a period of 31 years (1988–2018). The rainfall data were observed at 314 blocks scattered all over Odisha. The time-series data of June, July, August and September were studied for their spatial and temporal variations. The analysis of rainfall trend will help to facilitate decisions regarding the cropping pattern, sowing date, and other purposes. To detect any significant trend in the monsoon rainfall and its magnitude, non-parametric test viz. Mann–Kendall and Theil-Sen's slope was applied. Further, analysis was made of the trend with confidence interval at 95% level. As far as significant trend is concerned, the results indicate that, for the monsoon rainfall in June, there are increasing trends in 4 blocks and decreasing trends in 52 blocks, for July, there are increasing trend in 16 blocks and decreasing trends in 3 blocks, for August, there are increasing trends in 15 blocks and decreasing trend in 1 block and for September, there are increasing trends in 30 blocks and decreasing trend in 1 block. And for the total monsoon rainfall, there are significant increasing trends in 29 blocks and decreasing trends in 21 blocks. A significant decreasing trend in monsoon rainfall is observed during the months of June and August, whereas, a significant increasing trend is observed during the months of July and September. The present study is useful for planning and management of water resources to ensure sustainable availability and uses.

Keywords Monsoon rainfall Odisha · Mann–Kendall test · Trend analysis · Theil-Sen's slope · Rainfall variability.

T. Majumder · B. Das · J. Padhi (✉)
School of Civil Engineering, KIIT Deemed to be University, Bhubaneswar, Odisha 751024, India
e-mail: jyotiprakash.padhifce@kiit.ac.in

B. Das
e-mail: bdasfce@kiit.ac.in

B. B. Das et al. (eds.), *Recent Developments in Sustainable Infrastructure (ICRDSI-2020)—GEO-TRA-ENV-WRM*, Lecture Notes in Civil Engineering 207,
https://doi.org/10.1007/978-981-16-7509-6_39

1 Introduction

Rainfall is the most essential element in hydrometeorology, and much emphasis should be given in its study (Chowdhury et al. 2014). Recent studies have found that there are significant changes in rainfall patterns around the World (Hulme et al. 1998). Changes in rainfall patterns may lead to floods, drought, loss of agricultural productivity, and industrial productivity (Diaz et al. 1989; Kalra and Ahmad 2012). The most prominent feature of the rainfall in India is seasonality in nature which much depends on different climatic variables, at global and local levels. (Rind et al. 1989) discussed the various impact of climate change on precipitation trends. A study found that the coastal areas of India are under the risk of tropical cyclones (Pattanaik 2005). Also, in another study, it was found that there was a significant rise in extreme rain events such as flash flood and landslides (Goswami et al. 2006). Rainfall is the major source of river flow in India both on a monthly and seasonal time scale and also vital for rainfed crop production. Majority of the annual rainfall in India occurs during monsoon period starting from June till September. A study found that there has been an increase in pre-monsoon, post-monsoon and winter rainfall in India whereas the monsoon rainfall has decreased (Kumar et al. 1992). The overall rainfall trend in India has been decreasing, with a range of rainfall varying from −0.46 mm/year in Northeast India to 0.38 mm/year in Peninsular India (Mondol et al. 2014). Spatio-Temporal variation of monsoon rainfall affects significantly the national economy and day-to-day life in India.

A similar situation also exists for Odisha which is significantly influenced by the south-west monsoon. The state has a large variation in topography, while the northern portion of the state consists of hilly regions having hill peaks ranging from 1000 to 2000 m, the eastern portion of the state consists of coastal areas (Gouda et al. 2017). This study is based on the monsoon rainfall (June–September) as monsoon rainfall contributes to around 80% of India's annual rainfall (Kripalani et al. 2002). Analysis of rainfall data is important as it facilitates policy decisions regarding the cropping pattern, sowing date, providing drinking water to urban and rural areas, and other purposes. The variability of south-west monsoon is substantial, therefore quantification of the spatio-temporal variations of small domains is required. Hence, this study is carried out for the spatial temporal trend analysis of monsoon rainfall in Odisha using distributed rainfall measurement at 314 locations throughout the State using Mann-Kendall's (MK) trend test and Theil-Sen's slope estimator.

2 Data and Methodology

2.1 Study Area

This study is carried out for the 30 districts consisting of 314 blocks of Odisha (Fig. 1). Odisha is situated on the eastern part of India with a geographical area of 155,707

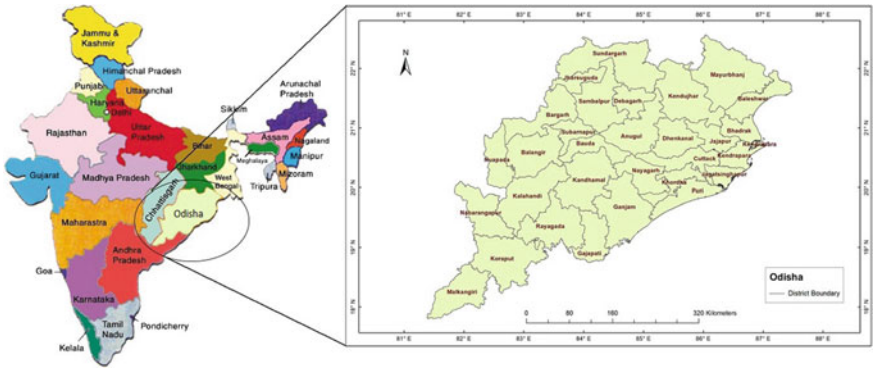

Fig. 1 District-wise map of Odisha

km^2. The geographical area of Odisha lies between (17.31°–22.31°) N latitude and (81.27°–87.29°) E longitude. The climate of the state is tropical with high temperature, high humidity, medium to high rainfall and short and mild winters. Severe events such as floods, droughts as well as cyclones occur frequently throughout the year with varying intensities. Due to these natural disasters, the agricultural production of the state is lower than the normal possible yield. The state has about 485 km of coastline along the Bay of Bengal, which extends from Balasore district to Ganjam district, including Bhadrak, Kendrapara, Jagatsinghpur, and Puri districts. During summer, the temperature rises to around (40–46) °C while in winter the minimum temperature is around 1 °C (Prabhakar et al. 2019).

2.2 Methodology

For the trend analysis, the monsoon rainfall data (June–September) over Odisha was obtained from Special Relief Commissioner (SRC) of Odisha for a period of 31 years (1988–2018). The time series rainfall data of 314 blocks (stations) were analyzed for any significant trend at a 95% confidence interval. The magnitude of these significant trends was quantified using Theil-Sen's slope estimator (Fig. 2).

2.3 Mann–Kendall (MK) Test

As the data used in this study is non-parametric (i.e. data is not normally distributed) therefore Mann-Kendall's trend test (MK) was adopted to detect any increasing or decreasing trend in the rainfall time series data. The main objective of the MK trend test (as proposed by Mann 1945 and Kendall 1975) is the statistical assessment of any monotonic rising or falling trend of the data over a time period.

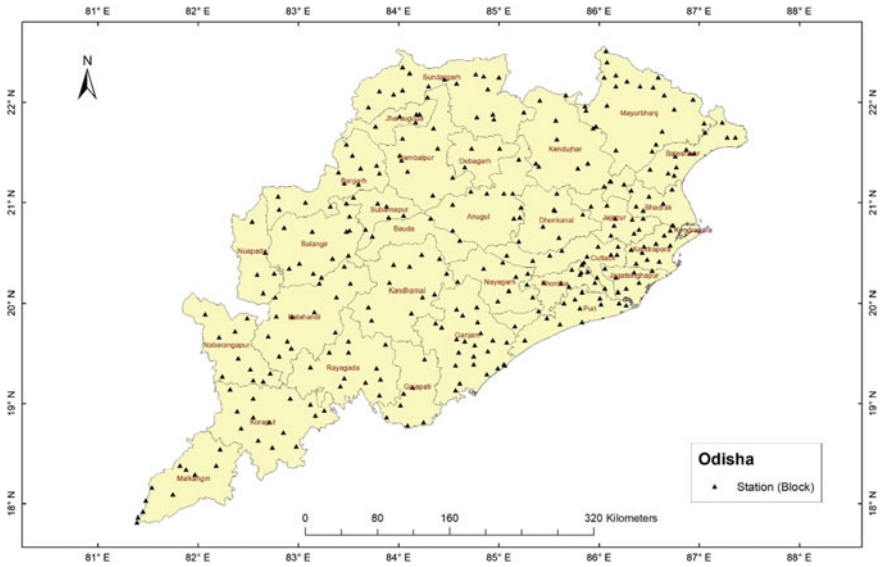

Fig. 2 Map displaying 314 stations (blocks) that were used in the study

The Mann-Kendall statistics S is calculated as;

$$S = \sum_{i=1}^{n-1} * \sum_{j=i+1}^{n} \operatorname{sgn}(y_j - y_i) \tag{1}$$

where y_i and y_j are time-series data having ranks from i = 1, 2, 3, …, (n − 1) and j = 1, 2, 3, …, (n). Every data point of the time series y_i is considered as a reference and is compared with the rest of the data points of y_j.

An upward trend or a downward trend can be identified if the S statistics value is either positive or negative respectively.

$$\operatorname{sgn}(y_j - y_i) = \begin{cases} +1, > (y_j - y_i) \\ 0, = (y_j - y_i) \\ -1, < (y_j - y_i) \end{cases} \tag{2}$$

Considering independent data having similar scattering, the variance of the S statistics can be calculated from the following equations,

The variance,

$$Var(S) = \frac{m(m-1)(2m+5)}{18} \tag{3}$$

Furthermore, for ties in the data series the expression for variance changes to,

$$Var(S) = \frac{m(m-1)(2m+5) - \sum_{i=1}^{n} t_i(t_i-1)(2t_i+5)}{18} \tag{4}$$

where the number of tied groups is represented by n and t_i is the number of data points in the ith tied group. The test statistics Z_c is computed using Eq. (5)

$$Z_c = \begin{cases} \frac{S-1}{\sqrt{Var(S)}} & when\ (S > 0) \\ 0 & when\ S = 0 \\ \frac{S+1}{\sqrt{Var(S)}} & when\ (S < 0) \end{cases} \tag{5}$$

The Z_c values $> +1.96$ and < -1.96 represents a significant upward and a downward trend in the time series (at 95% confidence level), respectively.

2.4 Theil-Sen's Slope

The Sen's slope estimator predicts the magnitude of the trend. This method is applicable if it is presumed that the trend is linear. The slope estimates (Q_i) of N data pairs is computed as

$$Q_i = \frac{y_j - y_k}{j-k}. \tag{6}$$

where the values at period j and k (j > k) is represented as y_j and y_k. The median of these N values of Q_i is Sen's estimator of slope

$$Q_i = \begin{cases} \frac{Q_{N+1}}{2} & if\ N\ is\ odd \\ \frac{1}{2}\left(\frac{Q_N}{2} + \frac{Q_{N+2}}{2}\right) & if\ N\ is\ even \end{cases} \tag{7}$$

Q_i value exceeding ± 1.96 are significant values (at $\alpha = 0.05$ level of significance).

MAKESENS excel template application (developed by Finnish Meteorological Institute, Finland) was used to calculate the trend of time series data. This template application performs two analyses, firstly it detects the existence of any rising or falling trend in the series using the MK trend test and later the magnitude of the slope using Sen's slope method.

3 Results and Discussion

The trend analysis of monsoon rainfall was done for 314 blocks (point rainfall daily data) of Odisha. The trend analysis was done for June, July, August, September and

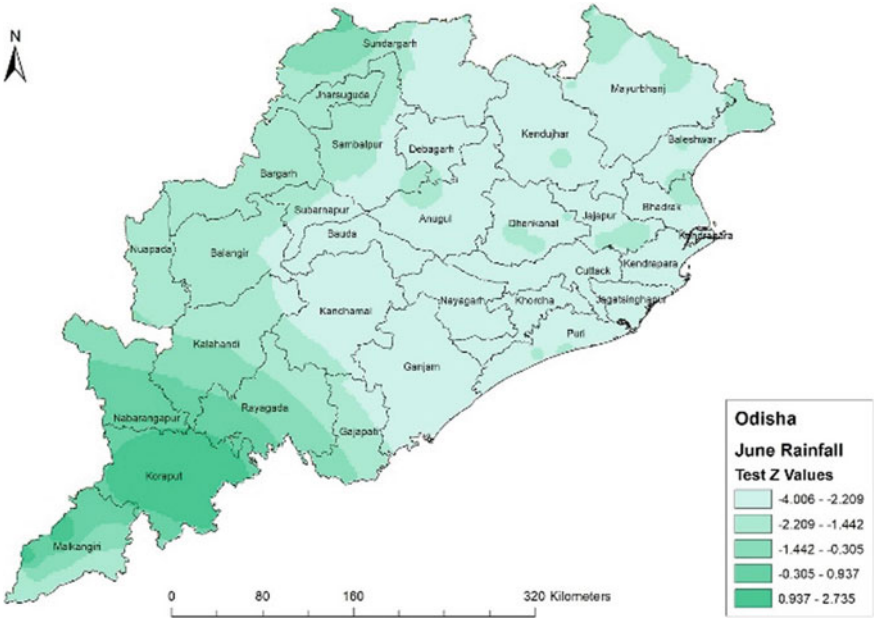

Fig. 3 Z statistics value for June rainfall over Odisha

total monsoon rainfall (i.e. cumulative rainfall for June, July, August and September). From the Mann-Kendall trend analysis performed at 95% significance level, the obtained Z statistics value of 314 blocks of Odisha for June, July, August, September and Total monsoon rainfall has been shown in choropleth maps (Figs. 3, 4, 5, 6, and 7). The Z statistics value for June rainfall varied from (−4.00 to 2.73), July rainfall varied from (−2.61 to 3.07), August rainfall varied from (−3.22 to 3.91), September rainfall varied from (−2.49 to 3.36) and total monsoon rainfall varied from (−3.19 to 5.31).

It was observed that the monsoon rainfall for 31 years (1988–2018) during the month of June has a significant decreasing trend over 52 blocks and a significant increasing trend over 4 blocks. The month of July has a significant decreasing trend over 3 blocks and a significant increasing trend over 16 blocks. The month of August has a significant decreasing trend over 18 blocks and a significant increasing trend over 15 blocks. The month of September has a significant decreasing trend over 1 blocks and a significant increasing trend over 30 blocks. For the total monsoon period (during 1988–2018), 21 blocks were having a significant decreasing trend and 21 blocks were having a significant increasing trend.

The graphs (Figs. 8, 9, 10, 11, and 12) provided below displays the number of blocks of each district exhibiting an increasing and decreasing trend of monsoon rainfall at 95% significance level for June, July, August and September as well as for Total monsoon rainfall period over Odisha for the time-period of 31 years (1988–2018).

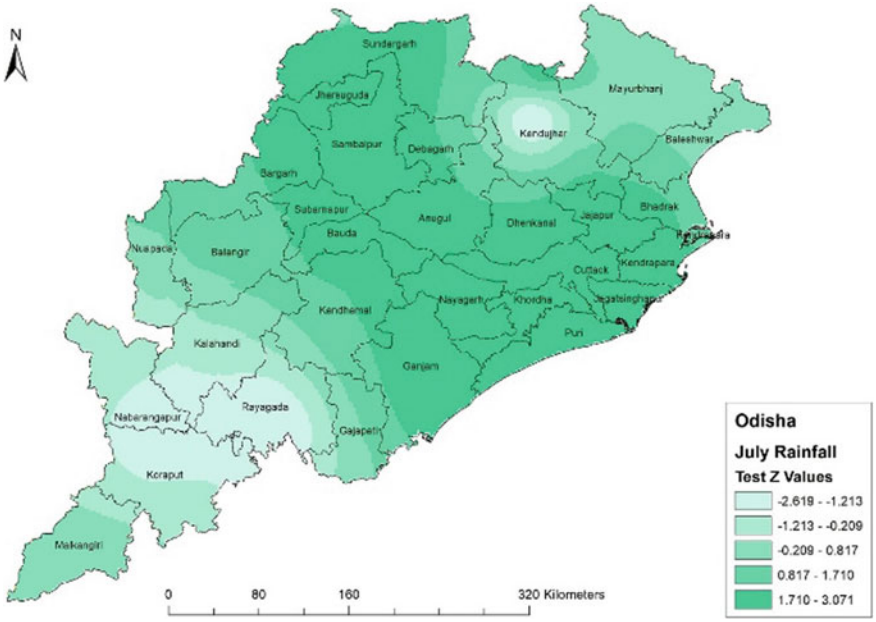

Fig. 4 Z statistics value for July rainfall over Odisha

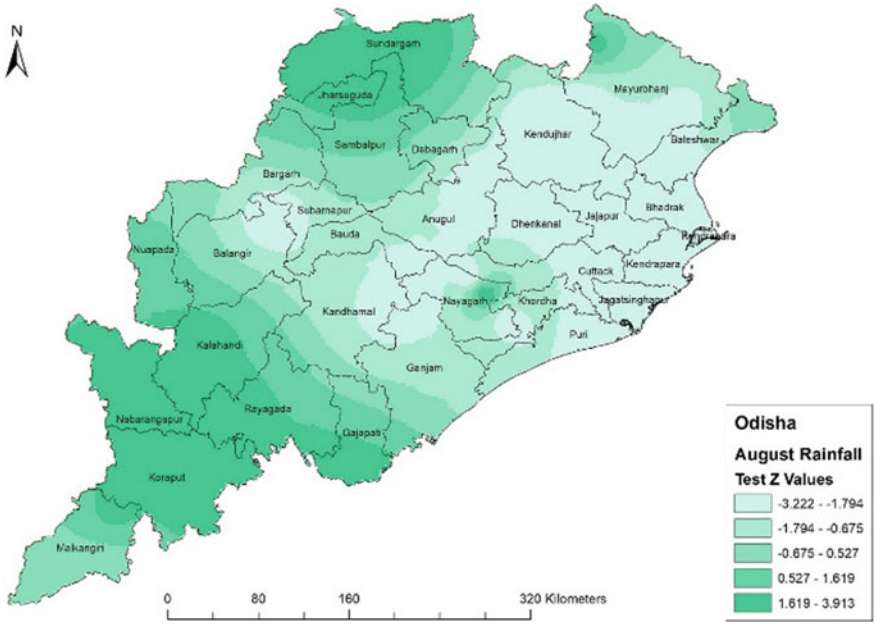

Fig. 5 Z statistics value for August rainfall over Odisha

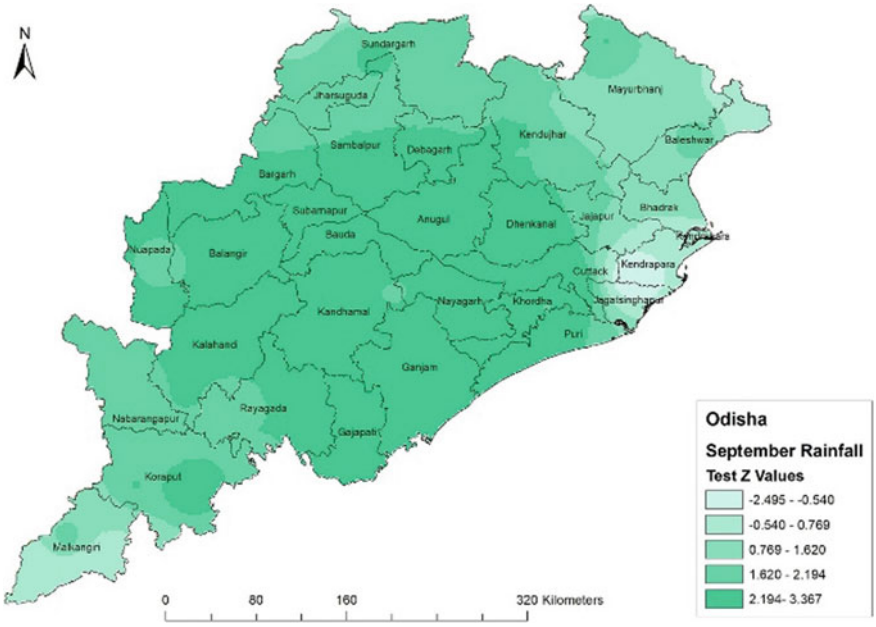

Fig. 6 Z statistics value for September rainfall over Odisha

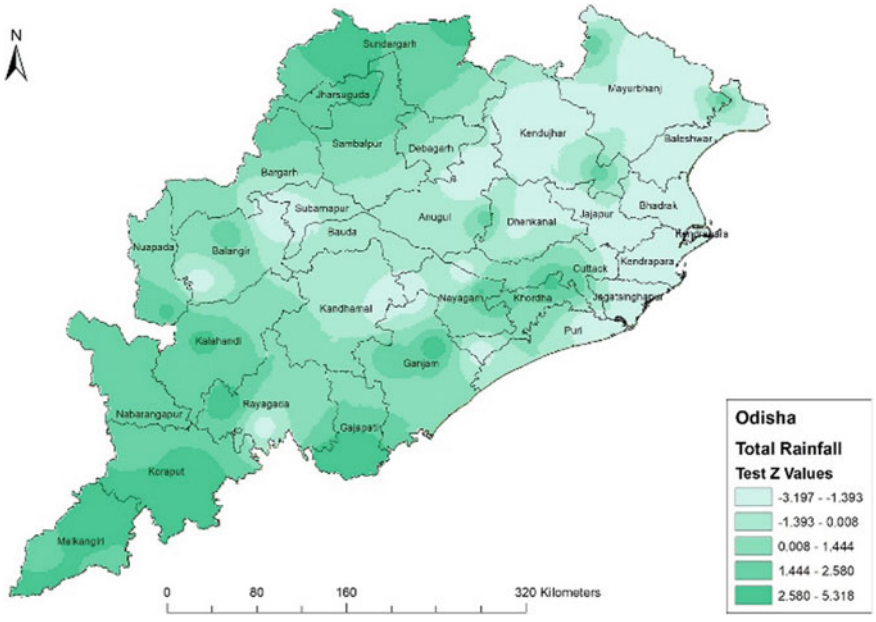

Fig. 7 Z statistics value for Total monsoon rainfall over Odisha

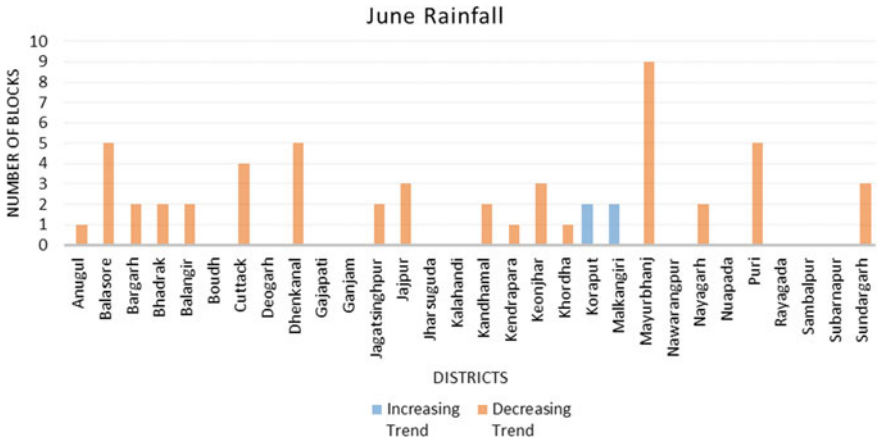

Fig. 8 Graphical representation of number of blocks having increasing and decreasing trend during June rainfall

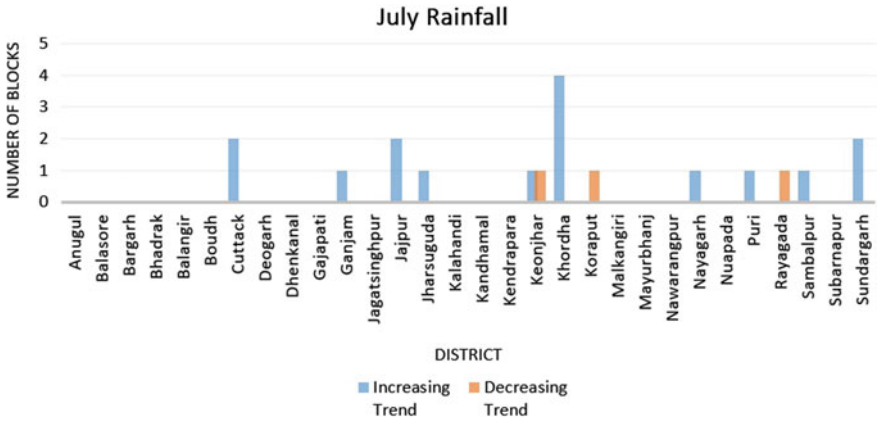

Fig. 9 Graphical representation of number of blocks having significant increasing and decreasing trend during July rainfall

4 Conclusions

- A significant decreasing trend in monsoon rainfall is observed during the month of June and August. Whereas, a significant increasing trend was observed during the month of July and September at 95% significance level.
- During the month of June, Mayurbhanj has 9 blocks are having significant decreasing trend of monsoon rainfall. Also, Balasore, Dhenkanal and Puri each have 5 blocks with a significant decreasing trend. These blocks need special attention regarding water usage policies.

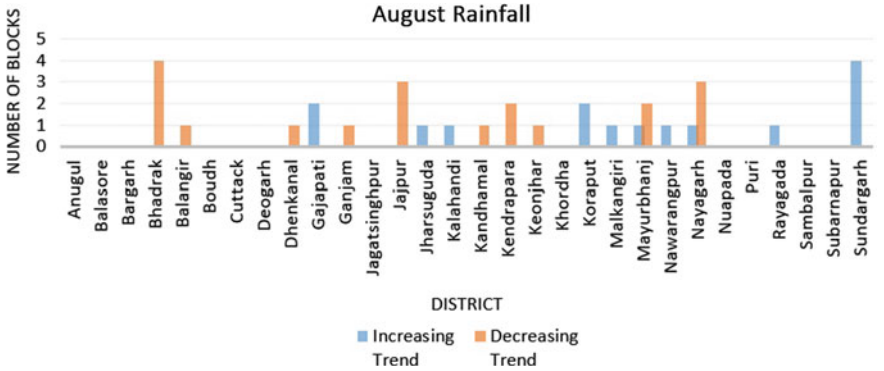

Fig. 10 Graphical representation of number of blocks having significant increasing and decreasing trend during August rainfall

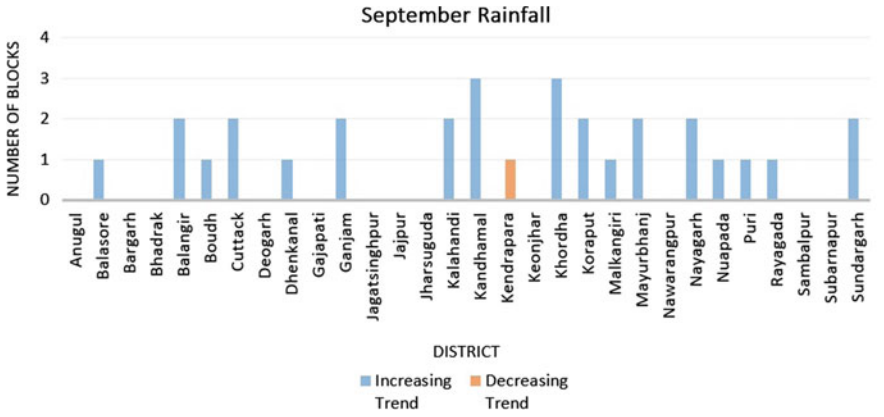

Fig. 11 Graphical representation of number of blocks having significant increasing and decreasing trend during September rainfall

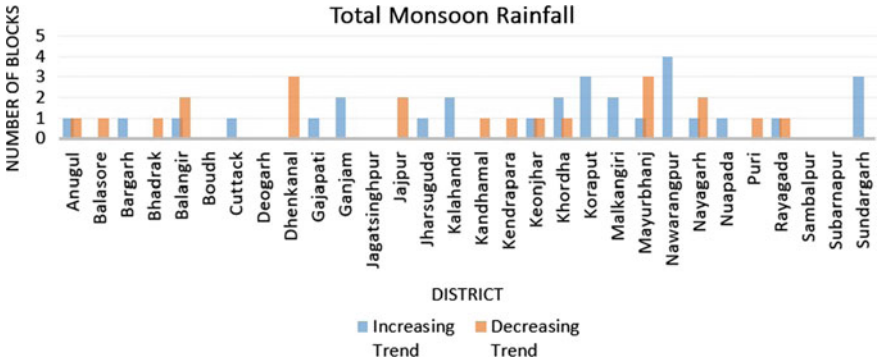

Fig. 12 Graphical representation of number of blocks having significant increasing and decreasing trend during Total monsoon rainfall

- For the monsoon rainfall, in June, 4 blocks have increasing trend, and 52 blocks have decreasing trend. In July, 16 blocks have increasing trend, and 3 blocks have decreasing trend. In August, 15 blocks have increasing trend, and 18 blocks have decreasing trend. In September, 30 blocks have increasing trend, and 1 block have decreasing trend. And for the total monsoon period, 29 blocks have increasing trend, and 21 blocks have decreasing trend.

References

Chowdhury MR, Kumar V, Sattar A, Brahmachari K (2014) Studies on the water use efficiency and nutrient uptake by rice under system of intensification. The Bioscan 9(1):85–88

Diaz HF, Bradley RS, Eischeid JK (1989) Precipitation fluctuations over global land areas since the late 1800's. J Geophys Res: Atmos 94(D1):1195–1210

Goswami BN, Venugopal V, Sengupta D, Madhusoodanan MS, Xavier PK (2006) Increasing trends of extreme rain events over India in a warming environment. Science 314:1442–1445

Gouda KC, Sahoo SK, Samantray P, Shivappa H (2017) Comparative study of monsoon rainfall variability over India and the Odisha state. J Clim (MDPI) 5(79):1–16

Hulme M, Osborn TJ, Johns TC (1998) Precipitation sensitivity to global warming: comparison of observations with HadCM2 simulations. Geophys Res Lett 25(17):3379–3382

Kalra A, Ahmad S (2012) Estimating annual precipitation for the Colorado river basin using oceanic-atmospheric oscillations. Water Resour Res 48(6):1–24

Kendall MG (1975) Rank correlation methods. Griffin, London

Kripalani RH, Kulkarni A, Sabade SS, Khandekar ML (2002) Indian monsoon variability in a global warming scenario. Nat Hazards 29:189–206

Kumar KR, Pant GB, Parthasarathy B, Sontakke NA (1992) Spatial and sub-seasonal patterns of the long-term trends of Indian summer monsoon rainfall. Int J Climatol 12:257–268

Mann HB (1945) Non-parametric tests against trend. Econometrica 13:245–259

Mondol A, Khare D, Kundu S (2014) Spatial and temporal analysis of rainfall and temperature trend of India. Theoret Appl Climatol 122:143–158

Pattanaik DR (2005) Variability of oceanic and atmospheric conditions during active and inactive periods of storms over the Indian region. Int J Climatol 25:1523–1530

Prabhakar AK, Singh KK, Lohani AK, Chandniha SK (2019) Assessment of regional-level long-term gridded rainfall variability over the Odisha state of India. J Appl Water Sci 9:93

Rind D, Goldberg R, Ruedy R (1989) Change in climate variability in the 21st century. Clim Change 14:5–37

Spatio-temporal Analysis of Monsoon Rainfall Over Odisha

Tanmoy Majumder, Bitanjaya Das, and Paromita Chakraborty

Abstract Climate change is a global issue which needs to be studied thoroughly especially in the context of rainfall. Rainfall plays a vital role in agriculture, and also it is the natural recharge process of the groundwater. Thus, seasonal uncertainty in the rainfall leads to irregular or insufficient recharge of the groundwater and also insufficient surface storage. Therefore, the occurrence and distribution analysis of monsoon rainfall in the country are very crucial. In this context, a study of monsoon rainfall of the state of Odisha is attempted using 31 years (1988–2018) of rainfall data. The state of Odisha is mostly influenced by the South-West monsoon. Administratively, Odisha has 30 districts consisting of 314 blocks. The analysis is carried out in terms of spatio-temporal variability and autocorrelation function (ACF) of rainfall time series for each block. The average total monsoon rainfall of the state is found to be 1147.9 mm with a standard deviation of ±400 mm during the study period. The variation of the rainfall over Odisha during monsoon period for individual months found to be much more in comparison to the analysis for the whole monsoon period cumulatively. Similarly, for each block level time series, the autocorrelation function is estimated for 12-time lags with a confidence interval of 95%. The results indicated that there is a significant number (more than 200) of blocks having favourable autocorrelation function values for lag 1, 2 and 3. This indicates non-randomness of the rainfall time series for monsoon period. The statistical analysis as well was autocorrelation function analysis can very well indicate how the monsoon rainfall is behaving in various locations and time-periods over Odisha. This provides useful data for effective planning and allocation of water in various regions of the state for sustainable usage.

Keywords Monsoon rainfall Odisha · Spatio-temporal rainfall distribution · Coefficient of variation · Monsoon rainfall · Autocorrelation function.

T. Majumder · B. Das · P. Chakraborty (✉)
School of Civil Engineering, KIIT Deemed to be University, Bhubaneswar, Odisha 751024, India
e-mail: paromita.chakrabortyfce@kiit.ac.in

B. Das
e-mail: bdasfce@kiit.ac.in

B. B. Das et al. (eds.), *Recent Developments in Sustainable Infrastructure (ICRDSI-2020)—GEO-TRA-ENV-WRM*, Lecture Notes in Civil Engineering 207,
https://doi.org/10.1007/978-981-16-7509-6_40

1 Introduction

Among the all hydro-climatic variables like temperature, evapotranspiration and humidity, the most essential variable is precipitation (Chowdhury et al. 2014). It has been studied that the significant changes in rainfall pattern are occurring globally (Diaz et al. 1989). The most prominent feature of the monsoonal areas of the world is the variation of seasonal rainfall. Monsoon rainfall contributes around 80% of India's annual rainfall (Kripalani et al. 2002). The South-West monsoon rainfall (June–September) extends from West Pakistan to Myanmar across northwest India and the northern Bay of Bengal (Mohapatra et al. 2003). The variability of southwest monsoon is large, therefore quantification of the spatio-temporal variations of small domains is required. In an analysis of rainfall characteristics and variability, it has been concluded that most of the regions of India will witness extreme variations in precipitation (Goswami et al. 2006).

The state of Odisha is situated on the eastern part of India and has a total area of 155,707 km^2. Odisha is divided into four physiographic zones: (i) Coastal plain, (ii) Northern upland, (iii) Central river basin and (iv) South-west hilly regions. The northern portion of the state consists of hilly regions having hill peaks ranging from 1000 to 2000 m and coast on the Eastern portion (Gouda et al. 2017). This large variation in topography affects the advancement and distribution of monsoon rainfall. Odisha has 485 kilometers long coastline along the Bay of Bengal. The state has 30 districts consisting of 314 blocks. Odisha is a coastal state and its economy mainly relies on agriculture, contributing around 30% of the Net State Domestic Product (NSDP) and providing employment to 73% of the state population (Patra et al. 2011). Therefore, rainfall plays a key role in the State's economy.

Urbanization plays an important role in climate change. Relationship between urbanization and climate change was analyzed and found that the two parameters have a certain degree of relationship (Kishtawal et al. 2010). Due to the rise in population, there is an increase in water demand in Odisha, and hence the availability of water should be estimated for the sustainability of the water resource. Rainfall is the major source of river flow in India as well as in Odisha. A detailed study of rainfall variation on the monthly and seasonal time scale is important as crop may fail due to drought as a result of low monsoon rainfall (Guhathakurta and Rajeevan 2008). Severe hydrological events like floods and droughts could occur due to large variability in rainfall. It has been found in a study that, due to an increase in the atmospheric moisture content because of global warming, the global mean precipitation may rise to a certain degree (Basistha et al. 2009). The statistical properties of rainfall (such as mean, standard deviation, variance, etc.) with time will be affected by any gradual or sudden spatio-temporal variation in rainfall (Kundzewicz and Robson 2004). Another study over the variations of precipitation over northern hemisphere regions in the mid-nineteenth century found a prominent rise in mid-latitude precipitation and simultaneously a fall in low-latitude precipitation (Kumar et al. 1992). The coastal areas of India are under the risk of tropical cyclones. These cyclones have their emergence over the north Indian Ocean and then intensifies as it moves towards

inland (Pattanaik, 2005). This can lead to a huge impact on agricultural production and the State's economy. Changes in rainfall pattern will eventually affect the crop grown in that region. In the Ganga basin where earlier sugar cane and peas were the dominant crop is now replaced with mustard and wheat because of less moisture (Kothyari and Singh, 1996). Rainfall is one of the essential climatic elements in hydro-meteorology and hence it is important to understand the characteristics of rainfall on spatio-temporal basis. Therefore, this study carried out for the spatial distribution and autocorrelation analysis of monsoon rainfall in Odisha.

2 Data and Methodology

2.1 Study Area

This study is carried out for the 30 districts consisting of 314 blocks of Odisha (Fig. 1). Odisha is situated on the eastern part of India with a geographical area of 155,707 km^2. The geographical area of Odisha lies between (17.310–22.31)° N latitude and (81.270–87.29)° E longitude. The climate of the state is tropical with high temperature, high humidity, medium to high rainfall and short and mild winters. Severe events such as floods, droughts as well as cyclones occur frequently throughout the year with varying intensities. Due to these natural disasters, the agricultural production of the state is lower than the normal possible yield. During summer, the temperature rises to around (40–46) °C while in winter the minimum temperature is around 1 °C (Prabhakar et al. 2019).

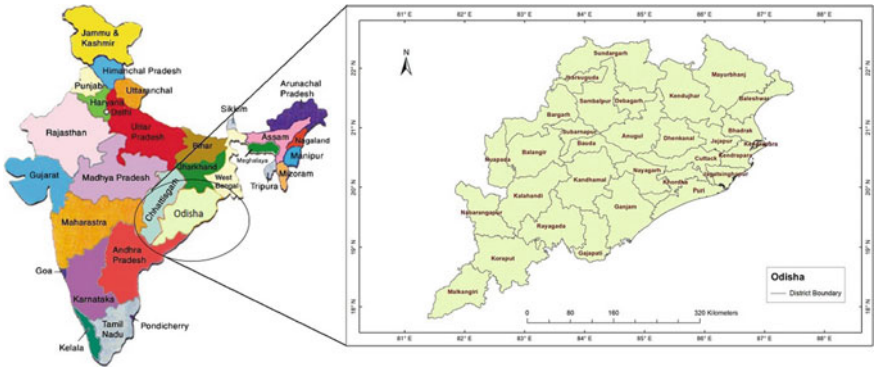

Fig. 1 District-wise map of Odisha

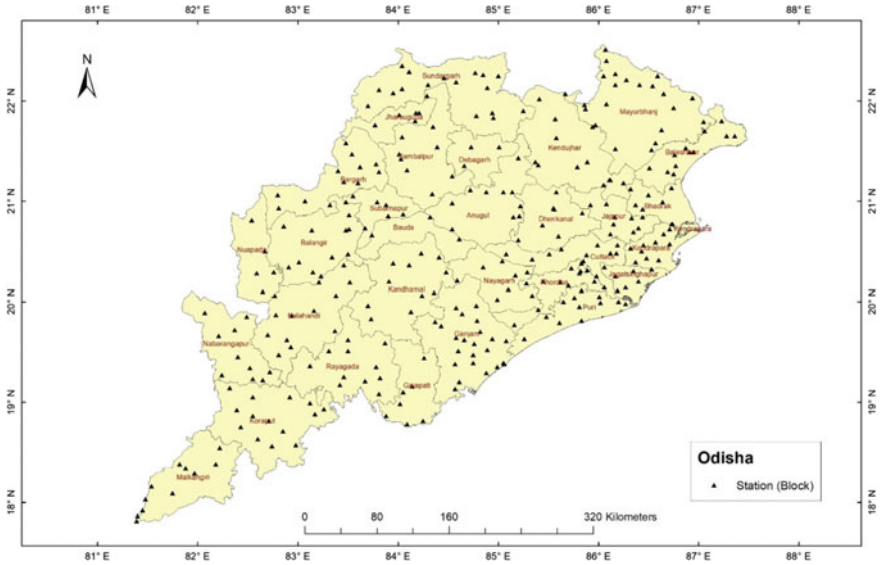

Fig. 2 Map displaying 314 stations (blocks) that were used in the study

2.2 Methodology

For the statistical analysis, the monsoon rainfall data (June–September) over Odisha was obtained from the Special Relief Commissioner (SRC) of Odisha for a period of 31 years (1988–2018). The time series rainfall data of 314 blocks (stations) were analyzed for any significant correlation at a 95% confidence interval using the Autocorrelation function (ACF) (Fig. 2).

For this study, monsoon rainfall data were analyzed, as around 80% of the total rainfall received by the state is during Southwest monsoon (June–September). The statistical properties of rainfall (such as mean, standard deviation, variance etc.) with time will be affected by any gradual or sudden spatio-temporal variation of rainfall (Kishtawal et al. 2010). The mean rainfall, standard deviation (SD) and coefficient of variation (CV) for each block were computed for the month of June, July, August, September and also for the total monsoon rainfall. Spatial maps of mean, SD and CV for the monsoon rainfall are prepared using the IDW method in ArcGIS 10.2. As the study contain long-term data series, therefore in order to test non-randomness of data, autocorrelation function (ACF) test was performed for each data series (i.e. June, July, August, September and Total monsoon rainfall). The autocorrelation function is expressed in the form of expression (1) as given below.

$$r_k = \frac{\sum_{i=1}^{N-K}\left(y_i - \overset{'}{y}\right)\left(y_{i+k} - \overset{'}{y}\right)}{\sum_{i=1}^{N}\left(y_i - \overset{'}{y}\right)^2} \tag{1}$$

where K represents Lags, N is the Sample size and $\overset{'}{y}$ denotes Mean.

Autocorrelation function was performed for 12-time lags with a confidence interval of 95%. For the test, α value was chosen to be 0.05 and degree of freedom (df) was 11.

$$df = (N - 1) \tag{2}$$

where N is the number of lags.

For 12 lags, the t-value taken from t-table was 2.201. The upper limit (UL) and lower limit (LL) of the ACF test were obtained by the following formulae.

$$UL = Mean + \left(2.201 \times \frac{Standard\ deviation}{\sqrt{N}}\right) \tag{3}$$

$$LL = Mean - \left(2.201 \times \frac{Standard\ deviation}{\sqrt{N}}\right) \tag{4}$$

The values exceeding the upper limit and lower limit are considered to be significant values. The significant values were compiled together according to their respective correlation lags.

3 Results and Discussion

The parameters such as mean rainfall, standard deviation, coefficient of variation and autocorrelation function calculated for the analysis of monsoon rainfall of Odisha. The mean, SD and CV during monsoon in Odisha was found to be 1147 mm, 252 mm and 29% respectively. The maximum mean of 1408.7 mm, SD of 569.8 mm and CV of 51.7% observed for the monsoon rainfall in Kalahandi and Sundergarh Districts respectively. Ganjam District experienced the lowest mean, SD and CV of monsoon rainfall. Maximum average rainfall observed in case of Balasore District for the months of June (268.4 mm) and September (317.3 mm) whereas Kalahandi District experienced highest mean rainfall in July (458.7 mm) and August (456.9 mm). Minimum mean rainfall occurred for Puri District in June (168.3 mm), Ganjam for July (238.8 mm) and August (261.27 mm) and Nuapada in September (193.11 mm). Highest SD value detected in case of Kalahandi for the months of June (136.7 mm) and July (208.3 mm), Kandhamal in August (186.9 mm) and Kendrapara for

September (134.6 mm). Khordha, Keonjhar, Ganjam and Rayagada District detected with minimum SD value in June (64.7 mm), July (89.0 mm), August (68.7 mm) and September (79.6 mm) respectively. Maximum CV value experienced by Kalahandi in June (57.4%), Sambalpur for the months of July (49.9%) and August (48.9%) and Nuapada in September (57.2%).

Maps were prepared to study the spatial variation of monsoon rainfall in the state (Figs. 3, 4, and 5). It can be observed from Fig. 3 that, mean monsoon rainfall varied from 129.1 to 487.0 mm over the 314 blocks of Odisha. Similarly, SD value varied from 69.2 to 363.0 mm (Fig. 4) and 36.4 to 104.2% for the CV value of the monsoon rainfall (Fig. 5).

Autocorrelation analysis of the state has been done block-wise by varying lag from 1 to 12 (Table 1). Lag 1 correlation corresponds to the relation of previous year rainfall data, likewise lag 2 correlation corresponds to two years previous rainfall data and lag 3 corresponds to three years previous rainfall data. Analysis has been done for all the 314 blocks of the state and was found that 219 blocks were having lag 1 correlation for total monsoon rainfall (i.e. for June, July, August and September). For June, July, August and September, the number of blocks having lag 1 correlation was 186, 169, 184 and 169 blocks respectively. Moreover, 216 blocks have lag 2 correlation for total monsoon rainfall and 204, 173, 169 and 191 blocks have lag 2 correlation for June, July, August and September respectively. This shows that the present data series has a strong correlation with previous year's data series, indicating non-randomness of rainfall series data. Autocorrelation analysis in Angul District

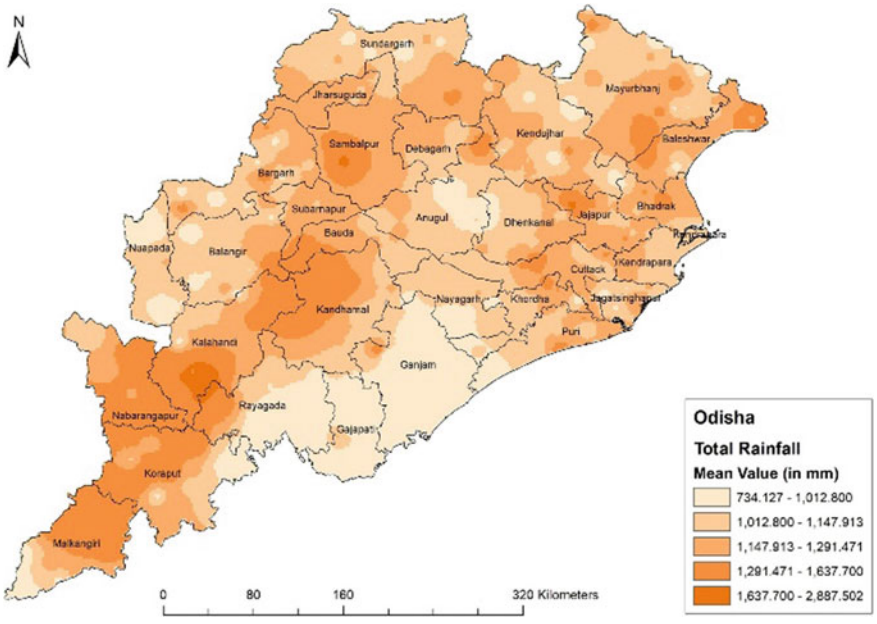

Fig. 3 Mean monsoon rainfall of 314 blocks of Odisha for 31 years (1988–2018)

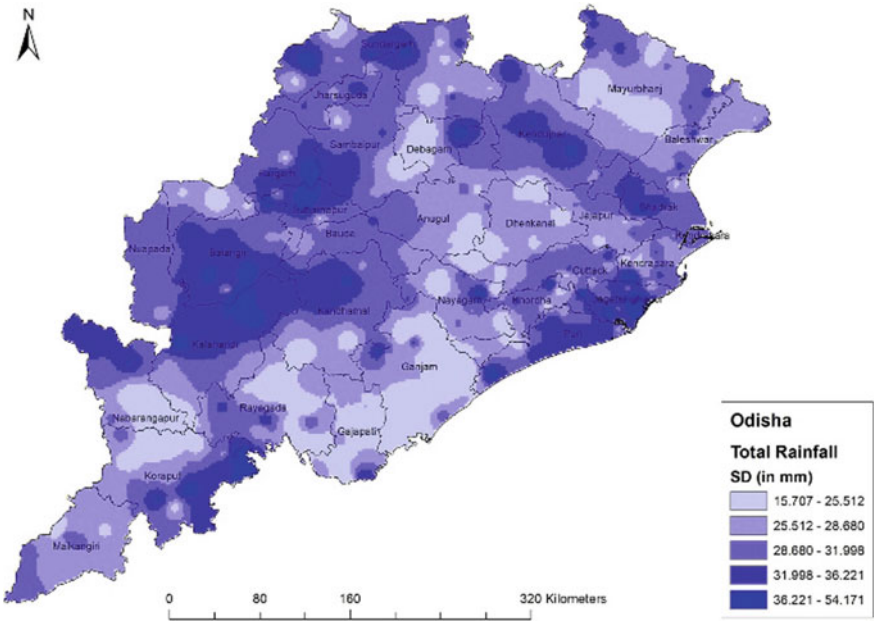

Fig. 4 Standard deviation of monsoon rainfall of 314 blocks of Odisha for 31 years (1988–2018)

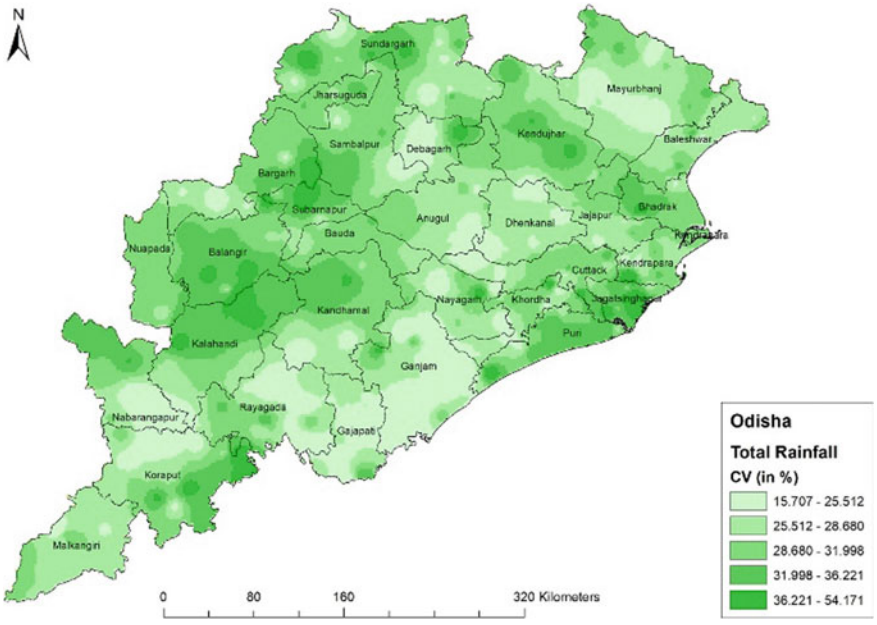

Fig. 5 Coefficient of variation of monsoon rainfall of 314 blocks of Odisha for 31 years (1988–2018)

Table 1 Autocorrelation analysis of monsoon rainfall of 30 districts of Odisha

Total monsoon rainfall (1988–2018)												
Sl. No.	District	Number of blocks having significant correlation										
		Lag 1	Lag 2	Lag 3	Lag 4	Lag 5	Lag 6	Lag 7	Lag 8	Lag 9	Lag 10	Lag 11	Lag 12
1	Angul	4	3	6	6	2	2	5	2	6	6	4	7
2	Balangir	8	7	7	7	6	6	5	6	7	7	12	10
3	Balasore	6	6	8	9	7	5	6	3	6	10	10	3
4	Bargarh	8	7	9	6	5	4	4	3	11	6	9	7
5	Bhadrak	3	7	4	4	3	1	3	5	4	5	5	6
6	Boudh	2	2	3	2	1	1	3	2	1	0	3	3
7	Cuttack	7	6	5	4	6	3	2	3	7	8	8	11
8	Deogarh	2	2	2	2	1	1	1	2	1	1	1	1
9	Dhenkanal	4	5	8	5	1	4	1	1	1	5	5	3
10	Gajapati	7	5	7	4	3	3	3	0	3	4	3	5
11	Ganjam	19	13	14	17	9	9	7	6	7	11	13	14
12	Jagatsinghpur	8	8	5	8	2	4	3	1	0	2	5	7
13	Jajpur	8	5	8	5	4	4	2	3	3	7	4	5
14	Jharsuguda	4	4	2	2	3	2	1	4	0	4	2	4
15	Kalahandi	11	9	4	8	7	10	6	7	7	4	8	7
16	Kandhamal	8	6	7	11	6	5	4	5	6	8	4	5
17	Kendrapara	6	4	6	3	4	5	5	4	6	6	5	5
18	Keonjhar	11	11	8	8	7	4	3	4	6	8	10	9
19	Khordha	9	8	5	7	5	5	3	2	4	3	4	4

(continued)

Table 1 (continued)

Total monsoon rainfall (1988–2018)												
Sl. No.	District	Number of blocks having significant correlation										
		Lag 1	Lag 2	Lag 3	Lag 4	Lag 5	Lag 6	Lag 7	Lag 8	Lag 9	Lag 10	Lag 11	Lag 12
20	Koraput	11	9	8	10	7	6	5	11	9	8	5	4
21	Malkangiri	5	7	6	4	2	5	2	4	3	3	2	6
22	Mayurbhanj	14	21	17	18	12	8	15	12	9	17	15	14
23	Nabarangpur	9	9	6	6	2	1	4	2	1	8	8	10
24	Nayagarh	7	8	6	3	1	4	4	2	2	5	6	7
25	Nuapada	4	4	5	3	2	1	2	2	1	4	3	5
26	Puri	5	9	7	5	4	9	2	8	5	5	6	6
27	Rayagada	9	9	10	4	3	3	3	2	4	7	9	11
28	Sabarnapur	4	3	2	5	5	2	1	3	3	3	3	4
29	Sambalpur	4	6	8	7	6	2	5	5	5	6	1	8
30	Sundergarh	12	13	11	10	6	9	7	13	10	11	9	11
	Total	219	216	204	193	132	128	117	127	138	182	182	202

for the monsoon rainfall have been presented in Fig. 6. Lag 1 correlation value of 314 blocks of Odisha (during 1988–2018) is presented through a spatial map (Fig. 7). It can be seen that lag 1 correlation value varied from −0.42 to 0.72 among the 30 districts of Odisha consisting of 314 blocks.

Number of blocks having significant correlation of monsoon rainfall for each districts for lag (1–12) has been represented in Table 1.

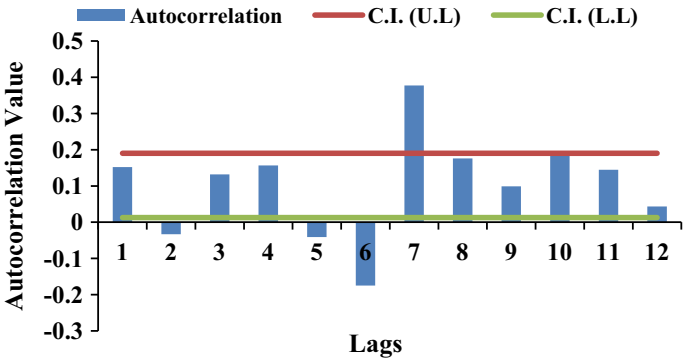

Fig. 6 Autocorrelation of total monsoon rainfall of Angul district

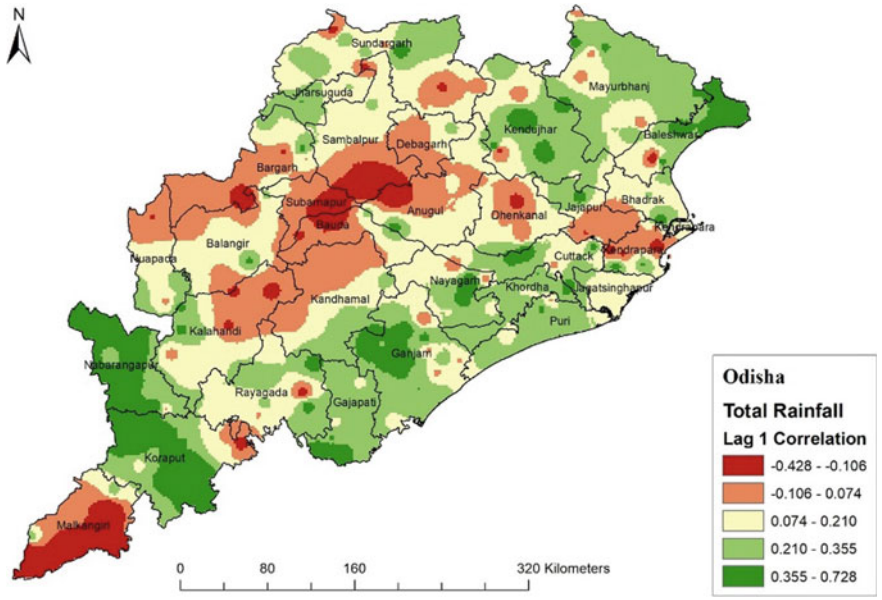

Fig. 7 Lag 1 correlation value of 314 blocks of Odisha for 31 (1988–2018) years

4 Conclusions

- In Odisha, there is a wide variation in the rainfall from region to region. The average total monsoon rainfall of the state was 1147.9 mm with a standard deviation of ±400 mm for 31 years (1988–2018).
- The maximum mean of monsoon rainfall has been observed in Kalahandi district whereas Sundergarh district experienced the highest value of both SD and CV.
- Ganjam District experienced the lowest mean, SD and CV of monsoon rainfall. Highest average rainfall occurred in Balasore District for June and September whereas Kalahandi District experienced maximum mean rainfall for July and August. Minimum mean rainfall detected for Puri district in June, Ganjam district for July and August and Nuapada district in September.
- Highest SD value of rainfall detected in case of Kalahandi district for June and July, Kandhamal district in August and Kendrapara district for September. Khordha, Keonjhar, Ganjam and Rayagada districts detected with minimum SD value of rainfall in June, July, August and September respectively.
- Maximum CV value of rainfall was experienced by Kalahandi district in June, Sambalpur district in July and August and Nuapada district in September. Spatial variation in mean, SD and CV value of monsoon rainfall was found among the 314 blocks of Odisha. Most of the western regions of Odisha receives more rainfall as compared to the southern and coastal regions of the state.
- Autocorrelation function showed a significant correlation of the monsoon rainfall time series for lag 1, lag 2 and lag 3 data. The present data series has a strong correlation with previous year's data series, indicating non-randomness of rainfall series data.

References

Basistha A, Arya DS, Goel NK (2009) Analysis of historical changes in rainfall in the Indian Himalayas. Int J Climatol 29:555–572

Chowdhury R, Kumar V, Sattar A, Brahmachari K (2014) Studies on the water use efficiency and nutrient uptake by rice under system of intensification. The Bioscan. 9(1):85–88

Diaz HF, Bradley RS, Eischeid JK (1989) Precipitation fluctuations over global land areas since the late 1800's. J Geophys Res: Atmos 94(D1):1195–1210

Goswami BN, Venugopal V, Sengupta D, Madhusoodan MS, Xavier PK (2006) Increasing trends of extreme rain events over India in a warming environment. Science 314:1442–1445

Gouda KC, Sahoo SK, Samantray P, Shivappa H (2017) Comparative study of monsoon rainfall variability over India and the Odisha state. J Clim (MDPI)

Guhathakurta P, Rajeevan M (2008) Trends in the rainfall pattern over India. Int J Climatol 28:1453–1469

Kishtawal CM, Niyogi D, Tewari M, Pielke RA, Shepherd JM (2010) Urbanization signature in the observed heavy rainfall climatology over India. Int J Climatol 30:1908–1916

Kothyari UC, Singh VP (1996) Rainfall and temperature trends in India. Hydrol Process 10:357–372

Kripalani RH, Kulkarni A, Sabade SS (2002) Indian monsoon variability in a global warming scenario. Nat Hazards 29:189–206

Kumar KR, Pant GB, Parthasarathy B, Sontakke NA (1992) Spatial and sub-seasonal patterns of the long-term trends of Indian summer monsoon rainfall. Int J Climatol 12:257–268

Kundzewicz ZW, Robson AJ (2004) Change detection in hydrological records—a review of the methodology. Hydrol Sci J 49(1):7–19

Mohapatra M, Mohanty UC, Behera S (2003) Spatial variability of daily rainfall over Orissa, India, during the south-west summer monsoon. Int J Climatol 23:1867–1877

Patra JP, Mishra A, Singh R, Raghuwanshi NS (2011) Detecting rainfall trends in twentieth century (1871–2006) over Orissa state, India. J Clim Change 111:801–817

Pattanaik DR (2005) Variability of oceanic and atmospheric conditions during active and inactive periods of storms over the Indian region. Int J Climatol 25:1523–1530

Prabhakar AK, Singh KK, Lohani AK, Chandniha SK (2019) Assessment of regional-level long-term gridded rainfall variability over the Odisha state of India. J Appl Water Sci 9:93

Cognizance of Rainwater Management System in Urban Areas (Pune City)—A Trial Study

J. S. Sudarsan, Harshavardhan, Kakuru Jyothi Priyanka Reddy, Ayushi, Manepalli Karun, and Sri Chaitanya Varma

Abstract Our environment is being subjected to drastic changes since past couple of years. The growing population in urban areas and their ever-increasing demand of basic resources like quality of food, air, water and hygiene surroundings are challenging. In urban cities like Pune, these requirements of human are not yet fully organized and managed. It can be said that the city is in a zone of earnest mismanagement. Lifestyle of users and increasing per-capita demand are projecting future years of water scarcity. Rigorous expansion in the urban cities are ravaging the existing local sources of water and polluting the water table. In addition to this, industrialization is integrating supplemental damage to water eco system. At the present rate of uncontrolled growth rate, expansions and behaviour of society, the water resources are in peril of depletion. In order to overcome such situations, the cognizance in people about rainwater harvesting system and storm water management system should be made realized. Because it is expressed that even in one tier cities like Pune, the cost-effective system such as both rainwater harvesting and storm water management is not sympathizing and is shooting problem in every monsoon season such as flooding and inundation. To ascertain its significance a questionnaire was floated with data in support of Rainwater harvesting importance, need and benefits among the local residence of Pune city. The bottom-line of the output is that more than 70% people residing in the city area are not aware of the rainwater harvesting system and its significance. To make them aware of the importance of the system, a trail study was initiated by considering an area of five towers of 5000 ft^2 and in addition it is assumed that the tower comprises of 5000 ft^2 of lawn in Nigdi locality of Pune. Rainfall data of the area for the year 2019 was accounted from the weather reports recorded. An estimation was done from the data collected of rainwater that could be harvested for the year 2019 from the 5 towers in the Nigdi area. The study also highlights the need for adopting the various smart technologies in managing the water scarcity, either the rainwater or the supplied potable water for efficient and controlled water management system.

J. S. Sudarsan (✉) · Harshavardhan · K. Jyothi Priyanka Reddy · Ayushi · M. Karun · S. Chaitanya Varma
National Institute of Construction Management and Research, Pune, India

B. B. Das et al. (eds.), *Recent Developments in Sustainable Infrastructure (ICRDSI-2020)—GEO-TRA-ENV-WRM*, Lecture Notes in Civil Engineering 207,
https://doi.org/10.1007/978-981-16-7509-6_41

Keywords Rain water harvesting system · Pune · Rainfall · Environment · Smart technology

1 Introduction

Rainwater harvesting is a technology that collects, conveys and retains rain from soundly neat surfaces such as a roof and land surface for later use. Water that is typically stored in the rain-water tank contributes to the resuscitation of groundwater. Another method of rain water harvesting that plays an important role in the management of storm water and the replenishment of groundwater levels is rainwater infiltration. Rainwater harvesting has been practised around the world for over 4000 years, historically in arid and semi-arid regions, supplying potable water, household water and minor irrigation. For the time being, rainwater harvesting as a new, water-saving and simple technology has gained much in significance (Patel et al. 2014).

The method of collecting rainwater from rainfall events can be categorized into two types: roof-based and land-based. When runoff from soil surface is captured by reservoirs, furrow dikes, dams, and tanks, land-based rainwater harvesting takes place. Rooftop-based rainwater harvesting involves the collection of rainwater runoff from roof surfaces, that generally gives an even more cleaner water supply which can also be used for drinking.

1.1 Need

The basic need for the rainwater harvesting system would be meeting the ever-increasing demand of the water in order to mitigate the water scarcity. Increase groundwater storage and monitoring the decrease in water levels would help to save more water. The groundwater quality and the reduction in soil erosion can be made possible by effective installation of the system (Kim et al. 2008). The system can help in reducing the soil erosion and flood hazards by collecting rainwater and reducing the flow of stormwater to prevent urban flooding. Most buildings that utilize rainwater harvesting systems have a built-in catchment area on top of the roof, which has a capacity of collecting large volumes of water in case of rainstorms.

In new and existing buildings, rainwater collection systems can be built as well as rainwater collected for various applications which do not require the quality of drinking water, such as flushing the toilet, watering the lawn, cleaning, irrigation and washing. In many parts of the world, harvested rainwater is also used as a source of drinking water. Washing and cleaning powder is also less used, as the rainwater is very warm. Savings in potable water can be as high as 50% with rainwater harvesting.

1.2 Components

1.2.1 Catchment

The region directly receiving rainfall is the rainwater collection system's catchment. The catchment area can be garden, terrace, open land, paved surface or unpaved surface. The terrace can be flat or sloping RCC/stone roof. Thus, the catchment is the zone that directly applies to the rainwater collection process.

1.2.2 First Flush

The first flush is an apparatus used in the first shower to flush the water. The first rain shower must be flushed off in order to prevent contamination of storable/rechargeable water by possible atmospheric pollutants and the roof for catchment. It also helps to clean silt and other resources accumulated during the dry weather. Arrangements should be made for the first rain separator on the outlet of each drainpipe.

1.2.3 Conveyance (Pipe)

Water pipes or drains are used to transfer water from rooftop to storage or harvesting system situated on the ground. The water pipes should be UV resistant with appropriate size. Gutters capture the water from sloping roofs and it is piped down. Could drain's mouth should have wire mesh on the terraces to limit floating material.

1.2.4 Filter

To effectively minimise turbidity, colour and micro-organisms, filters are used in water treatment. Water can pass through filters after the first flushing of rainfall or be deposited directly into the tank and filter before use. Mesh is construction by the use of different components such as gravel, sand and 'netlon' and the position of this mesh is kept on the top of the tank basically depending on the application.

1.2.5 Pressure Sand Filter

This filter comprises of a vertical or horizontal pressure tube fitted with a series of front pipe works and valves, graded silica quarts sand supported by graded bed layers of pebbles and gravel, a top distributor to spread the incoming water uniformity around the cross-section of the filter, and an under-drain system to collect filtered water.

Raw water passes through the filter bed downwards and is contained directly below the surface on the sand surface and between the sand grains as the suspended matter, which has traditionally been treated with the addition of a coagulant such as alum. As the filter process continues, the loss of head is steadily rising and the flow decreases as the filter drops excessive pressure (Mishra 2014).

1.2.6 Storage

Storage in this content generally refers that it stores the water that is received from the roof top and also stores the water that the filter collects. Different components used for small-scale storage of water are plastic containers, jerry cans, clay or cement pots, pottery pots and drums are used. A larger tank made of ferro cement or cement rings, or plain cement concrete or brick or stone, etc., will be required for the system with a cylindrical or rectangular or square shape. The storage tank is fitted with a top cover to avoid contamination of water from external sources. The storage tank is fitted at appropriate locations with pipe fixtures to draw water to clean the tank and dispose of waste.

1.2.7 Sustainability

Rainwater harvesting is one of the highest assuring and traditional options for water supply in contempt of rising water shortage and demand escalation which could be easily used for potable and non-potable purposes in residential uses. The onus on water sources, added on environmental accoutrements from major projects and decreasing water quality hinder the capacity to satisfy conventional freshwater demand. Rainwater harvesting provides an opportunity to increase water availability, allowing for autonomy and preservation at the same time. Substantial usage of water could stabilize balance between its demand and supply (Jain et al. 2015).

1.3 Advantages

Rainwater is a water source which is relatively clean and free. Harvesting rainwater provides a supply of water where it's needed. Socially, it is appropriate, and responsible for the environment. It enables autonomy and preserves energy for water. Rainwater is ideal for landscaping plants and gardens. Pollution from stormy water and non-point sources are minimised. Also includes quick, easy to manage, scalable technology. Provides potential cost savings, with rising water prices in particular. Provides clean, human consumption after adequate care, water (Milman and Short 2008).

2 Methodology

This paper briefs about the importance of rainwater harvesting, its need and how smart technologies will help in conserving water. It also introduces various components of rainwater harvesting unit. The runoff factor associated with different catchment areas were used for estimation of runoff that can happen over an area for the study. For this we choose five residential towers in Nigdi area of Pune city of Maharashtra. Of these five towers, the catchment area and surface characteristics were identified to estimate the rainfall runoff. The rainfall data of the year 2019 is collected from the weather Bureau. With all this data an estimation is done to calculate the amount of rainfall that could be harvested from those five residential towers. The volume thus calculated is analysed in water savings by implementing rainwater harvesting in particular premises. Further the data is interpretated as a supporting word to urge the public understand the importance of rainwater harvesting. The paper speaks about various smart technologies effective in saving water losses (Kimani et al. 2015).

3 Results and Discussions

A questionnaire was floated around Aundh area to know the awareness level of rainwater harvesting among the residents and according some of the responses received, majority of the population declared that they are unaware of most of the rainwater harvesting benefits and no proper system was installed in their residence. In order to project the benefits, five towers are selected with the runoff coefficient considered for calculating the rainwater harvesting system as shown in Table 1. In these two conditions were considered where condition 1 will be roof areas of 5 towers

Table 1 Runoff factors for various types of catchments

S. No.	Type of catchment	Coefficient
1.	Residential complexes in urban areas	
	1.1 Single family	0.3–0.5
	1.2 Multiunit, detached	0.4–0.6
	1.3 Multiunit, attached	0.6–0.75
2.	Lawns, sandy soil having slopes	
	2.1 Flat 2%	0.05–0.10
	2.2 Average 2–7%	0.1–0.15
	2.3 Steep 7%	0.15–0.2
3.	Lawns, clayey soil having slopes	
	3.1 Flat 2%	0.13–0.17
	3.2 Average 2–7%	0.18–0.22
	3.3 Steep 7%	0.25–0.35

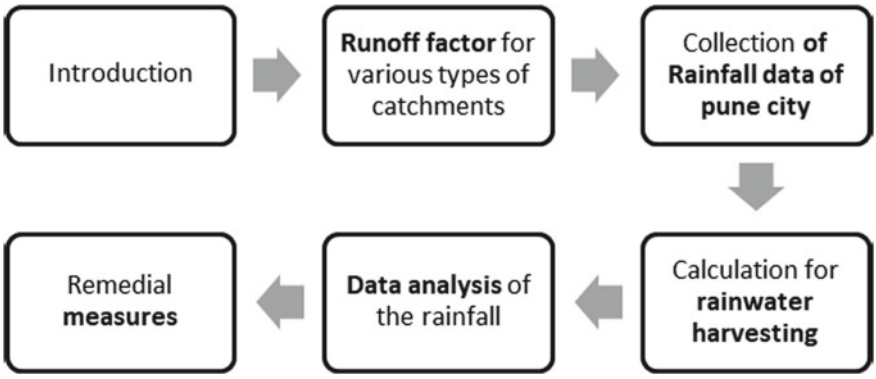

Fig. 1 Study methodology

that is 5000 m^2 each and condition 2 a 5000 m^2 of lawn in addition to each tower of 5000 m^2 roof area is considered. The lawns will have a sandy soil having slope 2–7% average (Kumar et al. 2010). The below Fig. 1 represents the study methodology which was followed in order to obtain the required data from the residents of the society.

3.1 Rainfall Data of Pune Area for the year 2019 month Wise

The highest number of days of rainfall observed was in the month of July—12.8 days and the lowest number of days, rainfall observed was January month—0 days and the same is expressed in Fig. 2 which contains the data of average no of days rainfall is observed of all months (Hajani and Rahman 2014).

After the average no of days in which rainfall is observed has been calculated the Maximum intensity of rainfall has also calculated and is observed that the highest rainfall is recorded in the month of July—187.2 mm and the lowest rainfall is recorded in the month of January—0 mm and Fig. 3 has the complete data of the rainfall intensity (Glendenning et al. 2012).

3.2 To Calculate Rainwater Probable to Harvest Will Be

Volume of rainfall likely to be collected will be equal to

$$V = I \times A \times C$$

I is intensity of rainfall in mm, A is area in m^2, C is runoff coefficient.

Table 2 gives the volume of rainwater that could be collected with the intensity

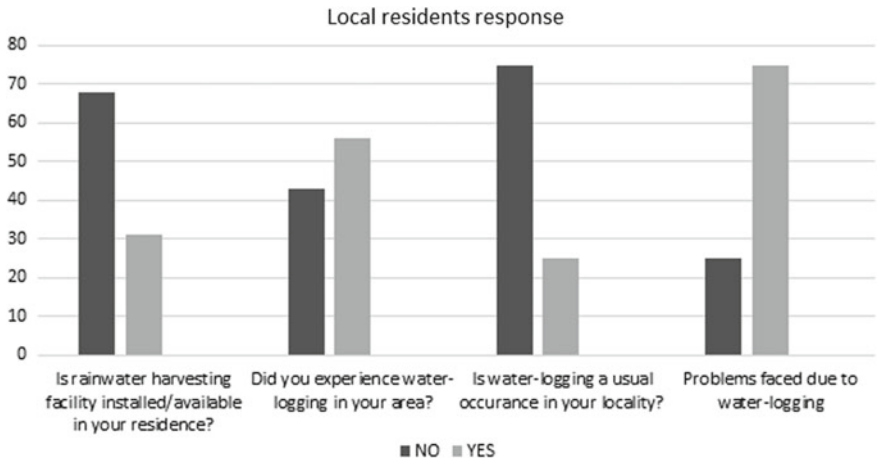

Fig. 2 Responses received from the local residents

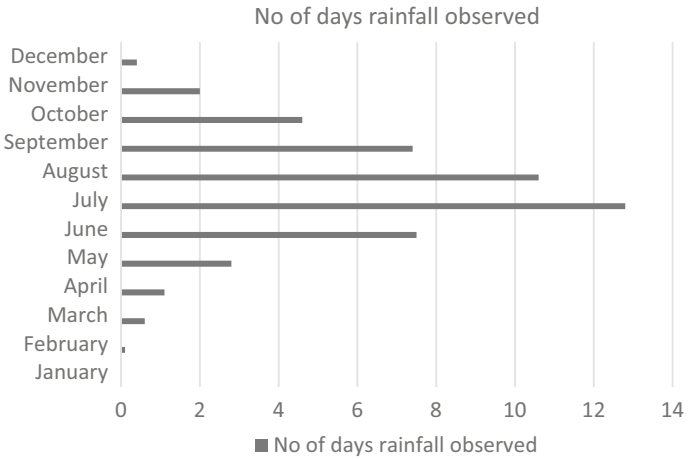

Fig. 3 Average No of days, rainfall observed in each month of 2019

of rainfall observed.

The above said table is the data calculated for one residential complex of area 5000 ft^2 with an open lawn of 5000 ft^2. So, the water harvestable from 5 towers will be 50.27 * 5, that is 251.35 m^3.

Therefore, 251.35 m^3. of water could be collected from the 5 residential complexes.

Rainwater collected in different seasons will be:

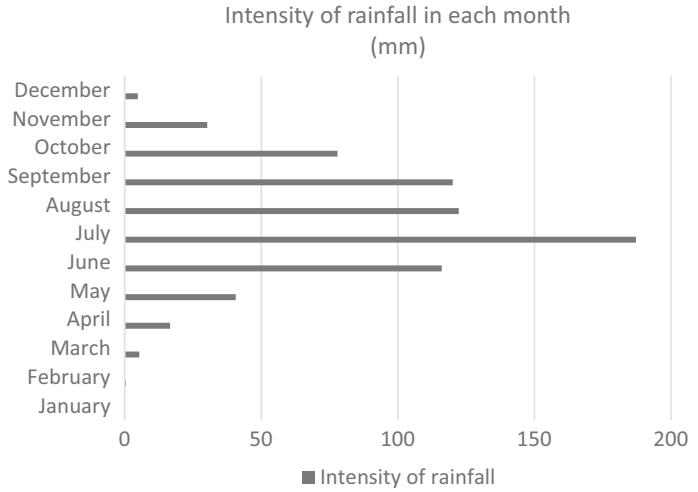

Fig. 4 Intensity of rainfall in each month of 2019 in mm is expressed through below Fig. 4

Table 2 Volume of rainwater

S. No.	Month	Rainfall in (mm)	Area (m^2)	Runoff factor	Collected rainwater (m^3)
1	Jan	0	464.5	0.15	0
2	Feb	0.5			0.03
3	March	5.3			0.36
4	April	16.6			1.15
5	May	40.6			2.82
6	June	116.1			8.08
7	July	187.2			13.04
8	Aug	122.3			8.52
9	Sep	120.1			8.86
10	Oct	77.9			5.42
11	Nov	30.2			2.10
12	Dec	4.8			0.36
Total					50.27

S. No.	Season	Volume of rainwater
1	Spring	2.0
2	Summer	60.35
3	Monsoon	149.64
4	Autumn	37.65

(continued)

(continued)

S. No.	Season	Volume of rainwater
5	Winter	1.67

The storage tank of the rainwater harvested must be such that it will be sufficient enough to serve water during the dry season. Tank volume V in litres = t × n × q,

where t is total no days in dry season, n is number of users, q is quantity of per capita consumption per day.

Dry days (t)	Population (p)	Avg. Per capita consumption (q)	Volume (v) Cu.M
91	1400	135	17,199

The average per capita consumption of residents, given by Pune Municipal Corporation is 194 lpcd and most of it is NRW

P = population intended to use the collected source, changes with no of units in an apartment and population in each house. Assuming 70 flats per tower and 4 persons per flat, total population will be 5 * 70 * 4 = 1400

Source http://www.pmc.gov.in/sites/default/files/project-glimpses/24x7_water_brochure.pdf

From this we can consider that, the size of tank must be sufficient to supply water during total dry season i.e., from April to June and the total quantity to be stored to supply the 91 days period will be 17,199 m^3. On average, the per day water required will be 189 m^3. Assuming the apartment has 5000 ft^2 tower area and 5000 ft^2 lawn area.

No of towers	Catchment area						Total volume (m^3)
	Volume arising from roof (m^3)	Runoff factor	Volume collected	Volume arising from Lawn (m^3)	Runoff factor	Volume collected	
5	1675.916	0.75	1256.75	1675.916	0.15	251.35	1508.1

Thus, out of 17,199 m^3 of water demand, 1508.1 m^3 can be availed from natural source which saves energy and cost in supply and monitoring.

4 Remedial Measures for Effective Water Management

Home automation was once a moon-shot, but it is getting common these days, with technological advancements we are able to control almost everything around us, one such kind of advancements are tracking water usage. Water being an important element in human life, appropriate usage of water is very crucial in order to avoid water shortage problems in the near future. To counter the problem of water wastage,

technological advancements have come up and are integrated into home automation with respect to household applications (Awuah et al. 2014).

When it comes to monitoring and control of water, the very first challenge starts with the age of infrastructure and components used in conveying the source from point of collection to point of delivery. New infrastructure arises new costs and old infrastructure limits the alterations to convert them into present required model for efficient management.

Some places are improving the existing facility and some are adopting the new generation models for future benefits. To support the constraint in improvements, technology offers many solutions depending on type of renovations (Norman et al. 2013).

The following are some of the useful technologies in water management.

4.1 Smart Sensors

In this system, sensors will be incorporated at regular intervals or at the nodes so as to detect the parameters associated with water. This will help us in measuring the pressure difference which probably indicates the losses. As we cannot visually access the underground pipe-lines, the sensors allow us to detect possible condition of those water lines by measuring the data in terms of volume of water flow—average flow, seasonal volume consumption, losses and also tracking of supplied water.

4.2 Smart Metering

This is a measurement device that is generally used for storing and transmitting the consumption with a certain frequency. So, to develop an effectual water management system, sensors and actuators have to be mounted to control the water system. Therefore, although the water bill generated by this manual reading can be used to read the water meter every month or once every two months, the smart water meter can obtain the water utilization from a long distance and at a high frequency, so as to provide customers and users with instant access information (Akpinar and Cecunjanin 2014). Advanced metering infrastructure is required for the management of this information. In order to increase water power and energy efficiency, achieve leakage protection and unauthorised connexions to water companies should also build this system.

4.3 Geographic Information System

This system plays a string role in the management of smart water, offering a full list of the components and their spatial locations throughout the network. GIS becomes essential for managing the water system, enabling spatial components to be used in an oriented model in order to enhance planning and management through a consistent evolution of the spatial components of the network. Simulation of reality based on data structure designed to capture, store, receive, exchange geographically suggested information is the main benefit component of GIS (Liaw and Tsai 2004).

4.4 Supervisory Control and Data Acquisition (SCADA)

The usage of memory and storage capabilities and the measurement of computers and servers that are exchanged and linked through the internet are referred to by following the network computing code. Cloud computing is described as "a new style of computing in which the resources are dynamically scalable and often virtualized being provided as a service over the internet". In order to maximise their use, such as vast collection of virtualized resources, hardware, development platforms and applications with easy access and dynamically optimised to respond to various workloads. In general, the majority of public water systems use a SCADA method to supervise, monitor and data management (Siderius et al. 2015).

4.5 Decision Support System and Optimization

Implementing a standard performance assessment system based on a collection of relevant metrics and data applications and interfaces used to support management decision making will enable stakeholders to assess, create confidence and track progress. Awareness of accurate short-term demand forecasting models is critical to the production of methodology models and thus to the real time implementation of active decision in the smart water system (Morey et al. 2016).

4.6 Leak Detectors

There exists two types of leaks in a water distribution system. 1. Static leaks 2. Dynamic leaks. Sensors can be installed in detecting and measuring the static leaks as they can be pin pointed and localized. Dynamic leak detection require movable devises and data can be measured when targeted the suspected zone or area. Geophones and hydrophones are commonly used devises in detecting leaks.

The importance of leak detectors is in identifying incognito water losses which in turn it will save consumption of water and saves water bills. So, a leak detector not only saves a distribution system in detecting water loss, but also the price consumer pays for unused water.

4.7 Smart Sprinkler Controller

The controller is completely cloud based, which could be operated by phone or similar devices. Which lets us select the nearby weather stations to know about weather forecasts which can help us in turning on/off the sprinkler to avoid water wastage (Ganguly et al. 2014).

4.8 Low Flow Faucets

The low flow faucets are the fixtures that reduces amount of water used for daily activities, which are enabled with sensors. In low flow faucets some of them offer touch sensitive flow control to regulate the use of water in daily activities.

5 Conclusion

Rainwater harvesting has benefits where people in the society are neglecting and exploiting ground water. May be the quantity collected will not serve every requirement of individual but can save in volume of collection, the supply boards are collecting to meet the per capita demand. From gardening to drinking purpose, if the water management board of a place has to supply from sources like rivers and borewells which involves huge cost, then we cannot sustain in the near future. Over-exploitation of ground and river water creates imbalances not only in terms of water table levels, but also for activities like agriculture and aqua culture and also for habitants.

Management of water has its importance in collection and supply as well. From point of collection to point of recycling or treatment, unless one becomes aware of alternatives, change in lifestyles or accountable for negligence and losses, and monitors, the population is going to suffer with water scarcity in future. Government and organizations should come forward in creating awareness among people. Associating water collecting capacities while designing infrastructure and buildings and accordingly water management plans must be developed.

References

Akpinar Ferrand E, Cecunjanin F (2014) Potential of rainwater harvesting in a thirsty world: a survey of ancient and traditional rainwater harvesting applications. Geogr Compass 8:395–413

Awuah E, Gyasi SF, Anipa HMK, Sekyiamah KE (2014) Assessment of rainwater harvesting as a supplement to domestic water supply: case study in Kotei-Ghana. Int Res J Public Environ Health 1:126–131

Ganguly R, Bansal A, Mishra M, Kumar A (2014) Application of rainwater harvesting scheme in Shimla Region. Hydrol Curr Res 5:34–42

Glendenning C, Van Ogtrop F, Mishra A, Vervoort R (2012) Balancing watershed and local scale impacts of rain water harvesting in India—a review. Agric Water Manage 107:1–13

Hajani E, Rahman A (2014) Reliability and Cost Analysis of a Rainwater Harvesting System in Peri-Urban Regions of Greater Sydney, Australia. Water 6:945–960

Jain S, Thakur P, Singh S, Srivastava M (2015) Design of rooftop rainwater harvesting tank for Katpadi Region, Tamil Nadu. SSRG Int J Civil Eng (SSRG-IJCE) 2:6–8

Kim Y et al (2008) Remote sensing and control of an irrigation system using a distributed wireless sensor network. IEEE Trans Instrument Measure 57:1379–1387

Kimani MW, Gitau AN, Ndunge D (2015) Rainwater harvesting technologies in Makueni County, Kenya. Res Inventy Int J Eng Sci 5:155–163

Kumar KK, Kamala K, Rajagopalan B, Hoerling MP, Eischeid JK, Patwardhan SK (2010) The once and future pulse of Indian monsoonal climate. Clim Dyn 36:2159–2170

Liaw C-H, Tsai Y-L (2004) Optimum storage volume of rooftop rain water harvesting systems for domestic use. J Am Water Resour Assoc 40:901–912

Milman A, Short A (2008) Incorporating resilience into sustainability indicators: an example for the urban water sector global environmental change. Global Envion Change 18:758–767

Mishra SS (2014) Rainfall analysis and design of water harvesting structure in water scarce Himalayan Hilly Regions. Int J Civ Struct Eng 5:29–41

Morey A, Dhurve B, Haste V, Wasnik B (2016) Rain water harvesting system. Int Res J Eng Technol (IRJET) 3:12–14

Norman ES, Dunn G, Bakker K, Allen DM, De Albuquerque RC (2013) Water security assessment: integrating governance and freshwater indicators water resources management. Water Resour Manage 27:535–551

Patel UR, Patel VA, Balya MI, Rajgor HM (2014) Rooftop rainwater harvesting (rrwh) at spsv campus, Visnagar: Gujarat - a case study. Int J Res Eng Technol 3:821–825

Siderius C, Boonstra H, Munaswamy V, Ramana C, Kabat P, van Ierland E (2015) Climate-smart tank irrigation: a multi-year analysis of improved conjunctive water use under high rainfall variability. Agric Water Manage 148:52–62

Effect of Aspect Ratio on Emergent Vegetated Flow Condition: A Semi-analytical Study

Deepika P. Palai, Sumanta Chaudhuri, Paromita Chakraborty, and Bitanjaya Das

Abstract Presence of vegetation in channels offers higher resistance towards the flow and affects the flow characteristics significantly, which ultimately influence local bed scouring, sediment transport, flow of pollutants, and bed shear. Initial research on this aspect focused on the bed resistance and provided few empirical relations for the resistance, which yielded the average velocity. However, for a better understanding of the flow characteristics, velocity distribution is needed; from which shear stress distribution and shear stress could be obtained. In view of that, several mathematical models, both numerical and analytical, were proposed for tackling the flow phenomenon. Numerical models generated results with higher accuracy, but their implementation required huge computational resources. Therefore, search for simpler analytical models are on and several analytical models were put forward. Experimental investigations were also carried out for validation of these numerical and analytical models. However, in the previous studies many important aspects are still unexplored and require further studies. One such factor is the effect of aspect ratio on the flow velocity and shear stress distribution. Effect of the aspect ratio will not have any effect on the flow if the channel width is large which usually occurs in case of rivers, wetlands etc. However, in case of flow through man-made channels, canals etc. channel width is not too large and can significantly affect the flow. In view of this, the present study attempts to analyze the effect of aspect ratio of the channel on the flow characteristics. Flow through emergent vegetation is studied for steady, incompressible, fully developed and laminar flow conditions. Although, laminar

D. P. Palai · P. Chakraborty · B. Das
School of Civil Engineering, KIIT-DU, Bhubaneswar, India
e-mail: 1881026@kiit.ac.in

P. Chakraborty
e-mail: paromita.chakrabortyfce@kiit.ac.in

B. Das
e-mail: bdasfce@kiit.ac.in

S. Chaudhuri (✉)
School of Mechanical Engineering, KIIT-DU, Bhubaneswar, India
e-mail: sumanta.chaudhurifme@kiit.ac.in

B. B. Das et al. (eds.), *Recent Developments in Sustainable Infrastructure (ICRDSI-2020)—GEO-TRA-ENV-WRM*, Lecture Notes in Civil Engineering 207,
https://doi.org/10.1007/978-981-16-7509-6_42

flow condition is not very practical but it provides insights, which are important for understanding the vegetated flow. A semi-analytical solution of the governing equation is obtained by employing the Least Square Method. The results indicate that velocity decreases significantly with changes in aspect ratio of the channel.

Keywords Vegetated flow · Velocity distribution · Bed shear · Semi-analytical solution · Least square method (LSM)

1 Introduction

Flow through vegetation has been an active area of research due to its importance in the fields wetland management, flood control, sediment transport etc. Presence of vegetation in channel flows, offers higher resistance towards the flow resulting in a higher drag. Understanding the flow characteristics of vegetated flow is important for a better control over sediment deposition, flood management.

Researchers, initially, focussed to estimate the resistance offered by the vegetation using empirical relations based on experiments. Gradually, however, researchers developed interest in obtaining the velocity distribution and the associated shear stress with the velocity. Several three dimensional models for turbulent flow were proposed by the researchers for analyzing flow through vegetation. K–ε, k–ω and Large Eddy Simulation (LES) are frequently employed models for describing the turbulent stress. But large computational resources were required for these three dimensional models, which motivated researchers to search for simpler analytical models without comprising the accuracy. As a result, various simplified one-dimensional models (Hsieh and Bolton 2007; Zhao et al. 2012) were put forward. In various studies (Kubrak et al. 2008; Huai et al. 2013), the drag experienced by the flow was estimated as the product of drag coefficient, area and square of velocity. Biot's poro-elastic theory, used in porous media flow, was employed by Hseish and Bolton (2007) for formulating the equations of flow through vegetation. This approach eliminated the need for estimating the drag coefficient. Later on, Chakraborty and Sarkar (2016) employed Biot's poro-elastic theory for analyzing flow through vegetation over a periodic bed. Guo and Zhang (2016) adopted a more general approach by employing Forchheimer law (1901) of porous media in flow through vegetation. The equation is as follows:

$$F_d = \frac{\mu}{k_p} V + \beta \rho V^2 \tag{1}$$

where, μ is the dynamic viscosity of the fluid, k_p is the intrinsic permeability of vegetation, β is the Forchheimer coefficient, ρ is the water density and V is velocity. Guo and Zhang reported that $k_p \neq$ infinity and $\beta = 0$ represents the case of laminar flow without separation. Several studies (Song and Huang, 2000; Hsieh and Shiu 2006; Hsieh and Bolton 2007; Zhao et al. 2012) can be viewed as the examples of this condition.

For artificially built channels, canals the lateral width of channel may not be very large compared to the depth of flow. Effect of the width or aspect ratio of the channel may be crucial on the flow characteristics. Effect of the aspect ratio of the channel is considered in the present study. Inclusion of the aspect ratio requires the formulation of the governing equation, where, the axial velocity is a function of both longitudinal and lateral coordinates. Forchhemier law, given by Eq. (1), is employed to describe the vegetation drag for the case of flow without separation. This is represented by $k_p \neq$ infinity and $\beta = 0$.Flow considered is steady, laminar, incompressible, fully developed and emerged. As mentioned by Guo and Zhang (2016) the condition of emerged flow is not practical, but it helps understanding the physics of flow. Least Square Method (LSM) is employed for obtaining a semi-analytical solution. LSM is a semi-analytical technique widely used by researchers (Hatami et al. 2014; Hatami and Ganji 2014). Results of the LSM are validated by comparing the same with the results of numerical solution, generated by using the finite difference technique. The results indicate that velocity decreases significantly with increase in the aspect ratio.

2 Problem Formulation

The physical problem, addressed in the present study, is presented in Fig. 1. The schematic of the emerged vegetated channel is shown in Fig. 1.

For steady flow case, the continuity equations is as follows:

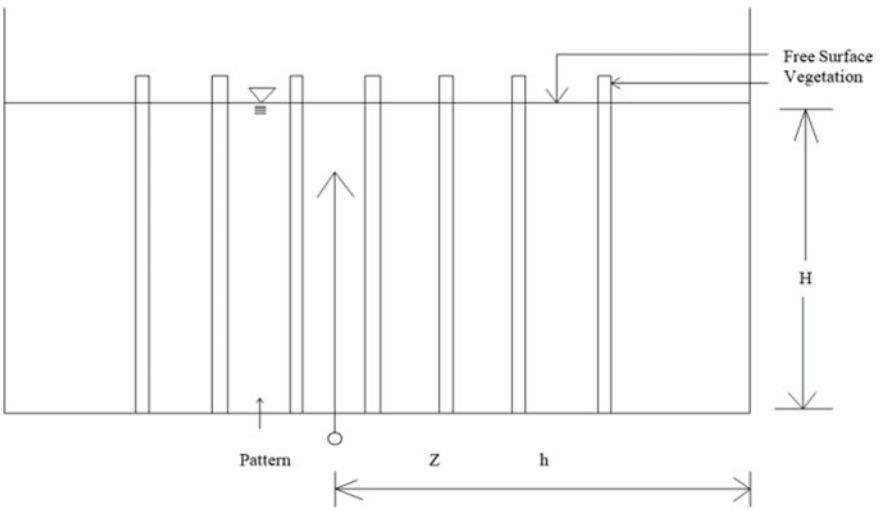

Fig. 1 Schematic of the emerged vegetated channel

$$\frac{\partial u}{\partial x} + \frac{\partial v}{\partial y} + \frac{\partial w}{\partial z} = 0 \tag{2}$$

where, x, y and z are the axial, vertical and transverse coordinate; u, v, and w are the corresponding velocity components along the axial, vertical and transverse directions. The flow considered is fully developed; only axial component of velocity exists. Therefore, Eq. (2) reduces to the following:

$$\frac{\partial u}{\partial x} = 0 \tag{3}$$

From Eq. (3) it can be concluded that the axial velocity is dependent of the vertical and transverse coordinates, which is expressed as follows.

$$u = u(y,\ z) \tag{4}$$

The momentum conservation equation employed by Guo and Zhang (2016), in its vector form, is given below:

$$\rho\left[\frac{\partial \vec{V}}{\partial t} + \left(\vec{V}\cdot\nabla\right)\vec{V}\right] = \rho\vec{g} - \nabla p + \nabla\cdot\sigma - \frac{\mu}{k_p}\vec{V} - \rho\beta\left|\vec{V}\right|^2 \tag{5}$$

$$V = \eta V_f \tag{6}$$

where, ρ is the density of the fluid, t is the time, g is the acceleration due to gravity, σ is the stress tensor, μ is the dynamic viscosity of fluid. V_f is the pore fluid velocity, η is the porosity. As per the assumption of the velocity in the present study, given by Eq. (4), Eq. (5) reduces to the following:

$$\frac{\partial^2 u}{\partial y^2} + \frac{\partial^2 u}{\partial z^2} - \frac{\mu}{k_p}u + \rho g \sin\theta = 0 \tag{7}$$

where, u is the velocity in the direction of flow, y and z are the coordinates in the vertical and lateral directions, respectively and θ is the slope of the channel. The boundary conditions required for solving Eq. (7) are as follows:

No slip boundary condition at the bottom of the channel

$$u(0, z) = 0 \tag{8a}$$

Negligible shear at the free surface, H is the depth of flow

$$\frac{\partial u(H, z)}{\partial y} = 0 \tag{8b}$$

No slip condition at the left wall of the channel

$$u(y, -h) = 0 \tag{8c}$$

where, h is the half width of the channel.

No slip condition at the right wall of the channel

$$u(y, h) = 0 \tag{8d}$$

For reducing Eq. (7) and Eq. (8a)–(8d) in their non-dimensional forms, following non-dimensional variables are introduced:

$$y^* = \frac{y}{H}, \quad z^* = \frac{z}{h}, \quad A = \frac{H}{h}, \quad K_1 = \frac{H^2}{kU_0}, \quad K_2 = \frac{\rho g \sin\theta H^2}{\mu U_0} \tag{9}$$

where, y^*, z^* are the non-dimensional variables in the vertical and lateral directions. A is the aspect ratio of the channel, K_1 is the porosity parameter, K_2 represents the gravity force parameter. Utilizing Eq. (9), Eq. (7) reduces to the following:

Boundary conditions:

$$\frac{\partial^2 u^*}{\partial y^{*2}} + A^2 \frac{\partial^2 u^*}{\partial z^{*2}} - K_1 u^* + K_2 = 0 \tag{10}$$

No slip

$$u\left(0, z^*\right) = 0 \tag{11a}$$

No shear

$$\frac{\partial u(1, z^*)}{\partial y} = 0 \tag{11b}$$

No slip at the left wall

$$u\left(y^*, -1\right) = 0 \tag{11c}$$

No slip at the right wall

$$u\left(y^*, +1\right) = 0 \tag{11d}$$

For convenience, asterisk is removed from the variables and the governing dimensionless equation reduces to the following form:

$$\frac{\partial^2 u}{\partial y^2} + A^2 \frac{\partial^2 u}{\partial z^2} - K_1 u + K_2 = 0 \tag{12}$$

2.1 Methodology (LSM)

The Least Square Method (LSM) is employed for solving Eq. (12). LSM is a semi-analytical technique, capable of generating solution to non-linear differential equations.

The detailed procedure of LSM is given below:

First, trial functions or base functions are selected which satisfy the boundary conditions, given by Eqs. (8a)–(8d). The approximate solution for Eq. (12) is assumed to be of the following form

$$u \approx v = \left(1 - z^2\right)\left[c_1\left(y - \frac{y^2}{2}\right) + c_2\left(y^2 - \frac{y^4}{2}\right)\right] \tag{13}$$

As the assumed solution for the velocity, does not satisfy Eq. (12) in all points of the domain, an error or residual will be generated upon substitution of Eq. (13) in Eq. (12), which is given as follows:

$$\begin{aligned} R_{err} = c_1&\left[-\left(1 - z^2\right) - 2A^2\left(y - \frac{y^2}{2}\right) - K_1\left(1 - z^2\right)\left(y - \frac{y^2}{2}\right)\right] \\ &+ c_2\left[\left(1 - z^2\right)\left(2 - 6y^2\right) - 2A^2\left(y^2 - \frac{y^4}{2}\right) - K_1\left(y^2 - \frac{y^4}{2}\right)\left(1 - z^2\right)\right] + K_2 \end{aligned} \tag{14}$$

In LSM, the principle is to minimize the square of error in the entire domain. Let sum of error be S, which is given as follows:

$$S = \int_0^1 \int_{-1}^{1} R_{err}^2 dydz \tag{15}$$

Summation of the error S is minimized with respect to the unknown constants c_1 and c_2. As the number of unknowns are two, two equations will be obtained as follows:

$$\frac{\partial S}{\partial c_1} = \int_0^1 \int_{-1}^{1} R_{err} \frac{\partial R_{err}}{\partial c_1} dydz = 0 \tag{16}$$

$$\frac{\partial S}{\partial c_2} = \int_0^1 \int_{-1}^{1} R_{err} \frac{\partial R_{err}}{\partial c_2} dydz = 0 \tag{17}$$

$$\frac{\partial R}{\partial c_1} = -\left(1 - z^2\right) - 2A^2\left(y - \frac{y^2}{2}\right) - K_1\left(1 - z^2\right)\left(y - \frac{y^2}{2}\right) \tag{18}$$

$$\frac{\partial R}{\partial c_2} = \left(1 - z^2\right)\left(2 - 6y^2\right) - 2A^2\left(y^2 - \frac{y^4}{2}\right) - K_1\left(1 - z^2\right)\left(y^2 - \frac{y^4}{2}\right) \tag{19}$$

From Eqs. (16) to (19), we obtain the following coupled linear equations:

$$a_{11}c_1 + a_{12}c_2 = b_1 \tag{20}$$

$$a_{21}c_1 + a_{22}c_2 = b_2 \tag{21}$$

where,

$$a_{11} = 1.733 + 1.778A^2 + 1.155K_1 + 0.711A^2K_1 + 2.08K_1^2 + 1.0667A^4 \tag{22}$$

$$a_{12} = 1.244A^2 + 0.404K_1 + 0.679A^4 + 0.458A^2K_1 + 1.245K_1^2 \tag{23}$$

$$a_{21} = 0.978A^2 + 0.819A^4 + 0.715K_1 + 0.546K_1A^2 + 0.249K_1^2 \tag{24}$$

$$a_{22} = 5.54 + 1.625A^2 + 0.679A^4 + 0.853K_1 + 0.453A^2K_1 + 0.09K_1^2 \tag{25}$$

$$b_1 = 1.33K_2 + 1.33K_2A^2 + 0.444K_1K_2 \tag{26}$$

$$b_2 = 0.466A^2K_2 + 0.311K_1K_2 \tag{27}$$

Solving Eqs. (20) and (21), c_1 and c_2 are evaluated as follows:

$$c_1 = \frac{b_1a_{22} - b_2a_{12}}{a_{11}a_{22} - a_{12}a_{21}} \tag{28}$$

$$c_2 = \frac{a_{11}b_2 - a_{21}b_1}{a_{11}a_{22} - a_{12}a_{21}} \tag{29}$$

2.2 *Numerical solution*

Results of the LSM solution are compared with that of the numerical solution for validation purpose.

Numerical solution is obtained by finite difference technique. Explicit scheme is employed. Equation (12) is discretized in the following form:

$$u_{i,j} = C\left[\left(u_{i+1,j}\right)\frac{1}{\Delta y^2} + \left(u_{i-1,j}\right)\frac{1}{\Delta y^2} + \left(u_{i,j+1}\right)\frac{A^2}{\Delta z^2} + \left(u_{i,j-1}\right)\frac{A^2}{\Delta z^2} + K_2\right] \tag{30}$$

$$C = \frac{1}{\frac{2}{\Delta y^2} + \frac{2}{\Delta z^2} + K_1} \tag{31}$$

where, $u_{i,j}$ represents the non dimensional velocity at i,j the node of the discretization domain, Δy and Δz are the lengths in y and z directions of the discretized element. A 50×50 grid is chosen after grid independence test. Tolerance level is fixed at 10–6, which is given as follows:

$$\text{error} = \sqrt{\sum_{j=1}^{50}\sum_{i=1}^{50}\left(u_{ij}^{k+1} - u_{ij}^{k}\right)^2} \tag{32}$$

where, k stands for the iteration step.

3 Results and Discussions

In this section, effect of parametric variation on the velocity is discussed. Values of the non-dimensional parameters are fixed based on the physically permissible values of the variables. K_p may vary from zero to infinity (Guo and Zhang 2016), μ is the viscosity of water (0.001 Ns/m^2), ρ is density of water (1000 kg/m^3), g = 9.81 m/s^2, and sin θ lies in the range of 0.00001–0.0001. Based on these values, in the present study, K_1 is considered to vary in the range 0.1–0.8 and K_2 is considered to be 10. Results of the present study are compared with that of the numerical solution and are found to be in close agreement, which demonstrates the suitability of the LSM for solving PDE. Figure 2 represents the comparison of the results of LSM and numerical solutions. It is evident from the Fig. 2 that the results are in close agreement. Effect of the increase in K_1 is presented in Fig. 3. It is evident from the figure that the velocity decreases with an increase in $K_{1.}$ Increase in K_1 signifies increase in the vegetation drag, which results in decreasing the velocity.

In Fig. 4, effect of the change in aspect ratio A on the velocity is displayed. The results indicate that as the aspect ratio increases, velocity decreases significantly. With an increase in the aspect ratio, resistance towards the flow increases which decreases the velocity.

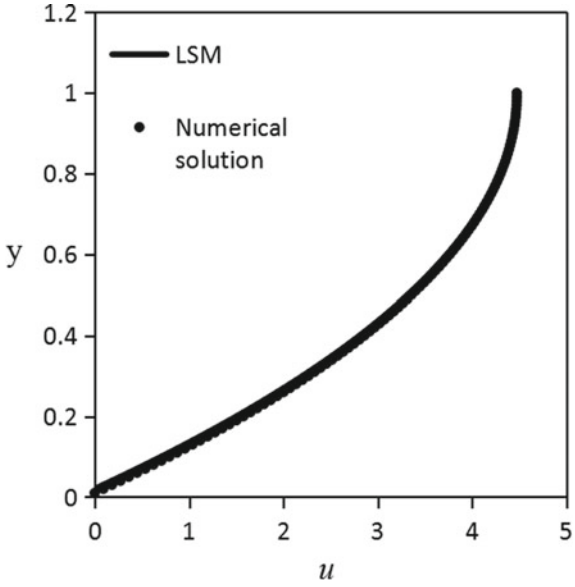

Fig. 2 Comparison of the results when $A = 0.1$, $K_1 = 0.9$, $K_2 = 10$

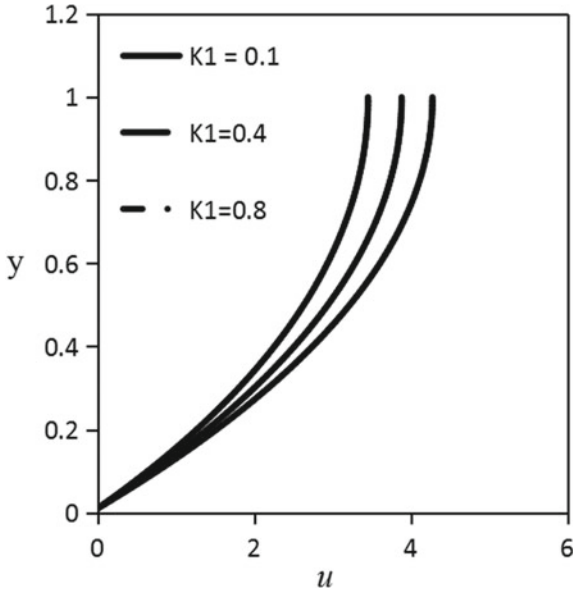

Fig. 3 Velocity distribution for different, K_1, When $A = 0.5$, $K_2 = 10$

4 Conclusions

Effect of the aspect ratio on the flow through vegetation in emerged condition is studied. The governing PDE is solved employing LSM. Further, numerical solution

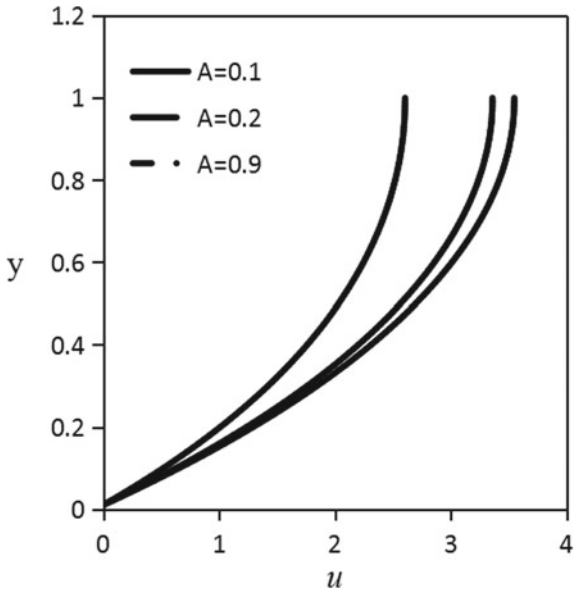

Fig. 4 Velocity distribution for different values of A when $K_1 = 0.9$ and $K_2 = 10$

of the governing equation is obtained for validation of the results generated by the LSM. The results indicate that the velocity decreases significantly with an increase in the aspect ratio and the porosity parameter K_1. In this study, drag is considered to be proportional to the velocity, which is valid for laminar flow without separation. Further studies can be carried out for vegetation drag proportional to the square of velocity.

References

Chakraborty P, Sarkar A (2016) Flow characteristics through submerged rigid vegetation over a sinusoidal perturbed bed. Int J River Basin Manage 14(3):255–266

Forchheimer P, Wasserwegung durch B (1901) Water flow through soil. Zeitschrift des Vereines Deutscher Ingenieure 45:1782–1788 (in German)

Guo J, Zhang J Velocity distributions in laminar and turbulent vegetated flows. J Hydraul Res 54(2)

Hatami M, Ganji DD (2014) Thermal and flow analysis of micro channel heat sink (MCHS) cooled by Cu-Water nano fluid by porous media approach and least square method. Energy Convers Manage 78:347–358

Hatami M, Sheikholeslami M, Ganji DD (2014) Laminar flow and heat transfer of nano fluid between contracting and rotating disc by least square method. Powder Technplogy 253:769–779

Hsieh PC, Bolton S (2007) Laminar surface water flow over vegetated ground. J Hydraul Eng 133(3):335–341

Hsieh PC, Shiu Y (2006) Analytical solutions for water flow passing over a vegetal area. Adv Water Resour 29(9):1257–1266

Huai W, Wang W, Zeng Y (2013) Two-layer model for open channel flow with submerged flexible vegetation. J Hydraul Res 51(6):708–718

Kubrak E, Kubrak J, Rowinski MP (2008) Vertical velocity distributions through and above submerged, flexible vegetation. Hydrol Sci J 53(4):905–920
Song CH, Huang LH (2000) Laminar poro-elastic media flow. J Eng Mech 126(4):358–366
Zhao MD, Huai W, Han J, Xie Z, Guo J (2012) Uniform laminar wetland flow through submerged and floating plants. J Hydraul Res 50(1):52–59

Landuse and Land Cover Change Detection Using Geospatial Techniques for Drought Studies in Chengalpattu District, Tamil Nadu, India

M. Kamalanandhini and R. Annadurai

Abstract Landuse and Landcover (LULC) practices vary from place to place which has an impact on natural resources such as water, vegetation, and soil. Change detection is useful for identifying the changes that have happened in a particular area by comparing the different periods. GIS and Remote Sensing techniques greatly involve in change detection process which helps in the management of natural resources. An attempt has been made to monitor the changes in land use and land cover pattern in the Chengalpattu District which helps in identifying the condition of drought. The Palar river is one of the major sources of water for the people in the district and the river is almost dry due to human activities. The study was carried out using geospatial techniques such as Remote sensing and GIS by using the Survey of India Toposheet and LANDSAT 8 OLI/TIRS satellite images for the classification of Landuse/Landcover. GIS software was used for the preparation of different thematic maps. The period from 2016 to 2020 was identified as moderate to severe drought conditions according to recent studies carried out in the district even though there was an occurrence of flood in 2015. The change detection process was carried for these six years to identify the major type of land use/land cover change. The results showed the reason for the changes that happened in the recent past. It is important to carefully monitor the changes in landuse and landcover to maintain a sustainable environment for the development of resources.

Keywords Landuse/landcover · Change detection · Remote sensing · GIS · Drought

M. Kamalanandhini (✉) · R. Annadurai
Department of Civil Engineering, SRM Institute of Science and Technology, Kattankulathur, Tamil Nadu, India
e-mail: kamalanm@srmist.edu.in

B. B. Das et al. (eds.), *Recent Developments in Sustainable Infrastructure (ICRDSI-2020)—GEO-TRA-ENV-WRM*, Lecture Notes in Civil Engineering 207,
https://doi.org/10.1007/978-981-16-7509-6_43

1 Introduction

Landuse and land cover changes are meant to be a most important issue in the environment (Halmy 2015). Land-use/land cover is decided based on the different environmental conditions, along with the slope and altitudes, the type of geological structure present in the region which creates an impact on the pattern of land-use and land cover (Rai et.al. 1994). Due to improper rainfall and over-exploitation of groundwater for various practices, the groundwater table will be affected. Detection of changes in the land use and land cover pattern will help to identify the cause or occurrence of various illnesses in the region. A natural hazard that has a slow onset and invisible, is the drought, which possess a serious threat to the environment. The identification of drought can be carried out using various techniques and also with different parameters such as rainfall, soil moisture, climate change, etc., which is highly independent. Drought is strictly dependent on these parameters, in such a way, when there is any deficiency in these parameters over a certain period, it will pave way for the occurrence of drought.

Landuse and Landcover change detection is mainly done to identify the changes that have happened during a period which will be easier for comparing it with the other period which shows the percentage of rise or fall of a certain feature. Afforestation or deforestation can be identified easily by calculating the area of forest cover change from one year to the other. Change in the shape of a water body can also be spotted out easily by adopting the change detection technique. Drought studies can be done by identifying the changes that had happened in a region over a period using the geospatial techniques such as Remote sensing and GIS which are two powerful tools for many applications. Remotely sensed images are widely used to map the landuse and landcover in the GIS environment. The information about the spatial and temporal scales of different Earth's surface features can be obtained easily with the help of remote sensing technique which is recognized as a powerful tool (Liang et al. 2015; Mohajaneet et al. 2018). Scientists used various techniques of remote sensing right from 1970, for acquiring satellite data from Earth observation satellites for identifying the Land-use/land cover changes (Townshend et al. 1983; Taylor et al. 2007). Recent studies by researchers have focused mainly on the assessment of possible satellites data for classification, monitoring, analyzing and quantifying the land use changes (Baumann et al. 2014). The main advantage of using the satellite data in concurrence with the geographical information system is to assist in the interpretation process and this is due to the developments in the remote sensing field (García-Mora et al. 2011; Mallupattu et al. 2013).

2 Study Area

Chengalpattu District is known for its agriculture and the major water supply was from the Palar river. The river is completely dry now and there is a lack of water supply

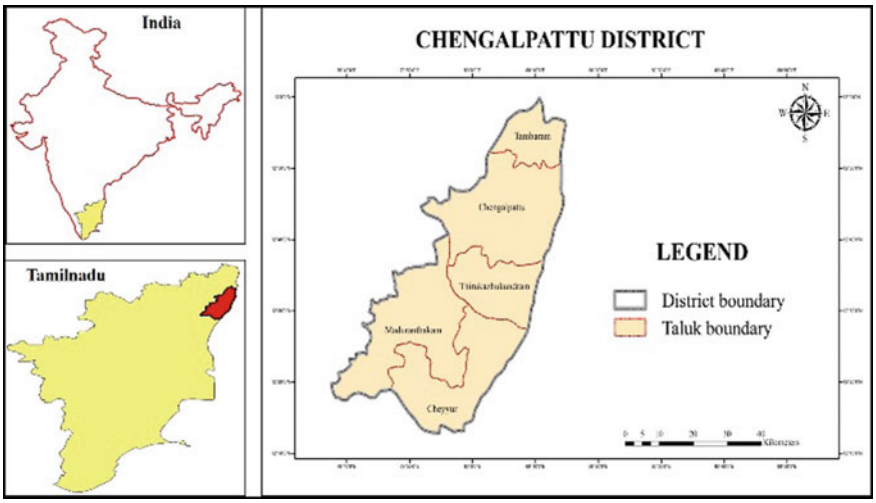

Fig. 1 Location map of study area

for the agricultural practices which has led the farmers to highly dependent on the groundwater. In recent past, the Chengalpattu district is exposed to certain boundaries of droughts having different intensities during several years (Esther Metilda et al. 2020). Remotely sensed images play an important role in landuse and landcover mapping and the change in area can be easily identified with the help of GIS. Landuse and landcover mapping is done to reflect the changes in the features such as waterbody, agriculture, forest cover, urban area, barren land, etc. The location map of study area represented in Fig. 1 shows that, the district has 5 taluks namely, Tambaram, Chengalpattu, Thirukazhukundram, Maduranthagam and Cheyyur.

The base map is prepared with 1:50,000 scale Survey of India (SOI) Toposheet no. D44T10, D44T11, D44T12, D44T14, D44T15, D44U1&5, D44U2, D44U3 covering the district boundary. The base map of Chengalpattu district shown in Fig. 2, represents the various features such as road networks, railway networks, waterbodies, plantation, reserve forest, agriculture, river, etc. The total area covered by the district boundary is nearly 2697.71 km^2. The region covers the National Highway (NH45), railway network, the Palar river, reserve forest and major tanks.

3 Materials and Methods

Landsat 8 with Operational Land Imager (OLI) and Thermal Infrared Sensor (TIRS) data is used for the landuse/landcover analysis. Landsat 8 has a 30-m spatial resolution for the OLI multispectral band, a 15-m resolution for the OLI panchromatic band and 100 m for TIRS thermal band. TIRS thermal band has been resampled to 30 m using cubic convolution resampling technique to match the multispectral band. There are

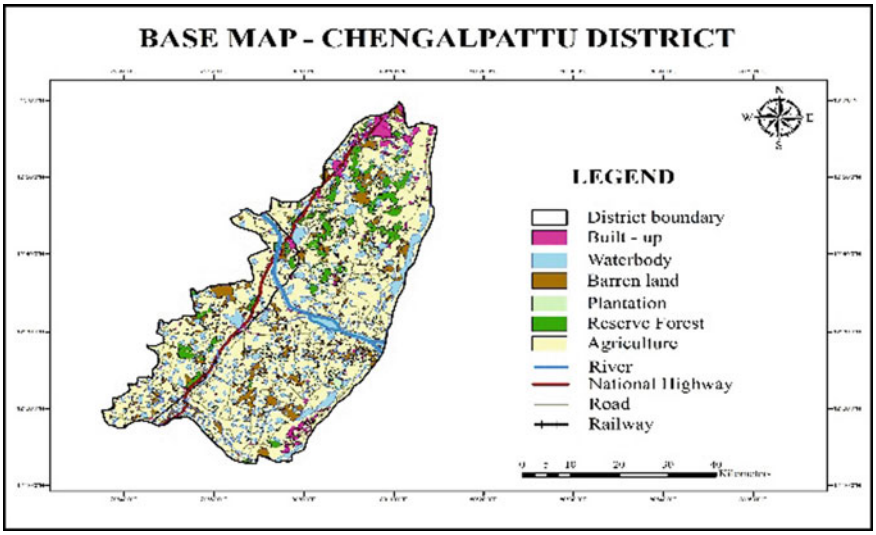

Fig. 2 Base map of study area

totally 11 bands in Landsat 8, in which band 2 to band 7 covers the visible, near infra-red and shortwave infra-red region in the electromagnetic spectrum, ranging from 0.45 to 2.30 μm. The band composite of these 6 bands are used for the landuse and landcover analysis. The methodology adopted for this study is represented as a flowchart in Fig. 3.

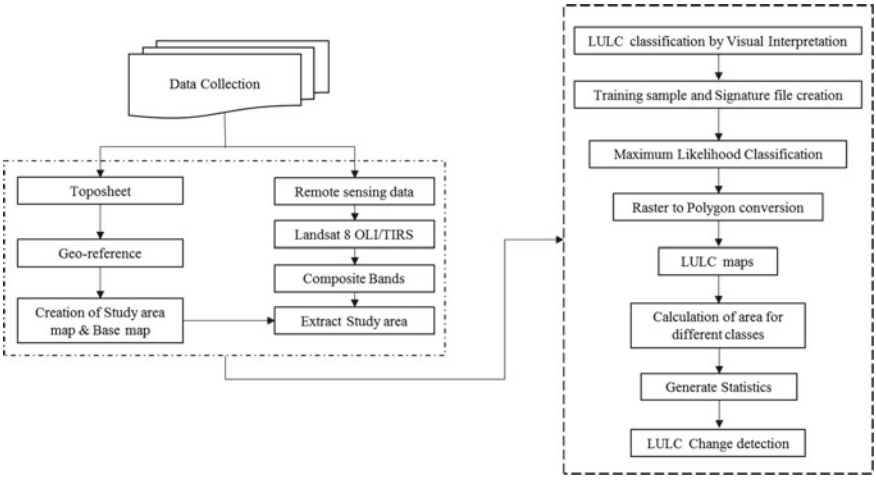

Fig. 3 Methodology flowchart

Preliminary data such as Toposheet and Satellite images for the study region has been collected and the digitization of study are boundary was done after georeferencing the Toposheet. Once the study area boundary is fixed, the base map pertaining to the region of interest was prepared. Landsat 8 OLI/TIRS data was obtained from USGS and the band composite was done followed by the extraction of data within the study area boundary. After the extraction process, the supervised classification technique was adopted to classify the land use and land cover of the region. The training sets were created for different land use classes such as waterbody, vegetation, urban, barren land and forest and saved as a signature file. This signature file is the input for the Maximum Likelihood classification and the land use classes were classified with respect to the training samples created earlier. The resultant will be in raster format and it needs a conversion to a vector. Once the conversion from raster to polygon is done, the area of each feature class can be determined by generating the statistics. This area calculation process helps to detect the changes that had happened in the past and will also help to compare it with the present data.

4 Results and Discussion

Change detection technique will be much helpful different applications such as urban sprawl detection, flood and drought studies, biomass identification etc. Drought is one of the natural disasters with a slow onset and possess a serious threat to the environment. Land use/ land cover change detection helps to determine the reasons for the occurrence of drought. Landsat 8 OLI/TIRS data was used for the landuse/land cover analysis. Four years' data namely 2016, 2017, 2019 and 2020 for Chengalpattu district were used for the change detection process. The Landsat data for the year 2018 was having more cloud cover, and thus it is not included for the LULC analysis. Figure 4 shows the land use/land cover classification of the study region for the selected years. WGS 1984 UTM Zone 44 N was the coordinate system and Transverse Mercator projection was done for the study area with the WGS 1984 as datum. The classification is limited to five classes namely, Urban, barren land, waterbody, forest and agriculture.

The area covered by each class is calculate using statistics option and this helps in detecting the differences from one year to another. The percentage of deviation in area of different class reveals the change that has occurred in those years. The total area of each landuse class along with the percentage of it with respect to the total area of the district is represented in Table 1.

The difference in the percentage of area of each land use class represents the changes happened in the region during a certain period comparing the other period. Barren land area during 2016 was 46.35% and the area got increased to 51.98% in 2017 but later on it was decreasing during 2019 and in 2020 it was 28.93%. Forest cover was 3.67% in 2016, 3.57% in 2017, 5.66% in 2019 and 12.13% in 2020, indicating a gradual increase its area. Urban area was 11.95% in 2016, 17.32% in 2018, 30.70% in 2019 and 10.39% in 2020 which shows that there was more

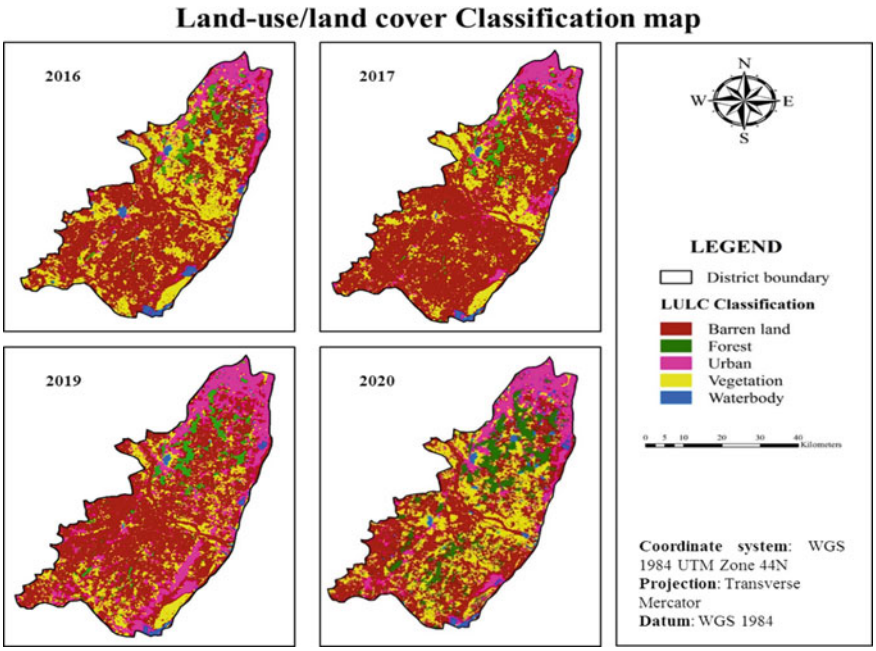

Fig. 4 Land-use/land cover classification map of Chengalpattu district

Table 1 Area and percentage of each landuse/land cover category

Landuse/land cover category	2016		2017		2019		2020	
	Area, km^2	% of land	Area, km^2	% of land	Area, km^2	% of land	Area, km^2	% of land
Barren land	1250.38	46.35	1402.30	51.98	1083.65	40.17	780.43	28.93
Forest	99.13	3.67	96.34	3.57	152.71	5.66	327.28	12.13
Urban	322.31	11.95	467.18	17.32	828.26	30.70	280.31	10.39
Vegetation	942.25	34.93	693.39	25.70	595.68	22.08	1267.20	46.97
Waterbody	83.64	3.10	38.51	1.43	37.41	1.39	42.49	1.58
Total	2697.71	100	2697.71	100	2697.71	100	2697.71	100

deviation in the urban development. Vegetation cover was 34.93% in 2016, 25.70% in 2018, 22.08% in 2019 and 46.97% in 2020 which had a fall from 2016 to 2019 and a slight increase in the year 2020. Waterbody was covering an area of 3.10% in 2016, 1.43% in 2017, 1.39% in 2019 and 1.58% in 2020 which is clear that the area of waterbody has been gradually decreasing in these years. The graph in Fig. 5 shows the deviations in the landuse/land cover classes from 2016–2020 in the district with respect to the area (km^2).

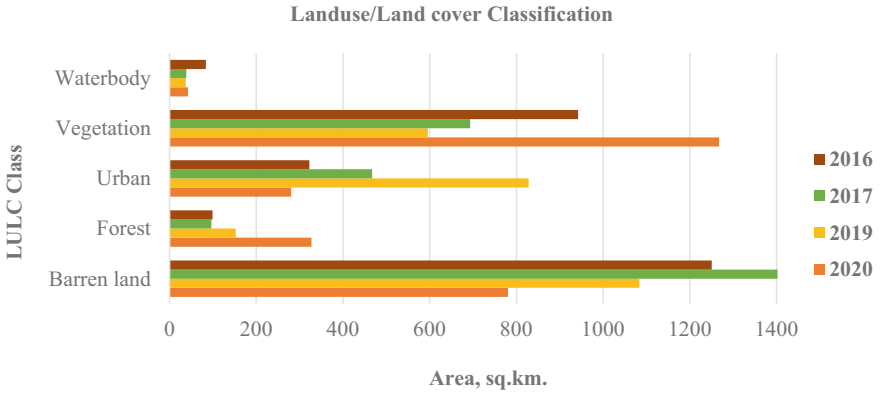

Fig. 5 LULC variation from 2016 to 2020 in Chengalpattu district by area (km^2)

While discussing the results obtained, it can be identified that, there is a decrease in area of waterbody, urban area and barren land and there is an increase in the vegetation and forest cover. Due to inadequate rainfall, poor drainage facilities and deviation in the climatic conditions, the region covering water is getting dried up soon. Even there is no water flowing in the major river which is contained in the district. The rainfall was just sufficient for the plant growth and due to poor drainage facilities, the groundwater potential is going down. This will lead to the over exploitation of groundwater thus using it for drinking and other purposes. Deviation in rainfall, climate and drainage system of a region will pave way for a drought to occur. Based on the previous research carried out in the district, it is proved that the meteorological indices showed a clear picture about the drought condition in the region. Indices such as SPI, RAI, DI, PNI and EDI was derived with the help of rainfall data which resulted in the moderate to severe drought condition, indicating a meteorological drought in the district.

5 Conclusion

Landuse/land cover change detection studies are done for various applications on the Earth. The scarcity of groundwater and rainfall creates an impact on the land use features which can be detected using the Earth observational satellites. These changes should be seriously monitored and preventive measures should be taken as a mitigation activity. Drought creates a long term impact on the groundwater which possess ill effects on the environment. Proper monitoring and management of drought can recover the situation and also help to create an alarm for the future events. Further studies can be carried out to identify the land surface temperature and groundwater potential of the region to clearly focus on the condition of drought.

References

Baumann M, Ozdogan M, Wolter PT, Krylov A, Vladimirova N, Radeloff VC (2014) Landsat remote sensing of forest windfall disturbance. Remote Sens Environ 143:171–179

Esther Metilda J, Annadurai R, Kamalanandhini M. (2020) Identification of soil moisture for drought assessment—a case study in Chengalpattu District, Tamil Nadu, India. Int J Adv Sci Technol 29(4s):699–704

García-MoraCentro TJ, Mas J-F, Hinkley EA (2011) Land cover mapping applications with MODIS: a literature review. Int J Digital Earth 5(1)

Halmy MWA, Paul E. Gessler, Jeffrey A. Hicke, Boshra B. Salem. "Land use/land cover change detection and prediction in the north-western coastal desert of Egypt using Markov-CA." *Applied Geography,* (2015), 101–112.

Liang D, Zuo Y, Huang L, Zhao J, Teng L, Yang F (2015) Evaluation of the consistency of MODIS land cover product (MCD12Q1) based on Chinese 30 m globeland 30 datasets: a case study in Anhui Province, China. ISPRS Int J Geo-Inf 4:2519–2541

Mallupattu PK, Reddy J, Reddy S (2013) Analysis of land use/land cover changes using remote sensing data and GIS at an urban area, Tirupati, India. Sci World J 6

Mohajane M, Essahlaoui A, Oudija F, El Hafyani M, El Hmaidi A, El Ouali A, Randazzo G, Teodoro AC (2018) Land use/land cover (LULC) using landsat data series (MSS, TM, ETM+ and OLI) in Azrou Forest, in the Central Middle Atlas of Morocco. Environments 5(12):131

Rai SC, Sharma E, Sundriyal RC (1994) Conservation in the Sikkim Himalaya: traditional knowledge and land-use of the Mamlay Watershed. Environ Conserv 30–34

Taylor P, Horler DNH, Ahern FJ (2007) Forestry information content of thematic mapper data. Int J Remote Sens 37–41 (2007)

Townshend JRG, Gayler JR, Hardy JR, Jackson MJ, Baker JR (1983) Preliminary analysis of LANDSAT-4 thematic mapper. Int J Remote Sens 4:817–828

Identification of Auto Regressive Model Parameter for Rainfall Forecasting in Baleswar District of Odisha

Ipsita Roy and Bitanjaya Das

Abstract Rainfall plays an important role in the success of agriculture through adequate surface storage and groundwater recharge. Besides, it also creates havoc due to high intensity rainfall coupled with cyclonic development leading to flood. Coastal Odisha stretches 450 km along the Bay of Bengal and several districts of Odisha directly in touch with the shoreline of Bay of Bengal. Primarily, Odisha receives more than 70% of its annual rainfall during monsoon time stretching from June till September. Monsoon induced rainfall coupled with low pressure and cyclonic development in Bay of Bengal leads to very high magnitude of rainfall in the coastal districts. At the same time, there is failure of monsoon rainfall in the coastal as well as interior districts of Odisha due to various climate change parameters. Such behavior of extremes is very much pronounced in coastal Odisha. Baleswar, which is a coastal district, has faced extremes which have lead to flood and drought. Besides, due to inadequate groundwater recharge, in this district, there is salinity ingress in to the aquifer. Such a critical district needs careful attention in terms of rainfall analysis and forecasting. Autoregressive (AR) models are very powerful tool/model to understand the behavior of time series and to forecast the rainfall using historical time series data. The model parameter depends on the past occurrences of rainfall and to the extent of past rainfall to be considered. This can be found out by estimating two important statistical parameters i.e. autocorrelation and partial autocorrelation. These two statistical parameters will indicate to what extent the past rainfall can be considered, which is otherwise known as "time lag". In the case of Baleswar district, rainfall data for the monsoon period was collected for 12 locations pertaining to 30 years i.e. 1990 to 2019. In each location, 5 time series were taken (June, July, August, September and full season) and autocorrelation and partial autocorrelation analysis was studied to find out the extent of lag that can be used in the auto regressive (AR) model. It is observed that at different locations and time periods, the lag is not consistent; rather it varies from location to location and for different time periods.

I. Roy · B. Das (✉)
School of Civil Engineering, KIIT Deemed to be University, Bhubaneswar, Odisha, India
e-mail: bdasfce@kiit.ac.in

I. Roy
e-mail: 1923003@kiit.ac.in

B. B. Das et al. (eds.), *Recent Developments in Sustainable Infrastructure (ICRDSI-2020)—GEO-TRA-ENV-WRM*, Lecture Notes in Civil Engineering 207,
https://doi.org/10.1007/978-981-16-7509-6_44

This estimate can help in accurate forecasting of the rainfall at 12 different locations and at different time periods.

Keywords Coastal Odisha · Autocorrelation · Partial autocorrelation · Auto regressive (AR) model · Rainfall forecasting

1 Introduction

Large parts of India, more than 70% of the annual rainfall happens during the four months from June to September, known as monsoon rainfall. The monsoon rainfall is an important phenomenon connected with the weather system. Agricultural activities throughout India and coastal Odisha are heavily dependent on the success or failure of monsoon rainfall. Hence, rainfall forecasting is an important issue for countries whose economies mainly depend on agriculture. Numerous efforts have been devoted for developing and improving the existing time series weather forecasting models by using different techniques. Since decades, many efforts have been made by researchers to identify the appropriate and reliable weather forecasting models. Rainfall forecast modelling is an important and significant study, and in most of the analysis attempts at advanced statistical approaches. In this study also, an attempt has been made to model the time series rainfall data for the Baleswar district of Odisha in order to forecast the rainfall based on the past historical data. In this district, daily rainfall data is collected at 12 different locations (administrative blocks) for the whole year starting from 1990 till 2019 (30 years). Being a coastal district, with 88 km stretch in direct contact with the Bay of Bengal, this district has experienced various climatic uncertainties in terms of cyclone land fall on several occasions, mostly in an around monsoon season. Besides, it has experienced deficit rainfall during the monsoon season also. In such scenario, it's a fitting case to model the rainfall which can be used for forecasting purpose by utilizing the historical data.

Auto regressive models are very powerful tool by which rainfall forecast modelling can be done. In this study, AR model is attempted for each month of the monsoon season i.e. June, July, August, September and whole season to fit AR model for each month for better forecasting of each month. In order to attempt the AR model, first of all autocorrelation and partial autocorrelation is estimated for each month and also for the whole season of the monsoon season with lag up to 10. Lag 10, takes care of the decadal aspect of the study. Autocorrelation depicts the degree of dependence of the time series and indicate whether the time series is auto regressive in nature or not. Partial autocorrelation estimates are used for identifying the order of an autoregressive model.

Various studies have been made in the past for time series analysis especially rainfall. S. Kokilavani et al. (2020) observed an empirical study for modelling and forecasting for the time series of monthly rainfall patterns for Coimbatore, Tamilnadu and this study has shown that the SARIMA model was appropriate for analyzing and forecasting the future rainfall patterns. Similarly Kaur et al. (2019) applied the

Seasonal Autoregressive Integrated Moving Average and Periodic autoregressive model to analyse the rainfall data of Punjab, obtained that PA model is more efficient than the other one. Shivare et al. (2018) considered Sixty-five years of daily meteorological data (1951–2015) of Varanasi and ARIMA model was compared with the observed values. This study showed that data mining techniques are straight-forward and helpful for forecasting future weather data. Patil et al. (2018) collected month wise ten year rainfall data from WALMI (Water and Land Management Institute) for Aurangabad division, Maharashtra state. In this paper, they set up various ARIMA models for prediction of rainfall from which derived predictive modelling of rainfall is very necessary criterion for water management resources. Basak (2016) described the parameters of AR model were computed for SWM rainfall of Barpeta, Digboi and Goalpara which is spread over hilly areas of Assam. It was observed that AR model up to order 1 have shows the good fit and correlation between the observed and predicted values. Dabral et al. (2016) developed monthly rainfall, maximum temperature and minimum time series models for Jorhat (Assam) using monthly rainfall, maximum temperature and minimum temperature data from the year 1965 to 2000, indicates that the climate at Jorhat (India) in next 04 decades will remain more or less stable. Meenakshi et al. (2014) examined the seasonal patterns of time series can be go through correlograms. Seasonality can be found by identifying those autocorrelation and partial autocorrelation coefficients and compared through graphs and residual plots. This study also reveals that the time series model SARIMA is very useful tool for prediction of rainfall in Tamilnadu. Babu et al. (2011) designed a proper rain flow system requires the prediction of average rainfall flow statistical parameters which is important for designing wind sensitive structures and for studying air pollution, obtained that ARMA is useful to study about the synthetic generation for the wind flow time series data analysis.

2 Materials and Methods

2.1 Study Area

The study was conducted for different blocks of Baleswar district of Odisha. This district is bounded by East and West Midnapore districts of West Bengal in its North, the Bay of Bengal in the east, Bhadrak district of Odisha in the South and Mayurbhanj & Keonjhar districts of Odisha in west. The district lies between 21° 3′ to 21° 59′ north latitude and 86° 20′ to 87° 29′ east longitude. The average altitude of the district is 19.08 m and the district has a total area of 3634 km^2. This district shares 88 km of coastal line with Bay of Bengal. It receives rainfall due to the influence of south west monsoon which occurs during the months of June, July, August and September. It gets highest rainfall 31% of south west monsoon rainfall in August month while the July month get 30% of the south west monsoon rainfall. June and September receive 18% and 21% of south west monsoon rainfall respectively. Also

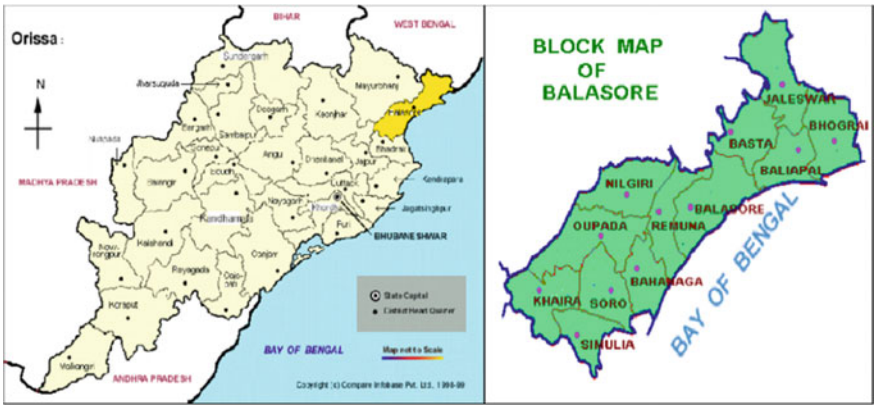

Fig. 1 Geographical location of study area, Baleswar

80% of annual rainfall receives during the southwest monsoon season only. The variability of monsoon and annual rainfall is also very less (15% and 14% respectively). The fate of the agriculture economy of the district is decided by the monsoon (Fig. 1).

2.2 Data Set

For this research work, daily rainfall data for 30 years (1990–2019) were collected pertaining to 12 different locations of Baleswar district from the website of Special Relief Commissioner, Odisa, where daily rainfall data of 314 locations (blocks) are available. Rainfall data for 12 blocks of Baleswar district was collected for the monsoon season i.e. June, July, August, September and full season.

2.3 Methodology

2.3.1 Basic Statistical Properties

The statistical characteristics of the rainfall data time series is calculated using the Eqs. (1), (2), and (3) as stated below;

The mean of rainfall time series is calculated as,

$$y' = \frac{1}{n}\sum_{i=1}^{n} y_i \tag{1}$$

The standard deviation of rainfall time series is computed using

$$\sigma_y = \sqrt{\sum (y - \overline{y})^2/(n-1)} \tag{2}$$

The coefficient of skewness of rainfall data is calculated as,

$$C_s = \frac{n \sum (y - \overline{y})^3}{(n-1)(n-2)(\sigma_y)^3} \tag{3}$$

where, $\acute{y}$ represents sample mean, n is the sample size and y_i represents rainfall data.

2.3.2 Autocorrelation Function (ACF)

The auto correlation function r_k at lag k of the variable y_t is obtained by

$$r_k = \frac{\sum_{t=1}^{n-k} (y_t - \overline{y})(y_{t+k} - \overline{y})}{\sum_{t=1}^{n} (y_t - \overline{y})^2} \tag{4}$$

where,

r_k autocorrelation function of time series y_t at lag k
y_t historical rainfall series
y mean of time series y_t
k lag of k time unit (1,2,3, …)
n total number of discrete values of time series y_t.

2.3.3 Partial Autocorrelation Function (PACF)

In time series analysis, the partial autocorrelation function (PACF) gives the partial correlation of a stationary time series with its own lagged values, regressed the values of the time series at all shorter lags. This function plays an important role in data analysis aimed at identifying the extent of the lag in an autoregressive model. The use of this function was introduced as part of the Box–Jenkins approach to time series modeling, whereby plotting the partial autocorrelative functions one could determine the appropriate lags p in an AR (p) model.

The following equation was used to calculate the partial autocorrelation function,

$$\text{PACF} = \frac{\text{cov}\left(y_i, y_{i-h} | y_{i-1,\ldots,} y_{i-h+1}\right)}{\sqrt{\text{var}\left(y_i | y_{i-1,\ldots,} y_{i-h+1}\right).\text{var}\left(y_{i-h} | y_{i-1,\ldots,} y_{i-h+1}\right)}} \tag{5}$$

where,

Cov covariance of time series
Var variance of time series

PACF partial autocorrelation
y_i historical rainfall time series.

Partial autocorrelation plots are a commonly used tool for identifying the order of an autoregressive model. If the sample autocorrelation plot indicates that an AR model may be appropriate, then the sample partial autocorrelation plot is examined to help identify the order. An approximate test that a given partial correlation is zero (at a 5% significance level) is given by comparing the sample partial autocorrelations against the critical region with upper and lower limits given by ±1.96 / Sqrt (N), $\pm\frac{1.96}{\sqrt{n}}$, where n is the record length (number of points) of the time-series being analysed.

2.3.4 Autoregressive Model

The pth order Autoregressive model AR (p), representing the variable y_t is in general represented as

$$y_t = \delta + \phi_1 y_{t-1} + \phi_2 y_{t-2} + \cdots + \phi_p y_{t-1} + A_t \tag{6}$$

where,

y_t time dependent series variable (say rainfall)
A_t White noise (randomness).

δ is defined by the following equation

$$\delta = \left(1 - \sum_{i=1}^{p} \phi_i\right)\overline{y} \tag{7}$$

3 Results and Discussion

The time series data pertaining to 12 locations (blocks) of the district was analyzed for basic statistical properties and the results of computation is presented in Table 1. The highest monthly mean value for the month of June, July August, September and full season are 286.4 mm in Oupada, 351.4 mm in Baliapal, 432.3 mm in Oupada, 366.9 mm in Opera and 1429.5 mm in Oupada blaock respectively. Similarly, the highest standard deviation for the months of June, July August, September and Full season are 152.3 mm in Basta, 174.4 mm in Remuna, 196.2 mm in Baliapal, 203.8 mm in Baliapal, and 448.4 in Remuna block respectively. The coefficient of skewness shows positive skewness in most locations and months except in Baleswar (September and full season) and Khaira in August (Table 2).

Table 1 Mean, standard deviation and skewness of rainfall data for the months of June, July, August, September, full season of different blocks of Baleswar for June, July and August

Name of block	June			July			August		
	Mean	SD	Skewness	Mean	SD	Skewness	Mean	SD	Skewnes
Hograi	276.9	117.1	0.55	307.5	124.9	0.85	336.9	179.5	1.41
Basta	234.1	152.2	2.72	276.2	140.7	0.98	305.1	130.4	0.37
Jaleswar	251.6	145.1	1.74	320.0	142.4	0.13	326.2	148.8	0.36
Baliapal	248.0	140.4	0.57	351.4	149.3	0.24	378.8	196.2	1.51
Baleswar	241.3	128.6	0.74	291.8	133.4	0.35	322.6	129.8	0.75
Remuna	258.1	133.2	0.56	325.9	174.4	1.03	357.5	178.1	1.68
Nilagiri	254.5	124.2	0.89	320.4	118.6	0.15	314.9	137.5	0.39
Soro	243.8	110.7	0.38	289.0	148.4	1.71	322.4	135.6	0.02
Bahanaga	239.0	140.0	0.59	264.7	125.3	0.49	308.7	132.6	0.72
Simulia	248.0	144.2	1.23	336.4	160.9	1.10	361.3	133.3	1.19
Khaira	252.9	149.9	1.70	320.7	133.4	0.12	368.8	125.5	−0.00
Oupada	286.3	138.3	0.11	343.8	159.7	0.92	432.3	155.1	0.45

Table 2 Mean, standard deviation and skewness of rainfall data for the months of June, July, August, September, full season of different blocks of Baleswar for September and full season

Name of block	September			Full season		
	Mean	SD	Skewness	Mean	SD	Skewness
Bhograi	337.9	167.7	1.05	1259.3	318.7	0.58
Basta	279.8	120.8	0.06	1095.3	305.9	0.65
Jaleswar	309.2	154.8	0.63	1207.0	329.2	0.67
Baliapal	366.1	203.8	0.91	1344.4	377.3	0.58
Baleswar	310.8	117.6	−0.54	1166.6	300.7	−0.02
Remuna	325.7	157.0	0.77	1267.5	448.4	1.07
Nilagiri	316.5	139.8	1.15	1206.4	311.0	0.41
Soro	299.3	127.0	0.51	1154.6	301.0	0.30
Bahanaga	296.0	152.5	1.02	1108.4	341.3	0.83
Simulia	311.9	171.6	1.14	1257.8	418.9	1.15
Khaira	335.7	164.5	0.51	1278.3	311.2	0.25
Oupada	366.9	188.2	0.78	1429.5	401.9	0.14

Autocorrelation measures the relationship between a variable's current value and its past values. The autocorrelation function values pertaining to different months and blocks of Baleswar district are calculated using Eq. 4 and a sample result pertaining to the full monsoon season of different blocks and different lags is presented in Table 3.

Table 3 ACF values of seasonal monsoon rainfall for different blocks of Baleswar district for different lags

Lag	Bhogarai	Basta	Jaleswar	Baliapal	Baleswar	Remuna
1	0.11	0.32	0.34	0.32	0.12	0.45
2	−0.04	−0.06	−0.09	0.01	−0.02	0.09
3	−0.12	−0.36	−0.10	0.04	−0.06	0.23
4	−0.13	−0.29	−0.29	−0.10	−0.17	0.14
5	−0.22	−0.04	−0.15	0.00	−0.27	−0.17
6	−0.11	0.13	0.16	0.26	−0.39	−0.30
7	−0.06	0.19	0.09	0.30	−0.03	−0.18
8	0.03	0.18	−0.06	0.16	−0.25	−0.13
9	0.14	0.07	−0.08	−0.09	0.14	−0.07
10	−0.05	−0.03	−0.24	−0.18	0.39	0.13
Lag	Nilagiri	Soro	Bahanaga	Simulia	Khaira	Oupada
1	0.27	−0.42	0.04	0.57	−0.11	0.17
2	0.00	0.40	0.22	0.32	0.19	0.35
3	−0.22	−0.24	−0.13	0.01	−0.06	−0.05
4	−0.16	0.15	−0.13	−0.14	−0.10	0.06
5	−0.17	0.02	−0.13	−0.45	0.14	0.07
6	−0.21	−0.19	−0.15	−0.38	−0.13	0.19
7	0.07	0.01	0.06	−0.29	0.20	0.12
8	0.03	−0.17	−0.02	−0.25	−0.11	0.05
9	0.05	−0.12	0.05	−0.28	−0.26	−0.14
10	−0.11	0.00	−0.04	−0.07	−0.13	−0.08

Partial autocorrelation plot is commonly used for identifying the order of an autoregressive model. Partial autocorrelation plot is examined to help identify the order of the autoregressive model. An approximate test that a given partial correlation is zero (at a 5% significance level) is given by comparing the sample partial autocorrelations against the critical region with upper and lower limits given by ± 1.96 / Sqrt (N), $\pm \frac{1.96}{\sqrt{n}}$, where n is the record length (number of points) of the time-series being analysed.

Sample values of PACF pertaining to full monsoon period for different blocks and at different lags are presented in Table 4. Similarly, for all blocks, all months and at different lags, PACF is computed and analyzed to see in which case the PACF is significant to be considered as the order of an autoregressive model. Such results are presented in Table 5. Further, the details of the significant PACF occurring in highest number of occasions in Soro and Simulia blocks are shown in Tables 6 and 7, and Figs. 2 and 3 respectively.

The least amount of significant PACF occurred in Nilagiri (one number), Oupada (two numbers) and Bhograi (four numbers). In can be said that the autoregressive

Table 4 PACF values of seasonal monsoon rainfall for different blocks of Baleswar district at different time lags

Lag	Bhogarai	Basta	Jaleswar	Baliapal	Baleswar	Remuna
1	0.11	0.32	0.34	0.32	0.12	0.45
2	−0.06	−0.18	−0.23	−0.10	−0.03	−0.14
3	−0.11	−0.32	0.02	0.07	−0.06	0.32
4	−0.11	−0.11	−0.33	−0.15	−0.16	−0.15
5	−0.21	0.05	0.09	0.10	−0.24	−0.21
6	−0.10	0.00	0.12	0.25	−0.40	−0.22
7	−0.10	0.04	−0.06	0.18	−0.06	0.00
8	−0.04	0.12	−0.13	0.02	−0.46	0.01
9	0.06	0.06	−0.06	−0.20	−0.06	0.18
10	−0.16	0.04	−0.18	−0.09	0.13	0.22
Lag	Nilagiri	Soro	Bahanaga	Simulia	Khaira	Oupada
1	0.27	−0.42	0.04	0.57	−0.11	0.17
2	−0.08	0.27	0.22	−0.01	0.18	0.33
3	−0.22	0.00	−0.16	−0.24	−0.03	−0.17
4	−0.05	−0.05	−0.18	−0.08	−0.15	−0.03
5	−0.13	0.15	−0.05	−0.42	0.14	0.17
6	−0.22	−0.24	−0.10	0.10	−0.06	0.17
7	0.15	−0.21	0.08	0.03	0.13	0.00
8	−0.11	−0.07	−0.01	−0.27	−0.06	−0.09
9	−0.06	−0.32	−0.04	−0.22	−0.35	−0.19
10	−0.13	−0.07	−0.06	0.06	−0.18	0.00

process in those blocks is not that much significant. In case of Soro and Simulia, there are several occasions when it shows significant PACF values indicating presence of autoregressive process for different lag values. In other blocks, it can be said that there exist auto regressive process of varying degree and AR process can be applied in such conditions having significant PACF.

4 Conclusion

In this study parameter estimation i.e. order of autoregressive model is made for application in monsoon rainfall forecasting of different blocks of Baleswar district.. This study further encompasses different time domain of monsoon season like June, July, August, September months and full season to ascertain the extent of order of the autoregressive process. Daily rainfall data for 30 years is used for 12 locations

Table 5 Significant PACF values for different blocks, months and time lags of Baleswar district estimated using limit $\pm\frac{1.96}{\sqrt{n}}$

Name of blocks	Significant PACF values to decide AR lag parameters	Total number of significant PACF
Bhograi	Lag 1 (July), Lag 4 (July), Lag 4 (September)	3
Basta	Lag 4 (July), Lag 4 (August), Lag 4 (September), Lag 1 (Total), Lag 3 (Full season)	5
Jaleswar	Lag 7 (June), Lag 1 (July), Lag 3 (July), Lag 7 (September), Lag 1 (Full season), Lag 4 (Full season)	6
Baliapal	Lag 7 (June), Lag 4 (July), Lag 10 (September), Lag 1 (Full season)	4
Baleswar	Lag 4 (July), Lag 5 (August), Lag 6 (August), Lag 6 (Total), Lag 8 (Full season)	5
Remuna	Lag 1 (August), Lag 6 (September), Lag 1 (Total), Lag 3 (Full season)	4
Nilagiri	Lag 10 (September)	1
Soro	Lag 2 (June), Lag 3 (July), Lag 4 (August), Lag 2 (September), Lag5 (September), Lag 7 (September), Lag 1 (Full season), Lag 9 (Full season)	8
Bahanaga	Lag 7 (July), Lag 10 (July), Lag 4 (August), Lag 4 (September)	4
Simulia	Lag 3 (June), Lag 6 (June), Lag 1 (July), Lag 3 (July), Lag4 (August), Lag 3 (September), Lag 1 (Full season), Lag 5 (Full season)	8
Khaira	Lag 6 (June), Lag 7 (June), Lag 10 (June), Lag 2 (July), Lag4 (August), Lag 9 (Full season)	6
Oupada	Lag 3 (September), Lag 2 (Full season)	2

(blocks) of the district to understand the order of the AR process in the spatio-temporal dimension. Mean, standard deviation, skewness is estimated for each block monthly data of monsoon period and for the full season. Most of the places showed positive skewness and only three locations in two blocks i.e. Balasore and Khaira showed negative skewness. Autocorrelation of the time series is estimated up to 10 time lags and subsequently partial autocorrelation function is estimated for 10 time lags also for all months and full season. PACF indicates about the order of the autoregressive process and significant PACF is estimated using 95% confidence interval. The result shows that Nilagiri is having the lowest occasion (only one) of significant PACF where as Soro and Simulia block show the maximum significant

Table 6 PACF values for Soro block for different months and time lags

Lag	June	July	August	September	Full season
1	−0.199	−0.068	−0.284	−0.241	**−0.422**
2	**−0.338**	0.056	0.094	**0.476**	0.270
3	0.060	**−0.306**	−0.086	−0.017	−0.005
4	0.123	−0.070	**−0.337**	−0.192	−0.045
5	−0.126	0.151	0.246	**0.437**	0.154
6	−0.037	−0.017	0.116	−0.100	−0.239
7	−0.028	−0.218	−0.132	**−0.388**	−0.207
8	0.017	−0.081	−0.041	−0.181	−0.073
9	0.042	0.032	−0.104	−0.091	**−0.320**
10	0.039	−0.157	0.004	−0.037	−0.066

The bold indicates the significance of PACF value which is judged by comparing whether the value is higher than +0.300 or less than −0.300

Table 7 PACF values for Simulia block for different months and lags

Lag	June	July	August	September	Full season
1	0.064	**0.309**	−0.042	0.242	**0.569**
2	−0.304	0.269	0.139	0.143	−0.012
3	**0.305**	**−0.335**	0.020	**−0.324**	−0.241
4	−0.009	−0.014	**−0.336**	0.018	−0.079
5	−0.184	−0.044	−0.035	−0.037	**−0.418**
6	**−0.328**	−0.289	−0.151	−0.133	0.102
7	−0.056	−0.183	−0.164	0.031	0.027
8	−0.159	−0.112	−0.053	−0.113	−0.272
9	−0.143	0.114	−0.071	−0.074	−0.216
10	−0.228	−0.040	−0.076	−0.126	0.060

The bold indicates the significance of PACF value which is judged by comparing whether the value is higher than +0.300 or less than −0.300

PACF on 8 different combinations of time lag and month. Such type of analysis can greatly help in the process of identifying the order of the auto regressive process in the spatio-temporal dimension which can help in the rainfall forecasting in the district.

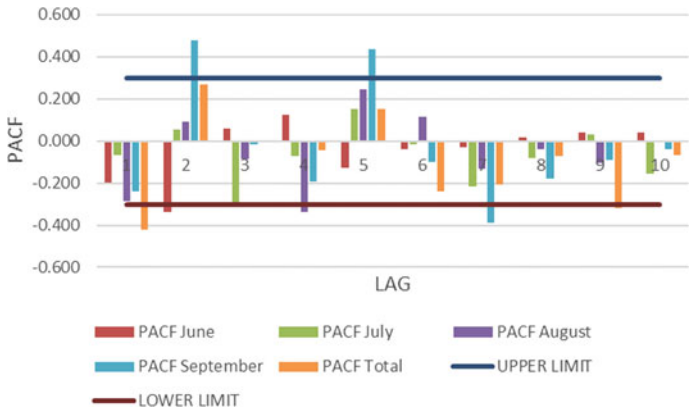

Fig. 2 PACF values at different lags and for different months in Soro block of Baleswar

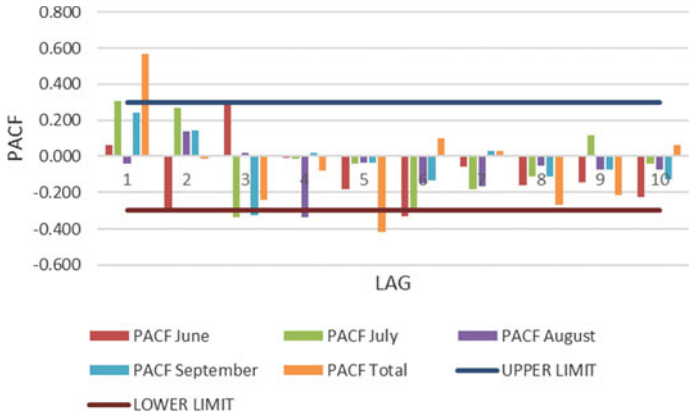

Fig. 3 PACF values at different lags and for different months in Simulia block of Baleswar

References

Babu SKK et al (2011) Prediction of rainfall flow time series using auto-regressive models. Pelagia Research Library 2(2)

Basak P (2016) Auto-regressive model development of some rainfall stations of Assam. Vayu Mandal 42(2)

Dabral PP et al (2016) Time series models of monthly rainfall and temperature to detect climate change for Jorhat (Assam), India. Global NEST J 18(3)

Kaur S, Rakshit M (2019) Seasonal and periodic autoregressive time series models used for forecasting analysis of rainfall data. IJARET 10(1)

Kokilavani S et al (2020) SARIMA modeling and forecasting patterns for Coimbatore, Tamil Nadu, India. Curr J Appl Sci Technol 39(8)
Patil R et al (2018) Predictive modelling of rainfall data for aurangabad region by using ARIMA method. Int J Eng Technol 7(4.10)
Shivhare N et al (2018) ARIMA based daily weather forecasting tool: a case study for Varanasi. MAUSAM 70(1)

Best Fitting of Probability Distribution for Monsoon Rainfall in Kalahandi District of Odisha

Abinash Mishra, Paromita Chakraborty, and Bitanjaya Das

Abstract KBK (Kalahandi, Bolangir, Koraput) districts of Odisha reels under various types of uncertainties during monsoon season rainfall and there by the agriculture and other water related activities suffers. These three districts of Odisha are further divided into eight (8) districts in the year 1992 like Kalahandi, Nuapada, Bolangir, Subarnapur, Koraput, Malkangiri, Nabrangpur, and Rayagada but the total geographical area remain as before. The uncertainty requires urgent attention to develop storage systems which can cater to the demand during the deficit rainfall. Water resources development of any locality depends on how much runoff being generated and accordingly the location and size of storage facilities are developed. These storage facilities serve the purpose for the future, and forecasting of the rainfall for such purpose is highly essential. The forecasting of the rainfall requires appropriate probability distribution has to be fitted to the historical time series of rainfall, and amongst various probability distributions the best one need to be selected and used. Rainfall varies in spatiotemporal dimension. Hence, the time series of rainfall cannot be fitted to a particular probability distribution model. In this study the best fitting probability distribution to time series of data collected from different locations in the Kalahandi district pertaining to one day maximum rainfall during the monsoon period i.e., June, July, August, September and the entire monsoon duration is attempted. The data was collected from 13 locations (thirteen blocks) of the Kalahandi district for a period of 30 years i.e., from 1990 to 2019. For each location 5 time series are analyzed and in total 65 time series are analyzed. Various probability distributions are applied to each time series and the best fitted probability distribution is found out for each time series. From the result, it is evident that the probability distribution of one day maximum rainfall varies spatially as well as temporarily.

A. Mishra · P. Chakraborty (✉) · B. Das
School of Civil Engineering, KIIT Deemed to be University, Bhubaneswar, Odisha, India
e-mail: paromita.chakrabortyfce@kiit.ac.in

A. Mishra
e-mail: 1923004@kiit.ac.in

B. Das
e-mail: bdasfce@kiit.ac.in

B. B. Das et al. (eds.), *Recent Developments in Sustainable Infrastructure (ICRDSI-2020)—GEO-TRA-ENV-WRM*, Lecture Notes in Civil Engineering 207,
https://doi.org/10.1007/978-981-16-7509-6_45

Such analysis can help in properly forecasting of the rainfall for each location using the appropriate probability distribution. This ultimately helps on appropriate water resources development planning.

Keywords KBK Districts of Odisha · One day maximum rainfall · Monsoon rainfall · Probability distribution · Water resources development

1 Introduction

Water is vital for any life process and there can be no substitute for it. Rainfall is the primary source of water in the tropical countries. However, the rainfall pattern is becoming very erratic in nature and prediction is becoming very much complicated. Such situations exist in the KBK districts of Odisha. The pattern of rainfall and its quantity is becoming very much unpredictable due to various climatic scenarios. The diversity of the region in getting rainfall during the monsoon season necessitates that the prediction should based on probabilistic analysis of rainfall in spatio-temporal dimension. Kalahandi is one of the districts where such type of uncertainties is being observed. Hence, it is pertinent to analyze the historical rainfall data for the monsoon period i.e., June, July, August, September, and for full season in order to ascertain the variation of probability distribution that can be fitted in various locations (13 locations) and for 5 different time series for each location. One day maximum rainfall was chosen to analyze the situation as such extreme can lead to various natural adverse situations. Such type of spatio-temporal analysis of best fit probability distribution can greatly enhance the prediction pattern of rainfall in various locations in the Kalahandi district of Odisha.

Singh et al. (2012) studied the probability analysis for estimation of annual one-day maximum rainfall of Jhalarapatan area of Rajasthan. Log-Pearson type-III distribution was found to be the best fitted to data. Amin et al. (2016) carried out the best-fit probability distribution for the estimation of rainfall in northern regions of Pakistan and concluded that the normal distribution and Log-Pearson type-III distribution are the best-fit probability distribution depending the location. Alam et al. (2018) performed the best fit probability distributions and return periods for maximum monthly rainfall in Bangladesh. Bhakar et al. (2008) researched the probability analysis of rainfall at Kota and concluded that for weekly maximum rainfall Weibull's distribution is found best fit distribution for rainy season and Gumbel distribution for non-rainy season. Sreedhar et al. (2019) researched the fitting of probability distribution for analyzing the rainfall data in the region of Andhra Pradesh and fitted log normal distribution as the best fitting probability distribution. Sharma et al. (2010) studied the use of probability analysis in the eastern zones of India and found Log normal and Gamma distribution as the best fit probability distributions. Arvind et al. (2017) carried out the statistical analysis of 30 years rainfall data using various distribution methods and concluded that that Gumbel Distribution (Extreme Value Type

I) is the best fit distribution type. Mohd et al. (2016) researched on the rainfall probability analysis in India using various distribution functions. They concluded that the Gumbel distribution was found to be the best model for India. Lairenjam et al. (2016) researched on the probability distribution of rainfall of North East Region (NER) of India using probability distributions and concluded that the monthly and annual rainfall for each station out of which 124 events have been fitted with Extreme Value Type I.

2 Materials and Methods

2.1 Study Area

Kalahandi district covering a geographical area of 7920 km^2 lies in between 19.175489° to 20.454517° North Latitude, and 82.617767° to 83.794874° East Longitude. It comprises of 13 blocks which are Narla, Lanjigarh, Thuamul Rampur, Dharmagarh, Junagarh, Kalampur, Jayapatna, Kokasara, Golamunda, Bhawanipatna, Kesinga, Kalramunda, Madanpur Rampur. The district occupies the South Western portion of Odisha. The climate of the Kalahandi District is of extreme type. It is dry except during monsoon. The maximum temperature of the district is 45 °C, whereas the minimum temperature recorded is 4 °C. The district experiences the average annual rainfall as 1378.20 mm. The monsoon starts late in June and generally lasts up to September (Fig. 1).

Daily rainfall data for 30 years (1990–2019) were collected from web site of Special Relief Commissioner, Odisha, where such data is maintained on daily basis for 314 locations (administrative blocks). The best fit probability distribution is performed for one day maximum rainfall for each month, and for the whole monsoon season for all 13 blocks in the district.

2.2 Methodology

2.2.1 Fitting of Probability Distribution

CUMFREQ is a data analyzer and simulation software which allows us to fit probabilistic distributions to given time series, simulate them, choose the best fitting sample, and implement the results of analysis to take better decisions. This software can be used as a Windows compatible program. Table 1 show different probability distributions that can be applied to the one day maximum rainfall data series and out of these the best probability can be found out using Chi-square test. Besides, the mean, standard deviation, coefficient of variation and coefficient of skewness of the data series were estimated.

Fig. 1 Map showing different blocks of Kalahandi district of Odisha

3 Results and Discussion

The main objective of this work is to identify the best-fit probability distribution for every block for 1-day maximum rainfall for each monsoon month as well as for the 1-day maximum rainfall for the whole monsoon season. This will indicate how such analysis can depict the spatio-temporal variation of the monsoon 1-day maximum rainfall in the Kalahandi district of Odisha. These estimates can provide useful guidance for policy making and decision purposes. Knowing the return period of such extreme events appropriate design decisions can be made for crucial hydraulic structures and also to assess the risk level of damage by extreme events e.g., rainfall and flood floods. First of all, the basic statistics like mean, standard deviation and skewness of all time series were estimated and presented in Tables 2 and 3.

After applying the CUMFREQ model and testing the all-possible probability distributions, the best fit probability distributions are found out for each block and each month as shown in Table 4.

The best fit probability distribution obtained for each time series of data based on average absolute difference between calculated and observed frequencies and return

Table 1 Various Probability Distributions attempted for finding best fit probability distribution for 1-day maximum monsoon rainfall

S. No.	Name of probability distributions
1	Normal distribution (symmetric)
2	Logistic distribution (symmetrical)
3	Cauchy distribution (symmetrical)
4	Exponential distribution, Poisson-type
5	Gamma (Erlang) distribution
6	Gumbel (Fisher-Tippet type I) distribution
7	Generalized Kumaraswamy distribution
8	Laplace distribution (composite, any skewness)
9	Student's t-distribution with 1 degree of freedom
10	Weibull distribution (skew to right)
11	Generalized Rayleigh distribution
12	Fréchet (Fisher-Tippet type II) distribution
13	Fisher-Tippet type III distribution
14	Generalized extreme value (GEV) distribution
15	Pareto-Lomax distribution (skew to right)
16	Burr (generalized Pareto-Lomax) distribution
17	Dagum (mirrored Burr) distribution (skew to left)
18	Generalized Gompertz distribution (any skewness)

Table 2 Basic statistical results of all 13 blocks of Kalahandi district for the month of June and July

S. No.	Blocks	June			July		
		Mean	SD	Skewness	Mean	SD	Skewness
1	Narla	72.39	62.01	2.26	132.98	127.78	1.82
2	Lanjigarh	64.02	43.6	1.46	97.5	63.81	1.49
3	Thuamul Rampur	149.13	154.15	2.16	240.21	167.9	2.18
4	Dharmagarh	61.14	53.74	1.75	77.08	68.2	3.21
5	Junagarh	69.68	59.88	2.21	104.07	63.23	1.79
6	Kalampur	97.9	87.39	2.26	131.98	94.17	1.84
7	Jayapatna	68.91	47.83	1.84	108.21	62.28	1.17
8	Kokasara	74.76	40.38	1.52	119.23	79.22	1.31
9	Golamunda	59.73	39.31	1.50	82.97	69.06	3.24
10	Bhawanipatna	58.00	54.77	2.29	109.40	82.72	1.48
11	Kesinga	69.88	74.10	2.69	108.56	73.35	1.24
12	Kalramunda	73.27	51.99	1.45	114.93	92.19	2.60
13	Madanpur Rampur	75.70	66.44	2.23	117.03	75.36	0.94

Table 3 Basic statistical results of all 9 blocks of Kalahandi district for the month of August and September

S. No.	Blocks	August			September		
		Mean	Sd	Skewness	Mean	Sd	Skewness
1	Narla	113.2	69.17	1.22	78.33	46.25	1.51
2	Lanjigarh	106.65	77.81	2.06	70.94	47.58	1.61
3	Thuamul Rampur	229.58	131.25	0.68	126.09	79.64	0.85
4	Dharmagarh	76.00	51.50	1.84	61.54	41.95	1.49
5	Junagarh	95.51	63.55	2.02	70.96	45.75	1.41
6	Kalampur	127.18	77.18	1.13	85.55	60.31	1.52
7	Jayapatna	115.47	64.22	1.70	74.73	50.43	1.41
8	Kokasara	101.15	41.22	0.64	71.45	42.28	1.32
9	Golamunda	85.53	55.64	1.05	65.84	47.45	1.79
10	Bhawanipatna	96.84	56.83	0.77	73.24	51.86	1.96
11	Kesinga	92.50	46.42	0.75	67.38	41.42	1.96
12	Kalramunda	124.94	74.59	1.30	83.92	59.70	1.89
13	Madanpur Rampur	137.37	88.30	1.67	91.03	85.99	3.45

periods for each month and for each location. The results are presented in Tables 5, 6, 7, 8 and 9.

In Fig. 2, one sample result is presented for Narla block pertaining to the time series of full monsoon period (June to September) which depicts the comparison of observed and estimated cumulative frequencies, return period, histogram and confidence interval of estimate at 90% limit.

4 Conclusions

The rainfall distribution varies spatiotemporally and need very careful analysis. During monsoon period also such phenomenon exists. In terms of selecting the best-fit probability distribution to model the one day maximum rainfall for 13 different locations of Kalahandi district, the result varied significantly in term of best fit probability distribution for different location and different time period. The practical result of this paper is that different probability distribution should be used to forecast rainfall for different locations and time period in order to obtain reliable result. It is observed that Burr distribution is the best fitted for the month of June and July followed by Generalized Laplace distribution, Fréchet (Fisher-Tippet Type 2) mirrored and Generalized exponential (Poisson-type) distribution for the months of August, September and full season respectively. The results of this study can be used

Table 4 Best fit probability distributions obtained for different monsoon months and blocks of Kalahandi pertaining to 1-day maximum rainfall

Name of the block	June	July	August	September	Full season
Narla	Log-normal distribution optimized	Frechet (Fisher-Tippet Type 2) distribution	Dagum distribution generalized	Frechet (Fisher-Tippet Type 2) distribution	Generalized exponential (poisson-type)
Lanjigarh	Generalized Laplace distribution	Dagum distribution generalized	Generalized Laplace distribution	Burr distribution	Generalized exponential (poisson-type)
Thuamul Rampur	Burr distribution	Dagum distribution generalized	Generalized Laplace distribution	Frechet (Fisher-Tippet Type 2) mirrored	Log-normal distribution optimized
Dharmagarh	Burr distribution	Burr distribution	Generalized Laplace distribution	Burr distribution	Dagum distribution generalized
Junagarh	Burr distribution	Dagum distribution generalized	Laplace distribution (standard)	Laplace distribution (standard)	Generalized Laplace distribution
Kalampur	Burr distribution	Generalized Laplace distribution	Gumbel distribution generalized	Dagum distribution generalized	Generalized exponential (poisson-type)
Jayapatna	Laplace distribution (standard)	Burr distribution	Dagum distribution generalized	Gumbel distribution generalized	Burr distribution
Kokasara	Burr distribution	Burr distribution	Laplace distribution (standard)	Generalized Laplace distribution	Frechet (Fisher-Tippet Type 2) distribution
Golamunda	Laplace distribution (standard)	Generalized Laplace distribution	GEV distribution	Generalized Cauchy distribution	Laplace distribution (standard)
Bhawanipatna	Dagum distribution generalized	GEV distribution	Frechet (Fisher-Tippet Type 2) mirrored	Generalized exponential (poisson-type)	Gumbel distribution generalized
Kesinga	Burr distribution	Burr distribution	Laplace distribution (standard)	Generalized Laplace distribution	Laplace distribution (standard)
Kalramunda	Generalized Laplace distribution	GEV distribution	Gumbel distribution generalized	Dagum distribution generalized	Dagum distribution generalized
Madanpur Rampur	Dagum distribution generalized	Generalized Laplace distribution	Laplace distribution (standard)	Burr distribution	GEV distribution

Table 5 Observed and calculated cumulative frequencies & return periods for the month of June

S. No.	Block	Differences between calculated and observed frequencies (%)	Efficiency coefficient (observed and calculated)	Differences between calculated and observed return periods	Efficiency coefficient (observed and calculated)
1	Narla	8.59	0.878	6.018	0.999
2	Lanjigarh	1.98	0.992	0.492	0.999
3	Thuamul Rampur	3.63	0.973	0.753	0.999
4	Dharmagarh	2.09	0.989	0.734	0.999
5	Junagarh	1.93	0.993	0.526	0.999
6	Kalampur	2.58	0.986	0.692	0.999
7	Jayapatna	1.86	0.993	1.357	0.999
8	Kokasara	2.79	0.984	2.814	0.999
9	Golamunda	2.02	0.990	0.292	0.999
10	Bhawanipatna	2.10	0.990	1.780	0.999
11	Kesinga	2.30	0.989	0.370	0.999
12	Kalramunda	2.11	0.991	0.780	0.999
13	MadanpurRampur	2.83	0.985	0.690	0.999

Table 6 Observed and calculated cumulative frequencies and return periods for the month of July

S. No.	Block	Differences between calculated and observed frequencies	Efficiency coefficient (observed and calculated)	Differences between calculated and observed return periods	Efficiency coefficient (observed and calculated)
1	Narla	2.29%	0.991	0.828	0.999
2	Lanjigarh	2.16%	0.989	1.165	0.999
3	Thuamul Rampur	2.22%	0.989	2.723	0.999
4	Dharmagarh	2.81%	0.985	1.562	0.999
5	Junagarh	2.61%	0.985	2.362	0.999
6	Kalampur	2.30%	0.989	1.556	0.999
7	Jayapatna	1.73%	0.993	0.348	0.999
8	Kokasara	2.55%	0.987	0.829	0.999
9	Golamunda	2.45%	0.988	1.294	0.999
10	Bhawanipatna	2.49%	0.987	0.999	0.998
11	Kesinga	1.68%	0.994	0.920	0.999
12	Kalramunda	2.33%	0.989	0.750	0.999
13	Madanpur Rampur	2.22%	0.980	0.920	0.999

Table 7 Observed and calculated cumulative frequencies and return periods for the month of August

S. No.	Block	Differences between calculated and observed frequencies (%)	Efficiency coefficient (observed and calculated)	Differences between calculated and observed return periods	Efficiency coefficient (observed and calculated)
1	Narla	2.05	0.992	0.949	0.999
2	Lanjigarh	2.22	0.989	1.675	0.999
3	Thuamul Rampur	2.19	0.989	1.232	0.999
4	Dharmagarh	2.26	0.989	1.063	0.999
5	Junagarh	1.91	0.992	1.473	0.999
6	Kalampur	2.23	0.989	0.456	0.999
7	Jayapatna	2.62	0.986	1.247	0.999
8	Kokasara	2.10	0.990	0.664	0.999
9	Golamunda	2.52	0.986	0.791	0.999
10	Bhawanipatna	2.94	0.982	0.800	0.999
11	Kesinga	2.07	0.988	0.530	0.999
12	Kalramunda	1.92	0.992	0.340	0.999
13	Madanpur Rampur	2.35	0.987	1.060	0.999

to develop bettermodels for analyzing one day extreme rainfall events. These analysis can help in proper forecasting of the event in a spation-temporal dimension in the whole district.

Table 8 Observed and calculated cumulative frequencies return periods for the month of September

S. No.	Block	Differences between calculated and observed frequencies	Efficiency coefficient (observed and calculated)	Differences between calculated and observed return periods	Efficiency coefficient (observed and calculated)
1	Narla	1.75%	0.994	0.490	0.999
2	Lanjigarh	2.51%	0.987	0.615	0.999
3	Thuamul Rampur	3.04%	0.982	0.616	0.999
4	Dharmagarh	1.92%	0.992	0.517	0.999
5	Junagarh	2.99%	0.983	0.951	0.999
6	Kalampur	1.53%	0.994	0.691	0.999
7	Jayapatna	2.03%	0.991	0.516	0.999
8	Kokasara	1.80%	0.993	0.522	0.999
9	Golamunda	2.35%	0.989	0.884	0.999
10	Bhawanipatna	3.72%	0.966	0.780	0.997
11	Kesinga	2.51%	0.988	1.480	0.999
12	Kalramunda	1.73%	0.993	0.490	0.999
13	Madanpur Rampur	2.09%	0.991	1.430	0.999

Table 9 Observed and calculated cumulative frequencies & return period for the full monsoon season

S. No.	Block	Differences between calculated and observed frequencies (%)	Efficiency coefficient (observed and calculated)	Differences between calculated and observed return periods	Efficiency coefficient (observed and calculated)
1	Narla	2.71	0.983	0.330	0.998
2	Lanjigarh	1.35	0.996	0.240	0.999
3	Thuamul Rampur	5.23	0.954	3.190	0.000
4	Dharmagarh	2.18	0.990	0.681	0.999
5	Junagarh	2.39	0.989	0.742	0.999
6	Kalampur	2.19	0.991	0.278	0.999
7	Jayapatna	2.17	0.991	0.531	0.999
8	Kokasara	1.43	0.995	0.492	0.999
9	Golamunda	2.87	0.985	1.575	0.999
10	Bhawanipatna	3.32	0.978	1.070	0.999
11	Kesinga	2.42	0.987	0.740	0.999
12	Kalramunda	1.67	0.994	0.490	0.999
13	Madanpur Rampur	1.65	0.995	0.530	0.999

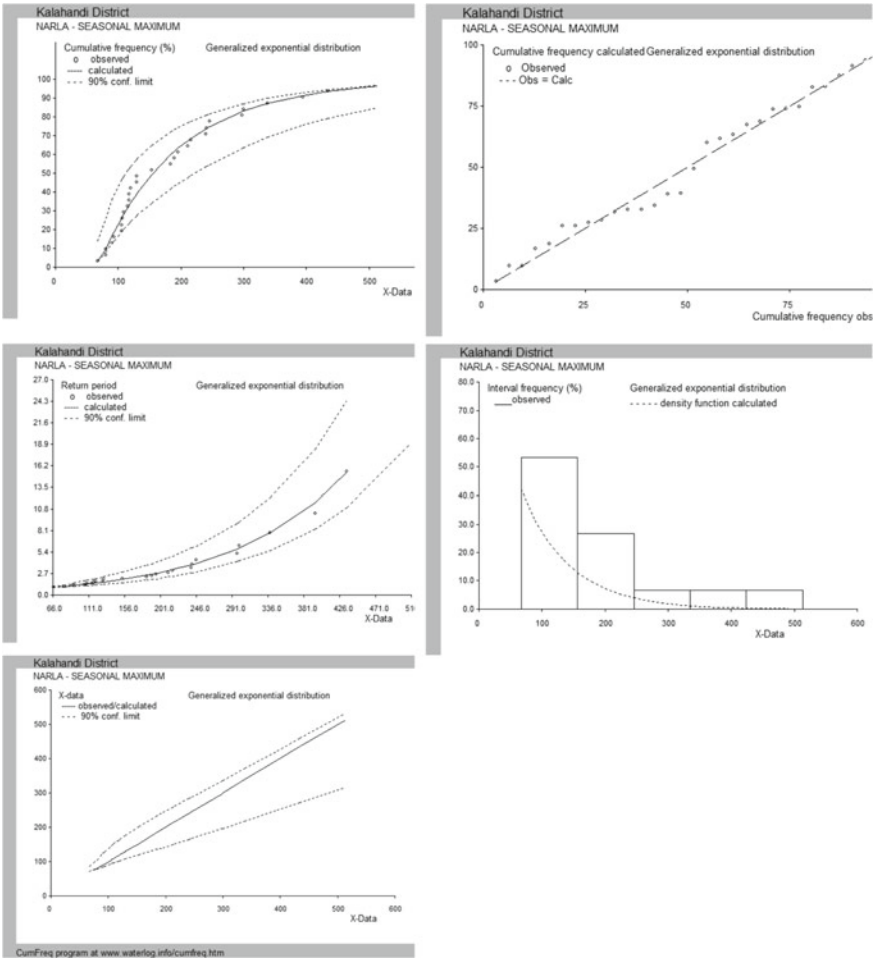

Fig. 2 Graph showing different aspects of best fitting probability distribution for 1 day maximum monsoon rainfall pertaining to full season for Narla block

References

Alam MA, Emura K, Craig F, Yuan J (2018) Best-fit probability distributions and return periods for maximum monthly rainfall in Bangladesh. Climate 6(1):1–16 (2018)

Amin MT, Rizwan M, Alazba AA (2016) A best-fit probability distribution for the estimation of rainfall in northern regions of Pakistan. Open Life Sci 11(1):432–440

Arvind G, Kumar A, Karthi G, Suribabu CR (2017) Statistical analysis of 30 years rainfall data: a case study. Earth Environ Sci IOP Conf Ser 80012067

Bhakar SR, Iqbal M, Devanda M, Chhajed N, Bansal AK (2008) Probability analysis of rainfall at Kota. Indian J Agric Res 42(3):201–206

Lairenjam C, Huidrom S, Bandyopadhyay A, Aditi B (2016) Assessment of probability distribution of rainfall of North East Region (NER) of India. J Res Environ Earth Sci 2(9):12–18

Mohd A, Nath S, Mehera B, Mohd N (2016) Study of rainfall probability analysis in India. Int J Agric Sci 8(53):2669–2672
Sharma M, Singh J (2010) Use of probability distribution in rainfall analysis. NY Sci J 3(9):40–50
Singh B, Rajpurohit D, Vasishth A, Singh J (2012) Probability analysis for estimation of annual one- day maximum rainfall of Jhalarapatan area of Rajasthan. Plant Arch 12(2):1093–1100
Sreedhar BR (2019) Fitting of probability distribution for analyzing the rainfall data in the state of Andhra Pradesh, India. Int J Appl Eng Res 14(3):835–839

Groundwater Evapotranspiration in Tropical Savanna Region of India

Ankita Manekar, Suraj Jena, and Rabindra Kumar Panda

Abstract Groundwater models are indispensable for water resources management in heavily stressed tropical aquifers. Though groundwater evapotranspiration (ET_G) contributes significantly to total evapotranspiration, ET_G has drawn less attention of groundwater hydrologists in physical based modelling. Regions with a shallow groundwater table, plant roots can penetrate the saturated zone and transpire water directly from the groundwater. The ET_G can be quantified for shallow groundwater areas employing groundwater level fluctuations. The previous studies mainly focus on the estimation of ET_G from the wetlands and drylands. In this study, the application of modified groundwater fluctuation method namely Modified White method was executed in varying land use/land cover over a tropical savanna region of India to quantify ET_G. This method uses the sine function to capture diurnal fluctuation of groundwater level and is capable in estimating daily to seasonal ET_G. The areas which were contributing to groundwater evapotranspiration were also verified using the extinction depth, as ET_G values decrease with an increase in depth to the water table. Results show that modified White method produced reasonably accurate results and ET_G obtained was nearly 50–70% of actual evapotranspiration. Besides, ET_G obtained were more for the pre-monsoon periods than other periods of the year, due to less availability of topsoil moisture during this dry period of the year. The modified White method gave a high r^2 value (0.88) than the simplified water table fluctuation method (0.40) when applied on a seven-day window. The range of extinction depth varied from 1 to 3 m for hard rock area and from 5 to 9 m for other parts of the region. Conclusively, modified White method provides reasonable ET_G, and can be applied successfully in shallow groundwater level regions for reducing groundwater model prediction uncertainty due to over simplification of water balance components.

A. Manekar (✉) · S. Jena · R. K. Panda
School of Infrastructure, Indian Institute of Technology Bhubaneswar, Odisha 752050, India
e-mail: am40@iitbbs.ac.in

S. Jena
e-mail: sj13@iitbbs.ac.in

R. K. Panda
e-mail: rkpanda@iitbbs.ac.in

B. B. Das et al. (eds.), *Recent Developments in Sustainable Infrastructure (ICRDSI-2020)—GEO-TRA-ENV-WRM*, Lecture Notes in Civil Engineering 207,
https://doi.org/10.1007/978-981-16-7509-6_46

Keywords Groundwater evapotranspiration · Modified white method · Soil moisture · Extinction depth · Groundwater table fluctuation

1 Introduction

Evapotranspiration (ET) is a key process in the regional as well as the local water cycle and is approximately 70% of global annual precipitation (Good et al. 2015). In India, nearly 40% of precipitation returned to the atmosphere through ET (Irmak 2008). There exist two major types of groundwater system in India, i.e., (i) deep aquifers, and (ii) shallow aquifers. In the shallow aquifers, plant roots penetrate the saturated zone below the water table and extract water from the groundwater system. Moreover, in conjunction with the shallow aquifer system the groundwater table rises during monsoon to intersect the root zone in many parts of the country and a reasonable portion of the groundwater contributes to the total ET, called as the groundwater evapotranspiration (ET_G) (Yeh and Famiglietti 2009). Sometimes ET_G exceeds 85% of potential ET (Sanderson and Cooper 2008), but undistinguished in many water balance studies. In many of the reported groundwater balance studies, the ET_G parameter has been either neglected or assumed to be a constant value, which induces uncertainty to the model predictions (Moreo et al. 2017). Thus, the estimation of ET_G carries indispensable importance in groundwater flow simulation as well as water balance studies at various spatio-temporal scales. In dry lands, deforestation results in the rise of water table with ET_G as 30–40% of the recharge (Lubczynski 2011). In arid and semi-arid regions, groundwater evapotranspiration is a major mechanism of groundwater fluctuations (Diouf et al. 2020). Additionally, ET_G decreases with an increase in water table depth (Cooper et al. 2006) and at a certain depth ET_G becomes zero, that depth is termed as extinction depth (ED) (Shah et al. 2007). ET_G and the ED have both spatial and temporal variability according to the change in vegetation cover, and soil physical properties (Diouf et al. 2020). Estimation of the ET_G and ED have paramount importance in groundwater resource management and accurate water budgeting. However, very little efforts have been reported at the basin scale to estimate these two parameters in varying atmospheric conditions, changing groundwater level, and heterogeneous land-use patterns (Carlson et al. 2014).

It is difficult to quantify ET_G directly due to its complex physical process and spatio-temporal variability (Orellana et al. 2012), few researchers studied ET_G from shallow water tables theoretically and experimentally in the laboratory or in-situ (Chimner and Cooper 2004). Another approach that is mostly used to quantify ET_G is analyzing the groundwater fluctuations in a shallow aquifer, introduced by White (1932). This method has been recognized by many researchers, as it is inferred to daily groundwater consumption by the vegetation which is evapotranspiration from the groundwater. White considered that plants transpire water during the day, causing an upward flow of groundwater due to the consumption by the plants which is much more than groundwater recovery leading to the decline of groundwater level. White also stated that during night time, photosynthesis ceases (midnight to 4 am) and

allowing the water level to increase gradually. Thus, groundwater water recovery and plant water use contribute to the pattern of diurnal fluctuations in the water table depth. The main advantage of estimating ET employing diurnal water table fluctuations is that the water loss due to groundwater consumption by phreatophytes is directly measured through water level change. This method also proved to be effective, less expensive, and involving simple calculations (Fahle and Dietrich 2014). Although there are advantages in the White method, many uncertainties were reported in different studies. Most of them were related to the specific yield calculation and short recovery interval (Gribovszki et al. 2008), thus the modification to the White method was carried out by applying time series function for 24 h window, which gives the measurement of ET_G on a weekly and monthly interval associated with water table fluctuations (Soylu et al. 2012).

In the current study, the Modified White method was applied to estimate ET_G on different land use/land cover for tropical savanna (tropical wet and dry) regions of India. The Rana groundwater basin of Odisha is observed with a shallow water level of less than 0.2–12 m below ground level. Such types of regions (Savanna) gain water during wet periods after rain and loses water during summer mainly due to ET_G. Thus, estimation of ET_G for such type of climate is imperative which is limited due to the non-availability of diurnal fluctuation data. This study includes the estimation of ET_G using monitored diurnal groundwater level fluctuation data and the assessment of extinction depth for different land-use/landcover for groundwater evapotranspiration.

2 Methodology

2.1 Study Area

Rana basin is located in the middle reach of the Mahanadi river basin extending from a latitude of 20.109°N to 20.413°N and longitude of 85.395°E to 85.631°E in Eastern India. The Mahanadi river is the longest river of Odisha. The study basin is extended over an area of 428.41 km^2. The site was selected based on depth to the water table, agricultural practice, and climatic conditions. The weather in Eastern India Odisha is greatly influenced by the coastal weather. This region falls under the Savannah type of climate with distinct wet and dry periods according to Koeppen's method, where it experiences very hot temperatures and rainfall of about 100–200 cm/year. The summer maximum temperature ranges between 35 and 40 °C and the low temperatures are usually between 12 and 14 °C. The region has a tropical climate, more specifically tropical wet and dry (tropical savanna), and receives an average annual rainfall of 1451.2 mm. A tributary of Mahanadi River, called Rana is flowing through the center of the groundwater basin from south to north, which is also seasonal in nature. The 70% of the average annual rainfall occurs in just 3–4 months of the year. Surface water availability in the region is therefore limited to those 3–4 months of

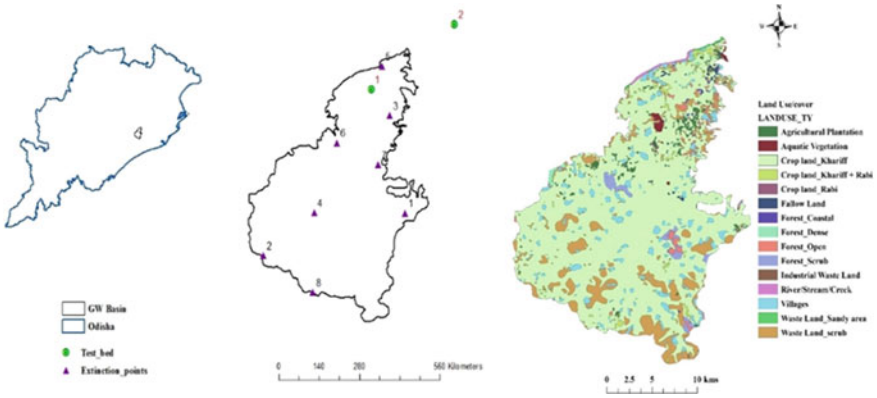

Fig. 1 **a** Study area, **b** land use/cover distribution in the study basin

monsoon period followed by the dry season during the rest of the year. After the withdrawal of the monsoon, this tributary is left with patches of stagnant water in its course. Therefore, the only alternative left is to use groundwater. The observed water table fluctuation data in 46 identified observation wells indicate that the groundwater level in the area varies between 0.2–12 m in monsoon and 4–21 m in the non-monsoon period.

The main activities in the basin are agriculture, forestry, and occupation. Most of the area is used for agricultural purposes. The main crop grown in these areas is rice, which requires stagnant water during the sowing period (June–July) and whose maximum root depth is 60 cm. The study area consists of high land at the southern part, most of the middle part is a crop-growing land, and the northern part of the basin is near to river bank. During the dry season, due to intense heating, evaporation, and rainfall deficit, most of the soil water dry up. Hence, during such periods, groundwater is of utmost importance for regional crops. Two observation wells were installed at Jorkul (20.367899°N, 85.557042°E) and Parthapur (20.439571°N, 85.666861°E) to observe groundwater fluctuations were used to estimate groundwater evapotranspiration (ET_G) for the year 2015–2016. The location of these two stations and the pattern of land use/land cover are shown in Fig. 1.

2.2 Data Required

Groundwater fluctuation data were collected using groundwater level recorder, conductivity temperature depth (CTD) sensors that were installed in two observation wells at two stations i.e. Jorkul and Parthapur. Data were recorded at 30-min intervals for both the stations. The specific yield (S_y) values were determined with the help of the pumping test and from CGWB Bhubaneswar for the entire study basin. Specific yield values used for Jorkul and Parthapur stations were 0.1 and 0.29 respectively.

The weather station was the source for weather data required such as solar radiation, temperature, and precipitation.

2.3 Modified White Method

A modified White method that includes the periodic nature of diurnal fluctuations in shallow groundwater levels has been proposed recently (Soylu et al. 2012). Very few studies have focused on this diurnal variation approach. Most of the studies based on groundwater level fluctuations were analyzed for wetlands, thus in this study, the application of the above method was observed on agricultural land and different land use. The diurnal fluctuation method offers a practical and simplified alternative method for estimating ET from vegetation (here we are determining mainly for agricultural land). White (1932) established a relation between specific yield, groundwater recovery, and ET_G. Loheide (2008) recommended some assumptions to ensure the validity of Eq. (1) which were considered in this study. ET_G was quantified using the following governing Equation suggested by White:

$$\frac{S_y dZ_{wt}}{dt} = r(t) - ET_G(t) \tag{1}$$

where, S_y = Specific yield; r = groundwater recovery; Z = height of water table.

Equation (1) is integrated over a time interval Δt to solve for total ET_G:

$$ET_G = S_y\left(r_{gw} \pm s\right) \tag{2}$$

where, ET_G is the daily total ET_G rate (mm/day), r_{gw} is estimated as the hourly rate of water table rise between midnight and 4:00 A.M. when transpiration is assumed to be negligible, and s is the daily change in storage that is estimated as the net rise or fall of the water table during the 24-h period (i.e. the net inflow rate signifying the difference between the incoming and outgoing flow). Positive or negative in Eq. (2) are used when water table fall or rise, respectively.

Soylu et al. (2012) suggested that the diurnal fluctuations in shallow groundwater levels often follow periodic and sinusoidal nature, thus it can be represented in the sinusoidal wave function. In the present study, diurnal variations of groundwater are used to represent the weekly and monthly ET_G. A sine function describing the streamflow was presented as time series function Eq. (3) by Czikowsky and Fitzjarrald (2004) where the various coefficients were calculated by empirically fitting the data.

$$Z(t) = At + D + B\sin\left[\frac{2\pi(t+E)}{24}\right] \tag{3}$$

where, Z is the stream discharge or stage (L), t is time (in units of hours), A is the 3-day trend (LT^{-1}), D is the mean bias (L), B is the diurnal amplitude (L), and E is the diurnal signal phase (T).

$$S_y \Delta Z_{wt}(t) = S_y[Z_{wt}(t) - Z_o] = \int_{\Delta t} (r - ET_G)dt = r\Delta t - \int_{\Delta t} ET_G dt \quad (4)$$

$$Z_{wt}(t) = Z_o + r_{gw}t - \frac{1}{S_y}\int_0^t ET_G dt = D + At + B\sin\left[\frac{2\pi(t+E)}{24}\right] \quad (5)$$

Estimation of ET_G using this approach is done by relating Eq. (4) to the governing equation for shallow groundwater fluctuations Eq. (2). In Eq. (5) D is accounted for the initial water level. The observed water level At represents the combined effects of both groundwater recovery and transpiration whereas the sine function represents the ET_G term $\int ET_G dt$. The trend in water level was contributed by ET_G, even when the groundwater recovery rate is zero, depicting the entire trend is the result of ET_G. The process of detrending is performed on the water level time series (removing $D + At$) in Eq. (5) will also remove some significant portion of the ET_G signal. The only term on the right-hand side of Eq. (5) that remains after the detrending process is the sine function with amplitude B (peak-to-trough $= 2B$). Simply equating the daily total transpiration to $S_y(2B)$, may result in significant underestimation of ET_G. This can be corrected by introducing a scaling factor (k) that is a function of solar radiation. Given hourly solar radiation values were accumulated over multiple days, then the scaling factor was evaluated (Soylu et al. 2012). The simplified ET_G Equation was established as a function of specific yield and scaling factor.

$$ET_G = S_y k(2B) \quad (6)$$

The variation of groundwater level and rainfall with time for the period of Jan–Dec 2016 is potrayed in Fig. 2a, it is visible that during the dry period, the depth of groundwater level increases, and in the monsoon season (Jul–Aug) with the effect of rainfall, the groundwater gets recharged and the water table becomes shallower. The

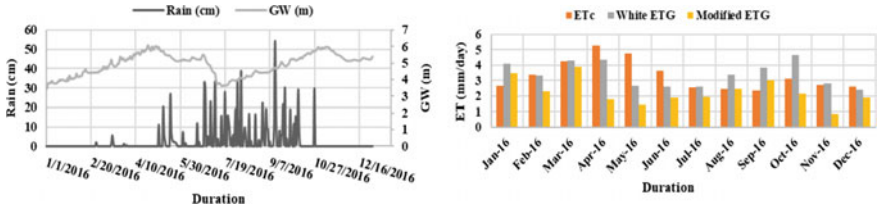

Fig. 2 **a** Variation of groundwater level (m) and rainfall (mm) during Jan–Dec 2016; **b** crop evapotranspiration (ET_C) and groundwater evapotranspiration (ET_G) for the period of Jan–Dec 2016 at Jorkul station (monthly average)

obtained ET_G results of Jorkul sites were compared with the crop evapotranspiration (ETc) obtained using potential evapotranspiration and crop coefficient. The method adopted for the calculation of daily ETo was Penman–Monteith Equation (Cai et al. 2007) and the crop coefficient (Kc) value was taken as 0.75 for rice crops and sub-humid climatic conditions (Allen et al. 1998).

2.4 Determination of Extinction Depth

In the tropical region, the depth to water table increases after monsoon and ET_G is assumed to decay with increase in water table depth, and when ET_G attains a value of zero, that depth is known as extinction depth (Shah et al. 2007). Landscapes where water table is near to root zone, vegetation can take water from both unsaturated vadose zone and saturated groundwater. Thus, extinction depth is used to verify that which portion is contributing to the groundwater extraction or from where ET_G is taking place. When the groundwater level is below extinction depth, then the contribution of groundwater to ET is very less or negligible. For practical purposes the depth at which groundwater contribution (ET_G) is 0.5% of crop ET, that depth is called as extinction depth. Extinction depth at different locations was analyzed in this study.

3 Results and Discussion

Daily ET_G was estimated using the groundwater fluctuation data that was obtained using the sensors installed in the observation wells at Jorkul station for the year 2016. The root system of vegetation in Jorkul site varies between 1 and 1.5 m for agriculture to 10 m for established vegetation. The plants' uptake water from groundwater as the depth of groundwater in the study area varies between 0.2 m and 12 m during monsoon to non-monsoon season. Figure 2a shows the variation of groundwater level and rainfall with time for the period of Jan–Dec 2016. It can be seen that during the dry period, the depth of groundwater level increases, and after the monsoon season with the effect of rainfall recharge, the groundwater level becomes shallower. The wet recharge period starting in June after the rainfall follows well with the rainfall pattern. During this period, ET_G will be less, as transpiration demands are satisfied by the surface and unsaturated zone moisture. For the period of Jan–Dec 2016, the range of water table depth varies from 3.44 m to 6.0895 m (May) in Jorkul. ET_G values increase after July–Aug 2016, as precipitation event occurred during June 2016 and delayed recharge causing root water uptake from groundwater. Moreover, the area being dominated by rice cultivation which starts during July month, during this period the topsoil contributes to the evapotranspiration as the maximum root zone depth of rice is 60 cm and waterlogging condition.

In Savannah type, the basin gains water after the rainfall happens and loses water in dry seasons due to variation in temperature and consumption of groundwater. The Rana groundwater basin has a shallow groundwater table, thus most of the ET is contributed from the groundwater. Groundwater ET computed using both White and Modified White (Eqs. 2 and 6) on a monthly mean time scale is shown in Fig. 2b. The maximum average ET_G attained was 3.7 mm/day and 4.65 mm/day during sunnier days with Modified White and White method respectively. Further, the minimum observed was 0.8 mm/day and 2.4 mm/day during the cloud cover period using the Modified White and White respectively when the groundwater level increased. It is observed from the Fig. 2b that the Modified white method gives considerably accurate results as ET_G obtained was nearly 50–70% of ETc which is reasonable for the actual condition. Whereas, the White method overestimated in some cases, resulting in undesirable ET_G values. The ET_G value increases after the monsoon as the water table becomes shallower due to rain and decreases during dry period (Nov–Dec, Apr–May), groundwater being at a deeper depth. Also, during Jan- Mar the ET_G values are higher as the topsoil moisture gets reduced giving rise to more root water uptake from groundwater. The ET_G rate decreases for the monsoon period because the rainfall gets entirely captured by the surface and unsaturated zone, leading to more contribution from the vadose zone for transpiration. In the wet season roots can uptake water from the moisture-rich topsoil with lower pressure, so the contribution of groundwater gets reduced. There was high variability of ET_G throughout the year (2016) because of the distinct wet and dry climatic conditions under the Savannah type climate. At the Jorkul site, statistical comparisons of estimated ET_G and observed ET values show higher r^2 values (Fig. 3) for the Modified white method (0.88) as compared to the White method (0.40) for the weekly time scale. The Modified White method also results in a reduction in ET_G RMSE from 0.64 in the White method to 0.27. It is evident from Fig. 3 that the use of a seven-day interval window, Modified white shows better correspondence with observed ET values. The results also indicate that the Modified white method provides an improved alternative to the

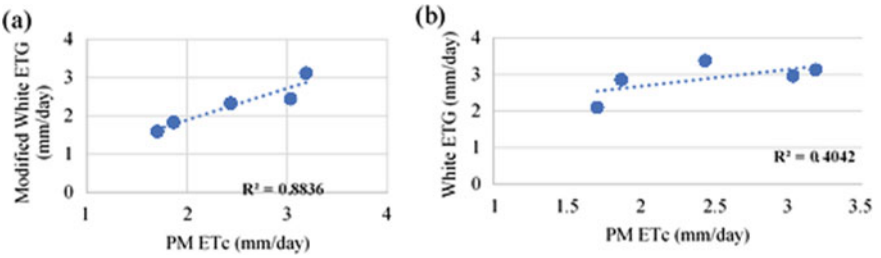

Fig. 3 Comparison of observed ET_C values at the Jorkul site (Penman Monteith method; x axis) with both of the diurnal water table fluctuation methods (y axis). ET_G comparisons from the 7-day White method and 7-day Fourier method are represented by panels in the right and left columns, respectively

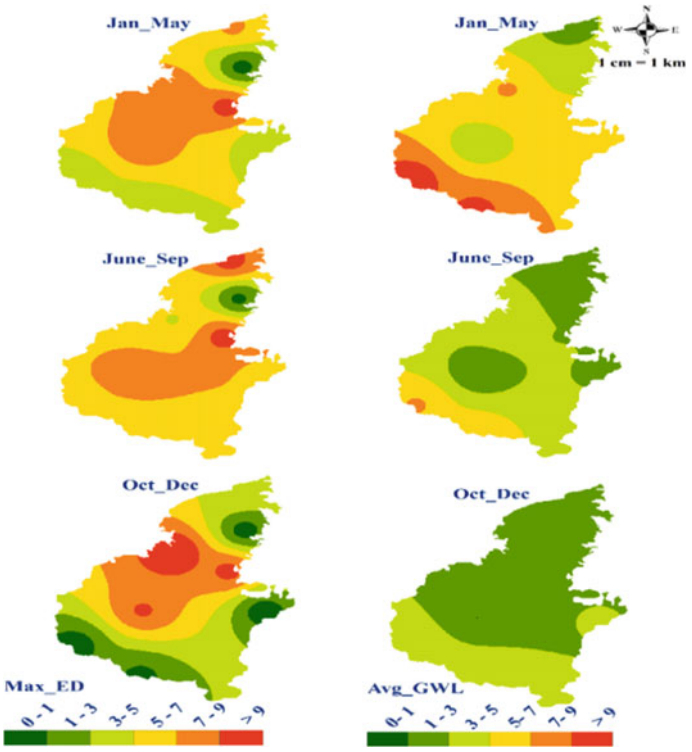

Fig. 4 Spatial distribution of maximum extinction depth (m) and average groundwater level (m) for the year 2016

White method in estimating groundwater evapotranspiration using water table fluctuations. Comparison of White and Modified white with observed monthly average values shows that the Modified method performs considerably better.

From Fig. 4, it can be interpreted that during the Jan–May period, which is the pre-monsoon period, the groundwater level is lower than the extinction depth in the southern portion of the basin, which indicates that the portion will have less/no contribution to the ET_G. The extinction depth in southern region found to be of 1–3 m and the groundwater level is much lower than this level, thus the ET_G will be less in this hard-rock area. In the upper region, the scenario is opposite to it, groundwater level is shallower (1–3 m) than the extinction depth (5–9 m), and it will contribute to the ET_G. The same is the case with the middle region (agricultural land), there will also be significant amount of ET_G in this region. During the month of Jun–September i.e. the monsoon period, there will always be some amount of ET_G, but the value of ET_G will be less as compare to other period of the year because of the more vadose zone ET. There is much variation in extinction depth for the period of Oct–Dec, as this is the post monsoon period.

4 Conclusions

White and Modified white approaches were used to estimate groundwater evapotranspiration (ET_G) which occurs in shallow water table environments. The study area falls under the Savannah type region with variable land use and seasonal change, plants withdraw groundwater during the dry period due to variability in temperature. During rainy season the topsoil moisture increases leading to smaller values of ET_G. After the rainy season the groundwater level rises due to the delayed recharge accelerating groundwater consumption by vegetation (ET_G). The White method stated that during night time, photosynthesis ceases and allowing the water levels to increase gradually. Thus, groundwater water recovery and plant water use contribute to the pattern of diurnal fluctuations in the water table depth. It was observed that the White method (simplified) sometimes overestimates the crop ET, which is not desirable. On the other hand, the Modified white method gives reasonable results and ET_G obtained was nearly 50–70% of ET_c. Also, the Modified white method gave a high r^2 value (0.88) than the White method (0.40) for a 7-day window. ET_G found in the dry period was more than the wet period of the year because the topsoil moisture gets reduced leading to less vadose zone contribution and consumption of groundwater increases by the vegetation. In the wet period, the rainfall causes the rapid increase of groundwater, but the transpiration demands of plants are satisfied by the surface and vadose zone. The Modified white method applied in this study enhances the accuracy of ET_G estimation from diurnal water table fluctuations. Furthermore, this method can be used to determine daily to monthly variations in ET_G. Additional studies should be performed to test these methods in other regions and under different environmental conditions. Extinction depth values changes based on land use type and the range of extinction depth for Rana basin varied from 1 to 3 m for hard rock area whereas from 5 to 9 m for other parts of the region.

References

Allen RG et al (1998) Crop evapotranspiration—guidelines for computing crop water requirements—FAO irrigation and drainage. FAO Food Agri Organ United Nations 300(56)

Cai J et al (2007) Estimating reference evapotranspiration with the FAO penman-monteith equation using daily weather forecast messages. Agri Forest Meteorol 145(1–2):22–35. https://doi.org/10.1016/j.agrformet.2007.04.012

Carlson M et al (2014) Estimating evapotranspiration and groundwater flow from water-table fluctuations for a general wetland scenario repository citation. Citation/Publisher Attribution: Ecohydrol Ecohydrol 7(2):378–90. https://doi.org/10.1002/eco.1356

Chimner RA, Cooper DJ (2004) Using stable oxygen isotopes to quantify the water source used for transpiration by native shrubs in the San Luis Valley, Colorado U.S.A. Plant Soil 260(1–2):225–236. https://doi.org/10.1023/B:PLSO.0000030190.70085.e9

Cooper DJ et al (2006) Effects of long-term water table drawdown on evapotranspiration and vegetation in an arid region phreatophyte community. J Hydrol 325(1–4):21–34. https://doi.org/10.1016/j.jhydrol.2005.09.035

Czikowsky MJ, Fitzjarrald DR (2004) Evidence of seasonal changes in evapotranspiration in eastern U.S. hydrological records. J Hydrometeorol 5(5):974–988. https://doi.org/10.1175/1525-7541(2004)005%3c0974:EOSCIE%3e2.0.CO;2

Diouf OC et al (2020) Modelling groundwater evapotranspiration in a shallow aquifer in a semi-arid environment. J Hydrol 587(April):124967. https://doi.org/10.1016/j.jhydrol.2020.124967

Fahle M, Ottfried D (2014) Estimation of evapotranspiration using diurnal groundwater level fluctuations: comparison of different approaches with groundwater lysimeter data, pp 273–86. https://doi.org/10.1002/2013WR014472

Good SP et al (2015) Hydrologic connectivity constrains partitioning of global terrestrial water fluxes. Science.Sciencemag.Org 349:175–77. https://doi.org/10.1002/2015GL064117

Gribovszki Z et al (2008) Riparian zone evapotranspiration estimation from diurnal groundwater level fluctuations. J Hydrol 6–17. https://doi.org/10.1016/j.jhydrol.2007.10.049

Irmak S (2008) Evapotranspiration. Encyclopedia Ecology, vol 2, Ecological Processes, pp 1432–38

Loheide SP (2008) A method for estimating subdaily evapotranspiration of shallow groundwater using diurnal water table fluctuations. Ecohydrology 1:59–66

Lubczynski MW (2011) Groundwater evapotranspiration—underestimated role of tree transpiration and bare soil evaporation in groundwater balances of dry lands. Climate change and its effects on water resources, Springer, pp 183–90

Moreo MT et al (2017) Groundwater discharge by evapotranspiration, flow of water in unsaturated soil, and stable isotope water sourcing in areas of sparse vegetation, amargosa desert, Nye County, Nevada

Orellana F et al (2012) Monitoring and modeling water-vegetation interactions in groundwater-dependent ecosystems. Rev Geophys 50(3). https://doi.org/10.1029/2011RG000383

Sanderson JS, Cooper DJ (2008) Ground water discharge by evapotranspiration in wetlands of an arid intermountain basin. J Hydrol 351(3–4):344–359. https://doi.org/10.1016/j.jhydrol.2007.12.023

Shah N et al (2007) Extinction depth and evapotranspiration from ground water under selected land covers. Ground Water 45(3):329–38. https://doi.org/10.1111/j.1745-6584.2007.00302.x

Soylu ME et al (2012) On evapotranspiration and shallow groundwater fluctuations: a fourier-based improvement to the white method. Water Resour Res 48(6):1–17. https://doi.org/10.1029/2011WR010964

White WN (1932) A method of estimating ground-water supplies based on discharge by plants and evaporation from soil: results of investigations in escalante valley, Utah. US Government Printing Office

Yeh PJF, Famiglietti JS (2009) Regional groundwater evapotranspiration in illinois. Journals.Ametsoc.Org 10(2):464–78. https://doi.org/10.1175/2008JHM1018.1

Damage Analysis of Seismic Response of Shallow Tunnels in Jammu

Abdullah Ansari, K. Seshagiri Rao, and A. K. Jain

Abstract There are lots of tunnel construction project is under progress in Jammu region of Indian Himalaya, at an expanding rate as a part of urban development and infrastructure design. Tunnel construction is playing vital role in urban and national transportation framework. Occurrence of any sort of seismic activity in Jammu and nearby areas may cause damage of these infrastructure. Hence, a careful consideration of the impacts of seismic loadings on the analysis and design of tunnels is needed as a part of damage evaluation. Different closed form analytical approaches exist, such as methods given by Wang and Penzien for seismic analysis of shallow tunnels. Ovaling deformations occur when seismic waves propagate perpendicular to the axis of tunnel and are therefore, designed for the transverse direction. In this paper, these two analytical solutions are used for the analysis of tunnel lining forces, constructed in soft to hard soil with various mechanical properties and constant shear strain. Seismic analysis carried out by means of selecting eight unique types of soil, very soft clay to highly dense sand. The study indicates a relative error in both analytical methods. It was found that the variations in thrust and bending moment are dependent on the flexibility ratio, thus, it is proposed that the stress distribution to be considered for analysis and design of tunnels lining. It is also seen that the induced circular stress in the tunnel liner is decreased with increasing soil stiffness.

Keywords Shallow tunnel · Seismic analysis · Jammu · Flexibility ratio

A. Ansari (✉) · K. S. Rao · A. K. Jain
Department of Civil Engineering, Indian Institute of Technology Delhi, New Delhi 110016, India
e-mail: ansariaa@civil.iitd.ac.in

K. S. Rao
e-mail: raoks@iitd.ac.in

A. K. Jain
e-mail: akjain@iitd.ac.in

B. B. Das et al. (eds.), *Recent Developments in Sustainable Infrastructure (ICRDSI-2020)—GEO-TRA-ENV-WRM*, Lecture Notes in Civil Engineering 207,
https://doi.org/10.1007/978-981-16-7509-6_47

1 Introduction

The geological strata found during tunnelling in the Jammu region of Indian Himalaya like seismically active region are relatively incompetent and influenced by a range of folds, faults and thrusts of varying magnitudes (Ansari et al. 2021). Tunnel alignments come across abrupt changes in strata from weak, broken, jointed rock mass to the competent rock mass, or through bands of different sediments. The fault, thrust, shear zones, squeezing and rock bursting are the most commonly encountered geological problems during tunneling in the Himalayan region (Ansari et al. 2017; Ameen 2018). The geological complexities involved in the Himalayan region, and the huge infrastructural projects under development in Jammu area coupled with the huge amount of instrumentation data available for each project, provides a good scope for the study of effect of seismicity on underground structures, especially transport tunnels in the region.

To understand the seismic response of the tunnels, different approaches are adapted including closed form analytical solution, numerical modelling and physical modelling (Ansari et al. 2022b). To estimate the seismic internal forces of tunnels' linings, many researchers proposed the analytical solutions under certain assumptions and conditions, e.g. elastic response of the soil and the tunnel lining and simulation of seismic loading in quasi-static fashion. The analytical solutions are useful, relatively fast and easy to use for preliminary seismic design of tunnels. In the present study, analytical solutions suggested by Wang and Penzien used to investigate the circular shaped shallow tunnel located in earthquake prone area having soil media. For this purpose, classified soils including clay, silt, sand and gravel with different Poisson ratio and elastic modulus considered. Effect of various soil parameters and maximum shear strain was evaluated using sensitivity analysis.

2 Modes of Tunnel Deformation Under Seismic Condition

There are three basic modes of tunnel deformation during seismic shaking including longitudinal compression or extension; longitudinal bending an ovaling or racking (Ansari et al. 2022a). The propagation of seismic waves propagate either longitudinal or transverse direction of the tunnel axis decide the expected mode of deformation (Owen and Scholl 1981). The first seismic design basis for tunnels was proposed based on Newmark's pioneering work based on slip between soil medium and tunnel (Newmark 1968; John and Zahrah 1987). For estimating the strains and curvature of the tunnel for ground motions propagating at an angle to the tunnel axis free field deformation approach used which further modified considering interaction between soil strata and tunnel. The soil tunnel interaction deals with two contact interface conditions, one for full slip and another for no slip (Wang 1993). Modified analytical solutions developed for thrust, shear force, and bending moment in the tunnel lining as a result of racking deformation (Penzien and Wu 1998). In case of no

slip condition, maximum thrust is much higher for Wang's solution (Hashash et al. 2001).

2.1 Wang's Analytical Solution for Tunnel Deformation Under Seismic Condition

The ovaling deformations due to earthquake loading proposed for both full slip as well as no slip condition (Wang 1993). Following set of equations can be use to calculate the maximum thrust (T_{max}) and moment (M_{max}) at the soil lining interface under seismic loading, where $\frac{\Delta d}{d}$ represents the diametric strain.

$$\frac{\Delta d}{d} = \frac{\mp K_l F}{3} \Upsilon_{max} \tag{1}$$

$$T_{max} = \mp \frac{K_l E_m}{6(1+\nu_m)} r \Upsilon_{max} \tag{2}$$

$$M_{max} = \mp \frac{K_l E_m}{6(1+\nu_m)} r^2 \Upsilon_{max} \tag{3}$$

$$K_l = \frac{12(1-\nu_m)}{2F+5-6\nu_m)} \tag{4}$$

$$F = \frac{E_m(1-\nu_l^2)R^3}{6E_l I(1+\nu_m)} \tag{5}$$

$$C = \frac{E_m(1-\nu_l^2)r}{E_l t(1+\nu_m)(1-2\nu_m)} \tag{6}$$

In above mentioned equations, E_m is molus of elasticity of the soil medium; E_l is modulus of elasticity of the tunnel lining; I is moment of inertia of the tunnel lining (per unit width) for circular lining R; F is flexibility ratio; C is = compressibility ratio; K_1 is full slip lining response coefficient; ν_m is Poisson's ratio of the soil medium and ν_l is Poisson's ratio of the tunnel lining.

Equation to calculate the maximum thrust for no slip assumption is suggested below:

$$T_{max} = \mp \frac{K_2 E_m}{2(1+\nu_m)} r \Upsilon_{max} \tag{7}$$

Here, K_2 is no slip lining response coefficient, which can be calculated as follows.

$$K_2 = 1 + \frac{F\,[(1-2\nu_m) - (1-2\nu_m)C] - \frac{1}{2}(1-2\nu_m)^2 + 2}{F\,[(3-2\nu_m) + (1-2\nu_m)C] + C\left[\frac{5}{2} - 8\nu_m + 6\nu_m^2\right] + 6 - 8\nu_m} \tag{8}$$

2.2 Penzien's Analytical Solution for Tunnel Deformation Under Seismic Condition

For both no slip and full slip condition under seismic loading, an analytical solution suggested to study ovaling and racking deformation in circular as well as rectangular shaped tunnel (Penzien 2000; Penzien and Wu 1998). The lining soil racking ratio can be estimated using below equation.

$$R^n = \frac{\mp 4(1-\nu_m)}{(\alpha_n + 1)} \tag{9}$$

$$\alpha_n = \frac{12E_l I(5-6\nu_m)}{d^3 G_m\left(1-\nu_l^2\right)} \tag{10}$$

In case of full slip condition, the analytical equations for thrust, bending moment, and shear force in circular tunnel linings suggested below.

$$\mp \Delta d^n_{lining} = \mp R^n \Delta d_{free-field} \tag{11}$$

$$T(\theta) = -\frac{12E_l I \Delta d^n_{lining}}{d^3\left(1-v_l^2\right)} \cos 2\left(\theta + \frac{\pi}{4}\right) \tag{12}$$

$$M(\theta) = -\frac{6E_l I \Delta d^n_{lining}}{d^2\left(1-v_l^2\right)} \cos 2\left(\theta + \frac{\pi}{4}\right) \tag{13}$$

$$V(\theta) = -\frac{24E_l I \Delta d^n_{lining}}{d^3\left(1-v_l^2\right)} \sin 2\left(\theta + \frac{\pi}{4}\right) \tag{14}$$

For the case of no slip condition, the equations are as follows:

$$\mp \Delta d_{lining} = \mp R \Delta d_{free-field} \tag{15}$$

$$T(\theta) = -\frac{24E_l I \Delta d_{lining}}{d^3\left(1-v_l^2\right)} \cos 2\left(\theta + \frac{\pi}{4}\right) \tag{16}$$

$$M(\theta) = -\frac{6E_l I \Delta d_{lining}}{d^2\left(1-v_l^2\right)} \cos 2\left(\theta + \frac{\pi}{4}\right) \tag{17}$$

$$V(\theta) = -\frac{24E_l I \Delta d_{lining}}{d^3\left(1-v_l^2\right)} \sin 2\left(\theta + \frac{\pi}{4}\right) \tag{18}$$

To calculate R and α, mathematical expression is given here:

$$R = \frac{\mp 4(1-v_m)}{(\alpha + 1)} \tag{19}$$

$$\alpha = \frac{24E_lI(3-4\nu_m)}{d^3G_m\left(1-\nu_l^2\right)} \tag{20}$$

3 Result and Discussion

Jammu city spreads over 167 sq. km and lies at uneven ridges of low heights at the Shivalik foot hills of the Himalayas falling in seismic zone IV (BIS 2002). It is surrounded by Shivalik range to the North, East and South East while the Trikuta range surrounds it in the North-West. The Tawi River separates the old city in the North from the new city in the south. A reference tunnel having 20 m depth from ground surface and 10 m diameter considered in Jammu area for study with region having earthquake magnitude $M_w = 7.8$, acceleration $a_{max} = 0.42$ g and 135 km source to site. Different soil models where Poisson ratio ranges between 0.2 and 0.45 and modulus of elasticity varies between 17,000 and 750,000 kPa considered for studying the effect of soil strength parameters on shear force, thrust and bending moment having maximum value of shear strain equal to 0.0023. Following Table 2 shows the calculated values of thrust, bending moment and shear force using Wang and Penzien method. The magnitude of error increases with increasing soil stiffness for both the methods having flexibility ratio less than 30. For soft clay to hard sand, the acceptable error would be less than 7%. The ΔT and ΔM are the magnitude of error between Wang and Penzien solution for thrust and bending moment, where subscript W–P refers to Wang and Penzien method (Table 1, 2 and 3).

For this study, maximum acceleration during earthquake activities at the ground level assumed 0.42 g which can be estimated based on soil layer strata. It can be observed that the values of shear modulus (G), maximum shear strain (γ_{max}) and C_m will change due to the value change of modulus of elasticity (E) and Poisson ratio (ν). The maximum shear strain (γ_{max}) increases with increasing modulus of elasticity (E) during starting phases which becomes constant for higher values of modulus of elasticity as shown in the Fig. 1. The variation of deformation parameters using Wang's method and Penzien's method presented in the following Fig. 2.

4 Conclusions

Tunnels constructed in Jammu area subjected to dynamic loading in terms of seismic forces as this area falls I seismic zone IV. Based on the nature in which seismic waves propagate in soil medium, the tunnels can undergo different form of deformation with full slippage or no slippage depending on the surficial behaviour. In this study, analytical solutions given by Wang and Penzien compared to understand the seismic response of tunnel lining considering different soil media for Jammu area. The soil

Table 1 Earthquake and soil parameters for classified soil models

Soil type	Model		a_{max} (g)	C_m (m/s)	V_S (m/s)	γ_m (kN /m^3)	ν_m	E_m (kPa)
Very soft clay	S1	Upper limit	0.25	180	0.45	17	0.45	159,732
Soft clay	S2		0.3	200	0.54	17.5	0.425	199,500
Medium clay	S3		0.325	230	0.58	18	0.4	266,616
Hard clay	S4		0.35	250	0.63	18.5	0.375	317,968.8
Dense sand	S5		0.35	290	0.64	19.2	0.325	427,900.8
Sand and gravel	S6		0.375	310	0.67	19.8	0.3	494,722.8
Dense sand and gravel	S7		0.4	330	0.73	20	0.275	555,390
Highly dense sand	S8		0.45	350	0.81	20.5	0.25	627,812.5
Very soft clay	S1	Lower limit	0.2	170	0.36	16	0.45	134,096
Soft clay	S2		0.25	190	0.43	16.5	0.425	169,760.3
Medium clay	S3		0.275	210	0.49	17	0.4	209,916
Hard clay	S4		0.3	230	0.54	17.5	0.35	249,952.5
Dense sand	S5		0.325	250	0.58	18	0.3	292,500
Sand and gravel	S6		0.35	270	0.63	18.5	0.275	343,905.8
Dense sand and gravel	S7		0.375	290	0.67	19	0.25	399,475
Highly dense sand	S8		0.4	300	0.72	19.5	0.2	421,200

stiffness has direct effect on the magnitude of error between these two methods but for hard soils, conservative results are achieved. Analytical solutions are not enough to calculate shear strain distribution, as thrust and bending moment are dependent on flexibility ratio. Due to which maximum shear strain can be evaluated based on real time seismic history. Earthquake induced stress distribution must be accounted for safe design of tunnels.

Table 2 Results of analytical Solution based on Wang and Penzien method

Method		Wang (1993)			Penzien (2000)				
Model		T_W (kN)	M_W (kN.m)	σ_W (kPa)	T_P (kN)	M_P (kN.m)	V_P (kN)	σ_P (kPa)	F
S1	Upper limit	29.98	119.94	7921.68	29.98	119.93	59.96	7921.69	19.16
S2		34.17	136.64	9012.11	34.17	136.63	68.23	9027.03	24.35
S3		33.95	135.11	8967.23	33.95	135.77	67.14	8967.89	33.12
S4		36.55	146.14	9655.31	35.03	140.81	70.21	9300.62	40.22
S5		34.18	136.71	9029.68	33.00	131.98	65.94	8718.53	56.17
S6		35.95	140.21	9402.78	34.40	137.62	68.33	9088.61	66.19
S7		36.11	147.32	9767.72	35.77	143.10	71.52	9451.27	75.75
S8		41.84	167.54	11,066.07	39.33	157.74	78.67	10,391.92	87.35
S1	Lower limit	25.13	100.50	6638.27	25.13	100.55	50.22	6638.63	16.08
S2		29.72	118.89	7852.54	29.72	118.89	59.45	7852.54	30.71
S3		31.15	124.56	8226.73	31.15	124.55	62.28	8226.98	26.07
S4		33.76	135.02	8918.27	33.75	135.03	67.52	8918.29	32.2
S5		36.38	145.52	9610.33	36.38	145.50	72.76	9610.39	39.14
S6		37.76	151.02	9974.92	37.75	151.02	75.51	9974.92	46.91
S7		39.12	156.48	10,335.51	39.12	156.48	78.23	10,335.59	55.58
S8		40.04	172.17	11,371.58	43.04	172.17	86.09	112,371.6	61.04

Table 3 Error between Wang and Penzien method

Soil type	Model	$\Delta T_{W\text{-}P}$ (%)	$\Delta M_{W\text{-}P}$ (%)	F_{avg}
Very soft clay	S1	1.47	5.61	17.51
Soft clay	S2	2.16	5.13	27.34
Medium clay	S3	1.87	4.14	29.31
Hard clay	S4	0.91	3.64	36.46
Dense sand	S5	1.84	4.36	47.5
Sand and gravel	S6	1.93	4.53	56.11
Dense sand and gravel	S7	2.91	4.38	65.14
Highly dense sand	S8	1.87	4.45	71.19

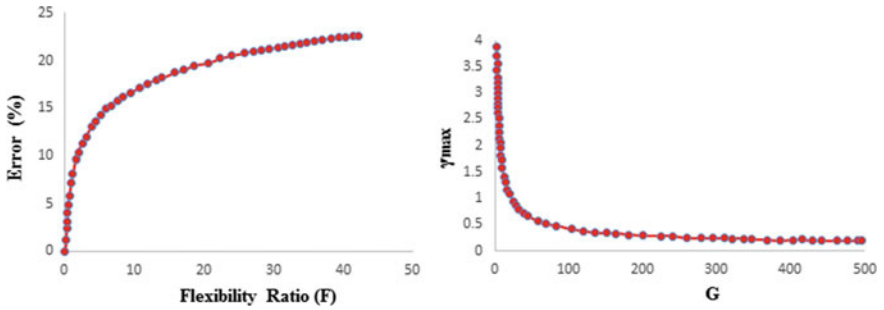

Fig. 1 **a** Variation of error between Wang and Penzien method versus flexibility ratio; **b** variation of maximum shear strain with shear modulus

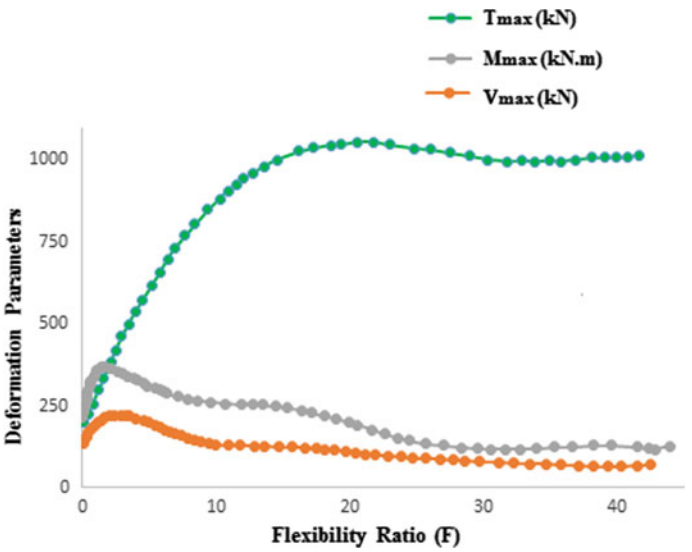

Fig. 2 Variation of deformation parameters with flexibility ratio (F)

References

Ameen AAMM (2018) Modeling the 2004 Andaman-Sumatra tsunami and historical tsunamis from Andaman and Nicobar Island: towards estimation of tsunami hazard along the adjoining areas of Indian Ocean. M.Tech., thesis, Indian Institute of Technology Kanpur, India

Ansari A, Satake K, Malik JN (2017) Modelling the 2004 Indian Ocean Tsunami to estimate tsunami heights and its amplitude and to study its effects on coastal areas. In: Proc. of the ERI Earthquake Conference, University of Tokyo, Japan

Ansari A, Rao KS, Jain AK (2021) Seismic hazard and risk assessment in Maharashtra: a critical review. In: Sitharam TG, Kolathayar S, Sharma ML (eds) Seismic hazards and risk. Lecture notes in civil engineering, vol 116. Springer, Singapore, pp 35–45. https://doi.org/10.1007/978-981-15-9976-7_4

Ansari A, Rao KS, Jain AK (2022a) Damage assessment of tunnels in seismic prone zone during earthquakes: a part of hazard evaluation, In: Sitharam TG, Kolathayar S, Jakka R (eds) Earthquakes and structures. Lecture notes in civil engineering, vol 188. Springer, Singapore, pp 161–169. https://doi.org/10.1007/978-981-16-5673-6_13

Ansari A, Rao KS, Jain AK (2022b) Seismic analysis of shallow tunnels in soil medium. In: Satyanarayana Reddy CNV, Muthukkumaran K, Vaidya R (eds) Stability of slopes and underground excavations. Lecture notes in civil engineering, vol 185. Springer, Singapore, pp 343–352. https://doi.org/10.1007/978-981-16-5601-9_29

BIS:1893 (2002) Indian standard criteria for earthquake resistant design of structures, Part 1—general provisions and buildings, Bureau of Indian Standards, New Delhi, India

Hashash YMA, Hook JJ, Schmidt B, Yao JIC (2001) Seismic design and analysis of underground structures. Tunn Undergr Space Technol 16(2):247–293

Newmark NM (1968) Problems in wave propagation in soil and rock. In: Proceedings of international symposium on wave propagation and dynamic properties of earth materials, New Mexico, University of New Mexico Press

Owen GN, Scholl RE (1981) Earthquake engineering of large underground structures. Report No. FHWA/RD-80/195, Federal Highway Administration and National Science Foundation, 279

Penzien J (2000) Seismically induced racking of tunnel linings. Earthq Eng Struct Dyn 29:683–691

Penzien J, Wu C (1998) Stresses in linings of bored tunnels. Earthq Eng Struct Dyn 27:283–300

St. John CM, Zahrah TF (1987) A seismic design of underground structures. Tunn Undergr Space Technol 2(2):165–197

Wang JN (1993) Seismic design of tunnels, a state-of-the-art approach. Monograph 7, Parsons Brickerhoff Quade and Douglas, Inc., New York

Full Scale Load Test on a Large Diameter Bored Cast Insitu Test Pile—A Case Study

R. Siddhardha, M. Prudhviraj, Manish Kumar Singh, and Jolsna Narayan

Abstract Piles are employed when subsoil strata proximate the ground surface is incompetent of bearing the superstructure loads. Notably, in view of installation and elimination of ground vibration bored cast insitu piles are often accustomed. Piles are designed by many methods namely, empirical, numerical, and analytical. Nevertheless, owing to a high degree of uncertainties such as subsoil conditions, laboratory testing, and variance in construction practices most of the codes worldwide recommend full scale insitu load testing preceding construction to double check the safe load. An Initial vertical maintained load test was performed as per guidelines of IS 2911(Part-4): 2013 for the proposed Eight Lane Dwarka Expressway project in Delhi-Haryana border by applying a 2.5 times safe load using a hydraulic jack by virtue of deriving the reaction from four temporary anchor piles. Dial gauges were installed on an independent datum to monitor the settlement under each increment of 20% of the safe load. The load settlement records were analysed and the safe load was computed using various approaches in the literature.

Keywords Bored cast insitu pile · Test pile · Safe load · Hydraulic jack · Load-settlement

1 Introduction

With the expeditious urbanization and infrastructure development worldwide, geotechnical engineers often face the challenge of designing safe and economical foundation systems. Moreover, the explorations leading to exact solutions involve

R. Siddhardha (✉)
Department of Civil Engineering, NIT Warangal, Warangal, India

M. Prudhviraj · M. K. Singh
Department of Civil Engineering, Sree Dattha Institute of Engineering and Science, Hyderabad, India

J. Narayan
Geotechnical Engineer, L&T Infrastructure Engineering Ltd, Chennai, Tamilnadu, India

B. B. Das et al. (eds.), *Recent Developments in Sustainable Infrastructure (ICRDSI-2020)—GEO-TRA-ENV-WRM*, Lecture Notes in Civil Engineering 207,
https://doi.org/10.1007/978-981-16-7509-6_48

profoundly robust state-of-the-art methods of sampling and testing, are seldom in practice. Also, the central problem is to inhibit settlements sufficient to cause damage to the structure or undermine its functions. Generally, the pile design as per static formula should be supplemented by conducting full scale insitu testing preceding construction to validate the geotechnical parameters, computation of safe load, and establishing the criterion for routine tests. Despite, they are exorbitant and cumbersome, they safeguard the cost-effectiveness of substructure. Indeed, design should be validated by full scale testing when safe load surplus of theoretical capacity is adopted. In the present study, an anchored reaction beam setup was used which draws the required reaction from four temporary anchor piles for applying load on pile head using a hydraulic system. The load settlement data was recorded and interpreted using various methods namely, De Beer's (1968), Double tangent (Hirany and Kulhawy 1988), and IS 2911(Part-4): 2013 for computation of safe load.

2 Project Description and Subsoil Profile

National Highways Authority of India (NHAI) entrusted in the development of highways and expressways across the nation undertake the project Construction of Eight Lane Dwarka Expressway (NH-248BB) Package-III of 10.2 km length from 9.50 to 19.70 km from Delhi-Haryana border to Basai Road over Bridge. For substructure, bored cast insitu piles were recommended. As a part of the sub-surface investigation and to observe, identify and study the nature of sub-soil conditions of the project location, geotechnical investigation was carried conformity with IS: 1892–1979. Mechanical shell and auger were used for drilling boreholes using 150 mm casing and bentonite slurry to prevent caving off sides of boreholes pursuant the prevailing soil conditions. Standard Penetration Tests were performed with 1.50 m spacing starting from 1.0 m depth conformity with IS: 2131–1981. Undisturbed samples were gathered by means of 450 mm height and 100 mm diameter mild steel tubes at every 3.0 m interval starting from 0.50 m depth conformity with IS: 2132–1986. A total of 133 nos. of boreholes (BH) were drilled at selected locations up to a depth of 45 m below existing ground level (EGL) nearby the proposed structural elements (piers) of the elevated corridor portion and is depicted in Fig. 1.

In light of the geotechnical examination, the summed-up stratigraphy at the proposed site is furnished below:

Stratum-1 Non-Plastic Sandy Silt/Silty Sand/ Silty Gravel (ML/SM/GM)

Stratum-2 Sandy Clay/Silty Clay of low to medium plasticity (ML-CL/CL/CI)

The typical bore logs for the project stretch is shown in Fig. 2.

The prevailing subsoil conditions at test pile location based on reference borehole (BH-P153) are presented in Table 1.

For design purpose, ground water table is assumed nearby pile cutoff elevation to account for seasonal fluctuations of water table level. Pile foundation was intended for bearing the superstructure with geometry of 1200 mm diameter and 27 m length.

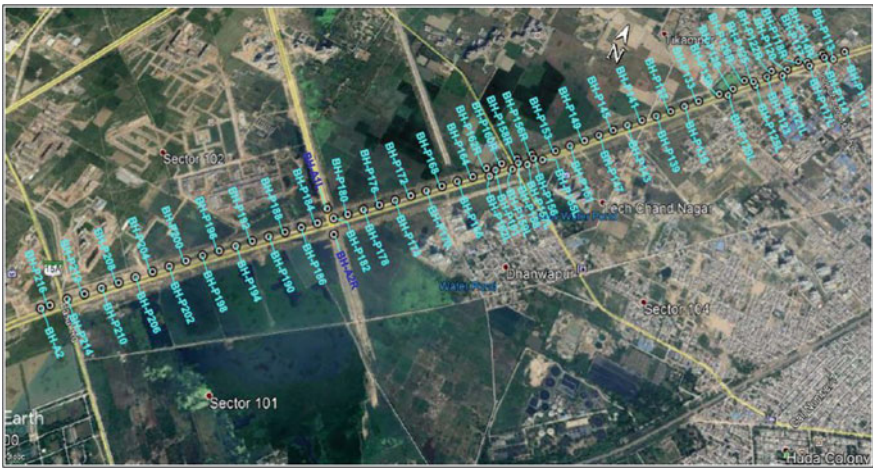

Fig. 1 Typical borehole location google image

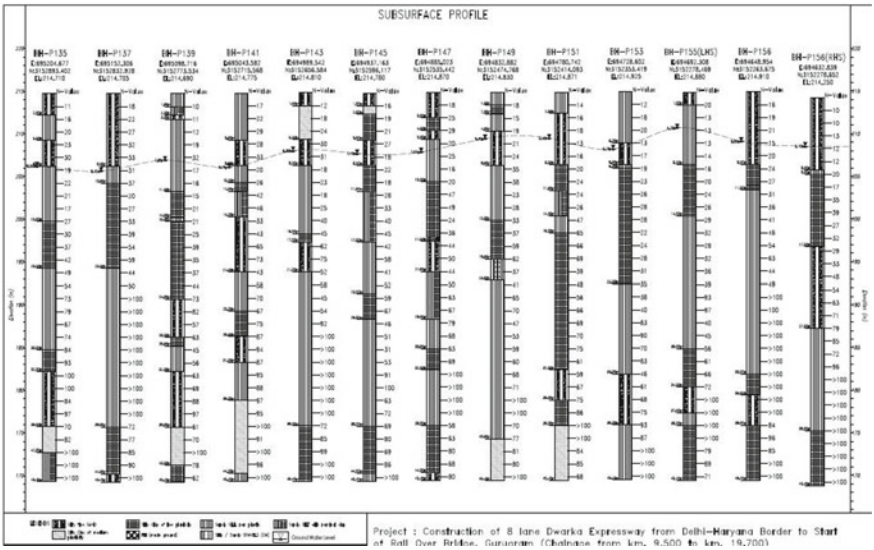

Fig. 2 Typical borelogs

Accordingly, pile capacity computed from static formula conformity with IS 2911 (Part 1/Sec 2): 2010 based on reference borehole works out as 650 Tonnes. To verify this capacity, it was recommended to conduct an Initial test on a test pile as per codal provisions.

Table 1 Subsoil profile at test pile location

Depth (from) m	Depth (to) m	Soil classification	Angle of internal friction (deg)	Cohesion (kPa)	Unit weight (kN/m^3)
0	5.50	ML	28.8	0	18.0
5.50	6.0	ML	29.4	0	18.4
6.0	8.50	SM	29.4	0	18.4
8.50	9.0	ML	30.5	0	19.4
9.0	18.0	CL	0	126	19.9
18.0	22.50	ML	30.0	0	19.9
22.50	27.0	ML	30.3	0	19.9
27.0	33.0	ML	31.0	0	19.9
33.0	39.0	SM	34.0	0	20.0
39.0	46.0	ML	34.0	0	20.0

3 Test Equipment

The setup comprises of a hydraulic jack, main beam, reaction beam, test pile, anchor piles, bearing plate, and dial gauges as depicted in the Fig. 3. The test was conducted on the casted M40 grade pile of 1200 mm diameter and 27 m length conformity with IS 2911(Part-4): 2013. The test pile was installed using similar construction methodology, same type of equipment as that of working piles. A static compression maintained load test was executed upon 28 days from the date of casting.

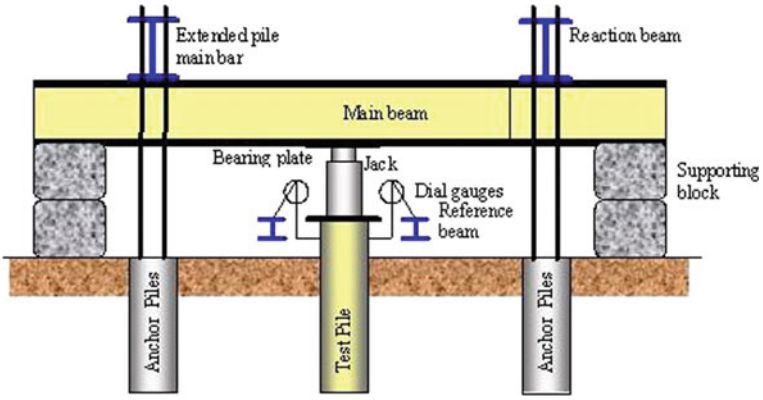

Fig. 3 Schematic setup of load test

Fig. 4 Anchored reaction beam setup

3.1 Anchor Pile Design

For the vertical load test, the required reaction for the test has been derived through 4 nos. of reaction piles as illustrated in Fig. 4. A spacing of three times the diameter of the test pile was kept between center to center distance of anchor and test piles. Anchor piles have been treated as temporary piles and pile length is worked out considering the factored skin friction resistance plus self-weight of the pile.

A total of 25% more than the test load has been made available as a reaction for the load test as per codal provisions. Accordingly, considering 4 nos. reaction piles, the load on each reaction pile is $1.25 \times (1625)/4 = 507$ tons; It was recommended to cast the equivalent length of test pile i.e. 27 m. The position of test pile accompanied by reaction piles, reference borehole in the project stretch is shown in Fig. 5.

3.2 Components of Test Setup

A hydraulic driven siphon having a potential of 2950 Tonnes was employed to deliver load on the test pile with the aid of jack configuration. A total of 6 nos. of rams were used for load test in the present study and the same is depicted in Fig. 6. A bearing plate and hydraulic jacks have been accommodated in the void amid the bottom of main beam and crest of pile head. The reaction beam which is in contact with the main beam transfers the load to anchor piles. As a result, anchor piles experience uplift force and therefore test pile undergo compression. Anchor piles have been coupled to the reaction beam using extended pile main bars which were designed

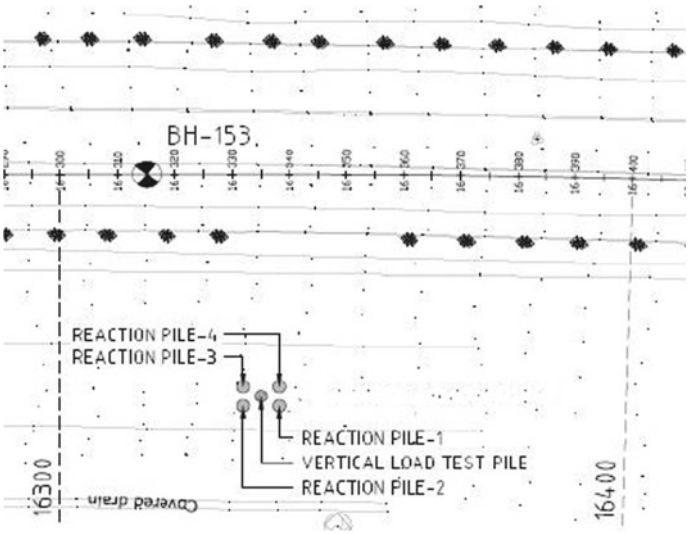

Fig. 5 Test pile location

Fig. 6 Hydraulic jack configuration

Table 2 Pile geometry and load test details

Dia of pile (mm)	Type of pile	Length below COL (m)	Working load (T)	Test load (T)
1200	Bored cast insitu	27	650	1625

to cater sufficient capacity to avoid slippage, or unwarranted deformation under test load. Four dial gauges each having 100 mm travel with 0.01 mm precision were installed to record the settlement during the test.

4 Methodology

The test pile head was chipped off to a flat level and the protruding reinforcement was cut-off and leveled with cement plaster. Six hydraulic jacks of 2950 Tonnes capacity were rested over the bearing plate as shown in Fig. 6 subsequent to attainment of required pile strength. Four number of anchor piles were casted similar to that of the test pile and reinforcement of anchor piles were tightly interlocked with reaction beam resulting net tension in anchor pile to impart the main beam adequate reaction capacity. The jack was coupled to siphon which was equipped with a force measure for noting the values. The test was started with 20% increments of the test load which was about two and half times of estimated safe load. Each increment has been kept till the settlement rate was less than 2 mm/hr or until 2 h had passed, whichever was earlier subjected to a least of 1 h. Upon, attaining the final test load, it shall be sustained minimum 24 h before recording the last value. Pile geometry and load test details are presented in Table 2.

5 Result and Discussion

The recorded data is represented in graphical form with load as abscissa and settlement as ordinate for computing of safe load as depicted in Fig. 7. The initial segment of the curve tends to be linear, until the full mobilization of skin friction, thereafter curve exhibits non-linear behavior. It is observed that pile has reached 10% of settlement before final test load i.e., 1625 Tonnes. Accordingly, a total settlement of 134.8 mm is recorded after 24 h of maintaining load of 1314 Tonnes as stipulated in codal provision.

Conformity with IS 2911(Part-4): 2013, Clause 7.1.5, for vertical load test on a large diameter pile the safe load should be minimum of the succeeding:

(a) $\frac{2}{3}$ of the load corresponds a total settlement of 18 mm or a peak of 2% of pile diameter (2013).

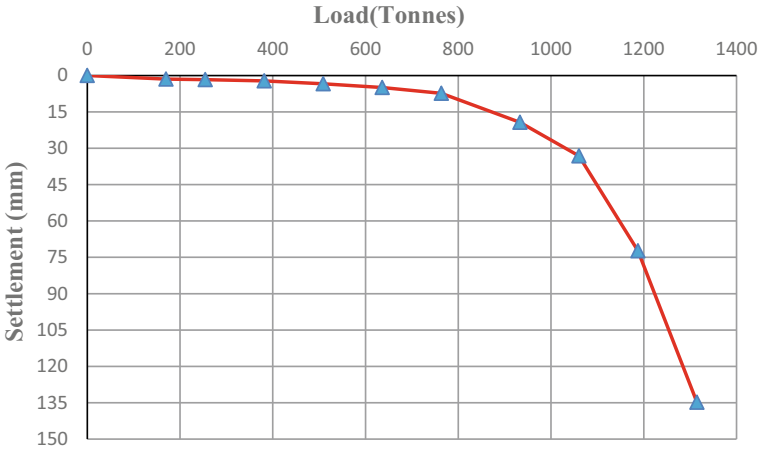

Fig. 7 Load versus settlement curve

- Load corresponds to 18 mm settlement from Fig. 7 equal to 900 Tonnes; (2/3) × 900 works out as 600 Tonnes.
- Load corresponds to 2% of pile diameter i.e., 24 mm equal to 960 Tonnes.

(b) 50% of the load corresponds a total settlement of 10% of the pile diameter (IS: 2013).

- 10% of pile diameter equal to 120 mm; load corresponds to 120 mm settlement from Fig. 7 yields 1280 Tonnes; 50% of 1280 Tonnes equal to 640 Tonnes.

Least of (a) and (b) works out as 600 Tonnes. Therefore, the final safe load obtained from the above interpretation is 600 Tonnes and is presented in Table 3.

The computed ultimate load of the pile using the following approaches i.e., De Beer's (1968) yield load criterion (Beer 1968), Double tangent method (Hirany and Kulhawy 1988), and IS 2911(Part-4): 2013, is furnished in Table 4. For ascertaining the ultimate load conformity with IS 2911(Part-4): 2013, a factor of 1.50 has been

Table 3 Safe load of the pile

Method	Safe load (Tonnes)
IS 2911(Part-4): 2013	600

Table 4 Ultimate load of the pile

Method	Ultimate load (Tonnes)
Dee Beer (1968)	800
Double Tangent	1040
IS 2911 (Part-4): 2013	900

considered on worked out safe load. In line with double tangent approach, two tangents were drawn from starting and latter straight-line segment of arc as depicted in Fig. 8 and intersection point of these lines yields the ultimate load.

Conformity with De Beer's (1968) criterion, recorded data is represented in log–log graph with load as abscissa and settlement as ordinate and the juncture point of two segments yields the ultimate load as illustrated in Fig. 9.

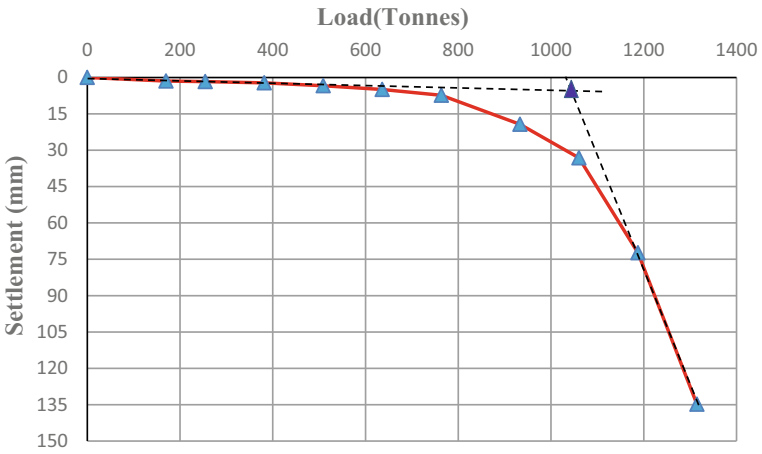

Fig. 8 Double tangent method

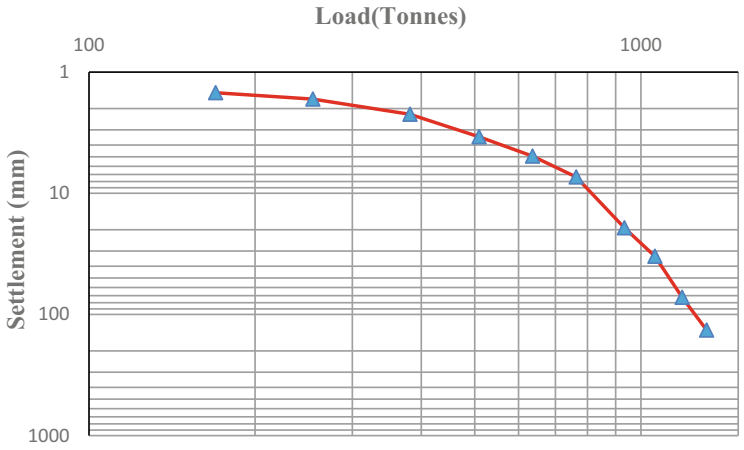

Fig. 9 Dee Beer yield load method

6 Conclusion

In-situ full scale maintained vertical load test is conducted on the test pile of 1200 mm diameter and 27 m length for the proposed project of Eight Lane Dwarka Expressway from Delhi-Haryana border to Basai Road over Bridge to ascertain the safe load. The recommended safe load of the pile is 600 Tonnes conformity with IS 2911(Part-4): 2013 and the ultimate load is 800 Tonnes, which is least of all methods furnished in Table 4.

Acknowledgements Authors are thankful to Associate Project Consultant, N. Shashanka Reddy, L&T Infrastructure Engineering Ltd, for providing the required data and valuable suggestions towards improving the quality of the manuscript.

References

De Beer EE (1968) Proefondervindlijkebijdrage tot de studie van het grensdraagvermogen van zandonderfunderingen op staal. Tijdshift der OpenbarVerken van Belgie, No. 6, (1967) and No. 4, 5, and 6

Hirany A, Kulhawy FH (1988) Conduct and interpretation of load tests on drilled shaft foundations: volume 1, detailed guidelines. Electric Power Research Institute, Palo Alto, CA (USA)

IS: 1892–1979. Code of practice for subsurface investigation for foundations

IS: 2131–1981. Method for standard penetration test for soils

IS: 2132–1986. Code of practice for thin walled tube sampling of soils

IS: 2911 (Part 1/Sec 2) (2010) Code of practice for design and construction of pile foundations-Bored cast in-situ concrete piles

IS: 2911 (Part 4) (2013) Code of practice for design and construction of pile foundations—Load tests on piles

Sustainable Solutions for Urban Public Transportation: A Case Study

Harish L. Reddy and Pradeepta Kumar Samanta

Abstract Urban areas are significant components for any developing and developed countries. Urban areas provide livelihood for majority of the country's population. Various service and manufacturing sectors concentrate in and around the urban areas. Numerous markets operate within the urban areas. Urban areas require efficient and sustainable transportation systems to enable the people to move for their needs and also to connect markets for transportation of goods. The public transportation in urban areas is mainly run by state governments and is meant to cater for majority of the general public. It is seen from various studies that for an urban area to have sustainable transportation system, emphasis has to be given to public transportation while limiting the use of private transportation. The present study investigates into the problems affecting public transportation in an urban area and finds solutions for improvement and also sets the direction for moving towards sustainable transportation system. Pune city is taken up as a case for studying urban transportation problems. A questionnaire survey was carried out among various commuters in Pune city. The survey was aimed to find the problems faced by the general public and which factors influence them to choose private transportation over public transportation. A total of 1180 responses were collected from residents of Pune city. The responses were subjected to descriptive analysis and reliability and validity tests. An exploratory factor analysis on the response data revealed nine key factors in choosing between public transportation and private transportation. The factors were (1) service between home and work, (2) Flexibility in travel, (3) Doorstep availability, (4) Minimal stops or delay, (5) Clear fare structure, (6) Easy to arrange transport, (7) Maintenance or quality, (8) Safety in travel and (9) Social status. Some of these factors can be addressed and resolved to improve the sustainability of public transportation. Whilst

H. L. Reddy
School of Construction Management, National Institute of Construction Management and Research (NICMAR), Pune, India
e-mail: hreddy@nicmar.ac.in

P. K. Samanta (✉)
School of General Management, National Institute of Construction Management and Research (NICMAR), Pune, India

B. B. Das et al. (eds.), *Recent Developments in Sustainable Infrastructure (ICRDSI-2020)—GEO-TRA-ENV-WRM*, Lecture Notes in Civil Engineering 207,
https://doi.org/10.1007/978-981-16-7509-6_49

some factors such as doorstep availability and flexibility in travel are distant possibilities of the future. Thus, this study finds key factors for the government departments to focus on improving urban public transportation and providing sustainability for the future.

Keywords Urban transportation · Sustainability · Factor analysis · Public transportation

1 Introduction

India as a country has many hurdles to overcome in its journey towards transforming from a developing country into a developed country. For one sector to flourish it is equally important for its supporting sectors to improve as well. The Indian transportation sector being large and diverse has been growing enormously catering needs of more than 1.3 billion people. Along with the movement of goods from one place to another, the urban transportation in India also plays a role in reduction of poverty by improving access to labour markets. Services and manufacturing sectors particularly concentrate around urban areas thus they require efficient and low cost transport systems to enable the workers to move and to connect them.

Urban public transportation includes the buses and metros run by the state government for conveyance of general public and private transportation include buses, taxis and autos run and administrated by private companies or individuals running their two wheelers and cars. There are various factors which might influence how an individual chooses whether to go for public or private transportation. It is by far considered by many experts and leading researchers that for transportation system to be sustainable there should be full emphasis on public transportation while discouraging the use of private transportation. Keeping this in mind, this research focuses on which influences the general public in choosing private transportation over public transportation. Also, to understand the expectations of the general public from public transportation thereby enabling arrival at solutions to reverse the choice of private transportation over public transportation.

2 Literature Review

Many peer reviewed research articles, newspaper articles, government publications and standards released by authoritative bodies were referred to understand the state of the art in public transportation.

Ranganathan (2003) in his report points out that urban transport is an important sector in the sustainable development of urban areas. Inadequate urban transport leads to a number of problems. First is congestion and delays, second problem is

accidents, third problem he has stated is that of pollution in cities and fourth problem is resources consumption like use of land, energy and capital etc.

Chopra (2003) points out that there has been a massive induction of personalized vehicles in all 23 urban areas in the country. As a result of this, the congestion on roads is increasing. He also mentions that a large scale of parking vehicles on road has not only reduced traffic capacity of existing roads but also has created safety problems as well. The author also mentions in his article that privatization of urban transportation would not release the pressure on the Government to allocate the capital resources for state run buses. He also recommends that public transport should attract car users and other personalized and hired mode of transport, by giving amenities in the form of bus terminals, queue shelters and suitable information system like display of route maps, time table etc.

Singh (1997) points out that the traffic in big cities is in a mess; the bigger a city, the greater the mess. According to the author following are some traffic congestion causes are private autos, Modern business and living styles, vast amounts of goods are needed to service a relatively high consumption urban population, Faulty city planning, Bad or inconsiderate driving and unsatisfactory or inadequate public transport.

Tripta (2003) presents a comparative study of assessment of the quality of service provided by private and public bus transport in Delhi. The study revealed that private buses are better than public buses in respect of service accessibility and reliability. Also, public buses have been rated better than private buses on safety service, information, comfort, convenience and journey time. The author has also stated that it is necessary to conduct periodical surveys to study the bus transport system in order to get the feedback from public for further improvement of the services.

Nandogopal and Chinnaiyan (2003) explained the-benefits of mini bus to commuters and owners. It was found that mini bus scheme is the solution to cover unserved area. Many of rural commuters can be benefited by mini bus scheme. And on the downside mini bus operators were not satisfied on the point of profit. Poor road condition higher fuel consumption and high maintenance cost were the major problems expressed by the owners.

3 Methodology

The methodology of this study is mainly focussed to acquire and analyze data from the regular commuters of Pune city, regarding the problems they face in public transportation and reasons behind increased preference towards private mode of transportation. A questionnaire survey was designed to collect information from the commuters of Pune city. A portion of the city, the Aundh-Baner-Balewadi (ABB) region was chosen as the sampling site for carrying out the survey. The sample size was found using Eq. (1). A total of 1180 responses were required for the survey, distributed uniformly across the survey area.

$$\text{Sample Size} = N = \frac{\left[Z^2 * P * (1 - p)\right]}{e^2} \quad (1)$$

wherein, 'e' is the desired level of precision (i.e. the margin of error),

'p' is the (estimated) proportion of the population which has the attribute in question.

The survey questionnaire was designed to capture information regarding following themes:

1. What will be the percentage of commuters using private mode of transportation and public transportation?
2. What are the reasons for opting to a particular mode of transportation?
3. Are there any problems faced while using public transportation?
4. What are parameters which commuters prefer while travelling?

The responses were analysed for completeness and completed responses were initially subjected to descriptive statistics. Exploratory factor analysis was then carried out on the responses. The Kaiser-Mayer-Olkin (KMO) test was administered for measure of sampling adequacy. This test provides for minimum standard to proceed for Factor analysis. Bartlett's test of sphericity provides for the validity of Factor analysis. Factor analysis looks for variables that correlate highly with a group of other variables, but correlate very badly with variables outside that group. This will find the underlying factors in commuter behaviour for choosing private transportation over public transportation.

4 Analysis of Data and Findings

A total of 1180 responses were collected from commuters in the Pune city. Among these responses, 101 were rejected because of errors in the response and remaining 1079 responses were considered for further analysis. Descriptive statistical analysis were carried out on the responses. The following sections summarize the results.

4.1 Descriptive Statistics

Table 1 shows the distribution of age of respondents. It is found that commuters in the age group of 15–45 make up for 77.6% of the total sample of commuters. This mostly includes college students and working professionals who rely on public transportation for their travel needs.

Table 2 shows the marital status of the respondents. The table shows that there is nearly equal distribution of single and married respondents among the sample.

Table 3 shows the working status of respondents. While students make up for

Table 1 Age group distribution of respondents

Age group	Frequency	Percent	Cumulative percent
15–25	344	31.9	31.9
25–35	276	25.6	57.5
35–45	217	20.1	77.6
45–55	176	16.3	93.9
55–65	49	4.5	98.4
>65	17	1.6	100
Total	1079	100	100

Table 2 Marital status of respondents

Marital status	No. of respondents	Percent	Cumulative percent
Single	473	43.8	43.8
Married	606	56.2	100.0
Total	1079	100.0	100.0

Table 3 Working status of respondents

Working status	No. of respondents	Percent	Cumulative percent
Student	397	36.8	36.8
Housewife	178	16.5	53.3
Employed	255	23.6	76.9
Others	249	23.1	100.0
Total	1079	100.0	100.0

36.8% of commuters, there is also 23.6% of employed professionals and 16.5% of house wives or homemakers. There is another 23.1% of commuters who are traveling for purposes such as businesses or contract works or for going out of station.

Table 4 shows the income range of the respondents. Nearly half of the respondents declined to disclose their income range, 40.2% of respondents were in the range of 1–7 lakh. There is very small percentage of respondents in the higher income category using public transportation for their travel needs.

Table 4 Annual income of respondents

Income range	Frequency	Percent	Cumulative percent
Undisclosed	511	47.4	47.4
1–5 lac	179	16.6	63.9
5–7 lac	255	23.6	87.6
>7 lac	134	12.4	100.0
Total	1079	100.0	100.0

Table 5 Primary mode of transportation

Transportation mode	No. of respondents	Percent	Cumulative percent
Public transport	386	35.8	35.8
Private vehicle/taxi	451	41.8	77.6
Other modes	242	22.4	100.0
Total	1079	100.0	100.0

Table 6 Frequency of travel in public transport

Travel frequency	No. of respondents	Percent	Cumulative percent
Daily	265	24.6	24.6
Weekly	223	20.7	45.2
Monthly	155	14.4	59.6
Occasionally	202	18.7	78.3
Rarely	234	21.7	100.0
Total	1079	100.0	100.0

Table 5 shows the primary mode of transport chosen by the respondents. The table shows that only 35.8% of respondents use bus as their primary mode of transport while the remaining respondents have the option to choose either bus or any other private mode of transport for their travel needs.

Table 6 shows the frequency of travel by the respondents. Nearly half of the respondents are occasionally using public transport for travel needs.

Table 7 shows the frequency of bus service in the selected area. Table shows that the bus service in the area is not as expected by the public. There are some parts, mainly in the outskirts which are not fully connected and serviced by the public transport. This reduces the frequency of bus service to these areas and can have negative consequences.

Table 7 Frequency of bus service

Frequency of bus service	No. of respondents	Percent	Cumulative percent
High	445	41.2	41.2
Low	634	58.8	100.0
Total	1079	100.0	100.0

4.2 Relative Importance Index (RII)

RII was used to rank the key service parameters (KSP's) influencing private and public transportation. The Rank of each parameter was found using Eq. (2), wherein W is the weight assigned by each respondent on a scale of 1–5, A is the highest weight and N is the total number of sample. The parameters are then arranged according to their rank as shown in Tables 8 and 9.

$$RII = \sum \frac{W}{A * N} \tag{2}$$

Table 8 shows the ranking of key service parameters rated for the public transportation system. The responses state that most of the service parameters are held important by the respondents. Similar observations can be made from Table 9 showing

Table 8 Rating of key service parameters for public transportation

Factors	No. of respondents					Mean of scores	RII
	1	2	3	4	5		
Safety during travel	8	44	257	406	364	3.99	0.80
Clear fare structure	11	68	279	475	246	3.81	0.76
Easy to arrange	12	71	274	497	225	3.79	0.76
Maintenance of system	29	89	270	434	257	3.74	0.75
Flexibility of travel	11	65	370	478	195	3.65	0.74
Service from work to home	31	78	357	388	225	3.64	0.73
Door step availability	15	79	382	414	189	3.63	0.73
Number of stops	17	91	355	441	175	3.61	0.72
Social status of system	101	102	275	341	260	3.52	0.70

Table 9 Rating of key service parameters for private transportation

Factors	No. of respondents					Mean of scores	RII
	1	2	3	4	5		
Safety	6	26	149	388	510	4.26	0.85
Clear fare structure	13	49	168	433	416	4.1	0.82
Very few stops	7	43	199	424	406	4.09	0.82
Maintenance	10	44	199	411	415	4.09	0.82
Easy to arrange	10	49	189	420	411	4.09	0.82
Social status	50	55	164	328	482	4.05	0.81
Service from work to home	12	47	234	457	329	3.97	0.79
Flexibility	11	43	233	504	288	3.94	0.79
Door step availability	9	28	2106	443	383	4.08	0.68

Table 10 Rating of bus services and bus stations

Factors	No. of respondents					Mean of scores	RII
	1	2	3	4	5		
Friendly customer service	112	280	393	240	54	2.86	0.57
Clear and helpful communication	102	310	394	240	33	2.81	0.56
Timely service	93	342	390	227	27	2.77	0.55
Ease in booking service	116	336	396	189	42	2.73	0.55
Error free time table	136	367	376	161	39	2.63	0.53
Arrival on time	127	399	361	157	35	2.61	0.52
Never breaking down of bus	134	388	376	142	39	2.6	0.52
Adequate resources	158	419	351	111	40	2.5	0.50
Attractive bus stop	123	507	302	125	22	2.46	0.49
Equipped with modern technology	155	496	304	93	31	2.4	0.48

ranking of key service parameters for the private transportation. This only indicates that satisfying one or two parameters is not sufficient to increase occupancy in public transportation. All the factors have more or less equal importance and the authorities should give importance to all the service parameters.

Table 10 shows the rating of existing bus service and bus stations by the respondents. It can be seen from the table that almost all of the service parameters have been given very low rating by the respondents. This indicates general low level of quality and dissatisfaction experienced by the commuters in public transportation systems.

4.3 Exploratory Factor Analysis

Table 11 shows the grouping of responses into six factors. These six factors explain a total variance of 59.68% for the preference of public towards private transportation. The Eigen values of these six factors are greater than one. Kaiser-Mayer-Olkin (KMO) test result was 0.841 indicating the sample was adequate for factor analysis. The Bartlett's test of sphericity value as shown in table proves the validity of factor analysis.

The six factors are named as stated below.

Factor 1: Hassle free travel
Factor 2: Punctuality
Factor 3: User specific services
Factor 4: Social status and safety

Table 11 Results of exploratory factor analysis (N = 1079)

Parameters	Factor 1	Factor 2	Factor 3	Factor 4	Factor 5	Factor 6
Easy to arrange	0.792					
Safety	0.771					
Very few stop	0.759					
Clear fare	0.757					
Maintenance	0.722					
Never break down		0.839				
Bus always arrive on time		0.759				
Error free timetable		0.702				
Marital status			0.872			
Working status			0.856			
Age group			0.849			
Annual income			0.774			
Safety				0.747		
Social status				0.636		
Communication clear and helpful					0.903	
Willing to help					0.837	
Service from work to home						0.936
Flexibility						0.807
% Variance Explained	**20.00**	**14.61**	**8.28**	**6.49**	**5.72**	**4.58**
Cumulative Variance Explained	**20.00**	**34.61**	**42.89**	**49.38**	**55.1**	**59.68**
Eigen Values	**7.00**	**5.11**	**2.90**	**2.27**	**2.00**	**1.61**
KMO = 0.841, Bartlett's Test of Sphericity $\chi^2 = 20{,}430.02$, $p < 0.001$						
Extraction Method Principal Component Analysis						

Factor 5: Friendly customer service
Factor 6: Flexibility in Travel.

5 Conclusions

The study finds six factors namely, Hassle free travel, Punctuality, User specific services, Social status and safety; Friendly customer service and Flexibility in Travel influence the choice of commuters towards private mode of transportation. These factors are very well covered and addressed by taxi operators such as uber and ola and probably is the reason for their increase in market share in transportation.

State transport authorities will now have to upgrade their systems to have customised travel arrangements for different regions of the city. There is need to improve the cleanliness and safety in bus travel. There is general need to upgrade the

social status and image of buses and the authorities will have to introduce multiple grade of buses to satisfy the commuter expectations.

It is reasonable to understand that in spite of several improvements in public transportation, some areas such as door step availability and flexibility of travel timing cannot be improved to compete with private mode of transportation and as such requires more changes in policies and attitude of people towards public transportation.

References

Chopra TS (2003) Emerging transportation scenario in Delhi. Urban transport—a book of reading. CIRT Pune pp 52–63

Goel T (2003) Urban bus transit system in Delhi—an assessment of the quality of service. Urban Transport—A Book of Reading, CIRT Publishers

https://www.pmc.gov.in

Nandgopal R, Chinnaiyan P (2003) Minibus operations in some districts of Tamil Nadu: a case study. Indian J Trans Manag 46:82–89

Ranganathan N (2003) India's urban transport scenario 2021: issues and perspectives in urban transport—a book of reading. CIRT Pune, pp 1–17

Singh M (1997) Traffic crisis in big cities causes and cures. Indian J Trans Manag March pp 78–80

Effect of Plastic Waste on Bituminous Mixture in Flexible Pavement

Setu Shubham, Shivam Kumar Singh, Vishal Kumar, and Sujit Kishor Chakraborty

Abstract For a past few decades, increase in infrastructure development has created pressure on the existing land space for a developing country like India. The exploration of new sites often emphasises the need for improving the existing sites by using appropriate ground improving techniques. A well connected road network is one of the basic infrastructure requirements, which plays a vital role for inter-regional traffic. One of the recent trends practiced for road improvement methods is the use of plastic, which brings into picture polyvinyl chloride (PVC), polyethylene terephthalate (PET or PETE), polypropylene (PP) and high and low density polyethylene (HDPE and LDPE). They offer benefits such as easy availability, eco-friendly, resistance to water and durability. The present study in this paper aims at exploring the possibilities of utilizing plastic for urban as well as rural roads. Plastic products that are very useful but plastic waste disposal has become a problem. The obvious solution to this problem is by recycling it by using it in bituminous pavement construction which results in reduction of permanent deformation by rutting of the pavement. The optimum bitumen content (OBC) was found out to be 5.9% in this research. The plastic was added in the proportions of 2, 4, 6, 8, 10% by weight of bitumen and the experiments conducted for this paper also showed that by addition of 5.5% plastic by weight of bitumen resulted in about 7.1% increase in the indirect tensile strength of modified bitumen.

Keywords Bitumen · Plastic · Road improvement · Indirect tensile strength · Optimum bitumen content

S. Shubham (✉) · S. K. Singh · V. Kumar · S. K. Chakraborty
Department of Civil Engineering, Asansol Engineering College, Asansol, India

B. B. Das et al. (eds.), *Recent Developments in Sustainable Infrastructure (ICRDSI-2020)—GEO-TRA-ENV-WRM*, Lecture Notes in Civil Engineering 207,
https://doi.org/10.1007/978-981-16-7509-6_50

1 Introduction

Bituminous plastic roads are made by the use of plastic added to bitumen or with composites of plastic with other materials used in the flexible pavement construction. The advantages of construction of plastic roads include better strength, better adhesion between aggregates and bitumen and durability characteristics as compared to conventional roads along with better drainage properties which can be very useful in areas of heavy rainfall. Bituminous roads are also preferred in hot and humid climatic conditions due to low temperature susceptibility. The recycling of plastic wastes for use as construction materials is an important part of achieving a sustainable and environmental friendly alternative, especially in construction of roads. The studies on various performance factors of bituminous pavements show that there has been a decline of 3–5 years in the life of the bituminous road with traditional non-modified binders in recent years for which heavy traffic and extreme climatic conditions are responsible. Polymer modified bitumen (PMB) known as higher performance binder, can be used to overcome these problems with ease and can be used to construct strong and durable flexible pavements.

2 Behavior of Non-modified Bitumen

Bitumen is a sticky, black and highly viscous liquid or semi-solid obtained from fractional distillation of crude oil. It is used as a binder in road constructions. The flexible pavement performance can be determined by the properties of the bitumen in continuous phase and the only deformable component. The disadvantages of using plain bitumen as binder are excessive rutting (furrow or track made in the ground made by passage of vehicles), stripping (loss of bond between aggregate and binder), seepage (percolation of water through the surface) and high cost of maintenance. The lower stability of road causes unravelling and flow of the surface. The strength of the conventional bitumen as given by Marshall Stability Value is 11.35KN (Nkanga et al. 2017). The Marshal Stability Value as found in this study is 1403.15 kg which is in accordance with the specified value in IRC: 111–2009. The Indirect Tensile Strength value as found in the experiment for this study is 456.01 kPa.

3 Effect of Addition of Plastic to Bitumen

The use of plastic is important as once it is discarded it becomes a pollutant and its use as a construction material especially in the construction of roads is a very efficient way of recycling it in an environmental friendly way. The disposal of plastic waste materials is a serious problem and waste plastic is burnt for disposal which causes environmental pollution (Chavan 2013). Apart from the modification of the

bituminous mixes for road construction for improved stability, the project aims at utilization of the waste plastic thus contributing to the recycling of accumulating plastic waste. Plastic and bitumen are both petroleum byproducts. When shredded recyclable plastic is added to a bituminous mix it dissolves completely. It functions in the same way as bitumen. A percentage of bitumen is saved and thus there is cost saving. Also, it reduces the stripping of bitumen from aggregates mix is immersed in water. The objective is primary to reduce plastic waste and bituminous plastic roads can incorporate extremely large quantities of plastic waste. It is also economical as compared to plain bitumen mix. The strength of the modified bitumen as given by Marshall Stability Value is 14.03KN–14.80KN (Nkanga et al. 2017). The Marshal Stability Value as found in this study is 3067.43 kg. The Indirect Tensile Strength (IDT) value for modified bituminous mix as found in the experiment for this study is 488.58 kPa. The advantages of using modified bitumen as binder are reduced rutting, reduced stripping, reduced seepage low cost of maintenance and eco-friendly and sustainable alternative.

4 Materials

The following materials have been used in the experiments conducted in this study.

4.1 Bitumen

The grade of bitumen used is A20. The penetration value is 20. Softening point of bitumen is 85 °C. Ductility value is 8.1 cm. Specific Gravity of bitumen is 0.99.

4.2 Aggregates

Crushing value is 11.435%, Impact value is 9.14%, and Los Angeles Abrasion Value is 28.62%, Flakiness Index and Elongation Index respectively are 30.49 and 42.40%. Specific Gravity of aggregates are listed in Table 1.

4.3 Plastic

The plastic used in the experiments for the study is Polyethylene Terephthalate. It is a low density polyethylene (LDPE). Specific gravity of plastic is 1.17. Size of the plastic is 4.75 mm passing and 2.36 mm retained.

Table 1 Specific gravity of aggregates

Sl. No.	Sample	Specific gravity
1	12.5 mm aggregate	2.82
2	10 mm aggregate	2.8
3	4.75 mm aggregate	2.749
4	2.36 mm aggregate	2.724
5	600-micron aggregate	2.69
6	300-micron aggregate	2.575
7	150 mm aggregate	2.518
8	75-micron aggregate	2.5
9	Stone dust (fillers)	2.5

5 Tests and Results

5.1 Tests Conducted on Bitumen

The results of the tests conducted on bitumen is given in the Table 2 (Figs. 1, 2, 3 and 4).

Table 2 Results of the tests conducted

Test results of the tests on bitumen	Plain bitumen	Bitumen with plastic
Penetration value	20	9
Softening point	8 °C	10 °C
Flash and fire point	20 °C, 22 °C	18 °C, 20 °C
Ductility value	8.1 cm	5.3 cm

Fig. 1 Penetration value of bitumen

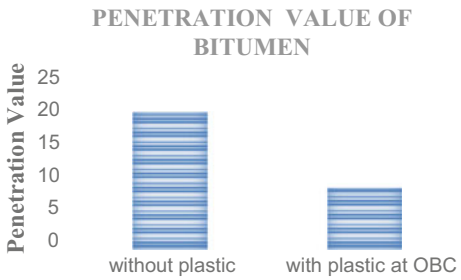

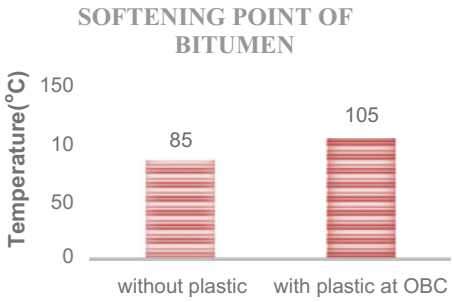

Fig. 2 Softening point of bitumen

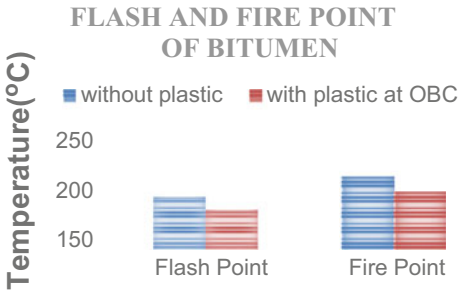

Fig. 3 Flash and fire point of bitumen

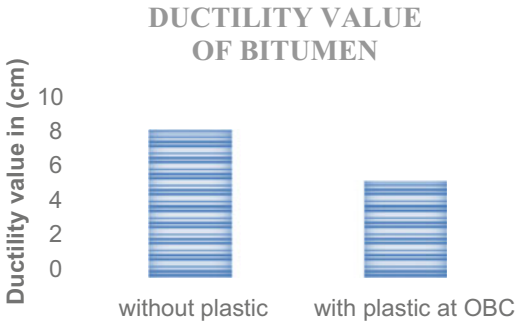

Fig. 4 Ductility value of bitumen

5.1.1 Indirect Tensile Strength (IDT) (ASTM)

IDT strength values are helpful to estimate the resisting against fatigue and rutting. The results of IDT are as given in Table 3.

5.1.2 Marshall Stability Test (IRC: 111-2009)

This test is conducted on compacted cylindrical specimens of bituminous mix of diameter 101.6 mm and thickness 63.5 mm.

Table 3 Results of indirect tensile strength of bitumen

Type of bitumen	Indirect tensile strength (KPa)
Plain bitumen	456.01
Bitumen with plastic of 5.5% at optimum bitumen content of 5.9% by weight as shown in Fig. 5	488.58

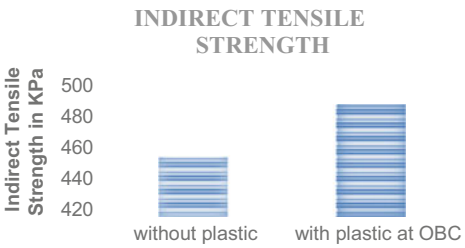

Fig. 5 IDT value of bituminous mix

5.1.3 Optimum Binder Content

Optimum binder content is the average binder content for maximum density, maximum stability and specified percent air voids in the total mix. The resulting graphical figures for all the findings are shown in Figs. 6, 7, 8 and 9 for plain bitumen (Table 4).

From the above graphs optimum bitumen content is found to be 5.9% of the weight of total mix (Figs. 10, 11, 12, 13 and Table 5).

From the Marshall stability test the optimum plastic content is calculated as 5.5% of bitumen content by weight.

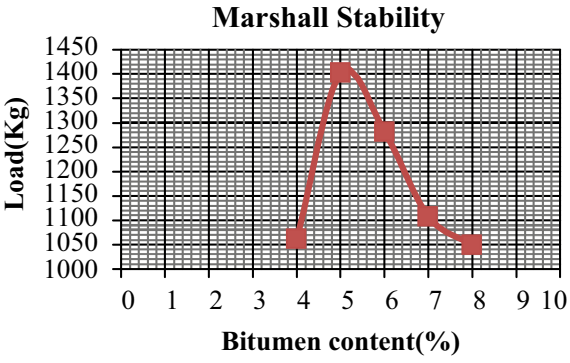

Fig. 6 Marshall stability graph for plain bituminous mix

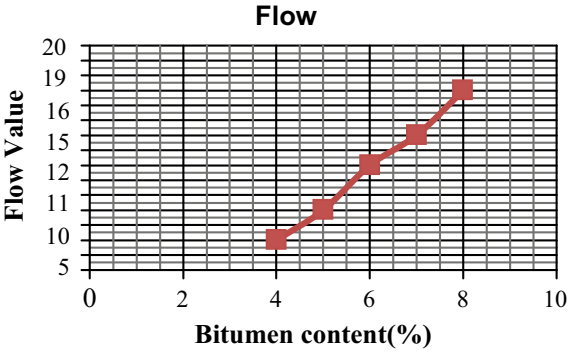

Fig. 7 Flow value graph for plain bituminous mix

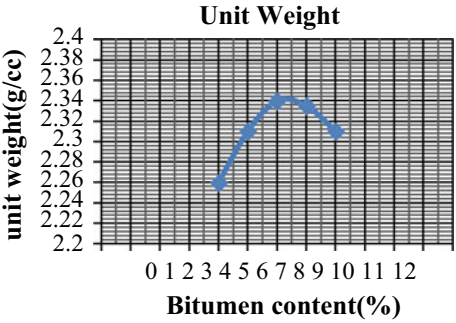

Fig. 8 Unit weight graph for plain bituminous mix

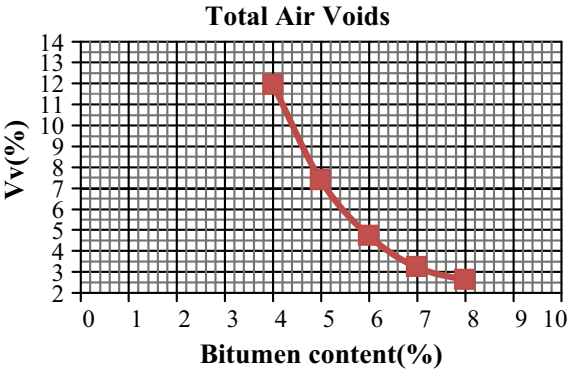

Fig. 9 Air voids graph for plain bituminous mix

Table 4 Marshall stability value for plain bituminous mix

Percentage of bitumen	4%	5%	6%	7%	8%
Stability (kg)	1061.5 0	1403 15	1281.3 7	1107.3 2	1049.0 4
Flow value	7	9	12	14	17
Unit weight (g/cc)	2.26	2.31	2.34	2.33	2.31
Air voids (%)	11.94	7.36	4.70	3.21	2.6

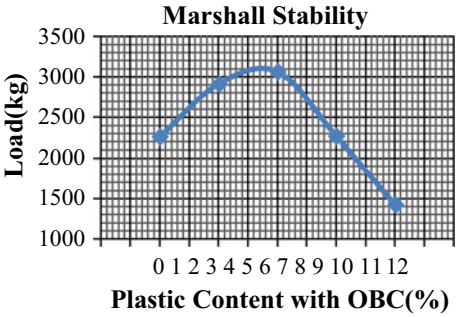

Fig. 10 Marshall stability graph for bituminous mix with plastic

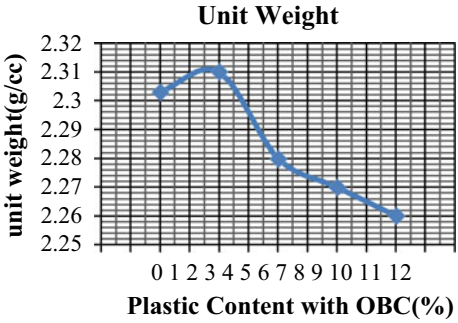

Fig. 11 Unit weight graph for bituminous mix with plastic

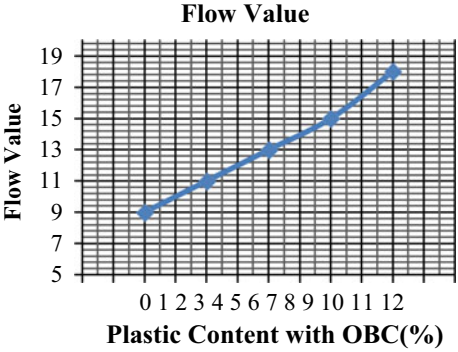

Fig. 12 Flow value graph for bituminous mix with plastic

Grain Size Analysis of Aggregates for Optimum Bitumen Content (OBC) of 5.9% by Weight of Mix (IS: 2386-PARTII-1963)

It is used to assess the gradation of a granular material. The test results are given in the Table 6 and the distribution is mentioned in Fig. 14.

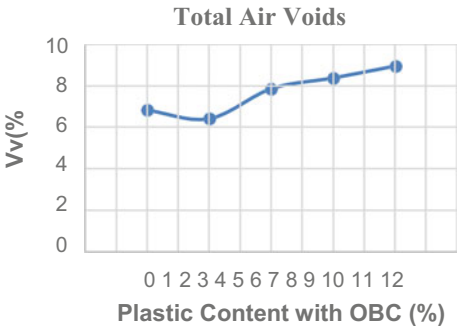

Fig. 13 Total air void graph for bituminous mix with plastic

Table 5 Marshall stability value for bituminous mix with plastic

Percentage of plastic at OBC	2%	4%	6%	8%	10%
Stability (kg)	2258.56	2913.35	3067.43	2268.64	1426.37
Flow value	9	11	13	15	18
Unit weight (g/cc)	2.3	2.31	2.28	2.27	2.26
Air voids (%)	6.82	6.4	7.85	8.37	8.94

Table 6 Grain size analysis of aggregates for optimum bitumen content (OBC) of 5.9% by weight of mix

Size of sieve (mm)	Weight retained (gm)	Cumulative weight retained (gm)	Cumulative percentage retained (%)	Cumulative percentage passing (%)
12.5	112	112	9.9185264	90.08147
10	196	308	27.275948	72.72405
4.75	255	563	49.858307	50.14169
2.36	169	732	64.824655	35.17535
0.6	191	923	81.739284	18.26072
0.3	55	978	86.609989	13.39001
0.15	59	1037	91.834927	8.165073
0.075	46	1083	95.908608	4.091392
Pan	46.2			
Total	1129.2			

6 Conclusions

The following specific conclusion can be drawn based on the test program for bituminous mix with or without plastic and the effect on stability value, indirect tensile strength value, penetration value, softening point etc. Due to replacement of bitumen with plastic is concluded as:

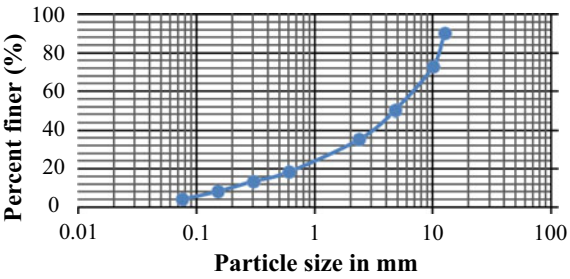

Fig. 14 Grain size analysis for 5.9% bitumen by weight of mix

1. The penetration value of plain and modified bitumen is 20 and 9 respectively.
2. The ductility value of plain and modified bitumen is 8.1 cm and 5.3 cm respectively.
3. The Softening point of plain and modified bitumen is 8 °C and 10°°C respectively.
4. The flash and fire point of plain bitumen is 20 °C and 22 °C respectively. Whereas for modified bitumen it is 18 °C and 20°°C respectively.
5. The optimum bitumen content (OBC) is calculated as 5.9% of the total weight of mix.
6. The optimum plastic content from the Marshall Stability test is calculated as 5.5% of the weight of the bitumen content.
7. The Marshall Stability value of plain and modified bitumen is 1403.15 kg and 3067.432 kg respectively.
8. The indirect tensile strength value of plain and modified bitumen is 456.01 kPa and 488.58 kPa respectively.
9. The crushing strength value of aggregate is 11.435%
10. The impact strength value of aggregate is 9.14%.
11. The Los Angles abrasion value of aggregate is 28.62%.
12. The Flakiness index values of aggregate is 30.49%.
13. The Elongation index value of aggregate is 42.40%.

The conclusions are summarized in the Table 7 as given below.

Table 7 Conclusions

Sl. No.	Properties	Bitumen with plastic	Plain bitumen
1	Marshall stability value	More	Less
2	Binding property	Better	Good
3	Softening point	More	Less
4	Penetration value	Less	More
5	Flash and fire point	Less	More
6	Indirect tensile strength	High	Less
7	Rutting	Less	More
8	Stripping	Less	More
9	Seepage	Less	More
10	Durability	Better	Good
11	Cost	Less	Normal
12	Maintenance	Less	More
13	Environment friendly	Yes	No

References

ASTM D6931–07. Standard test method for indirect tensile strength of bituminous mixture
Chavan AJ (2013) Use of plastic waste in flexible pavements. Int J Appl Innov Eng Manage (IJAIEM) 2(4):540–551
IRC: 111–2009. Specifications for dense graded bituminous mix
IS: 2386-PARTII-1963. Methods of test for aggregates for concrete
Nkanga UJ, Johnson A, Feyisayo V, Obioma U (2017) Characterization of bitumen/plastic blends for flexible pavement application. Procedia, Manuf 7:490–496

Estimating Uncertainty in Flood Frequency Analysis Due to Limited Sample Size Using Bootstrap Method

Tanmaya Kumar Sahoo and Rachita Panda

Abstract The prediction of magnitude of extreme flood events for a given return period is crucial for planning and designing of hydraulic structures. The most common method of estimating design flood value at a site for a given return period is by frequency analysis. As the method is based on the limited historical discharge data, the estimated design flood is associated with uncertainty. This uncertainty is represented by the confidence interval. In this paper, the annual maximum flow series for period 1972–2017 of Anandpur Discharge measuring site in Baitarani basin is fitted to Extreme Value Type-I (EV1) and Log Pearson Type-III (LP3) distribution models. The design flood and confidence interval corresponding to confidence level of 95% is calculated at various return periods using bootstrap method for both the distribution models from the original sample length and derived sub-sample length from original sample. The confidence interval obtained by bootstrap approach are compared with the analytical methods available in the literatures. Results of the study shows that the uncertainty in design flood magnitude estimate is dependent on sample size, sample statistical properties, probability distribution model used and return period considered. The study also suggests that the bootstrap method can be used for uncertainty estimate due to limited sample length.

Keywords Bootstrap method · Design flood · Confidence interval · Extreme value Type-I · Log Pearson Type-III

1 Introduction

Natural calamities like floods have a devastating effect on life and the economy. The structures built over rivers should have to be designed such that the risk of damages due to flood events should be minimum within the design life of the structure. Flood

T. K. Sahoo
Department of Water Resources, Government of Odisha, Bhubaneswar, India

R. Panda (✉)
K.I.I.T., Bhubaneswar, India

B. B. Das et al. (eds.), *Recent Developments in Sustainable Infrastructure (ICRDSI-2020)—GEO-TRA-ENV-WRM*, Lecture Notes in Civil Engineering 207,
https://doi.org/10.1007/978-981-16-7509-6_51

events are random in nature because of lack of information on underlying process generating the event. The Magnitude of a flood event for a given return period (T) is an important parameter in the design of hydraulic structures like bridges, weirs, barrages, dams, etc. The most common method for predictions of the magnitude of a flood event for a given return period (T) is done by frequency analysis. In frequency analysis, historical data are fitted to a probability distribution model for developing the relationship between flood magnitude with its probability of exceedance (=1/T). The most commonly used probability distribution models in flood frequency analysis are Extreme Value Type I (EV-I) and Log Pearson Type-III (LP-III) (Chow et al. 2010; Council 1981; Meylan et al. 2012). The population parameters of the probability distribution model are unknown, it has to be estimated from the available observed data samples. The discharge data used in flood frequency analysis is from the limited period of record, this limited sample size introduces uncertainty in the estimate of a flood magnitude for a given T. Due to this uncertainty, the value of flood magnitude for a given return period T (x_T) instead of a point estimate, should be represented as a range or confidence interval bounded by lower and upper confidence limits. This will give more reliability for design flood magnitude (Kite 1975). It is expected that the true value of x_T lies in the confidence interval for a given confidence level (β). Generally, in water resources engineering β value is taken as 90% or 95%. Researchers have used analytical methods estimating the confidence intervals in flood frequency analysis (Bao et al. 1987; Council 1981; Kite 1975). In analytical methods, an assumption is made on the probability distribution of x_T, based on which the confidence interval is obtained. Due to the parametric nature of this method, it becomes difficult to use, and any inappropriate assumptions or simplification may lead to misleading results (Davison and Hinkley 1997).

Recently, with the improvement in the computational power of computers, bootstrap methods have gained popularity for simplification of statistical computations (Davison and Hinkley 1997; Tibshirani and Efron 1993). Bootstrap is a computer-based statistical random resampling method used for quantile estimation of a random variable without using the knowledge of the underlying probability distribution model. This method has been used in estimation of the confidence intervals for design rainfall/storm events (Mamoon and Rahman 2019; Zucchini and Adamson 1989) and, flood frequency analysis (Hall et al. 2004; Rust et al. 2011; Schendel and Thongwichian 2015). The bootstrap method is flexible and easy to use and can be used with a minimum knowledge of statistics and probability.

In this paper, the effect of sample size and sample characteristics on confidence intervals of flood magnitude for a given T is studied using bootstrap resampling method for confidence level (β) of 95%. Two probability distribution models, i.e. EV-I and LP-III are used as candidate statistical models for flood frequency estimation. The confidence interval obtained from the bootstrap method is compared with the confidence interval derived from analytical methodology available in the literature (Council 1981; Kite 1977).

Table 1 Summary of sample statistics and sample notation

Sample record	Sample notation	Sample size	Coefficient of variation (cov)	Coefficient of skewness (c_s)
1972–2017	S0	46	0.611	0.724
1972–2012	S1	41	0.612	0.719
1972–2007	S2	36	0.576	0.879
1972–2002	S3	31	0.606	0.863

2 Study Area and Data Selection

The main assumption in frequency analysis is that the random variable are independent and identically distributed (Meylan et al. 2012). The annual maximum flood discharge (AMFD) data series satisfies this need, hence AMFD data is used for this study. The AMFD data of Anandpur Discharge measurement site located in Baitarani basin is taken from the Water Year Book published by the Central Water Commission (CWC) (Central Water Commission 2018). The study site is maintained by Central Water Commission and is located at latitude 21.209° N and 86.123° E longitude in the Odisha. The AMFD data for the study site is available from 1972 to 2017. The effect of sample length is studied from the original AMFD sample record of 1972 to 2017 with sub-sample lengths for sample records 1972 to 2012, 1972 to 2007 and 1972 to 2002. The summary of sample statistics and sample notations are given in Table 1.

3 Methodology

3.1 Overview of Methodology

Komogrov-Simrov (KS) tests (Massey Jr 1951) are performed at a significance level (α) of 0.05 on AMFD data samples S0, S1, S2 and S3 to assess the suitability of Extreme Value-I (EV-I) and Log Pearson, Type III distribution (LP-III) as candidate distribution in frequency analysis using the sample data. The flood frequency analysis methodology for EV-I and LP-III probability distribution model is explained in Sect. 3.2. The uncertainty in flood magnitude is estimated at different return periods, for EV-I and LP-III models using analytical and bootstrap methods using the methodology explained in Sects. 3.3 and 3.4 respectively.

3.2 Flood Frequency Analysis

The AMFD with a given return period is expressed as (Chow 1951):

$$x_T = \overline{x} + K_T s_x \tag{1}$$

In case of Log Pearson type-III (LP-III) the logarithmic transformation (y = $\log_{10} x$) is applied to the random variable, the expression of frequency analysis for LP-III is:

$$y_T = \overline{y} + K_T s_y \tag{2}$$

where

x_T AMFD at a return period T
$\overline{x}$ Mean of AMFD series
s_x Standard Deviation of AMFD series
K_T Frequency factor at return period T years.

For EV-I distribution the expression for frequency factor is given by (Chow 1953),

$$K_T = -\frac{6}{\pi}\left[0.5772 + \ln\left\{\ln\left(\frac{T}{1-T}\right)\right\}\right] \tag{3}$$

Approximate method for estimating frequency factor for LP-III distribution is given by (Kite 1977),

$$K_T = z + \left(z^2 - 1\right)k + \frac{1}{3}\left(z^3 - 6z\right)k^2 - \left(z^2 - 1\right)k^3 + zk^4 + \frac{1}{3}k^5 \tag{4}$$

where

z Standard normal variable at exceedance probability p $\left(p = \frac{1}{T}\right)$.
k $\frac{\text{Coefficient of skewness of log transformed variable}}{6}$.

3.3 Analytical Method for Confidence Interval Estimation

For confidence level (β) and significance level (α) is given by

$$\alpha = \frac{1-\beta}{2} \tag{5}$$

The upper and lower confidence limits for EV-I model at significance level (α) and return period (T) is given by (Kite 1977),

$$x_{U,\alpha,T} = x_T + s_e z_\alpha \tag{6}$$

$$x_{L,\alpha,T} = x_T - s_e z_\alpha \tag{7}$$

where

$x_{U,\alpha,T}$ Upper confidence limit at significance level (α) and return period (T)
$x_{L,\alpha,T}$ Lower confidence limit at significance level (α) and return period (T)
z_α Standard normal variable at significance level (α).

The expression for s_e for sample size (n) is given by S,

$$s_e = \left[\frac{1}{n}\left(1 + 1.1396K_T + 1.1000K_T^2\right)\right]^{\frac{1}{2}} s_x \tag{8}$$

For estimating upper and lower confidence limits for LP-III model at significance level (α) and return period (T) approximate method is developed by U.S. Water Resource Council (1981)

$$y_{U,\alpha,T} = \overline{y} + s_y K_{T,\alpha}^U \tag{9}$$

$$y_{L,\alpha,T} = \overline{y} + s_y K_{T,\alpha}^L \tag{10}$$

In which

$$K_{T,\alpha}^U = \frac{K_T + \sqrt{K_T^2 - \left[\left(1 - \frac{z_\alpha^2}{2(n-1)}\right)\left(K_T^2 - \frac{z_\alpha^2}{n}\right)\right]}}{\left(1 - \frac{z_\alpha^2}{2(n-1)}\right)} \tag{11}$$

$$K_{T,\alpha}^L = \frac{K_T - \sqrt{K_T^2 - \left[\left(1 - \frac{z_\alpha^2}{2(n-1)}\right)\left(K_T^2 - \frac{z_\alpha^2}{n}\right)\right]}}{\left(1 - \frac{z_\alpha^2}{2(n-1)}\right)} \tag{12}$$

3.4 Bootstrap Method for Confidence Interval Estimation

Let S is the sample containing n numbers of AMFD data, that is S = {x_1, x_2, … x_n}, where x_1, x_2 …. x_n are AMFD values. The steps for obtaining lower and upper confidence limits (for $\beta = 95\%$) of AMFD for a given T for sample S using bootstrap method are outlined below.

Step 1: Generate 100,000 samples (bootstrap samples) each of size n by random selection of elements from S with replacements.
Step 2: Estimate AMFD for return period (T) for all 100,000 bootstrap samples (using Eq. 1 for EV-I and Eq. 2 for LP-III model).
Step 3: Calculate the 2.5th and 97.5th percentile values using Weibull plotting position formula, which are the lower and upper confidence limits at 95% confidence interval.

The above steps are repeated for all the samples (i.e. S0, S1, S2, and S3) and for both EV-I and LP-III models.

4 Results and Discussions

The K-S test results are summarised in Table 2. It can be seen that all the AMFD samples fit to EV-I and LP-III model at 5% significance level (α). The best model is LP-III for all the samples, but as both the model satisfies the null hypothesis of K-S test, study is done using both the models.

For AMFD sample S0 comparison of uncertainty at 95% confidence interval (CI) by analytical (see Eq. 5–12) and bootstrap method for both the models (EV-I and LP-III) is shown in Fig. 1. It is observed that in both the models with increase in return period (T) the confidence band/interval becomes wider, and confidence band

Table 2 Summary of Kolmogorov–Smirnov (K-S) Test results

Sample	EV-I	LP-III	Critical value $\alpha = 0.05$
S0	0.073	0.058	0.200
S1	0.079	0.072	0.212
S2	0.084	0.081	0.221
S3	0.710	0.694	0.238

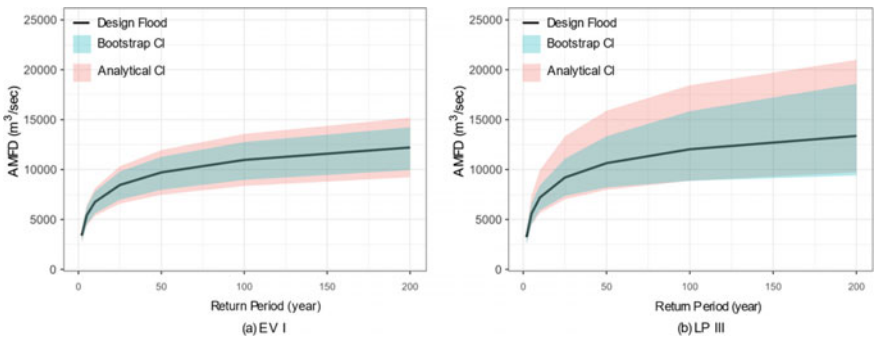

Fig. 1 Confidence band at 95% CI for sample S0 for **a** EV I model, **b** LP III model

estimated by bootstrap method is narrower than the confidence band estimated by analytical method. It can also be seen that in EV-I model the distribution of confidence band about the estimated design flood is fairly symmetric, while the confidence band for LP-III model is skewed towards the upper confidence level (UCL).

The effect of sample size and return period on lower and upper confidence level (LCL and UCL) at 95% confidence interval for return periods (T) 5 year, 50 year and 200 year are tabulated in Tables 3, 4 and 5 respectively. It is observed that in all the cases the confidence range increases with decrease in sample size, for any return period sample S3 has greater confidence range than sample S0. This increase

Table 3 Lower and upper confidence level (LCL and UCL) in m^3/s for return period T = 5 year at 95% confidence interval

Sample	Bootstrap method				Analytical method			
	EV-I model		LP-III model		EV-I model		LP-III model	
	LCL	UCL	LCL	UCL	LCL	UCL	LCL	UCL
S0	4523	6273	4558	6599	4388	6440	4476	7386
S1	4470	6321	4532	6683	4327	6505	4431	7628
S2	4392	6373	4489	6603	4284	6502	4425	7457
S3	4359	6580	4387	6846	4229	6752	4352	7912

Table 4 Lower and upper confidence level (LCL and UCL) in m^3/s for return period T = 50 year at 95% confidence interval

Sample	Bootstrap method				Analytical method			
	EV-I model		LP-III model		EV-I model		LP-III model	
	LCL	UCL	LCL	UCL	LCL	UCL	LCL	UCL
S0	7978	11,279	8210	13,338	7480	11,952	7977	15,894
S1	7864	11,403	8027	13,647	7354	12,101	7842	16,476
S2	7439	11,400	7318	13,165	7090	11,925	7492	15,432
S3	7507	11,888	7597	14,343	7083	12,581	7729	17,917

Table 5 Lower and upper confidence level (LCL and UCL) in m^3/s for return period T = 200 year at 95% confidence interval

Sample	Bootstrap method				Analytical method			
	EV-I model		LP-III model		EV-I model		LP-III model	
	LCL	UCL	LCL	UCL	LCL	UCL	LCL	UCL
S0	9953	14,235	9414	18,597	9238	15,187	9724	20,986
S1	9796	14,401	9026	19,196	9072	15,387	9497	21,672
S2	9168	14,360	8119	18,281	8679	15,111	8975	20,133
S3	9292	15,021	8518	20,807	8694	16,008	9456	24,382

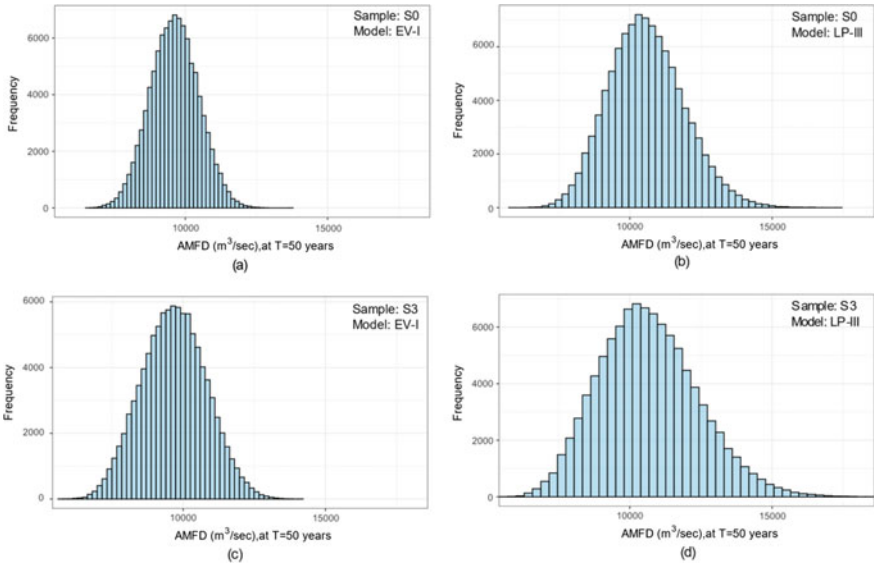

Fig. 2 Histogram of bootstrap sample AMFD in m^3/s at T = 50 year for **a** Sample S0, EV-I model, **b** Sample S0, LP-III model, **c** Sample S3, EV-I model, **d** Sample S3, LP-III model

in confidence range may be due to decrease in sample size and change in sample statistics. It is also seen that the LP-III model is more sensitive to sample size, as the sample size decreases the rate of increase in confidence range is greater for the LP-III model than the EV-I model. In most of the cases the confidence range predicted by analytical method (Eq. 5–12) is greater than that of bootstrap method.

Generally, design of smaller hydraulic structures is done for return period of 50 year. Figure 2 shows the histogram of bootstrap sample AMFD in m^3/sec of sample S0 and S3 for return period 50 year. It is seen that for EV-I model the bootstrap AMFD distribution at T = 50 year is more widely distributed for sample S3. For any sample, LP-III model shows more spread in AMFD, this means the AMFD estimated using LP-III model has more uncertainty associated than EV-I. This may be due to the fact that LP-III model depends on third order moment i.e. coefficient of skewness, which makes it more sensitive to sample size and gives a wider distribution.

5 Conclusions

The results of this study demonstrate that bootstrap method can be utilised for estimating uncertainty due to sample size in flood frequency analysis. It is also concluded that, with decrease in sample size of AMFD data the confidence range increases. The results reveal that at higher return period the uncertainty in estimation of AMFD

is also high. The confidence band estimated using analytical method is wider than confidence band estimated from bootstrap method. Further, it is concluded that uncertainty estimation in LP-III model is more sensitive to sample size than EV-I model. In smaller hydraulic structures where return period of 50 years or less is used for design purpose, uncertainty estimation of AMFD can be done by bootstrap method in replacement of traditional analytical methods.

References

Bao Y, Tung Y, Hasfurther VR (1987) Evaluation of uncertainty in flood magnitude estimator on annual expected damage costs of hydraulic structures. Water Resour Res 23(11):2023–2029

Central Water Commission (2018) Water Year Book (June 2017-May 2018) Baitarani, Subarnarekha & Burhabalang Basin. Ministry of Water Resources, River Development & Ganga Rejuvenation, Government of India

Chow VT (1951) A general formula for hydrologic frequency analysis. EOS Trans Am Geophys Union 32(2):231–237

Chow VT (1953) Frequency analysis of hydrologic data with special application to rainfall intensities. University of Illinois at Urbana Champaign, College of Engineering

Chow VT, Maidment DR, Mays LW (2010) Applied hydrology. Tata McGraw-Hill Education

Council, U. S. W. R. (1981) Guidelines for determining flood flow frequency. Bulletin 17B, US Govt.

Davison AC, Hinkley DV (1997) Bootstrap methods and their application. Cambridge University Press

Hall MJ, Van den Boogaard HFP, Fernando RC, Mynett AE (2004) The construction of confidence intervals for frequency analysis using resampling techniques. Hydrol Earth Syst Sci Discuss 8(2):235–246

Kite GW (1975) Confidence limits for design events. Water Resour Res 11(1):48–53

Kite GW (1977) Frequency and risk analyses in hydrology

Mamoon AA, Rahman A (2019) Uncertainty analysis in design rainfall estimation due to limited data length: a case study in Qatar. Extreme Hydrol Climate Variability 37–45

Massey Jr FJ (1951) The Kolmogorov-Smirnov test for goodness of fit. J Am Stat Assoc 46(253):68–78

Meylan P, Favre AC, Musy A (2012) Predictive hydrology: a frequency analysis approach. CRC Press

Rust HW, Kallache M, Schellnhuber HJ, Kropp J (2011) Confidence intervals for flood return level estimates using a bootstrap approach. Springer, Berlin, pp 61–81

Schendel T, Thongwichian R (2015) Flood frequency analysis: confidence interval estimation by test inversion bootstrapping. Adv Water Resour 83:1–9

Tibshirani RJ, Efron B (1993) An introduction to the bootstrap. Monographs on statistics and applied probability. Chapman and Hall, New York

Zucchini W, Adamson PT (1989) Bootstrap confidence intervals for design storms from exceedance series. Hydrol Sci J 34(1):41–48

Removal of Malachite Green from Spiked Pond Water Using Titanate Nanotubes

Saismrutiranjan Mohanty, Sanjib Moulick, and Sanjoy Kumar Maji

Abstract At room temperature of 25 ± 2 °C, spiked Malachite Green (MG) was tried to remove from pond water collecting from the KISS University on alkaline hydrothermally synthesized titanate nanotubes surfaces (TNTs) at 6.8 ± 0.2 pH using both adsorption and photodegradation techniques with water quality measures. Crystallinity, compositions, size and shapes of TNTs were understood using XRD, SEM/EDX and TEM. The final MG removal from spiked water sample was found to be ~ 98% following both the techniques at an agitation speed of 520 ± 20 rpm. Adsorption of MG on TNT surfaces followed Freundlich isotherm in a better way than the Langmuir isotherm. Adsorptive capacity of TNTs towards MG uptaking was understood from Langmuir adsorption isotherm and was found to be 5.8962 mg/g. Dimensionless equilibrium parameter value ($R_L = 0.0551 < 1$) and the Gibbs free energy changes value ($\Delta G^o = -0.6838$ kJ/mole) suggested that the adsorption process was favorable as well as spontaneous in nature following the pseudo-second order reaction kinetic model. Reuse of the exhausted adsorbent/photocatalyst was evaluated. Adsorption of MG on TNTs surfaces follows neither pore diffusion nor film diffusion. Probable photodegradation mechanism was proposed.

Keywords TNT · Hydrothermal treatment · Malachite green · Adsorption/photodegradation · Spiked dye sample

1 Introduction

Malachite green (MG), a triphenylmethane dye, is popularly used in paper, textile and leather industries. It is a type of non-biodegradable material and causes potential threat to the human reproductive and immune systems (He and Tian 2016). Therefore,

S. Mohanty · S. K. Maji (✉)
Department of Chemistry, School of Applied Sciences, KIIT Deemed to be University, Bhubaneswar, Odisha 751024, India

S. Moulick
School of Civil Engineering, KIIT Deemed to be University, Bhubaneswar, Odisha 751024, India

B. B. Das et al. (eds.), *Recent Developments in Sustainable Infrastructure (ICRDSI-2020)—GEO-TRA-ENV-WRM*, Lecture Notes in Civil Engineering 207,
https://doi.org/10.1007/978-981-16-7509-6_52

the elimination of MG dye from dye wastewater has drawn attention from the international society. There are numerous techniques proposed by the researchers for the dye removal. Flocculation, adsorption, biological treatment, reverse osmosis, photocatalysis and filtration are some commonly used treatment methods for removal of MG dye (Mohamed et al. 2019). We choose adsorption with photodegradation over other technique as adsorption is quite easier process and photodegradation helps to reduce the toxicity level. Commonly used photocatalysts are SnO_2, ZnO, TiO_2 (anatase, P25) etc. The band gaps for ZnO, SnO_2 and TiO_2 are 3.37 eV, 3.6 eV and 3.2 eV respectively. TiO_2 is used more frequently because of its low band gap as it helps in faster electron transfer to molecular oxygen leading to efficient photocatalytic degradation of pollutant. Moreover, TiO_2 is being popularly used due to its low-cost, easy availability, environmental friendly nature and photo-stability. In this present study, an initiative has been taken to remove Malachite green (MG) from aqueous media using synthesized Titanate Nanotube (TNT) (Synthesize from TiO_2 powder).

2 Materials and Methods

Analytical reagent grade chemicals were used in all the experiments. Stock solution of dye, MG (500 mg/L) was made with $C_{23}H_{25}ClN_2$ ($\lambda_{max} = 618$ nm) (Nice Chemicals) and diluted as per the requirement using double distilled water. Commercially available titanium dioxide (TiO_2, ~ 99% pure) was used. Concentrated HNO_3 and HCl, NH_4OH, NaOH, $MgCl_2.6H_2O$, NH_4Cl, 2-methoxy methanol, Erichrome black T were procured from J. T. Baker.

MG concentrations were measured at 618 nm (λ_{max}), using a UV–visible spectrophotometer (Shimadzu, UV-1800, Japan). Experimental apparatus used were cleaned properly using tap water followed by double distilled water after dilute acid treatment. A digital pH meter (Wensar, WPH-10) was used to measure the pH of the solutions. Weights were measured using Sartorius electronic balance, BSA224S-CW. Powder XRD analysis was conducted by means of an X-ray diffractometer (Shimazdu XRD 6100) with a Cu Kα radiation of wavelength $\lambda = 0.15406$ nm in the scan range $2\theta = 20°–80°$ (data acquisition rate of 0.033° per step) to understand the phase of the synthetic precursors. FEI-SEM (Apreo LoVac) was employed for SEM/EDX studies. TEM analysis was performed using JEM-1400, JEOL, Japan, at 120 kV. A hand-made UV-light (360 nm of 18 W, UV-C, make: Germany) set-up was used for the photodegradation of dye. The experimental arrangement was enclosed with a black textile to evade the radiation of harmful UV rays to the surroundings (Fig. 1).

The purchased TiO_2 powder (25 g) was blended with 100 mL of 10 M NaOH solution in a beaker and allowed to stir for 1 h placing on a magnetic stirrer (electrically operated, Remi, 2MLH) at 520–540 rpm to make a homogeneous suspension. The mixture was then hydrothermally treated using the Teflon-lined stainless-steel autoclave at temperature of 150 °C for 24 h to achieve the complete reaction between

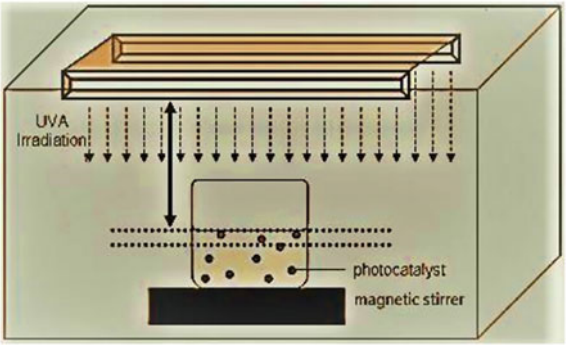

Fig. 1 UV-light set-up for photodegradation

the reactants. The hydrothermal heat treatment, over a long period of time, helps the layered $Na_2Ti_3O_7$ particles to exfoliate and form numerous sheet-like products, which finally produces nanotubes upon rolling (Fig. 2) (Wang et al. 2002; Sun and Li 2003). Alkaline hydrothermal heat treatment of anatase TiO_2 produces crystalline nanostructured titanate materials, though several controversial issues are there (Mohanty et al. 2020). The final obtained cooled product resembled a white-batten cotton wool. It was cleaned properly and frequently using double distilled water to attain pH ~ 7. It was subsequently dried at 100 °C for 6 h to produce TNT in solid residue form. Finally it was stored in a dry black bottle.

Acid treatment of TNT, was attempted to replace Na^+ by H^+ using dilute HCl (10^{-2} M). The resulting suspension was washed with double distilled water to attain pH ~ 7 and dried at 100 °C for 6 h. The final obtained material is termed as HTNT (Thorne et al. 2005). The characterization of the precursors was carried out using SEM/EDX, XRD and TEM. Experimental results at optimal conditions suggested

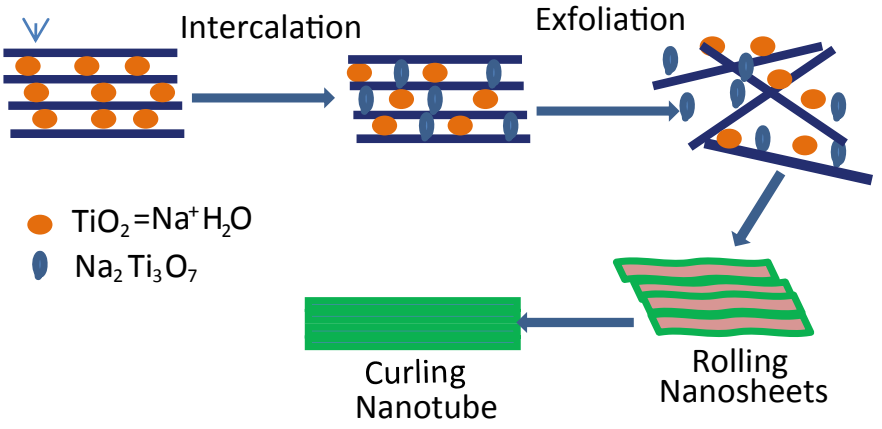

Fig. 2 Schematic diagrams for the synthesis of TNT

Table 1 Water quality parameters of dye-piked pond water pre- and post- treatment

Parameter	Before treatment	After treatment [MG] = 13 mg/L spiked sample
pH	8.2	8.8
EC (μs/cm)	288	300.0
Fe_{tot} (mg/L)	0.67	0.70
$C1^-$(mg/L)	230	235.0
D.O (mg/L)	6.1	5.2
TDS (mg/L)	47	49.0
Tem (°C)	27	29.0
ORP (mV)	98	105.0
Alkalinity (mg/L)	2.7	3.0
Hardness (mg/L)	78	80.0
Salinity (PSU)	0.15	0.4
Calcium (mg/L)	28.3	30.0
Magnesium (mg/L)	11.8	11.8
Sodium (mg/L)	16.6	17.0
Potassium (mg/L)	3.4	4.0
Bicarbonate (mg/L)	109	111.0
Chloride (mg/L)	33.7	34.0
Sulphite (mg/L)	4.6	4.6
Nitrate (mg/L)	22.2	22.5
Fluoride (mg/L)	5.8	5.4
		~98% removal

that, efficiency (% removal) of both synthesized materials is close to each other. Therefore, in this study, all the experiments were conducted using TNTs only.

The pond water sample was collected from the KISS University, Odisha. The water quality parameters were measured and are shown in Table 1. MG was then spiked to the collected water sample to achieve the desired concentration of dye to conduct the adsorption/photodegradation study by batch mode.

The 50 mL dye contaminated spiked water sample was taken in a 500 mL beaker (cross-sectional area 55.44 cm^2). The distance between the UV-light source to the surface of the water sample was kept at 13.2 cm. TNT was dispersed at a dose of 3 g/L. A magnetic stirrer for mixing the TNT with MG contaminated water was used at a stirring speed of 520–540 rpm at a room temperature of 25 ± 2 °C. The UV-light source (18 W, 360 nm, make: Germany) was put above the beaker as a source of photon. Adsorption studies were carried out in dark, but the photo-illumination studies were carried out in the presence of UV-light and sufficient air (oxygen) in the suspension. After achieving the desired adsorption and photo-irradiation time, Centrifuge (Remi-24) was used at 9000 rpm to separate the phases of the suspension (solid and liquid phase). An aliquot of 3 mL was taken out carefully (not filtered)

from the supernatant, and the dye concentration was measured using the standard drawn calibration of MG.

3 Result and Discussion

3.1 Analytical Method

To measure the residual MG concentration in the effluent after treatment, a standard calibration curve of MG ($\lambda_{max} = 618$ nm) was drawn (concentration ranges between 0 and 20 mg/L, air as blank). The calibration curve for the absorbance in linear form can be expressed as: Absorbance = 0.056 × MG concentration (mg/L) - 0.039 ($R^2 = 0.991$). This calibration curve was used for the entire study.

3.2 Characterization of Precursors

XRD (Fig. 3) and SEM/EDX (Fig. 4) analysis was conducted in order to understand the crystallinity and surface morphology with the composition of both synthesized precursors. TEM analysis was conducted to understand the shape and size (nanotubular with the radius of ~26 nm) for TNT only (Fig. 5) and the details were reported in our previous work (Mohanty et al. 2020). The XRD data was analyzed (JCPDF-00–044-0131) and shown in Table 2. With some impurities, EDX spec-

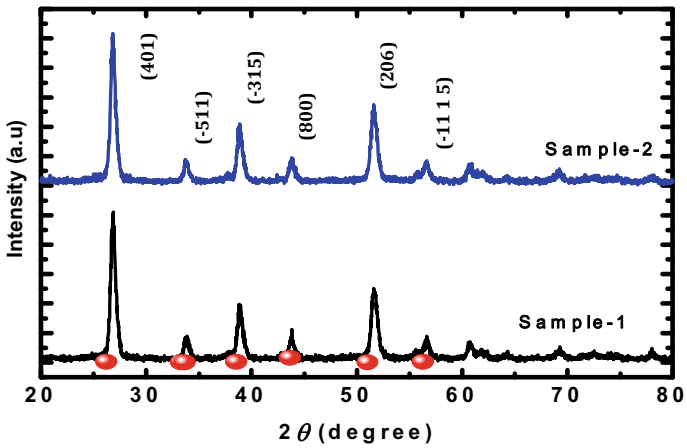

Fig. 3 X-ray diffraction (XRD) pattern of Sample-1 and Sample-2. The (red) solid dots represent the peak positions corresponding to monoclinic $H_2Ti_5O_{11}$, H_2O (JCPDF-00-044-0131)

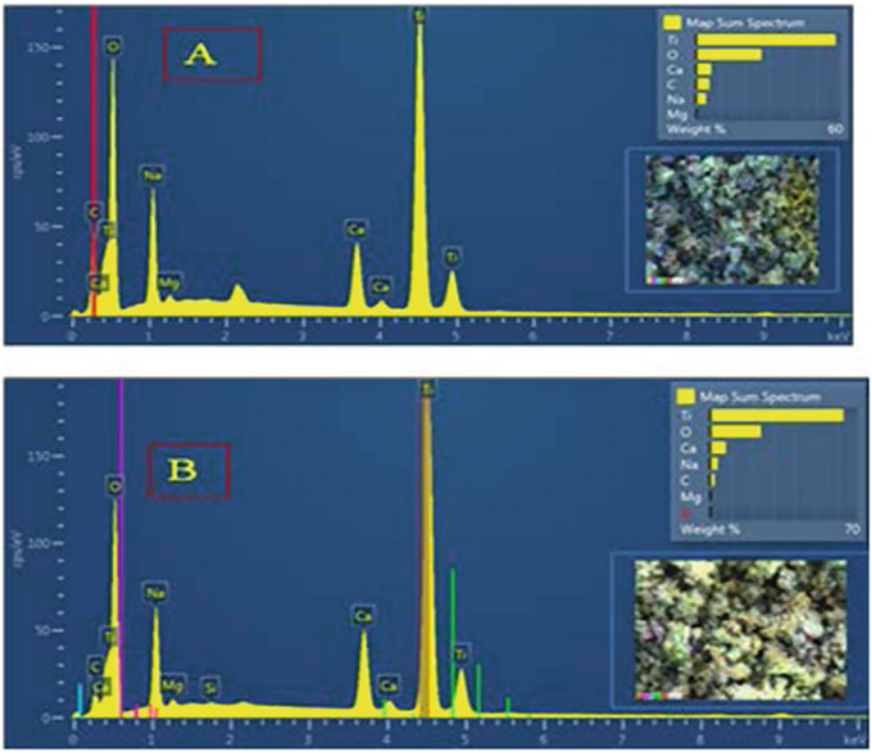

Fig. 4 **a**, **b** EDX spectrum of TNT and HTNT (Inset SEM image)

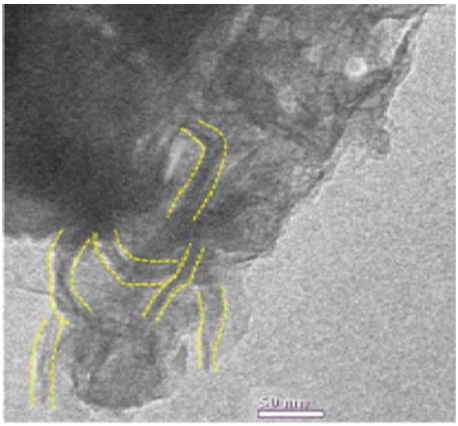

Fig. 5 TEM of TNT only

Table 2 Comparison between the observed 2θ values (in degree) and interplanar spacing (d_{hkl})

S. No.	Lattice planes	2θ value (in degree)			Interplanar spacing (d_{hkl}) in Å		
		Standard	Experimentally measured		Standard	Experimentally measured	
			Sample 1	Sample 2		Sample 1	Sample 2
1	(401)	26.197	26.87	26.92	3.399	3.315	3.310
2	(-511)	33.640	33.80	33.67	2.662	2.649	2.659
3	(−315)	38.525	38.87	38.96	2.335	2.315	2.310
4	(800)	43.627	43.76	43.87	2.073	2.067	2.062
5	(206)	51.008	51.70	51.50	1.789	1.766	1.773
6	(−1115)	56.253	56.59	56.60	1.634	1.625	1.625

trum suggested the composition of TNT and HTNT is mostly composed by titanium (Fig. 4), as P-25 is ~99% pure.

3.3 Determination of Optimal Conditions

To optimize the operational conditions for the maximum removal of MG from the spiked suspension, different concentrations of MG (1 to 20 mg/L) and different amounts of TNT (1 to 6 g/L) were considered. Experimental results suggested that TNT at a dose of 3 g/L can remove the maximum amount of MG (~98%) from the sample at the initial concentration of MG as13 mg/L followed by adsorption in the dark (1.75 h) and photo-irradiation (5.25 h), respectively. However, percent removal of MG decreased with the increasing concentrations.

To determine the time at which the maximum solute uptake on sorbent surfaces takes place, experiments were conducted for the following two cases: (a) adsorption followed by photodegradation and (b) simultaneous adsorption and photodegradation. In each case the TNT dose and MG concentration were kept at their optimum values—3 g/L and 13 mg/L respectively at pH of 6.8 ± 0.2 and room temperature of 25 ± 2 °C.

In dark (adsorption), maximum MG removal efficiency was found to occur within 1.75 h. (~87% removal) and photo-irradiation of the same suspension under UV-light. The final removal was achieved to be ~98% in the presence of sufficient quantity of oxygen in the suspension within 5.25 h of shaking time (Fig. 6). Fresh and active sites of the semiconductor photocatalyst, in the beginning, helps to adsorb the maximum amount of organic form the solution and then the remaining minimum numbers of active sites of the precursors surfaces which are may not be exposed, degrade the organic due to the transference of electron(s) from the valence band (VB) to conduction band (CB). In the second case, i.e. in complete photo-irradiation study, the organic removal efficiency (%) slowly increased to ~98%. The obtained results indicate that both the process of adsorption and photodegradation continued to take

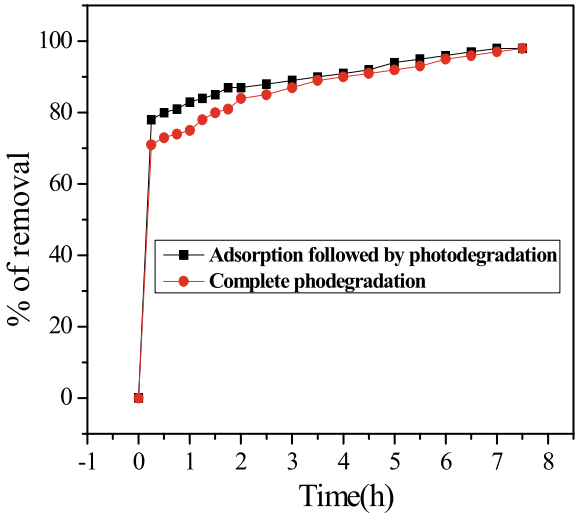

Fig. 6 Adsorption and photodegradation of MG spiked dye wastewater

place in the beginning as the precursors sites are fresh and active. However, solute uptaking capacity for any sorbent from the solution is completely depending on both the nature of the two as well as with the contact time between them.

4 Kinetics Study

In optimal operational conditions within 1.75 h of contact time between the sorbent and solute in dark, the maximum adsorption of MG was found to be ~87%, photo-irradiation of the same sample for another 5.25 h caused ~98% removal. Hence, in the beginning it is important to know the mechanism that followed the process. In this study, four different reaction models were analyzed namely, first order reaction model, pseudo-first order, second order reaction model and pseudo-second order reaction model (Hayeeye et al. 2017). Based on the specific relation co-efficient values (R^2), it can be noted that the pseudo-second order reaction model fitted in a better way than the other models analyzed (Table 3; Fig. 7). This reaction model in linear form can be depicted as:

$$\frac{t}{q_t} = \frac{1}{h} + \frac{1}{q_e}t \tag{1}$$

where, h = initial sorption rate constant = k q_e^2, terms and symbols are as usual.

Because dye removal initially followed adsorption and then photodegradation, so in adsorption it is important to know whether the process followed the pore diffusion or film diffusion and was evaluated using the overall first order rate const (Helfferich 1962; Michaels 1952) using the following equation:

Table 3 Linear four kinetic equations

Dye	Model	Equation of linear fit line	R^2
[MG] = 13 mg/L	First-order reaction model	In $C_t = -0.0064t + 1.4252$	0.9598
	Pseudo-first order reaction model	In $(q_{-1} - q_t) = -0.0137t - 0.2078$	0.9728
	Second-order reaction model	$1/C_t = 0.0019t + 0.2369$	0.9718
	Pseudo-second-order reaction model	$t/q_t = 0.21011 + 0.2286$	0.9996

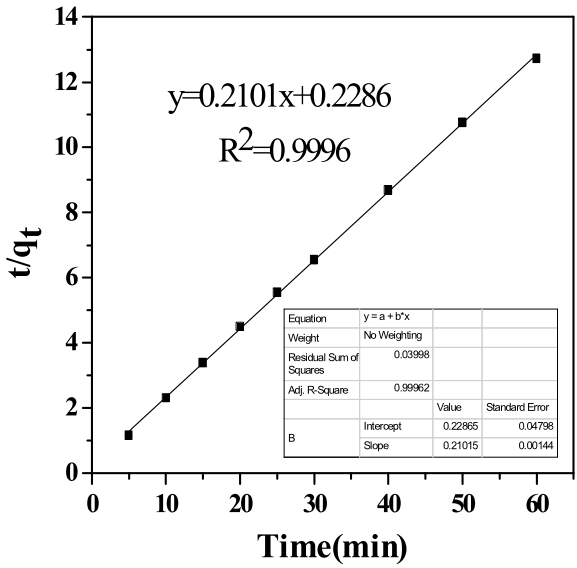

Fig. 7 Pseudo-second order reaction model of MG spiked dye wastewater

$$t_{\frac{1}{2}} = 0.030\frac{r^2}{D_p} \tag{2}$$

$$t_{\frac{1}{2}} = 0.23\frac{r\delta}{D_f} \times \frac{C_s}{C_e} \tag{3}$$

$t_{\frac{1}{2}}$ = half time, r = radius of the adsorbent unit (cm), D_p = pore diffusion coefficient (cm^2/s), D_f = film diffusion coefficient (cm^2/s), Cs = adsorbate concentration on the adsorbent at equilibrium (mg/L), Ce = adsorbate concentration in the solution at equilibrium (mg/L) and δ = thickness of film (0.001 cm). The half time ($t_{1/2}$) can be calculated (Maji et al. 2011) as:

$$t_{\frac{1}{2}} = -\frac{\ln(0.5)}{k_1} \tag{4}$$

Table 4 Diffusion constant values

Initial Dye	C_e (mg/L)	k_L (1/s)	$t_{L/2}$(S)	r (cm)	D_f (cm^2/s)	D_p (cm^2/s)
[MG] = 13 mg/L	~ 1.69	1.088×10^{-4}	6.398×10^{-3}	26×10^{-7}	6.25×10^{-13}	$3.16 \times 10^{-}17$

where, k_1 is the first rate constant.

In the present case, D_f and D_p values were evaluated to be 6.25×10^{-13} cm^2/s and 3.16×10^{-17} cm^2/s, which are not between the 10^{-6} to 10^{-8} cm^2/s (for D_f) or 10^{-11} to 10^{-13} cm^2/s (for D_p). Hence, it may be concluded that adsorption did follow neither film diffusion nor pore diffusion like heavy metal or metalloids (Table 4).

5 Isotherm Study

Isotherm studies viz., Langmuir, Freuindlich studies were conducted at the optimal conditions with varying the doses of the semiconductor adsorbent, TNT at the particular temperature of 25 ± 2 °C, in order to understand the adsorptive behavior of sorbent towards the contaminant (Fig. 8a, b). The feasibility of the adsorption process (mean free energy, E) was understood from D-R isotherm (Fig. 8c). The evaluated dimensionless equilibrium parameter ($R_L = 0.0551 < 1$) and the Gibbs free energy changes ($\Delta G^O = -0.6838$ kJ/mole) values suggested that the adsorption process was favorable and also spontaneous in nature. Calculated E value suggested (5.0403 kJ/mole < 8) the physisorption. The constant values of the Isotherm are presented in Table 5. The relations are as follows (Mohanty et al. 2020):

$$\text{Langmuir isotherm: } q_e = \frac{Q_{\max} b C_e}{1 + bC_e} \tag{5}$$

$$\text{Freundlich isotherm : } q_e = k_f C_e^{\frac{1}{n}} \tag{6}$$

$$\text{D - R isotherm : } \ln Q = \ln Q_m - k\varepsilon^2 \tag{7}$$

$$E = -(2k)^{-0.5} \tag{8}$$

$$R_L = \frac{1}{(1 + bC_0)} \tag{9}$$

$$\Delta G^o = RT \ln\left(\frac{1}{b}\right) \tag{10}$$

Impregnation of energy rich photon produced from UV light to the suspension, converted the dye molecules to its highly energetic activated species that are

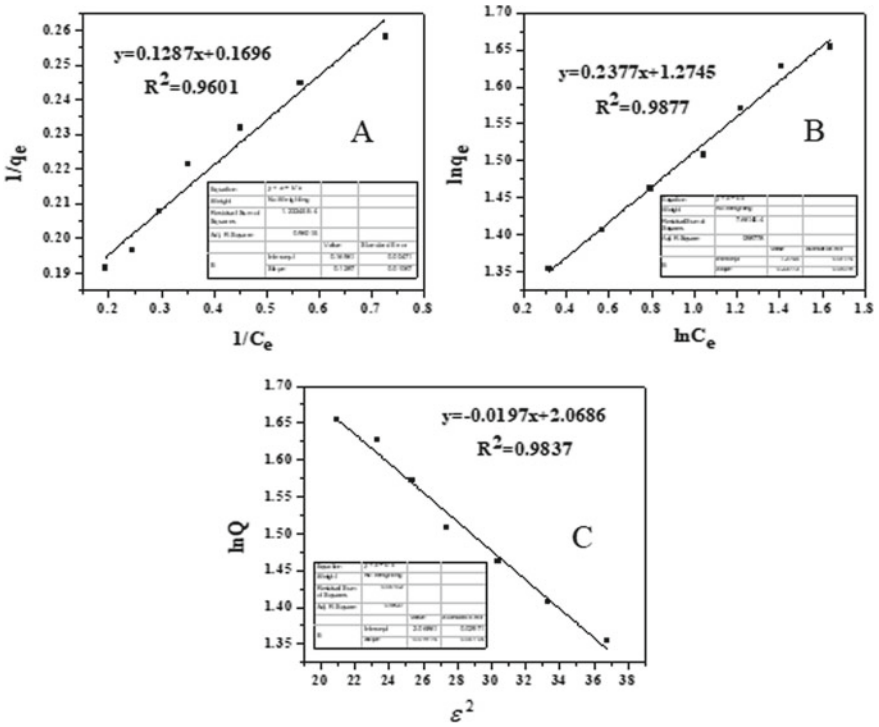

Fig. 8 **a–c** Adsorption Isotherms of MG on TNT surfaces

Table 5 Isotherm constant values

MG spiked sample (13 mg/L) (298 ± 2 K)	Langmuir isotherm		Freundlich isotherm		D-R isotherm	
	Q_{max} (mg/g)	5.8962	n	4.2069	E (kJ/mole)	5.0403
	b (L/mg)	1.3178	k_f	3.5769	Q (mg/g)	7.9137
	R_L	0.0551				
	R^2	0.9601	R^2	0.9877	R^2	0.9837
AG° (kJ/mole)	−0.6838					

short-lived radicals. These radicals in contact with TNT, transfer their negatively charged electron(s) to the semiconductor surfaces. These electron(s), may also join the conduction band of TNT by passing through the formed nanotube channels. The surface of the adsorbed O_2 molecules captured the injected electrons to finally produce $O_2^{\cdot -}$ and $HO^{\cdot}$ radical among other ions. The radicals also may mineralize the dye molecules (Mohanty et al. 2020). Photocatalyst TNT is having a low band gap between VB to CV of 3.2 eV. Hence, it is easier to transit the produced electron(s) from VB to CB in the presence of photon(s) produced from UV-light (in presence of oxygen) and during this process electron rich free radicals $O_2^{\cdot -}$ and $HO^{\cdot}$ are formed

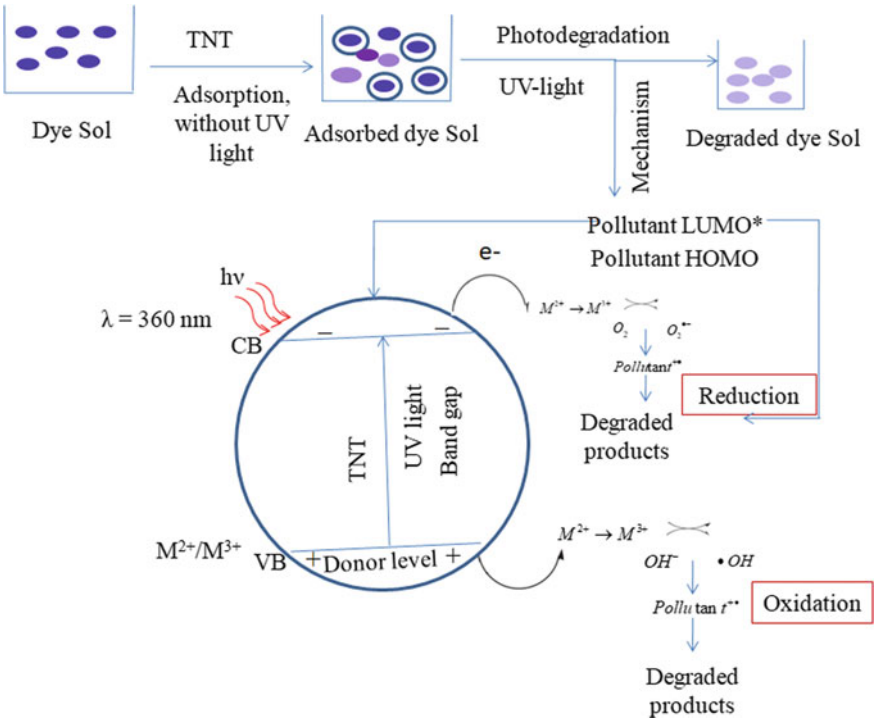

Fig. 9 Probable adsorption and photodegradation mechanism

as mentioned above. Due to the transference of electron(s) from HOMO to LUMO of organic dye MG, an oxidation or reduction or both may have taken place and degrades. The expected mechanism of adsorption and photodegradation of MG is presented in Fig. 9.

Two times turnover studies were conducted after successive washing the exhausted material with 100% EtOH (3 g in 10 mL alcohol) to recover the ~82% adsorbed MG, subsequently washing in double distilled water and drying at 80^0C in a hot air oven for 6 h, during photodegradation. Reduction in the efficiency of the dye degradation was noticed in each cycle (~71%, ~58%), because of blockage of the fresh and active sites of the precursors inhibiting the electronic transfer from the VB to the CB.

6 Conclusion

In this study, TNTs were synthesized under hydrothermal condition and also characterized using different instrumental techniques. These TNTs were utilized to remove MG from MG-spiked pond water at 25 ± 2 °C. Experimental results revealed that TNT, with a dose of 3 g/L, can remove ~98% organic from the aquatic system

followed by adsorption and photodegradation keeping the initial MG concentration at 13 mg/L and pH at 6.8 ± 0.2. The adsorption process followed Freundlich isotherm and Q_{max} was observed to be 5.8962 mg/g. Adsorption process found to be favorable, spontaneous with pseudo-second order reaction kinetics model. The mean free energy of adsorption suggested process is physisorption in nature. Adsorption didn't follow either pore diffusion or film diffusion model. Turnover study revealed the suppression of the degradation of organic. Plausible mechanism for adsorption/photodegradation was proposed.

Acknowledgements This work is financially supported by SERB, DST, Govt. of India, with contract number of ECR/2016/001315. For SEM/EDX, we sincerely acknowledge Dr. Rupam Goswami, BITS, Pilani.

References

Hayeeye F et al (2017) Kinetics and thermodynamics of Rhodamine B adsorption by gelatin/activated carbon composite beads. Colloid Surf A Physicochem Eng Aspects 513:259–266

He HY, Tian CY (2016) Rapid photo and photo-Fenton like catalytic removals of malachite green in aqueous solution on undoped and doped TiO_2 nanotubes. Desalin Water Treat 57(31):14622–14631

Helfferich F (1962) Ion exchange. McGraw Hill, New York, p 299

Maji SK, Kao Y-H, Liu C-W (2011) Arsenic removal from real arsenic-bearing groundwater by adsorption on iron-oxide-coated natural rock (IOCNR). Desalination 280(1–3):72–79

Michaels AS (1952) Simplified method of interpreting kinetic data in fix-bed ion exchange. Ind Eng Chem 44(8):1922–1930

Mohamed A et al (2019) A novel and highly efficient photocatalytic degradation of malachite green dye via surface modified polyacrylonitrile nanofibers/biogenic silica composite nanofibers. Sep Purif Technol 210:935–942

Mohanty S, Moulick S, Maji SK (2020) Adsorption/photodegradation of crystal violet (basic dye) from aqueous solution by hydrothermally synthesized titanate nanotube (TNT). J Water Process Eng 37:101428

Sun X, Li Y (2003) Synthesis and characterization of ion-exchangeable titanate nanotubes. Chem A Eur J 9(10):2229–2238

Thorne A et al (2005) Formation, structure, and stability of titanate nanotubes and their proton Conductivity. J Phys Chem B 109(12):5439–5444

Wang YQ et al (2002) Microstructure and formation mechanism of titanium dioxide nanotubes. Chem Phys Lett 365(5–6):427–431

Bearing Capacity and Settlement Analysis of Red Mud and RM-PA Mix Using GEO5

Vaibhav Vivek, Tawkeel Mukhtar Kiloo, and J. Sumalatha

Abstract Aluminium Industry is the second most important metallurgical industry in the world generating about 130 Million Tonnes per Year (Mtpy) of red mud as a residue. Storage and transportation of red mud is a serious problem. Red mud generated worldwide poses a severe environmental risk. Alkali Seepage into ground water, Safety storage problems, vast area of land required for disposal, alkaline airborne dust emission, soil contamination, trace heavy metal seepage into groundwater, fine particles suspension in the sea, etc. There is a need of utilization of red mud on large scale requiring research work which is by far very limited. This paper deals with the utilisation of red mud along with admixture pond ash for foundation analysis. The necessary data has been collected from the literature review and used in the analysis. In the present investigation using the data such as cohesion (C), angle of shearing resistance (ø), unit weight of soil (ɣ), moisture content (w), etc. provided as an input in the GEO5 software, foundation (Design bearing capacity, FOS) and settlement analysis were performed for different compositions of red mud and pond ash, the proportions being 100% RM + 0%PA, 90%RM + 10%PA, 80% RM + 20%PA, 70%RM + 30%PA, 60%RM + 40%PA and 50%RM + 50% PA. Using the data obtained from the software for various mixes, it can be deduced that the mix 80% RM + 20% PA showed good results. The design bearing capacity of 80%RM + 20%PA mix was higher and the settlement was lower. Further, the effect of GWT on the foundation was also studied considering the GWT below the footing, at the footing and above the footing.

Keywords Ground water table · Design bearing capacity · Red mud · Pond ash · Safety factor

V. Vivek (✉) · T. M. Kiloo · J. Sumalatha
Ramaiah Institute of Technology, Bengaluru, India

B. B. Das et al. (eds.), *Recent Developments in Sustainable Infrastructure (ICRDSI-2020)—GEO-TRA-ENV-WRM*, Lecture Notes in Civil Engineering 207,
https://doi.org/10.1007/978-981-16-7509-6_53

1 Introduction

Red mud is a bauxite residue generated during the production of Aluminium in the Bayer's Process. Alumina Production around the World is—130 Mtpy and in India—4 Mtpy leading to red mud generation of over 150 Mtpy globally and 9 Mtpy in India. For every ton of Alumina 1—2.5 Tonnes of red mud is produced depending upon the impurity of bauxite and the method of treatment involved (Rao and Reddy 2017; Sundaram and Gupta 2010; Reddy and Rao 2018; Sridevi et al. 2019; Sutar et al. 2014; Bhardwaj and Gupta 2019). This industry faces the biggest problem with the disposal of red mud produced. Around 2% of the total revenue is used alone in the disposal of red mud. The disposal of red mud still comes with the huge cost of the environment that can only be done away with appropriate and economical treatment of red mud and its proper utilization.

This paper mainly deals with two aspects i.e. the determination of Design Bearing Capacity followed by Ultimate Bearing Capacity and Safe Bearing Capacity (Theoretically) and also the Settlement Analysis of Red Mud along with Pond Ash (Stabilizing agent) using Geo5 Software.

For Design Bearing Capacity, Red Mud along with Pond Ash is taken in various proportions of 100%RM + 0% PA, 90%RM + 10% PA, 70%RM + 30%PA, 80%RM + 20%PA, 60%RM + 40%PA, 50%RM + 50% PA and finally the results for bearing capacity of RM-PA mixes are compared to find an optimum mix for the design of Spread Footings.

For the Settlement Analysis, a problematic soil (Clayey Soil) is taken in which Red Mud/ RM-PA mix is added to certain depths of 2.5 and 3.0 m and the settlement values are observed.

2 Aim and Methodology

- The aim of this project is to understand the use of red mud and red mud- pond ash mix as the foundation soil using GEO5 software.
- The data has been obtained from literature review (Bhumij 2015) and provided as an input in the software to carry out the analysis (Table 1).
- For a given depth of footing, thickness and reinforcement used the design bearing capacity of different RM – PA mixes where found out and an optimum mix among all the mixes is identified.
- The same data such as cohesion, angle of internal friction, depth of footing, etc. is used and theoretical value of the Ultimate Bearing Capacity and Safe Bearing Capacity is found out and compared with that of the software's value.
- The design bearing capacity was checked at different GWT i) below the base of the footing, ii) at the base of the footing and iii) above the base of the footing to understand the extent of effect of water table on the foundation.

Table 1 Engineering properties of different red mud—pond ash mixes

Proportions (%)		G	MDD	OMC	WL	WP	IP	C	Ø
Red mud	Pond ash		KN/m^3	(%)	(%)	(%)	(%)	KN/m^2	(°)
100	0	3	16.9	24.63	29	23	6	27.95	33.2
90	10	2.89	15.3	23.2	28.5	24.8	4	25.8	32.3
80	20	2.62	15.84	23.6	27.3	24	3	30.1	34.4
70	30	2.44	15.37	24.6	26.5	23.8	3	17.2	31.7
60	40	2.41	14.5	24	25.3	23	2	15.05	26.7
50	50	2.24	14.2	24.2	24.8	22.7	2	15.05	24.5

Table 2 Grain size distribution of 80% RM + 20% PA mix

Proportions (%)		Fines	Sand	Gravel
Red mud	Pond ash	(%)	(%)	(%)
80	20	91.45	8.55	0

- In order to analyse the settlement characteristics a problematic a soil was chosen i.e. Clayey Soil with high plasticity having depth from 0 to infinity then certain depth of problematic soil was replaced at the foundation with the effective red mud—pond ash mix say from 0 to 2.5 m and settlement characteristics are analysed in both the cases.
- Further the depth of the effective red mud—pond ash mix was increased say from 0 to 2.5 to 0 to 3 and the settlement characteristics are once again analysed using the software.
- The particle size distribution of RM—PA mix has been estimated using the data of the particle size distribution of individual materials. The data was needed for the settlement analysis of the foundation (Table 2).

3 Design Bearing Capacity

For the Determination of design bearing capacity of various RM-PA mixes, the Geo5 Software requires various parameters like cohesion (c), angle of internal friction (φ), unit, unit weight (γ) and saturated unit weight (γ_{sat}) for all the mixes and these values have been obtained literature review.

3.1 Analysis of Vertical and Horizontal Bearing Capacity Neglecting the Effect of GWT

For the analysis, RM-PA mixes from 100% RM + 0% PA to 50% RM + 50% PA is taken into consideration.

In a particular soil profile, the values of c, φ, γ, γ_{sat}, etc. are provided as a input then for a defined depth, loading and the thickness of the footing, etc. the software will automatically give us the Design Bearing Capacity (R_d), Safety Factor and other important parameters along with the dimensions of footing. The steps in brief have been explained:

(i) Firstly the standards are set to the Indian Standards, IS: 456-Concrete Structures and Analysis for drained conditions IS: 6403-1981.

Note: Usually, spread footings are analysed for drained conditions using the effective parameters of the soil (φ_{ef}, ς_{ef}). An analysis for undrained conditions is performed for cohesive soils and short-term performance using the total parameters of the soil (φ, ς).

(ii) In this next step enter the soil parameters i.e. unit weight, angle of internal friction, cohesion, saturated unit weight and assign them to the profile.

(iii) Choose type of footing, depth from the origin ground (OG) surface, etc. and specify the load.

Note: The analysis has been done using two load cases (Table 3) and the soil is automatically analysed for the worst load case scenario by the software and design load is used for the this analysis.

Note: The depth of the footing bottom depends on different factors, such as the natural and climatic factors, hydrogeology of the construction site and geological conditions.

(iv) Further M30 grade concrete was selected and Fe 415 grade steel was chosen for the foundation reinforcement.

Note: No surcharge was given. Surcharge around the foundation influences the analysis of the settlement and the rotation of the foundation but not the bearing capacity. In the case of vertical bearing capacity, it always acts favourably and no theoretical knowledge leads us to analyse this influence.

Table 3 Load cases used (in GEO5 software) for analysis

Name	N (kN)	(kNm)	(kNm)	(kN)	(kN)	Type
Load No. 1	1000	100	100	80	80	Design
Load No. 2	1200	100	100	100	100	Design

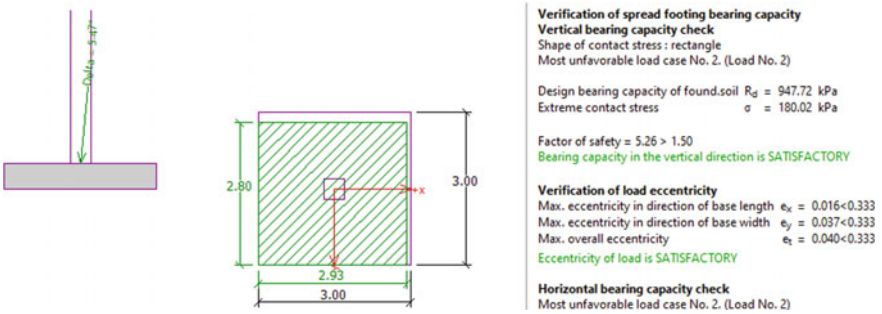

Fig. 1 Verification of bearing capacity of 3rd mix (80% RM + 20% PA)

Table 4 Footing design and design bearing capacity of the foundation

Soil type	Dimensions of the footing (m)	Design bearing capacity Rd (kPa)	Extreme contact stress σ (kPa)	Safety factor (SF)
100RM	3.00 × 3.00	851.60	181.49	4.69
90RM10PA	3.00 × 3.00	710.15	179.00	3.97
80RM20PA	3.00 × 3.00	947.72	180.02	5.26
70RM30PA	3.00 × 3.00	561.72	179.62	3.13
60RM40PA	3.00 × 3.00	337.42	178.49	1.89
50RM50PA	3.00 × 3.00	282.72	178.15	1.59

(v) Finally the design bearing capacity was calculated using the software tool (Fig. 1). The bearing capacities with respect to different dimensions of the footing were analyzed and are given in Table 4.

3.2 Theoretical Analysis of Red Mud RM- PA Mix

Terzaghi's Bearing Capacity Formula was used in order to find the ultimate bearing capacity and safe bearing capacity of the soil.

For Square Footing, ultimate bearing capacity, $q_u = 1.3CN_c + \gamma D_f N_q + 0.4\gamma BN_\gamma$

Net ultimate bearing capacity, $q_{nu} = q_u - \gamma D_f$

Net safe bearing capacity, $q_{ns} = \frac{q_{nu}}{F.S.}$

Considering Factor of Safety (F.S.) = 3, safe bearing capacity, $q_s = q_{ns} + \gamma D_f$

The ultimate and safe bearing capacities were estimated using the above equations for all the selected mixtures of soil (Table 5).

The bearing capacities thus obtained from the above analysis are compared with the design bearing capacities as shown in Fig. 2.

Table 5 Ultimate and safe bearing capacity of red mud and RM- PA mixes

Soil type	Dimensions of the footing (m)	Ultimate bearing capacity (kPa)	Safe bearing capacity (kPa)
100RM	3.00 × 3.00	3659.109	1240.765
90RM10PA	3.00 × 3.00	2992.832	1016.46
80RM20PA	3.00 × 3.00	4221.268	1426.635
70RM30PA	3.00 × 3.00	2335.249	797.551
60RM40PA	3.00 × 3.00	1211.78	421.906
50RM50PA	3.00 × 3.00	949.271	334.057

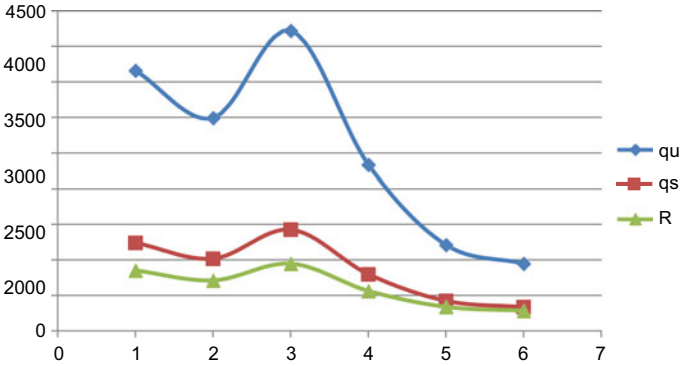

Fig. 2 Comparison of ultimate bearing capacity, safe bearing capacity and design bearing capacity of RM and RM- PA mixes (Rd)

3.3 Design Bearing Capacity of RMPA Mix with Ground Water Table Effect (GWT)

The design bearing capacity is calculated in a similar way as mentioned above with the introduction of GWT at three predefined depths i.e. below the footing, at the base of footing and finally above the base of footing (Table 6).

The effect of GWT on the mixes was then determined for the optimum mix (80% RM + 20% PA) keeping the footing design same.

Table 6 Effect of GWT on 80% RM + 20% PA mix

Depth (m)	Dimensions (m)	Rd (kPa)	σ (kPa)	SF
2.5	3.00 × 3.00	861.35	180.02	4.78
2.0	3.00 × 3.00	856.78	180.02	4.76
1.0	3.00 × 3.00	743.44	170.19	4.37

4 Settlement Analysis

In the Settlement Analysis Grading parameters (fine, sand and gravel particle percentage) and Moisture Parameters (sample moisture, liquid limit, plastic limit) of red mud and pond ash were required which was again taken from a literature paper.

By inputting the grading and moisture parameters, a particular type of mix is defined.

A problematic soil is defined using software and is replaced by RM-PA mix for a certain defined depth finally giving us Settlement values.

The load cases used in this analysis were same as that of design bearing capacity by after its conversion into service load obtained by dividing it by a factor of 1.5.

Note: In this analysis the bearing capacity of the soil was not stressed upon, the objective was just to understand the effect of red mud and RM- PA mixes on the settlement.

4.1 Spread Footing Settlement Analysis

In settlement analysis the distribution of the particle size of the 80–20 effective mix was calculated with the help of particle size distribution of the individual components of the mix using the formula:

$$x = \frac{x1y1 + x2y2}{y1 + y2}$$

where,

x percentage of fine/sandy/gravelly particle in the mix.
x1 percentage of fine/sandy/gravelly particle in red mud.
x2 percentage of fine/sandy/gravelly particle in pond ash.
y1 percentage of red mud present in the RM-PA mix.
y2 percentage of pond ash present in the RM-PA mix.

After entering soil type manually, the system automatically finds desired parameters for the soil to be used in the soil profile. The known parameters of the soil are kept as it is and unknown parameters are taken from the manual classification of the soil.

Note: While analysing settlement and rotational analysis, service load instead of design loads are used.

Similar process has been followed in order to find the settlement of the soil as that employed in finding the design bearing capacity of the soil.

Here, analysis of settlement for a problematic soil i.e. clayey soil with high plasticity is done using GEO5 Software and then comparing the results obtained with the settlement of RM80PA20 after replacement.

Case 1: **Settlement Analysis of Spread footing in Clayey Soil (CS), firm consistency**:

The soil i.e. Clayey Soil and its properties were directly obtained and then assigned into the profile by using soil database data in the GEO5 Software. The soil gave a settlement of 16.5 mm for a centric spread footing of dimensions 3 m × 3 m.

Case 2: **Settlement Analysis for spread footing in Clayey Soil soil filled with RM80PA20 up to 2.5 m from OG**.:

In this case Clayey Soil has to be replaced by RM80PA20 mix up to a depth 2.5 m from OG. The settlement of the centric spread footing of the same dimensions 3 m x 3 m was found to be 14.3 mm.

Again the depth of RM80PA20 mix replacing the Clayey Soil was increased and the amount of settlement was calculated (Fig. 3). Tabulated form of Data obtained in GEO5 Software for analysis of Settlement is given in Table 7.

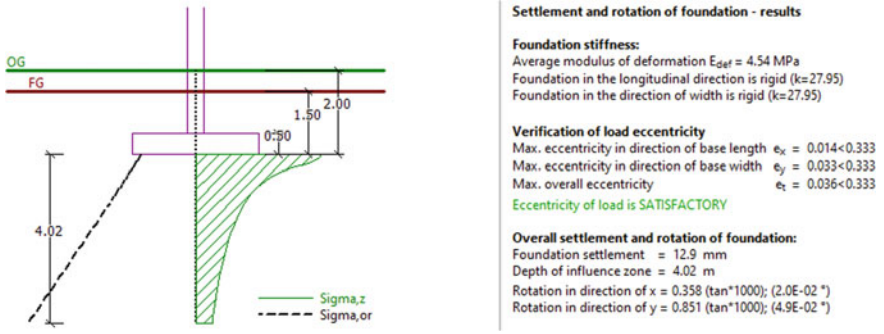

Fig. 3 Settlement analysis of spread footing in RM80PA20 (up to 3 m) and clayey soil (beyond 3 m)

Table 7 Result of the settlement analysis

Soil type	Depth (m)	Dimensions of S. footing	Settlement (mm)
Clayey soil (CH)	OG to ∞	3.00 × 3.00	16.5
RM80PA20 + CH	RM80PA20 up to 2.5 m CH beyond 2.5 m	3.00 × 3.00	14.3
RM80PA20 + CH	RM80PA20 up to 3.0 m CH beyond 3.0 m	3.00 × 3.00	12.9

5 Discussion

Although with the available data the ultimate and safe bearing capacity can be obtained theoretically but use of software can considerably reduce time and effort required in the analysis. The software analysis can be made more realistic by taking into account the effect of earthquake and can give solution to novel engineering problems and can be of great help in the times of crisis such as the current pandemic.

Terzaghi's formula can only be applied for vertical load and not for moments and horizontal force if any.

The difference in the values of the design bearing capacity of the software and safe bearing capacity (using Terzaghi's bearing capacity formula) can be due to the difference in methods applied for the analysis. The design bearing capacity gives a similar graph as obtained with the safe bearing capacity.

6 Conclusion

1. The design bearing capacity of red mud and red mud pond ash mixed were estimated and was found that the 80% RM + 20% PA mix showed best results.
2. The pond ash used in the red mud works as an stabilizer and in increases the bearing capacity of the soil upto 80% RM + 20% PA mix and further decreases with its addition.
3. The design bearing capacity is not same as the ultimate bearing capacity or safe bearing capacity of the soil and is subjected to change with the change in loading if all other parameters are fixed.
4. As the GWT rises the design bearing capacity of the red mud—pond ash mix reduces. The design bearing capacity is maximum when GWT is below the base of the foundation.
5. If in a region with problematic soil e.g. clayey soil or sandy clay, a portion of that soil is replaced by red mud the settlement of the foundation can be reduced. This settlement further reduces if 80RM 20PA mix is used instead of only red mud.
6. It was also found that as the depth of 80% RM + 20% PA mix replacing the Clayey Soil is increased (say from 2 to 3 m) the settlement of the foundation also decreases. The settlement of near about 4 mm was reduced merely by the substitution of 80% RM + 20% PA upto a depth of 3 m.
7. Further, the swelling potential of a soil basically depends upon its mineral composition along with the in situ moisture content and density. Soil permeability also affects the rate of swelling on site. In general, clays with plasticity indices > 25, liquid limits > 40, and natural water content near the plastic limit or less are more likely to swell.

   The plasticity of the red mud is 6 and 80 RM 20PA mix is 3 (from the literature) hence with this information it can be deduced that red mud and red

mud pond ash mix does not show swelling characteristics and hence can be used as a substitute for problematic soils (expansive soils).

8. Red mud when used alone causes more environmental problem due to its high pH as compared to red mud—pond ash mix as with increase in the percentage of the pond ash pH of RM-PA mix reduces.

References

Bhardwaj PS, Gupta S (2019) Utilization of red mud as a partial replacement of cement in concrete

Bhumij RK (2015) Compaction characteristics of red mud and pond ash mix as filling and embankment material (Doctoral dissertation)

Gangadhara Reddy N, Hanumantha Rao B. Effect of additives on consistency limits of red mud waste: a comparative study

Gangadhara Reddy N, Hanumantha Rao B (2016) Evaluation of compaction characteristics of treated and untreated red mud (August)

www.finessoftware.eu (GEO5 software, video tutorials, etc.)

Hanumantha Rao CHV et al. Relative performance of red mud over red soils as construction material

Hanumantha Rao CHV et al. Comparision of engineering properties of red mud an aluminium industrial waste with natural soils

Kaliakin VN (2017) www.sciencedirect.com Example problems related to compaction of soils. In: Soil mechanics

Rao BH, Reddy NG (2017) Zeta potential and particle size characteristics of red mud waste. In: Geoenvironmental practices and sustainability (pp 69–89). Springer, Singapore

Reddy NG, Rao BH (2018, October) Effect of additives on consistency limits of red mud waste: a comparative study. In: The international congress on environmental geotechnics (pp 234–241). Springer, Singapore

Sridevi G, Sahoo S, Sen S (2019) Stabilization of expansive soil with red mud and lime. In: Ground improvement techniques and geosynthetics (pp 259–268). Springer, Singapore

Sundaram R, Gupta S (2010) Constructing foundations on red mud. In: 6th international congress on environmental geotechnics (pp 1172–1175)

Sutar H, Mishra SC, Sahoo SK, Maharana HS (2014) Progress of red mud utilization: an overview

Surface Runoff Estimation of Rana Watershed in Mahanadi River Basin Using HEC-HMS

Chanchala, Jyotiprakash Padhi, and Bitanjaya Das

Abstract Due to unavailability, insufficient or of questionable quality and reliability of hydrological observations in small watersheds, it is difficult for the hydrologists to predict accurately hydrologic quantities like runoff, sediment, and nutrients etc. This issue is quite pronounced in developing countries like India, especially at the watershed (sub-catchment) level of large river basins, as these are ungauged. Thus, there is a need for methods that can be used for realistic estimation of such variables for ungauged catchments. Various researchers used HEC-HMS model due to its popularity in different studies of hydrology with respect to volume of surface runoff simulation for estimating flood peaks in flood forecasting. Therefore, an attempt has been made to predict the runoff in Rana sub-catchment in Mahanadi river basin of Eastern India through the integration of geographic information system (GIS) and a semi distributed hydrological model, HEC-HMS. Daily rainfall data of Rana watershed was collected over the period of 2000–2016. In the HEC-HMS model, SCS-CN method used for the computation of direct volume of runoff, SCS Unit Hydrograph method is used for converting the effective precipitation to runoff hydrograph and for the routing of the channel flow, Muskingum method is utilized. Simulation of runoff by HEC-HMS model in Rana basin is done by using the rainfall data, basin properties and SCS curve numbers. The sub basin characteristics of the Rana were found out with the help of HEC-GeoHMS through spatial analysis. Soil and LULC (Land use and Land cover) maps were used in HEC-GeoHMS for the determination of the CN (Curve number) for the loss model in order to compute the rate of loss and volume of runoff. Through the use of HEC-GeoHMS, hydrologic inputs were created that was used directly with the HEC-HMS model. Finally, HEC-HMS model was ran to estimate the direct surface runoff at the outlet of the Rana watershed. Surface runoff generated during monsoon months contribute to the maximum percentage of annual runoff in the Rana watershed. Average monthly runoff was found to be highest in the month of August and least for the month of December. By individually assessing

Chanchala · J. Padhi (✉) · B. Das
School of Civil Engineering, KIIT Deemed to be University, Bhubaneswar, Odisha, India
e-mail: jyotiprakash.padhifce@kiit.ac.in

B. Das
e-mail: bdasfce@kiit.ac.in

B. B. Das et al. (eds.), *Recent Developments in Sustainable Infrastructure (ICRDSI-2020)—GEO-TRA-ENV-WRM*, Lecture Notes in Civil Engineering 207,
https://doi.org/10.1007/978-981-16-7509-6_54

the runoff characteristics of other such sub-catchments in Mahanadi River Basin, accurate water resources analysis of the entire basin can be achieved.

Keywords Surface runoff · Ungauged sub-catchment · HEC-HMS · Hydrological model

1 Introduction

Availability of water resources affected due to increase in mean temperature, rainfall variation or rise in the level of sea through the manifestation of climatic change (Asokan and Dutta 2008). Mean yearly runoff will increase in the higher latitudes of equatorial Asia and Africa and mid latitudes as well as most of the sub tropic regions will experience decrease in runoff (Arnell 1999). Runoff plays an important role as it has a very substantial influence on various soil and water conservation practices. Estimation of runoff is a very critical hydrological process with respect to watershed management, which include the control and management of flood, irrigation and drainage network design, generation of hydropower and solid waste management.

Due to unavailability, insufficient or of questionable quality and reliability of hydrological observations, it is difficult for the hydrologists and water resources managers to predict accurately hydrologic quantities like runoff, sediment, and nutrients etc. This situation is particularly applicable for developing countries like India, where large number of watersheds are ungauged (Piman and Babel 2013). Runoff models based on rainfall developed recently have the capabilities for the representation of the variability in the properties of the landscape spatially (Refsgaard and Storm 1995; HEC 2000; Vieux and Vieux 2002). Integrating the precipitation data with the established models of runoff based on rainfall allows the hydrological scientists for the improved estimation of the volume of runoff from the watersheds (Hoblit and Curtis 2001). The representation of the spatial variability of factors controlling runoff is the advantage of distributed models. Considerable resources and attempt required for the preparation as well as modeling of data particularly in the developing countries because of the few monitoring as well as availability of data (Piman and Babel 2013). Practicing of the estimation of the flow at the ungauged sites of India could be beneficial, if there will be advanced assessment to the measured flow data in the gauged stations (Jha and Smakhtin 2008). The estimation of runoff in sub-catchments are being performed through various hydrological models.

Many authors in the past have also used hydrodynamic modeling approach to estimate hydrologic variables and developed rainfall-runoff for gauged as well as ungauged catchments. Various researchers used HEC-HMS model due to its popularity in different studies of hydrology with respect to volume of surface runoff simulation for estimating flood peaks in flood forecasting for the management and integration of watershed projects (Barik et al. 2017; Dariane et al. 2019; Thameemul Hajaj et al. 2019; Sai et al. 2017). HEC-HMS model designed for the simulation of the rainfall–runoff processes and forecast the flow of stream in the branched systems

of basin in the broad range of geographical areas such as small sized natural or urban watersheds and large river basins (Abushandi and Merkel 2013; Verma et al. 2010). The model provides number of options on hydrological modelling, with the key components focusing on the determination of hydrographs generated from runoff from the sub-basins and routing of hydrographs in channels to the study area's outlet (Beighley and Moglen 2003; Beighley et al. 2003). Preparation of the spatial data using the platform of GIS imported directly to HEC-HMS (Ali et al. 2011). Because of the lacking of adequate data and complex system of hydrology, the use of rainfall based runoff simulation models become inevitable and HEC-HMS comes up the best option through the integration of GIS and remote sensing (Ibrahim-Bathis and Ahmed 2016). Therefore, this study was undertaken for the estimation of the surface runoff in the Rana watershed.

2 Materials and Methods

2.1 Study Area

The river Mahanadi is the 3rd largest peninsula in India and also the largest river of Odisha state (Sundaray et al. 2014). Mahanadi River originates at the elevation of 442 m above MSL (Mean sea level) in the district Raipur of Chhattisgarh. The total drainage area of Mahanadi River was 141,589 km^2 covering Chhattisgarh, Odisha, Madhya Pradesh, Maharashtra and Jharkhand. Major part of the Mahanadi covers Odisha and Chhattisgarh whereas remaining portion of the basin is in Madhya Pradesh, Maharashtra and Jharkhand. In this study, Rana watershed (Fig. 1) was considered for estimation of surface runoff. Rana watershed is a right side tributary of Mahanadi river having Latitude of 20° 15′–20° 25′ N and Longitude of 85° 28′–85° 37′ E having geographical area of 500 km^2.

2.2 Methodology

DEM (Digital elevation model), LULC (Land use land cover) map, soil map, CN map and daily rainfall data of 17 (2000–2016) years and HEC-HMS model used for the estimation of surface runoff in the Rana watershed. DEM of Rana watershed was prepared from the SRTM (shuttle radar topography mission) 1 Arc-Second Global digital terrain elevation data (Fig. 2) having resolution of 30 m downloaded from the USGS Earth explorer website. After downloading, Arc Hydro tool of Arc GIS was used for the preparation of DEM of Rana watershed. Reconditioning, Fill sinks, Flow direction, Flow accumulation, Stream definition, Stream segmentation, Catchment grid delineation, Catchment polygon processing, Drainage line processing, Adjoint Catchment Processing, Drainage Point Processing, Locate Batch point and Batch

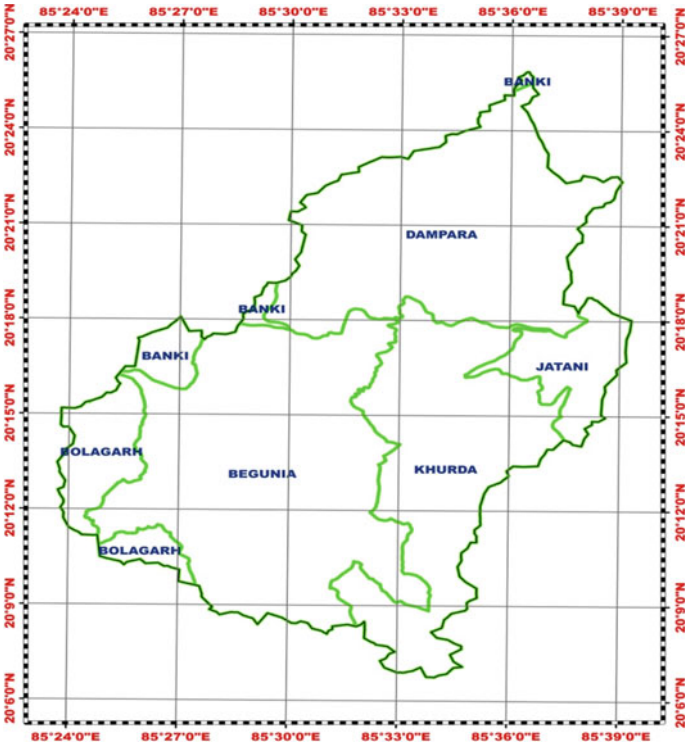

Fig. 1 Rana watershed

watershed delineation processes were performed for deriving the DEM (Fig. 2) from SRTM 1 Arc-Second Global data.

The Landsat satellite image was downloaded from the USGS Earth explorer website for the preparation of LULC map (Fig. 3) of the Rana watershed using Arc GIS. Maximum likelihood method of supervised classification in Arc GIS was used to classify the land use and land cover into five categories, vegetation, forest, bare land, water and built up area (Fig. 3). Soil classification file of the entire World was downloaded from the Food and Agriculture Organization (FAO) database for the preparation of the soil map (Fig. 4) of the Rana watershed. Major soils found in the area are sandy clay loam (47.36%), clay (26.31%) and sandy loam (21.05%). As per infiltration rate, they are further categorized into 4 HSGs (hydrological soil groups) A, B, C, D.

After the preparation of DEM of the watershed, data management, new project and generate project processes under the tab Project Setup performed in HEC-GeoHMS used for the generation of new project (Fig. 5). The sub basin characteristics of the Rana were found out with the help of HEC-GeoHMS through spatial analysis. Soil and LULC (Land use and Land cover) maps were used in HEC-GeoHMS for the determination of the CN (Curve number) for the loss model in order to compute the

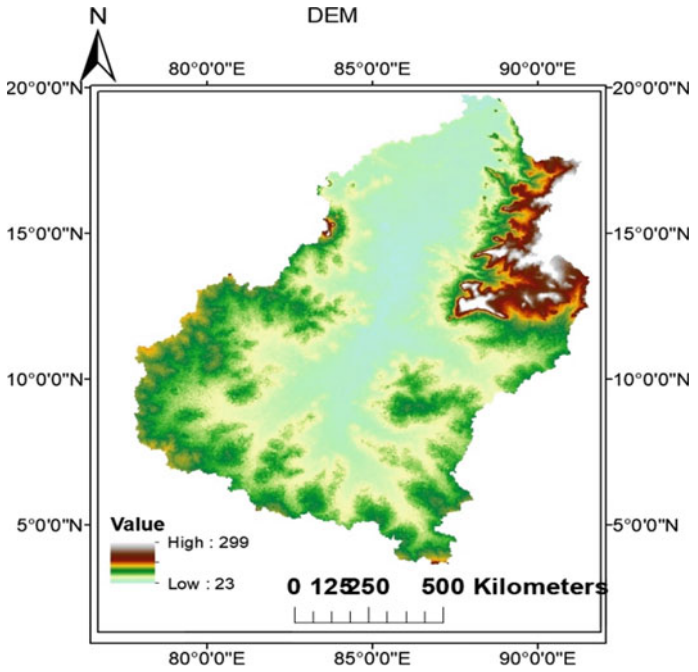

Fig. 2 DEM of Rana watershed

rate of loss and volume of runoff. CN grid (Fig. 6) of the Rana watershed generated through the utilization of soil map and LULC map. Then CN values were used as inputs into the Subbasin parameters through the use of CN Grid map. After that HEC-HMS project was generated by following the processes of data management, map to HMS units, HMS schematic, Toggle legend-HMS legend, add coordinate, prepare data for model export, background shape file, basin model file, met model file-specified Hyetograph under the tab HMS.

Through the use of HEC-GeoHMS, hydrologic inputs were created that was used directly with the model HEC-HMS. HEC-HMS is a semi distributed model developed by USACE (US Army Corps of Engineers). In the HEC-HMS model, SCS-CN method used for the computation of direct volume of runoff, SCS Unit Hydrograph method is used for conversion of effective rainfall to runoff hydrograph and for the routing of the channel flow, Muskingum method is used. Simulation of runoff by HEC-HMS model in Rana basin is done by using the rainfall data, basin properties and SCS curve numbers. Finally, HEC-HMS model was ran to estimate the direct surface runoff at the outlet of the Rana watershed.

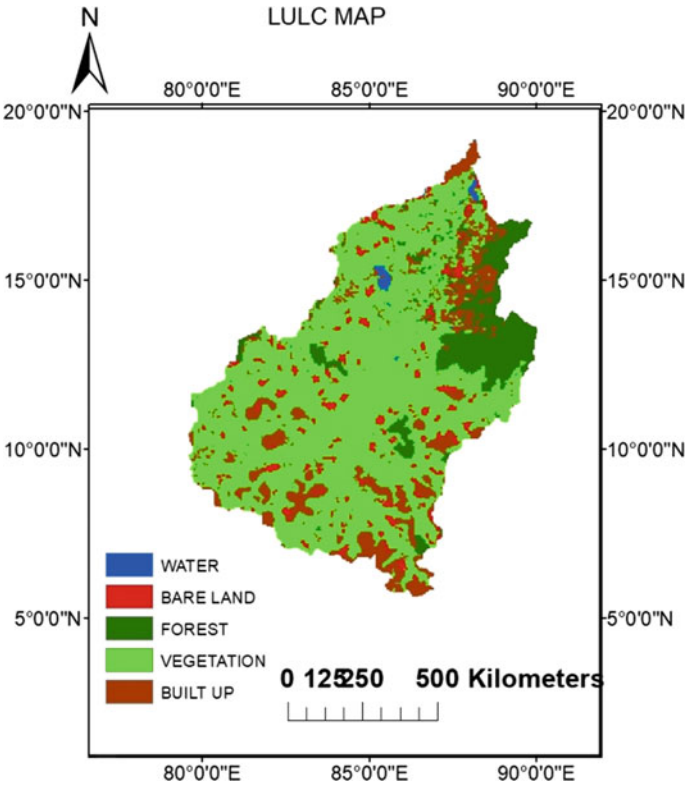

Fig. 3 LULC map of Rana watershed

3 Results and Discussion

3.1 Daily Runoff in Rana Watershed

DEM, Soil, LULC and CN maps generated through Arc Hydro and Geo-HMS, daily rainfall data of 17 (2000–2016) years and HEC-HMS model used for the generation of daily runoff in the Rana watershed for 17 years and presented in Fig. 7. Runoff pattern was not uniform across all the years for the Rana watershed (Fig. 7).

Daily maximum runoff amount of 31.6 m^3/s observed in the year 2009 in the month of July.

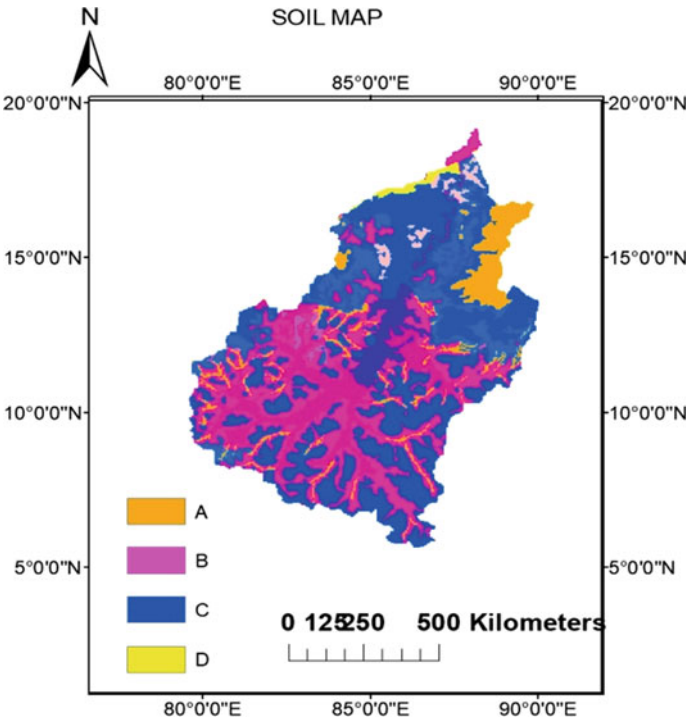

Fig. 4 Soil map of Rana watershed

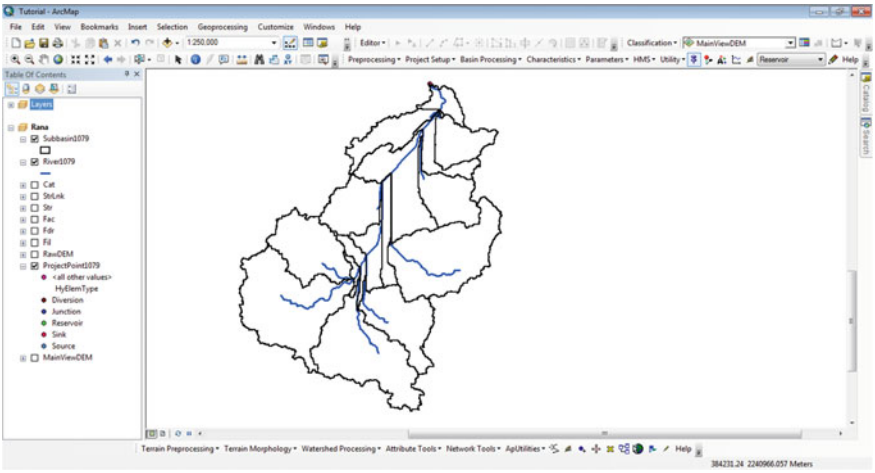

Fig. 5 Generation of new project using HEC-GeoHMS

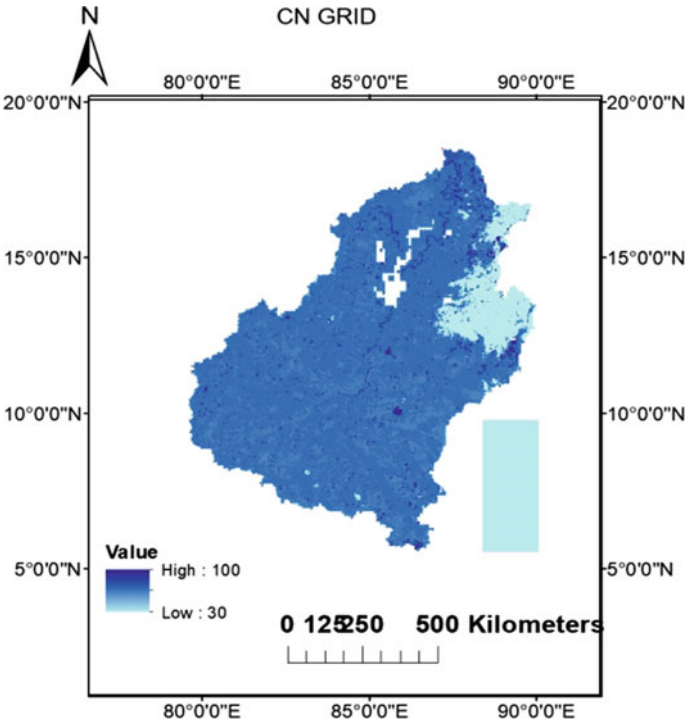

Fig. 6 CN Grid of the Rana watershed

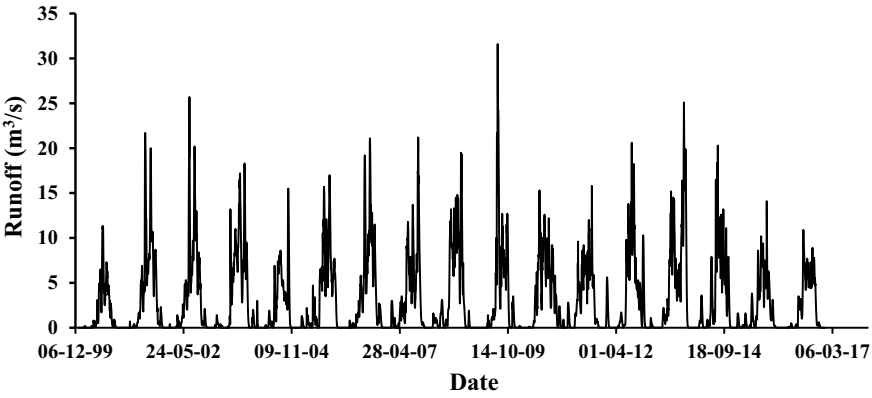

Fig. 7 Daily surface runoff of Rana watershed during 2000–2016

3.2 Annual Runoff in Rana Watershed

Maximum annual runoff of 1549.2 m^3/s occurred in the year 2013 whereas the year 2000 detected with lowest (558.2 m^3/s) amount of annual runoff (Table 1). Annual runoff categorized into monsoon (June, July, August and September) and non monsoon (January, February, March, April, May, October, November and December) runoff. Highest monsoon runoff of 1159.0 m^3/s found in the year 2008 whereas minimum monsoon runoff of 524.0 m^3/s experienced in the year 2000. Maximum (93.9%) percentage of annual runoff observed in the year 2000 as monsoon runoff whereas the year 2013 detected with lowest (56.6%) percentage of annual runoff. The year, 2013 detected with highest percentage of (43.4%) annual rainfall as non monsoon runoff and similarly minimum (6.1%) percentage of annual runoff found in 2000.

Table 1 Annual, monsoonal and non-monsoonal runoff in Rana watershed for individual year

Year	Runoff (m^3/s)		
	Annual	Monsoon	Non monsoon
2000	**558.2**	**524.0 (93.9%)**	**34.2 (6.1%)**
2001	1213.1	1034.1 (85.2%)	179.0 (14.8%)
2002	1210.9	1026.9 (84.8%)	184.0 (15.2%)
2003	1284.9	861.9 (67.1%)	423.0 (32.9%)
2004	742.1	520.7 (70.2%)	221.4 (29.8%)
2005	1189.0	843.0 (70.9%)	346.0 (29.1%)
2006	1255.3	1053.1 (83.9%)	202.2 (16.1%)
2007	1114.0	817.2 (73.4%)	296.8 (26.6%)
2008	1348.1	**1159.0** (86.0%)	189.1 (14.0%)
2009	1176.4	930.4 (79.1%)	246.0 (20.9%)
2010	1254.1	931.2 (74.3%)	322.9 (25.7%)
2011	978.5	775.5 (79.3%)	203.0 (20.7%)
2012	1213.4	899.8 (74.2%)	313.6 (25.8%)
2013	**1549.2**	877.0 **(56.6%)**	**672.2 (43.4%)**
2014	1147.5	904.5 (78.8%)	243.0 (21.2%)
2015	789.1	633.7 (80.3%)	155.4 (19.7%)
2016	797.2	636.6 (79.9%)	160.6 (20.1%)

Bold data indicating the maximum and minimum value for Annual, monsoonal and non-monsoonal runoff in Rana watershed

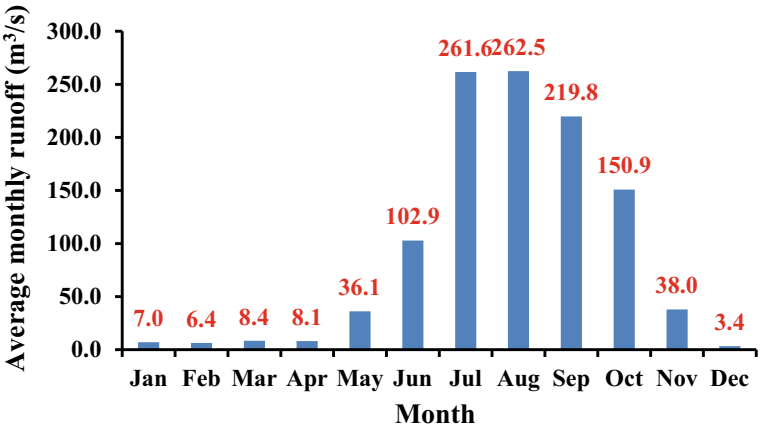

Fig. 8 Seventeen years monthly average surface runoff in Rana watershed

3.3 Average Monthly Runoff in Rana Watershed

Daily runoff data accumulated to get twelve number of monthly runoff data for each year and after that, average monthly runoff for the individual month calculated by taking the average of seventeen years monthly runoff data and presented in Fig. 8. Average monthly surface runoff value was found to be maximum (262.5 m^3/s) in the month of August followed by July (261.6 m^3/s) and September (219.8 m^3/s). Average monthly runoff value was least (3.4 m^3/s) in the month of December followed by February (6.4 m^3/s) and January (7.0 m^3/s).

3.4 Daily Runoff During Monsoon Period in Rana Watershed

Maximum percentage of annual precipitation occurred during the monsoon (June to September) season in India. As per the National Rainfed Area Authority (2012), mainly rainfed agriculture practiced in Odisha as major part of Odisha's cultivated area did not receive the irrigation water in spite of presence of lots of seasonal rivers in the State. Therefore, it is essential to know the pattern of runoff during 2000–2016 for the monsoon (June to September) period in the Rana watershed. The daily runoff value of Rana watershed during the monsoon period in the year 2000 presented in Fig. 9. Daily maximum runoff amount of 11.2 m^3/s found in the month of July for the year 2000 (Fig. 9).

The daily maximum, minimum and average runoff value for all the 17 years summarized in the Table 2. Daily maximum runoff varied from 8.6 to 31.6 m^3/s across all the years in the Rana watershed. Daily maximum runoff observed for 8 (2000, 2001, 2002, 2009, 2010, 2013, 2014 and 2016), 3 (2004, 2006 and 2012) and

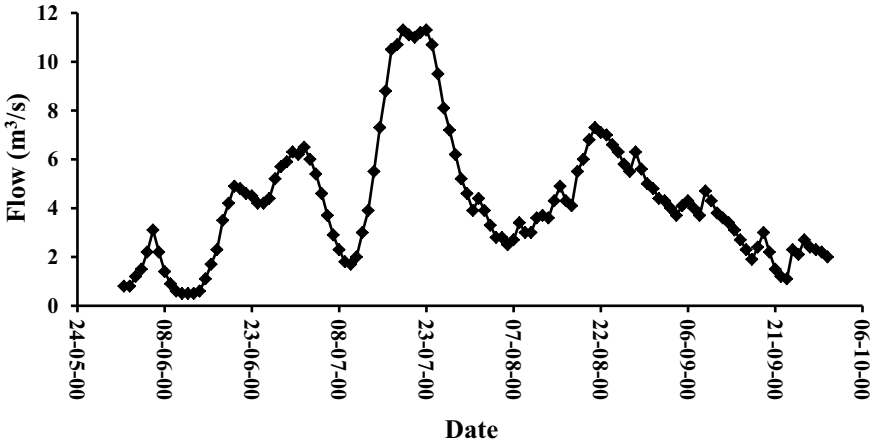

Fig. 9 Daily surface runoff of Rana watershed in the year 2000

Table 2 Daily maximum, minimum and average runoff value of the individual year during monsoon (June to September) and non monsoon (January to May and October to December) period

Year	Daily runoff (m^3/s) monsoon			Daily runoff (m^3/s) non monsoon		
	Maximum	Minimum	Average	Maximum	Minimum	Average
2000	11.3	0.5	4.3	1.8	0.0	0.1
2001	21.7	1.8	8.5	8.7	0.0	0.7
2002	25.7	2.0	8.4	7.8	0.0	0.8
2003	17.2	0.0	7.1	18.3	0.0	1.7
2004	8.6	0.0	4.3	15.5	0.0	0.9
2005	17.0	0.0	6.9	7.7	0.0	1.4
2006	21.1	1.7	8.6	11.2	0.0	0.8
2007	21.2	0.5	6.7	16.9	0.0	1.2
2008	19.5	1.2	9.5	7.2	0.0	0.8
2009	31.6	0.9	7.6	12.7	0.0	1.0
2010	15.3	1.4	7.6	9.2	0.0	1.3
2011	15.8	1.6	6.4	9.6	0.0	0.8
2012	20.6	0.1	7.4	10.3	0.0	1.3
2013	15.2	1.3	7.2	25.1	0.0	2.8
2014	20.3	0.4	7.4	11.1	0.0	1.0
2015	14.1	0.0	5.2	3.8	0.0	0.6
2016	10.9	1.0	5.2	7.8	0.0	0.7

6 (2003, 2005, 2007, 2008, 2011 and 2015) years in the month of July, August and September respectively. Similarly daily minimum runoff varied from 0.0 to 2.0 m^3/s and 4.3 to 9.5 m^3/s in case of average daily runoff during the monsoon periods over 17 years.

3.5 Daily Runoff During Non Monsoon Period in Rana Watershed

The daily maximum, minimum and average runoff value during non monsoon period for all the 17 years presented in Table 2. During the non monsoon period, surface runoff varied from 1.8 to 25.1 and 0.1 to 2.8 m^3/s for daily maximum and average runoff respectively.

3.6 Comparison of Daily Maximum and Average Runoff Between Monsoon and Non Monsoon months in Rana Watershed

It can be observed from the Fig. 10 that, daily maximum surface runoff was found to be more during the monsoon months as compared to the non monsoon months for all the years except in 2003, 2004 and 2013. Daily average surface runoff was found to be more in case of monsoon months with comparison to non monsoon months for all the seventeen years of the Rana watershed (Fig. 11).

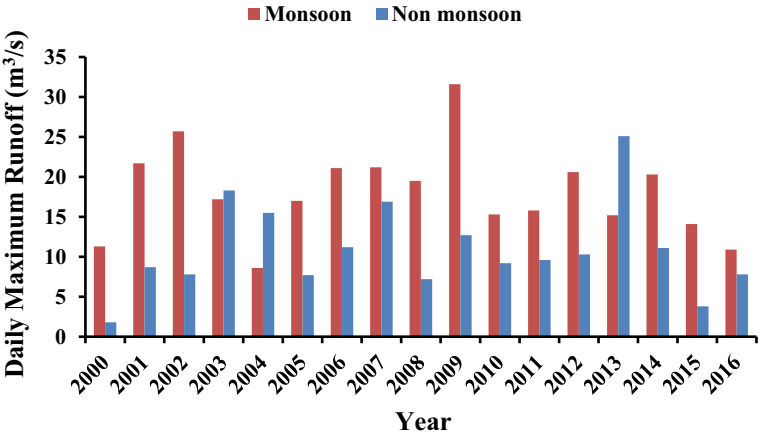

Fig. 10 Comparison of daily maximum surface runoff between monsoon and non monsoon months for all the 17 years of Rana watershed

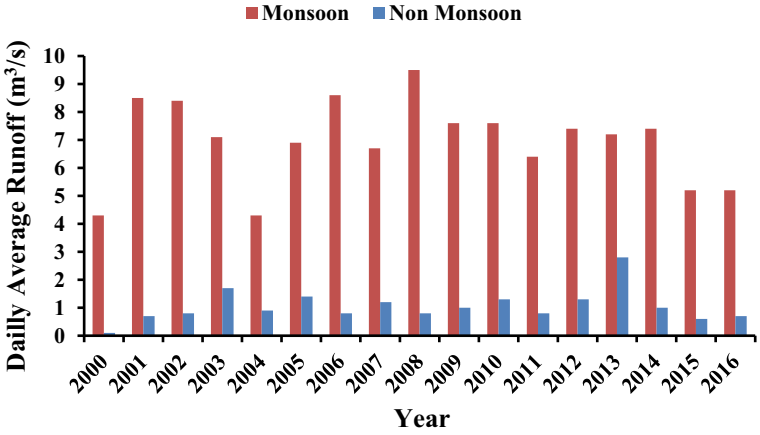

Fig. 11 Comparison of daily average surface runoff between monsoon and non monsoon months for all the 17 years of Rana watershed

4 Conclusion

DEM derived from SRTM, soil and LULC maps, CN grid maps generated through HEC-GeoHMS, seventeen years daily rainfall data and HEC-HMS model used for the computation of daily runoff in the Rana watershed during 2000–2016. Monsoon (June to September) months contributes maximum percentage of annual surface runoff in the Rana watershed as compared to non monsoon (January to May and October to December) months.

Average monthly runoff value were found to be more for the monsoon months as compared to non monsoon months and it was found to be maximum in the month of August. Daily maximum surface runoff was found to be more during the monsoon months as compared to the non monsoon months for all the years except in 2003, 2004 and 2013. However, the surface runoff generated by adopting this technique should be calibrated and validated by the measured data or through the regionalization and transposition techniques of basin similarity approach. The estimation of surface runoff through the integration of GIS technique and HEC-HMS model will be useful for those locations, where the gauge data is not available or difficult to collect information.

References

Abushandi E, Merkel B (2013) Modelling rainfall runoff relations using HEC-HMS and IHACRES for a single rain event in an arid region of Jordan. Water Resour Manage 27:2391–2409

Ali M, Khan SJ, Aslam I, Khan Z (2011) Simulation of the impacts of landuse change on surface runoff of Lai Nullah Basin in Islamabad, Pakistan. Landsc Urban Plan 102:271–279

Arnell NW (1999) Climate change and global water resources. Glob Environ Chang 9:S31–S49
Asokan SM, Dutta D (2008) Analysis of Water resources in the Mahanadi river basin, India under projected climate conditions. Hydrol Process 22(18):3589–3603
Barik DK, Singh AD, Sra MS (2017) Estimation of runoff and sediment yield from a small ungauged watershed using GIS and HEC-HMS. Int J Civ Eng Technol 8(6):517–527
Beighley RE, Moglen GE (2003) Adjusting measured peak discharges from an urbanized watershed to reflect a stationary land use signal. Water Resour Res 39:1093–1104
Beighley RE, Melack JM, Dunne T (2003) Impacts of California's climatic regimes and coastal land use change on streamflow characteristics. J Am Water Resour Assoc 39:1419–1433
Dariane AB, Bagheri R, Karami F, Javadianzadeh MM (2019) Developing heuristic multi-criteria auto calibration method for continuous HEC-HMS in snow-affected catchment. Int J River Basin Manag 18:69–80
Hoblit BC, Curtis DC (2001) GIS highlights importance of high resolution radar rainfall data. In: Proceedings of the 21st annual ESRI international user conference. ESRI, CA
Hydrologic Engineering Center (HEC) (2000) Hydrologic modeling system HEC-HMS user's manual—version 2, U.S. Army Corps of Engineers, Davis, CA
Ibrahim-Bathis K, Ahmed SA (2016) Rainfall-runoff modelling of Doddahalla watershed—an application of HEC-HMS and SCN-CN in ungauged agricultural watershed. Arab J Geosci 9:170
Jha R, Smakhtin V (2008) A review of methods of hydrological estimation at ungauged sites in India. IWMI working paper 130. International Water Management Institute, 24p
Piman T, Babel MS (2013) Prediction of rainfall-runoff in an Ungauged basin: case study in the mountainous region of Northern Thailand. J Hydrol Eng 18:285–296
Refsgaard JC, Storm B (1995) Chapter 23: Mike she. In: Singh VP (ed) Computer models of watershed hydrology. Water Resources Publications, Littleton, Co.
Sai M, Rahul KS, Mohanty B, Asadi SS (2017) Estimation analysis of runoff for Udaygiri Mandal using a potential method: a model study. Int J Civ Eng Technol 8(4):2062–2068
Sundaray SK, Nayak BB, Lee B-G, Bhatta D (2014) Spatio-temporal dynamics of heavy metals in sediments of the river estuarine system: Mahanadi basin (India). Environ Earth Sci 71:1893–1909
Thameemul Hajaj PM, Yarrakula K, Durga Rao KHV, Singh A (2019) A semi-distributed flood forecasting model for the Nagavali River using space inputs. J Indian Soc Rem Sens 47:1683–1692
Vieux BE, Vieux JE (2002) Vflo™: a real-time distributed hydrologic model. In: Proceedings of the 2nd Federal interagency hydrologic modeling conference, advisory committee on water information. U.S. Geological Survey, Reston, VA, pp 1–12
Verma AK, Jha MK, Mahana RK (2010) Evaluation of HEC-HMS and WEPP for simulating watershed runoff using remote sensing and geographical information system. Paddy Water Environ 8:131–144

Analysis of Annual and Seasonal Rainfall of Different Districts of Odisha

Sarthak Sahoo and Jyotiprakash Padhi

Abstract Temperature of the earth's surface increased over the last few decades because of global warming which effected the hydrological cycle and patterns of precipitation across World. Precipitation is one of the important parameter of water cycle which affects the agriculture by influencing the availability of water resources. The trend as well as pattern of the rainfall disturb significantly because of the climatic variability. This study carried out for finding the decadal changes of seasonal rainfall (monsoon), annual rainfall, and also the seasonality index (SI) along with annual as well as seasonal trend analysis rainfall for all thirty districts of Odisha. Daily rainfall data of thirty districts over 30 (1990–2019) years were collected and converted to annual rainfall and seasonal rainfall (monsoon) data, and was used for the analysis. Decade wise, Angul, Balasore, Dhenkanal, Jagatsinghpur, Jajpur, Kendrapara, Khordha and Puri Districts experienced decrease in average annual rainfall whereas Nawarangpur and Nayagarh Districts detected with increase in average annual rainfall. Decade wise, decrease in average monsoon rainfall is observed for Bhadrak, Bolangir aand Dhenkanal districts where as increase of average monsoon rainfall is observed in Gajapati, Ganjam, Koraput and Nuapada Districts. SI value was found to be lowest (0.76) in Gajapati district whereas maximum value of 1.13 in Bargarh district. Mann–Kendall test was performed for the seasonal as well as monsoon rainfall trend analysis. Amongst all districts, Koraput district experienced significant increasing trend for the annual rainfall. Significant increasing trend of seasonal (monsoon) rainfall observed for Koraput and Gajapati districts. Districts experiencing decreasing trend are critical from water resource management and crop planning view for annual and monsoon rainfall respectively.

Keywords Rainfall · Trend · Seasonality index · Water resources management

S. Sahoo · J. Padhi (✉)
School of Civil Engineering, KIIT Deemed to be University, Bhubaneswar, Odisha, India
e-mail: jyotiprakash.padhifce@kiit.ac.in

B. B. Das et al. (eds.), *Recent Developments in Sustainable Infrastructure (ICRDSI-2020)—GEO-TRA-ENV-WRM*, Lecture Notes in Civil Engineering 207,
https://doi.org/10.1007/978-981-16-7509-6_55

1 Introduction

The hydrological cycle as well as the patterns of precipitation across the world effected due to global warming because of the rise in the earth's surface temperature over the most recent decades (IPCC 2013). Water availability and the moisture level of the soil depends on the patterns of precipitation, which is a part of the terrestrial hydrological cycle (Pai et al. 2014). Changes in rainfall have affected directly drought, water resources, floods and ecosystem services as precipitation is one of the important component of the hydrological cycle (Wu et al. 2013). As per Pal and Al-Tabba (2011), rainfall's magnitude, frequency and intensity changes because of the change in climate. Further, the trend as well as pattern of the rainfall disturb significantly due to the variability in climate (Loo et al. 2015). Hydrologic cycle pattern may be changed due to changes in precipitation, which can impact the society and environment (Gajbhiye et al. 2016). Therefore, it is necessary for studying the rainfall variability characteristics (Ahmad et al. 2018). Country's food security and agricultural productivity would be adversely effected due to the change in the distribution of rainfall because of the climatic change (Gadgil and Gadgil 2006). As per the Ministry of Finance Report (2018), decrease in agricultural productivity can result in the increase of prices and distress of farmer in the country as 16% of the GDP depends on agriculture in India. For this reason, it is very important for investigating the variability and trend of rainfall for the assessment of the availability of water in the region affecting the agricultural productivity.

Various studies were carried out in the past for investigating the impact of change in climate on the variability and trend of rainfall in India (Dash et al. 2007; Ghosh et al. 2009; Kumar et al. 2010; Patra et al. 2012; Pai et al. 2015; Singh et al. 2020). Trend as well as distribution of rainfall are often utilized by the experts of climatology, hydrology and agriculture for the assessment of the effect of variability as well as climatic change around the World (Ghosh et al. 2009). It is found that, variability as well as trend on the basis of large scale may widely varied from scale on regional basis (Bisht et al. 2017; Taxak et al. 2014). For this reason, an improved understanding of the distribution as well as trend of rainfall in a particular location is important, mainly for the judicious use of water and adaptation of policies for the growing of major crops in the agricultural locations based on rainfall. As per the National Rainfed Area Authority (2012), mainly rainfed agriculture practiced in Odisha as major part of Odisha's cultivated area did not receive the irrigation water in spite of presence of lots of seasonal rivers in the State. For this reason, exploration of rainfall trend as well as pattern across the different parts of the Odisha is required for the successful management and planning of the cropping systems depend on rainfall. However, efficient management of water for agriculture requires the information on variability of rainfall region wise instead of providing the variability of rainfall over the entire State as a single unit. Therefore, this study is undertaken in the thirty districts of Odisha for investigating the decadal changes of seasonal rainfall (monsoon), annual rainfall, and also the seasonality index (SI) including the analysis of trend for seasonal as well as monsoon rainfall.

2 Materials and Methods

2.1 Study Area

Monsoon as well as annual rainfall analysis study was carried out for the thirty districts of Odisha (Fig. 1). Thirty districts of Odisha experineced ten different agro-climatic zones of Odisha.

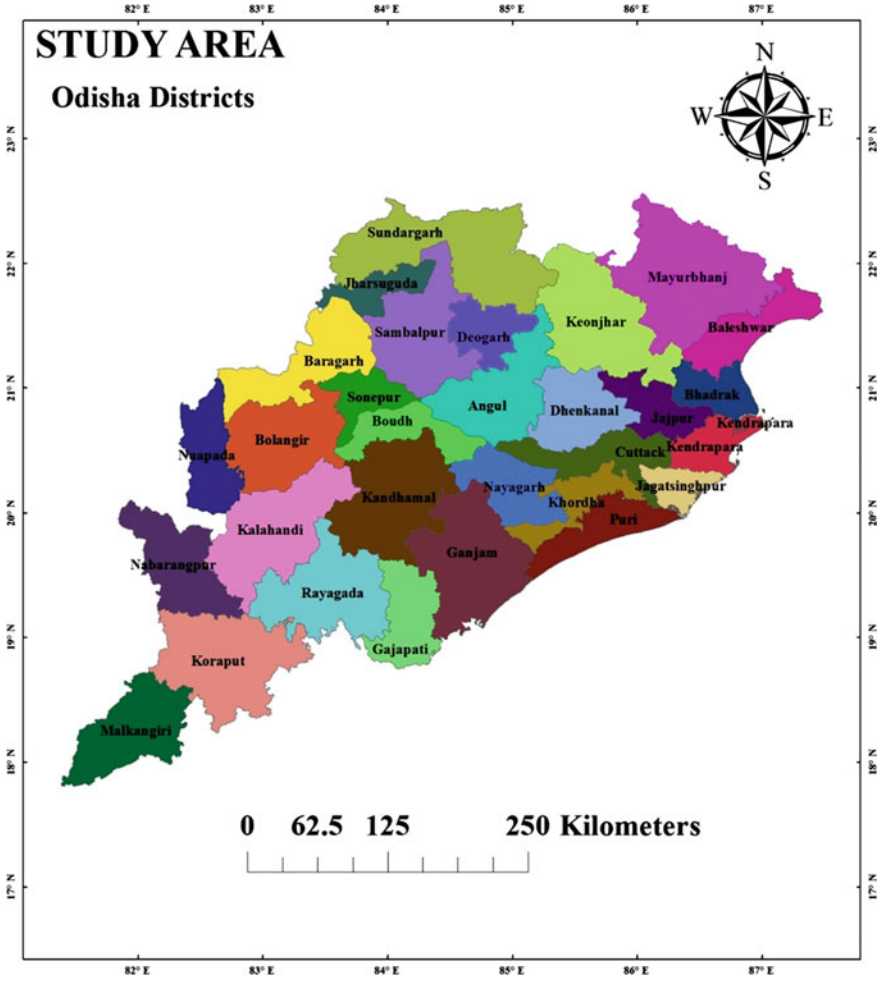

Fig.1 Geographical map of thirty districts of Odisha

2.2 Methodology

Daily rainfall data of thirty districts of Odisha for 30 (1990–2019) years collected from the Water Resources Department, Govt. of Odisha, India. Daily rainfall data converted to monthly rainfall data. Monthly rainfall data utilized for the estimation of monsoon and annual rainfall by cumulating the June to September and January to December rainfall respectively. 30 years of monsoon and annual rainfall data were utilized for the decadal, seasonality index (SI) and trend analysis of thirty districts of Odisha.

Thirty years (1990–2019) mean annual as well as monsoon rainfall value of all the districts of Odisha were estimated. With the purpose of finding the decadal effect of monsoon and annual rainfall, mean value were also computed decade wise during 1990–1999, 2000–2009 and 2010–2019 for both monsoon and annual rainfall. Identification of the regime of rainfall based on monthly rainfall distribution was done with the help of SI index. In addition to this, SI index also quantifies the variability of monthly rainfall all over the year. However, this index do not give any information on the magnitude and occurrence of rainfall. It is the summation of the absolute deviations of average rainfall on monthly basis from the long-term average monthly value, divided by the average yearly rainfall (Walsh and Lawer 1981; Guhathakurta and Saji 2013). SI is computed for thirty districts of Odisha by the formula given below:

$$\mathrm{SI} = \frac{1}{\overline{R}} \sum_{n=1}^{12} \left| \overline{x}_n - \frac{\overline{R}}{12} \right|$$

where $\overline{x}_n$ is average precipitation of the month n and $\overline{R}$ is average yearly precipitation of each district. SI can varied from zero, if all the months have the same amount of rainfall to 1.83 (if all of the precipitation events occur in single month) (Singh et al. 2020). SI classification limits along with their reimes of rainfall (Kanellopoulou, 2002) presented in Table 1.

Approaches for the detection of trend does not depend on the distribution of sample are useful and is choosen for the indication of the population behavior at present.

Table 1 Classification of SI index and the corresponding various regimes of rainfall

Regime of rainfall	SI
Very equable	≤0.19
Equable but with a definite wetter season	0.20–0.39
Rather seasonal with a short drier season	0.40–0.59
Seasonal	0.60–0.79
Markedly seasonal with a long drier season	0.80–0.99
Most rain in three months or less	1–1.19
Extreme, almost all rain in 1–2 months	≥1.2

For this reason, analysis of rainfall trend for long period is executed widely using Mann–Kendall test. Mann (1945) first used the non-parametric test based on rank whereas the statistical test developed by Kendall (1975). Computation of the trend slope in the sample data was performed by following the procedure of Sen's (1968) slope estimator, which is used for getting the trend magnitude obtained through Mann–Kendall test in the present study.

3 Results and Discussion

Average monsoon and annual rainfall for thirty districts of Odisha were estimated through the utilisation of 30 years of rainfall data and presented in Figs. 2 and 3.

Kalahanadi district experienced highest (1423.6 mm) amount of mean monsoon rainfall whereas minimum (304.8 mm) average monsoon rainfall observed in Balasore district (Fig. 2). It can be oberved from Fig. 3 that, the average annual rainfall was maximum (1803.8 mm) for the Cuttack district followed by Balasore district whereas Nuapada received lowest (1151.4 mm) amount of rainfall.

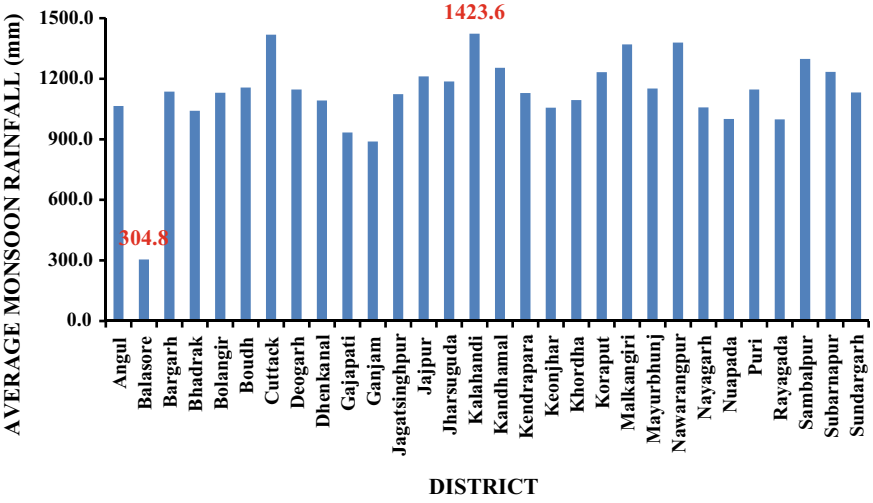

Fig. 2 Average monsoon rainfall of thirty districts of Odisha over 30 (1990–2019) years

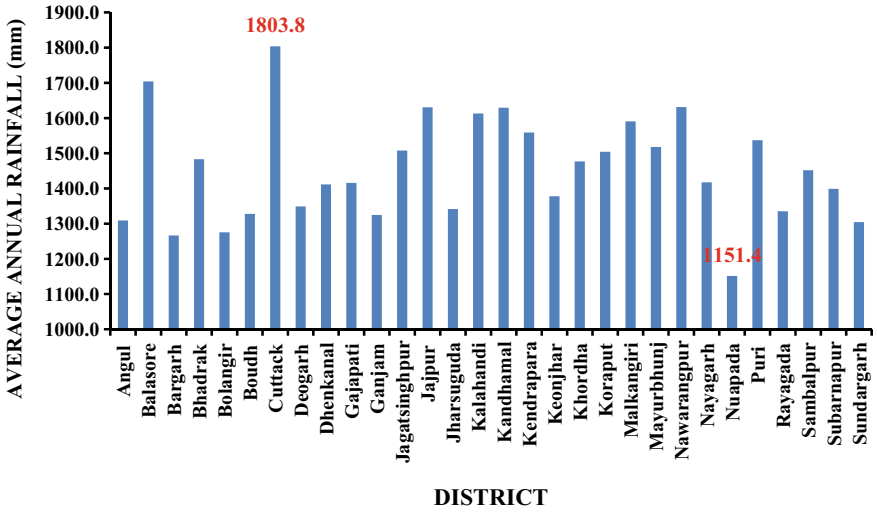

Fig. 3 Average annual rainfall of thirty districts of Odisha over 30 (1990–2019) years

3.1 Interpretation of the Decadal Changes of Average Monsoon and Annual Rainfall

The average monsoon and annual rainfall was computed decade wise for thirty districts of Odisha and presented in Table 2. Decrease in decade wise average monsoon rainfall observed for Bargarh, Bhadrak and Dhenkanal whereas Gajapati, Ganjam, Koraput and Nuapada districts experienced increase in average monsoon rainfall. No distinct pattern of average monsoon rainfall was observed among the remaining twenty three districts of Odisha.

Average monsoon rainfall reduced by 7.4, 11.2 and 10.1% in the last decade (2010–2019) with respect to the first (1990–1999) decade for Bargarh, Bhadrak and Dhenkanal respectively. Similarly, 11.7, 7.2, 18.7 and 8.7% increment in average monsoon rainfall detected for Gajapati, Ganjam, Koraput and Nuapada districts respectively. Decade wise, Angul, Balasore, Dhenkanal, Jagatsinghpur, Jajpur, Kendrapara, Khordha and Puri districts detected with decrease in average annual rainfall whereas increase in annual rainfall occurred for Nawarngpur and Nayagarh districts. Different districts have different pattern of monsoon as well as annual rainfall due to spatial and temporal variation of rainfall across the various parts of Odisha. Particularly, the districts experiencing decrease in average monsoon rainfall decade wise, proper steps should be taken for the efficient management of rainfall water.

Table 2 Decadal changes of average monsoon and annual rainfall of different districts of Odisha

District	Monsoon rainfall			Annual rainfall		
	1990–1999	2000–2009	2010–2019	1990–1999	2000–2009	2010–2019
Angul	1076.8	1131.6	988.2	1351.5	1331.9	1244.6
Balasore	1271.3	1289.4	1096.8	1841.8	1692.9	1577.5
Bargarh	1175.6	1143.6	1088.9	1340.8	1227.8	1231.2
Bhadrak	1100.2	1048.6	976.7	1635.3	1393.7	1421.0
Bolangir	1105.8	1231.3	1055.6	1289.5	1338.2	1198.3
Boudh	1035.1	1341.5	1092.4	1221.1	1482.0	1280.4
Cuttack	1076.1	1436.5	1201.4	1521.0	1744.4	1602.8
Deogarh	1244.7	1057.0	1138.7	1490.7	1214.5	1341.2
Dhenkanal	1138.5	1114.4	1023.3	1511.3	1361.6	1361.0
Gajapati	887.6	922.4	991.3	1412.9	1310.4	1524.0
Ganjam	853.3	900.6	914.5	1378.6	1233.0	1361.9
Jagatsinghpur	1162.9	1186.6	1022.9	1618.4	1481.6	1424.0
Jajpur	1211.9	1306.1	1118.1	1724.5	1593.6	1573.7
Jharsuguda	1178.8	1135.2	1246.1	1333.6	1291.5	1399.3
Kalahandi	1302.2	1610.3	1358.4	1556.6	1728.1	1555.1
Kandhamal	1174.0	1460.2	1128.7	1646.3	1758.7	1482.8
Kendrapara	1118.5	1211.7	1059.0	1662.5	1520.7	1494.0
Keonjhar	1009.8	1101.4	1058.4	1341.5	1394.3	1398.0
Khordha	1016.3	1202.6	1063.7	1487.1	1476.8	1466.6
Koraput	1138.9	1208.4	1352.0	1444.7	1420.7	1647.0
Malkangiri	1318.2	1266.5	1525.1	1609.7	1436.9	1725.9
Mayurbhunj	1129.2	1194.3	1133.7	1497.0	1533.0	1523.7
Nawarangpur	1226.5	1471.7	1439.8	1505.7	1677.1	1711.5
Nayagarh	958.3	1184.4	1031.9	1347.1	1450.7	1453.7
Nuapada	955.5	1008.2	1038.8	1163.2	1098.6	1192.4
Puri	1130.3	1221.8	1087.7	1624.7	1504.5	1482.1
Rayagada	936.4	1036.6	1023.2	1342.2	1293.0	1370.5
Sambalpur	1237.4	1362.0	1296.5	1380.5	1505.8	1469.2
Subarnapur	1239.0	1299.4	1163.9	1458.5	1410.5	1328.3
Sundargarh	1124.7	1139.9	1131.8	1316.7	1288.9	1307.5

3.2 Seasonal Index (SI)

Seasonal Index (SI) value calculated for the thirty districts of Odisha and presented in Table 3. SI value varied from 0.76 to 1.13 across the thirty districts. Angul, Balasore, Bhadrak, Cuttack, Dhenkanal, Ganjam, Jagatsinghpur, Jajpur, Kandhamal,

Table 3 Seasonal index (SI) value of thirty districts of Odisha

District	SI	Rainfall regime
Angul	0.97	Markedly seasonal with a long drier season
Balasore	0.82	Markedly seasonal with a long drier season
Bargarh	1.13	Most rain in three months or less
Bhadrak	0.83	Markedly seasonal with a long drier season
Bolangir	1.11	Most rain in three months or less
Boudh	1.08	Most rain in three months or less
Cuttack	0.93	Markedly seasonal with a long drier season
Deogarh	1.04	Most rain in three months or less
Dhenkanal	0.90	Markedly seasonal with a long drier season
Gajapati	0.76	Seasonal
Ganjam	0.82	Markedly seasonal with a long drier season
Jagatsinghpur	0.90	Markedly seasonal with a long drier season
Jajpur	0.86	Markedly seasonal with a long drier season
Jharsuguda	1.10	Most rain in three months or less
Kalahandi	1.10	Most rain in three months or less
Kandhamal	0.88	Markedly seasonal with a long drier season
Kendrapara	0.89	Markedly seasonal with a long drier season
Keonjhar	0.87	Markedly seasonal with a long drier season
Khordha	0.89	Markedly seasonal with a long drier season
Koraput	0.98	Markedly seasonal with a long drier season
Malkangiri	1.05	Most rain in three months or less
Mayurbhunj	0.86	Markedly seasonal with a long drier season
Nawarangpur	1.03	Most rain in three months or less
Nayagarh	0.87	Markedly seasonal with a long drier season
Nuapada	1.07	Most rain in three months or less

(continued)

Table 3 (continued)

District	SI	Rainfall regime
Puri	0.91	Markedly seasonal with a long drier season
Rayagada	0.84	Markedly seasonal with a long drier season
Sambalpur	1.13	Most rain in three months or less
Subarnapur	1.09	Most rain in three months or less
Sundargarh	1.07	Most rain in three months or less

Kendrapara, Keonjhar, Khordha, Koraput, Mayurbhanj, Nayagarh, Puri and Rayagada districts experienced markedly seasonal with a long drier season (SI value 0.80–0.99).

Most rain in three months or less rainfall regime (SI value 1–1.19) observed in Bargarh, Bolangir, Boudh, Deogarh, Jharsuguda, Kalahandi, Malkangiri, Nawarangpur, Nuapada, Sambalpur, Subarnapur and Sundargarh districts whereas Gajapati district detected with seasonal type of rainfall regime (SI value 0.60–0.79). Different rainfall regimes experienced by the different districts of Odisha due to non uniform distribution of rainfall across the different districts of Odisha. The knowledge of the pattern of seasonal precipitation and the identification of the changes in SI is beneficial for the planning of agriculture.

3.3 Trend Analysis of Monsoon and Annual Rainfall

Monsoon and Annual rainfall value during 1990–2019 were used for the determination of trend as well as magnitude through Mann–Kendall statistics and Sen's slope estimator method and presented in Figs. 4 and 5. It can be observed from Fig. 4 that, considerable variability of trend as well as magnitude of monsoon and annual rainfall observed among the thirty districts of Odisha.

No significant decreasing trend in monsoon rainfall observed for Angul, Balasore, Bargarh, Bhadrak, Bolangir, Deogarh, Dhenkanal, Jagatsinghpur, Jajpur and Subarnapur districts whereas Boudh, Cuttack, Ganjam, Jharsuguda, Kalahandi, Kandhamal, Kendrapara, Keonjhar, Khordha, Malkangiri, Mayurbhanj, Nawarangpur, Nayagarh, Nuapada, Puri, Rayagada, Sambalpur and Sundargarh districts detected with no significant increasing trend. Significantly increasing trend in monsoon rainfall experienced only in Gajapati and Koraput districts. Highest decrease (−1.21 mm/year) in monsoon rainfall magnitude of occurred in Deogarh district. Maximum increase (2.36 mm/year) in monsoon rainfall of magnitude observed for the Koraput district. Sixteen and thirteen districts of Odisha experienced no significant decreasing and increasing trend in annual rainfall respectively. Koraput district detected with significantly increasing trend in annual rainfall. Similarly, Kandhamal

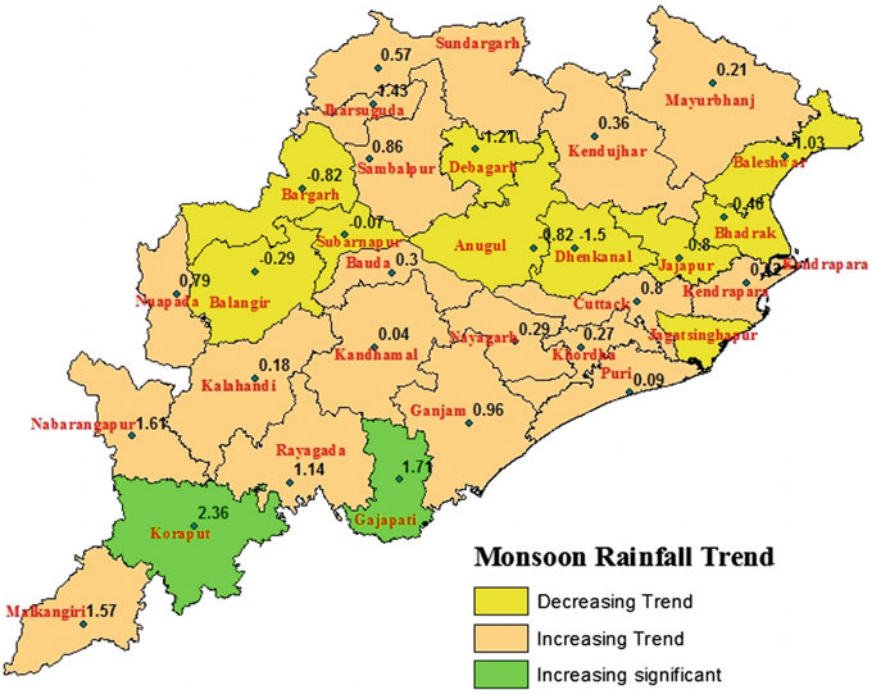

Fig. 4 Monsoon rainfall Trend of thirty districts of Odisha

district experienced maximum decrease (−1.28 mm/year) in annual rainfall whereas highest increase (1.86 mm/year) in annual rainfall detected for Koraput district.

4 Conclusion

Thirty years of precipitation data were utilized in order to interpret the effect of decadal changes of seasonal rainfall (monsoon), annual rainfall, and also the seasonality index (SI) along with trend analysis for annual and seasonal (monsoon) rainfall for all thirty districts of Odisha. Decrease in decade wise average monsoon and annual rainfall observed for three (Bargarh, Bhadrak and Dhenkanal) and eight (Angul, Balasore, Dhenkanal, Jagatsinghpur, Jajpur, Kendrapara, Khordha and Puri) districts respectively. Similarly, decade wise, Gajapati, Ganjam, Koraput and Nuapada districts experienced increase in average monsoon rainfall whereas Nawarngpur and Nayagarh districts detected with increase in average annual rainfall. Different regimes of rainfall observed across the thirty districts of Odisha based on seasonality index value. No significant decreasing trend observed for nine and sixteen districts whereas eighteen and thirteen districts detected with no significant increasing trend for monsoon and annual rainfall respectively. Significantly

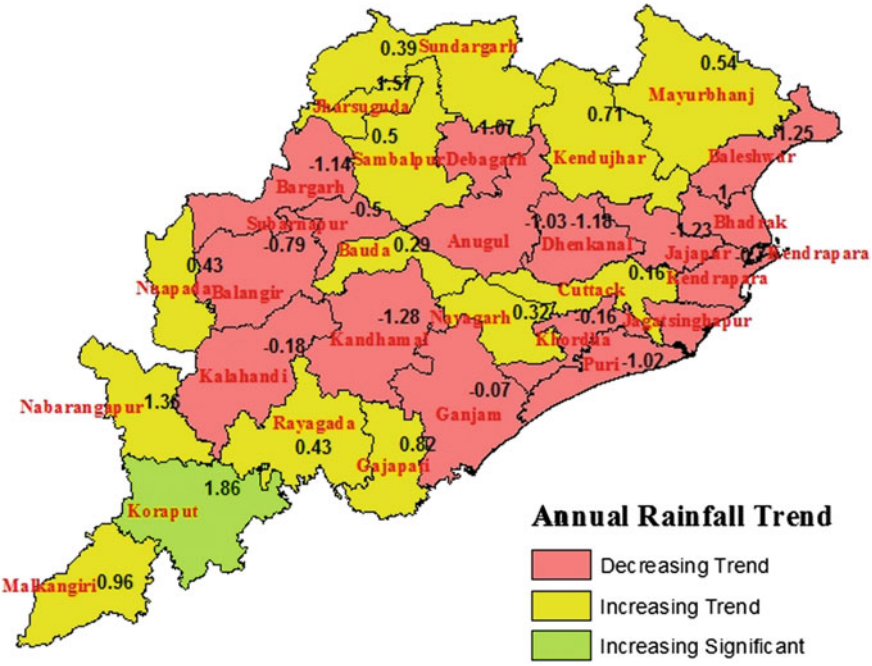

Fig. 5 Annual rainfall Trend of thirty districts of Odisha

increasing trend of monsoon rainfall experienced in Gajapati and Koraput districts whereas Koraput district detected with significantly increasing trend in annual rainfall. Therefore, the districts observed with decade wise decrease and also decreasing monsoon rainfall are critical from crop planning point of view. Therefore, cropping pattern should be modified and un utilized runoff water should be harvested during the monsoon season in order to cope with the drought in those districts. Similarly, districts experiencing decreasing trend in annual rainfall are critical from water resources management point of view. This study will be helpful for the management of monsoon and annual rainfall water for the efficient management and planning of cropping systems as well as water resources for the different districts of Odisha.

References

Ahmad I, Zhang F, Tayyab M, Anjum MN, Zaman M, Liu J, Farid HU, Saddique Q (2018) Spatiotemporal analysis of precipitation variability in annual, seasonal and extreme values over upper Indus River basin. Atmos Res 213:346–360

Bisht DS, Chatterjee C, Raghuwanshi NS, Sridhar V (2017) Spatio-temporal trends of rainfall across Indian river basins. Theoret Appl Climatol 132:419–436

Dash SK, Jenamani RK, Kalsi SR, Panda SK (2007) Some evidence of climate change in twentieth-century India. Clim Change 85:299–321

Gadgil S, Gadgil S (2006) The Indian monsoon, GDP and agriculture. Econ Pol Wkly 41:4887–4895
Gajbhiye S, Meshram C, Singh SK, Srivastava PK, Islam T (2016) Precipitation trend analysis of Sindh River basin, India, from 102-year record (1901–2002). Atmos Sci Lett 17:71–77
Ghosh S, Luniya V, Gupta A (2009) Trend analysis of Indian summer monsoon rainfall at different spatial scales. Atmos Sci Lett 10:285–290
Guhathakurta P, Saji E (2013) Detecting changes in rainfall pattern and seasonality index vis-a-vis increasing water scarcity in Maharashtra. J Earth Syst Sci 122(3):639–649
IPCC (2013) Summary for policymakers. In: Stocker TF, Qin D, Plattner G-K, Tignor M, Allen SK, Boschung J, Nauels A, Xia Y, Bex V, Midgley PM (eds) Climate change. The physical science basis. Contribution of working group I to the fifth assessment report of the IPCC. Cambridge University Press, Cambridge
Kanellopoulou EA (2002) Spatial distribution of rainfall seasonality in Greece. Weather 57:215–219
Kendall M (1975) Rank correlation methods. Charles Griffin, London
Kumar V, Jain SK, Singh Y (2010) Analysis of long-term rainfall trends in India. Hydrol Sci J 55:484–496
Loo YY, Billa L, Singh A (2015) Effect of climate change on seasonal monsoon in Asia and its impact on the variability of monsoon rainfall in Southeast Asia. Geosci Front 6:817–823
Mann HB (1945) Nonparametric tests against trend. Econometrica 13:245–259
Ministry of Finance Report India (2018) Climate, climate change, and agriculture, economic survey 2017–2018, vol 1, pp 82–101
National Rainfed Area Authority (2012) Prioritization of rainfed areas in India, study report 4. National Rainfed Area Authority, New Delhi, India 100p
Pai DS, Sridhar L, Rajeevan M, Sreejith OP, Satbhai NS, Mukhopadyay B (2014) Development of a new high spatial resolution (0.25° × 0.25°) long period (1901–2010) daily gridded rainfall data set over India and its comparison with existing data sets over the region. Mausam 65:1–18
Pai DS, Sridhar L, Badwaik MR, Rajeevan M (2015) Analysis of the daily rainfall events over India using a new long period (1901–2010) high resolution (0.25 × 0.25 degree) gridded rainfall data set. Clim Dyn 45:755–776
Pal I, Al-Tabbaa A (2011) Assessing seasonal precipitation trends in India using parametric and non-parametric statistical techniques. Theoret Appl Climatol 103:1–11
Patra JP, Mishra A, Singh R, Raghuwanshi NS (2012) Detecting rainfall trends in twentieth century (1871–2006) over Orissa State, India. Clim Change 111:801–817
Sen PK (1968) Estimates of the regression coefficient based on Kendall's Tau. J Am Stat Assoc 63:1379–1389
Singh G, Panda RK, Nair A (2020) Regional scale trend and variability of rainfall pattern over agro-climatic zones in mid-Mahanadi river basin of eastern India. J Hydro Environ Res 29:5–19
Taxak AK, Murumkar AR, Arya DS (2014) Long term spatial and temporal rainfall trends and homogeneity analysis in Wainganga basin, Central India. Weather Clim Extremes 4:50–61
Walsh RPD, Lawer D (1981) Rainfall seasonality: description, spatial patterns and change through time. Weather 36:201–208
Wu P, Christidis N, Stott P (2013) Anthropogenic impact on Earth's hydrological cycle. Nat Clim Chang 3:807–810

Study of Fatal Accidents Among Building Constructions Labours in Bangladesh

Shajahan Ali, Syed Ishtiaq Ahmad, and Md. Saddam Hossain

Abstract The building construction has a higher risk of accidents, and the fatality rate in this building construction is higher than in any other sector in most countries. Statistics suggest that construction workers are 3 to 6 times more likely to die from injuries at work than other workers. The building construction is considered one of the fastest-growing sectors in Bangladesh, contributing about 9% to the national economy of the country in terms of GDP, creating jobs for about 2.6 million people, which is about 4.4% of the total workforce of the country. In this area, however, very little research has been done to understand the trend of accidents and other mishaps prevalent in Bangladesh's construction industry. The purpose of this paper was to investigate the existence and reasons for the numerous fatal accidents prevalent in Bangladesh's building construction. For this reason, data is collected from the Occupational Safety, Health and Environment (OSHE) foundation, which collects data on occupational accidents. Data from the police authorities and news reported in various national daily newspapers were also collected. Data collected shows that over the last 12 years, there have been 1715 cases of fatalities in Bangladesh's building construction, one of the highest in the world. Examination of data also reveals that the two prime causes for building fatalities are falling from heights and electrocution, accounting for around 38.07% and 27.01% of all fatalities, respectively. Examination of the particular reasons for the two types of incidents reveals that enhancing the overall safety scenario for construction sites will easily avoid them.

Keywords Safety of construction · Fatal injuries · Falling · Electrocution

S. Ali (✉)
Department of Civil Engineering, Bangladesh Army University of Engineering and Technology, Natore, Bangladesh
e-mail: shajahan@bauet.ac.bd

S. I. Ahmad (✉) · Md. Saddam Hossain (✉)
Department of Civil Engineering, Bangladesh University of Engineering and Technology, Dhaka, Bangladesh
e-mail: siahmad@ce.buet.ac.bd

Md. Saddam Hossain
e-mail: saddam@ce.buet.ac.bd

B. B. Das et al. (eds.), *Recent Developments in Sustainable Infrastructure (ICRDSI-2020)—GEO-TRA-ENV-WRM*, Lecture Notes in Civil Engineering 207,
https://doi.org/10.1007/978-981-16-7509-6_56

1 Introduction

Construction is one of the largest and fastest growing industrial industries in the world. It is, however, one of the industry's most dangerous. Every year, at least 108 thousand employees are killed on site, representing around 30% of all workplace fatalities. The hazards are three to six times more likely than any other occupation (ILO 2015).The Bangladesh Bureau of Statistics (BBS) reveals that about 2.6 million people are working by construction in Bangladesh and contribute to 9% of GDP, amounting to US$ 12 billion (BSS 2019). Real Estate and Housing Association of Bangladesh (REHAB) shows that more than 1000 companies are involved in the construction business (Dewri 2012). The building construction is hazardous by nature (Ahmed et al. 2012) and is associated with low onsite efficiency, inadequate management and insufficient safety measures that cause fatal Injuries. Extensive research in this sector has been conducted around the world, but studies are restricted in Bangladesh and research cannot go far due to a lack of data, a lack of safety awareness and also a lack of enforcement of safety laws (Raheem et al. 2011). One of the few studies performed in this field is that of project work at the Bangladesh University of Engineering and Technology (BUET) Department of Civil Engineering (Sultana 2005).

2 Research Methodology

A variety of data is required to elaborate on the characteristics of fatal accidents in the building construction in Bangladesh. Data on deaths at building sites will be obtained from numerous potential sources for this report (Abas et al. 2015). First, the Dhaka Metropolitan Police (DMP) and other police authorities acquired data where construction injuries and deaths are reported. Fatal accidents are recorded either under the head of the unnatural death case or in cases allocated for negligence offences under the Penal Code 304A (Al Mamun et al. 2014). A record of 60 cases of deadly injuries have been reported to have occurred at building sites in the past five years, according to a police survey (Abdelhamid and Everett 2000). Even a conservative estimate on the number of fatal accidents is much higher. It is therefore obvious that the majority of accidents are usually not reported to the police (Hammond et al. 2015). This is primarily due to the fact that filing of criminal case needs to be solved in the court and is linked to legal proceedings which are long, hassling and tiring procedure in Bangladesh. So, the owner/contractor quietly settles the situation by giving the victim/victim's family a limited amount of money as compensation, which is inadequate in most cases (Hiyassat et al. 2016). Secondly, data are collected from Occupational Safety, Health and Environment (OSHE) foundation which collects and documents fatality events that are published in fifteen national daily newspapers on all the industrial accidents occurring in Bangladesh including construction fatalities.

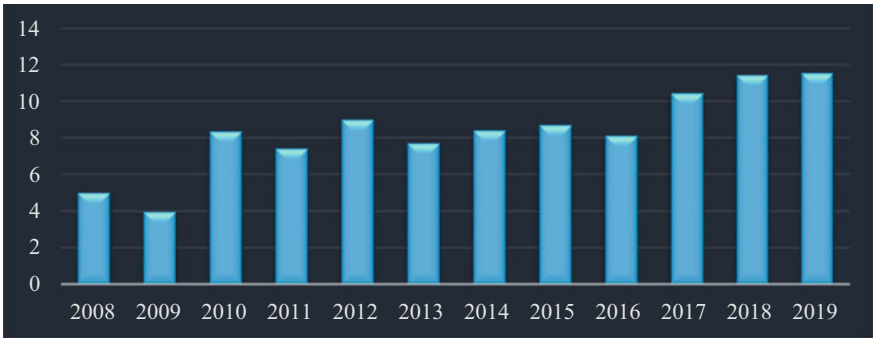

Fig. 1 Year basis spread of the number of fatal accident

Statistical research is carried out after data collection to analyze various facets of fatal incidents in Bangladesh affecting construction workers (Gunduz et al. 2017).

3 Overview of Collected Data

3.1 Year Basis Spread of the Number of Fatal Accident for Building Construction

The number of deaths in the Bangladesh construction section in the period from 2008 to 2019 is seen in Fig. 1. A total of 1715 people have died in Bangladesh's building construction for different reasons. This means that a total of 143 persons per year are killed averagely in the building construction, one of the largest in the country. The statistic also shows that the number of deaths in the last two years (2019 and 2018) has risen alarmingly, reaching nearly two hundred in both of those years. This suggests that in Bangladesh, the security situation at building construction sites is very bad (Table 1).

3.2 In Bangladesh, Division Wise Fatality Statics

It can be seen from Table 2, that Dhaka, the capital of Bangladesh and the key hub of the social and economic development of the country, has a maximum number of fatalities totaling 1026, which alone accounts for around 59.16% of all deaths. It is followed by about 15.16% of the port city of Chittagong. The economic centers of Khula and Rashahi, which are home to a significant number of factories and industries, are in third and fourth position on the list of fatalities. The remaining 27.57% of the fatality cases are shared by the remaining 6 divisions of Bangladesh.

Table 1 Year basis spread of the number of fatal accident

Year	Frequency	Percentage
2008	86	5.014
2009	68	3.96
2010	143	8.33
2011	127	7.40
2012	154	8.97
2013	132	7.69
2014	144	8.39
2015	149	8.68
2016	139	8.10
2017	179	10.43
2018	196	11.42
2019	198	11.54

Therefore, this analysis concentrated largely on the safety situation in the city of Dhaka, accounting for almost half of the overall number of casualties (Fig. 2).

3.3 Ratio of Gender in Fatality Statistics

It is understandable why most of the deaths are male workers, because most of the workers are males. Yet because of a lack of understanding and information about protection on building projects, female workers still die on the projects. It can be seen from Table 3, that about 13 female workers have lost their lives in the last 12 years, all of which were attributed to products falling on the body (Fig. 3).

3.4 Age-Wise Fatality Statistics

It was found from Table 4, that, relative to the other age groups during building, staff aged 21–30 are involved in most of the injuries. Young employees are more likely to perform dangerous tasks such as painting, plastering, ornamental exterior works, etc. And they also appear to operate without defensive measures such as a safety mask, harness, etc. As a consequence, this category is related to a higher trend of dropping collisions. About 20 and 30 years, this high frequency dominates. In comparison, construction experience for several years could be the key explanation for lower deaths in the higher age group (Fig. 4).

Table 2 Division basis distribution of proportion of fatal accident

Division	2008	2009	2010	2011	2012	2013	2014	2015	2016	2017	2018	2019
Dhaka	53.49	50.00	54.55	68.50	64.29	55.30	58.33	60.40	62.59	63.13	58.67	60.61
Barisal	1.16	7.35	2.10	4.72	1.95	3.79	2.78	2.01	2.88	0.56	4.08	3.03
Chittagong	19.77	16.18	17.48	14.96	16.23	15.15	11.81	13.42	13.67	17.32	13.78	12.12
Mymensingh	3.49	4.41	3.50	2.36	3.25	3.79	4.17	3.36	3.60	2.79	2.55	3.54
Khulna	6.98	7.35	7.69	1.57	5.84	7.58	6.94	8.72	8.63	3.91	6.12	9.09
Rajshahi	2.33	10.29	9.79	5.51	4.55	6.06	8.33	2.68	5.76	1.12	6.63	5.56
Rangpur	3.49	0.00	2.10	0.79	2.60	4.55	3.47	4.03	2.16	4.47	5.10	2.02
Sylhet	9.30	4.41	2.80	1.57	1.30	3.79	4.17	5.37	0.72	6.70	3.06	4.04

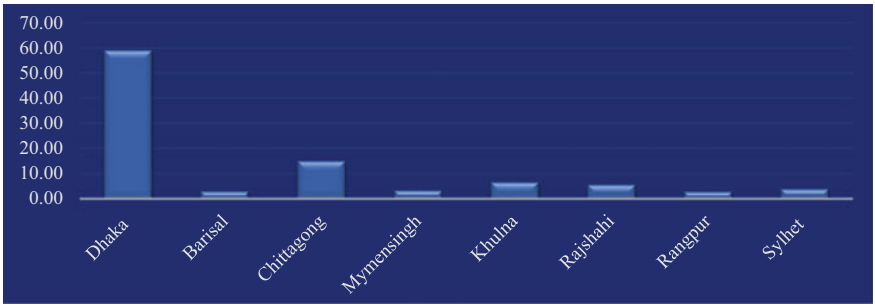

Fig. 2 Division basis distribution of proportion of fatal accident

Table 3 Gender basis spread of the fatal accident

Sex	2008	2009	2010	2011	2012	2013	2014	2015	2016	2017	2018	2019
Male	95.35	95.59	95.80	93.70	97.40	97.73	96.53	95.30	93.53	93.30	93.53	93.53
Female	4.65	4.41	4.20	6.30	2.60	2.27	3.47	4.70	6.47	6.70	6.47	6.47

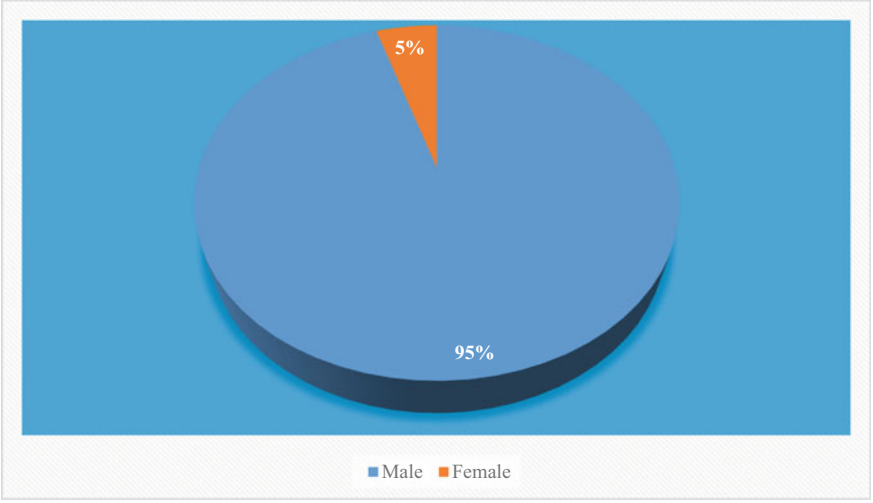

Fig. 3 Gender basis spread of the fatal accident

3.5 Month Wise Fatality Statistics

The timing of the injuries during both the day and throughout the year is seen in this segment. As seen in Fig. 5. July is the month with the highest number of casualties with 13.59% confirmed casualties during this month, while December is the month with the lowest number of fatalities with 4.13% injuries. The reasoning behind this

Table 4 Age basis spread of the fatal accident

Age range	2008	2009	2010	2011	2012	2013	2014	2015	2016	2017	2018	2019
0–10	0.00	1.47	2.10	0.00	0.00	0.76	0.69	0.00	0.00	0.56	0.00	0.56
11–20	19.77	22.06	17.48	23.62	20.13	18.94	13.89	18.12	16.55	20.67	16.55	20.67
21–30	46.51	42.65	41.96	43.31	42.86	43.18	44.44	40.94	46.76	43.02	46.76	43.02
31–40	17.44	20.59	25.87	18.90	22.08	24.24	27.08	23.49	20.86	20.67	20.86	20.67
41–50	11.63	10.29	11.89	9.45	10.39	9.85	13.19	16.78	12.23	10.61	12.23	10.61
51–60	4.65	2.94	0.70	3.94	3.90	3.03	0.69	0.67	3.60	3.91	3.60	3.91
61–70	0.00	0.00	0.00	0.00	0.65	0.00	0.00	0.00	0.00	0.56	0.00	0.56
71–80	0.00	0.00	0.00	0.79	0.00	0.00	0.00	0.00	0.00	0.00	0.00	0.00

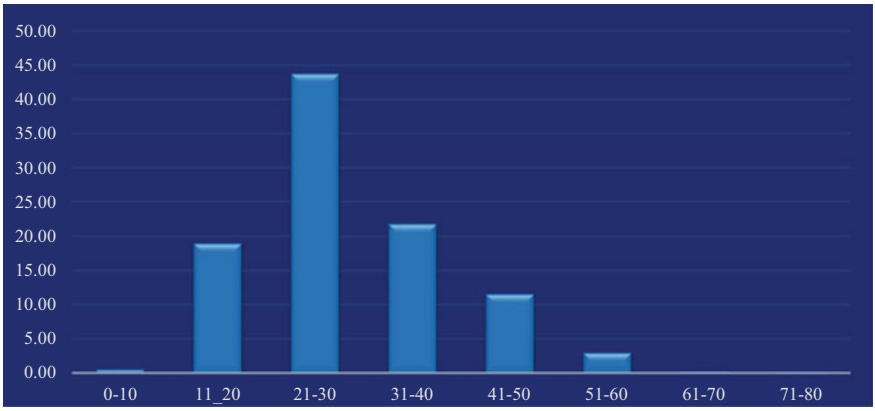

Fig. 4 Age basis spread of the fatal accident

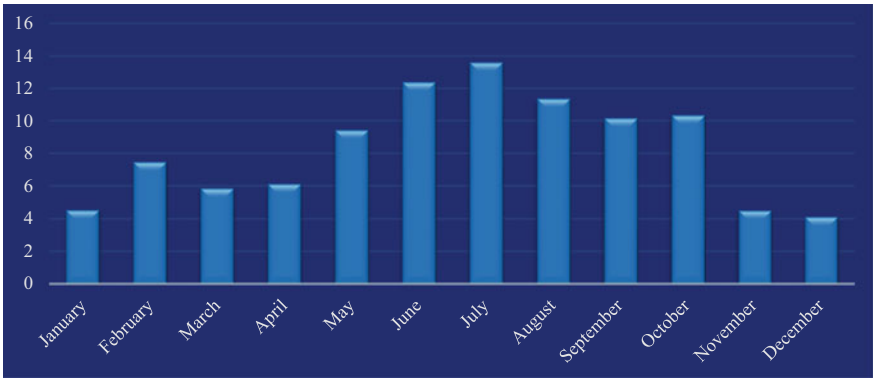

Fig. 5 Month wise fatality statistic

Table 5 Month wise fatality statistic

Month	2008	2009	2010	2011	2012	2013	2014	2015	2016	2017	2018	2019
January	4.65	2.94	4.20	7.09	3.25	5.30	2.78	6.04	3.60	5.59	3.60	5.59
February	10.47	2.94	9.09	6.30	6.49	4.55	10.42	7.38	9.35	6.70	9.35	6.70
March	11.63	5.88	3.50	7.87	4.55	6.82	2.78	5.37	6.47	4.47	6.47	4.47
April	3.49	5.88	6.99	11.02	5.19	3.03	7.64	3.36	7.91	5.59	7.91	5.59
May	9.30	7.35	12.59	7.87	7.14	7.58	9.03	10.07	12.23	8.94	12.23	8.94
June	19.77	10.29	10.49	7.09	11.04	9.85	12.50	13.42	13.67	13.41	13.67	13.41
July	8.14	19.12	11.89	13.39	12.99	18.94	15.97	15.44	10.79	12.85	10.79	12.85
August	8.14	14.71	13.29	12.60	9.09	12.88	9.03	7.38	12.95	11.73	12.95	11.73
September	12.79	13.24	5.59	10.24	13.64	13.64	7.64	9.40	7.91	10.06	7.91	10.06
October	5.81	10.29	12.59	9.45	12.99	12.12	10.42	12.08	8.63	10.61	8.63	10.61
November	4.65	4.41	4.20	2.36	6.49	3.03	4.86	4.03	2.88	7.26	2.88	7.26
December	1.16	2.94	5.59	4.72	7.14	2.27	6.94	6.04	3.60	2.79	3.60	2.79

can be attributed to the monsoon cycle that is normal during this season. On the other hand, the winter season is from November to January and the dry season is from February to April, with a slightly lower number of confirmed deaths. While construction activities during the winter and dry season are higher, most injuries occur during the monsoon time. This can be associated during the monsoon season with the strong rains. In addition, the financial year in our country begins and ends around the June–July time. There is also a hurry to finish the building work within the timeframe during this time, which provides a massive incentive to ignore and disregard the necessary safety measures (Table 5).

3.6 Distribution of Proportion of Fatalities Based upon Nature of Accident

A number of different kinds of incidents have been found to be responsible for fatal accidents in the construction sector of Bangladesh through the study of data obtained from the Police Authorities and OSHE. The percentile distribution of these causes of fatal injuries as shown in Fig. 6. It can be concluded from this statistic that falling from heights and electrocution are the two major causes of construction site fatalities. Together, they make up approximately 6872% of all deaths. With about 38% falling from heights, the fatality table leads, while electrocution is responsible for 28% of all deaths. The contribution of other causes of injuries varies from only 1.76–9.32%. It is also apparent that concentrating on the two primary causes of death, i.e. falling from heights and electrocution, will eliminate nearly two-thirds of building deaths in the construction industry (Table 6).

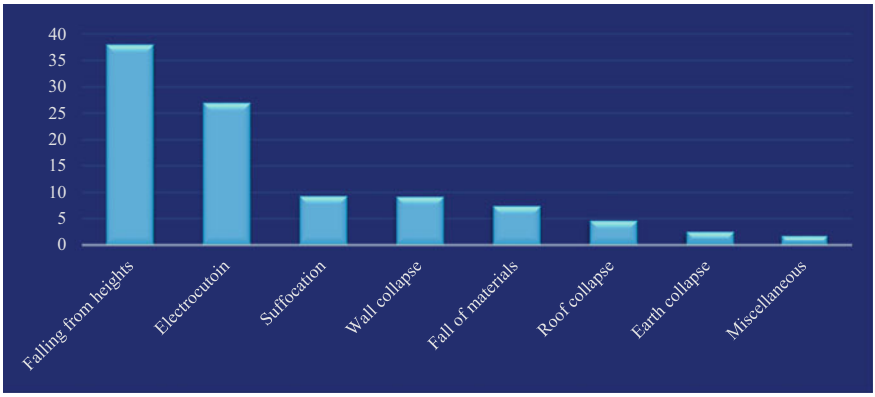

Fig. 6 Distribution of proportion of fatalities based upon nature of accident

4 Conclusion

Information on fatal accidents relating to construction sites in Bangladesh is obtained from different sources. From the information gathered, it can be seen that a total of 806 people have been killed in Bangladesh's construction sector throughout the last five years with different reasons. This means that a total of 135 persons per year are killed in the building industry, one of the largest in the country. The two key causes of deaths in the construction sector of Bangladesh account for 39% and 32% of overall deaths, among the distinct reasons for fatal accidents falling from heights and electrocution. More thorough study of dropping and electrocution injuries shows that, with the gradation of the overall safety condition of the building sites, their key factors are preventable.

Table 6 Distribution of proportion of fatalities based upon nature of accident

Cause of accident	2008	2009	2010	2011	2012	2013	2014	2015	2016	2017	2018	2019
Falling from heights	39.53	36.76	32.17	40.94	44.81	43.94	35.42	37.58	30.94	41.90	30.94	41.90
Electrocution	25.58	33.82	30.07	25.20	27.27	22.73	25.69	26.85	26.62	26.82	26.62	26.82
Suffocation	11.63	2.94	10.49	5.51	11.69	6.06	7.64	10.74	13.67	8.94	13.67	8.94
Wall collapse	6.98	11.76	13.99	6.30	5.19	6.82	11.11	14.77	12.23	4.47	12.23	4.47
Fall of materials	4.65	2.94	4.90	14.17	9.09	6.06	7.64	4.70	5.76	11.73	5.76	11.73
Roof collapse	3.49	5.88	4.90	3.15	1.95	10.61	7.64	2.01	6.47	1.68	6.47	1.68
Earth collapse	5.81	4.41	3.50	3.94	0.00	0.00	1.39	1.34	2.88	2.23	2.88	2.23
Miscellaneous	2.33	1.47	0.00	0.79	0.00	3.79	3.47	2.01	1.44	2.23	1.44	2.23

References

Abas M, Khattak S, Hussain I, Ishtiaq A, Maqsood S (2015) Evaluation of factors affecting the quality of construction projects. Tech J 20(2):115–120

Abdelhamid TS, Everett JG (2000) Identifying root causes of construction accidents. J Const Eng Manag 126(1):52–60

Ahmed MZ, Siddiquee MSA, Khan MS (2012) Reliability and construction practices in building construction industry of Bangladesh. In: Third international conference on construction in developing countries (ICCIDC–III), "Advancing and integrating construction education, research & practice", Bangkok, Thailand, 4–6 July 2012

Al Mamun A, Hoque BA, Islam FS (2014) Safety factors by BNBC and its practice in building construction: Uttara Zone, Dhaka. Bangladesh: Engineers Role in Ensuring Safety, Dhaka centre of the Institution of the Engineers

BBS, Labour Force Survey (LFS)—2003, 2006, 2010 and 2013 Bangladesh Bureau of Statistics (BBS). Retrieved from website: http://www.bbs.gov.bd/

Dewri LV (2012) A Comprehensive study on the real estate sector of Bangladesh. Real Estate and Housing Association of Bangladesh (REHAB), 12 July 2012

Gunduz M, Birgonul MT, Ozdemir M (2017) Fuzzy structural equation model to assess construction site safety performance. J Constr Eng Manage 143(4):04016112

Hammond JS, Keeney RL, Raiffa H (2015) Smart choices: a practical guide to making better decisions. Harvard Business Review Press, Boston, MA, USA

Hiyassat MA, Hiyari MA, Sweis GJ (2016) Factors affecting construction labour productivity: a case study of Jordan. Int J Constr Manage 16(2):138–149

ILO (2015) Construction: a hazardous work. International Labour Organization Document, © 1996–2013 International Labour Organization (ILO). Retrieved from website: http://www.ilo.org/, 15 June 2009

Raheem AA, Hinze JW, Azhar S, Choudhry RM, Riaz Z (2011) Comparative analysis of construction safety in Asian developing countries. In: Sixth international conference on construction in the 21st century (CITC-VI) "Construction challenges in the new decade", Kuala Lumpur, Malaysia, 5–7 July 2011

Sultana A (2005) A study on existing safety climate in building construction sites of Dhaka City. M. Engg. Project, Department of Civil Engineering, Bangladesh University of Engineering and Technology

Recent Developments in Deep-Water and Ultra-deep-Water Dynamically Installed Anchoring Systems

Soumya Sayan Pal and Satyajeet Nanda

Abstract The offshore industries have moved deeper into the ocean in search of natural resources. In their quest, they have felt the need for a cost efficient self-embedding anchor system which gave birth to the Dynamically Installed Anchors (DIAs) or Deep Penetrating Anchors (DPAs). Despite being came into existence a few decades ago DPAs are still not widely used. Various research is still going on to accurately predict their embedment depth which is directly related to their holding capacity. In this paper, recent scientific developments on this issue and the existing dilemma of having a wide range of the mathematical models available to predict their embedment depth are discussed.

Keywords Offshore geotechnical · Torpedo anchor · Dynamically installed anchor · Strain rate · Soil constitutive model

1 Introduction

As the natural resources get depleted gradually, the oil and gas industry has moved deeper into the ocean in search of more energy reserves. Consequently, the technologies required to extract those natural resources have evolved. From shallow depth (<300 m approximate) to deep water (>500 m approximate) and more recently ultra-deep water (>1500 m approximate) offshore platforms have moved from fixed to floating structures with different foundation technologies some of which can be seen in both the categories of superstructure. Floating structures require moorings to keep them in one place and moorings, require anchors on or inside the seabed. Anchoring systems, impart the resistance forces from soil to the mooring lines to keep the buoyant facilities in position and sometimes provide extra stability to fixed

S. S. Pal · S. Nanda (✉)
KIIT DU, Bhubaneswar, India
e-mail: satyajeet.nandafce@kiit.ac.in

S. S. Pal
e-mail: 1843002@kiit.ac.in

B. B. Das et al. (eds.), *Recent Developments in Sustainable Infrastructure (ICRDSI-2020)—GEO-TRA-ENV-WRM*, Lecture Notes in Civil Engineering 207,
https://doi.org/10.1007/978-981-16-7509-6_57

or flexible structures. Floating facilities come in many shapes and sizes with various degrees of functionality. Some examples include Floating Production Storage and Offloading platforms (FPSOs), Floating Production and Systems (FPSs), Single Point Anchor Reservoir (SPAR), Tension Leg Platforms (TLPs). All these types of platforms are moored with Catenary, Taut, Semi-Taut or Vertical moorings which requires foundations that have a vast range.

1.1 Types of Anchoring Systems

Although the deep-water anchoring systems vary widely, they can be divided into two broad categories: Surface or Gravity type anchor and Embedded anchors.

Gravity type anchors obtain their holding capacity mainly from the weight of the anchor and partly from the friction between the base of the anchor and the seabed. Gravity anchors are restricted to relatively shallow water and are limited by the practicality of their size and therefore holding capacity.

Embedded anchors are employed in situations where greater holding capacity is required than what is achievable through gravity anchors or the depth is too high. Embedded anchors comprise manly Driven or Drilled and Grouted Piles, Suction Caissons, and Drag anchors (fixed or flexible fluke). Also, worth mentioning is a proprietary anchor named OMNI-Max (Fig. 1).

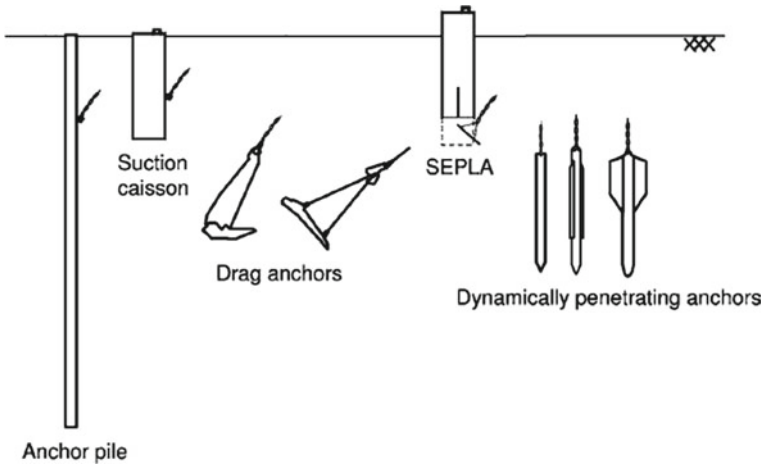

Fig. 1 Different types of Embedded anchors (Randolph and Gourvenec 2011)

1.2 Dynamically Installed Anchors

The huge cost of deep-water anchor installation led to the development of anchors that embed themselves under free falling action. These anchors are known as Dynamically Installed Anchors (DIAs) or Deep Penetrating Anchors (DPAs). This type of anchors is most recent and thus less used. DPAs are found in many shapes, sizes and weights depending on the requirement. Usual shapes include Torpedo anchors having conical tips or parabolic tip and proprietary OMNI-Max anchor (Fig. 2). Standard dimensions of Torpedo are shown in Fig. 3 and Table 1. They are designed to reach velocities of 25–35 m/s at the seabed during freefall through water (O'Laughlin et al. 2013), allowing tip penetrations of two to three times the anchor length and holding capacities after consolidation in the range of three to six times the weight of the anchor. They are by far the least costly anchoring solution invented to date. However, they are also not devoid of issues which are discussed in the next section.

Fig. 2 Different Variations of DPAs. (Top Left) Torpedo Anchor with conical tip, (Right) Torpedo Anchor with parabolic tip and (Bottom Left) OMNI-Max anchor (Randolph and Gourvenec 2011)

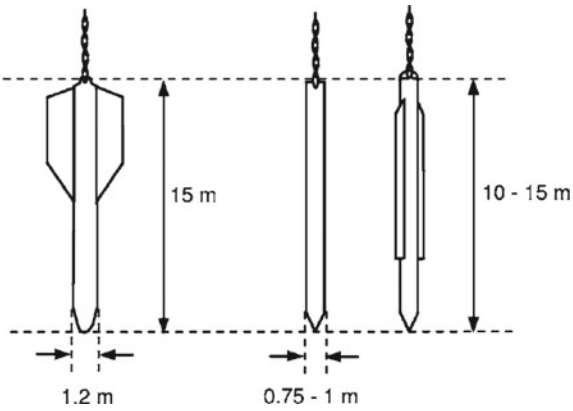

Fig. 3 Standard dimensions of Torpedo anchors (Randolph and Gourvenec 2011)

Table 1 Standard values of parameters related to torpedo anchors (Randolph and Gourvenec 2011)

Parameter	Standard Values
Diameter	0.75–1.2 m
Length	10–15 m
Weight	500–1000 kN
Fins	0–4 nos
Tip	Conical or parabolic
Release height	20–50 m

2 Theoretical Frameworks

The pull-out capacity of DIAs depends directly on the depth of their embedment in the seabed soil. Thus, accurate prediction of their embedment depths is of utmost importance. Studies have shown that typical embedment depths of DIAs range from 2 to 3 times the length of the anchor. Various mathematical models have been proposed over time by many researchers to predict their embedment depths accurately. O'Laughlin et al. (2004) reports that several analytical approaches were developed to predict the deceleration of DPAs inside the soil but their verification was difficult due to lack of reliable test data and poor understanding of soil response to dynamic penetrations.

2.1 DIA Penetration Models

An elementary approximation of the anchor embedment made by considering the resisting forces acting on the anchor during penetration was proposed by Arup (1982) and Freeman et al. (1984). The model they used was:

$$m\frac{dv}{dt} = W_S - \left(N_c s_{u,tip} A_{tip} - \alpha s_{u,side} A_{side}\right) \tag{1}$$

Arup (1982) proposed a dynamic bearing capacity factor of $N_C = 18$ while Freeman et al. proposed $N_C = 12$. However, True (1975) first considered a rational approach to the problem and proposed a mathematical model consisting an inertial drag term which is given below:

$$M^*\frac{dv}{dt} = F_D + W' - s_u S_C\left(N_c A_F + \delta\frac{A_s}{S_t}\right) - \frac{1}{2}\rho C_d A_F V^2 \tag{2}$$

where, F_D = Externally applied driving force, W' = buoyant weight of penetrator in soil, M* = penetrator mass and added mass, S_C = Factor accounting for soil strain rate effect (ratio of soil strength at a velocity to that of at zero velocity), ρ = fluid mass density, C_D = fluid drag coefficient based upon frontal area, A_F = penetrator frontal area, V = penetrator velocity, s_u = static undrained soil shear strength, N_C = bearing capacity factor, δ = side adhesion factor, A_S = penetrator side area, S_t = soil sensitivity (ratio of undisturbed to remoulded static shear strength).

O'Laughlin et al. (2004) used an improved model as

$$m\frac{dv}{dt} = W_S - R_f\left(F_b + F_f\right) \tag{3}$$

where,

W_S = Submerged anchor weight in water. R_F = Shear strain rate factor, F_b = Bearing Resistance, F_f = Frictional Resistance.

In this model they used the semilogarithmic formulation or power law formulation for the strain rate factor. Also, they omitted the buoyant force of the anchor from displaced soil.

Raie and Tassoulas (2009) used a similar model to O'Laughlin et al. (2004) and improved it further by changing the side adhesion factor from a constant value to

$$\delta = 1 - \exp\left[\frac{1}{8} - \frac{L}{40 \times D \times \tan(\alpha)}\right], \text{ for } \frac{L}{D \times \tan(\alpha)} \geq 5,$$
$$\text{and } \delta = 1, \text{ for } \frac{L}{D \times \tan(\alpha)} < 5 \tag{4}$$

where, D & L = penetrator diameter & length, α = penetrator nose half-angle.

However, they used fluid dynamics formulation for their analysis and concluded that the Herschel-Bulkley model needs to be modified to be used in this application. They modelled the remoulding effect as a reduction in yield stress by dividing the soil shear strength with soil sensitivity. Also, they introduced an ad-hoc increase in the yield stress based on the anchor end bearing capacity expression given by

$$\tau_{0_{tip}} = \frac{1}{\pi} \times \frac{A_F}{A_T} \times N_c \times S_u \tag{5}$$

where, τ_{0tip} = yield shear stress specified at the tip, N_C = Bearing Capacity Factor, S_u = static undrained shear strength of the soil, A_F and A_T = penetrator frontal area and projected area of the tip on a plane parallel to the penetrator longitudinal axis, respectively.

Chow et al. (2014) proposed a similar model as

$$ma = W - F_t - F_S - F_D - F_b \tag{6}$$

where, $F_t = R_f(S_u N_T A_T)$ and $F_S = R_f\left(\alpha S_{u,avg} A_T\right)$, W = Dry Weight of the Anchor, F_b = Buoyancy Force, calculated as the displaced volume of anchor multiplied by the total unit weight of the soil, F_t = Bearing Resistance along the tip of the anchor, F_s = Frictional Resistance along the shaft of the anchor, F_D = Hydrodynamic Drag Resistance.

In this model soil strength is taken at tip level for end bearing and average soil resistance is taken for skin frictional resistance.

Hossain et al. (2015) used similar model given by

$$m\frac{dv}{dt} = W_D + F_Y - R_f\left(F_b - F_f\right) \tag{7}$$

where, W_D = Dry Weight of the Anchor, F_Y = Buoyancy Force, calculated as the displaced volume of anchor multiplied by the total unit weight of the soil, F_b = Bearing Resistance along the tip of the anchor and the flukes, F_f = Frictional Resistance along the surface of the anchor shaft and the flukes, R_F = Shear strain rate factor.

Here, notably, they did not use the drag resistance force as the soil they experimented on was calcareous silt.

Kim et al. (2018) proposed a further illustrated model as

$$\mathrm{m}\frac{dv}{dt} = W_S + F_Y - R_{f_1}F_b - R_{f_2}F_f - F_D \tag{8}$$

where, W_S = submerged weight of anchor in water, F_Y = buoyant weight of soil displaced by the anchor, R_{f1} = strain rate factor applicable for end bearing resistance, R_{f2} = strain rate factor applicable for frictional resistance, F_b = end bearing resistance from tip (calculated at the junction of cylindrical anchor shaft and anchor tip) and fluke (calculated at the bottom of the flukes), F_f = frictional resistance from cylindrical anchor shaft (calculated at the centroid level of the shaft surface) and the flukes ((calculated at the centroid level of the flukes), $F_D = \frac{1}{2}\rho C_d A_P V^2$ = Inertial drag resistance force where, ρ = density of soil, C_d = drag coefficient, A_P = Frontal Projected area and V = Velocity of the anchor.

Liu et al (2016) used a model considering hydrodynamic drag too as

$$\mathrm{m}\frac{dv}{dt} = W_S + F_Y - R_{f_1}F_b - R_{f_2}F_f - F_D - F_{wd} \tag{9}$$

where, F_{wd} = Hydrodynamic drag calculated as $F_{wd} = \frac{1}{2}\rho_w C_{dw} A_P V^2$.

Almost all the models use a multipliable factor to define the strain rate dependency of soil and another factor to define the hydrodynamic drag force. These factors have also been defined by various authors in different times which are discussed in the next section.

2.2 Strain Rate Dependency Models

It has been established for a long time that the strength of the soil increases with strain rate. (Casagrande and Wilson 1951; Graham et al. 1983) And since during installation the velocity of the DPA stays in the range of 25–30 m/s the strain rate remains very high. The various predictive models that accounts differently for strain rate effects through soil mechanics framework or fluid mechanics framework is discussed as follows:

2.2.1 Soil Mechanics Framework

Most modern constitutive models based on the critical state concept for clays postulates a unique relationship between the shear strength, mean effective stress and water content (or void ratio) at failure (Roscoe et al. 1958; Schofield and Wroth 1968; Wood 1990). This concept is based on laboratory experiments and all loading paths during shearing end at critical state line which is given by

$$s_u = \frac{M}{2} p' \text{ with } p' = \exp\left(\frac{N - \upsilon}{\lambda}\right) \tag{10}$$

where s_u is the undrained shear strength of the clay (defined as the radius of the largest Mohr circle at failure); p' is the mean effective stress; υ is the specific volume (i.e. $\upsilon = 1 + e$, where e is the void ratio); and M, N and λ are soil constants.

Wroth and Wood (1978) proposed some assumptions which when adopted with correlations between soil strength and soil index properties along with the critical state concept yielded the following relationship:

$$S_u = 170 \exp(-4.6 L I) \text{ (kPa)} \tag{11}$$

The strain rate dependency of clay soil is usually expressed through a parameter μ to give the proportional change in shear strength for each order of magnitude change in strain rate. Semilogarithmic functions, power law functions or inverse hyperbolic sine functions have been used to define the strength of soil at a given strain rate.

Several researchers (Dayal and Allen 1975; Biscontin and Pestana 2001; Einav and Randolph 2005) proposed the semilogarithmic function which is expressed as follows:

$$s_u = s_{u,ref}\left(1 + \mu \log \frac{\dot{\gamma}}{\dot{\gamma}_{ref}}\right) \tag{12}$$

where $s_{u,ref}$ is the shear strength at the reference shear strain rate of $\dot{y}_{ref}$ and s_u is the shear strength at strain rate $\dot{y}$.

Alternatively, the power law formulation was proposed by (Biscontin and Pestana 2001) as:

$$s_u = s_{u,ref}\left(\frac{\dot{\gamma}}{\dot{\gamma}_{ref}}\right)^{\beta} \tag{13}$$

where β is the strain rate dependency factor.

Inverse hyperbolic sine functions have been proposed by Nanda et al. (2017) through laboratory tests using T-Bar penetrometer as

$$\frac{q_{T-bar}}{q_{T-ref}} = 1 + \mu \text{arcsinh}\left(\frac{v}{v_{ref}}\right) \tag{14}$$

where q_{T-ref} and v_{ref} are the reference penetration resistance and rate of penetration, respectively and μ is the soil rate coefficient. Or, in other words as mentioned by Einav and Randolph (2005):

$$s_u = s_{u0}\left[1 + \lambda' \text{arcsinh}\left(\frac{\dot{\gamma}}{\dot{\gamma}_0}\right)\right] \tag{14}$$

Apart from dependency to rate of strain, strength of a soil is also affected by the cumulative amount of applied strain. Generally, an intact soil exhibits a peak in mobilised stress during initial shearing, followed by a gradual decrease, owing to the destructuration of soil microstructure (such as chemical bonding), reorientation of clay particles, or the generation of excess pore pressure (Bokupeti et al. 2012). Einav and Randolph (2005) proposed to model this strength reduction through a simple exponential decay function as

$$s_u = \left[\delta_{rem} + (1 - \delta_{rem})e^{-3\xi/\xi_{95}}\right]s_{u,p} \tag{15}$$

where δ_{rem} is the inverse of the sensitivity, and ξ is the cumulative plastic shear strain, with ξ_{95} being the plastic shear strain required to achieve 95% remoulding.

2.2.2 Fluid Mechanics Framework

The behaviour of a fluid is described by a relation between its shear stress and rate of shear strain. The most common fluid flow model is Newton's law of viscosity. This model describes the shear stress as a multiple of a proportionality constant (called dynamic viscosity) times the shear strain rate. In Non-Newtonian fluids, for example

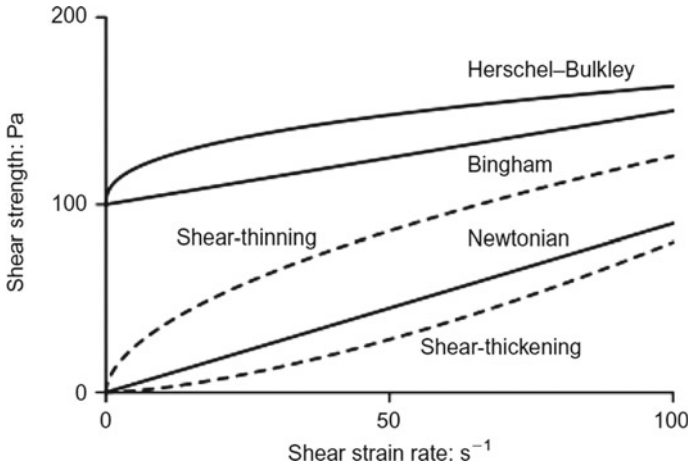

Fig. 4 Fluid models for viscous strength (Bokupeti et al. 2012)

suspensions of solids shear stress τ reaches a minimum value τ_y before flowing. This type of behaviour is called plastic and described by general equation

$$|\tau| = \tau_y + \eta|\dot{\gamma}|^n \tag{16}$$

where η represents the viscous property of the fluid. This equation is known as Hershel–Bulkley model (Herschel and Bulkley 1926) which gives a non-linear shear stress variation along with shear strain rate beyond the yield stress. The value of n in this formulation determines the nature of non-linearity observed in viscosity i.e. shear thickening (for $n > 1$) or shear thinning (for $n < 1$).

This equation reduces to a linear form with $n = 1$ which represents the Bingham fluid model. Bingham fluid model assumes a linear variation of shear stress along with shear strain rate beyond the yield stress (Fig. 4).

Bokupeti et al. (2012) presented a comparison between the two frameworks and concluded that the soil models described within the soil mechanics framework is better as it provides the ability to express the rate dependence in terms of dimensionless quantities.

2.3 Formulation of Drag

For the fluid mechanics drag term has been present in the mathematical models presented by different researchers for long despite of having any direct experimental proof of its existence. Different value of the drag coefficient C_D ranging from a constant value to a variable has been proposed over the time. True (1975) considered this term to be a function of surface roughness and penetrometer tip geometry with

a maximum value of 1 for blunt tip. He proposed an equation to account for the transition effect from during high velocities as:

$$C_d = C_{d,s} + \frac{C_{d,f} - C_{d,s}}{1 + \left(\frac{1}{v^f}\right)} \tag{17}$$

where $C_{d,s}$ and $C_{d,f}$ are the drag coefficients for soil and fluid respectively, and f is a function of tip geometry and soil sensitivity. However, he concluded that $C_D = 0.7$ can serve as a useful average approximation.

Freeman and Hollister (1989) suggested the drag coefficient in terms of L/d ratio of the penetrator as:

$$C_d = 0.030 + 0.0085\frac{L}{d} \tag{18}$$

where L is the length of the penetrator and d is the diameter.

O'Laughlin et al. (2009, 2013) used an average value of $C_D = 0.24$ in their formulation.

Zhu and Randolph (2011) reported that for the cases of slow flow of viscoplastic fluid around a circular cylinder, with negligible inertia effects, numerical simulations were carried out using Herschel–Bulkley model and Bingham model by de Besses et al. (2003) and Tokpavi et al. (2008) respectively. They expressed the drag coefficients as ratios of the force per unit area to either the viscous stress (C_D) or the yield stress (C_D^*) according to

$$C_d = \frac{F}{AK\left(\frac{v}{d}\right)^n} \tag{19}$$

and

$$C_d^* = \frac{F}{A\tau_0} = \frac{C_d}{Od} \tag{20}$$

where v is the velocity of the fluid far from the cylinder, and Od is the Oldroyd number (Od), the ratio of yield stress to viscous related shear stress, defined by

$$Od = \frac{\tau_0}{K\left(\frac{v}{d}\right)^n} \tag{21}$$

Oldroyd number represents the ratio of the yield stress to a viscous component of shear stress based on a nominal shear strain rate of v/d.

3 Experimental Works

Christians and Meisberger (1967), Scmid (1969), Young (1969) did some early works on the high-speed penetration of projectiles into earth. Migliore and Lee (1971) did field tests with instrumented penetrometers in Terrigenous Mud of Santa Barbara Channel. True (1975) first reported experiments on DIAs on silty clay soil of Seal Beach, California and gave a rational mathematical model for penetration. Beard (1984) presented seafloor penetrometer tests in clays, oozes and silts. Freeman et al. (1984), Freeman and Burdett (1986) presented model tests in the Great Meteor East and Nares Abyssal Plane of Atlantic Ocean. Medeiros (2002) published an overview on design and installation procedures, cost estimation, field and model tests results and applications of T-98 Torpedo anchors used by Petrobras in Campos Basin. De Araujo et al. (2004) described in detail about the first campaign of T-98 design, building process and the tests done. Chung et al. (2006) carried out laboratory test on various shaped penetrometers to determine effects of penetration rate on the penetration resistance in soft clay. Brandao et al. (2006) described in detail about the final campaign of T-98 at Albacora Leste Field. Zimmerman et al. (2009) introduced the novel OMNI-Max torpedo and discussed its installation. O'Laughlin et al. (2009, 2013) reported the results of centrifuge tests to inform about the expected anchor penetration in NC clay and attempted to form the basis for calibration of analytical models. Effect of soil variability on the penetration depth of DIAs via a sensitivity study and its effective application range was determined by Strum et al. (2011). Gaudin et al. (2013) investigated the penetration depth, anchor pull and anchor trajectory of OMNI-Max anchor in calcareous silt using centrifuge model tests. O'Beirne et al. (2015) provided insight into the hole closure phenomenon via centrifuge model tests. Centrifuge test on installation & pull out capacity of DPAs in lightly over-consolidated clay and calcareous silt was performed by (Hossein et al. 2014, 2015). Blake and O'Laughlin (2015) performed field tests on DEPLA and presented the net resistance and velocity profiles. Wang et al. (2016) proposed a single formula for calculation of penetration depth of torpedo anchor regardless of soil separation from free fall experiment observations as

$$D = \frac{V_i^2}{\left(1.172\frac{V_i}{V_0}N_C^{-0.376}\left(\frac{\delta}{S_i}\right)^{0.033}\left(\frac{S_u A_f}{mg}\right)^{-0.844}\left(\frac{S_u A_s}{mg}\right)^{-1.679}\left(\frac{L}{d}\right)^{-1.616}\left(\frac{d}{d_{50}}\right)^{-0.203} - 2\right)g} \tag{22}$$

A formula for undrained monotonic holding capacity of torpedo anchor was proposed by Wang et al. (2018) on the basis of free fall tests. Effect of fin length on torpedo anchor penetration was investigated using transparent soil substrate by Ads et al. (2020) and it was found that fin length is inversely related to penetration depth and directly related to pullout capacity.

4 Numerical Simulations

Zhou and Randolph (2007) conducted 3D LDFE Parametric analysis with RITSS approach using Modified Tresca and Hershel-Bulkley model to observe the Shear Band phenomenon. A Semi-logarithmic soil model expressing strain rate dependency with strain softening effect was later proposed by the same researchers by conducting LDFE analysis with RITSS approach (Zhou and Randolph 2009). Raie and Tassoulas (2009) used CFD modelling framework with modification to Bigham Fluid model with shear thinning effect. Side adhesion factor was modified to account for remoulding effect and the shear stress at tip region was increased to account for hardening due to strain rate effect. They concluded to Bingham model as unsuitable for effective geotechnical applications. Zhu and Randolph (2011) proposed Additive power law model for strain rate effect during DIA penetration using LDFE analysis with RITSS approach. Kim et al (2015) conducted 3D LDFE Parametric analysis with CEL approach using Modified Tresca and Hershel-Bulkley model considering strain rate and strain softening effect of soil and proposed a modification to the additive power law model for strain rate effect and suggested a procedure to calculate the depth of penetration using both Bearing resistance method and Modified energy method. Liu et al (2016) conducted LDFE Parametric analysis with CEL approach using Hershel-Bulkley model considering strain rate and strain softening effect of soil and Hydrodynamic Drag. A novel Fish DIA was evaluated for its penetration behaviour in calcareous silt using 3D LDFE analysis with CEL approach by Kim et al. (2018). Zhao et al. (2019) divided the whole installation and post-installation processes into 3 stages and used different methods and different approaches to simulate each stage and reported the comparison, advantages and disadvantages of each method in the different stages. Zhang and Evans (2019) used DEM analysis for analysing the micro-scale soil performance in the vicinity of the penetrating anchor in granular soil. Yi et al. (2020) used LDFE Parametric analysis with CEL approach to explore In-plane & out of plane pull out capacity. Parametric was also done to develop a design procedure.

5 Conclusion

Lots of research going on and immediate research gap is closing in fast. Most of the experimental works are being done in laboratory condition using scaled models. Although some of the field work has been done they are still a rare occurrence. Thus, many problems that are faced in the real-world scenario like anisotropy of soil, effect of installation errors, anchor capacity under dynamic loading are still not addressed properly. The need to estimate the penetration depth accurately still persists. Also, a sound design procedure to address the industry needs and regulatory restrictions are required. Most importantly, a less time-consuming computational method is the need

of the hour as none of the existing methods can fully address the vastness increasingly complex geotechnical problems and analyze them quickly and cheaply.

References

Ads A et al (2020) Visualizing the effect of Fin length on torpedo anchor penetration and pullout using a transparent soil. Ocean Eng 216:108021

Arup OP (1982) Penetrometer options—studies relevant to emplacement in deep ocean sediments. DOE report no. DOE/RW/82.102

Beard RM (1984) Expendable doppler penetrometer for deep ocean sediment strength measurements. No. NCEL-TR-905. Naval Civil Engineering Lab Port Hueneme CA

Biscontin G, Pestana JM (2001) Influence of peripheral velocity on vane shear strength of an artificial clay. Geotech Test J 24(4):423–429

Blake AP, O'Loughlin CD (2015) Installation of dynamically embedded plate anchors as assessed through field tests. Can Geotech J 52(9):1270–1282

Brandão FEN et al (2006) Albacora Leste field development-FPSO P-50 mooring system concept and installation. In: Offshore technology conference

Boukpeti N et al (2012) Strength of fine-grained soils at the solid–fluid transition. Géotechnique 62(3):213–226

Casacrande A, Wilson SD (1951) Effect of rate of loading on the strength of clays and shales at constant water content. Geotechnique 2(3):251–263

Chow SH, O'Loughlin CD, Randolph MF (2014) Soil strength estimation and pore pressure dissipation for free-fall piezocone in soft clay. Géotechnique 64(10):817–827

Christians JA, Meisburger EP (1967) Development of multi-leg mooring system, phase A explosive embedment anchor. Army Mobility Equipment Research and Development Center, Report 1909-A

Chung SF, Randolph MF, Schneider JA (2006) Effect of penetration rate on penetrometer resistance in clay. J Geotech Geoenviron Eng 132(9):1188–1196

Dayal U, Allen JH (1975) The effect of penetration rate on the strength of remolded clay and sand samples. Can Geotech J 12(3):336–348

de Araujo JB, Machado RD, de Medeiros Junior CJ (2004) High holding power torpedo pile: results for the first long term application. In: International conference on offshore mechanics and Arctic engineering, vol 37432

De Besses BD, Magnin A, Jay P (2003) Viscoplastic flow around a cylinder in an infinite medium. J Non-Newtonian Fluid Mech 115(1):27–49

Einav I, Randolph MF (2005) Combining upper bound and strain path methods for evaluating penetration resistance. Int J Numer Meth Eng 63(14):1991–2016

Freeman TJ, Hollister CD (1989) Modelling waste emplacement and the physical changes to the sediment barrier. In: Disposal of radioactive waste in seabed sediments: proceedings of an international conference. Society of Underwater Technology

Freeman TJ, Burdett JRF (1986) Deep ocean model penetrator experiments. No. EUR--10502. Commission of the European Communities

Freeman TJ et al (1984) Modelling radioactive waste disposal by penetrator experiments in the abyssal Atlantic Ocean. Nature 310(5973):130–133

Gaudin C et al (2013) The performance of dynamically embedded anchors in calcareous silt. In: International conference on offshore mechanics and Arctic engineering, vol 55409. American Society of Mechanical Engineers

Graham J, Crooks JHA, Bell AL (1983) Time effects on the stress-strain behaviour of natural soft clays. Géotechnique 33(3):327–340

Herschel WH, Bulkley R (1926) Measurement of consistency as applied to rubber-benzene solutions. Am Soc Test Proc 26(2)
Hossain MS, Kim Y, Gaudin C (2014) Experimental investigation of installation and pullout of dynamically penetrating anchors in clay and silt. J Geotech Geoenviron Eng 140(7):04014026
Hossain MS, O'Loughlin CD, Kim Y (2015) Dynamic installation and monotonic pullout of a torpedo anchor in calcareous silt. Géotechnique 65(2):77–90
Kim YH et al (2015) Numerical investigation of dynamic installation of torpedo anchors in clay. Ocean Eng 108:820–832
Kim YH, Hossain MS, Chang K (2018) Numerical investigation of novel dynamic installed fish anchors in clay and calcareous silt. Ocean Eng 163:29–39
Liu H, Xu K, Zhao Y (2016) Numerical investigation on the penetration of gravity installed anchors by a coupled Eulerian-Lagrangian approach. Appl Ocean Res 60:94–108
Medeiros Jr CJ (2002) Low cost anchor system for flexible risers in deep waters. In: Offshore technology conference
Migliore HJ, Lee HJ (1971) Seafloor penetration tests: presentation and analysis of results. No. NCEL-TN-1178. Naval Civil Engineering Lab Port Hueneme CA
Nanda S et al (2017) Effects of strain rates on the undrained shear strength of kaolin. Geotech Test J 40(6):951–962
O'Beirne C, O'Loughlin CD, Gaudin C (2015) Soil response in the wake of dynamically installed projectiles. Géotech Lett 5(3):153–160
O'Loughlin CD, Randolph MF, Richardson M (2004) Experimental and theoretical studies of deep penetrating anchors. In: Offshore technology conference
O'Loughlin CD, Richardson MD, Randolph MF (2009) Centrifuge tests on dynamically installed anchors. In: International conference on offshore mechanics and arctic engineering, vol 43475
O'Loughlin CD et al (2013) Penetration of dynamically installed anchors in clay. Géotechnique 63(11):909–919
Raie MS, Tassoulas JL (2009) Installation of torpedo anchors: numerical modeling. J Geotech Geoenviron Eng 135(12):1805–1813
Randolph M, Gourvenec S (2011) Offshore geotechnical engineering. CRC press
Roscoe KH, Schofield A, Wroth CP (1958) On the yielding of soils. Geotechnique 8(1):22–53
Schmid WE (1969) Penetration of objects into the ocean bottom (the state of the art)
Schofield A, Wroth P (1968) Critical state soil mechanics. McGraw-Hill
Sturm H, Lieng JT, Saygili G (2011) Effect of soil variability on the penetration depth of dynamically installed drop anchors. In: OTC Brasil. Offshore technology conference
Tokpavi DL, Magnin A, Jay P (2008) Very slow flow of Bingham viscoplastic fluid around a circular cylinder. J Non-Newtonian Fluid Mech 154(1):65–76
True DG (1975) Penetration of projectiles into seafloor soils (No. CEL-TR-822). Civil Engineering LAB (NAVY) Port Hueneme CA
Wang W, Wang X, Yu G (2016) Penetration depth of torpedo anchor in cohesive soil by free fall. Ocean Eng 116:286–294
Wang W, Wang X, Yu G (2018) Vertical holding capacity of torpedo anchors in underwater cohesive soils. Ocean Engi 161:291–307
Wood DM (1990) Soil behaviour and critical state soil mechanics. Cambridge University Press
Wroth CP, Wood DM (1978) The correlation of index properties with some basic engineering properties of soils. Can Geotech J 15(2):137–145
Yi JT et al (2020) Pull-out capacity of an inclined embedded torpedo anchor subjected to combined vertical and horizontal loading. Comput Geotech 121:103478
Young CW (19369) Depth prediction for earth-penetrating projectiles. J Soil Mech Found Div 95(3):803–817
Zhang N, Matthew Evans T (2019) Discrete numerical simulations of torpedo anchor installation in granular soils. Comput Geotech 108:40–52
Zhao Y et al (2019) Numerical advancements on the analysis of dynamically installed anchors. Ocean Eng 182:343–359

Zhou H, Randolph MF (2007) Computational techniques and shear band development for cylindrical and spherical penetrometers in strain-softening clay. Int J Geomech 7(4):287–295
Zhou H, Randolph MF (2009) Resistance of full-flow penetrometers in rate-dependent and strain-softening clay. Géotechnique 59(2):79–86
Zhu H, Randolph MF (2011) Numerical analysis of a cylinder moving through rate-dependent undrained soil. Ocean Eng 38(7):943–953
Zimmerman EH, Smith M, Shelton JT (2009) Efficient gravity installed anchor for deepwater mooring. In: Offshore technology conference

Cleaner City Through Lesser Noise: Traffic Noise Modelling

Animesh Maurya, Amina Khanam, and Malaya Mohanty

Abstract Noise is an unacceptable level of sound that creates annoyance, hampers mental and physical peace, and may induce severe damage to the health. Although there are many sources of noise, motorized traffic and their irresponsible honking is the major source of creating noise in urban areas. Past studies have shown that traffic flow, speed, and proportion of heavy vehicles are the principal parameters that affect the emission of noise. While most of the studies have been conducted in developed countries, the studies in developing countries are limited. Developing countries like India have completely different traffic scenarios consisting of mixed traffic conditions and absence of lane discipline. In the present study, traffic noise has been calculated using sound meter on 2-lane urban arterials across different traffic volumes. The effect of proportion of each category of vehicles and their counts on peak sound values has also been studied in detail. Subsequently, a mathematical equation has been developed to predict the minimum and maximum sound value using classified traffic volume, including the number of each category of vehicle plying on the road stretch as independent variables. A sensitivity analysis has also been performed to see the effect of each category of vehicle on the value of peak sound value. The study helps in predicting peak sound values at different traffic volume levels and also be useful in framing rules for prohibition of certain kind of vehicles or encouraging the movement of certain vehicles based on their contribution to noise pollution.

Keywords Noise pollution · Regression · Sensitivity analysis · Traffic flow

1 Introduction

As per the World Health Organisation (WHO), noise pollution stands second to air pollution on the effect which it causes to health. Traffic noise is the chief cause of environmental noise pollution, which gives rise to serious health issues and foreshortens the quality of life for residents of major urban cities (Nourani et al. 2018;

A. Maurya · A. Khanam · M. Mohanty (✉)
School of Civil Engineering, KIIT University, Bhubaneswar, India
e-mail: malaya.mohantyfce@kiit.ac.in

B. B. Das et al. (eds.), *Recent Developments in Sustainable Infrastructure (ICRDSI-2020)—GEO-TRA-ENV-WRM*, Lecture Notes in Civil Engineering 207,
https://doi.org/10.1007/978-981-16-7509-6_58

Lu et al. 2019; Gundogdu et al. 2005). With exponential rise in population and urbanisation, the urban vehicle ownership has also spiked up, thereby contributing towards the noise pollution (Yang et al. 2019; Zhao et al. 2015). The foremost step towards environmental management is to predict the traffic noise accurately (Li et al. 2016), so that the intricate nature of the traffic noise can be evaluated, monitored and modeled (Nourani et al. 2018). Mathematical simulations for the prediction of vehicular noise are dated back to 1950s as these models are much more efficient than physical measurements (Nourani et al. 2018). Further, traffic noise prediction models also aid in highway development and enhancement, designing new highways and other roads or redesigning vehicle flow in prevailing roads (Jamrah et al. 2006; Gundogdu et al. 2005).

Various trials have been performed worldwide to predict and reduce the vehicular noise emission levels (Singh et al. 2016). In 2001, Steele reviewed the six then frequently used models and also proposed the requirement for a model which could easily determine L_{max}, L_1, L_5, L_{10} and L_{90} apart from L_{eq}. Nourani et al. (2018) presented an analysis on the first implementation of the Emotional Artificial Neural Network (EANN) and justified its efficacy in correspondence to the traditional Feed-forward Neural Network (FFNN) adopting vehicular categorization and average speed as the input parameters for the first scenario and total traffic and percentage of hefty vehicles for the second scenario. In the case of developing nations like India, with the prevalence of heterogeneous traffic condition and absence of lane discipline, it is not possible to implement the models used for homogeneous traffic conditions (Kalaiselvi and Ramachandraiah 2016). Through field study, Kalaiselvi and Ramachandraiah (2016) instigated a new element for horn correction in connection with Level of Service (LOS) and validated it taking the support of noise-mapping review in soundPLAN software. Li et al. (2016) put forward a vehicular noise prognosis model established on the probability distribution model attained by Monte Carlo simulation; however, the suitability of the model was limited to the roads with less traffic flow. Using data from field measurements in Dalian city of China, Lu et al. (2019) generated structural equations to inspect the mediated effects of road characteristics on vehicular noise through traffic movement. Salomons and Pont (2012) established a relation between spatial diffusion of vehicular noise in a city and the dispersion of traffic volume and urban density; introducing the notion of urban traffic elasticity. Gaja et al. (2003) worked out to find the suitable measuring time, so that a 24-h noise level could be procured efficiently enough to represent the yearly equivalent level. Zhao et al. (2015) conducted a study to theoretically enhance the L_{eq} (20 s) models and also to corroborate its rationality by in-situ inspection. According to Fernandes et al. (2020), steady-state calculation and dynamic simulation are two of the most commonly used prediction models. Steady-state calculation relies on the aggregated kinematic information, namely traffic volumes and average speeds while the dynamic simulations involves detailed particulars about the vehicle activity data such as relative position of vehicles, acceleration and speed. Various researchers (Shalini and Kumar 2018; Morley et al. 2015; Suthanaya 2015) have used regression techniques to predict the noise. Regression model is basically a technique which

helps us to establish relationship between a dependent variable and a few independent variables (Shalini and Kumar 2018). Suthanaya (2015) developed a traffic noise model using multiple regression method for collector road in the city of Denpasar but the model was limited to the vehicles with the average speed lying between 23 and 49 km/h. According to Morley et al. (2015), traffic flow data is the most significant variable in deciding the performance of any traffic models.

The present paper attempts to derive a mathematical equation to predict the traffic noise using traffic volume and proportion of vehicles as independent variables. The category of vehicle plays a major role in heterogeneous traffic conditions that is prevalent in most of the developing countries like India. Microsoft Excel and SPSS software have been used for statistical analysis to develop simple yet efficient regression models which can be directly used on field. The developed equation can easily determine the volume at which the level of noise exceeds the safe levels and hence, certain amendments in rules and regulations with regards to traffic operations can be done to reduce the noise pollution and ensure healthy living conditions.

2 Data Collection and Extraction

In order to develop the regression model, various sites were selected. The field sections chosen for the present are undivided 2-lane road (width of 7 m) with a single carriageway. These type of roads were chosen for the present study as 55.5% of the roads in India are double lane (MORTH—2019). Shoulder of 2.5 m were provided on both sides of road across the whole stretchof test sections. The land use on both sides of the test sections consisted of University, hostels, street food corners, residential buildings and hospitals. Data collection was conducted with the help of camera for recording the videos and sound meter for collecting the sound data. The traffic volume during peak hours and during off-peak hours varied widely at this site and this was one of the reasons for selection of such site. Figure 1a shows the plan sketch of the test section while Fig. 1b and c show typical snapshots of test section in the early morning and night. A length of 15 m was marked on the road longitudinally with the help of measuring tape which signified the area (forming a rectangle EFGH) which was specifically covered for the observations (both volume and noise). At one of the corners of the rectangle formed, the camera (C1) was placed focusing towards the interior of the rectangle and turned at certain angle so that the whole of the traffic could be covered in the chosen area (as shown in Fig. 1a). The camera was positioned on a tripod in such a way that certain height could be provided to ensure that the incoming as well as the outgoing traffic is counted without any discrepancy and also none of the vehicle remains hidden because of the appearance of heavy vehicles in the way. It was necessary to keep a video record of the traffic volume alongside the manual instantaneous counting so that there would not be any chances of errors in the volume count. Parallely, the sound meter (S1) was arranged so that the noise readings could be taken simultaneously.

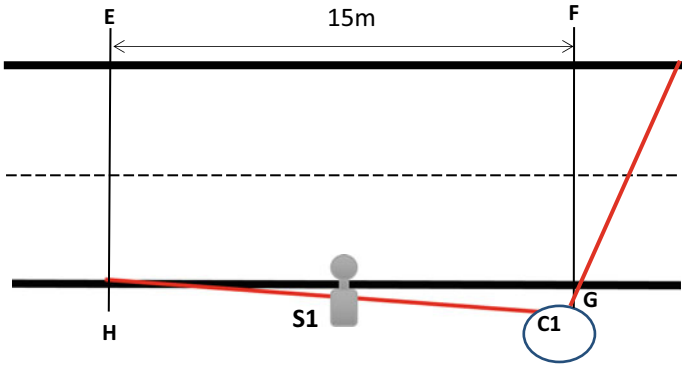

(a)

(b)

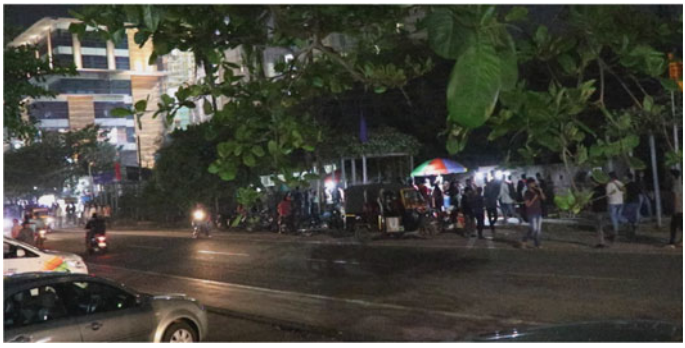

(c)

Fig. 1 **a** Camera setup for data collection; **b** A test section in early morning; **c** Data collection at night

The sound meter used here was IEC 61672 Type II, which had three levels of measurement ranging from 30 to 130 dB. During setting the sound meter, Type A was selected as it has been found that the A-scale on a sound-level meter best approximates the frequency response of the human ear. Sound pressure levels measured on the A-scale of a sound meter are abbreviated dB(A) (FHA 1995). The sound pressure level, generally indicated in units of dB(A) is the most appropriate criterion for drafting traffic noise emission (Nedic et al. 2014). Therefore, all sound pressure readings in the present study represented as dB actually represents dB(A).The sound meter was capable of catching the frequency from a distance of 15 m and hence with great ease the sound was recorded by positioning the meter nearby the camera so that both the processes continued simultaneously. The timings for recording the observation were chosen in a way such that data for a wide range of traffic volume along with noise is obtained, thereby enhancing the precision of the experiment. Further, the data collection require active involvement of atleast two persons. One has to set up the camera and record the field data while the other has to hold the sound meter upright and record the fluctuating readings of the sound meter. Video clips of 15–20 min duration have been recorded for both the parameters (traffic volume and traffic noise) and has to be dealt with great attention so that both the recordings starts and ends at same instant. From the videos, the number of vehicles has been counted for each time interval and is notedonan excel sheet. Similarly, the different composition of the vehicle such as 2 W, 3 W, 4 W and heavy vehicles have also been noted. Since the sound meter gave instantaneous readings, so average reading is calculated for each minute and is noted in a separate column corresponding to that particular minute's vehicle count. Further, percentages of different composition of vehicles are also extracted from the traffic videos. The following data were noted down for study and analysis.

- The number of vehicles
- The composition of vehicles
- Sound meter readings.

3 Results and Analysis

The data analysis involved the traffic recordings at various stretches of 2-lane undivided roads in the urban areas as mentioned in the previous section. The data for traffic flow, and percentage of different category of vehicles were extracted from the videos and noted down. Further, they were mapped with the noise values obtained from sound meter. In order to achieve this, the number of vehicles along with categories were calculated for every minute and this was mapped with the data from sound meter which gave the changing sound levels for every second for that respective minute. For every minute of traffic flow, the sound meter gave 60 values of noisevalues in decibels, which was then used to find the minimum, and the maximum sound value for that one minute time interval of traffic flow. Table 1 shows the traffic character-

Table 1 Traffic composition at various traffic volume levels

Traffic volume (vph)	Traffic composition											
	2-wheelers (%)			3-wheeler (%)			4-wheelers (%)			HV (%)		
	Max	Min	Avg	Max	Min	Avg	Max	Min	Avg	Max	Min	Avg
<1000	62.5	45.6	**57.4**	26.7	11.8	**15.4**	30.7	12.5	**18.7**	14.3	0.0	**8.5**
1000–2000	68.4	47.4	**61.0**	22.5	10.0	**13.2**	27.8	12.5	**18.5**	11.1	0.0	**7.3**
2000–3000	77.4	54.3	**67.7**	14.9	6.7	**9.2**	31.6	13.3	**18.9**	7.8	0.0	**4.2**
>3000	84.2	59.6	**72.6**	12.6	5.2	**7.7**	24.6	11.7	**17.7**	5.6	0.0	**2.0**

istics based on the traffic composition of different category of vehicles at various traffic volume levels.

It can be observed from the traffic composition that the composition of 4-wheelers (cars) remained more or less same across all the traffic volume levels. However, an increased number of 2-wheelers are found to ply on the road at higher traffic volume levels. Figure 2 presents a box plot showing the maximum, minimum, and average noise levels (in dB) at various traffic volume levels.

Figure 2 suggests as how traffic noise level increases with increase in traffic volumes. However, the figure gives the minimum, average and maximum sound value characteristics and not the detailed information about the variation in sounds across different traffic volume levels. Therefore, Fig. 3 depicts the minimum (S_{min}), average (S_{avg}), and maximum (S_{max}) noise levels on a scatter plot across various traffic volume levels.

The obvious remarks from Fig. 3 is that as the traffic volume increases, both the minimum, average, and maximum sound value increases. The 3 linear trends that is observed in the figure are as follows.

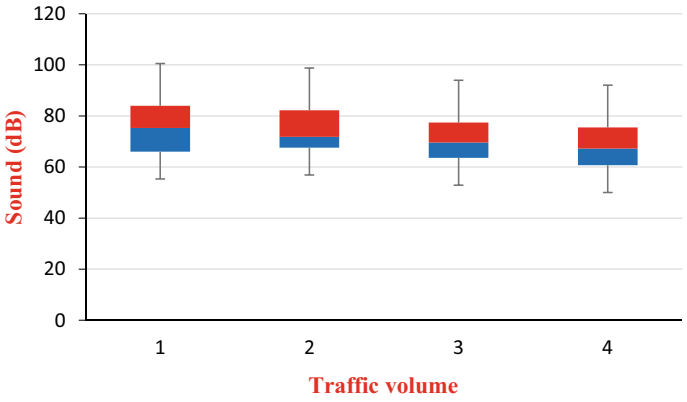

Fig. 2 Boxplots for noise levels at different traffic volume levels. *Note* 1 represents >3000 vph; 2 represents 2000–3000 vph; 3 represents 1000–2000 vph; and 4 represents <1000 vph

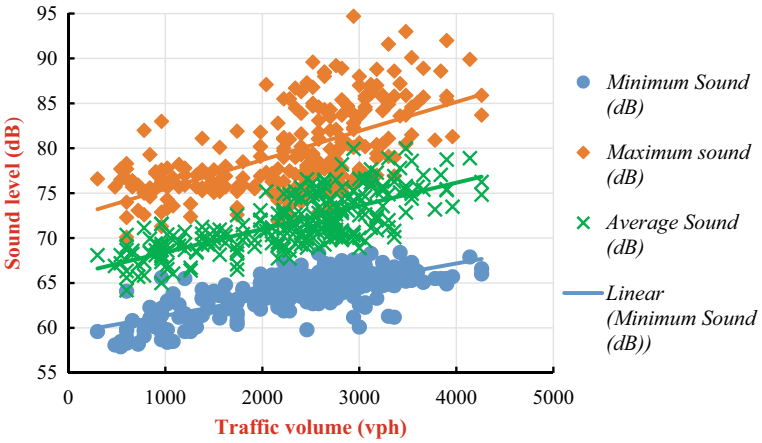

Fig. 3 Variation of minimum, and maximum sound levels at various traffic volumes

$$S_{\min} = 0.0019V + 59.427 \quad \left(R^2 = 0.548\right) \tag{1}$$

$$S_{\max} = 0.0032V + 72.243 \quad \left(R^2 = 0.362\right) \tag{2}$$

$$S_{avg} = 0.0026V + 65.835 \quad \left(R^2 = 0.541\right) \tag{3}$$

where,

$S_{\min}$, S_{avg}, and $S_{\max}$ represents the minimum and maximum sound value in decibels respectively.
V represents the traffic flow in vehicles per hour.

The vehicular movement on a road is usually considered a random phenomena (Mohanty et al. 2016). Therefore the value of R^2 in Eqs. (1) and (3) are somehow acceptable since its greater than 0.5 (Jamrah et al. 2006; Shan et al. 2013). However, the equation for determination of maximum sound value has a very less R^2 and may not be suitable for practical use. Further, the constant values in both the equations vary a lot. This constant value represents the sound value (in dB) when no vehicle is running on the road. In order to test this on actual field, another experiment was conducted at late night and during the dawn to record the sound value when no vehicles moveon the road. It was observed that the sound values ranged from 57 to 65 dB when there is no traffic on the road. This value is also correctly represented in Eqs. (1) and (3) where the constant values are in between the obtained ambient noise values. However, Eq. (2) grossly shows a very high value of constant. Hence, the interpretation shows that the regular regression equation can be used for predicting the minimum sound value at a road stretch for any traffic volume level with an acceptable degree of accuracy. In order to calculate the maximum sound value which

actually contributes more to noise pollution, the general regression equation cannot be used with a good field representative. Figure 3 also shows the same result i.e. the randomness of maximum sound value is very high as compared to the minimum sound value. It can be observed that at similar traffic volume levels, different maximum sound values are recorded by the sound meter. In order to understand this phenomena, a detailed analysis is conducted and one of the examples have been explained in the following paragraph. 2 data points from Fig. 3 has been taken for comparison and thorough investigation. The details about the data points are shown in Table 2.

The table clearly suggests that the maximum sound values are drastically different in 2 very similar traffic volumes. Microscopically, it can also be observed that slightly lower traffic volume has recorded higher S_{max}. In-depth analysis shows that the traffic composition plays a big role in this regard. It can be observed that in the first case (3480 vph), the percentage of Heavy vehicles (HV) are significantly higher as compared to the traffic flow of 3540 vph. These comparisons were also made across all the collected field data and and it was observed that for a definite traffic volume, the proportion of HV plying on the road stretch affect the maximum sound value (S_{max}) recorded in that road stretch. Further, the continuous 60 s recordings were also played along with the sound values obtained which showed the effect of HV and 3 W on the sound value. Figure 4 below shows the continuous data of sound for the 2 traffic volumes presented in Table 2.

Table 2 The details of maximum sound value and traffic volume for 2 time intervals

Traffic volume (vph)	Maximum sound (dB)	Traffic composition (%)			
		2 W	3 W	4 W	HV
3480	93	62.1	6.9	22.4	8.6
3540	81.5	67.8	5.1	23.7	3.4

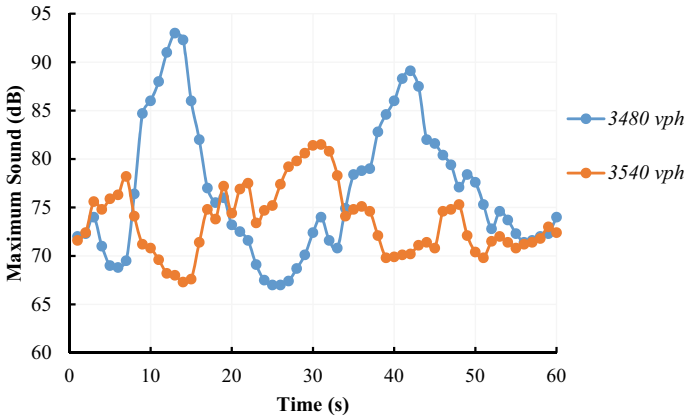

Fig. 4 Maximum sound recorded every second for one minute time interval

Figure 4 depicts the presence of 2 peaks (9–15 s and 38–43 s) in sound values for the traffic volume of 3480 vph, which is the same time when HVs are observed to be travelling on the stretch of road. Similarly, even in case of the curve for 3540 vph, a small peak is observed around 27-32 s. From the recorded video it was confirmed that during that time HV were travelling on the stretch of road. However, in the peaks of the curve for 3480 vph, the percentage of HV were higher as compared to the peaks of the curve for 3540 vph which is also presented in Table 1. In order to examine the effect of all the category of vehicles on maximum sound (S_{max}), a pearson correlation was conducted. All the variables, viz. S_{max}, traffic volume, and proportion of various categories of vehicles were used for the correlation test.

However, it can be noted that if percentage of HV is same for 2 completely different traffic volumes (like 1000 vph and 4000 vph), the effect on S_{max}. can't be ascertained. In other words, traffic volume directly has an effect on number of vehicles and S_{max}, but doesn't have effect on proportion of vehicles. For example, if the traffic volume is 3000 vph for one minute of traffic flow, and 10 HV were observed during that minute of traffic flow, then the proportion of HV is 20%. Similarly if in the next minute, only 20 vehicles move on road, the traffic flow is 1200 vph. Further out of those 20 vehicles, if only 6 vehicles are HV, then the proportion of HV becomes 30%. In these 2 scenarios, it can be noted that even though less number of HV are observed in the second scenario, the proportion of HV increases as the overall traffic volume is low. At similar ranged traffic volumes, proportion of category of vehicles won't affect the S_{max}; however at completely different traffic volume conditions, proportion of any category of vehicle will be practically wrong for statistical analysis. Therefore, either the traffic volumes need to be subdivided into groups for a definite range of flow or instead of pportion of vehicles, number of each category of vehicles plying on the road needs to be used for analysis. In the present study, the number of each category of vehicleshave been used for analysis as they can be directly obtained from field data, and don't need any further mathematical procedures. The pearson correlation table has been shown in Table 3.

The Pearson correlation table clearly indicates that all the variables i.e. traffic volume and number of different categories of vehicles (2 W, 3 W, 4 W, HV). However,

Table 3 Pearson correlation among all the variables

		S_{max}	Volume (V)	2 W	3 W	4 W	HV
S_{max}	Pearson Correlation	1	0.645**	0.622**	0.182**	0.397**	0.543**
	Sig. (1-tailed)		0.000	0.000	0.008	0.000	0.001
Volume (V)	Pearson Correlation	0.645**	1	0.957**	0.336**	0.723**	−0.042
	Sig. (1-tailed)	0.000		0.000	0.000	0.000	0.293

** Correlation is significant at the 0.01 level (1-tailed)

the second row indicates that the traffic volume is also significantly related to the number of 2 W, 3 W, and 4 W. Therefore, in a single mathematical model, either traffic volume can be used or the 3 different category of vehicles can be used. Both the variables can't be used at the same time. In the present analysis, the category of vehicles are taken as independent variables as the sum of these variables ultimately gives the traffic volume. The modelled regression equation is as follows

$$S_{\max} = 61 + (0.594 \times 2W) + (0.155 \times 3W) + (0.082 \times 4W) + (0.232 \times HV) \tag{4}$$

where,

$S_{\max}$ represents the maximum sound value (dB) for one minute time interval.
$2W$ represents the number of two wheelers plying on the road stretch in that one minute.
$3W$ represents the number of three wheelers plying on the road stretch in that one minute.
$4W$ represents the number of four wheelers plying on the road stretch in that one minute.
HV represents the number of heavy vehicles plying on the road stretch in that one minute.

The R-square for the equation is obtained to be 0.947 indicating a very good fit for the estimation of $S_{\max}$. The statistical parameters for the independent variables are provided in the Table 4. The p-values of all the variables are found to be less than 0.05 indicating significant effect of every independent variable on $S_{\max}$. Further, the p-value from the ANOVA analysis was found to be less that 0.05 signifying that there is no significant relation between independent variables. All four independent variables have a noteworthy effect on the result of the dependent variable (i.e. $S_{\max}$). Hence, it can be established that the mathematical regression is well-fitted and the developed model is statistically correct.

In order to verify the accuracy level of the equation, the values of $S_{\max}$ computed by the proposed equation were compared with those obtained from the sound meter from field as provided in Table 5.The recordings were done on a different road stretch having 2-lanes undivided carriageway, and data were extracted as explained in the "Data Collection and Extraction" section for the validation studies. A random sample of around 10 min were recorded and for every minute, the maximum sound value

Table 4 Statistical parameters for estimation of maximum sound value

Independent variables	Standardized coefficient	p-value	p-value for ANOVA
2 W	0.594	0.000	0.000
3 W	0.155	0.000	
4 W	0.082	0.028	
HV	0.232	0.000	

Table 5 Model validation

Minute	Composition of vehicles				Traffic volume (vph)	Value of S_{max}		MAPE (%)
	2 W	3 W	4 W	HV		Proposed model	Field observation	
1	25	0	14	6	2700	78.39	77.8	0.75
2	48	7	12	2	4140	92.04	89.9	2.38
3	19	2	4	2	1620	73.39	78.0	5.91
4	16	10	8	3	2220	73.41	78.2	6.13
5	28	4	13	1	2760	79.55	79.7	0.19
6	35	1	12	1	2940	83.16	77.8	6.89
7	31	3	6	4	2640	81.30	76.3	6.55
8	35	5	7	0	2820	83.14	78.2	6.31
9	31	5	8	3	2820	81.54	77.8	4.81
10	34	4	8	0	2760	82.47	77.1	6.97

and the number of different category of vehicles were noted. The data used for the validation are not used for development of the model. Figure 5 also presents the calculated and observed sound levels showing high rate of accuracy for the obtained results.

Figure 5 represents that the difference between calculated sound levels and sound levels observed from real field data is quiet close close to each other. However, the difference increases with increase in traffic volumes. This can be attributed to the fact that the obtained traffic volumes on field varied from 500 vph to maximum of 4500 vph. Therefore, the proposed equation also predicts the S_{max} accurately in this range of traffic volumes, and should be used when the traffic volume is less than 5000 vph on a 4-lane road. Further, inorder to calculate this difference, MAPE has

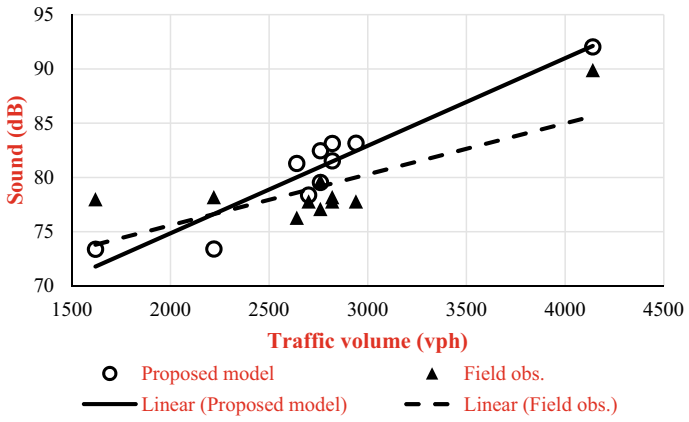

Fig. 5 Difference between model results and field data

been used in this study. Mean absolute percentage error (MAPE) is a good technique to predict accuracy for validation of models related to traffic studies (Liu et al. 2008). The equation for estimating MAPE is as follows

$$M = \frac{1}{n}\sum_{t=1}^{n}\left|\frac{A_t - F_t}{A_t}\right| \tag{5}$$

where,

A_t is the actual value; and
F_t is the model value and n represents the number of data used for validation.

Usually, a MAPE value less than or equal to 10% is considered to be good enough (Liu et al. 2008). The obtained MAPE values in the present study range from 0.19 to 6.97%, which indicates that the developed regression equation provides reasonable estimates of S_{max}.

A sound value of above 60 dB is usually considered as noise by World health Organisation (Menkiti and Agunwamba 2015). As discussed earlier, the traffic flow is the single largest cause for this noise pollution. Therefore, there is a need to decrease the dependency on vehicles and adopt other green means of transport to reduce high noise levels. A sensitivity analysis was conducted for all the independent variables i.e. category of vehicles to understand the impact of each vehicle on the peak sound (S_{max}) value. Figure 6 shows the pictorial representation of the change in number of 1 category of vehicle on the S_{max} value.

It is evident from Fig. 4 above that just 1 increase in the number of HV on road increases the peak sound value by 2.74 dB. Similarly, increase in one 2 W increases the noise value by 0.4 dB. This analysis would be really helpful for maintaining noise pollution under control in peak periods of the day.

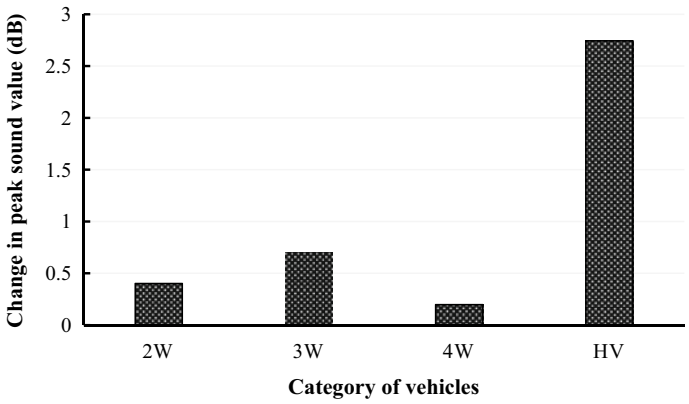

Fig. 6 Change in peak value of sound with change in number of vehicles

4 Implications of the Study

In the current urban transportation green development, effective reduction in traffic noise is the need of the hour. The various measures introduced by the government (namely speed and traffic limit etc.) have inevitable flaws which reduces the efficacy of road use and causes huge economic costs thereby inducing the need for improvement in noise prediction models (Chen et al. 2020). Although various models have been developed to predict the traffic noise, regression is one of the most common approaches which helps to establish relationship between a dependent variable and a few independent variables (Shalini and Kumar 2018). In the present study, post the regression modelling, a sensitivity analysis has been conducted to examine the contribution of each category of vehicle on peak noise levels. It is observed that the change in peak values are least affected by the change in 4 W numbers on road. The results show that prohibition of HVs like trucks during certain times of day can decrease the peak noise levels significantly. However, public buses should be used more. Although use of 1 bus will increase the peak noise level by 2.74 dB, it also carries atleast 40–45 passengers which otherwise would have used around 30 2 W for their movements on road. Considering increase of peak sound levels from movement of 2 W, the same 40–45 passengers would have caused a spike of around 12 dB in sound levels, which is much more than the public bus. Thus, considering different times of day, and different traffic scenarios, the results of present study can contribute significantly for framing rules to decrease the noise pollution in the urban areas. Further, the use of the proposed simple yet effective models can be directly applied on the field without much technical knowledge to control traffic noise in urban areas.

5 Conclusion

Any sound which is unwanted and causes discomfort and annoyance is termed as noise. With rapid increase in population and urbanization, the number of vehicles on the road has increased many fold. Although increase in vehicles increase connectivity and provide comfort to individuals travelling on them, but these overburdened traffic flow is also the chief source of noise pollution. In developing countries like India, where there is lack of lane-discipline and mixed traffic conditions, noise pollution is even more a cause for concern. The health of the population residing in cities with large levels of noise pollution are badly affected. The present study is aimed at predicting the level of sound based on the traffic flow on 2-lane undivided urban streets.

The study is conducted using video camera for recording the traffic flow and a sound meter. Initial impressions from the study made it clear that the increase in traffic volume leads to increase in both the maximum (S_{max}) and minimum (S_{min}) sound levels. It is also found that a regular regression equation can be used to predict the

S_{min} for any traffic volume. However, for the prediction of peak sound value (S_{max}), such general regression equation does not comply with a good field representation. In-depth analysis showed the importance of traffic composition in predicting S_{max}. A Pearson correlation was conducted which proved that S_{max} gets affected by the number of each category of vehicles plying on the road. Finally, a multiple linear regression has been developed and validated to predict S_{max} by noting the number of each category of vehicles plying on the roads. Sensitivity analysis showed that increase in one HV on the road spikes the value of S_{max} by almost 2.5 dB. Similarly, the increase in one 2 W and 3 W increases the S_{max} value by 0.4 and 0.7 dB respectively.

This study can help in framing rules for prohibiting or permitting the movement of different category of vehicles to control the traffic noise at different times of the day in urban areas. Further, in future these values can be analysed to optimise the movement of different category of vehicles on urban roads so that neither movement of people, nor the environment due to noise is hampered. The present study is limited to 2-lane undivided urban roads. Therefore, the volumes obtained from the study is less than 4500 vph for which the model is proposed. However, in future, the same studies can be conducted on different types of roads viz. national highways, state highways, rural roads with different lanes, geometrical features, and land use that shall provide more precise noise models which can be used on various types of roads across a wide range of traffic composition and volumes. Further, the traffic noise at intersections will surely be different and can be a subject of research in future.

Declaration (Ethical Approval, Availability of Data, Consent to Participate, Consent to Publish)

The authors would like to declare that no conflicting interests are present in the manuscript and all the authors have contributed to the manuscript.

All data and materials are available in the manucript itself. Further, if any detailed data is required, the authors agree to provide the raw data for publication and during the reviewing stage.

No funding has been received from any institution for the present research. However, both faculty members and students are a part of KIIT DU.

The authors approve for the use of data and study for research in public domain, if the manuscript gets accepted.

The authors give their consent for publishing under the guidelines laid down by the esteemed journal.

Authors Statement

Contribution of each author

1. ***Animesh Maurya***: Formal Analysis, Investigation, Data Curation, Writing—Original Draft, Validation
2. ***Amina Khanam***: Investigation, Resources, Writing—Original Draft, Writing—Review & Editing, Visualisation, Validation
3. ***Malaya Mohanty***: Conceptualization, Methodology, Software, Validation, Writing—Review & Editing, Supervision.

References

Chen L, Sun B, Wang H, Li Q, Hu L, Chen Z (2020) Forecast and control of traffic noise based on improved UE model during road network design. Appl Acoust 170:1–11

Federal Highway Administration (1995) Highway traffic noise analysis and abatement policy and guidance. US Department of Transportation

Fernandes P, Tomas R, Acuto F, Pascale A, Bahmankhah B, Guarnaccia C, Grana A, Coelho MC (2020) Impacts of roundabouts in suburban areas on congestion-specific vehicle speed profiles, pollutant and noise emissions: an empirical analysis. Sustain Cities Soc 62:102386

Gaja E, Gimenez A, Sancho S, Reig A (2003) Sampling techniques for the estimation of the annual equivalent noise level under urban traffic conditions. Appl Acoust 64:43–53

Gundogdu O, Gokdag M, Yuksel F (2005) A traffic noise prediction method based on vehicle composition using genetic algorithms. Appl Acoust 66:799–809

Jamrah A, Al-Omari A, Sharabi R (2006) Evaluation of traffic noise pollution in Amman, Jordan. Environ Monitor Assess 120(1–3):499–525

Kalaiselvi R, Ramachandraiah A (2016) Honking noise corrections for traffic noise prediction models in heterogeneous traffic condition like India. Appl Acoust 111:25–38

Li F, Liao SS, Cai M (2016) A new probability statistical model for traffic noise prediction on free flow roads and control flow roads. Transp Res Part D 49:313–322

Liu P, Lu JJ, Hu F, Sokolow G (2008) Capacity of U-turn movement at median openings on multilane highways. J Transp Eng—ASCE 134(4):147–154

Lu X, Kang J, Zhu P, Cai J, Guo F, Zhang Y (2019) Influence of urban road characteristics on traffic noise. Transp Res Part D 75:136–155

Menkiti NU, Agunwamba JC (2015) Assessment of noise pollution from electricity generators in a high-density residential area. Afr J Sci Technol Innov Dev 7(4):306–312

Mohanty M, Dey PP, Mishra A (2016) Reduction in flow due to U-turns at median openings. In: 96th annual meeting, Transportation Research Board, Paper no. 17-00195

Morley WD, de Hoogh K, Fecht D, Fabbri F, Bell M, Goodman SP, Elliott P, Hodgson S, Hansell A, Gulliver J (2015) International scale implementation of the CNOSSOS-EU road traffic noise prediction model for epidemiological studies. Environ Pollut 206:332–341

Nedic V, Despotovic D, Cvetanovic S, Despotovic M, Babic S (2014) Comparison of classical statistical methods and artificial neural network in traffic noise prediction. Environ Impact Assess Rev 49:24–30

Nourani V, Gokcekus H, Umar KI, Najafi H (2018) An emotional artificial neutral network for prediction of vehicular traffic noise. Sci Total Environ, 136134

Salomons EM, Pont MB (2012) Urban traffic noise and the relation to urban density, form and traffic elasticity. Landsc Urban Plan 108:2–16

Shalini K, Kumar B (2018) Development of traffic noise model (TNM) using regression analysis in Varanasi City, India. Int J Civil Eng Technol 9(4):70–76

Shan Z, Zhao D, Xia Y (2013) Urban road traffic speed estimation for missing probe vehicle data based on multiple linear regression model. In: 16th international IEEE conference on intelligent transportation systems (ITSC 2013). IEEE, pp 118–123

Singh D, Nigam SP, Agrawal VP, Kumar M (2016) Vehicular traffic noise prediction using soft computing approach. J Environ Manage 183:59–66

Steele C (2001) A critical review of some traffic noise prediction models. Appl Acoust 62:271–287

Suthanaya AP (2015) Modelling road traffic noise for collector road (case study of Denpasar City). In: The 5th international conference of Euro Asia civil engineering forum (EACEF-5), vol 125, pp 467–473

Yang W, Cai M, Luo P (2019) The calculation of road traffic noise spectrum based on the noise spectral characteristics of single vehicles. Appl Acoust, 107128

Zhao J, Ding Z, Hu B, Chen Y, Yang W (2015) Assessment and improvement of a highway traffic noise prediction model with L_{eq} (20 s) as the base vehicular noise. Appl Acoust 97:78–83

Assessment of Food Waste as Suitable Adsorbent for Removal of Chromium (vi) from Synthetic Waste Water

Manisha Mohanty and Ipsita Panda

Abstract Effluents from industries have created a congregation of mayhem worldwide as they carry a lot of heavy and virulent metals with them and contaminate the water when discharged to any water body. As per many sources effluents from industrial processes such as electroplating, mining, nuclear power operation, battery manufacturing, dye and pigments have been identified to contain high level of heavy metals and some heavy metals include Cr(III), Cr(VI), Zn, Cd, Cu, Ni, Hg and pb. Chromium as a metal has long been used in electroplating, leather tanning, metal finishing and many other manufacturing industries. It is found that effluents from these industries contain both trivalent chromium Cr(III), and hexavalent chromium Cr(VI) with concentrations ranging from tens to hundreds of mg/L. The aim of the current research work was pertinent to find a suitable sorbent for removal of chromium from waste water. Therefore naturally available resources like rice husk, saw dust, tea powder waste, banana peel and vegetable peel wastes viz. potato and carrot peel from kitchens are used as adsorbent for this study. A relative comparative study was done considering the effect of sorbent dose, sorbent concentration, pH of the solution and shaking time. Different adsorption isotherms was used to reckon the maximum uptake capacity. It was found from the study that percentage of metal uptake increased with the increase in sorbent dose, sorption of chromium increases with increase in pH for rice husk, tea waste, vegetable peels and decreased with increase in pH for saw dust and banana peel. Sorption of chromium was found to increase with increase in contact time specifically contact time is more for tea waste. Vegetable peel used was found to be more efficient in the adsorption of the metal ions than other adsorbents being used for this study. The results obtained from this work distinctly proved the efficacy of rice husk, saw dust, tea waste, banana peel and vegetable peel as effective adsorbents for chromium removal.

Keywords Adsorbent · Sorption · Concentration · Dose · Chromium

M. Mohanty
Synergy Institute of Technology, Bhubaneswar, India

I. Panda (✉)
School of Civil Engineering, KIIT University, Bhubaneswar, India
e-mail: ipsita.pandafce@kiit.ac.in

B. B. Das et al. (eds.), *Recent Developments in Sustainable Infrastructure (ICRDSI-2020)—GEO-TRA-ENV-WRM*, Lecture Notes in Civil Engineering 207,
https://doi.org/10.1007/978-981-16-7509-6_59

1 Introduction

As water constitutes a basic necessity in life, water pollution has become a great concern among human beings. The deliberate discharge of various types of pollutants into the environment especially in developing countries by the fast-paced industries such as metal mining, fertilizers, pesticides and paper industries have added pernicious effects in our ecosystem. Therefore among other issues, water contamination by heavy metals are more pronounced than any other pollutants especially when heavy metals are exposed to the natural ecosystem. 'Heavy metals' refers any elements with the atomic weights between 63.5 and 200.6 and a specific gravity greater than 5.0. Some of these heavy metal are also known to attack the active sites of enzymes in the body therefore inhibiting the enzymes (Olayinka et al. 2007). Most of the heavy metals salts are soluble in water and form aqueous solution and consequently cannot be separated by ordinary physical means of separation (Alkpokpodion et al. 2010). Chromium is normally concentrated in the ultramafic and ultra basic rocks and rocks like Dunite, peridotite, pyroxenite, and serpentine which has Cr level of 2400 ppm (Matzat and Shiraki 1974). The distribution of total Cr in natural ground waters was investigated by Barnes and Langmuir (1978) where they found total Cr thresholds, corresponding to the 97.7 percentile, of 10–19 ppb for 647 ground waters associated with carbonate rocks, sandstones (including quartzites, arkoses, grey wacks, and conglomerates), shales (comprising clays, siltstones, and slates), and felsic to intermediate igneous and meta-igneous rocks.

When the heavy metal concentration exceeds their permissible limit in the ecosystem it becomes very toxic and once they interrupt in human food chain they may affect the human body and possibly, cause severe health problems. Acidification of soil can also influence chromium uptake by crops. Chromium is not known to pile up in the bodies of fish, but high concentrations of chromium in a natural water body can damage the gills of fish that swim near the point of disposal. In both humans and animals chromium can cause respiratory problems, a lower ability to fight disease, birth defects, infertility and tumour formation. Breathing in high levels of Cr(VI) (>2 $\mu g/m^3$) containing dust particles in the form of compounds like chromic acid or chromium tri-oxide, can cause irritation to the respiratory system. The permissible limit of Cr(VI) in drinking water is 50 $\mu g/L$ and total Cr is 100 $\mu g/L$.

While hexavalent (CrO_2^{-4} and $Cr_2O_2^{-7}$) and trivalent (Cr^{+3} and $CrOH^{+2}$) species of chromium are prevalent in industrial waste solutions, the hexavalent form has been considered more hazardous to public health due to its mutagenic and carcinogenic properties. Its concentrations in industrial waste-waters range from 0.5 to 270.0 mg/l. The tolerance limit for Cr(VI) for discharge into surface waters is 0.1 mg/l and in potable water is 0.05 mg/l. Thence in order to comply with this limit, it is essential that industries must treat their effluents to reduce the Cr(VI) to acceptable levels before releasing it to nearby environment.

A wide range of physical and chemical processes are already available for the removal of Cr(VI) from waste water viz. electro-chemical, precipitation, ultrafiltration, ion exchange, electro-dialysis, reverse osmosis, chemical precipitation, and

adsorption. But the major drawbacks with these processes lies in its high cost, toxic sludge generation or incomplete metal removal. Adsorption has proved to be very effective and some commercial activated carbons as adsorbent for chemical modifications of Cr(VI). But cost effective techniques is still wanting. Many researchers are now adopting use of biomass from agricultural and livestock waste have captured many researchers attention. Mainly agriculture residues such as coconut husk, turmeric waste, ferronia shell waste Jatropha curcus seed shell waters, delonix shell waste, ipomea carnia stem, rice husk, jack fruit peel, bamboo, cow dung etc. have been tested for the bio-sorbent. Cr(VI) reduction rate by bio-materials at less acidic pH could be solved by screening a new efficient bio-material, banana skin, which has been considered as an useless agricultural waste (Park 2008; Memon 2009). Adsorption of Cr(VI) using activated neem leaves using kinetic studies (Babu et al. 2008). Tea waste has a moderate potential to remove Chromium (VI) (Saritha 2011; Bhavsar 2012; Attia, 2012).Sawdust and cardboard are the low cost, locally available material, and therefore could be used for the removal of heavy metals from the waste mine water (Radmila Markovic et al. 2011; Larous and Meniai (2012a, b).

Adhesion of atoms, ions, bimolecules or molecules of gas, liquid or dissolved solids to a surface is called adsorption. This process creates a film of the adsorbate the molecules or atoms being accumulated, on the surface of the adsorbent. The molecules of gases or liquids or the solutes in solutions adhere to the surface of the solids. In adsorption process, two substances are involved. One is the solid or the liquid on which adsorption occurs and it is called adsorbent. The second is the adsorbate, which is the gas or liquid or the solute from a solution which gets adsorbed on the surface. The substance on whose surface the adsorption occurs is known as adsorbent. Similarly, Biosorption is a metabolically passive process, meaning it does not require energy, and the amount of contaminants a sorbent can remove is dependent on kinetic equilibrium and the composition of the sorbents cellular surface. Bioaccumulation is an active metabolic process driven by energy from a living organism and requires respiration. Bioaccumulation occurs by absorbing contaminants which are transferred onto and within the cellular surface. Both bioaccumulation and biosorption occur naturally in all living organisms.

This study's first motive was to find a suitable sorbent for the removal of Chromium (VI) from waste-water. So, rice husk, saw dust, tea (*Camellia sinensis*), banana peel, vegetable waste (carrot and potato peels) was taken in dried form and adsorption studies were carried out by varying parameters like concentration of adsorbate and adsorbent, contact time and pH. Different adsorption isotherm equations such as Freundlich and Langmuir were tested. From the data obtained, it was found that R^2 values followed Langmuir absorption isotherm. Using Langmuir adsorption isotherm the maximum uptake capacity was calculated.

2 Materials and Methods

2.1 Materials

Five different biomass was taken for the preparation of activated carbon by following common method of activation, chemical method.

2.1.1 Rice Husk

It is a potential material and can be amenable for value addition. The chemical composition of rice husk is similar to that of many common organic fibers and it is comprised of 40–50% cellulose, 25–30% lignin, 15–20% ash and 8–15% moisture (Hwang and Chandra 1997). After burning, most of the components are evaporated slowly and the silicates are left. Rice husk was collected from a locally available rice mill at Remed, Sambalpur. It was washed thoroughly with tap water and then with distilled water to remove all extraneous dirt. Rice husk was dried in oven at 120 °C for 6 h. The dried materials was sieved by 599–853 μm sieve and kept in an air tight bottle.

2.1.2 Sawdust

Sawdust refers to the tiny-sized and powdery wood waste produced by the sawing of wood. In the field of compost science, sawdust being a ligno-cellulosic material has been referred to not only as a bulking agent but also as biomass material for the manufacture of woody compost due to its benefits in physical properties such as low apparent specific gravity (density), high porosity, high water retention, moderate water drainage, high bacteria tolerance, and biodegradability. Sawdust was collected from a nearby carpenter shop and sieved through 70–300 μm sieve. It was then washed with hot distilled water and dried in oven at 80ºC for 24 h to a constant dry weight and stored in an air tight bottle.

2.1.3 Tea Waste

Tea is one of the most popular beverages and about 3.5 million tons of tea was consumed annually in the world. As per few sources amount of tea powder waste produced per year after processing is about 190,400 tonnes in India alone. Insoluble cell walls of tea leaves are largely made up of cellulose, hemicelluloses, lignin, condensed tannins and structural proteins. For our experiment waste tea was collected from college hostel and washed using distilled water to remove color. It was dried at 105 °C for 24 h. Post drying, material was ground and sieved by 10 mesh sieve to

get the particle size of 149–297 μm. The powder was then further dried at 150 °C for 6 h and stored in a bottle at room temperature.

2.1.4 Banana Peel Waste

Banana Peel an aggro waste is discarded worldwide as an unusable material. On average, banana peels contain 6–9% dry matter of protein and 20–30% fiber (measured as NDF). The collected banana peel were cut into small pieces less then 5 mm, washed thrice with tap water and distilled water to remove any external dirt. The wet banana peels were air dried initially to remove water from surface and then dried in oven at 105 °C for 24 h. The dried banana peels were grounded into powder and kept in an air tight bottle for further experimental uses.

2.1.5 Vegetable Waste

Potato skins are a rich source of iron and skin and provides 88% of the total amount solid wastes from food processing industries. Similarly few investigators used carrot peels for the removal of heavy metals like copper, zinc and chromium. Vegetable wastes were collected from nearby hostel and thoroughly washed with distilled water and was oven dried at 60 °C for 48 h followed by fine grinding separately in a grinder. The ground peels were sieved using a 60 μ mesh size sieve. A homogeneous mixture of 1:1 ratio was prepared by taking equal amounts of sieved potato peel and carrot peel powders. The prepared mixture was stored in an air tight container which was placed in a desiccator for further experiments.

2.2 Methodology

2.2.1 Adsorbent Properties

The activated carbon prepared from biomass, used for adsorption process. Here five different materials are used for preparation of adsorbent and their characterizations are done.

Physio-Chemical Properties of Sorbent

Density, porosity, specific gravity, bulk density and dry density were determined with the help of specific gravity bottle of 50 ml capacity and calculated with empirical formulas.

2.2.2 Adsorbate

A pseudo industrial waste water was made ready by adding 1.414 g of potassium dichromate solution to 1 L of fresh distilled water to prepare a chromium enriched water of concentration 500 mg/l. This stock solution was used for all the experiments conducted for chromium removal process.

2.2.3 Adsorption Studies

Experimental Methodology Used for the Adsorption

Adsorption studies can be done by batch contact system method or continuous flow system method. In this study, all the studies of optimized operational variables including the adsorption kinetics, isotherms, thermodynamics were done in batch contact system method which was easy and uncomplicated to execute. Initially calibration curve was done before adsorption studies to generate the equation, which implied that absorbance is a function of concentration.

Batch Contact System Adsorption Studies

Mostly, in batch contact process, graphically determined amount of adsorbent is agitated with a specific volume of adsorbate solution with known concentration for a certain time period until the concentration of adsorbate in solution phase plummet to a desirable level. The removal rate of adsorbate mainly depends upon the driving force of the rate of adsorption as well as solution concentration. Few physical parameters like surface area, porosity of adsorbent, morphological parameters, chemical parameters like acidity or basicity nature of adsorbent are also essential. Preliminary experimental were done to optimize the adsorbent dose and agitation time.

In the present research, a series of batch adsorption experiments were conducted to determine the adsorption of chromium on rice husk, saw dust, tea waste, banana peel & vegetable peels. All the batch adsorption experiments were performed manually using 100 ml conical flasks with stopper containing 50 ml each of chromium solution. Experiments were performed at room temperature of 27 °C (300 K). The pH of the solution was maintained around 6–8 as well as checked periodically by pH paper and pH meter. Other parameters such as adsorbent doses, contact time were also either varied or kept at desired level as per the requirement. All solution samples post adsorption were filtered through syringe Wattman (0.45 μm) filter paper. The concentrations of chromium in treated samples were determined by UV spectrophotometer and by comparing with calibration equation (Figs. 1 and 2) shows the batch preparation.

Fig. 1 Cr(VI) stock solution

Fig. 2 Cr(VI) solution + adsorbent

2.2.4 Optimization of Operational Variables

Effect of various parameters or operational variable such as effect of adsorbent dose, contact time, pH, initial concentration and temperature on the adsorption of chromium by different adsorbent was examined. Kinetics studies for the removal of the dye under the given condition have also been done to understand the mechanistic role of the system. The experiments were repeated twice for substantiation and appropriate results was recorded.

Effect of Adsorbent Dose

Effect of adsorbent dose on the chromium adsorption was investigated by the varying the amount adsorbent dose of different adsorbent in 50 ml chromium solution. Adsorbent dose varied between 0.5 and 7 for rice husk and these experiments were carried out at pH 4 using 10 mg/L as initial chromium concentration with contact time 30 min. For saw dust, adsorbent dose varied between 0.5 and 5 and these experiments were carried out at pH 2 using 20 mg/l initial chromium concentration with contact time 60 min. For tea waste powder, adsorbent dose varied between 0.5 to 5 and experiment were carried out at pH 4 using 10 mg/l initial chromium concentration with contact time 60 min. For banana peel adsorbent dose varied 0.5 to 4 and experiment were carried out at pH 2 using 10 mg/l initial chromium concentration with contact time 60 min. Lastly, for vegetable peels adsorbent dose varied between 0.5 to 4 and experiment was carried out at pH 2 using 20 mg/l initial chromium concentration with contact time 30 min.

Effect of Contact Time

The effect of contact time on the adsorption of chromium on different adsorbent was studied in the range of 5 to 60 min (viz. 5, 15, 30, 60 min). Study was carried out for rice husk, dose concentration was kept at 2 g at pH 4 with 10 mg/l of chromium concentration of 50 ml solution. For saw dust, dose concentration was 1 g at pH 2 with 20 mg/l chromium concentration of 50 ml solution. For tea powder, dose concentration was 0.5 gm at pH 4 with 10 mg/l chromium concentration of 50 ml solution. For banana peel, dose concentration was 0.5gm at pH 2 with 10 mg/l chromium concentration of 50 ml solution. For vegetable peel, dose concentration was 1gm at pH 2 with 20 mg/l chromium concentration of 50 ml solution. As the time of agitation increased, the contact between sorbate-sorbent increased and all the pores of adsorbent was occupied by the adsorbate in mono-layer fashion.

Effect of pH

pH effect on the adsorption of chromium by different adsorbent was studied keeping pH range from 2.0 to 10. The pH of chromium solution was adjusted prior to the experiments using the 0.1 M NaOH and 0.1 M HCL. This study was carried out for rice husk keeping the dose concentration 2 g at 10 mg/l of chromium concentration of 50 ml solution with contact time 30 min. For saw dust, dose concentration was 1 g at 20 mg/l chromium concentration of 50 ml solution with contact time 60 min. For tea powder, dose concentration was 0.5 gm at 10 mg/l chromium concentration of 50 ml solution with contact time 60 min. For banana peel, dose concentration was 0.5gm at 10 mg/l chromium concentration of 50 ml with contact time 60 min. And lastly, for vegetable peel, dose concentration was 1gm at 20 mg/l chromium concentration of 50 ml solution with contact time 30 min. The pH values of the solution were

measured before and after the sorption process and change in pH was examined and noted.

Effect of Initial Concentration

The effect of initial adsorbate concentration (C_0) on the adsorption by adsorbent was examined by varying the initial concentration from 5 to 50 mg/l of 50 ml solution for rice husk, saw dust, banana peel, 5 to 60 mg/l of 50 ml for vegetable peel and 10 to 80 mg/l of 50 ml for tea waste. Similarly here experiments was carried out for for rice husk keeping the dose concentration at 2 g at pH 4 with contact time 30 min. For saw dust, dose concentration was 1 g at pH 2 with contact time 60 min. For tea powder, dose concentration was 0.5 gm at pH 4 with contact time 60 min. For banana peel, dose concentration was 0.5 gm at pH 2 with contact time 60 min. For vegetable peel, dose concentration was 1gm at pH 2 with contact time 30 min. The rate limiting step in the reaction is defined as the adsorption which is totally concentration dependent. When the kinetics of the reaction is dominated by intra-particle transport, variation in the reaction rate is not expected to be linear, rather the rates of the strictly adsorptive reaction and simple diffusion controlled procedure are expected to be proportional to the first power of the adsorbate concentration.

2.2.5 Modeling of Adsorption Isotherms and Its Studies

The process of adsorption is usually studied through graphs known as adsorption isotherm. It is the graph plot between the amounts of adsorbate (x) adsorbed on the surface of adsorbent (m) and pressure at constant temperature. In the process of adsorption, adsorbate gets adsorbed on adsorbent.

To determine the efficiency of the sorbents prepared, the equilibrium sorption of the chromium is studied as a function of concentration. Different equilibrium models have been developed to describe sorption isotherm relationships and here the sorption capacities of rice husk, saw dust, tea waste, banana peel waste and vegetable peels waste for chromium have been evaluated by Langmuir isotherm, Freundlich and Temkin isotherms.

Langmuir Isotherm

The most widely used isotherm equation for modeling of the adsorption data is the Langmuir equation, which is valid for monolayer sorption onto a surface with a finite number identical site and is given by following equation.

$$q_e = \frac{\text{Qmax} \,.\text{b.Ce}}{1 + \text{b.Ce}} \tag{1}$$

where,

Qmax = maximum adsorption capacity = monolayer adsorption capacity, (mg g^{-1}), signifies the solid phase concentration, corresponding to the complete coverage of available sorption site, can be evaluated from the slope of Langmuir isotherm plot (1/qe against 1/Ce) max Q.

b = Energy constant = Langmuir Isotherm constant, (L g^{-1}), this value corresponds to energy of sorption, calculated from the intercept of the linear plot of Langmuir isotherm.

For solid liquid systems, the Langmuir isotherm is expressed in the linear form as:

$$\frac{\mathrm{Ce}}{\mathrm{qe}} = \frac{1}{\mathrm{bQmax}} + \frac{\mathrm{Ce}}{\mathrm{Qmax}} \tag{2}$$

or

$$\frac{1}{\mathrm{qe}} = \frac{1}{\mathrm{Qmax}} + \frac{1}{\mathrm{bQmax}} \times \frac{1}{\mathrm{Ce}} \tag{3}$$

The essential characteristics of Langmuir isotherm can be expressed in terms of a dimensionless separation factor, R_L, which describe the type of isotherms and is defined by,

$$\mathrm{R_L} = \frac{1}{1 + \mathrm{bCo}} \tag{4}$$

where, b is Langmuir constant introduced in Eq. (4) and C_0 is the initial concentration. The parameters indicate the shape of the isotherm accordingly, if, R_L value lies in between 1 and 0, then it indicates favorable adsorption. If R_L value is greater than 1, it indicates unfavorable adsorption, whereas a value of 1 represents linear and unfavorable and 0 represents irreversible.

Freundlich Isotherm

The Freundlich isotherm model is derived by assuming a heterogeneous surface with a non-uniform distribution of heat of adsorption over the surface. The Freundlich model is non-linear & linear form can be expressed as

$$\mathrm{q_e} = \mathrm{K_f}(\mathrm{C_e})^{1/\mathrm{n}} \tag{5}$$

$$\ln \mathrm{q_e} = \ln \mathrm{K_f} + \ln \mathrm{C_e} \tag{6}$$

where,

K_f is the Freundlich characteristics constants and 1/n the heterogeneity factor of adsorption, obtained from intercept and slope of (ln(qe) vs. ln(Ce) linear plot) respectively. (4). Value of K_f is an indicator of adsorption capacity and thus can be used for relative measurement of the surface area. b and 1/n are related to enthalpy and intensity of the adsorption. 1/n value should be less than unity for high adsorption capacity.

Temkin Isotherm

The Temkin equation isotherm anticipates that the heat of adsorption of all the molecule in the layer attenuated linearly with coverage due to sorbent-sorbate interaction and that adsorption is characterized by uniform distribution of the binding energy, up to some maximum binding energy. The value of Temkin constant along with the coefficient of determination the Temkin isotherm can be expressed as

$$\mathrm{qe} = \frac{\mathrm{RT}}{\mathrm{bt}\ln(\mathrm{Kt.Ce})} \tag{7}$$

$$\mathrm{qe} = \mathrm{B1}\ln \mathrm{Kt} + \mathrm{B1}\ln \mathrm{Ce} \tag{8}$$

where,

b_t Temkin isotherm constant.
R universal gas constant (8.314 J/mol/K).
T Temperature at 298 K.

(B1 = RT/b) and Kt is the equilibrium binding constant (L/mg) corresponding to the maximum binding energy and the constant B1 is related to the heat of sorption (J/mol). A plot of (qe vs. ln(Ce)) enables the finding of the isotherm constant K_t and B1.

2.2.6 Adsorption Thermodynamics

Thermodynamics applies only to equilibrium adsorption isotherms. Since the adsorption is a kinetic process, removal rate can be increased or decreased by altering the system temperature. Gibbs free energy change (ΔG°) is calculated as per the following equation (Rout et al. 2014).

$$\ln = \frac{\Delta G^\circ}{\mathrm{RT}} \tag{9}$$

where R is the universal gas constant (8.314 J mol^{-1} K^{-1}) and T is the absolute temperature.

2.2.7 Adsorption Kinetics

The kinetic of sorption is important as it controls the process efficiency. Characterization of sorbent surface is a critical factor that affects the rate parameters and diffusion resistance also plays an important role in the overall transport of the solute. Here, kinetics of sorption was checked by the pseudo first order, pseudo second order models.

Pseudo First Order Model

The first order rate expression was given by Langergren

$$\log\left(q_e - q_t\right) = \log q_e - K_1\left(\frac{t}{2.303}\right) \tag{10}$$

where

qt and qe (mg g^{-1}) are, respectively, the adsorption capacity at any time t and at equilibrium, and k_1 is the first-order reaction rate constant (min^{-1}).

Using the kinetic equations, the overall rate constant, the forward and backward rate constants were calculated at variable parameter concentration and temperature.

Pseudo Second Order Model

The pseudo 2nd order model can be represent in the following form

$$\frac{dq1}{dt} = K_2\left(q_e - q_t\right)^2 \tag{11}$$

where,

K_2 is pseudo second order rate constant (g/mg min).

After integrating the equation for boundary conditions qt = 0 at t = 0 and qt = qt at t = t, the following equation is obtained

$$\frac{t}{qt} = \left(1/K_2.\, q_e^2\right) + \left(1/q_e\right)t \tag{12}$$

The initial Sorption rate, h (mg/g min), at $t \longrightarrow 0$ is defined as:

$$h = K_2.\, q_e^2 \tag{13}$$

The initial sorption rate h (mg/g min) and pseudo second order constant K_2 can be calculated from the slope and intercept of plot t/qt versus t.

Intra-Particle Diffusion Model

Theoretical treatments of intra-particle diffusion yield complex mathematical relationships which differ in form as functions of the geometry of the sorbent particle. If the Weber-Morris plot of qt versus t satisfies the linear relationship with the experimental data, then the sorption process is found to be controlled by intra-particle diffusion only however, if the data exhibit multi-linear plots, then two or more steps determine the sorption process. The initial curved portion reflects the film or boundary layer diffusion effect, and the linear portion represents the intra-particle diffusion effect (Vijaykumar et al. 2012).

The intra-particle diffusion equation can be written as

$$q_t = K_{ipd} t^{1/2} + C \tag{14}$$

where q_t is the amount of Cr(VI) adsorbed onto the adsorbent at time t (mg/g), C is the intercept, a constant that gives idea about the thickness of the boundary layer and K_{ipd} is the intra-particle diffusion rate constant (mg g^{-1} min^{-1}).

Elovich Model

The Elovich or Roginsky–Zeldovich equation is generally expressed as follows:

$$\frac{dqt}{dt} = \alpha \exp\left(-\beta\, q_t\right) \tag{15}$$

where q_t is the amount of Cr(VI) sorbed at a time t, α is the initial Cr(VI) sorption rate [mmol/(g min)] and β is the desorption constant (g/mmol) during any one experiment.

To simplify the Elovich equation, Chien and Clayton (1980) assumed $\alpha\beta t \gg t$, and on applying the boundary conditions $qt = 0$ at $t = 0$ and $qt = qt$ at $t = t$ in Eq. (15)

$$q_t = \ln(\alpha\, \beta) + \ln t \tag{16}$$

Thus the constants can be found from the slope and intercept of the linear plot of q_t versus ln t.

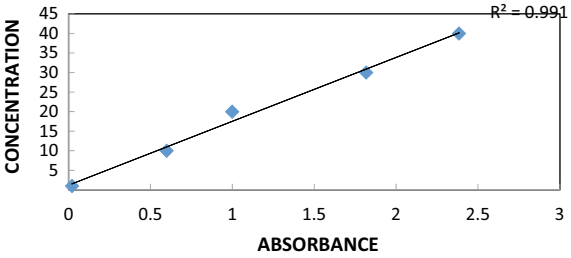

Fig. 3 Calibration of unknown chromium concentration in the water sample, Co = 1 mg/l– 40 mg/l, t = 27 °C, pH = 2

3 Results and Discussion

3.1 Calibration Curve

A calibration is a general method of determining the concentration of a substance in an unknown sample by comparing it with the known concentration having a set of standard sample (Fig. 3) shows the calibration of unknown chromium concentration in the water sample.

3.2 Analysis of Various Parametric Effects on the Adsorption of Chromium (VI)

3.2.1 Effect of Adsorbent Dose

Percentage removal of Cr(VI) from waste water was compared by varying the doses of different bio-adsorbent material (Fig. 4). It can be seen that the adsorption rate increases rapidly with increase in dose and this is due to availability of more surface

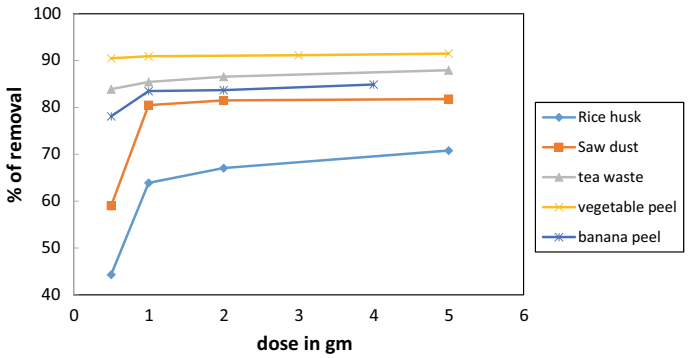

Fig. 4 Adsorbent doses versus % of removal

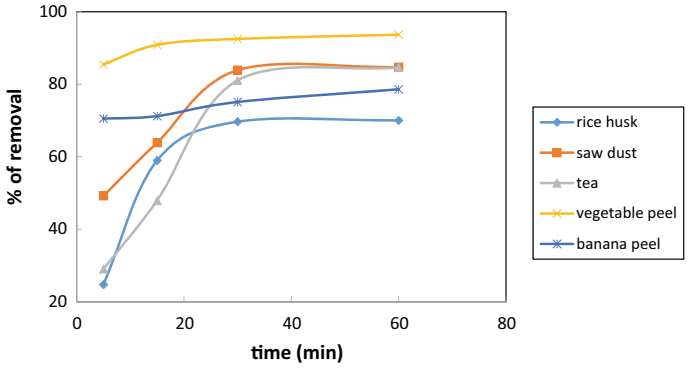

Fig. 5 Time versus % of removal of chromium

area and more adsorption functional sites. Concentration of rise husk was taken in the range of 0.5-7gm and percentage removal of Cr(VI) was found to be 67.06% at 2 gm. Concentration of saw dust, tea waste, banana peel, vegetable peel was taken in the range of 0.5-5gm and percentage removal of Cr(VI) was found to be 81.8%, 87.96%, 84.9% and 91.5% respectively. It was concluded that maximum percentage of chromium was removed using vegetable peels.

3.2.2 Effect of Contact Time

Percentage Removal of Cr(VI) from waste water was compared by varying the time of different bio-adsorbent material (Fig. 5). For rick husk saw dust, tea waste, banana peel, vegetable peel time was taken in the range of 5–60 min and percentage removal of Cr(VI) was found to be 70.02%, 84.7%,84.6%,78.6% and 93.67% at 60 min respectively. It was concluded that maximum percentage of chromium was removed using vegetable peels. A further increase in contact time over optimum contact time does not seem to have any significant impact on the equilibrium concentration.

3.2.3 Effect of pH

Percentage Removal of Cr(VI) from waste water was compared by varying the pH of different bio-adsorbent material (Fig. 6). pH of rise husk was taken in the range of 2–7 and percentage removal of Cr(VI) was found to be 71.7% at pH 7. pH of saw dust was taken in the range of 1–7 and percentage removal of Cr(VI) was found to be 85.4% at pH 2. pH of Tea waste was taken in the range of 2–9 and percentage removal of Cr(VI) was found to be 87.3% at pH 7. pH of banana peel and vegetable peel was taken in the range of 1 to 6 and percentage removal of Cr(VI) was found to be 84.3% at pH 2 and 92.8 at pH 4 respectively. It was again concluded that maximum percentage was found in vegetable peel.

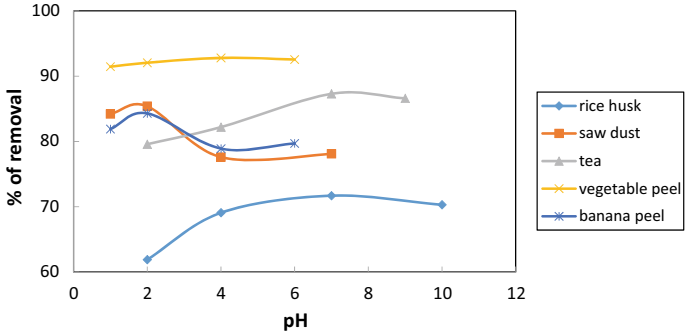

Fig. 6 pH versus % of removal of chromium

3.2.4 Effect of Initial Concentration

Percentage Removal of Cr(VI) from waste water was compared by varying the chromium concentration of different bio-adsorbent material (Fig. 7). It can be seen that the removal percentage decreases with increase in the initial concentration of Cr(VI) for rice husk and tea powder after a certain dose whereas it remained constant after a certain dose for saw dust, banana peel and vegetable peel. Chromium concentration for rice husk, saw dust, tea waste and banana peel was taken in the range of 5–50 mg/l and percentage removal of Cr(VI) was found to be 66.8%, 84.28%, 85.4% and 89.44% respectively. Chromium concentration of vegetable waste was taken in the range of 20–100 mg/l and percentage removal of Cr(VI) was found to be 98.7%. It was concluded that maximum percentage of chromium was removed using vegetable peels.

3.3 Adsorption Isotherm Study

Table 1 shows the physical and chemical properties of all the adsorbents chosen for

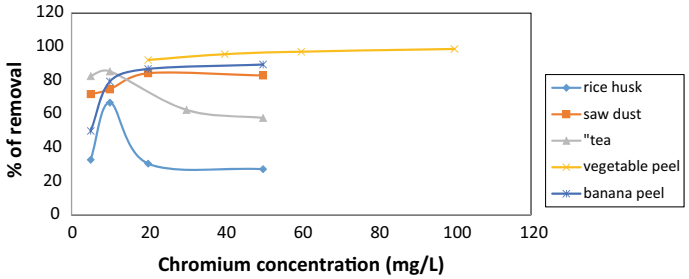

Fig. 7 Chromium concentration versus % of removal

Table 1 Physical and chemical properties of adsorbent

Properties	Rice husk	Saw dust	Tea waste	Banana peel	Vegetable peel
Particle size	599–853 μm	185 μm	149–297 μm	< 5 mm	60μ
Specific gravity	1.15	1.3	1.1	1.23	1.2
Bulk density	8.1	8.3	8.25	8.36	8.22
Dry density	5.7	5.9	5.42	5.47	5.82
Void ratio	0.78	0.776	0.794	0.775	0.793
Porosity	0.438	0.435	0.441	0.436	0.442
Surface area	512 cm^2/g	460 cm^2/g	495.54 cm^2/g	565.23 cm^2/g	549 cm^2/g
pH	6.43	6.49	6.35	6.54	6.7

Table 2 Langmuir adsorption isotherm

Langmuir model	Qm (mg/g)	b ($L\ g^{-1}$)	R^2	RL
Rice husk	1.18	1.48	0.903	0.063
Saw dust	0.98	2.23	0.981	0.021
Tea waste	1.67	1.23	0.895	0.016
Banana peel	0.4	4.5	0.822	0.021
Vegetable peel	0.2	5.2	0.896	0.009

Table 3 Freundlich adsorption isotherm

Freundlich model	Kf (L/mg)	n	R^2
Rice husk	0.62	3.448	0.935
Saw dust	0.435	1.68	0.906
Tea waste	0.23	1.293	0.994
Banana peel	0.58	1.5	0.957
Vegetable peel	0.26	0.46	0.939

the study. For the equilibrium study of the experimental work, three basic isotherm models were considered namely Langmuir, Freundlich and Temkin isotherm models. Isotherm constants of the models are summarized in Tables 2, 3 and 4.

3.3.1 Langmuir Isotherm

See Table 2.

3.3.2 Freundlich Isotherm

See Table 3.

3.3.3 Temkin Isotherm

See Table 4.

Compared with linearity by R^2 value for best fitting to adsorption isotherms is showed as,

- Rise husk and Tea waste—Freundlich isotherm > Langmuir isotherm > Temkin isotherm
- Saw dust—Langmuir isotherm > Freundlich isotherm > Tempkin isotherm
- Banana peel—Temkin isotherm > Freundlich isotherm > Langmuir isotherm
- Vegetable peel—Freundlich isotherm > Tempkin isotherm > Langmuir isotherm.

Higher value of Freundlich isotherm may indicate the predominance of multi-layer adsorption process over intra-molecular interactions among the adsorbed Cr(VI).Higher value of Langmuir isotherm may indicate the predominance of mono-layer adsorption process over intra-molecular interactions among the adsorbed Cr(VI).Higher value of Temkin isotherm may indicate the chemisorption process.

3.4 Adsorption Thermodynamics

See Table 5.

Table 4 Temkin adsorption isotherm

Adsorbant	Kt (L/mg)	bt (J/mol)	R^2
Rice husk	2.11	55.19	0.89
Saw dust	3.011	58.92	0.725
Tea waste	6.004	17.13	0.94
Banana peel	1.539	105.43	0.991
Vegetable peel	1.702	14.65	0.912

Table 5 Adsorption thermodynamics

Adsorbent	ΔG°(Kj/mol)
Rice husk	− 0.9778314
Saw dust	− 2.0003524
Tea waste	− 0.5163347
Banana peel	− 3.7514698
Vegetable peel	− 4.1120843

Table 6 Adsorption kinetic parameters

Adsorbent	qe(Exp) (mg/g)	qe(Cal) (mg/g)	k1	R^2	qe(Cal) (mg/g)	h (mg/g min)	k2	R^2
Rice husk	0.175	0.65	0.191	0.983	0.204	0.69	1.666	0.982
Saw dust	0.42	0.978	0.214	0.906	0.457	0.44	2.11	0.995
Tea waste	0.84	1.063	0.119	0.927	0.87	16.9	14.89	0.975
Banana peel	0.786	0.377	0.032	0.908	0.79	1.49	2.378	0.968
Vegetable peel	0.94	0.364	0.055	0.899	0.949	0.57	0.644	0.999

When ΔG° is negative, it indicated that adsorption process was spontaneous which necessarily represented the spontaneity of the Cr(VI) adsorption process by rice husk, saw dust, tea waste, banana peel, vegetable peel as an adsorbent.

3.5 Adsorption Kinetics

3.5.1 Pseudo-First Order Model and Pseudo-Second Order Model

Kinetic study of adsorption process is important as it gives an insight into the rate of adsorption process, which is helpful in finding out contact time required for adsorption to take place and also facilitates evaluation of reaction coefficients. To investigate the mechanism of adsorption kinetics of Cr(VI), two kinetic models, namely pseudo first-order and pseudo-second-order models were analyzed. The calculated kinetic parameters along with R^2 values for both the kinetic models are given in Table 6.

The qe, exp and the qe, cal values from the pseudo-second-order kinetic model are very close to each other. The calculated correlation coefficients are also closer to unity for pseudo-second-order kinetics than that for the pseudo first-order kinetic model.

3.5.2 Intra-Particle Diffusion Model

Intra-particle diffusion model for rice husk, saw dust, tea waste, banana peel and vegetable waste data are shown in Table 7.

It can be summarized that the correlation coefficient R^2 (0.952) of Banana peel is higher than other adsorbent but adsorption mechanism Kipd (0.105) in case of Tea waste found to be higher which is related to an improved bonding between Cr(VI) ions and the adsorbent Particles.

Table 7 Intra-particle diffusion model

Adsorbent	Kipd (mg g^{-1} min^{-1})	C	R^2
Rice husk	0.019	0.045	0.727
Saw dust	0.003	0.192	0.847
Tea waste	0.105	0.096	0.877
Banana peel	0.015	0.663	0.952
Vegetable peel	0.014	0.835	0.868

Table 8 Elovich model parameters

Adsorbent	α [mmol/(g min)]	β g/mmol	R^2
Rice husk	0.355	3.149	0.872
Saw dust	0.398	13.15	0.929
Tea waste	0.375	4.149	0.928
Banana peel	915.7×10^4	30.3	0.868
Vegetable peel	1318.1×10^4	30.3	0.957

3.5.3 Elovich Kinetics Model

Elovich model was used to explain Cr(VI) adsorption mechanism onto adsorbent. The two parameters (α and β) were calculated from the slope and intercept of the linear plot of qt versus ln(t) (Table 8).

It can be summarized that the correlation coefficient of vegetable peel was found to be 0.957 which was found to be higher among all the used adsorbent. From the Elovich equation calculation, the initial adsorption rate α is 1318.1×10^4 and desorption constant β is 30.3 of vegetable peel was found.

4 Conclusion

Removal of Cr(VI) from aqueous solutions by adsorption using food waste like rice husk, saw dust, tea waste, banana peel and vegetable waste was determined experimentally. The five different adsorbent prepared were characterized by multiple analysis and tests. From our survey it can be summarized that all of these adsorbents are quite promising as an effective material for removal of Cr(VI). Based open the experiment it can be calculated that by varying the pH, adsorbent dose, chromium concentration and contact time. The maximum percentage of removal of Cr(VI) for rice husk was obtained at pH 7, at 10 mg/l chromium concentration, at 2gm rice husk dose, and at 60 min and similarly maximum percentage removed for each parameter was 71.7%, 66.8%, 67.06% and 70.2% respectively. As pH is the most influencing parameter and at pH 7 as optimum value, adsorption for this

system took place in neither high acid medium nor high basic medium. Increase of chromium concentration and dose gave a consecutive higher value uptake capacity up to a certain period and then became constant. But, uptake capacity increased with increase in initial time. For saw dust, the maximum percentage of removal of Cr(VI) was obtained at pH 2, at 50 mg/l chromium concentration, at 2 gm saw dust dose, and at 60 min and similarly maximum percentage removed for each parameter was 85.4%, 84.9%, 81.5% and 84.7% respectively. Experiments for saw dust were done in high acidic medium and adsorption capacity rapidly increased with increase of chromium concentration up to a certain dose and then the concentration remained constant towards the end. For tea waste, the maximum percentage of removal of Cr(VI) was obtained at pH 7, at 10 mg/l chromium concentration, at 5gm tea waste dose, and at 60 min and similarly maximum percentage removed for each parameter was 87.3%, 85.4%, 87.9% and 81.6% respectively. Here, uptake capacity increased with increase in initial time and chromium concentration at basic medium of pH. For banana peels, the maximum percentage of removal of Cr(VI) was obtained at pH 2, at 50 mg/l chromium concentration, at 4gm banana peels waste dose, and at 60 min and similarly maximum percentage removed for each parameter was 84.3%, 89.44%, 84.9% and 78.26% respectively. At pH 2 being set as optimum value, adsorption for this system took place in highly acidic environment. The uptake capacity increased with increase in initial chromium concentration as well as time concentration. For vegetable peels waste, the maximum percentage of removal of Cr(VI) was obtained at pH 4, at 100 mg/l chromium concentration, at 5gm vegetable peels waste dose, and at 60 min and similarly maximum percentage removed for each parameter was 92.9%, 98.7%, 91.5% and 93.67% respectively. Experiments were done in acidic medium for vegetable peel waste and vegetable peel waste was found to be the most efficient in chromium removal among other four absorbent being taken as it removed maximum percentage chromium from synthetic waste water.

For best fitting to adsorption isotherms, the values were compared with linearity by R^2 value, which showed as, Freundlich isotherm > Langmuir isotherm > Temkin isotherm for rice husk, saw dust and tea waste, for banana peel Temkin isotherm > Freundlich isotherm > Langmuir isotherm and for vegetable peels Freundlich isotherm > Tempkin isotherm > Langmuir isotherm.

The kinetic of adsorption followed the pseudo second order kinetic model. Best fit to the pseudo-second order reaction kinetics indicated that both the concentration of adsorbate as well as adsorbent govern the Cr(VI) adsorption rate by bio-adsorbent. From the Elovich kinetics model the correlation coefficient, initial adsorption rate and the dispersion constant was found to be most favorable for vegetable waste. The value of adsorption mechanism demonstrate took a peak for banana peel in Intra-particle diffusion model. The experimental results of adsorption isotherm confirm that all adsorbents are spontaneous. Therefore, it can be proposed that all the five wastes (bio-sorbents) can be used as a low cost and highly efficient natural adsorbent for removal of chromium from industrial or any venomous waste water.

References

Ahn CK, Park D, Woo SH & Park JM (2009) Removal of cationic heavy metal from aqueous solution by activated carbon impregnated with anionic surfactants. J Hazard Mater 164(2-3):1130–1136

AIkpokpodion PE, Ipinmoroti RR and Omotoso SM (2010).Bisorption of Nickel (II) from aqueous solution using waste tea (Camella cinencis) materials. Am-Eurasian J Toxicol Sci 2(2):72–82

Attia HG (2012) A comparison between cooking tea-waste and commercial activated carbon for removal of chromium from artificial wastewater. J Eng Dev 16(1): 305–325

Babu BV (2008) Biomass pyrolysis: a state-of-the-art review. Biofuels, Bioproducts and Biorefining: Innovation for a sustainable economy 2(5):393–414

Barnes HL, Langmuir D (1978) *Geochemical prospecting handbook for metals and associated elements.* Annual Report AER77-06511 AO2, US National Science Foundation

Bhavsar K, Patel P (2012) Efficiency evaluation of tea waste for adsorption of hexavalent chromium from industrial effluent. Int J Sci Res (IJSR) (Impact Factor: 3.358)

Chien SH, & Clayton WR (1980) Application of Elovich equation to the kinetics of phosphate release and sorption in soils. Soil Sci Soc Am J 44(2):265–26

Hwang CL (1997) The use of rice husk ash in concrete. Waste materials used in concrete manufacturing. Chandra S (Ed)

Larous S, Meniai A-H (2012a) The use of sawdust as by product adsorbent of organic pollutant from wastewater: adsorption of phenol. Sci Direct Energy Procedia 18:905–914

Larous S, Meniai A-H (2012b) Removal of copper (ii) from aqueous solution by agricultural by-products sawdust. Sci Direct, Energy Procedia 915–923

Markovic R, Stevanovic J, Stevanovic Z, Bugarin M, Nedeljkovic D, Grujic A, Stajic-Trošic J (2011) Using the low-cost waste materials for heavy metals removal from the mine wastewater. Mater Trans 52(10):1849–1852

Matzat E, & Shiraki K (1974) Chromium. Handb Geochem 11(3):24(A)

Memon JR, Memon SQ, Bhanger MI, El-Turki A, Hallam KR, & Allen GC (2009) Banana peel: a green and economical sorbent for the selective removal of Cr (VI) from industrial wastewater. Colloids Surf, B: Biointerfaces 70(2):232–237

Olayinka KO, Adu T, & Alo BI (2007) Sorption of heavy metals from electroplating effluents by low-cost adsorbents II: Use of waste tea, coconut shell and coconut husk

Park D, Lim SR, Yun YS, Park JM (2008) Development of a new Cr(VI)-biosorbent from agricultural biowaste. Sci Direct Bioresour Technol 8810–8818

Rout PR, Bhunia P, & Dash RR (2014) Modeling isotherms, kinetics and understanding the mechanism of phosphate adsorption onto a solid waste: ground burnt patties. J Environ Chem Eng 2(3):1331–1342

Saritha B, & Sharmilaa G (2011) Treatability study of tannery effluent by using guargum with coagulants alum and Ferric Sulphate

Vijayakumar G, Tamilarasan R, & Dharmendirakumar M (2012) Adsorption, kinetic, equilibrium and thermodynamic studies on the removal of basic dye Rhodamine-B from aqueous solution by the use of natural adsorbent perlite. J Mater Environ Sci 3(1):157–170

Application of Bio-inspired Genetic Algorithm: A Case Study

S. N. Poojitha, Gagandeep Singh, and V. Jothiprakash

Abstract The paper presents the application of a bio-inspired evolutionary algorithm, a genetic algorithm (GA) for designing water distribution networks optimally. Six different models of GA are presented considering three different selection mechanisms, truncation, tournament and roulette wheel method, and their respective models with or without elitism operator. A real-life case study, the Gunsa water distribution network (GWD), in Silvassa city of Dadar and Nagar Haveli, the Union territory of India is considered for validating the developed models. On the application of the GA models to GWD, it is found that all the GA models are efficient in converging to an optimal cost. It is found that for all the models developed, the average optimal cost in 50 trials is found to have no much difference from the optimal cost. The computational results suggest that though the GA models are successful in reaching to the optimal cost they are less reliable considering the successful trials out of 50. From the analysis results, the study suggests for a more reliable model of GA with both solution precision and reliability, with more success rate.

Keywords Water distribution network · Optimization · Genetic algorithm · Gunsa water distribution network

1 Introduction

The maximum benefits with minimum cost spent is always an engineer's desire while designing any infrastructure, as the funds raised always fall scarce. This is where the design engineers use optimization techniques for optimally designing the infrastructures. The water distribution network (WDN) is an important water infrastructure. Its design and maintenance always involve a substantial investment. The traditional way of designing WDNs is based on engineer experience. At present, a vast literature is available considering a wide range of optimization techniques for

S. N. Poojitha · G. Singh · V. Jothiprakash (✉)
Department of Civil Engineering, Indian Institute of Technology Bombay, Powai, Mumbai, Maharashtra 400076, India
e-mail: vprakash@iitb.ac.in

B. B. Das et al. (eds.), *Recent Developments in Sustainable Infrastructure (ICRDSI-2020)—GEO-TRA-ENV-WRM*, Lecture Notes in Civil Engineering 207,
https://doi.org/10.1007/978-981-16-7509-6_60

WDN optimal design (for example Simpson et al. 1994; Vairavamoorthy and Ali 2000; Reca and Martinez 2006; Zheng et al. 2011; Ali et al. 2018, to name a few).

The design of WDN is in general the toughest task as has a complex structure with different design components and involves non-linear design equations. The WDN design problem is a familiar non- deterministic polynomial hard problem (Yates et al. 1984). Application of various metaheuristic optimization techniques and modification of existing ones for optimally designing WDNS is active research. Various optimization techniques have been formulated for their designs (Vairavamoorthy and Ali 2000; Geem 2006; Suribabu 2010; Ezzeldin et al., 2014; Zheng et al. 2014; Sheikholeslami et al. 2016; Fallah et al. 2019; Poojitha et al. 2020; and many more). In the present study, a widely studied, bio-inspired, evolutionary algorithm GA is considered.

Various GA models are proposed in the literature, for the optimal design of WDNs (Simpson et al. (1994); Vairavamoorthy and Ali (2000); Wu and Simpson 2001; Johns et al. 2014; Poojitha et al. 2020 to name a few). In the present study, different GA models are formulated considering three selection mechanisms alongside with or without elitism operator. To check the efficiency of the formulated models, they are applied to a real-life case study, Gunsa water distribution network (GWD). The structure of the paper is as follows. Initially, the methods and methodology adopted in the present study are discussed. Secondly, the details of the GWD are presented. Following this, thirdly, the results and discussions are presented. And finally, the highlights of the present study are discussed in the conclusions section.

2 Methods and Methodology

2.1 Methods

Genetic algorithm (GA) is a search based optimization technique, well explored in diverse engineering fields due to its versatility, adaptability, and ease in computations. In GA, over evolution, the search through the search space is governed by the natural heuristics, genetic inheritance (Goldberg and Kuo 1989). Unlike the conventional optimization techniques, in GA the search is with the population set in multiple directions, rather than a single population that follows ascending or descending gradients. The entire structure of GA is made with three simple and easy-to-computations operators, selection, crossover, and mutation. The selection mechanism is inclined to the fittest solutions, where the crossover operator generates the offsprings by exchanging the genes of the parent chromosomes. The mutation operator is the unary operator, where the genes are flipped based on the mutation probability (see Poojitha et al. 2020 for complete details of these six GA models).

In the present study, a simple real-coded GA with a single-point crossover, and a bit-wise mutation operator is used. Three different types of selection mechanisms, truncation, tournament, and roulette wheel method are considered. The respective

three models formulated are combined with the elitism operator to form three more elitist models. In total, six models, GA1 (with truncation method of selection), GA2 (with tournament method of selection), GA3 (with roulette wheel method of selection), EGA1 (elitist GA1), EGA2 (elitist GA2), and EGA3 (elitist GA3). The elitism operator helps in retaining the fittest solution without being distorted through the GA evolution process.

2.2 Methodology

WDN design is generally considered as the least cost, optimal design problem, where the design variables are the network pipes (see Savic and walters 1997; Vairavamoorthy and Ali (2000); ; Wu and Simpson 2001). The decision variable is the cost of the network, which depends on the length and diameter of the pipes. Though optimally designing the layout and pipe diameters of WDNs influences the later operation cost, the general practice is to consider only the design of pipe diameters. This is because the layout of the network strictly depends on the location's topological factors and the road network (Savic and Walters 1997). Therefore, in the present study, assuming that all the necessary data like the layout of the network, details of commercially available diameters, minimum pressure constraints are known, an optimization algorithm is used to choose the optimal set of diameters for the WDN. Since the optimization algorithm doesn't involve any cross verification of the operating conditions for a provided diameter set, in the present study, EPANET software (Rossman 2000) is used as a simulation model. Both the optimization algorithm and simulation model are combined using the MATLAB-EPANET toolkit. Thus, the optimization-simulation framework is used for optimally designing the WDN case study.

3 Case Study Considered, Gunsa Water Distribution Network

Gunsa water distribution network (GWN) is a branched network with 34 links and 35 nodes. GWN has a single reservoir. Initially, the head of the reservoir is taken as 124.57 m. But, while simulating the GWN using EPANET simulation model, the reservoir head considered is insufficient to fulfill all the design requirements. Therefore, the reservoir head is reconsidered to be 130 m. The layout of the GWN is shown in Fig. 1. The data on demand required at demand nodes, and link data is taken from the municipal corporation of Gunsa, Silvassa, Dadar and Nagar Haveli, Union territory, India (all these data is not presented here).

While designing the GWN, three design constraints are considered. They are (i) minimum nodal head requirement at the demand nodes, (ii) minimum head loss

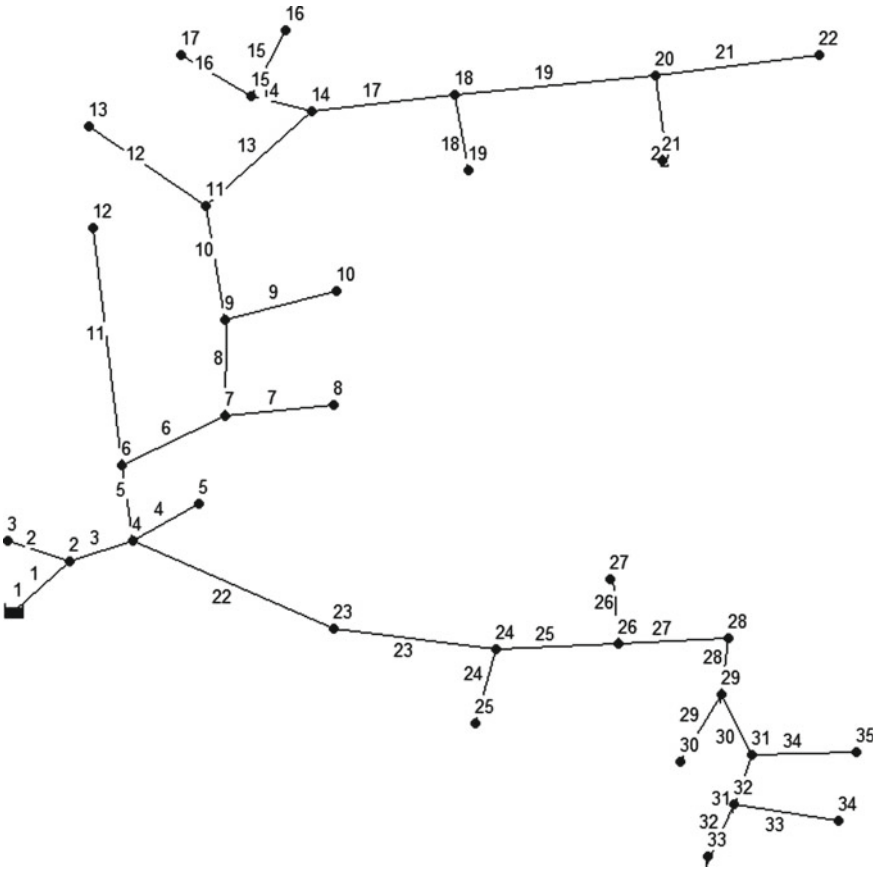

Fig. 1 Layout of Gunsa water distribution network

across each pipeline (m/km), (iii) maximum head loss across each pipeline (m/km). The head loss formula used in this study is the Hazen-Williams equation, and the Hazen-Williams constant considered is 140 for all the links of GWN. Table 1 entails the details of commercially available pipe diameters for the optimal design of the GWN. They are in total 12, and so each link of the GWN has 12 options each, making up a solution space 12^{34}.

Table 1 Details of commercially available diameters

Dia. (mm)	H-W Constant	Cost (Rs./m)
42.6	140	70
53.6	140	111
68.8	140	157
77.6	140	225
95	140	332
108	140	428
121	140	536
138.4	140	699
155.8	140	887
173.2	140	1093
194.8	140	1380
216.6	140	1700

4 Results and Discussions

4.1 Sensitivity Analysis Results

The GA parameters that need to be optimally chosen include population size, crossover, and mutation probability, generation size, and the penalty factor. The sensitivity analysis is performed for choosing the best values for these parameters. The guidelines given by Simpson et al. (1994) are followed to fix the ranges of these parameters. As there are three penalties levied, three penalty factors are considered. From the sensitivity analysis results, the population size is fixed as 100 and generation size as 800, for all the GA variants. The crossover, and mutation probability, and the penalty factors that are fixed through the sensitivity analysis are enclosed in Table 2

Table 2 Sensitivity analysis results

Methods	p_m	p_c	PM1	PM2	PM3
GA1	0.02	0.96	140,000	180,000	180,000
GA1E	0.02	0.96	140,000	180,000	180,000
GA2	0.02	0.96	140,000	180,000	180,000
GA2E	0.02	0.96	140,000	180,000	180,000
GA3	0.02	0.96	140,000	180,000	180,000
GA3E	0.02	0.96	140,000	180,000	180,000

4.2 Results of GA Models

Each GA model is optimized 50 times for 800 generations. It is interesting to note that all the GA variants are successful in converging to a minimum design cost of Rs. 1,710,215, at least once in 50 trials. This solution fulfills all the hydraulic constraints of the network. With the reservoir head of 124.57 m, the minimum cost, optimal solution obtained is Rs. 2,148,010. However, it is found to be infeasible. Thus, an increase in the reservoir head by 5.43 m saves Rs. 437,795 on the network cost and at the same time all the hydraulic requirements of the network are fulfilled. The optimal diameter set obtained for GWN using all the GA variants is provided in Table 3. The nodal head values corresponding to this optimal solution are presented in Table 3.

The computational results in terms of functional evaluation, the number of successful trials, the percentage of solution space explored before convergence, alongside the other important details are presented in Table 4. Of all the GA variants, GA3 converged to the optimal solution with lesser functional evaluations of 10,800 followed by EGA3 (17,300) and EGA1 (28,800). It is observed that EGA1 and EGA2 models achieved the optimal solution more times as compared to GA1 and GA2 models respectively. EGA2 and EGA3 achieved better average solution as compared to GA2 and GA3 respectively. Only EGA1 shows better performance in terms of both the average cost and probability of getting the optimal solution as compared to the GA1 model. And for all the models, the percentage of solution space explored for convergence to the optimal solution is very less as compared to the total solution space available (12^{34}) (see Table 4).

5 Conclusions

In the present study, six different models of GA are formulated considering different selection mechanisms, and incorporating an additional operator, an Elitism operation. On validating these models by applying it to the real-life case study, it is observed that all the GA models are efficient in converging to an optimal cost of Rs. 1,710,215. It is observed that although the models are successful in converging to the optimal cost, they are less reliable as out of the 50 trials conducted for each trial, the maximum successful trials are 7 (GA3). Though the deviation of average optimal cost from the optimal cost is less as compared to the other models, the most reliable model is always welcoming, when we deal with the large distribution networks. Therefore, the present study suggests for more reliable models that not only succeed in maintaining the solution precision but also, is reliable in converging to the optimal solution with more success rate.

Table 3 Optimal diameter set and nodal heads corresponding to the optimal solution for Gunsa water distribution network obtained using GA variants

Link	Length (m)	Dia (mm) (for all GA variants)	Node number	Pressure head (m)
1	30	138.4	2	25.34
2	50	42.6	3	26.83
3	55	138.4	4	44.11
4	100	53.6	5	27.28
5	155	108	6	41.42
6	275	95	7	35.77
7	85	42.6	8	30.82
8	350	108	9	37.30
9	250	68.8	10	16.16
10	245	95	11	37.35
11	810	42.6	12	44.68
12	285	53.6	13	42.78
13	670	77.6	14	29.44
14	85	53.6	15	29.86
15	30	42.6	16	29.72
16	95	42.6	17	29.85
17	65	95	18	26.86
18	130	53.6	19	7.52
19	325	68.8	20	15.87
20	60	53.6	21	10.00
21	590	42.6	22	5.70
22	925	95	23	37.92
23	715	95	24	21.55
24	420	42.6	25	29.34
25	180	95	26	23.18
26	25	53.6	27	23.08
27	305	77.6	28	15.17
28	280	53.6	29	18.48
29	80	42.6	30	20.85
30	295	53.6	31	28.43
31	140	53.6	32	25.20
32	40	42.6	33	23.24
33	85	42.6	34	17.15
34	160	42.6	35	9.77
	Cost (Rs.)	**1,710,215**		

Table 4 Computational results of GA variants

Methods	Gen. No	Aveg. Gen	Minimum functional evaluations	Optimal solution	Average solution	% by which avg. sol. is higher than optimal	%age of the solution space explored ($\times 10^{-33}$)	Successful trials out of 50
GA1	234	562	23,400	1,710,215	1,751,337	0.024	4.75394	3
EGA1	288	250	28,800	1,710,215	1,721,583	0.007	5.851	4
GA2	508	588	50,800	1,710,215	1,715,842	0.003	1.03205	2
EGA2	622	574	62,200	1,710,215	1,720,429	0.006	1.26365	3
GA3	108	201	10,800	1,710,215	1,725,392	0.009	2.19413	7
EGA3	173	226	17,300	1,710,215	1,724,110	0.008	3.51466	2

References

Ali MZ, Awad NH, Suganthan PN, Shatnawi AM (2018) An improved class of real-coded genetic algorithms for numerical optimization. Neurocomputing 275(2018):155–166

Ezzeldin R, Djebedjian B, Saafan T (2014) Integer discrete particle swarm optimization of water distribution networks. J Pipeline Syst Eng Pract 5(1):04013013

Fallah H, Kisi O, Kim S, Rezaie-Balf M (2019) A new optimization approach for the least-cost design of water distribution networks: an improved crow search algorithm. Water Resour Manage 33:3595–3613

Geem ZW (2006) Optimal cost design of water distribution networks using harmony search. Eng Optim 38(3):259–277

Goldberg DE, Kuo CH (1989) Genetic algorithms in pipeline optimization. J Comput Civ Eng 1(2):128–141

Johns MB, Keedwell E, Savic D (2014) Adaptive locally constrained genetic algorithm for least-cost water distribution network design. J Hydroinf 16(2):288–301

Poojitha SN, Singh G, Jothiprakash V (2020) Improving the optimal solution of Goyang network—using genetic algorithm and differential evolution. Water Supply 20(1):95–102

Reca J, Martinez J (2006) Genetic algorithms for the design of looped irrigation water distribution networks. Water Resour Res 42(5):W05416

Rossman LA (2000) "EPANET 2 Users Manual." US Environmental Protection Agency, Washington, DC, USA, EPA/600/R-00/057

Savic DA, Walters GA (1997) Genetic algorithms for least-cost design of water distribution networks. J Water Resour Plan Manag 123(2):67–77

Sheikholeslami R, Zecchin AC, Zheng F (2016) A hybrid cuckoo-harmony search algorithm for optimal design of water distribution systems. J Hydroinf 18(3):544–563

Simpson AR, Dandy GC, Murphy LJ (1994) Genetic algorithms compared to other techniques for pipe optimization. J Water Resour Plan Manag 120(4):423–443

Suribabu C (2010) Differential evolution algorithm for optimal design of water distribution networks. J Hydroinformatics 12(1): 66–82

Vairavamoorthy K, Ali M (2000) Optimal design of water distribution systems using genetic algorithms. Computer-Aided Civil Infrastruct Eng 15(5):374–382

Wu ZY, Simpson AR (2001) Competent genetic-evolutionary optimization of water distribution systems. J Comput Civ Eng 15(2):89–101

Yates DF, Templeman AB, Boffey TB (1984) The computational complexity of the problem of determining least capital cost designs for water supply networks. Eng Optim 7(2):143–155

Zheng F, Simpson AR, Zecchin AC (2011) A combined NLP-differential evolution algorithm approach for the optimization of looped water distribution systems. Water Resour Res 47:1–18
Zheng F, Simpson AR, Zecchin AC (2014) Coupled binary linear programming-differential evolution algorithm approach for water distribution system optimization. J Water Resour Plan Manag 140(5):585–597

Reduction of Sub Base Layer Using Bio-enzyme Treated Soil

R. Pradhan, T. Shil, S. Nanda, and B. G. Mohapatra

Abstract The performance of the various pavement layers relies very much on the strength characteristic of the subgrade soil. The Indian Road Congress (IRC) covers the precision of pavement layer construction strategies dependent on the subgrade strength that depends mainly on the CBR value for a laboratory or field specimen. The bio-enzyme is used to catalyze soil reactions, which is a different substance from the conventionally used road materials. Bio-Enzyme is a non-toxic, non-flammable, non-corrosive formulation of fluid enzymes fermented with extracts of vegetables that improve soil engineering capabilities. This present study provides an effective technique to reduce the thickness of the Sub Base layer in road construction. In this research, natural soil is mixed with three dosages of Terrazyme. The treated soils were characterized after seven and twenty-eight days of curing. The test results show that CBR value drastically changed with Bio-Enzyme, which reduces the thickness of the Sub Base layer in Flexible pavement.

Keywords CBR · Bio-enzyme · Soil stabilization · IRC

1 Introduction

The roads of India are a mixture of modern Highways, narrow and unpaved in rural areas and need to be strengthened to cater the ever growing traffic. A large part of soils in India consists of high silt and clay contents, low shear strength and bearing capacity. The quality of soil in subgrade layer affects the performance of the flexible pavement. Soils with inadequate bearing capacity are a challenge for construction Engineers. Continuous research has been carried out on various additives and stabilizers to improve the weak soil and reduce the excavation and hauling costs. Chemical

R. Pradhan · T. Shil · S. Nanda (✉) · B. G. Mohapatra
Bhubaneswar, India
e-mail: satyajeet.nandafce@kiit.ac.in

B. G. Mohapatra
e-mail: dean.civil@kiit.ac.in

B. B. Das et al. (eds.), *Recent Developments in Sustainable Infrastructure (ICRDSI-2020)—GEO-TRA-ENV-WRM*, Lecture Notes in Civil Engineering 207,
https://doi.org/10.1007/978-981-16-7509-6_61

Additives, both inorganic and organic, have also been used extensively to stabilize the soils to improve the strength and durability of the subgrade.

In soil stabilization, the properties of natural soil are enhanced by means of chemical or mechanical processes. The purpose of stabilization is to increase the load bearing capacity by increasing shear strength parameters, improve permeability and resistance to weathering due to traffic usage (Sherwood and Ryley 1966). Soil stabilization can be achieved in several ways like lime stabilization, asphalt stabilization, stabilization of fly ash, rice husk ash stabilization, bitumen stabilization, thermal stabilization, electric geo-Textile stabilization, and cloth stabilization, recycling and waste materials, and thermal stabilization. The traditionally used stabilizers like hydrated lime, Portland cement and bitumen are becoming costly and can produce shrinkage and cracking (Akinwumi 2015; Choudalakis 2009). Fly ash is also a good source for soil stabilization, but it is not practically applicable when the distance between the source of fly ash and the construction site is considerable.

Furthermore, the stabilizers mentioned above is of dry form; therefore, it requires proper mixing to archive the design strength. Contrary to the above mentioned stabilization agents, Bio-Enzymes based stabilization agents available in liquid form can be applied to the water used for soil compaction. It is also cost effective and safe to use in all construction environments. In literature, various studies have been reported (Gayatri and Shyla 2016; Saini and Vaishnava 2015; Shankar et al. 2009); however, these studies are inconclusive and there is a greater need for independent and neutral research (Kestler 2009).

Recently, a product market named "Terrazyme" was widely used to improve engineering properties of clayey soil consist of low to the medium liquid limit. Terrazyme is a Bio-Enzymes based liquid additive. The present research aims to study the change in strength characteristic of clayey soil by means of CBR value when treated with bio-enzymatic (Terrazyme) compound. The research also extended to determine the usability of Bio- enzyme-treated soil in road pavement construction. The methodology includes extensive laboratory experimentation.

2 Bio-enzyme Soil Stabilization

Clay particles consist of very small size particles (Less than 2η), large Specific surface and possess a significant amount of Cations exchange capabilities (Mitchell and Soga 2005). These properties of clay particles make them negatively charged particles and react with the dipolar water molecule. A thick water double layer formed around the clay particles, which consequently make the clay soil more compressible and weak in shear strength properties (Mitchell and Soga 2005). If the thickness of these double-layer water gets reduced by some means, then the compressibility of clay soil shall be reduced and the shear strength of soil may increase.

Enzymes are organic molecules that catalyze a particular chemical reaction if the condition is conducive to the response. They are used at low concentrations because the reaction does not consume them. Terazyme is a cation reactive synthetic

compound and it forms a protective layer on the surface of the soil which changes the hydrophobic nature to hydrophilic by eliminating the adsorption water layer. The treated material is less sensitive to water and easily compacted for better interlocking, thereby increasing internal friction, which improves soil bearing capacity.

Tingle and Newman (2007) conducted laboratory Experiments, including Image Analysis, physical and chemical analysis and revealed that, Enzyme catalyzed very specific reactions and it is difficult to establish a general stabilization Mechanism due to variations in particular soil reactions. Several experiments were conducted to investigate the effect of Bio Enzyme on the soil strength and reported that there is an increase in strength of fine grained soil and rate of improvement was proportional to clay content and significant improvement in unconfined strength and California Bearing ratio (CBR). AbouKhadra et al. (2018) conducted an experiment to investigate the effect of Bio Enzyme and found significant improvement in CBR and UCS in Bio Enzyme stabilized soil. Panchal (2017) conducted experiments with different dosages of Terazyme and found that CBR value was increased about 131.49% after two weeks curing period for the optimum dose of 900 ml per one cubic meter of soil. Table 1 shows the change in CBR value with the treatment of the Bio-Enzyme as reported in the literature. As it can be seen from Table 1 that there is nonuniformity in the calculation of doses. Furthermore, the observation reported by Gayatri and Shyla (2016) and Shankar et al. (2009) indicates a very significant increase in the CBR value, whereas Saini and Vaishnava (2015) did not find much increase in the CBR value. The observation reported in Table 1 is not very conclusive. However, it can be seen that the Bio Enzyme treated soil is sensitive to the doses and soil types.

Table 1 Percentage change CBR value with bio-enzyme treated soil

Author name	Type of soil	Dosage	CBR value of natural soil (%)	CBR value of bio-enzyme treated soil (%)
Gayatri and Shyla (2016)	Silty clay (CH-MH)	200 ml/3 m^3	1.49	8.18
Saini and Vaishnava (2015)	Clayey silt (CM)	3.0 m^3/200 ml	27.0	20.87
		2.5 m^3/200 ml		30.21
		2 m^3/200 ml		30.9
		1.5 m^3/200 ml		30.07
Shankar et al. (2009)	Lateritic soil	0.029 ml/kg	10	23
		0.0338 ml/kg		27
		0.0406 ml/kg		29
		0.050 ml/kg		31

Table 2 Summary of index properties of natural soil

S. No.	Physical property	Natural soil
1	Specific gravity	2.58
2	Soil classification	CI
3	Consistency limits	
	Liquid limit	35.5%
	Plastic index	16.5%
	Shrinkage limit	16.5%
4	Free swell index	21%
5	Optimum moisture content	15.78%
6	Maximum dry density	18.10 kN/m^3
7	Unconfined compressive strength	270 kN/m^2
8	California bearing ratio (soaked)	2.48

3 Materials and Methods

3.1 Collection of Materials

The soil used for this research was obtained from Nayagarh, Odisha (20.1654° N, 85.0233° E). Soil was transported to the Laboratory of the School of Civil Engineering, KIIT University, and kept in for air drying. Various laboratory tests were conducted to determine various index and strength parameters. These tests were conducted as per the IS 2720. The sieve analysis suggests the soil contains more than 60% of fine particles, out of which 45% of clay content. The soil is classified as CI and its liquid limits and plasticity index are 35.5 and 16.5, respectively. The soil used in this investigation is the same soil used in Shil et al. (2020). More detailed information about the soil characterization can be found in Shil et al. (2020). A summary of soil properties is given in Table 2.

Avijeet Agency Chennai supplied the Bio Enzyme used in this research. The trade name of this Bio Enzyme is Terazyme. The Bio Enzyme comes with a highly concentrated liquid form; therefore, it must be diluted with the water before use. It can store at normal room temperature and poses no harm to the environment.

3.2 Sample Preparation

The Bio Enzyme is diluted with the distilled water at the supplier's recommended Diluted Mass ratio of 1:1000. The Oven-dried soil mixed with diluted Enzyme treated with four dosages of Bio Enzyme at Optimum Moisture content of 15.78% and kept in tight polythene bags for 16 h mellowing period for intimate mixing. Sample were prepared in CBR moulds by standard proctor method and kept covering with Plastic

bags for testing in 7 days and 28 days Curing periods. The Plastic bags is cover with a wet jute bag to reduce the evaporation loss of moisture from the soil sample—Fig. 1 shown a photograph of just before the curing. After the curing period, the samples were soaked in a water tank for 96 h and then Tested for CBR at seven days and 28 days Curing.

Several CBR samples were prepared at various doses of Bio Enzyme. The idea was to perform several tests to understand the effect of Bio-enzyme on soil's CBR value and the optimum amount of Bio-enzyme for this particular soil. Details on the various doses used in this research are given in Table 3. Three different doses (5, 7. 5 and 10 m^3/l) of Bio-enzyme are used in this investigation. A total of eight sets of CBR tests were performed under shocking conditions after the curing period of 7 and 28 days. In each set of CBR test total, three number of sample was tested.

Fig. 1 CBR sample preparation

Table 3 Mix proportion of diluted bio-enzyme mixed with soil

Mix design	Dosage (m^3/l)	Dilution ratio	Amount of concentrated bio-enzyme (ml)	Amount of diluted bio-enzyme (ml)
Dosage 1	5	1:1000	0.109	109.23
Dosage 2	7.5	1:1000	0.073	72.82
Dosage 3	10	1:1000	0.055	54.61

4 Results and Discussions

Table 4 shown the shocked CBR test result after a quiring period of seven and twenty-eight days. The CBR test was conducted as per the recommendation given in IS 2720 (Part 16). The seven days and twenty days quiring period is adopted in this research as these curing days have been extensively used to study lime or cement-based stabilisation. Although Bio-Enzyme works completely differently from the lime or cement-based stabilisation, for a shake of comparison with other stabilisation agents, seven days and twenty days quiring period has been adopted. From Table 4, it can be clearly seen that the CBR value increased with the addition of Bio-Enzyme. The highest increased in CBR value was observed after 28 days and the increase is about 2.8 times the CBR value of untreated soil.

Figure 2 shown the CBR values observed after 7 and 28 days of curing. For untreated soil, there is a marginal increase in the CBR value after 28 days of curing. This is expected as any alteration in particles position or any strength gaining is a

Table 4 Comparison of CBR (soaked) test values at 7 and 28 days

Dosage	7 days curing	28 days curing
Natural soil	2.48	2.69
Soil + 5 m^3/l enzyme	2.69	7.02
Soil + 7.5 m^3/l enzyme	5.55	7.79
Soil + 10 m^3/l enzyme	3.47	6.07

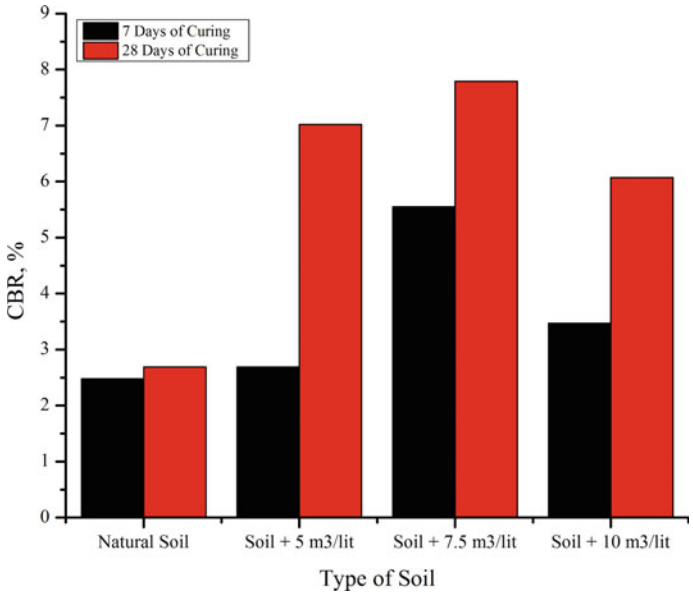

Fig. 2 CBR values at 7 and 28 days

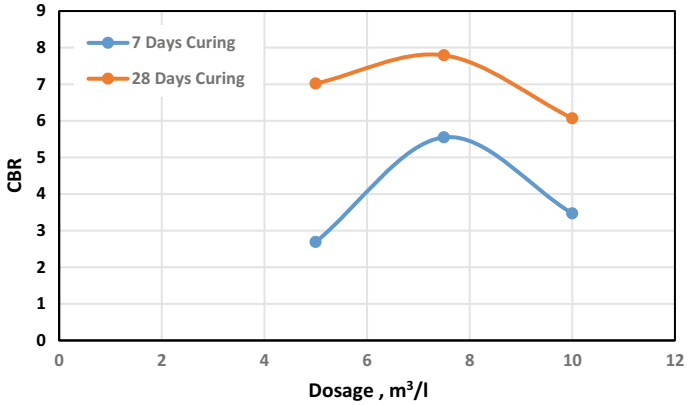

Fig. 3 Variation of CBR with dosage

prolonged process. In the Bio-Enzyme treated soil, a significant increase in CBR value increased in days of curing. The observation from Fig. 2 suggested that the elimination of observed water from the clay particles is not an instant process; rather, it can continue for months. The percentage increased between 7 and 28 days of curing is in the range or 40–160%. The highest percentage of increased CBR value between 7 and 28 days is 160% observed at a dose of 5 m^3/l.

Figure 3 shown variation in CBR value with the dosage of Bio-Enzyme. In Fig. 3, the x-axis represents Bio-Enzyme dosages in m^3/l and the the y-axis is the CBR value. Both 7 days and 28 days CBR test results are shown in Fig. 3. CBR value increased with the increase in the dosage of Bio-Enzyme up to a certain dose and after that, further increase in the dosage of Bio-Enzyme reduces the CBR value. The optimum dosage for both 7 and 28 days of curing is 7.5 m^3/l. A similar trend was also reported by Baby et al. (2016).

From Table 4 and Figures 2 and 3 it can be concluded that the Bio-Enzyme enhances the soil CBR value. This signifies that the addition of Bio-Enzyme effectively eliminates the absorbed water for the clay particles. Higher dosages of Bio-Enzyme may generate more free water, which consequently reduces the shearing strength of the soil. The Bio-Enzyme treated soil sensitive to the dosage and clay mineral types, as different clay minerals developed different thickness of absorbed water double layer. The increase in CBR value with the Bio-Enzyme treated soil is not as high as observed in other commonly used stabilizers like cement and lime. Still, it has other benefits, like the Bio-Enzyme treated soil is not so brittle as cement or lime treated soil. Also, Bio-Enzyme treated soil eliminates the possibility of shrinkage crack, which is very apparent in the case of cement or lime treated soil.

Table5 Comparison of thickness of pavement

S. No.	Type of soil	CBR value at 28 days curing period	Thickness as of pavement per IRC for 150–450 CVPD and tyre pressure 6 kg/cm^2 and wheel load 4100 kg	Thickness of pavement as per formulae developed by US crop of engineers for 150–450 CVPD and Tyre pressure 6 kg/cm^2 $t = \sqrt{P}\left[\frac{1.75}{\text{CBR}} - \frac{1}{p\pi}\right]^{1/2}$
1	Untreated soil	2.69	53.10 cm	49.50 cm
2	Treated with optimum dose of Terazyme	7.79	28.90 cm	26.52 cm
		189.59% increment	44% reduction	39% reduction

5 Utilization

To assess the usability of this research a flexible pavement analysis on a low volume road was performed using the method recommended by IRC and US Crop of Engineers. The tire pressure and wheel load are considered 6 kg/cm^2 and 4100 kg, respectively. Table 5 shows the details of pavement analysis. Around 40–44% of the reduction in subbase thickness can be achieved using Bio-Enzyme treated soil. The research suggests a substantial reduction in pavement thickness can be possible using Bio-Enzyme treated soil. Therefore the Bio-Enzyme may consider as a stabilizing agent for a road construction project.

6 Conclusion

A laboratory investigation and pavement analysis were performed to study the utilization of a Bio-Enzyme treated soil. From this research following conclusions can be drawn.

1. Bio-Enzyme treated soil shown an increase in the CBR value of about 2.8 times that of untreated soil.
2. Bio-Enzyme treated soil is dosage sensitive.
3. The curing period significantly influences the rate of increase in CBR value.
4. Using Bio-Enzyme treated soil about 39–44% reduction in the sub-base layer thickness can be achieved.

References

AbouKhadra A, Zidan AF, Gaber Y (2018) Experimental evaluation of strength characteristics of different Egyptian soils using enzymatic stabilizers. Cogent Eng 5(1):1517577. https://doi.org/10.1080/23311916.2018.1517577

Akinwumi AO II (2015) Effect of corncob ash on the geotechnical properties of lateritic soil stabilized with Portland cement. Int J Geomat Geosci 5(3):375–392

Baby M, Gowshik A, Karthick Rajeshwar AV, Mohanasundram M (2016) Experimental study of expansive soil stabilized with TerraZyme. Int J Eng Res Technol 5:897–899

Choudalakis GA (2009) Permeability of polymer/clay nanocomposites: a review. Eur Polym J 45(4): 967–984

Gayatri SN, Shyla AJ (2016) Effect of bio enzyme and geotextile on strength characteristics of sub grade soil. Int Res J Eng Technol 03:1891–1897

Kestler M (2009) Stabilization selection guide for aggregate and native-surfaced low volume roads. Forest Service, SanDimas Technology and Development Center, USA

Mitchell JK, Soga K (2005) Fundamentals of soil behavior, 3rd edn. Wiley

Panchal S (2017) Stabilization of soil using bio-enzyme. Int J Civ Eng Technol (IJCIET), 234–237

Saini V, Vaishnava P (2015) Soil stabilization by using terrazyme. Int J Adv Eng Technol 8(4):566

Shankar AU, Rai HK, Mithanthaya R (2009) Bio-enzyme stabilized lateritic soil as a highway material. Indian Roads Congr J 70(2)

Sherwood PT, Ryley MD (1966) The use of stabilized pulverized fuel ash in road construction. RRL report no. 49. Road Research Laboratory

Shil T, Pradhan R, Nanda S, Mohapatra BG (2020) Strengthening of soil subgrade using bio-enzyme. Rec Dev Sustain Infrastruct 13–25

Tingle JS, Newman JK (2007) Stabilization mechanisms of nontraditional additives. J Transp Res Board 2:59–67 (Transportation Research Board of the National Academies, Washington DC, 1989)

Behaviour of Surface Footing Resting on Reinforced Layered Soil

Bandita Paikaray, Benus Gopal Mohapatra, Sushree Barsha, and Apala Mohanty

Abstract The work presented here includes laboratory model testing on surface footing placed on sand overlying crusher dust—a two layer system of soil. The experimental work has been conducted on unreinforced and geosynthetic reinforced soil at loose and medium dense state condition. The reinforcement has been used at interface to find its effect on bearing capacity compared to unreinforced state of soil. For loose state, a relative density of 35% has been chosen and for medium dense state, a relative density of 67% has been taken for both sand and crusher dust. The effect of relative density, effect of reinforcement layer on bearing capacity of surface footing has been studied.

Keywords Model testing · Surface footing · Relative density · Crusher dust · Geosynthetic reinforcement · Bearing capacity

1 Introduction

In day today life, huge amount of waste materials are produced due to rapid industrialization. They are the main cause for environment pollution causing health hazards to a great extend. By utilizing these wastes such as red mud, fly ash, stone dust and marble dust in bulk below foundation, in embankment and in pavement construction, their adverse effect can be minimized. Crusher dust being an industrial waste produced hugely from construction site is used as a foundation material for the present study. Many research work has been conducted on sand as a foundation material to find bearing capacity of model footing. But as a natural source, keeping an eye on its depletion day by day is also causing a alarming situation for future. Hence to minimise its use in construction, crusher dust can be used as a complete substitute

B. Paikaray (✉) · B. G. Mohapatra · S. Barsha · A. Mohanty
School of Civil Engineering, KIIT DU, Bhubaneswar, India
e-mail: bandita.paikarayfce@kiit.ac.in

B. G. Mohapatra
e-mail: bmohapatrafce@kiit.ac.in

B. B. Das et al. (eds.), *Recent Developments in Sustainable Infrastructure (ICRDSI-2020)—GEO-TRA-ENV-WRM*, Lecture Notes in Civil Engineering 207,
https://doi.org/10.1007/978-981-16-7509-6_62

of sand or can be used in combination with sand. In the present study, crsuher dust is used as a bottom layer having sand as top in combination giving rise to a two layer soil condition. Many research work have been conducted in past on sand only Abtahi and Boushehrian (2020), Abu-Farsakh et al. (2013), Latha and Somwanshi (2009) and Yetimoglu et al. (1994). Also sand is used in two layer condition combined with different density of sand or with clay as a bottom layer with reinforcement at the interface. Ismail Ibrahim (2016) and Saha and Deb (2017). Also it has been used in stabilization process to soft or expansive soil in different proportion. Gupta et al. (2002) stabilized black cotton soil applying crusher dust. The optimum percentage of crusher dust used to reduce the liquid limit (LL) and shrinkage limit (SL) (Atterberg Limits) was found to be 40%. But the California bearing ratio (CBR) value and unconfined compressive strength (UCS) value increased in the same treatment. Gulsah (2004) treated expansive soil produced by adding kaolinite and bentonite and treated with the addition of crusher dust, rock powder and lime with fix proportion to reduce the swelling potential of soil. Stalin et al. (2004) used quarry dust and marble powder to expansive clay to reduce the liquid limit and swelling pressure (SP) of the soil. Soosan et al. (2005) utilized quarry dust as an additive to red earth, kaolinite and Cochin marine clay to improve their engineering property. Addition of stone dust and nylon fibers by 20% and 3% respectively to Black cotton soil reduced the swelling pressure of the expansive soil by about 48% (Jain and Jain 2006).

Research with crusher dust as a foundation material has not been reported till date except few Bai et al. (2013) and Paikaray et al. (2018, 2019).

2 Objective of the Study

The objective of the present study is to find the bearing capacity of surface footing placed on sand overlying crusher dust at relative density of 35 and 67% without reinforcement and with reinforcement at interface.

3 Literature Review

Sand as a foundation material has been taken in many model testing found in literature to find the bearing capacity of different types of footing at different relative density state. Yetimoglu et al. (1994) conducted model tests in laboratory to find the bearing capacity of rectangular footing on geogrid reinforced sand. A cubical tank of size 0.7 m (L) × 0.7 m (B) × 1 m (D) was used for model testing. The rectangular footing of size 127 mm (l) × 101.5 mm (b) × 12.5 mm (t) was placed over sand filled in the tank with a relative density of RD 73%. The top layer depth (u) of geogrid was optimized giving higher ultimate bearing capacity. The intermediate layer (h), number of layers (N) and geogrid size giving the maximum result was found out.

Latha and Somwanshi (2009) determined the bearing capacity of a square footing place on geosynthetic reinforced sand bed. The bearing capacity at reinforced stage was giving higher value than the unreinforced soil bed.

Abu-Farsakh et al. (2013) studied that the behaviour of square and rectangular footing on sand along with two reinforcements such as geotextile and geogrid. Square footing of size 152 mm (l) × 152 mm (b) × 25.4 mm (t) and rectangular footing of size 254 mm (l) × 152 mm (b) × 25.4 mm (t) were used in the test tank of size 1.5 m (L) × 0.91 m (B) × 0.91 m (D). The test showed better result of using geogrid than geosynthetic.

Abtahi and Boushehrian (2020) found the effect of contamination on bearing capacity of circular footing by adding gasoline and kerosene to the foundation sand bed. Similarly in two layer soil condition, sand has been used always with different density as a top layer to increase in bearing capacity of soft soil like clay. Also reinforcement like geosynthetic is used at interface to enhance the same at different layers towards top from the interface level. Roy and Deb (2017) have taken sand as top layer on clay using geosynthetic in many layers from the interface to find the bearing capacity of a rectangular footing. The effectiveness of multi-layer reinforcement was studied by comparing the bearing capacity improvement factor, settlement reduction factor, and load-spread angle. Bai et al. (2012) have only studied the effect of crushed stone as top layer over soft soil using geobelt as reinforcement. Similarly Paikaray et al. (2019) conducted model test on crusher dust as a foundation material for square footing at interference to find the ultimate bearing capacity. Also the effect of reinforcement layout has been studied at interference of footing on crusher dust (Paikaray et al. 2020a, b).

4 Methodology

The following procedure and methodology has been followed for conducting the present study. The model test was conducted in the specific research laboratory of school of civil engineering, KIIT University. The test tank used for this specific test is of 1.6 m (L) × 1.0 m (B) × 1.2 m (H). The model footing is of size 0.18 m (l) × 0.18 m (b) with thickness of 0.025 m. The tank was filled with crusher dust at the bottom up to a depth of 60% of the total height of the tank and the sand was filled upto the rest of the tank till the top. Sand behaving as a well graded material was placed at the top of the poorly graded crusher dust. The grain size distribution of both the materials are presented in Fig. 1 The coefficient of uniformity and coefficient of curvature of crusher dust are found to be 8,36 and 0.415 and for sand, it is of 2.28 and 1.03 respectively. As the sand carrying Cc as 1.03 considering as a well graded material was considered as the top layer over crusher dust. Both the materials were collected from Banki (sand) and Khurda (crusher dust) of Odisha (Fig. 2). Geosynthetic was used as reinforcement in between two layers of sand and crusher dust at the interface. It was collected from NTPC, Kanhia (Fig. 3). The tensile strength of geosynthetic was found to be 8.5 kN/m.

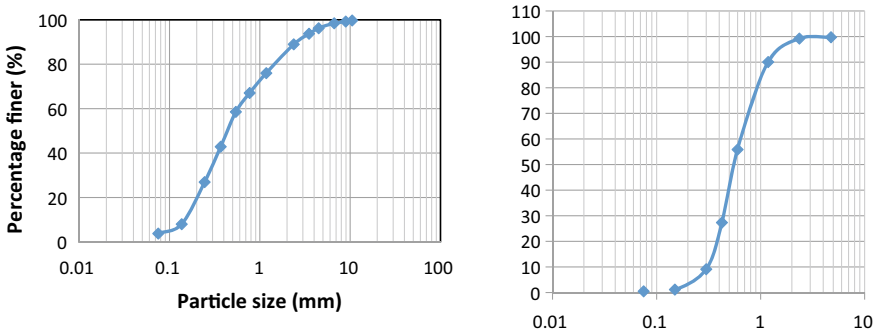

Fig. 1 Grain size distribution of crusher dust and sand

Fig. 2 Crusher dust and sand used as foundation material

Fig. 3 Geosynthetic used for present study

Fig. 4 Filling tank by sand rain technique

To maintain the relative density of the material such as sand and crusher dust, it was first filled in a small tank maintaining a particular height of fall each time and the dry density was measured. Different densities were obtained from different height of fall of the material. Based on the maximum and minimum dry density of the material, the relative density was achieved which was maintained in the final test tank. The crusher dust and sand were filled inside the test tank by using a funnel to flow the material from a fixed height to maintain the relative density by raining technique (Fig. 4).

At the top of the sand, the model footing was placed and set with LVDTs at its four corners to find the settlement at the time of testing. Similarly, a load cell was placed at the centre of the footing to apply the concentric load on the footing. The load-settlement data was obtained for different state of relative density with and without geosynthetic and graph was plotted to find the ultimate bearing capacity of footing.

The complete experimental set-up is presented by Fig. 5.

5 Results and Discussion

This chapter deals with the presentation of test result, and discussion of the present study. The results and analysis of the whole study is presented here in detail (Fig. 6).

Fig. 5 Load-settlement test on square footing

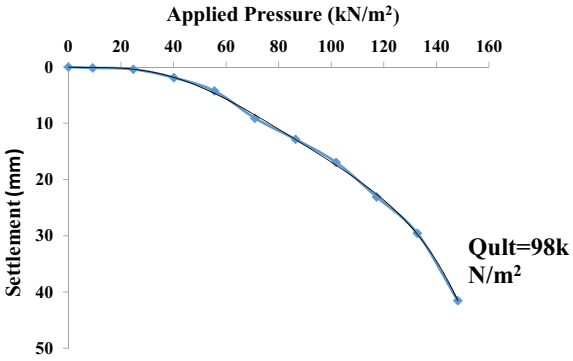

Fig. 6 Load-settlement curve for RD 35% CD and RD 35% sand without reinforcement

The load-settlement curve for reinforced crusher dust and sand at RD 35% is presented in Fig. 7.

In both the figures, the load-settlement curve for two layer soil is presented with and without reinforcement. Here the with reinforcement curve is becoming wider compared to unreinforced one for a higher ultimate bearing capacity that is achieved by using the reinforcement at the interface. The use of reinforcement acts as an tensile member to spread the load on a wider area as well as making the soil capable to take larger load at failure. Similarly for RD 65% CD and Sand with and without reinforcement test was conducted and the results obtained are presented in Table1.

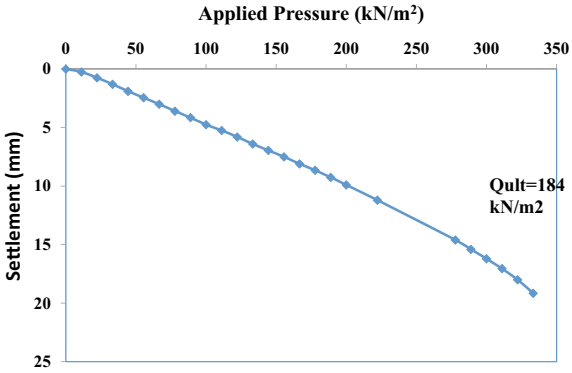

Fig. 7 RD 35% CD and RD 35% sand with reinforcement

Table 1 Ultimate bearing capacity values at different density with and without reinforcement

S. No.	Soil	Relative density (RD)	Footing	Reinforcement	Qult (kN/m^2)	Variation of Qult on same density (kN/m^2)
1	CD + Sand	35% + 35%	Square	Unreinforced	98	87.75
2		35% + 35%		Reinforced	184	
3		67% + 67%		Unreinforced	280	23.57
4		67% + 67%		Reinforced	346	

6 Implications on Society

Producing in huge quantity from the crusher units during the processing of aggregates, crusher dust is available plentily. Environment pollution is the main cause of its deposition. Using in bulk below foundation, in pavements, in embankments can reduce its bad effect which will be a great help to the society.

7 Conclusion

The present study summarizes the following conclusion.

1. The effect of two layer state of soil is giving better result of bearing capacity to crusher dust combination with sand than in isolation.
2. The Qult in unreinforced state of soil is giving less value than reinforced state at RD 35% with a percentage variation of 87.75%.
3. The Qult in unreinforced state of soil is giving less value than reinforced state at RD 67% with a percentage variation of 23.57%.

4. The variation of Qult at loose soil compared to dense soil in two layer condition is of 185% and 88% at unreinforced and reinforced soil.

References

Abtahi SA, Boushehrian AH (2020) Experimental behavior of circular foundations on oil contaminated sand. Sci Iranica A 27(1):80–87

Abu-Farsakh M, Chen Q, Sharma R (2013) An experimental evaluation of the behaviour of footings on geosynthetic-reinforced sand. Soils Found 53(2):335–348

Bai X-H, Huang X-Z, Zhang W (2013) Bearing capacity of square footing supported by a geobelt-reinforced crushed stone cushion on soft soil. Geotext Geomembr 38:37–42

Gulsah (2004) Stabilization of expansive soils using aggregate waste, rock powder and lime. A Master of Science thesis, submitted to the graduate school of natural and applied sciences of the Middle East Technical University

Gupta AK, Sachan AK, Sahu AK, Kumar S (2002) Stabilization of black cotton soil using crusher dust—a waste product of Bundelkhand region. In: Proceedings of Indian geotechnical conference, Allahabad, pp 308–311

Ismail Ibrahim KMH (2016) Bearing capacity of circular footing resting on granular soil overlying soft clay. HBRC J 12(1):71–77

Jain PK, Jain R (2006) Behaviour of black cotton soil with stone dust and nylon fiber. In: Proceedings of national conference on natural disaster management, Vizagapatam, pp 149–152

Latha GM, Somwanshi A (2009) Bearing capacity of square footings on geosynthetic reinforced sand. Geotext Geomembr 27(4):281–294

Paikaray B, Das SK, Mohapatra BG (2018) Interference of two shallow square footings on geogrid reinforced crusher dust. Lecture Notes in Civil Engineering this link is disabled 2019, 25, pp 41–60

Paikaray B, Das S, Mohapatra B (2019) Interference of two shallow square footings on geogrid reinforced crusher dust. In: Sustainable construction and building material, vol 25. Lecture notes in civil engineering, pp 41–60

Paikaray B, Das SK, Mohapatra BG (2020a) Effect of reinforcement layout on interference effect of square footings on reinforced crusher dust. Int J Geotech Eng. https://doi.org/10.1080/19386362.2020.1712531

Paikaray B, Das SK, Mohapatra BG, Swain SP, Swain S (2020b) Bearing capacity analysis based on optimization of single layer depth of reinforcement below rectangular footing. LNCE, pp 47–56. https://doi.org/10.1007/978-981-15-4577-1_4

Roy SS, Deb K (2017) Bearing capacity of rectangular footings on multilayer geosynthetic-reinforced granular fill over soft soil. Int J Geomech 17(9):04017069-1–04017069-15

Saha Roy S, Deb K (2017) Bearing capacity of rectangular footings on multilayer geosynthetic-reinforced granular fill over soft soil. Int J Geomech 17(9):04017069-1– 04017069-15

Soosan TG, Sridharan A, Jose BT, Abraham BM (2005) Utilization of quarry dust to improve the geotechnical properties of soils in highway construction. Geotech Test J 28(4):1–9

Stalin VK, Anu VJ, Sarvana Kumar R, Srinivasan V (2004) Control of swell potential of expansive clays using solid wastes. In: Proceeding of Indian geotechnical conference, Warangal, pp 155–158

Yetimoglu T, Wu TH, Saglamer A (1994) Bearing capacity of rectangular footings on geogrid-reinforced sand. J Geotech Eng ASCE 120(12):2083–2099

Detoxification of Accumulated Heavy Metals Residing in Construction Waste for a Safe Disposal

G. K. Monica Nandini

Abstract Day by Day, the pollution increases due to the intrusion of pollutants from various streams. In order to control the pollution, some remedial measures have to be taken keeping in view the environmental disposal standards. Here, we have focused on deducting the toxic heavy metals contamination in substances of construction and demolition waste category collected from nearby industrial sources. As the waste sample contains heavy metal contaminants, they cause severe air and land pollution to ambient environment. This work aims to study the detoxification and removal of the heavy metal pollutants in the construction waste. Toxic heavy metals such as Cadmium (Cd), Chromium (Cr), Copper (Cu), Lead (Pb), and Zinc (Zn) are to be identified in collected samples. These heavy metal contaminants can be reduced by certain chemical reagents such as Acetic acid, Citric acid, Hydrochloric acid, and Oxalic acid. With the combination of various heavy metals and chemical reagents, the process of detoxification is carried out in this work. By doing so the heavy metals deduction in the samples collected takes place and their removal also happens simultaneously, thus making the environment safe for the occupancies.

Keywords Cleaning · Construction waste · Heavy metals · Detoxification · Rinsing

1 Introduction

Developing an efficient green technology for detoxifying metal poisoning is the major concern for researchers in recent times. In Today's scenario, it is considered that the level of pollutants in the surrounding environment requires need of the hour measures (Kumar et al. 2017). The C&D waste is considered as the major outcome of speedy construction activities in major areas. This particular waste, using 3R concept can be used effectively in various ways. Though possibility of recycling and reuse available, landfilling is the most common disposal methods (Mah et al. 2018).

G. K. M. Nandini (✉)
Department of Civil Engineering, Sona College of Technology, Salem, India
e-mail: monicanandhini.civil@sonatech.ac.in

B. B. Das et al. (eds.), *Recent Developments in Sustainable Infrastructure (ICRDSI-2020)—GEO-TRA-ENV-WRM*, Lecture Notes in Civil Engineering 207,
https://doi.org/10.1007/978-981-16-7509-6_63

Numerous adsorbents have been suggested in the literature for the eradication of metals. These include activated carbon, natural zeolite, clays and biomass (Yaacoubi et al. 2014). Faced with more and more stringent regulations, these toxic heavy metals should be removed from the wastewater to protect the people and the environment (Dong et al. 2017). Heavy metals Cd, Ni, Cu, Pb, are common contaminants in ground, surface and wastewater (Danila et al. 2018) Heavy metals are elements having atomic weights between 63.55 and 200.59 and a specific gravity greater than 4.0. Inspite of its toxicity, living organisms require trace amounts of some heavy metals such as Co, Cu, Fe, Mn, Mo, V, Sr, and Zn. They are known as essential metals but their excessive levels can be detrimental to organisms (Ahmad et al. 2018). Humans are exposed to a range of "heavy metals" such as cadmium, mercury and its organic form methyl mercury (CH_3–Hg), uranium, lead, and other metals as well as metalloids, such as arsenic, in the environment, workplace, food and water supply (Dorne et al. 2011). Because of their high solubility in the aquatic environments, heavy metals can be absorbed by living organisms (Barakat 2011). Enormous works are undertaken for the removal of heavy metal ions, especially in the waste streams of Hydro-metallurgy and related industries and to reuse them.

Among various emerging industries such as electroplating industry, the sludge produced is of major concern contains heavy metals like Ni, Cu, Cr and Cd (Al-Hwaiti et al. 2015). The removal of heavy metals from the environment is of special concern due to their persistence (Karnib et al. 2014). Once the heavy metals are chemically stabilized, most pure salt of soluble form can be recovered (Rodella et al. 2017). Heavy metals could be classified as potentially toxic (e.g. arsenic, cadmium, lead, mercury), probably essential (e.g. copper, zinc, iron, manganese) (Suprapti et al. 2016). Whenever toxic heavy metals are released to the atmospheric air, bioaccumulation of the same happens in human beings through food web. Therefore, heavy metals should be prevented from reaching the natural environment (Abdul Salam et al. 2011). Among various emerging industries such as electroplating industry, the sludge produced is of major concern and contains heavy metals like Ni, Cu, Cd and Cr. Eliminating direct release of metal into the ambient area is highly desired in recent times (Su et al. 2016). Heavy metals are those with high density, atomic weight or atomic number. Generally, adsorptive removal of heavy metals in wastewater is obtained through activated materials such as Carbon, Alumina and other Polymeric resins, which are of cheap, cost effective and regenerable materials type (Sfaksi et al. 2014, Shen et al. (2012) and Winter et al. (2016). By selecting varieties of factors, designing experiment in groups and other methods, the cleaning and detoxification of chromium in construction waste has been studied in the yester year (Zhang et al. 2016). The chemical fixation could remediate the soil with low concentration contaminants; however, the bioavailability of fixed heavy metals may be changed with the environmental condition changing (Yao et al. 2012). Having extraction time and pH value as the key functions, heavy metals are extracted from different aggregate fractions (Ding et al. 2013). After studying various literatures, this work focuses on finding out suitable method of cleaning and detoxification of concrete samples collected from area surrounding a Paint industry located at Coimbatore.

2 Objectives

- To identify a suitable site surrounding an Industrial area for effective collection of the sample.
- To assess the toxicity of the heavy metals in the collected construction waste sample.
- To find out an appropriate solvent for effective cleaning and detoxification of the concentrated heavy metals such as Cu, Cr, Zn, and Pb in this work.

3 Materials and Methods

3.1 Materials

The construction waste samples were collected near a paint manufacturing unit located at Coimbatore. The samples were in different sizes and weighed around 5–6 kg. Then it has been crushed with a crushing machine into small size particles. Then the crushed samples were separated according to the required sizes of 1, 2, and 3 cm. Then the separated samples were washed with the distilled water and then rinsed with chemical reagents such as Citric acid, Oxalic acid, Hydrochloric acid and Acetic acid. After conducting trials at various concentrations of 0.5, 1, 1.5 and 2 M for above proposed solvents separately, 0.5 M has shown effective result and the same used throughout this work.

3.2 Experimental Contents

- Among various categories of C&D wastes, samples from concrete blocks of an old building surrounding a paint industry was collected and crushed to sizes of 1 cm, 2 cm, and 3 cm, respectively.
- Later, the samples were crushed and segregated to the sizes of 1, 2 and 3 cm and then washed separately with the distilled water to remove foreign substances.
- A quantity of 100 g of sample was soaked for one hour in the chemical reagents such as Citric acid, Oxalic acid, Hydrochloric acid and Acetic acid separately.
- After the first soaking, the sample solution was tested in UV spectrophotometer using appropriate wavelengths for Cu, Cr, Zn, and Pb followed by second soaking.
- Then the results after first and second soaking was compared to find the appropriate solvent and effective particle size for the detoxification of Heavy metals in collected concrete sample.

4 Results and Discussion

Each and every sample with the noted pollutants is tested on UV spectrophotometer. From that testing, the concentration of heavy metal contaminations have noted out. The following graphical diagrams show the rate of concentration of Cd, Cu, Pb and Zn in the samples after two successive rinsings.

Figures 1 and 2 shows that the samples were tested for Chromium (Cr) in UV–VIS spectrophotometer at a wavelength of 440 nm. The result of absorbance obtained after first and second rinsing for various sizes of particles such as 1, 2, and 3 cm showed almost similar results. After the first and second rinsing using Citric acid, the content of Cr which was initially in the range of 250–750 mg/kg after first rinsing was reduced completely below 400 mg/kg for the average particle size of 3 cm compared to 1 and 2 cm. On the other hand, Oxalic acid rinsing showed that the content of Cr was reduced substantially for the particle size of 1 cm and 3 cm, with no reduction for the 2 cm particle size. The rinsings of HCl and Acetic acid showed little effect on the removal of Cr content in the concrete samples taken.

Figures 3 and 4 shows that the citric acid after first rinsing showed that the Cu content was at the rate of 4000 mg/kg for 1 and 2 cm size particle compared to 3 cm particle having around 2500 mg/kg. On the other hand, oxalic acid was effective in the reduction of Cu content below 2000 mg/kg for 2 and 3 cm size concrete samples. HCl and Acetic acid was effective in the reduction of Cu below 3000 mg/kg after second rinsing with the same.

Figures 5 and 6 shows that the sample was tested for Lead (Pb) in UV–VIS spectrophotometer at a wavelength of 240 nm. For sample size of 2 and 3 cm, the citric

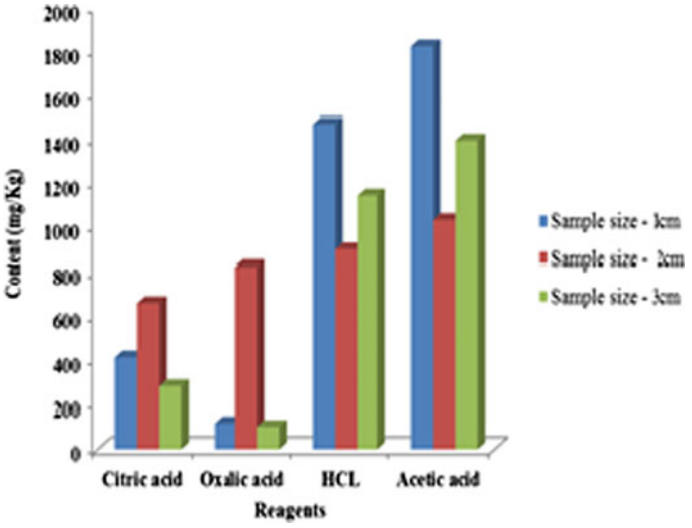

Fig. 1 Concentration of Cr after 1st rinsing

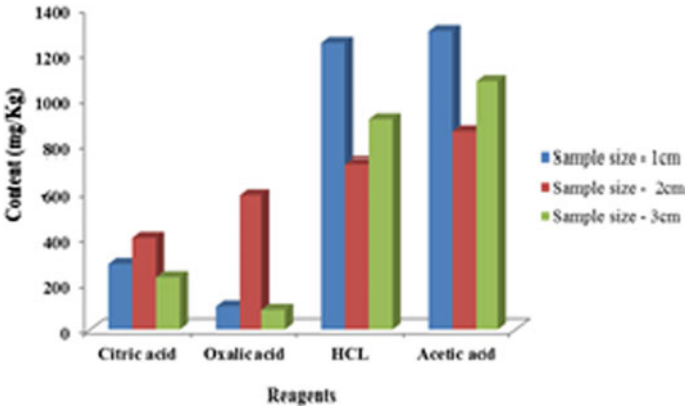

Fig. 2 Concentration of Cr after 2nd rinsing

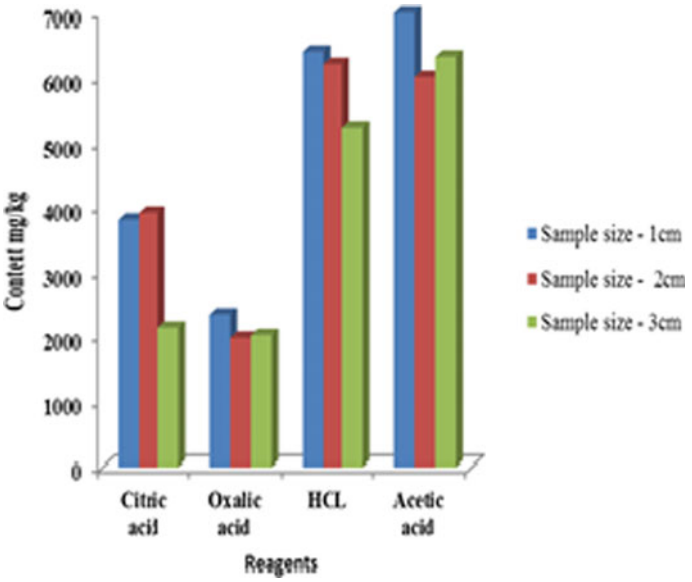

Fig. 3 Concentration of Cu after 1st rinsing

acid which was efficacious in removing pollutants at the range of 3500–5800 mg/kg for all the three sizes of particles to a level below 1500 mg/kg. Oxalic acid proved to be effective in removing the lead content from 3000 to 900 mg/kg after two successive rinsings. HCl and Acetic acid was capable of removing only a small quantity of Pb around 500 mg/kg.

Figures 7 and 8 shows that the sample was tested for Zinc (Zn) in UV–VIS spectrophotometer at a wavelength of 240 nm. For 1 and 2 cm particles, Citric acid,

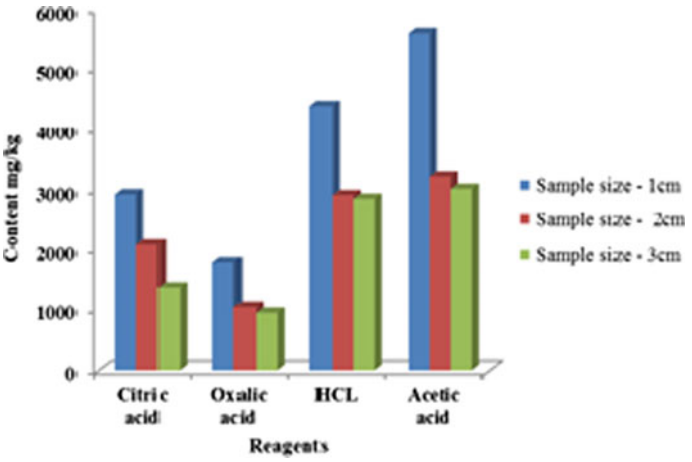

Fig. 4 Concentration of Cu after 2nd rinsing

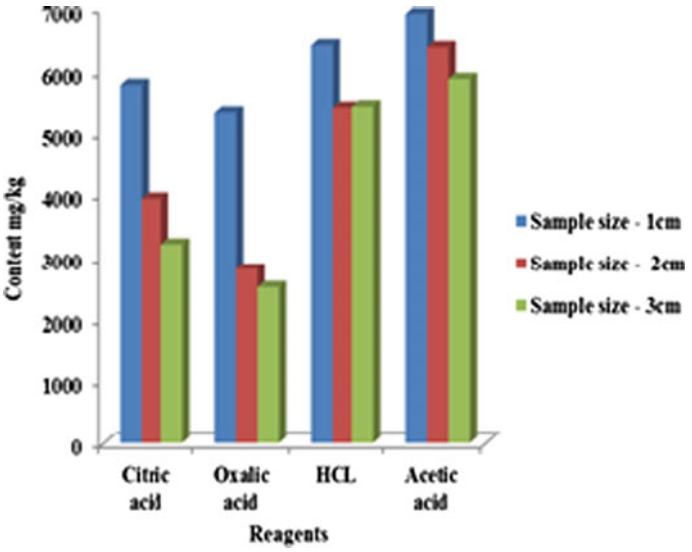

Fig. 5 Concentration of Pb after 1st rinsing

Oxalic acid was productive in removing Zn from 1700 mg/kg to an average level of 100 mg/kg after first and second rinsing. Zinc content was reduced from 2500 to 450 mg/kg when HCl was used after first and second rinsing. Acetic acid was productive in reducing the pollutants from 2500 to 900 mg/kg for all the three sizes of particles, giving only a minimal detoxification. Removal efficiency of citric acid and HCl was around 30% compared to other eluents on sample of size 1 cm; for 2 cm

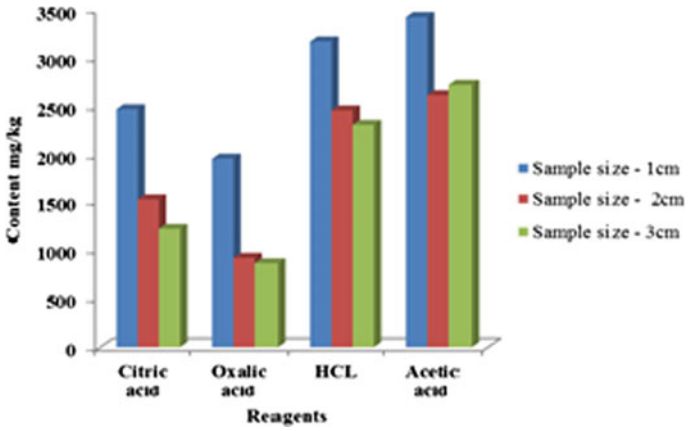

Fig. 6 Concentration of Pb after 2nd rinsing

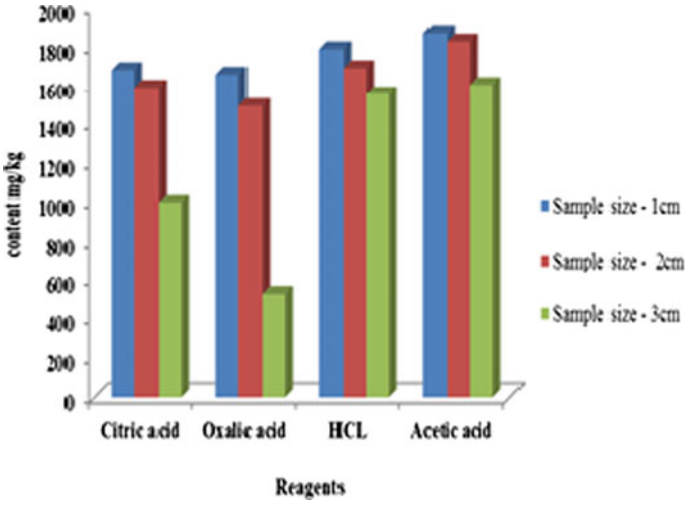

Fig. 7 Concentration of Zn after 1st rinsing

size particle, 40% removal efficiency was obtained when compared with the other solvents. The result of 3 cm size particle was not upto the mark.

From the perspective of Cu, sample of 2 and 3 cm size removal efficiency was around 50% in case of HCl, 48% in case of Oxalic acid, 46% in case of Acetic acid. Oxalic acid showed 63% removal for lead pollutants of 1 cm, 67% for 2 cm, 66% for 3 cm sample size, compared to other solvents namely citric acid, HCl and Acetic acids giving an efficiency of around 50% altogether. Zn pollutant was effectively removed by citric acid, Oxalic acid, Hcl at a rate of around 70%, 80%, 70% respectively compared to Acetic acid which has given only 55% for sample

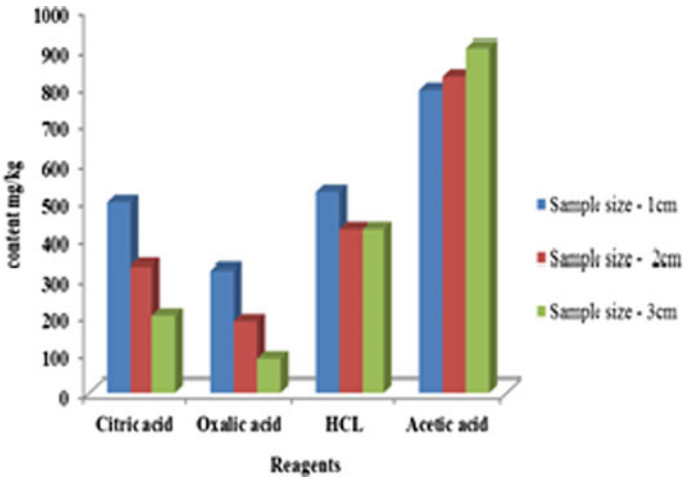

Fig. 8 Concentration of Zn after 2nd rinsing

of 1 and 2 cm size. For 3 cm size sample, no noteworthy result was found. From the enrichment factor, which helps in the detection of the presence and intensity of anthripogenic contaminant, it is understood that 85% EF factor for Cr shows that sample of 1 cm is highky enriched compared to 2 and 3 cm size sample of concrete.

Copper was significantly enriched in the sample size of 1, 2, and 3 cm with a EF below 20% on an average. Lead gave highly enriched factor of around 40% for all the three sample sizes. Zinc was also highly enriched for 1, 2, and 3 cm size particle. From the above enrichement factor and removal efficiency, it is understood that sample size plays a vital role in the accumulation of Heavy metals. Type of solvent and pH plays a significant role in detoxification of heavy metals such as Cr, Cu, Zn and Pb.

5 Conclusion

From the experimental work, it is understood that the contamination in construction wastes can be removed in an effective rate by the detoxification process. Heavy metals such as Cr, Cu, Pb, Zn occurs in the particles at different concentration possessing various enrichment factor without comprising the pH stability. pH value of Citric acid, Oxalic acid, Acetic acid and HCl was kept stabilized below 6 so that the redox potential obtained is greater than zero. After the second rinsing, the concentration rates of heavy metals such as Cr, Cu, Pb, Zn in the sample were reduced appropriately to cope up with the environmental disposal standards. The chemical reagents which were used in the process clearly explains that the rate of concentration differs for different reagents after the two consecutive rinsing with a stabilized pH. Thus

we conclude that the contamination of heavy metals in construction waste can be detoxified with the help of certain chemical reagents with a stable pH at different rates. This type of work can be adopted on large scale basis after a pilot scale study. Hence it proves to be a good way to reduce the massive dumping of the construction and demolition waste causing land and air pollution.

References

Abdul Salam OEA, Reiad NA, El Shafei MM (2011) A study of removal of heavy metals from waste water from low cost absorbents. J Adv Res 2:297–303

Ahmad I, Siddiqui WA, Qadir S, Ahmad T (2018) Synthesis and characterization of molecular imprinted nanomaterials for the removal of heavy metals from water. J Mater Res Technol 8(5), 4239–4252 (2019)

Al-Hwaiti M, Ibrahim KA, Harrara M (2015) Removal of heavy metals from waste phosphogypsum materials using polyethylene glycol and polyvinyl alcohol polymers. Arab J Chem 12(8), 3141–3150 (2019)

Barakat MA (2011) New trends in removing heavy metals from industrial wastewater. Arab J Chem 361–377

Danila V, Vasareviciusa S, Valskysb V (2018) Batch removal of Cd(II), Cu(II), Ni(II), and Pb(II) ions using stabilized zero-valent iron nanoparticles. Energy Proc 147: 214–219

Ding Z, Wang Q, Hu X (2013) Extraction of heavy metals from water-stable soil aggregates using EDTA. Proc Environ Sci 18, 679–685

Dong H, Fan Z, Wang B, Xue S, Zhao J, Song Y (2017) Hydrate-based reduction of heavy metal ion from aqueous solution. Energy Proc 105:4706–4712

Dorne JLCM, Kass GEN, Bordajandi LR, Amzal B, Bertelsen U, Castoldi AF, Heppner C, Eskola M, Fabiansson S, Ferrari P, Scaravelli E, Dogliotti E, Furst P, Boobis AR, Verger P (2011) Human risk assessment of heavy metals principles and applications. Metal Ions Life Sci 27–60

Karnib M, Kabbani A, Holail H, Olama Z (2014) Heavy metals removal using activated carbon, silica and silica activated carbon composite. Energy Proc 50:113–120

Kumar B, Smita K, Flores LC (2017) Plant mediated detoxification of mercury and lead. Arab J Chem 10:S2335–S2342

Mah CM, Fujiwara T, Ho CS (2018) Environmental impacts of construction and demolition waste management alternatives. Chem Eng Trans 63

Rodella N, Bosio A, Dalipi R, Zacco A, Borgese L, Depero LE, Bontempi E (2017) Waste silica sources as heavy metal stabilizers for municipal solid waste incineration fly ash. Arab J Chem S3676–S3681

Sfaksi Z, Azzouz N, Abdelwahab A (2014) Removal of Cr(VI) from water by cork waste. Arab J Chem, 37–42

Shen W, Li T, Chen J (2012) Recovery of hazardous metals from spent refinery processing solid catalyst. Proc Environ Sci 16:253–256

Su R, Lianga B, Guana J (2016) Leaching effects of metal from electroplating sludge under phosphate participation in hydrochloric acid medium. Proc Environ Sci 31:361–365

Suprapti NH, Bambang AN, Swastawati F, Kurniasih RA (2016) Removal of heavy metals from a contaminated green mussel using acetic acid as chelating agents. Aquat Proc 7:154–159

Winter SA, Dölling R, Knopf B, Mendelski MN, Schäfers C, Paul RJ (2016) Detoxification and sensing mechanisms are of similar importance for Cd resistance in *Caenorhabditis elegans*. Heliyon 3

Yaacoubi H, Zidania O, Moufliha M, Gouraib, M, Sebtib S (2014) Removal of cadmium from water using natural phosphate as adsorbent. Proc Eng 83:386–393

Yao Z, Lim J, Xie H, Yu C (2012) Review on remediation technologies of soil contaminated by heavy metals. Proc Environ Sci 16:722–729
Zhang W, Zhang M, Cai H, Liu A (2016) Experimental study on cleaning and detoxification of chromium in construction waste. Proc Environ Sci 31:247–254

IoT Based Irrigation System with Magnetic Water for High Crop Yielding

Rameshkumar Priyadharshini, Ramalingam Malathy, Karuppasamy Narayanan, Chandramoorthy Manimoliselvan, B. Dinesh Kumar, C. Ajay, and S. Manikandan

Abstract Water is a vital resource for human being, especially for Irrigation of crops. Resources of water are dramatically changing over the periods. Water quality and supply is greatly influenced by natural processes like amount of precipitation, temperature effects and sediment transport and such as farming and industrial development. Poor quality of water for irrigation has direct effects on crop productivity, crop quality, consumers health and farmers who are in direct touch with the irrigation water and also indirectly affects the amount of nutrients/organic matter present in soil. Magnetized or magnetic water possesses exclusive physical and chemical properties making it a dual-purpose compound with potential impact in medical treatment, industrial as well as environmental applications. The unique physical and electrochemical characteristics of Magnetic water have attracted research interests to develop different devices and techniques in agricultural and environmental applications. The purpose of this study is to discuss about enhance of nutrients like nitrogen, potassium, and phosphorus contents in soil by magnetizing the different sources of water which eventually results in improving the crop productivity and quality. Magnetic Field Treated Water (MFTW) can be achieved by passing water through the magnetic field of certain strength which is optimised through IoT Technology.

Keywords Magnetic water in agriculture · High crop yielding · IoT based irrigation system

R. Priyadharshini
Department of Computer Science and Engineering, Sona College of Technology, Salem, Tamil Nadu, India

R. Malathy (✉) · K. Narayanan · C. Manimoliselvan · B. Dinesh Kumar · C. Ajay · S. Manikandan
Department of Civil Engineering, Sona College of Technology, Salem, Tamil Nadu, India
e-mail: malathycivil@sonatech.ac.in

B. B. Das et al. (eds.), *Recent Developments in Sustainable Infrastructure (ICRDSI-2020)—GEO-TRA-ENV-WRM*, Lecture Notes in Civil Engineering 207,
https://doi.org/10.1007/978-981-16-7509-6_64

1 Introduction

Water is evidently the most vital element in the plant life. To attain maximum yield, it is mandatory to supply the optimum quantity of water in an efficient way with respect to climatic (or) seasonal rainfall and to maintain timing (Flórez et al. 2007; Yadollahpour and Rezaee 2014). Magnetic field treated water technology showcasing some new trends in the development crop yield in the irrigation field (Belyavskaya 2004). It improves the quality of water and quantity level of water usage; climate and water table level are monitored through IOT technology for optimizing the quantity of water with respect to that. IoT technology greatly helps the farmers to monitor the nutrients of crops and water for high yielding. Magnetic field treated water can be achieved by PERMAG magnet which produces magnetic intensity of 9000 gauss power with focused magnetic field. PERMAG is entirely made of strong rare earth magnet is called Neodymium (N406). Due to the effect of magnetic field, molecular group of normal water is broken down or damaged under the actions of lovenz force, without eliminating the mineral contents present in the water. It also helps to improve the activity of water for high crop yielding. It is observed that increase in magnetic intensity increases pH value but decreases conductivity and surface tension. The other chemical parameters were also studied by various testing like boron, Electrical Conductivity (EC), Total Dissolved Solids (TDS), chloride and sulphate limits as per IS 3025 to check Nitrogen Phosphorus Potassium (NPK) level before and after magnetization (Hasson and Bramson 1985; Wang 1997). To enrich the nutrients rate through NPK. Further this study is extended to investigate the quantity of water required for the different crop species through optimizing the water quantity with respect to climatic condition i.e., temperature, rainfall, humidity etc. Finally, water quality analysis and optimized water quantity is incorporated through IoT technology using arduino UNO board.

2 Components

The magnet which is used to create magnetic field in the flow of water is Permag. It is entirely made up of strong rare earth magnet called neodymium (N406). This magnet can be used to induce the high intense and focused magnetic field. In Fig. 1, it explains that Permag device is fitted on the pipeline, once water passes through the magnet, water gets magnetized. The sensors will be set in the delivery pipe which monitors and measures the amount of nutrients, and it will be programmed according to the crops and soil types to change the nutrients through optimum magnetic field with the help of IoT. Figure 1 shows the entire process of magnetization which is carried out with the components. For different intense of magnetic field, the quality of water will be changed. By observing the various types of quality, the final intensity can be set according to the requirements of the crop. The quality level of water is monitored by the incorporated sensors in the delivery pipe through IoT technology. For predicting

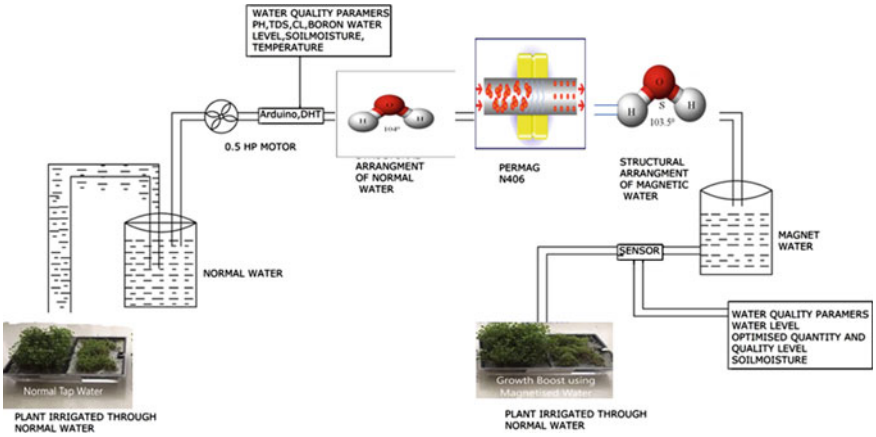

Fig. 1 Arrangement plan of magnetic water irrigation system

the climatic changes, DHT 11 weather sensor is used. Optical transducer has been used to measure NKP content present in the water which helps to analysis the changes in quality of water before and after magnetization of the respective water which passes through the created magnetic field. This study helps in understanding the performance of Permag Magnet in agriculture. The Components which have been used in the device long last for minimum 10 years with zero maintenance cost. It also acts as water purifier which has been more economical and affordable. IoT plays vital role in the analysis progress of Crops growth and periodical monitoring of the quality of water. Arduino board has been programmed with standard permissible limits of minerals, and with the help of sensor it stored the differences in cloud database at thinkspeak.com through IoT for analysis and then it recommends for corrective action in magnetic field. Application and uses of IoT can be discussed later as a separate topic.

3 Effect of Magnetic Field on Water

When bore well water seep through the magnetic field, the molecules arranged in the respective water will get affected by the enabled magnetic field intensity and have adversely affect on the water. In result, the molecules get rearranged inside the structure of the water molecules which also include increasing the count of crystallization centers and the changing the free gas content. In Fig. 2, it clearly explains the effect of magnetization in water that the water molecules are bond together which is in the form of water molecule clusters. When water molecule clusters are large, it is difficult to enter the root cells of plants. If the water is treated in the magnetic field, the water molecule clusters will break into smaller fragments or small hexagonal clusters. Both effects enhance the quality of water for irrigation. This

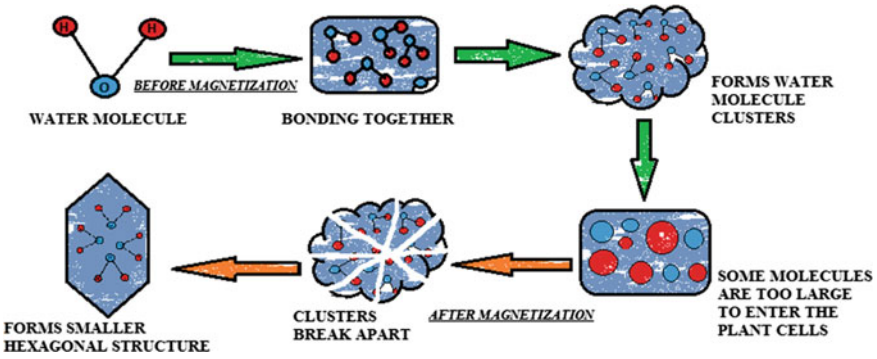

Fig. 2 Properties of magnetized water before and after magnetization

effect on water eliminates certain content like magnesium and chloride which creates hardness in the water and also add certain amount of mineral content in magnet like iron, potassium, phosphorous, and nitrogen which is add up from due to altering free flow of gas content in the water nucleus. This process helps water to carry the needed mineral content in high density and simultaneously, it reduces the hardness present in the water which also helps to carry soda content for soil. Henceforth, magnetic water leaches soil with high phosphorous content compared to the normal water. It also reduces the salt concentration which affects final germination of seeds. The reduction is important for high level of concentration (more than 5000 ppm). The concentration level in water can be monitored and controlled by changing intensity of permag magnet in further based on the requirement of certain crop for enriching with mineral contents. By this way, the amount of water is to be used for irrigation becomes minimal and enrich the content of water with necessary and required minerals in the short period of time and cost efficiency manner. In other words, the magnetic field purifies the bore well water for adopting proper and efficient irrigation system without affecting in the any form of Environment.

4 Effect of Magnetic Field Water on Soil

Soil is a significant part of successful agriculture and is the true source of the nutrients that we use to grow crops. The nutrients travel from the soil into plants that we take like tomatoes (Bogatin 1999). As previously discussed in the above topic, the magnetic field increased the nutrients in the water which also enriches the soil with the similar nutrient contents. Due to smaller hexagonal clusters of water molecules, it easily penetrates the soil and also results in increasing the permeability of soil content which also helps to the free flow of air in the Soil. The magnetic treatment of saline or bore well water is described as a valuable method for soil desalinization (Mostafazadeh-Fard 2010). Water treatment by magnetic field decreases the

hydration of salt ions and colloids that increases the salt crystallization, accelerated coagulation and salt solubility (Kronenberg 1985). The study showed that magnetic water increased leaching of excess soluble salts, lowered soil alkalinity and dissolved slightly soluble salts (Mohamed and Ebead 2013). To improve the plant growth, the soil needs to be fully enriched with NKP mineral content.

The role of NKP in soil:

- Nitrogen support to the enzymatic formation of proteins and is critical to the photosynthetic process. Crops will shift nitrogen around their plant systems from high-nitrogen density to areas deficient in the nutrient.
- Phosphorus plays a vital role in crop growth by aid in fruit production, stock growth, and root growth. A need of phosphorus in crop soil will produce weak plants that are prone to wilting, discoloration, and inadequate fruit.
- Potassium is important to the preservation and inclusion of water in crop soil. Good water saturation leads to strong and fit plants that resist disease and harm from heat.
- In addition to all of this, the magnetic water will drastically reduce the usage of fertilizer and pesticides in the irrigation field which results in organic yield. It helps to increase the water holding capacity of soil and maintains the necessary humidity for irrigation purpose. The magnetic water also enriches the soil with proper and required nutrient content for high crop yielding.

5 Effect of Magnetic Water on Plant Growth

Magnetic treatment in water carries adversely some positive effects for Plant growths. Since it purifies with required mineral content which gives necessary growth to the plant both theoretically and practically, the effect has been clearly showing comparison with previous yielding (Hilal and Hilal 2000). It also observed that the magnetic water increases the germination of seed. Similarly, in other field study indicates an important role of magnetic water irrigation of seeds in improving the growth of seedling. Further, Magnetic water treatment before sowing increases the number of pods per plant and decreased plant losses per unit area. Muraji et al. reported that the roots of maize plant have the highest growth rate under an Magnetic field intensity of 5 mT at 10^{17} Hz. In addition, Magnetic field has an important influence on dry weight of sunflower plants. The significant growth has been identified in maize, paddy, sugarcane, turmeric cultivation under the influence of magnetic water. The changed properties in magnetic water can alter the characteristics of plant, growth and production. Magnetic water changes several parameters that are related with the yield, growth characteristics, potassium, GA3, kinetin, nucleic acids (RNA and DNA), photosynthetic pigments and activity. Several studies revealed the enhancement of water productivity in crops and livestock production, flowers number and total fruits yield for various crops. In weak magnetic field, it adds the size and volume of mitochondria, calcium over-saturation in cytoplasm and disruptions in different metabolic systems including Ca^{2+} homeostasis in cells of root. The significant task

of magnetic water is to reduce the heat stress termination in various seedlings. The main effect of magnetic water in plants includes growth of plants, transplant leaf area, transplant dry weight and seed germination.

6 Prevention and Elimination of Scaling

An impurity like suspended particles, solids present in water give rise to issue in distribution system systems of irrigation or water networks. The scale deposition in distribution system can completely block running water. Accumulation of scale due to entrapped oxygen expands erosion (Busch and Busch 1997; Herzog 1989). At the point when the outside of any channel line or water utilizing frameworks gets scaled, this protecting scale diminishes the proficiency of the framework, builds fuel necessities and support. Hence the prevention and elimination of scaling technique demand evolved, not only economically but also to control the environmental pollution. The significant use of magnetic water is to prevent and eliminate the scale. This magnetic treatment provides effective savings in both production time and price. It has been concluded that the using of magnetic water reduce the mineralized coatings inside the pipes. Barrett and Parsons (1998) investigated the effect of magnetic water on calcium carbonate ($CaCO_3$) by suppressing nucleation and increasing the rate of crystal growth, and they observed scale reduction. The hexagonally organized of the magnetic water atom bunch would not permit the holding of minerals to it and expels scaling from pipes and would not permit new scaling to produce results. Henceforth, Magnetic water treatment is found to be useful for scale reduction, the exact mechanics of interaction between magnetic treatments and calcium carbonate in solution needs to be studied further (Vashisth and Nagarajan 2010). It can be conduct and studied in controlled laboratory is necessary. On behalf of it, some studies have been conducted on the effects of magnetic treatment of irrigation water on crop, soil, water, and yield (Maheshwari and Grewal 2009).

7 IoT in Irrigation System

Smart agriculture is a resolution to many global agricultural issues, like trending team productivity, monitoring results, communicating with other teams and sub-units, as well as calculating market tendencies. For the most of farms, the implementation of IoT agriculture begins with stylish irrigation. Optimizing the time frame and amount of water seep us to save resources and provide the finest care for crops. Sensor-based IoT technologies collect database about soil and update a crop review and transmit this information from sensors to farm irrigation systems (Yadollahpour and Jalilifar 2014), A. As soon as there is not enough water in the soil, a platform reacts to this alert and the water flow turns on. In Fig. 3, it shows the IoT device or component which have been used in our study to transmit data for analysis purpose. The data

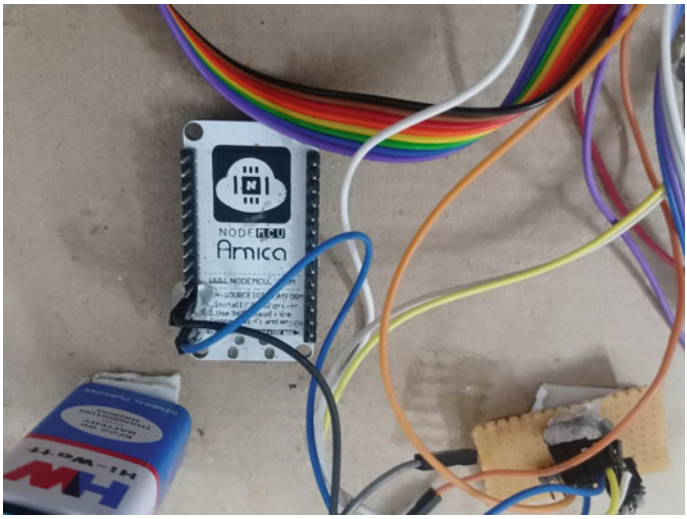

Fig. 3 An IoT hardware device used in the experimental study

used to transmit through wifi and stored in thingspeak.com, it is the cloud storage which has been used to collect and store the field data for some period.

Different crops have specific irrigation schedules according to their biological needs this is known as a precision agriculture approach, where farming activities such as irrigation or pesticide management is performed on-demand depending on the current soil and crop conditions. To make sure that each type of plant receives the best care, the irrigation system should recognize various zones depending on the sort of crop, soil, and weather conditions. Farmers should be able to set a separate schedule for each of these areas depending on the real-time sensor reads and install a separate irrigation valve for each of them. The system should notify the farmer about the start of watering and its finish, as well as send error alerts. In Figs. 4 and 5, it explains the analysis of water after magnetization and compares the data over different period in the form of chart for easy understanding on temperature, humidity, water level, pH, TDS, boron, chloride, sodium in the water.

If there is a technical problem, the system should be able to detect abnormalities in the irrigation flow and notify the farmer immediately. Water is the most crucial factor of the harvest's quality and health. Irrigation management controls the amount of used magnetic water and ensures that the crops receive the right dosage at the specific timeframe. The Internet of Things makes monitoring more accessible by connecting sensors and collecting all data on the Smartphone or laptop.

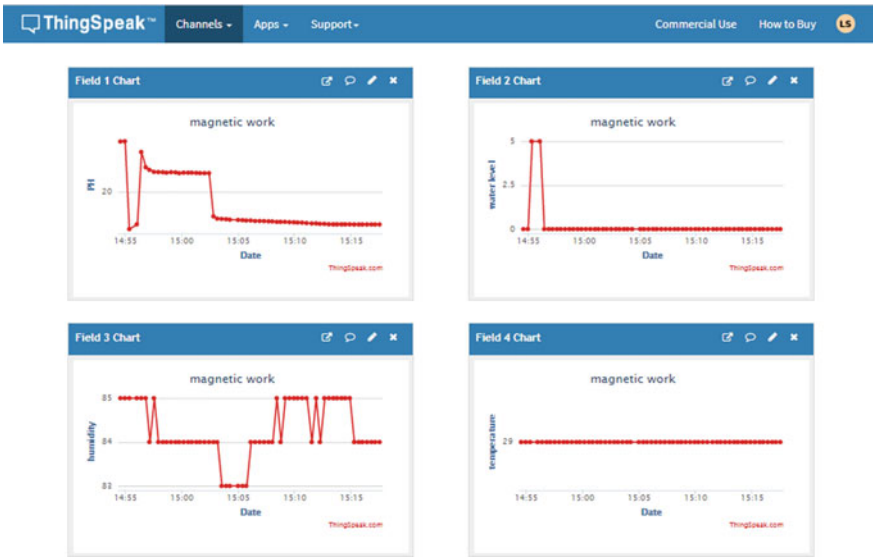

Fig. 4 Field analysis chart of pH, water level, humidity, temperature

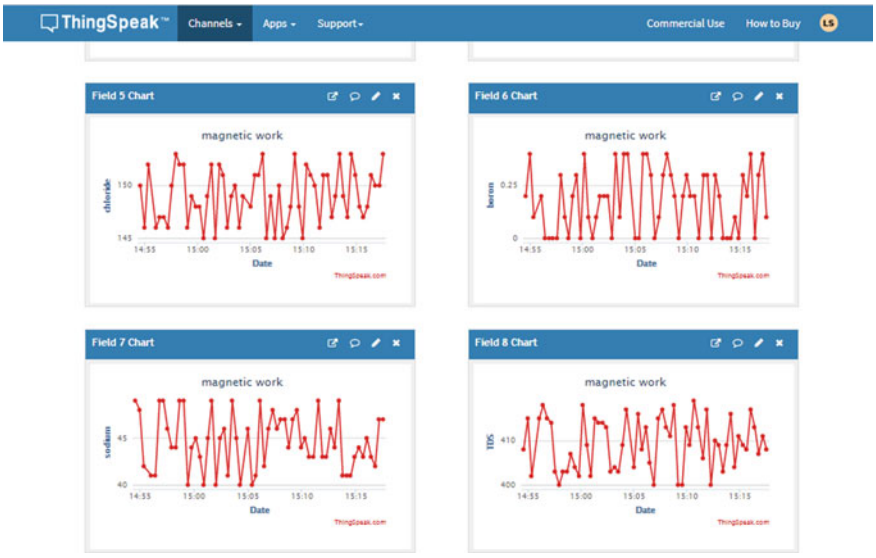

Fig. 5 Field analysis chart of chloride, boron, sodium, and TDS

8 Conclusion

Magnetic water treatment has opened to new research and taken one step forward to the modern way of agriculture. When this type of agriculture incorporated with IoT technology, it ensures the safety, compatibility, and productivity of crops. By using this IoT based magnetic water irrigation, the farmers can save production time, minimal usage of water, and can reduce the initiation cost. This method drastically reduces the use of fertilizers, and excessive use of watering which affects the growth of the crops. The Magnetic irrigation system increases high yielding of crops compared to the conventional water irrigation system. Magnetic water treatment method enhances irrigation water quality and quantity, crop yields and quality, soil improvement, scale prevention/elimination in water using systems and water saving are some of significant benefits in agriculture. In addition, magnetic fields have shown beneficial effects on the germination of seeds, plant growth and development, the ripening and yield of field crops. Magnetic water irrigation proves the growth in plant is purely based on organic manner and does not affect or harm the environmental at any cost. The crop yielded by using this method has enriched with high nutrient content and entirely it is safe and healthy. As it is embedded with IoT, it can reduce work and saves labor cost which can also monitor and controlled in remote without having any physical work.

References

Barrett R, Parsons SA (1998) The influence of magnetic fields on calcium carbonate precipitation. Water Res 32:609–612

Belyavskaya N (2004) Biological effects due to weak magnetic field on plants. Adv Space Res 34(7):1566–1574

Bogatin J et al (1999) Magnetic treatment of irrigation water: experimental results and application conditions. Environ Sci Technol 33(8):1280–1285

Busch KW, Busch MA (1997) Laboratory studies on magnetic water treatment and their relationship to a possible mechanism for scale reduction. Desalination 109(2):131–148

Flórez M, Carbonell MV, Martínez E (2007) Exposure of maize seeds to stationary magnetic fields: effects on germination and early growth. Environ Exp Bot 59(1):68–75

Hasson D, Bramson D (1985) Effectiveness of magnetic water treatment in suppressing calcium carbonate scale deposition. Ind Eng Chem Process Des Dev 24(3):588–592

Herzog RE (1989) Magnetic water treatment: the effect of iron on calcium carbonate nucleation and growth. Langmuir 5(3):861–867

Hilal M, Hilal M (2000) Application of magnetic technologies in desert agriculture. I-seed germination and seedling emergence of some crops in a saline calcareous soil. Egypt J Soil Sci 40(3): 413–422

Kronenberg KJ (1985) Experimental evidence for effects of magnetic fields on moving water. IEEE Trans Magn 21(5):2059–2061

Maheshwari BL, Grewal HS (2009) Magnetic treatment of irrigation water: its effects on vegetable crop yield and water productivity. Agric Water Manag 96(8):1229–1236

Mohamed AI, Ebead BM (2013) Effect of magnetic treated irrigation water on salt removal from a sandy soil and on the availability of certain nutrients. Int J Eng 2(2):2305–8269

Mostafazadeh-Fard B et al (2010) Effects of magnetized water and irrigation water salinity on soil moisture distribution in trickle irrigation. J Irrig Drain Eng 137(6):398–402
Vashisth A, Nagarajan S (2010) Effect on germination and early growth characteristics in sunflower (*Helianthus annuus*) seeds exposed to static magnetic field. J Plant Physiol 167(2):149–156
Wang Y (1997) Rapid onset of calcium carbonate crystallization under the influence of a magnetic field. Water Res 31(2):346–350
Yadollahpour A, Jalilifar M (2014) Electromagnetic fields in the treatment of wound: a review of current techniques and future perspective. J Pure Appl Microbiol 8(4):2863–2877
Yadollahpour A, Rezaee Z (2014) Electroporation as a new cancer treatment technique: a review on the mechanisms of action. Biomed Pharmacol J 7(1):53–62

Stabilization of Soil Sub-grade Using Plastic Waste and Effective Cost Analysis of Pavement Layers

Kalpana Sahoo, Satya Ranjan Panda, and Basudeb Munshi

Abstract People are now-a-days able to find instant solutions with the help of technology, plastic waste as a resources can be suitable used for the sidewalk construction. Plastic is a hazardous waste and very difficult to dispose. In this project plastic disposal glass is taken and it is cut into different aspect ratio (AR-1, AR-2, AR-3) and different proportion of plastic (0.1, 0.2, 0.3, 0.5, 0.7, 1.2% by weight of soil) mixed with soil and strength of soil is tested by CBR test. From the result the maximum CBR value was recorded for the reinforced soil. It is seen that CBR value different sample of reinforced soil increases with increase in addition of plastic sample and it increases up to certain limit and then decrease by adding more. Hence up to optimum value of addition of plastic waste giving maximum CBR and improve the strength of sub-bases, bases and sometimes surface courses, in case of low cost roads. The thickness of pavement layers is depending upon the CBR value of soil subgrade. So basically, this technique is an alternative to improve the economy of the country without having to harm the environment.

Keywords Waste management · Soil stabilization · Cost analysis

1 Introduction

Reliable road network is prime requirement for the process of any country. India is now the second largest road network in the world of total spanning about 5.89 million kilometer. This road network transport 64.5% of all goods. In coming two years government has set a target of constructing road of worth Rs. 15 lakh crore. A huge investment was increasing more than 3 times from 51,914 crore in 2014–2015 to 158,839 crore in 2018–2019. The expenditure related to the road construction must be minimum, according to economic point of view. In other hand, Plastics are

K. Sahoo
Department of Civil Engineering, KIIT, Bhubaneswar, Odisha, India

S. R. Panda (✉) · B. Munshi
Department of Chemical Engineering, NIT Rourkela, Rourkela, Odisha, India

B. B. Das et al. (eds.), *Recent Developments in Sustainable Infrastructure (ICRDSI-2020)—GEO-TRA-ENV-WRM*, Lecture Notes in Civil Engineering 207,
https://doi.org/10.1007/978-981-16-7509-6_65

the hazardous waste (Amrutha and Krishnan 2015) and due to huge amount of use of plastic create very difficult for disposal which causes environmental pollution. Use of plastic in a sub-grade soil of pavement not only increases the strength but also a best mode of disposal which reduces environmental pollution. Waste plastic of thickness 0.04 mm are taken and it is cut into different Aspect Ratio (AR-1, AR-2, AR-3) and different proportion of plastic (0.1, 0.2, 0.3, 0.5, 0.7, 1.2% by weight of soil) mixed with soil and strength of soil is tested by CBR test. It is seen that with increase in percentage of plastic, strength of soil increase and up-to certain value called optimum value, the strength of soil become maximum and then by adding more, the strength decrease. As the strength increase the thickness of flexible pavement required over it decreases. After getting maximum CBR value (Hansen 1959) and given load condition, Required thickness of flexible pavement corresponding value were calculated by using IRC-37 (2012) and cost analysis is done. It is seen that cost of stabilized pavement is considerable lesser than that of the unstabilized pavement. Hence, use of plastic not only better solution of disposal but also increases the strength of soil sub-grade. As a result thickness of pavement required over it decreases, which gives the economical benefit.

2 Methodology

The research is to find out the optimum combination of waste plastic and soil for road construction. Waste plastic is Purpose for stabilization of sub-grade soil and to provide a brief idea to road-way builders on merits and alternative use where soft sub-grade is encountered.

2.1 Subgrade Soil

In roads, the top 500 mm of the cutting or embankment at the formation level shall be considered as sub-grade. The sub-grade shall be compacted to utilize its inherent strength and prevent permanent deformation because of additional compaction by traffic.

2.2 IRC Specification

According to IRC-37, the permissible value of liquid limit is up to 70%.The allowable value of plasticity index should be greater than 8% and is allowable up to 45% and the soil whose value of plasticity index is greater than 8% is suitable for stabilization. The maximum dry density should not be less than 1.75 gm/cc and CBR value should be greater than 2%.

Table 1 Properties of unstabilized soil

Property	Soil
Maximum dry density in kN/m^3(by standard proctor compaction)	17.86
OMC (%) (by standard proctor compaction)	16
Maximum dry density in kN/m^3 (by modified proctor compaction)	18.6
OMC (%) (by modified proctor compaction)	14.5
CBR (%) (light compaction)	2
CBR (%) (un-soaked heavy compaction)	2.8
CBR (%) (soaked heavy compaction)	2.3
Liquid limit (%)	21.73
Plastic limit (%)	11.11
Plasticity index (%)	10.62
Unified soil classification (from sieve analysis test)	CL
Specific gravity	2.27
Typical name	Inorganic clay of medium plasticity

2.3 Materials and Testing

2.3.1 Sub Grade Layer and Material Selection

The soil was dug from a test pit in the Sadeipalli region in Burla. Through-out the project the characteristics of combination of soil was thoroughly studied. Different experiments were conducted hence-forth and the soil was finally conducted. Laboratory testing determined the index properties of all materials and test procedures were adopted as per the Bureau of Indian Standard (BIS). The soil was inorganic clay of high plasticity, properties of unstabilized soil is found out by carry out of different tests. The test result of the unstabilized soil is tabulated in Table 1.

2.3.2 Preparation of Soil Plastic Mixes

LDPE plastic strips having a thickness of 0.40 mm and width 12 mm were cut into length of 12 mm [Aspect Ratio (AR) = 1], 24 mm (AR = 2) and 36 mm (AR = 3). Aspect ratio is the length to width ratio of plastic. It is important to ensure that the mould diameter remains at least 4 times the maximum strip length, which will ensure that there is sufficient room for the strips to deform freely and independent of mould confinement. The waste plastic strips to be added to the soil were considered a part of the solid fraction in the void solid matrix of the soil. The content of the strip is defined here in as the ratio of weight of strips to the weight of dry soil. The tests were conducted at various strip contents of 0.0, 0.1, 0.2, 0.3, 0.5, 0.7 and 1.2%.

1. CBR Equipment and Test Procedure

CBR test is a penetration test which is done to find out the strength of soil at 2.5 mm or 5 mm penetration which value is greater is taken. A cylindrical mould of 175 mm internal diameter and 175 mm height with detachable extension collar height of 50 mm fitted with detachable base plate. Rammer weighing 2.6 kg and having a drop of 310 mm and a 50 mm diameter circular spacer disc is taken. Oven dried soil of passing through 4.75 mm IS sieve size is taken and plastic waste of different percentage by weight of soil and different aspect ratio were distributed evenly and mixed thoroughly with soil. Then optimum water content (16%) from standard proctor test is added to mixed soil. The test is done as per the I.S:2720-VII. The wet plastic-mixed soil was compacted in CBR mould in three equal layers by using rammers of weight 2.6 kg and free fall height of 310 mm and 56 no. of blows in each layers. Then mould was soaked in water for 4 days. After that the penetration value was found out by the California bearing ratio machine and from this value the CBR % was determined. Various graphs have been plotted for each aspect ratio and strip content versus penetration values. They have been shown in Figs. 1, 2, 3, 4, 5 and 6. CBR value is calculated by using the formula.

$$\text{CBR}\% = \frac{Load \times 6.681 \times 100}{STANDARD\ LOAD}$$

where

For 2.5 mm penetration, standard load is 1370 kg.
For 5.0 mm penetration, standard load is 2055 kg.

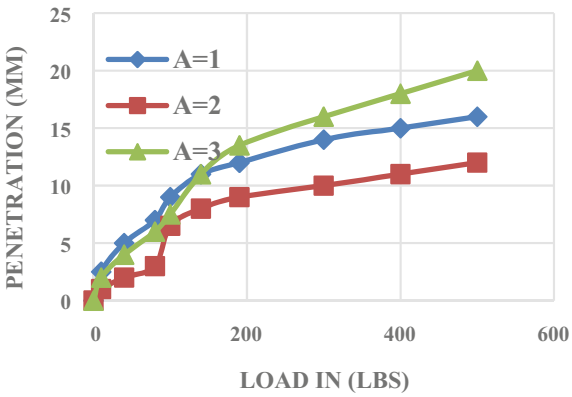

Fig. 1 Plastic content @ 0.1%

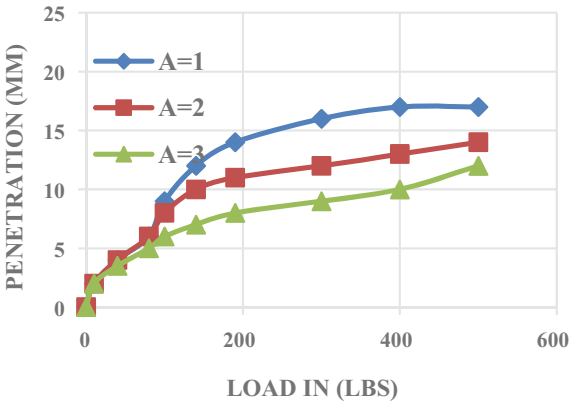

Fig. 2 Plastic content @ 0.2%

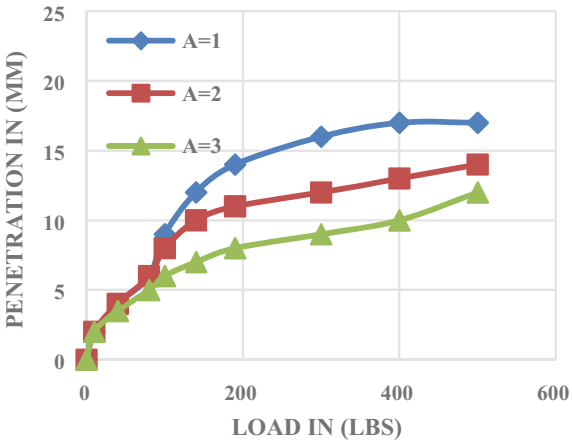

Fig. 3 Plastic content @ 0.3%

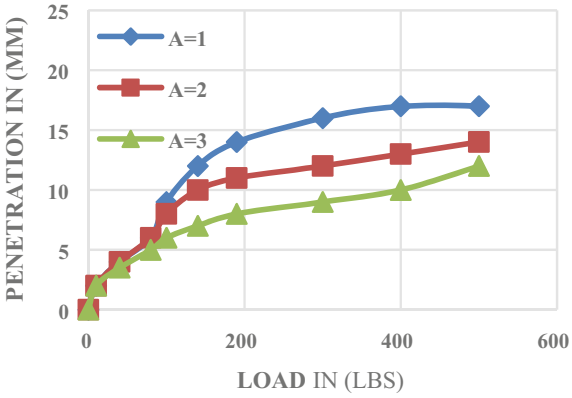

Fig. 4 Plastic content @ 0.4%

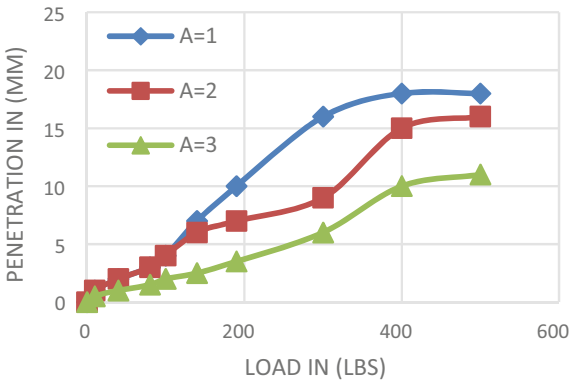

Fig. 5 Plastic content @ 0.7%

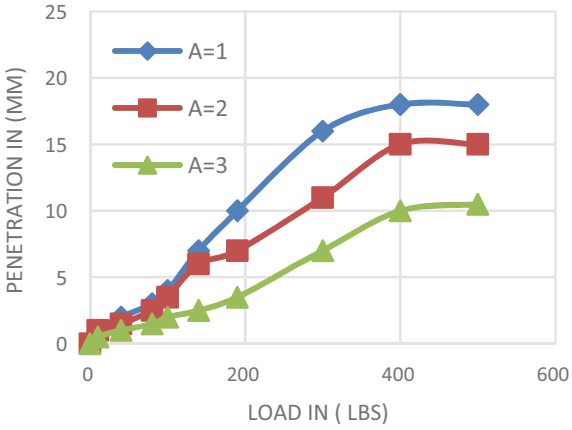

Fig. 6 Plastic content @ 1.2%

3 Experimental Observations

Variation of California Bearing Ratio (CBR) with different aspect ratio and at different plastic content.

Soil is mixed with plastic of different percentage and aspect ratio and this mixed soil is taken for the CBR test. Then graph is plotted with penetration value verses load applied in the soil sample which is called CBR graph is shown in above figure. The graph shows the comparisons of CBR value of soil of different aspect ratio. It is found that CBR value is decreases with increase in aspect ratio it is maximum for the aspect ratio-1 (AR-1) for any percentage of addition of plastic content. As the CBR is maximum for aspect ratio-1, hence the strength of soil will get more in aspect rato-1 of mixed plastic-soil. Hence minimum thickness of pavement layer can be constructed over the soil sub-grade which will be stabilized by mixed plastic wastes of AR-1 which will be economical (Fig. 7).

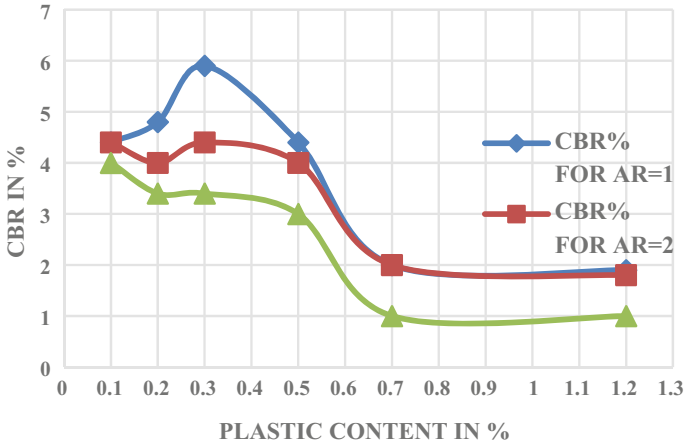

Fig. 7 Variation of plastic content and CBR

Again graph is plotted in CBR value verses plastic content (0.1, 0.2, 0.3, 0.5, 0.7, and 1.2%) with a particular aspect ratio. It is found that with increase in plastic content, the CBR value increases for certain limit and then further addition of plastic content, CBR value decreases. From the above result it is found that, the optimum plastic content at which the CBR value is maximum is 0.3% by weight of plastic strip of aspect ratio 1 (AR-1).hence strength of sub-grade soil will be more at that optimum value of plastic content and thickness of pavement layer will be decreased while constructing over the this type of stabilized soil sub-grade.

3.1 Design of Pavements

3.1.1 Sub-grade Strength Evaluation and Pavement Thickness Determination

The sub grade should be compacted 100% maximum dry density and optimum moisture content achieved by the standard proctor Test (IS2720- part 7). The material used for sub grade construction should have a dry unit weight of not less than 16.5 kN/m^3. for each of the soil groups does identified, at least one CBR test should be conducted with the soil compacted to the standard proctor density and at a moisture content considered in appropriate site condition. The laboratory CBR test was conducted according to IS 2720 part 16 on sub grade soil at different percentage of waste plastic. The results show that CBR value of sub grade soil increases with plastic content up to a certain extent then decreases.

3.1.2 Design for New Roads

For the pavement design of new roads the sub-grade strength needs to be evaluated in terms of CBR value. The CBR test should be conducted on representative samples of sub-grade soil impacted by static compaction 100% standard proctor dry density and tested at a moisture content corresponding to the wettest moisture condition likely to occur in the sub-grade during its service life. An average of test values obtained from the set of three specimens then an average of test values obtained from six specimens should be taken. For determining the CBR value in the laboratory the standard procedure laid down in IS 2720 (part 16) must be adopted.

3.1.3 Design Parameters

Traffic volume and its composition play a vital role in determining the pavement thickness and its composition. There is a wide variety motorized and non motorized vehicle running over the pavement surface. Hence the pavement layer should have sufficient strength to bear the existing load over the pavement. As per the code IRC-37 2012 for flexible pavements. The traffic load is calculated in terms of cumulative standard axle load by using the formula below

$$N = T_0 \times 365 \times \left[\frac{\{(1 + 0.01r)^n - 1\}}{0.01r} \right] \times L = T_0 \times 4811 \times L$$

where

T_0 = ESAL/day = no. of commercial vehicle per day in the year of opening × VDF.
VDF = vehicle damage factor.
L = lane distribution factor, n = design life, r = traffic growth rate.

3.2 Pavement Thickness Calculation

The CBR value of reinforced soil is found out to be 6%. For the payment thickness calculation we are referred the IRC-37-2012. For calculation of pavement thickness CBR and traffic parameter are important. Table 2 shows the variation of thickness of each pavement layers of flexible pavement according to cumulative standard axle load a specific CBR value. According to that total thickness of flexible pavement layer is calculated which is resting unstabilized soil sub-grade.

Table 2 Variation of CBR with AR and plastic strip

Plastic content (%)	CBR% for AR = 1	CBR% for AR = 2	CBR % for AR = 3
0.1	4.4	4.4	4
0.2	4.8	4	3.4
0.3	5.9	4.4	3.4
0.5	4.4	4	3
0.7	2	2	1
1.2	1.9	1.8	1

3.3 Layer Thickness Reduction

The laboratory CBR test was conducted on sub-grade soil at different percentage of plastic waste. The result shows that the CBR value of sub-grade soil increases with plastic content up to certain value and then decreases. Hence CBR value at optimum plastic content (0.3%) is taken for the analysis of pavement layers for stabilized soil for a traffic intensity of 2 msa 5 msa 10 msa 20 msa etc. as per the IRC 37-2012 in Table 3. For instance, combination of soil and plastic (100 + 0.3) for 2 MSA, the layer thickness of sub-grade, sub-base WPM, Bituminous surface treated WBM in 175 mm, 225 mm, 50 mm and 20 mm respectively and for 5 msa, 10 msa, 20 msa respective layer thickness are given in Table 4.

From the above table it found that at optimum plastic content the CBR value increases up to 6% which indicates the increase in strength of sub-grade soil. As strength of soil sub-grade increases, thickness of each pavement layer constructed over it can be decreased. If it is compared the Table 4 of the total thickness of each layers of flexible pavement to Table 3, it is found that thickness decreased for specific value of traffic load. The comparison of pavement thickness and un-stabilized soil and stabilized soil with plastic is shown in BAR graph (Fig. 8).

The above BAR graph shows the comparison between total thicknesses of flexible pavement laying over unstabilized soil to the total thickness of pavement layers

Table 3 Thickness of each layer of flexible pavement resting on an unstabilized sub-grade soil as code: (from IRC: 37:2012)

S. No.	CBR value (%)	Cumulative standard axle load in msa	Sub-grade thickness	Sub base (in mm)	WBM in mm	Bituminous surface in mm	Total thickness in mm
1	3	2	335	225	50	25	635
2		5	335	250	60	25	670
3		10	380	250	90	40	760
4		20	380	250	140	40	810

Table 4 Thickness of various layers and total thickness of payment resting on stabilized sub-grade soil

S. No.	Plastic waste (%)	Design effective CBR value (%)	Cumulative standard axle load in msa	Sub grade in mm	sub base (in mm)	WBM in mm	Bituminous surfacing in mm	Total thickness in mm
1	0.3	6	2	175	225	50	20	470
2			5	210	250	50	25	535
3			10	260	250	65	40	615
4			20	260	250	90	40	640
3			30	260	250	105	40	655

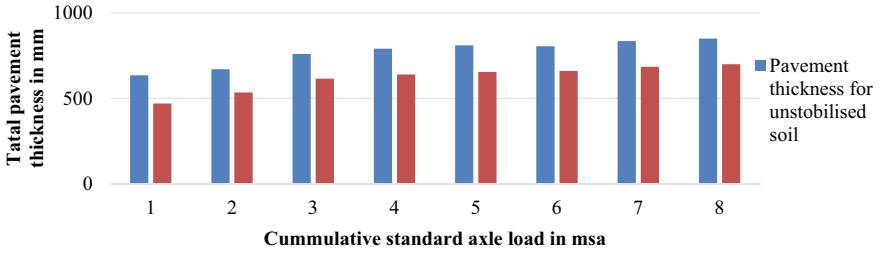

Fig. 8 Comparison of pavement thickness b/w ordinary soil and mixed soil

flexible pavement laying over unstabilized soil sub-grade. Hence there is considerable decrease in thickness of pavement layers which will give greater economical benefits.

3.4 Layer Wise Construction Calculation of Flexible Pavement Thickness

The construction cost of flexible pavement resting on stabilized sub-grade soil for different alternatives have been estimated in order to find out the most optimal design section based on economic aspects to stop the initial construction cost has been worked out for **1 km long, 7.5 m wide** pavement. The cost of the materials are given as per the data provide by R&B division, of a local area of Odisha. Various layers included in each design sections are as follows: the sub-grade, granular sub base (moorum), Water Bound Macadam WBM and bituminous surface treated WBM. From the above analysis the result was come out that there are considerable increases in CBR value after adding the plastic as stabilizer. As CBR value increases, the soil gains more stability hence there will be reduction of pavement thickness as per the IRC-37-2012.

Table 5 PWD schedule of rate: 2018–19, Govt. of Odisha

Items	Rates
Bituminous concrete	Rs. 7687/per m^3
Surface dressing	Rs. 97/per m^3
Water bound macadam	Rs. 1483 per m^3
Granular sub-base moorum	Rs. 1412 per m^3
Sub-grade with 5 km lead	Rs. 269 per m^3
Cost of capping layer (sand filling)	Rs. 400 per m^3
Compaction royalty soil, sand, dust, moorum	Rs. 28.8 per m^3
Dense bituminous macadam	Rs. 5946 per m^3

3.4.1 Structural Design

Structural strength is principle creation for determining the pavement thickness. The vertical compressive strength on the top of sub-grade composed by a standard axle load magnitude it should not exceed specified limit, otherwise it will cause the deformation in the sub-grade which is manifested in the form of rutting on the pavement surface. To test the strength of the sub-grade of flexible pavement, CBR test is done. Structural stability directly depends upon the strength of the material which can be compared from their CBR values. As per the IRC: 37-2012 if the CBR is less than 2% then capping layer should be provided having minimum hundred mm of modified soil (with CBR not less than 10) should be provided. For prepare cost analysis the reference has been taken from PWD schedule of rate, Govt. of Odisha (Table 5).

For cost consideration, we shall consider the following options:

(1) Only soil.
(2) Soil (100%) + plastic waste (0.3%, AR-1).

Let's consider width a pigment = 7.5 m.
Length of road = 1000 m.

4 Calculations for Cost Analysis for Unstabilised Soil CBR 3%

For Load 2 msa from IRC 37-2012

Pavement composition = Bituminous surface + WBM + GSB + SUBGRADE
= 25 + 50 + 225 + 33 = 635 mm
Cost for bituminous surface = 0.025 × 1000 × 7.5 × 97 = 0.0182 lakhs
Cost for WBM = 0.05 × 1000 × 7.5 × 1483 = 5.562 lakhs
Cost of GSB = 0.225 × 1000 × 7.5 × 1412 = 23.828 lakhs

Cost of sub-grade = 0.335 × 1000 × 7.5 × 269 = 6.759 lakhs
Cost of capping layer = 0.1 × 1000 × 7.5 × 400 = 3 lakhs
Total cost = 0.0182 + 5.562 + 23.828 + 6.759 + 3 = **39.1672** lakhs.

For Load 5 msa from IRC 37-2012

Total pavement thickness = 25 + 60 + 250 + 335 = 670 mm
Total cost calculation = 0.0182 + 6.673 + 26.475 + 6.759 + 3
= 42.92lakhs

For Load 10 msa from IRC 37-2012

Total pavement thickness = 40 + 90 + 225 + 380 = 760 mm
Total cost calculation = 0.0291 + 6.67 + 26.475 + 7.666 + 3
= 43.6951lakhs

For Load 20 msa

Total thickness = 40 + 140 + 250 + 380 = 810 mm
Total cost calculation = 0.0291 + 15.572 + 26.47 + 7.666 + 3 = 52.737 lakhs

Calculation for Plastic Waste Stabilised Soil CBR 6%

For Load 2 msa, IRC 37-2012

Total thickness = 20 + 50 + 225 + 175 = 470 mm
Total cost calculation = 0.0146 + 5.562 + 23.828 + 3.531 + 3
= 35.95 lakhs

For Load 5 msa, IRC-37-2012

Total thickness = 25 + 50 + 250 + 210 = 535 mm
Total cost = 0.0182 + 5.562 + 26.475 + 4.237 + 3
= 39.228 lakhs

For Load 10 msa, IRC-37-2012

Total thickness = 40 + 65 + 250 + 260 = 615 mm
Total cost = 0.029 + 7.223 + 26.647 + 5.245 + 3
= 39.14 lakhs

For Load 20 msa, IRC-37-2012

Table 6 Cost analysis per KM length of design of pavement

Soil type	CBR%	Cost according to traffic in lakh				Total cost in lakh
		2 msa	5 msa	10 msa	20 msa	
Only soil	3	39.1672	42.92	43.695	52.737	178.5192
Soil + plastic (0.3%)	6	35.95	39.22	39.14	41.87	156.18
Reduction in cost		3.217	3.7	4.555	10.867	22.3392
% Reduction of cost		8.22	8.62	10.42	20.6	17.55

Total thickness $= 40 + 90 + 250 + 260 = 640$ mm
Total cost $= 0.029 + 10.121 + 26.475 + 5.245 + 3$
$= 41.87$ lakhs.

Table 6 shows the total cost calculation for 1 km road length of flexible pavement layers laying over stabilized and unstabilized soil sub-grade for different traffic load conditions and the results show that there is considerable reduction of cost when pavement is constructed over stabilized soil sub-grade.

5 Conclusion

Local soil available test is inorganic clayey soil of medium plasticity properties taken and different test has been conducted for finding the property of unstabilized soil and the CBR test is done to find out strength of this soil. CBR value of UN-reinforced soil is found to be 3%. After adding plastic strip of different aspect ratio and different % by weight, the CBR of soil increase up to certain value and then decreases. The CBR value was found to be maximum 6% for 0.3% of plastic strip and aspect ratio-1. For cost analysis of pavement is done per KM of road length and it was observed that, the construction cost for pavement laying in unstabilized soil sub-grade is **39.1672 lakhs for 2 msa**, 42.92 lakhs for 5 msa, 43.6951 lakhs for 10 msa and 52.737 lakhs for 20 msa, Then the combination of 100% soil and 0.3% waste plastic gives the cost of 35.95 lakhs for load 2 msa, 39.228 lakhs for 5 msa, 39.14 lakhs for 10 msa and 41.87 lakhs for 20 msa. Hence there is reduction of cost corresponding loads are 3.217 lakhs, 3.7 lakhs, 4.555 lakhs and 10.876 lakhs respectively which gives total percentage of reduction of cost is 17.55% per km of road length. We can therefore conclude that base course thickness can be significantly reduced if waste plastic strip is used as stabilizing agent for sub-grade material. The use of plastic wastes as a stabilizer not only a best utilization of waste but also there is considerable reduction in cost which gives the huge economical benefits.

References

Amrutha TP, Krishnan A (2015) An overview on plastic waste as soil stabilizing agent. Int J Adv Res Trends Eng Technol 2(10):36–39

Hansen JB (1959) Developing a set of CBR curves. U.S. Army corps of engineers, Instruction report no. 4

Operational Effectiveness of Speed Humps in Urban Areas—A Review

Satya Ranjan Samal, Malaya Mohanty, and Dipti Ranjan Biswal

Abstract The effectiveness of the speed humps can be studied by the different static and dynamic characteristics of the vehicle. The heterogeneous traffic condition in India making things more complicated in the urban areas. In the past few years, accidents in India are increasing at an alarming rate due to the rapid growth of the motor vehicles. The number of accidents, drops only when there is a speed restriction of the different category of vehicles. Therefore, the reduction of speed of vehicles at some locations like approaches to level crossings, negotiating a sharp curve, approaching towards an intersection, accident prone locations, residential street, or near to schools and hospitals etc. become necessary for orderly traffic movement and from the safety point of view. The developing country like India, speed humps are primarily used as traffic calming devices. The present study reviews the available literature to understand the improvement in identifying the parameters influencing the effectiveness of speed hump characteristics. This paper has tried to review and recognise the gaps in research along with development of the future scope of study in this area. However, from the various literature the study found that most of the speed humps have faulty geometrical dimensions leading to various problems to the road users. Though speed humps reduce speed and increases safety, it has disadvantages like, increase in travel time, increase in the vehicle operating cost, decreases the capacity of roads and causes inconvenience to drivers and passengers.

Keywords Speed humps · Traffic calming devices · Accident · Traffic safety

S. R. Samal (✉) · M. Mohanty · D. R. Biswal
School of Civil Engineering, KIIT University, Bhubaneswar, India
e-mail: satya.samalfce@kiit.ac.in

M. Mohanty
e-mail: malaya.mohantyfce@kiit.ac.in

D. R. Biswal
e-mail: dipti.biswalfce@kiit.ac.in

B. B. Das et al. (eds.), *Recent Developments in Sustainable Infrastructure (ICRDSI-2020)—GEO-TRA-ENV-WRM*, Lecture Notes in Civil Engineering 207,
https://doi.org/10.1007/978-981-16-7509-6_66

1 Introduction

Road crashes are the ninth leading root cause of all deaths around the globe. Around 1.3 million people lose their lives on road due to road crashes each year, with about 20–50 million people inflicting serious injuries with negative health effects. More than 50% of all road crash related deaths are identified as susceptible road users, e.g. cyclists, pedestrians, and motorcyclists (WHO 2016). Road accidents are often caused by an accumulation of aspects where road users seem to be the most crucial (Domenichini et al. 2019). In a developing country like India, about 1.5 lakhs people die due to road accidents each year (MORTH 2017). According to MORTH 2017 data, over speeding and rash driving is the reason behind more than 70% of road crashes and 67% of road crash deaths. Among the numerous factors, speeding is considered to be a serious and hazardous factor for safety of road users since speeding lessens the drivers' reaction time as well as of pedestrians (Yeo et al. 2020).

Traffic engineers practice various diversified approaches in order to regulate vehicle speeds and to prevent crashes caused by over-speeding. One of the most commonly used traffic calming devices employed for the same is the placement of speed humps (Lav et al. 2018). Constructing speed humps to reduce speed is the most common type of traffic calming device due to their cheaper price and easy installation (Abdel-Wahed and Hashim 2017). In developing economies like India, a high proportion of the population use non-motorised vehicles like bicycle routinely (Patel and Vasudevan 2016). According to Patel and Vasudevan (2016), speed humps are placed mainly to increase safety of non-motorized vehicles and pedestrians by providing discomfort, through shocks and vibrations, to the passengers and drivers.

IRC 99-2018 is employed in India for construction and design of traffic calming devices like speed breakers. The guidelines in the code say that the minimum chord length for a speed hump should be 3 m and the maximum height for the same should be 0.1 m in order to decrease the speed of vehicles up to 20 kmph. However, if they are not designed properly, the vehicles moving towards the speed hump has to suddenly apply brakes in order to instantly reduce the speed which might lead to rear-end collision. According to Abdel-Wahed and Hashim (2017) the presence of faulty speed humps negatively affect the roadway level-of-service, since they increase delay due to increased travel times.

The operational effectiveness of the speed humps play a significant role in terms of traffic safety. Moreover, in developing economies, where mixed traffic is predominant, the research on the effect of speed humps on road users in terms of safety and comfort has been rare. Therefore, in the present study, a review of the literature has been conducted to have a comprehensive idea about the recent techniques adapted to evaluate the operational effectiveness of the speed hump characteristics. Various literature has been presented in the subsequent section and a detailed summary of all these literatures along with critical review has been presented in the study.

2 Review of Literature

Bennett, and Dunn (1995) examined the monitored driver deceleration behavior on a freeway in New Zealand. For the study, the researchers had placed a series of axle detectors over a 500 m interval and the speeds were recorded using a data logger. They have taken the speeds of the same vehicle at different stations along the road for over 1200 vehicles. They observed that the vehicles decelerated over the same distance irrespective of the initial speed. They concluded that the deceleration rate was proportional to the initial speed.

Dixon et al. (1997) illustrated the motorists' driving behavior as they move towards a pedestrian crossing in the presence and absence of speed humps. They hypothesized that the less risk as perceived by road users normally could be affected by the installation of tactile road stimuli like speed humps. They also employed an experimental design to quantify the reaction of motorists. Their results showed a robust relationship between driver behavior and the presence or absence of speed humps. They also opined that female drivers undertake more precautionary maneuvers than males.

Dixon and Jacko (1998) studied the effect of speed humps on motorists' behavior at pedestrian crossings. They observed 208 motorists at Florida International University in Miami, Florida for the study. They employed the experimental design to identify the motorists' reactions. Like the previous literature, their findings also concluded that female drivers take more preventive actions than male counterparts.

Barbosa et al. (2000) evaluated the impact of traffic calming measures on vehicles. A case study was conductedby them in the City of York (UK) focusing on traffic calming devices. They developed an empirical speed profile model by employing MLR techniques based on data collected at three sites.

Akçelik and Besley (2001) described the models of deceleration and acceleration. The researchers emphasized for calibration of a good model considering specific traffic facilities, various vehicle types, types of road, different levels of traffic demand, and an extensive range of initial and final speeds.

Elvik (2001) presented a detailed analysis of thirty three studies that evaluated the effects on road safety of area-wide urban traffic calming devices. The meta-analysis showed that area-wide urban traffic calming measures reduced the average number of injuries in accidents by fifteen percent.

Pau (2002) attempted a qualitative and quantitative approach towards drivers' behavior. The researcher conducted the study in Italy by observing more than twenty five thousand cars and motorcycles. He observed that apart from abrupt slow down, deceleration and acceleration before and after speed hump, the drivers tend to perform various other traffic maneuvers to minimize the uneasiness faced when travelling towards speed humps. Results disclosed that improper installation of speed bumps induced up to 50% car drivers and 85% motorcyclists to avoid the undulation in order to decrease the level of discomfort.

Wang et al. (2004) evaluated the general acceleration behavior of current passenger vehicles. They verified the model with the recent observations. They studied the

acceleration behaviors of both straight and turning movements as well as the impact of speed limits on rates of acceleration.

Galante et al. (2010) investigated drivers' behavior. Drivers' behavior was investigated by means of an experiment employing a driving simulator. They validated the simulation results by comparing the drivers' behavior in the real world scenario and in the driving simulator. They concluded more effective results in case of combined cluster analysis and statistical tests.

Bassani et al. (2011) evaluated the effectiveness of trapezoidal speed humps in reducing the operating speed of vehicles. In the city of Turin (Italy), with an average spacing of 147 m, which they monitored during two months and several speed profiles were collected with different measuring systems including a laser gun, a digital video camera and an instrumental vehicle. They developed a relationship which links operating speed measured at the midpoint between two consecutive humps to the hump spacing and lane width using multiple linear analysis. They reported that the *p*-value of the independent variable of the model are less than 0.05, indicating that the control variables affect significantly the operating speed in the middle point between two consecutive humps.

Garcia et al. (2011) evaluated the effect of traffic calming devices on their capacity and operating performance using traffic micro simulation VISSIM 5.1. They have calculated average delay and obtained the capacity of the road. They found that that the desired speed decision areas were defined from 25 m around the traffic calming devices, upstream and downstream.

Liu et al. (2011) assessed the influence of transverse rumble strips on road user safety on rural roads. The study area for speed measurement consisted of two numbers of hundred meters road sections on either side of a pedestrian crosswalks. From the t-tests results, they evaluated that transverse rumble strips are more effective in reducing road accidents in the vicinity of pedestrian crosswalks on rural roads.

Yu et al. (2011) developed a VISSIM module for simulation of highway traffic operations in the vicinity of speed humps. They collected the vehicle speed data at fifteen locations in the vicinity of speed humps. The researchers have used a genetic algorithm for calibration and validation of the RSA module.

Capri et al. (2012) focused on pedestrian safety. They evaluated the probability of collision between vehicle and pedestrian crossing. They have chosen a mathematical model. They used VISSIM 5.0 software for the micro simulation model.

Jain et al. (2012) proposed an early warning system that used an application employed on smart phones to alert the driver well in advance when the vehicle is moving towards a speed breaker. They also developed an application that constantly monitored the accelerometer on smartphone to detect beforehand unknown speed-breakers. They suggested that further improvement is required for accuracy while using multiple smartphones.

Antic et al. (2013) focused on the influences of speed bump heights with respect to the vehicle speed. The speed analysis has been conducted before and after placing the speed bumps. They have compared the 50th and 85th percentile speed. They found that speed humps in the range of 5–7 cm height should be provided in localities where vulnerable road users are highly endangered and speed bumps of 3 cm height

should be provided at less endangered locations. They also found that there had been no remarkable differences between vehicle speed ranging from the 1 day to 1 month.

Bekheet (2014) evaluated pavement performances in Alexandria Governorate. The researcher identified the patterns of pavement failure and also investigated the impact of illegal speed humps. He found that raveling was the most common distress found on the road surfaces. The researcher observed that inappropriate speed humps remarkably influenced the pavement condition.

Afrin et al. (2015) focused on the demerits caused by the excessive use of speed humps and the behavior of the driver at the faulty speed humps. They suggested that the use of real time monitoring of the driver can be more effective in the traffic monitoring and safety.

Patel and Vasudevan (2016) focused on the influence of speed humps on bicycle riders. They have taken the speed of the vehicle, geometry of the hump, and riding posture of driver to comprehend their distress levels. For the study, they recorded the vibrations by accelerometers installed on the handlebar, neck, and seat of the rider. They observed that bicyclists experienced more uneasiness as compared to motorized two-wheeler.

Abdel-Wahed and Hashim (2017) evaluated the impact of speed humps on pavement condition. For the study they have taken 52 speed. They have calculated pavement condition index (PCI). The researcher measured the characteristics, i.e. width, height, and distance from the preceding hump of each speed hump. They concluded that the conditions of pavement can play a major role for speed humps characteristics.

Arbogast et al. (2018) examined the pedestrian safety through speed humps and community engagement. They have examined the number of accidents involving vehicles and pedestrians. They observed that there was a 37.5% reduction in collisions. They suggested installation of proper speed humps near the schools and hospitals for better pedestrian safety.

Gonzalo-Orden et al. (2018) compared few traffic calming measures to assess the repeatability of their efficiency in various locality. They have compared the speed reduction of the existing traffic calming measures and evaluated the efficiency of traffic calming measure.

Lav et al. (2018) determined speed bump design that performs efficiently when drivers tried to reduce the speed of vehicles to safe levels. They have created a model to simulate the interchange between a car wheel and a speed bump. They determined the optimal design of a speed bump that will reduce the velocity of an incoming vehicle significantly without affecting the traffic safety.

Al-Obaedi (2019) evaluated the effectiveness of speed humps through real traffic data at the median U-turn. The researcher used video recordings for the data collection. He observed that the speed humps caused are markable reduction in average time spent for turning traffic. He developed regression models to evaluate merging time spent based on opposing flow rates.

Domenichini et al. (2019) assessed the interaction between driving behavior and psychological characteristics on the effectiveness of different types of traffic calming

devices at pedestrian crossings. The researchers employed 58 participants and categorized them into three groups, i.e. careful, worried and at risk. From the preliminary observation they observed that, all three groups changed their driving behavior, although they reacted differently.

Gedik et al. (2019) investigated the effect of parabolic speed hump profiles. They carried out the simulation tests to evaluate root-mean-square values. They observed that vehicle speed and height of the speed humps as the primary factors influencing comfort and safety. They suggested that parabolic speed humps are not effective beyond the vehicle speed of 25 km/h.

Abdulmawjoud et al. (2020) investigated three types of traffic calming measures located in Mosul city. They have collected the data like vehicle headways, travel times, delays, and driving speed at different locations. They observed that speed reduction for various types of speed humps ranged between 60 and 71%.

Yeo et al. (2020) analyzed the pedestrian crash near speed humps. They observed that there is a reduction of speed within thirty meters of a speed hump location and lesser pedestrian crashes occurred near speed humps. They suggested that speed humps on major roads were more effective measure for pedestrian safety.

3 Summary

The effectiveness of speed humps can be analyzed with its design, performance, impacts, operation and safety for road users, including the pedestrian, drivers as well as vehicles. The various effectiveness measures discussed here show that speed reduction, geometric features of the speed humps, vehicle and drivercharacteristics are most commonly used parameters by the researchers. Some of the recent methodologies like simulation of VISSIM software, vehicle headways consideration, parameters associated with pavement type and conditions, pedestrian and vehicle crash modeling, acceleration and deceleration phenomena have also been in the study. Almost all the factors related to speed humps have been studied by different authors.

Most of the researchers (Bennett and Dunn 1995; Dixon et al. 1997; Dixon and Jacko 1998; Pau 2002; Wang et al. 2004; Galante et al. 2010; Afrin et al. 2015; Domenichini et al. 2019) have evaluated the effectiveness of speed humps characteristics with respect to drivers as well as vehicle behavior. Although most of them have covered various parameters, but apart from few authors (Dixon et al. 1997; Dixon and Jacko 1998; Domenichini et al. 2019) none of them have taken the account of pedestrian crossing. After going through all the above mentioned road user behavior approach, it seems that the study by Domenichini et al. (2019) is the most reliable as it has considered the real-time information for road users with the driving behavior and psychological characteristics which helped to measure the effectiveness of sped humps. Nevertheless, they could have included the information like types of traffic calming devices and pavement performances. The study conducted by Pau and Angius (2001) and Bassani et al. (2011) evaluated the effectiveness of speed humps in reducing the operating speed of vehicles. The study conducted by

Bekheet (2014), Abdel-Wahed and Hashim (2017) evaluated the impact of speed humps on the performance of pavement condition, whereas Patel and Vasudevan (2016) focused on the effects of speed humps on bicycle riders.

Barbosa et al. (2000), Antic et al. (2013), Abdulmawjoud et al. (2020), and Yeo et al. (2020) investigated the influence of traffic calming measures on the vehicle speed profile. The study conducted by Antic et al. (2013) was an interesting study as it covered the geometrical features related to the speed humps. The studies conducted by researchers (Akçelik and Besley 2001; Garcia et al. 2011; Jain et al. 2012) are mostly based on the traffic simulation and modeling. Akçelik and Besley (2001) described the acceleration and deceleration models. Garcia et al. (2011) used traffic micro simulation VISSIM 5.1 to know the operational performance of the traffic calming devices, whereas Jain et al. (2012) used an early warning system that used a smartphone based application to alert the driver in advance when the vehicle is approaching a speed breaker.

Few of the articles (Jain et al. 2012; Pau 2002; Antic et al. 2013) have exhibited in their results about instantaneous and dangerous reduction in speed by vehicles while moving over the speed breakers. They opined that speed humps act as a hindrance to traffic flow resulting in an unnecessary undesirable traffic congestion scenario. Excluding Antic et al. (2013), very limited studies have tried to reconnoiter the reasons for this abrupt reduction of speed while moving on speed humps. Antic et al. (2013) concluded that at vulnerable road locations the height of speed humps should be less than 7 cm and at other less dangerous locations, the maximum height should be 3 cm. Furthermore, the safety characteristic of road users is needed to be explored more.

Fewresearchers (Elvik 2001; Johansson et al. 2011; Liu et al. 2011; Capri et al. 2012; Arbogast et al. 2018; Gedik et al. 2019) examined the impacts of traffic calming devices on traffic safety. Johansson et al. (2011), Capri et al. (2012) and Arbogast et al. (2018) focused on pedestrian safety. However, only Gedik et al. (2019) examined the consequence of speed breakers on riding comfort and safety under variable speeds, which can be considered as one of the most accurate approach and the result was found to be satisfactory with regards to the efficiency of the speed humps.

4 Conclusions

The operational effectiveness of traffic calming devices have become increasingly problematic for so many years across the globe. In developing economies, like India, the heterogeneous traffic conditions are further more complicated. The impact of traffic calming devices affect the health, environment, economy, and traffic safety, which is a major concern for researchers to address the issues and suggest comprehensive and new ideas to confront these challenges.

The presentreview is based on the operational efficiency of traffic calming devices with respect to the road uses characteristics and traffic safety. From various literatures, the researchers suggest that although there has been plenty of research in the

field of traffic calming measures, still many countries have not been able to solve the traffic calming measures associated problems. Many researchers have attempted to quantify the traffic calming measures of their respective countries with various parameters suiting to their traffic characteristics. Most of the researchers have adopted the drivers behavior and vehicle speed as a common method to study the effectiveness of traffic calming measures in terms of delays, pavement performance index, the rate of acceleration and deceleration, and pedestrian safety. It can also be seen that barring few, most of the researchers have not included the effect of non motorized vehicle in the evaluation of calming measures. Faulty design of the traffic calming measures and improper placing of road signs the are the main responsible factors for the operational effectiveness of the speed humps and traffic safety. Few researchers have also discussed about the performances of the pavement condition, which influences the traffic calming measures. Few studies also studied the impact of traffic calming measures on the road safety, mainly the safety of the pedestrians. Different methods have been suggested for proper utilization of the traffic calming measures. Most of the researchers have suggested the traffic calming measures in terms of proper design of speed humps, speed reduction implementation, proper use of road signs and marking ahead of the speed humps, and proper implementation of pedestrian safety.

It is detected that in developing countries as in India, mixed traffic scenario move on the road where lane discipline is not at all followed by the road users. The guidelines for various traffic rules and facilities are governed by different IRC codes. In this context, IRC 99:2018 provides the guidelines for design and construction of various traffic calming devices of which speed humps form the majority on Indian roads. The least reduced speed at which any vehicle should move towards a speed breaker is pegged at 20 kmph in the guideline. Similarly, a minimum value of chord length (3 m) and maximum height of the hump (0.1 m) has also been designated in the code. Since the design and operational characteristics of traffic calming measures are a widespread problem, many scopes for future studies open up in this field of research. The previous studies are primarily based on the drivers and vehicle behavior, which are practically good and economical; however, are getting old and outdated. New approaches like simulation by VISSIM software, vehicle headways consideration, parameters associated with pavement type and conditions, pedestrian and vehicle crash modeling, acceleration and deceleration phenomena are better alternatives as they are more accurate and user friendly. In a developing country like India, ITS techniques are usually not capable to solve the problems associated with traffic calming devices due to the high cost and mixed traffic conditions. Better traffic calming measures strategies with good traffic safety management system should be incorporated precisely to enhance the operational effectiveness of the speed humps and ensure a safe movement for vehicles.

References

Abdel-Wahed TA, Hashim IH (2017) Effect of speed hump characteristics on pavement condition. J Traffic Transp Eng (Engl Ed) 4(1):103–110

Abdulmawjoud AA, Jamel MG, Al-Taei AA (2020) Traffic flow parameters development modelling at traffic calming measures located on arterial roads. Ain Shams Eng J 12(1):437–444 https://doi.org/10.1016/j.asej.2020.04.014

Afrin M, Mahmud MR, Razzaque MA (2015) Real time detection of speed breakers and warning system for on-road drivers. In: 2015 IEEE international WIE conference on electrical and computer engineering (WIECON-ECE). IEEE, pp 495–498

Akçelik R, Besley M (2001) Acceleration and deceleration models. In: 23rd conference of Australian institutes of transport research (CAITR 2001), vol 10. Monash University. Melbourne, Australia, p 12

Al-Obaedi J (2019) Investigation the effect of speed humps on merging time of u-turn traffic. Ain Shams Eng J 10(1):1–4

Antic B, Pesic D, Vujanic M, Lipovac K (2013) The influence of speed bumps heights to the decrease of the vehicle speed–Belgrade experience. Saf Sci 57:303–312

Arbogast H, Patao M, Demeter N, Bachman S, Devietti E, Upperman JS, Burke RV (2018) The effectiveness of installing a speed hump in reducing motor vehicle accidents involving pedestrians under the age of 21. J Transp Health 8:30–34

Barbosa HM, Tight MR, May AD (2000) A model of speed profiles for traffic calmed roads. Transp Res Part A Policy Pract 34(2):103–123

Bassani M, Dalmazzo D, Riviera PP (2011) Field investigation on the effects on operating speed caused by trapezoidal humps. In: Proceedings of the transportation research board 90th annual meeting. Washington, DC, USA, pp 23–27

Bekheet W (2014) Short term performance and effect of speed humps on pavement condition of Alexandria Governorate roads. Alex Eng J 53(4):855–861

Bennett C, Dunn R (1995) Driver deceleration behaviour on a motorway in New Zealand. Transp Res Rec J Transp Res Board 1510:70–74

Capri S, Ignaccolo M, Inturri G (2012) Evaluating the effectiveness of traffic calming devices: using simulation to overcome analytical models assumptions. Int J Traffic Transp Eng (Rosemead, Calif) 1(3):45–51

Dixon MA, Jacko JA (1998) An investigation of tactile and visual stimuli in the roadway environment. Percept Mot Skills 87(2):387–394

Dixon MA, Alvarez JA, Rodriguez J, Jacko JA (1997) The effect of speed reducing peripherals on motorists' behavior at pedestrian crossings. Comput Ind Eng 33(1–2):205–208

Domenichini L, Branzi V, Smorti M (2019) Influence of drivers' psychological risk profiles on the effectiveness of traffic calming measures. Accid Anal Prev 123:243–255

Elvik R (2001) Area-wide urban traffic calming schemes: a meta-analysis of safety effects. Accid Anal Prev 33(3):327–336

Galante F, Mauriello F, Montella A, Pernetti M, Aria M, D'Ambrosio A (2010) Traffic calming along rural highways crossing small urban communities: driving simulator experiment. Accid Anal Prev 42(6):1585–1594

Garcia A, Torres AJ, Romero MA, Moreno AT (2011) Traffic microsimulation study to evaluate the effect of type and spacing of traffic calming devices on capacity. Proc Soc Behav Sci 16:270–281

Gedik A, Bilgin E, Lav AH, Artan R (2019) An investigation into the effect of parabolic speed hump profiles on ride comfort and driving safety under variable vehicle speeds: a campus experience. Sustain Cities Soc 45:413–421

Gonzalo-Orden H, Pérez-Acebo H, Unamunzaga AL, Arce MR (2018) Effects of traffic calming measures in different urban areas. Transp Res Proc 33:83–90

Jain M, Singh AP, Bali S, Kaul S (2012) Speed-breaker early warning system. In: NSDR

Johansson C, Rosander P, Leden L (2011) Distance between speed humps and pedestrian crossings: does it matter? Accid Anal Prev 43(5):1846–1851

Lav AH, Bilgin E, Lav AH (2018) A fundamental experimental approach for optimal design of speed bumps. Accid Anal Prev 116:53–68
Liu P, Huang J, Wang W, Xu C (2011) Effects of transverse rumble strips on safety of pedestrian crosswalks on rural roads in China. Accid Anal Prev 43(6):1947–1954
Mohanty M, Raj Y, Tiwary U, Roy S, Rout S, Samal SR (2021) Operational effects of speed breakers: a case study in India. Eur Transp 81(1):1–10 https://doi.org/10.48295/ET.2021.81.1
MORTH (2017) Road Accidents in India
Patel T, Vasudevan V (2016) Impact of speed humps of bicyclists. Saf Sci 89:138–146
Pau M (2002) Speed bumps may induce improper drivers' behavior: case study in Italy. J Transp Eng 128(5):472–478
Pau M, Angius S (2001) Do speed bumps really decrease traffic speed? an Italian experience. Accid Anal Prev 33(5):585–597
Wang J, Dixon KK, Li H, Ogle J (2004) Normal acceleration behavior of passenger vehicles starting from rest at all-way stop-controlled intersections. Transp Res Rec 1883(1):158–166
World Health Organisation (2016) Road traffic injuries, Factsheet
Yeo J, Lee J, Cho J, Kim DK, Jang K (2020) Effects of speed humps on vehicle speed and pedestrian crashes in South Korea. J Saf Res
Yu H, Liu P, Huang J, Zhang X (2011) Developing the simulation module of traffic operations in vicinity of speed bumps on highways in VISSIM. In: ICCTP 2011: towards sustainable transportation systems, pp 2375–2384

Monitoring of PM_{10} Aerosols in Outdoor Environment During Diwali Festival Over Bhubaneswar

Sushree Sasmita and Dudam Bharath Kumar

Abstract Studies on aerosol pollution monitoring gained considerable attention in recent decade, particularly, during the episodes of naturally and anthropogenically induced change in emission. The episodic events of PM_{10} aerosol levels in the ambient air were monitored during Diwali festival week. The activity of fire-works during the festival leads to the increase of pollution concentration levels (e.g. particulates, dust, gases), thereby worsening the air quality of the atmosphere. Present study was carried out from 5-11-2018 to 9-11-2018 on the terrace of KIIT, DU School of Civil Engineering, and Campus-3 in Bhubaneswar. The ambient concentrations of various air pollutants such as $PM_{10,}$ TSP was assessed during Pre-Diwali, During Diwali, Post Diwali for the present study. The analysis was carried out by using the instrument Respirable Dust Sampler for monitoring PM_{10} and TSP. The results showed that the mass concentrations of PM_{10} was found to be 50, 85.41 and 73.61 $\mu g\ m^{-3}$ on Pre-Diwali (5–6, November), During Diwali (on 7 November) and Post Diwali (8–9, November) days respectively. The 24 and 12 h N/D ratio are maintained on 5th and 9th of November 2018 and 12 h on 6th, 7th and 8th of November 2018. The corresponding 12 h ratio of PM_{10} between night time and daytime was calculated to be 2.33, 3.23 and 1.80 for the corresponding days. The prevailing meteorology and calm atmospheric condition was favourable for pollution after the fire event (Diwali) particularly on 9th of November 2018.

Keywords Diwali · PM_{10} aerosol · Outdoor

1 Introduction

The festival of lights Diwali is celebrated in India in usually the months of late October or early November and is known to be the festival of lights. Fire-crackers are burnt by people to celebrate the occasion. Fire-crackers release aerosol into the

S. Sasmita · D. B. Kumar (✉)
School of Civil Engineering, Kalinga Institute of Industrial Technology Deemed to be University (KIIT-DU), Bhubaneswar, Odisha 750124, India
e-mail: dudam.kumarfce@kiit.ac.in

B. B. Das et al. (eds.), *Recent Developments in Sustainable Infrastructure (ICRDSI-2020)—GEO-TRA-ENV-WRM*, Lecture Notes in Civil Engineering 207,
https://doi.org/10.1007/978-981-16-7509-6_67

atmosphere when they are burnt during any festival, New Year or celebration, sports event in any part of the world (Allan et al. 2010). During the festivals the mass concentrations of PM_{10} and $PM_{2.5}$ aerosols increases to more than ten times the normal concentrations due to burning of crackers (Gautam et al., 2018). Burning of firecrackers affects the human health severely especially in the children, women, and elderly people (Kannan et al. 2004). The smoke plumes arising from fire events raise the atmospheric particulate matter (PM) levels from tens to thousands of $\mu g\ m^{-3}$ (Joly et al. 2010), the fire emissions penetrates through the respiratory tract and causes health effects (Barnett et al. 2005; Hamad et al. 2016). The impact of Diwali on the atmosphere is very harmful due to the release of poisonous gases and particulate emissions. The Central Pollution Control Board (CPCB) has laid down 24 h National Ambient Air Quality Standards (NAAQS) for PM_{10} and $PM_{2.5}$ as 100 and 60 $\mu g/m^3$.

Bhubaneswar is a fast growing smart city with vegetation, infrastructure, roadways and rapidly increasing in developing technological advancements. During diwali the people burning fire-crackers is having an immense impact on the atmosphere and the increase in concentration of particulate emission is maximum during the nighttime of diwali which can be analyzed by considering the values obtained during the campaign.

2 Methodology

The monitoring was done by using Respirable Dust Sampler 460BL of Envirotech Pvt. Ltd. to monitor PM_{10} and TSP. Samples were collected during these days and measurements were done by gravimetric method to estimate the variations of particulate matter during the festival. The monitoring was done for 24 h during the first and last day of the campaign on 5th and 9th of November. The other three days were monitored for 12 h during day and night and samples were collected twice during 6th, 7th and 8th of the month. The samples were carefully and filter papers were measured before and after the monitoring to measure the particulate concentration. After the measurements samples were preserved for further analysis.

3 Site Description

3.1 Study Area-Bhubaneshwar

The capital of Odisha is Bhubaneswar. Bhubaneswar (refer Fig. 1) has its own geographic features that are distinct in nature. The present study is carried out in KIIT campus-3 in Bhubaneswar during 5th to 9th of November during 2018.

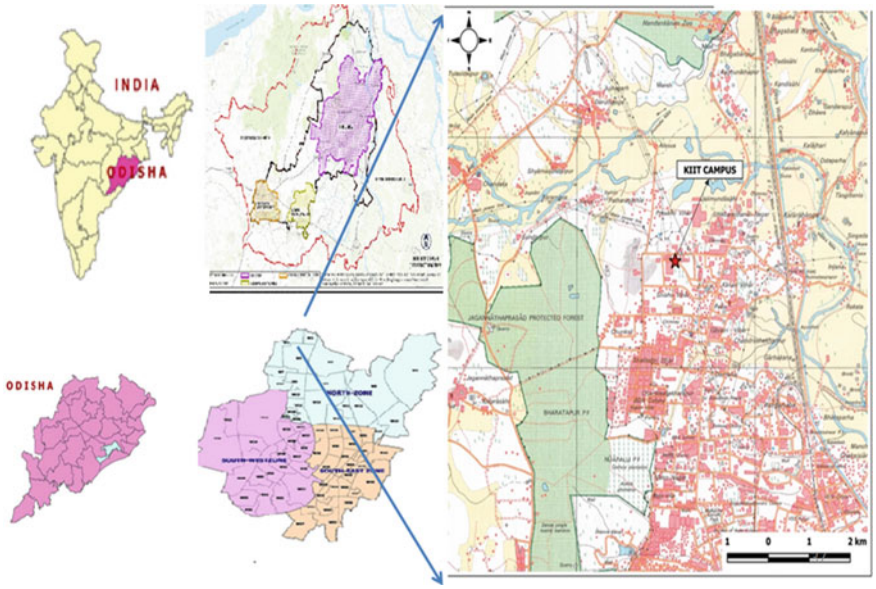

Fig. 1 Site location of ambient outdoor particulate matter concentration situate at KIIT Deemed to be University Bhubaneswar, Odisha, India (85.81° E, 20.25° N, 49 masl)

4 Results and Discussion

4.1 Surface Concentration of PM_{10} and Total Suspended Particulate (TSP)

Episodic quantities of surface particulate matter concentration was analyzed during Diwali festival days (2 days prior, during and 2 days after the festival) at two size bins namely particulate matter less than or equal to 10 μm (PM_{10}) and total suspended particulate matter (TSP). In order to investigate the day and night variability of pollution parameters, we monitored instrument for the collection of the target pollutants at two time periods (day: 8 am to 8 pm and night: 8 pm to 8 am). Ground based surface concentration of PM_{10} and TSP for whole day were observed to be highest in two episodic events including on diwali and after diwali events compared to that of prior diwali events. In particular, the corresponding night-time difference between during-diwali and post-diwali episodes exhibits 25–30 $\mu g\ m^{-3}$, respectively.

To investigate day/night differences of pollution generation in urban landscape on road side at the surface level, a ratio of surface concentration between daytime and nighttime values were used. The ratio of PM_{10} between night time and daytime was calculated to be 2.33, 3.23 and 1.80 for the corresponding days. Thus, in turn signifies the importance of accumulation of airborne particulates at the surface are

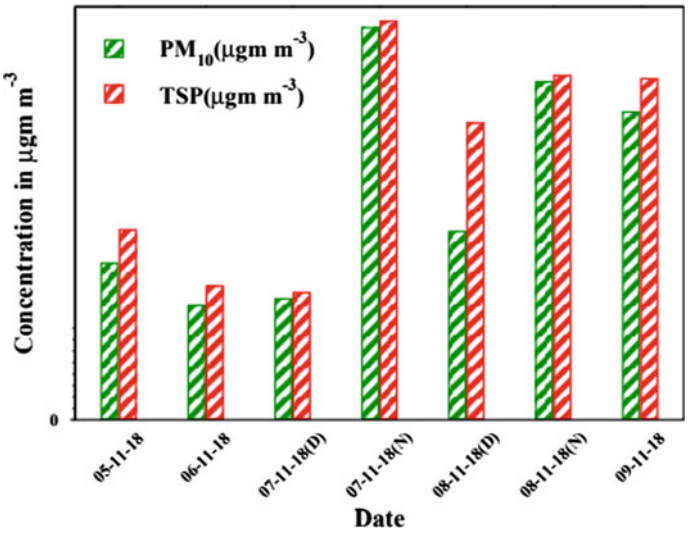

Fig. 2 Episodic events of pollution parameters (PM_{10} and TSP) observed at Bhubaneswar during (07-11-2018: day, D and night, N), pre- (05-11-2018 to 06-11-2018) and post-diwali (08-11-2018: day, D and night, N and 09-11-2018)

maximum during the night time. This may happens due to the fumigation effect of air parcel plumes that triggers the pollution accumulation at nighttime (Fig. 2).

4.2 Prevailing Meteorology

It is observed in our study meteorological parameters are likely to influence the pollution accumulation in urban locations in India, particularly, Bhubaneswar. We analyzed the episode-wise analysis of meterology influence on pollution by binning of meteorological parameters including temperature, relative humidity, wind speed along with pollution surface concentrations (PM_{10} and TSP). Results show that temperature and wind speed during pre-diwali days and on diwali day have constant values such as 28 °C and 2 m/s when compared to post-diwali days being relatively cool and stable (27 °C and 1 m/s, respectively). However, relative humidity was high during diwali day compared to that of other days that signifies the less dry weather on the festive day (refer Table 1).

Table 1 Episodic features of meterological parameters during, pre- and post-diwali days

Days	PM10	TSP	TEMP (C)	WS (m/s)	RH (%)
Pre-diwali	68	83	28	2	51
	50	58	28	2	54
During-diwali	112	115	28	2	54
Post-diwali	115	140	28	1	51
	134	149	27	1	50

5 Conclusion

The Diwali festival is celebrated every year among the people but the resulting impact on human and atmosphere is very severe. The particulate matter concentration is much higher during diwali day sample in comparison to pre- and post-diwali samples. The particulate matter and total suspended particles were found to be quite high in comparison to pre- and post-Diwali days which results in health impacts.

Acknowledgements This work was supported by the Kalinga Institute of Industrial Technology-Deemed to be University (KIIT-DU) Bhubaneswar.

References

Allan JD, Williams PI, Morgan WT, Martin CL, Flynn MJ, Lee J, Nemitz E, Phillips GJ, Gallagher MW, Coe H (2010) Contributions from transport, solid fuel burning and cooking to primary organic aerosols in two UK cities. Atmos Chem Phys 10:647–668

Barnett AG, Williams GM, Schwartz J, Neller AH, Best TL, Petroeschevsky AL, Simpson RW (2005) Air pollution and child respiratory health: a case-crossover study in Australia and New Zealand. Am J Respir Crit Care Med 171:1272–1278

Gautam S, Yadav A, Pillarisetti A, Smith K, Arora N (2018) Short-term introduction of air pollutants from fireworks during diwali in Rural Palwal, Haryana, India: a case study. Earth Environ Sci 120:1–6

Hamad S, Green D, Heo J (2016) Evaluation of health risk associated with fireworks activity at Central London. Air Qual Atmos Health 9:735–741

Kannan GK, Gupta M, Kapoor JC (2004) Estimation of gaseous products and particulate matter emission from garden biomass combustion in a simulation fire test chamber. Atmos Environ 38:6701–6710

Joly A, Smargiassi A, Kosatsky T, Fournier M, Dabek-Zlotorzynska E, Celo V, Mathieu D, Servranckx R, D'amours R, Malo A, Brook J (2010) Characterisation of particulate exposure during fireworks displays. Atmosp Environ 44(34):4325–4329